BRITISH JOURNAL OF
APPLIED PHYSICS

633

EDITOR

H. R. LANG

A.R.C.S., PH.D., F.INST.P.

Secretary of The Institute of Physics

VOLUME 9

1958

LONDON

THE INSTITUTE OF PHYSICS

EASTMAN KODAK CO.
RESEARCH LIBRARY
KODAK PARK

BRITISH JOURNAL OF APPLIED PHYSICS

ADVISORY COMMITTEE

for year ending 30 September, 1958

J. M. A. LENIHAN, M.SC., PH.D., A.M.I.E.E., F.INST.P., *Chairman*

C. B. ALLSOPP, M.A., PH.D., D.SC., F.INST.P., *Representing the British Institute of Radiology*

H. BARRELL, A.R.C.S., D.SC., F.INST.P.

W. BETTERIDGE, B.SC., PH.D., F.INST.P.

R. L. BROWN, M.A., F.INST.P.

A. B. D. CASSIE, C.B.E., M.A., PH.D., D.SC., F.INST.P.

W. H. J. CHILDS, PH.D., D.SC., F.INST.P., F.R.S.E., *Representing the Scottish Branch*

W. D. CORNER, B.SC., PH.D., F.INST.P., *Representing the North Eastern Branch*

J. E. GEAKE, M.SC., PH.D., A.INST.P., *Representing the Manchester and District Branch*

K. E. GREW, PH.D., D.SC., F.INST.P., F.R.S.E., *Representing the South Western Branch*

M. E. HAINE, D.SC., F.INST.P.

S. T. HENDERSON, M.A., PH.D., F.INST.P.

O. W. HUMPHREYS, C.B.E., B.SC., M.I.E.E., F.INST.P., *President, The Institute of Physics*

E. J. IRONS, PH.D., D.SC., A.M.I.E.E., F.INST.P., *Representing the Education Group*

O. P. T. KANTOROWICZ, D.PHIL., F.INST.P.

R. KING, B.SC., A.INST.P.

H. LIPSON, M.A., D.SC., F.INST.P., F.R.S.

M. MCCAIG, M.SC., PH.D., F.INST.P., *Representing the Yorkshire Branch*

J. W. MENTER, M.A., PH.D., F.INST.P., *Representing the Electron Microscopy Group*

F. OLDHAM, M.A., B.SC., F.INST.P., J.P.

E. A. OWEN, M.A., M.SC., SC.D., D.SC., F.INST.P., *Representing the Liverpool and North Wales Branch*

H. O. PULS, B.SC., PH.D., F.INST.P., *Representing the South Wales Branch*

T. LL. RICHARDS, B.SC., PH.D., F.I.M., F.INST.P., *Representing the Midland Branch*

G. D. ROBINSON, B.SC., PH.D., F.INST.P., *Representing the Royal Meteorological Society*

L. ROTHERHAM, M.SC., F.I.M., F.INST.P.

W. E. SCHALL, B.SC., F.INST.P., *Representing the Non-Destructive Testing Group*

H. SPOONER, B.SC., A.INST.P., *Representing the Stress-Analysis Group*

E. G. STANFORD, M.SC., PH.D., F.INST.P.

J. R. STANSFIELD, M.A., F.INST.P., *Representing the Applied Spectroscopy Group*

E. G. STEWARD, B.SC., PH.D., F.INST.P., *Representing the X-ray Analysis Group*

A. M. TAYLOR, M.A., PH.D., F.INST.P., *Representing the London and Home Counties Branch*

J. TAYLOR, M.B.E., PH.D., D.SC., F.R.I.C., F.INST.P., *Honorary Treasurer, The Institute of Physics*

J. THEWLIS, D.SC., F.INST.P.

S. TOLANSKY, PH.D., D.SC., F.INST.P., F.R.S., *Representing The Physical Society*

F. A. VICK, O.B.E., B.SC., PH.D., A.M.I.E.E., F.INST.P., *Honorary Secretary, The Institute of Physics*

R. G. WOOD, M.SC., A.M.I.E.E., F.INST.P.

D. A. WRIGHT, D.SC., F.INST.P., *Representing the Electronics Group and The Physical Society*

CONTENTS OF VOLUME 9

PAGE

JANUARY 1958

CONFERENCE REPORT

Summarized proceedings of a conference on biological structures and computational methods—London, November 1956. By J. Finch, D. W. Green, K. C. Holmes and A. C. T. North 1

ORIGINAL CONTRIBUTIONS

Measurement of elasticity and anelasticity of small disks by an inductor method. By G. Bradfield and F. A. Levi 13

The use of polytetrafluoroethylene as a lubricant. By E. Kay and E. D. Tingle 17

A technique for obtaining thin foils of aluminium and aluminium alloys for transmission electron metallography. By R. B. Nicholson, G. Thomas and J. Nutting 25

An overall test of equations of state of fluids. By N. Davy and Barbara M. Bell 27

The electric strength and molecular structure of liquids. By T. J. Lewis 30

Photoelastic investigation of stresses in composite models with notches and holes. By Heihachi Shimada . 34

The effect of specimen diameter on the straining of a cylindrical load-cell. By J. F. W. Bishop and M. T. Watkins 38

Determination of density of liquids under elevated gas pressure. By K. Goldman 40

NOTES AND NEWS

New books 43

FEBRUARY 1958

SPECIAL ARTICLE

Electroluminescence. By S. T. Henderson 45

ORIGINAL CONTRIBUTIONS

The thermal conductivity of nitrogen and argon in the liquid and gaseous states. By H. Ziebland and J. T. A. Burton 52

Reflexion electron microscopy at high angles. By D. H. Page 60

An improved spray droplet technique for quantitative electron microscopy. By H. L. Nixon and H. L. Fisher 68

A property of a buckled elastic rod. By G. A. Leaf . 71

The influence on the stress distribution in an adhesive lap joint of bending of the adhering sheets. By A. S. McLaren and I. MacInnes 72

NOTES AND NEWS

Correspondence

The sampling efficiency of the thermal precipitator. By H. H. Watson 78

New books 80

Notes and comments 84

PAGE

MARCH 1958

SPECIAL ARTICLE

A survey of exo-electron emission phenomena. By L. Grunberg 85

ORIGINAL CONTRIBUTIONS

Aluminosilicates and the high-temperature processing of microwave vacuum tubes. By M. Hillier and R. L. Bell 94

The particle size of some Witwatersrand mine dust. By H. St. G. Tucker 98

The synthesis of single crystals of the sulphides of zinc, cadmium and mercury and of mercuric selenide by vapour phase methods. By D. R. Hamilton . . 103

The low-temperature conductivity of oxide-coated cathodes. By G. S. Higginson 106

The indium–selenium system. By J. C. Brice, P. C. Newman and H. C. Wright 110

Temperature and pressure corrections to be applied to the shielded hot wire anemometer at speeds for which natural convective cooling is negligible. By C. F. Cowdrey 112

Magnetic anisotropy measurement with an oscillation magnetometer. By J. R. Macdonald 116

Transfer of tungsten carbide to soft metals during single-traverse and reciprocating sliding. By J. Golden and G. W. Rowe 120

NOTES AND NEWS

Correspondence

Temperature coefficient of maintenance potential of glow discharge voltage stabilizer and regulator tubes. From J. Smith 122

Comments on the A.S.T.M. Powder Data File—3. From J. W. Hughes, Isabel E. Lewis and A. J. C. Wilson . 123

New books 123

APRIL 1958

SPECIAL ARTICLE

The mechanical wear of metals. By W. Hirst . . . 125

ORIGINAL CONTRIBUTIONS

The geometry of twisted multi-filament structures. By G. J. Stansfield 133

Beam temperature, discharge lag and target biasing in some television pick-up tubes. By B. Meltzer and P. L. Holmes 139

An electrical analogue method of predicting the permeability of unsaturated porous materials. By M. C. Probine 144

A sintered nickel matrix cathode. By R. W. Fane . 149

The evaporation of sprays. By R. T. Jarman . . . 153

Measurements on the air-nuclei in natural water which give rise to cavitation. By K. S. Iyengar and E. G. Richardson 154

Measurements of pressure distribution between metal and rubber covered rollers. By G. J. Parish . . . 158

A method for determining ^{24}Na and ^{42}K when present together in liquid samples. By M. P. Esnouf . . 161

PAGE

NOTES AND NEWS

New books 163

Notes and comments 164

MAY 1958

SPECIAL ARTICLE

Physical methods of investigating chemical problems. By R. J. TAYLOR 165

ORIGINAL CONTRIBUTIONS

The photoelastic behaviour of cross-linked polymers. By Z. TUZI, K. KAWATA and I. HORI 173

Calculated and observed effects of texture on the magnetic properties and Young's modulus of nickel sheet. By E. R. W. JONES, C. A. CLARK and E. A. FELL . . . 178

Prismatic fin with non-linear heat loss analysed by resistance network and iterative analogue computer. By I. C. HUTCHEON and D. B. SPALDING 185

A portable lamination detector for steel sheet. By B. O. SMITH, A. P. H. JENNINGS and A. G. GRIMSHAW . 191

The high temperature stability of permanent magnets of the iron–nickel–aluminium system. By A. G. CLEGG and M. MCCAIG 194

A note on the adhesion of elastic solids. By K. L. JOHNSON 199

NOTES AND NEWS

Correspondence

A method for distinguishing between sources of noise in motor-cars. From A. E. W. AUSTEN and T. PRIEDE . 201

A rapid method for separating the principal stresses in plane photoelasticity. From I. BRODIE 201

Notes and comments 204

JUNE 1958

SPECIAL ARTICLE

Photoconductivity. By D. A. WRIGHT 205

ORIGINAL CONTRIBUTIONS

Sources of error in electron steremicroscopy. By R. I. GARROD and J. F. NANKIVELL 214

The pneumatic conveying of spheres through straight pipes. By J. A. HITCHCOCK and C. JONES . . . 218

NEW BOOKS SECTION (containing reviews of 49 books) 223

ORIGINAL CONTRIBUTIONS (*continued*)

Mechanical testing of materials in the transition region between steady flow and failure. By A. JOBLING and J. E. ROBERTS 235

The time-constant of carbon composition resistors. By G. H. RAYNER 240

Bonding optical components to metal mounts. By K. H. SPRING 242

The effective coefficient of friction for strings traversing cylinders transversely and slantwise. By C. MACK and C. RUBENSTEIN 247

A "super-elastic" single crystal calibration bar. By W. A. RACHINGER 250

PAGE

JULY 1958

SPECIAL ARTICLE

Recent developments in electron microscopy. By V. E. COSSLETT 253

ORIGINAL CONTRIBUTIONS

Thermionic and related properties of calcium oxide. By B. J. HOPKINS and F. A. VICK 257

The analysis of particle counts by the spray-drop method. By K. I. WILLIAMSON and W. B. TAYLOR 264

The chromatic field aberrations and their correction in a three-lens reflexion electron microscope. By D. H. PAGE 268

Solid angle corrections to single scattering. By F. F. HEYMANN and P. I. P. KALMUS 271

New techniques for the study of Bitter figures. By D. J. CRAIK and P. M. GRIFFITHS 279

A photoelastic technique for strain measurement on flat aluminium alloy surfaces. By H. FESSLER and D. J. HAINES 282

Stability and convergence limitations on the use of analogue computers with resistance network analogues. By M. E. FISHER 288

The performance of infra-red photoconductive cells. By D. H. ROBERTS and B. L. H. WILSON 291

NOTES AND NEWS

Correspondence

A note on the calculation of second moments of nuclear magnetic resonance absorption lines. From J. G. POWLES 299

AUGUST 1958

SPECIAL ARTICLE

Atmospheric pollution and the soiling of textile materials. By W. H. REES 301

CONFERENCE REPORT

Summarized proceedings of a conference on electron microscopy—Bangor, September 1957. By H. W. EMERTON 306

ORIGINAL CONTRIBUTIONS

The ratio of characteristic to white X-radiation from a copper target. By E. G. BENDIT 312

The ageing of vacuum standard lamps on a.c. and d.c. By W. BARNETT, R. G. BERRY and J. S. PRESTON . 317

The dependence of stress distribution on elastic constants. By MARGERY CLUTTERBUCK 323

Pulse-annealing technique for metals and alloys. By P. WRIGHT and K. THOMAS 330

A constant liquid flow device. By G. H. LAYCOCK . 333

The effect of gettering on the reflectivity of aluminium films. By L. HOLLAND 336

NOTES AND NEWS

Correspondence

Frictional behaviour and structure of the surface oxides of steel. From YASUKATSU TAMAI 338

Notes and comments 339

PAGE

SEPTEMBER 1958

SPECIAL ARTICLE

The physics of fibres with special reference to wool. By A. B. D. CASSIE 341

ORIGINAL CONTRIBUTIONS

Some developments and applications of microfocus X-ray diffraction techniques. By A. FRANKS 349
Temperature distribution throughout a stack of electrical sheet steel during annealing. By R. J. WAKELIN . 353
Heat-reflecting windows using gold and bismuth oxide films. By L. HOLLAND and G. SIDDALL 359
A general scheme for the examination of precipitates and inclusions in steels. By G. R. BOOKER and J. NORBURY 361
The performance of bismuth telluride thermojunctions. By H. J. GOLDSMID, A. R. SHEARD and D. A. WRIGHT 365
The flow of heat in a parallel-faced infinite solid. By T. P. NEWCOMB 370
Studies of the viscosity and sedimentation of suspensions. Part 4.—Capillary-tube viscometry applied to stable suspensions of spherical particles. By G. H. HIGGINBOTHAM, D. R. OLIVER and S. G. WARD 372
Energy balance in disk seal oscillators at ultra-high frequencies. By M. R. GAVIN and I. J. HERBST . . 377

OCTOBER 1958

ORIGINAL CONTRIBUTIONS

The influence of shear and rotatory inertia on the free flexural vibration of wooden beams. By R. F. S. HEARMON 381
Photoelastic properties of plasticised polymethyl methacrylate in the glassy state. By J. H. LAMBLE and E. S. DAHMOUCH 388
The theory of ballast tubes or barretters. By R. O. JENKINS 391
The bistable behaviour of the magnetic transductor. By E. H. FREI, S. SHTRIKMAN and D. TREVES 394

NEW BOOKS SECTION (containing reviews of 38 books) 396

ORIGINAL CONTRIBUTIONS (*continued*)

Proportional counters in X-ray spectro-chemical analysis. By T. MULVEY and A. J. CAMPBELL 406
The cleaning of glass in a glow discharge. By L. HOLLAND 410
Structure-cell data and expansion coefficients of bismuth telluride. By M. H. FRANCOMBE 415

NOTES AND NEWS

Correspondence

A note on the paper "The oxidation of evaporated barium films (getters)." From S. J. GREGG and W. B. JEPSON; R. N. BLOOMER 417
Selected area microdiffraction in the electron microscope. From A. W. AGAR 419

Notes and comments 420

PAGE

NOVEMBER 1958

ORIGINAL CONTRIBUTIONS

The relationship between surface texture and rolling resistance of steel. By J. HALLING 421
Apparent slip between metal and rubber-covered pressure rollers. By G. J. PARISH 428
The measurement of the strain-dependent damping of metals vibrating torsionally. By G. SUMNER and K. M. ENTWISTLE 434
Resonant cavity methods of measuring ferrite properties. By R. A. WALDRON 439
γ-ray yield and spectra produced by irradiating backing materials with protons. By S. E. HUNT, R. A. POPE, W. W. EVANS and D. A. HANCOCK 443
Crystallographic programmes for a computer. By J. C. GOWER and J. H. RAYNER 446
Stresses and strains in an infinite elastic sheet under a tension applied at two rigid pairs of square jaws. By DAPHNE G. PADFIELD and NORA B. DICKINSON . . . 448
The dielectric constant of zinc oxide over a range of frequencies. By N. H. LANGTON and D. MATTHEWS . 453
The radial flow of heat in an infinite cylinder. By T. P. NEWCOMB 456
The temperature dependence of noise temperature ratio in germanium diodes. By A. HENDRY 458

DECEMBER 1958

SPECIAL ARTICLE

The choice of resilient materials for anti-vibration mountings. By J. C. SNOWDON 461

ORIGINAL CONTRIBUTIONS

The performance of spark guards. By J. H. MCGUIRE and MARGARET LAW 470
Electrical properties of chalcopyrite. By B. DONOVAN and G. REICHENBAUM 474
A generalized theory of sedimentation. By A. D. MAUDE and R. L. WHITMORE 477
Resistance bias characteristic of the electron microscope gun. By M. E. HAINE, P. A. EINSTEIN and P. H. BORCHERDS 482
The friction of mineral particles. By R. T. SPURR . 486
The magnetic stabilization of low pressure d.c. arcs. By H. WROE 488
The grid emitting properties of titanium. By J. A. CHAMPION 491
The influence of the method of demagnetization on the reversible permeability of a high-permeability nickel-iron alloy. By R. C. JACKSON, E. W. LEE and A. G. H. TROUGHTON 495

NOTES AND NEWS

Correspondence

Deuterium-filled thyratrons. From K. G. COOK and G. G. ISAACS 497
Deuterium as a filling for high-voltage thyratrons. From R. J. ARMSTRONG and N. S. NICHOLLS 498

Notes and comments 500

SUBJECT INDEX TO VOLUME 9 501

AUTHOR INDEX TO VOLUME 9 506

INDEX TO VOLUME 9

SUBJECT INDEX

(SA) denotes special article, (CR) conference report, (C) correspondence.

Acoustics

Measurements on the air-nuclei in natural water which give rise to cavitation, K. S. Iyengar and E. G. Richardson 154
Method for distinguishing between sources of noise in motor-cars, A. E. W. Austen and T. Pride 201 (C)

Air measurements, pollution

Atmospheric pollution and the soiling of textile materials, W. H. Rees 301 (SA)
Evaporation of sprays, R. J. Jarman 153
Particle size of some Witwatersrand mine dust, H. St. G. Tucker 98
Physics of fibres with special reference to wool, A. B. D. Cassie 341 (SA)
Sampling efficiency of the thermal precipitator, H. H. Watson 78 (C)
Temperature and pressure corrections to be applied to the shielded hot wire anemometer at speeds for which natural convective cooling is negligible, C. F. Cowdrey 112

Biology

Recent developments in electron microscopy, V. E. Cosslett 253 (SA)
Reflexion electron microscopy at high angles, D. H. Page 60
Summarized proceedings of a conference on biological structures and computational methods—London, November 1956, J. Finch, D. W. Green, K. C. Holmes and A. C. T. North 1 (CR)

Book reviews

Achema Year Book 1956/1958 *European catalogue of apparatus and equipment* 405
Advances in electronics and electron physics. Vol. IX, by L. Marton 403
Analog computer techniques, by C. L. Johnson 226
Analytical design of linear feedback controls, by G. C. Newton, Jr., L. A. Gould and J. F. Kaiser 83
Angular momentum in quantum mechanics, by A. R. Edmonds 231
Applied mathematics and mechanics. Vol. 1. Gas dynamics, by Klaus Oswatitsch 82
Atomic energy in medicine, by K. E. Halnan 230
Basic automatic control theory, by G. F. Murphy 80
Chemical engineering practice. Vol. 4. Fluid state, edited by H. W. Cremer and T. Davies 401
Chemistry of the rare radioelements, by K. W. Bagnall 228
Comprehensive inorganic chemistry. Vol. 6. The alkali metals, by J. F. Suttle, and *Hydrogen and its isotopes*, by R. C. Brasted, edited by M. Cannon Sneed and R. C. Brasted 229
Computers, bibliographical series 83
Cosmic electrodynamics, by J. W. Dungey 398
Cosmic radiation, The, by J. E. Hooper and M. Scharff 398
Dictionary of physics, by H. J. Gray 403
Diffusion dans les métaux, La, edited by J. D. Fast, H. G. van Bueren and J. Philibert 124
Digital computer components and circuits, by R. K. Richards 399
Digital computer programming, by D. D. McCracken 124
Einführung in die Physik der magnetischen Werkstoffe, by Karl M. Koch and W. Jellinghaus 43
Electric contacts handbook. 3rd ed., by R. Holm, aided by Else Holm 234
Electrical discharges in gases, by F. M. Penning 82

Book reviews—*continued*

Electromagnetic isotope separators and applications of electromagnetically enriched isotopes, by J. Koch (Editor), R. H. V. M. Dawton, M. L. Smith and W. Walcher 397
Electron impact phenomena and the properties of gaseous ions, by F. H. Field and J. L. Franklin 228
Electronic semiconductors, by E. Spenke 404
Electrostatics in the petroleum industry, edited by A. Klinkenberg and J. L. van der Minne 230
Elektronik freier Raumladungen, by F. Ollendorff 404
Elements of heat transfer, by M. Jakob and G. A. Hawkins 83
Elsevier's dictionary of electronics and wave guides in six languages, compiled and arranged by W. E. Clason 232
Energy transfer in polyacene solid solutions: a guide to the literature to the end of 1956, by F. R. Lipsett 44
Erzeugung sehr tiefer Temperaturen, by H. Hausen 230
Évolution des sciences. No. 9. L'Automatique des informations, by F. H. Raymond 224
Experimental designs, by W. G. Cochran and G. M. Cox 80
Exploration of space by radio, The, by R. Hanbury Brown and A. C. B. Lovell 223
Exterior ballistics of rockets, The, by L. Davis, Jr., J. W. Follin, Jr., and L. Blitzer 399
Feedback theory and its applications, by P. H. Hammond 225
Ferroelectricity in crystals, by Helen D. Megaw 224
First nuclear engineering and science congress, The. Vol. 1. Problems in nuclear engineering, Vol. 2. Reactor operational problems, edited by D. J. Hughes, S. McLain and C. Williams 123
Flame photometry. A manual of methods and applications, by Burriel-Martí and J. Ramírez-Muñoz 400
Free radicals in solution, by C. Walling 401
Fundamental principles of transistors, by J. Evans 226
Fundamentals of electron devices, by K. R. Spangenberg 226
Fundamentals of optics, by F. A. Jenkins and H. E. White 228
Geometric integration theory, by H. Whitney 227
Grain boundaries in metals, by D. McLean 228
Grundprobleme der mathematischen Theorie elektromagnetischer Schwingungen, by C. Muller 226
Handbook of chemistry and physics, edited by C. D. Hodgman and others 232
1957 *Heat Transfer and Fluid Mechanics Institute* 232
Industrial electronics circuits, by R. Kretzmann 225
International Scientific Radio Union: Proceedings of the XIIth General Assembly. Vol. XI, Part I. Commission I: On radio measurements and standards 396
Kinetics of vinyl polymerization by radical mechanisms, The, by C. H. Bamford, W. G. Barb, A. D. Jenkins and P. F. Onyon 404
Light colour and vision, by Y. le Grand 223
Light scattering by colloidal systems, by M. M. Fishman 83
Light scattering by small particles, by H. C. Van de Hulst 81
Machinery's annual buyers' guide 232
Magnesium casting technology, by A. W. Brace and F. A. Allen 43
Magnetohydrodynamics, by T. G. Cowling 402
Mass spectroscopy, by H. E. Duckworth 234
Measurement of colour, The, by W. D. Wright 402
Measurement of soil properties in the triaxial test, The, by A. W. Bishop and D. J. Henkel 43
Mesure et détection des rayonnements nucléaires, by J. Sharpe and D. Taylor 404
Metallurgical progress—3.A. Third series of critical reviews 80

Book reviews—*continued*

Metallurgy of the rarer metals. No. 2. *Zirconium*, by G. L. Miller 163
Microwave measurements, by E. L. Ginzton 224
Missile engineering handbook, by C. W. Besserer 398
Modern electroanalytical methods, edited by G. Charlot 402
Neutron cross-sections, by D. J. Hughes 228
Nuclear engineering, edited by Charles F. Bonilla 82
Nuclear masses and their determination, by H. Hintenberger 398
Numerical analysis, by D. R. Hartree 399
Numerical solution of two-point boundary problems in ordinary differential equations, The, by L. Fox 80
Observation and interpretation, edited by S. Korner 232
Ondes centimétriques, Les, by G. Raoult 404
Particulate clouds: dusts, smokes and mists, by H. L. Green and W. R. Lane 43
Passive network synthesis, by J. E. Storer 82
Physics of clouds, The, by B. J. Mason 227
Physics of electrical contacts, The, by F. Llewellyn Jones 163
Physics of nuclear fission, translated from the Russian by J. E. S. Bradley 397
Piezoelectricity. Post Office Research Station: Selected engineering reports 225
Piles atomiques à neutrons lents, Les, by J. Maurin 404
Powder method in X-ray crystallography, The, by L. V. Azároff and M. J. Buerger 402
Proceedings of the congress on modern analytical chemistry in industry 396
Proceedings of the international conference on fatigue of metals, 1956 396
Proceedings of the international symposium on isotope separation, edited by J. Kistemaker, J. Bigeleisen and A. O. C. Nier 396
Proceedings of the sixth international conference on spectroscopy, edited by W. van Tongeren, F. Freese and E. H. S. van Someren 234
Progress in nuclear physics. Vol. 6, edited by O. R. Frisch 397
Propagation des ondes electromagnetiques de haute frequence, by J. Ortusi 43
Quantum mechanics, by E. Mandl 231
Radiation shielding, by B. T. Price, C. C. Horton and K. T. Spinney 43
Radioactive materials and stable isotopes. Catalogue No. 4 163
Radiography in modern industry 83
Rectifying semi-conductor contacts, by H. K. Henisch 227
Regelungstechnik. Moderne Theorien und ihre Vewendbarkeit 225
Reports on progress in physics. Vol. 20, edited by A. C. Stickland 233
Reproduction of colour, The, by R. W. G. Hunt 223
Rheology of elastomers, The, by P. Mason and N. Wookey 400
Rheology. Theory and applications. Vol. II, by F. R. Eirich 400
Russian–English atomic dictionary, by E. A. Carpovich 231
Sammlung Göschen. Vol. 728/728*a. Graphische darstellung in Wissenschaft und Technik*, by M. Pirani 83
Sciences of engineering materials, The, edited by J. E. Goldman 230
Scientific papers of Sir Geoffrey Taylor. Vol. 1. *Mechanics of solids, The*, edited by G. K. Batchelor 234
Semiconductor Abstracts. Vol. 3. 1955 *issue*, compiled by the Battelle Memorial Institute 82
Servomecanismes: Theorie et technologie, by M. Bonamy 229
Silicones, The, by P. Sykes 81
Solid state physics. Vol. 4. *Advances in research and applications*, edited by F. Seitz and D. Turnbull 231
Spectrochemical abstracts. Vol. 5. 1952–1953, by E. H. S. van Someren and F. Lachman 402
Structure reports for 1951. *Vol.* 15, by A. J. C. Wilson in association with N. C. Baenziger, J. Wyart and J. Monteath Robertson 233

Book reviews—*continued*

Surface chemistry. Theory and applications, by J. J. Bikermann 401
Television in science and industry, by V. K. Zworykin, E. G. Ramberg and L. E. Flory 403
Theoretical physics, by G. Joos, with the collaboration of Ira M. Freeman 228
Theoretische Physik, by F. Hund 44
Theorie der elektrizität, by R. Becker and F. Sauter 44
Theorie schallnaher Strömungen, by K. G. Guderley 233
Theory of dielectrics: dielectric constant and dielectric loss, by H. Fröhlich 400
Thermal stresses, by B. E. Gatewood 81
Thermodynamics of one-component systems, by W. N. Lacey and B. H. Sage 229
Transistor, Der, by J. Dosse 405
Transistor technology. Vol. 1, edited by H. E. Bridgers, J. H. Scaff and J. N. Shive 403
Ultra high frequency performance of receiving valves, The, by W. E. Benham and I. A. Harris 225
Vector analysis, by Louis Brand 44
World directory of crystallographers, compiled by W. Parrish 80
X-ray crystal structure, by D. McLachlan 224
X-ray microscopy and microradiography, edited by V. E. Cosslett, A. Engström and H. H. Pattee, Jr. 232

Capillarity

Electrical analogue method of predicting the permeability of unsaturated porous materials, M. C. Probine 144
Physics of fibres with special reference to wool, A. B. D. Cassie 341 (SA)
Studies of the viscosity and sedimentation of suspensions. Part 4. Capillary-tube viscometry applied to stable suspensions of spherical particles, G. H. Higginbotham, D. R. Oliver and S. G. Ward 372

Cavitation (*see* Liquids, cavitation)

Chemistry

Method for determining ^{24}Na and ^{42}K when present together in liquid samples, M. P. Esnouf 161
Physical methods of investigating chemical problems, R. J. Taylor 165 (SA)

Computers

Crystallographic programmes for a computer, J. C. Gower and J. H. Rayner 446
Electrical analogue method of predicting the permeability of unsaturated porous materials, M. C. Probine 144
Prismatic fin with non-linear heat loss analysed by resistance network and iterative analogue computer, I. C. Hutcheon and D. B. Spalding 185
Stability and convergence limitations on the use of analogue computers with resistance network analogues, M. E. Fisher 288
Summarized proceedings of a conference on biological structures and computational methods—London, November 1956, J. Finch, D. W. Green, K. C. Holmes and A. C. T. North 1 (CR)

Conference reports

Summarized proceedings of a conference on biological structures and computational methods—London, November 1956, J. Finch, D. W. Green, K. C. Holmes and A. C. T. North 1 (CR)
Summarized proceedings of a conference on electron microscopy—Bangor, September 1957, H. W. Emerton 306 (CR)

Crystallography (*see also* X-ray analysis)

Crystallographic programmes for a computer, J. C. Gower and J. H. Rayner 446
Structure-cell data and expansion coefficients of bismuth telluride, M. H. Francombe 415
Summarized proceedings of a conference on biological structures and computational methods—London, November 1956, J. Finch, D. W. Green, K. C. Holmes and A. C. T. North 1 (CR)
Summarized proceedings of a conference on electron microscopy—Bangor, September 1957, H. W. Emerton 306 (CR)
"Super-elastic" single crystal calibration bar, W. A. Rachinger 250
Synthesis of single crystals of the sulphides of zinc, cadmium and mercury and of mercuric selenide by vapour phase methods, D. R. Hamilton 103

Dielectric phenomena

Dielectric constant of zinc oxide over a range of frequencies, N. H. Langton and D. Matthews 453
Electric strength and molecular structure of liquids, T. J. Lewis 30
Resonant cavity methods of measuring ferrite properties, R. A. Waldron 439

Drops (*see* Particles, drops)

Elasticity

Apparent slip between metal and rubber-covered pressure rollers, G. J. Parish 428
Effective coefficient of friction for strings traversing cylinders transversely and slantwise, C. Mack and C. Rubenstein 247
Geometry of twisted multi-filament structures, G. J. Stansfield 133
Measurement of elasticity and anelasticity of small disks by an inductor method, G. Bradfield and F. A. Levi 13
Measurements of pressure distribution between metal and rubber-covered rollers, G. J. Parish 158
Mechanical testing of materials in the transition region between steady flow and failure, A. Jobling and J. E. Roberts 235

Stress, strain, photoelasticity

Calculated and observed effects of texture on the magnetic properties and Young's modulus of nickel sheet, E. R. W. Jones, C. A. Clark and E. A. Fell 178
Choice of resilient materials for anti-vibration mountings, J. C. Snowdon 461 (SA)
Dependence of stress distribution on elastic constants, Margery Clutterbuck 323
Effect of specimen diameter on the straining of a cylindrical load-cell, J. F. W. Bishop and M. T. Watkins 38
Influence of shear and rotatory inertia on the free flexural vibration of wooden beams, R. F. S. Hearmon 381
Influence on the stress distribution in an adhesive lap joint of bending of the adhering sheets, A. S. McLaren and I. MacInnes 72
Measurement of the strain-dependent damping of metals vibrating torsionally, G. Sumner and K. M. Entwistle 434
Note on the adhesion of elastic solids, K. L. Johnson 199
Photoelastic behaviour of cross-linked polymers, Z. Tuzi, K. Kawata and I. Hori 173
Photoelastic investigation of stresses in composite models with notches and holes, Heihachi Shimada 34
Photoelastic properties of plasticised polymethyl methacrylate in the glassy state, J. H. Lamble and E. S. Dahmouch 388
Photoelastic technique for strain measurement on flat aluminium alloy surfaces, H. Fessler and D. J. Haines 282
Property of a buckled elastic rod, G. A. V. Leaf 71
Rapid method for separating the principal stresses in plane photoelasticity, I. Brodie 201 (C)
Stresses and strains in an infinite elastic sheet under a tension applied at two rigid pairs of square jaws, Daphne G. Padfield and Nora B. Dickinson 448

Elasticity—*continued*

Stress, strain, photoelasticity—*continued*

"Super-elastic" single crystal calibration bar, W. A. Rachinger 250

Electrical and electronic devices and properties (*see also* Semiconductivity, photoconductivity)

Aluminosilicates and the high-temperature processing of microwave vacuum tubes, M. Hillier and R. L. Bell 94
Beam temperature, discharge lag and target biasing in some television pick-up tubes, B. Meltzer and P. L. Holmes 139 *erratum* 340
Deuterium as a filling for high-voltage thyratrons, R. J. Armstrong and N. S. Nicholls 498 (C)
Deuterium-filled thyratrons, K. G. Cook and G. G. Isaacs 497 (C)
Energy balance in disk seal oscillators at ultra-high frequencies, M. R. Gavin and L. J. Herbst 377
Grid emitting properties of titanium, J. A. Champion 491
Low-temperature conductivity of oxide-coated cathodes, G. S. Higginson 106
Magnetic stabilization of low pressure d.c. areas, H. Wroe 488
Sintered nickel matrix cathode, R. W. Fane 149
Temperature coefficient of maintenance potential of glow discharge voltage stabilizer and regulator tubes, J. Smith 122 (C)
Temperature dependence of noise temperature ratio in germanium diodes, A. Hendry 458
Theory of ballast tubes or barretters, R. O. Jenkins 391
Thermionic and related properties of calcium oxide, B. J. Hopkins and F. A. Vick 257
Time-constant of carbon composition resistors, G. H. Rayner 240

Electron microscopy, components

Analysis of particle counts by the spray-drop method, K. I. Williamson and W. B. Taylor 264
Chromatic field aberrations and their correction in a three-lens reflexion electron microscope, D. H. Page 268
Improved spray droplet technique for quantitative electron microscopy, H. L. Nixon and H. L. Fisher 68
New techniques for the study of Bitter figures, D. J. Craik and P. M. Griffiths 279
Recent developments in electron microscopy, V. E. Cosslett 253 (SA)
Reflexion electron microscopy at high angles, D. H. Page 60
Resistance bias characteristic of the electron microscope gun, M. E. Haine, P. A. Einstein and P. H. Borcherds 482
Selected area microdiffraction in the electron microscope, A. W. Agar 419 (C)
Sources of error in electron stereomicroscopy, R. I. Garrod and J. F. Nankivell 214
Summarized proceedings of a conference on electron microscopy—Bangor, September 1957, H. W. Emerton 306 (CR)
Technique for obtaining thin foils of aluminium and aluminium alloys for transmission electron metallography, R. B. Nicholson, G. Thomas and J. Nutting 25

Exo-electron emission

Survey of exo-electron emission phenomena, L. Grunberg 85 (SA)

Films, sheets, surfaces

Calculated and observed effects of texture on the magnetic properties and Young's modulus of nickel sheet, E. R. W. Jones, C. A. Clark and E. A. Fell 178
Effect of gettering on the reflectivity of aluminium films, L. Holland 336
Frictional behaviour and structure of the surface oxides of steel, Yasukatsu Tamai 338 (C)
Heat-reflecting windows using gold and bismuth oxide films, L. Holland and G. Siddall 359

Films, sheets, surfaces—*continued*

Magnetic anisotropy measurement with an oscillation magnetometer, J. R. Macdonald 116
Mechanical wear of metals, W. Hirst 125 (SA)
New techniques for the study of Bitter figures, D. J. Craik and P. M. Griffiths 279
Note on the paper "The oxidation of barium films (getters)," S. J. Gregg and W. B. Jepson; R. N. Bloomer 417 (C)
Photoelastic technique for strain measurements on flat aluminium alloy surfaces, H. Fessler and D. J. Haines 282
Relationship between surface texture and rolling resistance of steel, J. Halling 421
Technique for obtaining thin foils of aluminium and aluminium alloys for transmission electron metallography, R. B. Nicholson, G. Thomas and J. Nutting 25
Temperature distribution throughout a stack of electrical sheet steel during annealing, R. J. Wakelin 353

Fluids, flow (*see also* Liquids, cavitation)

Constant liquid flow device, G. H. Laycock 333
Electrical analogue method of predicting the permeability of unsaturated porous materials, M. C. Probine 144
Overall test of equations of state of fluids, N. Davy and Barbara M. Bell 27
Pneumatic conveying of spheres through straight pipes, J. A. Hitchock and C. Jones 218

Friction, lubrication, wear

Apparent slip between metal and rubber-covered pressure rollers, G. J. Parish 428
Effective coefficient of friction for strings traversing cylinders transversely and slantwise, C. Mack and C. Rubenstein 247
Frictional behaviour and structure of the surface oxides of steel, Yasukatsu Tamai 338 (C)
Friction of mineral particles, R. T. Spurr 486
Mechanical wear of metals, W. Hirst 125 (SA)
Photoelastic technique for strain measurement on flat aluminium alloy surfaces, H. Fessler and D. J. Haines 282
Relationship between surface texture and rolling resistance of steel, J. Halling 421
Transfer of tungsten carbide to soft metals during single-traverse and reciprocating sliding, J. Golden and G. W. Rowe 120
Use of polytetrafluoroethylene as a lubricant, E. Kay and E. D. Tingle 17

Heat, thermometry

Flow of heat in a parallel-faced infinite solid, T. B. Newcomb 370
Heat-reflecting windows using gold and bismuth oxide films, L. Holland and G. Siddall 359
Measurements of pressure distribution between metal and rubber-covered rollers, G. J. Parish 158
Mechanical wear of metals, W. Hirst 125 (SA)
Performance of bismuth telluride thermojunctions, H. J. Goldsmid, A. R. Sheard and D. A. Wright 365
Performance of spark guards, J. H. McGuire and Margaret Law 470
Prismatic fin with non-linear heat loss analysed by resistance network and iterative analogue computer, I. C. Hutcheon and D. B. Spalding 185
Radial flow of heat in an infinite cylinder, T. P. Newcomb 456
Structure-cell data and expansion coefficients of bismuth telluride, M. H. Francombe 415
Thermal conductivity of nitrogen and argon in the liquid and gaseous states, H. Ziebland and J. T. A. Burton 52

Liquids, cavitation (*see also* Fluids, flow)

Constant liquid flow device, G. H. Laycock 333
Determination of density of liquids under elevated gas pressure, K. Goldman 40
Electric strength and molecular structure of liquids, T. J. Lewis 30

Liquids, cavitation—*continued*

Evaporation of sprays, R. T. Jarman 153
Measurements on the air-nuclei in natural water which give rise to cavitation, K. S. Iyengar and E. G. Richardson 154
Method for determining ^{24}Na and ^{42}K when present together in liquid samples, M. P. Esnouf 161

Lubrication (*see* Friction, lubrication, wear)

Magnetism, nuclear magnetic resonance

Bistable behaviour of the magnetic transductor, E. H. Frei, S. Shtrikman and D. Treves 394
Calculated and observed effects of texture on the magnetic properties and Young's modulus of nickel sheet, E. R. W. Jones, C. A. Clark and E. A. Fell 178
High temperature stability of permanent magnets of the iron–nickel–aluminium system, A. G. Clegg and M. McCaig 194
Influence of the method of demagnetization on the reversible permeability of a high-permeability nickel–iron alloy, R. C. Jackson, E. W. Lee and A. G. H. Troughton 495
Magnetic anisotropy measurement with an oscillation magnetometer, J. R. Macdonald 116
Magnetic stabilization of low pressure d.c. arcs, H. Wroe 488
Measurement of elasticity and anelasticity of small disks by an inductor method, G. Bradfield and F. A. Levi 13
New techniques for the study of Bitter figures, D. J. Craik and P. M. Griffiths 279
Note on the calculation of second moments of nuclear magnetic resonance absorption lines, J. G. Powles 299 (C)
Resonant cavity methods of measuring ferrite properties, R. A. Waldron 439

Materials

Choice of resilient materials for anti-vibration mountings, J. C. Snowdon 461 (SA)
Dielectric constant of zinc oxide over a range of frequencies, N. H. Langton and D. Matthews 453
Electrical analogue method of predicting the permeability of unsaturated porous materials, M. C. Probine 144
Electrical properties of chalcopyrite, B. Donovan and G. Reichenbaum 474
Electroluminescence, S. T. Henderson 45 (SA)
Indium–selenium system, J. C. Brice, P. C. Newman and H. C. Wright 110
Influence of shear and rotatory inertia on the free flexural vibration of wooden beams, R. F. S. Hearmon 381
Mechanical testing of materials in the transition region between steady flow and failure, A. Jobling and J. E. Roberts 235
Performance of spark guards, J. H. McGuire and Margaret Law 470
Photoelastic behaviour of cross-linked polymers, Z. Tuzi, K. Kawata and I. Hori 173
Physics of fibres with special reference to wool, A. B. D. Cassie 341 (SA)
Survey of exo-electron emission phenomena, L. Grunberg 85 (SA)
Synthesis of single crystals of the sulphides of zinc, cadmium and mercury and of mercuric selenide by vapour phase methods, D. R. Hamilton 103
Transfer of tungsten carbide to soft metals during single-traverse and reciprocating sliding, J. Golden and G. W. Rowe 120
Use of polytetrafluoroethylene as a lubricant, E. Kay and E. D. Tingle 17

Mathematics, theories, calculations

Calculated and observed effects of texture on the magnetic properties and Young's modulus of nickel sheet, E. R. W. Jones, C. A. Clark and E. A. Fell 178
Effective coefficient of friction for strings traversing cylinders transversely and slantwise, C. Mack and C. Rubenstein 247

Mathematics, theories, calculations—*continued*

Flow of heat in a parallel-faced infinite solid, T. P. Newcomb 370
Generalized theory of sedimentation, A. D. Maude and R. L. Whitmore 477
Geometry of multi-filament structures, G. J. Stansfield 133
Note on the adhesion of elastic solids, K. L. Johnson 199
Note on the calculation of second moments of nuclear magnetic resonance absorption lines, J. G. Powles 299 (C)
Overall test of equations of state of fluids, N. Davy and Barbara M. Bell 27
Performance of infra-red photoconductive cells, D. H. Roberts and B. L. H. Wilson 291
Prismatic fin with non-linear heat loss analysed by resistance network and iterative analogue computer, I. C. Hutcheon and D. B. Spalding 185
Property of a buckled elastic rod, G. A. V. Leaf 71
Radial flow of heat in an infinite cylinder, T. P. Newcomb 456
Solid angle corrections to single scattering, F. F. Heymann and P. I. P. Kalmus 271
Sources of error in electron stereomicroscopy, R. I. Garrod and J. F. Nankivell 214
Stability and convergence limitations on the use of analogue computers with resistance network analogues, M. E. Fisher 288
Temperature and pressure corrections to be applied to the shielded hot wire anemometer at speeds for which natural convective cooling is negligible, C. F. Cowdrey 112

Metals, metallurgy

Apparent slip between metal and rubber-covered pressure rollers, G. J. Parish 428
Calculated and observed effects of texture on the magnetic properties and Young's modulus of nickel sheet, E. R. W. Jones, C. A. Clark and E. A. Fell 178
Frictional behaviour and structure of the surface oxides of steel, Yasukatsu Tamai 338 (C)
General scheme for the examination of precipitates and inclusions in steels, G. R. Booker and J. Norbury 361
Measurement of the strain-dependent damping of metals vibrating torsionally, G. Sumner and K. M. Entwistle 434
Measurements of pressure distribution between metal and rubber covered rollers, G. J. Parish 158
Mechanical wear of metals, W. Hirst 125 (SA)
Portable lamination detector for steel sheet, B. O. Smith, A. P. H. Jennings and A. G. Grimshaw 191
Pulse-annealing technique for metals and alloys, P. Wright and K. Thomas 330
Relationship between surface texture and rolling resistance of steel, J. Halling 421
"Super-elastic" single crystal calibration bar, W. A. Rachinger 250
Survey of exo-electron emission phenomena, L. Grunberg 85
Technique for obtaining thin foils of aluminium and aluminium alloys for transmission electron metallography, R. B. Nicholson, G. Thomas and J. Nutting 25
Temperature distribution throughout a stack of electrical sheet steel during annealing, R. J. Wakelin 353

Notes and comments

Bibliography on applications and properties of zirconium and alloys 84
British Group for computation and automatic control of the British Conference on automation and computation, The 84
British Nuclear Energy Conference: lecture symposium on the Geneva conference 420
Congress of the International Federation of Automatic Control, Moscow, 1960 500
Elections to The Institute of Physics 204, 339
Electronics exhibition and convention 204
Geophysical Journal, The 339
Instrument enquiries service 339

Notes and comments—*continued*

Instruments, Electronics and Automation Exhibition, 1958 164
International conference on the peaceful uses of atomic energy 339
Medical electronics discussion group 500
Molecular physics 164
New literature on atomic industry 164
Notes for prospective authors 339
Nuclear engineering monographs 164
Pakistan journal of scientific and industrial research 340
Physical Society's annual exhibition of instruments and apparatus, The 84, 500
Proceedings of the Royal Institution 420
Register of British manufacturers 84
Symposium on instrumentation and computation in process development and plant design 204
Symposium on nuclear fuel cycles 339
User-specification for high-temperature X-ray powder cameras 204
User-specification for sealed X-ray tubes for use in X-ray diffraction 420
Wear 340

Optics

Ageing of vacuum standard lamps on a.c. and d.c., W. Barnett, R. G. Berry and J. S. Preston 317
Bonding optical components to metal mounts, K. H. Spring 242
Chromatic field aberrations and their correction in a three-lens reflexion electron microscope, D. H. Page 268
Effect of gettering on the reflectivity of aluminium films, L. Holland 336
Electroluminescence, S. T. Henderson 45 (SA)
New techniques for the study of Bitter figures, D. J. Craik and P. M. Griffiths 279
Photoconductivity, D. A. Wright 205 (SA)
Sources of error in electron stereomicroscopy, R. I. Garrod and J. F. Nankivell 214

Particles, contamination, drops

Analysis of particle counts by the spray-drop methods, K. I. Williamson and W. B. Taylor 264
Atmospheric pollution and the soiling of textile materials, W. H. Rees 301 (SA)
Evaporation of sprays, R. T. Jarman 153
Friction of mineral particles, R. T. Spurr 486
Generalized theory of sedimentation, A. D. Maude and R. L. Whitmore 477
General scheme for the examination of precipitates and inclusions in steels, G. R. Booker and J. Norbury 361
Improved spray droplet technique for quantitative electron microscopy, H. L. Nixon and H. L. Fisher 68
Measurements on the air-nuclei in natural water which give rise to cavitation, K. S. Iyengar and E. G. Richardson 154
Particle size of some Witwatersrand mine dust, H. St. G. Tucker 98
Performance of spark guards, J. H. McGuire and Margaret Law 470
Pneumatic conveying of spheres through straight pipes, J. A. Hitchcock and C. Jones 218
Sampling efficiency of the thermal precipitator, H. H. Watson 78 (C)
Studies of the viscosity and sedimentation of suspensions. Part 4.—Capillary-tube viscometry applied to stable suspensions of spherical particles, G. H. Higginbotham, D. R. Oliver and S. G. Ward 372

Photoconductivity (*see* Semiconductivity, photoconductivity)

Radioactivity, α-, β-, γ-rays, isotopes

Gamma-ray yield and spectra produced by irradiating backing materials with protons, S. E. Hunt, R. A. Pope, W. W. Evans and D. A. Hancock 443

Radioactivity, α-, β-, γ-rays, isotopes—*continued*

Method for determing ^{24}Na and ^{42}K when present together in liquid samples, M. P. Esnouf 161
Solid angle corrections to single scattering, F. F. Heymann and P. I. P. Kalmus 271
Transfer of tungsten carbide to soft metals during single-traverse and reciprocating sliding, J. Golden and G. W. Rowe 120

Semiconductivity, photoconductivity

Electrical properties of chalcopyrite, B. Donovan and G. Reichenbaum 474
Indium–selenium system, J. C. Brice, P. C. Newman and H. C. Wright 110
Performance of bismuth telluride thermojunctions, H. J. Goldsmid, A. R. Sheard and D. A. Wright 365
Performance of infra-red photoconductive cells, D. H. Roberts and B. L. H. Wilson 291
Photoconductivity, D. A. Wright 205 (SA)
Structure-cell data and expansion coefficients of bismuth telluride, M. H. Francombe 415
Synthesis of single crystals of the sulphides of zinc, cadmium and mercury and of mercuric selenide by vapour phase methods, D. R. Hamilton 103
Temperature dependence of noise temperature ratio in germanium diodes, A. Hendry 458

Techniques

Bonding optical components to metal mounts, K. H. Spring 242
General scheme for the examination of precipitates and inclusions in steels, G. R. Booker and J. Norbury 361
Improved spray droplet technique for quantitative electron microscopy, H. L. Nixon and H. L. Fisher 68
Pneumatic conveying of spheres through straight pipes, J. A. Hitchcock and C. Jones 218
Pulse-annealing technique for metals and alloys, P. Wright and K. Thomas 330

Techniques—*continued*

Some developments and applications of microfocus X-ray diffraction techniques, A. Franks 349
Synthesis of single crystals of the sulphides of zinc, cadmium and mercury and of mercuric selenide by vapour phase methods, D. R. Hamilton 103
Technique for obtaining thin foils of aluminium and aluminium alloys for transmission electron metallography, R. B. Nicholson, G. Thomas and J. Nutting 25

Thermometry (*see* Heat, thermometry)

Vacuum techniques

Aluminosilicates and the high-temperature processing of microwave vacuum tubes, M. Hillier and R. L. Bell 94
Cleaning of glass in a glow discharge, L. Holland 410
Effect of gettering on the reflectivity of aluminium films, L. Holland 336
Note on the paper "The oxidation of evaporated barium films (getters)," S. J. Gregg and W. B. Jepson; R. N. Bloomer 417 (C)

Wear (*see* Friction, lubrication, wear)

X-ray analysis (*see also* Crystallography)

Diffraction, spectrometry

Comments on the A.S.T.M. Powder Data File—3, J. W. Hughes, Isabel E. Lewis and A. J. C. Wilson 123 (C)
Proportional counters in X-ray spectro-chemical analysis, T. Mulvey and A. J. Campbell 406
Ratio of characteristic to white X-radiation from a copper target, E. G. Bendit 312
Some developments and applications of microfocus X-ray diffraction techniques, A. Franks 349
Summarized proceedings of a conference on biological structures and computational methods—London, November 1956, J. Finch, D. W. Green, K. C. Holmes and A. C. T. North 1 (CR)

AUTHOR INDEX

(SA) denotes special article, (CR) conference report, (C) correspondence.

Agar, A. W., Selected area microdiffraction in the electron microscope 419 (C)
Armstrong, R. J., and N. S. Nicholls, Deuterium as a filling for high-voltage thyratrons 498 (C)
Austen, A. E. W., and T. Priede, A method for distinguishing between sources of noise in motor-cars 201 (C)

Barnett, W., R. G. Berry and J. S. Preston, The ageing of vacuum standard lamps on a.c. and d.c. 317
Bell, Barbara M., *see under* Davy, N.
Bell, R. L., *see under* Hillier, M.
Bendit, E. G., The ratio of characteristic to white X-radiation from a copper target 312
Berry, R. G., *see under* Barnett, W.
Bishop, J. F. W., and M. T. Watkins, The effect of specimen diameter on the straining of a cylindrical load-cell 38
Bloomer, R. N., A note on the paper "The oxidation of evaporated films (getters)" 417 (C)
Booker, G. R., and J. Norbury, A general scheme for the examination of precipitates and inclusions in steels 361
Borcherds, P. H., *see under* Haine, M. E.
Bradfield, G., and F. A. Levi, Measurement of elasticity and anelasticity of small disks by an inductor method 13
Brice, J. C., P. C. Newman and H. C. Wright, The indium–selenium system 110
Brodie, I., A rapid method for separating the principal stresses in plane photoelasticity 201 (C)
Burton, J. T. A., *see under* Ziebland, H.

Campbell, A. J., *see under* Mulvey, T.
Cassie, A. B. D., The physics of fibres with special reference to wool 341 (SA)
Champion, J. A., The grid emitting properties of titanium 491
Clark, C. A., *see under* Jones, E. R. W.
Clegg, A. G., and M. McCaig, The high temperature stability of permanent magnets of the iron–nickel–aluminium system 194
Clutterbuck, Margery, The dependence of stress distribution on elastic constants 323
Cook, K. G., and G. G. Isaacs, Deuterium-filled thyratrons 497
Cosslett, V. E., Recent developments in electron microscopy 253 (SA)
Cowdrey, C. F., Temperature and pressure corrections to be applied to the shielded hot wire anemometer at speeds for which natural convective cooling is negligible 112
Craik, D. J., and P. M. Griffiths, New techniques for the study of Bitter figures 279

Dahmouch, E. S., *see under* Lamble, J. H.
Davy, N., and Barbara M. Bell, An overall test of equations of state of fluids 27

Dickinson, Nora B., *see under* Padfield, Daphne G.
Donovan, B., and G. Reichenbaum, Electrical properties of chalcopyrite 474

Einstein, P. A., *see under* Haine, M. E.
Emerton, H. W., Summarized proceedings of a conference on electron microscopy—Bangor, September 1957 306 (CR)
Entwistle, K. M., *see under* Sumner, G.
Esnouf, M. P., A method for determining ^{24}Na and ^{42}K when present together in liquid samples 161
Evans, W. W., *see under* Hunt, S. E.

Fane, R. W., A sintered nickel matrix cathode 149
Fell, E. A., *see under* Jones, E. R. W.
Fessler, H., and D. J. Haines, A photoelastic technique for strain measurement on flat aluminium alloy surfaces 282
Finch, J., D. W. Green, K. C. Holmes and A. C. T. North, Summarized proceedings of a conference on biological structures and computational methods—London, November 1956 1 (CR)
Fisher, H. L., *see under* Nixon, H. L.
Fisher, M. E., Stability and convergence limitations on the use of analogue computers with resistance network analogues 288
Francombe, M. H., Structure-cell data and expansion coefficients of bismuth telluride 415
Franks, A., Some developments and applications of microfocus X-ray diffraction techniques 349
Frei, E. H., S. Shtrikman and D. Treves, The bistable behaviour of the magnetic transductor 394

Garrod, R. I., and J. F. Nankivell, Sources of error in electron stereomicroscopy 214
Gavin, M. R., and L. J. Herbst, Energy balance in disk seal oscillators at ultra-high frequencies 377
Golden, J., and G. W. Rowe, Transfer of tungsten carbide to soft metals during single-traverse and reciprocating sliding 120
Goldman, K., Determination of density of liquids under elevated gas pressure 40
Goldsmid, H. J., A. R. Sheard and D. A. Wright, The performance of bismuth telluride thermojunctions 365
Gower, J. C., and J. H. Rayner, Crystallographic programmes for a computer 446
Green, D. W., *see under* Finch, J.
Gregg, S. J., and W. B. Jepson, A note on the paper "The oxidation of evaporated barium films (getters)" 417 (C)
Griffiths, P. M., *see under* Craik, D. J.
Grimshaw, A. G., *see under* Smith, B. O.
Grunberg, L., A survey of exo-electron emission phenomena 85 (SA)

Haine, M. E., P. A. Einstein and P. H. Borcherds Resistance bias characteristic of the electron microscope gun 482
Haines, D. J., *see under* Fessler, H.
Halling, J., The relationship between surface texture and rolling resistance of steel 421
Hamilton, D. R., The synthesis of single crystals of the sulphides of zinc, cadmium and mercury and of mercuric selenide by vapour phase methods 103
Hancock, D. A., *see under* Hunt, S. E.
Hearmon, R. F. S., The influence of shear and rotatory inertia on the free flexural vibration of wooden beams 381
Henderson, S. T., Electroluminescence 45 (SA)
Hendry, A., The temperature dependence of noise temperature ratio in germanium diodes 458
Herbst, L. J., *see under* Gavin, M. R.
Heymann, F. F., and P. I. P. Kalmus, Solid angle corrections to single scattering 271
Higginbotham, G. H., D. R. Oliver and S. G. Ward, Studies of the viscosity and sedimentation of suspensions. Part 4.—Capillary-tube viscometry applied to stable suspensions of spherical particles 372
Higginson, G. S., The low-temperature conductivity of oxide-coated cathodes 106
Hillier, M., and R. L. Bell, Aluminosilicates and the high-temperature processing of microwave vacuum tubes 94
Hirst, W., The mechanical wear of metals 125 (SA)
Hitchcock, J. A., and C. Jones, The pneumatic conveying of spheres through straight pipes 218
Holland, L., The cleaning of glass in a glow discharge 410
Holland, L., The effect of gettering on the reflectivity of aluminium films 336
Holland, L., and G. Siddall, Heat-reflecting windows using gold and bismuth oxide films 359
Holmes, K. C., *see under* Finch, J.
Holmes, P. L., *see under* Meltzer, B.
Hopkins, B. J., and F. A. Vick, Thermionic and related properties of calcium oxide 257
Hori, I., *see under* Tuzi, Z.
Hughes, J. W., Isabel E. Lewis and A. J. C. Wilson, Comments on the A.S.T.M. Powder Data File—3 123
Hunt, S. E., R. A. Pope, W. W. Evans and D. A. Hancock, γ-ray yield and spectra produced by irradiating backing materials with protons 443
Hutcheon, I. C., and D. B. Spalding, Prismatic fin with non-linear heat loss analysed by resistance network and iterative analogue computer 185

Isaacs, G. G., *see under* Cook, K. G.
Iyengar, K. S., and E. G. Richardson, Measurements on the air-nuclei in natural water which give rise to cavitation 154

Jackson, R. C., E. W. Lee and A. G. H. Troughton, The influence of the method of demagnetization on the reversible permeability of a high-permeability nickel–iron alloy 495
Jarman, R. T., The evaporation of sprays 153
Jenkins, R. O., The theory of ballast tubes or barretters 391
Jennings, A. P. H., *see under* Smith, B. O.
Jepson, W. B., *see under* Gregg, S. J.
Jobling, A., and J. E. Roberts, Mechanical testing of materials in the transition region between steady flow and failure 235
Johnson, K. L., A note on the adhesion of elastic solids 199
Jones, C., *see under* Hitchcock, J. A.
Jones, E. R. W., C. A. Clark and E. A. Fell, Calculated and observed effects of texture on the magnetic properties and Young's modulus of nickel sheet 178

Kalmus, P. I. P., *see under* Heymann, F. F.
Kawata, K., *see under* Tuzi, Z.
Kay, E., and E. D. Tingle, The use of polytetrafluoroethylene as a lubricant 17

Lamble, J. H., and E. S. Dahmouch, Photoelastic properties of plasticised polymethyl methacrylate in the glassy state 388
Langton, N. H., and D. Matthews, The dielectric constant of zinc oxide over a range of frequencies 453
Law, Margaret, *see under* McGuire, J. H.
Laycock, G. H., A constant liquid flow device 333
Leaf, G. A. V., A property of a buckled elastic rod 71
Lee, E. W., *see under* Jackson, R. C.
Levi, F. A., *see under* Bradfield, G.
Lewis, Isobel E., *see under* Hughes, J. W.
Lewis, T. J., The electric strength and molecular structure of liquids 30

Macdonald, J. R., Magnetic anisotropy measurement with an oscillation magnetometer 116
MacInnes, I., *see under* McLaren, A. S.
Mack, C., and C. Rubenstein, The effective coefficient of friction for strings traversing cylinders transversely and slantwise 247

Matthews, D., *see under* Langton, N. H.
Maude, A. D., and R. L. Whitmore, A generalized theory of sedimentation 477
McCaig, M., *see under* Clegg, A. G.
McGuire, J. H., and Margaret Law, The performance of spark guards 470
McLaren, A. S., and I. McInnes, The influence on the stress distribution in an adhesive lap joint of bending of the adhering sheets 72
Meltzer, B., and P. L. Holmes, Beam temperature, discharge lag and target biasing in some television pick-up tubes 139
Mulvey, T., and A. J. Campbell, Proportional counters in X-ray spectro-chemical analysis 406

Nankivell, J. F., *see under* Garrod, R. I.
Newcomb, T. P., The flow of heat in a parallel-faced infinite solid 370
Newcomb, T. P., The radial flow of heat in an infinite cylinder 456
Newman, P. C., *see under* Brice, J. C.
Nicholls, N. S., *see under* Armstrong, R. J.
Nicholson, R. B., G. Thomas and J. Nutting, A technique for obtaining thin foils of aluminium and aluminium alloys for transmission electron metallography 25
Nixon, H. L., and H. L. Fisher, An improved spray droplet technique for quantitative electron microscopy 68
Norbury, J., *see under* Booker, G. R.
North, A. C. T., *see under* Finch, J.
Nutting, J., *see under* Nicholson, R. B.

Oliver, D. R., *see under* Higginbotham, G. H.

Padfield, Daphne G., and Nora B. Dickinson, Stresses and strains in an infinite elastic sheet under a tension applied at two rigid pairs of square jaws 448
Page, D. H., The chromatic field aberrations and their correction in a three-lens reflexion electron microscope 268
Page, D. H., Reflexion electron microscopy at high angles 60
Parish, G. J., Apparent slip between metal and rubber-covered pressure rollers 428
Parish, G. J., Measurements of pressure distribution between metal and rubber-covered rollers 158
Pope, R. A., *see under* Hunt, S. E.
Powles, J. G., A note on the calculation of second moments of nuclear magnetic resonance absorption lines 299 (C)
Preston, J. S., *see under* Barnett, W.
Priede, T., *see under* Austen, A. E. W.
Probine, M. C., An electrical analogue method of predicting the permeability of unsaturated porous materials 144

Rachinger, W. A., A "super-elastic" single crystal calibration bar 250
Rayner, G. H., The time-constant of carbon composition resistors 240
Rayner, J. H., *see under* Gower, J. C.
Rees, W. H., Atmospheric pollution and the soiling of textile materials 301 (SA)
Reichenbaum, G., *see under* Donovan, B.
Richardson, E. G., *see under* Iyengar, D. S.
Roberts, D. H., and B. L. H. Wilson, The performance of infra-red photoconductive cells 291
Roberts, J. E., *see under* Jobling, A.
Rowe, G. W., *see under* Golden, J.
Rubenstein, C., *see under* Mack, C.

Sheard, A. R., *see under* Goldsmid, H. J.
Shimada, Heihachi, Photoelastic investigation of stresses in composite models with notches and holes 34
Shtrikman, S., *see under* Frei, E. H.
Siddall, G., *see under* Holland, L.
Smith, B. O., A. P. H. Jennings and A. G. Grimshaw, A portable lamination detector for steel sheet 191
Smith, J., Temperature cofficient of maintenance potential of glow discharge voltage stabilizer and regulator tubes 122 (C)
Snowdon, J. C., The choice of resilient materials for anti-vibration mountings 461 (SA)
Spalding, D. B., *see under* Hutcheon, I. C.
Spring, K. H., Bonding optical components to metal mounts 242
Spurr, R. T., The friction of mineral particles 486
Stansfield, G. J., The geometry of twisted multi-filament structures 133
Sumner, G., and K. M. Entwistle, The measurement of the strain-dependent damping of metals vibrating torsionally 434

Tamai, Yasukatsu, Frictional behaviour and structure of the surface oxides of steel 338 (C)
Taylor, R. J., Physical methods of investigating chemical problems 165 (SA)
Taylor, W. B., *see under* Williamson, K. I.
Thomas, G., *see under* Nicholson, R. B.
Thomas, K., *see under* Wright, P.
Tingle, E. D., *see under* Kay, E.
Treves, D., *see under* Frei, E. H.
Troughton, A. G. H., *see under* Jackson, R. C.
Tucker, H. St. G., The particle size of some Witwatersrand mine dust 98
Tuzi, Z., K. Kawata and I. Hori, The photoelastic behaviour of cross-linked polymers 173

Vick, F. A., *see under* Hopkins, B. J.

Wakelin, R. J., Temperature distribution throughout a stack of electrical sheet steel during annealing 353
Waldron, R. A., Resonant cavity methods of measuring ferrite properties 439
Ward, S. G., *see under* Higginbotham, G. H.
Watkins, M. T., *see under* Bishop, J. F. W.
Watson, H. H., The sampling efficiency of the thermal precipitator 78 (C)
Whitmore, R. L., *see under* Maude, A. D.
Williamson, K. I., and W. B. Taylor, The analysis of particle counts by the spray-drop method 264
Wilson, A. J. C., *see under* Hughes, J. W.
Wilson, B. L. H., *see under* Roberts, D. H.
Wright, D. A., Photoconductivity 205 (SA)
Wright, D. A., *see under* Goldsmid, H. J.
Wright, H. C., *see under* Brice, J. C.
Wright, P., and K. Thomas, Pulse-annealing technique for metals and alloys 330
Wroe, H., The magnetic stabilization of low pressure d.c. arcs 488

Ziebland, H., and J. T. A. Burton, The thermal conductivity of nitrogen and argon in liquid and gaseous states 52

PRINTED IN GREAT BRITAIN BY UNWIN BROTHERS LIMITED, WOKING AND LONDON

Summarized proceedings of a conference on biological structures and computational methods—London, November 1956

The annual Autumn Conference of the X-ray Analysis Group of the Institute of Physics was held in London on 16 and 17 November, 1956. The three sessions dealt with crystallographic computing for large molecules; globular and fibrous proteins; and viruses and nucleic acids.

CRYSTALLOGRAPHIC COMPUTING FOR LARGE MOLECULES

Dr. D. W. J. CRUICKSHANK (University of Leeds) gave the first paper, entitled "Large scale crystallographic computing." He and his associates[1] had, in the past four-and-a-half years, worked on thirty-six crystal structures, using a total of 1500 h computing time on the Manchester University Computer. Most of the work had been the detailed refinement of small structures by means of programmes which calculate three-dimensional differential syntheses, and three-dimensional structure factors, including anisotropic temperature factors.

The facilities of the present Manchester machine (shortly to be replaced by a faster and more reliable one) were briefly described. The store is in two parts: a fast-access electrostatic store of eight "pages" each of thirty-two "words," and a magnetic drum with 512 tracks accommodating 16384 words, i.e. 655360 binary digits. Words on the magnetic drum have to be transferred to the rapid-access store before operations can be performed on them. This transfer is a slow process, taking about 50 ms for one track of thirty-two words. Addition and subtraction take 1·2 ms per operation, multiplication takes 2·2 ms.

For work on wet vitamin B_{12}[2] to be practicable with this relatively slow computer it was essential to use very efficient programmes. The rate determining operation in structure factor calculations was the computation of the trigonometric contributions. In space group $P2_12_12_1$ formulae of the type $\Sigma_r (\cos hx_r \cos ky_r \cos lz_r)$ were at least 7 times faster than $\Sigma_r \cos (hx_r + ky_r + lz_r)$. Including checking by repetition of each stage, the complete time for the calculation of 2600 A's and B's for 105 atoms in wet B_{12} was about 17 h. The corresponding Fourier map, calculated in fifteen sections each with 60×60 points, took about the same time. The large capacity of the drum store enabled each Fourier section to be computed in an efficient manner without any output of intermediate totals.

Referring to the new computers which would be available shortly, Dr. Cruickshank said that the main lesson which had been learnt was that programmes must be designed from the start to deal with every conceivable parameter in very large structures in general space groups.

The second paper "Crystallographic calculations for large molecules" was given by Prof. K. N. TRUEBLOOD (University of California at Los Angeles) to whom the Chairman, Prof. E. G. COX (University of Leeds) extended a special welcome as a representative of the foreign visitors to the Conference. Professor Trueblood described the computer SWAC, operated jointly by the University of California and the United States Office of Naval Research: it is a parallel-mode machine with a modified four-address command system. A high-speed store accommodates 256 words of thirty-six binary digits and sign, and is supplemented by a magnetic drum for 8192 similar words. Addition time is 64 μs; multiplication and division are somewhat slower. Drum transfers and input-output are appreciably less efficient operations and must therefore be minimized in programming for the machine.[3]

General programmes suitable for all space groups are usually used now, but the calculations for the hexa-carboxylic acid fragment of vitamin B_{12} were done with programmes modified somewhat to decrease the machine time required. For structures with about 100 or more atoms in the asymmetric unit the time factor becomes dominant in coding considerations, increasing, at least for structure factor calculations, roughly with the square of the number of atoms. Thus for such structures it is worth while to sacrifice the flexibility of general programmes for the efficiency of those written specially for the problem in hand. Professor Trueblood stressed the importance of programmes being written by crystallographers so that their form could be made sufficiently flexible to accommodate the unforeseen modifications almost invariably needed later on, and so that those actually using the programmes would completely understand them.

For the hexa-carboxylic acid derived from vitamin B_{12}, with seventy-three atoms and 3351 planes, structure factor calculations took about 7 h, an electron density map about $5\frac{1}{2}$ h, and a cycle of least squares refinement about 24 h. With more specific programming these times could have been reduced by 30–50%. Ten cycles of structure factor-Fourier synthesis calculations were done in establishing the structure, and refinement by least squares is now under way. Considerable care was needed in selecting new atomic positions at each stage of the determination; but it was encouraging to find that, among the Fourier peaks not representing atoms used in the phasing, those representing true atomic positions appeared persistently, even when spurious atoms were inserted by mistake. False detail disappeared almost completely in the later stages, even before refinement. It was usually possible to distinguish carbon, nitrogen and oxygen atoms purely by their peak heights if comparisons were made in regions of the molecule of comparable rigidity; because of large thermal vibrations, atoms in the side chains appeared with reduced height, the effect being more pronounced the longer the chain. The experience gained with 100-atom structures, together with foreseeable improvements in computers, indicated that the computing problem would present no serious difficulties for asymmetric units of as many as 1000 atoms.

The next speaker, Dr. A. S. DOUGLAS (University of Cambridge), discussed "The mechanical presentation of the results of Fourier series summation." He pointed out that machines now being designed would be of the order of 1000 times faster than the Manchester computer, and the output of results, their printing and plotting as contour maps, would then occupy much the largest proportion of the time required for a Fourier summation. A more direct form of output could be achieved by storing the table of results in the machine, and then using a programme to plot contours from this, either on a cathode-ray tube or with a pen-and-paper recorder of the type used in drawing weather maps

from signals received over a telephone line. Even with a grid of 1024 × 1024 points on a large cathode-ray tube one could not represent lines at small angles to the grid axes very satisfactorily.

The manner of presenting the results could have an important effect on the methods used in carrying out the Fourier summations. For example, if one could examine the effect of sign changes among a few Fourier terms on a directly presented electron density map, the initial summation of a large number of terms would, no doubt, be done by the usual Beevers–Lipson technique, but the effect of a sign change need not involve only a single-term Fourier calculation, which was more quickly done by a direct method. A point worth noting with the present machines was that reading from a punched tape or cards was always faster than output in this form, so it was better to split large calculations into small parts each of which could be completed within the capacity of the high-speed store, than to print out intermediate results which had later to be fed back into the machine, even though the initial table of F's might have to be re-read at the beginning of each part.

Dr. J. S. Rollett (University of Oxford) spoke on "Crystallographic calculations on Deuce." He had written programmes for three-dimensional electron density maps and structure factors in all space groups for the machine at the National Physical Laboratory, but there were several other Deuce machines in this country and overseas, and the programmes he had written would be available for use with them.

The structure factor programme worked directly from the general expression $F = \Sigma fT \cos(hx + ky + lz)$, which was slower than using the trigonometrical product formulae. However, this programme was still faster for most structures than that for the calculation of Fourier maps, and the use of the general expression made it easier to incorporate anisotropic temperature factors. The labour of inserting co-ordinates for all the equivalent points in the unit cell (X, Y, Z) was saved by generating them from the co-ordinates of one particular point (x, y, z) as follows: in all cases $X = C + V$ where C is one of the fractions 0, $\frac{1}{4}$, $\frac{1}{2}$, $\frac{3}{4}$, $\frac{1}{8}$, $\frac{3}{8}$, $\frac{5}{8}$, $\frac{7}{8}$; and V is one of $\pm(x, y, z, y-x)$, the selection depending on the space group. Overall computing times for three sets of structure factors were given in the following table:

	Space group	*Number of independent atoms*	*Number of reflexions*	*Time*
Vitamin B_{12}	$P2_12_12_1$	99	2500	11 h 0 min
Biotin	$P2_12_12_1$	16	1200	1 h 15 min
Cystine	$P6_12$	7	700	55 min

For the calculation of electron density maps each Fourier term was converted to binary in the form A, B, l, trig, in which trig was a symbol selecting the trigonometrical products appropriate to that term from the eight possibilities

$+A \cos hx \cos ky \cos lz$,
$-A \cos hx \sin ky \sin lz$, and its cyclic permutations,
$-B \sin hx \sin ky \sin lz$,
$+B \sin hx \cos ky \cos lz$, and its cyclic permutations.

The summation was carried out in sections by the Beevers–Lipson method, with the first summation performed as the data cards were read into the machine, a second summation for each change of k, and the third summation for each change of h. Computing times could be reduced by choosing h-indices to have the smallest range, and the number of plotting points along z to be as few as possible. The smallest interval at which the Fourier could be computed was 1/240th of the cell side, but any multiple of this could be chosen. Computing times for three Fourier series were given by the table:

	Space group	*Number of terms*	*Number of points*	*Total time*	*Punching time*
Vitamin B_{12}	$P2_12_12_1$	2500	60 × 60 × 15	8 h 30 min	2 h 0 min
Cocarboxylase	$P\bar{1}$	2000	30 × 30 × 15	3 h 20 min	20 min
Cystine	$P6_12$	1500	20 × 20 × 12	1 h 10 min	6 min

The programmes for Deuce were carefully written so that sequences of orders were in the most accessible positions at each stage, and the facilities of the machine were fully used all the time. This optimum programming led to great savings in computing time.

In speaking on "Calculations of theoretical electron distributions in molecules" Dr. W. Cochran (University of Cambridge) said that crystallographers had, in general, been interested only in the positions of the nuclei of atoms, though the scattering of X-rays was a function of the electrons. The calculation of electronic distributions in molecules, and comparison of the results with experimental measurements, was a neglected subject. In fact the approximation of a molecule by non-bonded atoms at the correct positions, and with some allowance made for thermal vibration, was very close to the truth, and there was little point in comparing the complete electron distributions in the observed and artificially constructed molecules ρ_0^m and ρ_c^m; differences would be more sharply revealed in comparing two difference density maps: the first representing the experimentally observed electron distribution in the molecule minus the densities from the appropriate non-bonded atoms $\rho_0^m - \rho_c^a$; the second the molecular density distribution calculated from a molecular orbital type approximation to the wave function minus the densities of the non-bonded atoms $\rho_c^m - \rho_c^a = D$. This paper was concerned with the calculation of D to a reasonable degree of approximation. Calculations of this type had been made before by March,[4] but could now be improved and extended with the use of electronic computers such as the EDSAC.[5]

For benzene, where experimental data were available from the accurate structure determination of salicylic acid, the electrons could be assigned to three groups:

(i) 12 (1s) electrons appearing unchanged in the molecular and atomic distributions, which could be left out of the calculations,
(ii) 24 σ-electrons in C–H and C–C bonds,
(iii) 6 π-electrons in C–C bonds.

In a section through the plane of the benzene ring the π-electrons did not appear, so one had

$$D_\sigma = \sum_{j=1}^{6} [D_\sigma(C_j - H_j) + D_\sigma(C_j - C_{j+1})]$$

Each of D_σ (C–H) and D_σ (C–C) was taken to have cylindrical symmetry about the bond. No allowance had been made at this stage for the effects of thermal vibration and zero-point energy of the molecule. The map of D_σ (Fig. 1) showed a peak on the C–H bond which did something to account for the shortening of the bond observed by experiment, but its size was not sufficient to account for the effect completely.

Calculation of a projection of the complete difference density on to the plane of the benzene ring had to include the π-electrons, but the work could be simplified by applying

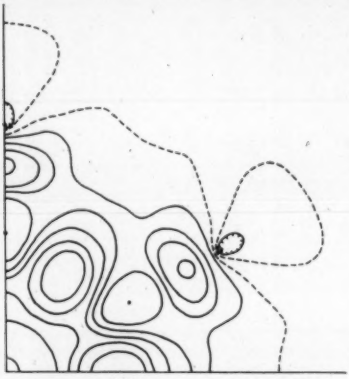

[Reproduced from *Acta Crystallographica*]

Fig. 1. Calculated difference density in the plane of the benzene ring. Contours every 0·1 e . A^{-3} from −0·1 to +0·5 e . A^{-3}

Fourier transform methods. The calculation was split into several parts each occupying a reasonably short time on the computer, and containing its own internal checks. First D_σ (C–C) and D_π (C–H) and their Fourier–Bessel transforms were worked out, then $\int D_\pi$ (C–C) dz and its transform. Then the transforms were multiplied by a temperature factor, and the appropriate sections put through a Fourier inversion to give the projected densities d_σ (C–H), d_σ (C–C), and d_π (C–C). The result was compared with the observed distribution (Fig. 2). Agreement or disagreement in detail was not significant because the method of calculation was comparatively crude, but the maps showed that the formation of covalent bonds between atoms led to very little distortion of their "unbonded" electron distributions; a rather surprising result.

In the discussion on Dr. Cochran's paper Dr. R. MASON (University College, London) said that with several structures containing benzene rings the experimental difference syntheses showed holes about 0·3 e/A^2 deep at the centre of the ring. He thought this might be an artefact which could be corrected by adjusting the screening constants used in calculating the wave functions and scattering factor curves of the non-bonded atoms.

Dr. Cochran agreed that adjustment of the screening constants might have a beneficial effect, but Dr. Cruickshank, who said that similar holes were found in the three-dimensional difference syntheses,[6] thought it unlikely that this would account for the phenomenon completely.

The last paper of the session, "Aspects or implications of high-speed automatic computing in the field of large-molecule X-ray crystallography," by Dr. A. D. BOOTH (Birkbeck College, London) was a survey of the rapid developments taking place at the present time, and an attempt to assess whether the facilities to be made available in the next year or two would be sufficient to meet the needs of crystallographers.

His estimates of computing times were based on operating times similar to those of the Deuce machines, which were unlikely to be bettered by commercially available machines within the next two years. Allowing 1 ms for multiplication, and compatible times for other operations, calculation of structure factors for a 100-atom structure with 1000 X-ray reflexions would take about 20 min, and a similar time would be required for a difference synthesis. A survey of the published work showed that something of the order of 100 structures might be solved each year, and the associated computing would apparently only occupy 100 days of machine

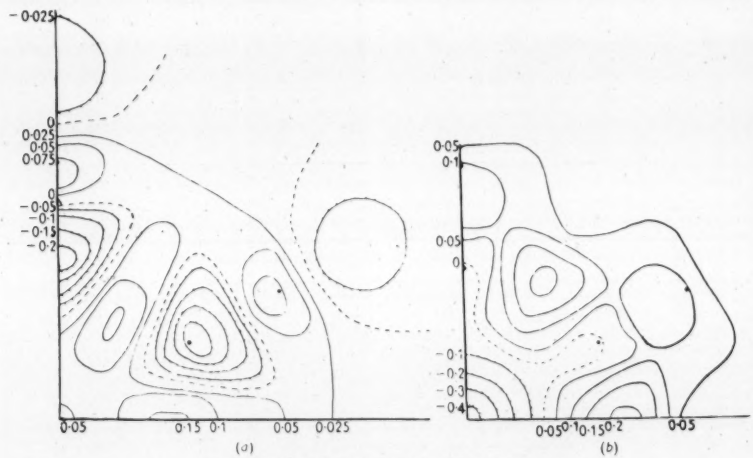

[Reproduced from *Acta Crystallographica*]

Fig. 2. (*a*) Calculated difference density in projection on the molecular plane, with allowance for temperature factor. (*b*) Measured density, for comparison with (*a*)

time. Analysis of protein structures with 1000 atoms and 10000 planes was a task of much greater magnitude: a year's machine time would be needed for ten three-dimensional Fouriers and the same number of stages of refinement by difference synthesis on two or three molecules. However, with several machines becoming available in university laboratories in a year or so, and the prospect of machines 100 times faster in two years' time, it seemed that the needs of crystallographers in this country were likely to be well provided for without a special computing centre being set up for their exclusive use.

Mr. J. H. WILKINSON (National Physical Laboratory) said that a computing service for crystallographers would be provided at the National Physical Laboratory with Dr. Rollett's programmes. The fee would be £15 an hour for university users, and £30 for industrial users plus, in each case, a royalty on the programmes of £3 an hour. Similar facilities would be available on the Deuce machines in Stafford and London.

Dr. J. H. RAYNER (Rothamsted Experimental Station) described programmes for the calculation of two-dimensional Fourier maps, structure factors, and *R*-factors on the Elliott 401 computer. For the structure factor calculations all structures were treated as if they belonged to the space group *P*1. The values were computed at the rate of one structure factor every $7N/80 + 3$ seconds, N being the number of atoms in the unit cell. The computer had a magnetic disk store for 3000 numbers, but the fast access store was limited to five registers, including the accumulator and multiplier. With this type of computer optimum programming was particularly important.

Dr. M. P. BARNETT (IBM United Kingdom, Ltd.) said that a programme written by Dr. D. Sayre (IBM, New York) would calculate structure factors, do least-squares refinement of atomic co-ordinates, and least squares refinement of individual isotropic temperature factors, for any space group. The number of atoms in the asymmetric unit could not exceed 176. The programmes had been used to date in calculations on some forty medium-sized molecules, the largest being aureomycin. The time required per least square iteration was approximately $1/1250 \times$ (number of atoms in the asymmetric unit) $\times$ (number of reflexions) min.

Dr. DOROTHY HODGKIN (University of Oxford), introducing the main discussion with some remarks about computing in the structure determination of vitamin B_{12}, said that with so many of those who had helped with the computing for vitamin B_{12} in the audience she would like to take the opportunity of expressing her thanks to them all. With the punched-card equipment used at first the computation of a set of three-dimensional structure factors for 100 atoms took many months, and it had been a great encouragement to know that with an electronic machine this could be reduced to a few hours' working time, though there might be long delays in getting the calculations on to the machine. At present the problem was still how to get started on the refinement of the structure; progress was not held up through any lack of computing facilities.

Professor Cox pointed out that to those concerned with smaller structures "refinement" meant improvements made after the main stereochemical configuration of a molecule had been established, whereas protein crystallographers used it to mean improvements made before that stage had been reached. He though it best to restrict the word to a precise connotation.

In reply to a question by Dr. H. J. GRENVILLE-WELLS (University College, London) Dr. Rollett said that the programmes for Deuce were equally applicable to two-dimensional refinement.

Professor Trueblood said that the computing times he had given for calculations on SWAC, which Dr. Douglas had thought rather optimistic, had not included the time required for punching the data and checking. Much time was also needed for the plotting and examination of the Fourier maps, and an accurate automatic method of plotting would be of the greatest use.

Dr. OLGA KENNARD (National Institute for Medical Research) put forward a renewed plea for the setting up of a centre for crystallographic computing, since she doubted whether a few more computers in university laboratories would greatly reduce present delays.

Dr. Dorothy Hodgkin and Dr. Booth said that with the services provided by the N.P.L. and the new machines in Manchester and London, all crystallographers in this country should be able to get their calculations done without undue delay.

Professor Cox summarized the expectations of computers by saying that in university laboratories, in addition to the machines already mentioned, there would be, in one or two years' time, Pegasus or Mercury computers at Oxford, Glasgow, Leeds, Sheffield, Southampton and Newcastle. No formal arrangements had yet been made, but fees would probably be standardized.

Dr. Douglas expressed doubts about the delivery dates which had been mentioned, but Dr. C. M. WILSON (Ferranti, Ltd.) assured him that promised dates of delivery for Pegasus machines would be adhered to.

GLOBULAR AND FIBROUS PROTEINS

Sir LAWRENCE BRAGG took the Chair in the afternoon session. In his opening remarks, he recalled the publication of a paper which proved that it was impossible to solve a structure involving more than five parameters. However, recent years had seen a great advance in structure analysis, and the afternoon's papers would show that a high peak had been reached in the study of complex substances. As an introduction to the papers, Sir Lawrence briefly described one method by which the shrinkage properties of the horse haemoglobin crystal had been used to trace nodes and loops along layer-lines, thus revealing relative phases of reflexions. The heavy-atom method of phase determination was proving very powerful, and Sir Lawrence illustrated its application to centro-symmetrical structures by diffraction patterns obtained with the Lipson optical diffraction instrument.

Dr. DOROTHY HODKGIN (University of Oxford) gave an account of the work of her group on vitamin B_{12}. The analysis had proceeded by parallel investigations of four different crystal structures:

(1) dry B_{12}, which contains about 111 atoms, not counting hydrogen,
(2) wet B_{12}, which contains an additional five or six molecules of water,
(3) the selenocyanide derivative of B_{12},
(4) a hexa-carboxylic acid, containing some 70 atoms, excluding hydrogen, which constitutes the so-called "red fragment" of B_{12}.

Initially, only the approximate empirical chemical formulae of these compounds were known. Other evidence, particularly on the presence of a nucleotide-like group, was obtained by chemical degradation experiments parallel with the X-ray analysis.

Three-dimensional Patterson distributions showed peaks arising from Co–Co vectors; neighbouring peaks indicated octahedral co-ordination about the cobalt atoms, and suggested the presence of something similar to a porphyrin ring. Three-dimensional electron-density distributions were calculated[2] for forms 1, 2 and 3, using phases derived from cobalt atoms (cobalt and selenium for form 3). These distributions were highly imperfect, the ratio $f_{Co}^2/\Sigma f_{rest}^2$ being only 0·14–0·21; they showed spurious peaks in addition to peaks which later proved to have been in correct positions. Among these it was possible to select a number which corresponded with the groups identified chemically, particularly the nucleotide-like structure. In addition, other peaks were selected; those around the cobalt atom composed four five-membered rings, similar to those of porphyrins except that two were linked directly together. However, it proved very difficult by cycles of structure factor and electron density calculation to decide which of the selected peaks were correct.

The isolation of the hexa-carboxylic acid, essentially B_{12} minus the nucleotide-like group, proved the turning point in the investigation. The first electron density distribution, computed again with phases derived from the cobalt atoms alone, showed the same porphyrin-like nucleus to be present in this compound as earlier recognized in B_{12}. Twenty-six atoms, including the cobalt, were selected and used for further phase angle and electron density calculations; they represented nearly 50% of the total scattering power. In the following electron density distribution all but a few atoms in the crystal could be clearly distinguished and the molecular structure as a whole could be written out in all but a few details.[7, 8]

With this knowledge of the major part of the B_{12} molecule, further refinement had now led to a complete description of the structure of the whole molecule and of the atomic arrangement in the different crystals, except for the positions of some water molecules.[9] The B_{12} molecules are very compact and almost spherical; they are in contact in the different crystals on all sides with neighbouring molecules through amide to amide, or phosphate hydrogen bonds. When water molecules are lost on drying, the whole molecule tilts and rotates through about 5° and two amide groups swing round to give closer packing.

Dr. M. F. Perutz (University of Cambridge) began his contribution with a summary of a recent series of papers describing how the signs of the *h*0*l* reflexions of horse methaemoglobin had been determined to a spacing of 6·5 Å.[10–15] The resulting Fourier projections on the *b* plane, though undoubtedly correct, had proved uninterpretable on account of inadequate resolution and of the great thickness of matter projected on to one plane. If it were possible to determine the signs to the limiting spacing to which reflexions can be observed, which is about 1·8 Å, the resolution of the projections could be much improved. Dr. Perutz then described an attempt by Miss Ann F. Cullis, Dr. H. M. Dintzis and himself to determine these signs by isomorphous replacement with heavy atoms. Three heavy atom compounds of haemoglobin had been prepared. In one compound each of two symmetrically disposed SH groups in haemoglobin was combined with one residue of mercuri-benzoate and in another with dimercuri-acetate. A third compound was made by combining two groups, probably consisting of mercuric tetraiodide ion, with one molecule of haemoglobin at sites whose chemical character was not yet known.

The positions of the mercury atoms in the mercuri-benzoate and dimercuri-acetate compounds were first found approximately from Patterson projections, using the squares of the differences in structure amplitude between the heavy atom compounds and normal haemoglobin as coefficients of the terms.[13] Signs were then calculated for the $F(h0l)$'s of each of the two compounds. The terms for which the signs derived separately from the two compounds agreed were used to calculate Fourier projections with the differences in structure amplitude as coefficients. These served to get accurate parameters for the mercury atoms. The mercuri–tetraiodide compound gave a poor difference Patterson; the positions of the heavy atom groups had to be found from a difference Fourier, using the signs already derived from the other two mercury compounds.

A plot of the reliability factors of the heavy atom contributions in the mercuri-benzoate and dimercuri-acetate compounds,

$$\frac{\Sigma\big||\Delta F_0| - |\Delta F_c|\big|}{\Sigma|\Delta F_0|},$$

showed that they rose from a value of about 0·3 for the inner reflexions above 6 Å spacing to about 0·6 at 3 Å spacing. Beyond this spacing the signs found from different heavy atom compounds ceased to be consistent, so that in haemoglobin the derivation of signs by the isomorphous replacement method seemed to be limited to reflexions of spacing larger than 3 Å.

The limiting circle of 3 Å spacing contains about 550 reciprocal lattice points. Eighty of these have F values too small to be measured leaving a total of 470 signs to be determined. Three hundred and forty of these had been found so far. The speaker then showed a comparison between the original Fourier projection of Bragg and Perutz,[15] calculated with only 94 terms, and a new projection calculated with 340 terms. The new Fourier projection showed much more detail than the old, but still contained no recognizable chemical features. However, Dr. Perutz pointed out that the four iron atoms in the haemoglobin molecule should be sufficiently prominent to show up in this projection, and that they might be recognized by suitable labelling with heavy atoms. Attempts to find the phases of complex structure amplitudes by direct methods were being made by Mr. D. M. Blow, but it was not sure as yet whether the accuracy of the phases would be good enough.

Dr. D. W. Green (Royal Institution, London) described work by himself and Dr. A. C. T. North on ox haemoglobin, an orthorhombic form. Chemical studies had shown ox and horse haemoglobins to be basically similar[16] and Patterson projections along the *a* axes of the two forms displayed similar features.[17] An isomorphous derivative with mercury atoms attached to the sulphydryl groups indicated that these groups occurred in the same part of the molecule as in horse haemoglobin. Fig. 3 represents diagrammatically the molecule as seen along the three principal directions in ox haemoglobin crystals and the positions of the SH sites, which have only been located in one projection in horse haemoglobin.

Fourier maps had been calculated for all three projections of the ox haemoglobin crystal structure to 6 Å resolution, containing terms representing about two-thirds of the total scattering power. Two of these projections were comparatively free of overlapping between neighbouring molecules, and were the two views at right angles to that seen in the horse haemoglobin projection. No molecular features could be recognized, but in both views there was a tendency to diad symmetry, which is not crystallographically required in ox

as it is in horse haemoglobin. This was another respect in which the molecules were similar.

The next paper was given by Dr. J. C. KENDREW (Cavendish

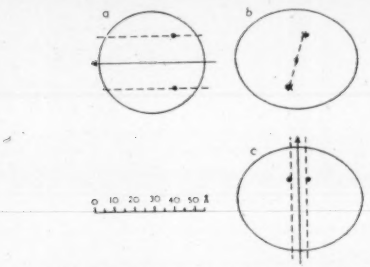

Fig. 3. Positions of the sulphydryl sites within the haemoglobin molecule, represented as an ellipsoid. The circles indicate the positions observed in ox haemoglobin, the crosses and broken lines the sites in horse haemoglobin, in which they have been located only in the *b*-projection

Laboratory, Cambridge) on "Phase determination in myoglobin." Of the twelve different crystal forms of myoglobin, most progress had been made with Type *A*, sperm whale myoglobin, which belonged to the space group $P2_1$, containing 2 molecules per unit cell. Unlike haemoglobin, myoglobin contained no sulphydryl groups, and it had been difficult to find specific binding sites which were satisfactory for the isomorphous replacement method to be used. Early attempts to attach suitable heavy atoms to the haem group had been unsuccessful, but Dr. H. M. Dintzis, Dr. G. Bodo and Dr. V. M. Ingram had eventually managed to prepare several heavy-atom derivatives, including one using mercuric tetra-iodide ion, $HgI_4^{''}$. It had been found that there were at least four different sites to which one or other of the heavy-atom complexes could be attached, as shown in Fig. 4. The

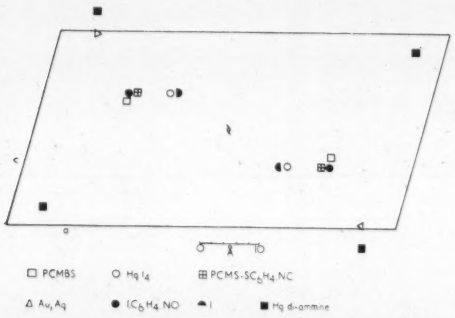

Fig. 4. Positions of heavy-atom sites in the unit cell of type *A* myoglobin

heavy-atom positions had been determined by difference-Patterson and difference-Fourier methods.

Signs had been deduced for most of the reflexions of the *h*0*l* zone out to 4 Å spacing, reliability factors between observed and calculated differences being generally about 0·30–0·33 for reflexions above 6 Å spacing. Two Fourier projections had been calculated, one to a resolution of 4 Å, the other to 6·6 Å; they showed little difference, probably because the real limit of resolution was the great depth of material in the direction of projection. It therefore appeared that, in myoglobin also, it would be necessary to work in three dimensions. In order to do this, the heavy-atom positions would have to be more closely defined; a difference-Patterson had been calculated with data out to 1·9 Å for the $HgI_4^{''}$ derivative and this resolved the separate atoms of the group. After placing atoms in the positions indicated by the Patterson, the reliability factor for reflexions greater than 6 Å was reduced to 0·23.

Dr. Kendrew intended to perform the three-dimensional analysis to a resolution of 6·3 Å in the first instance. To solve the complex phases, at least two, preferably three or four, different heavy-atom substitutions would be necessary; it was hoped that sufficient satisfactory substitutions had now been made. It was hoped to use the method of Perutz to measure the relative *b*-co-ordinates of the different heavy atoms. There were still various difficulties to be surmounted; in at least one case, PCMS, the heavy atom tended to migrate to a new site on prolonged irradiation; Friedel's law was found to break down for some of the derivatives, though it was hoped that this effect might be used as a check on phase-determination.

Dr. Kendrew also referred to work being done on two other myoglobin crystal forms, by Dr. Helen Scouloudi and Mr. P. J. Pauling at the Royal Institution.

Prof. J. D. BERNAL (Birkbeck College, London) described briefly the work on ribonuclease by Dr. C. H. Carlisle and his collaborators at Birkbeck College, London. A ribonuclease derivative containing mercury had been prepared; chemical analysis showed that two mercury atoms had combined with each protein molecule. The heavy-atom difference-Patterson maps were not as clean as those for haemoglobin and myoglobin. They appeared to show four mercury sites, but a difference-Fourier, based on these four positions, showed only two strong peaks, together with much background detail. It was concluded that the high background was due either to there being other possible mercury sites in the molecule in addition to the two favoured positions, or to distortion of the protein by the heavy metal complex; the latter explanation seemed more probable. Signs had been given to about forty reflexions, and a Fourier projection of the protein calculated. As with the haemoglobin and myoglobin Fourier projections, it showed no recognizable features, and the Birkbeck group also had come to the conclusion that a three-dimensional analysis alone would be informative.

Prof. W. T. ASTBURY (University of Leeds) surveyed "Recent trends in the study of fibrous proteins." One of the earliest results of the X-ray study of fibres had been the recognition that they were of the nature of molecular yarns. Only the simpler expressions of this concept had been identified in the earlier stages, but of recent years it had come to full realization in the discovery at molecular level also of "twist" and combinations of "twist." The general configuration of the fibre molecule, like so much else in nature, was helical, and sets of helical chains might also be twisted together to form compound helices or "coiled coils," and so on up to visible filaments.

According to another early X-ray conclusion in the field,[18] the three chief configurational classes of the fibrous proteins were: (*a*) and (*b*), the α- and β-forms of the *k*-*m*-*e*-*f* group,

the historical prototype of which was the protein (keratin) of unstretched and stretched mammalian hair; and (*c*), the collagen group. From the combined findings of many workers, it was seen now that: (*a*) was based on polypeptide helices (of about 3·6 amino acid residues per turn) held in shape by *intra*-chain CO . . . NH hydrogen bonds; (*b*) was based on opened-up (two-fold) helices linked together by *inter*-chain hydrogen bonds; and (*c*) was derived from the externally-bonded trigonal helices which were common to polyproline and polyglycine II. In (*a*) and (*c*) there were also superimposed the coiled-coil elaboration, in that at least two or three helices were twisted round one another in α-keratin and its analogues, while the configurational unit of the collagen group consisted of three of the polyproline-type trigonal helices twisted round one another so as to give now a repeat, not of nine, but of ten residues in three turns.

The great difficulty as things stood at present was the apparent conflict, or rather compromise, between geometry and stoichiometry; the macro-periods of the fibrous proteins had to be explained too. The coiled-coil systems were inherently capable of building up more or less specific macro-periods in the fibre direction, but regular sequences of residues must also have their effects. In α-keratin, for instance, where the macro-period (198 Å) might reasonably be interpreted on the basis of a two- or three-fold coiled coil so long as differences between side-chains were neglected, there were in actual fact too many observed meridional reflexions. Again, the 410 Å axial period of actomyosin could be dissolved out, so to speak: it had been shown to be associated both with the *F*-actin component and with the "light meromyosin" fraction of the myosin component. Indeed, when all the contributing factors and possibilities had been taken into consideration, the detailed working-out of the fibrous proteins seemed immensely complicated at the moment. We urgently needed more chemical data and the separation of constituents, especially in relation to the collagen group.

On the credit side, though, the application of optical transform methods was now proving extremely helpful in fibre studies.

Dr. PAULINE M. HARRISON (University of Sheffield) read the paper by herself and Dr. S. McGavin (King's College, London) entitled "The structure of collagen and its wider implications." The polypeptide chains of collagen have a distinctive and characteristic amino acid composition, including ~22% of proline and hydroxyproline and ~33% of glycine,[19] although there is a considerable compositional variation between collagens of different organs and between different species. High angle X-ray diffraction has shown that the chain-configurations of different collagens are nearly isomorphous, but the appearance of fibres in the electron-microscope reveals that there are differences in the relative arrangements of chains. Experiments on extracted collagens,[20] and on collagen solutions,[21] suggest that the fundamental collagen particle is 3000 Å long and of molecular weight 300000. These particles may be in a staggered array in the fibre, thus giving rise to the 640 Å fibre axis period observed by low-angle X-ray and electron microscope methods.

Determination of the polypeptide chain configuration of collagen had been aided in the past three-and-a-half years by: (1) work on small peptides and the α-helix, the development of Fourier-transform methods and of the optical diffraction technique, and improvement in X-ray tubes and cameras; (2) recognition of the helical nature of the collagen chain,[22, 23] revealed by the improved fibre diagram obtained under tension; (3) chemical evidence indicating that the sequence –glycine–proline–hydroxyproline–glycine– was important in collagen;[24, 25] and (4) synthesis of poly-L-proline[26] and the determination of its structure,[27] a three-fold spiral in which the proline imido groups are *trans* and planar, followed by the discovery of the similar backbone configuration of polyglycine II.[28]

Before the publication of the polyproline data, Ramachandran and Kartha had put forward a collagen structure[29] in which three chains, similar to those of poly-L-proline, were wound round one another to give a system of three coiled coils. Their structure was not correct in detail, but modified versions, such as those first published by Rich and Crick,[30] which would accommodate the –glycine–proline–hydroxyproline–glycine– sequence, were now accepted by all the main groups of collagen workers.[31, 32, 33] Dr. Harrison now favoured the version shown in Fig. 5, which gave

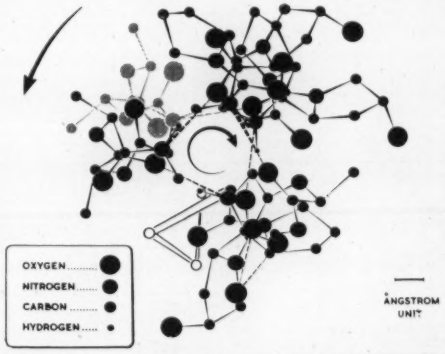

Fig. 5. Proposed structure of collagen, viewed along axis of helix. ("Clockwise" model)

reasonably good agreement between calculated and observed structure factors, as indicated by its optical transform in Fig. 6.

Now that the polypeptide chain configuration had been established with reasonable certainty, it might prove instructive to examine packing arrangements related to its symmetry, in order to explain the complex pattern given by fibres in their native moist condition.[34] The effects observed might be due to the crystallites involved containing only a limited number of chains. Alternatively, as Ramachandran had suggested,[35] the arrangement might be based on a cylindrical lattice; his proposed lattice was not entirely satisfactory, but it was possible that one of the other types of cylindrical or spiral lattice, as described by Whittaker,[36] would be better.

Dr. Harrison showed that the long fibre axis periodicity could be derived from the proposed three chain configuration, and suggested that the relative intensities of the low angle diffraction orders could be explained by the sequence of amino acid residues.

During the discussion Dr. W. TRAUB (Birkbeck College, London) described some X-ray studies of wheat protein done in collaboration with Dr. J. B. Hutchinson and other chemists at the Cereals Research Station, St. Albans. The elastic properties of wheat protein and the disoriented β-keratin X-ray diagram of the denatured material indicated that it was related to the *k-m-e-f* group of fibrous proteins.

Low angle photographs showed a sharp spacing at about 45 Å which had not been observed in other cereals. Furthermore, the low angle X-ray pattern was appreciably affected

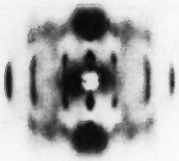

(*a*)

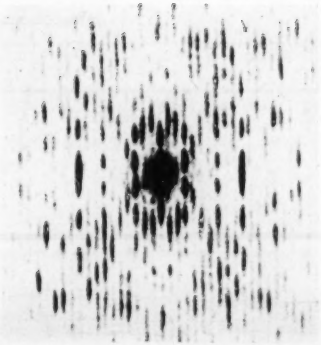

(*b*) [Photograph—Mr. R. E. Burge]

Fig. 6. (*a*) X-ray fibre diagram of dry rat tail tendon stretched 7·6%. (*b*) Optical diffraction pattern of the collagen model shown in Fig. 5. *L*-proline and hydroxy-*L*-proline side chains and one water molecule have been included; other side chains are omitted

by the processes of milling, wetting and doughing. Studies of materials extracted from wheat protein by chemical and enzymatic methods indicated that the 45 Å spacing was due to the presence of a fatty substance (probably a phospholipid) which was closely associated with the protein.

These results, together with the orientation of the 45 Å spacing in thin protein films, suggested that the protein structure was held together by layers of fat, and offered a qualitative explanation for the water-absorbing and elastic properties of wheat flour and its susceptibility to oxidation and mechanical working.

Dr. F. Happey (Bradford Technical College) believed that the differences between the X-ray fibre diagrams of natural and synthetic α-polypeptides could be explained in terms of the degree of crystallinity of chain packing, the chains themselves being basically the Pauling and Corey[37] α-helix in each case.[38] The simple synthetic polypeptides, such as poly-L-alanine, show a comparatively highly crystalline structure, based on α-helices in hexagonal array. Some polymers with long side-chains, synthetic copolymers[39] and natural α-fibres,[40] in which there are side-chains of different lengths, adopt less regular packing, resulting in diffuse X-ray reflexions. Long side-chains probably also cause relative displacement of adjacent helices in an axial direction, in order to achieve closer packing. Dr. Happey outlined the effect of such displacements on the spacings of meridional and near-meridional reflexions, and showed that the different spacings occurring in natural and synthetic α-polypeptides could be accounted for on this basis.

VIRUSES AND NUCLEIC ACIDS

On Saturday morning, Prof. Cox again took the chair. Dr. M. H. F. Wilkins (King's College, London) reported on work, being carried out at his College, on the structure of nucleic acids and nucleo-proteins. He pointed out that because of their very asymmetric shape deoxyribonucleic acid (DNA) molecules are of interest to physical chemists. They also have much biological interest, for, in living things it is DNA that carries the genetic information. This is assumed to be produced by the sequence of the four cyclic nitrogen bases that occur in DNA, attached to the sugar-phosphate backbone.[41] Therefore the structure of the molecule may show the connexion between the arrangement of bases and the genetic information.

The Watson-Crick[42] model suggests that a molecule is composed of two sugar-phosphate polymers intertwined, with the bases always occurring in certain pairs, giving a regular double helical arrangement. Empty regions on the diffraction photograph indicate that each of the basic units or nucleotides is rod shaped.

In the solid state the helix has two special configurations.[43,44] In the *A* form the nucleotide rods are at 70° to the helix axis, and in the *B* form they are perpendicular to this direction. Helices pack best when displaced relative to each other, and the sodium crystalline *A* form has eleven nucleotides per turn and forms a monoclinic lattice. The lithium salt (see Fig. 7) occurs in the *B* form, as it has ten nucleotides per repeat, and forms an orthorhombic lattice. At higher humidities crystals occur with nearest neighbour molecules displaced by one third of the pitch length, giving a hexagonally packed *B* form but with imperfect crystallinity.

The proposed model,[45] which is of a similar type to that of Watson and Crick, can be made to take up two special configurations. Optical transforms[46] (see discussion below) and calculated structure factors show reasonable agreement with the observed diffracted intensities from the *A* and *B* structures. To fit the observed to the calculated intensities the sodium atoms have to be specifically localized: these positions can be checked by using salts of potassium and rubidium in place of sodium. Ideally this isomorphous replacement might enable one to solve the structure by a Fourier synthesis, but the diffraction diagrams are not sharp enough in their outer regions to allow this.

Having determined this structure one would go on to see whether the knowledge helped in interpreting the diffraction patterns from more complicated and even living things. This had been attempted for nucleo-protamine,[45] both artificial and natural, which showed a hexagonal packing with the right kind of intensity distributions. Even from whole cells one could identify rings due to some of the DNA structure.

Dr. ROSALIND FRANKLIN (Birkbeck College, London) told of work being conducted by herself and her colleagues at Birkbeck College, London. Early work on tobacco mosaic

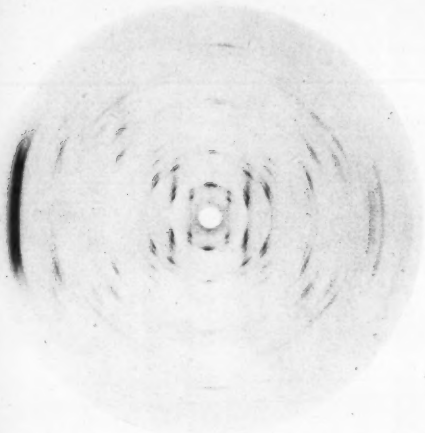

Fig. 7. Fibre diagram of the lithium salt of DNA at 66% relative humidity

virus (TMV), showed that it was a nucleoprotein of particle weight 40–50 million containing 6% ribonucleic acid (RNA). Bernal and Fankuchen[47] prepared orientated gels and obtained fibre photographs; Watson[48] employed helical diffraction theory to show that the virus contained $(3n + 1)$ equivalent sub-units in one repeat of three turns. This was confirmed by Franklin.[49] More recently photographs have been obtained with a focussing crystal monochromator.

A strong intensity modulation on the third layer line could be directly related to a helical groove round the outside of the particle.[50] The groove allowed the particles to interlock on drying, and therefore explained the previous lack of consistency between the observed diameter of single particles and particles in rafts in electron micrographs. The amplitude of the modulation suggested that the ridge and groove resulted from a set of protuberances.

In general, more information came from a comparison of TMV with related substances. Photographs of *U*2 and other strains, and of cucumber virus 4 yielded useful differences. The protein of TMV could be prepared free of RNA.[52] An isomorphous mercury derivative (mercury TMV) with one mercury per sub-unit had been prepared by Fraenkel-Conrat.

On the equator, the phases out to $R = 2 \sin \theta/\lambda = 0{\cdot}1$ Å^{-1} were all real. As the mercury atoms occurred once per sub-unit they were assumed to be in equivalent positions; therefore the contribution on the equator is $J_0(2\pi R r_{Hg})$ (where r_{Hg} is the real space radius). By comparing the logarithmic intensity plots from TMV and HgTMV the nodes of this function were found, giving $r_{Hg} = 57$ Å and hence the signs of the inner equatorial maximum. This was confirmed by amplitude difference plots. A radial density distribution (see Fig. 8) was calculated, which agreed with Caspar's independent work.[53] It was also calculated for some other strains, which all showed the same general features, and for the RNA-free protein. The most notable change in this was the replacement of the 40 Å peak by a hole. This showed, and the layer lines confirmed, the RNA to be deeply imbedded in the protein at a radius of 40 Å.

The number of sub-units in three turns $(3n + 1)$ should be determinable from the character of the $(3n + 1)$th layer line, but imperfections in orientation made this impossible. The mercury, however, gave rise to $J_{3n+1}(2\pi R r_{Hg})$ far out on the

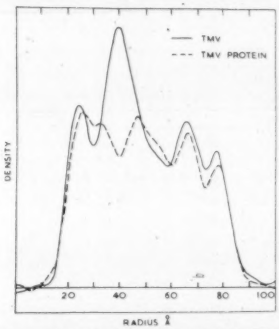

Fig. 8. The radial density distribution in (*a*) TMV (full curve); and (*b*) repolymerized, RNA-free, TMV protein (dotted curve). The curves show the difference between the electron density of the particles and that of water, plotted as a function of radial distance from the particle axis. The strong peak at 40 Å in (*a*) is absent in (*b*) and is therefore attributed to the virus nucleic acid

zero layer line and the observation of this fixed $(3n + 1)$ as 49. This was confirmed by measurements on the layer lines.[54]

The work was at an early stage. It was hoped that it would be possible to determine phases on layer lines by the method of isomorphous replacement, where one was aided by each layer line being a continuous part of the molecular transform.

Dr. F. H. C. CRICK (Cavendish Laboratory, Cambridge) described recent work[55] done in collaboration with Dr. J. D. Watson and Dr. D. L. D. Caspar, on the structure of "spherical" viruses. Electron microscopy has shown that small viruses are, in shape, either rods or approximate spheres. TMV, a typical rod virus, consists of sub-units related to each other by a screw axis, to form a helix. The small spherical viruses are usually of diameter 300 Å, and molecular weight about five or ten million, and like TMV contain RNA. The question arises whether these spherical viruses are also made up of sub-units related by symmetry elements. Early X-ray studies suggested that the spherical viruses might possess some symmetry since in a few cases cubic shaped unit cells were found. Certain types of symmetry can be ruled out—both mirror planes and centres of symmetry, since in biological molecules only one of the optical isomers occurs. This leaves only rotation axes. Apart from the simple rotation groups, the fact that from the sub-units is built a compact shell of protein suggests cubic point groups, and the possible ones are 23, 432 and 532.

The first X-ray diffraction photograph taken by Caspar was of a disordered crystal of tomato bushy stunt virus (BSV), which gave no sharp reflexions but a general impression of the reciprocal lattice. It had two rings of ten spots, indicating a possible five-fold symmetry. Dr. Caspar was later able to

obtain good single crystal precession photographs[56] out to 10 Å, and to show that the crystals were cubic and body-centred, having at each lattice point one virus particle, which therefore also had cubic symmetry. The extra symmetry of a virus particle having 532 symmetry would also be expected to show up in the X-ray photograph as spikes of intensity in the directions of the rotation axes, since, for example, on projecting atoms on to the five-fold axis, each atom occurs five times, and the diffraction in this direction would be, on the average, five times as strong as elsewhere. Caspar found the regions of strong intensity on the outer parts of his photographs to be in the directions of spikes expected from a virus particle having, at least in part, 532 symmetry (Fig. 9).

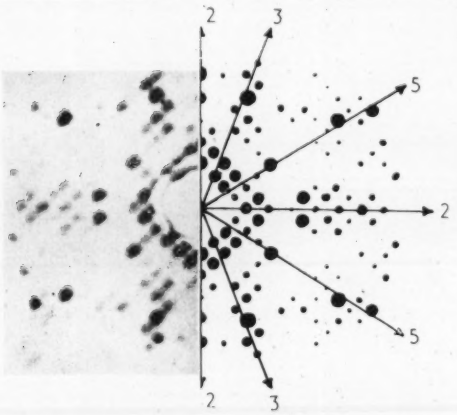

[Reproduced by permission of the Editors of *Nature*]

Fig. 9. Precession photograph by Caspar of the basal plane of the reciprocal lattice, normal to the cube edge of bushy stunt virus. On the right is a weighted reciprocal lattice net showing the orientation of the two-, three- and five-fold axes which lie in this plane

The cytoplasm of living cells contains many fairly uniform particles, similar to the spherical viruses in size, shape and amount of nucleic acid, and these are believed to be sites of protein synthesis. It will be interesting to see if these also can be crystallized and whether they have cubic symmetry. There is also the problem of putting a long fibrous molecule, as RNA is believed to be, into a particle and giving it cubic symmetry (although it may be a pseudo-symmetry) and the study of the arrangement of the RNA in spherical viruses, especially perhaps in turnip yellow mosaic virus (which exists in two forms, with and without nucleic acid) may help work on protein synthesis.

Dr. A. KLUG (Birkbeck College, London) then described some recent X-ray work on turnip yellow mosaic virus (TYMV). This contains 40% RNA which contributes a great deal to the X-ray scattering since it has higher electron density than the protein. The first X-ray work was done by Bernal and Carlisle who from powder photographs,[57] and later from single crystal "still" photographs,[58] determined that the unit cell was cubic and of side 706 Å. On account of the absence of the (222) reflexion, they suggested that there were eight virus particles in the unit cell, arranged as the carbon atoms in diamond.

Recently, low angle precession photographs have established that the crystals have the space-group $F4_13$, and that the virus particles have cubic symmetry (Fig. 10). The photo-

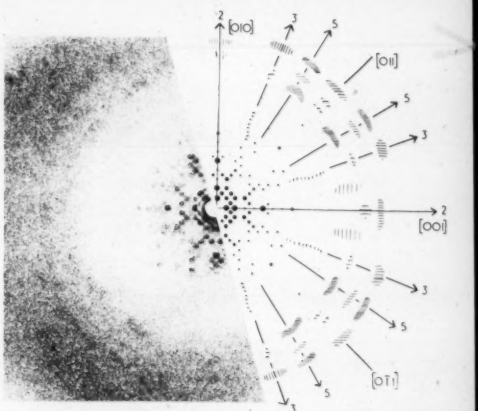

Fig. 10. Precession photograph of the basal reciprocal lattice plane, and parts of higher layer planes, normal to the cube edge of turnip yellow mosaic virus. On the right is a schematic impression of the reciprocal lattice net showing the orientation of the two-, three- and five-fold axes which lie in the basal plane. The shaded areas indicate the regions of strong intensity of the higher layer planes

graphs also show spikes of high intensity in non-crystallographic directions. This effect is as strong as that found by Caspar[56] in BSV, although in TYMV they do not stand out so clearly since the virus particle occurs in two orientations in the unit cell, and the number of spikes is doubled. The positions of the spikes agree with those expected from a virus particle having 532 symmetry. The first, low angle, precession photographs showed no reflexions with indices h, k, l, all odd, although a stronger exposure showed a few weak reflexions with odd indices; "still" photographs showed that they appear at higher angles. Reflexions of type $h + k + l = (4n + 2)$ are absent at least to spacings of 8 Å. The weakness of all non-$4n$ reflexions indicates a pseudo-body-centred cell of half the size of the true unit cell. This means that the true unit cell contains sixteen virus particles with their centres on a body-centred cubic lattice, but to preserve the true, large cell, alternate particles along a cube edge are turned through ninety degrees. This number of particles in a unit cell was confirmed from measurements of the ultra-violet absorption per unit path length through a single crystal, in collaboration with Dr. P. M. B. Walker of King's College, London.

To check the arrangement proposed above, optical transform work was done, with the virus particle represented by a 532 arrangement of points (the snub dodecahedron). With eight particles in a diamond type unit cell, reflexions of the type $h + k + l = (4n + 2)$ are absent at low angles, as is to be expected since the snub dodecahedron has fifteen two-fold

axes and hence a strong centrosymmetric tendency; reflexions with odd indices are however quite strong. With sixteen particles per unit cell, $(4n + 2)$ reflexions are strictly absent and odd reflexions only appear at high angles, as observed.

Virus protein particles free from nucleic acid are found accompanying the virus in nature.[59] Only small crystals of this form have been obtained, and these have been studied by powder photographs. The very low angle scattering agrees with the results of Schmidt and others[60] that the protein is in the form of a spherical shell as originally suggested by Markham.[61] The intensity at somewhat higher angles indicates that this shell is made up of discrete protein sub-units. This was illustrated formally by the calculation of the radial distribution function, which was found to be similar to that of sixty spheres arranged at the vertices of a snub dodecahedron.

In the discussion on these papers, Mr. C. W. HOOPER (King's College, London) described the photographic preparation of masks used in obtaining optical transforms. Kodalith stripping film could be used down to hole diameters of 70 to 100 μ.[46] Intensities measured on the optical pattern from a trial structure of DNA "*B*" agreed well with the calculated transform in the central region (Fig. 11) where

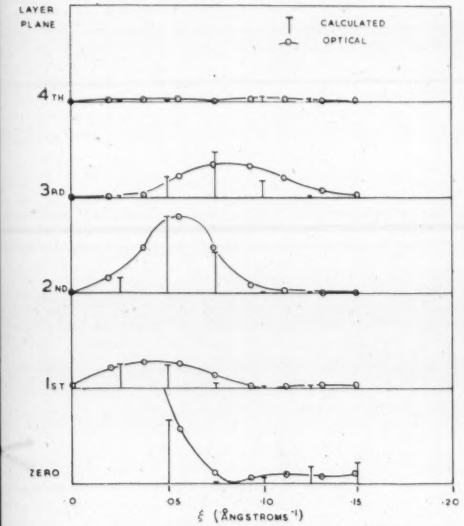

Fig. 11. A comparison of the optical and calculated structure factors for DNA trial structure BB_{10}

the number of projections used was sufficient to represent the cylindrically averaged structure.[62] Accurate Patterson maps had been obtained from masks representing weighted reciprocal lattice planes.

Summing up, Prof. Bernal showed how the new techniques dealt with, electronic computation, model building, phase determination by heavy element substitution, were all necessary to provide the precise solutions of complex structures which alone would give information on configuration beyond the reach of organic chemistry. So far, the model for this was the structure of vitamin B_{12} which had been discussed by Mrs. Hodgkin. The work reported on protein structures showed the necessity to push further the methods of multiple substitution and three dimensional analysis developed by Perutz and his school.

In view of the difficulties of determining the structure of protein molecules of weight of some tens of thousands, it was gratifying that such remarkable successes had been reached for structures of nucleic acids and virus nucleoproteins whose molecular weights run into tens of millions. This appeared to be due to the internal regularities of these larger structure compared with the highly heterogeneous peptide sequence of the proteins. The power of X-ray analysis in all these cases had been greatly increased by the extension of diffraction theory to cover non-crystallographic groups including spirals and higher point symmetries.

This could not, however, have produced results if the structures studied had not possessed a sequence of regularities on an ascending scale. Organic nature was far from a fortuitous concourse of atoms but rather an ordered sequence of aggregates, each one being constructed from units of the one immediately below. There were certain sticking points which rounded off a structure such as a protein at a molecular weight of some five to twenty thousands. Larger protein molecules such as haemoglobin seemed to be made out of agglomerations of these proto-proteins. Agglomerations of these in turn built up the virus protein in spiral or spherical cage-like form. At higher levels still, heterogeneous aggregation of protein with nucleic acids and lipids give regular structures coming well into the electron microscope range. As to the reasons for these definite discontinuities in the process of building up of biological micro-structures from their atoms, they were probably complex, partly depending on the enzymatic polymerization process by which the standard macromolecules were built up. Another part of the explanation, especially for the larger structures, might lie in pure geometry, as the Greeks had intuitively seen in creating their atomic theory. Certain regular arrangements fitted well and had consequently low energy. Thus it was easy to pack twelve equal spheres round another but difficult to pack eleven or thirteen. When any particular arrangement was completed independent units tended to form and in turn to agglomerate into large regular structures. The resulting regularities on a scale from several hundred to fifty Å units gave rise to strong X-ray reflexions. In fact the guiding idea of this extremely interesting, if somewhat sophisticated, meeting of the X-ray Analysis Group had been the possibility of analysing all structures which possessed regularity on any scale.

The evening discourse, given by Prof. Dame KATHLEEN LONSDALE (University College, London), entitled "Problems of simple structures," which was published in the Institute's *Bulletin* in July 1957, and which is not reported here in detail, was much appreciated by Members of the Conference.

J. FINCH
D. W. GREEN
K. C. HOLMES
A. C. T. NORTH

REFERENCES

(1) AHMED, F. R., and CRUICKSHANK, D. W. J. *Acta Cryst.*, **6**, p. 765 (1953).

(2) BRINK, C., HODGKIN, D. C., LINDSEY, J., PICKWORTH, J., ROBERTSON, J. H., and WHITE, J. G. *Nature* [*London*], **174**, p. 1169 (1954).

(3) SPARKS, R. A., PROSEN, R. J., KRUSE, F. H., and TRUEBLOOD, K. N. *Acta Cryst.*, **9**, p. 350 (1956).

(4) MARCH, N. H. *Acta Cryst.*, **5**, p. 187 (1952).

(5) COCHRAN, W. *Acta Cryst.*, **9**, p. 924 (1956).

(6) CRUICKSHANK, D. W. J. *Acta Cryst.*, **9**, p. 915 (1956).

(7) HODGKIN, D. C. *Bull. Soc. franc. Mineral Crist.*, **78**, p. 106 (1955).

(8) HODGKIN, D. C., PICKWORTH, J., ROBERTSON, J. H., TRUEBLOOD, K. N., and WHITE, J. G. *Nature* [*London*], **176**, p. 325 (1955).

(9) HODGKIN, D. C., KAMPER, J., MACKAY, M., PICKWORTH, J., TRUEBLOOD, K. N., and WHITE, J. G. *Nature* [*London*], **178**, p. 64 (1956).

(10) BRAGG, SIR LAWRENCE, and PERUTZ, M. F. *Proc. Roy. Soc. A*, **213**, p. 425 (1952).

(11) BRAGG, SIR LAWRENCE, HOWELLS, E. R., and PERUTZ, M. F. *Proc. Roy. Soc. A*, **222**, p. 33 (1954).

(12) PERUTZ., M. F. *Proc. Roy. Soc. A*, **225**, p. 264 (1954).

(13) GREEN, D. W., INGRAM, V. M., and PERUTZ, M. F. *Proc. Roy. Soc. A*, **225**, p. 287 (1954).

(14) HOWELLS, E. R., and PERUTZ, M. F. *Proc. Roy. Soc. A*, **225**, p. 308 (1954).

(15) BRAGG, SIR LAWRENCE, and PERUTZ, M. F. *Proc. Roy. Soc. A*, **225**, p. 315 (1954).

(16) INGRAM., V. M. *Biochem. J.*, **59**, p. 653 (1955).

(17) CRICK, F. H. C. *Ph.D. Thesis* (Cambridge University, 1953).

(18) ASTBURY, W. T. *Fundamentals of Fibre Structure*, p. 134 (London: Oxford University Press, 1933).

(19) BOWES, J. H., and KENTEN, R. H. *Biochem. J.*, **45**, p. 281 (1949).

(20) SCHMITT, F. O., GROSS, J., and HIGHBERGER, J. H. *Symp. Soc. Exp. Biol.*, **9**, 148 (1955).

(21) BOEDTKER, H., and DOTY, P. *J. Amer. Chem. Soc.*, **78**, p. 4267 (1955).

(22) COWAN, P. M., NORTH, A. C. T., and RANDALL, J. T. *The Nature and Structure of Collagen*, p. 241 (London: Butterworth's Scientific Publications, 1953).
COWAN, P. M., NORTH, A. C. T., and RANDALL, J. T. *Symp. Soc. Exp. Biol.*, **9**, p. 115 (1955).

(23) COHEN, C., and BEAR, R. S. *J. Amer. Chem. Soc.*, **75**, p. 2783 (1953).
BEAR, R. S. *Symp. Soc. Exp. Biol.*, **9**, p. 97 (1955).

(24) SCHROEDER, W. A., KAY, L. M., LEGETTE, J., HONNEN, L., and GREEN, F. C. *J. Amer. Chem. Soc.*, **76**, p. 3556 (1954).

(25) KRONER, T. D., TABROFF, W., and MCGARR, J. J. *J. Amer. Chem. Soc.*, **77**, p. 3356 (1955).

(26) BERGER, A., KURTZ, J., and KATCHALSKI, E. *J. Amer. Chem. Soc.*, **76**, p. 5552 (1954).

(27) COWAN, P. M., and MCGAVIN, S. *Nature* [*London*], **176**, p. 501 (1955).

(28) CRICK, F. H. C., and RICH, A. *Nature* [*London*], **176**, p. 780 (1955).

(29) RAMACHANDRAN, G. N., and KARTHA, G. *Nature* [*London*], **176**, p. 593 (1955).

(30) RICH, A., and CRICK, F. H. C. *Nature* [*London*], **176**, p. 915 (1955).

(31) COWAN, P. M., NORTH, A. C. T., and MCGAVIN, S. *Nature* [*London*], **176**, p. 1062 (1955).

(32) RAMACHANDRAN, G. N. *Nature* [*London*], **177**, p. 710 (1956).

(33) BEAR, R. S. *J. Biophys. Biochem. Cytology*, **2**, p. 363 (1956).

(34) NORTH, A. C. T., COWAN, P. M., and RANDALL, J. T. *Nature* [*London*], **174**, p. 1142 (1954).

(35) RAMACHANDRAN, G. N., and SASISEKHARAN, V. *Arch. Biochem. Biophys.*, **63**, p. 255 (1956).

(36) WHITTAKER, E. J. W. *Acta Cryst.*, **8**, p. 571 (1955).

(37) PAULING, L., and COREY, R. B. *Proc. Nat. Acad. Sci. U.S.A.*, **37**, p. 241, p. 729 (1951).

(38) HAPPEY, F. *Nature* [*London*], **179**, p. 194 (1957).

(39) BAMFORD, C. H., HANBY, W. E., and HAPPEY, F. *Proc. Roy. Soc. A*, **205**, p. 30 (1951).

(40) ASTBURY, W. T., and WOODS, H. J. *Phil. Trans A*, **232**, p. 333 (1933).

(41) WATSON, J. D., and CRICK, F. H. C. *Nature* [*London*], **171**, p. 964 (1953).

(42) WATSON, J. D., and CRICK, F. H. C. *Nature* [*London*], **171**, p. 737 (1953).

(43) WILKINS, M. H. F., STOKES, A. R., and WILSON, H. R. *Nature* [*London*], **171**, p. 739 (1953).

(44) FRANKLIN, R. E., and GOSLING, R. G. *Nature* [*London*], **171**, p. 740 (1953).

(45) FEUGHELMAN, M., LANGRIDGE, R., SEEDS, W. E., STOKES, A. R., WILSON, H. R., HOOPER, C. W., WILKINS, M. H. F., BARCLAY, R. K., and HAMILTON, L. D. *Nature* [*London*], **175**, p. 834 (1955).

(46) HOOPER, C. W., SEEDS, W. E., and STOKES, A. R. *Nature* [*London*], **175**, p. 679 (1955).

(47) BERNAL, J. D., and FANKUCHEN, I. *J. Chem. Physiol.*, **25**, p. 111 (1941).

(48) WATSON, J. D. *Biochim. Biophys. Acta*, **13**, p. 10 (1954).

(49) FRANKLIN, R. E. *Nature* [*London*], **175**, p. 379 (1955).

(50) FRANKLIN, R. E., and KLUG, A. *Biochim. Biophys. Acta*, **19**, p. 403 (1956).

(51) SCHRAMM, G. *Z. Naturforsch.*, **26**, p. 112, p. 249 (1947).

(52) FRANKLIN, R. E. *Nature* [*London*], **177**, p. 929 (1956).

(53) CASPAR, D. L. D. *Thesis* (*Yale University*). *Nature* [*London*], **177**, p. 928 (1956).

(54) FRANKLIN, R. E., KLUG, A., and HOLMES, K. C. *Ciba Foundation Symposium on the Nature of Viruses*, p. 39 (1956).

(55) CRICK, F. H. C., and WATSON, J. D. *Nature* [*London*], **177**, p. 473 (1956).

(56) CASPAR, D. L. D. *Nature* [*London*], **177**, p. 476 (1956).

(57) BERNAL, J. D., and CARLISLE, C. H. *Nature* [*London*], **162**, p. 139 (1948).

(58) BERNAL, J. D., and CARLISLE, C. H. *Disc. Faraday Soc.*, **11**, p. 227 (1951).

(59) MARKHAM, R., and SMITH, K. M. *Parasitology*, **39**, p. 330 (1949).

(60) SCHMIDT, P., KAESBERG, P., and BEEMAN, W. W. *Biochim. Biophys. Acta*, **14**, p. 1 (1954).

(61) MARKHAM, R. *Disc. Faraday Soc.*, **11**, p. 221 (1951).

(62) STOKES, A. R. *Acta Cryst.*, **8**, p. 27 (1955).

Measurement of elasticity and anelasticity of small disks by an inductor method

By G. BRADFIELD, B.Sc., and F. A. LEVI, Dott. Fisica,* National Physical Laboratory, Teddington, Middlesex

[*Paper first received* 10 *July, and in final form* 2 *September*, 1957]

An instrument is described operating on the inductor principle to set a small disk into radial vibration so that one of its elastic constants can be determined from its frequencies of resonance. The method of testing also permits the internal friction to be measured as the ratio Q_m of the real to the imaginary component of the elastic compliance. The accuracy of determination of the resonance frequency is to better than 1 part in 50000 and the determination of the internal friction ratio to better than 1 part in 50 in a typical case when, for example, the above ratio Q_m is about 3000. The elastic constant directly derived is the "sheet" modulus $E/(1-\sigma^2)$ where σ is Poisson's ratio and E is Young's modulus.

1. INTRODUCTION

This investigation forms an item of that part of the programme of research at the National Physical Laboratory which is devoted to the precise measurement of the elasticity and anelasticity of small specimens of solids in the form of plate or strip. This present item is confined to testing specimens having elastic isotropy in the plane of the plate or strip. The method was developed in 1950 and has already been mentioned briefly in a lecture given in 1952 recorded in a memorandum from these Laboratories,[1] and again briefly by the senior author in 1954[2] in the course of a general discussion of transducers. The dimensions of the specimens measured by this method are 2 cm in diameter and the thickness may vary from about 0·07 to 0·8 mm. The method devised was especially suitable for an investigation by one of the authors (F.A.L.) into the properties of electrolytically deposited copper. Such deposits are generally elastically isotropic in the plane of the sheet and the method devised, being an inductor method of circular symmetry, was especially suitable for testing disks made of these materials.

The method yields the "sheet" modulus $E/(1-\sigma^2)$, probably the most important elastic constant for sheet metals used in structures; Young's modulus E can be derived when Poisson's ratio σ is known.

2. DESCRIPTION OF PRINCIPLE AND CONSTRUCTION OF THE DEVICE

To avoid the setting up of bending and other modes of vibration in the disk, the tangential forces in the disk are developed in such a way that they are circularly symmetrical and also that they are equal on both sides of the disk. Examination of Figs. 1 and 2 with the help of the following description will show how this is accomplished. The large C-shaped permanent magnet in Fig. 1 established normal to the disk under test a flux of density 3400 G. This disk, which is 2 cm in diameter, rests on a central support consisting of three sapphire jewels, with ends of radius 25 μ set at the corners of an 0·65 mm equilateral triangle. It lies symmetrically between and concentric with two coils (each about 110 turns No. 42 double silk covered) which serve both to enable concentric circulating currents to be induced in the disk and, in turn, to have induced in them voltages due to the radial vibration of the disk in the magnetic field; these vibrations are, of course, caused by the interaction force of the magnetic field and the original induced currents. These voltages supplement those normally caused by the primary current flowing through the resistive and reactive components of the coils (which are in series) and cause an impedance

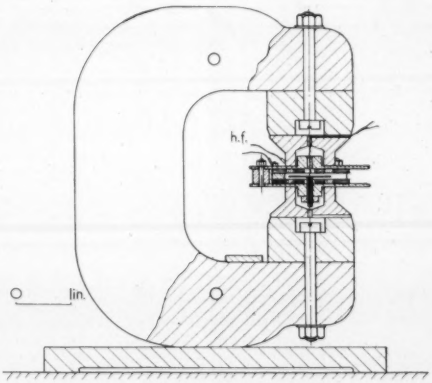

Fig. 1. Assembly of inductor-driven oscillating disk for damping measurement

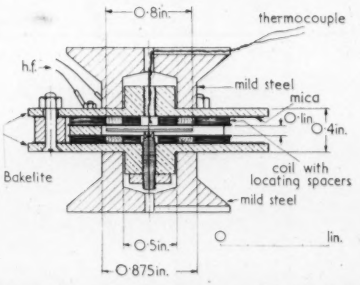

Fig. 2. Inductor-driven oscillating disk for damping measurements

* Now at University of Peruggia, Italy.

change which alters very rapidly as the frequency of excitation moves through the mechanical resonance frequency of the disk. Such impedance changes are readily observed by connecting the coils in a bridge circuit with a suitable out-of-balance indicator and varying the input frequency slowly and steadily. The approximate equivalent network of the device shown in Fig. 3 is valid over the frequency range

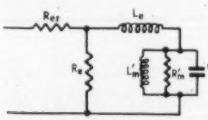

Fig. 3. Simplified equivalent circuit of disk inductor device

$R_{es} = 27{\cdot}1\ \Omega$ $R_e = 3760\ \Omega$ $R'_m = 33{\cdot}4\ \Omega$
$L_e = 392\ \mu H$ $L'_m = 0{\cdot}0145\ \mu H$ $C'_m = 108\ \mu F$

100 to 160 kc/s and, with suitable values of L'_m, C'_m and R'_m for a copper disk, corresponds with the Argand diagram of Fig. 4 which is based on an actual test using such a disk.

The elements L'_m, C'_m and R'_m of the network correspond to the mechanical resonance of the disk and are transformed from their mechanical counterparts of effective mass, compliance and resistance of the disk by the electro-mechanical transducer action of the inductor device. The theories concerning the latter have been summarized by Hueter and Bolt,[3] and Evison[4] has discussed the general case of driving a complex mechanical load.

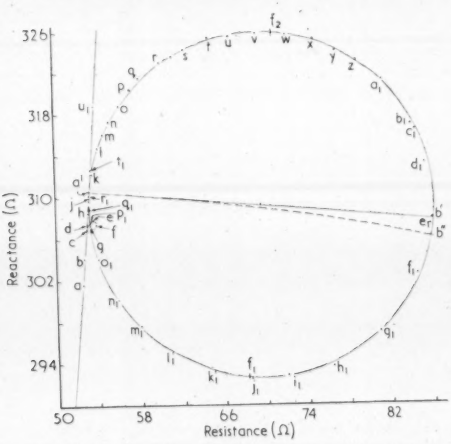

Fig. 4. Argand diagram for copper disk SVI. (Electrolytically deposited without ultrasonics.) The clamped impedance line is estimated to pass through a'. b'' is true resonance frequency of the disk

Frequency (c/s)	*Frequency* (c/s)	*Frequency* (c/s)
$a = 124001$	$q = 127449$	$g_1 = 127510$
$b = 125001$	$r = 127460$	$h_1 = 127516$
$c = 126001$	$s = 127466$	$i_1 = 127521$
$d = 126201$	$t = 127472$	$j_1 = 127526$
$e = 126294$	$u = 127476$	$k_1 = 127531$
$f = 126313$	$v = 127480$	$l_1 = 127542$
$g = 126354$	$w = 127483$	$m_1 = 127554$
$h = 126684$	$x = 127486$	$n_1 = 127574$
$i = 126935$	$y = 127488$	$o_1 = 127623$
$j = 127001$	$z = 127490$	$p_1 = 127752$
$k = 127265$	$a_1 = 127492$	$q_1 = 127908$
$l = 127358$	$b_1 = 127495$	$r_1 = 128087$
$m = 127390$	$c_1 = 127496$	$s_1 = 128250$
$n = 127409$	$d_1 = 127498$	$t_1 = 128920$
$o = 127428$	$e_1 = 127502$	$u_1 = 131281$
$p = 127442$	$f_1 = 127505$	

The acoustic load in the authors' case is that presented to a periodic radial force which acts at the periphery of the disk. It appears like a series combination of mass M, compliance S and resistance R_m and, in such a form, is inverted by the gyrator characteristics of the moving conductor transducer (to which the inductor device approximates) to yield the parallel combination of the elements L'_m, C'_m and R'_m in Fig. 3. When the loss in the vibrating disk is small, the mass reactance $j2\pi fM$ (where f is the frequency of excitation) is great compared with R_m, and R'_m in the inversion is great compared with $1/2\pi fC'_m$ so that the resonance frequency f_m of the disk is very closely given by $f_m = 1/2\pi(L'_mC'_m)^{\frac{1}{2}}$.

As has been discussed by Love[5] this resonance frequency f for a thin disk excited into radial resonance is given as the solution of the equation:

$$ka\,J_0(ka)/J_1(ka) = 1 - \sigma$$

$J_0(ka)$ and $J_1(ka)$ are zero and first order cylindrical Bessel functions of argument ka, where a is the radius of the disk, k is $2\pi f\,[\rho(1-\sigma^2)/E]^{\frac{1}{2}}$, ρ is the density of the disk, σ is the Poisson's ratio of the disk, and E is the Young's modulus of the disk.

Roots of this equation are given in Table 1 for various values of Poisson's ratio.

Table 1. *Roots of radial resonance equation for a thin disk*

	$\sigma =$	0·25	0·275	0·30	0·325	0·35	0·375
ka (first root)	=	2·020	2·037	2·053	2·070	2·084	2·098

The roots can be obtained to an accuracy of better than 1 in 10^6 using, for example, 11 or 15 place tables of Bessel functions.[6]

If typical figures are inserted for a copper disk: $a = 1{\cdot}036$ cm, $\rho = 8{\cdot}934$ g cm^{-2}, $\sigma = 0{\cdot}342$ and $E = 1{\cdot}298 \times 10^{-12}$ dyn cm^{-2}, the calculated resonance frequency is 130 kc/s and values quite close to this were found for such disks.

3. Additional Details of Operation of Disk Resonance Inductor Device

3.1 *Triple jewel support.* This is one of the most important features contributing to the successful operation of the device, for it was essential to find a method of support which would define the plane and centre of the disk accurately, yet would not contribute appreciably to the mechanical losses of the disk during vibration; the polished ends of the jewels assisted to reduce the latter but, in any case, the point of support was extremely close to the velocity node at the centre so that very little tangential movement occurred. The centring of the disk on the support was accomplished with the aid of screws which were withdrawn during test.

3.2 *Temperature control.* In order to realize the full accuracy of this instrument, the temperature needed to be maintained to an accuracy of $\pm 1/50^\circ$ C. This was accomplished by having a bell jar, thermally lagged on the outside, over the device and providing in it both a copper spiral to permit cooling water to be circulated and an electrical heating element to raise the temperature by as much as 30 or 40° C.

The bell jar could be evacuated but, in any case, the construction was such that the disk was well shielded from draughts; its temperature was read from several thermocouples inserted in the instrument in its immediate vicinity.

3.3 *Operation in a vacuum.* For an instrument of this precision it is desirable to eliminate the effect of the loading of the air on the frequency of vibration and on the damping of the vibrations. The wavelength in air at 130 kc/s is only 2½ mm so that the periphery of the disk is many wavelengths long and, at a thickness of 0·8 mm, the edge is radiating appreciably. The loading due to the air, because of the thinness of the disk, will be slightly reactive. The calculated ratio Q_m of a loss-free disk in these circumstances would be rather over $\pi/2$ × ratio of characteristic impedances of copper and of air, that is $(\pi/2) \times [(480\,000 \times 8{\cdot}9)/40] \simeq 170\,000$, so that the air damping may cause an error of about 2% where Q_m (as for a copper disk) is about 3000 or 10% where Q_m (as for an aluminium disk) is about 20 000.

The provision of a bell jar and vacuum tight joints through the base plate enabled these errors to be eliminated by operating in a vacuum.

3.4 *Anti-vibration mounting.* It was essential, in order to obtain the desired accuracy in measurement, to keep the position of the specimen unchanged in relation to the jewel support and the coils. This was achieved by mounting the device on a heavy steel block which itself rested on a heavy steel top supported by a slender tubular steel pillar. This system constituted a mechanical low-pass filter which prevented vibrations of the floor disturbing the measurements.

3.5 *The bridge-type vibration indicator.* It is possible to derive the mechanical resonance frequency of the disk rigorously from a detailed Argand diagram or by an approximation method, the latter involving much less labour. Discussing the rigorous method first, an equal ratio-arm bridge, the arms being 10 000 Ω, that is, over ten times the impedance of the coil system, has a calibrated variable inductance in series with a variable resistance in the arm balancing the coil impedance of the instrument. The impedance is therefore accurately determined at a series of frequencies and plotted as in Fig. 4.

Now this Argand diagram can be considered as the locus of the sum of two vectors represented by the clamped impedance circle (of diameter R_e) and the motional impedance circle, so that the true resonance frequency lies at the intersection of the latter with an arc drawn with centre R_{es}, O (see Fig. 3), through the point where the above two circles touch a'. This intersection occurs at b'' in Fig. 4 and interpolation gives the resonance frequency as 127 502·7.

In the approximation method we preferably constitute the balancing arm so as to have an impedance locus corresponding with the clamped impedance circle and use the out-of-balance voltage to indicate the vector of the motional impedance circle. The former is achieved by the use of an additional shunt resistive element for the balancing arm, and the latter is achieved by the use of high resistances for the ratio arms of the bridge so that the currents through the balancing arm on through the instrument impedance are substantially unaffected by the variations in these relatively low impedance elements. Then at the maximum value of the out-of-balance voltage, the frequency f_m' is very close to the true value of f_m. (A further correction is, however, possible as will be seen later.) Now vary the values of the reactance and resistance given by the bridge for a balance at frequencies $f_m' \pm 1$ kc/s, $f_m' \pm 2$ kc/s and record the results. By linearly interpolating between the first two pairs and between the second two pairs and averaging, then adjusting resistance and reactance on the bridge to these values, a more accurate value of f_m can be obtained at the maximum vector of the out-of-balance voltage. Leaving the bridge adjustments untouched, the frequency is varied so that the vector is $1/\sqrt{2}$ of this maximum vector and the frequencies f_1, f_2 at which this occurs are recorded. The value of Q_m is $(f_1 + f_2)/[2(f_1 - f_2)]$.

The correction $b'b''$ in Fig. 4 is only 1 part in 120 000 and as this is substantially independent of the quality factor Q, this proportion can be added in all cases of copper disks of the same conductivity.

4. MEASUREMENTS MADE ON THE EQUIPMENT AND DISCUSSION OF ERRORS

4.1 *Evaluation of the circuit elements of the equivalent network of Fig.* 3. The value of R_{es} is determined with the coils out of the magnet system by extrapolating the arc of the Argand diagram with the disk in position, but at well below resonance, for there the shape is determined almost entirely by R_{es} and L_e. The disk approximately halves the impedance of the coils. When the coils are assembled in the magnet system, loss occurs due to eddy currents in the pole pieces and this is included in resistance R_e. A slight modification to L_e also occurs and these changes are determined from the Argand diagram, again at low frequencies, but with the coils assembled and the disk in position. Some of the measurements made are given in Tables 2 and 3.

Table 2. *Impedance of coils (away from magnet and pole pieces; disk not in position)*

Frequency (kc/s)	*R resistance (series)*	*X reactance (series)*	$X\ 2\pi f$ $(10^{-6}H)$
100	32·5	558	888
120	35·8	693	918
125	36·8	728	927
127·5	37·4	746	932
130	38·0	765	937
150	92·4	923	979

Table 3. *Impedance of coils (assembled in magnet and pole pieces; disk not in position)*

Frequency (kc/s)	*R resistance (series)*	*X reactance (series)*	$X\ 2\pi f$ $(10^{-6}H)$
100	92·9	501	797
120	108·5	608	805
125	112·1	635	809
127·5	114·1	649	810
130	116·4	665	815
150	133·3	785	834

4.2 *Measurements on a copper disk.* The Argand diagram of Fig. 4 applied to a copper disk electrolytically deposited without ultrasonics, 0·33 mm thick and 2·030 cm in diameter at a temperature of 20·0° C. In accordance with the discussion above, the resonance frequency f_m of this disk was at point b'' on the figure, i.e. at 127 502·7 c/s. Assuming Poisson's ratio to be 0·342, by the use of Table 1, ka is obtained as 2·074. Since $a = 1{\cdot}015$ cm and f_m is 127 502·7, $[E/\rho(1 - \sigma^2)]^{\frac{1}{2}}$ is 391 970 cm/s and, using the above value of Poisson's ratio and taking a value for the density of 8·934 gm cm^{-3}, the value of E, Young's modulus, is $1{\cdot}212 \times 10^{12}$ dyn cm^{-2}.

It will be quite close to the truth if the mechanical quality factor Q_m is derived from the values of f_1, f_2 (see Section 3.5) on the orthogonal diameter to $a'b'$. These two frequencies

are 127 525·8 and 127 481·6 respectively yielding a value of Q_m of 127 502·7/44·2 = 2880.

4.3 *Accuracy of determination of "sheet" modulus $E/(1-\sigma^2)$ and of the mechanical quality factor Q_m.* The assumption will be made in this section that the disk is thin and isotropic and that its density, temperature and Poisson's ratio are known accurately. Each of the frequency points on the Argand diagram can be ascertained to an accuracy of $\pm 0{\cdot}3$ cycle by averaging ten or more readings, since the frequency counter used in this work was capable of reading to an accuracy of 1 c/s. The values of resistance and reactance could be accurate to $\pm 0{\cdot}2\,\Omega$ and this error did not limit the accuracy obtainable. On the above assumptions, the accuracy of deducing the frequency of resonance would be about 1 part in 200 000 and hence, if the radius of the disk be accurately known, the "sheet" modulus $E/(1-\sigma^2)$ can be calculated to 1 part in 10^5.

Assuming an error of 0·3 cycle in determination of the orthogonal points for determination of the quality factor Q_m, with a frequency difference of 44 cycles as above, an error of about 2% is to be expected.

4.4 *Measurements on an aluminium disk.* A measurement was made on an aluminium disk of diameter 2 cm and thickness 0·75 mm. The value obtained for the mechanical quality factor Q_m was 20 000 in air. As discussed in Section 3.3, about 10% of the loss so measured must have been due to the damping of the air. It seems doubtful whether the friction at the supports would be responsible for more than 1 or 2% but clearly, if disks of such low decrement are under investigation, an evaluation of the support loss would be necessary.

4.5 *Measurements on a very thin silver disk.* In order to explore the capabilities of the instrument a flat disk of silver foil only 0·075 mm thick and 2 cm diameter was tested in the equipment. A good clear resonance was obtained from which the mechanical quality factor Q_m could be derived.

4.6 *Discussion of results and conclusion.* For a copper disk the calculated errors are 1 in 100 000 for Young's modulus and 2% for the mechanical quality factor Q. The real accuracy will depend on the possibility of obtaining specimens perfectly homogeneous in properties (see Sections 5 and 6) and on systematic errors such as that for the effect of the supports; the latter is thought to be very small, but could be evaluated approximately by replacing the existing triple jewel support by one with a wider separation of the jewels. The systematic errors arising from air damping can be, if necessary, evaluated by testing in air and in a vacuum. The estimate in Section 3.3 is probably of the right order of magnitude.

5. A NOTE ON THE PREPARATION AND CUTTING OF THE DISK SPECIMENS

It should be recognized that great care is necessary when cutting materials like copper or considerable errors will result in the mechanical quality factor Q_m. If the investigation concerns texture, thorough annealing is often not permissible because of the great changes of texture which this may cause.(7) As an example, a disk cut with some care had $Q_m = 2000$ but the normal annealing processes which proceed on copper even at room temperatures, permitted the strains to be reduced in six months storage so that the factor Q_m rose to 3000. [Since this work was done, a method of cutting the discs by a spark erosion process has been devised by one of the authors (G.B.).]

6. A NOTE ON THE EFFECT OF ANISOTROPY OF THE DISK

Owing to the very great anisotropy of single copper crystals (their Young's modulus can vary from $6{\cdot}7 \times 10^{11}$ to $19{\cdot}0 \times 10^{11}$ dyn cm^{-2} according to direction of cut(8)), a small departure from a random texture can cause serious elastic anisotropy. Although the instrument described will still yield clear, sharp resonances in the presence of considerable anisotropy in the plane of the disk so that the quality factor Q_m seems meaningful, the elastic constant then derived is not. However, for elastic anisotropy with circular symmetry about the normal to the disk, the instrument will yield useful information concerning the elasticity.

7. THE EFFECT OF DEFECTS IN A DISK

In Fig. 4, a loop about thirty times smaller than the main loop is seen. Experience seems to indicate that the presence of a small hole or defect in the disk is accompanied by a subsidiary loop of the type illustrated at *efg*; such a defect was visible in the specimen under test.

ACKNOWLEDGEMENTS

This work was carried out as part of the research programme of the National Physical Laboratory and is published by permission of the Director. One of the authors (F.A.L.) acknowledges the help of the British Council who provided a grant during most of the duration of the work.

REFERENCES

(1) BRADFIELD, G. *N.P.L. Memo. No. PHYS/U8.* (Lecture given at Elasticity Symposium at the National Physical Laboratory, 20 March, 1952.)
(2) BRADFIELD, G. *Acustica*, **4** (1), pp. 171–181 (1954).
(3) HUETER, T. F., and BOLT, R. H. *Sonics.* 1st Ed., pp. 168, 218 (London: Chapman and Hall Ltd., 1955).
(4) EVISON, F. F. *Proc. Phys. Soc.* [*London*] *B*, **64**, pp. 311–22 (1951).
(5) LOVE, A. E. H. *A Treatise on the Mathematical Theory of Elasticity*, p. 498 (Cambridge: University Press, 1927. Reprinted New York: Dover Publications, 1944).
(6) CAMBI, E. 11 *and* 15 *Place Tables of Bessel Functions of the First Kind to all Significant Orders* (New York: Dover Publications, 1948).
(7) BRADFIELD, G., and PURSEY, H. *Phil. Mag.*, **44**, p. 437 (1953).
(8) BARRETT, C. S. *Structure of Metals.* 2nd Ed., p. 533 (London: McGraw-Hill Publishing Co. Ltd., 1952).

The use of polytetrafluoroethylene as a lubricant

By E. Kay, B.Sc., A.Inst.P., and E. D. Tingle, Ph.D.* Royal Aircraft Establishment, Farnborough, Hants

[*Paper received* 16 *January*, 1957]

The use of the polymer polytetrafluoroethylene (P.T.F.E.) in bulk form as a bearing is limited by its low strength and poor thermal conductivity. Experiments are described in which these difficulties are overcome by the deposition of thin films of P.T.F.E. on to metal substrates.

Frictional tests under a variety of conditions show that tenacious films of low frictional coefficient and high load-carrying capacity can be prepared. These properties are considerably enhanced by using a surface phosphating treatment prior to application of the P.T.F.E.

Earlier work on the comparatively new polymer polytetrafluoroethylene (P.T.F.E.) demonstrated its inherently good frictional properties. Unfortunately the use of the bulk polymer as a bearing is limited by its low strength and poor thermal conductivity. These difficulties may be largely overcome by impregnating a substance of higher strength and conductivity, usually phosphor-bronze, with the material, or alternatively depositing thin films on to metal substrates. An extensive investigation has been made using bearings prepared by the second method.

THE FRICTIONAL PROPERTIES OF THIN FILMS OF P.T.F.E.

The frictional properties of thin deposited films of P.T.F.E. on metals have been evaluated on three machines, the Bowden–Leben machine,[1] an extensively modified Wells machine[2] and a Shell four-ball machine.[3] The films were deposited by brushing an aqueous suspensoid of P.T.F.E. on to the clean metal substrate, draining off the excess and drying in air. The best films were produced with a suspension containing 6% solid by weight. A higher concentration resulted in a tendency to "mud cracking" and peeling of the film. Films for test on the Bowden–Leben machine were sintered in air at a temperature of 350° C, which is above the transition point of the polymer. In the case of copper, rapid oxidation of the metal at this temperature, which tended to lead to break-up of the film with a concentrated suspension, was overcome by heating the specimen to the required temperature in a bath of tetracresyl silicate followed by rapid cooling in a second bath of the liquid. Tests on the Wells machine and the four-ball machine showed that preliminary sintering of the film was unnecessary, since at the higher speeds used the frictional heat was sufficient to cause sintering of the film.

In the Bowden–Leben apparatus the friction is measured between a lower plane surface moving at a slow uniform speed and a hemispherical slider pressed against it by a known load. The temperature of the sliding surfaces can be raised to a maximum of about 300° C. In the present investigation both sliding surfaces were of copper, the applied load 4 kg and the sliding speed 0·1 cm/s.

The endurance of films sintered in air and in the tetracresyl silicate was assessed by making the slider traverse the same track several times the coefficient of friction being measured at intervals. The results are shown in Table 1.

The effect of temperature was studied by measuring the coefficient of friction of test surface *A* whilst its temperature was raised to 300° C. Sliding was smooth throughout the test and the wear slight. The coefficient of friction rose from an initial value of 0·13 to 0·20 at 100° C when "stick slip" motion set in, and then remained constant at a value of 0·17 up to 200° C.

The essential parts of the modified Wells machine are the lower and upper friction surfaces. The lower friction member consists of a metallic disk mounted in a horizontal plane on a spindle which rotates at speeds up to 20 rev/min (corresponding to a sliding speed of 5 cm/s). The upper friction member is a heavier metal disk, faced with three, equally spaced, raised, knife-edge sections, which bear on the lower rotating disk with a load of 3 kg. Both test specimens are cleaned so as to be completely free of grease before test. Comparative tests were made of two hours duration at a sliding speed of 5 cm/s between a deposited film of P.T.F.E. and a film of an extreme pressure oil (specification OEP. 71 to M.O.S. specification DED 2479/1). The bearing combinations used were stainless steel sliding on stainless steel (B.S. specification S62), hard steel sliding on hard steel (B.S. specification S11) and copper sliding on copper (specification B.S. 1433). Continuous records were made of the coefficient of friction. At the conclusion of the test, both surfaces were examined under the microscope and a surface profile obtained from two separate portions of the wear track on the lower surface. This specimen was also photographed using a Vickers projection microscope at a magnification of ×500 by the Tolansky multi-profile technique.[4] Fig. 1 shows the multi-profile photographs of wear tracks on copper for the two lubricants. The black lines follow the surface contours of the specimen, valleys and hills being indicated by deviations to the right and left respectively. The magnification in depth is ×1000. Frictional results of these tests are summarized in Table 2.

Table 1. *Endurance characteristics of sintered P.T.F.E. films*

No. of traversals of track	1	2	3	10	20	50	100	200	300	400	500	750	1000
Coefficient of friction (μ) *for test surface A*	0·06	0·05	0·04	0·04	0·06	0·07	0·07	0·10	0·11	0·14	0·09	0·12	0·13
Coefficient of friction (μ) *for test surface B*	0·04						0·05				0·11		

Test surface *A*: P.T.F.E. film sintered in air.

Test surface *B*: P.T.F.E. film sintered in tetracresyl silicate.

* Now at Road Research Laboratories, Harmondsworth, Middlesex.

Table 2. *Frictional properties of air-dried films of P.T.F.E. and an extreme pressure lubricating oil (OEP71)*

Metal Combination	*Lubricant*	*Coefficient of friction (μ)*	*Type of motion*	*Remarks*
Hard steel/hard steel	P.T.F.E.	0·08	Initially smooth. Signs of breakdown after 30 min	Polished. Discontinuous film P.T.F.E. Slight brown discoloration
Stainless steel/stainless steel	P.T.F.E.	0·07	Initially smooth. Signs of breakdown after 45 min	Similar to above with slight wear of metal
Copper/copper	P.T.F.E.	0·10 → 0·13	Smooth running throughout	Polished. Film patchy, slightly discoloured. A few faint wear lines. Scuffing at isolated points
Hard steel/hard steel	OEP 71	0·15 → 0·05	Motion slightly irregular	Wear resistance good
Stainless steel/stainless steel	OEP 71	0·10 → 0·05	Motion slightly irregular	Wear resistance good
Copper/copper	OEP 71	0·15 → 0·07	Motion slightly irregular	Wear moderate

All tests carried out for 2 h, load 3 kg.

Table 3. *Frictional properties of air-dried P.T.F.E. films on various metals*

Metal combination	*Speed (cm/s)*	*Coefficient of friction (μ)*	*Type of motion*	*Endurance*	*Wear resistance*
Aluminium/aluminium	0·26	>0·30	Stick slip	Almost immediate seizure	
Phosphor-bronze/phosphor-bronze	5	0·15–0·20	Tendency to stick slip	>90 min	Good Slight polishing
Naval brass/naval brass	5	0·10	Slight tendency to stick slip	>90 min	Good Polishing
Stainless steel/phosphor-bronze	5	0·10	Smooth	>90 min	Good Polishing
Stainless steel/naval brass	5	0·08	Smooth	>90 min	Good Brown patches on P.T.F.E. film
Hard steel/phosphor-bronze	5	0·10	Smooth	>90 min	Good Dark patches on P.T.F.E. film
Hard steel/naval brass	5	0·08	Slightly irregular	>90 min	Good. P.T.F.E. film brownish colour in patches

Load in all tests 3 kg.

Table 4. *Frictional properties of air-dried P.T.F.E. films on treated surfaces*

Metal combination	*Surface treatment*	*Coefficient of friction*	*Motion*	*Wear resistance*
Hard steel/hard steel	Phosphated	>0·5	Immediate seizure	
Hard steel/hard steel	Phosphated, plus P.T.F.E. film	0·10	Smooth	Very good
Hard steel/hard steel	Phosphated* plus P.T.F.E. film	0·10–0·15	Slightly irregular towards end of test	Very good
Stainless steel/stainless steel	Polymerized silicone	>0·5	Immediate seizure	
Stainless steel/stainless steel	Polymerized silicone, plus P.T.F.E. film	0·10	Smooth	Good
Hard steel/hard steel	Polymerized silicone, plus P.T.F.E. film	0·10	Slightly irregular	Good
Copper/copper	Polymerized silicone, plus P.T.F.E. film	0·10	Smooth	Good

* Test of 8 h duration.

All tests for 2 h at 5 cm/s; load 3 kg.

In a second series of tests, air-dried films of P.T.F.E. on leaded brass, phosphor-bronze and aluminium were run under similar conditions, the tests being terminated after ninety minutes (Table 3). Experiments were also made using lower specimens which had been phosphated before application of the P.T.F.E. Results of two tests, one run for two and the other for eight hours, are given in Table 4.

Table 4 also contains some interesting results which were obtained when the phosphates film was replaced by a film of polymerized silicone. Silicone fluid was brushed on to the clean metal surface, which was maintained at a sufficiently high temperature until polymerization occurred, when a tough tenacious film was obtained. The P.T.F.E. was applied in the same way as before.

In the Shell four-ball machine a $\frac{1}{2}$ in. diameter steel bearing ball is rotated at a speed of 1500 rev/min on three similar balls rigidly clamped in a cup filled with the lubricant under test. Normal loads up to 800 kg can be applied through a lever system. An average value of the diameters of the resulting wear scars on the lower balls is taken as a measure of the effectiveness of the lubricant. Mean Hertz load[5] determinations were made for: (1) P.T.F.E. dry; (2) P.T.F.E. dry on phosphated balls; (3) phosphated balls, dry; (4) P.T.F.E. with a plain mineral oil; (5) the plain mineral oil alone; (6) phosphated balls with a plain mineral oil; (7) P.T.F.E. on phosphated balls with a plain mineral oil. These values are tabulated in Table 5 and the wear-scar diameter after the ten seconds run plotted against load in Fig. 2.

The ten seconds run used in determining the mean Hertz load may be of value as a measure of the anti-seize properties of a lubricant, but is of very little aid in assessing its endurance. Hence wear scar diameters and coefficients of friction were measured for a range of lubricants after running for (*a*) 30 min under a load of 40 kg; (*b*) 30 min under a load of 100 kg; (*c*) 15 min under a load of 300 kg. Tests were made on both phosphated and unphosphated balls (Tables 6, 7). Figs. 3(*a*) and (*b*) show the four balls after the 300 kg test, using an extreme pressure mineral oil as lubricant with and without P.T.F.E. In the case where the oil was used alone there was almost immediate seizure between the upper ball and the three lower ones.

Table 5. *Mean Hertz load for various lubricants*

Lubricant	*Mean Hertz load (kg)*
P.T.F.E. dry	67
P.T.F.E. dry on phosphated balls	61
Phosphated balls, dry	32
Mineral oil (OM62)	28
Mineral oil (OM62) on phosphated balls	67
P.T.F.E. plus mineral oil (OM62)	67
P.T.F.E. plus mineral oil (OM62) on phosphated balls	>73

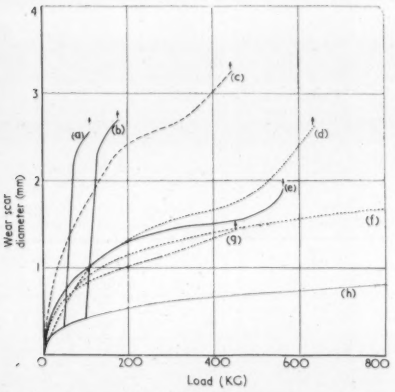

Fig. 2. Curves of relationship between wear scar diameter after ten seconds and load on the Shell four-ball machine for various lubricants

Curve (*a*) mineral oil; (*b*) extreme pressure oil; (*c*) phosphated surfaces (dry); (*d*) P.T.F.E. on phosphated surfaces (dry), (*e*) phosphated surfaces plus mineral oil; (*f*) P.T.F.E. on phosphated surfaces plus mineral oil; (*g*) P.T.F.E. dry; (*h*), Hertz diameter.

DISCUSSION OF RESULTS

Although the conditions of test on the Bowden–Leben machine do not simulate normal practice, the results indicate that:

(1) a tenacious and enduring film of P.T.F.E. can be obtained on copper if the film is prepared from a latex of suitable concentration;

(2) the slight copper oxidation obtained on sintering in air has no harmful effect on the lubricating ability of the film;

(3) effective lubrication is obtained up to temperatures of 300° C;

(4) the coefficient of friction decreases with increasing temperature up to 300° C.

The wear process for surfaces lubricated with an oil or grease under boundary conditions in a mechanism such as the Wells machine is rather different from that for a solid lubricant. In the former case metal-to-metal contact occurs to a higher or lower degree during the whole time of sliding. With a solid lubricant on a metal substrate, no wear of the metal occurs until the lubricant breaks down. The results for steel confirm this, but an anomalous result was obtained with copper. In this case the amount of wear was comparatively large, although the coefficient of friction curve remained smooth. Microscopic examination of lower surfaces of copper and copper bearing alloys, particularly after running with steel as a mating surface, showed fragments and smeared patches of bright yellow metal adhering to the underside of the P.T.F.E. film which had been pushed to the inside and outside edges of the track (Fig. 4). This rather puzzling observation (see also Rabinowitz and Shooter[6]) is an extreme example of the "pick-up" of a hard material by a softer one and may be compared with the "pick-up" of steel by copper as observed by Bowden, Moore and Tabor.[7]

As can be seen from Table 3, effective lubrication was obtained under the conditions of test for all the bearing combinations used, with the exception of aluminium, in which case almost immediate seizure resulted. When P.T.F.E. was applied to an aluminium specimen phosphated electrolytically, a bearing surface of comparatively long life was obtained. Table 4 shows the advantage of surface treat-

Table 6. *Four-ball machine endurance tests. Plain steel bearing balls*

Lubricant	Wear scar diameter (mm)			Coefficient of friction					
				30″ at 40 kg		30″ at 100 kg		15″ at 300 kg	
	30 min 40 kg	30 min 100 kg	15 min 300 kg	μ_1	μ_2	μ_1	μ_2	μ_1	μ_2
OEP 71	0·53	2·44	W	0·12	0·12	0·14	0·15	—	—
OEP 71 + P.T.F.E.	0·51	1·03	2·00	0·09	0·12	0·10	0·11	0·13	0·11
OM 62	0·54	2·65	W	0·12	0·12	0·14	0·13	—	—
OM 62 + P.T.F.E.	0·55	1·47	W	0·12	0·12	0·12	0·10	—	—
Liquid paraffin	0·52	3·84*	W	0·12	0·12	0·45	—	—	—
Liquid paraffin + P.T.F.E.	0·60	1·03	W	0·12	0·12	0·13	0·12	—	—
Silicone (DC200/20)	2·12	3·28†	W	0·30	0·40	0·42	—	—	—
Silicone + P.T.F.E.	2·08	3·48†	W	0·25	0·40	0·38	—	—	—
DTD 577 grease	0·54	2·06	W	0·12	0·30	0·12	0·07	—	—
DTD 577 + P.T.F.E.	0·60	1·20	W	0·18	0·50	0·07	0·10	—	—
DTD 825 grease	0·66	W	W	0·12	0·12	—	—	—	—
DTD 825 + P.T.F.E.	0·70	1·96	2·84	0·12	0·12	0·09	0·10	0·19	0·10

* test stopped after 2 min.
† test stopped after 7 min.

μ_1, coefficient of friction 30 s after beginning of test.
μ_2, coefficient of friction 30 s before end of test.

OEP 71, mineral oil containing an extreme pressure additive.
OM 62, plain mineral oil.
DTD 577, petroleum base grease.
DTD 825, synthetic base grease.
W, welded immediately or during test.

Table 7. *Four-ball machine. Endurance tests. Phosphated steel bearing balls*

Lubricant	Wear scar diameter (mm)			Coefficient of friction					
				30″ at 40 kg		30″ at 100 kg		15″ at 300 kg	
	30 min 40 kg	30 min 100 kg	15 min 300 kg	μ_1	μ_2	μ_1	μ_2	μ_1	μ_2
OEP 71	1·24	1·64	2·48	0·06	0·06	0·14	0·15	0·12	0·15
OEP 71 + P.T.F.E.	0·96	1·24	1·96	0·05	0·05	0·12	0·14	0·14	0·13
OM 62	1·16	1·20	1·60	0·07	0·07	0·14	0·11	0·09	0·09
OM 62 + P.T.F.E.	0·96	1·20	1·40	0·09	0·09	0·13	0·12	0·10	0·10
Liquid paraffin	1·04	1·36	W	0·08	0·05	0·16	0·12	—	—
Liquid paraffin + P.T.F.E.	0·84	1·12	1·40	0·05	0·05	0·15	0·10	0·12	0·09
DTD 577	0·96	1·60	W	0·07	0·07	0·14	0·11	—	—
DTD 577 + P.T.F.E.	1·08	1·56	W	0·06	0·06	0·12	0·10	—	—
DTD 825	1·28	1·32	W	0·05	0·05	0·10	0·08	—	—
DTD 825 + P.T.F.E.	1·20	1·40	W	0·05	0·05	0·09	0·08	—	—

ment before application of the polymer. One of the phosphated steel surfaces was run for eight hours without any breakdown of the P.T.F.E. film.

Referring to Fig. 2, curve (*a*) is characteristic of mineral oils and other liquid lubricants. The initial part of the curve lies either on, or near to, the curve of the Hertz diameter, which is the diameter of the area of contact between upper and lower balls under the static applied load. At the point of incipient seizure the curve rises almost vertically and then lines parallel to the initial part when the lubricant film is re-established. A further slight increase in slope indicates the approach of the "weld load." The relationship between Hertz diameter and load is a cubic one, so that the curve becomes linear when plotted on a log-log scale. A mineral oil containing an extreme pressure additive will have a higher incipient seizure point than a plain mineral oil and also a higher weld load.

As one would expect, a solid lubricant has a different characteristic curve. It is found to have an S-shape both in the presence and absence of oils. This latter fact would suggest that the oil mainly acts as a coolant in conducting heat away from the bearing surfaces.

At low loads the wear-scar diameter is higher for the solid lubricant than for the oil. In the case of P.T.F.E. on phosphated steel with a mineral oil, no welding occurred at a load of 800 kg, which is the maximum obtained on the machine.

The results of the endurance tests, in which effective lubrication was obtained at 100 kg even with paraffin (which has a poor load-carrying capacity), illustrate the excellent

The use of polytetrafluoroethylene as a lubricant

By E. KAY, B.Sc., A.Inst.P., and E. D. TINGLE, Ph.D.

See pages 17–25

(*a*)

(*b*)

Fig. 1. Photomicrographs of wear tracks on copper lubricated with (*a*) an extreme pressure oil O.E.P. 71, and (*b*) P.T.F.E. ×500 laterally, ×1000 in depth

***

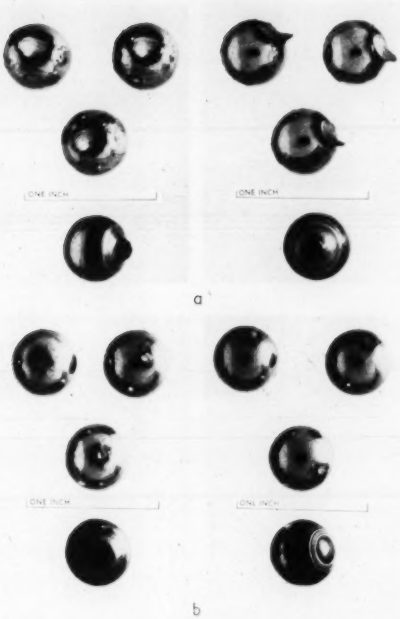

Fig. 3. Comparison of wear scars obtained after an endurance test on the Shell four-ball machine with an extreme pressure oil, (*a*) alone, load 300 kg, immediate seizure; and (*b*) in conjunction with P.T.F.E., load 300 kg, after 15 min.

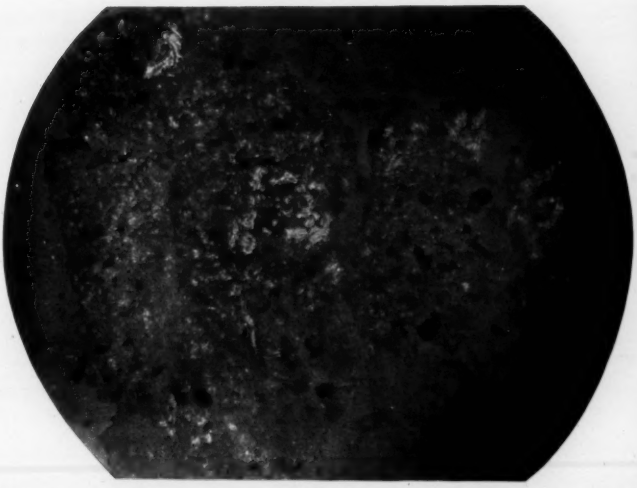

Fig. 4. Photomicrograph of copper "pick-up" on P.T.F.E. film stripped from edge of wear track on copper substrate

Film taken from specimen illustrated in Fig. 1 (*b*) × 100

A technique for obtaining thin foils of aluminium and aluminium alloys for transmission electron metallography

By R. B. Nicholson, B.A., G. Thomas, B.Sc., Ph.D., and J. Nutting, M.A., B.Sc., Ph.D.

See pages 25–27

Fig. 1. Grain boundary in pure aluminium. Thin foil (×25 000)

Fig. 2. Al–4% Cu alloy solution treated and subsequently aged for ½ h at 340° C. Thin foil (×2000)

Fig. 3. Al–4% Cu alloy solution treated and subsequently aged for three days at 160° C (peak hardness) showing bands of preferential precipitation of θ' phase. Thin foil (×3500)

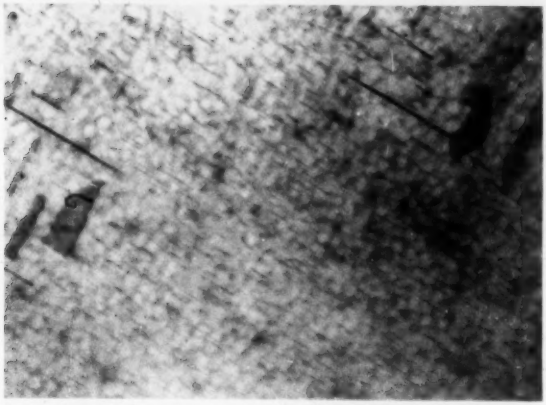

Fig. 4. Same specimen as Fig. 3 but showing fine precipitates of G.P. [2] zones. Thin foil (×80000)

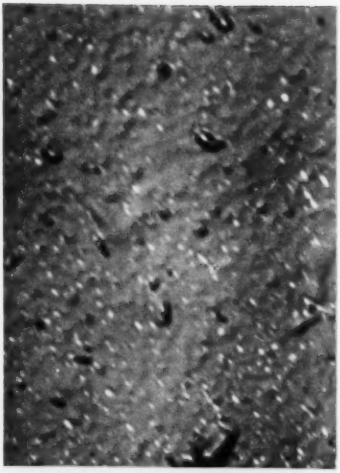

Fig. 5. Complex Al–Mg–Zn–Cu alloy solution treated and subsequently aged for ten days at 160° C. Oxide replica (×40000)

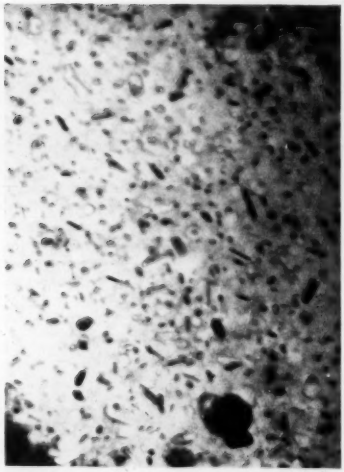

Fig. 6. As Fig. 5, but showing precipitated particles not revealed by the oxide replica. Thin foil (×40000)

anti-seize properties of P.T.F.E. and confirm that the main role of the oil is that of coolant. The silicone fluids in conjunction with P.T.F.E. fail as lubricants. The P.T.F.E. film is porous when applied and it appears that the silicone fluid penetrates the pores and displaces the P.T.F.E. from the surface. Evidence obtained on the Wells machine indicates that silicones will produce a decrease in the coefficient of friction of non-porous P.T.F.E. films.

THE USE OF P.T.F.E. AS A GELATOR IN GREASE

Because of its thermal and chemical stability, it seemed worth while to explore the possibilities of using P.T.F.E. as a gelling agent in the preparation of high temperature greases. The silicone fluids have many of the desirable properties of a good high temperature lubricant, i.e. little change in viscosity with temperature and good temperature stability. It was hoped that by gelling these fluids with P.T.F.E., a grease combining these desirable characteristics with the good boundary lubricating properties of the P.T.F.E. would be produced.

The method employed was to heat the fluid to a temperature of a little over 100° C, effective agitation of the liquid being maintained by an electric stirrer. A small quantity of the diluted suspensoid of the polymer was then added and the source of heat removed. Stirring was continued until gelation occurred. By this means grease with a fibrous structure was obtained. Boundary lubrication tests on the Wells machine were disappointing. This may be attributed to the stronger affinity of the silicone constituent for the metal substrate, thus preventing the adhesion of the P.T.F.E. Greases were also prepared from fluorocarbon oils by this technique, the boundary lubricating properties of which were satisfactory. It was thought that these might be used for high temperature applications, but the idea was abandoned when it was found that the volatility of fluorocarbons was much higher than would be anticipated from their high boiling points (see, however, Ref. 8).

APPLICATION OF P.T.F.E. IN THE FIELD OF LUBRICATION

At the present time cost alone would preclude the use of P.T.F.E. from applications where the more conventional oils and greases are adequate. However, it should be of value as a safeguard against seizure when extreme conditions prevail and the normal type of lubricant would break down. Other applications where P.T.F.E. might prove of value are:

(1) where components are required to function without relubrication after long periods of storage;
(2) where use of a grease or oil would attract abrasive dust;
(3) where temperatures are very high or very low;
(4) under reduced atmospheric pressures where oils or greases would be too volatile;
(5) in the presence of acids or other corrosive media;
(6) in watches and other clockwork mechanisms, where oils and greases creep away from the bearings and, in particular, those required to work over a wide temperature range;
(7) under tropical conditions where high humidity produces an increased tendency for corrosion.

REFERENCES

(1) BOWDEN, F. P., and LEBEN, L. *Proc. Roy. Soc. A*, **169**, p. 371 (1939).
(2) TINGLE, E. D. *Unpublished Ministry of Supply Report.*
(3) BOERLAGE, G. D. *Engineering*, **136**, p. 46 (1933).
(4) TOLANSKY, S. *Nature* [*London*], **169**, p. 445 (1952).
(5) *U.S. Fed. Spec.* "*Load carrying capacity mean Hertz load.*" U.S. Federal specification VV-L-791d, Method 650.3 (20 June, 1950).
(6) RABINOWITZ, E., and SHOOTER, K. V. *Proc. Roy. Soc. B*, **65**, p. 671 (1952).
(7) BOWDEN, F. P., MOORE, A. J. W., and TABOR, D. *J. Appl. Phys.*, **14**, p. 8 (1943).
(8) IRWIN, C. F. *U.S. Patent* 2576837 (27 November, 1951).

A technique for obtaining thin foils of aluminium and aluminium alloys for transmission electron metallography

By R. B. NICHOLSON, B.A., G. THOMAS, B.Sc., Ph.D., and J. NUTTING, M.A., B.Sc., Ph.D., Department of Metallurgy, University of Cambridge

[*Paper first received* 24 *June, and in final form* 1 *September*, 1957]

The structural changes produced by ageing aluminium–copper and aluminium–magnesium–zinc–copper alloys have been investigated by examining foils of these alloys in the electron microscope. The foils have been obtained by mechanical reduction in thickness followed by controlled electropolishing and chemical dissolution of the remaining oxide film.

INTRODUCTION

There are many advantages to be gained from the direct examination in the transmission electron microscope of thin metal specimens, rather than replicas of metal surfaces, but until recently no satisfactory methods were available for obtaining specimens 100–500 Å thick. Although Heidenreich[1] obtained thin aluminium foils in 1949, the first outstanding advance was made by Castaing[2] who bombarded aluminium and aluminium–copper alloys with ionized air at a potential of 3 kV thereby reducing the specimen thickness from 100 μ to 200 Å in 24 hours. The surfaces obtained by ionic bombardment are clean and free from oxide layers whilst uniformly thin specimens may be produced. Hirsch, Horne and Whelan[3] have used a method of chemical solution for obtaining thin foils of aluminium and an electropolishing technique has been used by Bollmann[4] for preparing stainless steel.

The chief disadvantage of using chemical thinning methods for alloys containing precipitated phases is that chemical attack occurs preferentially at either the matrix or the pre-

cipitated phases; thus with aluminium alloys, chemical solution, e.g. 1% hydrofluoric acid, invariably leaches out the second phases so that the resulting thin films are not satisfactory for electron microscopy. The present technique of thinning by controlled electro-polishing has been devised to overcome these difficulties.

EXPERIMENTAL METHOD

The technique for preparing thin foils of aluminium and aluminium alloys involves the following sequence of operations:

(1) Primary reduction to a thickness of about 0·025 mm is carried out by cold rolling or other mechanical treatments such as grinding.
(2) The foil is heat treated. This may be either annealing or solution treatment and ageing.
(3) A short electro-polish of the whole sample is carried out in a standard perchloric acid–ethyl alcohol bath.
(4) A small area of the specimen is electro-polished in a solution devised by Lenoir[5] until holes appear.
(5) The polished sample is immersed in phospho-chromic acid solution to dissolve away any oxides.
(6) The sample is washed in distilled water and regions adjacent to the holes cut into 2 mm^2 specimens suitable for mounting and subsequent examination in the electron microscope.

If the primary reduction in thickness is to be carried out by rolling it is convenient to start with strips about 10 × 2 cm. These can readily be reduced to a thickness of less than 0·025 mm without an intermediate anneal in the case of aluminium, but for aluminium alloys intermediate solution heat treatment followed by quenching may be necessary.

At this stage the aluminium is annealed at 600° C for 1 h to remove the effects of cold work. The aluminium alloys are heated to a temperature at which all the components are taken into solid solution (solution treated), quenched to produce a supersaturated solid solution and then aged to bring about precipitation of the secondary phases. It is better to carry out the heat treatment of the alloys at this stage as the results obtained are then representative of bulk material, for it has been found that very thin sections age more slowly than thick sections. Furthermore, any oxide layers produced during heat treatment can be removed before the final thinning. The oxide removal is accomplished by a short electro-polish of the whole specimen using a standard technique which also cleans the surface.

The edges and other parts of the specimen are covered with polystyrene deposited from a solution in benzene to leave areas of about 1 cm^2 centrally situated on both sides of the specimen. These areas are completely immersed in Lenoir's solution (817 cm^3 orthophosphoric acid (d 1·57), 134 cm^3 sulphuric acid, 156 g chromic oxide, 40 cm^3 water) and a slow controlled electro-polishing is carried out at a potential of 10–12 V and a current of 0·1 A, the bath temperature is maintained at 70° C. Depending upon the thickness of the specimen and the alloy composition holes appear in the polished area after 5–30 min. The regions adjacent to these holes are then suitable for examination in the electron microscope.

The specimen is removed from the electro-polishing bath and washed carefully in distilled water. It is then immersed in cold phospho-chromic acid solution (350 cm^3 orthophosphoric acid (d 1·71), 160 g chromic oxide, 650 cm^3 water) for 10–15 min to dissolve any oxide layers and again is washed in distilled water. Samples suitable for examination in the electron microscope are then cut from the regions adjacent to the holes. The samples should be about 1–2 mm^2 and are caught on copper mounting grids which previously have been coated with a layer of polybutene deposited from a 1% solution in xylol, to make them sticky.

With the more complex aluminium alloys, many intermediate solution treatments may be required to obtain thin sections by cold rolling. Thicker sections may be used therefore and the thinning by dissolution in the ethyl alcohol–perchloric acid bath is continued for a longer period until holes appear in the specimen. The final thinning is then continued as before in Lenoir's solution. With aluminium–copper alloys it is better to avoid if possible any polishing in the perchloric acid–ethyl alcohol bath, as this leaves a deposit of copper on the specimen surface which, although it may be removed by treatment of the specimen in concentrated nitric acid or ammonia, leaves the surface in an unsatisfactory condition for subsequent treatment. The Lenoir solution leaves no copper deposit on the alloys after thinning.

RESULTS

The results to be described have been obtained by examining thin foils of aluminium and aluminium alloys in the Siemens electron microscope (type Elmiskop 1) operated at a beam voltage of 80 kV.

A grain boundary in pure aluminium is shown in Fig. 1. The black lines running to the boundary are extinction contours and the structure within the grains results from the electro-polishing. The micrograph is essentially similar to those shown by Hirsch, Horne and Whelan,[3] but as the specimen has been annealed at a higher temperature and has had initially a much smaller amount of deformation, the dislocation density is low and dislocation movements are only infrequently observed.

The precipitates obtained by ageing an aluminium–4% copper alloy at 340° C for ½ hour are shown in Fig. 2. The particles within the grains and lying parallel to the surface of the section are seen to be disc shaped whilst the particles perpendicular to the section surface appear as needles but with enhanced contrast. If the alloy is aged at a lower temperature the θ' phase (metastable $CuAl_2$) is precipitated preferentially on dislocations to give the structure shown in Fig. 3. Similar structures have been observed by Thomas and Nutting[6] when examining oxide replicas from this alloy. The light areas around the large particles of the θ' phase result from denudation of the matrix with respect to copper. Both Figs. 2 and 3 illustrate the fact that useful metallurgical information may be obtained by examining thin foils at relatively low magnifications. In the regions between the bands of large θ' precipitates, there is a much finer precipitate, the structure of which is shown in Fig. 4. This corresponds to the formation of Guinier–Preston zones 2 (G.P. [2]) in the matrix. The width of some of these zones is as small as 15 Å—i.e. about four lattice spacings, whilst the θ' precipitates in the same specimen have a thickness of 100–200 Å. The light regions in the background are probably due to electro-polishing.

The microstructures revealed by oxide replicas and thin foils may not be the same, since the origins of contrast in the electron optical images are different. This difference in microstructure is clearly shown in Figs. 5 and 6 which are

micrographs of an oxide replica and a thin foil taken from a specimen of a complex aluminium–magnesium–zinc–copper alloy after solution heat treatment and ageing. With an oxide replica the contrast in the image can result from differences in oxide film thickness which are in turn related to differences in rates of oxidation of the matrix and precipitated phases. The contrast obtained when examining thin foils of alloys containing precipitated phases depends chiefly upon the relative scattering powers of the atomic species forming the matrix and the precipitates. In the aluminium–magnesium–zinc–copper alloy the precipitated phase, which is thought to be zinc rich, does not oxidize at a rate different from the matrix; there is therefore no clear evidence of precipitates in Fig. 5. But in Fig. 6 the precipitates are clearly observed as a result of the enhanced scattering from the zinc rich areas.

ACKNOWLEDGEMENTS

The authors would like to thank Professor G. W. Austin for his interest and encouragement. One of them (R. B. N.) gratefully acknowledges financial support from the Department of Scientific and Industrial Research.

REFERENCES

(1) HEIDENREICH, R. D. *J. Appl. Phys.*, **20**, p. 993 (1949).
(2) CASTAING, R. *Rev. Univ. Mines*, **12**, p. 454 (1956).
(3) HIRSCH, P. B., HORNE, R. W., and WHELAN, M. J. *Phil. Mag.*, **1**, p. 677 (1956).
(4) BOLLMANN, W. *Phys. Rev.*, **103**, p. 1588 (1956).
(5) LENOIR, G. *Rech. Aéronautique*, **36**, p. 35 (1953).
(6) THOMAS, G., and NUTTING, J. *Inst. Metals Monograph and Report Series No.* 18, p. 57 (1955).

An overall test of equations of state of fluids

By N. DAVY, D.Sc., and BARBARA M. BELL, M.Sc., Grad.Inst.P., Physics Department, University of Nottingham

[*Paper received* 1 *May*, 1957]

An equation of state of a fluid can usually be expressed in the form $f_1(V, T) = P$. When the reduced form of the equation exists, it may be expressed as $f_2(v, t) = p$, where p, v, and t are the reduced values of P, V and T. Since the critical volume cannot be measured with precision, the recent fashion is to use, instead of v, the accurately obtainable pseudo-reduced volume ϕ, leading to a reduced equation $f_3(\phi, t) = p$. It is now suggested that a calculation and plot of the quantity $Y = 100[f_3(\phi, t)/p - 1]$ against $X = p$ (t constant) or $X = t$ (p constant), using experimental values of p, ϕ, and t for some real fluid, will reveal in a quantitative manner the discrepancy between the experimental behaviour of that fluid, and of a fluid obeying the particular equation of state under consideration. A set of graphs at various constant temperatures or pressures may be drawn.

TEST OF VAN DER WAALS' EQUATION

The symbols P, V and T are here used for ordinary pressures, volumes and absolute temperatures, and p, v and t for their reduced values. Van der Waals' equation is

$$(P + a/V^2)(V - b) = RMT/W = KT \qquad (1)$$

where R is the universal gas constant, M the mass, and W the molecular weight, and $K = RM/W$. The usual reduced form is

$$(p + 3/v^2)(3v - 1) = 8t \qquad (2)$$

Recognizing that the critical volume cannot be measured accurately, authors such as Su[1] and Ghosh[2] have used, instead of v, the quantity

$$\phi = P_c V/RT_c \qquad (3)$$

ϕ is called the pseudo-reduced volume. Hence

$$v = V/V_c = RT_c\phi/P_c V_c \qquad (4)$$

Substituting this quantity in equation (2) and re-arranging, we get

$$8t/(8\phi - 1) - 27/64\phi^2 = p \qquad (5)$$

as the reduced equation. Noting that the left-hand side is a function of ϕ and t only, it is now proposed to calculate and use the quantity

$$Y = 100\left\{\frac{1}{p}[8t/(8\phi - 1) - 27/64\phi^2] - 1\right\} \qquad (6)$$

If van der Waals' equation is true, the left-hand side of equation (5) should equal p, and Y should equal zero. If in the expression for Y we substitute experimental values of p, t and ϕ, the numerical result will not usually equal zero. We may regard Y as the percentage excess of the quantity $8t/(8\phi - 1) - 27/64\phi^2$, with experimental values of t and ϕ substituted in it, over the experimental value of p.

Experimental data are available as sets of values of P and V, each set being measured at some constant value of T. From one of these sets we calculate values of p, ϕ and t, and Y. Then plot a graph of this value of Y against $X = p$. Such a graph is an isothermal, and similar isothermals are plotted for other available temperatures. Obedience to van der Waals' equation would be indicated by the coincidence of a graph, at any temperature, with the axis of X. This does not occur, but the ordinates of any graph, i.e. the values of Y, give at a glance a quantitative measure of the discrepancy between the real fluid under consideration, and a van der Waals' substance.

In this paper the fluid considered is carbon dioxide, and the experimental data include those of Amagat,[3] Michels

and others,[4, 5] and MacCormack and Schneider.[6] It has been thought sufficient to exhibit four diagrams, Figs. 1 to 4, corresponding to the four reduced temperatures $t = 1{\cdot}000$,

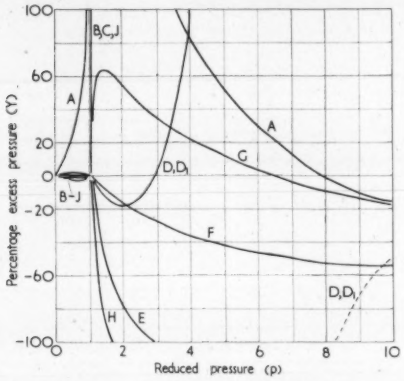

Fig. 1. Isothermals of carbon dioxide at the critical temperature $t = 1{\cdot}000$ (31·04° C = 304·20° K)

A, perfect gas; *B*, Berthelot; *C*, Dalton; *D*, Dieterici; D_1 = Porter; *E*, Wohl; *F*, Su–Chang; *G*, Beattie–Bridgeman; *H*, Lees; *J*, van der Waals.

1·226, 1·549 and 1·746, respectively, and in each case the range of pressure is $0 < p < 10$.

Values of that quantity which correspond to the above value of Y, predicted by nine other equations of state, are plotted as ordinates on Figs. 1 to 4, so that their claims can

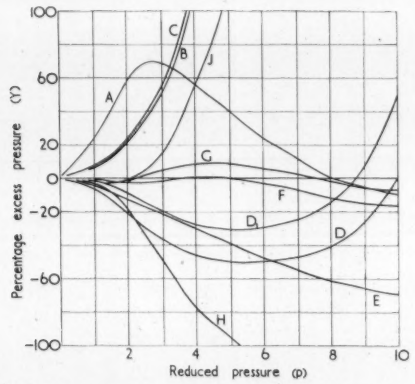

Fig. 2. Isothermals of carbon dioxide at $t = 1{\cdot}227$ (100° C = 373·16° K)

be compared directly and quantitatively. From a general point of view, the quantity plotted is

$$Y = 100[f(\phi, t) - p]/p \qquad (7)$$

against $X = p$; $f(\phi, t)$ is that function of ϕ and t which, according to a particular equation of state, should equal p. Such values of Y, for the other nine equations of state, are given below.

TESTS OF NINE OTHER EQUATIONS OF STATE (Figs. 1–4)

Berthelot equation. To test the Berthelot equation

$$(P + a/V^2T)(V - b) = KT \qquad (8)$$

plot

$$Y = 100\left\{\frac{1}{p}[8t/(8\phi - 1) - 27/64\phi^2 t] - 1\right\} \qquad (9)$$

against $X = p$.

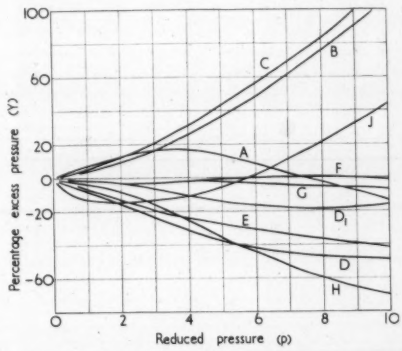

Fig. 3. Isothermals of carbon dioxide at $t = 1{\cdot}549$ (198° C = 471·16° K)

Dalton equation. To test the Dalton equation

$$\{P + a \exp[\beta(T_c - T)]/V^2\}(V - b) = KT \qquad (10)$$

plot

$$Y = 100\left(\frac{1}{p}\{8t/(8\phi - 1) - [27 \exp(1 - t)]/64\phi^2\} - 1\right) \qquad (11)$$

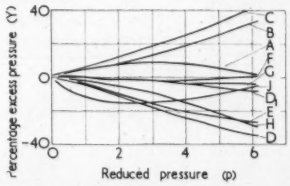

Fig. 4. Isothermals of carbon dioxide at $t = 1{\cdot}746$ (258° C = 531·16° K)

Dieterici equation. To test Dieterici's equation

$$P(V - b) = KT \exp(-a/KTV) \qquad (12)$$

plot

$$Y = 100\left\{[t \exp(-0{\cdot}5414/\phi t)]/[p(\phi - 0{\cdot}135)] - 1\right\} \qquad (13)$$

Porter–Dieterici equation. To test Porter's modification of Dieterici's equation

$$P(V-b) = KT\exp(-a/KT^{5/3}V) \tag{14}$$

plot

$$Y = 100\left\{[t\exp(-0{\cdot}5414/\phi t^{5/3})]/[p(\phi-0{\cdot}135)]-1\right\} \tag{15}$$

Wohl equation. To test Wohl's equation

$$P = KT/(V-b) - a/V(V-b) + c/V^3 \tag{16}$$

plot

$$Y = 100\left\{\frac{1}{p}[t/(\phi-0{\cdot}0667) - 96/225\phi(\phi-0{\cdot}0667) + 256/3375\phi^3] - 1\right\} \tag{17}$$

Su and Chang equation. To test Su and Chang's equation, which is commonly quoted in the reduced form

$$p = t[\phi + 0{\cdot}160(1 + 0{\cdot}190/\phi)]/\phi^2 - 0{\cdot}472/\phi^2 \tag{18}$$

plot

$$Y = 100\left\{t[\phi + 0{\cdot}160(1 + 0{\cdot}190/\phi)]/p\phi^2 - 0{\cdot}472/p\phi^2 - 1\right\} \tag{19}$$

Beattie–Bridgeman equation. To test the Beattie–Bridgeman equation (reduced)

$$p = t(1 - 0{\cdot}050/\phi t^3)[\phi + 0{\cdot}18764(1 - 0{\cdot}03833/\phi)]/\phi^2 - 0{\cdot}4758(1 - 0{\cdot}1127/\phi)/\phi^2 \tag{20}$$

plot

$$Y = 100\left\{t(1 - 0{\cdot}050/\phi t^3)[\phi + 0{\cdot}18764(1 - 0{\cdot}03833/\phi)]/p\phi^2 - 0{\cdot}4758(1 - 0{\cdot}1127/\phi)/p\phi^2 - 1\right\} \tag{21}$$

Lees equation. To test Lees' equation

$$(P + aP^{1/3}/TV^{5/3})(V-b) = KT \tag{22}$$

note that on account of the presence of the factor $P^{1/3}$ in one term, we are compelled to express p as a function of t, ϕ and p itself. Assume this to be reasonable and plot

$$Y = 100\left\{15t/[p(15\phi-1)] - 4^{5/3}/15^{5/3}p^{2/3}t\phi^{5/3} - 1\right\} \tag{23}$$

Perfect gas equation. To test the equation of state of a perfect gas

$$PV/MT = R/W \tag{24}$$

note that this equation does not envisage a critical state, and plot

$$Y = 100(RMT/PVW - 1) \tag{25}$$

In this case, for the isothermal at the critical temperature, $t = 1$, (31·04° C), we put $T = 304{\cdot}20$ and substitute the various values of P and V obtained by Michels and co-workers at that temperature, up to values of $P = 730$ atm., $p = 10$. Plot $X = p$ as in all the other cases.

COMMENTS ON THE GRAPHS

All four diagrams are drawn on the same scale. In passing from Fig. 1 to Fig. 4 the temperature is rising from $t = 1{\cdot}00$ to $t = 1{\cdot}746$, and it is seen that the sheaf of graphs gradually closes in towards the X-axis. On the whole, the equations are obeyed more closely by carbon dioxide at higher temperatures than at low ones.

Graphs for $t = 1{\cdot}000$, the critical temperature, i.e. 31·04° C or $T = 304{\cdot}20$° K are shown in Fig. 1. In the perfect gas equation test, the value of Y starts at zero when $p = 0$, and rises to a high positive maximum excess of 386% when $p = 1{\cdot}115$, later falling through zero to negative values, i.e. carbon dioxide is transitorily a true perfect gas when $t = 1$ and $p = 8$ approximately ($P = 584$ atm). May not this effect be due to the gradual decrease of average distance from centre to centre of two molecules, as the pressure is increased, so that at a certain stage the attraction between two molecules changes to a repulsion? An elementary calculation gives the cube root of the average volume occupied by a molecule of carbon dioxide when $t = 1, p = 8, \phi = 0{\cdot}123$ as $1{\cdot}91 \times 10^{-8}$ cm.

All the other graphs pass through the point $X = p = 1$, $Y = 0$. Since $t = 1$, the van der Waals, Berthelot and Dalton graphs coincide. The Dieterici and the Porter–Dieterici graphs also coincide with each other. Fig. 1 therefore shows the perfect gas equation graph and six others, and all the six have a cusp at $X = p = 1$, $Y = 0$. This cusp would seem to be due to a transition from liquid to gas, and suggests that the temperature taken as $t = 1$ was actually very slightly below the critical point. It is hard to see how a single gas or vapour phase would exhibit the abrupt change of density implied by the cusp.

The positive value of Y in the case of the perfect gas equation suggests that the equations of van der Waals, Berthelot, Dalton and Beattie–Bridgeman, when $1 < p < 6{\cdot}5$, for which Y is also positive, do not contain terms allowing sufficiently for attractions between molecules. The equations of Lees and Wohl perhaps allow too much for such attractions, i.e. contain terms representing attractions which are too large, or terms representing repulsions which are too small. The Dieterici and Porter–Dieterici graphs behave like those of Lees and Wohl at first, but at about $p = 2{\cdot}9$ begin to give increasing positive values of Y, going to infinity, like those of van der Waals. The graphs which do this reappear for higher values of p, with infinite negative values of Y; Y then comes up from $-\infty$ towards zero, but the points are mostly outside the range of the figures.

Inspection of Fig. 1 shows that when $t = 1{\cdot}000$ and when $0 < p < 1$, the Beattie–Bridgeman equation fits best. From $1 < p < 2{\cdot}15$ the Su–Chang equation, from $2{\cdot}15 < p < 3{\cdot}4$ the Dieterici equation, from $3{\cdot}4 < p < 7{\cdot}4$ the Beattie–Bridgeman again, and from $7{\cdot}4 < p < 10$ the perfect gas equation fits best.

Graphs at $t = 1{\cdot}226$, $1{\cdot}549$, and $1{\cdot}746$ are shown in Figs. 2, 3 and 4. When $t = 1{\cdot}226$ all the cusps have disappeared and the graphs bend inwards towards the X-axis. The height of the hump on the perfect gas graph is considerably reduced. The value of Y of the Su–Chang graph is less than 2% from $p = 0$ to $p = 6$, while from $p = 6$ to $p = 10$ the lowest value of Y, that of the Beattie–Bridgeman graph, is under 4%. When $t = 1{\cdot}549$, the Su–Chang discrepancy is under 2% over the whole range $0 < p < 10$. The reduced spread of all the graphs is marked. When $t = 1{\cdot}746$, the data available do not extend beyond a pressure of 450 atm, $p = 6{\cdot}17$, but it is evident that Su and Chang's equation is almost perfectly obeyed by carbon dioxide, and for all the other equations Y is numerically less than at the lower temperatures.

FURTHER APPLICATIONS OF THE METHOD

As far as the available data goes, Su and Chang's equation of state appears to represent the behaviour of carbon dioxide fairly well at the lower, and very well at the higher temperatures.

In work to be published elsewhere the above method has been applied also to various fluids. Applying one and the same equation, at a common reduced temperature, to several gases, the isothermal graphs, drawn as above, provide evidence as to the existence of corresponding states. If two gases give the same graph under these circumstances, it may be said that they then exist in corresponding states. Or, two fluids exist in corresponding states at the same reduced temperature if they have the same value of Y. If the graph happens to be a straight line or other recognizable curve, we can calculate an equation of state which it will obey with considerable precision.

In the present paper only isothermals have been exhibited. Isobars and isometrics (ϕ constant) may also be used. In fact, six types of graph in all can be obtained, for any one of the three variables p, t and ϕ can be chosen as abscissa, and then one of the two remaining ones must be made constant. These graphs are exhibited elsewhere.

Another test, based on the Joule–Thomson effect, can also be applied. A general equation of state usually gives rise to three equations connecting p and t, t and ϕ, and ϕ and p, holding when Joule–Thomson inversion occurs. In a paper to be published elsewhere a percentage excess pressure Y, derived from the inversion equations of van der Waals, Berthelot and the rest, is calculated for one given fluid, and plotted against $X = p$. As in the present paper, this is believed to show graphically which equation is most nearly obeyed by the given fluid.

REFERENCES

(1) Su, G. J., and Chang, C. H. *Industr. Engng Chem.*, **38**, pp. 800–806 (1946).
(2) Ghosh, B. *Trans Indian Inst. Chem. Engng*, **6**, pp. 76–81 (1953–4).
(3) Amagat, E. H. *International Critical Tables*, **3**, pp. 11–13 (New York: McGraw-Hill, 1928).
(4) Michels, A., and Michels, C. *Proc. Roy. Soc. A.*, **153**, p. 201 (1935).
(5) Michels, A., Michels, C., and Wouters, H. *Proc. Roy. Soc. A*, **153**, p. 214 (1935).
(6) MacCormack, K. E., and Schneider, W. G. *J. Chem. Phys.*, **18**, p. 1269 (1950).

The electric strength and molecular structure of liquids

By T. J. Lewis, M.Sc., Ph.D., A.M.I.E.E., Department of Electrical Engineering, Queen Mary College, London

[*Paper first received* 20 *December*, 1956, *and in final form* 21 *June*, 1957]

Further measurements of the electric strength of liquids are used to support the theory of a breakdown criterion, suggested in an earlier paper, in which conduction electrons in the liquid excite molecular vibrations associated with individual groups within the molecules. It has been demonstrated that collision cross-sections could be assigned to these groups and the breakdown strength derived. This criterion is used to relate the breakdown strengths of a series of alkyl benzenes recently measured by Sharbaugh, Crowe and Cox and a cross-section for the benzene ring is determined. The additive effect of the various group cross-sections is found as before, but it is necessary to consider dipole effects as well as liquid structure in order to explain the increased cross-section values for the alkyl groups.

The general correctness of the concept is further demonstrated by measurements of the strength of a series of dimethyl siloxanes. It is assumed that cross-sections are to be associated with the oxygen sites and also with the methyl groups. The value of the methyl cross-section determined in this case is identical with that found from the previous measurements on the alkanes. Lastly, the presence of a puckered ring structure as well as steric hindrance is suggested as the cause of the strength of cyclohexane calculated from alkane measurements being different from the measured value.

It has been suggested[1] that one major factor determining the electric strength of a pure liquid alkane is the energy loss incurred by conduction electrons in interactions with the molecules of the liquid. These interactions are considered to excite molecular vibrations and thereby to cause an energy loss. Provided that this loss is greater than the energy gain from the applied field, ionizing collisions will be infrequent and breakdown will not occur. If an adequate supply of electrons is available from the cathode, a breakdown criterion can be found from the electron energy balance equation for the gain and loss. This has been obtained previously[1] in the form

$$F = kN\Sigma n_i Q_i \qquad (1)$$

in which F is the breakdown field strength, N is the number of molecules per cm^3 and n_i is the number of i'th groups per molecule for which the cross-section of the electron/molecule collision process involved is Q_i. The constant k includes a factor determined by the experimental conditions and also the frequency ν of the molecular vibrations involved. The author has suggested that ν for the alkanes is that of the carbon–hydrogen stretching frequency (of the order of 3000 cm^{-1}) and has also demonstrated that the Q_i's can be associated with the CH_3, CH_2 and CH groups present in the molecules; these groups acting as independent collision centres assumed to have a uniform distribution in the liquid phase. Spectroscopic evidence supports the assumption of an independent vibrational behaviour of these groups.

More recently, experimental results have become available for aromatic hydrocarbons[2] and also for certain dimethyl

siloxanes. It is the purpose of the present paper to show that the theory can be applied to these new molecular types which contain groups not present in the alkanes, giving thereby additional support for a vibrational energy loss criterion for breakdown in pure liquids.

AROMATIC HYDROCARBONS

Sharbaugh, Crowe and Cox[2] have measured the electric strengths of a series of alkyl benzenes as well as benzene itself, employing microsecond pulse techniques previously used for a range of alkanes. These liquids are listed in Table 1 and each contains the benzene ring having a cross-section Q_b together with the various alkyl groups CH_3, CH_2, CH having cross-sections Q_3, Q_2 and Q_1.

The benzene ring is to be considered as one interacting unit rather than as a set of carbon-hydrogen linkages. Evidence from other fields of investigation concerning the electronic configuration, the binding forces and the nature of the bonds involved, justifies considering it as a single entity in the collision processes. In any case its CH bonds, if considered separately, would not be expected to offer the same cross-section as the CH bonds present in the chain structure of the alkanes. We therefore consider the benzene ring as a single collision centre and assign it a cross-section Q_b. Regarding the vibrations set up by the colliding electrons, spectroscopic evidence indicates that a frequency close to 3000 cm^{-1} corresponding to a CH stretching mode will be a principal frequency to be associated with the benzene ring. This same frequency can also be assigned to the alkyl groups since they will also have a CH stretching mode as in the alkanes.

In addition to the numbers of groups present in the various molecules, Table 1 also gives the quantity F/N, F being

Table 1. *Data for the alkyl benzenes, from microsecond pulse measurements of Sharbaugh, Crowe and Cox*[2]

	Number of groups				F	F/N	Dipole moment
	$n_0(Qr)$	$n_3(Q_3)$	$n_2(Q_2)$	$n_1(Q_1)$	(MV/cm)	(MV/cm^2)	(Debye units)
Benzene	1				1·63	144	0
Methyl–benzene	1	1			1·99	211	0·37
Ethyl–benzene	1	1	1		2·26	276	0·58
n-Propyl–benzene	1	1	2		2·50	347	
iso-Propyl–benzene	1	2		1	2·38	331	0·65
n-Butyl–benzene	1	1	3		2·75	426	
t-Butyl–benzene	1	3			2·22	343	0·70

obtained from the experiments of Sharbaugh, Crowe and Cox. Using equation (1), plots as shown in Fig. 1 can be drawn. Fig. 1(*a*) is obtained by considering molecules for which $n_3 = 1$ and $n_1 = 0$ and Fig. 1(*b*) by considering molecules in which $n_1 = n_2 = 0$. Both plots and especially the second are practically linear. A linear relationship has also been noted by the previous authors[2] but only for the normal alkyl benzenes. It can be associated with the progressive increase of CH_2 groups (Fig. 1*a*) in accordance with equation (1). Even more convincing is the excellent agreement found in Fig. 1(*b*) for the additive effect of methyl groups to the benzene ring, *t*-butyl benzene fitting easily into this scheme. By considering the slopes and intercepts, it is possible to obtain for the two plots respectively, kQ_2 and $k(Q_b + Q_3)$ and kQ_3, kQ_b. The cross-section values found are listed in

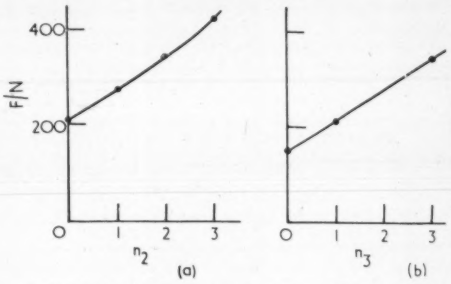

Fig. 1. Plots according to equation (1) for the alkyl-benzenes
(*a*) $n_1 = 0$, $n_3 = 1$.
(*b*) $n_1 = n_2 = 0$.

Table 2 in which kQ_1 has been calculated from the results for the one liquid *iso*-propyl benzene in Table 1. This latter value may be very doubtful therefore.

The estimate of kQ_b for the benzene ring, which is non-polar, can now be used to calculate the breakdown strength to be expected from static measurements which will be

Table 2. *Estimates of group cross-sections, based on microsecond pulse measurements of Sharbaugh, Crowe and Cox*[2]

	From alkyl benzenes	From alkanes: According to Ref. (1)	From alkanes: Branched chain alkanes alone
kQb	145		
kQ_3	65, 66	30	35·5
kQ_2	70	38, 42	35·5
kQ_1	56	30	19

Table 3. *Electric strength data for the silicones*

Silicone	n	Specific gravity 25°/25° C	Number of groups $n_0(Q_0)$	$n_3(Q_3)$	F (MV/cm) (d.c. value)	F/Nn_3	n_0/n_3
Dimer	0	0·761	1	6	0·84	30·0	0·167
Trimer	1	0·818	2	8	0·88	32·0	0·250
Tetramer	2	0·852	3	10	0·95	34·6	0·300
Pentamer	3	0·871	4	12	0·99	36·4	0·333

different from that from the pulse measurements made by Sharbaugh, Crowe and Cox. The different values of k required to account for the differing conditions of the pulse and static measurements have been discussed by Lewis[1] and the relative values of k obtained from alkane measurements would indicate that kQ_b for static breakdown measurements should be about two-thirds of that given in Table 2 or, in other words, the static breakdown value of benzene should be 1·1 MV/cm which is in excellent agreement with the mean value, 1·8 MV/cm found by Salvage[3] using techniques similar to Lewis. Lewis obtained 0·84 MV/cm which is not in agreement, but this low value has been considered unreliable.[4]

The new estimates of the cross-sections Q_3, Q_2 and Q_1 are considerably larger than those obtained from the alkane measurements of Crowe, Sharbaugh and Bragg[5] either by

the procedure adopted by Lewis[1] earlier, or by an alternative procedure of solving equation (1) simultaneously from data based on branched chain alkanes alone. Both sets of values for the alkanes are given in Table 2 and although these differ, showing that too great a significance cannot be attached to numerical estimates based on limited data, there is a definite distinction between the alkane and alkyl benzene values. It is necessary to offer some explanation of this difference.

Dipole and associated effects. Unlike the alkanes, the alkyl benzenes are polar although benzene itself has zero moment (Table 1). Addition of an alkyl radical to the carbon ring causes a modification of the electronic orbits of both the alkyl and aromatic parts of the molecule with an effective shift of negative charge to the ring, causing a dipole moment directed along the molecule. The modified electron configurations can be expected to result in changes in the collision cross-sections. Further, the electro-negativity of the alkyl group would increase the interaction with free electrons and would cause an increase in the cross-sections. The increase in dipole moment through the series suggests that the cross-sections might also change progressively. For instance, a CH_2 group might be expected to change its cross-section as its proximity to the benzene ring changes. At the same time each substitution can modify the ring structure so that Q_b will change. It is not unlikely that the departure from linearity in Fig. 1(*a*) is due to these causes, but a larger number of liquids would need to be investigated to show this effect clearly.

There is another factor which may contribute to the difference. The various estimates of Q_l in Table 2 are based on the assumption of a uniform distribution of collision centres which, in fact, may not be occurring in these liquids.

Local molecular arrangement is known to exist in the non-polar liquid alkanes in which the molecules pack with their long axes parallel, X-ray evidence having been furnished by Stewart[6, 7] and others. At room temperature the molecules are free to rotate about their long axes and the arrangement in a local grouping would be somewhat as illustrated in Fig. 2, the distances between molecules and between groups

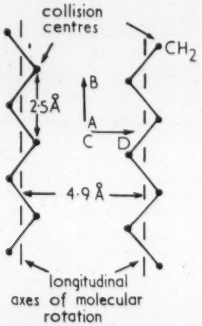

Fig. 2. Schematic arrangement of collision centres in a cybotactic group in a liquid *n*-alkane

within the molecules being approximate only. It is seen that in a local ordered region the density of alkyl collision centres is greater in the chain direction *AB* than at right-angles to it *CD*. An electron travelling in the direction *AB* experiences greater energy loss than when travelling along *CD*. If the molecules were arranged randomly, or if the local cybotactic groupings believed to exist have random orientations, then the estimated collision cross-sections for the alkanes in Table 2 are averaged in some way over all electron paths between the extremes *AB* and *CD*. In liquid benzene, the ring structures can also pack parallel to each other with a spacing of the order of 3·4 Å which is less than that for the alkanes. The attachment of a benzene ring to an alkyl group introduces a dipole effect which would upset the packing, producing an arrangement differing from that of a straight-chain alkane. This can change the effective mean free path of an electron from that assumed for equation (1).

If this picture is accepted, then we have for the alkyl benzenes a consistent set of results which can be interpreted in terms of group cross-sections with the benzene ring as a single group. On this basis it is significant that the pulse and static breakdown strengths of benzene can be related with a high degree of accuracy. The differences between cross-sections in the alkanes and alkyl benzenes can be reasonably resolved by including the polar nature of the latter, which will alter the electronic structure of the groups and, by changing the local molecular arrangements, will alter the electron mean free path also.

SILICONES

The dimethyl siloxane liquids have molecular structures similar to the straight-chain alkanes. The main skeleton consists of silicon-oxygen linkages rather than the carbon linkages of the straight-chain hydrocarbons and methyl side groups are added at the silicon atoms. Fig. 3 illustrates the

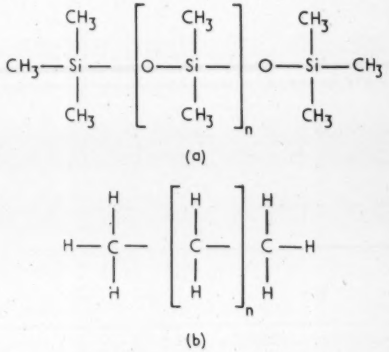

Fig. 3. Structural formulae for silicone and *n*-paraffin molecules. The length of the molecule is determined by the integer *n*

main features of the silicone and *n*-paraffin molecules. The important difference between the two structures is that, whereas the skeleton is well shielded by hydrogen atoms in the *n*-paraffins, the siloxane skeleton is comparatively exposed at the oxygen sites. The similarities illustrated in Fig. 3 make it interesting to compare the electric strengths of the siloxanes with corresponding alkanes on the basis of group cross-sections.

For this purpose, the d.c. electric strengths of the first four members of the dimethyl siloxane series were obtained under

conditions corresponding to those for d.c. measurements of the hydrocarbons previously reported.[4] Experiments had to be limited to the first four members because these were the only silicones easily obtainable with sufficient purity. The results of the measurements are given in Table 3. It is logical to compute the strengths on the basis of two cross-sections, Q_3 of the CH_3 group and Q_0 to be associated with the exposed oxygen atoms of the skeleton. The number of centres of each type is given in Table 3 and referring back to equation (1) we now write

$$F = kN(n_0Q_0 + n_3Q_3) \qquad (2)$$

The plots of F/Nn_3 against n_0/n_3 should be linear which is confirmed by Fig. 4. From the intercept and slope of the

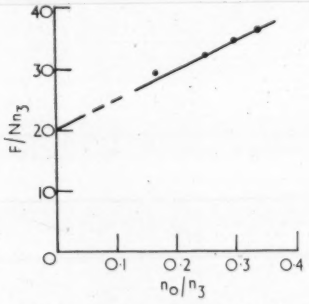

Fig. 4. Plot according to equation (2) for the silicones

curve, we obtain $kQ_3 = 20$ and $kQ_0 = 47{\cdot}5$. The value of kQ_3 is identical with that obtained earlier from the d.c. breakdown measurements on the alkanes[1] and must be considered as strong support for the breakdown model assumed. That the oxygen centre should have a comparatively large cross-section is possibly associated with the polar nature of the silicon–oxygen bond. In this connexion it is interesting to note that infra-red spectral analysis[8] has shown a strong band due to the silicon–oxygen linkage and a weaker one due to the carbon–hydrogen linkage of the CH_3 groups at a wavelength close to that found for the same vibration in the hydrocarbons. In Fig. 4 the dimer lies off of the linear plot. This exceptional behaviour of the dimer is typical and has been noticed in other physical properties of these silicones.

CYCLOHEXANE

Lastly, it is interesting to speculate on the possible behaviour of cyclohexane. The cyclohexane molecule C_6H_{12} has a closed hexagonal ring structure with a CH_2 group at each corner, and if we consider that each of these has a cross-section such that kQ_2 has the same value as that for the straight-chain hydrocarbons, then, using $kQ_2 = 27$ as found earlier,[1] the d.c. breakdown strength is 1·62 MV/cm which should be compared with the experimental value of 1·04 MV/cm.[4] The agreement is very poor and indicates that if the CH_2 groups are to be considered as separate collision centres in cyclohexane, then kQ_2 must be much smaller than the value above. This may indeed be the case, because both the molecular and liquid structures will not be the same in cyclohexane as in, say, *n*-hexane. The puckered ring structure of cyclohexane will pack differently from a straight-chain hydrocarbon, the latter being free to rotate about its long axis at normal temperatures.[7] Steric hindrance will also be effective in the case of the rigid cyclohexane, but hardly important for the chain molecules. This latter factor alone could cause the CH_2 group in cyclohexane to offer quite a different mean collision cross-section to an electron. Further ring compounds need to be investigated to give further evidence on this matter.

CONCLUSION

The evidence presented here supports that given in the earlier paper for a theory of electrical breakdown in liquid dielectrics based on electron energy loss by excitation of molecular vibrations. On the basis of independent molecular groups having characteristic collision cross-sections, measurements on a wide range of pure liquids subjected to both static and impulse stress can be correlated satisfactorily. More work is required, however, on dipole effects in polar liquids and also on ring compounds before a complete theory could be evolved. The present postulates yield a reasonable explanation of the behaviour of the bulk of the liquid away from the test electrodes.

ACKNOWLEDGEMENT

The author acknowledges the award of a Turner and Newall Fellowship by the University of London which has made this work possible.

REFERENCES

(1) Lewis, T. J. *J. Appl. Phys.*, **27**, p. 645 (1956) and references therein.
(2) Sharbaugh, A. H., Crowe, R. W., and Cox, E. B. *J. Appl. Phys.*, **27**, p. 806 (1956).
(3) Salvage, B. *Proc. Instn Elect. Engrs.*, **98**, p. 227 (1951).
(4) Lewis, T. J. *Proc. Instn Elect. Engrs.*, **100**, (IIa), p. 141 (1953).
(5) Crowe, R. W., Sharbaugh, A. H., and Bragg, J. K. *J. Appl. Phys.*, **25**, p. 1480 (1954).
(6) Stewart, G. W. *Phys. Rev.*, **31**, p. 174 (1928).
(7) Moore, R. J., Gibbs, P., and Eyring, H. *J. Phys. Chem.*, **57**, p. 172 (1953).
(8) Wright, N., and Hunter, M. J. *J. Amer. Chem. Soc.*, **69**, p. 803 (1947).

Photoelastic investigation of stresses in composite models with notches and holes

By HEIHACHI SHIMADA, B.Eng., Faculty of Engineering, Tohoku University, Sakurakoji, Sendi, Japan

[*Paper first received* 18 *February, and in final form* 23 *July*, 1957]

The object of the work described was to obtain information about the stresses in stiffened plastic bars. Tests were carried out under tension on a composite bar with a circular hole, and under bending, on a composite bar with a semicircular notch. The bars were of epoxy resin stiffened with duralumin strips. Graphs were obtained from which the stress-concentration factors of the stiffened models may be deduced from those in similar unstiffened models.

The stress concentrations in bars with notches and holes have been investigated by various authors, all of whom considered only bars of homogeneous material. The use of resins has been developed in recent years and stiffened resins are frequently employed in engineering structures, especially in aircraft.

In this investigation bars of epoxy resin are bonded to duralumin stringers by Araldite type 121, using the techniques developed by Mylonas and others.[1, 2] Bars stiffened along both edges and having a central circular hole were tested under tension, while bars with one stiffened edge having a semicircular notch in the other edge were tested under bending. The observations were made in a simple polariscope.

METHOD OF EXPERIMENTS

The resin used for the bars was epoxy resin KT-102, the stringers were of duralumin, and the bonding medium Araldite 121, which sets at room temperature. Very small initial bonding stresses were introduced.

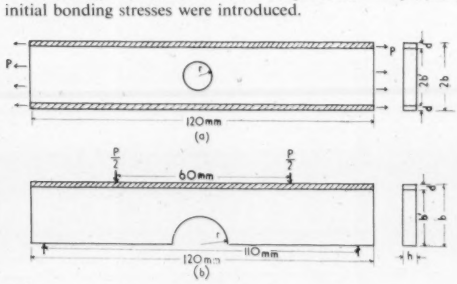

Fig. 1. The shapes of the models

The shapes and dimensions of the models used are shown in Figs. 1(*a*) and 1(*b*) and Table 1. The methods of applying the loads in the two types of model are shown in Fig. 2. Fig. 3 shows the isochromatic fringes in the loading ends.

In a model of the first type without a hole the disturbance due to application of the load extends to a distance of about $1{\cdot}0\,b$; in the second type the distance is $0{\cdot}75\,b$. These results indicate that the conditions in the "test" area are not influenced by end-loading conditions. Fig. 4 shows a part of the isochromatic fringes of the test pieces. The relative-retardations were measured from the isochromatic fringes, with fractional measurements by the Tardy method where necessary.

STRESSES IN TENSION BARS WITH HOLE

Fig. 5 shows values of the ratio σ/σ_n round the hole boundary in one model for a range of values of r/b,

where σ = tangential stress in model
σ_n = nominal mean applied stress = $P/2bh$
P = applied axial load
r = radius of hole
$2b$ = breadth of model
$\lambda = r/b$

In the figure the broken line gives the theoretical values for the unstiffened model with $\lambda = 0{\cdot}5$, taken from Howland.[3] Stresses on the minimum section are shown in Fig. 6.

In order to study the effect on the stress concentration factor K of the reinforcement, values of the ratio K/K_0 are considered, where K is the stress concentration factor in the composite model and K_0 is the factor in an unreinforced model having the same size of hole. For this comparison the values of K_0 used are taken from Howland.[3]

The results are shown in Fig. 7, K/K_0 being shown as a

Table 1. *Dimensions of test pieces*

(*a*) *First type* (*units in mm*)

No.	l_0	$2b$	$2b'$	d	h	r
1	120	21·01	20·01	0·50	5·92	3·00, 4·99, 7·00, 8·99, 9·50
2	120	22·01	20·01	1·00	5·80	3·00, 5·00, 7·01, 9·00, 9·50
3	120	24·01	20·01	2·00	5·75	3·00, 5·01, 7·00, 9·00, 9·50
4	120	22·02	20·02	1·00	5·81	3·00, 5·01, 7·00, 9·00, 9·50

(*b*) *Second type* (*units in mm*)

No.	l_0	b	b'	d	h	r
1	120	22·01	20·01	2·00	5·80	2·98, 6·01, 10·00, 14·01, 18·00, 19·00
2	120	21·17	20·17	1·00	5·88	3·00, 6·00, 10·00, 14·00, 18·01,
3	120	22·00	20·00	2·00	5·80	3·01, 6·01, 10·00, 14·00, 17·99, 18·99
4	120	21·00	20·02	1·00	5·88	3·00, 6·00, 10·00, 14·00, 18·00,

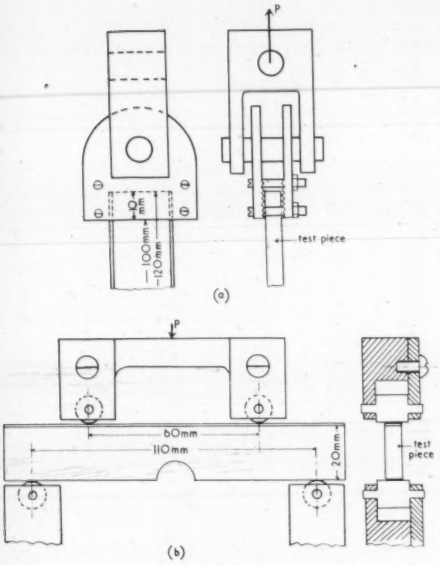

Fig. 2. The methods of applying the loads in the two types of model
(*a*) Pure tension; (*b*) pure bending.

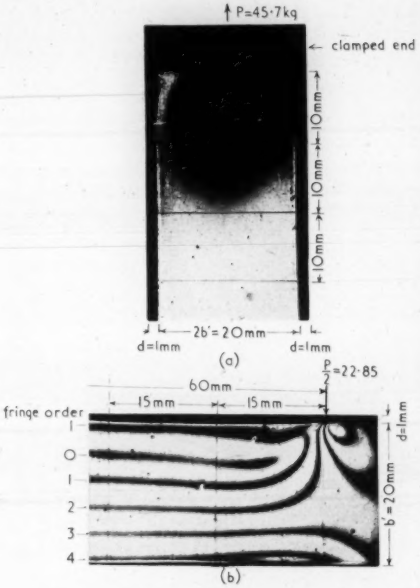

Fig. 3. The isochromatic fringes in the loading end
(*a*) Pure tension; (*b*) pure bending.

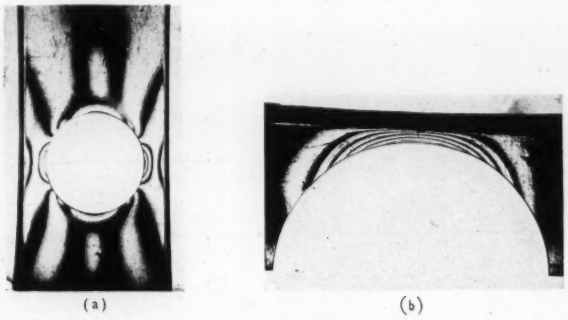

Fig. 4. The isochromatic fringes of the test pieces
(*a*) First type: $d/b' = 0{\cdot}05$, $\gamma = 0{\cdot}7$; (*b*) Second type: $d/b' = 0{\cdot}1$, $\sigma = 0{\cdot}9$.

function of $\gamma = r/b'$, for three values of d/b'. It is seen that K/K_0 is sensibly constant over the range $0 \leqslant \gamma \leqslant 0{\cdot}5$, but decreases rapidly as γ increases further and the influence of the reinforcement is felt directly at the point of stress concentration. When γ tends to $1{\cdot}0$, the strains in the duralumin and in the resin at the hole boundary will tend to equal values, and the value of K then tends to the ratio of the Young's moduli of resin and duralumin, namely $320/700 = 0{\cdot}0475$. This conclusion is confirmed by the experimental data as shown in Fig. 7. When γ tends to zero, we assume a limiting condition of uniform strain across resin and duralumin. Then if the total load is P, and if P_r and P_g are

the loads carried by resin and duralumin, and E_r and E_g the Young's moduli of resin and duralumin,

the strain $$\epsilon = \frac{P_r}{E_r 2b'h} = \frac{P_g}{E_g 2dh}$$

and since $$P = P_r + P_g$$

we have $$P_r/P = E_r B'/(E_g d + E_r B')$$

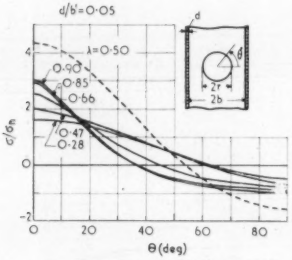

Fig. 5. Values of σ/σ_n round the hole boundary

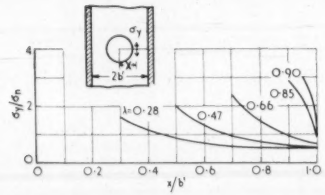

Fig. 6. Stresses on the minimum section for various values of λ

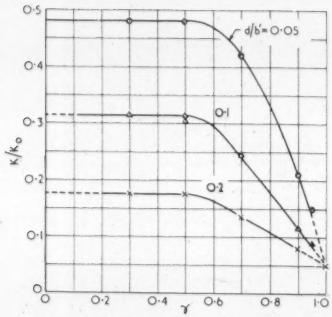

Fig. 7. Values of K/K_0 as a function γ

The ratio of stress concentration factors should then be equal to the ratio P_r/P. The values of this ratio for the models tested are shown in Table 2, and these agree very closely with the experimental values of K/K_0 for values of $\gamma \leqslant 0{\cdot}5$.

We may therefore consider that K/K_0 is defined for this range of γ by the formula given for P_r/P.

Table 2. *Calculated values of Pr/p for first type models*

d/b'	P_r/P
0·05	0·478
0·10	0·314
0·20	0·186

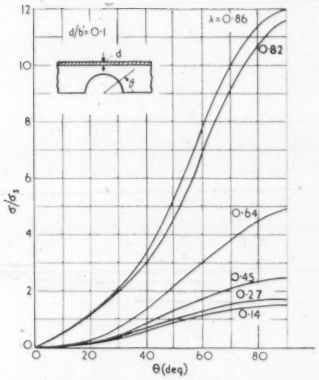

Fig. 8. Values of σ/σ_s on the boundary of the semi-circular notch in composite models, for $d/b' = 0{\cdot}1$

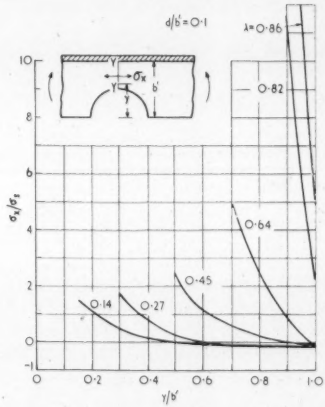

Fig. 9. Values of σ/σ_s on the minimum section for various values of λ

STRESSES IN BARS WITH SEMICIRCULAR NOTCHES IN BENDING

Fig. 8 shows values of σ/σ_s at points on the boundary of the semicircular notch in composite models for which $d/b' = 0{\cdot}1$, for a series of values of λ,

where σ = tangential stress of boundary
$\sigma_s = M/b^2h$
M = applied bending moment
$\lambda = r/b$

Fig. 9 shows values of σ_x/σ_s on the minimum section for various values of λ. The values of σ_x were obtained by use of the "shear-difference" method.[5]

As in the tension model, values of K/K_0 were calculated and these are shown in Fig. 10 as a function of $\gamma\ (= r/b')$.

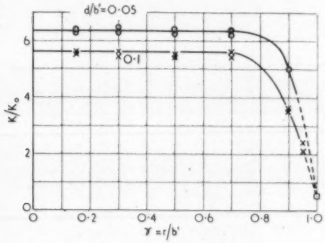

Fig. 10. *Values of K/K_0 as a function γ, for $d/b' = 0{\cdot}05$ and $0{\cdot}1$*

The ratio in this case is found to be sensibly constant for the range $0 \leq \gamma \leq 0{\cdot}7$, and to fall rapidly as γ increases further. The values of K_0 used were taken from Leven and Frocht[6] and others.[7, 8] As in the previous case, when γ tends to unity the ratio K/K_0 tends to the ratio of the Young's moduli. When γ tends to zero, the ratio tends to the value of σ_c/σ_m, where σ_c is the boundary stress in the unnotched composite model, and σ_m that in the unstiffened model. The calculation of σ_c is by the method given by Timoshenko,[9] and values of σ_c/σ_m for the two models tested are given in Table 3.

Table 3. *Compare with σc/σm and K/Ko for second type models*

d/b'	σ_c/σ_m (calculation)	$K/K_0 (0 \leq \gamma \leq 0{\cdot}7)$ (experiment)
0·05	0·635	0·630
0·10	0·560	0·555

From the results shown it can be seen that there is good agreement between theoretical and experimental values for values of γ less than 0·7. For this range therefore the stress concentrations in the composite model may be deduced from those in an unstiffened model by using Timoshenko's result for the unnotched bar.

ACKNOWLEDGEMENT

The author wishes to express his thanks to Prof. Emeritus Seiichi Higuchi of the Tohoku University for his advice and encouragement throughout the progress of the investigation.

REFERENCES

(1) D'Agostino, J., Drucker, D. C., Liu, C. K., and Mylonas, C. *Proc. Soc. Exper. Stress Anal.*, **12**, p. 123 (1955).
(2) Mylonas, C. *Proc. Soc. Exper. Stress Anal.*, **12**, p. 129 (1955).
(3) Howland, R. C. J. *Phil. Trans A*, **229**, p. 67 (1930).
(4) Timoshenko, S. *Strength of Materials*, pt. 1 (London: Macmillan and Co., 1955).
(5) Frocht, M. M. *Photoelasticity*. Vol. 1, p. 252 (London: Chapman and Hall Ltd., 1949).
(6) Leven, M. M., and Frocht, M. M. *Proc. Soc. Exper. Stress Anal.*, **11**, p. 179 (1954).
(7) Tamate, O. *Technol. Rep. Tohoku Univ.*, **16**, p. 34 (1952).
(8) Nishida, M. *Soc. Pap. Inst. Phys. and Res. (Tokyo)*, **23**, No. 3 and 4 (1944).
(9) Timoshenko, S. *Strength of Materials*, pt. 2 (London: Macmillan and Co., 1955).

The effect of specimen diameter on the straining of a cylindrical load-cell

By J. F. W. Bishop, Ph.D., and M. T. Watkins, B.Sc., A.Inst.P., Mechanical Engineering Research Laboratory, East Kilbride, Glasgow

[*Paper received* 5 *April*, 1957]

Theoretical and experimental results on the surface axial distortion of a cylindrical load-cell loaded by circular punches of differing diameters are given. It is concluded that a height to diameter ratio of about 7 : 4 is required to eliminate end effects and the effect of specimen diameter on the loads recorded near its centre.

The problem considered in this paper arose in an experimental investigation into the loads occurring in the drop-forging of (short) right-circular cylindrical specimens. The specimen is placed centrally on top of a cylindrical column or load-cell, to the periphery of which electrical resistance strain gauges are attached. It is then given a heavy plastic deformation under an impact load and the (elastic) distortion of the column obtained from photographic records of the behaviour of the strain gauges. The problem is to interpret the (axial) strain at the surface of the load-cell in terms of load. Since the specimen undergoes heavy plastic deformation, the load-cell is loaded over an area which is initially the cross-sectional area of the specimen and which gets continuously larger until it is the final area of the distorted specimen. This problem is not, of course, essentially one of dynamic loading. In this paper the quasi-static loading problem is considered in which the complications introduced by impulsive forces are absent.

PREVIOUS WORK

From Saint Venant's principle it is known that the statically equivalent forces and not the detailed distribution of loads determine elastic deformation except in the reasonably close neighbourhood of constraints, etc. This fact is demonstrated by Frocht's photoelastic method.[1] His examples of a column under point load (p. 22), a disk compressed by a pin and a flat plate at opposite ends of a diameter (p. 27), and a "semi-infinite" plate under different types of edge loading (pp. 42, 69, 74) are elegant and conclusive. The question of interest in the current investigation is how *far* from the point of application of the load it is necessary to be before the details of the loading become unimportant in so far as the loads measured are concerned.

The problem of elastic deformation in circular cylinders has received considerable attention in the literature. Although the problem treated in this paper does not appear to have been considered, many of the results obtained have a direct bearing on it. Filon[2] has considered the problem of a cylinder compressed between rigid dies where the frictional constraint at the ends is just large enough to inhibit relative motion between the perimeter of the end of the bar and the dies. With a zero constraint at the ends the stress and axial strain would be uniform throughout the bar. The surface axial strains in a short bar of length/diameter ratio (L/D) approximately unity as a multiple of the strain produced in a uniform compression under the same load is shown in Fig. 1. It is seen that the strain is sensibly uniform at the centre of the bar with a peak at the ends. The uniform strain is approximately 90% of its value without end constraint. In long bars the effect of end constraint will be similar with the non-uniform strain confined to the neighbourhood of the ends. Other types of end constraint with rigid dies can be obtained by superposition of the two types mentioned. The effect of the difference between constant displacement and constant pressure at a die can be inferred from the photoelastic patterns given by Frocht (Ref. 1, pp. 69, 74). It can be seen there

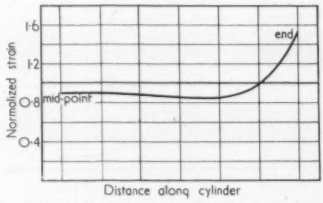

Fig. 1. Surface axial strain in a short cylindrical specimen (Filon)

that, except in the immediate neighbourhood of the die, the effect is a second-order one in relation to the stresses due to the total load. It would therefore appear that, for all practical purposes, the problem can be reduced to that of finding the deformation in a circular cylinder loaded uniformly over one end and uniformly over a smaller concentric circular area at the other.

The work of Sims, Place and Morley has a bearing on the problem considered. They were interested in the design and performance of an industrial load-meter for use in rolling mills. The L/D ratio was of order unity and they investigated the effects of varying loading area and eccentricity of loading. Their results will be considered later in this paper.

EXPERIMENTAL WORK

In the current investigation the surface axial strains in a cylinder of L/D ratio 2·5 were investigated for three different loading areas and two types of end constraint. The effect of eccentricity of loading was examined.

A tool-steel cylinder 10 in. long and 4 in. in diameter was ground all over and lapped at the ends. This was mounted on a 10 in. diameter ground tool-steel block and loaded through punches of 1 and 2 in. diameter and through an over-hanging punch. The loads were applied to the punches in a fifty-ton hydraulic press through a spherical head.

In order to obtain a comprehensive picture of the strain distribution in the load-cell, twenty-two pairs of electrical resistance strain gauges of half-inch gauge length were used. Four gauges were mounted symmetrically on the curved surface at the top, centre and bottom of the load-cell and the

remaining sixteen pairs mounted spirally at opposite ends of diameters at equal intervals along the length. Temperature-compensating gauges were mounted on an (unstressed) block placed adjacent to the load-cell. The out-of-balance method of measuring strain was employed since it had advantages of simplicity and speed of measurement. A comprehensive series of tests was conducted to determine the reproducibility of the experimental technique. The order of reproducibility determined for a series of tests repeated at different times for each diameter tool was $\pm 3\%$. Axiality of loading was checked from the strains recorded on the four gauges at the top of the block in the earlier tests until the effects of eccentricity had been investigated.

The results for direct contact between the load-cell and the punch and base platen are given in Fig. 2. It will be seen that

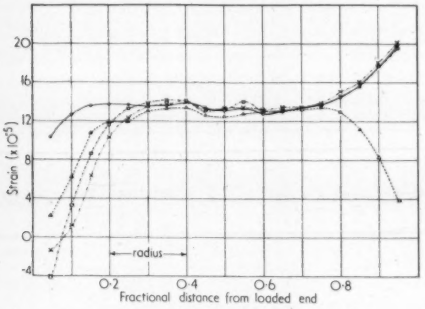

Fig. 2. Experimental surface axial strains

○ = 4 in. punch, direct contact.
□ = 2 in. punch, direct contact.
× = 1 in. punch, direct contact.
△ = 4 in. punch, rubber mats at ends of cell.

the strains differ markedly up to nearly a diameter from the loaded end and then are sensibly equal. At the supported end the effect of end constraint results in a peak axial strain.

A series of tests was carried out with an overhanging platen and stiff rubber mats $\frac{1}{4}$ in. thick interposed at the ends of the load-cell. The mean results for two series are also given in Fig. 2. The effect of end-support on the strains is clearly demonstrated, although the strain in the centre is virtually unaltered.

To examine the effect of eccentricity of loading, the mean strain registered on opposite ends of the diameter passing through the centre of a loaded, off-set punch was recorded. The method of loading and the measured strains are shown in Figs. 3 and 4. Also shown are the strains due to axial

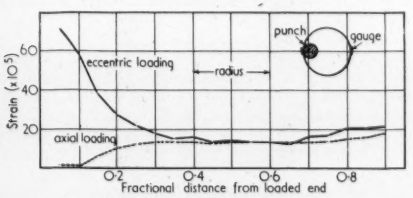

Fig. 3. Surface axial strains under eccentric loading

loading through punches of the same diameter. It can be seen that even with a 1 in. diameter punch located at the extremity of the diameter, the effect of this gross eccentricity on the mean strain is negligible at distances greater than a diameter from the loaded end.

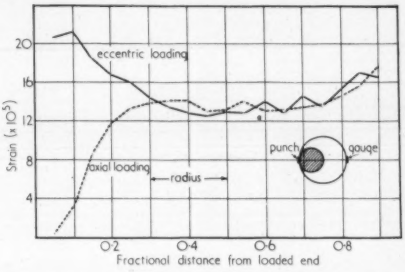

Fig. 4. Surface axial strains under eccentric loading

THEORETICAL INVESTIGATION

Southwell[4] has shown how problems of axially-symmetric elastic deformation can be formulated in terms of two partial differential equations involving two stress functions. The stresses and strains can be obtained from these functions by a single partial differentiation. This formulism is very convenient for a relaxation solution as shown, for example, by Allen, Fox and Southwell.[5] Details of the method used for the current investigation can be found in Allen.[6]

Calculations were made for uniformly distributed applied loads and supporting forces for a block of L/D ratio 2·5. The punch radius to block radius R was taken as 0·25, 0·5 and 0·75. The results are given in Fig. 5, with the strain

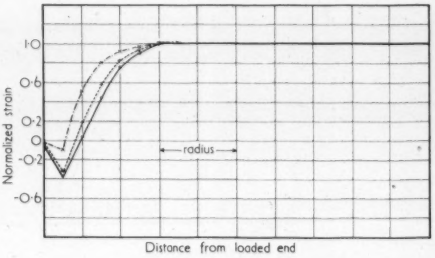

Fig. 5. Calculated surface axial strains

○, $R = 0{\cdot}25$.
+, $R = 0{\cdot}50$.
×, $R = 0{\cdot}75$.

shown as a multiple of the strain due to a uniform stress corresponding to the same load. The relaxation solution was continued until the derived forces on the curved surface (known to be zero) were not more than 1% of the uniform supporting pressure. The sharp knee in the curves near the loaded end is not a real effect and arises from the difference method of solution. The first pairs of points are joined by straight lines since curves could only be put in arbitrarily.

DISCUSSION OF RESULTS

The results obtained in the last section are in close agreement with the experimental results. Sims, Place and Morley found that, with gauges located three-quarters of the way down the cell from the loaded end, there was virtually no effect of punch diameter for an L/D ratio of 1·095, but a 10% variation in strain in changing the diameter from 1 to 4 in. (the cell was 4 in. diameter) for $L/D = 0{\cdot}906$. This agrees very closely with the theoretical results obtained here. The plane stress photoelastic results of Frocht (Ref. 1, p. 30) are qualitatively in agreement with the results obtained. Fisher[7] has examined the deformation of a cylindrical strut using the photoelastic method. For uniformity of *stress* (as opposed to constant axial strain) he finds a length to diameter ratio of about 9 to 4 is required.

On the basis of all the results considered it would appear that the minimum L/D ratio permissible is 7/4 with the gauges mounted one diameter from the loaded end. This location allows for localized loading due to small punches with a more uniform distribution of forces at the supporting end. For ratios larger than this the effect of loading area, support conditions and eccentricity of loading should be negligible as far as the strains measured are concerned and having regard to the reproducibility of the technique.

ACKNOWLEDGEMENTS

The authors wish to acknowledge the assistance of Messrs. F. P. Bolger and T. R. Cook with the experimental work. The work described forms part of the research programme of the Mechanical Engineering Research Board of the Department of Scientific and Industrial Research. It was carried out in the Plasticity Division of the Mechanical Engineering Research Laboratory and is published by permission of the Director.

REFERENCES

(1) FROCHT, M. M. *Photoelasticity* (New York: J. Wiley and Sons Inc., 1949).
(2) FILON, L. N. G. *Phil. Trans Roy. Soc. A*, **198**, p. 147 (1902).
(3) SIMS, R. M., PLACE, J. A., and MORLEY, A. D. (Report MW/A/15/50 (London: British Iron and Steel Research Association, 1950).
(4) SOUTHWELL, R. V. *Proc. Roy. Soc. A*, **180**, p. 367 (1942).
(5) ALLEN, D. N. de G., FOX, L., and SOUTHWELL, R. V. *Phil. Trans Roy. Soc. A*, **239**, p. 501 (1945).
(6) ALLEN, D. N. de G. *Relaxation methods* (London: McGraw-Hill, 1954).
(7) FISHER, W. A. P. A.R.C., R and M, No. 2532 (1951).

Determination of density of liquids under elevated gas pressure

By K. GOLDMAN, B.Sc., British Oxygen Research and Development Ltd., London.

[*Paper first received* 14 *March, and in final form* 15 *May*, 1957]

A new method of density measurement using an open-end hydrometer has been developed for liquids under elevated gas pressure. It has been successfully employed for determining densities of high vacuum oil (Apiezon A), saturated with nitrogen, at 25° C in the pressure range 1–300 atm. The estimated accuracy of determination was better than 1 in 1000.

LIST OF SYMBOLS

m = weight of the hydrometer
ρ_L = density of oil at pressure P and temperature T
ρ_g = density of nitrogen at P and T
σ = surface tension of oil
θ = angle of contact of oil
V = volume displaced by main body of the hydrometer
v = volume displaced by 1 cm of the stem
l = total length of the stem
l_1 = length of the stem immersed in oil
l_2 = length of the stem above the surface of oil ($l_2 = l - l_1$)
v_2 = volume of aluminium alloy used in the main body of the hydrometer
v_3 = volume of steel used in 1 cm of the stem
r = outer radius of the stem

INTRODUCTION

In the work undertaken to determine the viscosity of gases at high pressures by a transpiration method, the pressure difference across the capillary tubes was measured by means of a manometer filled with high vacuum oil. Since no data of the change of density of the nitrogen-saturated oil with pressure were available, subsidiary experiments for their determination were carried out.

THEORETICAL

Under isothermal conditions, two factors can affect the density of a liquid: (1) compressibility of the liquid; and if pressure is applied through the gas phase, (2) solubility of the gas in the liquid.

In the case of Apiezon A oil the effect of both factors is not very large at moderate pressures (1–300 atm) and a sensitive method was therefore required to determine the variation of the oil density with pressure. The open-end hydrometer was then adopted. According to our literature survey, this method has never been used before.

All forces acting downwards are considered positive and those acting upwards are negative.

(1) Force due to gravity: m. (2) Surface tension acting on the stem: $2\pi r\sigma\cos\theta$. (3) Buoyancy: $-\rho_L(V + l_1 v) + \rho_g[(V - v_2) + l_1(v - v_3) - l_2 v_3]$.

It is assumed that the materials used in making the hydrometer are incompressible.

In equilibrium we have

$$m + 2\pi r\sigma\cos\theta - \rho_L(V + l_1 v) + \rho_g[(V - v_2) + l_1(v - v_3) - l_2 v_3] = 0$$

hence
$$\rho_L - \rho_g = \frac{m + 2\pi r\sigma\cos\theta - \rho_g(v_2 + l v_3)}{V + l_1 v} \qquad (1)$$

Equation (1) determines the differential density of oil and nitrogen for the viscosity calculations. As the density of nitrogen is known, the absolute density of nitrogen-saturated oil can be readily obtained.

EXPERIMENTAL

Hydrometer design and construction. The open-end hydrometer differs from the ordinary hydrometer by the fact that the pressure inside and outside is equalized. This was essential for our high pressure measurements where a light thin-wall hydrometer (which would float in the oil) was the appropriate type. This would not be possible in the case of the closed-end hydrometer made to withstand high pressure, i.e. robust and strong. The hydrometer is depicted in Fig. 1.

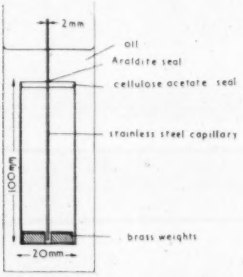

Fig. 1. Diagram of open-end hydrometer

The main body of the hydrometer was made of aluminium alloy. The neck was made of fine stainless steel tube passing through the centre of a screwed cap and cemented to it with Araldite. Brass weights were placed inside the hydrometer, at the bottom. In order to prevent any leakage through the threaded cap, the thead was covered with a thin film of cellulose acetate and then the cap was screwed up. After the cellulose had dried, the hydrometer was weighted and placed in a glass vessel containing the investigated oil. The glass vessel was then accommodated in a stainless steel enclosure which had a row of sight glasses along its whole height. The enclosure formed a part of the viscosity measurement apparatus and was capable of withstanding a pressure of 300 atm.

Measurement techniques. The steel enclosure and the gas reservoir were situated in a tank filled with water (Fig. 2) and the temperature maintained at approximately 25° C by means of a bimetal strip regulator. The water was stirred by a fast circulating pump and the variation of water temperature was $\pm 0{\cdot}1$° C. The temperature within the enclosure was measured by a platinum resistance thermometer placed close to the vessel containing the oil. The temperature variation within the enclosure was not more than $\pm 0{\cdot}02$° C.

The apparatus was first evacuated and then filled with nitrogen, the nitrogen pressure being raised slowly until the hydrometer submerged. The pressure balance valve was then opened. When the oil temperature became steady, the pressure was slightly adjusted by opening the fine control valves (1) and (2), depending whether an increase or decrease of pressure was required, until the hydrometer was floating with its stem partly immersed in oil. The travelling microscope was focused on either the top or the bottom of the hydrometer, depending upon the convenient position seen through the windows, and its position measured. The hydrometer was illuminated by an electric lamp placed under

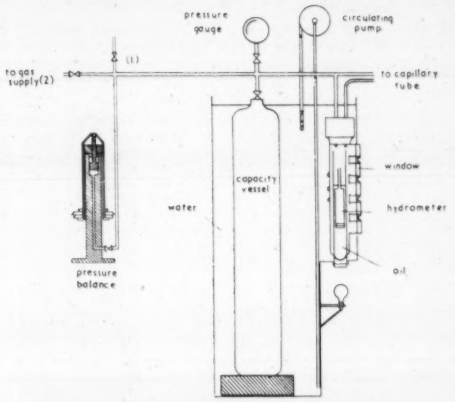

Fig. 2. Diagram of viscosity measurement apparatus

the bottom window, When the pressure was raised initially, it was found necessary to operate above the pressure actually required for the partial immersion of the stem of the hydrometer in order to overcome the effect of surface tension.

Preliminary experiment has shown that the oil became saturated with the dissolved gas within one hour. However, in the course of the main experiment, in order to allow at least three measurements of different stem immersion to be taken, the oil was kept under approximately the same pressure and temperature for several hours. A typical example of the results obtained for one pressure is demonstrated in Table 1. The time given in the table is only approximate and is measured from the final adjustment of the pressure.

Table 1. *Saturation of oil with gas*

Time (*h*)	*Temperature* (° C)	*Pressure* (*atm*)	$(\rho_L)_{25°\,C}$ (*g*/*cm*³)
$\frac{1}{2}$	25·02	124·9	0·8594
1	25·02	124·7	0·8593
$1\frac{1}{2}$	25·02	124·7	0·8593
2	25·02	124·5	0·8593
3	25·00	122·8	0·8583

Calibration. The hydrometer was calibrated by floating it in water in the same apparatus at atmospheric pressure applying equation (1). The calibration was repeated at several temperatures. The accuracy of determination of the main displacement of the hydrometer is shown in Table 2.

Table 2. *Volume of the hydrometer*

Temperature *T* (°C)	*Volume V at temperature T* (*cm*³)	*Volume V at 25° C* (*cm*³)
27·80	29·1197	29·058
26·95	29·1158	29·057
28·16	29·1214	29·059

mean = 29·058 cm³.

The stem of the hydrometer was calibrated by inserting weighed segments of wire through its open end and measuring the depth of immersion when it was stationary. The volume of water displaced by 1 cm of the stem was 0·029 cm^3.

The surface tension of the oil was determined by a capillary rise method, the mean of several determinations being 29 dyn/cm. Since the value of surface tension was used only in a small correction term, it was unnecessary to determine it very accurately. The angle of contact between glass and oil and also between steel and oil was assumed to be zero. The density of high pressure nitrogen was obtained from the data of Michels and others.[1–3]

RESULTS AND DISCUSSION

The experimental results of the density measurements are given in Table 3.

Table 3. *Variation of oil density with pressure*

Pressure (atm)	*Temperature (° C)*	$(\rho_L - \rho_g)$ 25° C (g/cm^3)	(ρ_L) 25° C (g/cm^3)
140·0	25·19	0·7041	0·8612
106·5	25·09	0·7376	0·8590
44·3	25·00	0·8046	0·8556
25·5	25·09	0·8258	0·8548
74·3	24·95	0·7721	0·8574
124·7	25·02	0·7183	0·8593
292·7	25·07	0·5732	0·8677
196·6	25·02	0·6496	0·8634
1·0	24·94	0·8542	0·8554
9·1	24·62	0·8556	0·8552

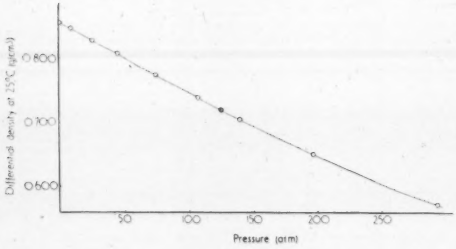

Fig. 3. Differential density of Apiezon A oil and nitrogen at 25° C at pressures of from 1 to 300 atm.

Both the differential density $(\rho_L - \rho_g)$ 25° C and the absolute density (ρ_L) 25° C of nitrogen-saturated oil were plotted against the pressure (Figs. 3 and 4).

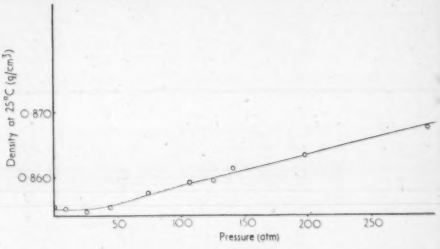

Fig. 4. Density of Apiezon A oil at 25° C at pressures of from 1 to 300 atm.

There are two causes of the change in oil density: (*a*) compressibility of oil, and (*b*) solubility of nitrogen in the oil.

As the pressure is raised, the oil becomes more compressed and also more gas is dissolved in it. It is believed that the dissolved gas has a swelling effect on oil and, therefore, diminishes somewhat its density. This is supported by the flattening of the density-pressure curve (Fig. 4) at the lower pressure range (1–50 atm.) At comparatively low pressures the effect of compressibility is small and the swelling due to the dissolved gas is more pronounced. As the pressure goes up, the compressibility becomes the dominant factor.

It is believed that, although the open-end hydrometer method of density measurements is not a rapid one, it is capable of high accuracy. The calculated overall accuracy is better than 1 in 1000.

ACKNOWLEDGEMENT

The author wishes to thank the Directors of British Oxygen Research and Development Ltd. for permission to publish this paper.

REFERENCES

(1) MICHELS, WOUTERS and DE BOER. *Physica*, **1**, p. 587 (1934).
(2) MICHELS, WOUTERS and DE BOER. *Physica*, **3**, p. 585 (1936).
(3) OTTO, MICHELS and WOUTERS. *Phys. Z.*, **35**, p. 97 (1934).

New books

Particulate clouds: dusts, smokes and mists. By H. L. GREEN and W. R. LANE. (London: E. and F. N. Spon Ltd., 1957.) Pp. xix + 425. Price 70*s*.

It is not generally realized by industrialists or by academic and research workers how much is known about the properties and behaviour of gas-borne particles of solids and liquids and that the basic phenomena may enter into many different processes. For example the theory of the impaction of particles on obstacles, which was first investigated in connexion with the icing of aircraft, is relevant to the effectiveness of insecticidal aerosols, the removal of smokes and dusts by filters, the capture of wind-borne pollen, and the growth of raindrops. A consequence has been the investigation by workers in one field of problems solved in another field. This book on the properties and behaviour of gas-borne suspensions of particles, which contains a critical and selective account of the literature, should do much to prevent unnecessary duplication of research effort.

The first part is concerned with the physics of particles and contains chapters dealing with: the production of particulate clouds; their physical characteristics, the scattering and absorption of light; coagulation and adhesion; and sedimentation, impaction and diffusion. The treatment is from the theoretical point of view, but the authors have been at pains to ensure a high degree of clarity in their exposition. The first part ends with chapters on the sampling and sizing of gas-borne particles and on diffusion in the atmosphere.

The industrial and environmental aspects are discussed in Part II. The chapter on collection of smokes and dusts by cyclones, filters and electrostatic precipitators, is the least successful because there is here a wider divergence between the industrial plant and the model system that can be treated theoretically. The last four chapters discuss: health hazards including fire and explosion hazards; atmospheric pollution; aerosols in nature; and uses of particulate clouds including inhalation therapy, screening and signal smokes and agriculture and pest control.

The book deserves to be widely read and indeed would fail in its purpose if it were not studied by workers concerned in any way with solids or liquids in particulate form.

P. G. W. HAWKSLEY

The measurement of soil properties in the triaxial test. By A. W. BISHOP and D. J. HENKEL. (London: Edward Arnold Ltd., 1957.) Pp. viii + 190. Price 70*s*.

Important engineering data on soil stability and deformation can be obtained from a triaxial test in the laboratory, the behaviour of a cylindrical specimen being observed in a cell where it is subjected to radial fluid pressure while another load is applied along the axis of the cylinder. Bishop and Henkel, writing for fellow experts, have set out the various possible forms of test and the practical details that need attention to obtain satisfactory results.

The book carries its own internal standard. For those to whom the Mohr stress circle is a familiar concept and working tool this survey of techniques will be very valuable, not least in the multiplicity and clarity of its diagrams. For others who may want an entry to the fascinating field of classical physics applied to an awkward raw material, some other gate is advised.

H. L. PENMAN

Magnesium casting technology. By A. W. BRACE and F. A. ALLEN. (London: Chapman and Hall, Ltd., 1957.) Pp. 174. Price 21*s*.

The unique combination of lightness with strength attainable with the alloys of magnesium must commend their use for many applications over the whole field of scientific instrument manufacture, and indeed for camera components and binocular casings (to take two examples) the advantages to be gained are already well recognized.

This book is primarily an exposition of the principles and practice of producing magnesium alloy castings, aimed at foundrymen, but it will at the same time prove readable by, and instructive to, instrument designers who wish to make the most effective use of a still somewhat unfamiliar range of light alloys.

G. L. J. BAILEY

Einführung in die physik der magnetischen werkstoffe. By KARL M. KOCH and W. JELLINGHAUS. (Vienna: Franz Deuticke, 1957.) Pp. vii + 208. Price 52*s*. (approx.).

This book, which is one of a series dealing with the physics of materials of electrotechnical interest, is a scholarly little work which gives, within a modest compass, an admirable summary of modern magnetism. It could be very useful to the advanced student and young graduate. The first chapter deals with formal classical theory and the second with atomic theory, including descriptions of antiferromagnetism and ferrimagnetism. In the next four chapters the process of magnetization, domain theory, anisotropy, alternating current properties and magnetic resonance are all treated very well within the space available, and there is a useful little excursion into the metallurgy of some of the simpler two-component systems. The last chapter deals with measurements of technical magnetic properties.

The book is set out in c.g.s. units, but the relevant aspects of the m.k.s. system are well summarized in an Appendix.

N. F. ASTBURY

Propagation des ondes electromagnetiques de haute frequence. By J. Ortusi. (Paris: Societe Francaise de Documentation Electronique, 1957.) Pp. 320. Price 3100 fr.

This book on high frequency wave propagation is the first volume in a new series of monographs on radio under the editorship of Dr. M. Ponte. It is divided into five main sections, the first of which establishes the basic theory for the propagation of electromagnetic energy. Part two deals with guided waves in isotropic media and is followed by a section on propagation in ferrites. The fourth part covers the effects of branches and discontinuities in guides, and the final section discusses propagation around the earth's surface. Although this is a fairly advanced text it is written clearly, attractively and authoritatively, with frequent appeal to basic principles. The rather large list of errata on page 313 might have been placed more prominently.

M. R. GAVIN

Radiation shielding. By B. T. PRICE, C. C. HORTON and K. T. SPINNEY. (London: Pergamon Press Ltd., 1957.) Pp. ix + 350. Price 60*s*.

This is a very impressive work. The authors have crammed a large amount of information into a moderate sized book and the claim inside the dust cover that this is the most

comprehensive reference work on the subject so far published is probably justified. It is, however, only natural that an engineer should feel that there is too much emphasis on the physics of the subject and not enough on the engineering aspects.

Understandably there are one or two errors. In Fig. 2.10.1, for instance, there is no curve for U_{233} although it appears in the caption. And in table 3.6.2 the first reaction is wrongly printed. It is a pity that some of the graphs are rather crowded and on a small scale. On the other hand, the list of references is magnificent and leaves the reader no reason to doubt that the book took about three years to produce. It should become an essential companion for anyone who works in the field of radiation shielding.

W. BONSALL

Theoretische physik. By F. HUND. (Stuttgart: B. G. Teubner, 1957.) Pp. x + 364. Price DM. 29.40.

This work has much the same scope as the book by Becker–Sauter noticed above, but tends to have a slightly more experimental bias. The treatment of electrostatics is fuller and there are four pages on experimental magnetism. There is, however, in the present work, some one hundred and fifty pages on optics and a fairly full treatment of elementary relativity theory.

In both works the printing and the preparation of diagrams conform with the normal German standards, i.e. they are very good indeed.

J. D. CRAGGS

Theorie der elektrizität. By R. BECKER and F. SAUTER. (Stuttgart: B. G. Teubner, 1957.) Pp. 302. Price DM. 29.

This work follows on the famous book by Abraham and Becker of nearly 30 years ago, which was, and still is, a standard work for European connoisseurs of textbooks on electricity. The present work, as we should therefore expect, gives a mathematical account to advanced degree standard, and it embraces firstly a general introduction (42 pp.) to vectors, vector fields and tensors (the latter are used in many places later in the book), then a full classical treatment of electrostatics (some 57 pp.), electric currents and magnetic fields (some 120 pp.), and relativity theory (60 pp.). There are collections of questions and answers, and a summary of formulae with commonly used equations.

This scholarly work should be read by students and teachers in British universities. But can they and will it?

J. D. CRAGGS

Energy transfer in polyacene solid solutions: a guide to the literature to the end of 1956. By F. R. LIPSETT. (Ottawa: National Research Council, 1957.) Pp. 64. Price 50*c*.

This useful guide to the literature on the transfer of absorbed energy of radiation from "host" to "impurity" molecules in the polacenes is collected under six main headings: books; theories on spectra; experiments on spectra; energy transfer; related subjects and experimental. The volume also contains thirty-three sub-headings. A large number of the references deal with subjects related to energy transfer rather than with the transfer process itself, i.e. molecular structure and photo- and semi-conduction, and a brief text is given which outlines the history of research on energy transfer and current views on the transfer process, as well as suggesting starting-points in reading for research workers new to the field.

Vector analysis. By LOUIS BRAND. (New York: John Wiley and Sons Inc.; London: Messrs. Chapman and Hall Ltd., 1957.) Pp. xiii + 282. Price 48*s*.

Starting from the vector as a directed line segment, the subject is developed as far as is required in a course up to first degree level.

Five chapters deal with general theory as far as the fundamental integral theorems of Gauss, Green and Stokes. The use of dyadics enables some of the later results to be expressed very neatly. Three chapters then illustrate the application to dynamics, fluid mechanics, and electrodynamics. A return to theory is made in the final chapter which introduces abstract vector spaces.

The treatment is clear with plenty of examples and this book is strongly recommended.

A. W. GILLIES

Journal of Scientific Instruments

Contents of the January issue

SPECIAL ARTICLE

Silicones and their applications. By J. Ames.

ORIGINAL CONTRIBUTIONS

Papers

A rhodium-plated kata thermometer for measuring true air velocity. By Walter Koch and Deborah Kaplan.
A 20 ft Ebert grating spectrograph. By G. W. King.
Correction due to aperture in transmission interference microscopes. By E. Ingelstam and L. P. Johansson.
A total-absorption Čerenkov counter for photons of about 100 MeV energy. By J. Moffatt and M. W. Stringfellow.
A d.c. and square wave a.c. resistance and voltage comparator. By T. M. Dauphinee and H. Preston-Thomas.
A gas target and nuclear plate camera. By D. L. Booth, R. S. Hill, F. V. Price, D. Roaf and G. L. Salmon.
Automatic temperature programming and recording for a platinum–rhodium furnace. By J. M. Cutter and R. Derry.
An apparatus for the determination of dynamic elastic moduli at low strains. By E. V. Vernon.
A note on progressive codes for positive and negative indication. By W. T. Bane.

Laboratory and workshop notes

A stabilizer for large sub-standard lamps. By A. W. S. Tarrant.
A precise reference inductor. By D. Gugan.
Injecting trace impurities into a gas stream. By P. Hersch and J. E. Whittle.
Grinding hemispheres of germanium and silicon. By D. B. Gasson.

NOTES AND NEWS

Correspondence

Lattice parameter determination from broad diffraction lines. From E. R. Pike.
A scale for solid-stem thermometers. From E. Greil.
The a.c. properties of resistors. From A. C. Lynch; G. H. Rayner and L. H. Ford.
A method of preparing and filling plastic tubes for specimens for X-ray powder photographs. From W. E. Armstrong and R. J. Davis.

New instruments, materials and tools

THIS JOURNAL is produced monthly by The Institute of Physics, in London. It deals with all branches of applied physics (including theory and technique).

All rights reserved. Responsibility for the statements contained herein attaches only to the writers.

EDITORIAL MATTER. Communications concerning editorial matter should be addressed to the Editor, The Institute of Physics, 47 Belgrave Square, London, S.W.1. (*Telephone:* Belgravia 6111.) Prospective authors are invited to prepare their scripts in accordance with the *Notes on the preparation of contributions*. (Price 2*s*. 6*d*. including postage.)

REPRODUCTION. The Institute of Physics is a signatory to The Royal Society's Fair Copying Declaration. Details may be obtained upon application from The Royal Society, London, W.1.

ADVERTISEMENTS. Communications concerning advertisements should be addressed to the agents, Messrs. Walter Judd Ltd., 47 Gresham Street, London, E.C.2. (*Telephone:* Monarch 7644.)

CLAIMS FOR MISSING JOURNALS. Claims from regular subscribers to this *Journal* for missing numbers will only be considered if received within 60 days of the date of mailing plus normal outward time of transit and time for lodging the claim. Losses attributable to failure to notify a change of address or to similar omissions will not be considered.

SUBSCRIPTION RATES. A new volume commences each January. The charge is £5 per volume ($14.25 U.S.A.), including index (post paid), payable in advance. Single parts, so far as available, may be purchased at 10*s* each ($1.50 U.S.A.), post paid, cash with order. Orders should be sent to The Institute of Physics, 47 Belgrave Square, London, S.W.1, or to any bookseller.

Electroluminescence*

By S. T. Henderson, M.A., Ph.D., F.Inst.P., Thorn Electrical Industries Ltd., Enfield

An account is given of the present state of field-controlled luminescence, with references to the earlier experiments using additional forms of excitation, and to carrier injection luminescence. Intrinsic electroluminescence is dealt with at greater length, the main aspects considered being the phosphor, the voltage against brightness relation, and emission wave-forms. Theoretical discussions of the process and practical applications are reviewed.

INTRODUCTION

Electroluminescence is a subject that can be well illustrated in the lecture room. A written discussion without the demonstrations may be less convincing, for it is difficult to do more than add another to the reviews published in recent years.[1–3] Progress has reached a point where the comparatively simple improvements in technique have been made, practical applications are well in hand, but further desirable advances depend on that kind of effort which is required, for instance, to discover new phosphors for various purposes. This is not exactly empirical work, but it needs investigations which are not informed by any very useful theory. In other words, progress in electroluminescence is slow and there is not much to report since the first review mentioned. It will be assumed in the following that the reader has some knowledge of the historical and practical details, and attention will now be given to some important aspects of the subject. These will deal largely with the behaviour of zinc sulphide phosphors, in particular the copper-activated material with green luminescence.

EARLY EXPERIMENTS

It has been suggested by Walsh that the term electroluminescence ought to be used for all direct conversions of electrical energy to light, while the most widely known and practised form, variously known as the Destriau effect, "true" or "intrinsic" electroluminescence, ought to be called "condenser" luminescence.[4] The last term is indeed an apt description of the usual electroluminescent cell or plate, with its sandwich of phosphor and dielectric between two close conducting plane surfaces. This type of construction may be used to demonstrate a number of the earlier experiments on phosphors which were simultaneously, or successively, under two forms of excitation, as we now regard them, though at that time the electric field was not recognized as a form of excitation in its own right. The effects described by Gudden and Pohl, Schmidt, Hinderer and others are now of little more than historical interest; there have been some more recent examinations of them.[5–9] In the early work phosphors were used which had stored up energy during a prior excitation by light, and the light subsequently emitted was not derived from the electric field. There is a resemblance to the effect of infra-red stimulation and quenching in these field effects on non-electroluminescent phosphors, for by itself the infra-red quantum is insufficient to cause excitation but needs to be added in some way to existing stored energy to produce light in the visible spectrum. In "true" electroluminescence the phosphor begins in the unexcited ground state and all the light energy is derived from the field.

The Gudden and Pohl effect is easily demonstrated. Their original experiments were made on thin layers of dry phosphors, but it is more convenient to coat a thin layer of a long afterglow ZnS . Cu phosphor (not an "electroluminescent" preparation) in an alkyd resin on to the surface of a glass plate previously made conducting by spraying, at its softening point, with a dilute solution of a tin salt in alcohol. A second conducting layer of graphite or evaporated metal on the back forms a condenser which is waxed on the back and along the edges to exclude moisture. Exposed to long ultra-violet radiation and examined in the dark, this plate will show a gradually decaying phosphorescence, and if a connexion is made between the plates and a 200–300 V dry battery, a momentary flash of brighter phosphorescence is seen. This may be repeated at intervals during the decay (see Fig. 1). Krautz has shown[8] how rapidly these flashes

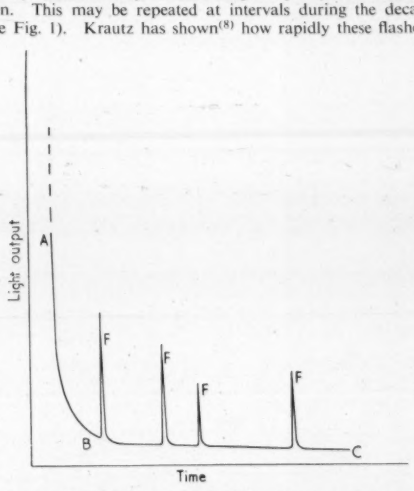

Fig. 1. Flash effect of d.c. field on phosphorescence of ZnS . Cu (diagrammatic)

ABC, normal decay; *FF*, momentary application of field. [After *Gudden and Pohl*.]

rise and fall (rise ~30 μs, fall ~1 ms). The corresponding flash on switching off the field is slower and more difficult to observe. In some cases, particularly ZnS . Cu . Mn of yellow electroluminescence, quenching may be observed after the flash and while the field is still on. With a.c. fields more complicated effects occur, partly due to the periodic relaxation

* Based on a lecture given to the Electronics Group of the Institute of Physics on 15 January, 1957.

of polarized conditions in the crystal, partly due to "intrinsic" electroluminescence. Quenching may be observed with ZnS . Cu during the period of maintained a.c. field, as well as flashes on switching on. In general, the fields used in the above experiments are of the order of 10^4–10^5 V/cm. Infra-red analogies are evident in the phenomena. If infra-red irradiation is added to an existing field, the general result is that the infra-red effects are accelerated, either in quenching or stimulation.

Next we may consider the experiments where excitation and electric field are applied together. These lead to some interesting effects which should have practical applications, even if their theoretical interpretation is not altogether clear by reason of the involved nature of the procedures and the marked differences caused by more or less uncontrollable variations in phosphors.

DUAL EXCITATIONS

Matossi and Nudelman have devoted much attention to the case of ultra-violet excitation of ZnS . Cu with simultaneous electric fields.[10, 11] A simplified scheme of the variation of light output with time is shown in Fig. 2. The dotted lines

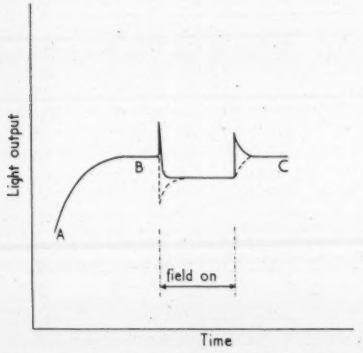

Fig. 2. Quenching effect of field on phosphor excited by ultra-violet

AB, rise under excitation; *BC*, steady level under u.v. alone. [After *Matossi* and *Destriau*.]

show alternative behaviour seen in other phosphors. The important effect to notice is the quenching, which is described (but not explained) by saying that the field induces radiationless transitions of excited electrons. The small peaks in Figs. 1 and 2 are attributed to freeing of trapped electrons by the field. This idea is, however, by no means generally accepted, and it evidently does not apply to the continuous stimulation, or rather enhancement, of photoluminescence seen in the Cusano amplifier.[12, 13] In this device the material is a 10 μ thick evaporated layer of ZnS . Mn . Cl having a moderate ultra-violet fluorescence which is greatly increased by a d.c. field of $\sim 10^5$ V/cm applied across the phosphor layer; it appears that the energy represented by this extra light is derived from the field though controlled by the incident ultra-violet.

Till recently only manganese-activated phosphors were known to show enhancement under any radiation. Arsenic and phosphorus have now been used instead of manganese to activate evaporated phosphors for this "photoelectroluminescence."[14] Other methods of showing this increase of emission under a field (see Fig. 3) are by a primary

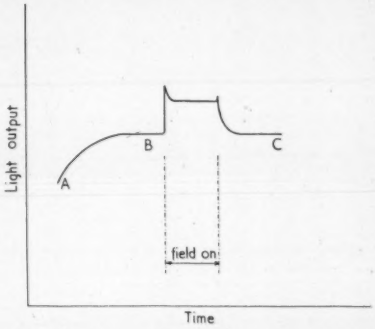

Fig. 3. Enhancement effect of field on phosphor excited by X-rays

AB, rise under excitation; *BC*, steady level under X-rays alone. [After *Destriau*.]

excitation with X-rays, α-rays or cathode-rays. An a.c. field of the order of 10^4 V/cm is particularly effective on a screen of ZnS . CdS . Mn under X-rays, the light output being more than doubled;[15] a d.c. field merely gives flashes at switching on and off. The a.c. effect depends on the spectral region observed, and it is improved if the phosphor also incorporates small amounts of gold.[16] The possibilities of a practical device, which would be of great value in medical practice, have been recognized in recent patents.[17] The converse effect of field quenching under ultra-violet instead of X-rays could be used in a radiation detector with image reversal.[18]

Enhancement of α-ray fluorescence in an a.c. field has been demonstrated with ZnS . Mn . Ag. The effect could be distinguished from intrinsic electroluminescence occurring at the same time.[19] The last example to be given here is of ZnS . CdS . Mn under a cathode-ray beam, which showed increased emission when the phosphor layer was subjected to an a.c. field of the order of 10^4 V/cm. Frequency of the applied field was important.[20] Compare a d.c. effect on the cathodoluminescence of magnesium oxide.[21] It is interesting that X-rays or α-rays can be used for the primary excitation in the Gudden and Pohl type of experiment. Energy can be stored and released by later application of a field.[22]

CARRIER INJECTION LUMINESCENCE

Turning to cases where no preliminary phosphor excitation is necessary, there are two well defined types and perhaps a few border-line cases. The first type is appropriately called carrier injection luminescence, first observed for carborundum (SiC) by Lossev, and since then in a variety of other crystalline powders or single crystals, such as $CaWO_4$,[23] ZnS and CdS,[24] SnO_2,[25] and C (diamond).[26] The effect may be seen by applying a few hundred volts d.c. between two sheets of conducting glass enclosing a layer of coarse carborundum powder in castor oil. Bright points of light are seen where the crystals are suitably orientated. Efficiency is low and this

visible emission is so far of no practical importance. Rectifying properties are often found in this group, and the processes involved, at any rate with d.c. fields, have been explained adequately by recent semi-conductor theory. When the crystal is specifically *p* or *n* in constitution, forward or reverse bias produces contrasted effects, for example in carborundum. Sometimes the peak light emission corresponds more or less exactly in frequency to the forbidden band separation, and, as with crystal phosphors, some widening of the emission to a band occurs. The emission is infra-red for hole injection into *n*-germanium. Red or infra-red emission of similar type occurs in the III–V compounds like GaSb, InP, etc.,[27] in GaP,[28] and in the II–VI compound CdTe.[29] In other cases a complex band structure arises from foreign impurity levels in the forbidden band, as with SiC. Similarly for boron nitride, with the difference that a.c. fields are required, in contrast to d.c. for the other materials listed.[30] This is a border-line case resembling the intrinsic type by operating without electrode contact to the phosphor powder. CaF_2 appears to be similar in behaviour.[31]

INTRINSIC ELECTROLUMINESCENCE

The second main type of electroluminescence is that discovered by Destriau in 1936. In practical applications, dating from about 1950, the flat plate condenser with a dispersed phosphor layer is basic to nearly all designs, the light being emitted either through a conducting glass electrode, or through transparent fused ceramic layers if the condenser is built up on a metal backing plate. A white reflector layer is usually incorporated, and this may have electrical as well as optical advantages.[1] The only other practical detail calling for comment here is the very difficult exclusion of all traces of moisture from the completed lamp by embedding in wax or a synthetic resin; even then it is not certain that internal generation of water does not occur, and since water in traces will reduce the phosphor efficiency, this represents a serious hazard in manufacture. The ceramic type of plate appears to be fairly immune to the effects of external water.

Wherever phosphors are used in light-producing devices, their efficiency is apt to be the limiting factor on what can be achieved, and many devices of standardized design have been improved by work on the phosphor component. This is true of electroluminescence, where only a very limited selection of phosphors has been found adequate to produce the accepted light levels, low as those are at present. Almost all current work is done with zinc sulphides and selenides with copper as impurity activator and other co-activators or additions such as halides, Al, Ga, Pb and ZnO. Manganese is an extra activator for yellow emission. Zinc oxide has a special significance historically, for its incorporation as such or by partial oxidation of the phosphor was formerly the main method of conferring electroluminescent properties on zinc sulphide. The cubic (zinc blende) form is usual but not essential to electroluminescence in ZnS, and some experimental evidence has recently been produced on the mechanism of incorporation of Cu in the crystal,[32] and the influence of Cl content on the emission bands developed.[33] Otherwise not a great deal of effort has been devoted to the study of emission band shapes, positions and movements with temperature. The green and blue emission bands commonly found in electroluminescent ZnS . Cu are very similar though probably not identical with those produced by ultra-violet excitation.[34] Electroluminescent sulphides are photoluminescent unless poisoned for special purposes,[35] conversely few photoluminescent sulphides exhibit electroluminescence.

The arrangements of crystallites in dielectric-coated phosphors is believed to be important, and may account for the initial increase in light output in thermoplastic-bonded phosphors in the glass type of plate. Deliberate alinement has been proposed to give enhanced light output. Much attention has been paid to the more fundamental problem of the nature of the barrier layers on the crystallite surfaces, postulated in some current theories. Conducting phases like ZnO, Cu_2S, evaporated Cu,[36] and ionizable salts suitably deposited[37] are known promoters of electroluminescence, while the recent discovery that admixed sharp metal particles will induce electroluminescence in sulphides and other phosphors not normally responding[38] suggests that carrier injection and intrinsic electroluminescence are more closely allied than was previously thought, and may sometimes exist together and be confused.[39] Lehmann in fact believes exhaustion barriers to be less important in the "intrinsic" case than local field intensifications caused by mere contact of the ZnS crystals with particles of higher conductivity. Internal barriers in electroluminescent crystals are also presumed to exist.[40, 41] They cause the non-homogeneous light output characteristic of crystals examined microscopically and their peculiar dielectric properties. This behaviour has to be remembered when means of improving the phosphors are considered.

The possibility of non-sulphide phosphors has not been realized in a useful form. An obvious difference is that few, if any, other phosphors show the well-developed crystal forms of ZnS. However, the addition of CdS promotes crystal growth, but by introducing deep traps speedily reduces electroluminescence; therefore, good crystallization is not all that is required. The way in which the lattice is built up seems to be a more important factor. The use of lead salts in the preparation of the sulphides may be an empirical means of attaining the correct structure, for very little lead is left in the finished product; on the other hand these traces may have some activator or sensitizer-like action.

Electrical behaviour. The electroluminescent plate combines capacitative with non-ohmic resistive properties. Attempts have been made to give equivalent circuits. Resonant effects produced by an inductance in the circuit have an important bearing on light output,[42] but the overriding electrical factor which limits the performance is the low power factor of the electroluminescent plate ($\sim 0{\cdot}1$–$0{\cdot}2$). In certain cases this may have value, for example, in permitting the operation by a transistor oscillator circuit, powered by low voltage dry batteries. Circuit analogies do not appear to have any value in the study of the mechanism or prediction of performance under stated conditions. A more useful approach to the electrical properties is through the dielectric characteristics.[43–45]

Voltage relations. A specific electrical parameter, namely the voltage (or field strength) applied to the plate, has been very extensively used in relation to light output. Many formulae have been proposed to express the superlinear light output by exponential or power functions of voltage. A formula holding over a wide range can be used as a check on the theory of electroluminescence mechanism. Many interesting individual pieces of work have been done, but there is still diversity of view and discrepancies among experiments. The accurate measurement of electroluminescence looks at first more hopeful experimentally than for phosphor emission under, say, cathode-rays, where similar quantitative attempts have been made despite the varying penetration of the exciting agent, which makes it difficult to measure true light production in the powder layer, as contrasted with light

emitted after variable internal scattering. However, each crystal shows electroluminescent emission at many spots, not all in phase and with varying voltage thresholds, hence the least involved case is the measurement of light from a single spot. This, of course, is very difficult. In fact most of the measurements made have been on powder layers. Yellow emitting ZnS . Cu . Mn behaves differently from green-emitting ZnS . Cu in its voltage characteristic and so offers another unsolved problem.

The most favoured expression for average light output or luminance at voltage V has been $L = a \exp(-b/\sqrt{V})$.[46] Not all types of powder layer conform. If account is taken of the non-homogenous emission in the crystals, and the assumption made that L tends to a limit as $V \to \infty$, for which there is some experimental justification, then a relation of the type $L = a \exp(-b/V)$ is more probable.[47] This is a return to one of the earliest formulae, which has some other theoretical justification from the mean free path of the conduction band electrons.[48]

Emission wave-forms. A topic which has attracted much attention is that of the variation with time of the light output (the emission wave-form) and its dependence on the wave form of the applied field. Some progress has thus been made in understanding the mechanism of light emission, even if most of the information refers to the mean output from heterogeneous assemblies of crystals, each of which has a non-uniform response to the field. This averaged response could, of course, appear either less or more complex than that of a single electroluminescent spot according to the distribution of fields, phasing and so on. An example of the value of time-averaged measurements will be seen later in the work of Waymouth and Bitter.

In general, intrinsic electroluminescence is out of phase with the excitation if this is sinusoidal, though under some circuit conditions with high frequency operation the light output may be very closely sinusoidal and in-phase. Some typical wave forms for powder layers are shown in Figs. 4–6 with the corresponding sinusoidal voltage waves producing them. Changes occur with voltage, type of electrode, temperature and nature of phosphor. It is also necessary to distinguish between experiments on phosphor powders embedded in plastic dielectrics (the more common case), layers of powder without binder, and single crystals. It should be noted that oscilloscope traces of emission wave-forms are often published without zero levels, suggesting that the light output returns to zero at each half cycle. This is not strictly true, even at low frequencies, while at high frequencies the modulation is much reduced. The reason is in part the overlap in light emission of numerous out-of-phase spots in each small crystal. This also produces the two main peaks per cycle in Figs. 4–6 instead of one given by each emitting spot.

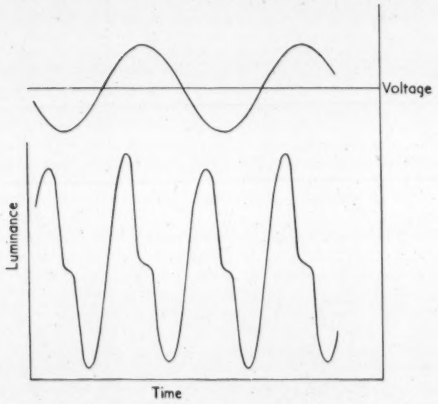

Fig. 4. Wave-forms of emission and voltage for low frequency excitation of ZnS . Cu
[After *Destriau*, *Mattler*, *Luyckx* and others.]

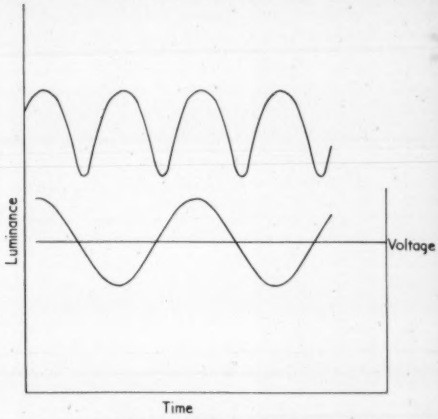

Fig. 5. Wave-forms of emission and voltage for high frequency excitation of ZnS . Cu
[After *Destriau* and others.]

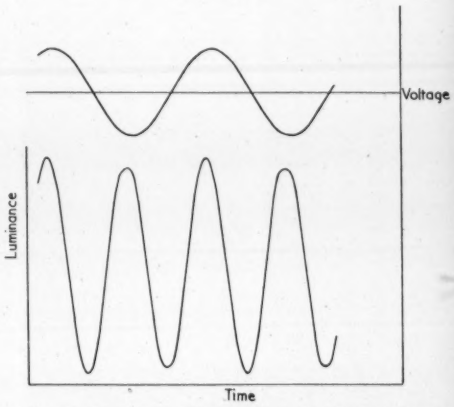

Fig. 6. Wave-forms of emission and voltage for low frequency excitation of ZnS . Cu . Mn
[After *Luyckx*, *Mattler* and others.]

Different spectral bands may be emitted at different points in the voltage cycle, and there is a marked difference between the wave-forms of ZnS with Cu and Mn as the main emitting centres respectively. From manganese-activated phosphors only one (nearly symmetrical) wave per half cycle is observed, as in Fig. 6, another instance of manganese "abnormality."[49] The wave-forms are not established instantaneously.[50] Full light output requires several cycles of voltage, and there is often a continuing slow rise over hours or days of operation, with an eventual fall possibly due to electrolysis.[51]

When the applied voltage wave-form is altered a great variety of results may be obtained. Evidence is available for pulsed d.c. with varied pulse and interval lengths, sinusoidal a.c. with varied amounts of rectification, square-topped a.c. pulses, saw-tooth a.c. and so on. These excitations were used to alter the emission wave-forms mainly for theoretical reasons, though practical advantages have not been overlooked.[52] There is difficulty in reconciling the single crystal results with those of dielectric-embedded powders, especially as the single crystals may be susceptible to carrier injection from the electrodes as well as showing intrinsic electroluminescence. The discrepancies mainly concern the phase relations of different parts of the emission wave and the effects of electrode polarity at any given moment. (See a discussion on p. 1922 of Ref. 2.) For the usual type of layer it has been claimed that the volume luminescence is nearly symmetrical while the light from near the electrodes contributes the unsymmetrical effects. To summarize the deductions from many studies of emission waves, it may be said that they show the electroluminescent process to consist of a primary excitation, when the field is high, during which light may or may not be emitted; and a relaxation process following the reduction or extinction or reversal of the field as the a.c. cycle is continued or the d.c. pulse removed, when the main luminescence occurs.

Frequency is important in all a.c. operation. Its primary effect is simply that it controls the number of emitting states occurring per second: the length of the "on" period seems less important. Very roughly the light output is proportional to frequency over small ranges, and the log-log plot of luminance against frequency is linear up to kilocycle frequencies. Voltage, frequency and temperature are closely interconnected and it is not possible to isolate the effects of any one of these parameters.

Temperature effects. Temperature changes have been a powerful if not always controllable tool in the study of luminescence under conventional excitations. The same applies to electroluminescence, and the variations of light output above and below 0° C differ much as for photoluminescence. Temperature affects the resistivity and dielectric constant of the binder in powder layers if these are used, temperature quenching effects on the phosphor occur, hence the pure electroluminescence is not easy to isolate.[53] It appears to increase with temperature rise, though the overall effect on an electroluminescent cell, or a single crystal, is of a maximum output at some point below 200° C, but often above 0° C, depending on frequency and voltage.[54]

Phosphors containing ZnO have been claimed to behave differently, first by a rising emission below 0° C, and second in the sense that their temperature-luminance curves below 0° C depend on whether the temperature is rising or falling during the measurements. Thus a kind of glow curve with peaks was obtained on heating, provided the electric field was present, and provided that a liquid silicone dielectric was used.[55, 56] The normal thermoluminescence, observed in the glow experiment, may be involved in some way. This is a suitable point to mention another aspect of electroluminescence, namely the enhancement of thermoluminescence light sum at low temperatures by a d.c. field. This was observed for single crystals of ZnS which may simultaneously show carrier injection luminescence;[57] apart from this complication the process is a kind of refrigerated Gudden and Pohl experiment.

Temperature effects emphasize the importance of electron traps in the phosphor, but trapping is of a more general importance in electroluminescence considered theoretically.

THEORETICAL ASPECTS

It has already been suggested that there are large differences of opinion on the interpretation of electroluminescence data, often because similar phosphors give dissimilar response to the same experimental conditions. The same differences are naturally found in general theories of electroluminescence. A few basic principles are widely accepted, and their combination into plausible schemes offers scope for much ingenuity and some controversy. It is not yet possible to deduce further consequences for experimental test from these theories. In fact they are mostly no more than hypotheses, but encouraging agreement with experiment has been reached in a number of attempts, even if they are not always mutually compatible.

The luminescence of ZnS . Cu involves the presence of electrons in the conduction band of energy levels in the crystal. Intrinsic electroluminescence has already been distinguished from the carrier injection process, and it is agreed that one other possible source of conduction electrons is extremely unlikely, namely those excited directly across the forbidden band from the valency band or activator centres not far above the latter. This would require fields a thousand times higher than those applied in the usual electroluminescence experiments (10^3 V/cm upwards). There remain as the primary source of electrons the electron traps or donor states in the forbidden zone between valency and conduction bands. If these electrons can be raised into the conduction band, they will be accelerated by the field till they have enough energy to cause multiplication of carriers by collision and to excite or ionize the activator centres (also in the forbidden zone), and so initiate the luminescence process. Even so the calculated fields are much higher than the average fields applied, or than the calculated fields in the phosphor particles,[58] consequently local concentrations of field have to be invoked, usually in the form of electronic barriers of the exhaustion type located in the crystal surfaces. This has already been mentioned in the discussion of phosphors. At this point speculation becomes more prominent in the argument.

Opinions differ on the type and distribution of donor levels necessary. Levels located at imperfections of a crystal surface in contact with the cathode, and energetically at a very small depth below the conduction band level, could provide the necessary electrons for acceleration by the local high field.[59] Deeper donor levels are also considered necessary by some authors to account for barrier formation and in particular for voltage against luminance data,[60, 61] while various distributions in depth have also been proposed. The extent of thermal as opposed to field ionization of donors is doubtful,[62, 63] and the effects of temperature on voltage and frequency behaviour have been interpreted in different ways which cannot be briefly summarized. Various ideas on the complementary functions of positive holes are also current. As an example of the complexity and limitations of the theoretical approach, Zalm's very complete discussion may be

mentioned.[3] Among the subjects it deals with specially is the relation of powder layers in a dielectric to single crystals in contact with electrodes.

A different method has been used by Nagy and by Goffaux, from the Fröhlich conception of free electron temperature in relation to lattice temperature. Electron multiplication can be explained, and semiquantitative agreement with experiment found for voltage against luminance,[64] and for frequency dependence and several other relations.[50] Another interesting study is that of Ince and Oatley, whose measurements of the low frequency dielectric dispersion which is characteristic of electroluminescent sulphides imply the presence of mobile ions.[44] These may have some subsidiary influence on the process.

These generalized ideas on mechanism are insufficient to account for the detail of the emission process. Certain aspects have already been discussed, and are not very difficult to explain. Thus the blue and green bands in ZnS . Cu arise from electronic transitions of different type and speed, they are therefore differently affected by change of exciting field frequency and give different wave-forms.[65] Manganese activation has a different effect, since its emission is nearly if not exactly in phase with the field (Fig. 6).

It is, however, from the special voltage wave-forms, and in particular the pulsed type of excitation, that electroluminescence has been clearly seen to consist of an excitation process followed by emission at a time interval controlled by the instant of field suppression as well as by the inherent phosphor processes. Temporary space charges are built up, and the importance of more permanent internal polarization has been stressed by Waymouth and Bitter in their work on integrated light output under d.c. pulses.[66] Incidentally they found once again that the manganese emission differs from that of copper, confirming that different emission processes are involved.

With the many possible qualitative ideas on the successive stages of electroluminescence, and the large approximations that have to be made in any quantitative studies of solid state processes, no theory can be expected to give an exact account of the phenomena, and to decide between alternative theories may be difficult. Fresh advances will, of course, be made by new experiments, though the directions of progress cannot be foreseen at this time.

APPLICATIONS OF INTRINSIC ELECTROLUMINESCENCE

Applications of electroluminescence are of importance, if only to sustain the considerable research and development effort which has been made since 1950, mostly in commercial laboratories, to bring the phenomenon into the class of useful light sources. At present general lighting is not practicable because of the low power input and low efficiency of plates operated at mains frequency and voltage. Even with voltages stepped up to 600 V, a convenient limit if organic dielectrics are used, the surface brightness is no more than 1% of that of a fluorescent lamp. Luminous efficiency in lumens per watt is less than 10% of that of the fluorescent lamp. There are situations where illumination at low levels by uniform large areas is valuable, for example in photographic work. The probability of improvement by an interesting factor does not seem very large, at any rate for low frequency working. Experimentally a luminance similar to that of a fluorescent lamp surface (0·5–1·0 stilb) has been achieved at high frequencies and voltages.[2] In view of the lowered efficiency in lumens/watt at high frequencies the power input must be enormous and the continued operation of such plates a matter of doubt.

Light output in practicable electroluminescent plates has been improved by moderate frequency increase. If the appropriate supply is available, for example the usual 400 c/s of aircraft, useful brightness levels can be obtained for the operation of information and warning signs. Oscillator circuits with transistors will provide adequate power for portable devices or instrument panels on vehicles. It has also been possible to fill a demand for compact indicator lights in a circuit-testing computer, by constructing moulded blocks with five separately switched circular spots in each, to work at kilocycle frequencies and several hundred volts.

The colour limitations on electroluminescent devices are well known. Green is the usual colour, derived from ZnS . Cu, with variations towards blue according to relative excitations of the two bands centred near 4500 and 5200 A (increased frequency favours the blue). A blue without the green band is also possible in ZnS . Cu, and a yellow by ZnS . Cu . Mn. Mixtures give "near-whites" but colours are apt to vary with the electrical conditions. No efficient red is known by direct excitation, and filters or cascade processes have to be used to produce a reasonable output.

In U.S.A. the ceramic-embedded phosphor is largely used instead of the type described in this article. Vitreous enamelling techniques are used to build up the condenser on a steel backing plate, which may be of any shape, with holes if required, and not necessarily plane, and hence much more flexible in design.

The possible combination of photoconductor surfaces with electroluminescent plates, with or without feedback, in order to make light switches, information storage devices, amplifiers, radiation detectors and converters for light and X-rays have been well explored in theory.[67, 68] There is much work in progress on the development of workable arrangements of this kind. The Cusano amplifier is the simplest that has been demonstrated, its main limitation is long response time; in this it resembles the Nicoll and Kazan amplifier which uses a photoconductor detector layer.[69] The inherently slow luminescent process in the zinc sulphides is also serious for many possible applications. The way these devices will work is known, but their realization depends on specific advances in both photoconductor and phosphor research, for example, the development of evaporated layers is one attractive line of work. While such advances cannot be prophesied with any confidence, interest in the applications of electroluminescence is likely to persist for a long time, if only because the exciting agent, the electric field, is so universally available.

REFERENCES

(1) Henderson, S. T. *Research*, **8**, p. 219 (1955).
(2) Destriau, G., and Ivey, H. F. *Proc. Inst. Radio Engrs*, **43**, p. 1911 (1955).
(3) Zalm, P. *Philips Res. Rep.*, **11**, pp. 353, 417 (1956).
(4) Walsh, J. W. T. *Light and Lighting*, **49**, p. 256 (1956).
(5) Gudden, B., and Pohl, R. *Z. Phys.*, **2**, pp. 181, 192 (1920).
(6) Schmidt, F. *Ann. Phys., Lpz.*, **70**, p. 161 (1923).
(7) Hinderer, H. *Ann. Phys., Lpz.*, **10**, p. 265 (1931).
(8) Krautz, E. *Z. Naturforsch.*, **4a**, p. 284 (1949).
(9) Asagoe, K., and Tani, N. *Sci. of Light*, **4**, p. 7 (1955).
(10) Matossi, F. *Phys. Rev.*, **98**, pp. 434, 1545 (1955).
(11) Matossi, F., and Nudelman, S. *J. Electrochem. Soc.*, **103**, p. 122 (1956).
(12) Cusano, D. A. *Phys. Rev.*, **98**, p. 546 (1955).

(13) MATOSSI, F. *Phys. Rev.*, **99**, p. 1332 (1955).
(14) CUSANO, D. A. *Phys. Rev.*, **106**, p. 604 (1957).
(15) DESTRIAU, G., MATTLER, J., DESTRIAU, M. and GUMLICH, H. E. *J. Electrochem. Soc.*, **102**, p. 682 (1955).
(16) DESTRIAU, G. *Electrochem. Soc. meeting*, May 1957, paper 24.
(17) Westinghouse Electric International Co. British Patent 772572, appl. 28.5.1954.
(18) DIEMER, G., ZALM, P., KLASENS, H. A., and PHILIPS. S. Afr. Pat. Appl. 2234/56.
(19) MATTLER, J. *J. Phys. Radium*, **17**, p. 758 (1956).
(20) JAFFE, P. M. *Electrochem. Soc. meeting*, May 1957, paper 26.
(21) WOODS, J., and WRIGHT, D. A. *Proc. Phys. Soc. B*, **68**, p. 566 (1955).
(22) MATTLER, J., and CURIE, D. *C.R. Acad. Sci., Paris*, **230**, p. 2086 (1950).
(23) GÜNTHERSCHULZE, A., and GERLACH, M. *Z. Phys.*, **88**, p. 355 (1934).
(24) SMITH, R. W. *Phys. Rev.*, **100**, p. 760 (1955); **105**, p. 900 (1957).
(25) EGYESÜLT IZZOLAMPA. British Patent 761961, appl. 22.12.1953.
(26) WOLFE, R., and WOODS, J. *Phys. Rev.*, **105**, p. 921 (1957).
(27) BRAUNSTEIN, R. *Phys. Rev.*, **99**, p. 1892 (1955).
(28) WOLFF, G. A., HEBERT, R. A. and BRODER, J. D. *Phys. Rev.*, **100**, p. 1144 (1955).
(29) VAN DOORN, C. Z., and DE NOBEL, D. *Physica*, **22**, p. 338 (1956).
(30) LARACH, S., and SHRADER, R. E. *Phys. Rev.*, **104**, p. 68 (1956).
(31) SCHARF, K. *J. Phys. Radium*, **17**, p. 723 (1956), discussion.
(32) MCKEAG, A. H., and STEWARD, E. G. *J. Electrochem. Soc.*, **104**, p. 41 (1957).
(33) TOMLINSON, T. B. *J. Electronics*, **2**, p. 293 (1956).
(34) WAYMOUTH, J. F. *J. Electrochem. Soc.*, **100**, p. 81 (1953).
(35) LEHMANN, W. *Phys. Rev.*, **101**, p. 489 (1956). Belg. Patent 549390.
(36) DIEMER, G. *Philips Res. Rep.*, **10**, p. 194 (1955).
(37) BOWTELL, J. N., and BATE, H. C. *Proc. Inst. Radio Engrs*, **44**, p. 697 (1956).
(38) LEHMANN, W. *J. Electrochem. Soc.*, **104**, p. 45 (1957).
(39) HAHN, D., and SEEMAN, F. W. *Z. Phys.*, **146**, p. 644 (1956).
(40) LOEBNER, E. E., and FREUND, H. *Phys. Rev.*, **98**, p. 1545 (1955).
(41) DIEMER, G., and ZALM, P. *Physica*, **22**, p. 561 (1956).
(42) LUYCKX, A., WEILER, M., and STOKKINK, A. J. *J. Phys. Radium*, **17**, p. 769 (1956).
(43) ROBERTS, S. *J. Opt. Soc. Amer.*, **43**, p. 590 (1953).
(44) INCE, A. N., and OATLEY, C. W. *Phil. Mag.*, **46**, p. 1081 (1955).
(45) LEHMANN, W. *J. Electrochem. Soc.*, **103**, p. 24 (1956).
(46) ZALM, P., DIEMER, G., and KLASENS, H. A. *Philips Res. Rep.*, **10**, p. 205 (1955).
(47) LEHMANN, W. *J. Electrochem. Soc.*, **103**, p. 667 (1956).
(48) CURIE, D. *J. Phys. Radium*, **14**, p. 510 (1953).
(49) MATTLER, J. *J. Phys. Radium*, **17**, p. 725 (1956).
(50) GOFFAUX, R. *Bull. Acad. Roy. Belg. Cl. Sci.*, **40**, p. 808 (1954). *J. Phys. Radium*, **18**, p. 1 (1957).
(51) THORNTON, W. A. *J. Appl. Phys.*, **28**, p. 313 (1957).
(52) PHILIPS. British Patent 774314, appl. 7.10.1953.
(53) HAAKE, C. H. *J. Electrochem. Soc.*, **104**, p. 291 (1957).
(54) ALFREY, C. F. *J. Phys. Radium*, **17**, p. 719 (1956).
(55) GOBRECHT, H., HAHN, D., and GUMLICH, H. E. *Z. Phys.*, **136**, p. 623 (1954).
(56) HAHN, D. *J. Phys. Radium*, **17**, p. 748 (1956).
(57) NEUMARK, G. F. *Phys. Rev.*, **98**, p. 1545 (1955); **103**, p. 41 (1956).
(58) ROBERTS, S. *J. Opt. Soc. Amer.*, **42**, p. 850 (1952).
(59) BURNS, L. *J. Electrochem. Soc.*, **100**, p. 572 (1953).
(60) HOWARD, B. T. *Phys. Rev.*, **98**, p. 1544 (1955).
(61) PIPER, W. W., and WILLIAMS, F. E. *Brit. J. Appl. Phys., Suppl.* 4, **6**, S 39 (1955).
(62) JOHNSON, P. D., PIPER, W. W., and WILLIAMS, F. E. *J. Electrochem. Soc.*, **103**, p. 221 (1955).
(63) THORNTON, W. A. *Phys. Rev.*, **102**, p. 38 (1956).
(64) NAGY, E. *Acta Phys. Hungar*, **6**, p. 153 (1956).
(65) NUDELMAN, S., and MATOSSI, F. *J. Electrochem. Soc.*, **101**, p. 546 (1954).
(66) WAYMOUTH, J. F., and BITTER, F. *Phys. Rev.*, **95**, p. 941 (1954).
(67) LOEBNER, E. E. *Proc. Inst. Radio Engrs*, **43**, p. 1897 (1955).
(68) GARLICK, G. F. J. *J. Sci. Instrum.*, **34**, p. 473 (1957).
(69) KAZAN, B., and NICOLL, F. H. *Proc. Inst. Radio Engrs*, **43**, p. 1888 (1955).

The thermal conductivity of nitrogen and argon in the liquid and gaseous states

By H. Ziebland, Dipl.Ing., A.M.I.Mech.E., and J. T. A. Burton, Explosives Research and Development Establishment, Waltham Abbey, Essex

[*Paper first received* 19 *July, and in final form* 6 *September*, 1957]

The thermal conductivity of nitrogen and argon was measured with a vertical coaxial cylinder apparatus. The investigation included the critical region and covered the temperature range 85 to 200° K at pressures between 1 and 135 atm. The results obtained in this research agree well with those obtained by most other authors.

The investigation reported here is part of a research programme on the molecular transport properties of air and its constituents. In an earlier paper[1] the authors described the measurement of the thermal conductivity of oxygen. Except for a few minor modifications the same apparatus has been used for nitrogen and argon.

There have been several previous investigations[2, 6] on the thermal conductivity of nitrogen within the temperature range covered in this paper but only two of these, by Borovik[2] and by Uhlir,[3] covered the critical region and showed the effect of pressure on thermal conductivity. The only previous extensive research on argon at low temperatures is by Uhlir.[3]

A knowledge of the thermal conductivity of the constituents of air over a wide range of pressure and temperature is not only of importance for the solution of practical problems, but is also of considerable theoretical interest, particularly if the measurements include the critical region of the substances investigated. Very few previous investigators studying the thermal conductivity of either organic or inorganic materials have extended their research into the critical region. In the present work, particular attention was paid to obtaining data as close as possible to the critical point.

EXPERIMENTAL

For details of the apparatus and the experimental method the reader should refer to the authors' paper on oxygen.[1] For the work on nitrogen and argon some modifications were introduced, mainly to facilitate the operation of the metal block thermostat and to improve the accuracy and reproducibility of the temperature measurements in the conductivity cell.

The Dewar vessel containing the conductivity apparatus and the thermostat had a cylindrical extension fifteen inches long fitted to its upper part. This extension was filled with Santocel (by Monsanto Ltd.), an insulating powder, and had the effect of considerably reducing the heat inleak to the apparatus. The amount of liquid nitrogen required for the refrigeration of the apparatus was considerably reduced and consequently enabled the apparatus to be run for longer periods without suffering the disturbance caused by replenishment of the liquid nitrogen store.

To provide automatic control of temperature an electric heater was wound on the outside of the refrigerated aluminium cylinder surrounding the autoclave which contained the conductivity cell. A platinum resistance thermometer served as the temperature sensitive element and was fitted in a hole in the aluminium cylinder drilled between the cast-in refrigerating coil and the electric heating element. The thermometer was connected to an electronic thermostat (by Fielden Electronics Ltd.) which controlled the current to the heater winding. This arrangement enabled the temperature of the conductivity cell to be maintained constant within a few hundredths of a degree for a period of several hours. This was a great improvement over the manual control used previously, as the greater temperature stability enabled the guard ring heaters to be matched more accurately and the time required to complete a measurement was appreciably reduced.

During the measurements on oxygen some difficulty was experienced from parasitic e.m.f.'s in the thermocouple circuits and from condensation of moisture, and also at the lowest temperature, of air into the stainless steel tubes containing the thermocouple wires. Parasitic e.m.f.'s were almost completely eliminated by making the thermocouples of multi-stranded wire connected in parallel. Sealing the thermocouple wires with a thermo-setting resin at the point where they emerged from the stainless steel tube prevented the previously observed effects of atmospheric condensation.

Purity of argon and nitrogen. The gases used in this research were taken from commercial cylinders supplied by British Oxygen Gases Ltd. According to the manufacturer's specification the nitrogen had a purity of 99·5 and the argon a purity of 99·95%.

RESULTS

The thermal conductivity of the fluid in the annulus between the emitting and receiving cylinder was computed from the following equation

$$k = Q \ln (r_2/r_1)/2\pi L(T_1 - T_2)$$

where k (cal cm^{-1} deg C^{-1} s^{-1}) is the thermal conductivity, Q (cal/s) is the radial heat flow through the annulus, r_1 and r_2 (cm) are the radii of the emitting and receiving cylinders respectively, T_1 and T_2 (° K) are the temperatures of the emitting and receiving surfaces respectively and L (cm) is the length of the emitting cylinder. A conversion factor of 1 cal = 4·184 joule was used.

The experimental results for nitrogen and argon are tabulated in Tables 1 and 2 and are plotted in Figs. 1 and 2 respectively. The measurements were made at pressures which were simple fractions or multiples of the appropriate critical pressures to facilitate comparison of the results with those of previous observers. For the sake of clarity the values obtained at pressures of one quarter of the critical pressure were not plotted in Figs. 1 and 2. The critical pressures and temperatures were taken from a National Bureau of Standards circular.[7]

Each value of the thermal conductivity given in the tables is the mean of several determinations at the same temperature and pressure; individual determinations did not differ from the mean value by more than 1%. The guard ring corrections, i.e. corrections for axial heat flow between the emitting cylinder and the guard rings due to imperfect matching of their temperatures, were very small and in almost all experiments amounted to less than 1% of the reported thermal conductivity.

The effect of convection on the measurement of thermal conductivity was discussed in the paper on oxygen.[1] Lack of pertinent physical data, however, prevented the evaluation

Table 1. *Thermal conductivity of nitrogen*

Pressure (atm)	*Nominal reduced pressure*	*State*	*Temperature (° K)*	10^4k *(cal cm^{-1} deg C^{-1} s^{-1})*	*Mean ΔT (deg C)*	*Number of determinations*
1·0	1/33·5	gas	125·9	0·300	5·730	3
			134·1	0·315	5·340	3
			158·6	0·370	4·517	3
			172·3	0·400	4·228	2
			187·9	0·430	3·935	6
			202·0	0·460	3·747	2
8·4	¼	liquid	88·2	2·79	2·399	5
		gas	158·5	0·385	4·402	4
			172·2	0·410	4·103	2
			187·9	0·440	3·840	3
			201·9	0·470	3·683	2
16·8	½	liquid	87·7	2·84	2·159	4
			105·8	2·07	1·448	4
		gas	124·7	0·365	4·789	3
			133·4	0·360	4·711	3
			158·3	0·400	4·172	3
			172·0	0·425	3·949	3
			187·4	0·455	3·726	4
			201·8	0·480	3·586	2
27·6	1	liquid	80·9	3·18	2·019	4
28·1			80·7	3·19	2·009	4
31·3		gas	164·2	0·460	6·000	3
			188·8	0·490	3·073	4
			202·5	0·510	5·357	3
33·5		liquid	87·7	2·90	2·154	4
			105·8	2·17	1·391	4
			114·6	1·810	0·881	4
			116·1	1·750	1·710	5
			120·6	1·555	1·086	3
			124·1	1·410	0·542	4
			124·1	1·415	1·185	3
			124·2	1·390	0·851	3
		gas	128·4	0·660	1·038	3
			129·9	0·600	1·873	3
			131·2	0·565	2·983	2
			138·3	0·475	3·318	2
			147·0	0·470	3·424	3
			157·6	0·460	3·625	3
			171·6	0·475	3·560	3
			187·3	0·495	3·440	3
			201·5	0·515	3·360	3
50·3	1½	liquid	105·9	2·25	1·335	3
			116·4	1·830	1·530	2
			125·9	1·440	1·217	2
			127·0	1·380	1·964	3
			128·4	1·330	0·543	3
			128·9	1·355	0·849	3
			129·5	1·335	1·258	4
			136·2	1·085	1·440	2
			136·9	0·890	0·811	3
			139·0	0·835	0·480	3
			139·0	0·885	1·304	1
			139·3	0·805	0·919	3
			139·4	0·810	1·362	1
			147·3	0·645	2·468	3
			156·9	0·555	2·995	2

Table 1 (continued)

Pressure (atm)	*Nominal reduced pressure*	*State*	*Temperature (° K)*	*$10^4 k$ (cal cm^{-1} deg C^{-1} s^{-1})*	*Mean ΔT (deg C)*	*Number of determinations*
67·0	2	liquid	87·3	2·98	2·055	5
			98·3	2·60	2·708	4
			105·6	2·32	1·302	3
			116·4	1·935	1·490	3
		gas	126·8	1·555	1·796	3
			145·1	0·940	1·695	3
			155·3	0·730	1·686	4
			171·1	0·620	2·694	5
			186·5	0·595	2·822	4
			201·0	0·600	2·874	2
100·5	3	liquid	87·2	3·08	1·984	4
			98·2	2·70	2·571	3
			105·6	2·46	1·232	5
			116·1	2·11	1·334	4
		gas	126·6	1·755	1·591	4
			145·1	1·275	1·315	2
			155·2	1·065	1·590	2
			170·9	0·845	1·987	4
			185·8	0·755	2·255	3
			200·5	0·710	2·417	3
134·0	4	liquid	87·3	3·16	2·124	5
			97·9	2·82	2·470	4
			105·4	2·57	1·167	3
			114·5	2·24	0·785	5
		gas	126·3	1·935	1·426	4
			144·8	1·530	1·100	2
			154·9	1·260	1·349	3
			170·5	1·040	1·620	4
			185·5	0·915	1·871	4
			200·8	0·840	2·067	3

of Rayleigh's criterion for the occurrence of convection. The reliability of the data in the range most likely to be affected, i.e. the critical region, was checked in the present research by carrying out experiments with different temperature differences across the fluid-filled annulus. Absence of convection was regarded as proved if the thermal conductivity at constant pressure and temperature was independent of the temperature difference across the annulus.

On approaching the critical point along the critical isobar it was found that, within a narrow temperature range around the critical temperature, guard ring matching became extremely difficult, although the temperature difference appeared to be small enough to prevent convection in the fluid-filled annulus. Despite the Fluon filler pieces (by Imperial Chemical Industries Ltd.) above and below the conductivity cell, which were arranged to reduce the free volume in the autoclave; the thicknesses of the various liquid layers through which heat had to be conducted from the cell to the autoclave walls were several times larger than the width of the measuring annulus itself. Natural convection, dependent on the third power of the thickness of the liquid layer, was therefore the most probable cause of the observed difficulties which prevented reliable measurements within about 3° K above and below the critical point. In a redesign of the guard ring configuration of the conductivity cell, consideration

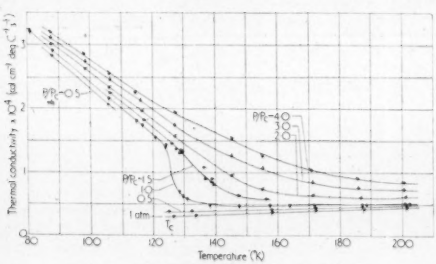

Fig. 1. Thermal conductivity of nitrogen
$T_c = 126{\cdot}1_{35}$° K.
$P_c = 33{\cdot}49$ atm.

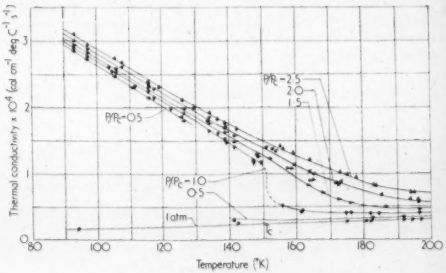

Fig. 2. Thermal conductivity of argon
$T_c = 150{\cdot}6_5$° K.
$P_c = 48{\cdot}0$ atm.

Table 2. *Thermal conductivity of argon*

Pressure (atm)	*Nominal reduced pressure*	*State*	*Temperature (° K)*	10^4k *(cal cm^{-1} deg C^{-1} s^{-1})*	*Mean ΔT (deg C)*	*Number of determinations*
1·0	1/48	gas	93·4	0·160	5·273	4
			142·1	0·230	6·725	3
			175·1	0·275	3·827	5
			181·0	0·275	3·799	3
			182·4	0·280	2·464	3
			191·5	0·295	5·466	5
			194·3	0·300	3·488	4
			196·1	0·300	1·650	3
12·0	¼	liquid	93·6	2·81	2·283	1
			98·0	2·68	2·451	3
			106·1	2·44	2·262	4
		gas	138·9	0·245	3·419	3
			182·4	0·295	2·508	3
			196·0	0·320	1·586	2
19·3	½	liquid	111·1	2·31	1·860	8
			117·2	2·16	3·104	4
			125·7	1·880	1·565	5
		gas	141·1	0·285	5·530	4
24·0		liquid	93·6	2·84	2·261	4
			98·0	2·71	2·429	3
			106·1	2·47	2·253	3
			116·1	2·16	2·077	2
			126·3	1·840	2·458	3
		gas	182·6	0·315	2·362	4
			191·6	0·330	4·949	3
47·3	1	liquid	105·5	2·52	2·588	4
			111·6	2·33	2·750	4
			122·6	1·995	3·096	5
			136·5	1·628	0·975	4
			139·2	1·485	2·014	5
		gas	161·6	0·425	1·648	5
			161·7	0·430	2·270	3
			174·9	0·380	2·697	2
			184·5	0·380	2·782	5
47·9	1	liquid	93·4	2·90	2·231	3
48·0			97·9	2·75	2·406	3
			104·5	2·58	2·229	3
			106·2	2·52	2·329	2
			115·9	2·23	2·014	6
			126·1	1·925	2·379	2
			133·8	1·665	1·724	3
			138·6	1·540	1·011	2
			142·5	1·385	1·223	2
			147·5	1·220	0·678	4
			147·6	1·200	1·304	4
			149·2	1·195	1·396	4
			149·2	1·365	1·616	2
		gas	155·4	0·515	1·518	2
			176·0	0·390	4·127	3
			181·8	0·380	1·944	3
			195·7	0·380	1·257	2
70·7	1½		165·3	0·884	2·962	5
72·0		liquid	93·4	2·93	2·195	2
			97·8	2·80	2·365	4
			105·9	2·58	2·300	3
			115·8	2·30	1·957	4
			126·2	1·985	2·274	3
			133·8	1·765	1·632	4
			138·3	1·650	0·950	2
			142·3	1·470	1·147	2

Table 2 (continued)

Pressure (atm)	Nominal reduced pressure	State	Temperature (°K)	10^4k (cal cm^{-1} deg C^{-1} s^{-1})	Mean ΔT (deg C)	Number of determinations
		liquid	148·9	1·300	1·720	2
			149·3	1·280	1·314	3
		gas	152·0	1·220	0·613	2
			158·2	1·075	1·466	4
			159·2	1·075	1·460	3
			164·5	0·775	0·955	5
			164·7	0·845	1·873	4
			167·5	0·685	1·094	3
			173·0	0·570	1·331	4
			176·1	0·525	3·062	4
			186·4	0·480	3·320	2
			195·7	0·450	1·034	2
95·5	2	liquid	115·8	2·33	1·856	2
			117·7	2·25	2·841	3
			129·1	1·995	1·124	2
			133·4	1·805	1·200	4
		gas	150·7	1·395	1·785	5
			152·2	1·375	1·222	7
			165·8	1·000	1·329	7
			173·3	0·810	1·497	3
			195·4	0·555	2·323	5
96·0		liquid	93·3	2·97	2·195	2
			97·7	2·84	2·348	3
			107·6	2·57	2·654	3
			115·7	2·36	1·906	4
			133·7	1·850	1·565	5
			138·2	1·720	0·950	4
			138·3	1·705	0·923	2
			142·3	1·560	1·090	2
		gas	152·9	1·335	0·542	2
			159·5	1·155	1·373	4
			164·5	1·040	1·524	5
			172·6	0·825	0·929	3
			173·9	0·845	1·898	4
			185·5	0·635	2·522	4
			193·8	0·570	0·883	3
			195·6	0·535	0·844	3
118·1	2½		178·1	0·925	2·966	5
			183·9	0·825	1·147	4
120		liquid	93·3	3·04	2·612	2
			97·6	2·89	2·327	3
			105·6	2·69	2·057	4
			107·5	2·63	2·596	4
			118·8	2·28	3·093	4
			125·7	2·11	2·172	4
			133·7	1·915	1·548	5
			136·1	1·835	2·569	3
			138·2	1·775	0·879	2
			138·2	1·765	0·898	2
			142·7	1·655	1·032	2
		gas	153·8	1·440	1·105	2
			154·8	1·400	1·129	1
			159·3	1·300	1·222	4
			164·1	1·200	1·351	3
			173·6	1·005	1·607	3
			175·2	0·980	2·959	2
			183·5	0·825	1·959	2
			193·8	0·705	0·731	3
			194·5	0·700	2·325	2
120		solid	83·6	4·27	1·507	4

will be given to this point and it is hoped to approach the critical point even closer. However, an analysis of the results obtained on the critical isobar indicated that the interpolation between the experimental values near the critical point, and thus the critical conductivity itself, is not likely to be seriously in error.

At the critical temperature two factors in the Rayleigh criterion, namely, the specific heat at constant pressure and the thermal expansion coefficient, fall rapidly from infinity at the critical pressure to finite values with increasing pressure. For pressures higher than the critical pressure, all the terms in the Rayleigh criterion remain finite and the maximum value of the criterion decreases and occurs at higher temperatures as the pressure is increased.

On the reduced isobar 1·5, for example, it was possible to obtain convection-free data at the critical temperature itself, but not in the interval 5 to 15 deg C above it. No difficulties were experienced in obtaining reliable data (at any temperature level) at reduced pressures larger than two. This is discussed further below.

Nitrogen. The results obtained for nitrogen at the critical pressure ($P_c = 33{\cdot}49$ atm) and about 2 deg C below the critical temperature are not likely to have been affected by convection, since the three measurements at 124° K give values of thermal conductivity which agree to within ±1% although they were obtained with different temperature differences across the annulus. Similarly three values on the same isobar near 130° K obtained with temperature differences from 1 to 3 deg C lie on a smooth curve and do not display the steep increase of thermal conductivity characteristic of the onset of convection. Lack of time prevented a more extensive exploration of this region.

On the reduced isobar 1·5 (50·3 atm) five values between 125 and 130° K obtained with temperature differences from 0·5 to 2 deg C do not exhibit a trend that would indicate the presence of thermal convection. There are six results on the same isobar between 136 and 140° K and the first of these, at 136·2° K seems to be too high. This might be due to convection as this point was obtained with a temperature difference of 1·440 deg C whereas the next point at 136·9° K,

Table 3. *Comparison of results for nitrogen with those of other authors*

		Thermal conductivity × 10^4 (cal cm^{-1} deg C^{-1} s^{-1})							
Pressure (atm)	*Temperature (° K)*	*Eucken (12)*	*Keyes (11)*	*Powers et al (5)*	*Borovik et al (6)*	*Borovik (2)*	*Uhlir (3)*	*Hammann (4)*	*This Research*
1·0	130	0·288	0·280						0·310
	200	0·440	0·420						0·450
Saturation	85			3·08	3·26		2·90 (extra-pol.)	4·90 (extra-pol.)	2·90
33·5	85					3·31	3·02		3·01
	90					3·05	2·83		2·81
	100					2·60	2·45		2·40
	110					2·12	2·05		1·990
	120					1·58	1·65		1·580
	130					0·62	0·55		0·600
	140					0·52	0·475		0·475
	150					0·48	0·44		0·455
	160					0·46			0·460
	170					0·47			0·470
50·3	120					1·72			1·690
	130					1·20			1·280
	140					0·73			0·800
	150					0·64			0·610
67·0	85					3·38	3·13		3·08
	90					3·15	2·95		2·89
	100					2·70	2·60		2·53
	110					2·26	2·24		2·16
	120					1·82	1·89		1·795
	130					1·36	1·53		1·445
	140					1·03	1·18		1·110
	150					0·84	0·88		0·810
	160					0·72	0·72		0·680
	170					0·61	0·64		0·630
100·5									
	90					3·25			2·975
	100					2·83			2·635
	110					2·40			2·295
	120					2·01			1·965
	130					1·67			1·655
	140					1·37			1·390
	150					1·13			1·167
	160					0·95			0·980
	170					0·81			0·855

Table 4. *Comparison of results for argon with those of other authors*

Pressure (atm)	*Temperature (° K)*	*Thermal conductivity × 10⁴ (cal cm⁻¹ deg C⁻¹ s⁻¹)* *Eucken (12)*	*Keyes (11)*	*Uhlir (3)*	*Kannuluik and Carman (13)*	*This research*
1·0	90·0	0·140	0·145		0·140	0·150
	170·0	0·255	0·255	0·23	0·255	0·260
	190·0	0·285	0·280	0·26	0·280	0·290
12·0	90·0		2·82 (10·2 atm)			2·93
	110·0		2·29 (10·2 atm)			2·32
24·0	90·0			2·87		2·95
	130·0			1·74		1·740
48·0	90·0			2·90		2·98
	100·0			2·63		2·69
	110·0			2·35		2·40
	120·0			2·08		2·10
	130·0			1·81		1·790
	140·0			1·54		1·470
	145·0			1·40		1·310
	155·0			0·50		0·520
	170·0			0·39		0·390
	180·0			0·38		0·380
	190·0			0·37		0·375
96·0	90·0			2·96		3·08
	100·0			2·70		2·78
	110·0			2·45		2·49
	120·0			2·20		2·20
	130·0			1·94		1·925
	140·0			1·70		1·650
	145·0			1·57		1·520
	155·0			1·32		1·270
	170·0			0·93		0·910
	180·0			0·71		0·710
	190·0			0·61		0·590

obtained with a temperature difference of 0·811 deg C, is consistent with the others in this region. As the maximum value of the isobaric specific heat at this pressure occurs in the region of 136° K, Rayleigh's criterion for convection would also reach a maximum near this temperature.

There is no evidence of the results at higher pressures having been influenced by convection. Although they were obtained with various temperature differences across the annulus they all lie on smooth curves.

Argon. Similar considerations apply to the case of argon. The experimental values on the critical isobar ($P_c = 48·0$ atm) are certainly free from convection up to 148° K. Two values obtained at 147·5° K with different temperature differences agreed within ±0·8%. Above the critical temperature, measurements were carried out sufficiently removed from the critical point to ensure absence of convection.

On the reduced isobar 1·5 the two points at 158·2 and 159·2° K seem to be too high, probably due to convection. On the same isobar there are three values near 165° K obtained with successively larger temperature differences, and it can be seen that this has led to convection and anomalously high values of thermal conductivity. Extrapolation of the available experimental data towards diminishing temperature differences suggests a probable value of $(0·73 \pm 0·01) \times 10^{-4}$ cal cm^{-1} deg C^{-1} s^{-1} at 165° K.

At reduced pressures higher than 1·5 the experimental data do not appreciably deviate from the smoothed isobars of Fig. 2, in spite of considerable variations in the temperature difference across the annulus. One determination was made of the thermal conductivity of solid argon at 83·6° K at 120 atm. A value of $4·27 \times 10^{-4}$ cal cm^{-1} deg C^{-1} s^{-1} was found which compares favourably with a value reported by Uhlir[3] of $(4·2 \pm 0·2) \times 10^{-4}$ cal cm^{-1} deg C^{-1} s^{-1} at 77° K at an unspecified pressure.

DISCUSSION

In Tables 3 and 4 values of the thermal conductivity taken from the smoothed plots of Figs. 1 and 2 are compared with the smoothed data of other observers.

Nitrogen. Considering the different techniques and types of apparatus used by the various authors the agreement between previous research[2, 3, 5, 6] and this work can be regarded on the whole as satisfactory. Very good agreement, however, exists between Uhlir's data[3] and this work. Discrepancies between the two investigations rarely exceed 4%.

Compared with Borovik's data[2] somewhat larger discrepancies have been observed which occur in two temperature regions. At about 85° K the results by Borovik and others[2, 6] are between 6 to 12% higher than those by Powers and others,[5] by Uhlir[3] and by the authors of this paper. Data found in the latter three investigations agree at this tem-

perature level within $\pm 3\%$. Larger deviations have also been found in the critical temperature range where some of Borovik's results are lower than those by Uhlir and by the present authors. These latter discrepancies might have their origin in some corrections Borovik had to apply to his measurements. Although the type of apparatus used in his research should have precluded convection (flat plate heated from above) natural convection took place and the observed apparent conductivity was a function of the temperature difference across the fluid layer. In order to arrive at the true thermal conductivity, measurements were carried out at several temperature differences and the results thus obtained were extrapolated graphically to zero temperature difference. This method implies that convection would occur as long as there is a finite temperature difference between the heat emitting and heat receiving plates. This is in contrast to Rayleigh,[8] and Kraussold[9] from whose researches it follows that convection must disappear at finite values of temperature difference. Borovik's extrapolation to zero temperature difference leads, therefore, to an over-correction for convection and his values are likely to be too low wherever he applied this technique. In the same paper[2] Borovik also reports some values of the thermal conductivity of gaseous oxygen at $T = 156°$ K, i.e. about 1·2 deg C above the critical temperature, and pressures up to 100 atm. These data, too, are lower than those reported by the present authors in a previous paper[1] and are also lower than the values reported recently by Tsederberg and Timrot[10] whose data agree well with the present authors' previous research.

Previously[1] a value of $3{\cdot}28 \times 10^{-4}$ cal cm^{-1} deg C^{-1} s^{-1} had been reported for the thermal conductivity of liquid nitrogen at 80° K and 33·5 atm by the authors of this paper. This agrees well with the value of $3{\cdot}22 \times 10^{-4}$ cal cm^{-1} deg C^{-1} s^{-1} at the same temperature and pressure obtained from Fig. 1. As has been stated already by other authors, Hammann's data[4] are grossly in error.

Argon. The thermal conductivity of liquid argon has been measured before only by Keyes[11] and Uhlir.[3] The values reported by these authors differ by less than 4% from the present data. As errors in measurement may amount to 2%, this agreement is considered to be excellent.

The apparatus used in this research was intended primarily for use with liquids. When used for substances of low conductivity, i.e. for gases, there is some loss of accuracy, since small errors in determining axial heat losses or gains, through imperfect guard ring matching, correspond to considerably larger ratios of axial to radial heat flow than when the fluid in the annulus has a higher thermal conductivity. Such measurements therefore provide a very sensitive test for the accuracy of the data obtained. As can be seen from Table 4 the gas-phase data on argon at 1 atm agree well with those by four other observers. Similar data on gaseous nitrogen obtained in this research again appear to be slightly too high, in comparison with Keyes's[11] and Eucken's[12] results. The maximum deviation from the mean values found from both the above references and this research is less than 6%.

The opportunity is taken to note the very good agreement between Keyes's data for liquid oxygen[11] and those reported earlier by the present authors.[1] They are compared in Table 5.

Table 5. *Comparison of results for oxygen*

Pressure (atm)	*Temperature (° K)*	*Thermal conductivity* $\times 10^4$ *(cal cm^{-1} deg C^{-1} s^{-1})* *Keyes (11)*	*Ziebland and Burton (1)*
7·4	85·7	3·72	3·74
10·5	110·4	2·98	2·94

ACKNOWLEDGEMENTS

The authors wish to acknowledge the assistance of Mr. E. Speller, who carried out some of these measurements. Crown copyright is reserved. This paper is reproduced with the permission of the Controller, H.M.S.O.

REFERENCES

(1) Ziebland, H., and Burton, J. T. A. *Brit. J. Appl. Phys.*, **6,** p. 416 (1955).

(2) Borovik, E. *J. Phys., USSR*, **11,** p. 149 (1947).

(3) Uhlir, A. *J. Chem. Phys.*, **20,** p. 463 (1952).

(4) Hammann, G. *Ann. Phys., Leipzig*, **32,** p. 593 (1938).

(5) Powers, R. W., Johnston, H. L., and Mattox, R. W. *Proceedings 8th Int. Congr. Refrig. London* 1951, p. 186 (III) (London: Institute of Refrigeration, 1951).

(6) Borovik, E., Matveev, A., and Panina, E. *J. Tech. Phys., USSR*, **10,** p. 988 (1940).

(7) N.B.S. *Circular* 564, *Tables of Thermal Properties of Gases* (Washington: National Bureau of Standards, 1955).

(8) Rayleigh, Lord. *Phil. Mag.*, **32,** p. 529 (1916).

(9) Kraussold, H. *Forsch. Ing. Wes.*, **5,** p. 186 (1934).

(10) Tsederberg, N. V., and Timrot, D. L. *Zh. Tekh. Fiz.*, **26,** p. 1849 (1956).

(11) Keyes, F. G. *Trans Amer. Soc. Mech. Engrs*, **77,** p. 1395 (1955).

(12) Eucken, A. *Phys. Z.*, **12,** p. 1101 (1911).

(13) Kannuluik, W. G., and Carman, E. H. *Proc. Phys. Soc. B* [*London*], **65,** p. 701 (1952).

Reflexion electron microscopy at high angles

By D. H. PAGE, M.A., British Paper and Board Industry Research Association, Kenley, Surrey

[*Paper first received* 24 *July, and in final form* 20 *September*, 1957]

A commercial electron microscope has been adapted for use as a reflexion instrument with an angle of beam deviation of 26·5°. The resolution is, in general, severely limited by the chromatic aberration arising from excessive energy losses suffered by electrons scattered through large angles. However, when both the axial and field components of the aberration are minimized, within the limits imposed by the use of a commercial instrument, a resolution of 600 Å is attained. Although this is inferior to the resolution of the reflexion microscope at low angles of deviation, the high depth of field and the greatly reduced foreshortening give rise to a highly informative and readily interpreted image. Micrographs illustrate the method applied to specimens in the chemical, biological and metallurgical fields.

The first attempts to image electrons reflected from a specimen were made by Ruska[1] and later by Ruska and Müller.[2] In the latter case the specimen was illuminated at a glancing angle and the electrons scattered normally were focused. However, the resolution obtained was inferior to that of the light microscope, being limited by the chromatic error arising from the high energy losses suffered by electrons scattered through large angles. Von Borries[3] showed that, by illuminating and viewing specimens at glancing angles, the energy spread in the scattered beam could be reduced sufficiently to give a resolution of a few hundred Ångströms. However the image then suffers from a severe foreshortening, and, because glancing angles are used, the method is applicable only to the smoothest surfaces. Interest in reflexion work lapsed, therefore, with the advent of more refined replica techniques but again revived with the work of Kushnir and others,[4] Fert and Saporte,[5] Menter,[6] and Haine and Hirst.[7] In all this work the proposal of Von Borries was followed and the total beam deviation was kept low. Incident angles (θ_1) of 0·1–2° and viewing angles (θ_2) of 4–8° were common. The desirability of increasing these angles to reduce the foreshortening and the amount of information lost in shadow is, however, apparent. Menter[8] concluded that no serious loss in resolution occurs for angles of beam deviation as high as 14°. In this laboratory a beam deviation of 17° has been employed for some time for the examination of the comparatively rough surfaces of pulp fibres and paper.[9, 10] It was considered that an even larger angle would have been desirable for this study but a limitation was imposed by the loss of intensity at higher viewing angles.[7] Such a loss may be counteracted by an increase in incident illumination but this would aggravate the effect of beam damage which, in the case of cellulosic specimens, is already disturbing.[9] This difficulty was eliminated when Bradley[11,12] devised for reflexion work a technique for producing solid metal replicas that would withstand the full intensity of the electron beam. At about this time Fert and co-workers[13] showed that the poor resolution obtained when examining metal specimens at high angles is due to the high energy losses suffered by electrons in passing through the layer of carbonaceous contamination. Furthermore, they showed that if the layer is removed continuously during examination by bombardment from an ion gun, a resolution of 350 Å may be achieved. Such an approach, however, has the limitation that the use of a commercial instrument is excluded and that examination is confined to those surfaces unaffected by ion bombardment, that is, the surfaces of certain metals. An attempt was made at this laboratory[10] to evaluate high-angle work without the aid of ion bombardment so that the method could be applied to metal replicas of biological and other specimens and metal surfaces in general. In this early work poor results were obtained because the objective lens was operated at long focal length in order to keep instrumental modifications to a minimum. This condition aggravated the chromatic error. In the work about to be described, a preliminary account of which has appeared elsewhere,[14] great care has been taken to minimize the effect of chromatic aberration within the limits imposed by the use of a commercial instrument.

INSTRUMENTAL MODIFICATIONS

The main requirement in this modification was that the instrument should be readily returnable to transmission working conditions. The Metropolitan-Vickers type EM3 microscope was therefore modified in a manner similar to that described by Menter,[6] a hollow metal wedge being inserted between the specimen chamber and the gun alinement section. The choice of the angle of beam deviation for this work was governed partly by the design of the specimen chamber. At an angle of deviation of 22° the incident beam is intercepted by the upper flange of the chamber, but if this flange is filed away as far as the O-ring recess, angles of up to 28° are permitted. Further increase in this angle is not readily possible. The angle chosen was 26·5° and a wedge giving this deviation was constructed. A specimen stage designed in this laboratory[15] for reflexion work was employed. By filing away part of the specimen carriage, variability of tilt with respect to the microscope axis was increased to 26°.

Because of the high angle of tilt of the gun axis and the great weight of the gun and condenser sections there is a large bending moment at the gun alinement section. This impedes the easy operation of the gun lateral controls used in reflexion to scan the specimen. A counterbalancing force was therefore provided by means of a weighted rope, passed over a pulley, and attached to the condenser lens section.

THEORETICAL CONSIDERATIONS

In reflexion work, because of the large voltage spread of scattered electrons, the resolution is determined by the chromatic aberration of the objective lens. The radius of the disk of least confusion d is given by

$$d = \alpha C_c \delta V / V \qquad (1)$$

where α is the semi-angular aperture of the beam accepted by the lens, C_c is the chromatic aberration constant of the lens, δV is the half width of the energy spread of electrons accepted by the aperture and V is the accelerating voltage.

There is an optimum value of α for which the effect of chromatic aberration is balanced by that of diffraction. However, because of the relatively large value of $\delta V/V$, the optimum aperture is very small and would give an impossibly low illumination on the screen. In practice, C_c is made small by choosing the shortest practicable working distance. For the best resolution α is then chosen so that the image is just bright enough to be focused and recorded at the necessary magnification. In reflexion at low angles the best resolution achieved is in the region of 200–250 Å. Typical values giving such a resolution are:

$$C_c = 1 \text{ cm}; \alpha = 1{\cdot}5 \times 10^{-3}; \delta V/V = 0{\cdot}0015$$

As the resolving power of the reflexion method is at present limited by the inability to focus and record low intensity images, it is of interest to consider the relationship between the theoretical resolving powers that may be attained at high and low angles for a given screen illumination. The intensity I of the electron beam on the specimen is related to the intensity I_s on the screen by the equation:

$$I_s \propto M^{-2}\alpha^2\phi I$$

where M is the magnification and $\alpha^2\phi$ is the fraction of incident electrons accepted by the aperture. If the magnification is adjusted so that the plate is just able to record the smallest resolved distance d, then, for a given plate, M is inversely proportional to d.

Hence
$$I_s \propto d^4(\delta V/V)^{-2}\phi I$$

Putting suffixes h and l to indicate high and low angle conditions respectively we have for constant screen illumination:

$$\frac{d_h}{d_l} = \left(\frac{I_l \cdot \phi_l}{I_h \cdot \phi_h}\right)^{\frac{1}{4}} \left[\frac{(\delta V/V)_h}{(\delta V/V)_l}\right]^{\frac{1}{2}} \tag{2}$$

It has been estimated from an investigation of the chromatic field aberrations that, provided the specimen is not heavily contaminated, $(\delta V/V)_h$ is approximately 0·01 when θ_2 is 21° and V is 60 kV. Ratio ϕ_l/ϕ_h may be obtained from data due to Haine and Hirst,[7] and is approximately 5 for viewing angles of 6° and 21° respectively, being independent of the angle of illumination. For similar values of I this gives $d_h/d_l = 3{\cdot}8$ suggesting a resolution d_h of about 800 Å with an objective aperture of $8{\cdot}0 \times 10^{-4}$. In practice it has been possible to use a slightly smaller aperture of $6{\cdot}0 \times 10^{-4}$ yielding a resolution of 600 Å.

Equation (2) implies that the loss in resolution at high angles is accounted for largely by the increase in $\delta V/V$. The resolution is, however, dependent on the square root of this quantity and is not affected as adversely as might be expected. The resolution is proportional to the fourth root of the intensity of the scattered beam so that the lower intensity at high angles is not disturbing. Equally, no great improvement in the resolution is to be expected from an increase in the incident beam intensity followed by an adjustment of the magnification and the aperture angle.

The axial distance in object space D_p, within which the specimen is focused with a resolution better than $p(>d)$, is given by the equation:

$$D_p = 2(p - d)/\alpha \tag{3}$$

When $p = 2d$, D_p is commonly termed the depth of field D

Therefore
$$D = 2d/\alpha = 2C_c\delta V/V \tag{4}$$

For the high-angle conditions quoted this gives the exceptionally large value of 200 μ compared with 30 μ for the typical low-angle case. Moreover, because of the reduced foreshortening, the extent of the well-defined region on the plate is greatly increased. The magnification M that is just high enough to permit the plate to record the full available resolution d of the image is given by the equation $M = kd^{-1}$ where k is the limit of resolution of the plate.

The length L of the in-focus image on the plate is then $MD \tan \theta_2$.

Hence from equation (4) we have

$$L = 2k \tan \theta_2/\alpha \tag{5}$$

Putting in a typical value for k (40 μ) this gives $L = 5$ cm, showing that the majority of a lantern plate is in good focus. This is a considerable improvement on low-angle reflexion work in which only a relatively narrow band across the centre of the plate is focused. Moreover L in equation (5) is independent of the magnification, implying that most of the plate shows a well-defined image at all magnifications, even when the resolution is limited by the grain of the plate.

So far consideration has only been given to the effect of the axial chromatic error of the objective lens. There are, however, field aberrations that affect the definition of abaxial points. These aberrations, which are usually of little importance in electron microscopes in transmission or low-angle reflexion conditions, become of overriding importance in reflexion at high angles when $\delta V/V$ is large, and, in general, severely limit the sharply-focused area. A three-lens microscope may be adjusted so that these aberrations are compensated and it was found essential in this work to do this.

The coefficient of chromatic difference of magnification in a three-lens reflexion electron microscope may be determined as a function of the focal length of its lenses, the separation m and n between them, and the axial position of the objective aperture.[16] It may be shown that, for a thin lens system, this coefficient vanishes at the approximate condition

$$f(m + n) = \gamma mn \tag{6}$$

where f is the focal length of the intermediate lens and γ is a constant depending on the position of the objective aperture; γ is 2·0 when the aperture is at the centre of the lens and 1·5 when it is in its back focal plane.

The chromatic aberration of rotation is given by the equation

$$2\delta\psi/\psi = \delta V/V \tag{7}$$

where ψ is the total rotation of the image and $\delta\psi$ is the rotational aberration due to the energy spread δV. The aberration becomes insignificant when $\delta\psi$ is less than $1{\cdot}5 \times 10^{-3}$ and, putting in typical values, this implies that ψ should be less than 20°.

PRACTICAL CONSIDERATIONS

The focal length of the intermediate lens required for the correction of the magnification error has been found by the following procedure. Assuming the focal length to be inversely proportional to the square of the lens current, the constant of proportionality may readily be found (for example, by noting the current when the objective aperture is focused on the screen with the other lenses switched off and applying the thin lens formula). The current in the lens may then be set to give the focal length required from equation (6). This

method does not give the correct value sufficiently accurately and a series of micrographs must be taken with current settings on either side of the theoretical value and the best setting selected. The determination is quite critical, a change in the lens current of as little as 4% having a noticeable effect on the image quality. However, once this procedure has been carried out the same setting gives satisfactory results for some time without adjustment. The effect of a gross mis-setting of the lens current, 18% higher than the required value, is shown in Fig. 1. Only a very small central region of the image is of value.

The condition for the correction of the rotational aberration is fortunately not so critical. In the type EM3 microscope the image rotation is less than the necessary value of 20°, within the magnification range used, provided that the intermediate and projector lenses are excited in opposition to the objective lens. With the focal lengths of the other two lenses fixed by previous considerations the projector lens may be used to vary the magnification. A minor modification of the lens current circuit has been made to permit continuous variation of the magnification in the range ×300–1200. The pincushion distortion at these magnifications is fortunately not excessive.

The illumination under these conditions is very low and a period of dark adaptation is necessary before an image magnified 500 times can be focused on the screen even with the condenser lens set at critical illumination. This difficulty has been overcome to some extent by a method due to Menter.[6] The objective aperture is raised for focusing, thus increasing the angular aperture and hence the illumination. It is then lowered for micrography. In reflexion at high angles, however, this procedure upsets the condition for correction of the magnification aberration, for γ in equation (6) is altered by an axial movement of the aperture. The method, while being useful, is not then entirely satisfactory for high-angle work. It should be noted that some electron microscopes permit the interchange of objective apertures during operation and such a facility would be very desirable for this work. The replacement of an aperture by one of larger size decreases the resolving power and increases the illumination. However, the depth of focus, and hence the effect on the image of a change in objective current, is independent of the aperture size as can be seen from equation (4). It seems, therefore, that the small aperture required for micrography could be replaced for focusing by an aperture so large that the operation could be carried out with the same ease as the focusing of a light microscopical image. The necessity of recording the image is therefore the ultimate factor affecting the lowest tolerable illumination. With the conditions previously mentioned exposure times are commonly of two minutes duration at a magnification of about 800 times using Rapid Process Experimental plates (by Ilford Ltd.). It seems unlikely that a fainter image could be satisfactorily recorded.

For the best resolution the objective aperture must be centred accurately. The method of centration described below was devised independently by the author, and although it is known to be in use at other laboratories, it has not to his knowledge been published elsewhere. The method is similar to the alinement of the gun tilt in transmission work. On taking the objective current through focus the image rotates and the centre of rotation may be brought to the centre of the screen by adjusting the position of the aperture. Using a ×10 telescope for viewing the image, the aperture may be centred with an accuracy of a few microns and it is essential for good results to achieve this accuracy. Alinement of the aperture by variation of the accelerating voltage has also been employed but it appears to give the same results as the above procedure. Moreover, the voltage alinement procedure is more difficult in practice, as a change in the accelerating voltage defocuses the beam incident on the specimen and consequently reduces the illumination on the screen.

The contamination forming on the specimen affects the resolution of the image noticeably after about two minutes' exposure to critical illumination. The effect is seen clearly in the highlights of Fig. 6. To reduce the effect a method has been adopted that was originally proposed by Chapman and Menter[17] for the prevention of beam damage when examining fibrous specimens. Focusing is carried out on an area to the side of the specimen and the area of interest is moved into the beam immediately prior to taking the micrograph. During the exposure the condenser lens is over-focused sufficiently to give even illumination over the field of view so that the contamination formed is not appreciable.

The use of a small angle of illumination (between 1 and 3°) is stated by Fert[18] to be essential for a good resolution. However this does not seem to be the case for this work. Angles of illumination have commonly been about 5°, and in some cases angles as high as 10° have been employed without a serious deterioration of the image quality.

DISCUSSION

The relative merits of this and other microscopical methods may now be critically discussed. The image is very similar to that produced by the scanning reflexion electron microscope.[19, 20] The great depth of field and the oblique viewpoint in both instruments permit a specimen to be observed in what is, for many purposes, its most informative aspect. The contrast mechanism is, however, different from that produced in the scanning microscope in which detail may be seen in the shadowed regions. While in many instances this

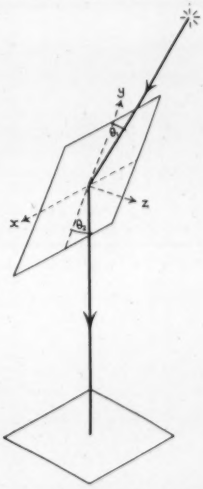

Fig. 2. Relation between resolution in object and image space

The magnification of Figs. 3–7 is indicated by the scale ellipse, of diameter shown, in accordance with Emerton's system [*Research*, 7, p. S 56 (1954)]

Fig. 1. Specimen support grid, 200 bars per inch, showing effect of chromatic magnification aberration

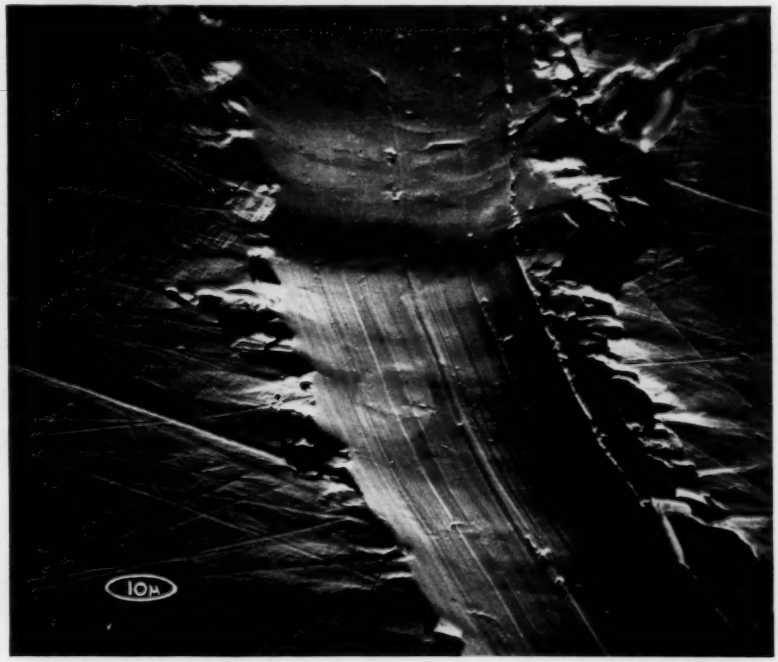

Fig. 3. Scratch on mechanically polished brass

****

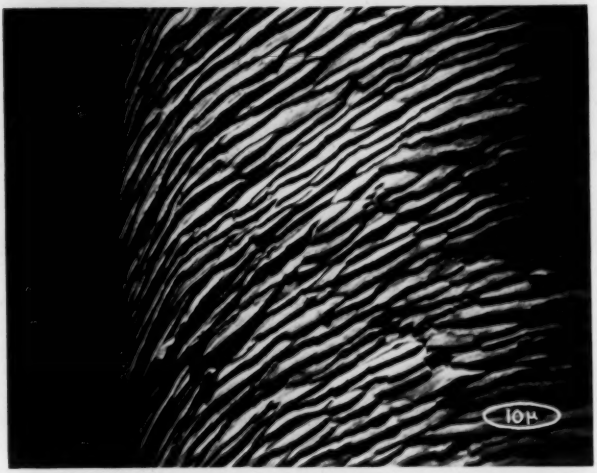

Fig. 4. Human hair

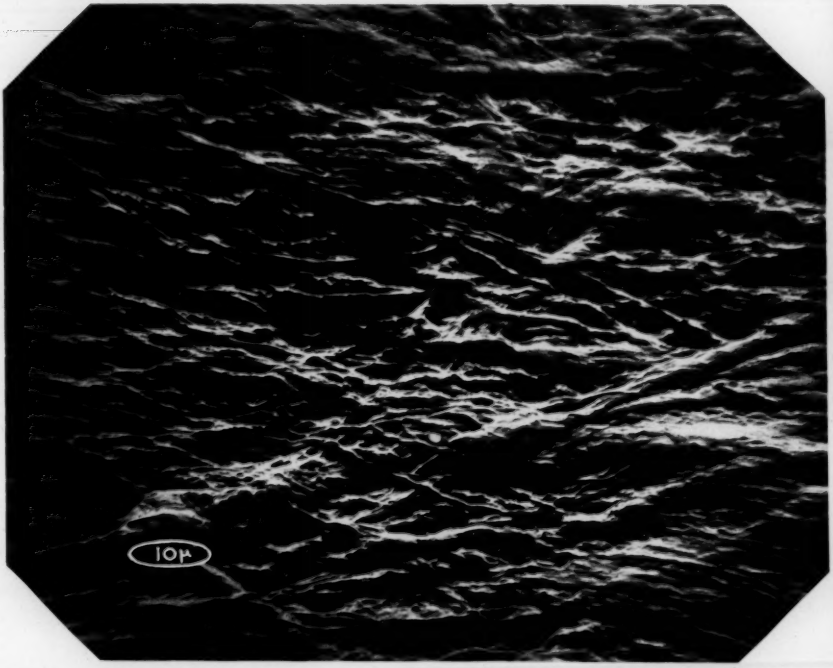

Fig. 5. Tissue paper

Fig. 6. Growing face of copper sulphate crystal

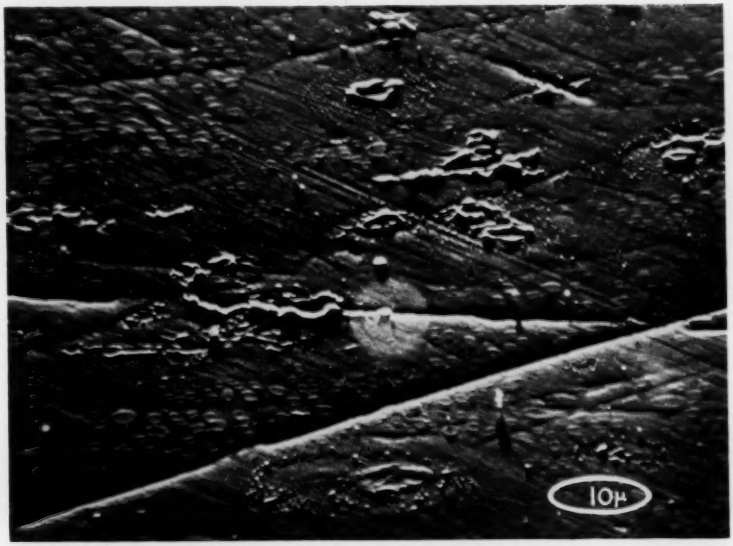

Fig. 7. Polished brass surface after passage of spark discharge

An improved spray droplet technique for quantitative electron microscopy

By H. L. Nixon, M.A., and H. L. Fisher, B.A.

See pages 68–70

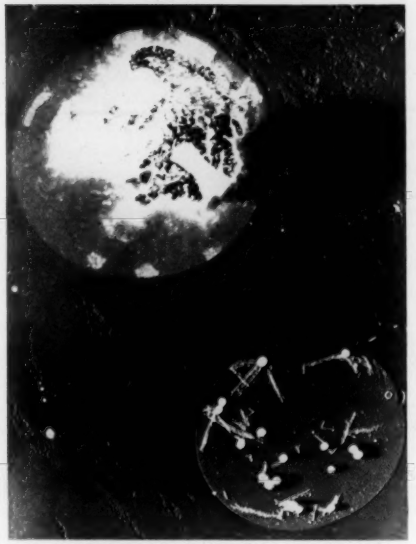

Fig. 1. Field showing large droplet which has been in contact with the wall of the apparatus and become contaminated with calcium chloride and Teepol R. The smaller droplet trace shows partly aggregated tobacco mosaic virus and latex particles

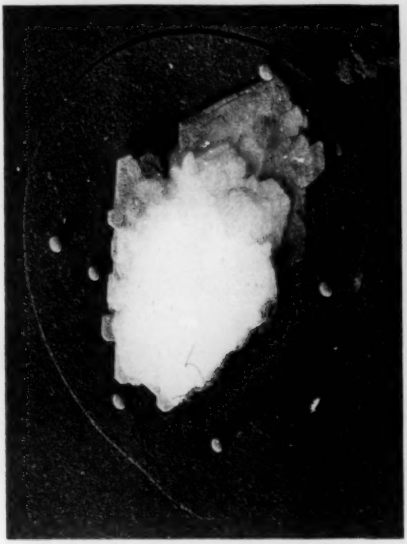

Fig. 4. Trace containing a large aggregate of kaolin flakes

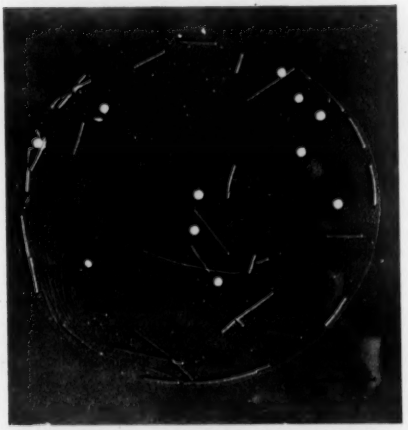

Fig. 2. Typical droplet trace suitable for counting. Note clear outline, the result of including bovine serum albumen in the sprayed fluid. The albumen layer is puckered in the lower left corner

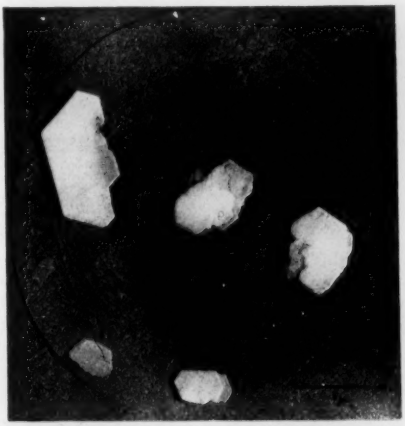

Fig. 5. Trace from a similar kaolin preparation, dispersed by treatment with sodium hexametaphosphate

extra information is valuable, the image may not then be so readily interpreted. Moreover, loss of information in shadow is only a serious drawback at very low angles of illumination and such a restriction has not been found necessary in this work.

The ability to resolve a feature in the reflexion microscope is dependent on the orientation of the feature in the specimen plane. If d is the resolving power of the microscope and d_x, d_y, d_z the smallest resolved distances in the x, y, z directions (Fig. 2) we have

$$d_x = d$$
$$d_y = d \operatorname{cosec} \theta_2$$

Features in the z direction are recognized by their shadow and the ability to resolve such a feature may be considered as the ability to resolve its shadow.

Hence $$d_z = d \sin \theta_1 \operatorname{cosec} (\theta_1 + \theta_2)$$

The table gives the three resolutions attained in typical cases of low-angle and high-angle reflexion and in the scanning reflexion electron microscope. It will be seen that the

Resolution of different reflexion instruments

Type of reflexion microscope	θ_1	θ_2	d_x	d_y	d_z
High angle	2°	24°	600	1500	50
Low angle	2°	6°	250	2400	65
Scanning	—	25° (say)	250	600	250

scanning microscope, when used under its highest resolution conditions, has a superior resolution to both reflexion microscopes. However, because it lacks the shadow magnification effect it is inferior in resolving small features in the z direction. In spite of the intrinsically higher resolution of the low-angle reflexion microscope, because of the considerable foreshortening d_y and d_z are inferior to the high-angle case.

The micrographs (Figs. 3–7) illustrate the high-angle method applied to subjects taken from biological, metallurgical and chemical fields.

Fig. 5 shows the surface of a tissue paper made for use as a capacitor dielectric. The surface is sufficiently rough to prevent useful observation by the conventional low-angle method. Angles θ_1 and θ_2 were approximately 8 and 18·5° respectively.

The growing face of a copper sulphate crystal is shown in Fig. 6. The smallest growth step visible is approximately 200 Å high.

A spark discharge was allowed to pass between the brass surface shown in Fig. 7 and a probe held above it. The crater in the top centre of the micrograph and the spherical particles are typical of the disturbance of the surface caused by this treatment. It seems likely, though it is by no means certain, that the transparent bubbles seen on parts of the surface are an oxide layer formed during the discharge. The presence of such bubbles or blisters, not so perfectly formed as in this micrograph, has been demonstrated by Hirst and Halliday[21] in their study of oxide films in the reflexion electron microscope.

In Figs. 4–6 the specimen has been replicated in copper-backed silver by Bradley's replica method.[11, 12]

CONCLUSION

A commercial electron microscope used in reflexion at high angles represents an additional microscopical method that may be of value in many fields. The reduction of the foreshortening to a more reasonable value, combined with the great depth of focus, give the image a realistic three-dimensional appearance that is comparable only with that produced by the scanning electron microscope. Because of the higher angles of illumination and viewing, rougher surfaces may be more usefully examined. The method has a resolving power of 600 Å in the direction perpendicular to the plane of incidence. While this is inferior to that claimed by Fert using ion bombardment, the method is more versatile, being applicable to the study of all metal surfaces and metal replicas. Moreover, the method can be used by the simple adaptation of a commercial instrument, and although more attention must be paid to the reduction of the chromatic error, it is not appreciably more difficult in operation than conventional reflexion work.

ACKNOWLEDGEMENT

I am indebted to Mr. H. W. Emerton for useful discussions during the early stages of this work.

REFERENCES

(1) RUSKA, E. *Z. Phys.*, **83,** p. 492 (1933).

(2) RUSKA, E., and MÜLLER, H. O. *Z. Phys.*, **116,** p. 366 (1940).

(3) VON BORRIES, B. *Z. Phys.*, **116,** p. 370 (1940).

(4) KUSHNIR, YU. M., BIBERMAN, L. M., and LEVKIN, N. P. *Bull. Acad. Sci., URSS Fer. Phys.*, **15,** p. 306 (1951).

(5) FERT, C., and SAPORTE, R. *C.R. Acad. Sci., Paris*, **235,** p. 1490 (1952).

(6) MENTER, J. W. *J. Inst. Metals*, **81,** p. 163 (1952).

(7) HAINE, M. E., and HIRST, W. *Brit. J. Appl. Phys.*, **4,** p. 239 (1953).

(8) MENTER, J. W. *J. Phot. Sci.*, **1,** p. 12 (1953).

(9) AMBOSS, K., EMERTON, H. W., and WATTS, J. *Proceedings of the International Conference on Electron Microscopy, London*, 1954, p. 560 (London: Royal Microscopical Society, 1956).

(10) EMERTON, H. W., PAGE, D. H., and WATTS, J. *Electron Microscopy. Proceedings of the Stockholm Conference, September* 1956, p. 287 (Stockholm: Almqvist and Wiksell, 1957).

(11) BRADLEY, D. E. *Research*, **8,** p. S12 (1955).

(12) BRADLEY, D. E. *Brit. J. Appl. Phys.*, **6,** p. 191 (1955).

(13) FERT, C., MARTY, B., and SAPORTE, R. *C.R. Acad. Sci., Paris*, **240,** p. 1975 (1955).

(14) PAGE, D. H. *Research*, **10,** p. 120 (1957).

(15) AMBOSS, K. *J. Sci. Instrum.*, **32,** p. 116 (1955).

(16) PAGE, D. H. *Brit. J. Appl. Phys.* To be published.

(17) CHAPMAN, J. A., and MENTER, J. W. Unpublished work.

(18) FERT, C. *Electron microscopy, Proceedings of the Stockholm Conference, September* 1956, p. 8 (Stockholm: Almqvist and Wiksell, 1957).

(19) MCMULLAN, D. *Proc. Instn Elect. Engrs*, **100,** (II), p. 245 (1953).

(20) SMITH, K. C. A., and OATLEY, C. W. *Brit. J. Appl. Phys.*, **6,** p. 391 (1955).

(21) HALLIDAY, J. S., and HIRST, W. *Proc. Phys. Soc. [London] B*, **68,** p. 178 (1955).

An improved spray droplet technique for quantitative electron microscopy*

By H. L. Nixon, M.A., and H. L. Fisher, B.A., Plant Pathology Department, Rothamsted Experimental Station, Harpenden, Herts.

[*Paper received* 9 *October*, 1956]

Improvements are described to the spray droplet method of Backus and Williams[1] for direct particle counting by electron microscopy. Decreasing the droplet size makes it possible to use much higher magnifications without sacrificing the ability to photograph each droplet trace entire on one frame, and droplets of the desired size are sorted and collected in a reproducible manner in a cascade impactor. The technique is also useful for studying the state of aggregation of a suspension.

Some factors affecting the accuracy of measurement of the polystyrene latex standard particles are discussed. Different methods yield different values, and there is at present no valid basis for selecting the best estimate.

A number of different techniques have been proposed for making estimates of particle concentration by electron microscopy. In all these methods except one[1, 2] the sampling unit is the field of view of the electron microscope in use, and the main intention of the technique is to ensure that the particles are uniformly distributed over the mount so that randomly selected fields of view may contain a random sample of the material.[3–6] However, the very nature of the specimen preparation process, involving the formation of a dry mount from a liquid suspension, makes this essential condition very difficult to satisfy and always a little uncertain of achievement.

The spray droplet technique of Backus and Williams[1, 2] avoids all these difficulties by transferring the sampling from the electron microscope mount to a spray gun, which is used to make droplets small enough for a single dried trace, containing both unknown and standard particles, to be photographed entire on one frame. The volume of the droplet when it left the spray gun and the concentration of the unknown particles may then be estimated from the known concentration of standard particles by counting each species in each of a number of droplet traces. Williams and his co-workers have since shown that the method is capable of a precision limited only by statistical considerations and the accuracy with which the concentration of standard particles is determined.[2, 7–10] Nevertheless, there are some practical limitations which make the method difficult to apply as a research tool, and the main purpose of this paper is to describe modifications by which these limitations can be overcome.

The shortcomings of the original method are: (i) nearly all the droplet traces are too large to permit the use of adequate magnification and at the same time retain the essential convenience of photography of each trace entire on one frame;

(ii) the catching of a suitable density of droplets of a convenient size on filmed grids is a highly uncertain process, as the spray gun is merely directed towards the grids from a distance of some feet over open bench. A low pressure, low velocity sprayer (atomizer), although easier to use,[2] is no real answer to the problem because it produces a higher proportion of larger, unwanted droplets;

(iii) the standard particles are too large for counts of maximum accuracy with minimum labour, for which it is necessary to have the two species present in roughly equal numbers. This limitation becomes more serious as the droplet size is reduced, when the standard particles, if too large, come to occupy a high proportion of the area of the trace, and small unknown particles may be missed in counting when they lie under the edges or in the shadow of the much larger standard particles.

* Originally presented at the Annual Conference of the Electron Microscopy Group of The Institute of Physics held in Reading, July 1956.

DROPLET SIZE AND TRACE DIAMETER

The upper limit to the trace diameter is set by the field of the microscope, coupled with the necessity to use a high enough magnification to ensure proper resolution of the detail desired.[11] For counting plant viruses, electron optical magnifications of 8–12 000 have proved suitable, and this permits the photography of circular droplet traces up to about 3·5 μ in diameter in a frame 5 cm square. Experiments indicate that, under our conditions, such traces arise from droplets which are about 2 μ in diameter immediately before impaction on the supporting film.

The deposition of small spherical particles on surfaces of various kinds has been studied by Gregory,[12, 13] using a wind tunnel. He found that the trapping efficiency of a surface goes down as the area of the surface increases, as the size of particle being caught becomes smaller and as the wind speed decreases, so that the efficiency of an extended surface, such as an electron microscope specimen grid resting on a glass slide, is vanishingly small for 2 μ particles in winds of only a few metres per second. It is therefore clear that, even if the air close to the grids contains a high proportion of droplets of the desired size, only very few will be caught on grids merely exposed in the open; under these conditions the grids will always catch a high proportion of larger, unwanted droplets for which their surface is a more efficient trap. Some device to select out and catch droplets of the desired size is therefore necessary. These requirements are met by the cascade impactor,[14] which we have used for the purpose. The instrument is easily adapted to the needs of electron microscopy by attaching one or more filmed grids to the desired slide by means of cellulose tape arranged to secure the grids by one edge so that the centre of the trace produced by the impactor passes through a diameter of each grid. Either collodion or formvar membranes may be used, but not unsupported carbon films as these are destroyed by the high velocity air stream in the impactor.

THE STANDARD PARTICLES AND THEIR MEASUREMENT

Probably the most important source of error in a method of this kind lies in the determination of the concentration of the standard particles. We have used as a source of standard particles the smallest of a new series of polystyrene latexes

made by the Dow Chemical Co., Midland, Michigan, U.S.A., and designated by them LSO40A. It has spherical particles nominally 880 ± 80 Å in diameter,[15] a size convenient for work with plant viruses. This value for the diameter was obtained by measurement of electron microscope images obtained under carefully controlled conditions, and similar measurements in this laboratory have yielded an estimate of 850 ± 33 Å for unshadowed particles under conditions of minimum electron bombardment. It is possible to make a rough estimate of the reliability of these measurements by examining the much larger body of data for the original Dow polystyrene latex 580G, the diameter of which is generally accepted to be 2590 Å. The large difference in particle size may alter the relative importance of the many factors affecting the measurements, but it is reasonable to assume that broadly similar considerations apply to both cases. The value of 2590 Å is the mean of a number of estimates made in different laboratories,[16] but there are on record a number of discrepant estimates, also obtained by electron microscopy in various other laboratories.[17–21] Low molecular weight material in the latex suspensions may coat the particles and cause the diameter to be overestimated,[21] and similar errors may result from electron-beam induced contamination.[15] Errors in the opposite sense may be caused by exposure to an intense electron beam without previous irradiation at a lower intensity.[20]

Because the measurements which went to make up the 2590 Å value were in good agreement with each other, it is hard to escape the conclusion that the particles were, in fact, close to 2590 Å in diameter when they were photographed. The 2590 Å value may therefore be acceptable for use when the particles are to serve as an internal standard of magnification and shadow angle, within the limits imposed by the necessity to keep both the duration and the intensity of electron irradiation to a minimum. However, for the present purpose it is the diameter in liquid suspension which is required, and measurements which lead directly to this without the complications involved in electron microscopy are therefore of special interest. There is an estimate at 2720 Å by light scattering,[22] but the method is not accurate enough to enable the value to be distinguished clearly from the 2590 Å one derived from electron microscopy. Sedimentation in the ultra-centrifuge yielded a value of 2520 ± 20 Å, and the method is an attractive one because of the simplicity of the assumptions involved.[23] The interparticle distance has also been measured by X-ray methods, yielding results of 2740 Å,[24] 2731 ± 3 Å,[25] 2687·5 ± 1·2 Å[26] and 2830 ± 20 Å.[27] The question of what is really measured in this way, and its relation to true particle diameter, is complex, since interparticle spacing is clearly a different quantity to particle diameter.

From this review we conclude that there are good reasons for thinking that the accepted value of 2590 Å for the Dow 580G latex particle may be a much less accurate estimate than it was first thought to be. At present there is no satisfactory way of telling which of the many estimates is closest to the true value. For the LSO40A latex which we have used, a corresponding uncertainty in the measurement of diameter would lead to an error of up to 30% in the mean particle mass, and hence also in all particle counts. In these circumstances we have thought it best to accept, for the time being, the electron microscope value of 880 ± 80 Å for the mean diameter of the LSO40A latex.[15] Making this assumption, and taking the density of polystyrene to be 1·05 g/cm^3, the mean mass of a single LSO40A particle is $3{\cdot}75 \times 10^{-16}$ g.

THE SPRAY SOURCE

We have tried a wide variety of home-made and proprietary sprayers of both high and low velocity patterns, and although all have given some droplets of the desired size, we have found the type A54 air brush (by The Aerograph Co. Ltd.) to be the most satisfactory. This is a high pressure spray gun, made of metal, and intended to work with small samples. The cup holds only 1·0 ml., and 0·2 ml. is quite sufficient to operate the instrument and prepare mounts.

EXPERIMENTAL METHODS

The air brush is arranged to deliver spray into one end of a cylindrical glass mixing chamber, 15 cm long and 5 cm in diameter. Here it is mixed with additional air drawn in from the room through a jet dust trap, as the cascade impactor requires a flow of 17·5 l./min, and the air brush only provides 1–4 l./min according to setting. The impactor is fitted to a rubber stopper which closes the end of the mixing chamber remote from the air brush, and the suction line to it passes through a flow meter (by The Rotameter Co. Ltd.) so that the rate can be set to the value desired. It is usually convenient to use stage 3 of the impactor, although there is, of course no reason why any other stage should not be used if required. Stages earlier than the one in use are fitted with blank slides wrapped in filter paper, and these, together with the whole of the inside of the mixing chamber and impactor, are coated with a mixture of Teepol R (by Shell Chemicals Ltd.) and calcium chloride, so that droplets which come into contact with the walls of the apparatus, and thereby become contaminated, can be easily recognized and rejected from the counts (Fig. 1, p. 66). Unless this is done, statistical tests indicate that a small proportion of droplets have had their origin in a material with a different composition from the majority. Such droplets are possibly formed as satellites on the impaction of much larger, unwanted droplets in stages 1 and 2 of the impactor, and perhaps also on the walls of the mixing chamber. The specimen for spraying should contain, in addition to the "unknown" particles, about 10^{11} latex particles per ml., and approximately 1 part in 3000 of bovine serum albumen.[1] If it is not already substantially free of dissolved salts it must be dialyzed against water or against a volatile salt such as ammonium acetate, benzoate, chloride, carbonate, or succinate.[1] If this is not done the presence of salt crystals may interfere with counting. Spraying times are of the order of one to five seconds for the sizes of mixing chamber given, with the air brush adjusted so that the emerging spray is just visible in a good light. Under these conditions it takes about one second for the mist to pass from the air brush to the impactor, and there is a concentration of 70 : 1 as a result of evaporation of water from the droplets in flight. This factor may be increased if desired by lengthening the mixing chamber, but the conditions then become very critical, and any slight alteration, for instance in room temperature or humidity, may result in total evaporation of the wanted droplets prior to collection. It is usually advantageous to shadow the mounts before examining them in the electron microscope, and if it is known that they will only be required for counting and not for detailed morphological studies, recognition and counting are made easier if the shadow layer is rather thicker than usual. Counting may be done from photographs, or, if the numbers of particle are small, it may be possible to count directly from the viewing screen of the microscope.

The χ^2 test is a useful one for testing the validity of the assumption that all the droplet traces selected for counting

have come from a common source, and we have found it convenient to accept values of χ^2 which correspond to values of p which are greater than 0·05. A further check on a long series of counts is given by the distribution of p.[28] The fact that the cascade impactor selects only a very narrow size fraction from the wide range produced by the air brush makes it necessary to check that there is no change in the ratio of standard to unknown particles over a wide range of droplet sizes before it can be assumed that the common source indicated by the χ^2 test is, in fact, the fluid sprayed. Careful tests have failed to show any variation of ratio with droplet size, and nothing in our experience with the method has suggested that there is any reason for suspecting trouble of this kind. Estimates of error may be made by any of the usual methods, or by the rapid approximate method of R. A. Fisher.[28]

The method as described was intended for counting plant virus particles. Nevertheless, the most rigorous check on the actual counting technique is made by counting a number of samples forming a dilution series of one polystyrene latex, the "unknown," against another latex, the "standard," having a different particle size, and present in each sample at the same known concentration. This avoids any complications over purification, aggregation or disintegration of a labile virus particle, and has the added advantage of checking at the same time the calibration of one latex against the other. The results of such an experiment are shown in Fig. 3. Here the concentration of LSO55A particles, 1880 ± 80 inÅ diameter,[15] as determined by electron microscope particle counts using the LSO40A latex as a standard, is plotted against the concentration of LSO55A particles added, as calculated from the known diameter and the dry weight present. The apparent departure from complete recovery is almost certainly due to a difference in the calibration of the two latexes, and not to an actual loss of particles in the analyses.

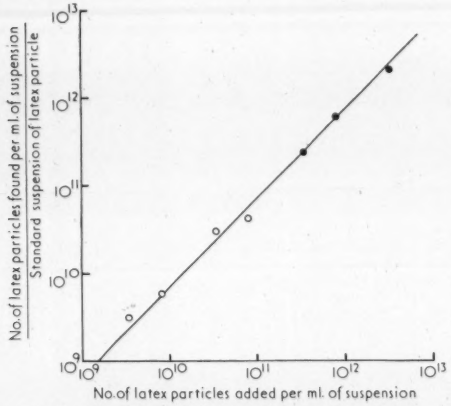

Fig. 3. Number of LSO55A latex particles added, per ml. of suspension, calculated from dry weight present, *versus* numbers of LSO55A particles found, per ml. of suspension, by electron microscope counting against standard suspension of LSO40A latex particles

○ = points obtained by visual counting on electron microscope screen.

● = points obtained by counting from photographic plates.

The same technique is also a useful one for studying the stage of aggregation of a suspension. Using conventional "gross drop" mounting techniques, it is impossible to be sure whether an observed aggregate was existing as such in the liquid suspension, or whether it was formed during the drying of the liquid on the mount. Using the spray droplet method, and working at very high dilution so that there is an average of fewer than one particle (or aggregate) per droplet trace, it is certain that any aggregate found was present as such in the liquid. Figs. 4 and 5 (see p. 66) show droplet traces made from kaolin suspension before and after dispersion with sodium hexametaphosphate.

ACKNOWLEDGEMENTS

We are indebted to the Dow Chemical Co. for samples of polystyrene latex, to Dr. A. Kleczkowski for advice on statistical matters and to Mr. R. D. Woods for technical assistance.

REFERENCES

(1) BACKUS, R. C., and WILLIAMS, R. C. *J. Appl. Phys.*, **21**, p. 11 (1950).
(2) BACKUS, R. C., and WILLIAMS, R. C. *J. Amer. Chem. Soc.*, **71**, p. 4052 (1949).
(3) SHARP, D. G. *J. Appl. Phys.*, **19**, p. 1188 (1948).
(4) SHARP, D. G. *J. Appl. Phys.*, **23**, p. 162 (1952).
(5) BEARD, J. W., and SHARP, D. G. *Proc. Soc. Exper. Biol. Med.*, **81**, p. 90 (1953).
(6) HARTMAN, R. E., GREEN, T. D., BATEMAN, J. R., SENSENEY, C. A., and HESS, G. E. *J. Appl. Phys.*, **24**, p. 90 (1953).
(7) STEERE, R. L. *J. Appl. Phys.*, **21**, p. 70 (1950).
(8) STEERE, R. L. *Amer. J. Bot.*, **39**, p. 211 (1952).
(9) STEERE, R. L., and WILLIAMS, R. C. *Phytopathology*, **42**, p. 518 (1953).
(10) WILLIAMS, R. C., BACKUS, R. C., and STEERE, R. L. *J. Amer. Chem. Soc.*, **73**, p. 2062 (1951).
(11) HAINE, M. E., and MULVEY, T. *Proceedings of International Conference on Electron Microscopy, London* 1954. To be published by Royal Microscopical Society, London.
(12) GREGORY, P. H. *Ann. Appl. Biol.*, **38**, p. 357 (1951).
(13) GREGORY, P. H., and STEDMAN, O. J. *Ann. Appl. Biol.*, **40**, p. 651 (1953).
(14) MAY, K. R. *J. Sci. Instrum.*, **22**, p. 187 (1945).
(15) BRADFORD, E. B., and VANDERHOFF, J. W. *J. Appl. Phys.*, **26**, p. 864 (1955).
(16) GEROULD, C. H. *J. Appl. Phys.*, **21**, p. 183 (1950).
(17) SCOTT, G. D. *J. Appl. Phys.*, **20**, p. 417 (1949).
(18) COSSLETT, V. E. *Proceedings of International Conference on Electron Microscopy, Delft*, 1949.
(19) KERN, S. F. and KERN, R. A., *J. Appl. Phys.*, **21**, p. 705 (1950).
(20) WATSON, J. H. L., and GRUBE, W. *J. Appl. Phys.*, **23**, p. 157 (1952).
(21) ELLIS, S. G. *J. Appl. Phys.*, **23**, p. 728 (1952).
(22) DANDLIKER, W. B. *J. Amer. Chem. Soc.*, **72**, p. 5110 (1950).
(23) SHARP, D. G. *J. Appl. Phys.*, **21**, p. 71 (1950).
(24) YUDOWITCH, K. L. *J. Appl. Phys.*, **22**, p. 214 (1951).
(25) LEONARD, B. R., ANDEREGG, J. W., KAESBERG, P., and BEEMAN, W. W. *J. Appl. Phys.*, **23**, p. 152 (1952).
(26) DANIELSON, W. E., SHENFIL, L., and DUMOND, J. W. M. *J. Appl. Phys.*, **23**, p. 860 (1952).
(27) HENKE, B. L. *Chem. Eng. News*, **32**, p. 2272 (1954).
(28) THORNTON, H. G., and GRAY, P. H. H. *Proc. Roy. Soc. B*, **115**, p. 522 (1934).

A property of a buckled elastic rod

By G. A. V. Leaf, B.Sc.,* Hosiery and Allied Trades Research Association, Nottingham

[*Paper first received* 25 *June, and in final form* 30 *July*, 1957]

One shape assumed by a perfectly elastic rod buckled by appropriate forces and couples at its ends is studied. It is shown that the ratio of maximum height to maximum width is independent of the material of the rod. Also, this ratio is linearly related to the distance between the ends of the rod expressed as a fraction of its length, provided the fraction is roughly less than one half.

THEORETICAL INVESTIGATION

When a pair of balancing forces, with or without a pair of balancing couples, act at the ends of a perfectly elastic and naturally straight rod, so as to buckle it, the form of the curve assumed by the deformed rod is called an elastica. In this note we shall investigate a property of the particular elastica shown in Fig. 1. Here the naturally straight rod ABA' is

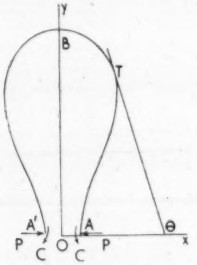

Fig. 1. The elastica

bent by two equal and opposite forces P, whilst the tangents to the curve at A and A' are kept parallel, and perpendicular to the line of action of P, by the application of equal and opposite couples C, as shown.

Take rectangular axes Oxy with origin O at the mid-point of AA', and Ox along the line of action of the forces P. Let T be any point of the elastica, where arc $AT = s$; and let θ be the angle between the tangent to the curve at T and the positive direction of Ox. The length of the rod is L and $AA' = aL$.

Taking moments about T for the portion AT of the elastica gives

$$Bd\theta/ds = Py - C$$

where B is the flexural rigidity of the rod, assumed to be constant throughout its length. Writing

$$b^2 = B/P,\ c = C/P,$$

this equation becomes

$$b^2 d\theta/ds = y - c. \tag{1}$$

Now $dy/ds = \sin\theta$, and equation (1) becomes, after integration,

$$y^2 - 2cy = -2b^2 \cos\theta,$$

since, at A, $y = 0$ and $\theta = \pi/2$.

Adding c^2 to both sides of this equation gives

$$\begin{aligned}(y - c)^2 &= c^2 - 2b^2 \cos\theta \\ &= c^2 + 2b^2 - 4b^2 \cos^2\theta/2.\end{aligned}$$

Let $\cos\alpha = c^2/2b^2$, and write

$$\cos(\theta/2) = k \sin\phi \tag{2}$$

where $k = \cos(\alpha/2)$. Then

$$y - c = \pm 2bk \cos\phi \tag{3}$$

If $\phi = \phi_0$ when $\theta = \pi/2$ at A, then from (3),

$$-c = \pm 2bk \cos\phi_0 \tag{4}$$

since $y = 0$ at A. Thus equation (3) may be written

$$y = \pm 2bk(\cos\phi - \cos\phi_0). \tag{3a}$$

Again, from (1) and (3),

$$b^2 d\theta/ds = \pm 2bk \cos\phi$$

and from (2),

$$d\theta = -2k \cos\phi\, d\phi/(1 - k^2 \sin^2\phi)^{\frac{1}{2}}$$

Therefore

$$ds = \mp b(1 - k^2 \sin^2\phi)^{-\frac{1}{2}} d\phi.$$

Integration gives

$$s = \mp b \int_{\phi_0}^{\phi} (1 - k^2 \sin^2\phi)^{-\frac{1}{2}} d\phi,$$

no integrating constant being needed since $s = 0$ when $\phi = \phi_0$. This expression for s may be written

$$s = \mp b[F(k, \phi) - F(k, \phi_0)], \tag{5}$$

where $F(k, \phi)$ is an elliptic integral of the first kind with modulus k.

Now at the point B of the elastica, $s = L/2$; also $\theta = \pi$ and accordingly $\phi = 0$. Putting these values in (5) gives

$$L/2 = \mp b[-F(k, \phi_0)] \tag{6}$$

The left hand side of this equation is always positive and, since b and $F(k, \phi_0)$ are positive also, the upper sign in equations (6), (5), (3) and (3a) must be taken. Equation (6) then gives

$$b = L/2F(k, \phi_0), \tag{6a}$$

and from (4),

$$\cos\phi_0 = -c/2bk. \tag{4a}$$

Next we have

$$dx/dy = \cot\theta$$

Thus $dx/d\phi = \cot\theta\, dy/d\phi$

$$= b[2(1 - k^2 \sin^2\phi)^{\frac{1}{2}} - (1 - k^2 \sin^2\phi)^{-\frac{1}{2}}] \tag{7}$$

Integrating,

$$x = b[2E(k, \phi) - F(k, \phi)] \tag{8}$$

where $E(k, \phi)$ is an elliptic integral of the second kind with

* Now at Leicester College of Technology.

modulus k. No integrating constant is necessary since $x = 0$ and $\phi = 0$ at B.

At A, $\phi = \phi_0$ and $x = aL/2$, and from (8),

$$aL/2 = b[2E(k, \phi_0) - F(k, \phi_0)].$$

Substitution for b from equation (6a) gives

$$a = [2E(k, \phi_0) - F(k, \phi_0)]/F(k, \phi_0) \qquad (9)$$

Now consider the maximum value of x for the case in which it is greater than OA. This maximum value occurs when $dx/d\phi = 0$, or

$$2(1 - k^2 \sin^2 \phi)^{\frac{1}{2}} - (1 - k^2 \sin^2 \phi)^{-\frac{1}{2}} = 0$$

from (7). This leads to

$$\sin \phi_m = 1/k\sqrt{2}, \cos \phi_m = c/2bk,$$

where ϕ_m is the value of ϕ when x is a maximum. The positive sign is taken since $\phi_m < \pi$ and $\phi_m \neq \phi_0$. If d is the greatest total width of the elastica,

$$d = 2b[2E(k, \phi_m) - F(k, \phi_m)]$$

The maximum height D of the elastica is equal to OB, and is found by putting $\phi = 0$ in (3a). This gives

$$D = 2bk(1 - \cos \phi_0)$$

Thus $$D/d = k(1 - \cos \phi_0)/[2E(k, \phi_m) - F(k, \phi_m)] \qquad (10)$$

Equations (9) and (10) may be regarded as parametric equations for the relationship between D/d and a, the parameter being k. It follows that D/d is independent of the elastic properties of the rod.

Numerical calculation shows that this relationship is linear so long as $d \geqslant aL$ (i.e. if $a \leqslant 0{\cdot}46$). The equation of the relationship is

$$D/d = -2{\cdot}72a + 2{\cdot}08 \qquad (11)$$

From this equation it can be seen that if $a = 0$, i.e. if the two ends of the elastica are brought together, the ratio $D/d = 2{\cdot}08$, irrespective of the material or length of the rod.

EXPERIMENTAL CONFIRMATION

The above theory was checked by experiment. Strips made from materials with entirely different elastic properties were used, namely (i) spring steel, (ii) phosphor bronze, (iii) acetate film, (iv) drawing paper. Values of D/d were obtained for several values of a in each case and the results

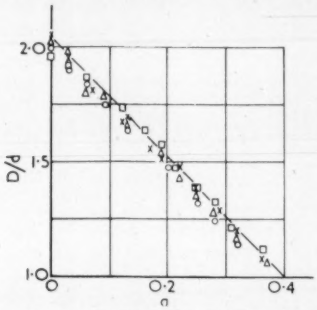

Fig. 2. Relation between D/d and a
×, spring steel; ○, phosphor bronze; □, acetate film; △, drawing paper.

are plotted in Fig. 2. The line given by equation (11) is drawn on this figure and it will be seen that the experimental results are in good agreement with it.

ACKNOWLEDGEMENTS

The author wishes to thank his colleagues, Mr. D. L. Munden and Mr. T. S. Nutting, for suggesting this type of investigation, and Miss M. Williams for performing the experiment. Thanks are also due to the Director of Research and Council of the Hosiery and Allied Trades Research Association for permission to publish this paper.

The influence on the stress distribution in an adhesive lap joint of bending of the adhering sheets

By A. S. McLaren, B.Sc., A.Inst.P., and I. MacInnes, A.R.C.S.T., Grad.Inst.P., The Royal College of Science and Technology, Glasgow

[*Paper first received* 22 *July, and in final form* 30 *August*, 1957]

The mathematical analysis of Goland and Reissner of the effect of deformation due to load is examined photoelastically and extended to cover a wider range of suchlike deformations. It is shown that introduction of a bending moment in the sheets opposite to that occurring in the conventional joint can produce a stress distribution on the glue line free from high normal stresses and fairly uniform in shear. A modified design of lap joint to ensure this is proposed.

INTRODUCTION

The normal adhesive lap joint, whether of wood to wood or metal to metal will usually consist of a thin layer of synthetic resin adhesive between much thicker adhering sheets, or adherends, the length of the overlap being again large in comparison with the sheet thickness. It cannot be assumed that the load is evenly distributed over the adhesive area and photoelastic examination of the stress distribution in an enlarged adhesive layer between steel bars had shown that serious stress concentrations are liable to arise on the free end surfaces of the adhesive, particularly at the leading corners.[1] The position and magnitude of the stress concentration was shown to depend particularly on the contact angle of the adhesive to the adherend. Apart from this end effect, the adhesive appeared to be in a state of fairly uniform shear throughout the length of the overlap.

Mathematical attempts to deduce the stress distribution, in particular by Volkersen[2] and by Goland and Reissner,[3] assume uniformity of stress across the thickness of the layer and so are not capable of resolving the factors leading to variation across the free end surface. Nevertheless, they do discuss the variations along the length of the joint in a manner

which should give values which bear some relationship to the mean stresses. Both papers allow for the effect on stress of some of the resulting deformation, Volkersen for the lengthwise stretching of the adherends [Fig. 1(*a*)], assumed to

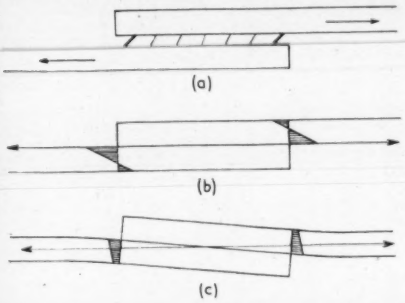

Fig. 1. Effect of elastic deformation of joint considered by (*a*) Volkersen, (*b*) and (*c*) Goland and Reissner. Normal boundary stresses on joint shown in (*b*) and (*c*)

remain straight, and Goland and Reissner for the rotation of the joint with the bending of the overlapped, and hence not collinear, adherends [Fig. 1 (*b*) and (*c*)]. Both papers find that the particular stresses considered should, in general increase on going from the centre towards the end of the adhesive, but Goland and Reissner show that the greater the bending produced by the applied load, the less should be this relative increase.

The photoelastic examination described in this paper centres around the significance of this last point. Mylonas's tests,[1] using steel adherends of Young's modulus and flexural rigidity of a very much higher order than that of the adhesive layer do not allow the effects of load deformation to be observed. Substitution of the steel adherends by similarly dimensioned ones of elasticity more comparable with the adhesive allows the effect of the bending to be examined directly. The effect of stretching is, however, likely to be of no significance in a joint sufficiently enlarged in thickness as to be examinable photoelastically. The analysis of Goland and Reissner, therefore, is followed exclusively.

Goland and Reissner consider the two extreme cases where due to variations in elastic moduli and dimensions of adherends and of adhesive, the strain energy can be regarded as being localized in (*a*) the adherends, and (*b*) the adhesive layer. In the former, where the adhesive is relatively unstrained this layer is thought merely to transmit stress applied to one side to the other and so this layer is omitted in the analysis. The problem becomes then the stress distribution in a beam of thickness $2t$ and length $2c$ due to the loads applied by the adherends of thickness t and off centre at the ends, it being appreciated that the two applied tensions must be collinear and pass through the centre of the joint. In case (*b*) the main difference is the presence of a central layer of thickness η of different elasticity (Fig. 2).

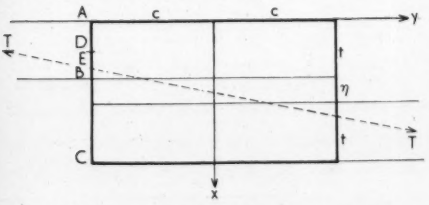

Fig. 2. Diagram of joint to which load is applied as a distributed boundary stress by adherend

The resultant force T applied by the adherend to the face ABC is analysed into a longitudinal tension, which can be taken as T for a long joint and acting at D, the mid-point of AB, a shear force V_0 and a moment M_0; M_0 will be the bending moment in the adherend just free of the joint. As the adherends are regarded as cylindrically bent plates, the linear stress distribution from tension at one side to equal compression on the opposite associated with a bending moment M_0 in such a plate is assumed to exist across AB. M_0 is put equal to $K(T \times \frac{1}{2}t)$ and so the boundary loads applied to the joint in cases (*a*) and (*b*) are:

$$\text{at } y = -c \qquad (a) \qquad (b)$$

$$\sigma_y \begin{cases} = p + pK\left(6\frac{x}{t} - 3\right) & 0 \leqslant x < t \quad 0 \leqslant x < t \\ = 0 & t < x \leqslant 2t \quad t < x \leqslant 2t + \eta \end{cases}$$

$$\text{at } y = +c$$

$$\sigma_y \begin{cases} = 0 & 0 \leqslant x < t \quad 0 \leqslant x < t + \eta \\ = p + pK\left(9 - 6\frac{x}{t}\right) & t < x \leqslant 2t \quad t + \eta < x \leqslant 2t + \eta \end{cases}$$

and the stresses are calculated on the assumption that no deformation enters to alter these. It is assumed that the only effect of the load on the geometry of the problem is to produce a rotation of the joint about its centre and relative to the line of action of the load [Fig. 1(*c*)], this rotation reducing the factor K. The shear forces are omitted from the calculation, being reckoned small.

Now it is apparent that as the line of action of the applied loads T passes through E on AB that the factor $K = DE/DB$ and that the effect of variation of K can be tested just as correctly by changing the direction of the applied loads as by loading the adherends centrally and allowing bending to take place. As will be discussed later, this allows exploration of a wider range of values of K than could be produced by bending alone and was used to broaden the examination of stress systems in joints.

EXPERIMENTAL

Two series of tests were performed. In the first, the lap joint consisted of adherends each $\frac{1}{4}$ in. thick, adhesive layer of thickness varying between zero and $\frac{1}{2}$ in., the whole model being cast in one of Araldite (by Aero Research Ltd.) (100 parts F, 20 parts 33/980, 11·5 parts Hardener 951). In the second, intended to simulate more closely Redux-bonded aluminium, where the adhesive layer has a Young's modulus about 1/20th that of aluminium, the adhesive layer was cast instead from Araldite consisting of 100 parts F, 70 parts 33/980 and 9 parts 951. In the former, the effect of thickness of adhesive and of direction of applied load were examined, a more detailed study being made where the adhesive had zero thickness. In the latter, the effect of angle of inclination of free end of adhesive surface was also studied.

Technique. A suitable mould was prepared by pouring Vinamold (by Vinatex Ltd.) HMC.18 around a replica of the whole model, or adherend or adhesive as required. Araldites

F and 33/980 were premixed by tumbling in a two-thirds filled sample bottle at about 10 rev/min for about two hours and thereafter freed from bubbles by evacuating on a water pump for about the same period. The hardener necessary was added and tumbled and rolled by hand for around 12 min, or until a rise in temperature was just perceptible, care being taken to minimize the introduction of air bubbles. The poured model was allowed to set overnight at room temperature inside a box containing calcium chloride.

For composite models either two selected adherends were placed in the mould for the whole model and the space for the adhesive poured and again allowed to set overnight or the procedure was reversed; both methods were successful. The complete model was turned smooth on both sides and polished.

The loaded model was viewed immersed in a mixture of around 2/1 of 1-bromonaphthalene and liquid paraffin. The load was applied through brass stirrups attached to the ends and designed to allow the direction of the load to be chosen approximately and adjusted freely. The direction of the load was indicated by a loop of thread passing round both load pins and held taut, and in contact with the pins, by an elastic band attached to one end. The model was normally photographed in mercury green monochromatic light in a dark-ground circular polariscope, but when directions of principal stresses were required, the image was projected on to a suitable screen, plane polariscope setting being used.

Observations. Homogeneous models (i.e. single castings) in which the adhesive layer was rectangular and ran the whole length of the overlap showed the same type of pattern of fringes for all thicknesses of "adhesive layer." Zero thickness was therefore chosen for special examination as this conformed to the simpler pattern analysed by Goland and Reissner. In all cases where $K > 0$ the fringe pattern had the same general character, the order being a minimum at the centre of the joint and increasing along the glue layer towards a peak at the joint edge. The free end surface of the adherend was in tension, this increasing regularly across the end to the same peak value at the end of the glue line [Fig. 3(*a*), (*b*) and (*c*)]. Change of K value with the same load produced an approximately proportional change in the peak fringe value while not appearing to affect the order at the centre.

Extension of the examination of the effect of change of bending moment in the negative range showed that for K less than $-0{\cdot}5$ approximately, the stress on the free end of the adherend is compressive and increases in magnitude with further reduction of K. The normal or "tearing" stress at the end of the glue line appears to pass through zero for a

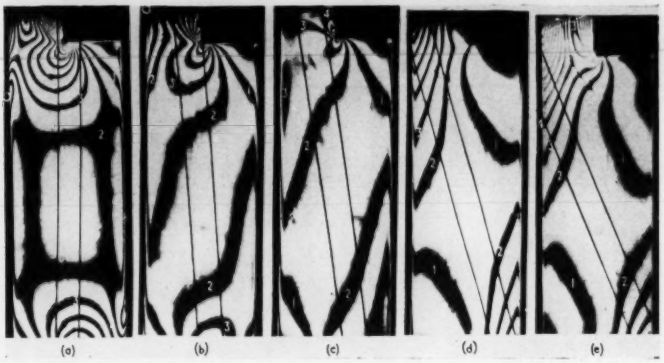

Fig. 3. Fringe pattern in homogeneous joint without adhesive layer. Bending moment factor K is (*a*) $+1{\cdot}2$, (*b*) $+0{\cdot}6$, (*c*) $+0{\cdot}2$, (*d*) $-0{\cdot}5$, (*e*) $-1{\cdot}3$. The parallel lines are the thread loop between the loading pins

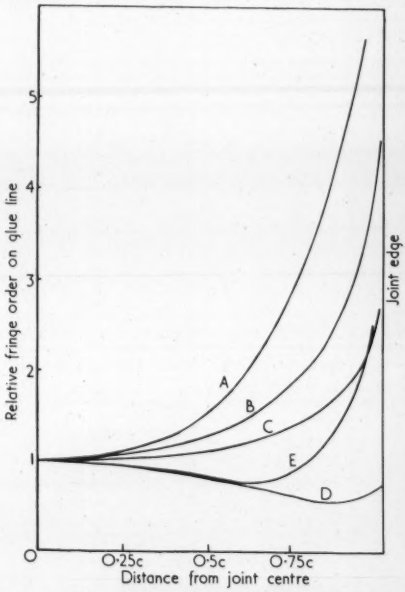

Fig. 4. Fringe order on glue line relative to fringe order at centre; from Fig. 3

value of K of approximately $-0{\cdot}5$. Under this loading the fringe value on the glue line rises to a maximum at the centre (Figs. 3 and 4) and the end of the glue line seems to have lost its significance as the point of greatest stress.

Stress trajectories for values of K of $+1$ and $-0{\cdot}5$ show that the line of application of the load coincides with a stress trajectory for a considerable distance each side of the centre [Figs. 5 (*a*) and (*b*)]. In the particular case of $K = +1$ the

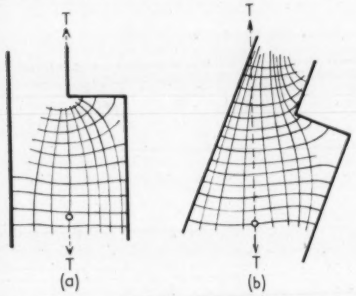

Fig. 5. Stress trajectories, homogeneous models, K values (*a*) $+1{\cdot}0$, (*b*) $-0{\cdot}5$, *o*, joint centre

stress along the central region of the glue line must be therefore a combination of longitudinal tension and normal or "tearing" stress; no transference of load from one adherend to the other by shear could take place across the glue line around its centre. This is in agreement with the deductions of Goland and Reissner.

Line integration analysis along the glue line is not capable of yielding high accuracy in the presence of a high stress concentration at the end, but was considered justified for the particular cases of $K = -0{\cdot}5$ and $K = 0$. Fig. 6 shows

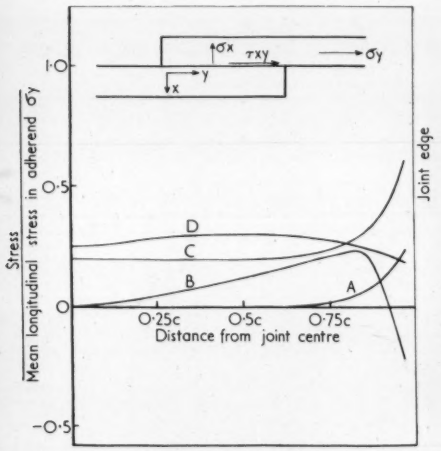

Fig. 6. Stresses on glue line

Tearing stress σ_x (*A*) $K = 0$, (*B*) $K = -0{\cdot}5$.
Shear stress τ_{xy} (*C*) $K = 0$, (*D*) $K = -0{\cdot}5$.

the distributions of shearing and of "tearing" or normal stress obtained.

In the composite models which were geometrically similar to the homogeneous ones the fringe patterns were fairly similar in some important aspects, allowance being made for the fringe value of the adhesive being around one quarter of that of the adherends. Comparison is best made between models with a thick adhesive layer not running the full length of the overlap (Fig. 7). Thus for K positive, the fringe order

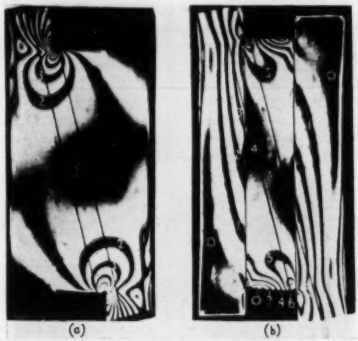

Fig. 7. Fringe patterns, models with thick adhesive layer, $K = 1$

(*a*) adhesive homogeneous with adherends.
(*b*) adhesive of Young's modulus approximately 1/20th that of adherends.

rose from a minimum at the centre of the adhesive layer to a highest value at the leading corner. The high tension in the free surface at the leading corner fell away on traversing the end, but gave way to slight compression at the other extreme. Increase in K again produced no change at the centre, but an increase in rate of rise towards the increased value at the leading corner (Figs. 8 and 10).

Examination of direction of stresses showed a striking change. While the principal stresses in the adherends adjacent

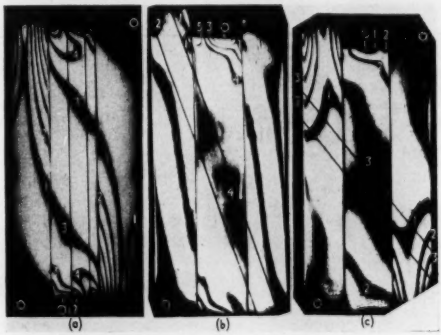

Fig. 8. Fringe pattern in composite model with flexible adhesive layer. Bending moment factor K, (*a*) $+2{\cdot}0$, (*b*) $0{\cdot}0$, (*c*) $-3{\cdot}0$

to the adhesive layer were parallel and perpendicular to the adhesive-adherend boundary over the main extent of the joint clear of the ends, the trajectories in the corresponding region of the adhesive lay very nearly at 45° to this direction right across the thickness of the layer (Fig. 9). This indicates that the adhesive is, in the main, in longitudinal shear as was the case with steel adherends.[1]

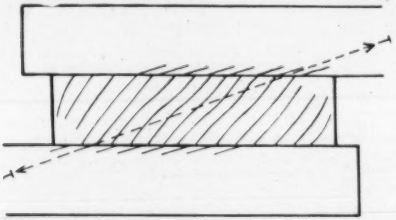

Fig. 9. Stress trajectories (single set) in central region of adhesive and adjacent edges of adherends. (Corners of adhesive left blank)

Change in angle of inclination of the adhesive free surface to the adherend gave effects very like those found by Mylonas as the stress concentration moved out of the leading corner to near the trailing corner somewhere between a contact angle of 50° and 40° (Figs. 10 and 11). For angles less than this transition value the fringe order now fell away towards the leading corner both along the free surface of the adhesive and along the whole adhesive-adherend boundary. Increase in K did not seem to have any readily measurable effect on the value of this transition angle but, for angles less than this, reduced the extent of the fall towards the leading corner, thus giving an apparently more uniformly stressed adhesive.

For negative values of K again there is some similarity to the stresses produced in the homogeneous models. Thus, when K becomes sufficiently negative the highest fringe order appears at the centre of the adhesive layer and there is a general fall in order towards the free surfaces. But the general nature of the stress distribution over the free surface of the adhesive does not seem to change in that the isotropic point of zero stress persists, only moving somewhat towards the leading corner and retaining on each side regions of tensile

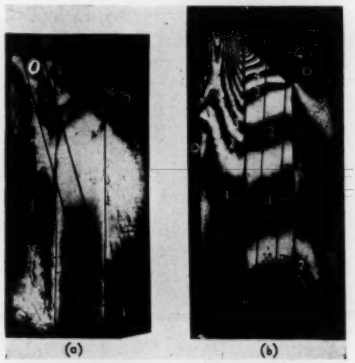

Fig. 10. Fringe patterns; contact angle 50°. Bending moment factor K, (*a*) +0·3, (*b*) +2·5

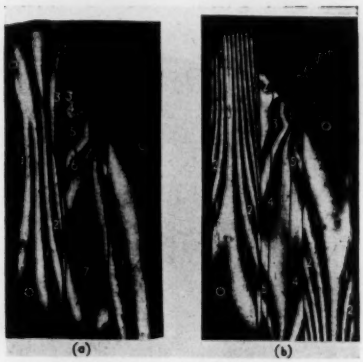

Fig. 11. Fringe patterns; contact angle 40°. Bending moment factor K, (*a*) +0·3, (*b*) +2·1

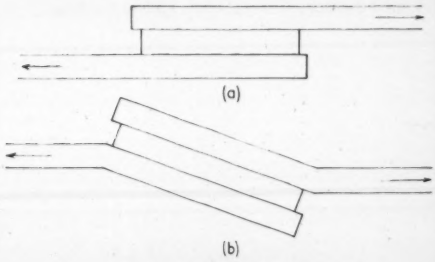

Fig. 12. Design of lap joint
(*a*) conventional.
(*b*) proposed, to give negative bending moment factor.

Fig. 13. Fringe pattern in "reverse bent" model as proposed in Fig. 12

and of compressive stress respectively. Thus, even up to $K = -3$ we appear to have a tensile tearing stress at the leading corner. Nevertheless, this stress appears to fall to a value lower than that persisting at the centre of the adhesive layer and so would appear to have lost its significance as a stress concentration [Fig. 8(*c*)].

The foregoing tests suggest that a lap joint with K negative would have certain merits and a simple trial of a joint so designed as shown in Fig. 12 was undertaken. The stress pattern shown in Fig. 13 confirms the expectations in that the stress, or at least, the fringe order, is greatest at the centre of the adhesive layer (strictly on the adhesive-adherend surfaces) and falls towards each free surface which is in a state of low stress, tensile towards the leading corner, compressive towards the trailing corner.

DISCUSSION OF RESULTS

The main outcome of this work is a clarification of the significance of bending of the adherends. Goland and Reissner examine special cases of the conventional lap joint and bending enters as a factor which, through causing rotation of the joint, modifies the boundary loading assumed in the stress analysis and, hence, also the calculated stresses. It would appear that their general conclusions are correct in so far as they deduce tensile and tearing stresses increasing towards the joint edge, these increases being reduced by the bending under load.

The deliberate rather than the incidental change in the bending has shown this to be a primary factor in the distribution of stress in the adhesive, it being possible virtually to eliminate and also to reverse the increases in stress towards the joint edges solely by the controlled variation of the bending moment in the adherends. Thus, it appears possible to produce a loaded joint where the stress distribution in the adhesive layer has certain sought-after features such as freedom from stress concentrations on the free surface and a high degree of uniformity. It might be possible, by detailed study of such joints, to lay down criteria for the optimum design of joints.

The work to date suggests that the optimum loading is produced by making the bending moment factor of Goland and Reissner approximate to $-0{\cdot}5$ for joints where the adhesive has the same elastic properties as the adhering sheets and probably somewhat less when the adhesive is more flexible. Although negative values do not enter into Goland and Reissner's considerations there does not appear to be any inconsistency produced by substituting such values in their calculations as K enters as a factor in their chosen boundary loading and there is then no reason to limit its range of possible values. It is not easy, in their presentation of their calculations, to test the effect of putting $K = -0{\cdot}5$ approximately except in one case, equation (49), which gives an analytic expression for the shear stress in a flexible adhesive layer

$$\frac{\tau_0}{p}\cdot\frac{c}{t} = -\frac{1}{8}\left[\frac{\beta c}{t}(1+3K)\frac{\cosh\dfrac{\beta c}{t}\cdot\dfrac{x}{c}}{\sinh\dfrac{\beta c}{t}} + 3(1-K)\right]$$

where x is the distance from the centre of the adhesive layer measured along the layer and it is seen that putting $k = -\frac{1}{3}$ gives τ_0 uniform throughout the joint. It seems doubtful if the allied statement that the tearing stress is a maximum at the joint end would be valid for negative values of K, equation (54). The formula as simplified by Mylonas for long joints gives

$$\sigma_{max}/p = (0{\cdot}485K + 0{\cdot}015)\gamma \text{ where } \gamma^4 = 6E_a s/Ed$$

which suggests compression is introduced when $K = -\frac{1}{3}$. The corresponding equation by Plantema[4] who allows both for bending and stretching of adherends shows

$$\tau_{max}/\tau_{mean} = \sqrt{\tfrac{1}{2}\Delta}(1+3K)\coth\sqrt{\tfrac{1}{2}\Delta}(1+3K) \to 0 \text{ as } K \to -\tfrac{1}{3}$$

i.e. non-uniform distribution along length of joint, stress apparently falling from centre outwards.

The boundary loading of the joint assumed by Goland and Reissner is as stated in the introduction. $K = -\frac{1}{3}$ is clearly a case of special interest as it produces loading as shown in Fig. 14.

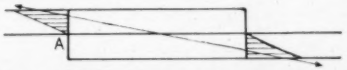

Fig. 14. Boundary loading of joint when $K = -\frac{1}{3}$

In this there is no discontinuity at A in the boundary load. Also, there is no applied load at A, the point in the adhesive usually associated with the highest stress concentration. Physically this means that the adherend is unstressed at the point A where it meets the adhesive layer. It seems desirable to consider the relevance of these concepts to the production of optimum loading, i.e. freedom from stress concentrations and most uniform distribution of load over the adhesive surface.

The experimental work on homogeneous models lacking an actual adhesive layer and, in particular, the results shown in Fig. 6 do suggest a high measure of agreement between measured stresses and those predicted by these considerations.

Interpolation between $K = 0$ and $-0{\cdot}5$ for some value closer to the latter would give a tearing stress zero at the end of the glue line and nowhere more than about a quarter of the longitudinal stress in the adherends as well as a shear stress showing a high measure of uniformity with freedom from localized peak values. It is also clear that making K less than $-\frac{1}{3}$ would produce in Goland and Reissner's boundary load a compressive stress at A. Experimentally, we see that a "holding on" rather than a "tearing" stress results on the glue line at A for $K = -0{\cdot}5$ and presumably more negative values.

Models representing the behaviour of a more flexible adhesive layer on the other hand, while showing the same general trend with reduction of K towards optimum stress distribution in the adhesive, have not shown an actual change of tearing stress to a compressive one, but only a reduction in tension sufficient to eliminate the usual stress concentration at the end.

REFERENCES

(1) MYLONAS, C. *Proc. Soc. Exp. Stress Analysis*, **12**, p. 129 (1955).

(2) VOLKERSEN, O. *Luftfahrtforschung*, **15**, p. 41 (1938).

(3) GOLAND, M., and REISSNER, E. *J. App. Mech.*, **7**, p. A17 (1944).

(4) PLANTEMA, F. J. Report 1181, Nat. Luchtvaartlaboratorium (Amsterdam, 1949).

Correspondence

The sampling efficiency of the thermal precipitator

Prewett and Walton[1] have obtained experimental data on the efficiency with which the thermal precipitator[2, 3] gives the number concentration of an aerosol in the particle size range of 2·5 to 30 μ diameter. Shellac spheres, of density close to 1·0 g/cm^3, were produced by means of a spinning top atomizer[4] and were sampled with a sedimentation cell (considered to be an absolute standard) and in turn with each of five different thermal precipitators (T.P.'s). The results obtained, with a heating current of 1·2 A and at a sampling rate of 6·75 cm^3/min, are summarized in columns 1 and 2 of Table 1.

The efficiencies reported were considered[1] to represent a balance between *losses* to (*a*) walls (small), (*b*) through the dust-free space[5] and (*c*) on to the wire, and *over-sampling* due to sedimentation into the sampling orifice. For particles larger than 10 μ this over-sampling is not able to compensate for the losses, which are clearly size dependent.

The over-sampling ratio, which is also size dependent, is expressed as $(v_s + v_1)/v_1$, where v_s is the terminal velocity of the particle size being considered and v_1 is the velocity of the air entering the sampling orifice. Walton[6] has shown that the effective sampling orifice of the T.P. is the rectangular opening at the top of the parallel channel running through the body of the instrument. Thus, at a sampling rate of 6·75 cm^3/min, the value of v_1 is 2·56 cm/sec.

The instrument losses should be related to the actual number of particles approaching the hot wire, a number dependent on the product of the airborne concentration and the over-sampling ratio (Table 1).

Table 1. *Experimental results of Prewett and Walton,[1] together with calculated percentage loss within T.P., taking into account the over-sampling ratio*

Particle diameter (μ)	*T.P. efficiency*[1] *S* (%)	*Over-sampling ratio* ($\times 100$)	*Loss, L* (%), *of particles approaching wire**
2·5	99	100·7	1·7
5	92	102·9	10·6
10	100	111·8	10·6
15	93	126·4	26·4
20	73·5	147·0	50·0
25	63·5	173·4	63·5
30	53	205·9	74·2

* Values of L in column 4 are given by

$$\frac{\text{Col. 3} - \text{Col. 2}}{\text{Col. 3}} \times 100$$

The figures given in column 4 of Table 1 can be represented generally by the empirical equation

$$E = (100 - L) = [1 - \phi(p)] \times 100 \qquad (1)$$

where E is the percentage efficiency with which particles of a given size are deposited on the cover-glasses; $\phi(p)$, or L, can be expressed as a function of the non-dimensional particle parameter, p, given by

$$p = \rho d^2 V / 18 \eta D \qquad (2)$$

where ρ is particle density, d is the diameter of particle (sphere), η is the viscosity of the air, D is a characteristic length (the size of the gap between hot wire and cover-glasses), and $V = v_s + v_2$, where v_2 is the mean velocity of the air past the wire (5·00 cm/s at a sampling rate of 6·75 cm^3/min).

The actual T.P. recording efficiency, S (column 2 of Table 1), is thus given by

$$S = \frac{v_s + v_1}{v_1}[1 - \phi(p)] \times 100 \qquad (3)$$

If we know how $\phi(p)$ depends on p we can obtain an estimate of the apparent T.P. efficiency at different sampling rates for particles of different sizes and densities. The relationship between $\phi(p)$ and (p) given in Fig. 1 has been derived from the experimental values of L [column 4 in Table 1 and equation (1)].

To test the validity of equation (3) and the curve in Fig. 1 over a wider range of conditions, two T.P.'s were set up side by side in a horizontal rectangular duct, 20 by 10 in., along which a well-mixed dust was passed. Simultaneous samples

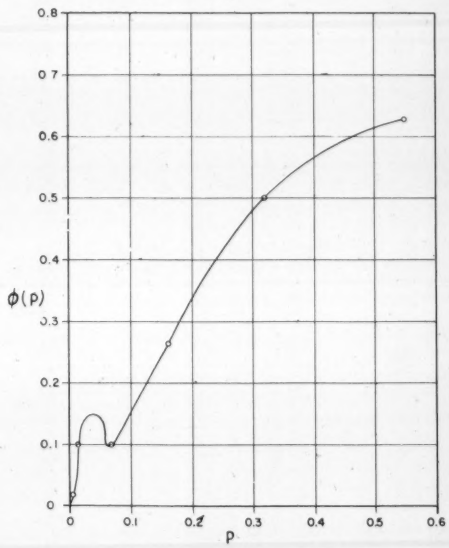

Fig. 1. Relationship between $\phi(p)$ and p

were taken, one T.P. sampling at a rate above the standard one of 6·75 cm³/min, the other at a lower rate. The heating current was 1·2 A. Runs were made as shown in Table 2.

Table 2. *Details of experiments*

Run no.	*Dust*	*Sampling rate (cm³/min)* *Fast*	*Slow*
1	plastic spheres	7·98	2·54
2	coal dust	9·60	3·96
3	coal dust	9·60	4·44

The results, given as ratios of the corresponding particle counts on the two T.P.'s at the two sampling rates, are presented in Table 3. Particle sizes used to calculate the expected ratios are given in terms of Stokes's diameters d_s, where

$$d_s = \rho^{\frac{1}{2}} d_p / f \qquad (4)$$

d_p being the mean projected diameter of an irregularly-shaped particle (coal dust) and f a shape factor.[7] The densities of the plastic material and the coal dust were 1·19 and 1·29 g/cm³ respectively. For a sphere, $f = 1$; the mean value for the coal dust particles has been found to be 1·35.[7]

Table 3. *Comparison between equation* (3) *and experiment of the ratios of the T.P. counts at different sampling rates*

Mean projected diameter (μ)	*Ratio of count on fast T.P. to slow T.P.* *Experimental*	*Equation* (3)
Run 1		
15·6–20·8	0·52	0·46
20·8–26·0	0·40	0·36
26·0–32·5	0·36	0·30
32·5–39·0	0·37	0·30
Run 2		
2·1– 3·1	0·87	0·98
3·1– 4·3	1·06	0·95
4·3– 8·6	1·05	0·90
8·6–13·0	0·77	0·95
13·0–17·3	0·63	0·76
17·3–21·8	0·61	0·53
21·8–27·0	0·51	0·49
27·0–32·4	0·53	0·46
32·4–43·2	0·41	0·42
Run 3		
2·1– 3·1	0·90	0·99
3·1– 4·3	1·06	0·95
4·3– 8·6	1·04	0·92
8·6–13·0	0·86	0·97
13·0–17·3	0·62	0·76
17·3–21·8	0·47	0·58

The overall mean ratio of the count on the fast T.P. to that on the slow T.P. is 1·024 with a standard deviation of 0·144.

When the results are taken as a whole, agreement between experiment and prediction is quite good for this kind of work. The effects of sampling rate and of Stokes's diameter on S are presented graphically in Fig. 2, calculations being made from

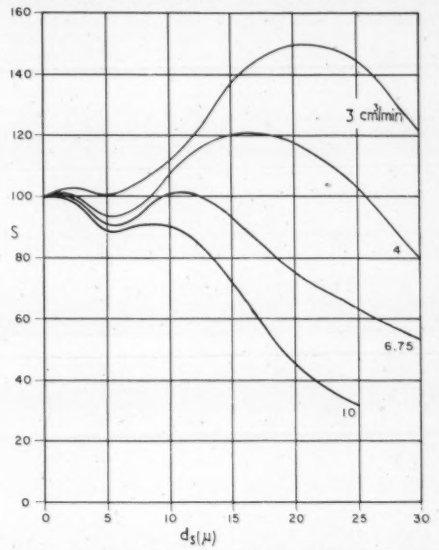

Fig. 2. Calculated values of S for different Stokes's diameters at various sampling rates

equation (3) and Fig. 1. These curves give a guide as to the optimum sampling rates for different particle sizes.

Thanks are due to Mr. D. F. Mulford who made the microscope counts of the T.P. records obtained.

Suffield Experimental Station, Ralston, Alberta, Canada.

H. H. WATSON

[22 May, 1957]

REFERENCES

(1) PREWETT, W. C., and WALTON, W. H. *Ministry of Supply unpublished report* (1948).
(2) GREEN, H. L., and WATSON, H. H. *Medical Research Council Special Report Series No.* 199 (1935).
(3) WATSON, H. H. *Trans Instn Min. Metall.*, **46**, p. 155 (1936–37).
(4) WALTON, W. H., and PREWETT, W. C. *Proc. Phys. Soc. [London], B*, **62**, p. 341 (1949).
(5) WATSON, H. H. *Trans Faraday Soc.*, **32**, p. 1073 (1936).
(6) WALTON, W. H. *Symposium on particle size analysis*, p. 140 (Institution of Chemical Engineers and Society of Chemical Industry, 1947).
(7) WATSON, H. H. *Brit. J. Phys. Med.*, **17**, p. 275 (1954).

New books

Metallurgical progress—3.A. Third series of critical reviews. (London: Iliffe and Sons Ltd., 1957.) Pp. 88. Price 6*s*.

The first three of these reviews dealing with refractories, non-destructive testing and metallurgical coke are by members of the Staff of the Metallurgy Department of the Royal Technical College, Glasgow, while the remaining ones dealing with cast iron foundry problems are by members of the Staff of the British Cast Iron Research Association. All the reviews are good substantial accounts of recent work with comprehensive references and are very useful for providing an encyclopaedic background to their subject rather than inspiring reading.

M. W. THRING

Basic automatic control theory. By G. J. MURPHY. (New Jersey: D. Van Nostrand Co. Inc.; London: D. Van Nostrand Co. Ltd., 1957.) Pp. xi + 557. Price 67*s*. 6*d*.

As a subject becomes accepted as a part of the corpus of educated knowledge, the presentation which it receives tends to simplify. The theory of automatic control is no exception and the present book attains a satisfying degree of lucidity without in any way detracting from the rigour of the treatment. There are eleven chapters and four appendices, the whole making the book independent of outside sources of more advanced mathematical technique.

After an introductory chapter on terminology and methods, there follow two chapters on the theory of physical analogues and their characteristics respectively. The fourth chapter derives such Laplace transform theory as is required and this is augmented by Appendix III in which selected transforms are listed. The fifth and sixth chapters consider transfer functions, block schematics and types of control systems, and lead naturally to chapters seven and eight where stability criteria and frequency response are examined. Chapters nine and ten discuss time response and its correlation with frequency response; they contain the only real deficiency noticed by the reviewer—the almost incomprehensible application of conformal transformation to the Nyquist diagram on pp. 464–465. Chapter eleven describes some typical electronic analogue computer applications. The first Appendix discusses the solution of polynomial equations and the treatment of Lin's method is one of the clearest which the reviewer has seen. The second Appendix summarizes complex variable theory and the fourth discusses graphical methods. The text is lavishly illustrated with examples, both worked and for exercise, and the book can be unreservedly recommended.

A. D. BOOTH

World directory of crystallographers. Compiled by W. PARRISH. (New York: Philips Laboratories, 1957.) (Available from: Polycrystal Book Service, 84 Livingstone Street, Brooklyn 1, New York, U.S.A.) Pp. xvi + 79. Price $1.50.

This directory contains short biographical data of 2260 crystallographers from 54 nations. The Directory is arranged in alphabetical order by nations, and individuals within the nations. It gives (i) the full name and title of the crystallographer; (ii) information on the field of study, the university and year of the highest degree; (iii) present position, name of institution and address; (iv) in some cases a permanent or personal address; and (v) major crystallographic interests. Statistical data is also included.

Biographical details for the Directory were obtained by means of a questionnaire sent to persons known to be crystallographers and it includes all details submitted for publication by 20 May, 1957. Additional questionnaires and names received up to 3 June, 1957, are included in a special Late Arrivals section.

The numerical solution of two-point boundary problems in ordinary differential equations. By L. FOX. (London: Oxford University Press, 1957.) Pp. xi + 371. Price 60*s*.

The position of the boundary conditions is a major factor governing the choice of a numerical method to evaluate a solution of a differential equation. The author is concerned solely with problems in which there are conditions to be satisfied at both ends of the range of integration. These are called boundary-value problems to distinguish them from initial-value problems in which all conditions are specified at one point. A basic feature of nearly all the methods described is that the differential equation is replaced by a set of algebraic equations arising from the replacement of derivatives by their finite-difference equivalents. Accordingly, there are introductory chapters on finite-differences and the numerical solution of algebraic equations. Subsequent chapters deal with a selection of well-tried, boundary-value methods of obtaining numerical solutions of differential equations of orders one to four, including problems of eigen-value type. Both linear and non-linear cases are considered and special attention is given to the proper numerical treatment of various possible types of boundary conditions. There is a whole chapter on the accuracy of the solutions so obtained. Initial-value techniques are also applied to boundary-value problems and a final chapter deals with miscellaneous methods and comments.

The methods are described in great detail with the practical computer always in mind. Each fresh point is illustrated by a worked example. Not unnaturally, the author seizes the opportunity to suggest once again the desirability of using a large finite-difference interval together with a "difference correction" to take care of truncation errors—an approach he has long advocated.

There is no other book to compare with this and no one is more qualified to have written it than Dr. Fox who has worked in this branch of numerical analysis for many years. The book is certain to become a classic in the subject. It is produced in the impeccable style which is so characteristic of the Oxford University Press.

J. CRANK

Experimental designs. By W. G. COCHRAN and G. M. COX. Second Edition. (New York: John Wiley and Sons Inc.; London: Chapman and Hall Ltd., 1957.) Pp. xiv + 609. Price 82*s*.

With their increasing participation in industrial problems physicists in common with other scientists are devoting more attention to the principles of experiment design. These are, briefly, that an experiment should provide its own, and a valid, estimate of that residual variability which tends to mask the effect being studied; that, in order that its results should be generally applicable, an experiment should cover a wide range of conditions; and yet, in spite of this last, its residual variability should be low. The effects of variability

are reduced by skilful grouping and selection of material to which the different "treatments" being studied are to be applied. These principles are especially required in the development type of experiment. The laboratory type of experiment is usually only exempt because there the emphasis is on the method of measurement or on the maintenance of special conditions. It is this inevitable narrowness of the laboratory experiment which creates the need for complementary development work.

The book under review was originally written as the result of frequent requests to the authors for detailed designs and instructions for the subsequent analysis of the results. It will, therefore, serve well as a reference work for anyone in a similar position; the beginner would perhaps be daunted by the seventeen chapters and the variety of designs of increasing complexity. The authors do not claim to have catered entirely for the student: they recommend some supplementary teaching on the analysis of variance which is the basis of all designs. The first three chapters, amounting to ninety-two pages, on initial steps in planning, on methods for increasing precision, and on analysis are, however, admirably informative.

Those who are already familiar with the first edition will want to know what this, the second, contains. It has one hundred and fifty more pages including two new chapters (labelled 6A and 8A to leave the paragraph numbering of the remainder the same), one of which is devoted to fractional replication, useful in exploratory research, and the other to the strategy of sequential experiment in finding optima (of yield, for example). There are several new sections on new incomplete block designs. One of the features of the book is the setting out of designs of the incomplete block and latin square type so that they are ready for the random choice of the experimenter.

Experiments, especially industrial ones of the development type, tend nowadays to be costly so that thought given to good design can be well repaid by the resulting economy of tests and material quite apart from the advantage of unambiguity.

E. D. VAN REST

The silicones. By P. SYKES. (London: John Murray Ltd., 1957.) Pp. 16. Price 1*s.* 6*d.*

This short monograph provides a useful introduction to the methods of preparation and the properties of the simple polysiloxanes for the teacher or the student of chemistry, for whom it is evidently intended. The absence of much important physical data, however, limits its interest for the physicist or the user of silicones.

The trade name "Silastomer" is incorrectly used as a general term for silicone rubbers.

J. AMES

Thermal stresses. By B. E. GATEWOOD. (New York: McGraw-Hill Book Co. Inc.; London: McGraw-Hill Publishing Co. Ltd., 1957.) Pp. xv + 232. Price 56*s.* 6*d.*

The development of thermal stresses in structures, parts of which are heated to high temperatures, is becoming a problem of increasing practical importance in connexion with heat effects in supersonic flight and in turbines and nuclear reactors. The use of algebraic equations and numerical methods for evaluating the stresses do not involve any new fundamental principles, but provides some very interesting applications of mathematical techniques which are comprehensively surveyed in this book. The author, who is Research Co-ordinater and Professor at the Air Force Institute of Technology in Ohio, has obviously very considerable experience in the solutions of problems of this type and his preferred method of attack on a problem is to set up the complete equations, simplify them by well-chosen physical assumptions, and so obtain an analytical solution for the simplified problem. This enables the effects of the variables to be readily calculated and presented in chart form and then the solution for some particular cases can be refound by eliminating the simplified assumptions. This is certainly the best procedure when an analytical solution can be obtained without excessive simplifying assumptions, and he shows that this can in fact be done.

The presentation of the book and the illustrations are up to the usual high standard which one expects from McGraw-Hill, and the text is illustrated both with worked examples and stated problems. It is interesting that it shows examples of the increasing divergence between the American and the English languages, as in the sentence "the two bars may move some before they restrain each other," or the use of the plural "formulas." There are good references at the end of each chapter, but it is probable that it would not be necessary to refer to those to solve any of the problems dealt with in the text, which is just as well as in some cases there are over 100 references at the end of one chapter.

M. W. THRING

Light scattering by small particles. By H. C. VAN DE HULST. (New York: John Wiley and Sons Inc.; London: Chapman and Hall Ltd., 1957.) Pp. xiii + 470. Price 96*s.*

The author has confined this treatise to single scattering by independent particles, thus excluding co-operative phenomena and multiple scattering. Modulated scattering (Raman effect) has also been regarded as outside the scope of the book. On the other hand, the term "small particles" covers a wide range of sizes, from small fractions of a wavelength to high multiples of it. The reader will be on familiar ground at either end of this scale; for the Rayleigh scattering caused by the smallest particles, and for diffraction phenomena due to large particles. In the critical range where wavelength and particle size are comparable, the phenomena are complex but of considerable practical importance. One has to abandon familiar textbook concepts and go back to Maxwell's equations with the appropriate boundary conditions. The basic assumptions and final results of these rather involved theories are presented clearly, with the aid of tables and graphs, and with full references to the original literature.

In Part I the problem of scattering is treated in a general way, and the "amplitude functions" are introduced. Part II forms the bulk of the book and deals with the calculation of the actual amplitude functions for various shapes and sizes of particles. Simple shapes, especially spheres and cylinders, are treated in greater detail. Part III deals with applications to various fields of Physics, Chemistry, Meteorology and Astronomy.

Readers will sometimes find explicit answers to their questions in Part III. Others will require more detail or a more thorough insight by turning to Part II, and many Physicists will mainly study the fundamentals contained in Part I. In a field where elementary textbooks are of little use and where the literature is scattered over a wide range of periodicals, this up-to-date, authoritative book will be invaluable for anyone who has to deal with scattering or diffraction of light. The reader will feel grateful for the great care taken by the author in producing this clear and systematical treatment of a highly complex subject.

H. G. KUHN

Semiconductor Abstracts. Vol. 3, 1955 issue. Compiled by the Battelle Memorial Institute. (New York: John Wiley and Sons Inc.; London: Chapman and Hall Ltd., 1957.) Pp. viii + 322. Price 80*s*.

The present volume is the third of a series, the previous two dealing with abstracts of papers mainly published in 1953 and 1954. Papers covered by the present volume appeared mainly in late 1954 or 1955. A few earlier papers have also been included, and, while this is desirable to complete the coverage of the subject, it leads to some confusion when searching for a particular abstract. The abstracts deal with fundamental research on semiconductors and luminescent materials and various devices in which they are used. This is now a very wide field in which there is great activity as can be seen from the increased number of abstracts included in this third volume, 775 in Vol. 1, 765 in Vol. 2, and 1258 in Vol. 3. To accommodate this increase and also to improve the appearance and usefulness of the volume a more robust binding has been used.

The abstracts vary in length and quality, but on the whole are quite good and aim at giving the essential results of each paper, including numerical values in many instances. Libraries attached to laboratories engaged in research in this field will certainly wish to have all the volumes of this series and a number of research workers will feel it worth while having their own copy.

R. A. SMITH

Electrical discharges in gases. By F. M. PENNING. (Eindhoven: Philips Technical Library; London: Cleaver-Hume Press Ltd., 1957.) Pp. viii + 78. Price 15*s*.

This essay, by a great master in the field, appears some four years after the author's death. It is a fairly elementary but typically clear account of transient (40 pp.) and self-maintained (30 pp.) electrical discharges. There is, for example, a brief account of some of the properties of positive columns in the latter part of the book, but Townsend discharges and breakdown not unnaturally receive most attention.

J. D. CRAGGS

Applied mathematics and mechanics. Vol. 1. Gas dynamics. By KLAUS OSWATITSCH. English version by G. KUERTI. (New York: Academic Press Inc.; London: Academic Books Ltd., 1957.) Pp. xv + 610. Price 96*s*.

This book assumes no previous knowledge of gas dynamics but demands a graduate standard of mathematics. An introductory chapter on thermodynamics is followed by the theory of steady and unsteady quasi-one-dimensional flow processes including shock waves, cylindrical and spherical waves, and flow through nozzles, together with a readable account of the method of characteristics. The integral theorems and general equations of the mechanics of compressible fluids are then obtained without the use of vector or tensor analysis, and applied to a few particular problems such as jets, thermodynamic propulsion, and flow through a cascade. Particular exact solutions are derived for steady inviscid plane and axisymmetric flows preparatory to subsequent chapters on steady inviscid subsonic, supersonic and transonic flows. These chapters are concerned mainly with shock waves, and flows past airfoils and axisymmetric bodies. There is one chapter on steady and unsteady three-dimensional flow problems including the delta wing. Boundary layer theory is presented very briefly and confined to flow with an adiabatic wall. A final chapter on experimental techniques is concerned mainly with steady flow measurements.

Every chapter except the first has an extensive and up-to-date reference list of English, German and American papers. Throughout the whole book the physics of the problems considered is kept to the fore and never lost sight of through preoccupation with mathematical analysis.

Although the author does not claim that it is an encyclopaedic treatise, it covers, nevertheless, a wide range of topics very thoroughly and should be of great use to anyone concerned with the fundamental problems of gas dynamics.

G. D. SMITH

Nuclear engineering. Edited by Charles F. BONILLA. (New York: McGraw-Hill Book Co. Inc.; London: McGraw-Hill Publishing Co. Ltd., 1957.) Pp. xi + 850. Price 94*s*.

The declared aims of this book are to assist in the training of engineers in the field of nuclear-power-plant design, and to serve as a reference work for those already engaged in this field. Its scope is deliberately restricted to the reactor in operation; all such preliminary stages as the manufacture of reactor components and reactor construction, and subsequent operations including processing of fuel elements are not dealt with.

Following a short introduction, the basic nuclear physics of reactors is outlined in three chapters, dealing in turn with nuclear particles, nuclear radiation, and their detection and measurement. A chapter each is devoted to health physics, reactor physics and shielding. A detailed treatment of the fundamental engineering aspects of reactors then takes up half the book. The editor contributes the sections on fluid flow and heat transfer; other sections deal with thermal stress analysis, instrumentation and control, and the economics of power generation. The metallurgy of uranium and its alloys form the subject-matter for another chapter. Following a descriptive account of existing and projected types of reactors, the book ends with a section on the law concerning nuclear power, naturally of purely American interest.

This book is successful in its first aim, and provides a useful introduction to nuclear engineering; the engineering sections in particular contain much fresh material, including the flow and heat-transfer properties of slurries, two-phase flow and the effect of plastic flow on stresses in fuel elements. Its value as a reference work would be enhanced if more space were given to reactor materials other than uranium and its alloys, including the effect of radiation and corrosion.

More careful proof reading of the second chapter would have prevented the appearance of several errors in the equations, e.g. the Klein–Nishina formula on p. 43.

J. WOODROW

Passive network synthesis. By J. E. STORER. (New York: McGraw-Hill Book Co. Inc.; London: McGraw-Hill Publishing Co. Ltd., 1957.) Pp. x + 319. Price 64*s*.

This detailed and scholarly work by an industrial scientist, be it noted, is probably too advanced and specialized for undergraduate physicists in general, even where such mundane matters as low pass filters are concerned. Here the use of transmission matrices may present difficulties to such students, although advanced engineering undergraduates (to whom I commend this book) would probably not bat an eyelid, since elegant mathematical techniques in physics schools seem sometimes to be reserved for nuclear studies.

The present work can be recommended to graduates interested in an integrated general treatment of filter theory. There are groups of chapters on impedance synthesis, network synthesis using image parameters, modern realization methods for two-terminal-pair networks and rational fraction approximations.

J. D. CRAGGS

Computers, bibliographical series. Vol. C-I, No. 1. October, 1957. (London: The Bureau of Technical Information, 1957.) Pp. 29. Subscription £6 6*s*. p.a.

A list of 159 papers, books, reports and films dealing with the design and application of digital and analogue computers. There are also references to 35 patents, and a list of educational course on computers, meetings, trade literature, and available reprints. An author index is provided.

The coverage appears to be fair, although several omissions were noticed even on casual examination. A. D. BOOTH

Elements of heat transfer. By M. JAKOB and G. A. HAWKINS. 3rd ed. (New York: John Wiley and Sons Inc.; London: Chapman and Hall Ltd., 1957.) Pp. xxv + 317. Price 54*s*.

This book is primarily written for the engineering student rather than the physics student and the emphasis is accordingly on the practical formula from which heat transfer may be calculated. Nevertheless, the authors are interested in the fundamental mechanism of heat transfer so that, for example, while heat transfer by free convection is primarily dealt with by the use of dimensional analysis which enable large scale results to be derived from small scale experiments, it is pointed out that dimensional analysis does not really explain the phenomena, and the existence of a thin layer of stagnant gas on the surface is postulated. However, a physicist would like to see a treatment of how the Grashof number appears as a natural ratio in terms of this theory.

In a similar way, it is stated that the fourth power law of black body radiation can be derived from thermodynamics, whereas a text book for physicists would give the derivation.

Thus, it may be concluded that the book is of great practical value of use in engineering teaching, whereas its main use to the physicist is when he comes up against a heat transfer problem for which he has to find a solution in order to design his apparatus. M. W. THRING

Light scattering by colloidal systems. By M. M. FISHMAN. (New Jersey: Technical Service Laboratories, 1957.) Pp. 84. Price (including supplement) £1 8*s*.

This annotated bibliography, together with a recently issued supplement, is intended to provide a source of reference for the increasing number of investigators in the field of application of light-scattering techniques to the study of colloidal systems. Providing, as it does, a comprehensive guide to light-scattering literature from 1869 up to, and including, 1956, this volume will surely fulfil its purpose.

Within the main heading are covered the following subjects: Gases; Vapours; Solutions; Rayleigh's Law; Mie theory; Tyndall spectra; Molecular weight; Size and shape of molecules; Dissymmetry and Depolarization. These combine to make over 850 references, each of which is abstracted, together with the names of over 750 authors which are fully indexed.

Analytical design of linear feedback controls. By G. C. NEWTON, Jr., L. A. GOULD and J. F. KAISER. (New York: John Wiley and Sons Inc.; London: Chapman and Hall Ltd., 1957.) Pp. xi + 419. Price 96*s*.

The widespread use of feedback control systems needs no emphasis, but it may cause amused surprise, to those unenlightened in the art, to learn that probably the first application of the art is Babylonian and about 4000 years old. This was the irrigation of land, which involved the opening and closing of ditches to appropriate amounts, governed by soil moisture content. After this initiation we readily pass from the float control of water clocks (Arabic) through the mechanism for turning windmills, so as to face upwind, to the design of an azimuth drive for a 140 ft. radio telescope, of which a quite detailed treatment is given.

It would be wrong to suggest that this work, by three members of the MIT staff, consists of a hot potch of oddities. On the contrary, it gives a very basic and general analytical treatment of control systems, illustrated by a few examples.

There are groups of chapters on a general review of the control art, on the minimizing of integral-square errors, on stochastic signals, on the minimizing of mean square errors, on the limitation of saturation tendencies, on the design of control systems for minimum bandwidth and, finally, on the radio telescope problem. About 100 pages are devoted to appendices on mathematical treatments (although the whole of the book is strictly analytical) and there are about 20 pages of problems.

This book is a welcome and worthy addition to the extensive literature on the subject. J. D. CRAGGS

Sammlung Göschen. Vol. 728/728a. Graphische darstellung in wissenschaft und technik. By M. PIRANI. (Berlin: Walter de Gruyter and Co., 1957.) Pp. 216 + 15. Price DM. 4.80.

The third and revised edition of this book is prepared by Johannes Fischer, an engineer and a Member of the German Academy of Science, Berlin. It deals comprehensively with the technical details of graphical representation and is subdivided into two main sections dealing respectively with the representation of functions containing two variables, whose functional dependence is either unknown or known, and of functions containing three or more variables. Although some theory of graphs, which will interest the mathematician and physicist, is included, the author's intention in the first place is to give the man of applied science, i.e. the engineer, a guide to the understanding and the layout of graphs and to their useful interpretation. Many examples taken from engineering processes are included in the text. A knowledge of mathematics required for the General Certificate of Education, Advanced Level, or for the Higher National Certificate is all that is demanded of the reader.

H. D. FELDHEIM

Radiography in modern industry. (New York: Eastman Kodak Co.) Pp. 136. Price 35*s*.

This book contains an outline of the knowledge necessary for efficient radiographic practice, covering all aspects from the radiation source to film processing. It includes up-to-date information on gamma and high voltage radiography. The "arithmetic" of exposure and the factors governing exposure are dealt with from first principles and the sensitometric characteristics of X-ray films are clearly explained, and detailed for the Company's products. The chapters on scattered radiation and radiation screens are also of especial interest. A chapter on radiation protection includes a useful bibliography of American literature on the subject, but a chapter giving brief details of special radiographic techniques could well have been extended, and would have been of more value with additional references. An appendix lists the possible sources and results of the more common faults in radiographic practice.

The book is very well produced, has extremely lucid diagrams and tables throughout and deserves a place in every industrial radiographic department for reference and for training purposes. R. S. SHARPE

Notes and comments

The British Group for computation and automatic control of the British Conference on automation and computation

The rapid growth of automation, in which is comprised computation, process control and data processing generally, led to a decision by some twenty bodies of the learned society type having interests in these fields, or in their social and economic implications, to set up a central organization to provide more effective liaison between the interested bodies, to be known as the British Conference on automation and computation. This has been organized in three Groups, (*A*) The British Group for the engineering applications of automation, (*B*) The British Group for computation and automatic control and (*C*) The British Group for the sociological and economic aspects of automation techniques.

At a meeting held on 20 December, 1957, Group B was formally constituted, comprising as its members twenty-three societies and institutions including the Institute of Physics.

The objects of the Group are: "(*a*) to foster the development and applications of automatic controls, computing and data processing equipment and programming techniques, (*b*) to afford a common meeting ground for the adhering organizations whereby such of their activities as fall within the purview of the Group can, if so desired, be co-ordinated and extended, (*c*) to maintain, as may be desirable, liaison with other Groups of the British Conference on automation and computation by direct contact and by representation on the General Committee of the British Conference, (*d*) to encourage and, if desired, to co-ordinate the presentation at International Conferences of British papers whose subjects fall within the purview of the Group, and (*e*) through the General Committee of the British Conference on automation and computation, to maintain, as may be desirable, liaison with corresponding National Committees of other countries which support such International Conferences."

The executive committee of the Group consists of the Honorary Officers together with the representatives of six of the constituent bodies, including the Institute of Physics.

The Group constitution provides for the election of additional member societies: those interested should communicate with the Honorary Secretary, B.C.A.C., Group B, c/o The Institution of Electrical Engineers, Savoy Place, London, W.C.2.

Bibliography on applications and properties of zirconium and alloys

A seven-page bibliography gives complete and up-to-date source material available on the properties of zirconium and its alloys. This material has been compiled by the Columbia-National Corporation and the *Bibliography* is available free on request from: Mr. J. W. Blanton, Columbia-National Corporation, 70 Memorial Drive, Cambridge 42, Massachusetts, U.S.A.

The Physical Society's annual exhibition of scientific instruments and apparatus

The Physical Society announces that its forty-second annual exhibition will be held at the Royal Horticultural Society's Old and New Halls, Westminster, London, S.W.1, from 24–27 March, 1958 (inclusive).

Entrance to the exhibition is by ticket only and these may be obtained, free of charge, from the offices of the Society, 1 Lowther Gardens, Prince Consort Road, London, S.W.7. Members of The Institute of Physics may obtain tickets from the Institute's office. The handbook of scientific instruments and apparatus published in connexion with the exhibition is available from the Society, price 6*s*.; by post 7*s*. 8*d*.

Register of British manufacturers

The 1958 edition of the F.B.I. register of British manufacturers provides a comprehensive guide to a substantial cross-section of British industry, listing the products and services of over 7500 firms who are members of the Federation of British Industries, under more than 5400 alphabetical headings. The headings used are: products and services, addresses, trade associations, brands and trade names, trade marks. In addition there are language glossaries in French, German and Spanish.

The register is published by Kelly's Directories Ltd., and Iliffe and Sons Ltd., Dorset House, Stamford Street, London, S.E.1. The price is 42*s*.

Journal of Scientific Instruments

Contents of the February issue

ORIGINAL CONTRIBUTIONS

Papers

New types of recording differential thermobalances. By P. L. Waters.
A linear, unidirectional anemometer of rapid response. By R. J. Taylor.
A magnetic gauge utilizing the magnetron effect. By W. Fulop.
A high-resolution grating spectrometer for the infra-red region. By M. A. Ford, W. C. Price and G. R. Wilkinson.
Modifications to a travelling microscope used for measuring X-ray powder photographs. By W. E. Armstrong and R. J. Davis.
An oxidizing atmosphere furnace for use with an X-ray diffractometer By S. W. Kennedy and L. D. Calvert.
The recording of pressure distributions in porous media during fluid flow experiments. By T. O'Donnell, D. H. Edwards, N. Collis-George and E. G. Youngs.
A simple method of monitoring ultra-violet light. By C. K. Coogan.
A laboratory electron bombardment furnace. By P. G. England and H. N. Jones.
A combined liquid nitrogen cryostat, furnace and liquid helium bath. By M. J. Stubbs and M. W. Thompson.

Laboratory and workshop notes

A simple centrifugal circulating pump. By M. M. Benarie, I. Amariglio and M. Mokady.
A simple gas inlet for use with vacuum systems. By J. Almond.
A greaseless vacuum seal for rotating shafts. By E. A. Billett and J. Bishop.
The protection of glass apparatus by embedding in transparent resin. By F. Jones.
A modification for use with wire resistance strain gauge circuits. By J. Halling.
An instrument to trim specimen blocks prior to ultra-microtomy. By A. L. Sims.
Simple refractory-metal and glass-metal seals. By W. D. Jamieson.
The preparation of spherical single crystals for X-ray diffraction work. By K. S Revell and R. W. H. Small.

NOTES AND NEWS

New instruments, materials and tools
New books Manufacturers' publications Notes and Comments

THIS JOURNAL is produced monthly by The Institute of Physics, in London.

It deals with all branches of applied physics (including theory and technique). All rights reserved. Responsibility for the statements contained herein attaches only to the writers.

EDITORIAL MATTER. Communications concerning editorial matter should be addressed to the Editor, The Institute of Physics, 47 Belgrave Square, London, S.W.1. (*Telephone:* Belgravia 6111.) Prospective authors are invited to prepare their scripts in accordance with the *Notes on the preparation of contributions*. (Price 2*s*. 6*d*. including postage.)

REPRODUCTION. The Institute of Physics is a signatory to The Royal Society's Fair Copying Declaration. Details may be obtained upon application from The Royal Society, London, W.1.

ADVERTISEMENTS. Communications concerning advertisements should be addressed to the agents, Messrs. Walter Judd Ltd., 47 Gresham Street, London, E.C.2. (*Telephone:* Monarch 7644.)

CLAIMS FOR MISSING JOURNALS. Claims from regular subscribers to this *Journal* for missing numbers will only be considered if received within 60 days of the date of mailing plus normal outward time of transit and time for lodging the claim. Losses attributable to failure to notify a change of address or to similar omissions will not be considered.

SUBSCRIPTION RATES. A new volume commences each January. The charge is £5 per volume ($14.25 U.S.A.), including index (post paid), payable in advance. Single parts, so far as available, may be purchased at 10*s*. each ($1.50 U.S.A.), post paid, cash with order. Orders should be sent to The Institute of Physics, 47 Belgrave Square, London, S.W.1, or to any bookseller.

SPECIAL ARTICLE

A survey of exo-electron emission phenomena

By L. GRUNBERG, D.Sc., M.Sc., Mechanical Engineering Research Laboratory, East Kilbride, Glasgow

"Exo-electron" emission phenomena are reviewed. Kramer's original hypothesis that exo-thermal processes are the cause of the effect is no longer considered valid and it is now widely accepted that particularities of the crystal lattice, such as crystal imperfections are present in surfaces showing electron emission after mechanical deformation, X- or ultra-violet irradiation, electron bombardment, etc. Apparently spontaneous emission during phase changes of metals requires the presence of surface films. Oxygen must be present for emission to occur after the mechanical deformation of metals and photo-electric emission measurements suggest that certain surface oxides then contain negative-ion vacancies (*F'*-centres). The emission from ionic materials, such as alkali halides, depends on the presence of colour centres. The importance of crystal imperfections is brought out by the parallelism between luminescence and exo-electron emission. The latter depends only on the presence of donor-centres, but not on the activator centres necessary for the former to occur. Various applications of exo-electron phenomena and the question of nomenclature are discussed.

INTRODUCTION

The term "exo-electron emission" was practically unknown before 1950, yet to-day a large number of workers are studying this phenomenon with materials which have been subjected to a great variety of treatments, such as mechanical deformation, irradiation by X-rays and ultra-violet light, electron bombardment, electric gas discharges and additive coloration. The factor which is common to all these studies is that they concern themselves with the measurement of small emission currents which are obtained only if the materials have been subjected to certain treatments and hence are a measure of the structural changes brought about by the latter.

It appears natural that a subject of such recent date should be yet imperfectly understood and still somewhat controversial. Sufficient experimental evidence is however available, mainly due to considerable research efforts of Continental workers, to place the subject into its proper perspective. In the present survey mainly a historical approach was chosen, since it enabled the development of the subject to be traced and attention to be focused on yet unsolved problems. Within the framework of the present article it would be impossible to describe the whole volume of evidence which has become available and reference will be made only to work which in the opinion of the writer has decisively influenced the interpretation of the phenomena observed.

EXO-ELECTRON EMISSION FROM METALS

It has been known for a considerable time that freshly-manufactured Geiger–Müller counters may give an abnormally high background count, which decreased as the counter aged. The first indication that this phenomenon may be caused by the mechanical deformation processes to which the metals used for the construction of counters had been subjected was obtained by Lewis and Burcham.[1] These workers observed that abraded or scratched specimens of aluminium, copper, brass and nickel when introduced into a counter triggered off a large number of pulses. They suggested that the pulses may be due to ionization phenomena accompanying the reaction of oxygen with the deformed metal surface. The experiments by Lewis and Burcham remained unnoticed for a considerable period of time. Kramer was the first to draw attention to the fact that this phenomenon afforded a means of investigating metal surfaces. Although most of Kramer's work was done during the last war, it was not until 1950 that he published a comprehensive account of his investigations in the form of a monograph.[2] The work covered an enormous number of experiments in which metals were subjected to various treatments and then investigated with the aid of a "Spitzenzähler" (point counter). This is a rather simple instrument and consists of a fine anode wire terminating in a small metal sphere or a fine point surrounded by an open-ended cathode cylinder. It can be operated in air at atmospheric pressure, but requires high anode voltages (2000–4000 V). It is not a very stable instrument and has a narrow plateau characteristic, so that quantitative measurements are made only with some difficulty. In his experiments Kramer placed worked metal specimens under the counter anode, to form part of the cathode and observed a considerable counting rate, which decreased in the course of time. Fig. 1 shows the type of record obtained when abraded aluminium was investigated in this manner.

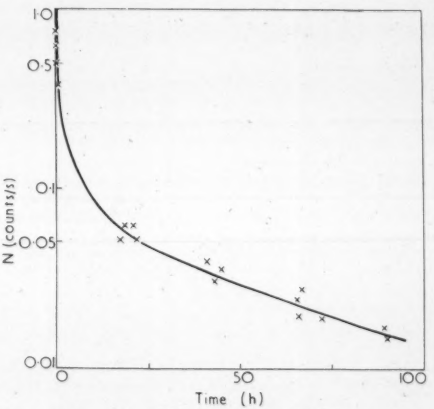

[Reproduced from *Der metallische Zustand.*]

Fig. 1. Decay curve from an abraded aluminium surface. Background count has been subtracted[2]

Experiments of the type shown in Fig. 1 appeared impossible to explain in a simple way, since, although undoubtedly negative charge carriers (oxygen ions or electrons) migrated from the deformed metal surface into the counter, externally, no energy had been supplied to the emitting specimen and the emission was apparently spontaneous. Amongst the various experiments which Kramer performed was one which lead him to the formulation of a hypothesis about the origin of the emission currents. The results of this experiment are shown in Fig. 2. Wood's metal when melted in front of the counter opening produced only few counts. However, when afterwards allowed to cool in that position a surge of pulses was observed when solidification commenced. This emission current again subsided at temperatures below the freezing point. Kramer believed that this experiment provided a clue to the apparently spontaneous emission from worked metal surfaces. Solidification is an exo-thermal process and the emission of electrons during this stage could be thermal caused by the latent heat of fusion. Kramer suggested that all the emission phenomena he had observed were due to exo-thermal processes and he termed electrons emitted in this

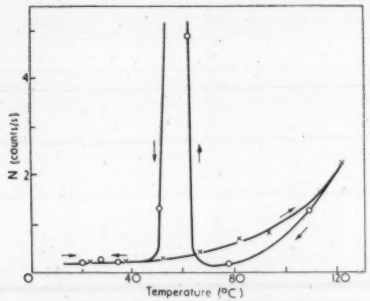

[Reproduced from *Der metallische Zustand.*]

Fig. 2. Melting and solidification of Wood's metal in a point-counter[2]

manner *exo-electrons*. This is then the origin of the term exo-electrons, meant in the first instance to describe electrons emitted from surfaces when exo-thermal processes are taking place. For abraded or otherwise deformed metal surfaces Kramer suggested the presence of a non-metallic phase of the metal. This phase was thought to be thermodynamically unstable above a certain critical temperature and then reverted to the normal metallic phase. The latent heat of phase change was suggested to be the cause of the emission of exo-electrons. Kramer has now abandoned this hypothesis and the term exo-electrons is at present used only for historical reasons. It will be shown later that it describes structure-sensitive emission phenomena, rather than those associated with exo-thermal processes. There exists, however, further evidence that apparently spontaneous electron emission occurs during phase changes of metals. Futschik[3] confirmed Kramer's experiment with Wood's metal and showed that the solidification of mercury also lead to electron emission. Most striking, however, were experiments by Futschik, Lintner and Schmid[4] with a series of lead–tin alloys. Using a Geiger–Müller counter with a hydrogen-ethanol filling, these workers found a perfect correlation to exist between the phase diagram and temperatures at which emission maxima occurred during cooling cycles. Crossing of the liquidus line, of the demixing line or the eutectic point on the phase diagram corresponded to the appearance of emission maxima. This is illustrated in Fig. 3 for an alloy containing 10% tin. Recently Steiner[5] observed an emission peak during the $\beta \rightarrow \alpha$ transition of thallium.

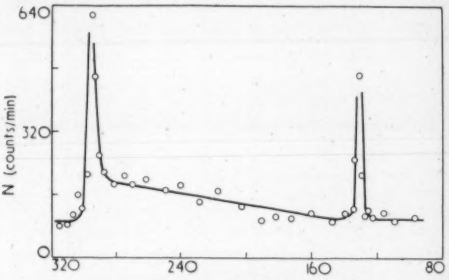

[Reproduced from *Zeitschrift für Physik.*]

Fig. 3. Exo-electron emission during the cooling of a lead–tin alloy, containing 10% tin[4]

Although the above evidence about emission during phase changes of metals appears conclusive, in the light of other experiments it cannot be attributed solely to the exo-thermal nature of the processes. Bathow and Gobrecht[6] have conclusively shown that emission during phase changes is not observable if sufficient care is taken to free the surface of the specimen from surface films and it is kept in a high vacuum (better than 10^{-6} mm of mercury). These workers overcame a difficulty which is inherent in the use of point counters or counting tubes for the observation of emission currents, namely the necessity of exposing the surface to air or to the counting gas. They enclosed the specimen in a specially shaped vacuum chamber and electron-optically focused the emission current into a counter. The latter was separated from the vacuum vessel by a glass membrane less than 1000 Å thick, permeable to electrons of 6 kV and yet capable to withstand a counting gas pressure of 4 cm of mercury. With this apparatus they were able to show that thorough cleaning of the specimen surface eliminated electron emission during solidification. If the vacuum was imperfect ($> 10^{-5}$ mm of mercury) emission currents were observable. This also was the case if the specimen was exposed to the atmosphere prior to investigation in a high vacuum.

The emission of exo-electrons hence appears to be connected with the presence of surface films or possibly with the interaction between gas molecules (i.e. oxygen) and the metal surface. The hypothesis that *chemisorption* of oxygen provided the energy of electron-emission was suggested by Haxel, Houtermans and Seeger.[7] By gradually raising the temperature of specimens in a gas-quenched Geiger–Müller counter they observed several emission maxima at definite temperatures. These maxima were attributed to adsorption centres having different energies of activation. Other workers went even further in this direction and suggested that the chemical reaction between oxygen and the metal surface provided the energy of electron emission so that the process was one of *chemo-emission*. Roubinek and Seidl,[8] who advocated this interpretation found that the presence of

oxygen was necessary for emission to be observed. This fact was again demonstrated in a very elegant manner by Lohff.[9] Metal specimens were scratched *in vacuo* ($>7 \times 10^{-5}$ mm of mercury) with a steel brush and the emission currents appearing after the admission of oxygen to a definite pressure, were detected with the aid of an electron-multiplier. Fig. 4 shows emission decay curves obtained from scratched aluminium at various oxygen pressures. The emission currents obtained at an oxygen pressure of 10^{-4} mm of

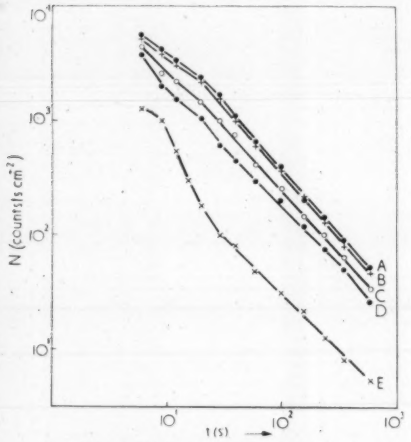

[Reproduced from *Zeitschrift für Physik*.]

Fig. 4. Decay curves from aluminium at 22° C after scratching with a steel-brush at different oxygen pressures.[9] (Pressure of oxygen in mm of mercury: curve *A*, 1×10^{-4}; curve *B*, 5×10^{-5}; curve *C*, $2{\cdot}5 \times 10^{-5}$; curve *D*, $1{\cdot}5 \times 10^{-5}$; curve *E*, 7×10^{-6})

mercury were very much greater than at a pressure of 7×10^{-6} mm of mercury. The role which oxygen plays is still more clearly brought out by results for zinc shown in Fig. 5. On admission of oxygen the emission passes through a maximum and then decays. The intensity of emission is greater and the time interval for reaching the maximum is shorter at higher oxygen pressures. Similar results have since been obtained by Wüstenhagen (private communication) with evaporated aluminium films.

The experiments so far described show that whatever the origin of the emission currents may be, it cannot be ascribed to instrumental causes, such as the bombardment of the specimen surface by positive ions or metastable atomic or molecular particles. Such events, whilst possible or even likely when a specimen is exposed to a point counter or is introduced inside a Geiger–Müller counter, could not occur with the closed counter used by Bathow and Gobrecht[6] or in the electron-multiplier used by Lohff.[9] The above experiments were mainly designed to discover an exo-thermal process which would enable thermal emission from the metal to occur. A fact which seems to have been overlooked in this approach to the problem is that the work function of most metals is usually greater than the energies which can be associated with phase changes or chemical reactions. The latent heat of fusion of metals for instance is of the order of 0·1 eV, i.e. about 1/40 of the work function. It appeared possible that working of the surface may lead to a general decrease of the work function. This problem was investigated by

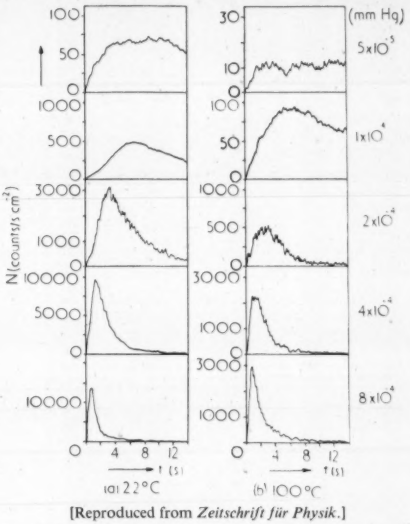

[Reproduced from *Zeitschrift für Physik*.]

Fig. 5. Exo-electron emission from zinc after scratching with a steel-brush at different oxygen pressures[9]

Edlinger and Müller,[10] who studied the photo-electric emission from abraded aluminium and zinc in the near ultraviolet range as a function of the wavelength. Fig. 6 shows the results obtained with aluminium. Those for zinc follow a similar pattern. The figures on the curves denote the time which had elapsed since abrasion. The photo-electric threshold appears to have been shifted to longer wavelengths by several hundred Ångstrom units and this shift receded with time. There are however serious doubts whether this effect can really be ascribed to the metal proper, since it may

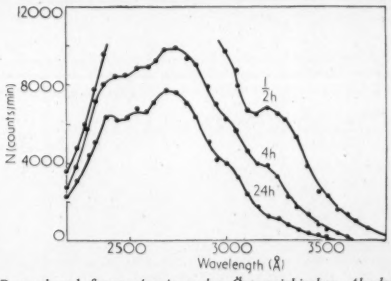

[Reproduced from *Anzeiger der Österreichischen Akademie der Wissenschaften*.]

Fig. 6. The dependence of photo-electric emission from abraded aluminium on the wavelength[10]

be due to a surface film created during the abrasion process. Seeger,[11] for instance, has clearly shown that thermal emission from aluminium, after stimulation with ultra-violet light is associated with the presence of an oxide film.

The work of Grunberg and Wright shed considerable light on the structures produced on metal surfaces by deformation. In 1952 these workers found that an abraded zinc surface gave photo-electric emission when illuminated in the visible range of wavelengths.[12] A thorough investigation[13] of the photoelectric response from freshly abraded metal surfaces revealed that oxidizable metals such as aluminium, magnesium, zinc, copper, brass, lead, indium, gallium, cadmium, iron, nickel, tin and titanium showed, after abrasion, emission below 3700 Å, i.e. in the range of wavelengths investigated by Edlinger and Müller.[10] Since the emission appeared to be independent of the nature of the metal or oxide involved, an interpretation of emission in this range of wavelengths as a shift of photo-electric threshold of the metal seems difficult to accept. Grunberg and Wright further found that a group of metals such as aluminium, magnesium and zinc, known to give excess-metal oxides, gave after abrasion a sharp and strong electron-emission peak at 4700 Å and subsidiary peaks at 5200 Å and above 6000 Å (Fig. 7).

described the decay process, where a and n are constants, the latter being of the order of unity. Equation (1) is obviously incapable of describing the initial conditions and Hanle[14] has recently suggested a modification

$$N = N_0(a + bt)^{-n} \tag{2}$$

Grunberg and Wright, however, found that the kinetic equation which described the decay of the emission peak at 4700 Å was greatly dependent on the ambient atmosphere to which the metal surface was exposed. In the absence of oxygen

$$N = N_0 \exp(-k_1 t) \tag{3}$$

whilst in the presence of oxygen

$$N_0/N = (1 + k_2 t)^2 \tag{4}$$

The reaction velocity constant k_2 was found to be directly proportional to the partial pressure of oxygen. Grunberg and Wright also found that the emission current was dependent on the electric field above the specimen surface. If a grid at earth potential was interposed between the counter and the earthed specimen then no counts could be registered. If a negative bias of the order of a few volts was placed on the

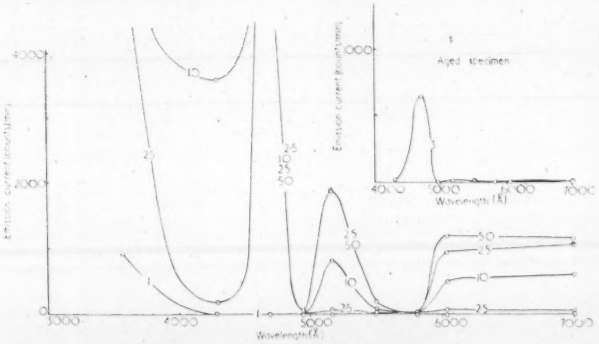

[Reproduced from *Proceedings of the Royal Society*.]

Fig. 7. Emission current against wavelength for abraded aluminium. Inset shows curve for aged specimen. The numbers on the curves indicate negative potential on specimen in volts[13]

Such emission peaks could be associated with the existence of definite electronic energy levels in the forbidden band of the oxide and could not be attributed to the metal. Isolated energy levels could be due to the presence of crystal imperfections and since the selective photo-electric effect was only observable with metals giving excess-metal oxides and for various other reasons the energy level responsible for the emission at 4700 Å was attributed to the presence in the oxide of negative-ion vacancies trapping two electrons. Owing to the similarity with such centres known to exist in alkali halide crystals, the crystal imperfections were termed F'-centres. Grunberg and Wright also investigated the decay of the emission currents. Most other workers had until then contented themselves with plotting the emission current, N *versus* the time t on double-logarithmic graph paper and obtained near enough straight lines as can be seen in Fig. 4 and it was generally assumed that an equation of the type

$$N = at^{-n} \tag{1}$$

specimen and the grid kept at earth potential then the emission current could be observed (see Fig. 7). The emission current increased with the applied voltage V according to

$$N = \alpha(V - V_0)^2 \tag{5}$$

where α = a constant and V_0 = the voltage at which no measurable emission current was observed. The reason for this voltage dependence of the emission current is not yet fully understood although two important conclusions can readily be drawn from it: (i) the electrons leave the surface with a negligible energy content and (ii) in experiments in which the specimen is directly exposed to the field of the counter anode or of the first dynode of an electron multiplier the magnitude of the measured current would depend on the intensity of this field. Recent experiments (Grunberg and Wright unpublished) seem to indicate that the voltage dependence may be connected with the heterogeneous nature of the surface on which "patch-fields" may exist, from the action of which electrons must escape before they can be

drawn into the counter. The applied negative voltage lowers the patch-field potential and thus increases the probability of escape of electrons. For this interpretation to be correct a saturation effect should be observable, particularly with weakly-emitting surfaces. This has indeed been observed experimentally. The emission current was also found to increase with increasing light intensity I according to

$$N = \beta I^m$$

where β and m are constants, the latter being somewhat greater than unity (between 1·25 and 1·33). In recent experiments Grunberg and Wright[15] were able to show that the electron emission spectra were independent of the method of introducing centres into the surface. The same spectra were obtained from abraded, extended and evaporated aluminium.

The excitation of definite electronic energy levels in surface oxides can also be achieved thermally by gradually raising the temperature of the specimen and observing the appearance of electron emission maxima at definite temperatures. This technique is similar to that used in taking a glow-curve from thermo-luminescent phosphors and the term *electron emission glow-curve* is now generally in use in this connexion.[14] Seeger,[16] with the aid of an electron-multiplier was able to show that the surface of tungsten subjected to electron bombardment was activated more strongly by oxidation, followed by abrasion than by either processes separately. This can be seen from the results shown in Fig. 8. Both optical and thermal exo-electron emission currents from metal surfaces thus appear to depend on the presence of highly deformed oxide films.

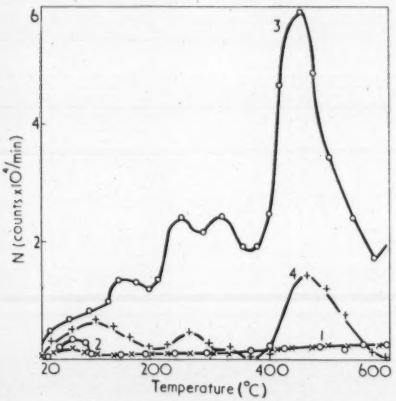

[Reproduced from *Zeitschrift für Physik*.]

Fig. 8. Electron emission from tungsten after electron bombardment. Curve 1, after heating sample for 30 min *in vacuo* at 1000° C; curve 2, as for 1, but subsequently oxidized in air for 15 min at 100° C; curve 3, as for 2, but then abraded in air; curve 4, abraded without prior oxidation[16]

EXO-ELECTRON EMISSION FROM NON-METALS

The work on exo-electron emission from metals has shown that the presence of non-metallic surface films was necessary for emission to occur. This finding was fully supported by the evidence which accumulated about exo-electron emission from non-metallic materials. At an early stage Kramer[17] was able to show that a number of minerals, such as fluorspar, corundum, pyrites, potassium orthoclase and others gave, after mechanical disintegration, a definite counting rate when investigated with the aid of a point-counter. The decay of the emission appeared to follow equation (1) and there was therefore a great similarity between the emission obtained from metallic and non-metallic materials. Kramer[18] was further able to show that emission from abraded non-oxidizable metals was due to contamination with non-metallic particles of abrasive and was not due to the metal itself. Mechanical deformation was not the only means of producing exo-electron emission in minerals. Pyrites, after irradiation with X-rays, behaved in a manner very similar to the mechanically deformed mineral.[19] Kramer also showed that quartz acquired emissive properties after X-irradiation and potassium sulphate after irradiation with ultra-violet light. X-irradiated gypsum when heated gradually underneath a point-counter gave rise to a number of emission peaks.[20] The exo-electron emission glow-curves obtained were greatly dependent on the tempering conditions and this

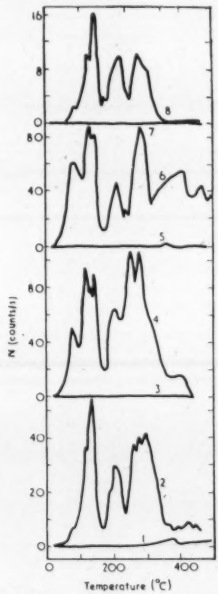

[Reproduced from *Zeitschrift für Physik*.]

Fig. 9. Exo-electron emission glow curves from gypsum and calcium oxide as affected by tempering. Curves 1 and 2, tempered at 640° C (1 without stimulation, 2 after X-ray stimulation); curves 3 and 4, as 1 and 2, but tempered at 940° C; curves 5 and 6, as 1 and 2, but tempered to 1240° C; curves 7 and 8, similar measurements on calcium oxide[20]

could partly be due to the formation of calcium oxide as suggested by the results shown in Fig. 9.

The deliberate supply of energy to specimens in the form of heat in order to study definite electronic energy levels present constituted a definite advance of the subject. It lead to the suggestion that the interpretation of the emission phenomena from non-metallic materials could best be achieved in terms of the presence of colour centres or other imperfection in ionic crystals. Bohun[21] was amongst the first to realize this. Since a great deal was known about the properties of colour centres in alkali halides he investigated these materials in detail. With photo-chemically coloured (X-irradiated) rock-salt, thermal emission glow curves revealed a number of emission peaks which Bohun[22] was able to assign to various types of colour centres known to exist in rock-salt. In a further detailed investigation Bohun[23] used rock-salt crystals coloured by additive coloration, i.e. by exposure to sodium metal vapour. Fig. 10 shows the electron emission glow-curve obtained with this material. The emission maximum

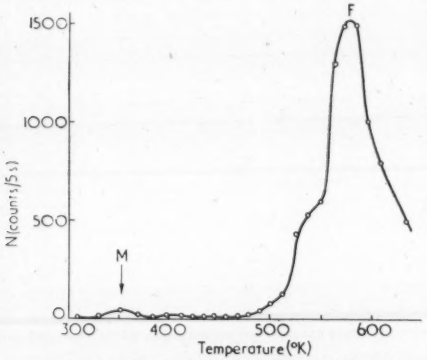

[Reproduced from *Czechoslovak Journal of Physics*.]

Fig. 10. Exo-electron emission glow-curve from additively coloured rock-salt[23]

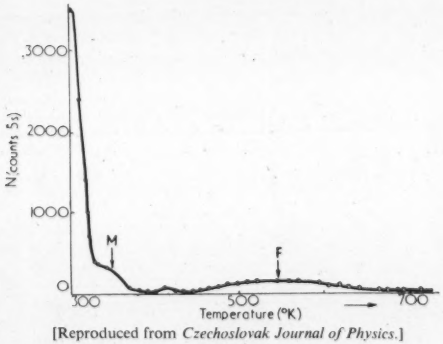

[Reproduced from *Czechoslovak Journal of Physics*.]

Fig. 11. Exo-electron emission glow-curve from additively coloured rock-salt with simultaneous illumination in the *F*-band[23]

at 560° K which can be assigned to *F*-centres (negative ion-vacancies trapping one electron) is clearly discernible, as is a smaller maximum at 350° K attributed to *M*-centres (combination of a vacancy pair and an *F*-centre). Bohun was able to show that optical bleaching of the *F*-centres reduced the peak at 560° K. Fig. 11 shows how illumination with light containing the *F*-band lead to strong emission at room temperature. If the temperature of the specimen was raised the *M*-peak could still be seen, but the *F*-peak had been flattened, possibly under the formation of *F'*-centres (negative ion-vacancies, trapping two electrons). More recent experiments by Kramer[24] demonstrated that the emission from *F'*-centres was enhanced by illumination in the *F*-band (4750 Å) and that these centres were bleached by illumination in the *F'*-band (7290 Å). Kramer also investigated the formation of colour centres in potassium bromide as a function of the energy level of the ultra-violet light used. Colour centres, giving exo-electron emission, were only obtained if the stimulation energy was greater than that corresponding to the light absorption edge, which suggests a mechanism of formation involving excitons. The experiments reported in this section clearly demonstrate the connexion between exo-electron emission and colour centres. The importance of crystal imperfections and impurity centres is shown by the relationship between exo-electron emission and luminescence which will be discussed in the next section.

EXO-ELECTRON EMISSION AND LUMINESCENCE

In 1954 Kramer[25] pointed to the similarity which existed between exo-electron emission and luminescence phenomena and a year later experimental evidence became available of a most striking parallelism between the two phenomena. Lepper[26] showed that, if exo-electronic emission and phosphorescence were observed simultaneously, then the two phenomena followed the same decay law. Fig. 12 shows the

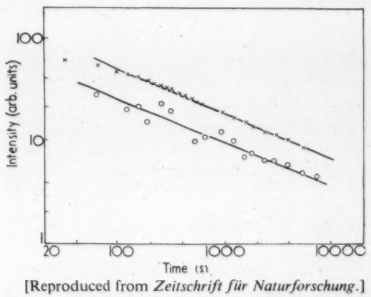

[Reproduced from *Zeitschrift für Naturforschung*.]

Fig. 12. Decay curves of exo-electron emission (circles) and of phosphorescence (crosses) of $CaSO_4$. Mn[26]

observed decay curves of exo-electron emission and phosphorescence from a calcium sulphate . manganese phosphor after X-ray stimulation. Equation (1) is apparently followed by both these phenomena and the slopes of the lines are identical. Similar results were obtained with a crystal of sodium chloride + 1·5% silver chloride. The parallelism between exo-electronic emission and luminescence was found to be fully evident also when the respective glow-curves were observed simultaneously. This can be seen in Fig. 13 for

X-ray stimulated NaCl.Ag. The maxima of thermo-exo-electron emission and thermo-luminescence occur at identical temperatures. Bohun[23, 27] independently discovered the parallelism between electron emission and luminescence and investigated the simultaneous glow-curves for a number of phosphors, in particular rock-salt containing various foreign ions and fluorspar.

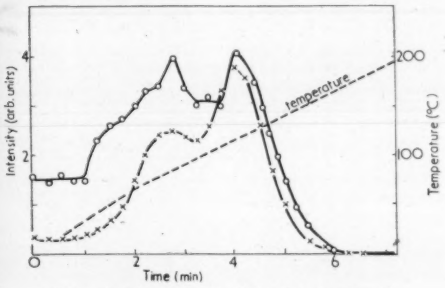

[Reproduced from *Zeitschrift für Naturforschung.*]

Fig. 13. Glow-curves of electron emission (circles) and luminescence crosses from an X-ray stimulated NaCl + +1·5% AgCl.[26] Temperature shown by dashed curve

The electronic transitions involved in thermo-luminescence are now well understood. Reduced to its simplest terms thermo-luminescence requires the presence of two types of electron-trapping levels in the forbidden energy gap of an insulator. Donor levels, lying sufficiently close to conduction levels are thermally excited and dissociated. Electrons enter the conduction band and some of these may recombine in radiationless transitions with empty donor levels. Other electrons may drop from the conduction band, under the emission of light quanta to empty activator levels, lying close to the valency band of the crystal. The activator levels are often associated with the presence of foreign atoms in the crystal. The parallelism between exo-electron emission and luminescence raised the question whether or not both types of electron-trapping centres are involved in the electron emission process. The answer to this question was provided by Lepper.[26] Calcium sulphate in its pure state is not a phosphor and requires the presence of manganese to provide the activator levels. Pure calcium sulphate gave the same electron emission glow-curve as $CaSO_4$. Mn, but thermo-luminescence could only be obtained from the latter. The results of these experiments are shown in Fig. 14. It can thus be concluded that exo-electron emission requires the presence of donor levels, but not of activator levels.

A large number of new results on the simultaneous observation of thermo-luminescence and electron emission were presented by Gourge and Hanle.[28] Activator levels can interfere with the parallelism between the two phenomena. This is illustrated by Fig. 15 showing results obtained with strontium sulphate.manganese. At lower temperatures the curves show maxima at identical temperatures, but at higher temperatures the electron emission curve shows maxima which do not appear on the luminescence curve. The effect is interpreted as due to a gradual filling-up of the activator levels by electrons from the valency band. Gourge and Hanle also investigated glow-curves starting from liquid air temperature. A number of maxima below room temperature were found with NaCl.Ag and $SrSO_4$.Mn. In general it can be said that exo-electron emission now provides a useful tool for the investigation of electronic energy levels in phosphors, which would remain undetected if luminescence alone would be observed.

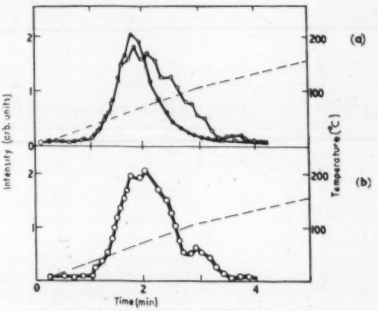

[Reproduced from *Zeitschrift für Naturforschung.*]

Fig. 14. Glow-curves from (*a*) $CaSO_4$.Mn and (*b*) pure $CaSO_4$, both tempered at 850° C. Electron emission (circles) is shown by both materials, luminescence (solid circles) only by (*a*).[26] Temperature shown by dashed curve

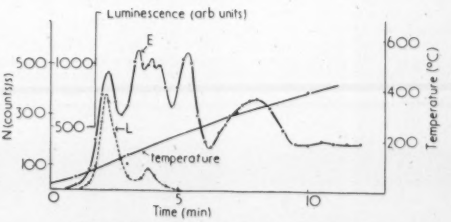

[Reproduced from *Acta Physica Austriaca.*]

Fig. 15. Glow-curves of electron emission *E* and luminescence *L* from $SrSO_4$.Mn (1%). Tempered at 900° C, irradiation dose 250r[28]

THE MECHANISM OF EXO-ELECTRON EMISSION

The experiments on luminescence and exo-electron emission and those on exo-electron emission from ionic materials containing colour centres have shown that donor levels must be present for the phenomenon to occur. The mechanism by means of which electrons are emitted from the crystal is however not fully explained by this finding. It seems fairly easy to understand that on reaching a certain temperature or on absorbing light of a certain wavelength donor centres are excited and dissociated. Electrons are then raised into the conduction levels, but there appears to be no well-established mechanism by means of which they could leave the crystal. Nassenstein[29] suggested that electrons arising from the dissociation of centres located close to the surface are capable of leaving the crystal *via* the conduction band.

Since the energy bands are likely to be modified at the crystal boundary this explanation does not describe the emission process in detail. According to Lepper[26] the electrons are raised into the conduction band and then diffuse into a surface energy band from which they are emitted thermally. The filling of such surface states would depend on the electron affinity of the crystal (i.e. the depth of the conduction levels) a higher electron affinity making exo-electron emission more difficult. Bohun,[30] however, has shown that the emission was relatively independent of the electron affinity of the crystal, since silver halides with an electron-affinity of about 3 eV respond as readily as rock-salt with an electron-affinity of 0·5 eV. Grunberg and Wright[13] put forward a mechanism suggested by Mott for the photo-electric emission from deformed metal surfaces containing F'-centres. Absorption of light in the F'-band (4700 Å) leads to the excitation of F'-centres. The energy of excitation can be transferred by direct interaction to shallow centres over a distance of between 30 to 40 Å. If the shallow centres are actually on the surface then electrons will be ejected from them out of the crystal. According to recent evidence (Grunberg and Wright, unpublished) the shallow surface centres appear to be adsorbed oxygen. This explanation of the emission mechanism eliminates the difficulty of having to consider the electron-affinity of the crystal and provides a reasonable interpretation of the fact that exo-electron emission can only be observed above a certain partial pressure of oxygen. An indication that exo-electron emission depends on the presence of centres which do not partake in luminescence can be deduced from measurements of the intensity of the first electron emission and luminescence maximum as a function of the X-ray dose used for stimulating $CaSO_4$.Mn. Whilst electron emission becomes saturated after a dose of 1000r luminescence continues to increase even after a dose of 3000r.[28] This result can be interpreted as showing that after high X-ray doses the exo-electron emission intensity becomes independent of the concentration of donor centres and is then governed by the concentration of surface centres, which would be relatively independent of the X-ray dose.

APPLICATIONS OF EXO-ELECTRON EMISSION

Since exo-electron emission appears to be so strongly connected with the presence of crystal imperfections the study of semi-conductors may greatly benefit from the application of this new technique. The application to luminescence has already been described in a previous section and recently attempts have been made to study intrinsic semi-conductors with this method. Gourge and Hanle[28] investigated *p*-silicon after X-ray stimulation. An emission maximum was observed at 100° C, which could possibly be due to surface oxide, although the measurements were carried out in a high vacuum. Seeger[31] investigated polycrystalline and single crystals of germanium after electron-bombardment in an electron multiplier at 10^{-6} to 10^{-7} mm of mercury. Polycrystalline germanium gave two maxima, a strong peak at −150° C and a weaker peak at +175° C. Single crystals of *n*-germanium gave a number of emission peaks, which were stronger with etched than with rough surfaces. Seeger also carried out some photo-electric emission measurements on germanium.

Fields of study which largely depend on the properties of solid surfaces may be advanced by the investigation of exo-electron emission. Foremost amongst these are chemisorption and catalysis. In the latter field a start has already been made by the work of Nassenstein and Menold.[32] Using silver catalysts of the same chemical composition, but different methods of preparation, they were able to show that differences in yield of between 90 and 0% in the reaction between ethylene and oxygen could be associated with different electron emission glow-curves from the catalysts. The study of deformed metal surfaces has been advanced by electron emission investigations and useful applications may be envisaged in the field of lubrication in which the structure and the mechanical properties of such surfaces are of significance. It must also be considered that such surfaces may initiate chemical reactions in the medium with which they are in contact. Grunberg[33] for instance has shown that measurable quantities of hydrogen peroxide are formed from water and oxygen on metal surfaces which one would expect to give exo-electron emission.

Various applications of direct practical interest have been suggested.[34] The efficiency of grinding of ball-mills can be followed by exo-electron emission and the optimum grinding time for oil absorption of titanium oxide in paint manufacture seems to correspond to the greatest possible exo-electron emission obtainable from this material. Similarly the sintering ability of metal powders used in powder metallurgy was said to find an expression in the intensity of exo-electron emission obtainable. It has also been suggested that the tendency of certain minerals to cause pneumoconiosis may be related to the presence of colour centres.

NOMENCLATURE

Earlier in this survey the origin of the term "exo-electrons" has been described. Although many problems still remain to be solved it seems now fairly clear that the original interpretation of the phenomenon as a consequence of exo-thermal processes is no longer tenable. On the occasion of the Discussion Meeting "Exo-electrons" held under the auspices of the Austrian Physical Society at Innsbruck in September 1956 the question of nomenclature was discussed in an informal meeting under the chairmanship of Prof. W. Hanle (Giessen). Workers from many countries interested in the subject attended and it was agreed that in view of the great contribution which Dr. J. Kramer has made "structure-dependent" electron emission should henceforth be known as the "Kramer Effect" and that the electrons be known as "exo-electrons" quite independently of the means of exciting the emission centres.

Owing to the analogy between exo-electron emission and luminescence the system describing in a short manner the stimulation method (i.e. the creation of centres) and of causing the emission of light quanta used in luminescence work should be adapted to describe exo-electron emission. Details of the system are given in the proceedings of the discussion meeting.[14, 35] A few examples will suffice to illustrate the system. Photo-electric emission from previously abraded surfaces should be described as "tribo-stimulated post-photo-electron emission," photo-electric emission during extension of metals as "plasto-stimulated co-photo-electron emission" and the observation of a glow-curve from X-irradiated materials as "X-radio-stimulated post-thermo-electron emission." These terms whilst precise in their meaning were not used in the present survey in order not to create difficulties for the uninitiated reader.

REFERENCES

(1) Lewis, W. B., and Burcham, W. E. *Proc. Camb. Phil. Soc.*, **32**, p. 503 (1936).

(2) KRAMER, J. *Der metallische Zustand.* (Göttingen: Vandenhoeck and Ruprecht, 1950.)

(3) FUTSCHIK, F. *Thesis* (Vienna, 1955); According to BRUNA, O., LINTNER, K., MÜLLER, H., and SCHMID, E. *Z. Phys.*, **136**, p. 605 (1954).

(4) FUTSCHIK, F., LINTNER, K., and SCHMID, E. *Z. Phys.*, **145**, p. 48 (1956).

(5) STEINER, H. *Acta Phys. Austriaca*, **10**, p. 401 (1957).

(6) BATHOW, G., and GOBRECHT, H. *Z. Phys.*, **146**, p. 1 (1956).

(7) HAXEL, O., HOUTERMANS, F. G., and SEEGER, K. *Z. Phys.*, **130**, p. 109 (1951).

(8) ROUBINEK, F., and SEIDL, R. *Czech. J. Phys.*, **2**, p. 84 (1953).

(9) LOHFF, J. *Z. Phys.*, **146**, p. 436 (1956).

(10) EDLINGER, W., and MÜLLER, H. *Anz. d. Österr. Akad. Wiss.*, **91**, p. 89 (1954).

(11) SEEGER, K. *Z. Phys.*, **135**, p. 152 (1953).

(12) GRUNBERG, L., and WRIGHT, K. H. R. *Nature* [*London*], **171**, p. 890 (1953).

(13) GRUNBERG, L., and WRIGHT, K. H. R. *Proc. Roy. Soc. A*, **232**, p. 423 (1955).

(14) HANLE, W. *Acta Phys. Austriaca*, **10**, p. 339 (1957).

(15) GRUNBERG, L., and WRIGHT, K. H. R. *Acta Phys. Austriaca*, **10**, p. 375 (1957).

(16) SEEGER, K. *Z. Phys.*, **141**, p. 221 (1955).

(17) KRAMER, J. *Z. Phys.*, **128**, p. 538 (1950).

(18) KRAMER, J. *Acta Phys. Austriaca*, **10**, p. 392 (1957).

(19) KRAMER, J. *Z. Phys.*, **129**, p. 34 (1951).

(20) KRAMER, J. *Z. Phys.*, **133**, p. 629 (1952).

(21) BOHUN, A. *Czech. J. Phys.*, **3**, p. 2 (1953).

(22) BOHUN, A. *Czech. J. Phys.*, **4**, p. 91 (1954).

(23) BOHUN, A. *Czech. J. Phys.*, **5**, p. 64 (1955).

(24) KRAMER, J. *Acta Phys. Austriaca*, **10**, p. 327 (1957).

(25) KRAMER, J. *Naturwissenschaften*, **41**, p. 169 (1954).

(26) LEPPER, J. *Z. Naturforsch.*, **10***a*, p. 47 (1955).

(27) BOHUN, A. *Czech. J. Phys.*, **5**, p. 224, p. 429 (1955).

(28) GOURGE, G., and HANLE, W. *Acta Phys. Austriaca*, **10**, p. 427 (1957).

(29) NASSENSTEIN, H. *Z. Naturforsch.*, **10***a*, p. 944 (1955).

(30) BOHUN, A. *Czech. J. Phys.*, **4**, p. 88 (1954).

(31) SEEGER, K. *Acta Phys. Austriaca*, **10**, p. 448 (1957).

(32) NASSENSTEIN, H., and MENOLD, R. *Acta Phys. Austriaca*, **10**, p. 452 (1957).

(33) GRUNBERG, L. *Proc. Phys. Soc.* [*London*] *B*, **66**, p. 153 (1953).

(34) Dechema Discussion Meeting, Frankfurt, 21 October, 1955. Reported in *Chemie-Ing.-Techn.*, **27**, p. 799 (1955).

(35) LINTNER, K., and SCHMID, E. *Acta Phys. Austriaca*, **10**, p. 313 (1957).

Aluminosilicates and the high-temperature processing of microwave vacuum tubes

By M. Hillier and R. L. Bell, Ph.D.,* Services Electronics Research Laboratory, Baldock, Herts.

[*Paper first received* 7 *June, and in final form* 17 *September*, 1957]

The application of high temperature glass techniques to the construction and processing of microwave vacuum tubes is described. An increase in bake-out temperature is shown to have a profound effect on the running pressure, cathode life and other properties which may depend on tube vacua.

Tubes for microwaves often have metallic envelopes to promote cooling of internal parts. This prevents the outgassing of these parts during processing by the normal means of eddy-current heating or electron bombardment and it is usual to outgas the complete valve by baking on the pump at as high a temperature as possible. With the borosilicate glasses commonly used for the insulating parts of the envelope, softening of the glass sets a limit of about 450° C to the bake-out temperature. In some cases even a very long bake at this temperature is insufficient to prevent the subsequent release of occluded gas. This may limit the useful life of the tube since cathode activity is destroyed by ion bombardment.

Means are continually being sought of raising the bake-out temperature so that all occluded gas in the tube components is effectively removed on the pump. The use of ceramic envelope materials is one approach to this problem, but the technology of vacuum-tight ceramics and ceramic-to-metal seals is not yet as reliable a laboratory process as a glass/metal structure.

The problem has been solved in the case of a millimetre wave klystron recently developed at this Laboratory[1] by evolving a fabrication technique using molybdenum and high melting point aluminosilicate glass. This paper describes the glass-to-metal sealing techniques and discusses some of the factors affecting choice of bake-out temperature.

MATERIALS

Some properties of useful aluminosilicates are shown in the table. H26X is made by the Osram/General Electric Co. Ltd., Glassworks, Wembley, and C37 and C46 by The British Thomson-Houston Co. Ltd., Rugby. Included in the table are the dielectric constants and power factors measured by the authors at 8·6 mm wavelength. Comparison with the kovar-sealing borosilicate Kodial (by Plowden and Thompson Ltd., Stourbridge, Worcs.), power factor 0·013, shows that aluminosilicates should make useful window materials. Measurements at a low frequency[2] on glasses very similar to H26X and C37 show good stability of dielectric loss against temperature rise. This, combined with their high softening temperature, suggests the possibilities of high power handling capacity of aluminosilicate windows, but no work has been done on this. The table shows that their maximum bake-out temperature will be between 700 and 800° C, provided that rapid changes of temperature over the annealing range are avoided; sealing temperatures are around 1200° C.

Properties of the materials

	Molybdenum	*C37*	*C46*	*H26X*
Thermal expansion (50–400° C) × 10^7	55	42·5	43	46
Melting point	2620° C			
Log. direct current resistivity at 300° C		12·0	11·9	11·4
500° C				8·8
Dielectric constant at 1 Mc/s			5·9	
Dielectric constant at 35 000 Mc/s		4·2		4·1
Specific gravity	10·2	2·55	2·62	2·30
Power factor at 1 Mc/s			0·001 9	
Power factor at 35 000 Mc/s		0·009		0·012
Refractive index				1·535
Composition (%): silica		55·8	54·5	54·25
alumina		23·0	23·5	22·0
boric oxide		5·1	—	7·5
calcium oxide		13·0	11·3	13·25
barium oxide		3·1	6·3	3·0
magnesium oxide		—	0·5	—
phosphorus pentoxide		—	3·8	—
Upper annealing temperature (° C)		775	790	725

The aluminosilicates are designed for sealing to molybdenum, which, for the success of the technique, must be capable of fabrication into vacuum-tight cups, cylinders, etc. The ductility of molybdenum rises markedly with temperature[3] around room temperature, and deep drawing is facilitated by using heated tools. However, it was found possible[4] to draw cups from good quality sheet of 0·010 thickness at

* Now at Varian Associates, Palo Alto, California, U.S.A.

room temperature provided the material was kept under tension by pressure pads.

GLASS-TO-METAL SEALS

Molybdenum heated in air readily forms the dioxide and trioxide at low temperatures, and the latter is volatile above about 700° C. The impossibility of making large seals in air will be appreciated; heating in pure nitrogen is also undesirable due to embrittlement by formation of the nitride above 1100° C. Much of the sealing is therefore done in dry de-oxidized cylinder argon, heating the metal parts by radio frequency induction.

The molybdenum parts are prepared for sealing by first furnacing in wet hydrogen at 900° C, and the edges to be glassed are deplated in a weak chromic/sulphuric acid solution. The parts are then oxidized for five minutes at 580° C in air or oxygen. A certain amount of trioxide is formed during this process and must be evaporated by heating to about 1000° C in dry argon, leaving the adherent brown-purple dioxide required for glass sealing. Particular care is taken in handling the glass to avoid contamination from fingers near the parts to be melted. Failure to observe these precautions may result in a discoloured, unreliable seal.

A typical component with cylindrical seals is shown in Fig. 1. This is assembled in a sealing-jig (Fig. 2) which

Fig. 1. Disk seals (half size)

consists of a long water-cooled induction coil mounted on an insulating base and provided with a concentrator which can be moved up and down the vertical axis of the coil by means of a cam arrangement under the base. A glass bell jar encloses the coil and is clamped to the base to form a gas-tight enclosure. Argon is passed into the working space by means of a tube through the base. The prepared glass and metal parts are stacked vertically on the axis of the coil in a jig which applies compression by means of a guided top weight whose fall can be stopped at pre-set heights.

In making the seals, the apparatus is flushed with argon, and the useful parts are gradually heated to about 1000° C, when the weight begins to sink as the glass melts on to the metal, the amount of glass at each seal being controlled by

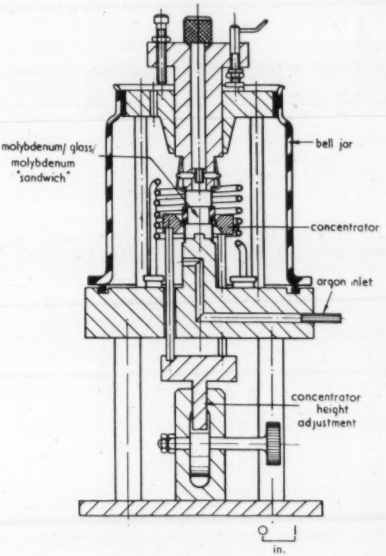

Fig. 2. Sealing jig

the jig. After the weight has fallen its pre-set amount, the individual seals are heated to about 1200° C, when the glass wets the metal, as seen by a change in the contact angle.

The metal is now covered with a thin, tenacious layer of dioxide, which is very difficult to remove chemically without damaging the seal. However, this is rendered unnecessary if the assembly is removed from the jig while still warm and annealed in hydrogen (or cracked ammonia). The oxide on exposed metal is reduced but the oxide of the seal is unaffected. It is found sufficient to anneal the seals by cooling at a uniform slow rate from the upper annealing temperature of the glass—2° C/min is adequate for the assembly described. In normal glass working, aluminosilicates should be heated slowly in the oxidizing tip of a bushy oxygen-air-coal gas

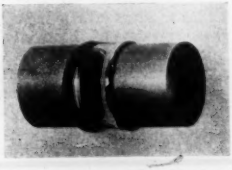

Fig. 3. Cylindrical seals (half size)

flame to avoid decomposition. They can be sealed directly to Pyrex.

Figs. 1 and 3 show typical seals which have been made successfully in numbers and baked at 700° C without failure. Fig. 4 shows a millimetre wave window, made by sealing a

Fig. 4. Millimetre wave window (full size)

0·010 in. thick slip of aluminosilicate over a 0·200 in. hole in the end of a cup of 0·010 in. molybdenum. Such a window of C37 has been baked at 780° C without failure.

SINTERED BASE

The sintered "button" base technique is easily applied to the aluminosilicate/molybdenum combination. A crushed glass aggregate, with particle sizes up to about 32 mesh, is loaded into a good quality carbon mould together with molybdenum rods pre-oxidized as described above; a compacting pressure of about 7 g/cm^2 is applied by means of a carbon weight sliding freely on the rods. The sintering is conveniently done by induction heating of the carbon mould to about 1200° C in an atmosphere of dry de-oxidized tank argon, when the seals are made and a fairly robust button base is produced. A typical sample is shown in Fig. 5; here the carbon mould has been shaped to provide some sintered-on sheathing and so obtain increased insulation—in this case up

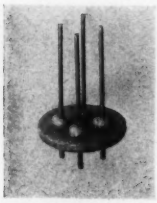

Fig. 5. Sintered pinch (half size)

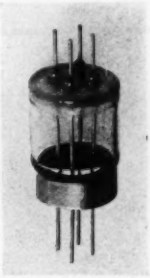

Fig. 6. Sintered pinch assembly (half size)

to 9 kV between adjacent wires. It was not found possible to make a reliable metal to glass seal at the periphery of the button, but the sealing of a glass tube to the base as a separate operation is easily accomplished in another induction-heated carbon jig. Fig. 6 shows a completed base in which the glass tube has been previously sealed to a molybdenum tube. The final structure is annealed as described previously.

BRAZING

Molybdenum can be plated with nickel or copper.[5-7] A nickel-plating process used by N. Rain of this Laboratory is given in the Appendix. The metal parts can then be brazed into the tube using any of the conventional brazing alloys—copper–silver, copper–gold, etc. A thickness of nickel of 0·0003 in. is found to be about optimum from the point of view of adherence of the plate combined with good protection of the molybdenum.

Molybdenum itself can be wetted by palladium–nickel, platinum–nickel or platinum–silver alloys, and a braze can be effected if the parts can be raised to around 1200° C in a reducing atmosphere. The titanium hydride technique can also be used to braze copper or silver or their alloys directly to molybdenum.

BAKING TEMPERATURE

Gases dissolved in the materials of the tube components diffuse out at a rate depending on the gas and material and cannot be entirely removed from metals without melting them. However, a few hours bake at 700° C was found sufficient to degas the tube mentioned in Ref. (1) to a satisfactory degree and no obvious improvement in tube performance resulted from longer bakes. To remove the same amount of gas at 400° C might take several weeks, diffusion rates varying exponentially with temperature. An increase in the bake temperature to 800° C might thus give a further factor of improvement of between 3 and 10 times depending on the gases present.

One consequence of speeding up the diffusion process at high temperatures is that gases from the atmosphere are able to dissolve in the metal envelope and diffuse through to the inside causing a deterioration in the tube exhaust vacuum. For this reason it is necessary to bake in a vacuum oven. The process of solution in metals is one of chemical combination, molecular gases at the hot surface dissociating into atoms and working their way through the metal lattice. At high pressures this process leads to a law of variation of the rate of diffusion with the square root of external pressure, but at pressures of the order of 1 mm of mercury the surface ceases to be completely covered by a layer of gas. The fraction of the surface covered then depends on the pressure and the rate of diffusion is approximately proportional to the external pressure. Clearly it is worthwhile reducing this pressure as much as possible.

Fig. 7 shows diagrammatically a pump set utilized for the tube of Ref. (1). The tube itself is evacuated by a fractionating oil pump capable of an ultimate vacuum better than 10^{-7} mm of mercury while the bell jar surrounding the tube and oven is pumped out by a separate high speed oil diffusion pump to about 10^{-5} mm of mercury. The oven consists of a self-supporting zig-zag cut from 0·010 in molybdenum sheet; the tube is inside this and the whole is surrounded by a nickel heat shield and finally by a bell jar.

The effect of high temperature baking on the activity of an oxide cathode is strikingly illustrated by the performance of the cathode in the tube of Ref. (1). This is required to run at a high emission density (0·6 A/cm^2). Tubes processed at 400° C failed by cathode poisoning after a few tens of hours; processing at 700° C in a vacuum oven gave lives of about 1000 hours.

The limit on baking temperature is not set by the glass alone for this is safe at least up to 800° C. The length and intensity of the bake will generally be governed by the effect of temperature on the properties of commonly-used materials. For example, the vapour pressures of metals or their oxides may be quite high—silver and copper have vapour pressures of 10^{-4} and 10^{-5} mm of mercury at 700° C—and conducting

films may be built up on windows and insulators. At this temperature also the yield strength of metals is only a fraction of their cold strength. Hence the design of metallic springs for use as retaining elements in tube structures presents a problem. Tungsten and the Nimonic series of alloys (by

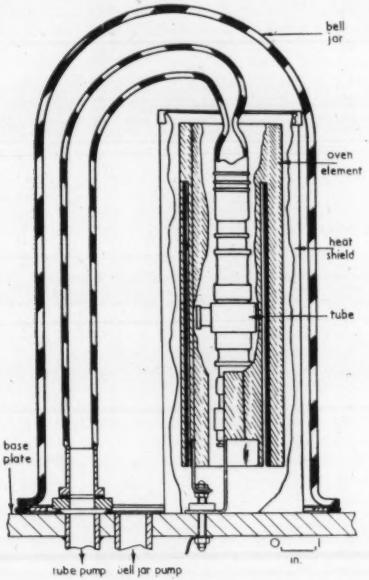

Fig. 7. Pumping set

Henry Wiggin and Co. Ltd., Birmingham) have been used but, in our experience, torsional creep in wires of these materials is more severe than the longitudinal variety and difficulty is found in making a spring which is of adequate strength above 700° C without being embarrassingly bulky.

CONCLUSIONS

The use of high melting point molybdenum-sealing aluminosilicate glasses in the construction of microwave tubes has opened the way to better outgassing by high temperature baking on the pump; significant increases in cathode performance have been achieved by this method. The method has several advantages over the ceramic technique, particularly in reliability and adaptability. In addition it seems likely that the aluminosilicates will make useful microwave window materials. The technological difficulties of forming molybdenum, making large glass-to-metal seals with it, and protecting it during the bake have been overcome.

ACKNOWLEDGEMENT

The authors are indebted to the Admiralty for permission to publish this paper.

REFERENCES

(1) BELL, R., and HILLIER, M. *Proc. Inst. Radio Engrs*, **44**, p. 1155 (1956).

(2) STEVELS, J. M. Progress in the Theory of the Physical Properties of Glass, p. 68 (London: Elsevier Publishing Co. Inc., 1948).

(3) BECHTOLD, J. H. *J. Metals*, **5**, p. 1469 (1953).

(4) DUCKWORTH, F. *Machinery*, **84**, p. 389 (1954).

(5) KORBELAK, A. *Plating*, **40** (10), p. 1126 (1953).

(6) VAALER, L. E., SUAVELY, C. A., FAUST, C. L. *Battelle Memorial Institute, BM.* I–813 (1953).

(7) HANSEN, ROBERT M. *Adherent Electroplating on Molybdenum* (New Jersey: Newark College of Engineering, 1952).

APPENDIX

The nickel plating of molybdenum. As mentioned in the text, molybdenum parts can be silver brazed if first plated with nickel. For a vacuum-tight seal, of course, it is desirable that the nickel should be securely bonded to the base metal. Thus it seemed logical to consider a process which would ensure an adherent plate—even if the adherence was initially only superficial—and which allowed for diffusion bonding by means of a short heat treatment in a reducing or inert atmosphere without either blistering or peeling.

In the process now to be described, the technique concentrated on an efficient cleaning cycle, followed by a Wood's chloride nickel strike, then a nickel plate in a type of bath which would give a soft ductile deposit. After plating the components were given a heat treatment in cracked ammonia gas or hydrogen for a short period at a temperature of 650–700° C. This served two purposes; it bonded the deposit to the base metal, and/or gave a check on the quality of the plating, as unsatisfactory deposits blistered. It was found incidentally that temperatures as low as 500° C gave evidence of diffusion bonding.

The cleaning treatment is critical, as in all electroplating techniques, and it is essential to maintain all solutions in a good condition. The acid cleaning bath and anodic electrocleaning bath should be frequently renewed; care should be taken with the nickel strike bath particularly in regard to its acid content which should never be allowed to become exhausted.

The exact cycle is as follows:

(1) Degrease.
(2) Immerse in acid cleaning bath at room temperature for 20 s.
(3) Rinse in tap water.
(4) Electroclean anodically in the 3% sulphuric/chromic bath for 1 min at a current density of 0·200 A/cm^2.
(5) Rinse in tap water.
(6) Nickel strike for 1 min in Wood's bath at a current density of 0·100 A/cm^2.
(7) Nickel plate at current density suitable for bath used.
(8) Rinse in running water, finally in distilled water and dry.
(9) Furnace in cracked ammonia or hydrogen for 10 min at 650°–700° C.
This should result in a firmly bonded, blister-free plating.

**

The particle size of some Witwatersrand mine dust

By H. St. G. Tucker, M.A., Chamber of Mines, Johannesburg, S. Africa

[*Paper first received* 21 *March*, 1956, *and in final form* 6 *July*, 1957]

The size distribution of mine drilling dust is examined and the use of Gaudin's relation to describe it proposed. The literature is reviewed and it is inferred that this is the true distribution for any dust of this kind.

In connexion with the dust hazard in mining operations, it became clear that obtaining a measure of dustiness independent of the particular situation and the instruments employed, in fact the choice of instruments for sampling and assessment, called for a knowledge of the size distribution of the dust.[1] To determine this, however, seemed to present some difficulty in view of the very large uncertainties associated with sampling a dusty atmosphere. A search of the literature revealed no agreement on this question. Roller, of the U.S. Bureau of Mines Research Station, advanced a relation for the weight (dM) of the fraction of size (a) of the form

$$\int^{a} \frac{dM}{da} da = Aa^{\frac{1}{2}} \exp(-B/a) \qquad (1)$$

where A and B are constants.[2] More recently Wynn and Dawes arrived at a radically different type of relation between the particle count (dN) and size

$$dN/da = A \exp(-Ba) \qquad (2)$$

where A and B are again constants, for the airborne dust in British collieries.[3] They argued that rock dust would be of the same form. Roller expected his relation to hold for industrial dust in general; in fact his result was actually derived from fine-grinding data.

That a basic size-distribution applying to dusts and fine-ground products generally existed appeared to be commonly accepted in the literature; also that it must be related to the mechanism effecting comminution—an obvious starting point for an attack on the production of dust. In view of the availability of several thousand thermal precipitator sample counts of mine dust, compared with the 130 used by Wynn and Dawes, it was therefore decided to investigate their size distribution.

EXPERIMENTAL DATA

The material consisted of a collection of nearly 1500 sample counts taken in the course of some "Jackhammer" drilling tests underground, from 1939 to 1943. The amount of water used in drilling was varied. A number of working places, on different mines, were used. In most cases they were ventilated from the downcast shaft.

The thermal precipitator cover slips were ignited and then washed in 50% hydrochloric acid to remove carbonaceous matter and salts originating in the drilling water. The dust particles were counted under the microscope as having a diameter of less than 0·2, 0·2, 0·4, 0·8, 1·2, 1·6, 2·0, 2·5, 3, 4 or 5 μ and above, using the Patterson–Cawood graticule. The two end classes were rejected as inevitably introducing a spurious curvature.[4] The majority of the samples were counted twice: before and after acid treatment.

It was assumed that the collecting efficiency of the thermal precipitator is independent of particle size for the range $0{\cdot}1 < a < 4{\cdot}5\ \mu$.[5] The acid treatment can cause a mechanical loss of particles, which may be size-selective.

This material was selected because (i) it constituted the largest single dust sampling project, (ii) the drilling dust might be expected to exhibit the basic "breakage" pattern comparable with other comminution studies, and (iii) for the importance commonly ascribed to drilling in the creation of dangerous dust in mining.

PROCEDURE

The treatment of an experimental size analysis was described in detail by Martin[4] and has been reviewed more recently by Work,[6] Austin[7] and Ratcliffe,[8] among others.[9–14]

The relative number of particles in unit size interval was plotted against size.[4] Plotting 1233 samples, ignited only, on a logarithmic scale, yielded an almost rectilinear figure in two parts, with a break at a particle size $a \simeq 2\ \mu$. A peculiarity at the large size end in one block of 230 samples was apparent, and was traced to a faulty counting procedure. When this material was subtracted, leaving 1000 "good" counts, a very nearly linear plot was obtained. This indicates a very simple equation of the form

$$a^{m}(dN/da) = \text{const.} \qquad (3)$$

where dN is the number of particles to be found in the size range a to $a + \delta a$. When a similar plot was made of 1480 counts following both ignition and acid treatment neither component of the distribution was removed: the figure was similar but for some change in slope and improvement in its rectilinear appearance. For the benefit of the large-size end 386 faulty counts were subtracted, as above, leaving 1094 "good" counts.

These curves are given in Fig. 1. The values indicated for the exponent (m) are:

	$a < 2\ \mu$	$a > 2\ \mu$
Ignition	2·50	7·7
Ignition and acid	2·00	10·5

To show that relation (3) is a necessary and sufficient description of the data, the average deviation was estimated, point by point, for the two curves (the broken lines in Fig. 1). Fifty per cent of the counts fall within these limits. It can be seen that a two-part rectilinear figure is the simplest consistent with the information.

Both parts of the distribution are therefore rock particles. In order to investigate the composition of the distribution further, the totals were extracted under several headings. The evidence of these smaller groups should be treated with caution. There were a number of samples taken in the drilling excavation itself, and a number taken in the air leaving it. In addition there were a number of samples of the "clean" air entering the working place. The numbers of samples were 289, 280, 296 and 340, 333, 315, counted before and after acid treatment, respectively. With ignition only, the break at $a \simeq 2\ \mu$ is rectilinear for the drilling point

samples, less strikingly so for the return air. The incoming ventilation, which in most cases should have been air relatively uncontaminated by other mining operations, exhibited the same type of dust content. To check this result all the material was divided into two categories according as to whether the total concentration of rocky particles alone was greater, or less than, 100 particles per cm^3. Experience in this laboratory advised that the latter category must consist of overwhelmingly "intake" air, or, if not, arise from working in an excess of water effectively flooding the drilling point (some of the tests involved such conditions) so that virtually "clean" air passed over into the "return" airway. This comparison utilized 733 and 961 counts of more than 100 particles per cm^3, and 500 and 519 of lesser concentrations, with and without acid treatment, respectively. Both curves were similar to those already described. Further, all the material was divided into twenty-seven groups by dust concentration, from 40 to 4000 particles per cm^3, the lowest concentrations being, of course, ordinary air. The form of the curves was seen to be independent of the dust concentration, apart from some rounding off of those for the very lowest dust contents where the statistical sampling errors are rather large.

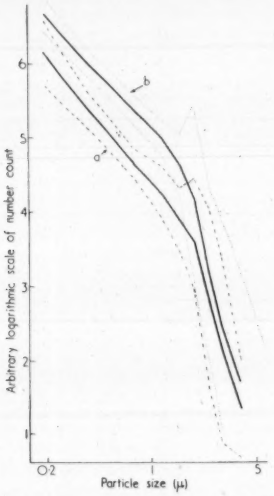

Fig. 1. The particle size distribution of the dust
a, ignited; *b*, ignited and acid treated.

Comparison of the counts before and after acid-treatment shows some excess of water-borne salts towards the lower end of the size range in the less than 100 particles per cm^3 material. A concentration of salts towards both ends of the range is suggested by the slopes of the curves of Fig. 1 already noted. Acid treatment reduces the curve for the drilling point material to near coincidence with that for samples from the "return" airway, both in distribution and absolutely, suggesting the composition of the drill mist constituent. Similarly, the greater part of the "dust" content of the incoming air is shown to consist of salts. Thus the small salt species seems to originate in the incoming air (the usual atmospheric nuclei?) and the large from the drilling water.

The distribution curves applicable before and after acid treatment are shown in Fig. 1. Other curves may be reproduced from the table. Some electron microscope observations in this laboratory suggest that the form of the curve below 2 μ is the same down to about 0·01 μ. With regard to Fig. 1 it may be remarked that the deviation from a straight line noticeable in the region of 1·2 μ is exactly removed if we suppose that the microscopist has made no correction for the diffraction disk down to this point.

Summary. From the foregoing observations it is clear that relation (3) is a suitable description of the dangerous dust broken by the drill for use in the kind of evaluation mentioned at the beginning. There is also some suggestion of generality in that the same form is observed in the incoming air. In addition it may be remarked that a small number (316) of counts from some other work suggests the same curve; as do some from rock-loading (182) and blasting (58), though with different constants.

The size-analyses of the drilling dust

Item	*No. of samples*	*Normalized count/0·1 μ size interval* 0·2	0·4	0·8	1·2	1·6	2·0	2·5	3	4 μ
Total ignited only	1233	147·5	1·1	4·60	1·83	0·76	0·46	0·065	0·03	0·01
less faulty material	1000	134·24	21·66	4·52	1·87	0·77	0·40	0·064	0·014	0·0023
Total ignited and acid treated	1480	44·73	8·96	2·43	1·04	0·50	0·28	0·029	0·039	0·027
less faulty material	1094	30·66	7·67	2·15	0·96	0·41	0·15	0·015	0·0019	0·0002
Air entering working place ignited only	296	58·70	8·83	1·55	0·85	0·42	0·22	0·045	0·012	0·0037
ignited and acid treated	315	12·81	2·47	0·82	0·41	0·15	0·062	0·013	0·0017	0·0035
Working place ignited only	289	151·3	27·0	5·64	2·55	1·07	0·64	0·073	0·026	0·0059
ignited and acid treated	340	40·02	9·65	2·46	1·18	0·57	0·25	0·019	0·0078	0·0035
Air leaving working place ignited only	280	125·5	20·97	4·04	1·69	0·77	0·37	0·055	0·015	0·0021
ignited and acid treated	333	33·66	8·17	2·25	1·06	0·49	0·20	0·019	0·013	0·012
More than 100 particles per cm^3 ignited only	733	178·59	29·31	6·54	2·65	1·17	0·65	0·090	0·046	0·016
ignited and acid treated	961	62·51	12·44	3·08	1·39	0·71	0·39	0·041	0·057	0·039
Less than 100 particles per cm^3 ignited only	500	102·50	9·28	1·76	0·63	0·33	0·175	0·029	0·022	0·0078
ignited and acid treated	519	10·82	2·49	0·73	0·31	0·12	0·062	0·0066	0·0077	0·0056
Other drilling dust ignited only	200	32·75	10·45	2·26	0·85	0·38	0·18	0·09	0·031	0·028
ignited and acid treated	116	12·3	3·8	0·88	0·45	0·14	0·042	0	0	0

"BREAKAGE"

The distribution observed for the rock dust below $2\,\mu$

$$a^2(dN/da) = \text{const.} \tag{4}$$

i.e. $a.N = \text{const.}$

has some plausibility as a size-frequency on general grounds.[13] But is must be made clear that nothing has been said thus far about the "true" size-frequency of the dust, which cannot be obtained empirically but only analytically[15, 16] as will now be reviewed.

It has been mentioned above that a size-frequency is commonly considered to reflect the mechanism of "breakage." The obvious analysis of a repeated fracture process leads to the exponential form[4, 17] adduced by Wynn and Dawes in support of their result.[3] The present results were therefore something of a surprise. It seemed necessary to investigate whether a "true" size-frequency of this form [relation (3)] were possible.

Another point: while Roller's and the present material would seem suitable for this mode of analysis, the coal dust samples studied by Wynn and Dawes were not ignited to remove ordinary smoke; their smaller component resembles smoke. They obtain a two-term distribution, but the physical basis they offer for it would not account for the similar feature in the present results.

SIZE DISTRIBUTIONS

There is a great deal of information available on this subject which does not seem to have been brought together in this connexion before. If our interest is confined to dust-size products smaller than, say, $10\,\mu$, it is a question of comminution products inferior to the grain size of the massive rock, and the mechanism is likely to be largely independent of the size-reducing agency; the interpretation of the results of the many studies of size-reduction processes and the like is much simplified.

The sizing of crushed rock was extensively investigated by Martin for the British Portland Cement Association.[4, 18–21] He put forward a size-distribution of the form

$$dN/da = A \exp(-Ba) \tag{2}$$

where dN is the number of particles in the size range a to $a + \delta a$, and A, B are constants. However, Rosin and Rammler reported to the German State Coal Board that this distribution was unsatisfactory, at least for the finer products of coal.[22] They proposed the form

$$\int_a \frac{dM}{da} da = A \exp(-Ba^c) \tag{5}$$

i.e.
$$dN/da = A' a^{c-4} \exp(-Ba^c) \tag{5a}$$

where dM is the weight fraction in the size range a to $a + \delta a$ and A, A', B, c are constants.[23–35] Meanwhile a third form, associated with the name of Gaudin, had been reported[17, 36]

$$dM/da = Aa^B \tag{3a}$$

i.e.
$$dN/da = A' a^{B-3}$$

where A, A' are constants and m of relation (3) has been replaced by $(3 - B)$.

THE INFORMATION AVAILABLE FROM SIZE-DISTRIBUTION STUDIES

The general form of size-distribution for the product of a size-reduction process is probably as illustrated in Fig. 2,[13] in which portions A and B may be thought of as representing "primary action" and "secondary action" respectively.[10] The relative importance of portions A and B varies greatly with the process,[8] the portion B being predominant in percussion processes[37] or in any process involving a high reduction ratio.[17] Particles smaller than $10\,\mu$ probably always fall into the region. From another point of view, when a massive lump is shattered, the product may be classified as consisting of a small number of large pieces ("residue") and fines ("complement").[16, 38–41]

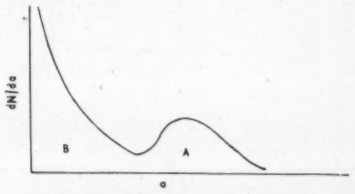

Fig. 2. The general form of a comminution product

The exponential size-frequency of Martin implies the fracture of particle diameter in all proportions with equal probability.[3] It was derived from a model of successive particle division and applied to finely-reduced rock,[4, 18] crushed anthracite, coal, cork, peat, etc.[42]; rejected for coal[15, 22, 41]; and revived for coal dust.[3] It has been identified with the coarser products of size-reduction processes generally,[10, 12] or with the "primary action."[10] It has been linked with particle fracture[4, 12] yet considered proper to the products of granular source materials above the grain size.[40, 41] Though unsatisfactory for coal it has been accepted as describing the product of a single "stage" in its crushing, succeeding products evolving into the form (5).[41, 43] It has been applied to the sizes of rain-drops.[44, 45]

A rationalization of form (3a) has been offered[46] and a mechanism[8, 10]; it has been derived from an equipartition law, or Rittinger's law.[47–49] It was originally proposed for the finer products of grinding processes, the whole product sometimes conforming in the case of high reduction ratios.[17] This form has been fitted to the "complement" in shattering a homogeneous non-granular solid, or the sub-grain products of granular solids.[40, 41] It can apply, it seems, to the fracture of a single crystal over a wide size range,[50] contrary to the hypothesis as to the basis of relation (2).[3, 4, 12] It seems justifiable to identify this form with "secondary action,"[10] in preference to the more cautious statement that "secondary action" amounts to a combination of types (2) and (3a).[6] It is certainly associated with percussion processes,[37] another example of high reduction ratios. For fine comminution we find that B in relation (3) equals, or is slightly less than, unity,[37, 47, 50] particularly for quartz[37] and quartzite.[46] So far as they go some figures for Belgian colliery dust conform to this pattern,[51] though in Britain this dust is reported as obeying relation (2).[3]

This type (3a) of size-distribution has a much wider significance.[8] It has been found to describe the whole range of "natural" aerosol particles and condensation nuclei in the atmosphere as rendered by the thermal precipitator,

(Aitken) nucleus counter and ion counter together in the size range $0{\cdot}05 < a < 20\ \mu$, in agreement with optical measurements of visibility, sky colour, polarization, etc.[52–59] In this case we find $-1 < B < 1$.[53, 55, 60, 61]

In practical size reduction the object is to obtain a product of the desired size efficiently and the "feed" size and machinery used can be adapted to this purpose. Relation (5) was advanced by Rosin and Rammler on the basis of a resemblance between plots of their crushing products and the distribution of the log-normal curve about its modal peak. Transforming relation (5) into

$$dM/da = A''a^{c-1} \exp(-Ba^c) \qquad (5b)$$

it appears that since $c \simeq 1$[41] it might better be put forward as an empirically adjusted exponential in weight, analagous to relation (2), and on a similar basis, implying "random breakage" in volume. A fundamental significance was attributed to this form, and a very wide validity claimed.[10, 12, 15, 16, 23–35, 37, 40–42] It has been widely employed, applied to the size range $20 < a < 150\ \mu$ for many materials,[15] particularly those of a granular nature (e.g. dolomite) when fine-ground, to silica powders $2 < a < 100\ \mu$.[41] It is probably appropriate to the grain size of some photographic emulsions,[62] although the Rosin–Rammler distribution was not known to these investigators. It has been applied to the drop-size of rain.[63]

DISCUSSION

It may be noticed that for small a relation (5) becomes relation (3*a*), while for large a the exponential term predominates and we have the analagous form to (2). For a single "stage" of crushing $c = 1$,[41] i.e. "random breakage" in volume. With further crushing we find some departure from unity: the emergence of the function (a) of relation (3*a*). For the initial product, where $c = 1$, at small a we have, transforming,

$$dN/da = A'a^{-3}$$

i.e. relation (3*a*) once more, and precisely the result of Gates and Gaudin.[17, 36] The general application claimed for relation (5) arises logically from its containing the large- and small-size relations (2) and (3*a*).[51] And, further, the fact of $c = 1$ for the initial "breakage," together with a moment's consideration of the analogy with form (2), suggests the status of form (5) as a combination of a "primary action" [relation (2): the "Gaussian" component,[37, 41] Gaudin's "paraboloid loop," Bennett's "residue"] and a "secondary action" [relation (3*a*): "free fracture,"[37] Bennett's "complement."][10] In general, over a sufficient range, it looks as if we may expect to find the coarser product obeying relation (2), while the finer sizes conform to relation (3*a*), the intermediate form (5) being an attempt to cover both ranges at once. In other words the initial "breakage" is defined by relation (2) (presumably, implying Kick's law); further action introduces a size-frequency of the form (3*a*) (obeying Rittinger's law), spreading from the small-size end so that that part of the total product nearest the "feed" size, though somewhat modified,[41] continues to be dominated by the form (2),[10, 17, 47] until, after a very great reduction, the whole product is transformed into the form (3*a*).[17] In fact, a recent study of shattering water drops produced a size distribution clearly divisible into two portions, one Martin—and one Gaudin—type.[64]

This interpretation of the "general curve" differs from that[16, 38] according to which it consists of a "Gaussian" (presumably log-normal[65]) part,[11, 19, 41] together with a Gaudin-type component[37]; or with a Gaudin component in the case of a homogeneous parent material and a Rosin–Rammler-type component in the case of a granular material.[41] On the basis of the preceding analysis this view appears to involve a mathematical contradiction, apart from some obscurity, and a difficulty in the derivation[38] of relation (5) "from probability considerations"[35] in that where the starting assumptions would seem to be best fulfilled—for homogeneous massive material—relation (3*a*) is actually observed.[41] A similar point was noted in the previous section and also emerged in connexion with Wynn and Dawes's work. It is for this reason that no reference has been made to the tedious question of assigning "breakage" probabilities proportional to particle size—or even inverse size[43]—and an inductive approach adopted.

The implied criticism of relation (2) is that it obscures the mechanism and for this reason has, in fact, proved barren of interpretative value.[41] But as a convenient description of the intermediate region of relation (2) and (3*a*) is it not practically useful? The answer is that it is not.[66] This conclusion may be illustrated by referring again to the intermediate-type distribution due to Roller[2, 12, 66] given in equation (1) which was tested on some of the same data as relation (5) and a similar general import claimed for it. Work[6] claimed that this relation had been proposed by him.[10] Actually it contradicts his argument in that paper, differing as it does from the form (5) in that here the exponential term is important at small values of a. The fact is that the form of relations (1) and (5) is such that with the ordinary experimental gradings it is difficult to decide that a significant measure of fit has been obtained. A test of some U.S. Bureau of Mines data[67] illustrated this particularly well.

Several other relations have been proposed by various authors[11, 42, 68] to fit certain results. There is no convincing case of the natural occurrence of the log-normal form reported.[3, 8, 66] That the forms (2) or (3*a*) when truncated as by a screening operation generate a log-normal distribution has yet to be shown.

CONCLUSION

The interpretation of the "most general distribution" which has been offered may be contained by implication in a purely mathematical paper by Lienan.[69] It differs from previous treatments [e.g. Refs. (1), (10), (38), (41)] in its conclusions. It suggests that fine airborne dust from the shattering of rock may be expected to have a Gaudin-type size-frequency. It suggests that the same form may be anticipated from ordinary air. Atmospheric salt nuclei have this characteristic, sometimes two-part.[53, 56] In equation (3*a*) we find $-1 < B < 1$.

All this is in agreement with the results obtained for drilling dust, except for the value of B for $a > 2\ \mu$. Since this pattern is so general it suggests a fairly invariant dust form. Changes in the processes producing it are unlikely to affect it.[70]

ACKNOWLEDGEMENT

Permission from the Transvaal and Orange Free State Chamber of Mines to publish this report is gratefully acknowledged.

In addition acknowledgement is due to the members of the staff of the Dust and Ventilation Laboratory of the

Transvaal and Orange Free State Chamber of Mines responsible for the collection and assessment of the thermal precipitator samples.

REFERENCES

(1) SVENSSON. *Trans Roy. Swedish Inst. Technol., No.* 88 (1955).

(2) ROLLER. *J. Franklin Inst.*, **223,** p. 609 (1937).

(3) WYNN and DAWES. *Safety Mines Res. Establ. Res. Rep.* 28 (1951).

(4) MARTIN. *Trans Ceram. Soc.*, **23,** p. 61 (1923–24).

(5) GREEN. *Trans Faraday Soc.*, **32,** p. 1091 (1936).

(6) WORK. *Bull. Amer. Ceram. Soc.*, **17,** p. 1 (1938).

(7) AUSTIN. *Industr. Engng Chem.* (Analyt. Ed.), **11,** p. 334 (1939).

(8) RATCLIFFE. *Proc. Instn Mech. Engrs*, **162,** p. 378 (1950).

(9) LOVELAND and TRIVELLI. *J. Franklin Inst.*, **204,** p. 193 (1927).

(10) WORK. *Trans Amer. Soc. Mech. Engrs* (*Res. papers*), **110,** pp. 55–6 (1932).

(11) DRINKER and HATCH. *Industrial Dust* (New York: McGraw-Hill Book Co. Inc., 1936).

(12) ROLLER. *Proc. Amer. Soc. Test Materials*, **37** (II), p. 675 (1937).

(13) DALLAVALLE. *Micromeritics* (New York: Pitman Publishing Corp., 1943–48).

(14) HERDAN. *Small Particle Statistics* (Amsterdam: Elsevier Publishing Co., 1953).

(15) BENNETT. *J. Inst. Fuel*, **7,** p. 109 (1933).

(16) BENNETT, and others. *J. Inst. Fuel*, **14,** p. 111 (1941).

(17) GAUDIN. *Trans Amer. Inst. Min. Metall. Engrs*, **73,** p. 253 (1926).

(18) MARTIN. *Trans Ceram. Soc.*, **25,** p. 51 (1925–26).

(19) MARTIN. *Trans Ceram. Soc.*, **25,** p. 63 (1925–26).

(20) MARTIN. *Trans Ceram. Soc.*, **27,** p. 247 (1927–28).

(21) MARTIN. *Trans Ceram. Soc.*, **27,** p. 259 (1927–28).

(22) ROSIN and RAMMLER. *German State Coal Board Rep. No.* C52 (1933).

(23) ROSIN and RAMMLER. *Z. Verein Dtsch Ingen* [*VDI*], **71,** p. 1 (1927).

(24) ROSIN and RAMMLER. *Zement*, **16,** p. 820 (1927).

(25) ROSIN and RAMMLER. *Zement*, **16,** p. 840 (1927).

(26) ROSIN and RAMMLER. *Zement*, **16,** p. 871 (1927).

(27) ROSIN and RAMMLER. *Zement*, **16,** p. 897 (1927).

(28) ROSIN and others. *Zement*, **19,** p. 189 (1930).

(29) ROSIN and others. *Zement*, **19,** p. 214 (1930).

(30) ROSIN and RAMMLER. *Zement*, **20,** p. 210 (1931).

(31) ROSIN and RAMMLER. *Zement*, **20,** p. 240 (1931).

(32) ROSIN and RAMMLER. *Zement*, **20,** p. 311 (1931).

(33) ROSIN and RAMMLER. *Zement*, **20,** p. 343 (1931).

(34) ROSIN and RAMMLER. *Zement*, **22,** p. 100 (1933).

(35) ROSIN and RAMMLER. *J. Inst. Fuel*, **7,** p. 29 (1933).

(36) GATES. *Trans Amer. Inst. Min. Metall. Engrs*, **52,** p. 875 (1915).

(37) PIRET. *Chem. Engng Progr.*, **49,** p. 56 (1953).

(38) BENNETT. *J. Inst. Fuel*, **10,** p. 22 (1936).

(39) BENNETT and others. *J. Inst. Fuel*, **14,** p. 135 (1941).

(40) TAYLOR. *J. Inst. Fuel*, **26,** p. 133 (1953).

(41) TAYLOR. *J. Inst. Fuel*, **27,** p. 249 (1954).

(42) HEYWOOD. *J. Inst. Fuel*, **6,** p. 241 (1933).

(43) PONCELET. *Trans Amer. Inst. Min. Metall. Engrs*, **169,** p. 37 (1946).

(44) LAWS and PARSONS. *Trans Amer. Geophys. Union*, **24** (II), p. 452 (1953).

(45) MARSHALL and others. *J. Meteorol.*, **11,** p. 362 (1954).

(46) COGHILL. *Engng Min. J.*, **126,** p. 934 (1928).

(47) GAUDIN. *Trans Amer. Inst. Min. Metall. Engrs*, **169,** p. 67 (1946).

(48) GAUDIN. *Trans Amer. Inst. Min. Metall. Engrs*, **169,** p. 88 (1946).

(49) GRIFFITH. *Canad. J. Res. A*, **21,** p. 57 (1943).

(50) GAUDIN. *Min. Technol.*, **8** T.P., p. 1779 (1944).

(51) HOUBERECHTS and others. *I.H.M. Hasselt Comm. No.* 118 (1954).

(52) DESSENS. *La Meteorologie*, **17,** p. 321 (1947).

(53) MOORE and MASON. *Quart. J. Roy. Meteorol. Soc.*, **80,** p. 583 (1954).

(54) JUNGE. *Chr. Ber. Dent. Wetterd. U.S. Zone*, **35,** p. 261 (1952).

(55) JUNGE. *Tellus*, **5,** p. 1 (1953).

(56) GILBERT. *Condensation Nuclei of the Los Angeles Region* (University of California, 1954).

(57) HOLL and MUHLEISEN. *Geofis. Pura Appl.*, **31,** p. 115 (1955).

(58) VOLZ. *Geofis. Pura Appl.*, **31,** p. 119 (1955).

(59) AVY. *Les Aerosols* (Paris: Dunod, 1956).

(60) JUNGE. *J. Meteorol.*, **12,** p. 13 (1955).

(61) Conference Report. *Nature* [*London*], **177,** p. 320 (1956).

(62) LOVELAND and TRIVELLI. *J. Franklin Inst.*, **204,** p. 377 (1927).

(63) MEETHAM. *Quart. J. Roy. Meteorol. Soc.*, **76,** p. 16 (1950).

(64) MAGARVY and TAYLOR. *J. Appl. Phys.*, **27,** p. 1129 (1956).

(65) EPSTEIN. *J. Franklin Inst.*, **244,** p. 471 (1947).

(66) ROLLER. *J. Phys. Chem.*, **45,** p. 241 (1941).

(67) GATES. *U.S. Bureau of Mines Rep. Invest.*, p. 3549 (1941).

(68) HATCH. *J. Franklin Inst.*, **215,** p. 27 (1933).

(69) LIENAN. *J. Franklin Inst.*, **221,** p. 673 (1936).

(70) *Brit. N.C.B. Science Bull.* (Spring 1956).

The synthesis of single crystals of the sulphides of zinc, cadmium and mercury and of mercuric selenide by vapour phase methods

By D. R. HAMILTON, M.A., Ph.D.,* Department of Physics, The University of Birmingham

[*Paper first received* 24 *July, and in final form* 9 *October*, 1957]

Experiments with the Reynolds–Czyzack method of growth are described for zinc sulphide and cadmium sulphide. A new application of the method to the crystallization of mercuric sulphide is discussed. Single crystals of mercuric selenide have been produced by a vapour phase reaction and similar experiments attempted with mercuric telluride. The conditions of growth are examined in the light of recent theory; estimates of surface free energies are obtained.

1. INTRODUCTION

The study of conductivity and luminescence among members of the zinc sulphide (ZnS) family has been greatly facilitated by the synthesis of crystals of controlled composition. Since the reintroduction of the Lorenz method for cadmium sulphide (CdS) by Frerichs[1] in 1947, a variety of alternative sublimation techniques have been advanced. It is the purpose of this paper to describe growth of crystals by the method of Reynolds and Czyzack.[2] The experimental results are discussed in terms of current theories of crystal growth.

2. EXPERIMENTAL

Growth of zinc sulphide and cadmium sulphide crystals. Powdered zinc sulphide or cadmium sulphide was placed in a fused quartz tube and heated in a furnace with two independent sections (see figure). The temperature of the powder

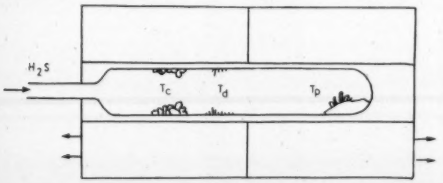

The two-section furnace showing the habit of cadmium sulphide crystals in a typical run

T_p was controlled by the first section. The other section was used to establish a temperature gradient along the length of the quartz tube. The crystals formed in the apparatus as shown. The crystals deposited in the vicinity of the temperature T_c will be called the normal growth and comprise the larger part of the yield. Crystals grown at the temperatures T_d and T_p are less numerous, and will be discussed in detail in Sections 3 and 4. The experimental details are collected in Table 1.

An atmosphere of 10–20 cm of hydrogen sulphide, prepared by triple vacuum distillation, was maintained in the quartz tube. This gas dissociated appreciably above 1100° C. The sulphur deposited in cooler regions of the system and the atmosphere became slightly reducing. Even with several litres of hydrogen sulphide and frequent gas changes crystals of apparently reduced composition were found during runs above 1100° C. The dissociation alters the nature of chemical equilibrium above the growing crystals which in turn may effect a change in growth rate. In this connexion it was found that the growth rate was reduced when inert gases were used.

Mercuric sulphide. The apparatus used for the crystallization of mercuric sulphide (HgS) was similar to that shown in the figure. Since the temperatures employed were below 550° C (Table 1) a glass tube was substituted for the quartz tube. It is likely that runs at lower pressures and temperatures would prove equally satisfactory.

Table 1. *Physical conditions for growth of sulphide crystals*

	T_p (° C)	T_c (° C)	dT/dx (° C/cm)	*Pressure* (H_2S in cm)	*Run time* (h)
ZnS	1180	1100	15	10	100
CdS	980	910	10	20	100
HgS	490	440	8	35	50

The runs times indicate the lower limit for growth of crystals of approximately 20 mm^3 volume.

Mercuric selenide and mercuric telluride. Direct application of a Reynolds–Czyzack method to mercuric selenide (HgSe) and mercuric telluride (HgTe) is complicated by several factors. Neither material is readily available, and synthesis in a melt is reputedly violent. Stoichiometry is consequently difficult to control. Hydrogen selenide or hydrogen telluride would have to be used in the atmosphere; both gases are very toxic.

Mercuric selenide was crystallized by a method analogous to that of Frerichs for cadmium sulphide. A two-section furnace was again employed. A flowing atmosphere of oxygen-free nitrogen was passed successively over mercury and molten selenium. The temperature of each metal was adjusted so that its equilibrium vapour pressure was 10 cm. The details are shown in Table 2. A maximum temperature of 600° C was reached a few centimetres beyond the selenium; although the point was not investigated, it is thought this was not essential. Crystals deposited in a fashion similar to that of the sulphides.

Table 2. *Physical conditions for growth of mercuric selenide and telluride crystals*

	T of Hg (° C)	*T of Se or Te* (° C)	T_c (° C)	dT/dx (° C/cm)	*Run time* (h)
HgSe	255	560	350	10	18
HgTe	255	840	see text	8	18

The rate of flow of N_2 was approximately 1 cm^3/sec.

Mercuric telluride did not condense in single crystal form, although polycrystalline material deposited at temperatures about 400° C. Dendrites of tellurium were recovered below 400° C.

* Now at Westinghouse Research Laboratories, Churchill Borough, Pittsburgh 35, Pennsylvania.

3. RESULTS

Crystal habit. Two distinct habits were found among crystals of zinc sulphide and cadmium sulphide. The crystals which deposited at T_c and T_p were hexagonal columns, a few millimetres long and one to two millimetres thick. The principal axis of the column is [0001]. The sides of the column are rarely good {0110} planes, for microscopic examination reveals the presence of numerous growth sheets. These advanced from the base and edges of the column towards the top. High index surfaces were frequently found at the top of the column.

The second habit was principally dendritic and was found in the region of the temperature T_d. The crystals grew up to two millimetres in length, with small cross-section. As a consequence, recovery was difficult. The dendrites were often thickened by the growth of thin sheets parallel to the unique axis.

Crystals of mercuric sulphide grew only in the columnar habit described above. The side faces were poorly developed and it was often not possible to determine structure from casual inspection. The principal form was hexagonal. Dendrites were not observed.

Mercuric selenide deposited as flat hexagonal or near hexagonal plates. The basal [0001] face is well developed. Oriented overgrowths can be found on this face, and growth sheets on all faces.

Regions of deposit. The growth rate of crystals of normal habit decreased rapidly as the temperature of the deposition region increased above T_c. At temperatures 10° above T_c the growth rate of this habit was negligible. The dendritic habit formed at still higher temperatures; this behaviour will be considered in Section 4. Crystals of normal habit deposited in the vicinity of T_c greatly decreased the concentration of sublimate molecules in the atmosphere. Because of this, few crystals grew in cooler parts of the apparatus. It has also been noted that considerable crystal growth may occur directly on the powder mass at the temperature T_p. These crystals are of normal habit, but, as will be shown later, cannot grow by the same mechanism as those at the temperature T_c.

Experiments under various conditions have shown that for small changes of the temperature T_p, the difference in temperature $T_p - T_c$ remains nearly constant. When T_p (and hence T_c) was increased the normal deposit consisted of a small number of larger crystals. Higher deposition temperatures favoured growth of crystals with better developed faces and greater size. This behaviour is well known in the growth of crystals from solution, but, to the author's knowledge, has not been reported for growth from the vapour phase. This observation has led to the use of higher temperatures for zinc sulphide than normally employed. Shorter runs were possible and losses through failure of the quartz vessel were reduced.

Crystal purity. The sulphide crystals were examined for luminescence excited by ultra-violet light at liquid oxygen temperatures. These tests showed that chlorine was present in low concentrations. Although the starting materials were free from heavy ion impurities, the respective chlorides were found in considerable quantities. In one lot of starting material the chlorine content was as high as 10% by weight! This content was reduced by repeated washing and by the following preliminary heat treatment. The washed powder was heated in a stream of nitrogen at 300–400° C for an hour or two. Low boiling-point components were removed at this stage. The system was next pumped out to a rough vacuum. The temperature was then raised to 550° C and 650° C for cadmium sulphide and zinc sulphide respectively. One hour at these temperatures distilled out all but a few hundred parts per million of the chloride from the sample. Although longer heating further reduced the chloride content, it was found impossible to reduce the figure below a hundred parts per million if the initial concentration was above 1%. However, further purification could be obtained by vacuum distillation. For cadmium sulphide and zinc sulphide, temperatures of 650° C and 750° C were used. Such a distillation reduced the chlorine content by a further factor of five. The sublimed deposit was largely polycrystalline. Dendrites were found in the distillation tube between the polycrystalline deposit and the precipitate.

A similar purification took place during runs of the Reynolds–Czyzack type. Thus the actual quantity of chlorine incorporated into the crystals grown at T_c was small, less than ten parts per million. In spite of the preliminary treatment and this subsequent purification crystals grew to a greater size if the starting material contained a high initial chlorine content. The columns were shorter and thicker. The presence of chlorine evidently alters the relative growth rates along the different crystallographic directions. A similar effect has been noted by Kroger and others[3] during experiments with deliberate introduction of chlorine.

As noted earlier, a few crystals of the sulphides showed apparent reduction in varying degrees. It was estimated from the resulting luminescence that the deviation from stoichiometry was of the order of one part in 10^5. The banded appearance of the luminescence of these crystals suggested a periodic change in conditions. This periodicity is thought to correspond to the changing of the hydrogen sulphide atmosphere. Hydrogen from dissociated hydrogen sulphide may have been the reducing agent.

The chemistry of mercuric sulphide as a phosphor is not known. However, the occurrence of luminescence at $2{\cdot}2\ \mu$[4] is indicative of a moderate degree of purity. The starting materials used for the growth of mercuric selenide were not of high purity; no analysis was attempted.

4. DISCUSSION

There are two current theories applicable to the growth of crystals from the vapour phase. The theory of Volmer, Becker and others[5] depends upon the formation of a two-dimensional seedling to serve as a nucleus for the growth of a new crystalline layer. The theory of Frank and others[6] postulates growth with the help of a spiral dislocation. The dislocation presents a self-perpetuating step at which growth takes place.

It is assumed in the former theory that a certain energy W is required to establish a two-dimensional seedling large enough to survive. The rate of formation of seedlings N is related to W by a Boltzmann expression

$$N = B \exp(-W/kT) \qquad (1)$$

where B is a binary collision factor of the order of $10^{20}\ \mathrm{s}^{-1}$. Now it can be shown that

$$W = \tfrac{1}{2}\sigma\pi r^2 \qquad (2)$$

where σ is the surface free energy and r the radius of the seedling. It can also be shown from purely thermodynamic considerations that

$$RT \log p/p_o = RT \log \alpha = \sigma M/r\rho \qquad (3)$$

where ρ is the density and M the molecular weight. The

supersaturation ratio $\alpha = p/p_o$, where p is the actual pressure above the crystal and p_o the equilibrium vapour pressure. From equations (2) and (3)

$$\frac{W}{kT} = \frac{1}{2}\frac{\pi r^3 \rho}{m} \log \alpha \qquad (4)$$

where m is the molecular mass. If it is assumed that $r = 2a$, then the nucleation rate equation may be written in the form used by Sears[10] and in the present work, namely

$$N = B \exp\left(\frac{-\pi a m}{\rho \log \alpha}\right)\left(\frac{\sigma}{kT}\right)^2 \qquad (5)$$

Veselovsky and Rinse[7,8] have published vapour pressure data for the sulphides over the majority of temperature range of interest. This data permits calculation of the supersaturation ratio providing the pressure is not reduced by diffusion. Reasonable numerical estimates suggest diffusion is not important in this connexion. From the observed growth rate it is estimated that $N \sim 10^3$ cm^{-2} sec^{-1}. An average value is used for the layer spacing, since both σ and α may be functions of direction in the crystal. It is thus possible to use the equations to obtain estimates of the surface free energy, assuming that two dimensional nucleation was taking place. The results are collected in Table 3 for crystals grown at T_c. The values are of the correct order of magnitude, and the variation with molecular weight is in the right direction. It is therefore concluded that two-dimensional nucleation may have been operative in these experiments.

A rough theoretical estimate of the surface free energy may be made by the method of Harkins.[9] It is assumed that the bonding is covalent and involves nearest neighbour interactions only. Knowledge of the density of bonds and the standard free energy then allows assignment of an energy per bond. Since the number of bonds across a given plane in the crystal is known, an estimate can be made of the energy required to break these bonds. The surface free energy is half this figure; the calculated values are shown in Table 3.

Table 3. *Comparison of experimental values of surface free energy*

	α	$a = \frac{1}{2}(c_0/2 + a_0\sqrt{3}/2)$ (Å)	*experimental* (ergs/cm^2)	*Harkins* (ergs/cm^2)
Zns	3·74	3·22	700	1200
CdS	3·25	3·45	500	800
HgS	3·52	4·46	300	300

The sulphide crystals are intermediate in bonding between ionic and covalent, the degree of covalency increasing with molecular weight. Since the Harkins calculation assumes complete covalency, it is not surprising that mercuric sulphide displays the best agreement between theoretical and experimental surface energies. The theoretical values for zinc sulphide and cadmium sulphide are high due to neglect of the ionic repulsive component.

The experimental values of σ have been used to calculate N for the crystals grown at T_d. For both zinc sulphide and cadmium sulphide $N_{calculated} \sim 10^{-10}$, while the observed rate is $N \sim 10^2$ cm^{-2}. It is concluded that a screw dislocation mechanism must be operative. This observation is in agreement with the proposals of Sears[10] for dendrites generally, and for cadmium sulphide in particular.

In the case of the crystals grown at T_p, the supersaturation is not well defined. Experimentally, it could not have exceeded 1·1. In order to account for the observed rate of growth, two-dimensional nucleation would require a supersaturation of $\sim 10^7$. Consequently, if these crystals grew by sublimation, then they must have grown with the aid of screw dislocations. However, it was observed that the crystals grew only on the powder mass and not on the nearby walls of the quartz vessel. This suggests that surface diffusion may have played a role in the crystal growth. One can only conclude that two-dimensional nucleation did not play a part in the growth of crystals at T_p.

Crystals of zinc sulphide and cadmium sulphide were examined for spiral growth features using a conventional microscope with a narrow parallel beam of light for illumination. Spirals were not observed. However, the sensitivity of this method of observation is rather low, and spirals with shallow steps may well have been present on the samples examined. In any case, spirals have been observed on natural zinc sulphide crystals. Thus the apparent absence of this type of surface feature on crystals grown at T_p or T_d is not significant.

5. CONCLUSIONS

The principal features of the growth of crystals of the zinc sulphide family may be explained by either a two-dimensional nucleation mechanism or by a screw dislocation theory. Calculations based on the former theory give 700, 500 and 300 ergs cm^{-2} as the surface-free energies of the sulphides of zinc, cadmium and mercury.

The author acknowledges with pleasure the help and encouragement of Prof. G. F. J. Garlick during the course of this work.

REFERENCES

(1) FRERICHS, R. *Phys. Rev.*, **72**, p. 594 (1947).

(2) REYNOLDS, D. C., and CZYZACK, S. J. *Phys. Rev.*, **79**, p. 543 (1950).; *ibid*, and ALLEN, R. C., REYNOLDS, C. C. *J. Opt. Soc. Amer.*, **44**, p. 864 (1954); *ibid.*, *J. Opt. Soc. Amer.*, **45**, p. 136 (1955); CZYZACK, S. J., CRAIG, D. J., MCCAIN, C. E., and REYNOLDS, C. C. *J. Appl. Phys.*, **23**, p. 932 (1952).

(3) KROGER, F. A., VINK, H. J., and VAN DEN BOOMGAARD, J. *Z. Physikalische Chemie*, **203**, p. 1 (1954).

(4) DUMBLETON, M. J., and GARLICK, G. F. J. *Proc. Phys. Soc. B*, **67**, p. 442 (1954).

(5) See BUCKLEY, H. E. *Crystal Growth* (London: Chapman and Hall Ltd., 1951) for an extensive bibliography.

(6) FRANK, F. C. *Advances in Physics*, **1**, p. 91 (1952).

(7) VESELOVSKY, B. K. *J. Appl. Chem. U.S.S.R.*, **15**, p. 422 (1942).

(8) RINSE, J. *Rev. des Travaus Chim. des Pays Bas*, **47**, p. 28 (1928).

(9) HARKINS, W. D. *J. Chem. Phys.*, **10**, p. 268 (1942).

(10) SEARS, G. W. *Acta Metal*, **3**, pp. 361, 367 (1955).

(11) VOTAVA, E., AMELINCKX, S., and DEKEYSER, W. *Physica*, **19**, p. 1163 (1953).

The low-temperature conductivity of oxide-coated cathodes

By G. S. HIGGINSON, B.A., Ph.D.,* Physics Department, University College of North Staffordshire

[*Paper received* 27 *August*, 1957]

Measurements of electrical conductivity in the temperature range 300–700° K employing probe-diodes reveal that, in addition to pore-conduction, at least two conduction processes operate in parallel at temperatures below 700° K. It is suggested that one of these is movement of barium ions over interior crystallite surfaces and the other is electronic conduction limited by electron trapping, e.g. by oxygen, at crystal–crystal interfaces.

In recent years several authors have reported measurements of the conductivity of oxide-coated cathodes. The work of Loosjes and Vink[1] demonstrated that two conduction processes operate simultaneously, one of which, pore conduction, becomes the predominant process at temperatures above approximately 700° K. Fig. 1 shows the type of curve obtained by plotting $\log \sigma$ *versus* $1/T$ in the temperature range 500 to 1000° K. The pore conduction hypothesis has been substantiated by Hall effect measurements,[2] by poisoning experiments[3] and by extensive conductivity measurements employing various techniques.[4,5,6]

The nature of the conduction process which predominates below 700° K is not so well understood. Loosjes and Vink pointed out that it might be conduction through the crystallites limited by barriers between the crystals. Some authors[5] have associated this with "normal semi-conduction" whereas others[7] have proposed a barium film on the cathode surface to account for the low activation energies of conduction which are encountered.

In the work described below some experiments are reported which help to elucidate the nature of the conduction mechanism at temperatures in the range 300–700° K. Evidence is afforded which suggests that both "bulk" conductivity of the crystallites and a modified form of surface conductivity contribute to the conduction mechanism.

EXPERIMENTAL

Coating conductivity and thermionic emission measurements were made employing diodes with cylindrical symmetry containing a helical probe wire embedded in the oxide coating. Such diodes have been described in the literature from time to time.[3] In each cathode the probe to base-metal distance was approximately 50 μ, the total thickness of the oxide layer was approximately 100 μ, and the emitting area approximately 2·0 cm^2.

Both the probe wire (diameter 0·0005 in.) and the cathode base-metal were of "0" nickel, cleaned by washing in hot distilled water and heating to redness in a stream of hydrogen for five minutes. All the metal parts of each tube were cleaned in a similar manner before assembly and subsequently were handled only with clean pliers. Cathodes were prepared by spraying on to the nickel base a mixture consisting of equal proportions of barium and strontium carbonates suspended in amyl acetate. A fairly wet spray was employed in order to give a uniform but thin coating over which the probe wire could be wound. After assembly and sealing into the vacuum tube, outgassing of the glassware was accomplished by baking at 450° C for six hours. The metal parts were then outgassed by eddy-current heating. Breakdown of the carbonates was prolonged over a period of twenty-four hours to prevent disruption of the coating. During this period the anode was frequently heated and towards the end of the breakdown schedule, maintained at about 100° C higher than the cathode temperature. This ensured that the anode was free from contaminants, no current decay being observed on subsequently applying a potential to the anode. After breakdown, when no further carbon dioxide was evolved, the cathode temperature was maintained at 1200° K for six hours. The two barium getters were then fired and the tube sealed off at an indicated pressure of 10^{-6} mm of mercury. The cathode was then aged by drawing an emission current at 1200° K with 100 V applied to the anode until a stable emission was obtained.

Conductivity measurements were made in two ways, either by applying small d.c. potentials from 0 to 100 mV between the probe and the cathode core in each direction, or by applying up to 10 V r.m.s. at 1000 c/s, and photographing the current-voltage characteristic displayed on a cathode-ray oscillograph. Either method ensured that rectification effects would have been observed; these were not seen, and the two methods gave similar values for the coating conductivity at temperatures below 600° K.

Cathode temperature was measured by means of a thermocouple, the hot junction of which consisted of a fine tungsten wire welded internally to the centre of the "0" nickel cathode base. The potential difference developed between this and a similar junction in melting ice was measured by means of a Muirhead potentiometer, enabling the temperature to be estimated to better than ± 1° C.

RESULTS

1. *Conductivity measurements*

Measurements of conductivity *versus* temperature were made on six cathodes coated with the mixed oxides (BaSr)O. In each case the conductivity line in the temperature range

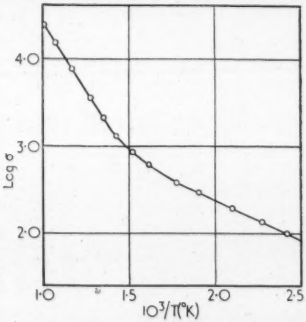

Fig. 1. Conductivity line for an oxide-coated cathode

* Now at Physics Department, Queen's University, Belfast.

1000–500° K (Fig. 1) had shape corresponding closely to that described by Loosjes and Vink and other authors.

In the course of investigating the effect of admitting oxygen to the cathode at temperatures below 500° K, very careful measurements were made of the conductivity of a well-activated (BaSr)O cathode in the temperature range 500–300° K. The resulting conductivity line is shown in Fig. 2.

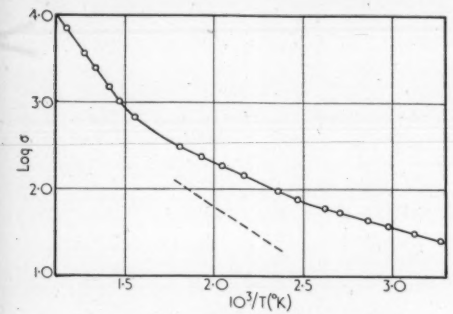

Fig. 2. Conductivity line for cathode BS9

The log σ *versus* $1/T$ relationship was not a linear one, but appeared to consist of two linear sections intersecting at a value of $1/T$ corresponding to approximately 400° K. This additional "bend" in the conductivity line had not been encountered either in previous measurements or in the literature, owing to the fact that usually only a few points were plotted in the temperature range below 600° K. Accordingly, conductivity measurements were made in this temperature range on a number of (BaSr)O cathodes. The resulting conductivity line in each case exhibited a bend at approximately 400° K. Table 1 gives the values of the activation energies Q and L obtained from the slopes of the two sections of each conductivity line.

Table 1. *Activation energies for conductivity in (BaSr)O cathodes*

	Activation energies (eV)		
Cathode	300–400° K *L*	400–600° K *Q*	*corrected Q* *Q**
BS4	0·12	0·15	0·24
BS5	0·14	0·17	0·23
BS6	0·12	0·20	0·27
BS7	0·09	0·15	0·20
BS9	0·12	0·18	0·22

The values of Q and L in Table 1 are spread over quite a wide range. This is not unusual in work on oxide cathodes. It is thought to arise from the extent to which each cathode is activated, which will depend upon the ultimate vacuum in the tube and the processing schedule. Although every attempt was made to produce similar cathodes by careful control of the spraying and processing, it is clear that many variables are involved, some of which cannot be controlled, and thus reproducible results were not obtained.

The additional "bend" in the conductivity line at approximately 400° K may be interpreted in a manner analogous to that used by Loosjes and Vink to interpret the bend in the conductivity line which occurs at approximately 700° K; namely, that two conduction processes operate in parallel. It is then necessary to correct the values of Q in Table 1 to account for the parallel low temperature conduction process, of activation energy L, and thus obtain a more accurate value for Q, the activation energy of the conduction process predominant between 400 and 700° K. A simple method was employed to do this. The lower section of the conductivity line in Fig. 2 was produced to meet the ordinate axis. At a number of temperatures, the conductivity obtained from this line was subtracted from the measured conductivity at that temperature. The logarithmic value of the resulting conductivity was plotted at the corresponding temperature and a new conductivity line produced. This is shown as a broken line in Fig. 2. The slope of this broken line gives the required corrected activation energy (Q^*). Table 1 also gives the corrected values for each cathode.

This simple method of correction was justified by constructing theoretical curves based on an equation for the conductivity of the following form,

$$\sigma = \sigma_1 \exp(-E_1/kT) + \sigma_2 \exp(-E_2/kT)$$

Values were assigned to E_1, E_2 and σ_1/σ_2 in order that log σ *versus* $1/T$ could be plotted in the range $300 < T < 600$° K so as to give curves very similar to those obtained by measurement. The slopes of the theoretical curves were very different from the values of E_1 employed to construct them. However, correction by the method outlined above gave agreement to within 10% between E_1 and the corrected slope of the theoretical conduction line. Agreement to within about 10% was obtained between E_2 and the slope of the theoretical line at the lowermost temperatures. Accordingly, correction of the values of L in Table 1 was not attempted.

Prolonged activation experiments. In order to investigate the effect of further activation upon cathodes exhibiting the bend in the conductivity line at 400° K, several cathodes were operated under activating conditions, namely, cathode temperature 1200° K, anode potential 100 V, for a period of 200 hours. At the end of this period the anode current had stabilized in the region of 120 mA. Conductivity measurements revealed that little change had occurred in some of the cathodes but for cathodes BS8 and BS5 completely linear conductivity lines below 700° K were obtained. Fig. 3 illustrates the change in the conductivity *versus* temperature

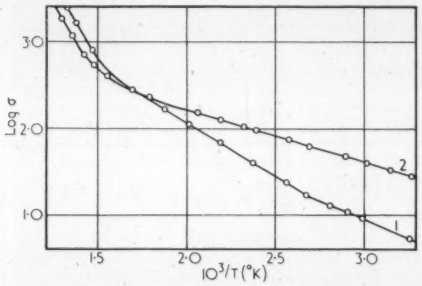

Fig. 3. Conductivity lines for cathode BS8
Curve (1) before, and curve (2) after 200 h activation.

behaviour of BS8 as a result of the prolonged activation procedure. Table 2 gives the activation energies of each section of the conductivity lines for all the cathodes employed in these measurements.

Table 2. *Activation energies at different states of activation*

	Activation energies (eV)			
	before prolonged activation		after prolonged activation	
Cathode	Q^*	L	Q^*	L
BS5	0·23	0·14	—	0·16
BS6	0·27	0·12	0·27	0·12
BS7	0·20	0·09	0·25	0·12
BS8	0·25	0·17	—	0·12
BS9	0·22	0·12	0·23	0·12

The absence of the bend at 400° K in the conductivity line of some well-activated cathodes (BS5 and BS8) observed in these experiments may be a partial explanation of why this bend has not been observed previously. It is clear that under certain conditions of activation, the low temperature conductivity line is quite linear, possibly because one of the two conduction processes becomes predominant throughout the temperature range 300–700° K.

2. *Barium deposition experiments*

In the course of activating a cathode at a temperature above 1200° K by drawing an anode current in excess of 140 mA, it was noted that the anode became red hot and that a bright green discharge developed between the anode and cathode. This discharge was attributed to the presence of ionized barium, removed from the hot anode by electron bombardment. The effect of this liberated barium upon the coating conductivity was investigated by allowing the discharge to continue for two minutes and then cooling the cathode over a period of fifteen minutes to a temperature of 600° K, after which conductivity measurements were made. Fig. 4,

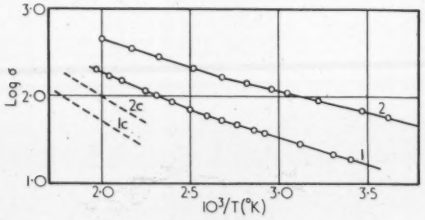

Fig. 4. Conductivity lines for cathode BS9
Barium deposition experiment.
Curve (1) before, curve (2) after barium deposition.

curve (1) shows the conductivity line for cathode BS9 prior to barium deposition and curve (2) the enhanced state of conductivity resulting from the presence of barium on the cathode. Fig. 5 gives Richardson plots of the cathode emission prior to and after the barium deposition. Table 3 indicates the changes in activation energies as a result of the deposition. This table reveals that the process most affected by barium deposition is the low temperature conduction process of activation energy L. Conductivity, at temperatures below 400° K, is enhanced by the presence of barium on the cathode.

Operation of the cathode at 1200° K without anode potential for a period of thirty minutes, after passing the green discharge for two minutes, and then cooling to 600° K as before gave a conductivity line identical with curve (1) in Fig. 4. This removal of the deposited barium by operation of the cathode at high temperatures for a short interval suggests that most of the deposited barium was located on the surfaces of the oxide particles rather than incorporated into the crystal lattice of the oxide.

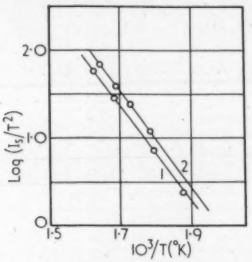

Fig. 5. Richardson lines for cathode BS9
Barium deposition experiment.
Curve (1) before, curve (2) after deposition.

Table 3. *Changes in activation energy due to barium deposition*

Cathode	Activation energies (eV)		
BS9	Q^*	L	r_1/r_2
Before Ba dep.	0·25	0·13	1·1
After Ba dep.	0·24	0·10	1·1

3. *Oxygen poisoning experiments*

The phenomenon of deactivation of an oxide-cathode (poisoning) by admitting oxygen gas to the vacuum tube is one which has received considerable attention in the literature. The effect of oxygen poisoning on the conductivity of the oxide-layer at temperatures below 700° K has not been studied however. The experiments reported here were designed to investigate the change in slope of the conductivity line when a cathode was poisoned by different quantities of oxygen.

A technique similar to that employed by Shepherd[3] was used to produce oxygen within the vacuum tube. The extent of poisoning was controlled by observing the decrease in thermionic emission as oxygen was admitted to the cathode. The emission was reduced to 66, 30, and 10% of its initial value in successive experiments. At the conclusion of conductivity measurements in the poisoned state, reactivation was accomplished by raising the cathode temperature to 1100° K and applying an anode potential of 50 V. Under these conditions recovery to the initial state of activation occurred within a few minutes, the emitted oxygen being taken up by the two getters.

Cathode BS8 was employed in these experiments. This cathode possessed a higher conductivity than others that were available; moreover, in the fully activated state, the conductivity line was linear at temperatures below 700° K [Fig. 6, curve (1)]. After each poisoning experiment the state represented by curve (1) could be reproduced by following the recovery procedure described.

Curves (2), (3) and (4) of Fig. 6 are the conductivity lines obtained when the emission was poisoned to 66, 30 and 10% of its initial value. The bend at 400° K observed in measurements on other cathodes is evident in all three of these curves, but is quite pronounced in the more poisoned states. Table 4 lists the activation energies obtained from the slopes of the two sections of each conductivity line, those listed

under Q^* being corrected as described previously. The table indicates that L is affected by small additions of oxygen whereas larger quantities appear to affect Q. In each case the activation energy is increased by admitting oxygen, implying that both conduction processes are impaired by the presence of oxygen.

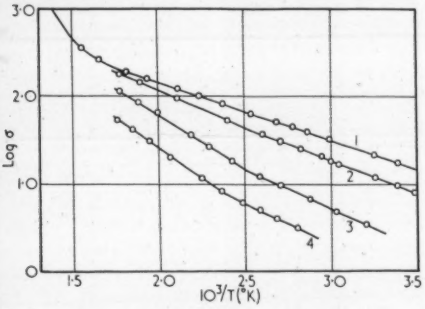

Fig. 6. Conductivity lines for cathode BS8

Oxygen poisoning experiments.

Curve (1) fully activated state; curves (2), (3) and (4) after poisoning to 66%, 30% and 10% of initial value.

Table 4. *Activation energies after poisoning*

Curve no. Fig. 6	Poisoned to % init. Ia	Activation energies (eV) Q^*	L
1.	Act.	—	0·12
2.	66	0·26	0·15
3.	30	0·27	0·18
4.	10	0·34	0·19

4. *Summary of results*

(i) The log σ *versus* $1/T$ relationship for an oxide-coated cathode in the temperature range 600–300° K is not always linear as higherto supposed. The results described here indicate that the curve consists of two linear sections which intersect at a value of $1/T$ corresponding to approximately 400° K. This suggests that more than one conduction process contributes to the total conductivity mechanism in this temperature range.

(ii) In order that a value of the activation energy of each conduction process may be obtained from the conductivity lines a form of correction has to be employed. Corrected values of Q, the activation energy in the temperatures range 600–400° K, obtained from measurements on six cathodes lie in the range 0·22 to 0·27 eV. The activation energy at temperatures below 400° K (L) was found to be in the range 0·10–0·14 eV.

(iii) Deposition of barium on to a cathode gives rise to enhanced conductivity. The activation energy L is reduced, but Q does not appear to be affected appreciably by the presence of barium. The excess barium is readily evaporated by raising the cathode temperature to 1200° K for a few minutes.

(iv) Prolonged activation of a cathode which exhibits a bend in the conductivity line at approximately 400° K may occasionally result in a completely linear line between 700 and 300° K. This is probably due to one conduction process becoming predominant throughout the temperature range. The admission of small quantities of oxygen to the cathode results in a reappearance of the bend. Controlled oxygen poisoning experiments indicate that both L and Q are increased by the presence of oxygen, L appearing to be more sensitive to small quantities.

DISCUSSION

The results reported here strongly suggest that two conduction processes operate in parallel in oxide-coated cathodes at temperatures in the range 600–300° K. It has been assumed in the past that conduction below the bend or knee of the conductivity line in Fig. 1 is controlled by the semi-conducting nature of the oxide; barium oxide being an excess *N*-type semiconductor due to the presence of a stoichiometric excess of barium in the crystal lattice. However, the oxide cathode consists of a large number of very small crystals and therefore conduction through the mass of crystallites is limited by barriers at crystal–crystal contacts. Furthermore, the oxide layer is very porous and hence the surface to volume ratio will be quite large. Conduction processes on the surfaces of the crystallites may largely determine the behaviour of the oxide cathode at temperatures below 700° K.

There is some evidence from oxygen and sulphur poisoning experiments previously reported[8] to suggest that surface conduction processes are important at temperatures below 700° K. The initially rapid reduction in conductivity on admitting oxygen or sulphur to a cathode indicates a surface as opposed to a bulk conduction process. Further evidence is afforded by the conductivity measurements and barium deposition experiments described here. The conductivity at temperatures below 400° K is enhanced by the addition of barium to the cathode. This could be accounted for if conduction were due to the movement of barium ions over the surfaces of the crystallites. Addition of barium would increase the conductivity by increasing the surface concentration. Re-evaporation of the added barium, which would not be tightly bonded to the crystal lattice, should be comparatively easy. Experiment shows that this is the case.

A charge-transporting barium diffusion process over the surfaces of barium oxide crystals has been reported by Redington.[9] The activation energy, 0·16 eV for this process, compares favourably with the values obtained for the conduction process predominant below approximately 400° K. Therefore it is reasonable to suggest that the conduction process predominant at temperatures below 400° K is one of movement of barium ions over the surfaces of the crystallites of which the oxide layer is composed.

The parallel conduction process, with activation energy Q, may be identified with *N*-type semi-conduction within the crystallites, limited by barriers at the interfaces between the crystallites. Conduction at temperatures below 700° K will be a combination of both of these processes in addition to pore conduction. Under certain conditions the concentration of barium on the crystallite surfaces becomes sufficiently great for the ionic process to become the predominant conduction process at all temperatures below 700° K. The conductivity line is then quite linear and the slope usually less than 0·16 eV. This explanation overcomes the difficulty, cited by Hughes and Coppola,[7] of interpreting the low values of activation energy obtained in conductivity measurements in terms of *N*-type semi-conduction. In addition this explanation, involving ionic and electronic conduction processes in parallel, may account for the departure from linearity of the current-voltage characteristics at low temperatures reported by King.[10]

Oxygen poisoning at temperatures below 700° K is explained partly by impaired barium ion movement, due to the presence of oxygen ions on the crystallite surfaces, and partly by increased electron trapping at crystal–crystal contacts. Poisoning is thus almost entirely a surface phenomenon and an explanation involving the reoccupation by oxygen of vacant lattice sites is unnecessarily involved.

CONCLUSIONS

There is evidence from measurements of the conductivity of oxide cathodes in the temperature range 300–600° K to suggest that at least two processes contribute to the conduction mechanism. One of these may be identified with the movement of barium ions over the surfaces of the minute crystallites which constitute the oxide coating. The other process is thought to be electronic conduction, the oxide particles being *N*-type excess semi-conductors, limited by barriers, e.g. electron traps due to oxygen, between the crystallites. Oxygen poisoning in this temperature range may then be explained by impaired movement of barium ions on the crystallite surfaces and by increased electron trapping at crystal–crystal interfaces.

ACKNOWLEDGEMENTS

The author wishes to thank Prof. F. A. Vick for helpful advice and discussion during this work and the University College of North Staffordshire for the laboratory facilities provided. The gift of valve stems and materials by Siemens-Edison-Swan Ltd. is also gratefully acknowledged.

REFERENCES

(1) LOOSJES, R., and VINK, H. J. *Philips Res. Rep.*, **4**, p. 449 (1949).
(2) FORMAN, R. *Phys. Rev.*, **96**, p. 1479 (1954).
(3) SHEPHERD, A. A. *Brit. J. Appl. Phys.*, **4**, p. 70 (1953).
(4) YOUNG, J. R. *J. Appl. Phys.*, **23**, p. 10 (1952).
(5) TOMLINSON, T. B. *J. Appl. Phys.*, **25**, p. 720 (1954).
(6) TOMLINSON, T. B., and KING, R. E. J. *Brit. J. Appl. Phys.*, **7**, p. 268 (1956).
(7) HUGHES, R. C., and COPPOLA, P. P. *Phys. Rev.*, **88**, p. 364 (1952).
(8) HIGGINSON, G. S. *Brit. J. Appl. Phys.*, **8**, p. 148 (1957).
(9) REDINGTON, R. W. *Phys. Rev.*, **87**, p. 1066 (1952).
(10) KING, R. E. J. *Research*, **9**, p. S9 (1956).

The indium-selenium system

By J. C. BRICE, B.A., Grad. Inst.P., P. C. NEWMAN, M.A., A.Inst.P., and H. C. WRIGHT, B.Sc., A.Inst.P.,
Mullard Research Laboratories, Salfords, Surrey

[*Paper received* 13 *September*, 1957]

Polycrystalline specimens of In_2Se_3, InSe and In_2Se were prepared by direct fusion. Electrical and physical measurements were made which indicated a phase change in In_2Se_3 at 196° C.

In this article, the symbols In_2Se_3, InSe, and In_2Se will be used for indium sesquiselenide, indium monoselenide, and indium subselenide respectively.

The possibility that In_2Se_3 might be a useful semi-conducting material was suggested by the properties of compounds analogous to it, such as gallium sesquitelluride (Ga_2Te_3).[1] The last comprehensive work on the indium–selenium system was that of Klemm and von Vogel[2] in 1934 and hence a survey of the whole system was undertaken. Three compounds, In_2Se_3, InSe and In_2Se are said to occur, and comparison with the indium–tellurium phase diagram[3] indicates that In_2Se may have an incongruent melting point.

EXPERIMENTAL

The compounds were prepared by direct fusion of stoichiometric amounts of spectroscopically-standardized elements (by Johnson, Matthey and Co. Ltd.) in sealed, evacuated,

Physical properties of the indium-selenium compounds

	In_2Se_3 High temp. phase	In_2Se_3 Low temp. phase	InSe	In_2Se High temp. phase	In_2Se Low temp. phase
Composition (% Se)	50·79	50·79	40·76	25·60	25·60
Melting point (° C)	890 ± 10[1]		660 ± 10[1]		
Specific gravity		5·48	5·44		6·15
Optical energy gap (eV)		1·2	1·05		See Fig. 2
Electron mobility at 300° K ($cm^2\ V^{-1}\ s^{-1}$)		30	900		1
Carrier density at 300° K (cm^{-3})		10^{14}	10^{14}		10^{16}
Donor levels (eV)	0·26*		0·32		

Temperature of phase change (°C) by:			
(*a*) Dilatometry	192 ± 2		
(*b*) Thermal e.m.f.	213 ± 5		
(*c*) D.T.A. Heating at 15 C°/min	190 ± 2		Heating and Cooling
(*c*) D.T.A. Cooling at 1·5 C°/min			120 ± 2
(*d*) Resistance/temperature	197 ± 1		
(*e*) Weighted mean	196		

* Values varied from specimen to specimen. This is a mean value.

silica tubes. The specimens were all polycrystalline. Mobilities and carrier concentrations at room temperature were deduced from measurements made with a conventional d.c. Hall apparatus. The specimens had Leitsilber painted current-contacts, and indium-tipped tungsten probes were sparked on. Donor levels were deduced from resistivity/temperature plots obtained by immersing specimens in a heated bath of MS550 silicone oil (by Midland Silicones Ltd.).

An anomaly in the curve obtained with In_2Se_3 was further investigated by differential thermal analysis (D.T.A.) (using a standard apparatus by A. Gallenkamp and Co. Ltd.), thermal e.m.f. curves, and dilatometry (using a specially constructed pyknometer). These investigations confirmed the existence of two phases of In_2Se_3 as reported by Miyazawa and Sugaike.[4] The results are shown in the table and Fig. 1.

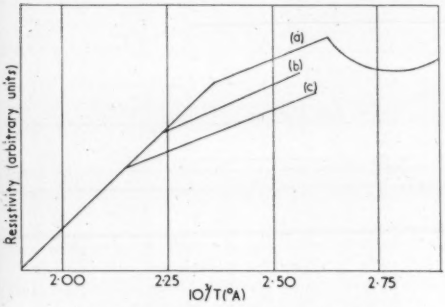

Fig. 1. Temperature/resistivity plot for In_2Se_3

(*a*) Rate of cooling 6° C/min.
(*b*) Rate of cooling 3° C/min.
(*c*) Held 15 min at each temperature.

Spectral absorption curves were taken either on powdered specimens using a Uvispek spectrophotometer (by Hilger and Watts Ltd.) with diffuse reflectance attachment, or by specular reflexion from polished surfaces using a type D247 monochromater (by Hilger and Watts Ltd.). The results of the diffuse reflexion measurements for In_2Se_3 and InSe were interpreted on Moss's[5] theory. The values obtained do not differ appreciably from those which result from using Fochs's[6] method. Fig. 2 shows the direct reflexion curve obtained for In_2Se. Interpretation of this is doubtful since it seems possible that the necessary polishing may have left a film of indium over the reflecting surface which would obscure the absorption curve by interference phenomena.

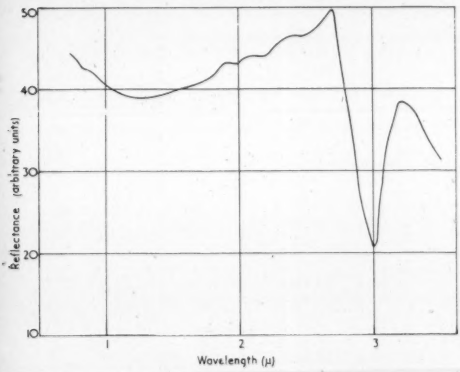

Fig. 2. Absorption spectrum of In_2Se

DISCUSSION

The findings of Miyazawa and Sugaike[4] and Goryunova and others[7] that In_2Se_3 and InSe are semi-conductors were confirmed. The preparation of In_2Se as a single phase was not achieved. Some samples of In_2Se appeared to be homogeneous by inspection, but X-ray analysis showed the existence of two or three phases, one of which was free indium. Results quoted for In_2Se were those taken on the most homogeneous specimens. Difficulty was experienced in determining the type of carrier in InSe (see Damon and Redington[8]). One sample appeared to be definitely *n*-type by Hall measurement and *p*-type by thermoelectric e.m.f. sign. Russian workers[9-10] have found only *p*-type carriers.

The phase change in In_2Se_3 appeared at various temperatures according to the method of observation used. The idealized temperature-resistance curves in Fig. 1 show how the apparent temperature of the phase change varies with rates of cooling. The differential thermal analysis results, unlike the work of Miyazawa and Sugaike indicate an exothermic change on heating. No effect was observed on cooling; this suggests a supercooling phenomena which might be expected from an exothermic change.

ACKNOWLEDGEMENT

The assistance of many members of the Solid State Physics Division of these Laboratories is gratefully acknowledged.

REFERENCES

(1) HARBEKE, C., and LAUTZ, G. *Z. Naturf.*, **11***a*, p. 1015 (1956).

(2) KLEMM, W., and VON VOGEL, H. U. *Zeit. anorg. u. allgem. Chem.*, **219**, p. 45 (1934).

(3) HANSEN, M. *Aufbau der Zweistofflegierungen* (Berlin: Springer, 1936).

(4) MIYAZAWA, H., and SUGAIKE, S. *J. Phys. Soc. Japan*, **12**, p. 312 (1957).

(5) MOSS, T. S. *Photoconductivity in the Elements* (London: Butterworth's Scientific Publications, 1952).

(6) FOCHS, P. D. *Proc. Phys. Soc. B*, **69**, p. 70 (1956).

(7) GORYUNOVA, N. A., GRIGOR'EVA, U. S., KONOVALENKO, B. M., and RYVKIN, S. M. *Zh. tekh. Fiz. (Moscow)*, **25**, p. 1675 (1955).

(8) DAMON, R. W., and REDINGTON, R. W. *Phys. Rev.*, **96**, p. 1498 (1954).

(9) RYVKIN, S. M. *Zh. tekh. Fiz. (Moscow)*, **18**, p. 1521 (1948).

(10) ARSEN'EVA GEIL, A. M. *Doklady Akad. Nauk SSSR*, **68**, p. 254 (1949).

Temperature and pressure corrections to be applied to the shielded hot wire anemometer at speeds for which natural convective cooling is negligible

By C. F. Cowdrey, B.Sc., National Physical Laboratory, Teddington

[*Paper first received* 23 *August, and in final form* 11 *November*, 1957]

The form of the law of cooling of a shielded hot wire anemometer should not differ greatly from the normal laws of cooling of heated cylinders. By using the law propounded by Hilpert,[3] a method is devised to allow for changes in ambient temperature and pressure when a hot wire anemometer is used at speeds for which the cooling can be considered as entirely due to forced convection. This method is then used to derive the corrections needed in the measurement of air flow over the range of variation of atmospheric conditions normally experienced. However, with slight modifications to allow for changes in the values of the physical constants, it should be possible to use the general method to cover all "perfect" gases at various ambient conditions. A number of experimental results are included in support of the theory.

A simple circuit is indicated in the Appendix, based on that outlined by Simmons,[1] by which the useful range of the instrument is greatly increased.

INTRODUCTION

The cooling of a small diameter wire heated by an electric current has been used for a long time as a measure of the speed of the air passing across the wire. Readings can be taken at a considerable distance from the instrument if required and, being of small dimensions, it will have very little effect on the general flow. Furthermore, since the sensitivity increases with decreasing speed, it is often the best instrument for measuring very low speeds. It has been impossible, however, to design a simple hot wire anemometer which would retain its calibration over a considerable period of time. As it is desirable to keep the diameter of the wire small, in order that the current needed to produce satisfactory heating should not be too large, small dust particles which settle on the wire have a large effect on the calibration. The use of such an instrument is possible in a wind tunnel, where repeated recalibration can be carried out, but is not of great value in the field. In 1948, Simmons[1] produced a special form of the instrument based on one he had designed in collaboration with Mr. E. Ower.

The Nichrome heater wire was threaded through one bore of a short length of twin bore silica tubing and a junction of a Nichrome-constantan thermocouple was arranged approximately at the centre of the other. To prevent relative movement, the diameter of the wires was only slightly less than that of the bores. Lengths of thick Nichrome wire fused to the ends of the heater wire, which was kept taut, served both as electrical leads and as supports for the head of the instrument. The free ends of the thermocouple were soldered to two copper prongs and the junctions were bent outwards away from the influence of the heater. They would thus be at the temperature of the surrounding air and would, in fact, form the cold junction of the couple. The four prongs were firmly attached to a block of insulating material and the whole formed an anemometer of very small size. Thus, the effective diameter of the heater was increased about threefold and the influence of dust particles practically eliminated.

Simmons also demonstrated that, over the range of speeds for which an appreciable proportion of the cooling was due to natural convection, the calibration, in terms of thermocouple e.m.f., was unchanged by variations of at least 30° C in the ambient temperature. When used with a careful understanding of the principles involved, this instrument has proved admirable for very low speed measurements where other methods have often been impracticable.

CORRECTIONS FOR AMBIENT TEMPERATURE AND PRESSURE VARIATIONS AT SPEEDS FOR WHICH NATURAL CONVECTIVE COOLING IS NEGLIGIBLE

A rough empirical correction was suggested by Simmons, but no reliable theoretical treatment has been developed so far. It was appreciated that the law of forced convective cooling of a shielded hot wire anemometer should not differ greatly in form from the usual laws pertaining to heated cylinders and numerous attempts have been made to solve this problem on the basis of the law propounded by King.[2] However, it was thought possible that a simpler form of correction could be derived from the form of the law put forward by Hilpert.[3]

It is to be remembered that the e.m.f. generated by a thermocouple is a function not only of the temperature difference between its junctions, but also of the actual temperature of the cold junction (in this case, of the ambient temperature) a point that appears to have been overlooked. By using this fact in conjunction with Hilpert's law of cooling, a simple method of correcting the calibration of a shielded hot wire anemometer has now been worked out and is presented in this report.

Theoretical treatment.

List of symbols used:

d = mean diameter of the silica tube
H = rate of heat transfer
t = temperature of the air in ° C
θ = temperature of the outer wall of the silica tube above that of the surrounding air
P = absolute pressure of the surrounding air
k = thermal conductivity of air
ρ = density of air
μ = viscosity of air
C_v = specific heat of air at constant volume
V = velocity of the air
e = net e.m.f. generated by the thermocouple
R = Reynolds number $= Vd\rho/\mu$
(Nu) = Nusselt number $= Hd/k\theta$

C and m are constants depending on R. A table of values of C and m is shown at the end of the paper. Suffixes refer to the ambient temperature in degrees Centigrade.

Hilpert's law of cooling states that

$$(Nu) = C(R)^m$$

i.e. $$\frac{Hd}{k\theta} = C\left(\frac{\rho V d}{\mu}\right)^m$$

But, $k = 1{\cdot}603\,C_v\mu$ and C_v can be taken as constant at the temperatures and pressures likely to be encountered in atmospheric variations.[4]

Therefore $$\frac{Hd^{(1-m)}}{1{\cdot}603C\cdot C_v} \times \frac{1}{\mu^{(1-m)}\theta} = (\rho V)^m$$

If Nichrome is used for the heater wire, the resistance will not vary appreciably with temperature and, if the current through the wire is kept constant, H will also be constant.

Let $$F = \frac{Hd^{(1-m)}}{1{\cdot}603C\cdot C_v} \qquad \text{(which is constant)}$$

Then $$\frac{F}{\mu^{(1-m)}\theta} = (\rho V)^m \qquad (1)$$

When changes in pressure alone are to be considered, μ is constant and θ is a function of e. Thus e is a function of ρV and a unique calibration curve is obtained, independent of pressure, by plotting e against ρV (or more conveniently, $\rho/\rho_0 V$, where ρ_0 is the air density at some standard temperature). If, however, changes in ambient temperature, as well as pressure, have to be taken into account, no such simple form of correction is in general possible. Consider equation (1) for two different values of the ambient temperature 0° C and t° C and two wind speeds V_0 and V_t such that e is the same in both cases

then $$F/[\mu_0{}^{(1-m)}\theta_0] = (V_0\rho_0)^m$$

and $$F/[\mu_t{}^{(1-m)}\theta_t] = (V_t\rho_t)^m$$

therefore $$\left(\frac{\mu_t}{\mu_0}\right)^{(1-m)}\frac{\theta_t}{\theta_0} = \left(\frac{V_0\rho_0}{V_t\rho_t}\right)^m$$

Let $$\left(\frac{\mu_t}{\mu_0}\right)^{(1-m)}\frac{\theta_t}{\theta_0} = (A_t)^m \qquad (2)$$

then $$V_0 = A_t\left(\frac{\rho_t}{\rho_0}\right)V_t \qquad (3)$$

and $$V_t = \frac{1}{A_t}\left(\frac{\rho_0}{\rho_t}\right)V_0 \qquad (4)$$

It is now necessary to determine the value of A. To the accuracy needed, $\mu_t/\mu_0 = (1 + 0{\cdot}0028t)$ for the range of temperatures of at least 0–100° C[4] and, for practical purposes, m can be taken as 0·466. Finally, by using the Law of Intermediate Temperatures, θ_0 and θ_t (and hence θ_t/θ_0) can be calculated for various values of e and t, if an accurate calibration of the thermocouple employed in the anemometer is known.

In practice Nichrome-constantan is used, for which a typical calibration was supplied by the Physics Division of the N.P.L. This calibration was reduced to the equations

$$\theta = 22{\cdot}92e - 0{\cdot}5716e^2 + 0{\cdot}0279e^3 - 0{\cdot}000\,743e^4 + + 0{\cdot}000\,004\,72e^5$$

$$e = 0{\cdot}0436\theta + 0{\cdot}000\,049\,2\theta^2 - 0{\cdot}000\,000\,035\,5\theta^3$$

The values of A were then derived analytically, neglecting the slight temperature difference between the thermocouple junction and the outer wall of the silica tube. Curves of A against e for ambient temperatures of 10, 20, 30, 40 and 50° C are shown in Fig. 1. The choice of metals used for the thermocouples of the shielded hot wire anemometers is extremely fortunate as changes in the readings due to variations of the viscosity of the air are almost entirely neutralized by the changes in the calibration of the thermocouple. It is for this reason that all the curves of Fig. 1 pass so remarkably nearly through unity when $e = 7$ mV and that none of the curves diverges from unity by more than 5% over the whole range considered.

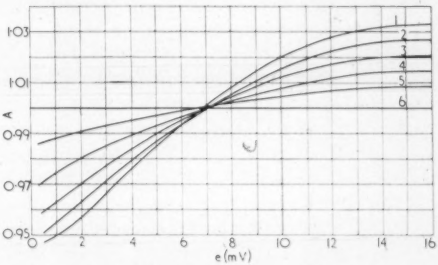

Fig. 1. Values of correction factor A for Nichrome-constantan thermocouple

Curve 1, $t = 50$° C; curve 2, $t = 40$° C; curve 3, $t = 30$° C; curve 4, $t = 20$° C; curve 5, $t = 10$° C; curve 6, $t = 0$° C.

A being known, a calibration of the instrument can be reduced to a standard form by applying the result of equation (3) and this standard calibration can be used, in conjunction with equation (4), to deduce the value of V_t corresponding to an observed value of e.

Experimental details. To test the accuracy of the theory a shielded hot wire anemometer was calibrated under various conditions of ambient temperature and pressure and the results reduced to a "standard" form by application of equation (3). The instrument used was one of a type now produced commercially. It differed from that originally used by Simmons only in the geometric design, the silica tube being longer and the diameters of the wires slightly less so that, for the same current, higher temperatures were produced and the e.m.f. generated was increased. Also, the axis of the silica tube was parallel to that of the insulating support and not perpendicular to it as in the original design.

In the first set of tests, to investigate the effect of pressure changes, the instrument was calibrated against a vane anemometer in the Compressed Air Tunnel of the N.P.L. at a number of pressures up to a maximum of approximately 6 in. of mercury above normal atmosphere. It will be appreciated that evacuation of the tunnel, to represent pressures below that of the atmosphere, is not practicable. The hot wire anemometer was set up, with the silica tube vertical, at a point one foot upstream of the vane anemometer, both instruments being on the centre line of the tunnel. In deciding the exact positions of the instruments, reference was made to a previous investigation of the flow distribution, to make sure that they were in regions of equal velocity. This was not, however, really necessary as the absolute calibration was not needed and a small percentage error in the measurement of the wind speed would not appreciably affect the changes likely to be produced by the variations in pressure. The temperature remained constant throughout.

The second set of readings, in which the effects of changes of ambient temperature were studied, were taken in a return

flow tunnel of one foot square working section. The temperature of the air in the tunnel was varied by six 1 kW cylindrical heaters set up horizontally one above the other just behind the fan which was a long way upstream of the working section. This gave the maximum possible time for the air temperature to become evenly distributed at the working section. Two, four or six of these heaters could be switched in as required and, by this means, the temperature could be controlled to within less than 1° C. This tunnel, unlike the Compressed Air Tunnel, had no convenient speed indicator and, without making special provision, it would have been difficult to keep the velocity steady enough for the length of time needed to read the vane anemometer. It was therefore decided to use a pitot static tube connected to a 13 in. Chattock gauge instead. The hot-wire anemometer was placed 4 in. upstream of the pitot static tube, the instruments being staggered 1 in. either side of the centre line to minimize interference. The air temperature was taken as the reading of a mercury thermometer projecting 3 in. into the tunnel slightly downstream of the pitot static tube. A preliminary test showed no difference, over the full range of temperature and velocity, between this thermometer and a similar one, placed in turn in the positions to be occupied by the anemometers. The pressure remained constant throughout.

Three values of heater current were used in all the tests, namely 0·5, 1·0 and 1·5 A.

Experimental results. The first series of experiments was undertaken in order to determine the effect of pressure variations of up to approximately 20% above normal atmosphere; for these, no correction for temperature was necessary as this remained the same throughout. The results for a heating current of 1·0 A are shown in Fig. 2, where the e.m.f.

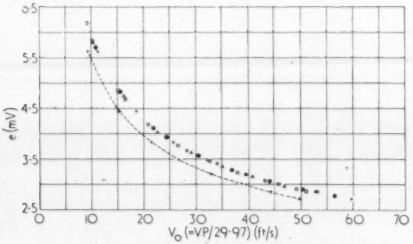

Fig. 2. Effect of pressure

Heating current = 1·0 A.
$P \simeq 30{\cdot}0$ in. mercury ○ (no correction required).
$P \simeq 31{\cdot}4$ in. mercury □.
$P \simeq 32{\cdot}0$ in. mercury △.
$P \simeq 34{\cdot}1$ in. mercury ●.
$P \simeq 35{\cdot}9$ in. mercury ×.
$P \simeq 35{\cdot}9$ in. mercury uncorrected + – – – +.

generated by the thermocouple is represented as a function of $V_0(P/29{\cdot}97)$. It will be seen that all the points taken lie on the same curve to the degree of accuracy to be expected in the calibration of a hot wire anemometer. The results obtained for the other two currents are equally satisfactory, so that the pressure correction would appear to be very well defined.

In Fig. 3, the results of the second series of results, for the same heater current, are shown. In this case e is plotted against $V_0 (= A\frac{\rho}{\rho_0}V)$ where V_0 refers to 0° C and 29·97 in. of mercury pressure (in this case, although P remained constant, the readings were corrected to standard conditions on the evidence of the previous tests). Here, again, all the points lie very nearly on one curve. This also applies to those obtained with heating currents of 0·5 and 1·5 A, except for the corrected observations with the smaller current and 40° C ambient temperature which are very slightly

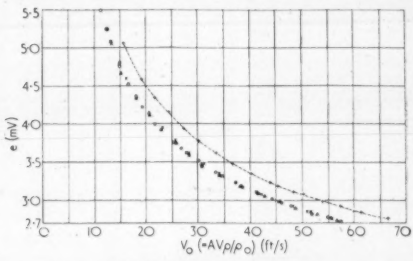

Fig. 3. Effect of temperature

Heating current = 1·0 A.
$t \simeq 10°$ C ○.
$t \simeq 20°$ C □.
$t \simeq 30°$ C △.
$t \simeq 40°$ C ×.
$t \simeq 40°$ C uncorrected + – – – +.

displaced. This is probably due to the lack of accuracy in the estimation of A at the low values of e, which is to be expected since the thermocouple calibration was given at intervals of 10° C and the interpolation was of a much lower order of accuracy. No attempt has been made to rectify this as the errors arising are not of great importance, and it is extremely unlikely, anyway, that such a low value of heating current would be employed in this range of wind speed. Thus, the correction for temperature is amply confirmed.

In each of the graphs of the corrected results, the uncorrected values for the maximum deviation from standard conditions are shown to illustrate the magnitude of the improvement.

TEMPERATURE CORRECTION FACTOR FOR OTHER STANDARD CONDITIONS

Reference to Fig. 1 will show that the value of A can be taken as unity over a large range of the ambient temperature, especially as is often the case, if not more than 2 or 3% accuracy is required. It may be of advantage to use another standard temperature nearer to the mean of those normally encountered, for example 15° C. The values for this new value of standard temperature can be calculated as follows.

Taking A' as the new factor, for a given value of e

$$(A_t')^m = \left(\frac{\mu_t}{\mu_{15}}\right)^{(1-m)} \frac{\theta_t}{\theta_{15}} \qquad \text{from equation (2)}$$

But
$$(A_t)^m = \left(\frac{\mu_t}{\mu_0}\right)^{(1-m)} \frac{\theta_t}{\theta_0}$$

Therefore
$$\left(\frac{A_t'}{A_t}\right)^m = \left(\frac{\mu_0}{\mu_{15}}\right)^{(1-m)} \frac{\theta_0}{\theta_{15}}$$
$$= (1/A_{15})^m$$

and
$$A_t' = A_t/A_{15} \qquad (5)$$

GENERAL ACCURACY

It is appreciated that there are several possible sources of error in the theoretical treatment, but these are considered to be too small to matter, a conclusion amply borne out by the experimental results. For example, the hot junction of the thermocouple is not at the circumference of the silica tube and the temperature difference of the thermocouple junctions will be slightly in excess of θ. The difference is estimated to be of the order of 1% for the highest temperature used and is insignificant. Again, if the hot wire temperature were excessively high, an appreciable loss of heat by radiation would result and a different law of cooling would be needed in deducing the errors likely to arise in the calibration. This, obviously, would become important if too high a current were used, but the experimental results indicate no appreciable effect at the maximum hot wire temperature used.

Within the limits of the investigation, and probably to a large extent outside these limits, the results suggest that any further refinement of the proposed corrections is unnecessary. Even under laboratory conditions, other errors of measurement would normally be at least of the same order as, and probably larger than, any uncertainty that might still remain.

CONCLUSIONS

When the e.m.f. generated is in the region of 7 mV, it measures ρV directly. For other values than this, an added correction of up to a few per cent may be necessary as shown in Fig. 1. To the order of accuracy likely to be required, a unique calibration curve is obtained if e is plotted against $A\frac{\rho}{\rho_0}V$. By using this calibration, the errors arising out of changes in ambient temperature and pressure are reduced to the order of those in the original calibration.

The experimental results show excellent agreement with the theory and, although they only cover a range of speeds of about 10 ft/s to 60 ft/s, a fair amount of extrapolation should be permissible. Furthermore, since no account was taken in the theory of the geometric design of the instrument, the theory should hold for all types of shielded hot wire anemometer utilizing the same thermocouple. The special circumstances when natural convection is significant have been examined by Simmons.[1]

ACKNOWLEDGEMENTS

The author wishes to acknowledge the assistance given by Mr. P. G. G. O'Neill of the Aerodynamics Division during the wind tunnel experiments.

The work described was carried out in the Aerodynamics Division of the National Physical Laboratory; it is published on the recommendation of the Aeronautical Research Council and by permission of the Director of the Laboratory.

REFERENCES

(1) SIMMONS, L. F. G. *J. Sci. Instrum.*, **26**, p. 407 (1949).
(2) KING, L. V. *Phil. Trans.*, **214**, p. 273 (1914).
(3) HILPERT, R. *Forch. Gebiete Ingenieurwes*, **4**, p. 215 (1933).
(4) KAYE, G. W., and LABY, T. H. *Physical and Chemical Constants* (London: Longmans, Green & Co., 1911).

APPENDIX

Modified circuit for use with the shielded hot wire anemometer. It is very desirable to be able to dispense with such a bulky and expensive instrument as a potentiometer for measuring the e.m.f. generated by the thermocouple and a simple circuit was indicated in Ref. 1 whereby the deflexion of a galvanometer was used to record the velocity. This circuit is reproduced in Fig. 4. A small part of the potential

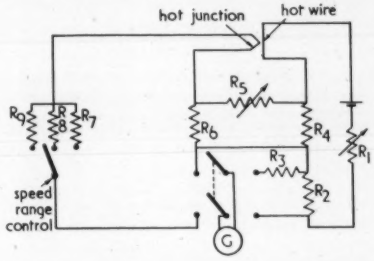

Fig. 4. Simple circuit for hot wire anemometer

difference across a fixed resistance R_4 in the heater circuit, is used to balance out the thermocouple e.m.f. at zero wind speed. To allow for the small day-to-day variations which are found to occur in the zero setting, small adjustments are made in the value of the resistance R_5. This is carried out, prior to using the instrument, by placing a box over the anemometer and allowing the natural convective currents to become settled. It should be emphasized that this adjustment is purely empirical and is made under conditions of wholly natural convective cooling. The extent to which it compensates for atmospheric variations, at speeds for which there is appreciable cooling by forced convection, has not been examined. Furthermore, with the circuit shown in Fig. 4, only a limited range of velocity is practicable at maximum sensitivity of the galvanometer and, to increase the range of use, one of a number of fixed resistances can be introduced, in series with the galvanometer, to reduce its sensitivity.

In Fig. 5, an improved circuit is shown in which the voltage fed into the thermocouple circuit can be varied, in stages,

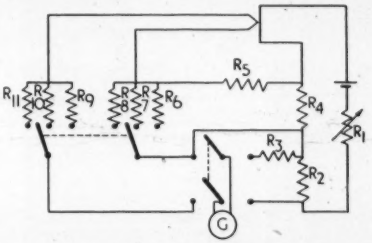

Fig. 5. Modified circuit for hot wire anemometer for extended speed range

so that it is possible to obtain zero deflexion of the galvanometer at any number of pre-arranged speeds. At the same time, a resistance (R_9, R_{10} or R_{11}), automatically switched into the galvanometer circuit, determines the velocity for

maximum deflexion. Thus, increased range of use of the instrument is introduced without loss of sensitivity as in the previous circuit, since these series resistances can be as low as required. This arrangement has been conveniently used for speeds of the order of 50 ft/s, both in the wind tunnel and in the field, where sensitivity with the original circuit is inadequate.

At speeds for which the new circuit was primarily designed, there would be no cooling by natural convection and it is doubtful if the method used in the original circuit for allowing for day-to-day variations would have been of any great value. Furthermore, the galvanometer deflexion is a measure of the e.m.f. generated by the thermocouple, but to a different scale depending on the pre-arranged speed range selected and a calibration curve in the form of deflexion against $A\frac{\rho}{\rho_0}V$ is applicable to all ambient conditions. Therefore, no variation is made in the value of the resistance R_5 and all corrections are carried out by calculation.

Values of constants used in Hilpert's law of cooling cylinders by forced convection

R	C	m
1–4	0·891	0·330
4–40	0·821	0·385
40–4000	0·615	0·466
4000–40 000	0·174	0·618
40 000–400 000	0·024	0·805

Magnetic anisotropy measurement with an oscillation magnetometer

By J. R. Macdonald, D.Phil., Texas Instruments Inc., Dallas 9, Texas, U.S.A.

[*Paper first received* 27 *June, and in final form* 20 *September*, 1957]

A method of using an oscillation magnetometer to determine magnetic anisotropy factors in the plane of a thin disk-shaped sample lying in the $X - Z$-plane is described. Both the saturation magnetization, M_0, and the factor $(N_x - N_z)M_0$ may be obtained independently; N_x, N_y and N_z are demagnetization factors which include all contributions to magnetic anisotropy such as those arising from stress, magnetocrystalline anisotropy and shape. These results are correlated with previous work on a somewhat different type of oscillation magnetometer used to determine $(N_y - N_z)M_0$, and it is shown that a correction must be applied for both types of magnetometer when the oscillation amplitude exceeds a degree or two. Finally, it is shown that the oscillation magnetometer can be employed to determine the details of any angular dependence of magnetic anisotropy in the plane of the sample if such anisotropy is sufficiently large. These measurement techniques are particularly applicable to the determination of any dependence of M_0 on film thickness in thin ferromagnetic evaporated films, and to the determination of magnetic anisotropy in thin films evaporated and/or annealed in a magnetic field.

Some time ago an oscillation magnetometer was described by Griffiths and the author[1, 2] which allowed the factors M_0 and $(N_y - N_z)M_0$ to be obtained for an ellipsoidal ferromagnetic disk or thin film. Here M_0 is the saturation magnetization of the ferromagnetic material and N_y and N_z are demagnetization factors in the Y and Z directions, respectively. In operation, a disk-shaped specimen is supported in a saturating, homogeneous magnetic field in such a way that it can rotate about its X-axis and with the plane of the disk, which contains both X- and Z-axes, parallel to the magnetic field direction at equilibrium. When equilibrium is very slightly disturbed, the specimen will oscillate about its equilibrium position with a period (neglecting damping) of $2\pi[J/\mathscr{T}]^{\frac{1}{2}}$, where J is the moment of inertia of the disk and its container about the X-axis and $\mathscr{T}$ is the restoring torque per unit angular displacement. In general, the period will depend on disk volume, saturation magnetization, magnetic anisotropy and the applied static field H_0.

The terms $(N_y - N_z)M_0$ and $(N_x - N_z)M_0$ appear in ferromagnetic resonance experiments and are composed of possible contributions from shape anisotropy, magnetocrystalline anisotropy in single-crystal samples and stress anisotropy.[3] Without independent knowledge of these factors, ferromagnetic-resonance g values cannot be obtained. By making both ferromagnetic resonance and oscillation magnetometer measurements on the same sample, the author showed that g and M_0 were independent of the thickness of evaporated nickel films down to the smallest thickness measured, 870 Å, and that such evaporated films were usually considerably stressed.[1, 4, 5]

When the g value and saturation magnetization of a material are known, the factors $(N_y - N_z)M_0$ and $(N_x - N_z)M_0$ may be experimentally determined from resonance measurements alone. There is currently a great deal of interest, however, in thin alloy films for which g and M_0 may not be accurately known, especially in regard to possible dependence of M_0 on film thickness for very thin films[6] for use in fast switching and computer storage applications.[7, 8] The combination of resonance and oscillation magnetometer measurements on such films should be a powerful means of investigating their magnetic properties, since the oscillation magnetometer may be used to determine both $(N_y - N_z)M_0$ and $(N_x - N_z)M_0$.

The oscillation magnetometer is not generally as accurate as a good torque magnetometer,[9] nor can it measure the angular dependence of anisotropy as accurately as can a torque magnetometer or ferromagnetic resonance experiments. However, it is considerably simpler, cheaper and easier to set up and use than either of the other methods, and it yields useful quantities of direct experimental interest. In many cases, oscillation magnetometer measurements on thin films evaporated and/or annealed in a magnetic field[10] to enhance their switching properties are quite sufficient to give all needed information on the isotropic and anisotropic magnetic properties of the film. Whenever there is a variation in magnetic properties through the thickness of a disk sample, magnetometer and resonance measurements may yield somewhat different values for $(N_y - N_z)M_0$, $(N_x - N_z)M_0$ and M_0. The magnetometer yields values for the above quantities averaged through the entire thickness. On the other hand, if the film thickness is greater than a resonance skin depth or so, resonance results pertain only to an

exponentially weighted part of the film within approximately a skin depth of the side being measured. Thus, the combination of oscillation magnetometer measurements and resonance measurements made separately for each surface of a film or disk can yield information concerning variation of magnetic properties in the thickness dimension. In the next section, it is shown how an oscillation magnetometer can be used to obtain $(N_x - N_z)M_0$ and M_0; then, in the final section some of the anisotropy factors which can be determined by oscillation magnetometers are tabulated.

DETERMINATION OF PLANAR ANISOTROPY

In the usual operation of an oscillation magnetometer, the rotation axis is the X-axis, taken along a diameter of the disk-shaped sample, and $(N_y - N_z)M_0$ and M_0 may be determined. This type of operation is termed the X-mode. There exists another type of operation, the Y-mode, however, which can yield information about anisotropy lying entirely in the plane of the disk. The disk again lies in a magnetic field with its plane parallel to the field direction, but rotation is now about the Y-axis passing through the centre of the disk. As shown below, the Y-mode of oscillation allows $(N_x - N_z)M_0$ and M_0 to be determined. If there is no planar anisotropy, any rotational position of the disk about the Y-axis will be a position of equilibrium and no oscillation will occur when the disk is slightly rotated. However, when planar anisotropy is present, there will exist one or more stable equilibrium positions and the disk and its container can be set into oscillation about such a position.

A scheme somewhat similar to the Y-mode of operation of an oscillation magnetometer has been suggested by Dahl and Pfaffenberger,[11] but was not used by them to obtain quantitative measurements of anisotropy. In the absence of damping, the period of oscillation for infinitesimal amplitude is given by the expression already presented. Damping arises from several sources. By using long thin Nylon threads for support, the damping and restoring torque from this source can be made negligible. Also air damping can be minimized by making the sample support rotationally symmetric. Finally, eddy-current damping is negligible at the frequencies of oscillation used, and rotational hysteresis[12] is zero as long as the magnetization of the specimen is saturated. It will, therefore, be a good approximation to neglect damping effects.

The calculation of Y-mode torque with damping neglected is carried out in the Appendix yielding, for a volume V,

$$L \simeq \frac{V(N_x - N_z)M_0^2 H_0}{H_0 + (N_x - N_z)M_0}\left(\frac{\sin 2\theta}{2}\right) \equiv \mathscr{T}_0\left(\frac{\sin 2\theta}{2}\right) \qquad (1)$$

where θ is the angle in the $X - Z$-plane, in which the specimen lies, between the Z-axis, fixed in the disk, and H_0, the applied field. This result is a good approximation as long as H_0 is appreciably larger than the anisotropy field $(N_x - N_z)M_0$ and the oscillation amplitude is of the order of 20° or less. To this approximation the system satisfies a simple pendulum equation in 2θ and the period of oscillation (for non-infinitesimal excursions) is[13]

$$\tau = 4K(k)\sqrt{(J/\mathscr{T}_0)} \qquad (2)$$

where $K(k)$ is the complete elliptic integral of the first kind, $k = \sin\theta_0$, and θ_0 is the amplitude of oscillation. For infinitesimal amplitude equation (2) becomes $\tau_0 = 2\pi\sqrt{(J/\mathscr{T}_0)}$.

Equation (2) can be rewritten in the useful form

$$\left[\frac{M_0 V}{16K^2(k)J}\right]\tau_e^2 = [(N_x - N_z)M_0]^{-1} + H_0^{-1} \qquad (2a)$$

where $\tau_e(\theta_0)$ is the experimentally determined period. Since J, V, τ_e, θ_0 and H_0 will be known in an experiment, this linear relationship between τ_e^2 and H_0^{-1} shows that both $(N_x - N_z)M_0$ and M_0 can be independently determined by plotting τ_e^2 *versus* H_0^{-1} for H_0 values sufficiently large for saturation to be maintained and for equation (1) to be a good approximation. Alternatively, if either of the above quantities is known, the other can be calculated from a single measurement of τ_e. For highest accuracy, it is still desirable, however, to measure τ_e up to as high fields as practical and extrapolate the resulting τ_e^2 dependence on H_0^{-1} to infinite field strength. If we further extrapolate the straight line obtained for high field strengths to the point where it cuts the negative H_0^{-1} axis, the quantity $(N_x - N_y)M_0$ is obtained directly from the H_0^{-1} axis intercept without any need to know the values of V, J and θ_0, provided θ_0 is the same for each τ_e measurement. It is of interest that for non-infinitesimal oscillations the time-average value of H_z is less than H_0, although the time average of H_x over an oscillation period is zero. The time dependence of θ is of the form $\theta(t) = \theta_0 \cos^{-1}\left\{dn[\sqrt{(\mathscr{T}_0/J)}t]\right\}$, where dn is a Jacobian elliptic function. When $\cos\theta$ is averaged over a period, given by equation (2), we obtain $\langle \cos\theta \rangle = \pi/2K(k) = 1 - (k/2)^2 \ldots$ Thus, $\langle H_z \rangle = \pi H_0/2K(k)$.

Equation (2a) is of the form previously obtained[1, 2] for the X-mode oscillation magnetometer with $4\pi^2$ here replaced by $16K^2(k)$ and $(N_y - N_z)M_0$ replaced by $(N_x - N_z)M_0$. Exclusive of stress and magnetocrystalline anisotropy differences between the latter two quantities, there is an important difference arising from shape effects for a circular disk-like sample. For a sample approximated as a spheroid very oblate in the Y-dimension, the shape contributions to the demagnetization factors are[3] $(N_x^s - N_z^s)M_0 = 0$ and $(N_y^s - N_z^s)M_0 \simeq (4\pi - 3\epsilon\pi^2)M_0$, where ϵ is the ratio of disk thickness to disk diameter. Thus, one measures $4\pi M_0$ plus small shape, magnetocrystalline anisotropy and stress terms in the X-mode, but only the latter terms in the Y-mode. Therefore, the Y-mode yields a more sensitive measure of anisotropy than does the X-mode, but the Y-mode period of oscillation is correspondingly greater.

The above difference may be illustrated by a comparison for nickel films between the X-mode period for $(N_y - N_z)M_0 = 4\pi M_0 \simeq 6100$ G and the Y-mode period with $(N_x - N_z)M_0 = 10$ G, produced by uniaxial stress or magnetocrystalline anisotropy. Consider a disk 1·6 cm in diameter and 0·1 μ thick and a container having a moment of inertia of 1 g cm^2 in either the X- or Y-mode. This value of J is near the minimum value obtainable with convenient sizes using container material with a density near unity. The X-mode period is 1·14 s, while that for the Y-mode is 19·9 s. An applied field H_0 of 6000 oersteds was used for these calculations. A period of 20 s is too long for both convenience and accurate measurement, but it can be reduced by making the container of low-density material such as foamed polystyrene which has a density of only about 0·03. With a moment of inertia of only 0·03, the above Y-mode period is reduced to 3·45 s, a practical value. A reduction of this order of magnitude has been observed experimentally using a foamed polystyrene sample holder. An accurate and convenient way to determine τ_e is to apply a low-frequency external torque coupled magnetically or electrically to the specimen or its holder, then vary the applied frequency until

resonant oscillation is noted, using optical-lever magnification of the motion.

These results indicate that anisotropy contributions of as little as 10 G in films $0{\cdot}1\ \mu$ thick or less can be detected in the Y-mode of operation. It should be noted, however, that equation (2) cannot be used to obtain both M_0 and $(N_x - N_z)M_0$ accurately and independently when $(N_x - N_z)M_0$ is much less than the saturation field strength of the material. Since the equation applies only for static field strengths greater than that required for saturation, within the applicable range H_0^{-1} will be almost negligible compared to $[(N_x - N_z)M_0]^{-1}$ for the above case. Nevertheless, if either M_0 or $(N_x - N_z)M_0$ is known, the other can still be determined from equation (2). Such determination, in conjunction with ferromagnetic resonance measurements,[10] should allow both quantities to be separately and unambiguously determined.

ANISOTROPY FACTORS

The table summarizes some of the relations between experimentally determined $(N_x - N_z)M_0$ and $(N_y - N_z)M_0$ factors and possible physical causes of anisotropy. It has been formed using results of a previous paper where the pertinent relations are derived for ferromagnetic resonance experiments.[3] In the table, stress results are given for polycrystalline material only and involve the isotropic magnetostriction constant λ. The results of Ref. 3 may be used when isotropic magnetostriction is not a good assumption. The stress T_0 is isotropic in the plane of the sample, while T is a directed stress lying in this plane parallel to the Z-axis. The stresses are positive for tension and negative for compression. The angle θ is measured in the plane from the Z-axis, and the stable equilibrium values of θ for a circular disk-shaped sample in the Y-mode are shown in column three of the table. Note that when $\lambda T < 0$, the Z anisotropy axis is a hard rather than easy magnetization axis, and equilibrium is then found at right angles to this axis. The internal fields $3\lambda T/M_0$ or $3\lambda T_0/M_0$ arising from stress in thin films can be as large as 10^3 G.[1, 4, 5] Only first order magnetocrystalline anisotropy constants K_1' and K_1 appear in the table for $(N_x - N_z)M_0$. The substitution of these values in equation (1) is only valid when $2K_1'/M_0$ and $2K_1/M_0$ are considerably less than the applied static field H_0, as pointed out in the Appendix. Further, the absence of the second-order magnetocrystalline anisotropy constants K_2' and K_2 in $(N_x - N_z)M_0$ is contingent upon either measurements with infinitesimal oscillation amplitude or the additional conditions $K_2' \ll K_1'$, $K_2 \ll K_1$.

Anisotropy type	*Y-mode* $(N_x - N_z)M_0$	*Stable equilibrium positions, θ*	*X-mode* $[(N_y - N_z) - 4\pi]M_0$
Isotropic plane stress ($X - Z$ plane)	0	All values	$\dfrac{3\lambda T_0}{M_0}$
Directed stress (Z-axis)	$\dfrac{3\lambda T}{M_0}$	$0, \pi \quad \lambda T > 0$ $\pm\dfrac{\pi}{2} \quad \lambda T < 0$	$\dfrac{3\lambda T}{M_0}\cos^2\theta$
Uniaxial magneto-crystalline anisotropy (Z-axis)	$\dfrac{2K_1'}{M_0}$	$0, \pi \quad K_1' > 0$ $\pm\dfrac{\pi}{2} \quad K_1' < 0$	$\dfrac{2K_1'}{M_0}\cos^2\theta + \dfrac{K_2'}{M_0}\sin^2 2\theta$
Cubic magneto-crystalline anistropy	$\dfrac{2K_1}{M_0}$	$0, \pm\dfrac{\pi}{2}, \pi \quad K_1 > 0$ $\pm\dfrac{\pi}{4}, \pm\dfrac{3\pi}{4} \quad K_1 < 0$	$\dfrac{K_1}{2M_0}(3 + \cos 4\theta) + \dfrac{K_2}{2M_0}\sin^2 2\theta$
Shape anisotropy $a \gg b \gg c$	$\dfrac{4\pi cM_0}{ae^2}\left[\dfrac{(2 - e^2)E - 2(1 - e^2)K}{(1 - e^2)^{\frac{1}{2}}}\right]$	$0, \pi$	$\left(\dfrac{-4\pi cM_0}{a}\right)\left[\dfrac{E - (1 - e^2)K}{e^2(1 - e^2)^{\frac{1}{2}}}(1 + \sin^2\theta) + \dfrac{K - E}{e^2}(1 - e^2)^{\frac{1}{2}}(1 + \cos^2\theta)\right]$

Except in the limit of high field strengths, the introduction of the N_x, N_y and N_z general demagnetization constants to describe second-order uniaxial magnetocrystalline anisotropy or first- and second-order cubic magnetocrystalline anisotropy is an approximation. For example, the effective internal field arising from uniaxial magnetocrystalline anisotropy with the anisotropy axis along the Z-axis may be written[3]

$$ {}^iH = {}^iH_z i_z = \underbrace{\left\{(2K_1'/M_0) + (4K_2'/M_0)[1 + (M_z/M_0)^2]\right\}}_{(M_z/M_0)i_z} $$

where i_z is a unit vector along the Z-axis. Since the second-order term involves $(M_z/M_0)^3$, ${}^iH_z$ cannot, in general, be set equal to $-N_zM_z$. If one attempts to calculate the torque for the oscillation magnetometer in the manner of the Appendix, but using the above expression for ${}^iH_z$ instead of $-N_zM_z$, one is led to an eighth-degree equation for M_z, analogous to the fourth-degree equation otherwise present. By making measurements at sufficiently high field strengths and extrapolating to infinite field strength if necessary, these difficulties may be avoided and the results given in the table will hold. The results for cubic magnetocrystalline anisotropy apply when the [001] crystal direction coincides with the Z-axis and when the plane of the disk is the (010) crystal plane. For other directions and planes the pertinent results may be obtained from Ref. 3.

The last row in the table applies to ellipsoidal samples of dimensions a, b, c along the Z-, X- and Y-axes, respectively. The demagnetization constants have been obtained from the work of Osborn[14]; the factors K and E are complete elliptic

integrals of the first and second kinds, both having the argument $e = [1 - (b/a)^2]^{\frac{1}{2}}$. For a circular disk $b = a$, and these results reduce to $(N_x - N_z)M_0 = 0$ and

$$[(N_y - N_z) - 4\pi]M_0 = -3\pi^2 cM_0/a$$

For an elongated ellipsoid with b appreciably smaller than a but still much larger than c, $(N_x - N_z)M_0$ reduces to approximately $(c/b)4\pi M_0$. If this quantity is of the order of 5 or 10 G, it should be possible to measure M_0 in a thin film of this shape quite accurately using the *Y*-mode of operation. Generally, however, other anisotropy effects in thin films will outweigh that of shape even in an elongated sample.

For the *X*-mode column, the values of $[(N_y - N_z) - 4\pi]M_0$ have been listed rather than $(N_y - N_z)M_0$. The $4\pi M_0$ factor is almost always the dominant term in $(N_y - N_z)M_0$. Therefore, the values listed in the last column usually represent relatively small corrections to $4\pi M_0$, and themselves cannot be determined as accurately as the corresponding factors in the *Y*-mode. However, angular dependence can be determined in the *X*-mode but not in the *Y*-mode. Here again θ measures the angle in the $X - Z$ plane between the applied magnetic field direction (no *X*-mode oscillation) and the *Z*-axis, fixed in the sample. By carrying out *X*-mode observations with a circular sample securely fixed in various angular positions with respect to the applied field direction, the correction terms listed in the last column of the table may be determined, provided their amplitudes are of the order of $0{\cdot}01(4\pi M_0)$ or greater.

REFERENCES

(1) MACDONALD, J. R. D.Phil. Thesis (University of Oxford, 1950).

(2) GRIFFITHS, J. H. E., and MACDONALD, J. R. *J. Sci. Instrum.*, **28**, p. 56 (1951).

(3) MACDONALD, J. R. *Proc. Phys. Soc.* [*London*] *A*, **64**, p. 968 (1951).

(4) MACDONALD, J. R. *Phys. Rev.*, **81**, pp. 312*A*, 329*A* (1951).

(5) GRIFFITHS, J. H. E. *Physica*, **17**, p. 253 (1951).

(6) CRITTENDEN, E. C., JR, and HOFFMAN, R. W. *Rev. Mod. Phys.*, **25**, p. 310 (1953).

(7) CONGER, R. L., and ESSIG, F. C. *Phys. Rev.*, **104**, p. 915 (1956).

(8) SMITH, D. O. *Phys. Rev.*, **104**, p. 1280 (1956).

(9) WILLIAMS, H. J. *Rev. Sci. Instrum.*, **8**, p. 56 (1937).

(10) MACDONALD, J. R. *Phys. Rev.*, **106**, p. 890 (1957).

(11) DAHL, O., and PFAFFENBERGER, J. *Z. Phys.*, **71**, p. 93 (1931).

(12) BRAILSFORD, F. *J. Instn Elect. Engrs*, **83**, p. 566 (1938).

(13) WOODS, F. S. *Advanced Calculus*, p. 370 (Boston: Ginn and Co., 1934).

(14) OSBORN, J. A. *Phys. Rev.*, **67**, p. 351 (1945).

(15) LANDAU, L., and LIFSHITZ, E. *Phys. Z. Sowjet.*, **8**, p. 153 (1935).

APPENDIX

Torque calculation for the Y-mode

The restoring torque $\boldsymbol{L}$ is given by

$$\boldsymbol{L} = V\boldsymbol{M} \times \boldsymbol{H}_0 = -V\boldsymbol{M} \times {}^i\boldsymbol{H} \tag{3}$$

where ${}^i\boldsymbol{H}$ is that part of the internal field not including the external field. The direction of the magnetization vector may be determined from the Landau–Lifshitz equation[15] which reduces very closely to

$$\boldsymbol{M} \times \boldsymbol{H}^i = \boldsymbol{M} \times (\boldsymbol{H}_0 + {}^i\boldsymbol{H}) = 0 \tag{4}$$

in the present low-frequency case. Its magnitude satisfies $|\boldsymbol{M}|^2 \equiv M_0^2 \simeq M_x^2 + M_z^2$, since M_y is very nearly zero. The total internal field components in the present case are $H_x^i = H_0 \sin\theta - N_x M_x$, $H_y^i \simeq 0$, $H_z^i = H_0 \cos\theta - N_z M_z$. Equations (4) now yields

$$M_x H_z^i = M_z H_x^i = M_x[H_0 \cos\theta - N_z M_z] = \\ = M_z[H_0 \sin\theta - N_x M_x] \tag{5}$$

or

$$M_x = \frac{M_z H_0 \sin\theta}{H_0 \cos\theta + (N_x - N_z)M_z} \tag{6}$$

On using the second part of equation (3), introducing the internal field expressions, and making use of equation (6), one finds

$$L = L_y = V(N_x - N_z)M_x M_z = \\ = \frac{V(N_x - N_z)M_z^2 H_0 \sin\theta}{H_0 \cos\theta + (N_x - N_z)M_z} \tag{7}$$

Finally, using equation (6) and the saturation condition, the equation determining M_z is found to be

$$[H_0 \cos\theta + (N_x - N_z)M_z]^2 = \\ = \left(\frac{M_z}{M_0}\right)^2 \left\{[H_0 \cos\theta + (N_x - N_z)M_z]^2 + H_0^2 \sin^2\theta\right\} \tag{8}$$

This is a fourth-degree equation in M_z. It may be readily solved to first-order in $[(N_x - N_z)M_0/H_0]$ provided this quantity is appreciably less than unity. The result is

$$M_z \simeq M_0 \cos\theta\left[1 + \frac{(N_x - N_z)M_0}{H_0} \sin^2\theta\right] \tag{9}$$

The torque L thus becomes, approximately

$$\left.\begin{aligned} L &\simeq \frac{V(N_x - N_z)M_0^2 H_0 \cos^2\theta \sin\theta\left\{1 + [(N_x - N_z)M_0/H_0] \sin^2\theta\right\}^2}{H_0 \cos\theta + (N_x - N_z)M_0 \cos\theta\left\{1 + [(N_x - N_z)M_0/H_0] \sin^2\theta\right\}} \\ &\simeq \frac{V(N_x - N_z)M_0^2 H_0 (\sin^2\theta/2)\left\{1 + [2(N_x - N_z)M_0/H_0] \sin^2\theta\right\}}{H_0 + (N_x - N_z)M_0 + [(N_x - N_z)M_0]^2 \sin^2\theta/H_0} \end{aligned}\right\} \tag{10}$$

This equation is correct to second-order in $[(N_x - N_z)M_0/H_0]$. Since, however, the terms in the numerator and denominator proportional to $[(N_x - N_z)M_0/H_0]^2$ are multiplied by sinusoidal factors which will be small for relatively small oscillation amplitude, these terms may usually be neglected. Equation (10) then reduces to equation (1) of the text.

Transfer of tungsten carbide to soft metals during single-traverse and reciprocating sliding

By J. Golden, B.Sc., Ph.D., and G. W. Rowe, M.A., Ph.D., Tube Investments Research Laboratories, Hinxton Hall, Cambridge

[*Paper received* 4 *September*, 1957]

This paper describes experiments in which a small radioactive tungsten carbide hemisphere was slid slowly over copper and steel plates. The tungsten carbide transferred to the plates was assessed by counting and autoradiography. On well-prepared copper about 50×10^{-12} g was transferred steadily to each millimetre of track during a single traversal. This carbide was firmly embedded in the copper, even after several traversals in each direction over the track. Single traversals on mild and stainless steels also produced steady embedded wear. However, when reciprocating traversals were made a considerable proportion of the transferred carbide was scattered loosely on the surface. It is suggested that the difference between the first and subsequent traversals on steels is due to the embedded particles acting as abrasives. It is thus important to distinguish between these two phases of wear.

It has long been known that when two metal specimens are rubbed together metal is transferred from one to the other and it has been demonstrated that fragments of a soft copper slider can be plucked out and will remain firmly attached to a hard steel plate.[1] Further experiments using radiotracer techniques[2] have shown that steel fragments may be transferred to copper. It has been shown that steel fragments transferred to steel are generally tightly adherent.[3]

Some recent experiments have shown that even such a hard material as tungsten carbide can be steadily worn away by copper, and that the transferred particles remain adhering to the copper. Stainless and mild steels also cause wear, but the transferred particles are loose when the slider reciprocates over the same track.

RESULTS

Tungsten carbide on copper. A small spherically-ended slider of tungsten carbide (94% tungsten carbide, 6% cobalt) was activated in a pile to give strong W187 activity. The slider was then carefully degreased and ten identical sliding tracks were made under a load of 1·5 kg on a smooth degreased copper block. Each track was about 2·25 cm long and the slider passed only once over each. The amount of activity transferred was assessed with a scintillation counter and an autoradiograph was also made by placing a photographic film in close contact with the block for several hours. When the film was developed it showed uniform blackening over the whole track region. Fig. 1(*a*) is a print of such an autoradiograph. The track images are white. It is found in other experiments that this smooth wear is common on well-prepared surfaces but that quite small defects such as pits, scratches, or inclusions could cause severe local increase in the wear.

The counter was calibrated with a small fragment of known weight, identical in composition with the slider, which had been activated at the same time. It was then found that the total amount of tungsten carbide which had been transferred to the block during sliding was 10^{-8} g. The resolution of the autoradiographic film is such that it is possible to detect irregularities in blackening greater than 20 μ across. The blackening nevertheless appears uniform in general, so we may consider the rate of wear as $10^{-8}/225$, or about 45×10^{-12} g/mm of sliding. To give an idea of the magnitude, if we assumed the wear to be absolutely uniform this would correspond to a layer about 2 Å thick.

Tracks were made on other similar copper blocks, which were then counted and showed about the same wear. The blocks were then subjected to mechanical shocks of increasing violence, ending with sharp hammer blows and a drop from one metre on to a steel plate. The amount of transferred tungsten carbide which could be detached from the blocks in these ways amounted to less than 4% of the total wear on any given block.

Tracks were then made with ten traversals of the slider in each direction. Again the amount of loose wear did not exceed a few percent. Fig. 1(*b*) shows the wear distribution on this specimen. The small areas of heavier wear represent the ends of the wear tracks.

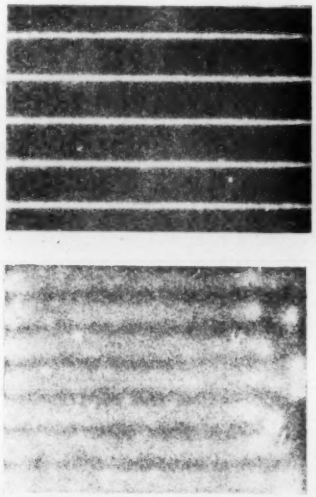

Fig. 1. An autoradiograph positive print showing transferred active tungsten (white regions). × 6

(*a*) A small tungsten carbide slider produced the tracks on smooth copper by sliding once over each.

(*b*) Transfer of carbide on to copper in tracks traversed ten times in each direction.

Tungsten carbide on mild steel. Similar tests were made with ten single traverses on mild steel blocks. Again a smooth steady wear was found on well prepared blocks [Fig. 2(*a*)] and the amount of transferred tungsten carbide which could be detached by mechanical shock was again not more than a few percent. The total wear on mild steel was found to be less than on copper, about 6×10^{-12} g/mm of sliding under comparable single-traverse conditions.

Fig. 2(*b*) shows that the character of the wear was changed when ten traversals in each direction were made on each sliding track. A considerable proportion of the wear was loose and was scattered over the block, no longer conforming to the sliding tracks. Indeed, the autoradiograph emulsion itself detached many of the loose fragments from the block.

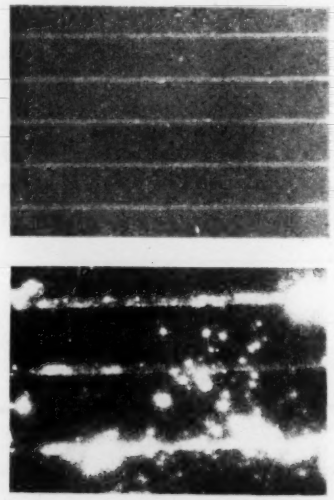

Fig. 2. Autoradiograph positive print showing transfer to mild steel

(*a*) Single traverses on each track.
(*b*) Ten traverses in each direction on each track.

Tungsten carbide on stainless steel. Fig. 3(*a*) shows the smooth wear produced by traversing a tungsten carbide slider once over each track on a stainless steel block. The amount of wear was comparable with that found on mild steel and only about one-fifth of that on copper. Again almost the whole of the transferred carbide was strongly bonded to the block.

The autoradiograph Fig. 3(*b*) shows that the wear is very uneven when a carbide slider is traversed ten times in each direction over each track. The total wear is very much heavier than that found on copper and loose fragments are scattered all over the block. About 30% of the total wear was removed by a small suction nozzle passed slowly over the block.

DISCUSSION

These experiments suggest that when copper, mild steel or stainless steel specimens are carefully prepared with mechanically smooth surfaces the wear of a tungsten carbide slider is sensibly uniform and that the transferred carbide is strongly bonded to the surface. Small defects, however, cause sharp local increase in wear and this may explain why

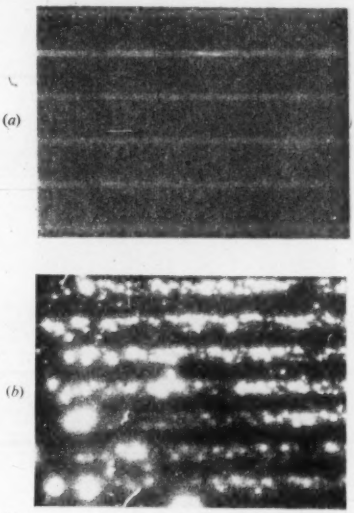

Fig. 3. Autoradiograph positive print showing transfer to stainless steel

(*a*) Single traverses on each track.
(*b*) Ten traverses in each direction on each track.

second and subsequent traversals over the same track give uneven wear. Small fragments of tungsten carbide left behind by the first traversal are embedded in the track and act as minute abrasives, which may knock fragments out by a mechanical action during further sliding. Such chips are apparently scattered freely over the surface and do not adhere to it. It is possible that with copper, which is much softer than steel, a greater number of these abrasive particles are pushed down well into the substrate material and so cause less damage to the carbide slider.

The wear process must this be considered to have two phases: (*a*) the initial steady wear on virgin metal, and (*b*) the more complicated adhesive and abrasive wear régime in subsequent sliding over the same track.

ACKNOWLEDGEMENTS

We wish to thank the Chairman of Tube Investments Ltd. for permission to publish this communication.

REFERENCES

(1) BOWDEN, F. P., MOORE, A. J. W., and TABOR, D. *J. Appl. Phys.*, **14**, p. 80 (1943).
(2) RABINOWICZ, E., and TABOR, D. *Proc. Roy. Soc. A*, **208**, p. 455 (1951).
(3) RABINOWICZ, E. *J. Appl. Phys.*, **24**, p. 367 (1953).

Correspondence

Temperature coefficient of maintenance potential of glow discharge voltage stabilizer and regulator tubes

The temperature coefficient of maintenance potential of a glow discharge tube refers to the effect of ambient temperature changes on the maintenance potential V_m of a tube run at a constant current. It is usually measured as dV_m/dT_e where T_e is the temperature of the outside of the tube envelope. Temperature coefficient effects were first studied by Jurriaanse[1] using a temperature range 20 to 40° C. The coefficients were negative and approximately constant. Jurriaanse calculated the variation in gas density in the vicinity of the cathode and showed that this could explain the observed variations in V_m. Measurements have since been made on a number of commercial voltage stabilizer and regulator tubes, mainly of the miniature type taking less than 60 mA current.[2,3] Water baths, oil baths or electric furnaces were used. The temperature was raised a few degrees and, after a fixed interval of time, V_m was measured. This procedure was repeated over the required temperature range. Although the coefficients below 100° C for most commercial tubes were negative, some positive coefficients were obtained.

Elevated temperatures cause drifting of V_m in some tubes, and a disadvantage of this method is that recorded changes in V_m are due not only to the temperature, but also to the length of time held at that temperature. In the present work the tube is normally held in a reference oil bath at 35° C. It is then plunged into one of six baths each held at a constant temperature covering the range 20 to 110° C. Variations in V_m are continuously recorded. After five minutes the tube is returned to the 35° C bath and allowed to return to the reference state. Cumulative drift effects are therefore avoided.

A number of commercial, miniature-type, voltage regulator and stabilizer tubes have been measured by this method over their current ranges given in published data. In most cases, as the temperature increases, the temperature coefficient commences negative, becomes zero at a critical temperature T_c, and is then positive. Benson reports cases in which a second reversal occurs. The value of T_c varies with gas composition and pressure, cathode material, tube geometry and discharge current. Temperature coefficients measured by Jurriaanse were approximately constant because the values of T_c applicable were much in excess of the highest temperature used.

The manner in which V_m reaches its equilibrium value on sudden increase of T_e is of interest. For most tubes an initial rapid decrease in V_m is followed by a slow increase. Special tubes in which the cathode temperature rises quickly to its new equilibrium value do not show this overshoot effect. The final value equals that obtained by slowly increasing T_e to the same temperature. A typical result for a type 85A2 tube at 5·5 mA is shown in Fig. 1. The effect is reversible.

Transient density changes are the most likely cause of this effect. The majority of voltage stabilizers and regulators are designed to have no anode fall. The greater part of V_m therefore appears across the cathode dark space, and will be dependent upon the gas density in this region of the tube, ρ_c. Sudden heating of the gas adjacent to the tube envelope will cause it to expand and increase ρ_c. The latter will then decrease according to two time constants owing to: (i) the gas quickly reaching a quasi-equilibrium state, and (ii) the cathode temperature slowly rising by an amount approximately equal to the change in envelope temperature. The final value of ρ_c will be greater than the initial value; i.e. $d\rho_c/dT_e$ is positive, ρ_c approaching a constant value, that for zero density gradient within the tube, as T_e approaches infinity. $dV_m/d\rho_c$ can be shown to be negative and therefore dV_m/dT_e, if caused by density changes only, would be negative,

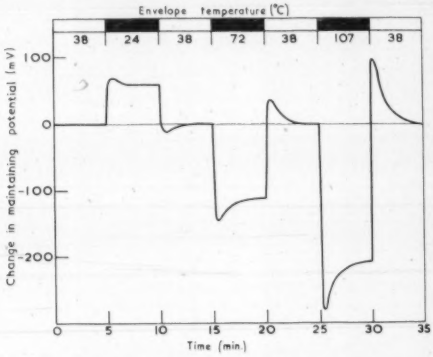

Fig. 1. Effect of changes in envelope temperature on maintaining potential for a type 85A2 tube

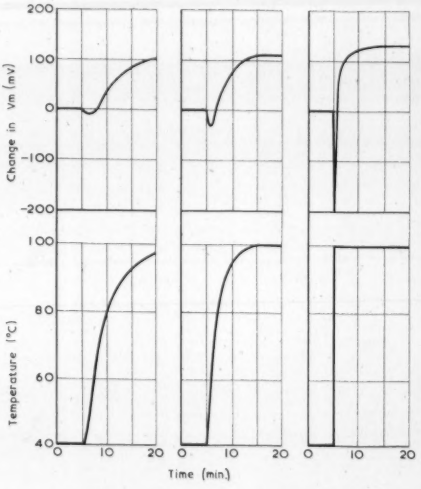

Fig. 2. Effect of rate of rise of envelope temperature on maintaining potential for a type 150B2 tube

approaching zero as T_e approaches infinity. We conclude that, although the phenomenon described indicates that density changes can cause appreciable changes in V_m and must be a contributory cause of temperature coefficient, there must be other effects present which tend to increase V_m as T_e is increased. Explanations based upon the release of contamination from the walls of the tube on increase of T_e are not consistent with the reversible nature of the effect.

An interesting result of the phenomenon is that sudden changes in T_e will cause V_m to alter over a range greater than that previously observed for gradual changes in T_e. Changes in V_m for a type 150B2 tube at 10·0 mA with different rates of rise of T_e are shown in Fig. 2. For high rates of change, V_m alters over a range greater than twice the difference between the equilibrium values.

Acknowledgements are made to the Director of Mullard Research Laboratories for permission to publish this note.

Mullard Research Laboratories, Salfords, Surrey.

J. SMITH

[12 November, 1957]

REFERENCES

(1) JURRIAANSE, T. *Philips Res. Rep.*, **1**, p. 407 (1946).
(2) KIRKPATRICK, G. M. *Proc. Inst. Radio Engrs*, **35**, p. 485 (1947).
(3) BENSON, F. A., and BENTAL, L. J. *Wireless Engr*, **33**, p. 33 (1956).

Comments on the A.S.T.M. Powder Data File—3

The writers have now prepared a third booklet, bearing the above title, which contains further additions to the lists previously published and described in the Institute's journals.* Copies of the present booklet are being distributed in the same way as were the others. Those who do not receive copies of the booklet in this way may obtain them (free of charge) on request from the Institute or from us.

It is hoped that similar lists of comments will be published at approximately annual intervals. Users of the Data File are urged to send to the writers any material that they feel should be included in future issues.

Viriamu Jones Laboratory, University College, Cardiff, S. Wales.

J. W. HUGHES
ISABEL E. LEWIS
A. J. C. WILSON

[12 February, 1958]

* HUGHES, J. W., LEWIS, ISABEL E., and WILSON, A. J. C. *J. Sci. Instrum.*, **34**, p. 211 (1957). *Brit. J. Appl. Phys.*, **8**, p. 173 (1957).

New books

The first nuclear engineering and science congress. Vol. 1. Problems in nuclear engineering. Vol. 2. Reactor operational problems. Edited by D. J. HUGHES, S. MCLAIN and C. WILLIAMS. (London: Pergamon Press Ltd., 1957.) Pp. Vol. 1, 365. Vol. 2, 278. Price: £6 per volume, £10 per set.

Each of these two companion volumes consists of a collection of papers grouped into sections covering various nuclear reactor problems. The Engineers Joint Council in the U.S.A. —comprising the major institutions in the field—organized a meeting held in December, 1955, closely following the International Conference in Geneva that year, which was designed for American scientists and engineers and to supplement the Geneva papers with others of a more engineering flavour. Many of the papers have appeared individually in various journals, but the publishers intended these volumes to be a collection of the most significant and original ones, and set their editors the invidious task of making a suitable selection from the 358 papers presented at the Congress. It is not possible within the scope of a review notice to examine each paper and to give detail comment on such a range of material. Attention will therefore be directed to the general content of the papers selected and any of outstanding interest.

Volume 1 consists of four sections, the first of which is entitled "site selection, safety and economics". There are in fact no papers on economics and those on site selection are of an introductory nature only. In addition to some general discussions of factors affecting safety, there is an elementary paper on shielding design and one on health precautions. A further paper outlines the mode of working of the Reactor Safeguards Committee in the U.S.A., but for the design engineer perhaps the most interesting article discusses "a proposed structural design basis for nuclear reactor pressure vessels". The editors admit that this section has two noticeable gaps—the first a lack of information on hazards due to chemical fires with reactor materials, the second the design of the containment vessel, a universal item in all major reactors in the U.S.A.

The second section is entitled "material," and by intent deals with materials and their properties rather than testing methods. It is much more technical in nature than the first section, containing some quite specialized papers as well as the review type. Various fuel materials, mainly uranium and its alloys but including ceramics, are discussed, structural materials are considered, and there are two papers on graphite. Only one paper on thorium is presented. Liquids are represented by discussion of water decomposition by fission recoils, and by several papers on liquid metals and their corrosion characteristics. The editors must have had considerable difficulty in making their selection for this section.

The heading for the third section is "design" and it illustrates in some respects the difficulty that always exists in writing about design. The papers range from detailed discussion of components to analysis of power cycles and general surveys of reactor types. Two interesting papers deal with zirconium welding, and the fabrication of the zirconium core tank for the ORNL homogeneous reactor. Two literature surveys rather surprisingly complete the section.

A short section of heat transfer papers concludes this volume. Two papers deal with experimental results, one on boiling in horizontal channels, one on heat transfer for water flowing parallel to a bank of tubes. Two analytical papers consider stability of flow in parallel channels, and there is one dealing with calculation of heat generation by radiation in reactor components, a complicated subject which it is hardly possible to do justice to in such compass.

Volume 2, entitled somewhat strangely "reactor operational problems," contains four sections, the first of which deals largely with waste disposal. There is some duplication of the material here, and the papers are mainly of the general survey type, covering water treatment and waste processing,

storage and disposal problems, and finally fall-out monitoring, and a survey of health physics literature.

The second section contains sixteen papers on chemical processing, ranging from dissolution of solid fuels through chemistry and engineering of aqueous processing to the special processing of fluid fuel systems of the aqueous and liquid metal types, and ending with papers on pyrometallurgical and electrolytic processing, and on fluoride volatility methods. There is a paper on design of active plant for maintenance, and one on pulsed column operation.

In the third section are papers on reactor physics, including critical assemblies and exponential experiments. General items are on experimental comparison of U^{235} and U^{233}, reactor kinetics and determination of source strengths. Sub-critical and critical assemblies are examined for their use as measuring devices for sections of other fuel elements and lattices, and there are two papers on the determination of breeding ratio referring to EBR.I which are of interest.

The final section on control and instrumentation is a rather mixed selection covering some general papers on instruments and their use, the considerations needed in devising a reactor control system, including a paper on calculation of control rod effectiveness, and some studies of overall power cycle control systems.

In compiling these volumes, the editors have selected about one quarter of the papers originally presented; even though they have obviously made an effort to balance the contents, it is inevitable that some unevenness is still present, and in places some overlapping. The range of subject-matter is very wide and the range in paper content from the elementary survey to the highly technical in the various areas make it a little uncertain as to the reader at whom these books are aimed. Interesting though many of the papers are, it is unlikely that more than a fraction will become works of reference, and in such a developing field, the price will force the private reader to consider carefully whether he can afford to have these volumes to dip into as needed for general interest, since such collections are scarcely in the nature of genuine textbooks.

J. SMITH

La diffusion dans les metaux. Edited by J. D. FAST, H. G. VAN BUEREN and J. PHILIBERT. (Eindhoven: Philips Technical Library, 1957.) Pp. 124. Price 37*s*. 6*d*.

In this book are published eleven papers originally presented at a colloquium at Eindhoven in September 1956. The introductory survey by A. D. Le Claire deals briefly with the theoretical and practical bases of the study of diffusion in a manner which many lecturers and young research workers will find attractive. Similarly, P. Lacombe gives an authoritative account of diffusion in grain and low-angle boundaries and its relationship to their structure. It is fairly easy to show preferential grain-boundary diffusion and its qualitative dependence upon orientation difference between grains, but refinement of techniques will be necessary in order to test the hypotheses which are advanced. J. L. Meijering discusses how our detailed knowledge of the diffusion of interstitial atoms in binary solid solutions may be used in the study of more complicated systems.

The remaining papers present new experimental results on the Kirkendall Effect, grain-boundary diffusion, interstitial diffusion, and the effect of elastic strain upon diffusion. Needless to say, the contributions are of variable quality but all merit the serious attention of specialists in the field of diffusion.

The book is attractively produced but its price seems rather high.

T. BROOM

Digital computer programming. By D. D. MCCRACKEN. (New York: John Wiley and Sons Inc.; London: Chapman and Hall Ltd., 1957.) Pp. vii + 253. Price 62*s*.

This is a well written and attractively produced text on the elementary aspects of computer programming, but the reviewer would join issue with the author and the publishers on the following points. Firstly, because it is untrue to claim, as is done on the dust jacket, that this is "The first general introduction in book form . . .", and secondly, because the author's invention of an artificial machine for his illustrations means that readers will have to re-learn the coding process for any machine which they actually use, particularly in Europe where decimally based machines are rare.

The author mentions the handbooks supplied by machine manufacturers, and the fact that these usually cover the same ground as the book and are issued without charge will combine with the high price in restricting its interest in this country.

A. D. BOOTH

Journal of Scientific Instruments

Contents of the March issue

ORIGINAL CONTRIBUTIONS

Papers

The Venturi pneumatic pyrometer. By A. M. Godridge, R. Jackson and G. G. Thurlow.

A nuclear magnetometer. By G. S. Waters and P. D. Francis.

The emergent column correction in mercury thermometry. By J. A. Hall and Vera M. Leaver.

A vibrating condenser manometer. By J. L. Williams and G. F. Eveson.

A simple tensile testing machine for very fine wires. By A. E. Widdowson.

Diffusion measurements by a sampling technique. By P. H. Elworthy.

An airflow interrupter for respiratory work. By L. E. Mount.

Anti-reflexion coatings for indium antimonide and other semi-conductor filters. By S. D. Smith and T. S. Moss.

A feedback-controlled Pirani gauge. By J. H. Leck.

Laboratory and workshop notes

A graphite resistance furnace for physicochemical studies up to 2200° C. By J. D. Mackenzie and J. O'M. Bockris.

An X-ray collimator for single-crystal goniometers. By E. N. Maslen.

The reduction of misalignment voltage in Hall measurements. By L. W. Davies.

An insulated vacuum lead-in using an O-ring. By W. D. Edwards.

An electron gun alinement and mounting technique. By L. C. Robinson.

The closure of high pressure vessles; a hydraulic high-torque torque wrench. By E. Whalley, A. Lavergne and R. Goton.

Removal of signal fluctuations in a photoelectric polarimeter. By A. R. Downie.

A variable ratio, tape-coupled, recording microdensitometer. By P. C. Russell and J. E. Wilson.

NOTES AND NEWS

Correspondence

A method for measuring transistor current gain at radio frequencies. From F. J. Hyde.

A digital recording system for measuring the electrical properties of semiconductors. From R. H. A. Carter, D. J. Howarth and D. H. Putley.

The sectioning of hard keratinous substances. From F. Happey and J. H. Keighley.

New instruments, materials and tools — New books

Manufacturers' publications — Notes and comments

THIS JOURNAL is produced monthly by The Institute of Physics, in London. It deals with all branches of applied physics (including theory and technique).
All rights reserved. Responsibility for the statements contained herein attaches only to the writers.
EDITORIAL MATTER. Communications concerning editorial matter should be addressed to the Editor, The Institute of Physics, 47 Belgrave Square, London, S.W.1. (*Telephone:* Belgravia 6111.) Prospective authors are invited to prepare their scripts in accordance with the *Notes on the preparation of contributions*. (Price 2*s*. 6*d*. including postage.)

REPRODUCTION. The Institute of Physics is a signatory to The Royal Society's Fair Copying Declaration. Details may be obtained upon application from The Royal Society, London, W.1.

ADVERTISEMENTS. Communications concerning advertisements should be addressed to the agents, Messrs. Walter Judd Ltd., 47 Gresham Street, London, E.C.2. (*Telephone:* Monarch 7644.)

CLAIMS FOR MISSING JOURNALS. Claims from regular subscribers to this *Journal* for missing numbers will only be considered if received within 60 days of the date of mailing plus normal outward time of transit and time for lodging the claim. Losses attributable to failure to notify a change of address or to similar omissions will not be considered.

SUBSCRIPTION RATES. A new volume commences each January. The charge is £5 per volume ($14.25 U.S.A.), including index (post paid), payable in advance. Single parts, so far as available, may be purchased at 10*s*. each ($1.50 U.S.A.), post paid, cash with order. Orders should be sent to The Institute of Physics, 47 Belgrave Square, London, S.W.1, or to any bookseller.

SPECIAL ARTICLE

The mechanical wear of metals*

By W. Hirst, B.Sc., Ph.D., F.Inst.P., Associated Electrical Industries Ltd., Aldermaston, Berks.

The design of fundamental experiments for examining the wear phenomena encountered in the conditions of speed and loading of industrial machines is discussed. Apparatus is described in which nominal point or nominal line contact can be maintained indefinitely, and some of the phenomena observed when a lubricant is used are discussed. With carefully run-in specimens, the hydrodynamic condition of lubrication is maintained up to very heavy loads; a method of measuring the thickness of the oil film in line contact conditions is outlined and some results given. In unlubricated conditions the phenomena of wear can be studied using simpler equipment. The main phenomena, the laws and the mechanisms of wear in unlubricated conditions are discussed, and the present state of development of theories of wear is outlined. In conclusion, some suggestions are made about the directions in which fundamental studies of wear need to be pursued.

Mechanical wear takes many forms and its study is confused by the large number of factors which influence a wear rate. In compensation there are large rewards to be obtained, for it is one of the few subjects in which a tenfold improvement can sometimes reasonably be expected. This is because the wear rates of materials range so widely. In unlubricated conditions the range is as much as a millionfold, whilst for an individual combination of materials a small change in the rubbing conditions may change the wear rate by one or two orders of magnitude.

Wear is a problem of great practical importance; the depreciation due to wear and tear in man's total accumulated capital assets, at a rate of several per cent per annum, constitutes one of the largest costs of this industrial civilization; depreciation due to mechanical wear comprises an important part of this. Although it can be argued that it is desirable to replace plant and equipment periodically in the interests of efficiency, it is nevertheless better to be able to do this when one chooses than to have it forced upon one by wear and tear. Because of its practical importance a great many investigations of mechanical wear have already been made, but the subject is still receiving far less attention from scientists than its importance merits. The weakness of the subject is that, whilst there is a most voluminous literature amply illustrating its complexity, an underlying framework of scientific principles has not clearly emerged. This is probably because the amount of effort exerted on empirical testing has far outweighed that put into studying the fundamentals of the subject.

Previous investigations fall into three classes—those using full or reduced-scale machinery, those using test rigs designed to simulate practical operating conditions, and fundamental investigations. Work with full-scale machinery gives information which can be applied directly to practice. This method is convenient when one is interested in relatively small machines, such as motor car engines, but it is less so for examining the behaviour of large components such as marine gears. Large systems are more conveniently studied by means of a test rig which simulates the operating conditions, but the use of this method confronts the experimenter with a paradox. Full-scale testing and simulated testing are commonly employed when the operating conditions are thought to be too complicated for fundamental study. The paradox is that without the fundamental understanding it remains uncertain whether or not the test rig succeeds in simulating the operating conditions.

Early fundamental investigations of wear were primarily devoted to determining the manner in which variables such as load, speed and atmosphere affect the wear rates. It was soon learned that the number of variables is considerable and the picture of wear phenomena which emerged showed little discernible pattern. In the years since the war there has been a renewed interest in the fundamental approach. This interest is timely for, with the development of the techniques of electron microscopy and of radioactive tracers, it has at last become possible to examine in detail the mechanisms by which wear occurs. In this article, the approach developed by the author and his colleagues is described. The objective was to extend fundamental investigations to provide a background of knowledge against which the behaviour of machinery could be considered.

CHOICE OF EXPERIMENTAL METHODS

In designing experiments it needs to be remembered that the wear phenomena in a machine may change during its working life, that machines often operate at high speeds and that their elements have various shapes. The first requirement, therefore, is that an experiment must continue for an adequate period of time and during this period the surfaces will wear to some extent. This introduces a difficulty, particularly when a lubricant is used, if it is desired to obtain fundamental information. The nature of the difficulty is most readily seen by considering an example. Fig. 1 depicts a simple rubbing system consisting of a flat block *a* loaded against a rotating ring *b* and lubricated with oil from a bath *c*.

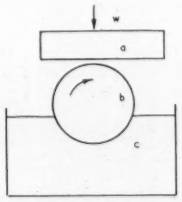

Fig. 1. A simple wear apparatus

a, flat block; *b*, rotating ring; *c*, oil bath; *w*, load.

* Based on a lecture given to the London and Home Counties Branch of The Institute of Physics in Aldermaston on 31 October, 1956.

Initially contact is made along a line and the local stresses in the block and ring are high. As wear occurs, a scar forms on the block, its size increasing with time, and the stresses diminish. Simultaneously, the proportion of the load supported hydrodynamically by the oil changes so that the remaining load, which alone produces wear, changes also. The magnitude of the hydrodynamic lift depends upon the size of the wear scar, on its conformity to the ring, and on the clearance. The clearance depends upon the surface finish which in turn is related to the manner in which the materials wear. It is clear that whilst experiments using this system might be useful as empirical tests, they are of little fundamental value except when the lubricant is omitted or at speeds so small as to render hydrodynamic effects insignificant: otherwise not only do the conditions change with time, but it is also practically impossible to determine what they are. The first problem therefore is to devise methods of making extended experiments in definable conditions despite the fact that the materials wear.

Since machine elements have various shapes, wear experiments are needed in systems having different geometry. Fortunately, it may not be essential to study many systems. Machine elements either conform or they do not. If they do not, nominally they engage either along a line or at a point. If they conform, they will either be separated by a relatively thick oil film, as in full hydrodynamic lubrication, or will be in local contact, as in thin film or boundary lubrication or when running without lubricant. In full hydrodynamic conditions, wear is negligible but otherwise it occurs mainly where raised features on the surfaces make local encounter. The majority of these local contact areas will again approximate to lines or points. However, with conforming surfaces there may be complications owing to the fact that the total applied load is supported upon a distribution of contacts instead of on a single one. These arguments suggest that a great many of the elementary features of the operation of machines could be examined by making experiments in line and also point contact provided these conditions could be maintained. In addition special problems with distributed contacts might require separate study.

ROLLING AND SLIDING

Machine elements operate with a variety of motions and this has to be considered also. Conforming surfaces can only slide but non-conforming surfaces also roll. Some non-conforming machine elements, such as gear teeth, engage with a motion which is a combination of both rolling and sliding. One of the main features characterizing these forms of motion is the distance a point on one surface slides over the other during the engagement. In rolling it is nominally zero but it increases as the motion changes towards pure sliding. The distance of sliding has an important influence on the tendency of the surfaces to become damaged whilst they are in contact.

The importance of the sliding distance can be illustrated by considering the nature of the damage between surfaces which are loaded together normally and the change which occurs when they are displaced tangentially. Holm[1] has shown that when clean degassed metals are placed in contact in a vacuum, they will adhere. Usually the adhesive forces are not very great but Bowden and Rowe[2] have shown that they can be raised to an appreciable fraction of the loading force by annealing the metals whilst they remain in contact. However, admission of a trace of air before contact allows a thin oxide layer to form on the metal surfaces and destroys adhesion. Metal surfaces as used in engineering are generally covered with relatively thick films of oxide or other contaminant and in general do not adhere. The adhesion is destroyed because under normal load only, surface films remain intact. Thus Cocks,[3] from measurements of the electrical contact resistance, calculated the maximum extent of breakdown of the oxide films on metals normally loaded together, and quite commonly derived values less than 10^{-7} of the total contact area. Even with surfaces so rough that the surface markings were visibly deformed, values between 10^{-2} and 10^{-7} were obtained. There is, therefore, little tendency for the metals underlying the surface films to break through them and weld together. Kerridge[4] demonstrated this directly by measuring the extent of metallic transfer after a radioactive copper hemisphere had been loaded against an inactive copper flat. Degreased specimens showed no significant transfer at loads up to 30 kg, whilst even at 160 kg it amounted to only $2{\cdot}7 \times 10^{-9}$ g, despite the fact that there had been sufficient bulk flow of the copper to form a dent $1{\cdot}9$ mm^2 in area. In contrast it may be noted that, in sliding, under a load of only 1 kg, the transfer was about 1×10^{-6} g/cm.

This small degree of penetration of the surface film, despite extensive bulk flow, appears surprising, but an argument due to Crook[5] helps to show why it can happen. When curved surfaces are loaded together the point of maximum shearing stress lies beneath the surface,[6, 7] and at a sufficient load this is the point where flow begins. It has generally been supposed that when the load is increased further the plastically deformed zone spreads above and below this point. Crook, however, points out that the effect of flow is, in fact, to relax the surface stresses and they remain within the elastic limit. The plastically distorted zone does not rise but instead penetrates deeper and deeper into the material. With materials which work-harden this simple picture is modified somewhat because of the increase in the yield stress as deformation proceeds.[8] Fig. 2 shows a metallographic section

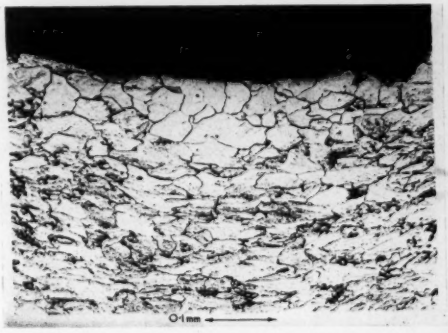

Fig. 2. Normal section through an impression in Armco iron produced by a $\frac{1}{8}$ in. diameter ball bearing at a load of 2000 lb

by Dr. Welsh taken through an impression in Armco iron produced by loading a $\frac{1}{8}$in. diameter ball bearing against it with a force of 2000 lb. Although this load is some hundreds of times greater than that needed to initiate flow and produces very severe deformation in the iron, the photograph

shows clearly that there is a thin layer near the surface in which the crystalline structure remains almost unaffected.

In sliding, the friction superposes a tangential component on to the stress distribution and in these circumstances the shearing stress in the surface may become very close to the maximum shear stress.[9] It is then to be expected that the surface films will become disrupted and extensive inter-metallic contact will occur. Experiment shows[10] that when the normal load is sufficient to cause extensive bulk flow, large scale, continuous rupture of the surfaces results. When the load is within the elastic limit, the stresses at some surface irregularity may, nevertheless, locally exceed the yield stress, and a small weld may form and then grow as sliding continues. From this it follows that the frictional forces at the onset of sliding are typical of contaminated surfaces, and that as sliding proceeds the coefficient of friction in general changes.

Different frictional phenomena and different degrees of surface damage are therefore to be expected in mechanical systems in which the sliding distance is short, as with a pair of spur gears, from those in which it is long, as with a piston in a cylinder. The effect of sliding distance is conveniently studied in a friction apparatus in which the specimens are cylinders, one inclined at 45° to the direction of sliding, the other being mounted on a turntable (Fig. 3). The sliding distance is varied by rotating the turntable. Such an apparatus has been designed by Dr. Archard and results obtained with it show that the influence of the sliding distance can indeed be very great (Fig. 4). This, therefore, is a factor which must be borne in mind when attempting to design experiments intended to show the probable behaviour of a material in a particular type of machine. The dependence of the extent and nature of the surface damage on the distance of sliding is probably the main reason for the well-known difference between the behaviour of materials in rolling and in sliding. In pure sliding very effective lubrication must be provided, whereas rollers will often operate satisfactorily with hardly any lubrication at all. Moreover, the stresses which can safely be imposed on sliding elements are very small in comparison with those which can be carried by rollers.

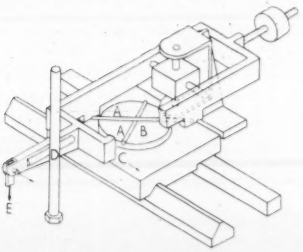

Fig. 3. Crossed cylinder friction apparatus

AA', cylindrical specimens; *B*, turntable; *C*, direction of sliding; *D*, friction measuring element; *E*, point of application of the load.

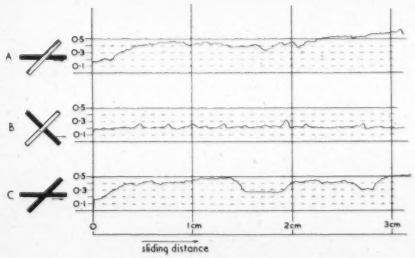

Fig. 4. Crossed cylinders friction apparatus

Friction records corresponding to the specimen arrangements shown at *A*, *B* and *C*. With *A* and *C* the sliding distance is long, with *B* it is short. Upper specimen 0·4% carbon steel; lower specimen 1·5% nickel, 1% chromium steel unlubricated. Speed 0·05 cm/s. Loads: *A*, 10 kg; *B*, 7·5 to 25 kg; *C*, 10 kg.

CONTINUOUS RUBBING IN CONDITIONS OF POINT CONTACT

To maintain nominal point contact conditions indefinitely a fairly complicated apparatus is required. Dr. Archard and Mr. Tillen have designed a machine in which the test specimens are cylinders both rotating with their axes crossed at 90°. Simultaneously, one cylinder reciprocates in a direction at 45° to its axis (Fig. 5), the reciprocating motion being deliberately

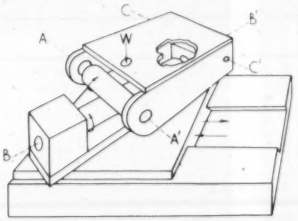

Fig. 5. Schematic diagram of crossed cylinders wear machine

AA', upper specimen axis; *BB'*, lower specimen axis; *CC'*, fixed pivot axis, *W*, load.

unrelated to the speed of rotation. Each point of the surface of each cylinder therefore rubs against the other, so that although the specimens wear they retain their cylindrical form. In this way point contact conditions are maintained and, since wear changes the diameter of the cylinders very little, the stresses are also effectively constant. The sliding distance can be varied by varying the speed of rotation of one cylinder with respect to the other.

Exploratory experiments with this apparatus show that at light loads, after careful running-in, the electrical contact resistance between lubricated specimens can be very high, some tens of thousands of ohms. As the load is increased the oil film begins to break down locally giving temporary excursions of the contact resistance to low values, one ohm or less. Eventually at heavy loads low resistances below one ohm are observed all the time. At sufficiently heavy loads, the lubrication fails and the surfaces become heavily damaged; this is commonly termed "scuffing." This general pattern of events is influenced by the speed; at low speeds the low resistance region extends over a considerable range of loads, but at higher speeds scuffing may follow almost immediately after the electrical resistance begins to fluctuate to low values. The variation of the scuffing load with speed is shown in

Fig. 6. The experiments show two rather surprising effects. The first is that although point contact conditions are not favourable for good lubrication, nevertheless, when enough care is taken to run-in the surfaces, loads sufficient to cause extensive plastic flow can be supported over long periods of

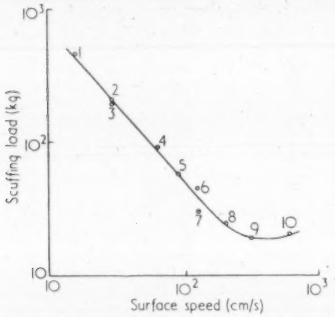

Fig. 6. Scuffing loads of 3·8 cm diameter mild steel specimens as a function of speed: The average values of the electrical resistance for the experimental points are as follows:

1, $\ll 0{\cdot}1\ \Omega$; 2 and 3, $< 0{\cdot}1\ \Omega$; 4, 50 Ω; 5, not measured; 6, 100 Ω; 7, $3 \times 10^4\ \Omega$; 8 and 10, $10^4\ \Omega$; 9, $2 \times 10^3\ \Omega$.

running without the surfaces seizing. Examples of the flow produced are shown in Fig. 7. The second point is that the very high electrical contact resistances which can be observed clearly denote some form of hydrodynamic lubrication. Simple hydrodynamic theory, assuming rigid bodies and an

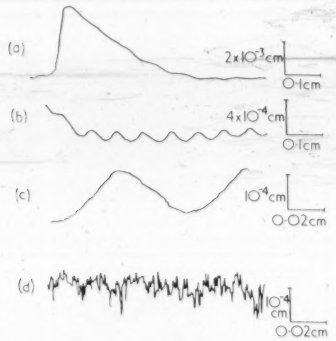

Fig. 7. Plastic flow in mild steel without scuffing

(*a*) Accumulation of material at the end of track.
(*b*) Plastic flow in track.
(*c*) Surface finish of track.
(*d*) Original surface finish.

oil of constant viscosity, predicts that the load which can be supported in point contact conditions is given by[11]

$$W = 2{\cdot}4\eta VR\left(\frac{2R}{h_0}\right)^{\frac{1}{2}} \qquad (1)$$

where η is the oil viscosity, V is the sum of the surface velocities at the contact (i.e. the rate at which oil is dragged into the contact), R is the local relative radius of curvature of the surfaces and h_0 is the minimum thickness of the oil film. A high resistance film has been observed at loads up to some tens of kilograms and, on substituting the experimental values for W, η, V, and R in the formula, one obtains a value for h_0 of about one ångström unit. This value is incompatible with a condition of hydrodynamic lubrication and, clearly, hydrodynamic theory for point contact conditions requires considerable development.

LINE CONTACT

Phenomena in conditions of line contact are conveniently studied in a disk machine of the type described by Merritt[12] and illustrated in Fig. 8. The disks are loaded together at the periphery and, by controlling their speeds independently, either rolling or rolling with sliding may be obtained.

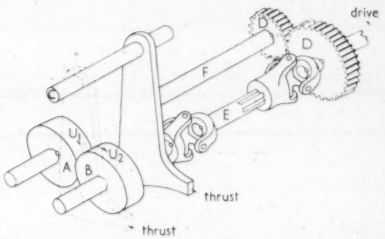

Fig. 8. Disk machine

A, fixed cylinder; *B*, cylinder suspended from pivot *C*; *D*, gears determining slide/roll ratio; *E*, cardon shaft; *F*, fixed shaft, U_1, U_2, disks.

Machines of this kind are often used for simulating the conditions at a chosen instant during the engagement of a pair of spur or helical gear teeth. In these gears pure rolling occurs at the pitch line, but above and below this line sliding also occurs, the direction of sliding reversing at the pitch line.

For many years the mechanism of lubrication of gears has been a subject for argument. The practical fact that gears often show the original machining marks after many years of running suggests that they operate in conditions of hydrodynamic lubrication, and electrical contact resistance measurements using a disk machine[13] support this suggestion. Nevertheless, elementary hydrodynamic theory[14] assuming rigid disks gives the following expression,

$$F = 2{\cdot}448\eta r(u_1 + u_2)/h_0 \qquad (2)$$

where F is the load per unit face width, η is the viscosity of the oil, r is the relative radius of curvature of the disks, u_1 and u_2 are their peripheral speeds and h_0 is the minimum film thickness. If values corresponding to practical operation are inserted, the calculated film thickness is usually about 10^{-5} in. or even less. The inaccuracies in manufacture exceed this value so that one might expect the surface irregularities to penetrate the films and the gears to operate under conditions of boundary lubrication.

However, the inadequacy of the simple theory is shown by the fact that it predicts the development of pressures in the

oil film of the same order of magnitude as the elastic limit of the disk materials. Under such stresses, the disks would deform and the hydrodynamic forces therefore ought to be calculated for the deformed shape. Moreover, pressure changes the viscosity of oils and a complete mathematical analysis of the problem needs to allow for this also; it should, moreover, allow for the viscosity change due to the heat generated by the shearing of the oil film and for the conduction of some of this heat into the material of the disks. Very serious attempts have been made to give consideration to these factors,[15] but no complete solution of this extremely complicated problem has yet been obtained.

Crook[16] has found recently that it is possible to measure the oil film thickness between the disks by a method which does not rest upon the uncertainties in these theories. If the capacitance between the disks is measured, the film thickness can be derived once the dielectric constant of the oil and the shape of the gap is known. The dielectric constant of a non-polar oil is not likely to be changed by the temperatures and pressures by more than say 20%; the main problem is that the shape of the gap is unknown. Fortunately, after passing between the conjunction of the disks, the oil film divides to form thin sheets of oil on the surface of each disk. Very lightly loaded plane pads can be made to float upon these films and the capacitance between these pads and the disks can be measured. Because there is no appreciable load, the pads remain sensibly undeformed; the shape is therefore known and the film thickness can be derived. Therefore, from the capacitance between the disks and the pads, a measure of the oil film thickness at the conjunction of the loaded disks may be derived. A check on the method is provided by measuring the capacitance between the disks themselves when they are loaded so lightly as to be sensibly undeformed. This also provides a means of determining for the first time the range of validity of Martin's elementary theory.

Dr. Crook's experiments show that as the load is increased the first departure from elementary theory arises from the increase in viscosity of the oil due to the pressures developing. Later the pressures rise sufficiently to cause the disks to deform noticeably and, finally, the oil film thickness becomes independent of load. In the last stage an increase in load increases the width of the flattened conjunction of the disks sufficiently to compensate for the tendency to diminish the oil film thickness. Fig. 9 shows the variation of film thickness with load for rolling conditions. A particularly interesting feature of Dr. Crook's work is that he shows that the film thickness is influenced far more by changes in the overall temperature of the disks, than by changes in the temperature in the heavily loaded zone where the properties of the oil are so abnormal. This suggests that the oil film thickness is primarily determined by the hydrodynamic phenomena at the entry side of the disks. If this were to be confirmed it might speed the development of an adequate theory of line lubrication because it is at the entry side, before the oil drastically changes its properties, that the conditions are definable with least uncertainty.

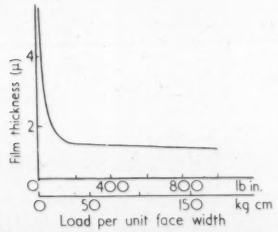

Fig. 9. The thickness of the hydrodynamic film between rolling disks as a function of load

Disk diameter, 3 in.; peripheral speed 597 cm s^{-1}; oil to Admiralty specification OM100; inlet temperature of oil 50° C; viscosity of inlet oil 0·4 P.

THE LAWS OF UNLUBRICATED WEAR AND THE INFLUENCE OF MATERIAL PROPERTIES

The above experiments have also shown that hydrodynamic support up to heavy loads can only be obtained on carefully prepared or run-in specimens. If a heavy load is applied to a rough surface immediately after the onset of running, the subsequent events depend on the manner in which the materials wear. If the surface irregularities reduce in size as the experiment proceeds hydrodynamic conditions will ultimately be achieved. If this does not happen the usual consequence is early catastrophic failure. It is clear, therefore, that the achievement of adequate lubrication depends on the properties of the solid materials as well as on the properties of the oil.

Wear experiments in lubricated conditions are very sensitive to the conditions of lubrication, and it is easier to obtain a picture of the way in which material properties influence wear from experiments made in unlubricated conditions. Also, of course, the study of the wear of unlubricated materials has its own intrinsic importance. The apparatus needed is simpler and many useful conclusions can be drawn from experiments using a pin and ring apparatus such as is shown in Fig. 10. Two general types of wear can be observed, a

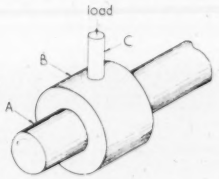

Fig. 10. Schematic diagram of pin and ring wear machine

A, rotating shaft; *B*, ring, $\frac{5}{16}$ in. diameter; *C*, flat-ended $\frac{1}{4}$ in. diameter pin, pressed under load against ring.

mild type and a severe type. In severe wear the surfaces remain metallic in appearance; there is extensive tearing, the wear fragments are of the order of tenths of a millimetre in size, and the structure of the rubbing metals is disrupted to a comparable depth. In mild wear, the surfaces often become discoloured, the wear fragments are usually smaller than one micron and, in a normal section, there is no distortion of the underlying structure visible in the optical microscope. Fuller descriptions of these two forms of wear have been given by Archard and Hirst.[17]

In general, the change in the nature of the surfaces produced by rubbing causes the wear rate to change with time, until an equilibrium surface condition has been achieved,[18] but thereafter it becomes constant and independent of the apparent area of contact. This behaviour has now been

observed a great many times and the author believes that the statement "In constant surface conditions, the wear rate is independent of the apparent area of contact" can be regarded as a law of wear. A second law follows from this if it is taken together with the fact that reproducible wear rates can be obtained. Two wear machines running side by side would together give twice the wear in either. But since the wear rate is independent of the apparent area of contact, the load on one could be transferred to the other and the wear rate remain the same; i.e. the wear rate should be directly proportional to the load. This behaviour is not generally observed because increasing the load on a specimen may change the surface conditions, notably by changing the temperature. However, Dr. Lancaster[19] has measured the wear rates in severe conditions for a number of materials at slow speeds so as to minimize frictional heating. Fig. 11 shows that in

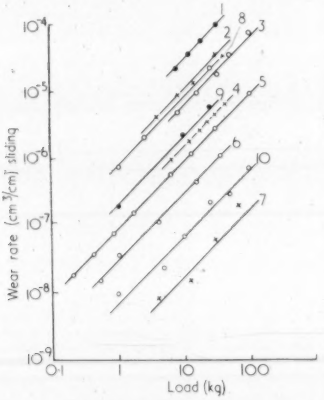

Fig. 11. Variation of severe wear rate with load

35 cm/s: Curve 1, cadmium on tool steel; curve 2, silver on copper; curve 3, zinc on tool steel; curve 4, 0·5% tellurium–copper on tool steel; curve 5, 60/40 leaded brass on tool steel; curve 6, titanium on tool steel; curve 7, stellite 12 on tool steel. 0·15 cm/s: Curve 8, gold on nickel; curve 9, platinum on nickel; curve 10, tungsten on stellite 20.

these conditions quite accurate proportionality between wear rate and load may often be observed.

Mild wear seems to occur when rubbing produces a surface skin which protects the underlying metals against welding. Thus severe wear tends to occur more readily when running in evacuated vessels, whilst if it already occurs under normal atmospheric conditions, it may be inhibited by raising the temperature. Fig. 12 shows an example of results obtained in a wear apparatus which could be heated by means of a surrounding electric furnace; the wear rates start to increase when the metal is made sufficiently hot to begin to soften, but on heating further oxidation phenomena predominate and the wear rate drops by the order of a thousand.[20] As is well known, at high speeds of sliding, frictional heating alone is sufficient to induce high temperatures at localized regions of the surface,[21] and at these temperatures the surface layers may not only react with the atmosphere, but also undergo phase transformations. On steels the changes may be very marked and Fig. 13 shows an example of a martensitic layer formed on the surface of 0·8 carbon steel. The original surface hardness was raised by a factor of about three whilst the wear rate was reduced some thirty times.[8]

The development of radioactive tracer techniques and availability of facilities for irradiation of metal specimens in

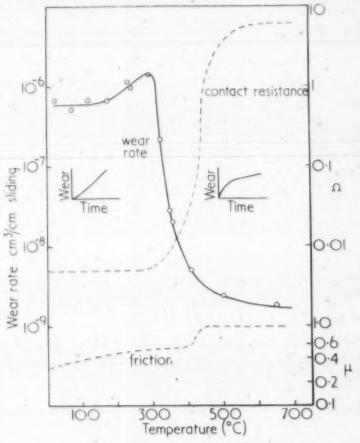

Fig. 12. Variation of wear rate with temperature for 60/40 brass on tool steel

the pile has now made it possible to determine the details of the mechanism of wear processes. Three detailed studies have been made,[22, 23, 24] and it appears that wear particles may sometimes be the result of a sequence of processes and are not always the product of a single event. Thus, in a study of the severe wear of brass on steel Kerridge and

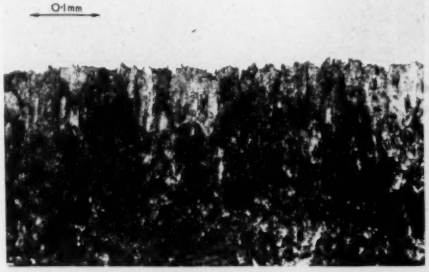

Fig. 13. Martensitic layer formed on the surface of 0·78% carbon steel after sliding unlubricated at 200 cm/s under a load of 1 kg

Lancaster[23] found that small fragments of brass were transferred to the steel, other fragments subsequently transferred adding to the original one, and finally the whole aggregate

was knocked off to form a loose wear particle. These authors also obtained a measure of the size of the individual contact regions supporting the load by a method devised by Dyson and Hirst.[25] The size of the individual fragments transferred was considerably greater, indicating that during the instant of transfer the load tended to become concentrated at the region of damage. This is one of the ways in which phenomena with distributed loads can differ from those when the load is supported upon a single point. In a study of the mild wear of tool steel on itself, Archard and Hirst[24] observed that the mechanism of wear changed with time. Initially it appeared similar in mechanism to that of brass, but on a reduced scale. The scale of the wear processes diminished with time ultimately reducing to events occurring on a scale of size of the order of a hundred ångström units; wear was then mainly due to a process of abrasion. To examine the later stages in the wear process, the electron microscope had to be used.

In the sequence of processes leading to the production of a wear particle, one stage in the sequence may exert predominating control of the overall wear rate. However, these three investigations show that wear particles may be produced in more than one way and by more than one sequence of ways. Investigations of this kind could with profit be extended until the main types of wear mechanism are understood in detail. Without this knowledge it seems difficult to envisage how to determine what are the minimum values to which it is in principle possible for the wear rates of materials to be reduced or how to try in practice to approach these rates as nearly as possible.

THEORIES OF WEAR

Holm[1] made the first attempt to develop a theory of wear. In its original form it related the wear rate to the number of interatomic encounters occurring during sliding, but as Holm recognized, the treatment was capable of extension as experimental information about the nature of wear became available. The hypotheses introduced by Archard[26] now seem to provide the best basis for the interpretation of the experimental evidence. Archard's theory rests on the fact that the true area of contact between surfaces is generally small compared with the apparent area, so that during sliding there is a series of encounters as localized regions of the surfaces come temporarily into true contact. The essential concepts of the theory are that at each encounter a wear particle either forms or does not, the magnitude of the probability of formation being represented by a constant K, and that the wear particle is a lump of material with dimensions comparable with those of the local contact area. If the wear particle is assumed to be a hemisphere with a radius equal to that of the contact region, assumed circular, the wear rate W equals KPs/p_m where s is the sliding distance, P the applied load and p_m is the flow pressure of the softer material.

The theory therefore predicts that the wear should be directly proportional to the sliding distance and the load, and independent of the apparent area of contact. With the qualifications given earlier, this is in conformity with the experimental evidence. The theory does not give any direct indication of the expected variation of wear rate with hardness because the probability constant K may also be expected to depend upon the material. When different metals are examined in similar states of wear[27] it is observed experimentally that there is a general tendency for K to decrease with hardness. Experiment also shows[17] that the value of K is always very small, ranging from 10^{-2} to 10^{-7}, so that any individual localized area in the surface must be loaded many times without suffering damage by wear.

Archard's treatment clearly requires modification to allow for the fact that the wear process may involve several stages and in a recent theory by Rightmire[28] the wear process studied by Kerridge has been examined. In Kerridge's experiment the wear of a soft tool steel pin loaded against a hardened tool steel ring was studied. The wear process comprised three stages, transfer from pin to ring, oxidation of the transferred material, and rubbing-off of the oxide to form a loose wear product. Rightmire was able to formulate by statistical methods an expression for the rate of removal of the layer as oxide, assuming that this occurred by a succession of small stages. The numerical constants in his expression were determined from the experimental transfer/time curve and the diameter of the wear particles could then be predicted to be about fifty ångström units; this value was in accord with his estimates of the thickness of oxide film which would grow in the intervals between its removal as wear particles. It is to be expected, as more becomes known about the sizes and distribution of the individual areas of true contact between loaded surfaces, that the use of statistical methods will be extended and that theories of the collision processes will be developed analogous to those of collision processes in other conditions. The predominant problem remaining, and one which a complete theory will have to solve, is to account for the absolute magnitude of the wear rate. All existing theories of wear merely relate the number of collisions to the rate of wear. Some additional physical postulates concerning the difference in nature between the collisions which do and those which do not produce a wear particle now need to be introduced.

DISCUSSION

Although the experiments and results referred to above provide only a mere outline of wear phenomena, they nevertheless appear to the author to provide a basis from which a fundamental background to the subject can be developed. The crossed cylinders wear apparatus provides a method of maintaining point contact conditions despite wear, and enables protracted experiment to be made under conditions of constant stress. It thus combines the precision and control required in a fundamental experiment with the facility to operate with the speeds and loadings used in machinery. This apparatus appears to offer a better means than has existed previously for determining the phenomena of wear quantitatively in relation to the speed, temperature, load, stress and material properties, and for determining which of these, or other variables are to be regarded as independent.

The disk machine, although originally devised as a practical test for examining the behaviour of gear materials, has also proved suitable for fundamental work. It provides an excellent experimental method for studying the fundamentals of hydrodynamic lubrication in thin film conditions, and Dr. Crook's work indicates that it will be possible to develop a very complete picture of the phenomena which occur in these conditions. His work needs, however, to be extended to include other oils with different pressure viscosity relationship and metals of varying resistance to deformation.

The studies of unlubricated wear show that in certain conditions the rules of wear are extremely simple, i.e. the wear rate is independent of the apparent area of contact

and is directly proportional to the load. It is also possible to study the mechanisms of wear in detail and preliminary attempts have been made to develop theories of wear. The next experimental objective appears to be to investigate systematically over a wide range of load, speed and temperature, and in different atmospheres, the wear characteristics of materials. This should show the main phenomena of wear, and it is to be hoped that it would also show the manner in which wear rates depend upon the properties of the rubbing materials. Theoretically, the important problem is to find how to predict the absolute magnitude of a wear rate.

REFERENCES

(1) HOLM, R. *Electric Contacts* (Uppsala: Almquist and Wiksells, 1946).

(2) BOWDEN, F. P., and ROWE, G. E. *Proc. Roy. Soc. A*, **233**, p. 429 (1956).

(3) COCKS, M. H. *Proc. Phys. Soc.* [*London*] *B*, **67**, p. 238 (1954).

(4) KERRIDGE, M. *Proc. Isotopes Techniques Conference, Oxford*, 1951, vol. II (London: H.M. Stationery Office, 1952).

(5) CROOK, A. W. *Nature* [*London*], **178**, p. 755 (1956).

(6) HERTZ, H. *Miscellaneous papers* (London: Macmillan, 1896).

(7) TIMOSHENKO, S. *Theory of Elasticity*, pp. 337, et seq. (New York: McGraw Hill Book Co. Inc., 1934).

(8) WELSH, N. C. *Proc. Conference on Lubrication and Wear*, I.Mech.E. (London: Institution of Mechanical Engineers, October 1957).

(9) PORITSKY, H. *J. Appl. Mech.*, **17**, p. 191 (1950).

(10) HIRST, W., and LANCASTER, J. K. *Proc. Roy. Soc. A*, **223**, p. 324 (1954).

(11) HOWLETT, J. *J. Appl. Phys.*, **17**, p. 137 (1946).

(12) MERRITT, H. E. *Proc. Instn Mech. Engrs*, **129**, p. 146 (1935).

(13) CROOK, A. W. *Proc. Instn Mech. Engrs*, **171**, p. 187 (1957).

(14) MARTIN, H. M. *Engineering*, **102**, p. 119 (1916).

(15) GRUBIN, A. N. *Central Scientific Research Institute for Technology, and Mechanical Engineering, Book No.* 30 (Moscow, 1949).

(16) CROOK, A. W. *Phil. Trans Roy. Soc.* In press.

(17) ARCHARD, J. F., and HIRST, W. *Proc. Roy. Soc A.*, **236**, p. 397 (1956).

(18) HIRST, W., and LANCASTER, J. K. *J. Appl. Phys.*, **27**, p. 1057 (1956).

(19) LANCASTER, J. K. *Proc. Conference on Lubrication and Wear* (London: Institution of Mechanical Engineers, October 1957).

(20) LANCASTER, J. K. *Proc. Phys. Soc.* [*London*] *B*, **70**, p. 112 (1957).

(21) BOWDEN, F. P., and RIDLER, K. E. W. *Proc. Roy. Soc. A*, **154**, p. 640 (1936).

(22) KERRIDGE, M. *Proc. Phys. Soc.* [*London*] *B*, **68**, p. 400 (1955).

(23) KERRIDGE, M., and LANCASTER, J. K. *Proc. Roy. Soc. A*, **236**, p. 250 (1956).

(24) ARCHARD, J. F., and HIRST, W. *Proc. Roy. Soc. A*, **238**, p. 515 (1957).

(25) DYSON, J., and HIRST, W. *Proc. Phys. Soc.* [*London*] *B*, **67**, p. 309 (1954).

(26) ARCHARD, J. F. *J. Appl. Phys.*, **24**, p. 981 (1953).

(27) HIRST, W. *Proc. Conference on Lubrication and Wear* (London: Institution of Mechanical Engineers, October 1957).

(28) RIGHTMIRE, B. G. *Trans A.S.M.E.*, **79**, p. 1242 (1957).

The geometry of twisted multi-filament structures

By G. J. STANSFIELD, Dunlop Cotton Mills Ltd., Rochdale

[*Paper first received* 27 *September, and in final form* 5 *November*, 1957]

A self-consistent geometry of cords made from multi-filament yarns is derived from the assumption that all filaments in a cord follow an epihelical path. This path is defined mathematically using a definition of ply twist not considered before, which leads to simpler formulae than those developed by previous workers. Formulae for changes in ply length, ply twist and cord length on cording are derived which enable the retraction of cords and yarns on twisting to be predicted accurately. An experimental method of cord twisting (simple twisting) is described which enables a simple experimental verification of this theory of twist to be carried out.

LIST OF PRINCIPAL SYMBOLS

α, yarn constant, proportional to yarn radius.
a, cord radius.
b, ply or yarn radius.
n, ply twist.
n, s, ply or yarn twist.
s, initial yarn twist.
N, cord twist.
ρ_n, ρ_s, ply or yarn retracted length per unit untwisted yarn length.
P, cord retracted length per unit untwisted ply length.
θ, cord folding angle.
r, radius of filament helix.
ϕ, angular position of ply axis.
ξ, angular position of filament with respect to ply axis.
σ, filament length.
λ, ply axis length.
z, cord axis length.
ψ, angle between filament and ply axis.
γ, initial parameter of epihelix.
y, untwisted yarn length.

A large proportion of industrial textiles is used as reinforcement material for rubber and plastics. These textiles are principally used in cord form, these cords consisting of two or more twisted plies twisted together. In the study of properties of textile cords such as strength, elongation and modulus it is necessary first to establish a system of co-ordinates which will enable the geometrical form of the cords to be characterized unambiguously. This paper establishes such a system of co-ordinates for multi-ply multi-filament cords, whose number of filaments (greater than 400) per ply is much greater than the number of plies (two to five).

It should be noted that this geometry applies only to systems which may be described as bundles of continuous strings, a string being defined as a body capable only of sustaining a tensile force and not a torsional or flexural couple. The theory probably does not apply exactly to a system of corded monofilament rubber, for example.

The differential geometry of the non-uniform simple helix and epihelix is first discussed in this paper and the equations obtained are then applied to derive relations between the lengths and twists of cords and their plies using an idealized model of a cord, in which it is assumed that the filaments follow epihelical paths. Experiments on the retraction of rayon tyre cords are described and it is shown that their results support the formulae derived from the mathematical model. It is concluded that this model represents the materials considered, within close limits.

It is first necessary to define precisely the meaning of twist in a ply of a multi-ply cord. This definition must (*a*) conform with intuitive ideas concerning twist in yarns, (*b*) lead to mathematically consistent formulae and (*c*) lead to experimentally correct formulae. Intuitively the idea of twist for a continuous filament yarn may be obtained by considering an ordinary twist tester. In this instrument a measured length of twisted yarn is fastened between a rotatable clamp and a movable carriage, the carriage being loaded to secure a uniform tension in the yarn. The yarn is now untwisted by rotating the clamp until the filaments in the yarn are parallel to each other. The number of revolutions necessary to untwist the yarn is then taken to be the turns of twist in the yarn and the "twist" is defined as the number of turns of twist per unit twisted length of yarn.

This intuitive definition of twist in a single yarn leads to the mathematical one. Consider one filament in a yarn, RPQ (Fig. 1), then each point on the filament can be fixed by the length of EP and the angle which EP, perpendicular

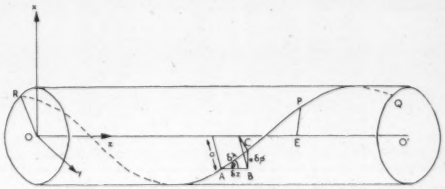

Fig. 1. A simple helix

to the yarn axis OO', makes with an initial line OR in the Oxy plane.

If ξ is the angle between OR and EP, then the filament would have made $\xi/2\pi$ revolutions between O and E. If λ is the length of the yarn axis between O and E the twist of the yarn is $(1/2\pi)(\xi/\lambda)$. This is the mean yarn twist between O and E. The twist at a point may be defined as $(1/2\pi)(d\xi/d\lambda)$. It is now necessary to extend this concept to a yarn, the axis of which is twisted into a helix, that is, a yarn made into the ply of a cord.

In Fig. 2(*a*), CC' is the axis of a cord ply, the cord axis of which is OO'. The filament RP is twisted round the ply

axis CC' which is itself twisted round the cord axis OO'. If $OO' = z$ and $O'C'$ makes an angle ϕ with OC, then the cord twist may be defined by analogy with the yarn twist as $(1/2\pi)\,(d\phi/dz)$. The ply twist is now defined as $(1/2\pi)\,(d\xi/d\lambda)$ where λ is the length of the ply axis from C to C' and ξ is the angle through which the radius vector generating the filament rotates between $C'P$ and CR.

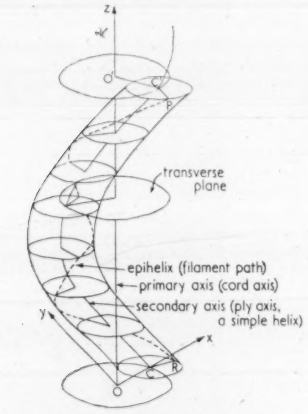

(*a*)

(*b*)

Fig. 2. (*a*) An epihelix. (*b*) Model used to illustrate the definition of ply twist

The above definition of cord twist agrees with those previously adopted by Woods,[1] Treloar[2] and others, but the ply twist definition does not. It has been customary to define ply twist in terms of the tortuosity of the ply axis and the torsion in the ply. This is equivalent to defining the ply twist as $(1/2\pi)\,(d\xi/d\lambda)$ where ξ is the angle turned through by a vector perpendicular to the ply axis and passing through the filament as that vector passes along the ply axis from C to C'. It will be seen from Fig. 2 that the vector used for defining ply twist in this paper is perpendicular to the cord axis and not the ply axis. A simple model may be constructed to illustrate the position of the plane containing the radius vector generating the path of a filament.

Two bundles of braided spindle band were prepared, each containing several strings. Each bundle was then twisted separately in the same direction and the same amount. A circle was then marked round one of the bundles in a plane perpendicular to the axis of the bundle. Finally the two bundles were twisted together to make a cord. The result of these operations is shown in Fig. 2(*b*).

It can be seen that the circle of section remained approximately perpendicular to the cord axis and not the ply axis throughout the cording operation. This suggests that the path of the filament should be described by vectors rotating in a plane perpendicular to the cord axis (the transverse plane) and not the ply axis.

Imagine any cord crossed by two transverse planes a distance δz apart. Let the length of ply axis of any ply intercepted between these planes be $\delta\lambda$ and let the untwisted length of yarn in the ply intercepted between these two planes be δy.

Then $(\delta z/\delta y)$, $(\delta\lambda/\delta y)$ both exist as the planes move together and ultimately coincide. Hence we define the following parameters of the cord *at that transverse plane*.

$$P = dz/dy \text{ the cord retracted length}$$

$$\rho_n = d\lambda/dy \text{ the ply retracted length}$$

$$n = (1/2\pi)(d\xi/d\lambda) \quad N = (1/2\pi)(d\phi/dz) \text{ the ply and cord twists} \qquad (1)$$

and θ the folding angle, which is the angle between the ply axis and the cord axis at that transverse plane.

THE SIMPLE NON-UNIFORM HELIX

This helix is generated by a rotating vector of length a advancing along the Oz axis rotating at a rate $d\phi/dz$ which need not necessarily be constant. At any transverse plane on the Oz axis (that is, any plane parallel to the Oxy plane) the helix makes an angle θ with the Oz axis.

Imagine two transverse planes δz apart along the Oz axis and an arcual length $\delta\lambda$ apart along the helix itself. We then have a differential triangle ABC (Fig. 1) in the surface of the cylinder on which the helix is drawn where $CB = a\delta\phi$, $AB = \delta z$, $AC = \delta\lambda$ and angle $CAB = \theta$. So

$$\tan\theta = a\frac{d\phi}{dz} \quad \sin\theta = a\frac{d\phi}{d\lambda} \quad \cos\theta = \frac{dz}{d\lambda} \qquad (2)$$

THE NON-UNIFORM EPIHELIX

Having defined the simple non-uniform helix above and derived the geometrical properties of it necessary to the discussion in this paper, the curve which is postulated to be the path of a filament in a multi-filament structure is now studied. It has been suggested that the curve be called a non-uniform epihelix.

The epihelix is generated by a vector of length r which, whilst remaining throughout in a plane parallel to the Oyz plane, rotates about a point, the locus of which is a simple non-uniform helix with the properties discussed above.

In any transverse plane the parametric equations of the epihelix are:

$$x = a\cos\phi + r\cos(\gamma - \xi)$$

$$y = a\sin\phi + r\sin(\gamma - \xi)$$

Where ϕ, ξ are the angles made by the simple helix vector and the epihelix vector with the Ox axis and γ is the initial value of ξ at $z = 0$ (ϕ and ξ are measured in opposite senses). If σ is an arcual length measured along the epihelix

$$\left(\frac{d\sigma}{d\lambda}\right)^2 = \left(a\frac{d\phi}{d\lambda}\right)^2 + \left(r\frac{d\xi}{d\lambda}\right)^2 - 2ar\frac{d\xi}{d\lambda}\frac{d\phi}{d\lambda}\cos(\phi + \xi - \gamma) + \left(\frac{dz}{d\lambda}\right)^2$$

Hence substituting relations (2)

$$\left(\frac{d\sigma}{d\lambda}\right)^2 = 1 + \left(r\frac{d\xi}{d\lambda}\right)^2 - 2ar\frac{d\xi}{d\lambda}\sin\theta\cos(\phi + \xi - \gamma) \quad (3)$$

As y varies from 0–2π this equation gives the value of $(d\sigma/d\lambda)^2$ at the transverse plane for the family of epihelices which pass through the circumference of a circle of radius r, the centre of the circle being on the simple helix.

Hence the mean value of $(d\sigma/d\lambda)^2$ for all such epihelices is:

$$1 + [r(d\xi/d\lambda)]^2 \quad (4)$$

Since the mean value of $\cos(\phi + \xi - \gamma)$, as γ varies from 0–2π, is zero [see Appendix (iii)].

MODEL OF A CORD

A cord is assumed to consist of plies, the axes of which describe helices about the cord axis whose filaments describe epihelices about the ply axes.

The following further assumptions are made:

(i) the "m" filaments are distributed uniformly across the cross-section of a ply, that is, the number of filaments crossing unit cross-section of the ply is the same for all parts of that cross-section;

(ii) the parameters of each epihelix described by a filament, i.e. $d\phi/dz$ and $d\xi/d\lambda$ are the same;

(iii) the ply retracted length ρ_n is a mean* of the components of length along the ply axis per unit ply axis length of all the filaments.

We can on these assumptions obtain a relation between ρ_n, the ply retracted length, and n, the ply twist.

Consider a transverse plane of a cord and an annulus of the ply, drawn in that plane, of radius r (less than the ply radius) and thickness dr. This annulus contains $2\pi mrdr/\pi b^2$ filaments [by assumption (1)] and since, by assumption (2), the twists of all the filaments is then the same for the filaments in this annulus, the mean value of $(d\sigma/d\lambda)^2 = 1 + 4\pi^2n^2r^2$ by definitions (1) and formula (4).

Hence a mean value* of $d\lambda/d\sigma$ for these filaments is $1/\sqrt{(1 + 4\pi^2n^2r^2)}$.

Hence a mean value* of $d\lambda/d\sigma$ for all the filaments in the ply

$$= \frac{1}{m}\int_0^b \frac{2mrdr}{b^2\sqrt{(1 + 4\pi^2n^2r^2)}} = \frac{2}{(2\pi nb)^2}\left\{\sqrt{[1 + (2\pi nb)^2]} - 1\right\}$$

and by assumption (3)

$$\rho_n = \left(\overline{\frac{d\lambda}{d\sigma}}\right) = \frac{2}{(2\pi nb)^2}\left\{\sqrt{[1 + (2\pi nb)^2]} - 1\right\} \quad (5a)$$

Inverting this equation and writing $\alpha = 2\pi b$ we get

$$\alpha n = (2/\rho_n)\sqrt{(1 - \rho_n)} \quad (5b)$$

* This mean value is not an arithmetic mean—see Appendix (i).

This equation gives the relation between ρ_n and n involving only one experimental constant, α, which is proportional to ply radius.

Also from definitions (1) and relations (2)

$$\tan\theta = 2\pi aN \quad (6)$$

and

$$P = \rho_s\cos\theta \quad (7)$$

These three last equations are the fundamental geometrical relations for a cord and are applicable at any transverse plane of the cord *even though the cord be irregular.*

TWIST CHANGES DURING CORDING

Consider two yarns each having s turns of twist per unit length lying parallel to each other and fixed rigidly together at each end. Let one end of this combination be fixed and the other end rotated about an axis mid-way between the yarns. Consider two transverse planes δz apart in the cord.

Fig. 3 shows one of the transverse planes, cord axis O, ply axis C_1 and filament P where OX is a line parallel to the

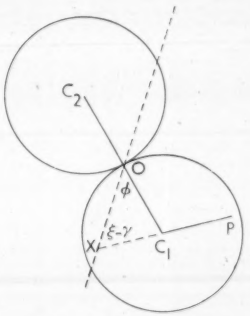

Fig. 3. A transverse plane

Ox axis. For the process of twisting decribed above (which we call compound cord twisting) the angle OC_1P is unchanged during the twisting. It follows that since C_1P, OC_1 make angles ϕ, $\xi - \gamma$ with the Ox axis, where ξ is measured in the opposite direction to ϕ, then $\phi + \xi - \gamma = c$ where c is a constant independent of the cord twist for a compound twisting operation.

By the definition of n, ρ_n, N and P [equations (1)]

$$n\rho_n + NP = \frac{1}{2\pi}\left(\frac{\partial\xi}{\partial y} + \frac{\partial\phi}{\partial y}\right)$$

Differentiating with respect to cord twist, N

$$\frac{\partial}{\partial N}(n\rho_n + NP) = \frac{1}{2\pi}\frac{\partial}{\partial N}\left(\frac{\partial\xi}{\partial y} + \frac{\partial\phi}{\partial y}\right) = \frac{1}{2\pi}\frac{\partial}{\partial y}\left(\frac{\partial\xi}{\partial N} + \frac{\partial\phi}{\partial N}\right)$$

[see Appendix (ii)].

But $\phi + \xi$ is independent of cord twist for compound twisting.

Hence $$(\partial/\partial N)(n\rho_n + NP) = 0$$

So $n\rho_n + NP$ is independent of cord twist.

Now, since $n = s$ and $\rho_n = \rho_s$ at $N = 0$ then

$$n\rho_n + NP = s\rho_s \quad (8)$$

for compound cord twisting.

The calculation of ply length and ply twist at any cord twist can be done as follows: equation (5*b*) gives

$$\alpha n = (2/\rho_n)\sqrt{(1 - \rho_n)}$$

Therefore $$1 - \rho_n = \tfrac{1}{4}\alpha^2 n^2 \rho_n^2$$

but from equation (8)

$$\alpha^2 n^2 \rho_n^2 = \alpha^2 (s\rho_s - NP)^2$$

Therefore $$\rho_n = 1 - \tfrac{1}{4}\alpha^2 (s\rho_s - NP)^2 \qquad (9)$$

which enables the ply retracted length ρ_n to be calculated from experimental data on cord retraction.

The ply twist can now be calculated using equation (8) in the form:

$$n = (2/\alpha\rho_n)\sqrt{(1 - \rho_n)} \qquad (10)$$

Further, equation (7) gives

$$\rho_n = P \sec\theta$$

So, using equation (9)

$$\sec\theta = (1/P)(1 - \tfrac{1}{4}\alpha^2 [s\rho_s - NP]^2) \qquad (11)$$

So the folding angle can be calculated from retraction data.

CORD RETRACTION EQUATION

By equation (11)

$$P \sec\theta = 1 - \tfrac{1}{4}\alpha^2 (s\rho_s - NP)^2$$

but since

$$\alpha n = \frac{2}{\rho_n}\sqrt{(1 - \rho_n)},\ \alpha s = \frac{2}{\rho_s}\sqrt{(1 - \rho_s)} \text{ or } 1 - \tfrac{1}{4}\alpha^2 s^2 \rho_s^2 = \rho_s$$

then

$$P \sec\theta = \rho_s + \tfrac{1}{2}\alpha^2 s\rho_s NP - \tfrac{1}{4}\alpha^2 N^2 P^2 \qquad (12)$$

Arranging as a quadratic equation and solving for P,

$$P = \frac{2\sec\theta - \alpha^2 s\rho_s N}{\alpha^2 N^2}\left\{\left[1 + \frac{4\alpha^2 N^2 \rho_s}{(2\sec\theta - \alpha^2 s\rho_s N)^2}\right]^{\frac{1}{2}} - 1\right\} \qquad (13)$$

which may be written

$$P = \frac{2\rho_s}{2\sec\theta - \alpha^2 s\rho_s N} F\left(\frac{2\alpha N\sqrt{\rho_s}}{2\sec\theta - \alpha^2 s\rho_s N}\right) \qquad (14)$$

where $$F(x) = \frac{2}{x^2}\left[(1 + x^2)^{\frac{1}{2}} - 1\right]$$

THE RETRACTION OF A SINGLE YARN

The retracted length ρ_n of a ply of twist n in a cord is given by $\alpha n = (2/\rho_n)\sqrt{(1 - \rho_n)}$ [equation (5*b*)] and, since a yarn may be regarded as a cord with zero cord twist, this equation gives the relation between the retracted length of a yarn and the yarn twist. Equation (5*b*) may, however, be derived separately for a yarn.[3]

We assume that the filaments are arranged in simple helices about the axis of the yarn and that the retracted length of the yarn is the mean axial component of the filament length per unit filament length. For a filament tracing a helix of radius r, if the filament is of length σ in a yarn of length l, then axial component of filament length equals $\sigma\cos\psi$ where ψ is the angle the filament makes with the yarn axis. Also $\tan\psi = 2\pi nr$ as in equation (3).

So $$\cos\psi = (1 + 4\pi^2 n^2 r^2)^{-\frac{1}{2}}$$

Therefore, the axial component of filament length at radius r is $\sigma(1 + 4\pi^2 n^2 r^2)^{-\frac{1}{2}}$. In an annulus of the yarn cross-section of radius r and thickness dr there are $2\pi r dr m/\pi b^2$ filaments if m is the number of filaments in the yarn and b is the radius of the yarn.

Therefore, mean axial component of filament length per unit filament length

$$= \rho_n = \frac{1}{b^2}\int_0^b 2[1 + (2\pi nr)^2]^{-\frac{1}{2}} r\,dr$$

So $$\rho_n = \frac{2}{(2\pi nb)^2}\left\{\sqrt{[1 + (2\pi nb)^2]} - 1\right\}$$

Writing $2\pi b = \alpha$ and re-arranging.

$$\alpha n = (2/\rho_n)\sqrt{(1 - \rho_n)} \quad \text{as in equation (5}b\text{).}$$

EXPERIMENTAL WORK

In this experimental work we are assuming that the yarns and cords involved are uniform.

(*a*) *Yarn retraction.* Using the apparatus illustrated diagrammatically in Fig. 4, an untwisted yarn was attached at one end to one of the rotatable clamps *B* and at the other end to the carriage *A*, the yarn being tensioned by a weight

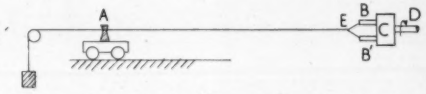

Fig. 4. Apparatus for the measurement of yarn and cord retraction

of about 50 g. The yarn length could be read off on a scale parallel to the yarn and the number of turns of twist inserted, on a counter coupled to shaft *D*.

About 180 in. of 1650 denier continuous filament rayon yarn was given various twists up to about 15 turns/in. and the retracted length ρ_n of the yarn was measured for each value of the twist n. A graph was then plotted of $(1/\rho_n)\sqrt{(1 - \rho_n)}$ against n for each yarn and the results are shown in Fig. 5.

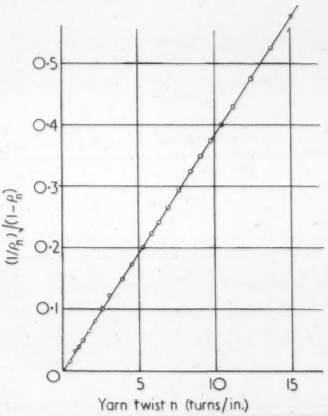

Fig. 5. Graph of $(1/\rho_n)\sqrt{(1 - \rho_n)}$ against yarn twist n

The graph is a straight line through the origin, showing that the relation between ρ_n and n is of the form $\alpha n = (2/\rho_n)\sqrt{(1-\rho_n)}$ where $\alpha/2$ is the gradient of the line. Using the value of α obtained above and equation (5*a*) the graph of Fig. 6 was drawn showing the theoretical retraction curve and the experimental points. Good agreement is shown between the theoretical curves and the practical points.

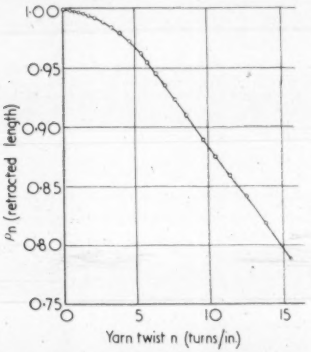

Fig. 6. Retracted length curve for 1650 denier rayon yarn

○, experimental points; ——, theoretical curve.

(*b*) *Cord retraction.* From a cord retraction experiment the quantities which can be measured are: s, the yarn singles twist before cord twisting; ρ_s, the retracted yarn length before cord twisting; α, the yarn constant; N, the cord twist; and P, the cord retracted length.

Using equation (11) $\sec\theta = (1/P)[1 - \frac{1}{4}\alpha^2/(s\rho_s - NP)^2]$, θ can be calculated from the retraction data for all values of N and P. A graph of $\tan\theta$ against N can, therefore, be plotted. Such a graph for a 2/1650 rayon cord is shown in Fig. 7.

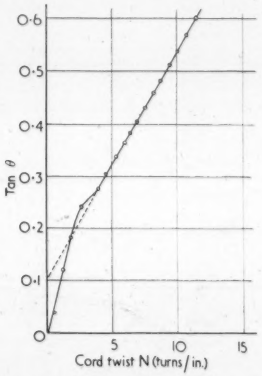

Fig. 7. Graph of tan (folding angle) against cord twist, for compound cord twisting

– – –, continuation of the linear portion of the experimental results.

But $\tan\theta = 2\pi aN$ by equation (3). Since the graph of $\tan\theta$ against N is not a straight line the ratio $\tan\theta/N$ is not constant for all N, that is, the cord radius a varies during the cording operation.

However, since the graph of $\tan\theta$ against N is linear after about $N = 2$–3 turns/in. a straight line can be fitted to the points of the experimental graph. The result of calculating the cord retracted length for a range of N from 0–15 turns/in., using the cord retraction equation (14) with α obtained from a preliminary yarn retraction experiment and θ, as obtained from the $\tan\theta$ *versus* N graph as above, is shown in Fig. 8. It can be seen that the theoretical curve gives a good fit to the experimental points.

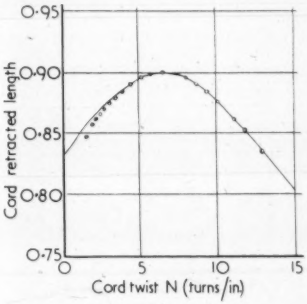

Fig. 8. Graph of cord retracted length against cord twist

○, experimental points; ——, theoretical curve.

VARIATION OF CORD RADIUS, *a* WITH TWIST

In the preceding section it is shown that the cord radius a varies with twist. It is interesting to enquire whether the radius depends upon the ply twist, the cord twist or a combination of the two. An experiment was therefore designed in which the cord twist could be varied without varying the ply twist.

Simple cord twisting. A cord AE has one end A fixed on a carriage which can move in the direction AD (Fig. 4). The ends B, B' of the yarns constituting the cord are attached to two yarn clamps B and B', which are geared to an axle D through a twisting head C in such a manner that the end of the cord at $B\,B'$ can be rotated about the axis AD without rotation of the yarn clamps $B\,B'$ about their own axes. This manner of twisting a cord is called simple twisting in contrast to the usual (twist tester) method, which may be called compound twisting.

If we consider any transverse plane of a cord which is being simply twisted, then (see Fig. 3) the angle between the direction C_1P and a fixed line OX is constant throughout the twisting where C_1 is the ply axis, P any filament and O the cord axis.

It follows that for simple twisting $\xi - \gamma$ is independent of the cord twist N. Hence at any transverse plane $(1/2\pi)(d\xi/dy)$ is independent of N since y, the untwisted length of the yarn in the ply, is also independent of N. Hence the product $n\rho_n = (1/2\pi)(d\xi/dy)$ is independent of the cord twist N for simple twisting.

**

Now at any transverse plane in the cord

$$\rho_n = 1 - \tfrac{1}{4}\alpha^2 n^2 \rho_n^2 \quad \text{from equation (5}b\text{)}$$

So since $n\rho_n$ is independent of N, so also is ρ_n and hence n. We may therefore state:

"if the ply radius parameter $\alpha(=2\pi b)$ is constant for all forms of cord twisting, then both the ply retracted length ρ_n, and the ply twist n, of a cord are independent of the cord twist N for simple twisting." (15)

Experimentally it is impossible to twist a cord in a simple manner because this operation involves the sliding of one ply over another throughout the length of the cord during the simple twisting operation, and this sliding is prevented by inter-ply friction. It is, however, possible to untwist a cord simply.

The procedure is to make a cord in the ordinary manner and connect it to the apparatus in Fig. 4. About a hundred turns of cord twist, say, are simply removed from the cord and then the twist is evened out along the cord by untwisting the whole cord in a compound manner and re-twisting it to restore the cord twist as it was immediately after the simple untwisting. The length of the cord L and the cord twist N for various values of N are found in this manner.

If y is the untwisted length of the yarn from which the cord was made, then $P = L/y$ at all points in the cord if we assume the cord was twisted uniformly.

So from equations (6) and (7)

$$\sqrt{[(y^2\rho_n^2/L^2) - 1]} = 2\pi aN \qquad (16)$$

For simple twisting, if the statement (15) is true, then $y\rho_n$ is constant for all N and is the length of the cord when it is completely untwisted simply.

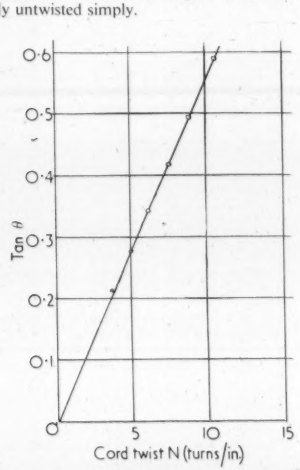

Fig. 9. Graph of tan (folding angle) against cord twist for simple cord twisting

A graph of $\tan\theta \equiv \sqrt{[y^2\rho_n^2/L^2) - 1]}$ against N for a 2/1650 denier rayon cord is shown in Fig. 9. Since this graph is a straight line through the origin we may conclude that (i) a the cord radius is constant for simple twisting, and (ii) ρ_n the ply retracted length is constant for simple twisting. This corroborates the deductions and assumption in statement (15).

CONCLUSIONS

(1) The model of a cord proposed in this paper yields a set of self-consistent formulae for cord retraction.

(2) A definition of ply twist is proposed which is consistent with the model and enables the mathematics to be considerably simplified.

(3) An alternative cord twisting process (simple twisting) is defined, which yields simpler formulae than those for compound twisting and which facilitates experimental study of the structure of a yarn in a cord.

(4) The formulae developed are a good fit to the experimental data of yarn retraction and the cord retraction for both simple and compound twisting.

ACKNOWLEDGEMENTS

The author would like to express his thanks to Dr. L. R. G. Treloar of the British Rayon Research Association for helpful criticism.

The author also wishes to thank Mr. W. L. Jackson, Senior Physicist, and Mr. G. F. Morton, Research Manager, for many valuable discussions during the course of this work. Thanks are due to Mr. L. F. Pickup, Technical Manager, for his continued interest and to him and his colleagues on the Management Board of the Dunlop Cotton Mills Ltd. for permission to publish this work.

REFERENCES

(1) Woods, H. J. *J. Text. Inst. Manchr*, **24**, p. T317 (1933).
(2) Treloar, L. R. G. *J. Text. Inst. Manchr*, **47**, p. T348 (1956).
(3) Treloar, L. R. G. *J. Text. Inst. Manchr*, **47**, p. T357 (1956).

APPENDIX

(i) *The mean of* $d\lambda/d\sigma$

In the derivation of the formula $\alpha n = 2/\rho_n\sqrt{1 - \rho_n}$, having defined the cord model such that $\rho_n(=-dz/d\lambda)$ is a mean value of $d\lambda/d\sigma$, it is necessary to enquire as to the meaning of "a mean" in this connexion.

To obtain the relation (4) we show that the mean of $(d\sigma/d\lambda)^2$ in an annulus of radius r of the ply is $1 + [r(d\xi/d\lambda)]^2 = 1 + 4\pi^2 n^2 r^2$.

Hence a mean value of $d\lambda/d\sigma = (1 + 4\pi^2 n^2 r^2)^{-\frac{1}{2}}$. This mean value is the root mean harmonic square defined by the equation:

$$\text{r.m.h.s. of } x_1 x_2 x_3 \ldots x_n = 1/\sqrt{\left(\frac{1}{n}\sum\frac{1}{x^2}\right)}$$

This method of estimating a mean of $d\lambda/d\sigma$ cannot be justified mathematically, beyond the definition, and the question as to its appropriateness depends upon the experimental applicability or otherwise of the final result.

(ii) *The proof of* $n\rho_n + NP = s\rho_s$

In this proof we assert that

$$\frac{\partial}{\partial N}\left(\frac{\partial\xi}{\partial y} + \frac{\partial\phi}{\partial y}\right) = \frac{\partial}{\partial y}\left(\frac{\partial\xi}{\partial N} + \frac{\partial\phi}{\partial N}\right) \qquad (17)$$

and this is true providing $(\partial\xi/\partial y) + (\partial\phi/\partial y)$ is not zero throughout the range considered (for compound twisting). Since $(\partial\xi/\partial y) + (\partial\phi/\partial y) = 2\pi(NP + n\rho_n)$ equation (17) is true providing $NP + n\rho_n$ is not zero for all N. But at $N = 0$, $n\rho_n = s\rho_s$, so $NP + n\rho_n$ can only be zero at $N = 0$ if $S = 0$, in which case the cord would no longer exist in the geometrical

form postulated, and so the case of $S = 0$ is excluded from the discussion.

(iii) *Note on equation* (4)

The mathematics from which this equation is derived depend upon the epihelix having a constant secondary generating vector r. In practice, since the ply cross-section is slightly elliptical r is not strictly constant. However, if this proof is written with r varying as the radius vector of an ellipse, then the eccentricity terms occur only in products with $\sin(\phi + \xi - \gamma)$ and $\sin(\phi + \xi + \gamma)$, and so are eliminated during the averaging process.

Beam temperature, discharge lag and target biasing in some television pick-up tubes

By B. MELTZER, B.Sc., Ph.D., F.Inst.P., Department of Engineering, University of Edinburgh, and P. L. HOLMES, B.Sc., Research Laboratories of Electric and Musical Industries Ltd., Hayes, Middlesex

[*Paper first received* 2 *September, and in final form* 30 *October*, 1957]

Discharge lag in pick-up tubes, particularly of modern cathode-potential-stabilized type, and its relation to the acceptance of the electron beam by the target are analysed. Measurements of beam acceptance as a function of target potential reveal effective beam temperatures substantially equal to cathode temperature at low beam currents, but higher and multi-valued at high currents. These temperatures set a limit to the possible reduction of lag without target biasing; this limiting lag, referred to as Maxwellian lag, is calculated and presented graphically. Direct measurements of lag are compared with the limiting values. Target biasing, the application of a small positive potential to the target face, reduces this limitation. Results of electron-optical measurements, throwing some light on the anomalous beam temperatures, are presented.

The requirement that a television picture should be reproduced accurately in time as well as in space imposes limitations on camera tube design. In a perfect camera tube of the full-storage type, ideally the output signal should depend solely on the illumination during the previous frame. However, in practice this is not the case, and a bright image takes some time to build up or to decay. Decay lag is usually longer than build-up lag and is more objectionable in normal television practice, as a moving bright object will leave a characteristic trail behind it. However, the lag effect has been put to use in some storage tubes.[1]

Lag may arise from several causes—e.g. delayed photoconductive effect,[1] dielectric hysteresis, or "burn-in" as in the image orthicon.[2] These effects may be circumvented, but the form of lag investigated in this paper, which has been given the name "discharge lag," is inherent in the mechanism of charge-restoration by a low-energy electron beam, a type of scanning employed in all modern camera tubes. It is, in fact, dependent on the energy-spread of electrons in the beam; a factor which is not altogether under control. During an investigation aimed at producing improved camera tubes,[3, 4] measurements of the acceptance of a low-energy beam by a target at varying potentials were made, and hence expected values of lag were calculated and compared with measured values.

BEAM ACCEPTANCE AND BEAM TEMPERATURE

During the operation of a cathode-potential stabilized television camera tube, the potential of the target is always within a few volts of that of the cathode of the electron-gun. In order to measure the amount of beam actually accepted by the target of a tube, special tubes were made similar to the C.P.S. Emitron (type 5954),[5] but with the photoemissive mosaic replaced by a continuous film, usually of gold. Photoemissive layers give identical measurements at low energies (< 2 eV). The current accepted by this film was measured as a function of the potential difference between film and gun cathode with the tube in the normal operating condition for use as a camera tube. A preliminary experiment had shown that if the tube controls were set to predetermined average values, and then adjusted slightly to maximize accepted beam, the beam was then correctly focused on the target and alined perpendicularly to it.

Twenty-nine curves were obtained on nine tubes. The factors varied were: beam current (controlled by the modulator electrode), a.c. or d.c. heater current (for possible magnetic effects), size of limiter aperture, limiter anode potential, gun type, strength of focusing magnetic field, target material, and gun alinement.

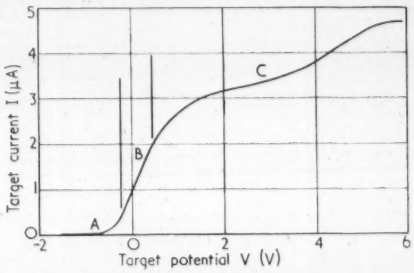

Fig. 1. The three main regions of a beam acceptance curve. Exponential region, *A*. Linear region, *B*. Secondary emission region, *C*

Fig. 1 shows a typical beam acceptance curve, and Fig. 2 shows the lower-potential end with current plotted to a logarithmic scale. It will be noted that the curve in Fig. 1 can be divided into three main regions—a linear region, which is modified at higher voltages by secondary emission and by saturation to give a second region, and, at low

energies, a third exponential region, which is best seen in Fig. 2: this exponential region is very important in the production of lag (see below).

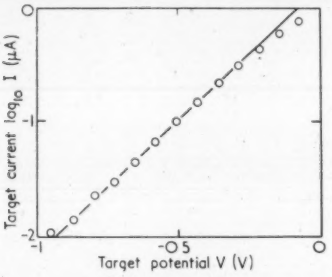

Fig. 2. Exponential region of beam acceptance curve plotted on logarithmic scale

Exponential region. Here $I = I_0 \exp(aV)$, where I_0 is a constant and $2{\cdot}303a$ is the slope of the linear portion of the $\log_{10}I$ against V curve. This resembles the Maxwellian law, $I = I_0 \exp(eV/k\theta)$, for an electron gas, where $-e$ is the electron charge, k is Boltzmann's constant and θ the absolute temperature. We may say that the beam temperature is: $\theta = e/ka = 11\,600/a$ (V in volts). Fig. 3 shows θ against I_B, where I_B is the maximum current of the beam acceptance curve and is an approximate measure of the total current in the beam; its value is less because of secondary emission, but it gives a useful measure for the present purpose.

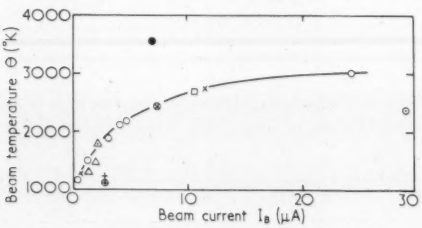

Fig. 3. Beam temperature against beam current

○, Tube G.20. Standard gun (0·002 in. diameter limiter)
□, Tube G.20. d.c. heater
△, Tube G.20. Beam misalined
●, Tube G.20. Modulator positive
+, Tube G.20. Limiter potential ÷ 5, focus field normal
⊕, Tube G.20. Limiter potential ÷ 5, focus field ÷ 3
⊙, Tube G.21. Standard-type gun with 0·017 in. diameter limiter
⊗, Tube H.36. Wehnelt gun
×, Tube H.37. Wehnelt gun
△, Tube G.29. Standard gun, photoemissive-layer target

At low beam currents, for all guns of the two types used, θ approaches cathode temperature, which is estimated from pyrometer measurements to be approximately 1 100° K in all cases. At higher beam currents, the beam temperature increases. Surprisingly, the points for the standard gun and a very different gun employing a Wehnelt cylinder (see Fig. 3) lie on the same line. Some points are, however, anomalous, and it is evident that beam current is not the only important parameter. The points with modulator positive and with large limiter hole appear less anomalous when θ is plotted against modulator potential (Fig. 4). It is possible that the important factor is the space-charge density near the cathode and target.

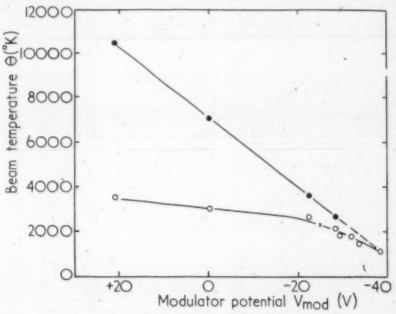

Fig. 4. Beam temperature against modulator potential

○, Primary exponential region (standard tube G.20)
●, Secondary exponential region (G.20)
×, Primary exponential region (tube G.21: large diameter limiter)

Secondary exponential region. When $I_B > 4\mu$A, another exponential region corresponding to a higher temperature arises at the lower end of the curve. Fig. 5 shows this phenomenon in well-developed form. The corresponding

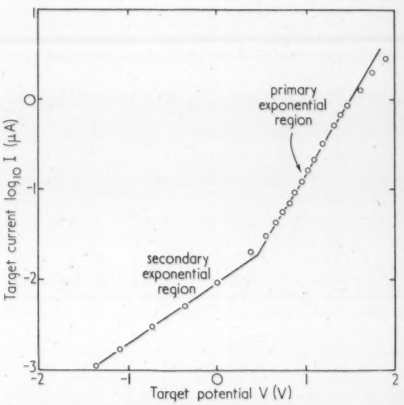

Fig. 5. Beam acceptance curve with two exponential regions ($I_B = 24{\cdot}3\ \mu$A)

secondary beam temperatures as well as the primary ones are plotted for a particular standard gun in Fig. 4, not against I_B, but against gun modulator potential V_{mod}: and it is notable that both secondary and primary beam temperatures appear to tend to the temperature of the thermionic cathode as the beam current is decreased towards zero. The cause of large

and dual beam temperatures is not known, but the phenomenon has been met in diodes and may be caused by space-charge oscillations near the cathode or target.

Linear region. Above the exponential region, a linear region follows at once without discontinuity of slope. It can be shown on plausible assumptions (see Meltzer[6]) that the exponential law $I = I_0 \exp(eV/k\theta)$ would be expected to hold for $V < 0$, and be followed by a linear region $I = I_0[1 + (eV/k\theta)]$ when $V > 0$, where V is the potential of the target minus V_c, the contact potential of the target with respect to cathode. For both portions of the curve, when $V = 0$, $I = I_0$ and $(dI/dV) = I_0 e/k\theta$, so the curve and its slope are continuous, agreeing with observation. As a test of this law, the slopes of the straight portions of the exponential and linear plots were determined, giving $e/k\theta$ and $I_0 e/k\theta$ and hence I_0. The intercepts of these two lines on the potential axis then gave two values of V_c. This test was applied to six curves, and in no case did the two values differ by more than 3% (0·06 V). Beyond the linear region the curve depends on the electron optics of the system and on secondary emission.

DISCHARGE LAG

In a cathode-potential-stabilized television camera tube,[5] under steady illumination an equilibrium state is reached in which the target is restored to the same potential after every scan. For moving scenes, if the scanning beam restored the target to exactly the same potential whatever the light intensity, the signal would depend on the light incident during the preceding frame period only. This is not the case in practice, however, and an image takes some time to build up or decay.

The potential excursion during a frame period is fixed by the light intensity, being equal to the product of light flux and photosensitivity divided by target capacity. The component beam-electrons do not all have the same speed normal to the target, owing to their initial emission energy and the converging action of the electron gun, so the target accepts more current at higher potentials than at lower; for steady illumination the restoration potential is then determined by the requirement that in equilibrium the charge accepted during a scan must equal the photoelectric charge stored during a frame.* If the light is now removed, the successive decay lag signals produced in successive frame periods may be found from the restoration potential and the beam acceptance characteristic.

A complete treatment of target-discharge would be complicated, involving the distribution of beam density over the spot, overlap of adjacent scan-lines, interlace and inter-element capacity. It will be assumed that the spot discharges all points, on the centre of lines or midway between lines, with the same efficiency, a condition known as "flat field"—see Zworykin.[7] The beam then discharges an elementary area A' as though the whole beam were concentrated on it for time $T' = TA'/A$, where T is the frame period and A the scanned area of the target. With sequential scanning, all neighbouring points in a uniformly illuminated region have the same potential, unless the beam is close by. The target then resembles a parallel plate condenser, and the capacity of the elementary area is $C' = CA'/A$, where C is the capacity of the scanned area. While the element is being scanned, some neighbouring points will have higher potential and some lower, but this will tend to average out, and the potential of the element will still be supposed to be determined solely by its own charge and the capacity C'.

If the current I accepted by the target is given as a function of its potential V by $I(V)$ and, during scan, the element has potential V at time t, then $I(V) = -C'(dV/dt)$. So

$$\int_{V_2}^{V_1} \frac{dV}{I(V)} = \frac{T'}{C'}; \text{ and } \int_{V_2}^{V_2+S_1} \frac{dV}{I(V)} = \frac{T}{C'} \qquad (1)$$

where V_1, V_2 are respectively the target potential before and after scanning and $S_1 = V_1 - V_2$. Fig. 6 shows a typical reciprocal beam acceptance curve, a plot of $1/I$ against V. The potential V_2 to which the target is restored may be found

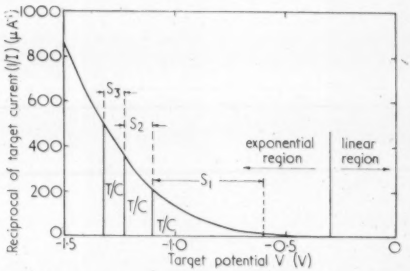

Fig. 6. Calculation of lag from reciprocal beam acceptance curve

for any potential swing S_1 from the condition that the area under the curve between V_2 and $(V_2 + S_1)$ is T/C. If the light is now removed immediately after a scan, successive lag signals $S_2 = V_2 - V_3$, etc., are found by marking off areas T/C to the left of V_2. In Fig. 6, if $S_1 = 0{\cdot}5$ V, then $S_2 = 0{\cdot}132$, $S_3 = 0{\cdot}089$, $S_4 = 0{\cdot}07$. The lag has fallen to noise level in three frame periods. If the light is removed at some instant between scans, the lag signals will be less: decay time is indeterminate to the extent of one frame period.

MAXWELLIAN LAG

In the C.P.S. Emitron, beam currents of at least a few microamperes are required for stable operation. The exponential region then extends to values of I sufficiently high for the area under the rest of the $(1/I)$ against V curve to be much less than T/C (see Fig. 6). The exponential region also extends to currents so low that lag signals produced in the secondary exponential region are near or below the noise level of the amplifier (0·005 μA) and are negligible, for beam currents normally used. The lag observed should therefore approach the value calculated on the assumption that the primary exponential law is obeyed at all values of V; this will be referred to as Maxwellian lag. The Maxwellian lag corresponding to cathode temperature is the lowest lag attainable in the sense that it does not seem possible to achieve a lower value by altering the electron-optical design of the gun.

* Lateral leakage on the target is negligible if the picture-definition is good. Any continuous spray of charge on to the target (e.g. ion spot) may be treated in its effect on lag as though due to a light source superposed on the viewed scene. The possibility of leakage through the target to the opposite face will be considered later.

From equation (1)

$$\int_{V_2}^{(V_2+S_1)} \frac{dV}{I_0 \exp(aV)} = \frac{T}{C}$$

$$\exp[-aV_2] - \exp[-a(V_2 + S_1)] = aTI_0/C \qquad (2)$$

At the next scan,

$$\exp[-a(V_2 - S_2)] - \exp[-aV_2] = aTI_0/C \qquad (3)$$

Hence,

$$\exp[aS_2] = 2 - \exp[-aS_1] \qquad (4)$$

The lag signal S_2 depends only on S_1 and the beam temperature and not on I_0 or (T/C). When $S_1 > 1$ V, S_2 is close to the constant value: $\theta/16\,700$ V. It follows that the lag signal of a bright object on a black background in the C.P.S. Emitron cannot be reduced below 0·06 V, or 1/70 of the tube's peak signal. The curves of Figs. 7, and 8 show the Maxwellian lag for different beam temperatures. S_2/S_1 is plotted as this gives an indication of the visibility of decay lag on a black background. The same curves give S_3/S_2 in terms of S_2, etc.

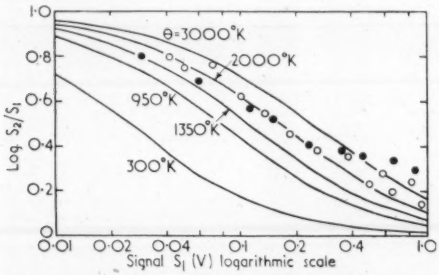

Fig. 7. Direct lag measurements for 0·016 μF target tube superposed on Maxwellian lag curves
○, $V_{mod} = -13$; ●, $V_{mod} = -32$.

DIRECT MEASUREMENT OF LAG

A small neon lamp on a dark background is viewed by the camera-tube to be tested. A line-selector presents on a monitor a line passing through the image of the lamp. The lamp is automatically switched each time the line is scanned, so the line is illuminated only during alternate frames. Two traces corresponding to S_1 and S_2 appear on the monitor and are measured on the calibrated Y-shift. Noise causes difficulty in measuring the lower signals. The points on Fig. 7 were obtained on a tube with high capacity (0·016 μF) which produced a higher signal for given S_1. The points on Fig. 8 were obtained on a standard 0·001 μF target with the noise cut by reducing the bandwidth. At low values of S_1, the agreement with the theoretical curves is good. At higher signals the lag is somewhat greater than expected. When the modulator is at -31 V, the beam current is abnormally low and the tube is close to instability; for large signals the area T/C (see Fig. 6) may not then lie in the exponential region, and this would explain the high values of lag in this case. The lag is, however, nowhere less than the Maxwellian lag.

REDUCTION OF LAG BY TARGET BIASING

Lag is reduced when an object is moving on a background which is not completely black. The target potential cannot become more negative than the restoration potential under the background light, and the tube operates in the region where the Maxwellian lag is relatively low. It has been found

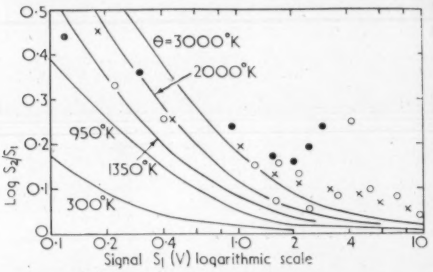

Fig. 8. Direct lag measurements for 0·001 μF target tube superposed on Maxwellian lag curves
○, $V_{mod} = -13$; x, $V_{mod} = -22$; ●, $V_{mod} = -31$.

possible to reduce substantially the lag on a black background by illuminating the mosaic from a small lamp in the camera, and subtracting the resulting uniform signal by means of the lift control.[3] The mosaic may also be biased by leakage from the signal plate if the target is of slightly conducting glass.[4] If the biasing produces potential swing v at the target, equation (2) is replaced by

$$\exp - (aV_2) - \exp[-a(V_2 + S_1 + v)] = aTI_0/C$$

and equation (3) by:

$$\exp[-a(V_2 - S_2)] - \exp[a(V_2 + v)] = aTI_0/C,$$

where S_1, S_2 are the signals after subtraction of v in the lift.

Hence:

$$\exp(aS_2) = 1 + [1 - \exp(-aS_1)] \exp(-aV) \qquad (5)$$

When $v = 0$, the lag for large signals is $\theta/16\,700$ V. The table gives the corresponding value for various v when $\theta = 1\,160°$ K, expressed as a percentage of the value when $v = 0$.

Dependence of lag on biasing

v (volts)	*Greatest S_2*
0	100
0·05	68
0·1	45
0·2	18
0·3	7
0·4	2·6
0·5	1

The maximum bias which can be applied depends on

(i) the finite stable working range of target potential,

(ii) the uniformity with which the bias can be applied. It would be desirable to increase the target capacity so as to increase the amount of light the tube could handle (i.e. the contrast range) without excessive excursions of target

potential; S_1 would then be reduced for a given amount of light so the lag would be increased. The possibility thus appears of overcoming this increase in lag by means of target biasing.[3]

FURTHER CONSIDERATIONS ON BEAM ACCEPTANCE CURVES

The anomalous beam temperatures are not understood, but a few observations were made which probably have some bearing on them. Secondary exponential regions appear when the beam current is increased beyond 4 μA, as is shown in the lower curve of Fig. 9, which plots the

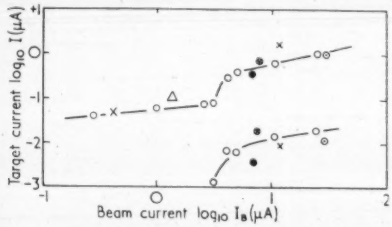

Fig. 9. Limits of exponential regions at various beam currents. Symbols as in Fig. 3

limits of the primary and secondary exponential regions of the beam acceptance curves. At $I_B = 4\ \mu$A, too, there are signs of a discontinuity in the upper curve (G.20 points). Fig. 10 shows, as a function of modulator current, the target potential at which the maximum occurs in the beam acceptance curve. The latter may be taken as an indication of the maximum lateral energy of beam-electrons, and here again there appears to be a discontinuity when $I_B = 4\ \mu$A which corresponds to a modulator potential of -31 V.

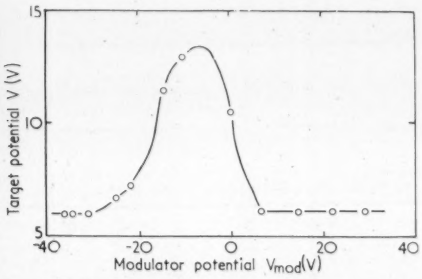

Fig. 10. Potential corresponding to maximum current on beam acceptance curve against modulator potential

In Fig. 1 there are signs of a subsidiary maximum just below 2 V. As the modulator potential approaches zero, a definite maximum develops and finally rivals the main maximum. This suggests that the beam consists of two groups of electrons with different lateral energies. Confirmation was obtained by momentarily pulsing a gun, and allowing the beam to pass through a field-free region on to the storage mesh of a VCRX350.[1] The stored image was then read off and examined at leisure. At the more positive modulator potentials, the beam consisted of a hollow shell, sometimes with a central spot, the two groups of electrons having different lateral energies. Fig. 11 shows tracings made from a line monitor of a line passing through the centre of the pattern, for various modulator potentials V_{mod}. The maximum lateral energies V_L are shown by the width of the spot; heights are arbitrary. Possibly the double

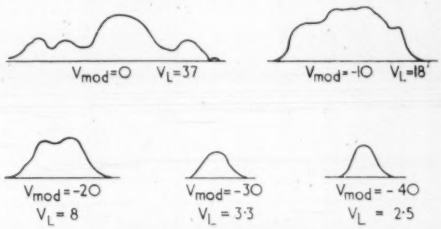

Fig. 11. Beam density profiles

exponential regions arise through the two groups having different beam temperatures. Hollow beams may be produced by spherical aberration in the gun (see Klemperer[8]); there is no convincing evidence that they arise from space-charge oscillations.

ACKNOWLEDGEMENTS

The work described was carried out, most of it some years ago, in the Electric and Musical Industries Research Laboratories, and the authors wish to thank the present Director—Dr. L. F. Broadway—for initiating, encouraging and permitting publication of it. The results were summarized in a short talk to the Physical Society Meeting on Recent Research in Electron Optics in 1953, and some have been referred to by McGee[9] and by Webley and others.[1] Thanks are due, for useful discussions as well as technical help, to Dr. H. G. Lubszynski, Professor J. D. McGee, Messrs. A. H. Atherton, W. E. Turk, H. Cassman, C. A. Johnson, R. S. Webley, A. E. Jennings, J. A. Lodge, and others. In particular, the basic relationship between lag and beam acceptance had been worked out earlier by Dr. Lubszynski, although independently found by the authors.

REFERENCES

(1) Webley, R. S., Lubszynski, H. G., and Lodge, J. A. *Proc. Instn Elect. Engrs*, **102**, p. 401 (1955).
(2) Janes, R. B., Johnson, R. E., and Moore, R. S. *R.C.A. Review*, **10**, p. 191 (1949).
(3) Meltzer, B., Cassman, H., and Holmes, P. L. Brit. Pat. No. 728,050 (1952).
(4) Lubszynski, H. G., McGee, J. D., Turk, W. E., and Cassman, H. Brit. Pat. No. 683,603 (1948).
(5) McGee, J. D. *Proc. Instn Elect. Engrs*, **97**, p. 377 (1950).
(6) Meltzer, B. *J. Electronics and Control*, **3**, p. 355 (1957).
(7) Zworykin, V. K., and Morton, G. A. *Television*, Chap. 5, 2nd Ed. (London: Chapman and Hall Ltd., 1954).
(8) Klemperer, O. *Proc. Phys. Soc. B*, **64**, p. 790 (1951).
(9) McGee, J. D. *Arch. d. Elektr. Übertrag.*, **9**, p. 355 (1955).

An electrical analogue method of predicting the permeability of unsaturated porous materials

By M. C. PROBINE, M.Sc.(N.Z.), Dominion Physical Laboratory, Department of Scientific and Industrial Research, Lower Hutt, New Zealand

[*Paper first received* 21 *November*, 1956, *and in final form* 25 *July*, 1957]

The manner in which the permeability of unsaturated porous materials varies with moisture content has been investigated, using an electrical analogue technique. The hydraulic resistance of a water channel in the porous material has been represented by an electrical resistor, and the three dimensional network of channels by a corresponding three dimensional resistance network. With all the resistors in circuit the electrical resistance across opposite faces of the network is assumed to be inversely proportional to the saturated permeability. Empty channels are not effective in transporting liquid so that drying of the material is simulated by progressively removing resistors representing the largest of the remaining water-filled channels. In this way the decreasing permeability of the material as it dries out can be related to its moisture content. The predictions by the analogue method agree very well with the experimentally determined values.

INTRODUCTION

The flow of fluids in unsaturated porous media is of importance in agricultural and engineering problems. When the porous material is saturated, all of the pores and channels are filled and the transport of water is proportional to the pressure gradient (Darcy's law), viz.

$$q = k \text{ grad } \phi$$

where q is the quantity of water crossing unit area perpendicular to flow in unit time,
ϕ is the hydraulic potential
and k is the permeability.

When the porous material is not fully saturated some of the pores are empty and since water cannot pass through empty pores the permeability to water flow is reduced. The permeability is therefore a function of the moisture content of the material and this leads to a non-linear differential equation for flow. In order to solve the equation it is necessary to know the relationship between moisture content and permeability.

It is difficult to measure the relationship between moisture content and permeability experimentally, the difficulty being to maintain a small pressure gradient over a finite region. A small gradient is required since one does not wish the permeability to change appreciably over the region being considered, and permeability is a function of water pressure. It is therefore desirable to have an indirect method of estimating the permeability as a function of moisture content.

Earlier workers have attempted to deduce the permeability from a knowledge of the particle size distribution (mechanical analysis) and formulae have therefore been developed relating permeability to particle size, e.g. Kozeny's equation[1] may be expressed in the form:

$$k = cd^2p^3/(1 - p)^2$$

where p is porosity,
d is a measure of particle size,
and c is a constant.

The limitations of this equation and other similar equations have been discussed by Childs and Collis-George,[2] and they have shown quite clearly that the equations can have only very restricted validity. Childs and Collis-George advance the idea that since the permeability is largely determined by the voids, it is more rational to attempt to calculate the permeability from the pore size distribution rather than the particle size distribution.

The pore spaces of a porous material are continuous, consisting of a set of pores of various sizes, interconnected by narrow channels. The pores have a certain size distribution and they are randomly distributed in space. Water is retained in them by surface tension and the tension that is needed to empty a pore is inversely proportional to its radius. Since water is retained by surface tension and this tension becomes smaller with increasing pore size, the larger pores will lose their water at a lower tension and will therefore empty first.

Childs and Collis-George proposed a method whereby the permeability may be deduced by computation when the distribution of pore sizes is known. They used the moisture content/water tension curve to derive the pore size distribution, and a simple statistical theory was used to calculate the permeability based on the probability of occurrence of sequences of pores of all possible sizes, and of the contribution to the permeability as a sum of a series of terms. A weakness of their approach is that by considering only the probability of occurrence of a pore sequence, they have ignored the effect of parallel pores and the by-passing of a pore sequence by larger pores.

In this paper the problem has been treated using an analogue technique. The three-dimensional effect of the actual material is preserved as well as taking into account the probability of occurrence of a pore sequence. One would therefore expect it to be more accurate and to be applicable to a wider range of materials.

ELECTRICAL ANALOGUE

If one considers first the simple case of cuboidal packing of uniform spheres, then there is a pore at the middle of every four spheres connected to the adjacent pores through the six channels between contacting spheres. In the flow through such pores the main resistance will be produced by these narrow entry channels. Each pore with its related channels can be represented electrically by a network of six resistors joined at a common point (Fig. 1*b*). When the pore empties, the six entry channels are isolated from one another and this may be simulated by opening the circuit of the six resistors at the common point. In rhombohedral packing, which is the closest type of packing of uniform spheres, there are two types of pore; a rhombohedral pore and a tetragonal pore. Each rhombohedral pore has eight points of entry and each tetrahedral has four points of entry. In a random packing

of non-uniform spheres, the number of entry points may differ from these examples given above, but it would not be expected that it would vary greatly from the figure of six, and the six terminal network of resistances (Fig. 1*b*) could therefore be expected to represent a single pore reasonably well.

An electrical analogue of a porous medium can therefore be built up by connecting a number of these networks representing single pores into a three dimensional array representing a multi-pored material.

DESIGN OF THE ANALOGUE

Applying Poisseuille's law to flow through the entry channels, the rate of flow in each is proportional to r^4 per unit potential gradient (where r is the radius of the channel), i.e. resistance to flow is proportional to r^{-4}. Converting this to its electrical equivalent:

Electrical resistance of a pore unit, $R = kr^{-4}$
where k = a scaling factor,
r = radius of entry channel.

It is assumed that the dimensions of a pore are proportional to the dimensions of its entry. Therefore the volume of a pore will be proportional to r^3. As the material dries out, a pore just emptied by water tension P will have an entry channel of radius which is proportional to S/P where S is the surface tension. Since S is a constant, a "hydraulic radius" r of the pore can be defined, such that $r = 1/P$. Therefore, if the moisture content is plotted against $1/P$, the volume of water held in pores between the limits r_n and r_{n+1} can be tabulated. Since the volume contribution of each group, of mean radius r, is known, we can calculate the "number" of pores in the group. It is equal to the volume of water held between the limits r_n and r_{n+1} divided by r_i^3 (where r_i is the mean radius). Thus the frequency distribution of the number of pores is obtained as a function of radius, r, and this leads directly to a frequency distribution of hydraulic resistance, r^{-4}. Only a limited number of resistance units can be used in the analogue and it is necessary to normalize the calculated number of pores to the number of resistance units required in the analogue, by allocating resistance units in the proportion which the number of pores in the group bears to the total number of pores.

Since pores of different size are distributed randomly in a porous material, it is necessary to devise some method whereby resistance networks can be randomly distributed in a three dimensional network. This is done by allocating each resistance network a number in a series, which ranges from unity for the resistor of lowest value, to n for the highest (n = total number of resistance units in the network). Resistors are selected for insertion in the network in an order determined by the order in which their numbers occur in a table of random numbers. The selected resistors are plugged into the network in sequence. For example, suppose the numbers occurring in a table of random numbers are 16, 37, 4, 8, 64, 45, etc., then a convenient sequence for placing the resistors is say, No. 16 in the $x_1 y_1 z_1$ position; 37 in $x_2 y_1 z_1$; 4 in $x_3 y_1 z_1$; 8 in $x_4 y_1 z_1$; 64 in $x_1 y_2 z_1$; 45 in $x_2 y_2 z_1$, . . . etc., until all the spaces in the $x_n y_m z_1$ plane are full (where n and m have values of 1, 2, 3 or 4). The $x_n y_m z_2$, $x_n y_m z_3$ and $x_n y_m z_4$ planes are then filled in their turn.

Thus we have resistance units randomly distributed in the three-dimensional analogue, the number of resistance units of each value being proportional to the number of pores of radius "r" and the value of resistance proportional to r^{-4}. A resistance measurement between opposite faces of the cube is inversely proportional to the permeability, so that with all the resistors in circuit we obtain a measure of the saturated permeability.

As the moisture content falls, the suction pressure will rise until it reaches a value at which channels of radius r can no longer remain open. The associated pores, together with those of radius greater than r, which are already empty, will no longer conduct water, and this situation is simulated in the analogue by removing these pore networks from the array. The permeability is inversely proportional to the resistance measured across the faces of the cube. In practice the resistance is measured in the three principal directions and the mean of the permeability values obtained is taken to represent the permeability at that moisture content.

In the analogue there is, of necessity, a discontinuous range of pore sizes, pores within a discrete radius group being assigned a resistance value related to the *mean* radius of the

Extract from a calculation for graded sand—1 mm to ½ mm

(1) $1/P = r$ (reciprocal of tension)	(2) Moisture content % by vol. M	(3) Vol. contribution of pore group $\Delta M_{r_n}^{r_{n+1}}$	(4) Mean radius of pore group r_i	(5) Volume of pore r_i^3	(6) No. of pores $(\Delta M_{r_n}^{r_{n+1}}/r_i^3 = N$	(7) Number normalized to 64 $64\,N_i/\Sigma N$	(8) $1/r_i^4$	(9) Resistance, R ($k\Omega$) $R = k(1/r_i^4)$ ($k = 10^{-2}$)
0·0295	3·45							
0·0305	3·465	0·015	0·030	27×10^{-6}	560	1	$12{\cdot}3 \times 10^5$	12
0·0315	3·485	0·02	0·031	29·8	700		11·2	
0·0325	3·50	0·015	0·032	32·8	460		9·5	
0·0335	3·52	0·02	0·033	35·9	560		8·4	
0·0345	3·55	0·03	0·034	39·3	760		7·5	
0·0355	3·60	0·05	0·035	42·9	1200	1	6·7	6·8
0·0365	3·67	0·07	0·036	46·7	1500		6·0	
0·0375	3·79	0·12	0·037	50·6	2400	1	5·3	5·6
0·0385	3·96	0·17	0·038	54·8	3100	1	4·8	4·7 (*Y*)
0·0395	4·17	0·21	0·039	59·3	3500	1	4·3	4·7 (*R*)
0·0405	4·41	0·24	0·040	64·0	3750	1	3·9	3·9
0·0415	4·70	0·29	0·041	68·9	4200	1	3·5	3·3 (*Y*)
0·0425	5·05	0·35	0·042	74·1	4700	1	3·2	3·3 (*R*)
0·0435	5·47	0·42	0·043	79·5	5300	2	2·9	2·7 (*Y*)

Note (1) In general "preferred types" of resistors have been used.
(2) The code, *R*, *Y*, is to distinguish resistors of same value.

group. Therefore, when a set of resistors representing a particular radius group is removed, the resistance increases stepwise (permeability decreases). Once this group has been removed, only the remaining pores contribute to the permeability. Hence, the moisture content which corresponds to the predicted permeability is the moisture content corresponding to the lower radius boundary of the group removed (or what is the same thing, the moisture content corresponding to the higher radius boundary of the group not yet removed).

A portion of the specimen calculations is given in the accompanying table. The basic information from which the table is prepared is the moisture content/water tension curve for the material (Fig. 2). The reciprocal of the water tension (hydraulic radius) is entered in column (1), and the corresponding moisture content M is listed in column 2. The volume of water held between the limits of each radius group can be derived from column 2 ($\Delta M_{r_m}^{r_m+1}$). The fineness of subdivision of the hydraulic radius is chosen to limit the volume contribution of any one pore group to not more than two or three percent. The mean radius of the group r_i is listed in column (4), and using these values, the mean volume of the pores in each group r_i^3 can be calculated (column 5). The number of pores of each size is calculated by dividing the volume contribution of the group ($\Delta M_{r_m}^{r_m+1}$) by the mean volume of a single pore in the group r_i^3 (column 6 and Fig. 3). The total number of pores is normalized to the number of resistance units required in the analogue (64 in this case), by allocating resistance units in the proportion which the number of pores in the group bears to the total number of pores. The number of units in group i is given by $64\ N_i/\Sigma N$. The hydraulic resistance r_i^{-4} is calculated from column (4), and a scaling factor chosen which gives convenient electrical resistance values. In all cases the nearest "preferred" values to the calculated values of resistance are used.

AN ALTERNATIVE MODEL

In the preceding discussion we have built up an electrical analogue by imagining a porous material as being composed of an aggregation of spherical particles in which water moves through the voids and connecting channels between contacting spheres. This concept leads to the adoption of a six-terminal resistance network to represent a single pore. We might call this the packed sphere model (Mk I).

A porous material may also be thought of as a three-dimensional network of inter-connecting capillary tubes. In this case a single pore could be represented by a single resistor presenting the hydraulic resistance of a capillary tube (Fig. 1*a*). We might call this the capillary model (Mk II). The arguments put forward in the previous sections, for the calculation of pore size distribution and hydraulic resistance, apply equally well in this case. The assembled pores lead to an array of resistors which at first sight is identical to that for the packed sphere model. In the capillary model, however, each resistor represents a single pore and the emptying of a pore is simulated by opening the circuit at points *a* and *b* in Fig. 1(*a*). In the case of the packed sphere model, the circuits are broken at points *a*, *b*, *c*, *d*, *e* and *f* (Fig. 1*b*). This is the essential difference between these two analogues.

In the experimental section of this paper, analogues based on both models are applied to predicting the permeability of porous materials comprised of packed spheres.

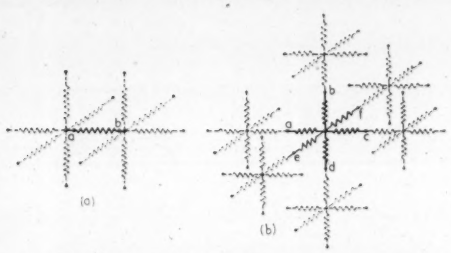

Fig. 1. (*a*) Heavy line delineates resistor representing a capillary tube in the capillary type model. Dotted lines indicate the position of adjacent resistors (or capillary tubes). To simulate the emptying of a pore as material dries out the circuit is broken at points *a* and *b*.

(*b*) Heavy line delineates network representing a single pore in packed sphere type of model. Dotted lines indicate the position of adjacent networks (or pores). To simulate the emptying of a pore as material dries out the circuit is broken at points *a*, *b*, *c*, *d*, *e* and *f*.

EXPERIMENTAL VERIFICATION OF THE ANALOGUES

Analogues based on both the capillary tube model and the packed sphere model have been tested against actual permeability measurements on each of two granular-type porous materials. Since Childs and Collis-George have very fully reported their figures, analogues of each type have been constructed which are based on the moisture characteristics of their 1 mm to ½ mm graded sand (material *A*). The moisture characteristic is shown in curve (*a*), Fig. 2, and the pore-size distribution derived from it is shown in curve (*a*), Fig. 3.

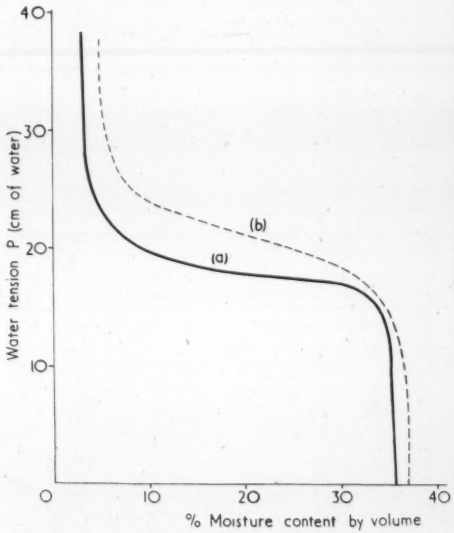

Fig. 2. Moisture characteristic of materials *A* and *B*

——— Material *A*, graded sand (1 mm to ½ mm).
– – – – Material *B*, ungraded glass beads.

Since material *A* is a graded sand, it contains a very narrow range of pore size. In addition, therefore, analogues of each type have been set up for a material having a wider range of pore size (material *B*)—see curve (*b*) in Figs. 2 and 3.

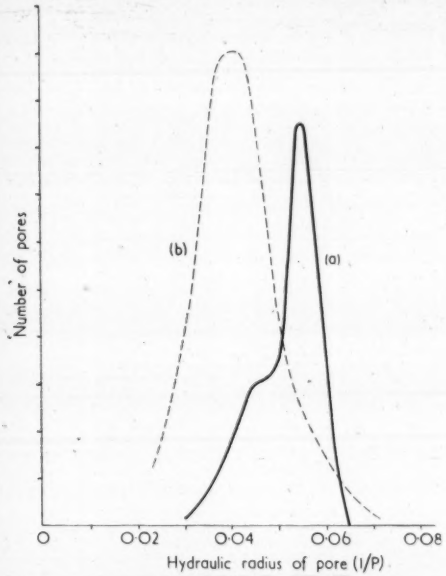

Fig. 3. Pore-size distribution of materials *A* and *B*

——— Material *A*, graded sand (1 mm to ½ mm).
– – – – Material *B*, ungraded glass beads.

The results of the analogue predictions of the permeability function for materials *A* and *B* are shown in Figs. 4 and 5 respectively. In each case these have been compared with the measured permeability and the permeability computed by the method of Childs and Collis-George.

DISCUSSION

For material *A* the packed sphere model and the computation method give very similar results and both are considerably closer to the measured curve than the capillary model. Although the analogue prediction is very good, it is not significantly better than the computation method. The assigning of confidence limits to the analogue curves will be discussed later. A possible reason for the difference between the measured and analogue curves is that the pore-size distribution is calculated on the assumption that the volume contribution of each radius group is due to the complete emptying of pores whose radius lies between the limits for the group. In addition, however, some water will be withdrawn from pores already partially empty in such a way as to maintain an equilibrium curvature at all points in the medium. The number of pores in a particular radius group will therefore be over-estimated since this latter source of water has been ignored in the computation. The resulting error in the calculated number of pores will increase from a minimum near saturation to a maximum at the pendular stage (Haines[3]), i.e. the stage at which all remaining water is held in the points of contact between adjoining particles. Since the calculated proportion of small pores will be greater than the actual number, one would expect that, at a given moisture content, the model would predict a higher unsaturated/saturated

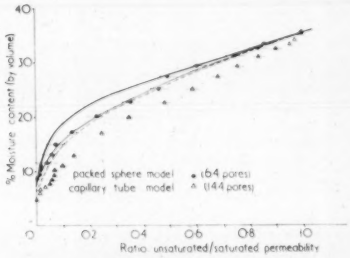

Fig. 4. Permeability ratio for material *A*

——— Measured by Childs and Collis-George.
– – – – Computed by Childs and Collis-George.

Note. (1) Permeability made equal to unity at saturation (35·7%).
(2) The limits shown are the 95% confidence limits for one construction of the model (see text).

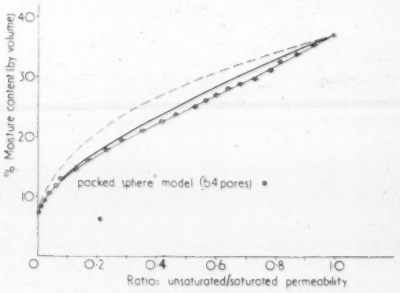

Fig. 5. Permeability ratio for material *B*

——— Measured by the author.
– – – – Computed by the Childs and Collis-George method.

Note. (1) Permeability made equal to unity at saturation (37%).
(2) The limits shown are the 95% confidence limits for the mean of ten determinations (see text). The limits for one determination are of the same magnitude as those in Fig. 4 for the packed sphere model.

permeability ratio than is obtained by measurement, i.e. there is a higher proportion of smaller pores, and the number of possible flow paths through the material is not reduced as rapidly with falling moisture content in the analogue as in the actual material. Further, the radius calculated from the suction pressure will be the radius of the *largest* entry channel to the pore. Two sources of error arise from this fact. Firstly the channel radius has been used to calculate the volume of the pore and hence the pore-size distribution.

Whilst for a specified type of packing of uniform spheres there is a known proportional relationship between the "neck" radius and pore radius, there is no such relationship in a randomly packed medium and there will be a further error in the calculated pore size distribution.

The second source of error is that in the analogue the pore, with its connecting channels, is represented as a six-terminal network with equal resistors and these are proportional to the hydraulic resistance of the largest channel. In practice, of course, the channels may be of different size depending on the size of the adjoining pores. Just how serious this error is, is hard to assess.

The permeability of the material *B* falls off less rapidly with falling moisture content than it does for material *A*. The reason is probably similar to that given above for the difference between the measured and analogue predicted curves, viz. material *B* has a wider range of pore size than material *A*, and the number of possible flow paths through the material is not reduced as rapidly with falling moisture content. This, too, is probably the reason why the computation method fails to give as good a prediction in this case. Childs and Collis–George have considered only the probability of occurrence of a pore sequence and its contribution to the permeability. They have ignored the effect of parallel pores and by-passing of pore sequences by larger pores.

It is found that the difference between the two types of analogues is not as marked for material *B*. The reason for the smaller difference is probably that in randomly packed *ungraded* material the argument requiring six entry points (based on ideal packing) will no longer be completely valid. The capillary tubes concept probably becomes more nearly correct.

The packed sphere model, however, seems to be more generally applicable to granular materials; and for graded granular materials, in particular, the capillary concept is quite inadequate.

VARIABILITY

Since there are only sixty-four pores in this construction of the packed sphere analogue, i.e. only sixteen attached to any one face, it might be supposed that the results obtained would depend a good deal on the randomly determined order of placing resistances in the network.

This variation has been assessed by constructing ten models from the same set of resistors (actually Material *B*, Mk I type model), the only difference between constructions being the random order in which the resistors were put into the network. The permeability versus moisture content function was derived from the analogue for each of these ten sets of data and a polynomial of sixth degree fitted to each curve by the method of least squares. The curve was constrained to pass though a value of unity for the unsaturated/saturated permeability ratio. Coefficients of powers higher than the sixth were found to be randomly distributed and a sixth degree equation gave an adequate representation of the curve.

The mean value of the variance of the permeability ratio about the portion of the curve from 0·06 to 0·9 is 0·000455, i.e. the standard deviation is 0·0213. On this basis, therefore, there is a 95% probability that a single construction of the model will predict a function whose values will be within ±0·048 of the mean over the greater part of the curve. These results apply to the Mk I type of model which has 64 pores. It seems a reasonable assumption that, in the case of the Mk II model, which has 144 pores, the standard deviation will be reduced to two-thirds of this value ($\sqrt{64/144}$). This assumption has been made in assigning limits to the Mk II curve in Fig. 4.

In spite of its limitations, the method does appear to have some advantage over the method of Childs and Collis–George and gives a very good intuitive physical picture of the conduction process in the soil. Further, the predictions by the analogue method fit the experimental facts fairly well, and it seems to be more generally applicable than the computation method.

ACKNOWLEDGEMENT

The assistance of Mr. W. B. Taylor, of the Applied Mathematics Laboratory, with the statistical treatment, is gratefully acknowledged.

REFERENCES

(1) KOZENY, J. *S.B. Akad. Wiss. Wien*, *A*, **136**, p. 271 (1927).
(2) CHILDS, E. C., and COLLIS–GEORGE, N. *Proc. Roy. Soc. A*, **201**, p. 392 (1950).
(3) HAINES, W. B. *J. Agr. Sci.*, **30**, p. 97 (1930).

A sintered nickel matrix cathode

By R. W. Fane, M.Sc., A.Inst.P., English Electric Vacuum Physics Research Unit, Great Baddow, Chelmsford, Essex

[*Paper received* 18 *September*, 1957]

A study of a cathode containing alkaline earth carbonates and boron has shown that lives of at least 8000 hours may be obtained at d.c. current densities in excess of $\frac{1}{2}$ A/cm^2. The cathode also exhibits good pulse emission properties. Processing schedules and operating temperatures are similar to those of a normal oxide-coated cathode. Experiments carried out in an attempt to elucidate the mechanism of operation are described.

Many of the limitations inherent in the oxide-coated cathode have been overcome by the development of the atomic film emitter in various forms known as the "L,"[1] metal capillary[2] and impregnated cathodes[3] and a considerable amount of information has been published on these. An alternative approach, using oxide cathode materials has been briefly reported by the Bell Laboratories[4] and termed the "molded" or matrix cathode. The comparatively low operating temperature combined with favourable electrical and mechanical properties makes this type of particular interest. Details of a study made on one such system are given below.

SELECTION OF BASIC MATERIALS USED IN CATHODE PREPARATION

Carbonyl nickel powder and co-precipitated (Ba, Sr, Ca)CO_3 are used, the methods of powder metallurgy being employed to form the cathode into the desired shape and size. For ease of activation some reducing agent, capable of reacting with barium oxide (and strontium and calcium oxides) to produce free barium (strontium and calcium), must be included either pre-alloyed to the nickel or added to the cathode mixture as a fine powder. The latter method was chosen since powdered nickel alloys are not readily available and the impurity content can be varied and controlled accurately in this way. The selection of the reducing agent is governed by several considerations namely:

(i) there must be little or no sublimation at the operating temperature, which will necessarily be somewhat higher than for the oxide-coated cathode;

(ii) the pressure of barium produced by the reaction

$$R + BaO \rightleftarrows RO + Ba$$

where R is the reducing agent, must be sufficient to activate the cathode but not too high or excessive barium evaporation would result;

(iii) no deleterious reactions between the agent and (Ba, Sr, Ca)CO_3 must occur at the sintering temperature (as is the case with tungsten, for example).

A thermodynamic analysis of the reactions involved in oxide cathodes has been given by Rittner[5] and has been used as a guide when considering condition (ii). In the present investigations boron has been used as the reducing agent, although practically no information exists as to the behaviour of nickel-boron cathode alloys.

PREPARATION OF THE CATHODE MIXTURE

The constituents used are as follows:—

Carbonyl nickel powder (analysis: carbon, 0·05–0·1%; sulphur, 0·001–0·002%; silicon, titanium, aluminium, 0·0001%; oxygen, 0·1%; iron, 0·02%).

Particle size 3–5 μ, 68% by weight.

Co-precipitated (Ba, Sr, Ca)CO_3 (in the ratio 45·5 : 45·5 : 9) 30·6% by weight. The particle size is shown by an electron micrograph to be approximately 1 μ.

Boron less than 300 mesh, 0·4% by weight.

Barium stearate, to serve as binder and lubricant during pressing, 1% by weight.

The powders are ball-milled together for 24–72 hours. It has not been found necessary to take any special precautions in storing the mixture.

Pressing and sintering cathodes. Cathode pellets, usually about 4 mm in diameter, consisting of a layer of cathode material approximately 0·010 in. thick and a layer of nickel 0·030 in. thick, are formed by pressing the materials in a hardened steel die at 50 t/in.^{2} Sintering is carried out in a hydrogen atmosphere. Several firing schedules have been used but the one most generally employed consists of maintaining the cathodes at 1000° C for 15 min followed by 30 min at 1100° C.

CATHODE PROCESSING AND PERFORMANCE CHARACTERISTICS

The sintered cathodes, after spot welding into a molybdenum or nickel retaining sleeve, are mounted in small planar diodes with an anode dissipation of about 6 W; anode-cathode spacing is kept small so that fairly large current densities may be drawn at convenient anode voltages. These valves have generally been pumped on a three-stage oil diffusion pump to a pressure of about 5×10^{-5} mm of mercury followed by a bake at 400° C. After induction heating the electrode structure, the cathode temperature is slowly raised to 1050–1075° C and maintained for about 5 min, the pressure never exceeding 5×10^{-4} mm of mercury at this stage. Activation is then continued at 1000–1050° C, the pressure having fallen to 5×10^{-6} mm of mercury. After gettering and seal-off, ageing of the valves is continued for 24–48 hours gradually reducing the temperature to the required operating value. Variations in the above procedure have not caused any marked changes in cathode characteristics. An extensive study of the effect of the activation treatment has not, however, been carried out.

A pulsed emission Schottky plot of a typical cathode is shown in Fig. 1. The zero field emission at various temperatures, obtained by extrapolating the linear portion of the curves, has been used to give a Richardson line with slope 1·07 eV. Values ranging from slightly less than this figure to about 1·15 eV have been obtained. These values are in close agreement with those found by Balas, Dempsey and Rexer[6] for their oxide-impregnated nickel matrix cathode.

Approximate d.c. emission currents obtained are 1 A/cm^2

at 840° C and 2–3 A/cm² at 900° C. While values up to 8 A/cm² have been obtained, no life studies have been made at these high current densities. Cathodes, polished using the technique as for microscopic examination (see subsequent section), have given substantially the same results as unpolished ones. Further, exposure to air at atmospheric pressure after activation causes no permanent deterioration, thus making the cathodes useful for testing electron-optical devices in demountable vacuum systems.

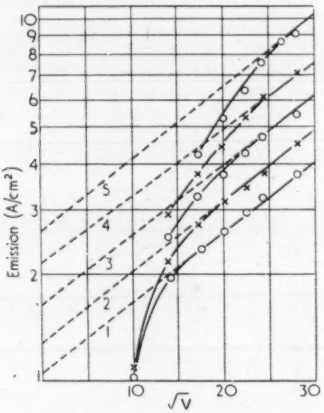

Fig. 1. Schottky curves of a typical cathode

Curve (1), 808° C; curve (2), 830° C; curve (3), 852° C; curve (4), 873° C; curve (5), 885° C.

Limited thermionic and spectrochemical analysis of the evaporation products indicate a total barium evaporation rate of $1{\cdot}5 \times 10^{-1}$ μg/cm² × h at 900° C, a temperature at which about 2½ A/cm² is available. Similar figures have been given by Brodie and Jenkins[7] for their impregnated cathodes.

LIFE TESTS

Using the small diodes mentioned above the emission life has been tested by operating the cathodes at 850–900° C while drawing a space-charge limited current of the order of 0·5 A/cm². The decrease in d.c. emission over 5000 hours has not been more than 20% of the initial value and usually considerably less than this. Periodically the valves are further tested, at 940° C, by applying a 1 kV, 2 μs pulse (250 pulses/s) thus ensuring temperature-limited emission. Typical results are shown in Fig. 2. More recently the time taken to reach a stable emission has been reduced by the adoption of the ageing technique referred to above.

Life tests under more stringent conditions have been carried out in valves employing a copper water-cooled anode. One such valve, operating at 835° C drawing a "knee" emission of 1 A/cm² at an anode voltage of 1 kV, has shown a 25% decrease in emission in 10000 hours.

Results recently announced by Hadley, Rudy and Stoeckert[8] for their "molded" cathodes operating under similar conditions show a 30% decrease in d.c. emission and a 50% decrease in pulse emission currents over a period of 1000 hours. Using similar constituents but different sintering techniques, Beck, Brisbane, Cutting and King[9] quote lives of 5000 hours at 1 A/cm² and 1000° C. Experimental results obtained by these latter authors indicate, however, that the mechanism of operation in this case is that of an atomic film emitter rather than emitting oxide grains within a nickel matrix.

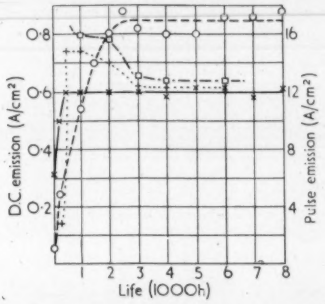

Fig. 2. Emission density variation with life

——— diode *A*, d.c. emission. ..... diode *B*, d.c. emission.
– – – diode *A*, pulse emission. —·— diode *B*, pulse emission.

At present only limited life test information on cathodes mounted in microwave valves is available, but polished cathodes, mounted in travelling-wave tubes, have shown no deterioration in emission current or noise factor over periods in excess of 2000 hours.

METALLOGRAPHY OF THE CATHODE

Attempts to prepare active oxide cathodes by mixing various powdered reducing agents with (Ba, Sr)CO_3 have been unsuccessful.[10] This finding has been substantiated in the case of boron. Oxide coatings containing boron supported on a pure nickel base show little thermal activation when maintained at 900° C for several hours. Activation by drawing current followed a similar course to cathodes prepared in an analogous manner but without the inclusion of boron. A knowledge of the location and form of the boron in the sintered cathodes is, therefore, important in considerations of the mechanism of operation.

The relevant part of the nickel-boron equilibrium diagram is shown in Fig. 3. It is seen that an intermetallic compound, Ni_2B, is formed at about 92% nickel and the solid solubility of boron in nickel is negligible. There is also a eutectic point at composition 96% Ni, 4% B.

In order to determine whether the boron in the cathode exists as free boron or in combination with nickel as Ni_2B, alloys of composition Ni/4% B and Ni/0·4% B were prepared: (*a*) by melting and casting into small ingots and; (*b*) by pressing and sintering the powdered materials. Sections were polished using graded emery paper followed by two grades of diamond dust (6 and 1 μ).

From Fig. 3 it will be seen that the Ni/4% B alloy melts at 1140° C while the Ni/0·4% B alloy is not wholly liquid until a temperature of over 1400° C is reached. At a sintering temperature of 1150° C the Ni/4% B would be above its melting point and the resulting pellet would appear similar to the melted and cast ingots; the Ni/0·4%B alloy, however, would still be partly solid.

Microscopic examination of the cast ingots after etching with Carapella's reagent (ferric chloride 5 g, concentrated hydrochloric acid 2 cm^3, ethyl alcohol 99 cm^3) showed a typical eutectic structure (Fig. 4) for the Ni/4%B alloy consisting of alternate plates of nickel (light) and Ni_2B (dark). The Ni/0·4%B alloy (Fig. 5) showed nickel grains with dark Ni_2B in the boundaries. The sintered Ni/4%B alloy was similar in appearance (Fig. 6) to the cast structure, but the Ni/0·4%B alloy showed light, outlined, particles within the nickel grains (Fig. 7). Since Ni_2B etches dark, it was concluded that the light particles were of unreacted boron, this conclusion being supported by the absence of such particles in a polished section of a sintered pellet of pure nickel.

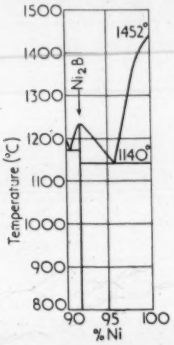

Fig. 3. Nickel/boron equilibrium diagram (nickel rich)

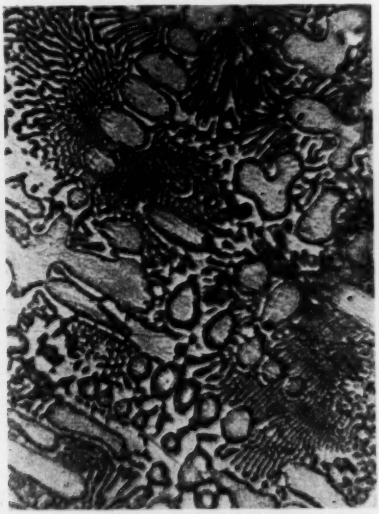

Fig. 4. Microstructure of melted and cast Ni/4%B ingot (Ni_2B dark, Ni light). (×320)

Fig. 5. Microstructure of melted and cast Ni/0·4%B ingot (dark Ni_2B in Ni grain boundaries). (×320)

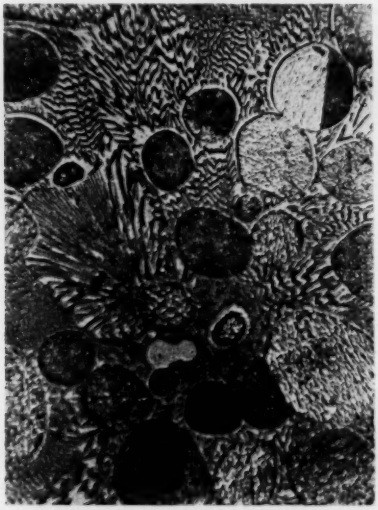

Fig. 6. Microstructure of sintered Ni/4%B (Ni_2B dark, Ni light). (×320)

Fig. 7. Microstructure of sintered Ni/0·4%B showing boron grains (light, outlined) with dark etch pits in a nickel matrix. (×320)

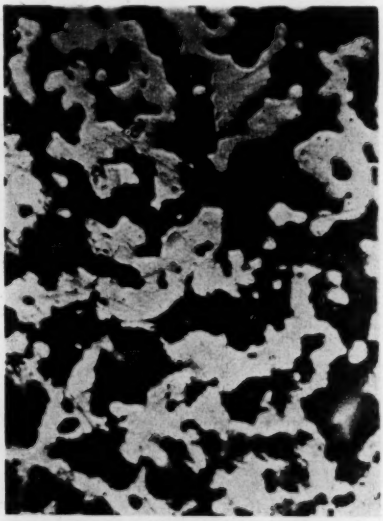

Fig. 8. Microstructure of cathode surface showing small outlined particles of boron in nickel grains. (×720)

Examination of a cathode pellet containing carbonates showed the existence of small outlined particles (Fig. 8). These particles and also the nickel grains are much smaller than in the corresponding carbonate free pellet (Fig. 7), but this observation is consistent with the inhibition of grain growth by a second phase, in this case, the carbonates. It was therefore concluded that the boron in a cathode pellet is present mainly as free boron with possibly some Ni_2B.

To show that Ni_2B is capable of reducing the alkaline earth oxides, conventional oxide-coated cathodes were prepared using three different base metals, namely, Ni/4%B, Ni/0·4%B and pure nickel. The cathodes were activated by a thermal process emission being checked periodically for brief intervals of time. Whereas the pure nickel-based cathodes showed no increase in emission density beyond about 50 m A/cm^2 over 40 min heating time, the eutectic-based cathodes gave 0·5 – 1 A/cm^2 in 10–20 min. Intermediate values were obtained for the 0·4%B-based cathodes. Boron may therefore prove to be a useful addition to oxide-cathode base alloys. This finding is, however, contrary to one test made by Sylvania[11] using a 0·08% boron base alloy.

From these various investigations it may be concluded that free barium may be produced in the cathode by the pure boron in the nickel or by Ni_2B. Probably the higher barium pressure produced by the pure boron is important in the early stages of cathode operation with some contribution from the Ni_2B during life.

CONSTITUTION OF THE EMITTING SURFACE

After activation the cathode surface consists of approximately 20–25% nickel, the remainder being mixed alkaline earth oxides. Assuming the nickel to have a monatomic coverage of barium, the work function, ϕ, of these grains would be about 1·7 eV while for the oxide grains the value would approximate to 1 eV. The average work function for the complete surface would then be 1·1–1·2 eV in reasonable agreement with measured values. Assuming the nickel grains to remain free of barium ($\phi = 4{\cdot}6$ eV) the average work function would be nearer 2·0 eV. This suggests that the cathode consists of emitting oxide grains within a nickel matrix, the work function of the nickel being reduced by at least a partial barium coverage. Considerably more information is required regarding the migration of barium on nickel, the location and size of the pores, and the electron velocity distribution before an accurate physical picture of the mechanism can be obtained.

CONCLUSION

A description of a matrix type cathode together with some experiments to elucidate the mechanism of operation has been given. Several characteristics such as mechanical strength, machinability, recovery from gas poisoning and ion bombardment and good life at high current densities make it superior to the oxide cathode in applications where the demands on the cathode are severe, e.g. backward-wave oscillators and high-power pulse valves. More experimental work on the nature of the evaporant, correlated if possible with some parameter such as porosity, is required, in addition to more life studies at high pulse densities and d.c. current values in excess of 1 A/cm^2, before a final assessment of the relative merits of this cathode can be made.

ACKNOWLEDGEMENTS

Acknowledgement is made to Dr. E. Eastwood, Director of the English Electric Vacuum Physics Research Unit, for

permission to publish this paper. The author is also grateful to his colleagues at the Marconi Research Laboratories, Great Baddow, for many helpful discussions and in particular, to Mr. R. E. Adlington for his assistance in taking the various photographs.

REFERENCES

(1) LEMMENS, H. J., JANSEN, M. J., and LOOSJES, R. *Philips Tech. Rev.*, **11**, p. 341 (1950).
BRODIE, I., and JENKINS, R. O. *J. Electronics*, **2**, p. 33 (1956).
RITTNER, E. S., AHLERT, R. H., and RUTLEDGE, W. C. *J. Appl. Phys.*, **28**, pp. 156, 167 (1957).
(2) KATZ, H. *J. Appl. Phys.*, **24**, p. 597 (1953).
(3) LEVI, R. *J. Appl. Phys.*, **24**, p. 233 (1953); *Instn Radio Engrs Conv. Record*, **1**, Pt 6, p. 40 (1953).
(4) COOMES, E. A., and FORSBERGH, P. W. *U.S. Patent No.* 2 543 439.
MACNAIR, D., LYNCH, R. T., and HANNAY, N. B. *J. Appl. Phys.*, **24**, p. 1335 (1953).
(5) RITTNER, E. S. *Philips Res. Rep.*, **8**, p. 184 (1953).
(6) BALAS, W., DEMPSEY, J., and REXER, E. F. *J. Appl. Phys.*, **26**, p. 1163 (1955).
(7) BRODIE, I., and JENKINS, R. O. *J. Electronics*, **2**, p. 457 (1957).
(8) HADLEY, C. P., RUDY, W. G., and STOECKERT, A. J. *Abstract* 84, Washington Meeting of Electrochemical Society (May 1957).
(9) BECK, A. H., BRISBANE, A. D., CUTTING, A. B., and KING, G. *Vide*, **9**, p. 302 (1954).
(10) RITTNER, E. S. *Philips Res. Rep.*, **8**, p. 184 (1953).
NOTTINGHAM, W. B., CARDELL, J., and LEVY, I. E. *Report on contract N7onr-389: Fundamental research on raw materials used for electron emissivity on indirectly heated cathodes* (1951).
(11) BENDER, H. *Vide*, **11**, p. 112 (1956).

The evaporation of sprays

By R. T. JARMAN, M.Sc., A.Inst.P., D.I.C., A.R.C.S.,* Colonial Insecticides Research Unit, Porton Down, Wilts.

[*Paper received* 23 *October*, 1957]

The rate of evaporation of an aircraft spray of kerosene droplets in the atmosphere has been measured, and was found to approximate to the theoretical estimates.

The rate of evaporation of spray droplets has been deduced theoretically by Probert,(1) while Sacks(2) measured the rates of evaporation of kerosene sprays in a small chamber and found them to be about 1% of the theoretical values. Recently, while assessing the performance of certain aircraft sprays,(3) the evaporation of a dyed kerosene spray in the atmosphere was measured. Although the scatter of the results was not small, it was found that the rate of evaporation was close to the theoretical values.

Probert took the droplet size distribution to follow the Rosin–Rammler relation,

$$R = \exp\left[-(x/\bar{x})^n\right] \tag{1}$$

where R is the volume fraction of the spray composed of droplets greater in diameter than x, $\bar{x}$ is a mean droplet size, and n a measure of droplet uniformity. With the rate of evaporation of droplets given by the relation,

$$\frac{d}{dt}(x^3) = -\frac{2}{3}\lambda x \tag{2}$$

where λ is a constant independent of droplet size, dependent on humidity, etc., and equal for all droplets, Probert showed that the percentage of the spray remaining T seconds after emission is

$$\int_{\sqrt{\lambda T}}^{\infty} (-100n)\frac{x^{n-4}}{\bar{x}^n}(x^2 - \lambda T)^{3/2} \exp\left[-(x/\bar{x})^n\right]dx \tag{3}$$

He integrated this graphically for various values of $\sqrt{\lambda T}/\bar{x}$ and n. Langmuir(4) showed that for stationary droplets in still air,

$$\lambda = 8\Delta Mp/R\rho T \tag{4}$$

where Δ is the diffusion coefficient, M the molecular weight of the vapour, p the vapour pressure of the liquid, R the gas constant, ρ the liquid density and T the absolute temperature. Using this equation the rate of evaporation of kerosene was computed taking

$\Delta Mp/RT = 1{\cdot}3 \,.\, 10^{-6}$ g s^{-1} cm^{-1} (Sacks(2))
$\rho = 0{\cdot}807$ (Sacks(2))
$\bar{x} = 200$ to $280\ \mu$
$n = 2{\cdot}5$
} see field experiment described below.

It is shown as a full line in the figure.

In the field assessments the aircraft, an Auster J.5G was flown straight and level at a height of 40 ft, across wind, over a slightly contoured surface of short grass. Kerosene (tractor vapourizing oil) dyed with 1% of Waxoline Red Dye (by Imperial Chemical Industries Ltd.) was emitted for 30 s at 10 gals/min producing a line source of spray which drifted downwind. Filter papers were laid in a downwind line at 10-yard intervals in the centre of this line of spray. The droplets deposited on them, and by measuring the stain sizes visually, and the dye deposited colorimetrically,(3) the (percentage) volumes remaining at various distances downwind were found. They are plotted in the figure. The droplet size distribution of the deposit was measured at various distances downwind and found to approximate to the Rosin–Rammler relation. While n was approximately 2·5 from 25–110 m downwind, $\bar{x}$ decreased from 280 μ at 25 m to 200 μ at 110 m. The large droplets deposited on average nearer to the aircraft track, but the range of droplet sizes found at various distances was similar. The wind speed was 3 m/s.

Comparing the theoretical and measured values we see that they are of the same magnitude, but there was appreciable scatter of the observations. The deposited spray characteristics were used in the calculation, not the emitted (pre-evaporation) spray, but the error arising in this way would probably be small. The smaller decrease of evapora-

* Now at Chesterford Park Research Station.

tion with distance found in the measurements shown by the dotted line through the points could be due to the dyed tractor vapourizing oil being a mixture in which the less volatile components evaporated off early in the flight leaving the less volatile residues (including the dye) to reduce the

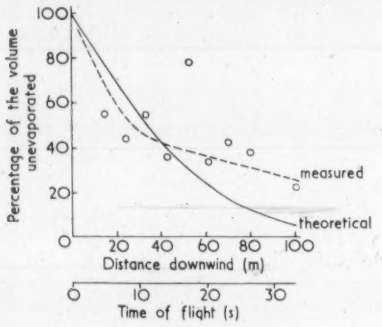

The volume lost by evaporation

evaporation rate, or because the theory treats the droplets as stationary. The relative motion of individual droplets and air increases the rate of evaporation by a factor[5]

$$1 + 0{\cdot}276\, Re^{\frac{1}{2}}(\nu/\Delta)^{\frac{1}{3}} \qquad (5)$$

where Re is the Reynolds Number of the droplet (due to its falling relative to the surrounding air) and ν the kinematic viscosity of the liquid (tractor vapourizing oil = 1·8 centistokes) the Reynolds Number is given by the relation

$$Re = vx/\nu' \qquad (6)$$

where v is the relative velocity of droplet and air (here the terminal velocity) and ν' is the kinematic viscosity of air. As v increases with x, Re increases with droplet size (equation 6) and so does the increase in the rate of evaporation (equation 5). The magnitude of the factor for kerosene is 1·01 for a 10 μ diameter droplet, 1·55 for 200 μ and 2·49 for 500 μ. Therefore this mechanism could also cause the evaporation to decrease more rapidly with distance, than the simplified calculations indicated.

The experiments[2] in a small chamber used such slow airflow that the theoretical evaporation rate would have produced approximately saturated air. As the theoretical treatment is for negligible vapour concentration, and appreciable quantities of vapour could reduce the rate of evaporation, the chamber results were less than the calculated values. From the present measurements it is clear that the simplified theoretical treatment gives the right order of magnitude for the rate of evaporation of kerosene in the atmosphere when the vapour concentration is small.

REFERENCES

(1) Probert, R. P. *Phil. Mag.*, **37**, p. 94 (1946).
(2) Sacks, W. *N.R.C. (Canada). Div. of Mech. Eng. Rpt. No. M.F.* –2816 (July 1950).
(3) Hill, R. F., and Jarman, R. T. *J. Agric. Eng. Res.*, **4**, p. 243 (1957).
(4) Langmuir, I. *Phys. Rev.*, **12**, p. 368 (1918).
(5) Froessling, N. *Gerlands Beitrage zur Geophysik*, **52**, p. 170 (1938).

Measurements on the air-nuclei in natural water which give rise to cavitation

By K. S. Iyengar, M.Sc., Ph.D., and E. G. Richardson, B.A., Ph.D., D.Sc., King's College, Newcastle upon Tyne

[*Paper received* 11 *November*, 1957]

Measurements are described on the detection by physical means of the gaseous nuclei in water which are responsible for the water cavitating when the pressure is reduced. For measuring the critical pressures for cavitation an ultrasonic excitation is used. To estimate the size and number of the nuclei, methods based on the reverberation and optical scattering are used. The changes in cavitation potential of aerated water with time and the effect on the nuclei of subjecting the water to prolonged excess pressure are described.

1. Introduction

Whilst an extensive literature exists on the subject of the development and disappearance of vacuous or gas-filled cavities in water, there still remain gaps in our knowledge of the mechanism of initiation of cavities. In particular, there remain unresolved difficulties in reproducing results reported from one laboratory in others, which suggest that there are latent differences in the nature of different specimens of water which make them more or less susceptible to cavitation. About twenty years ago Harvey[1] and others suggested that such differences were to be ascribed to the presence or absence in the liquid of nuclei on which cavities could develop and put forward as evidence for their ideas the fact, now well established, that the subjecting of the liquid to prolonged high pressure inhibited the subsequent formation of cavities even after the pressure was reduced, the nuclei presumably having been driven into solution by the applied pressure. Yet the means of measuring, even of detecting these nuclei, has been lacking. It was in the hope of being able to make such measurements and to be able to assess, in advance of their use in hydraulic machines, the cavitating propensities of water specimens that this research was undertaken. During the course of the work, there emerged fundamental physical data on the nature of the cavitation process and of the meaning of the term "solution," as applied to gas in liquid. These will be discussed subsequently in another paper.

2. CAVITATION THRESHOLD POTENTIAL

It was decided, in repeating the experiments of Harvey and others, that a method of initiating the cavitation should be used which would allow a "critical potential" for cavitation to be quoted for each liquid tested. One operation which lends itself readily to this usage is the application of ultrasonics. The electric potential in volts applied to a piezoelectric or magneto-strictive transducer in contact with the liquid can generally be taken as a measure of the alternating sound pressure amplitude set up in its vicinity. When this method was tried, an effect already noticed by previous workers in ultrasonic cavitation was observed. It was found impossible to express "cavitation potential" as a single parameter, the time to cavitate being also involved.

The bubbles that appear at the onset of cavitation are generally of two kinds, gas (air)-filled bubbles and vacuous or more exactly vapour-filled bubbles. Gas-filled bubbles grow to visible size and then remain stable while vapour-filled bubbles expand and collapse explosively in a sound field. The term cavitation in respect of hydraulic machinery is normally applied to the formation of vapour-filled cavities, these being the ones whose collapse causes erosion. But this distinction is not critical as both kinds of cavitation must in the last analysis originate from microscopic cavities already existing in the liquid. When the liquid contains dissolved gases these will diffuse into the growing nucleus and give rise to gaseous cavitation. During the progress of this cavitation, vapour-filled bubbles are also seen to grow and collapse so that the two types of cavitation can exist side by side.

Our measurements of cavitation potential were performed using a focused sound beam in a cavitation tank (Fig. 1)

Fig. 1. Tank for observation of cavitation
T, transducer; *R*, reflector; *A*, absorber.

consisting of a rectangular box made of Perspex sheets 26 × 15 × 15 cm open at the top. A 442 kc/s barium titanate saucer-shaped transducer is set into one end with its inner surface (8·7 in. diameter) in contact with the liquid in the tank. The connexions from the plated faces of the transducer are led to a power oscillator which is capable of delivering a maximum electrical output of 100 W. To absorb the waves at the far wall a pad of glass wool was used; otherwise a concave reflector (two watch glasses enclosing an air-film) could be interposed to double the effect at the focus. In order to determine the sound intensities at the focus of the transducer, the radiation pressure on a small steel bead 1·6 mm diameter suspended by a nylon thread in this region was measured. A microscope was used to watch the bead and adjust its position in the focus.

The power to the transducer was gradually increased and at every step the reading of an electronic voltmeter connected to it was noted. From the force required to restore the bead to its original position, the intensity of the sound field or peak pressure at the focus was measured and compared with the reading of the voltmeter. A peak pressure of 1·6 atm at the focal point of the (progressive) sound field corresponded to a potential of 5 V on the transducer.

3. OBSERVATION OF CAVITATION INCEPTION

The onset of cavitation was recognized by two methods. In the first method a microscope was used to observe the bubbles. (The smallest bubble that could be seen through it was of a radius of 10 μ.) At the onset of cavitation in aerated water, bubbles of this size suddenly appear one after another in rapid succession at the focus which is a pressure antinode. They start rising in an oblique direction towards a pressure node. On the way the smaller bubbles coalesce to form larger ones, but more often the individual bubbles grow in size as they move forward and finally join larger bubbles.

The second method of detecting the onset of cavitation was through the noise the bubbles make while they are growing in a sound field. This noise is picked up by the same bowl transducer which provides the acoustic energy to start cavitation and is detected through the modulation which it produces in the circuit driving the transducer, seen on an oscillograph or heard in a pair of headphones attached thereto. This method of detecting gaseous cavitation is quite sensitive, as even before the bubbles become visible in the microscope, the onset of cavitation can be heard.

In the main, the methods of measuring nuclei resolve into two types: (1) acoustical, and (2) optical.

4. ACOUSTICAL MEASUREMENTS

The absorption of sound waves in degassed distilled water is small at frequencies below 2 Mc/s. At these frequencies, the presence of small quantities of air entrained in water, however, considerably increases the absorption. One convenient way of measuring this excess absorption is to employ the reverberation technique (compare Mulders[2]).

In this method measurement is made of the rate of decay of a diffuse sound field established in the liquid. The attenuation is caused by absorption in the liquid itself and also by energy losses associated with the vessel. The vessel losses are determined by using a liquid for which the coefficient of absorption of sound is known.

In this work both spherical and cylindrical glass vessels were employed as containers of water. They were suspended by thin twine in a constant temperature enclosure. The source of sound was a small barium titanate transducer attached to the outer wall of the vessel. A similar transducer served to pick up the decaying sound field. The experimental details of this apparatus will be found in a paper by Lawley and Reid.[3]

The reverberation vessel is first filled with degassed water which has been kept standing for several days and the reverberation times are determined at a number of frequencies. Then tap water—or other specimen—is substituted. The difference in the reciprocal of reverberation time—the "decay factor" δ—is a measure of the sound absorption due to air bubbles. The results for tap water are shown in Fig. 2. The curves shown represent the fact that the bubbles cover a range of size, peaks being associated with the existence of bubbles of diameter d having a resonant frequency f_0(c/s) according to Minnaert's[4] formula: $f_0 d = 652$. (At 165 kc/s this diameter is 40 μ.)

It will be noted that the prominent peak in curve (*a*) is absent in curve (*b*) which was recorded half an hour later. The larger bubbles disappear at first, then the smaller ones, and so the decay constant continues to fall, until finally after 20 hours it becomes almost identical with that of degassed water. Applying Stokes' law we arrive at an estimate of the

size of the bubbles which can reach the surface at the end of this period. It is of the order of a micron.

It is possible to associate a maximum of decay constant with the size which resonates to the pulsing frequency and the height of the peak with the total resonating volume. If the Q of the bubbles was infinite then graphs such as those of Fig. 2 would delineate, with appropriate change of

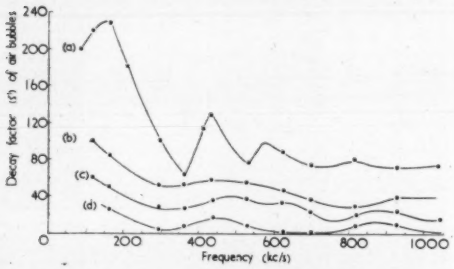

Fig. 2. Decay factor of air bubbles in tap water
(*a*) on filling; (*b*) after ½ h; (*c*) after 1 h; (*d*) after 20 h.

abscissae according to the above formula, the size distribution curve. Unfortunately for this simple viewpoint, the bubbles can be in forced vibration at frequency f off resonance. The formula derived by Pfriem[5] accounts for thermal damping and viscous damping, the most relevant to this case:

$$\delta = 4{\cdot}45 \times 10^{-4} f_0^{\frac{1}{2}}/f$$

Thus at *resonance* the radiation damping is independent of frequency, whereas that due to heat conduction is proportional to $\sqrt{f_0}$ and at kilocycle frequencies is much greater than the radiation damping. This predicted rise in overall damping with frequency has been confirmed by Meyer and Tamm,[6] Carstensen and Foldy,[7] and others. Lauer[8] measured the amplitude of single bubbles over a range of forcing frequencies. At a resonant frequency of 1500 c/s (radius 2 mm) the amplitude fell to $\sqrt{2}$ times the maximum at about 20 c/s higher, corresponding to a change in δ according to Pfriem's formula.

This frequency-dependence of the damping makes it impossible to derive *precisely* the size distribution of the gaseous nuclei, though curves such as those of Fig. 2 could be corrected for frequency dependence.

5. TESTS OF PRESSURIZED WATER

The propensity of natural samples of water to cavitation was then tested in the ultrasonic apparatus. The tank was filled with de-aerated water so that gaseous cavitation would not take place even at maximum sound intensities (40 atm). A clean thin-walled glass bulb was filled with tap water and introduced into the tank at the focus. The cavitation threshold was observed. The bulb with the water was then transferred to a pressure vessel in which hydrostatic pressures up to 10000 lb/in.^{2} could be applied with the help of a hydraulic pressure intensifier. (Actually pressures from 100 lb/in.^{2} onwards were applied for 3 to 5 min.) The pressure was then released and the bulb with the contents was again introduced into the tank at the focus. The thresholds observed in this manner are shown in Fig. 3 for different air contents. These graphs, which are linear, show a rapid increase of threshold with the degree of undersaturation. In the case of tap water the threshold pressure is nearly equal to the hydrostatic pressure. The time-effect of pressurization was also studied. Fig. 4 shows two curves

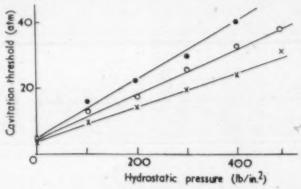

Fig. 3. Cavitation thresholds after pressurization
× represents 100% air-saturated, ○ represents 90% air-saturated, • represents 83% air-saturated.

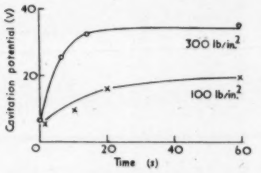

Fig. 4. Potential required to produce cavitation at various times after application of pressure

representing pressurization at 100 lb/in.^{2} and 300 lb/in.^{2} The reverberation time of the liquid was also determined before and after pressurization. Curve (*a*) of Fig. 5 shows the condition of water before and curves (*b*) and (*c*) after pressurization. The total volume of "free-air" in the water used in these experiments was measured on the M.E.R.L. modification of the van Slyke apparatus (9). The *total* air content was unchanged. The decrease in absorption indicated by curves (*b*) and (*c*) is due to the entrained air going into solution. The interesting feature of these curves is the finite amount of absorption still remaining, particularly in the neighbourhood of 1 Mc/s.

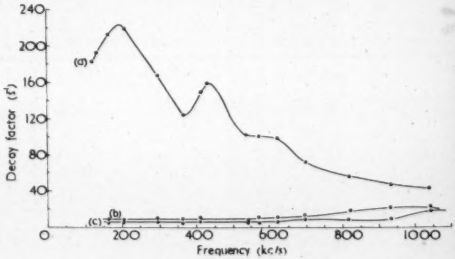

Fig. 5. Effect of pressurization on decay factor of air bubbles in water
(*a*) at start; (*b*) 5000 lb/in.^{2} applied for 24 h; (*c*) 10000 lb/in.^{2} applied for 24 h.

Many other samples of water were investigated. All natural waters contain more or less solid matter in suspension as well as dissolved gases and salts. Two samples of sea water collected near the shore on different days were subjected to cavitation. They showed a low threshold, lower than tap water. The water was allowed to remain undisturbed for a few days. But once again at the end of the period they showed the same threshold. On examination of the air content of the samples they showed undersaturation, the percentage saturation being 85%. It appeared that they contained some air in undissolved form probably entrained by the action of waves or produced by organisms near the surface. The sea water samples were pressurized at 100 and 200 lb/in.^{2} At the lower pressure they cavitated at 15 atm, while at the higher pressure no cavitation could be effected.

In tap water *vaporous* cavitation starts at a threshold pressure of 4·1 atm. The individual bursts of bubbles are just perceptible and they occur roughly at the rate of one per minute. The amount of dissolved air has no effect whatever on this threshold. The threshold for vaporous cavitation goes up quite considerably even for such small applications of pressure as 50 to 100 lb/in.^{2}, but it is not possible to state these thresholds after pressurization precisely as in the case of gaseous cavitation.

6. OPTICAL MEASUREMENTS

Detection of the nuclei by the light (or X-rays) transmitted or scattered by them is an obvious method, but one fraught by grave theoretical and optical difficulties, when, as in this case, the objects to be detected cover a range of size. An assessment of the difficulties in obtaining a size distribution curve for a *solid* suspension by optical means will be found in a paper by Ellison.[10]

Experience with nuclei in the acoustical methods of detection had taught us that some sorting of sizes with time would occur from the differential rate of rise of the bubbles in the liquid and this suggested the use of an optical method which would apply to the delineation of bubble size a combination of Mie's and Stokes' laws.

The characteristic pattern of light of wavelength λ scattered by a particle of diameter d depends on the relative refractive index m of the particles and the medium and the parameter $\gamma = \pi d/\lambda$. When $d \ll \lambda$ the intensity of the scattered light is proportional to $1 + \cos^2\theta$ where θ is the angle between the directions of the incident and the scattered light, and so is symmetrical about the direction of the incident light—as well as about a perpendicular direction. As d approaches λ more light is scattered in the forward than in the backward direction.

The scattering envelope of a sample of purified water is shown in Fig. 6. After aeration at a pressure of 15 lb/in.^{2}, the scattering is shown in the same figure for different intervals of time. The curves are typical of many observations made. They reveal the following features:

(*a*) The curves are disymmetrical about an axis perpendicular to the light path, the scattering in the forward direction being much larger.

(*b*) The minimum of the envelope is displaced in the backward direction. The magnitude of this displacement decreases progressively with increasing time.

(*c*) The symmetry which is the characteristic of purified water is not attained even after long standing.

Depending on the number of the largest bubbles present, the minimum will be shifted from the 90° position in the backward direction. After the large bubbles have risen, the smaller bubbles which are left behind, while scattering less light, will give rise to a minimum which is nearer the 90° position. This process will continue until the smallest bubbles are left in the liquid.

Tables for the coefficient k which, on the basis of the theory of Mie for a refractive index of 0·8, must be used to multiply the surface of a bubble to give its effective scattering area in the expression for the obliteration of the light (i.e. $k\pi d^2/4$), have been constructed by Lowan *et al.*[12] From these, it is apparent that the correction for the value of k being different from that pertinent to geometrical optics becomes necessary when $d < 5\lambda$. (The theory, of course, still requires that the concentration of bubbles should not be so great that one individual can interfere with the shadows of others in the light beam.)

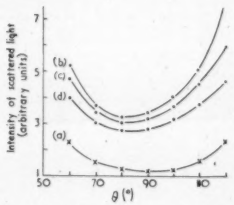

Fig. 6. Variation of intensity of scattered light (λ = 4080 Å) in water

(*a*) degassed; (*b*) aerated, at start; (*c*) aerated, after 1 h; (*d*) aerated after 10 h. The readings on curve (*a*) are magnified five fold.

In order to estimate the size of the bubbles it is necessary to compare the curves of Fig. 6 with those of the theory. From the position of the minimum and the amount of asymmetry in the experimental curve the estimated bubble size is 0·8 μ in long standing water.

Attempts to estimate the number of bubbles in unit volume of water based on light *transmission* measurements, have shown that in freshly drawn tap water the number increases with decreasing bubble size and reaches a maximum for a bubble diameter in the neighbourhood of 40 μ. The number of smaller bubbles rapidly falls until it is one (or less) per cubic centimetre below a size of 30 μ. It is interesting to note that the maximum number of bubbles has a diameter round about 40 μ which confirms the observation made earlier using the reverberation method (maximum decay rate at 165 kc/s).

7. CONCLUSION AND ACKNOWLEDGEMENTS

The acoustic method is superior to the optical method in precision, and is, in fact, well suited to the estimation of gaseous nuclei in water. Nevertheless the separate estimation of *both* their mean size and number remains a difficult and tedious process.

This work was carried out under contract to the Mechanical Engineering Research Laboratory (D.S.I.R.) and is published with the permission of the Director.

REFERENCES

(1) HARVEY, E. H. *J. Amer. Chem. Soc.*, **67**, p. 156 (1945).
(2) MULDERS, C. E. *App. Sci. Res. B*, **1**, pp. 149, 341 (1949).

(3) LAWLEY, L., and REID, D. C. *Acustica*, **5**, p. 316 (1953).
(4) MINNAERT, M. *Phil. Mag.*, **16**, p. 235 (1933).
(5) PFRIEM, H. *Akust. Z.*, **5**, p. 202 (1940).
(6) MEYER, E., and TAMM, K. *Akust. Z.*, **4**, p. 146 (1939).
(7) CARSTENSEN, E., and FOLDY, L. L. *J. Acoust. Soc. Amer.*, **19**, p. 481 (1947).
(8) LAUER, H. *Akust. Beihefte*, **1**, p. AB 12 (1951).
(9) MCNULTY, P. J. *M.E.R.L. Fluids Mem. No.* 35 (1955).
(10) ELLISON, J. M. *Brit. J. Appl. Phys.*, **5**, Suppt. 3, p. 66 (1954).
(11) MIE, G. *Ann. d. Physik.*, **25**, p. 377 (1908).
(12) LOWAN, A. N. (Ed.). *Scattering of Radiation from Circular Cylinders and Spheres*, Rep. U.S. Navy (1946).

Measurements of pressure distribution between metal and rubber covered rollers

By G. J. PARISH, B.Sc., The British Cotton Industry Research Association, Shirley Institute, Manchester

[*Paper received* 17 *September*, 1957]

Measurements of pressure distribution in the nip between a metal roller and a roller consisting of a thin rubber cover on a metal shell under various conditions of load, cover hardness and cover thickness are described. The results, although in qualitative agreement with Hannah's theory, show appreciable deviations from the quantitative theoretical predictions, and the possible causes of this discrepancy are discussed.

An experimental study has been made of the pressure distributions in nips between two rotating rollers where one of the rollers is of metal and the other consists of a metal shell carrying a relatively thin rubber cover. The apparatus with which the measurements were carried out has been described in a previous paper[1]; a pressure-transmitting pin is carried in a radial hole in the metal roller with its outer end flush with the roller surface and its inner end in contact with a glass block on the roller axis. The photoelastic effect is used to convert the load variations on the pin as it passes through the nip into intensity variations in a beam of polarized light passing along the roller axis. The light falls on a photocell and the resulting voltage variations are amplified and displayed on a cathode-ray tube. The rollers employed in the experiment were typical of those in use for mangling in the textile industry, but as similar roller systems are used in many other industrial processes the results should be of more general application.

All the measurements to which this article refers were made without any material interposed between the rollers; experiment having shown that the properties of the nip are governed primarily by the properties of the "soft" roller, and the presence of a textile fabric of normal thickness introduces only minor differences.

THEORIES

The theory of stress distribution between two bodies in contact was first investigated by Hertz,[2] and his results have been quoted by several writers.[3] This theory applies in general to the stationary contact of homogeneous bodies when the dimensions of the contact region are small compared with the dimensions of the bodies. The case of two rollers, one of which is assumed perfectly hard, in contact with their axes parallel is a particular form of this problem; it has been investigated by Thomas and Hoersch.[4] Their solution is given for conditions of plane strain.

The important features of a nip between two rollers are the nip width (the width of the contact region in the direction of rolling) and the form of the pressure distribution through the nip. With one hard and one homogeneous elastic roller the nip width is given by

$$h_0^2 = \frac{2WD(1-\eta^2)}{\pi E} \qquad (1)$$

assuming plane strain,

where $2h_0$ is the nip width,
W is the applied load per unit length of the rollers,
E is the Young's modulus of the elastic roller,
η is its Poisson's ratio, and

$1/D = 1/D_1 + 1/D_2$, D_1 and D_2 being the roller diameters.

The form of the pressure distribution through the nip is

$$P(x) = P_m[1 - x^2/h_0^2]^{\frac{1}{2}} \qquad (2)$$

where x represents distance measured from the centre line of the nip ($-h_0 \leqslant x \leqslant h_0$),
$P(x)$ is the pressure at point x, and
P_m is the maximum value of this pressure ($x = 0$).

Since it is assumed that the roller diameters are large compared with the nip width, the shape of the pressure distribution curve is independent of the values of the nip parameters.

A treatment of the problem when the soft roller is not homogeneous but consists of a thin elastic cover on a hard supporting core has been given by Hannah.[5] It is shown that both the nip width and the form of the pressure distribution now depend upon the additional parameter, the cover thickness, b. The change in nip width is given by the ratio h/h_0 for given values of the nip parameters, where $2h$ denotes the nip width obtained with a cover of thickness b. The change in shape of the pressure distribution curve is conveniently shown by using the ratio peak pressure/mean pressure, $P_m/\bar{P}$, as a measure of this shape. Its value for a homogeneous elastic roller (equation 2) is $4/\pi$ (1·27).

Hannah's treatment leads to the conclusion that the two factors h/h_0 and $P_m/\bar{P}$ depend only on the ratio nip width/cover thickness, $2h/b$ (Hannah, in fact, uses $K = h/2b$ as the appropriate factor; in the present article $2h/b$ will be used). As $2h/b$ increases from zero Hannah predicts a

decrease in h/h_0 and an increase in $P_m/\bar{P}$; her results, however, are quoted for conditions of generalized plane stress. Since the present experimental conditions must correspond much more closely to plane strain it was thought desirable to obtain results appropriate to these conditions, particularly since any difference between results on the two assumptions will be at its greatest for a material, like rubber, which has a Poisson's ratio of almost 0·5.

Making the usual modification of the elastic constants,* results have been computed from Hannah's solution for conditions of plane strain with a material of Poisson's ratio 0·5. The computation has been carried out for three values of $2h/b$, and the results are shown in Table 1. Comparison with the results given by Hannah will show that the assumption of plane strain increases somewhat the deviations of h/h_0 and $P_m/\bar{P}$ from the values appropriate to homogeneous rollers. The theoretical curves shown in the figures in this paper are derived from the data given in Table 1.

Table 1. *Nip parameters for conditions of plane strain and Poisson's ratio of* 0·5

K	0·4	0·7	1·0
$2h/b$	1·6	2·8	4·0
a_1	0·136	0·481	0·928
a_2	0·008	0·030	0·052
a_3	−0·001	−0·005	−0·009
$\frac{P_m}{\bar{P}}\left[=\frac{4}{\pi}C_2(K,0)\right]$	1·31	1·39	1·45
$\frac{h}{h_0}[=C_1(K)]$	0·80	0·62	0·50

The symbols K, a_1, a_2, a_3, $C_1(K)$, $C_2(K,0)$ are those used by Hannah.[5]

EXPERIMENTAL PROCEDURE

The machine on which the experiments were made has been fully described in the paper referred to above[1]; it is hydraulically loaded and accommodates three rollers, the centre one of which is the soft roller. The pressure pin is carried in the top roller which is of mild steel and 14 inches in diameter. This roller alone is positively driven.

Two rubber-covered rollers of different diameters and cover hardnesses were used in the experiments, and the cover thicknesses were changed by grinding, one roller being used at two cover thicknesses, the other at three. These rollers were constructed in the normal manner with a thin layer of hard vulcanized rubber, about $\frac{3}{16}$ in. thick, between the metal shell and the softer rubber cover. It has been assumed that only the outer rubber layer contributes to the nip forming properties of the system; that is, the cover thickness, b, has been taken as the thickness of this layer. The hardnesses of the covers were measured, on the rollers, with a Wallace Pocket Hardness Meter reading in ° B.S. hardness, and a load/extension curve for one of the rubber mixes was also available.

The majority of the measurements were carried out at a roller surface speed of 7 ft/min, but a few were made at higher speeds, up to 42 ft/min. Three or four pressure distributions were recorded during each run, and a mean curve was obtained from these. The correction for compression of the pressure pin assembly under load was applied where necessary.[1]

RESULTS

Examination showed that all the pressure distribution curves were very closely symmetrical in shape and that their peaks lay on the line of centres of the rollers within the accuracy of measurement of the position of this line. A change in roller speed was found to have no significant effect on the shape or magnitude of the pressure curve. Most of the pressure distributions were noticeably different in shape from the theoretical distributions. Fig. 1 shows a typical pressure distribution curve, obtained with a value of $2h/b$ of about 4, compared with the theoretical curves.

The ratios $P_m/\bar{P}$ can be computed directly from the shapes of the pressure curves, and the curves also give the nip width

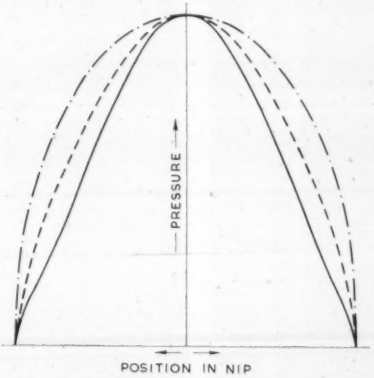

Fig. 1. Comparison of pressure curve shapes

Both pressure and position in nip are shown in normalized co-ordinates.
———: recorded curve, roller A2, $2h/b = 4{\cdot}03$.
— — —: Hannah's theory, $2h/b = 4$, plane strain, $\eta = 0{\cdot}5$.
—·—·—: Simple theory.

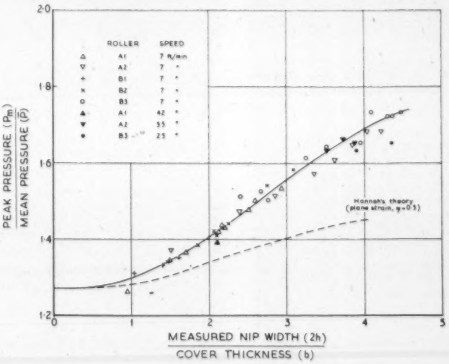

Fig. 2. Variation of $P_m/\bar{P}$ with $2h/b$

* In the present instance the change from generalized plane stress to plane strain is made by replacing $\sigma[=\eta/(1+\eta)]$ by η and E by $E/(1-\eta^2)$ in Hannah's equation (10).

Table 2. *Details of rubber covered rollers*

Roller	Diameter (in.)	Cover thickness (in.)	Hardness by Wallace meter (° B.S.)	Corresponding Young's modulus (lb. in.$^{-2}$)	Young's modulus from load/extension Curve (lb. in.$^{-2}$)	Selected Young's modulus (lb. in.$^{-2}$)
*A*1	18·9	0·38	88	2600	2550	2600
*A*2	18·5	0·19	88	2600		2600
*B*1	11·0	1·25	71	900		900
*B*2	9·75	0·62	72	950		900
*B*3	8·8	0·15	78	1300		1200

for the calculation of $2h/b$; these results are presented in Fig. 2. To make a comparison of nip widths it is necessary to know the Young's modulus of the rubber cover for the determination of h_0. The hardness meter readings can be used to give a value for Young's modulus[6]; values calculated in this way were found to be in good agreement with the value from the load/extension curve where the comparison could be made. The results are shown in Table 2 which also includes other details of the rollers. The increased hardness reading shown by *B*3 is probably due to some extent to the thinness of the cover affecting the meter reading but must be largely due to a true difference in hardness (possibly the result of increased curing near the metal shell). The selected Young's modulus has been adjusted to allow for the probable proportions of these two factors, but this value must be somewhat less accurate than the others.

The value of h_0 is calculated from equation (1) using the appropriate value of E and putting $\eta = 0{\cdot}5$, and with W determined from the area under the pressure curve (a check on this value is provided by measurement of the hydraulic line pressure); a plot of h/h_0 against $2h/b$ is shown in Fig. 3.

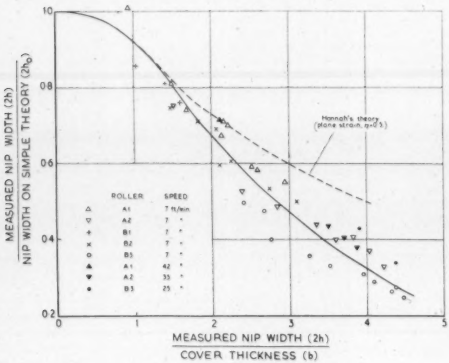

Fig. 3. Variation of h/h_0 with $2h/b$

DISCUSSION

The experimental results shown in Figs. 2 and 3 are in qualitative agreement with Hannah's theory in that the values of $P_m/\bar{P}$ and h/h_0 are determined by the value of $2h/b$ and in the direction of the change of these ratios with change in $2h/b$, but quantitatively the changes produced are significantly greater than predicted.

The h/h_0 results show somewhat more scatter than the $P_m/\bar{P}$ results, as is to be expected since they involve not only the uncertainties in the value of Young's modulus, but also the errors in absolute measurement by the pressure recording apparatus (for the determination of W).

There is some evidence for branching of the empirical curves at high values of $2h/b(>3)$, but the results in this range were all obtained with very thin covers, the thickness of which is difficult to measure accurately. In fact, because of slight distortion of the vulcanite layer during the rubber curing process, this thickness has no unique value. There seems therefore no good reason for drawing other than the single curves shown in the figures. In view of the qualitative agreement between the experimental results and the theory, these curves have been drawn so as to agree in the limit with the theoretical values for homogeneous rollers.

Several possible reasons for the discrepancy between the experimental and theoretical results can be envisaged. The theoretical treatment is based on the following assumptions, none of which is satisfied exactly by the experimental conditions:

(*a*) the nip width and the cover thickness are small compared with the roller diameters,
(*b*) strains are infinitesimal,
(*c*) the material of the cover possesses linear elastic properties, and
(*d*) the rollers are stationary.

It should be pointed out that the suggested agreement between the theoretical and experimental results at very small values of $2h/b$ does not itself rule out any of these assumptions as the source of the discrepancy, since all the covers are relatively thin and therefore small values of $2h/b$ can only be obtained from very small nip widths; that is, under conditions in which the first three theoretical assumptions are more nearly satisfied.

The results show no evidence that the discrepancy is due to the relative sizes of nip width or cover thickness and roller diameter; for example, the largest values of $2h/D$ are shown by rollers *B*1 and *B*2 which give a value of $0{\cdot}33$ at $2h/b = 1{\cdot}6$ and $3{\cdot}1$ respectively; the values given by *A*2 and *B*3 (at $2h/b = 4{\cdot}2$, $4{\cdot}5$) are appreciably smaller than this. A similar consideration rules out the finite strains; if the magnitude of the maximum rubber indentation divided by the cover thickness is taken as a measure of the strain, the largest values are again shown by rollers *B*1 and *B*2.

The most likely cause of the discrepancy is non-linearity in the elastic properties of the rubber. The load/extension curve for the rubber mix used for roller *A* shows a certain amount of curvature, and it is possible that the curvature is increased under dynamic conditions. Any other effect due to the experiments being performed with the rollers rotating does not seem likely; a significant tangential force at the nip would be expected to distort the pressure distribution curve and also to vary with speed. It may be added that the characteristic curvature of a rubber stress/strain curve in compression (towards the stress axis) is of the correct form to account qualitatively for the observed behaviour as

regards the shape of the pressure distribution through the nip.

In conclusion it may be stated that the empirical curve in Fig. 3 has been applied to the calculation of nip widths on a considerable number of textile mangles having rubber-covered rollers and has given results in good agreement with measured nip widths.

ACKNOWLEDGEMENTS

The author's thanks are due to the Dunlop Rubber Company who carried out the covering of the rollers used in these experiments and provided the load/extension curve. Acknowledgement is also due to the Director of the Shirley Institute for permission to publish this paper.

REFERENCES

(1) PARISH, G. J. *Brit. J. Appl. Phys.*, **6**, p. 256 (1955).
(2) HERTZ, H. *J. f. Math. (Crelle)*, **92**, p. 156 (1881).
(3) E.g. LOVE, A. E. H. *Mathematical Theory of Elasticity*, p. 193 (London: Cambridge University Press, 1927).
(4) THOMAS, H. R., and HOERSCH, V. A. *Univ. Ill. Eng. Exp. Sta. Bull.*, **212**, p. 7 (1930).
(5) HANNAH, M. *Quart. J. Mech. Appl. Math.*, **4**, p. 94 (1951).
(6) SODEN, A. L. *A Practical Manual of Rubber Hardness Testing*, pp. 6, 7 and Appendix III (London: Maclaren and Sons Ltd., 1951).

A method for determining ^{24}Na and ^{42}K when present together in liquid samples

By M. P. ESNOUF, M.A., B.Sc.,* Department of Biochemistry, University of Oxford

[*Paper first received* 30 *September, and in final form* 19 *December*, 1957]

A simple method has been described for the separate determination of ^{24}Na and ^{42}K in liquid samples, which is based on the differential absorption of β-particles. The relative concentrations of the isotopes are estimated from the difference in the observed counting rates of a sample when it is measured in a type M6 tube and in a modified M6 tube. Details are given for the necessary modification of the M6 tube.

In a study of the movement of sodium and potassium in tissues by means of isotopes, the long lived isotope ^{22}Na (half-life 2·6 years) and the short lived isotope ^{42}K (12·4 hours) have been used. However, since ^{22}Na is not cheap, experiments were conducted to test whether a method could be devised whereby ^{42}K could be estimated in the presence of a short lived isotope of sodium ^{24}Na (half-life 15·06 hours). The physical methods available for the individual determination of mixture of two isotopes depend on a difference either between the half-lives, or between the characteristics of the emitted radiation. In the case of these two isotopes, which have similar half lives, the first technique is not practical. On the other hand there is a difference between the emitted radiation of ^{24}Na (2·76 MeV γ ; 1·36 MeV γ : 1·39 MeV β in coincidence),[1] and ^{42}K (82% 3·58 MeV β : 18% 2·04 MeV β + 1·51 MeV γ).[2] An analysis of the γ-ray spectrum revealed that the isotopes could be estimated to an accuracy of not greater than 10% and, since only 18% of the disintegrations of ^{42}K resulted in the emission of γ-rays, the estimation of ^{42}K in the presence of a high proportion of ^{24}Na was unreliable.

Because of this an attempt was made to differentiate between the two isotopes, taking advantage of the different energies of the β-particles. Since it was desirable to determine the concentration of the isotopes in liquid samples, experiments were performed employing a counting tube of the type described by Veall.[3] It was found impracticable to determine the composition of mixtures of the two isotopes from the difference in the counting rates obtained by using absorbers of different thicknesses. The effect of increasing the size of the annular liquid space on the counting rate was calculated for both ^{24}Na and ^{42}K.[4] It was found (see figure) that, while at a liquid space of 2 mm ^{24}Na was counted at almost infinite thickness, an enlargement of the space resulted in an increase in the counting rate in the case of ^{42}K. From this it appeared that, if the isotopes were counted

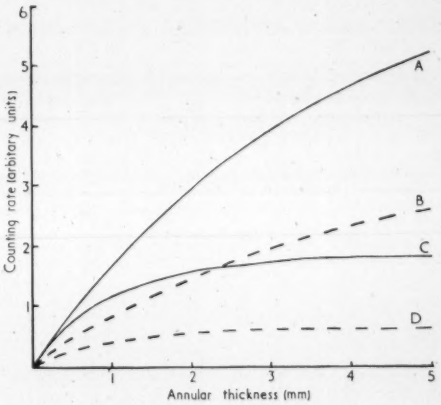

Effect of the annular space on the observed counting rate in a liquid counting tube

A, ^{42}K; *B*, ^{42}K + 80 mg/cm² Al; *C*, ^{24}Na; *D*, ^{24}Na + 80 mg/cm² Al.

* Now at Nuffield Institute for Medical Research, Oxford.

at two different thicknesses of liquid, then the proportion of each isotope present in a mixture could be calculated from the increase in the counting rate. Therefore, the solutions were counted in two counting tubes, one of which had a wider annular space than the other.

Since this method depended on the self-absorption of the solutions it was necessary that the densities of the standard and unknown solutions were approximately equal. This did not affect the difference in the counting rates for solutions containing ^{24}Na when measured at liquid thicknesses greater than 2 mm. However, there were small differences in the counting rates for samples containing ^{42}K. In order to reduce this dependence on density an absorber (80 mg/cm^2) was introduced into the counting tube with the larger annular space.

The percentage decrease in the counting rate which resulted from an increase in the density of the liquid was the same whatever the counting rate. Therefore, when the counting rate was reduced by one-half by the absorber, the loss in total counts was also reduced by one-half, and the error brought about by differences in the densities of the liquids was reduced to the same extent.

Accordingly, a modified type M6 counting tube was constructed with the co-operation of 20th Century Electronics Ltd. In this tube the thickness of the glass window of the counter was increased from 35 to 115 mg/cm^2 and the annular space from 2 to 3·5 mm. These changes made it necessary to reduce the diameter of the counting element from 16 to 12 mm so that it could be used in a conventional lead castle. The reduction in the diameter of the counter did not reduce the counting efficiency for β-particles, but brought about a small decrease in the sensitivity of γ-rays. The volume of solution required for this special counting tube was 17 ml.

The apparatus was calibrated using solutions of $^{24}Na_2CO_3$ and $^{42}K_2CO_3$ dissolved in hydrochloric acid. The salts were provided by the Isotope Division, Atomic Energy Research Establishment, Harwell.

The counting rate for a particular sample was measured simultaneously in the special tube and a type M6 tube (by 20th Century Electronics Ltd.) using two scalers for which the dead time had been adjusted to 300 μs. A single scaler could be used, however, provided that the activities were determined within a short time of each other. The samples were counted to an accuracy of 1% (10000 counts) and corrected for background and dead time. From the difference in the ratio of the activities measured in the two counting tubes (Table 1) it was possible to determine the relative activities of ^{24}Na and ^{42}K in the mixtures by using equations (1) and (2) (Table 2):

Counts/min observed with M6 = sum of counting rates due to

$$^{24}Na + {}^{42}K \qquad (1)$$

Counts/min observed with special tube = 0·315 ^{24}Na +

$$+0{\cdot}722\ {}^{42}K \qquad (2)$$

Since this technique depended partially on the self-absorption of the liquid sample, the solutions which were used for calibrating the apparatus were made to have the same density as the solutions used in subsequent experiments.

Table 1. *Comparison of the counting rates of samples of ^{24}Na and ^{42}K measured with the special and M6 counting tubes*

	Counts/min		
	M6	Special	Mean ratio special/M6
	6597·5	2055·8	
	6598·7	2067·3	0·315
^{24}Na	6473·6	2042·4	±0·0023
	6497·8	2092·8	
	5779·4	4225·5	
	5727·2	4172·7	0·722
	5711·4	4088·7	±0·0044
^{42}K	5633·8	4020·4	

Table 2. *Analysis of mixtures of ^{24}Na and ^{42}K*

Calculated Counts/ml.		Observed Counts/ml.	
Na	*K*	*Na*	*K*
1101	3427	1029	3513
2063	1428	2117	1337
83·5	3430	98·9	3451
3968	175	3904	180
835·4	2800	807	2834
2924	1050	2944	1045

ACKNOWLEDGEMENTS

I wish to thank Dr. P. F. D. Shaw, of the Clarendon Laboratory, Oxford, for much helpful discussion, and Dr. L. A. Stocken of this Department for his encouragement during the course of this work.

REFERENCES

(1) HOLLANDER, J. M., PECKMAN, I., and SEABORG, G. T. *Rev. Mod. Phys.*, **25**, p. 469 (1953).

(2) *Nuclear Science Abstracts.* New Nuclear Data, **8** (1954).

(3) VEALL, N. *Brit. J. Radiol.*, **21**, p. 347 (1948).

(4) COOK, G. B., and DUNCAN, J. F. *Modern Radiochemical Practice*, p. 246 (London: Oxford University Press, 1952).

New books

The physics of electrical contacts. By F. LLEWELLYN JONES. (Oxford: The Clarendon Press; London: Oxford University Press, 1957.) Pp. xii + 219. Price 35*s*.

This book is an addition to the well-known series of Monographs on the Physics and Chemistry of Materials, and is concerned with the fundamental physics of a subject of very great practical importance. The reliability of the automatic telephone service, for example, is a tribute to the technical efficiency of many designs of contacts, but in the search for solutions of a large number of immediate individual practical problems some of the fundamental physics of the processes involved have received inadequate attention. There has been some improvement in the position recently due, among others, to a group at Swansea under Professor Llewellyn Jones who is, therefore, well qualified to write a guide book for those wishing to learn more about the physics of contacts.

The author first states the problems involved, and points out that when a circuit is broken the behaviour of the contacts involves physical properties of the electrode materials right up to their boiling points. Indeed, Chapter VI is concerned with the properties of metals at high temperatures, and how the study of a fine metal bridge between two large masses of the same metal can give information on these properties. Such a bridge may be formed during the operation of a make-and-break contact, and chapters are devoted to the theories of their formation, to the general study of transfer of metal from one electrode to the other, and to erosion. There is an informative chapter on discharge phenomena, with particular reference to erosion, containing a clear and concise account of the main factors involved. With relatively high-power high-voltage d.c. circuits the formation of an arc discharge is considered to be practically certain, so that the chief design problems are to extinguish it as soon as possible and to minimize the cumulative damage caused by the arc. To solve these problems an understanding of the basic physics must be alloyed with a knowledge of good engineering practice. The last chapter is concerned with various contact phenomena ascribed to surface films.

In the book as a whole, there is a good balance between theory and experiments, with the main emphasis on recent work. There is a useful bibliography, and some excellent photographs. There are remarkably few slips and misprints, and the production is well up to the normal high standards of the Clarendon Press.

F. A. VICK

Radioactive materials and stable isotopes. Catalogue No. 4. (Harwell: Atomic Energy Research Establishment, Isotope Division, 1957.) Pp. 221. Free on application.

It is not often that one meets with what is, in effect, a commercial catalogue and price list but which contains such a mass of detailed information that it can serve as a most useful work of reference.

The book under review gives details of the radioactive isotopes offered by A.E.R.E. Harwell and their cost to the user. Of its 221 pages, 139 are devoted to the 136 isotopes of 74 elements. The details given are the half-life, the type and energy of radiation, the process by which the isotope is produced, and a list of the isotopes which may occur as impurities. Details also appear of the material of which the irradiated target consists and the maximum quantity which can normally be irradiated at one time. There follow the thermal neutron absorption cross-section, the excitation cross-section and specific activity produced after one week or four weeks of irradiation or at saturation. Finally there is the price per irradiation unit after one or four weeks' irradiation.

In addition to this information about the actual articles which constitute the catalogue, and the commercial details concerning sales conditions overseas, packing, transport, etc., which one expects in such a book, there are short notes on the preparation of radioisotopes, health hazards, an explanatory guide to the terms used in the book, and data which are necessary in regard to those isotopes which are used for gamma radiography and therapy.

In the article on health hazards the reviewer feels that it would be of help to many readers if, in a future edition, it were possible to define what is meant by "very high," "high," "moderate" and "low" toxicity. To the layman such terms are probably more indefinite than to the doctor or health officer, and some indication of permissible concentration would be very useful.

The book is sure to be a helpful work of reference in a difficult and rapidly growing subject.

W. E. SCHALL

Metallurgy of the rarer metals. No. 2. Zirconium. 2nd ed. By G. L. MILLER. (London: Butterworth's Scientific Publications, 1957.) Pp. xxi + 548. Price 70*s*.

Zirconium may with justice be said to have, out of all the members of its group of refractory metals, a special claim on the attention of the physicist. It shares with titanium, tantalum and niobium exceptional resistance to corrosion at temperatures up to about 400° C (through the existence of a tough, adherent, self-healing surface film of oxide), but it also, when free from hafnium, has the extremely low absorption cross-section for thermal neutrons of 0·18 barn. It thus has been of considerable interest as a material of construction in atomic reactors and their related equipment as well as in thermionic values and in other applications where its resistance to chemical attack is put to good account.

In the short period since the publication of the first edition of this excellent monograph (in 1954), there has been a considerable relaxation in the controls on "classified" information regarding many aspects of the properties and use of zirconium. As a consequence, Dr. Miller has found it necessary to increase the number of pages from 382 to 548, and a comparison of the two editions makes it evident that considerable re-writing has been undertaken to incorporate much new information and to bring the matter up to date. In the general revision, the somewhat artificial distinction between physical and structural properties has been abandoned and both are now considered in one chapter, with advantage of clarity and logical order. This new edition should enhance the reputation which this volume already has gained as a comprehensive, critical and authoritative survey of present-day knowledge of this interesting metal. It can be unreservedly recommended as a source book and a wholly reliable work of reference.

J. C. CHASTON

Notes and comments

Molecular physics

We have received the first issue of a new quarterly periodical entitled *Molecular physics*, edited by Professor H. C. Longuet-Higgins of Cambridge, and published by Taylor and Francis Limited. The group of scientists from different countries, to whom the journal owes its establishment, felt the need for bringing together papers on the physics of molecules which might otherwise be missed. The new journal will deal particularly with: (1) molecular structure and dynamics, (2) the electric and magnetic properties of molecules, and the processes of molecular excitation, ionization and dissociation, and (3) the equilibrium, transport and relaxation properties of molecular assemblies.

The price of the annual volume is £4 15*s*. ($13.30) including postage, and single parts £1 5*s*. ($3.50) plus postage. Orders should be sent to the publishers, but those originating in U.S.A. and Canada should be sent to the Academic Press Inc., 111 Fifth Avenue, New York 3, N.Y., U.S.A.

We wish the latest of the many additions to our contemporaries all success.

Nuclear engineering monographs

A new series of monographs on nuclear engineering subjects has been issued under the general editorship of Mr. W. K. Mansfield, of the Nuclear Engineering Laboratory, Queen Mary College, London. The monographs are intended for university and technical college students, research assistants and qualified technicians who require a broad understanding of those topics of nuclear engineering outside their own field of study. The depth of treatment in the specialized works currently available is often too great and the cost too high for this category of reader and in producing this relatively inexpensive series in association with their monthly journal, *Nuclear Engineering*, the publishers have attempted to meet the requirement of low cost and at the same time provide a broad treatment ranging from elementary principles to up-to-date summaries of more advanced theories. The first three titles received are *Elementary nuclear physics*, by W. K. Mansfield (price 10*s*. 6*d*.); *Nuclear reactor theory*, by J. J. Syrett (price 12*s*. 6*d*.); and *Reactor heat transfer*, by W. B. Hall (price 10*s*. 6*d*.). The monographs are published by Temple Press Books, Bowling Green Lane, London, E.C.1.

Instruments, Electronics and Automation Exhibition, 1958

The Instruments, Electronics and Automation Exhibition, to be held at Olympia, London, from 16–25 April next, will show the latest advances in scientific instruments—laboratory, industrial and medical, automation and industrial control equipment, telecommunications, radar and navigational aids, computers and many other applications of electronics and instrumentation.

Admission to the exhibition will be by tickets to be distributed by the exhibiting firms or upon payment of 2*s*. 6*d*. at the door; it will be open from 10 a.m. to 6 p.m. daily, except on Friday, 18 April, and Wednesday, 23 April, when the Exhibition will remain open until 9 p.m. There will be lectures each day on subjects relative to the exhibition.

New literature on atomic industry

The Atomic Industrial Forum has announced the availability of papers from sessions of its recent conference on "The 1957 nuclear industry." The papers cover 20 primary areas of interest to individuals involved in nuclear development today, or those who are planning activity in this field in the future.

The subject areas for which sets of papers are available include: research and test reactor progress, uranium production, radiation applications, appraisal of the atomic industry, U.S. power reactor experience, reactor fuel reprocessing, instrumentation responsibilities, financing, U.S. power reactor programme in review, reactor fuel manufacture and handling, progress in nuclear standardization, legal problems, atomic activities outside the United States, reactor components and accessories manufacture, economic incentives in the nuclear industry, information and training, factors affecting power reactor construction, marketing, financial protection against nuclear liability and advanced reactor concepts. An average of five individual papers are listed under each subject area.

A complete conference paper catalogue is available from the offices of the Atomic Industrial Forum, 3 East 54th Street, New York, U.S.A.

Journal of Scientific Instruments

Contents of the April issue

ORIGINAL CONTRIBUTIONS

Papers

An improved Czochralski crystal-pulling furnace. By K. H. J. C. Marshall and R. Wickham.
An a.c. velodyne integrator. By J. B. Sharp and R. W. Williams.
The flash photography of a deep field of view. By F. de S. Barros, D. M. Binnie and B. D. Hyams.
A simple instrument for the periodic application of controlled bi-axial strains. By P. U. A. Grossman.
An automatic quartz-fibre electrometer. By M. C. B. Russell and J. Leng.
Decade flux linkage generators. By T. M. Palmer.
A recording double-beam attachment for the Unicam type SP500 spectrophotometer. By J. L. Hales.

Laboratory and workshop notes

Magnetic measurements with the bridged-T network. By J. K. Choudhury and P. C. Sen.
An adjustable geared coupling for misalined shafts. By A. L. Sims.
Apparatus for measurement of thermal E.M.F. in semi-conductors. By J. C. Brice and H. C. Wright.
A sensitive and quickly made water flow switch. By G. W. Green.
A device for the preliminary cutting of single-crystal metallic rods to a desired orientation. By T. B. Vaughan.
Preparation of fine wires for metallographic examination. By G. L. Davis.
An economical safe hand-controlled device for raising small quantities of liquids by compressed air. By W. S. Sebborn.

NOTES AND NEWS

Correspondence
On the optical properties of a biprism combined with a coarse grating. From G. M. Sreekantath and C. A. Verghese.
New instruments, materials and tools
Manufacturers' publications
Notes and comments

THIS JOURNAL is produced monthly by The Institute of Physics, in London. It deals with all branches of applied physics (including theory and technique). All rights reserved. Responsibility for the statements contained herein attaches only to the writers.

EDITORIAL MATTER. Communications concerning editorial matter should be addressed to the Editor, The Institute of Physics, 47 Belgrave Square, London, S.W.1. (*Telephone:* Belgravia 6111.) Prospective authors are invited to prepare their scripts in accordance with the *Notes on the preparation of contributions*. (Price 2*s*. 6*d*. including postage.)

REPRODUCTION. The Institute of Physics is a signatory to The Royal Society's Fair Copying Declaration. Details may be obtained upon application from The Royal Society, London, W.1.

ADVERTISEMENTS. Communications concerning advertisements should be addressed to the agents, Messrs. Walter Judd Ltd., 47 Gresham Street, London, E.C.2. (*Telephone:* Monarch 7644.)

CLAIMS FOR MISSING JOURNALS. Claims from regular subscribers to this *Journal* for missing numbers will only be considered if received within 60 days of the date of mailing plus normal outward time of transit and time for lodging the claim. Losses attributable to failure to notify a change of address or to similar omissions will not be considered.

SUBSCRIPTION RATES. A new volume commences each January. The charge is £5 per volume ($14.25 U.S.A.), including index (post paid), payable in advance. Single parts, so far as available, may be purchased at 10*s*. each ($1.50 U.S.A.), post paid, cash with order. Orders should be sent to The Institute of Physics, 47 Belgrave Square, London, S.W.1, or to any bookseller.

SPECIAL ARTICLE

Physical methods of investigating chemical problems*

By R. J. Taylor, B.Sc., F.Inst.P., Research Department, Unilever Limited, Port Sunlight, Cheshire

The scope that exists for physicists in chemical research is greater than many physicists realize. Applications of physical methods to chemical problems have increased rapidly during recent years and a wide literature has grown up around them. A brief review of physical techniques in current use is given, together with a detailed illustrative study of two problems, the removal of fishy flavour from vitamin A oils, and the relationship of polymorphic form to the characteristics of glyceride oils. The study is treated discursively to bring in matters of related interest.

INTRODUCTION

In these days when nuclear physics is so much to the forefront it may seem a little mundane to consider an aspect of research in which physics serves—at least superficially—more as a handmaid to chemistry in the sense that the problems to be solved are basically chemical in nature. It is not really mundane: the problems may not have the glamour of those of nuclear physics, but they are not dull or unimportant. There are many problems—even in industrial chemical research—that cannot be solved by chemical methods alone, or would need a long time for solution, and it is here that physical methods are providing the more powerful tools of research. One may instance the structures of penicillin[1] and vitamin B12[2] as two problems of much scientific interest that have been solved in this way, in part by infra-red analysis but mainly by X-ray analysis.

CONTRIBUTIONS OF PHYSICS AND PHYSICISTS TO CHEMICAL RESEARCH

The recognition that physics can contribute usefully to chemical research is a comparatively recent phenomenon. In fact, it was not until the emergence of spectrophotometry in the 1930's that the star of the physicist began to rise in the chemical world. It is difficult to realize this today when one considers the techniques that have since been introduced and are now well established. Next to visible and ultra-violet spectrophotometry, X-ray spectrometry and electron microscopy have probably served longest in this field, followed more recently by infra-red and Raman spectrometry and by mass spectrometry. Other useful but more limited techniques are those of differential thermal analysis, thermal diffusion and zone melting. One must mention also the various techniques that are ancillary to chromatographic methods of separation: the Schlieren optical system and the differential refractometer used in adsorption or partition chromatography, and the catharometer, gas density balance and ionization gauge used in vapour phase chromatography. There are the newer techniques of magnetic resonance—already being actively developed in America and to a lesser extent in this country—which will be of further valuable help to chemical research. Finally, and in a slightly different capacity, there is radio tracer work which calls for a close fusion of the efforts of physicists and chemists.

Moreover, advances in instrumentation in the older techniques have made their usefulness more generally acceptable. One may think nostalgically of the old visible region spectrophotometer with its optical principles barely hidden from the inquiring eye—still good for teaching or for demonstrating to V.I.P.'s—or of the drill necessary with the ultra-violet photographic instrument; but the introduction of photoelectric instruments marked a significant advance, particularly in quantitative accuracy, although one might sometimes miss fine absorption structure that would be immediately obvious in a photograph. Now the age of recording spectrophotometers has been reached, and the spectrum can be scanned automatically from 1850 Å through the ultra-violet and visible regions to the near infra-red as far as 2·5 μ. Not in one run, of course, for different light sources are required, but a quite complicated spectrum that formerly would take up to two hours to map manually now takes only twenty minutes, with no fine structure missed.

Instrumentation, however, is a dangerous word for physicists for often it obscures the role they play. One is tempted at times to pose the question, "When is a physicist not a physicist?" in order to provoke the answer "When he is an instrument technologist." For it is in the guise of instrument technology that many of the contributions of physics are being introduced to the chemical world. Paradoxically, one could just as reasonably ask, "When *is* a physicist a physicist?" for although the methods of attack are those of physics the reasoning and deductions are often those of chemistry.

A physicist in the present context needs to maintain his knowledge on a wider basis than the man whose research is physics. He needs to recognize what physical methods may be applied to the problem in hand and how to apply them. He is concerned with both methods of isolation and non-destructive methods of identification. He needs to assess new physical methods that may be developed in relation to the problems awaiting solution. And he needs to know a little chemistry. While it is true that instruments and apparatus have been developed that can be operated by trained assistants—and chemists—the basic understanding of the methods and their uses rests with the physicists.

There is already an adequate literature on the applications of physical methods and there is no need here to state more than that it exists. Moreover, merely to describe methods and their uses would leave no clear picture of their usefulness and so, to present them in another, less detached manner just two examples will be given of industrial research problems within the experience of the author. They will be used as a kind of framework on which to hang a number of comments not wholly relevant to the problems themselves but quite consistent with the theme of the paper. The first concerns vitamin A, and the second the glycerides of natural fats.

A PROBLEM OF VITAMIN A OILS AND FISHY FLAVOUR

Vitamin A is a substance of some importance to our well-being but of little obvious interest to physicists. Yet it is to

* Based on a lecture given to the Liverpool and North Wales Branch of The Institute of Physics in Liverpool on 8 February, 1957.

vitamin A that physicists owe the initial industrial interest in spectrophotometers, which created a demand for the now ubiquitous photoelectric model. Vitamin A in its simplest terms is an unsaturated alcohol having in its structure five conjugated trans* double bonds and five branched methyl groups [Fig. 1(*a*)].

The conjugated system of five double bonds gives rise to the strong spectral absorption band [Fig. 1(*b*)] in the region of 325 mμ that is characteristic of vitamin A; and a quite

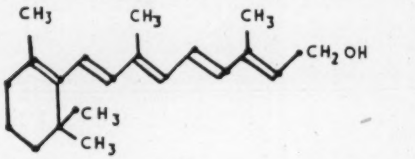

(*a*)

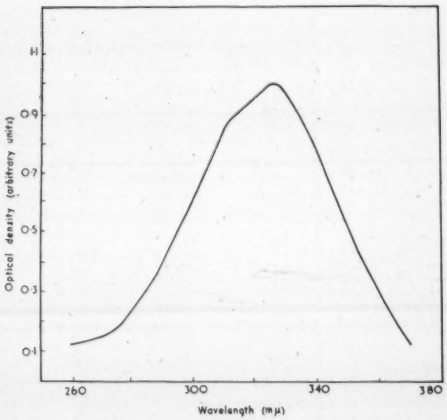

(*b*)

Fig. 1. Vitamin A alcohol. (*a*) Structure; (*b*) Spectral absorption curve in solvent in the region 260–380 mμ

fantastic amount of work has been done in delineating, in a most precise manner, the absorption curves of the alcohol and its esters, in all manner of solvents, for in any quantitative evaluation the proof of identity and purity lies in the precision of fit of the unknown to the known. Vitamin A is a costly commodity and the quantitative capabilities of spectrophotometry must be stretched to their limit for the sake of accountancy.

Until recent years, the sole source of vitamin A was liver oils, obtained either from whales or a variety of fish; and a major problem, particularly with fish oils, was to refine them sufficiently to provide a palatable product for human consumption. At the time in question (1939) whale liver oil was in diminishing supply; hence the need for an efficient refining method for fish liver oils was paramount. Nowadays synthetic vitamin A is used almost universally in food for human consumption; and this, in the American scene, has given rise to some delightfully uninhibited advertising, with "No Fishy Burp" as its theme. The problem here then was the removal of fishy burp from natural sources of vitamin A without destroying the vitamin to any significant extent in the process.

There was some work being carried out in America, and it is worth referring to it here because it provides a classic example of the elevation of a comparatively simple physical technique to the status of a major American industry. It originated with Kodak and there is a possibly apocryphal story that it was primarily concerned with the instantaneous drying of photographic film, for which a molecular still was required. Wishing to test the efficiency of the still, the operator took the nearest thing to hand, a large bottle of medicinal cod liver oil, and found to his surprise that he could separate and concentrate both vitamin A and vitamin D. From this developed a large molecular distillation industry turning out concentrates of many natural products of physiological importance. The technical advances that were made thereby in the process of molecular distillation were reflected in the research laboratory in the provision of a remarkably neat laboratory cyclic still (Fig. 2) of advanced design, utilizing a

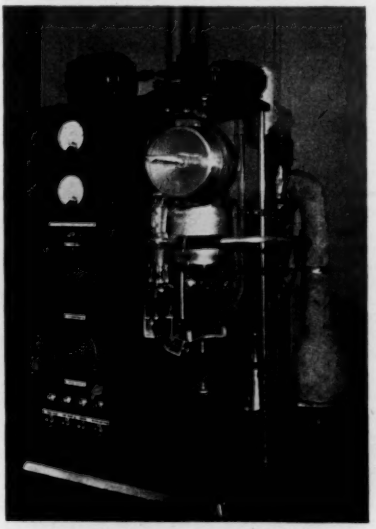

Fig. 2. CMS-5 Laboratory molecular still (by Distillation Products Inc.). The photograph shows the centrifugal disk on which distillation occurs. The distillate is collected on the domed glass face and drained into the receiver

centrifugal disk to obtain the uniformly thin film of distilland so necessary for effective distillation. A particular advantage of this form of still is that the material is held at the distilling temperature for only a second or so.

* By "conjugated" is meant that the double bonds alternate with single bonds, and by "trans" that the hydrogens at the ends of a double bond are directed spatially away from each other.

For several reasons this lead was not followed here. The results of molecular distillation had been studied in the laboratory, and American samples were intermittently examined, and it seemed that the desired edible quality of oil could not be achieved by this means. Furthermore there were difficulties in translating the process to large scale in this country, not least of which were the succession of patents being taken out by the Americans; and the costs of the process were high. So a solution was sought elsewhere.

The standard refining process, which is the basis of all edible oil work, is one in which caustic soda is added to neutralize free fatty acids in the oil. The finely dispersed soap so formed is allowed to settle and then separated from the oil. The improvement in appearance and edible quality of the oil, however, is greater than would be expected from a mere removal of free fatty acid, and examination of the soap-stock confirms that other noxious substances have been removed. What one has in fact is a mild adsorptive process in which the dispersed soap particles act as the adsorbent. It was natural, therefore, to consider alternative methods of adsorption, particularly the newer chromatographic techniques which were then in course of development.

Much is known now about the chromatographic treatment of oils. At that time it was an adventure into the unknown. A survey of available adsorbents showed alumina to be the most promising. Liver oil contains not only vitamin A but also other trace constituents like sterols and tocopherols, combined in ester form. When the oil, dissolved in light petroleum, was passed through a column of alumina the trace constituents of the oil were virtually unadsorbed by the alumina in the presence of the glycerides. They fell comparatively freely through the glycerides and concentrated at the leading edge of the chromatogram. But they could not pass through the leading edge into the free solvent beyond. This suggested two interesting possibilities: (1) to obtain a concentrate of vitamin A in the oil by isolating the lower fraction of the chromatogram; (2) to introduce a bland oil into the column immediately prior to the vitamin oil, and so obtain a transfer of vitamin A to the bland oil. Both proved feasible but uneconomic; nevertheless it was interesting, in view of the decision to use chromatographic methods rather than those of molecular distillation, to meet these words some years later in the preamble to a patent taken out by the exponents of molecular distillation: "This invention relates to improved procedure for the concentration of vitamin A esters, in particular by methods involving chromatographic adsorption. . . ."

The chosen route[3] did not lead to any significant concentration of vitamin A, although concentration could be achieved by modifying the operations. There were difficulties, because in the first case the adsorption affinity of those substances responsible for the "burp" was not greatly stronger than that of vitamin A and a delicate balance between the various factors was required, and in the second it was by no means a simple proposition to provide large quantities of cheap alumina of uniform activity. The crux of the problem turned out to be the lack of knowledge of the state of the alumina most suitable for the process. Only by giving attention to this was it possible to control the product and to produce activated alumina at a cost that made the process economical. That is to say, the problem was no longer one of chemistry but of physics.

There were two main aspects to the problem, the first relating to particle size and the other to a basic understanding of the process of activation. In any industrial process involving flow rates, time is an important factor in costing and one must provide the freest flowing column compatible with adsorptive efficiency. It was necessary, therefore, to know the particle size distribution of the starting product—particularly that fraction known as the sub-sieve fraction ($< 60\ \mu$ in size) which largely governs the flow rates—and the effects of activation upon it. The starting product was the alumina trihydrate, gibbsite, seeded from a supersaturated solution of sodium aluminate, which could be converted to an active alumina by furnace heating; and since the hydrate is a poor conductor of heat, it was conceivable that the application of heat could set up disruptive stresses in the particles and so lead to breakdown in size. Particle size is of immense importance to a number of industries, such as the cement and pottery industries, and much literature has been published on it, including the proceedings of an Institute symposium.[4] Methods for determination of size are all based on Stokes' law for falling bodies. There are sedimentation methods in which one weighs the sedimenting material *in situ* or on withdrawal, or measures the photo-extinction of a beam of light on passing through a dispersion of the particles after fixed intervals of time from the moment of uniform dispersal in a liquid. And there are elutriation methods in which the particles are segregated by an upward flow of air or liquid through a series of vessels of increasing diameter. For a $2\times$ cut in particle size the diameters must vary in the ratio of $\sqrt{2}$. In the Canadian mining industry the principle of air elutriation has been explored exhaustively, and a most efficient but awe-inspiring machine developed called the Infrasizer.[5] To prevent particle adhesion to the sides of the machine it is raised and dropped rhythmically like a hydraulic ram, and so it is preferably housed in a sound-proof room! It has been pointed out[6] that ideally such machines should have expanding cones with an angle not greater than 10°, and stilling lengths of 60 pipe diameters. The machine would then "look like a church organ and require a laboratory the size of a small cathedral to house it!" Nevertheless, air elutriation is the only method suitable when examination of the various size-fractions is required, and a simply-constructed glass laboratory-apparatus can yield useful information.

For this phase of the investigation[7] the hydrate was subjected to a variety of heat impacts, at different temperatures and for different periods of time, in the extreme instance feeding a very thin stream of particles continuously through a furnace held at 900° C, but there was no change in size distribution due to any of the treatments. This meant that an alumina of sufficiently uniform particle size distribution could be ensured merely by specifying the required distribution for the hydrate.

The experiment carried out at 900° C was of particular importance. In investigations of this sort where an understanding of a phenomenon is sought it sometimes happens that as the investigation develops one experiment will yield unexpected evidence that gives a clue to the whole phenomenon and indicates just what pattern of further experiments is required to reach an understanding. So it was here. The furnace was a simple laboratory-made affair, the hydrate trickling from a tiny hopper on to a stainless steel ribbon and moving almost instantaneously into the heated zone in which it remained for about three minutes. As stated, there was no breakdown in particle size but, surprisingly, the anhydrous material was extremely active; more active than alumina heated at this temperature in the more normal manner for several hours; and more active than one might expect from a reading of the literature. It was immediately obvious that if a number of samples were taken, small enough to ensure

rapid temperature equilibration but adequate for subsequent examination; and if these were heated in sets, each at a different temperature and each member of the set for a different period of time, then a study of the dehydration, surface activity and crystal structure of the samples should present a clear picture of the process of activation.

Now it was interesting to observe, when the literature was searched, that although the heat transformations of alumina and its hydrates had preoccupied workers for over 30 years—and the struggle to unravel them still goes on—no work had been carried out on the integrated relationship of the three properties referred to above.

The dehydration studies of the hydrate showed that loss of water of hydration commenced at about 150° C, and that up to 225° C it was progressive over a number of hours and represented a systematic conversion from trihydrate to monohydrate. Between 300° C and 500° C dehydration proceeded more rapidly to a state of equilibrium, which was then maintained over long periods of heating at the same temperature even though dehydration was not complete. At 500° C and higher only anhydrous alumina was obtained.

Activity studies, based on dye adsorption from solution, showed that the trihydrate and monohydrate were completely inactive. The partially anhydrous samples, that is those heated at temperatures between 225° C and 500° C (Fig. 3),

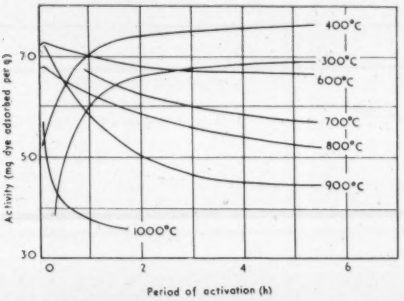

Fig. 3. Activated alumina. Activities of the heat transformation products of γ-alumina trihydrate in the temperature range 300–1000° C

exhibited activity increasing asymptotically to a maximum as the time of heating was increased. The anhydrous samples showed a sharp initial rise in activity corresponding, one presumes, to the dehydration phases, then decreased asymptotically to a steady value. The decrease was more marked as the temperature was increased. At 1400° C wholly inactive alumina was obtained.

The X-ray pattern was consistent with the dehydration and activity curves. It could be interpreted as showing first, at temperatures up to 225° C, the gradual change from trihydrate to monohydrate, both completely defined crystalline forms giving sharp diffraction lines. Between 225° C and 500° C, there was a gradual conversion to γ-alumina, a highly disordered and near-amorphous state yielding a diffuse pattern superimposed on that of the monohydrate. As the temperature of treatment of the wholly anhydrous state was increased, there was a gradual sharpening of the first γ-alumina lines and an emergence of new lines, which were interpreted as a partial orientation leading to a growth of crystallite size within the particle and a consequent reduction of active surface. At temperatures in the region of 1400° C, there was a complete orientation of structure to α-alumina, which provided again a sharply defined X-ray pattern and was completely inactive.

It was plausible, therefore, to associate activity with this highly disordered but controllable state of anhydrous alumina, and to explain the reduction in activity in terms of a gradual orientation towards a more ordered structure. That is to say, one could think of activated alumina as a continuously variable transitional product in a heat-controlled transformation. It must be admitted, however, that other workers[8, 9] claim that the transformation is not continuously variable but includes a number of recognizable crystalline states. As in mathematics, one may consider any variable function in terms of discrete steps and no more may be involved here than a matter of definition. Or it may depend on whether one views things either as a crystallographer or with a primary interest in surface functions. It is difficult to imagine truly crystalline structures with the surface activity of γ-alumina; but these facts are mentioned primarily to show that, although an insight into the phenomenon of activation was obtained that was adequate for its purposes, what in fact does occur may be considerably more complex.

It followed from the activity curves that to obtain a uniformly activated product one must heat the alumina for a sufficient time to ensure that the whole charge has reached the steady state, i.e. not less than 5 h at activation temperature. Once the optimum activity had been determined, all that was then needed was a furnace whose temperature could be controlled and held steady at the predetermined value. For some time use was made of an idle pottery furnace of the continuous type. It was convenient but not ideal for the purpose for, when lit, it took a week to come into equilibrium, and over 90% of the mass passing through the furnace was dead weight to be heated and cooled for no useful purpose. When these furnaces reverted to their legitimate use at the end of the war, a more convenient continuous electric furnace was designed and constructed (Fig. 4). With a uniform supply of alumina assured the most serious problem of the process was eliminated.

It may be of interest to give a brief description of the process[10] because, from 1942 until the introduction of synthetic vitamin A in 1950, it was used to treat a quite significant proportion of the vitamin A oils that went into the nation's margarine.

Basically it consisted of passing a solution of the oil in benzine through a tube packed with activated alumina. There were two critical factors affecting the efficiency of the process in removing the fishy flavour with a minimal loss of vitamin A. One was the concentration of oil in solvent (25% w/v) and the other the ratio of oil to alumina (1 : 3). There was the equally important economic aspect to be considered. Two factors bearing on this were (1) the flow rate of oil solution, governed by the particle size distribution of the alumina, and (2) the cost of alumina, required in a ratio of three times the weight of oil processed. It was necessary to maintain this ratio in any one cycle of operations if fishy flavour was to be removed, but the ratio could be effectively reduced by "revivifying" the alumina after each cycle for further use. To do this, adsorbed oil was stripped from the alumina with a mixture of benzine and alcohol, and the alumina was heated *in situ* and blown free of solvent, particularly of alcohol whose removal was essential to any re-use of the alumina.

Another problem peculiar to this process was to determine the optimum size of column. The first impulse in any large-

scale application of chromatographic methods is to increase the dimensions of the tube, but such a procedure was not feasible here, not least because of the difficulty of adequate heat transfer in the revivification stage. Moreover, it is not really the most efficient method of scaling-up for it can be demonstrated readily that the time required for the cycle of operations is increased disproportionately as the column dimensions are increased. It was reasoned that for large-scale work one could with advantage use a multiplicity of small columns and operate them as a single column by

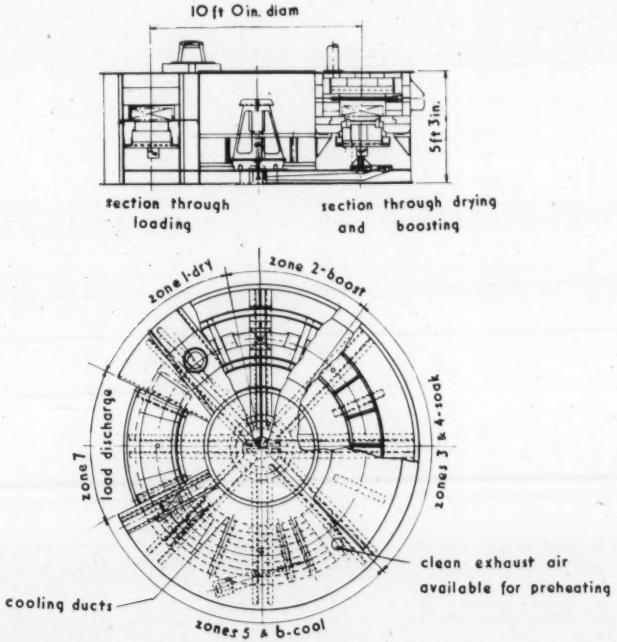

Fig. 4. Activation furnace for alumina. Electrically-heated continuous furnace of circular construction with heating, soaking and cooling sections. The design makes it possible to load and unload at the same point

employing the principle of the calandria (Fig. 5). This was perhaps the most novel feature of the process and it was useful for three reasons: (1) the conditions for operating the calandria could be determined precisely in the laboratory with a single small tube, (2) the time cycle of operations was the same as that of the small tube, (3) revivification of the alumina could be effected between cycles by having the necessary steam and water connexions to the calandria jacket. Only one difficulty was encountered and that was in convincing certain patent examiners that this was a plant for chromatographic processes and not a common heat exchanger!

A PROBLEM OF GLYCERIDE OILS AND THEIR POLYMORPHIC FORMS

Patents have a habit of obscuring their contents by the generality of their titles. The same might be said of this section of the paper. In less scientific terms its title would be: Why is chocolate hard and lard soft?

The consistency of fat products such as chocolate, butter, margarine, pastry shortenings and confectioners' fats is largely determined by the content of solid crystals in the fat and by the physical properties of these crystals. Nature makes use of a wide range of acids in building up its glycerides but considerately uses only saturated C_{16} and saturated and unsaturated C_{18} acids for the major part of them, so simplifying the task of the investigator. Nevertheless, the combinations and permutations of even this limited series of fatty acids in a glyceride molecule are many. One may have a monoglyceride with one fatty acid group and two free hydroxyl groups; a diglyceride with two fatty acid groups, or a triglyceride. The glyceride may be wholly saturated like tri-stearin, or wholly unsaturated like tri-olein. It may be a saturated mixed glyceride, and symmetrical like palmito-stearo-palmitin (PSP) or unsymmetrical like dipalmitostearin (PPS). Or it may be a symmetrical (POS) or unsymmetrical (OPS) mixed saturated/unsaturated glyceride. A basic understanding of the behaviour of simple and mixed glycerides and of mixtures of them is therefore important in the oils and fats industry; and so also is an ability to identify the glyceride structure of commercially important fats. It will be obvious that a knowledge of the existence of polymorphic forms induces caution in interpreting evidence of glyceride structure.

The conventional method of studying the component glycerides of fats is one of fractional crystallization from solvent and this has been widely used.[11] It is particularly suited to those glycerides containing wholly saturated acids

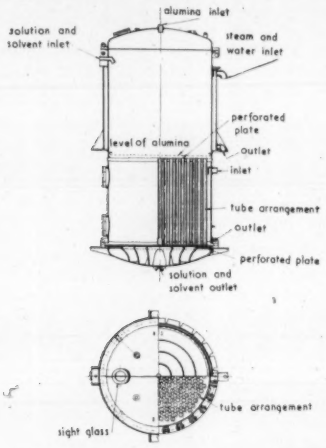

Fig. 5. Calandria for chromatographic treatment of oils. The design shows the disposition of the vertical chromatographic tubes. The head space allows a complete solvent charge to be introduced. The calandria operates under a pressure of 30 lb/in^2

or only one unsaturated acid. The difficulties of separation become greater as both the number of unsaturated acids in the glyceride molecule and the degree of unsaturation increase, but more recently the method of discontinuous countercurrent separation has been applied with considerable success. This technique is without doubt one of the most powerful tools to have been made available to the research laboratory and it is well worth considering for a few moments for, strangely, it is one of those beautifully simple techniques that has been neglected in this country until recently. If a solute is soluble in two immiscible liquid phases, then it will distribute itself between them. Suppose for simplicity that equal volumes of solvent have been taken, and that the solute distributes equally, i.e. each phase contains 50% of the solute. Suppose now that a second container is taken with an equal volume of fresh lower phase. The upper phase of the first container is transferred to it, and fresh upper phase is added to the first container. If both containers are then shaken, the solute will redistribute and there will be 25% in each phase in both containers. If a third container is now taken and a similar set of transfers undertaken, then on further redistribution there will be 12½% solute in each phase in the first and third containers and 25% in each phase in the second container. In other words, there is a moving zone whose peak after two transfers is in the second container. On the other hand, a solute with a partition in favour of the upper phase will form a zone moving faster than that with a 50 : 50 partition; and, conversely, if the partition is in favour of the lower solvent, it will move more slowly. Finally, if the three solutes are together initially, then they will separate as the process of partitioning and transferring is continued.

It can readily be shown that the distribution is binominal and of the form $\left(\frac{1}{K+1}+\frac{K}{K+1}\right)^n$, where K is the partition ratio for the upper phase and n is the number of transfers. For an ideal distribution, therefore, the shape of the distribution can be traced; but in practice distributions are rarely ideal because of solute-solute interaction. Nevertheless, an estimate can be obtained of the number of transfers required for the separation of solutes.

To proceed in the manner described would be extremely laborious, but Craig[12] designed a machine (Fig. 6) in which all shaking, and transferring, is carried out simultaneously, and elaborated it later to make it wholly automatic in working. The technique thus becomes analogous to partition chromatography, but with certain advantages: greater amounts of material can be dealt with; there can be no adsorption effects;

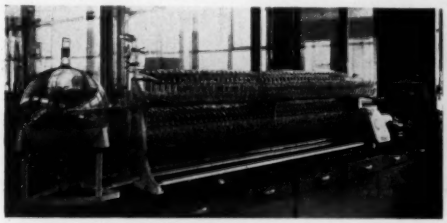

Fig. 6. Craig countercurrent distribution apparatus, fully automatic type. Lower solvent is distributed throughout the tubes at the start of any experiment. Upper solvent is transferred in fixed aliquots from the large reservoir on the left

components that are well separated can be removed from the system; components that are difficult to separate can be circulated within the system until separation is achieved; and the entire distributed sample can be recovered.

The method is being used to investigate the physiologically important products of fat metabolism such as phospholipids and sterol esters and there is also an expanding interest in work on component glycerides of fats. The work of Dutton and Cannon[13] on linseed oil demonstrates clearly the possibilities of the method. Linseed oil contains a large proportion of unsaturated acids, including oleic acid with one double bond, linoleic acid with two double bonds and linolenic acid with three double bonds, and separation of the more unsaturated glycerides has hitherto presented an intractable problem. With the aid of two partition systems, light petroleum 50: furfural 50 and light petroleum 50: furfural 25: nitroethane 25, Dutton and Cannon have succeeded in separating the glycerides into groups containing 9, 8, 7, etc., double bonds [Figs. 7(*a*) and (*b*)]. Those containing 9 and 8 double bonds can each be assigned only one structure, namely, trilinolenin (LeLeLe) and linoleo-dilinolenin (LLeLe or LeLLe), but for the remaining groups combinations of two or more structures are possible. Nevertheless, by first determining the mean unsaturation and then inducing conjugation in the material, so that those acid radicles with two double bonds absorb at 230 mμ and those with three at 270 mμ, it is possible to calculate the proportions of the

possible glycerides in each fraction and so arrive at a total distribution. Investigations of this nature will lead to clearer ideas on the distribution of fatty acid radicles among the glycerides.

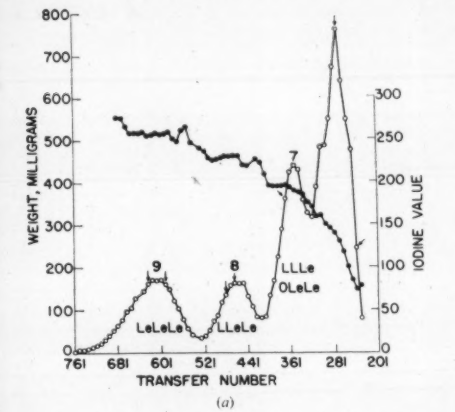

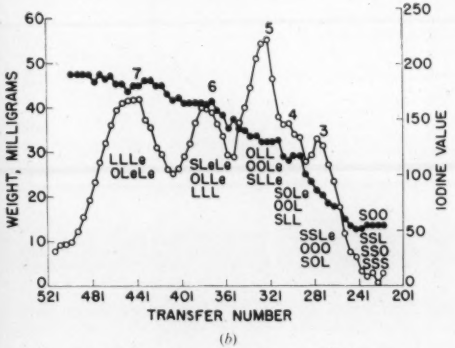

[Reproduced from *Journal of the American Oil Chemists' Society*.]

Fig. 7. Countercurrent separation of glycerides of linseed oil

(*a*) Distribution in system pentane–hexane/furfural, and (*b*) distribution in system pentane–hexane/furfural nitroethane. ○, weight curve; ●, iodine value curve.

Turning now to polymorphism, a great deal of circumstantial evidence of the different forms can be obtained by simple thermometric and dilatometric methods. More fundamental work has been carried out by X-ray diffraction methods,[14] by Malkin in this country and by Lutton in America; but the precise pattern of polymorphism is at present controversial. Recently, Chapman[15] has been applying infra-red techniques to the study of polymorphism; and it would appear that here is a tool which in some ways is complementary to X-ray analysis and in others is superior to it. One can, for example, follow transitions as they occur, by holding a thin film of the fat in a thermally-controlled cell and scanning the requisite portion of the spectrum repeatedly.

When the early work on polymorphic forms was carried out, an unsatisfactory nomenclature was introduced. Only two forms were recognized, and the lower melting form was designated α and the higher melting form β. The application of X-ray analysis has led to the probability of two α-forms, α and sub-α, and the certainty of two β-forms, β and β'. The higher melting forms are the more stable. In some cases only one of the two β-forms can be obtained, e.g. SPS gives β, PSP gives β'.

Crystallographically, the transitions to the higher melting forms are related to a more ordered packing of the lattice. Chapman,[16] from a study of the 700 cm^{-1} region of the infra-red, suggests that the α-form (720 cm^{-1}) is due to hexagonal packing, the β'-form (720 and 730 cm^{-1}) to orthorhombic packing and the β-form (717 cm^{-1}) triclinic packing of the hydrocarbon chains.

In a well-diversified fat mixture polymorphic changes will of course be smoothed out to some extent; but conversely, a fat exhibiting polymorphism is likely to have either a simplified glyceride structure or a dominant glyceride grouping. Two such fats are cocoa butter and lard, dissimilar in physical appearance and behaviour yet hitherto supposed to contain the same dominant glyceride OPS. These glycerides have been investigated recently by Chapman, Crossley and Davies.[17] The methods used were those of dilatometry, cooling curves, X-ray diffraction and infra-red analysis. For dilatometry and X-ray diffraction the samples were brought into the most stable crystal form. It could be accepted that the three fatty acid radicles of the major glycerides in each case had been correctly identified in earlier work, and so for this investigation the three isomeric configurations—OPS, OSP and POS—were prepared. These were examined alone and in various mixtures aimed to simulate possible constitutions of the two materials. The dilatometric measurements and cooling curves suggested that whereas the dominant

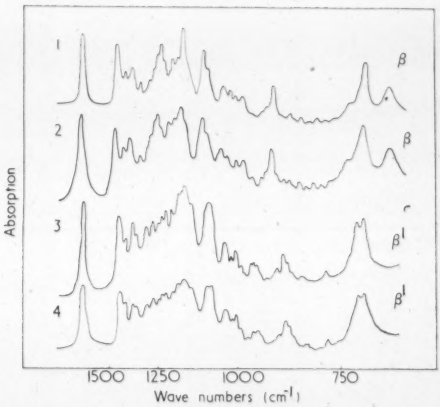

Fig. 8. Characterization of major glycerides of cocoa butter and lard. Infra-red spectra of most stable polymorphic form

1, 2-Oleopalmitostearin (POS); 2, cocoa butter; 3, 2-palmitooleostearin (OPS); 4, lard fraction.

glyceride of lard was OPS as stated, that of cocoa butter was POS and not OPS. X-ray and infra-red data confirmed these views. Fig. 8 illustrates the closely parallel behaviour of cocoa butter and POS, the most stable form of the glyceride being β. In OPS, on the other hand, the β'-form was the most stable; and comparison of this with a lard fraction (Fig. 8), obtained by solvent crystallization, showed it to be the dominant disaturated glyceride of lard.

CONCLUSION

It will be seen then from just these two problems of industrial chemistry how the methods of physics have played a dominant role in their solution. One problem was concerned with vitamin A and with the fishy factor, both trace constituents of glyceride oils, and the other with the behaviour and identification of major constituents of glyceride oils. The problems of trace constituents today are perhaps the most fascinating of all; for it is now possible not only to isolate the constituents but also to apply critical tests of identification to minute quantities of them. It is here that the non-destructive methods of physics are invaluable since cumulative evidence can be obtained by a variety of physical measurements on the same small sample.

The particular problem considered in this paper was not concerned with identification, for vitamin A was known, and it was sufficient to remove the fishy material without identification. But there are many current problems, for example, the identification of by-products of chemical processes, and of the constituents of natural flavours, waiting to be solved. It is worth noting in closing that of all the physical methods that have been mentioned two are emerging in partnership and providing perhaps the most powerful general method of attack. These are vapour phase chromatography and mass spectrometry. It is a curious partnership for they were originally rival techniques, with vapour phase chromatography proving itself the simpler, cheaper and more effective method of determining the number of components of a mixture. In doing so it has simplified and made more effective the contribution of the mass spectrometer, for one can now feed the separated components to it and attach to the results a correspondingly greater significance.

REFERENCES

(1) CROWFOOT, D. (HODGKIN) AND CO-WORKERS. *Chemistry of Penicillin*, p. 310 (Princeton University Press, 1949).

(2) HODGKIN, D. C. *Acta cryst.*, **7**, p. 616 (1954).

(3) UNILEVER LTD., and TAYLOR, R. J. British patent 631722: 1949.

(4) *The physics of particle size analysis*, *Brit. J. Appl. Phys.*, Supplement No. 3 (1954).

(5) HAULTAIN, H. E. T. *Trans Can. Inst. Mining Met.*, **40**, p. 229 (1937).

(6) ROSE, H. E. *The measurement of particle size*, p. 47 (London: Constable and Co. Ltd., 1953).

(7) TAYLOR, R. J. *J. Soc. Chem. Ind.*, **68**, p. 23 (1949).

(8) STUMPF, H. C., AND CO-WORKERS. *Industr. Engng Chem.*, **42**, p. 1398 (1950).

(9) DAY, M. K. B., and HILL, V. J. *J. Phys. Chem.*, **57**, p. 946 (1953).

(10) UNILEVER LTD., TAYLOR, R. J., and THOMPSON, T. British patent 649583: 1951.

(11) HILDITCH, T. P. *The chemical constitution of natural fats*, 3rd Ed., p. 291 (London: Chapman and Hall Ltd., 1956).

(12) CRAIG, L. C., and CRAIG, D. *Technique of organic chemistry*, Vol. III, 2nd ed., p. 171 (London: Interscience Publishers Ltd., 1950).

(13) DUTTON, H. J., and CANNON, J. A. *J. Amer. Oil Chem. Soc.*, **33**, p. 46 (1956).

(14) BAILEY, A. E. *Melting and solidification of fats*, p. 123 (London: Interscience Publishers Ltd., 1950).

(15) CHAPMAN, D. *VIth International Spectroscopic Colloquium*, Amsterdam (1956), p. 609 (London: Pergamon Press Ltd., 1957).

(16) CHAPMAN, D. *J. Chem. Soc.*, p. 4489 (1957).

(17) CHAPMAN, D., AND CO-WORKERS. *J. Chem. Soc.*, p. 1502 (1957).

The photoelastic behaviour of cross-linked polymers

By Z. Tuzi, D.Eng., K. Kawata, B.Eng., and I. Hori, Scientific Research Institute, Tokyo, Japan[b]

[*Paper first received* 11 *October*, 1954, *and in final form* 9 *July*, 1957]

The photoelastic and mechanical properties of various cross-linked polymers have been studied over a wide range of temperature. A large change of the stress-optical coefficient was observed in the second order transition region. At temperatures above that region, suitably cross-linked polymers show a photoelastic behaviour corresponding to nearly perfect entropy-elasticity. The effect of cross-linkage on the stress-optical coefficient has been studied in styrene–divinylbenzene copolymers. The DVB content affects the coefficient considerably in the entropy-elasticity region, but negligibly in the glassy state.

From photoelastic data, one may derive the value of the optical anisotropy ($\alpha_1 - \alpha_2$). The value of $\Delta n/S$ extrapolated to zero degree of cross-linkage agrees well with that of the linear polymer.

Experimental evidence is given that polymers formed by polymerization or addition reactions are preferable to those formed by condensation as materials for the stress-freezing method.

1. Introduction

Photoelastic effects in various polymers have been widely used as a means of stress analysis in structural members. Photoelastic stress analysis is an important application of the photoelastic effect, and a study of the effect within the temperature range of entropy-elasticity of polymers may also contribute to an understanding of their molecular structure. For three-dimensional studies of stress distribution, using the stress-freezing method, it is important to know the photoelastic behaviour of materials over a wide temperature range.

The authors have studied this behaviour, principally in cross-linked polymers, and find that there is a marked variation of the stress-optical coefficient in the second order transition region. Suitably cross-linked polymers show a photoelastic effect based upon nearly perfect entropy-elasticity at sufficiently high temperatures. It is also found that the stress-optical coefficient of styrene–divinylbenzene copolymers in the entropy-elasticity range increases linearly in magnitude with decreasing content of divinylbenzene, until for zero content of the latter it attains the value for polystyrene.

There is some experimental evidence that the heat edge effect is dependent on the type of chemical reaction involved in the preparation of the polymer. Materials formed by addition or polymerization reactions are preferable to those formed by condensation reactions.

2. The temperature variation of photoelastic and mechanical properties of cross-linked polymers

To observe the temperature variation of the properties of various polymers, an air thermostat having two glass windows was placed in the light beam ($\lambda = 5461$ Å) of a photoelastic apparatus. Tension test-pieces of uniform cross-section were stretched in the thermostat and the mechanical deformation and the stress birefringence observed.

The materials studied were phenolic resin (Phenolite); epoxy resin; diallylphthalate polymer (DAP); styrene-divinylbenzene copolymers (S-DVB); and styrene–polyester copolymer; all prepared by the authors. The phenolic resin was prepared from phenol and formaldehyde in equimolecular proportions, with ammonia as a catalyst, and the (S-DVB) copolymer from styrene and Koppers' DVB in the various proportions mentioned in Section 3. The styrene–polyester copolymer was prepared from a mixture of 48% by weight of styrene with 52% of an ester (diethylene glycol fumarate/adipate) prepared with the following molar proportions: fumaric acid, 0·3; adipic acid, 0·2, diethylene glycol, 0·5.

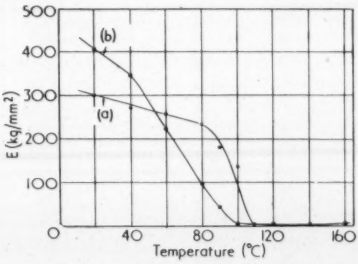

Fig. 1. The variation of Young's modulus with temperature for (*a*) an epoxy and (*b*) a phenolic resin

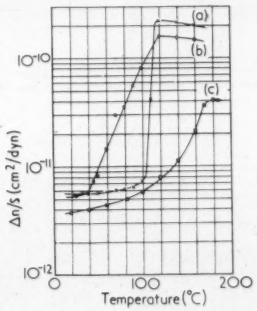

Fig. 2. The variation of the stress-optical coefficient $\Delta n/S$ with temperature for (*a*) an epoxy and (*b*) a phenolic resin, and for (*c*) DAP polymer

Some typical results are given in Figs. 1 and 2, in which the variation with temperature of Young's modulus E and the stress-optical coefficient are shown. The latter coefficient is defined as $\Delta n/S$, while the photoelastic sensitivity α is defined as

$$\alpha = 9{\cdot}8 \times 10^{14} \Delta n/\lambda S \text{ (mm/kg)}$$

where Δn = birefringence, S = stress in dyn/cm^2, and λ = the wavelength used, in Ångström units.

It is clear from Fig. 1 that at low temperatures E decreases gradually with increasing temperature. At somewhat higher temperatures E falls rapidly with increasing temperature and a noticeable creep is present. At still higher temperatures E becomes very small but shows a slight increase with increasing temperature.

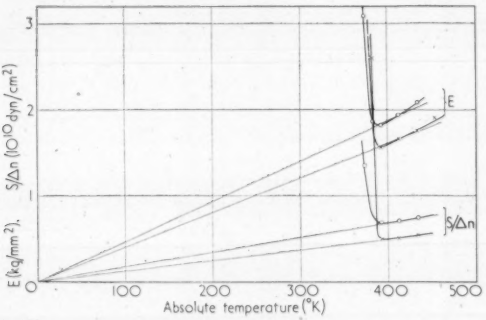

Fig. 3. The variation of Young's modulus and of $S/\Delta n$ with absolute temperature for an epoxy and a phenolic resin

○—○ = epoxy.
—×—× = phenolic resin.

Some properties of photoelastic materials, measured by the authors, with light of wavelength 5461 Å

Material		*Type of reaction*	*Temp.* (° C)	$\Delta n/S$ (cm^2/dyn) ($\times 10^{12}$)	α (mm/kg)	E (kg/mm^2)	αE (mm^{-1})
Phenol–formaldehyde		Condn.	20	5·3	0·96	410	—
			120	160	29	1·8	52
Epoxy		Addn.	20	5·2	0·94	300	—
			120	225	40	1·6	64
Diallylphthalate polymer		Polym.	20	3·7	0·67	390	—
			180	41	7·4	6·6	48
Styrene–divinyl–benzene copolymers	I	Polym.	20	1·1	0·19	290	—
			130	370	67	0·26	17
	II	Polym.	20	0·9	0·16	270	—
			130	320	57	0·51	29
	III	Polym.	20	1·0	0·18	280	—
			130	205	36	1·5	54
Styrene–polyester copolymer		Polym.	100	50	9	2·9	26

In Fig. 3 the values of E and of $S/\Delta n$ are plotted against the absolute temperature. At the higher temperatures, the values of these two quantities lie on straight lines passing through the origin. The theory of rubber-like elasticity predicts the relation[1]

$$E = KT \qquad (1)$$

where T is the absolute temperature and K a constant. The values of E shown in Fig. 3 agree well with this equation at the higher temperatures, and the behaviour of these polymers in this temperature region should be considered as due to entropy-elasticity, while the temperature range in which E changes abruptly corresponds to the second order transition range.

The theory of rubber-like elasticity also predicts the following relation[2–4]

$$\frac{\Delta n}{S} = \frac{2\pi}{45} \cdot \frac{(n_0^2 + 2)^2}{n_0 kT} (\alpha_1 - \alpha_2) \qquad (2)$$

where in addition to the previous definitions n_0 = the refractive index in the unstressed state, α_1 and α_2 = the principal polarizabilities of the equivalent statistical link, and k = Boltzmann's constant.

Since n_0, α_1 and α_2 are constant for a given material, equation (2) can be expressed in the form

$$\Delta n/S = C/T \qquad (2a)$$

where C is another constant. Further, from equations (1), (2a) and the definition of α already given, one can derive

$$\Delta n/\sigma = 1{\cdot}02 \times 10^{-15} \lambda \alpha E = CK = \text{const} \qquad (3)$$

where σ is the strain and αE is the so-called "figure of merit" in the freezing method.

In Fig. 3, $S/\Delta n$ is proportional to the absolute temperature, which agrees with equation (2). Thus, not only the mechanical but also the photoelastic behaviour agrees with the entropy-elasticity theory at sufficiently high temperatures. A marked change of the stress-optical coefficient occurs in the second order transition region, similar to the change already known in other properties such as Young's modulus, thermal expansion, etc.

With phenolic and epoxy resins, and the diallylphthalate polymer, the stress birefringence remains of the same sign in both the glassy and the rubber-like states, but a reversal of the sign was observed in the transition region for styrene-polyester and styrene–divinylbenzene copolymers.

As indicated by equation (3), $\Delta n/\sigma$, and therefore the figure of merit αE, are constant within the entropy-elasticity region. The experimental values of $\Delta n/S$ and αE given in Table 1 confirm the predicted constancy.

All the polymers studied here, with the exception of the diallylphthalate polymer, are relatively lightly cross-linked. They show nearly perfect entropy-elasticity at high temperatures, although glassy at lower temperatures. The diallylphthalate polymer, however, is cross-linked at many places, and for this material equations (1) and (2) do not hold strictly. As indicated in Figs. 2 and 4, the behaviour of DAP does not tend toward perfect entropy-elasticity at high temperatures. The authors conclude that the behaviour of a cross-linked polymer in the rubber-like state is influenced by the degree of cross-linkage.

3. THE EFFECT OF DEGREE OF CROSS-LINKAGE ON THE STRESS-OPTICAL COEFFICIENT

Observations were made of the photoelastic and mechanical properties of styrene–divinylbenzene copolymers in which the content of the cross-linking agent (DVB) was varied. These measurements were intended to reveal the effect of the degree of cross-linking over a wide temperature range.

Materials I, II, and III were prepared, containing respectively 5, 10 and 20% of Koppers' "divinylbenzene 40–50%" as the cross-linking agent, the remainder being styrene.

The composition of Koppers' DVB, in volume percentage, is as follows:

divinylbenzene	46·6
ethylvinylbenzene	40·5
diethylbenzene	5·9
high boiling components	7·0
benzene, toluene, styrene, ethylbenzene	Nil

The variation with temperature of E and $\Delta n/S$ for these materials is shown in Figs. 4 and 5, from which it is clear that the variation is similar to that observed with the epoxy and phenolic resins. The behaviour at high temperatures is again attributable to entropy-elasticity. However, in these copolymers a reversal of sign of the stress-optical coefficient was observed in the second order transition region (see the enlarged scale insert at the top of Fig. 5). The temperature at which this reversal occurred tended to decrease slightly with decreased rate of loading.

The dependence of E and $\Delta n/S$ upon the percentage of cross-linking agent (DVB) is shown in Figs. 6 and 7. From either Fig. 5 or Fig. 6 it will be seen that the dependence of $\Delta n/S$ upon the degree of cross-linking is small at low temperatures, but considerable in the entropy-elasticity region.

In Fig. 8 the variation of E and $\Delta n/S$ with content of DVB is plotted for a fixed temperature of 130° C. The absolute value of $\Delta n/S$ decreases linearly with DVB content, while E increases nearly linearly.

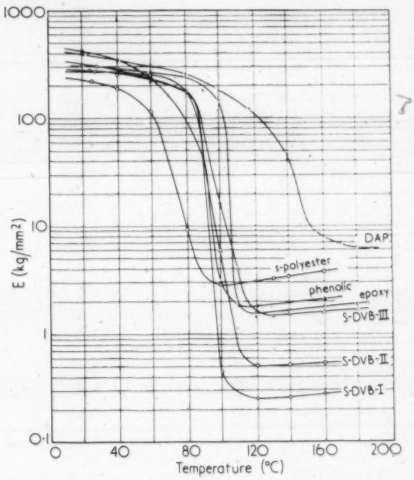

Fig. 4. The variation of Young's modulus with temperature for various cross-linked polymers and copolymers: epoxy and phenolic resins; DAP; S-DVB; and styrene–polyester

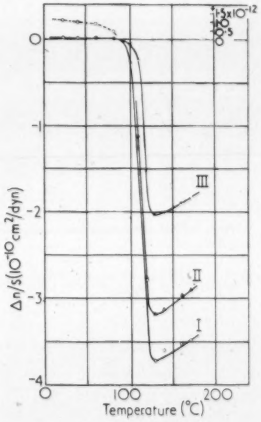

Fig. 5. The variation of the stress-optical coefficient $\Delta n/S$ with temperature for styrene–divinylbenzene copolymers I, II and III. For the dotted curve the scale is inset on the right-hand side

The theory of entropy-elasticity predicts the relation[5]

$$E = \text{const } NkT \qquad (4)$$

where N is the number of chains per unit volume of the network. The results of Fig. 8 confirm, approximately, a linear relation between E and N.

On the other hand, the values of $\Delta n/S$ in the high temperature region depend significantly on the degree of cross-linking, whereas equation (2) predicts that they should be independent of this factor. In earlier work,[6] it was found that the value of $\Delta n/S$ for a pure rubber-sulphur compound increased linearly with increasing degree of cross-linkage, but for the authors' (S-DVB) copolymers the variation is of opposite sign from this. Presumably, the divinylbenzene modifies the polarizability of the equivalent statistical link in the polystyrene chain. If the anisotropy $(\alpha_1 - \alpha_2)$ of the equivalent statistical link is derived by extrapolating the value of $\Delta n/S$ to zero content of DVB, the following values are obtained (for 130° C):

$$\Delta n/S = -4{\cdot}28 \times 10^{-10}\ \text{cm}^2/\text{dyn}$$
$$\alpha_1 - \alpha_2 = -1{\cdot}31 \times 10^{-23}\ \text{cm}^3$$

It is interesting to find that the value of $(\alpha_1 - \alpha_2)$ coincides with that obtained from polystyrene itself.[7]

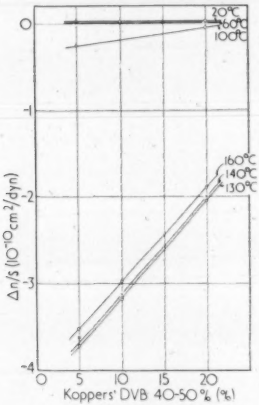

Fig. 6. The variation of the stress-optical coefficient $\Delta n/S$ of S-DVB copolymers with varying content of "Koppers' DVB 40–50%"

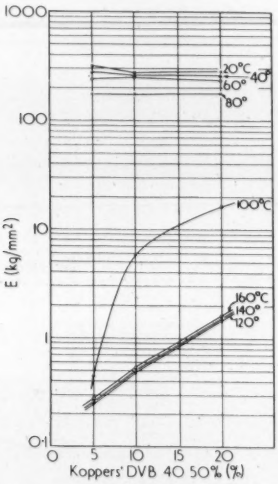

Fig. 7. The variation of Young's modulus of S-DVB copolymers with varying content of Koppers' DVB 40–50%

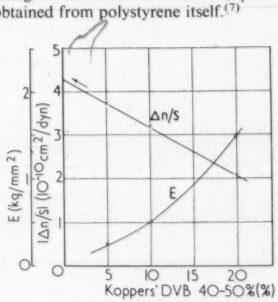

Fig. 8. The variations of Young's modulus and of the absolute value of the stress-optical coefficient $|\Delta n/S|$ at 130° C with varying content of Koppers' DVB 40–50%

Values of the elastic modulus and of the photoelastic constants of the materials tested are collected in the table, for room temperature and for one selected temperature in the entropy-elasticity region.

4. THE "HEAT EDGE EFFECT" IN POLYMERS

The stress-freezing method of using polymers for stress analysis depends upon fixing the orientation of molecular chains, imposed at temperatures above the second order transition region, by slow cooling to temperatures below that region. For polymers in which the transition is above room temperature, the process is therefore one of heating, loading, and cooling. With some polymers, however, a considerable "heat edge effect" occurs in the course of heating, and introduces a serious error into the stress analysis. The effect in an otherwise unstressed specimen of phenol–formaldehyde resin is shown in Fig. 9.

The authors have measured the heat edge effect in a number of polymers by observing the change of fringe order, caused by the birefringence, between the edge and interior of the block. Specimens of the materials were prepared, with dimensions 15 by 30 mm and 5·5 mm thick, by carefully filing the edges to expose new material free from any "time edge effect." Sets of these specimens were heated at 125° C for periods of 1·5, 3·5, 6, and 13 hours respectively, and were allowed to cool to room temperature while still in the thermostat.

The change of fringe order caused by each of the heat treatments is plotted in Fig. 10. The largest effect occurred

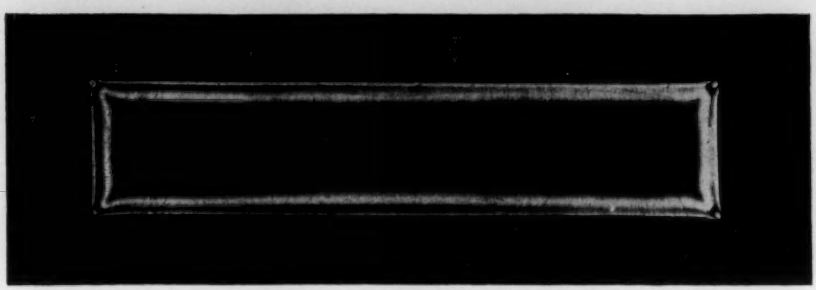

Fig. 9. The heat edge effect in a phenolic resin

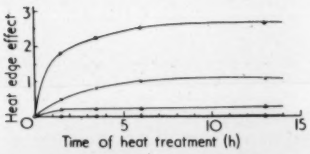

Fig. 10. The heat edge effect in various polymers. The ordinates show the birefringence, in terms of fringe order, caused at a free boundary by heat treatment

—○— = phenolic resin.
—×— = DAP-I.
—△— = DAP-II.
—●— = epoxy resin; polymethylmethacrylate; styrene–polyester copolymer; S-DVB I; methylmethacrylate—DAP copolymer.

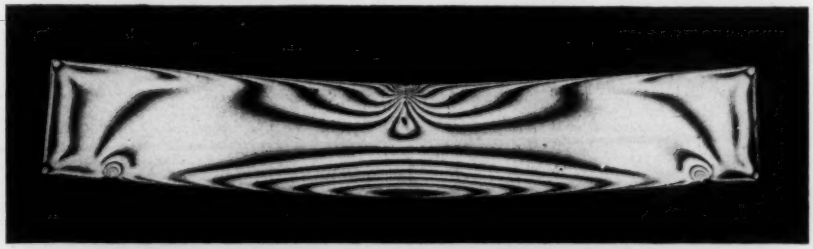

Fig. 11. A fringe pattern of frozen-in stress in a phenolic resin, showing a large heat edge effect

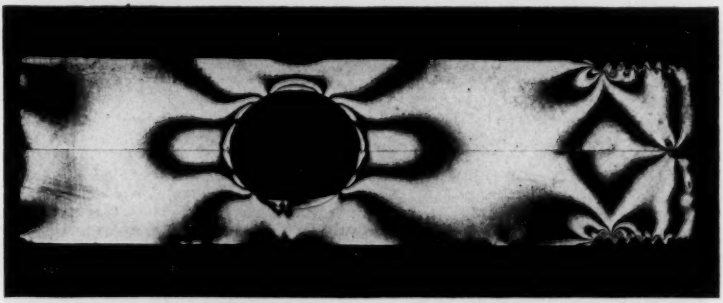

Fig. 12. A fringe pattern of frozen-in stress in an epoxy resin showing little heat edge effect. The pattern shows the stress distribution in the central section (thickness 2 mm) of a circular cylinder containing a spherical cavity, when in axial tension

**

with the phenolic resin. The next largest occurred in a sample of diallylphthalate resin which had been under-polymerized. A small effect was still observable in the same resin when fully polymerized. No measurable effect was observed in polymers or copolymers of the following: epoxy resin; methylmethacrylate; styrene–polyester; styrene–DVB I; methylmethacrylate–DAP.

Fig. 11 shows the stress pattern in a bent beam, as distorted by a large heat edge effect in the phenolic material used.

Fig. 12 shows a stress pattern undistorted by edge effect, obtained by using an epoxy resin. The pattern represents the stress in the central plane of a solid cylinder containing a spherical cavity, when subjected to axial tension.

The authors' studies indicate that the heat edge effect is smaller in resins formed by polymerization or addition reactions than in those formed by condensation. For example, glyptal (BT-61-893) belongs to the latter class, and it is well known that it shows a large effect. Polymers which are insufficiently polymerized also show a large effect, even though they belong to the former class. Complete reaction and freedom from cracks and bubbles are more easily obtained with the former class than with the latter. For these reasons the authors recommend the use, in the stress freezing method, of polymers formed either by polymerization or addition reactions.

ACKNOWLEDGEMENTS

The authors express their thanks to Dr. S. Sakurai for valuable advice on the preparation of various polymers, and also to the Ministry of Education (of Japan) for a grant.

REFERENCES

(1) GUTH, E., and JAMES, H. M.: *Industr. Engng Chem.*, **33**, p. 624 (1941); *Rubb. Chem. Techn.*, **14**, p. 596 (1941).
(2) KUHN, W., and GRÜN, F.: *Kolloid Z.*, **101**, p. 248 (1942).
(3) KUBO, R. *J. Phys. Soc. Japan*, **2**, p. 84 (1947).
(4) TRELOAR, L. R. G. *Trans Faraday Soc.*, **43**, p. 277 (1947).
(5) TRELOAR, L. R. G. *The Physics of Rubber Elasticity* (London: Oxford University Press, 1949).
(6) THIBODEAU, W. E., and MCPHERSON, A. T.: *J. Res. Nat. Bur. Stand.*, **13**, p. 887 (1934).
(7) STEIN, R. S., and TOBOLSKY, A. V.. *J. Polymer Sci.*, **11**, p. 285 (1953).

Calculated and observed effects of texture on the magnetic properties and Young's modulus of nickel sheet

By E. R. W. JONES, M.A., F.I.M., C. A. CLARK, Ph.D., A.Inst.P., and E. A. FELL, B.Met., A.I.M., The Mond Nickel Co. Ltd. Birmingham 16

[*Paper received* 2 *September*, 1957]

Relative values of Young's modulus, magnetostrictive coupling coefficient and initial and maximum permeabilities are calculated for various textures in nickel, an approximate model being used for magnetic properties.

Experimental values are given for high purity polycrystalline nickel sheet produced by powder metallurgy and annealed in purified hydrogen. Comparison between theory and experiment indicates good agreement for Young's modulus and fair agreement for magnetic properties. The textures were determined by X-ray photographic techniques and it was shown that strip possessing a cube recrystallized texture gave lower properties than recrystallized strip having a random grain orientation. It was also found, in agreement with previous work on copper, that the perfection of the cube texture was mainly governed by the temperature of anneal.

It is well established that the magnetic domains in annealed ferromagnetic materials are alined as far as possible along preferred crystallographic directions. Practical application of this effect is illustrated by the deliberate production of cube texture in 3% silicon–iron[1] and 50% nickel–iron alloys.[2] The cubic orientation may be produced in face-centred cubic metals by a heavy cold reduction and subsequent high temperature anneal, the annealing temperature for best results often being rather critical. In iron, 3% silicon–iron alloy and 50% nickel–iron alloy, the cube edge is the easy direction of magnetization and the production of a cube texture improves the maximum permeability of the material.

Little work has been done, however, on the dependence of magnetic properties on texture in sheet material for which the ⟨111⟩ direction is the easy direction of magnetization, as in nickel, although the roll and recrystallization textures for face-centred cubic metals generally have been investigated by several workers.[3]

It was therefore decided to investigate the processing and annealing treatments required for the production of nickel strip, with and without texture, and then to determine the average magnetic properties of the material, with particular reference to the initial magnetization curve, hysteresis loop, electromechanical coupling coefficient and dynamic Young's modulus.

THE MAGNETIZATION PROCESS IN NICKEL

In order to eliminate errors due to demagnetizing effects, it is desirable to use toroidal ring cores. An explanation of the results obtained in this way was attempted by using a simple model based on domain theory.

When a small magnetic field is applied to a stress-free ferromagnetic material, the initial stage of magnetization occurs primarily by 180° domain boundary movement, no appreciable work being required to overcome magnetocrystalline anisotropy or magnetostrictive stress. Higher applied field strengths result in magnetostrictive strain, since the domain walls move in such a way that the domain magnetization vectors become parallel to that easy direction of magnetization nearest to that of the applied field. Finally, above the "knee" of the magnetization curve, the magnetization of each grain

is rotated out of easy directions of magnetization, the approach to magnetic saturation being accompanied by linear magnetostriction and also being opposed by magnetic crystal anisotropy.

The relative magnetic properties for the various textures were calculated by assuming that the magnetization processes described above do not overlap. The first two stages are then amenable to calculation since they do not involve the magnetic anisotropy of the material. The magnetic induction at the end of the first and second stages is taken as proportional to initial permeability μ_0, and maximum permeability μ_m, respectively.

It is more convenient in practice to determine the electromechanical coupling coefficient K, rather than magnetostriction. It has been shown that the two quantities are related by the following equation[4]

$$K = \frac{4\pi}{l}\left(\frac{\partial l}{\partial H}\right)_p \sqrt{\left(\frac{E}{4\pi\mu_p}\right)} \qquad (1)$$

where $\frac{1}{l}\left(\frac{\partial l}{\partial H}\right)_p$ = incremental magnetostriction per unit field at constant stress; μ_p = incremental permeability at constant stress; and E = Young's modulus.

The maximum value of the electromechanical coupling coefficient determined in the experiments occurs at d.c. polarizing fields corresponding to the second stage of the magnetization

Table 1. *Variation of property in sheet with angle measured from rolling direction*

Rolling plane and direction	*Texture* Major roll (110) [$\bar{1}$12]	Minor roll (112) [11$\bar{1}$]	Cube (001) [100]
Initial permeability	$\frac{\sqrt{2}}{3}\cos\theta + \frac{1}{4}\sin\theta$, $0 \leqslant \theta \leqslant \cos^{-1}\sqrt{\frac{1}{3}}$. $-\frac{1}{3\sqrt{2}}\cos\theta + \frac{5}{12}\sin\theta$, $\cos^{-1}\sqrt{\frac{1}{3}} \leqslant \theta \leqslant \cos^{-1}\frac{1}{3}$. $\frac{1}{2}\sin\theta$, $\cos^{-1}\frac{1}{3} \leqslant \theta \leqslant \pi/2$.	$\frac{1}{2}\cos\theta$, $0 \leqslant \theta \leqslant \cos^{-1}\sqrt{\frac{6}{7}}$. $\frac{1}{3}\cos\theta + \sqrt{\frac{1}{6}}\sin\theta$, $\cos^{-1}\sqrt{\frac{6}{7}} \leqslant \theta \leqslant \pi/2$.	$\sqrt{\frac{1}{3}}\cos\theta$, $0 \leqslant \theta \leqslant \pi/4$. $\sqrt{\frac{1}{3}}\sin\theta$, $\pi/4 \leqslant \theta \leqslant \pi/2$.
Maximum permeability	$\frac{2\sqrt{2}}{3}\cos\theta$, $0 \leqslant \theta \leqslant \cos^{-1}\sqrt{\frac{2}{3}}$. $\sqrt{\frac{2}{3}}\cos\theta + \frac{2}{3}\sin\theta$, $\cos^{-1}\sqrt{\frac{2}{3}} \leqslant \theta \leqslant \cos^{-1}\sqrt{\frac{1}{3}}$. $\sin\theta$, $\cos^{-1}\sqrt{\frac{1}{3}} \leqslant \theta \leqslant \pi/2$.	$\cos\theta$, $0 \leqslant \theta \leqslant \cos^{-1}\sqrt{\frac{3}{5}}$. $\frac{1}{3}\cos\theta + \sqrt{\frac{2}{3}}\sin\theta$, $\cos^{-1}\sqrt{\frac{3}{5}} \leqslant \theta \leqslant \pi/2$.	$\sqrt{\frac{2}{3}}\sin(\theta + \pi/4)$.
Magnetostriction	$\frac{1}{4} + \frac{7}{12}\cos 2\theta$, $0 \leqslant \theta \leqslant \cos^{-1}\sqrt{\frac{2}{3}}$. $\frac{1}{4} - \frac{1}{4}\cos 2\theta + \frac{1}{3\sqrt{2}}\sin 2\theta$, $\cos^{-1}\frac{2}{3} \leqslant \theta \leqslant \cos^{-1}\sqrt{\frac{1}{3}}$. $\frac{1}{4} - \frac{3}{4}\cos 2\theta$, $\cos^{-1}\sqrt{\frac{1}{3}} \leqslant \theta \leqslant \pi/2$.	$\frac{1}{4}(1 + 3\cos 2\theta)$, $0 \leqslant \theta \leqslant \cos^{-1}\sqrt{\frac{3}{5}}$. $\frac{1}{12} - \frac{5}{12}\cos 2\theta + \sqrt{\frac{2}{3}}\sin 2\theta$, $\cos^{-1}\sqrt{\frac{3}{5}} \leqslant \theta \leqslant \pi/2$.	$\frac{1}{2}\sin 2\theta$.
Young's modulus, direction cosine term only	$\frac{7}{32} - \frac{1}{24}\cos 2\theta + \frac{7}{96}\cos 4\theta$	$\frac{7}{32} + \frac{1}{24}\cos 2\theta + \frac{7}{96}\cos 4\theta$	$\frac{1}{8}(1 - \cos 4\theta)$

process, e.g. about 6 oersteds for annealed strip, so that for comparative purposes it is justifiable to neglect the third stage.

The relative values of permeability are obtained by resolving the magnetization vectors into the field direction and summing the components. In calculating the magnetostriction, the change in length in a given direction is required when the direction of magnetization of the domain changes from one easy direction to another. If unit spherical volume in the non-magnetic state transforms into an ellipsoid of revolution in the magnetic state, it may be written as

$$\frac{x^2}{(1-\epsilon)^2}+\frac{y^2}{(1-\epsilon)^2}+\frac{z^2}{(1+2\epsilon)^2}=1 \qquad (2)$$

The length of a radius vector making an angle θ with the z-axis is then $1+\epsilon(3\cos^2\theta-1)$, neglecting quantities of the order of ϵ^2. The change in length when a domain magnetization vector changes from making an angle θ_1 with the field direction to making an angle θ_2 is, therefore, proportional to $\cos^2\theta_2-\cos^2\theta_1$.

Calculations of this type have been made for four possible orientations of the crystals in nickel sheet; random orientation, major roll texture (110) [$\bar{1}$12], minor roll texture (112) [11$\bar{1}$], and cube texture (100) [001]. The accuracy of the description of roll textures in terms of (110) [$\bar{1}$12] and (112) [11$\bar{1}$] has been confirmed by Jones and Fell.[5] Calculations for the minor roll texture are given in detail in Appendix I; the calculations for major roll and cube texture are similar, although in the case of the major roll texture allowance must be made for symmetry about the roll direction. The calculations for random orientation are somewhat different, in that the variation of properties is calculated for a field direction making an arbitrary angle with the crystal axes. The values so obtained are averaged over all possible orientations of the field direction.

It was considered that the model described above, although over-simplified, could be expected to yield fairly accurate relative values of the magnetic properties for different textures.

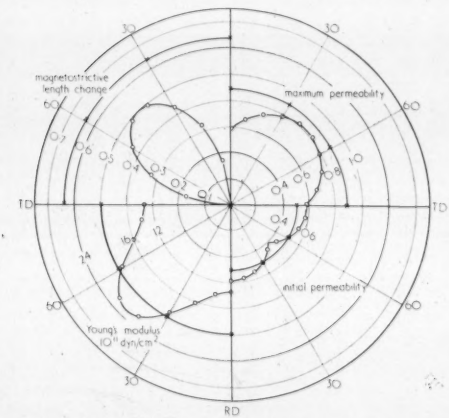

Fig. 1. Variation of property with direction for cube texture. Magnetostrictive length change, maximum permeability and initial permeability in arbitrary units ○—○ cube texture; ×—× random; *RD*, rolling direction; *TD*, transverse direction.

The Young's modulus may be calculated exactly in terms of the elastic coefficients C_{11}, C_{12} and C_{44}, as described in Appendix II.

The expressions for the angular dependence of property relative to the roll direction are given in Table 1 for the four textures and, together with the average values, are plotted as a polar diagram in Fig. 1. The calculated average magnitudes round a ring are given in Table 2.

Table 2. *Average value of property round a ring*

	Major roll	*Minor roll*	*Cube*	*Random*
Initial permeability (arbitrary units)	0·502	0·493	0·540	0·500
Maximum permeability (arbitrary units)	0·887	0·883	0·735	0·883
Magnetostriction (arbitrary units)	0·701	0·832	0·318	0·637
Young's modulus $\times 10^{-11}$ dyn/cm^2	20·8	20·8	16·6	19·8

EXPERIMENTAL TECHNIQUE

Two types of nickel were available for this work, cast ingots and powder metallurgy compacts. It is known that a heavy cold reduction in strip rolling is needed to give marked texture and that cast material cannot conveniently be given such a reduction, although the softer powder metallurgy compacts can. Further, preliminary experiments showed that texture develops in strip made from sintered compacts at reductions which would be inadequate for cast material: appreciable roll texture is developed at 50% reduction in strip made from compacts, whereas, according to Barrett,[3] cold reductions in excess of 90% are needed for conventionally made materials, presumably because of the higher impurity content resulting from the air-melting process. It was therefore decided to use sintered compacts as the starting material.

Two samples of 0·004 in. thick strip which had been cold-rolled by 96 and 99% respectively, were obtained for the experiments. Since it was found impossible to induce random or recrystallized roll textures in this strip by any annealing schedule, a further sample, 0·004 in. thick, was produced with a random grain orientation. The "randomized" strip was obtained by reducing 0·008 in. thick strip to 0·004 in. in two reductions of 0·002 in. with an anneal at 700° C prior to each reduction.

The textures were determined using a Unicam single-crystal goniometer. The pole figures were obtained photographically and by this method no significant differences could be detected between the textures of samples reduced by 96 and 99% respectively.

Several heat treatments were used to determine the conditions necessary to obtain a good cube texture. Pole figures for the as-rolled condition and for three of the heat treatments are given in Fig. 2 for the nickel strip which had received 99% cold reduction. The ideal textures are included for comparison. From these results it was deduced that a good cube texture could be obtained in heavily cold-rolled strip by annealing at 1050° C, but that it was impossible to obtain a recrystallization texture free of cube orientation by annealing the heavily cold reduced strip even at temperatures as low as 250° C.

As internal stress has a large effect on magnetic properties determined at low and medium field strengths, the results for as-rolled strip could not be directly compared with those for

strip in the recrystallized stress-free condition. Since it was impossible to retain the roll texture during annealing, it was decided that the magnetic properties of annealed nickel strip possessing a cube grain orientation should be compared with those of "randomized" material, although it was not expected that the differences would be so marked. Random orientation was therefore induced in a sample of nickel strip by the method already described.

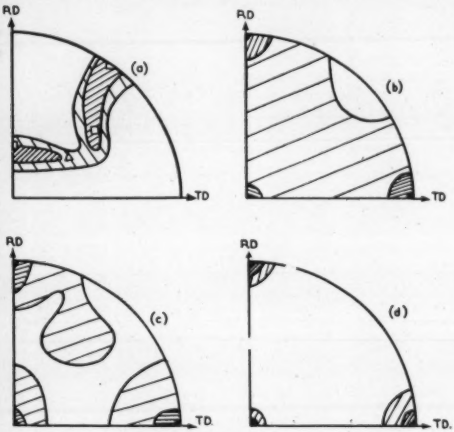

Fig. 2. (200) pole figures for various conditions

(*a*) As rolled; (*b*) annealed 500° C for 2 h; (*c*) annealed 1050° C for 1 h; (*d*) annealed 1050° C for 3 h.

Ideal orientations: △ (110) [$\bar{1}$12] major roll texture.
□ (112) [11$\bar{1}$] minor roll texture.
● (100) [001] cube texture.

The cores for the magnetic tests each consisted of fifteen ring laminations of 5 cm outer diameter and 4 cm inner diameter. The rings fitted loosely into a plastic box, on which were wound two coils, one to supply a polarizing field and the other for the alternating field. Initial permeability was determined at a test frequency of 2 kc/s, and the maximum electromechanical coupling coefficient corresponding to optimum polarizing field and the resonance frequency were determined by measuring the variation of core impedance with frequency, as described by Clark.[4] The hysteresis loops and initial magnetization curves were determined ballistically in the usual way. The Young's modulus was deduced from the equation

$$E = \pi^2 d^2 f_0^2 \rho \qquad (3)$$

where ρ is the density, d is the mean diameter and f_0 is the resonance frequency. The annealing treatments used and the resultant textures are given in Table 3.

EXPERIMENTAL RESULTS

The roll texture developed in the cold-rolled nickel strip is of the usual type for face-centred cubic metals,[3] i.e. a mixture of major and minor roll textures consisting of (110) [$\bar{1}$12] and (112) [11$\bar{1}$], respectively. The recrystallization textures developed on annealing the cold-rolled strip were all of the (100) [001] type, even at as low a recrystallization temperature as 250° C. At the lower annealing temperatures the texture was poorly defined and cube texture improved as the annealing temperature was increased, as shown in Fig. 2. It was found also that a good cube texture could be obtained if a substantially random specimen, which had been recrystallized at a low temperature, was re-annealed for three hours at 1050° C, and that the degree of perfection

Table 3. *Magnetic properties of nickel sheet*

		D.C. results					*A.C. results*†								
										Stress sensitivity		*Young's modulus* $\times 10^{-11}$ *dyn/cm²*		*Incremental permeability at Resonance frequency*	
Production schedule*	*Texture*	*Thickness of strip (cm)*	*Maximum permeability*	*H for μ_{max} (oersteds)*	*Remanence (G)*	*Coercive force (oersteds)*	*Initial permeability (at 2 kc/s)*	*Coupling coefficient* K_r	K_m	Ω_r $\times 10^7$	Ω_m $\times 10^7$	E_r	E_m	*Remanence*	*Optimum polarization*
99% cold reduction	Normal roll	0·0100	69	62	3440	46	26	0·06	0·07	7·6	8·5	21·6	21·3	25	26
99% cold reduction, 2 h at 500° C	Mixed roll and cube	0·0100	625	4·7	3230	3·3	142	0·22	0·23	57	52	19·1	18·8	105	75
99% cold reduction, 3 h at 1050° C	Cube	0·0100	1390	2·0	3410	1·30	149	0·16	0·21	44	79	17·1	17·1	102	59
96% cold reduction, 3 h at 1050° C	Cube	0·0098	1450	1·0	3430	1·17	163	0·21	0·25	61	50	18·0	18·2	121	61
25% cold reduction, anneal, 20% cold reduction, 3 h at 1050° C	Random	0·0099	2100	1·4	3480	0·92	207	0·25	0·28	76	64	20·3	20·6	151	86
99% cold reduction, 2 h at 500° C + 3 h at 1050° C	Cube	0·0100	1400	1·8	3300	1·33	166	0·21	0·23	65·5	59·6	17·4	17·5	134	93

* Annealing atmosphere was purified hydrogen.
† The subscripts *r* and *m* denote properties determined at remanence and with optimum polarizing field respectively.

of this texture was apparently independent of the previous heat treatment.

The main magnetic properties are shown in Table 3. It is seen that the initial and maximum permeabilities of annealed strip with random texture are respectively 30 and 50% higher than those of strip in which a cube texture has been induced. The electromechanical coupling coefficient and Young's modulus are also seen to be texture dependent, the values being lowest for the material with cube texture.

DISCUSSION

An interesting feature of the X-ray photographs is that they indicate the presence of some cube texture after an anneal at only 250° C. In addition, heavily cold-rolled strip, recrystallized at 500° C and subsequently annealed at 1050° C, appeared to possess just as good a cube texture as the same strip annealed only at 1050° C. The magnetic tests confirm this finding. It is concluded therefore that the recrystallization texture is dependent solely on the maximum temperature of anneal and not on any prior anneal at a lower temperature, and that texture, once induced, cannot be eliminated by heat treatment alone. This result has also been found recently by Merlini[6] in copper.

The relative magnetic properties for nickel sheets possessing random and cube grain orientation respectively, depend qualitatively on the recrystallization texture as predicted, although the numerical agreement is not particularly good. The ratio of magnetic properties for random and cube textures in nickel sheet are given in Table 4, (*a*) as predicted

Table 4. *The ratio random: cube of properties for nickel sheet possessing random and cube texture*

Property	*Calculated ratio*	*Experimental ratio* 96% *reduction*	99% *reduction*
Initial permeability	0·92	1·27	1·39
Maximum permeability	1·20	1·45	1·51
Incremental magnetostriction	2·00	1·25	1·47
Young's modulus	1·23	1·13	1·20

theoretically and (*b*) as determined by experiment. The incremental magnetostriction was calculated from experiment by assuming equation (1) and using the measured values of Young's modulus, incremental permeability and electromechanical coupling coefficient. In view of the necessarily simple model which was chosen as a basis for calculation and because of possible imperfections in the recrystallization textures, the agreement between theory and experiment is probably as good as can be expected. Although the X-ray work revealed no obvious differences between recrystallized strip reduced by 96 and 99% respectively, the magnetic results appear to indicate that the 99% reduction yields magnetic properties inferior to those given by the 96% reduction, which implies a more perfect cube recrystallization texture in nickel strip reduced by 99%. The magnetic test is apparently more sensitive than photographic X-ray techniques. Good agreement was obtained between the calculated values for Young's modulus and those obtained from impedance measurements.

CONCLUSIONS

An investigation of the conditions under which roll and recrystallization textures are produced in nickel has shown that, after very heavy reduction, the recrystallization texture invariably contains some cube texture, even when low annealing temperatures have been used. In addition, it has been shown that the final cube texture is dependent solely on the highest recrystallization temperature and not on any previous heat treatment.

Typical magnetic properties have been determined on nickel strip after various processing and annealing schedules. In particular, it has been shown that ring samples, possessing respectively random and cube recrystallization textures, exhibit quite different magnetic properties and also different Young's modulus values.

The ratio of average magnetic properties for random and cube texture is in qualitative agreement with calculated values based on a simple model of the domain magnetization process. The ratio of Young's modulus for these textures is in good agreement with calculated values.

ACKNOWLEDGEMENTS

The authors wish to thank the Mond Nickel Co. Ltd. for permission to publish this paper.

APPENDIX I

Calculations for the magnetic model on minor roll texture

Since there is symmetry about both the rolling and transverse directions, only one quadrant need be considered. The direction of the field can be specified by the angle θ, measured anti-clockwise, which it makes with the rolling direction [11$\bar{1}$]. To specify the domain vector two further angles are needed, ϕ and ψ. These are defined in Fig. 3. If ξ is the angle between

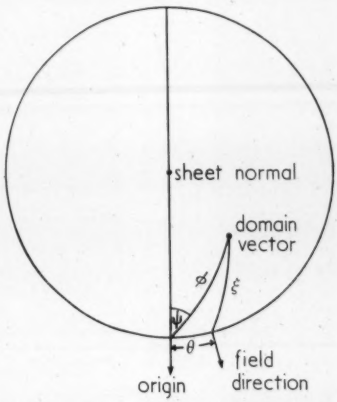

Fig. 3. Stereogram showing definition of angles used in the calculations for the magnetic model

the field and the domain vector, then $\cos \xi = \cos \phi \cos \theta + \sin \phi \sin \theta \sin \psi$.

The values of the function of the angles for various directions are given in Table 5.

Initial permeability. In the calculation of the induction, those domains which have an antiparallel component must be reversed and the magnetic induction of all the domains resolved into the field direction. Two cases must be considered which arise from reversal of [1$\bar{1}\bar{1}$] to [$\bar{1}$11]. While

the field direction is nearer to $[1\bar{1}\bar{1}]$ than to $[\bar{1}11]$ the domain vector will be in $[1\bar{1}\bar{1}]$ and conversely. The change-over will come when the field is along $[13\bar{2}]$ which is perpendicular to $[1\bar{1}\bar{1}]$.

Table 5. *Functions of the angles for various directions in sheet possessing minor roll texture*

Direction	*Cos* ϕ	*Sin* ϕ	*Sin* ψ
111	$\frac{1}{3}$	$\frac{2\sqrt{2}}{3}$	0
$1\bar{1}\bar{1}$	$\frac{1}{3}$	$\frac{2\sqrt{2}}{3}$	$-\frac{\sqrt{3}}{2}$
$\bar{1}1\bar{1}$	$\frac{1}{3}$	$\frac{2\sqrt{2}}{3}$	$\frac{\sqrt{3}}{2}$
$\bar{1}11$	$-\frac{1}{3}$	$\frac{2\sqrt{2}}{3}$	$\frac{\sqrt{3}}{2}$
$11\bar{1}$	1	0	0
$13\bar{2}$	$\sqrt{\frac{6}{7}}$	$\sqrt{\frac{1}{7}}$	1

If the induction from each domain is taken as one unit then there are the following contributions (putting in the values from Table 5)

from $[11\bar{1}]$ and $[\bar{1}\bar{1}1]$, $2\cos\theta$

from $[111]$ and $[\bar{1}\bar{1}\bar{1}]$, $2\cdot\frac{1}{3}\cos\theta$

from $[\bar{1}1\bar{1}]$ and $[1\bar{1}1]$, $2\left[\frac{1}{3}\cos\theta+\frac{2\sqrt{2}}{3}\sin\theta\left(\frac{\sqrt{3}}{2}\right)\right]$

from $[1\bar{1}\bar{1}]$ and $[\bar{1}11]$, $2\left[\frac{1}{3}\cos\theta+\frac{2\sqrt{2}}{3}\sin\theta\left(\frac{-\sqrt{3}}{2}\right)\right]$,

$$0\leqslant\theta\leqslant\cos^{-1}\sqrt{\frac{6}{7}}$$

or

$$2\left[-\frac{1}{3}\cos\theta+\frac{2\sqrt{2}}{3}\sin\theta\left(\frac{\sqrt{3}}{2}\right)\right],\qquad\cos^{-1}\sqrt{\frac{6}{7}}\leqslant\theta\leqslant\frac{\pi}{2}$$

adding these

$$\text{induction}=4\cos\theta,\qquad 0\leqslant\theta\leqslant\cos^{-1}\sqrt{\frac{6}{7}}$$

$$=\frac{8}{3}\cos\theta+\frac{8}{\sqrt{6}}\sin\theta,\quad\cos^{-1}\sqrt{\frac{6}{7}}\leqslant\theta\leqslant\frac{\pi}{2}$$

If all the magnetization vectors are alined in the field direction, the maximum possible value is, in the authors' units, 8, and working in terms of this as unity,

$$\mu_0=\frac{1}{2}\cos\theta,\qquad 0\leqslant\theta\leqslant\cos^{-1}\sqrt{\frac{6}{7}}$$

$$=\frac{1}{6}(2\cos\theta+\sqrt{6}\sin\theta),\quad\cos^{-1}\sqrt{\frac{6}{7}}\leqslant\theta\leqslant\frac{\pi}{2}$$

In practice, sheet material is often used in the form of rings. In this case θ takes all values from 0 to $\pi/2$. We therefore require the average value which is

$$\bar{\mu}_0\simeq 0{\cdot}493$$

Maximum permeability. In calculating the induction it is assumed that all the domain vectors swing into that $\langle 111\rangle$ direction nearest to the field. It can be shown that there are two possibilities, either along $[11\bar{1}]$ or $[\bar{1}1\bar{1}]$. The change-over will come when $\xi_{11\bar{1}}=\xi_{\bar{1}1\bar{1}}$, i.e.

when $\cos\theta=\sqrt{\frac{3}{5}}$.

Therefore, working in the same units as for μ_0,

$$\mu_{max}=\cos\theta,\qquad 0\leqslant\theta\leqslant\cos^{-1}\sqrt{\frac{3}{5}}$$

$$=\frac{1}{3}\cos\theta+\sqrt{\frac{2}{3}}\sin\theta,\quad\cos^{-1}\sqrt{\frac{3}{5}}\leqslant\theta\leqslant\pi/2$$

The average is

$$\bar{\mu}_{max}\simeq 0{\cdot}883$$

Magnetostriction. Here the sum of the changes in length due to swinging from the original to final domain vector orientation is required, and again there are two possible final orientations, depending on whether θ is greater or less than $\cos^{-1}\sqrt{\frac{3}{5}}$.

$$0\leqslant\theta\leqslant\cos^{-1}\sqrt{\frac{3}{5}}$$

All domains will swing to $[11\bar{1}]$, the contributions being:

$$\text{from }[111],\ \cos^2\xi_{11\bar{1}}-\cos^2\xi_{111}=\cos^2\theta-\frac{1}{9}\cos^2\theta$$

$$\text{from }[1\bar{1}\bar{1}],\ \cos^2\xi_{11\bar{1}}-\cos^2\xi_{1\bar{1}\bar{1}}=\cos^2\theta-\left(\frac{1}{3}\cos\theta-\sqrt{\frac{2}{3}}\sin\theta\right)^2$$

$$\text{from }[\bar{1}1\bar{1}],\ \cos^2\xi_{11\bar{1}}-\cos^2\xi_{\bar{1}1\bar{1}}=\cos^2\theta-\left(\frac{1}{3}\cos\theta+\sqrt{\frac{2}{3}}\sin\theta\right)^2$$

Summing, linear magnetostriction λ is given by

$$\lambda=k\left(\frac{8}{3}\cos^2\theta-\frac{4}{3}\sin^2\theta\right)\quad\text{where } k \text{ is a constant.}$$

If the maximum possible value is taken as unity, the constant of proportionality is $\frac{3}{8}$, therefore $\lambda=\cos^2\theta-\frac{1}{2}\sin^2\theta$.

Similarly

$$\cos^{-1}\sqrt{\frac{3}{5}}\leqslant\theta\leqslant\pi/2,\ \frac{8}{3}\lambda=3\cos^2\xi_{\bar{1}1\bar{1}}-\cos^2\xi_{111}-\cos^2\xi_{1\bar{1}\bar{1}}-\cos^2\xi_{11\bar{1}}$$

Therefore

$$\lambda=\frac{1}{2}\sin^2\theta+\sqrt{\frac{2}{3}}\sin\theta\cos\theta-\frac{1}{3}\cos^2\theta$$

The average is then

$$\bar{\lambda}=0{\cdot}832$$

APPENDIX II

Variation of Young's modulus with stressing direction in textured sheets of cubic materials

It can be shown, e.g. Wooster,[7] that the Young's modulus E in a direction making angles $\cos^{-1}\alpha_1$, $\cos^{-1}\alpha_2$ and $\cos^{-1}\alpha_3$

with the axes of a cubic crystal with elastic coefficients c_{11}, c_{12} and c_{44} is given by

$$\frac{1}{E} = \frac{c_{11} + c_{12}}{(c_{11} - c_{12})(c_{11} + 2c_{12})} - \left(\frac{2}{c_{11} - c_{12}}\right)(\alpha_1^2\alpha_2^2 + \alpha_2^2\alpha_3^2 + \alpha_3^2\alpha_1^2)$$

This may be written as

$$1/E = a - bf(\alpha)$$

where a and b are constants for the material and $f(\alpha)$ is the direction cosine term. Taking the mean of the values given for nickel by Bozorth and others,[8] and Neighbours and others,[9] gives $1/E = 0{\cdot}758 - 1{\cdot}273\, f(\alpha)\,.\,10^{-12}$ cm^2/dyn.

In the case of a crystal having some prescribed orientation with respect to a plane in which the stress axis must lie, the direction cosines are definable in terms of the orientation of the crystal and the angle between the stress axis and a reference direction. The way in which the Young's modulus varies with direction is therefore defined by the orientation of the crystal in the sheet.

Table 6. *Direction cosine scheme*

	Reference direction	*Transverse direction*	*Plane normal*
x_1	α_{11}	α_{12}	α_{13}
Crystal axes x_2	α_{21}	α_{22}	α_{23}
x_3	α_{31}	α_{32}	α_{33}

If the direction cosines are as given in Table 6, the direction cosines of the stress axis which makes an angle θ with the reference direction are given by

$$\alpha_1 = \alpha_{11}\cos\theta + \alpha_{12}\sin\theta$$
$$\alpha_2 = \alpha_{21}\cos\theta + \alpha_{22}\sin\theta$$
$$\alpha_3 = \alpha_{31}\cos\theta + \alpha_{32}\sin\theta$$

Substituting these values gives

$$f(\alpha) = A_0 + A_2\cos 2\theta + A_4\cos 4\theta + B_2\sin 2\theta + B_4\sin 4\theta$$

where

$$A_0 = \frac{5}{16} - \frac{3}{16}(\alpha_{13}^4 + \alpha_{23}^4 + \alpha_{33}^4)$$

$$A_2 = \frac{1}{4}[(\alpha_{12}^4 - \alpha_{11}^4) + (\alpha_{22}^4 - \alpha_{21}^4) + (\alpha_{32}^4 - \alpha_{31}^4)]$$

$$A_4 = \frac{1}{16}[3 - 4(\alpha_{11}^4 + \alpha_{21}^4 + \alpha_{31}^4) - 4(\alpha_{12}^4 + \alpha_{22}^4 + \alpha_{32}^4) + 3(\alpha_{13}^4 + \alpha_{23}^4 + \alpha_{33}^4)]$$

$$B_2 = \frac{1}{2}[\alpha_{11}\alpha_{12}\alpha_{13}^2 + \alpha_{21}\alpha_{22}\alpha_{23}^2 + \alpha_{31}\alpha_{32}\alpha_{33}^2]$$

$$B_4 = \frac{1}{4}[\alpha_{11}\alpha_{12}(\alpha_{12}^2 - \alpha_{11}^2) + \alpha_{21}\alpha_{22}(\alpha_{22}^2 - \alpha_{21}^2) + \alpha_{31}\alpha_{32}(\alpha_{32}^2 - \alpha_{31}^2)]$$

Now the rolling process imposes symmetry about the rolling direction, but for the single-crystal equation given above this is not the case. The equation must, therefore, be averaged with that for the mirror image orientation, which is equivalent to suppressing the sine terms.

If, as in the text, Young's modulus is measured by determining the resonant frequency of a ring, then an average value is required. There are many possible averages, of which that corresponding to uniform stress is the easiest to determine, since it merely involves averaging $f(\alpha)$. This gives the average value of E, $\bar{E} = 1/(a - A_0 b)$. For the cases of interest, the value so determined is a few per cent different from that obtained by numerical integration of E, which corresponds to uniform strain. The uniform stress value is therefore a sufficiently good approximation for our purpose.

It is also interesting to note that, if a $\langle 111\rangle$ direction lies in the sheet, $\alpha_{13}^4 + \alpha_{23}^4 + \alpha_{33}^4 = \frac{1}{2}$ for all orientations of the sheet. In this case $A_0 = 7/32$ and the average value of Young's modulus round a ring is independent of the texture, so that it cannot be used to distinguish between various possible descriptions of the texture.

REFERENCES

(1) Paxton, W. S., and Nilan, T. G. *J. Appl. Phys.*, **26,** p. 994 (1955).

(2) Crede, J. H., and Martin, J. P. *J. Appl. Phys.*, **20,** p. 966 (1949).

(3) Barrett, C. S. *Structure of Metals*, Chap. 18 (New York: McGraw-Hill Book Co., 1943).

(4) Clark, C. A. *Brit. J. Appl. Phys.*, **7,** p. 355 (1956).

(5) Jones, E. R. W., and Fell, E. A. *Acta Metallurgica*, **5,** p. 689 (1957).

(6) Merlini, A. *Trans Amer. Inst. Min. Met. Eng.*, **206,** p. 967 (1956).

(7) Wooster, W. A. *Crystal Physics*, p. 252 (London: Cambridge University Press, 1949).

(8) Bozorth, R. M., Mason, W. P., McSkimin, H. J., and Walker, J. G. *Phys. Rev.*, **75,** p. 1949 (1954–1955).

(9) Neighbours, J. R., Bratten, F. W., and Smith, C. S. *J. Appl. Phys.*, **23,** p. 389 (1952).

Prismatic fin with non-linear heat loss analysed by resistance network and iterative analogue computer

By I. C. Hutcheon, M.A., A.M.I.E.E., A.M.I.Mech.E., G. Kent Ltd., Luton, Beds.,
and D. B. Spalding, M.A., Ph.D., A.M.I.Mech.E., Imperial College of Science and Technology, London, S.W.7

[*Paper received* 16 *October*, 1957]

The paper analyses heat flow by natural convection from a fin of uniform conductivity and cross-sectional area, fixed at one end to a hot wall and immersed in a cooler fluid. A resistance network analogue is used in conjunction with a new type of iterative analogue computer to determine the temperature distributions and fin efficiencies for a variety of fin proportions, on the assumption that heat loss is proportional to the local temperature to the power 5/4. Results are compared with the case of linear heat loss.

The theory of heat transfer from secondary surface elements (fins) has been extensively developed with the assumptions of: (i) fixed fin root and surrounding fluid temperatures; (ii) fin temperature dependent only on distance from the root; (iii) heat flux from the fin surface proportional to difference between local fin temperature and fluid temperature (see, for example, Schneider[1] for references, and Kayan[2]).

When the fin projects into a fluid, the bulk of which is at rest, heat transfer results by natural convection; the heat flux is then proportional to the local temperature to the power 5/4 under common conditions, in contrast to assumption (iii) above. Because of the resultant non-linearity of the heat-flow equation, this case appears not to have been analysed, despite its practical relevance.

The present paper analyses heat flow by natural convection from a fin of uniform conductivity and cross-sectional area. It is supposed that the heat flux is the same non-linear function of temperature difference at all points. Temperature distributions and fin efficiencies have been determined by an automatic electrical analogue technique, and are compared with the results of the linear theory. Heat loss from the end of the fin is taken into account.

It is recognized that the present one-dimensional problem could be solved by numerical computations without excessive difficulty. The problem has been solved by resistance network analogue however, as a demonstration, on an example of engineering interest, of the new method of dealing with non-linearity. The present technique is applicable without modification to two- and three-dimensional problems, the numerical solution of which would involve prohibitive labour.

LIST OF SYMBOLS

Thermal quantities

A, cross-sectional area of fin.
C, heat loss per unit surface area of fin divided by $(T - T_f)^{5/4}$.
h, length of block in terms of y ($= 1/7$ in present example).
j, suffix designating block, numbering from wall.
k, thermal conductivity of fin.
K, non-dimensional fin parameter, $= l^2pC(T_w - T_f)^{1/4}/Ak$.
l, length of fin.
p, perimeter of fin cross-section.
q, rate of heat loss from whole fin.
T, temperature (local) of fin, assumed uniform over a cross-section.
T_f, fluid temperature.
T_w, wall (fin-root) temperature.
x, distance of fin cross-section from wall.
y, non-dimensional distance from wall, $= x/l$.
θ, non-dimensional fin temperature, $= (T - T_f)/(T_w - T_f)$.
θ_0, θ at fin root, $= 1$.
η, fin efficiency, $= q/[pl(1 + A/pl)C(T_w - T_f)^{5/4}]$.

Electrical quantities

g, function generator coefficient.
i, current withdrawn from network point.
i_o, current supplied to whole network.
j, suffix denoting network point.
R, resistance in cathode circuit of current-controlling element.
r, resistance between adjacent network points.
V, voltage across R.
V_b, h.t. supply voltage.
v, voltage at network point, representing $T - T_f$.
v_0, voltage representing $T_w - T_f$.

HEAT TRANSFER THEORY

Fig. 1 illustrates the system considered. The fin has length l, cross-sectional area A and perimeter p. Its conductivity is k, and the heat loss per unit surface area is taken as $C(T - T_f)^{5/4}$ where C is a constant derived from natural

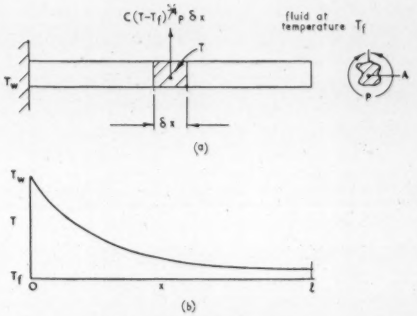

Fig. 1. The heat-flow problem
(*a*) Prismatic fin immersed in a fluid.
(*b*) Temperature distribution.

convection theory, T is the local fin temperature, and T_f is the fluid temperature. At the fin root, where it abuts the wall, the fin temperature is T_w. The problem is to determine the temperature distribution in the fin and the total heat loss to the fluid.

Differential equation. The Fourier heat-conduction equation, combined with the condition that the state is steady, leads to

$$Ak(d^2T/dx^2) = pC(T - T_f)^{5/4} \tag{1}$$

where x is the distance from the fin root.

Introducing the dimensionless quantities

$$\theta = (T - T_f)/(T_w - T_f),$$
$$y = x/l,$$
$$K = l^2pC(T_w - T_f)^{1/4}/Ak,$$

equation (1) becomes

$$d^2\theta/dy^2 = K\theta^{5/4} \tag{2}$$

Boundary conditions. At the fin root ($y = 0$), we have $\theta = \theta_0 = 1$ by definition.

At the fin end ($y = 1$), we have

$$Ak(dT/dx) = -AC(T - T_f)^{5/4},$$
$$\text{i.e. } d\theta/dy = -K(A/pl).\theta^{5/4} \tag{3}$$

Finite difference form. The electric analogue involves the supposition that the fin can be "lumped" into a number of blocks of uniform temperature connected by "resistances" to heat transfer. The "lumping" diagram is given in Fig. 2 and

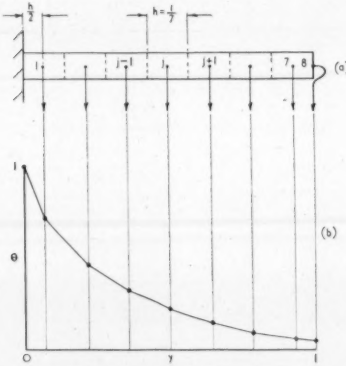

Fig. 2. Method of lumping

(*a*) Fin.
(*b*) Temperature distribution in dimensionless form.

is for seven blocks. The differential equation and boundary conditions must therefore be approximated by finite difference equations as follows.

For blocks away from the fin extremities

$$\frac{\theta_{j+1} + \theta_{j-1} - 2\theta_j}{h^2} = K\theta_j^{5/4} \tag{4}$$

For the first block ($j = 1$)

$$\frac{1}{h}\left[\frac{(\theta_2 - \theta_1)}{h} - \frac{(\theta_1 - \theta_0)}{h/2}\right] = K\theta_1^{5/4} \tag{5}$$

where $\theta_0 = 1$ by definition of θ.

For the last block ($j = 7$)

$$\frac{1}{h}\left[\frac{(\theta_8 - \theta_7)}{h/2} - \frac{(\theta_7 - \theta_6)}{h}\right] = K\theta_7^{5/4} \tag{6}$$

At the right-hand extremity

$$\frac{\theta_8 - \theta_7}{h/2} = -K(A/pl)\theta_8^{5/4} \tag{7}$$

Here subscript j indicates the location of the block, numbering from the fin root, h is the block length (there are $1/h = 7$ blocks altogether), and θ_8 is the temperature of the end face of the fin.

The mathematical problem. The task is to solve the system of simultaneous non-linear equations (4), (5), (6) and (7) for various values of K and of A/pl. The first of these factors measures the ease of heat loss from the surface relative to the ease of axial heat conduction; the second is the ratio of the area of the end of the fin and the remainder of the exposed area. Of special importance is the heat-transfer q, across the fin root, which equals the total heat loss from the fin. In differential form this is given by

$$\dot{q} = -kA\left(\frac{dT}{dx}\right)_{x=0}$$
$$= -kA\frac{(T_w - T_f)}{l}\left(\frac{d\theta}{dy}\right)_0 \tag{8}$$

In finite difference form this becomes

$$\dot{q} = \frac{kA(T_w - T_f)}{l}\frac{(\theta_0 - \theta_1)}{h/2} \tag{9}$$

The performance of a fin is usually expressed in terms of the "fin efficiency" η, defined as the actual heat transfer from the fin surface, divided by the heat transfer which would occur if the whole surface were at the wall temperature. From equation (8), therefore

$$\eta = \frac{-(d\theta/dy)_0}{(1 + A/pl)K} \tag{10}$$

THEORY OF THE ELECTRICAL ANALOGUE

The electrical analogue used to solve the problem is shown in Fig. 3. The seven uniform-temperature blocks are considered as concentrated at points 1 to 7 and separated from each other by six equal resistances r. Separation from the ends is by two further resistances $r/2$. Fin temperature is represented by electrical potential along the network of resistances, and heat flow in the fin by electric current through the network. Currents $i_1 - i_8$ simulate heat loss from the fin surface and free end, and are controlled by an iterative analogue computer comprising eight thermionic valves and a scanning and current-adjusting circuit.

The following equations hold for the analogue under equilibrium conditions, i.e. when there is no accumulation of charge (representing heat) at any point.

For points away from the extremities

$$\frac{v_{j+1} + v_{j-1} - 2v_j}{r} = i_j, \tag{11}$$

for the first point

$$\frac{v_2 - v_1}{r} - \frac{v_1 - v_0}{r/2} = i_1, \tag{12}$$

for the seventh point

$$\frac{v_8 - v_7}{r/2} - \frac{v_7 - v_6}{r} = i_7, \tag{13}$$

while at the right-hand extremity

$$\frac{v_8 - v_7}{r/2} = -i_8, \tag{14}$$

and at the left-hand extremity

$$\frac{v_1 - v_0}{r/2} = -i_0. \tag{15}$$

Comparing equations (11), (12), (13) and (14) with (4), (5), (6) and (7) we see that the similarity is complete and the problem is solved provided that v/v_0 is interpreted as θ and the currents are adjusted to have the values

$$i_j = \frac{h^2 v_0 K}{r}\left(\frac{v_j}{v_0}\right)^{5/4}, \tag{16}$$

for $j = 1$ to 7, and

$$i_8 = \frac{h^2 v_0 K}{r}\frac{A}{plh}\left(\frac{v_8}{v_0}\right)^{5/4}. \tag{17}$$

Values of θ along the fin are thus given by values of v/v_0 along the analogue, while the temperature gradient at the left-hand extremity is, from equation (15),

$$\frac{\theta_1 - \theta_0}{h/2} = -\frac{r\, i_0}{h\, v_0}, \tag{18}$$

where $\theta_0 = 1$. It may be noted that this is also the mean gradient between points 0 and 1.

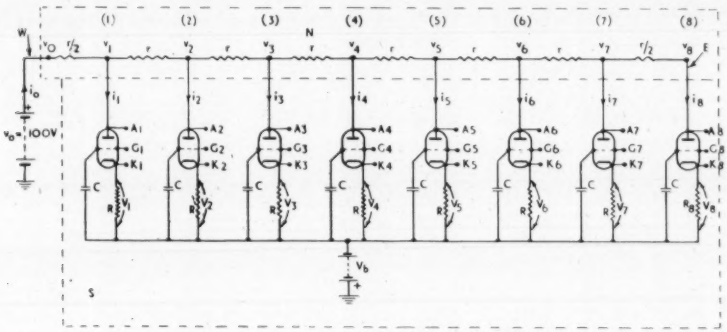

Fig. 3. Resistance analogue with current-controlling elements

W = wall. E = free fin end.
N = resistance network simulating fin. S = elements simulating surface heat loss.

THE PROBLEM OF NON-LINEARITY

Conventional solution. To satisfy equations (16) and (17), the eight currents must be adjusted to be in the correct (5/4 power) relation to the local voltages. The method most usually adopted in this type of problem is to make the adjustments manually, each current being supplied from a high-impedance source so as to be relatively unaffected by changes in the network voltage. However, this method is tedious because the adjustment of any one current modifies the potentials throughout the network and upsets all the other adjustments. An iterative procedure is thus rendered necessary, whereby every adjustment is repeated several times until all are simultaneously correct.

Display technique. Liebmann and Bailey[3] have described a scanning technique whereby the errors in adjustment are displayed on a cathode-ray screen. This enables the larger errors to be picked out and reduced first, considerably easing the adjustment procedure which is, however, still manual. The method does not seem to have been applied to cases where the current-voltage law is non-linear.

Use of non-linear resistors. The difficulties of manual adjustment can be overcome by attaching a suitable non-linear resistance element to each point on the network. For example, Lawson and McGuire[4] have used non-linear resistors of Metrosil combined with ohmic resistors to approximate a desired law in solving heat flow problems, while McIlroy[5] uses some two hundred varieties of tungsten-filament lamp to simulate the pressure-flow characteristics of fluids flowing in pipe networks.

This approach is simple in principle but somewhat inflexible in practice unless a large stock of non-linear resistors is made up to provide a range of coefficients. An alternative in the present case would be to construct several (linear) networks, each of different resistance, so as to enable several different sets of results to be obtained with a single set of non-linear resistors. But this would still be tedious. Another disadvantage of the method is its limited accuracy owing to the difficulty of obtaining the desired law over a sufficiently wide range of voltages.

Use of conventional analogue computers. A different approach has been described by Karplus,[6] who connected a complete analogue computer unit of conventional type to each node of a network of resistors so as to maintain continuously the desired non-linear relation between each current and the associated voltage. In a typical case involving four computer units, each comprised three high-gain d.c. amplifiers, a servo-amplifier, and a motor-driven three-gang potentiometer. This system is rapid in operation and adjusts the currents with an accuracy of about 1%, but it clearly becomes costly if there are more than a few network points.

ITERATIVE ANALOGUE-COMPUTER SOLUTION TO THE PROBLEM OF NON-LINEARITY

Principle of the system. In the present case, an iterative automatic system has been adopted for adjusting the currents

withdrawn from the network. As shown in Fig. 3, each current flows through a triode valve connected as a cathode-follower and having a 1 μF capacitor connected to its grid. The current through each triode depends primarily on the grid potential, which is held substantially constant for several seconds by the capacitor when no other connexion is made to the grid, and only slightly on the anode potential.

The triodes thus constitute a set of current-controlling analogue memory units which are adjusted in turn according to the output of a function generator, the input of which scans the network potentials.

The scanning and adjusting circuit is shown in Fig. 4 and contains an a.c.-coupled amplifier connected in a null-balance arrangement to amplify the control signals and hence minimize the errors in adjustment. Operation of this system is described in detail by Hutcheon.[7] In principle, the apparatus makes a "first guess" at the appropriate potential

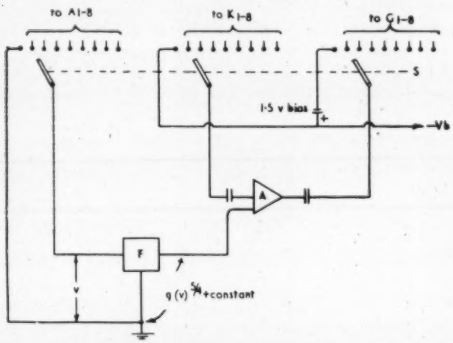

Fig. 4. Scanning and current-adjusting circuit

S = continuously rotatable three-gang switch.
F = function generator.
A = amplifier.

at each network point and then, as the scanning switch is continuously rotated, adjusts the currents and improves the guess on successive cycles until equilibrium is reached and the solution is available in the form of voltages along the network.

The system is relatively simple, since only the memory units are duplicated. The valve characteristics do not have to be accurately matched, and it is necessary merely to make all the cathode resistances equal in order to ensure that each unit has the same current-voltage law as every other one, while local modifications to this law can be made, if desired, by adjusting the individual cathode resistances. It is also flexible, since different laws can be introduced simply by modifying the characteristics of the single function generator, a change in coefficient in particular requiring merely the adjustment of a gain control in the generator. The experimental computer contains a hand-rotated switch, and solutions are reached after several cycles. This takes several seconds, but much faster operation could clearly be obtained by the use of a motor-driven switch of suitable design. Some details of the amplifier and function generator are given below.

Amplifier. The amplifier has only two stages, one of which is a cathode-follower to provide a low output impedance and enable the memory capacitors to be charged rapidly. The gain was normally set near its maximum of about fifty: the circuit is shown in Fig. 5.

In order to avoid the errors inherent in alternative circuits using, for example, differential amplifiers, the whole amplifier was designed to "float" at the function generator output

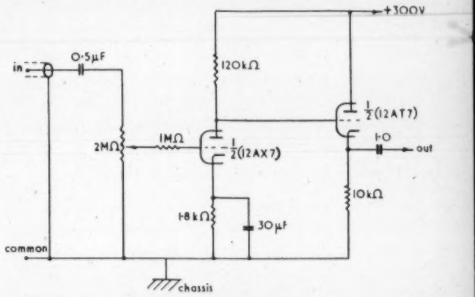

Fig. 5. Amplifier

potential. The chassis was connected to the low-impedance input terminal and isolated from earth, while the h.t. transformer was fitted with a double inter-winding screen to minimize the stray a.c. flowing to earth *via* the function generator.

Function generator. The function generator, Fig. 6, comprises a biased-diode network arranged to approximate the law.

$$\text{Output voltage} = g(v)^{5/4} + \text{constant} \qquad (19)$$

where v is the input voltage, by four straight-line segments, g being variable from zero up to a maximum of 0·1 by means of the calibrated 5 kΦ output potentiometer. The cathode-follower output stage presents a low-impedance path to

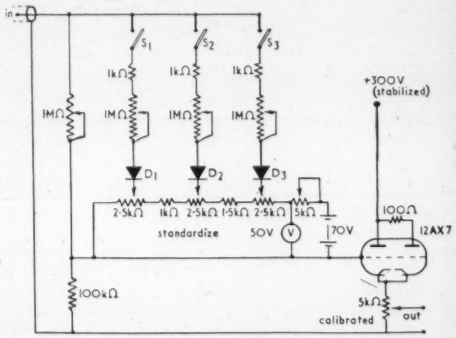

Fig. 6. Function generator

D_{1-3} silicon diodes: Ferranti ZS10A.

earth for stray currents from the amplifier, and enables the potential of the whole amplifier to be changed rapidly.

The ideal curve was first plotted for $g = 0{\cdot}1$, and four break-points chosen slightly off the curve to give segments

deviating from the curve by not more than about ¾% of full output. Thus:

Table 1. *Function generator characteristic*

v (V)	$0.1\,v^{5\cdot4}$ (*calculated*)	*Output at break points* (V)
0	0	0 + constant
10	1·778	1·7 + constant
30	7·021	6·9 + constant
60	16·70	16·6 + constant
100	31·62	31·5 + constant

The 1 MΩ potentiometers were adjusted to set the slopes of the segments, being first shorted in turn while the 2·5 kΩ potentiometers were adjusted to set the break points. The constant component of the output arises in the cathode-follower, but is eliminated by the zeroing action of the current-adjusting circuit.

Scale factors. When the analogue solution has been set up, the currents withdrawn from the network are given by

$$i_j = \frac{V_j}{R} = \frac{g v_j^{5\cdot4}}{R} \quad \text{for } j = 1 \text{ to } 7$$

$$i_8 = \frac{V_8}{R_8} = \frac{g v_8^{5\cdot4}}{R_8}$$

whence it can be seen, by comparison with equations (16) and (17) that the problem is solved for the following conditions

$$K = \frac{g}{h^2}\frac{r}{R}(v_0)^{1/4} \tag{20}$$

$$\frac{A}{pl} = h\frac{R}{R_8} \tag{21}$$

The following values of circuit parameters gave a range of values of K from zero to 12·5 and of A/pl from zero to 1/3·5:

$g = 0$ to 0·1 adjustable
$h = 1/7$
$r = 5\ \text{k}\Omega \pm 0{\cdot}1\%$
$R = 10\ \text{k}\Omega \pm 0{\cdot}1\%$ or $6{\cdot}2\ \text{k}\Omega \pm 1\%$
$v_0 = 100$ V
$R_8 =$ infinity or R or $R/2$

RESULTS

Voltage measurements along the network are plotted as ratios in Figs. 7 [(*a*), (*b*), and (*c*)] and represent dimensionless temperature distributions along the fin for various conditions. The general shape of these curves is similar to the well-known case of linear heat loss.

Fig. 8 shows the fin efficiency as ordinate plotted against $(1 + A/pl)\sqrt{K}$ as abscissa. Values of $(d\theta/dy)_0$ used in calculating the fin efficiency by equation (10) were derived according to equation (18) from measurements of the current i_0 supplied to the high-voltage end of the network. The quantity plotted as abscissa is related to the geometry, etc., by

$$(1 + A/pl)\sqrt{K} = l(1 + A/pl)\sqrt{[pC(T_w - T_f)^{1/4}/Ak]} \tag{22}$$

and is chosen because $l(1 + A/pl)$ is the "effective fin length" introduced by Harper and Brown[8] to bring fin data of various A/pl values approximately on to a single curve; $l(1 + A/pl)$ represents the length of a fin of the same cross-sectional shape and exposed area as the given one, but with an insulated free end.

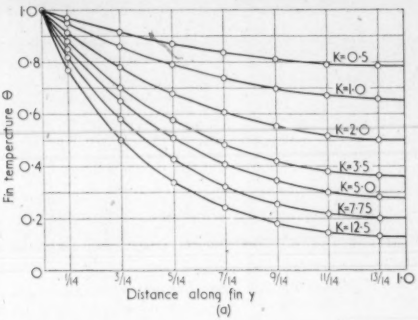

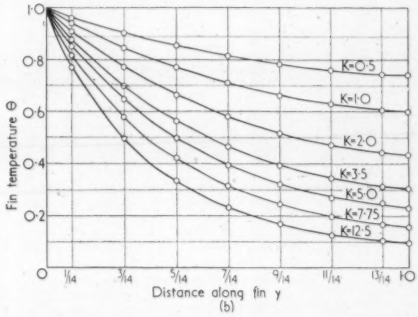

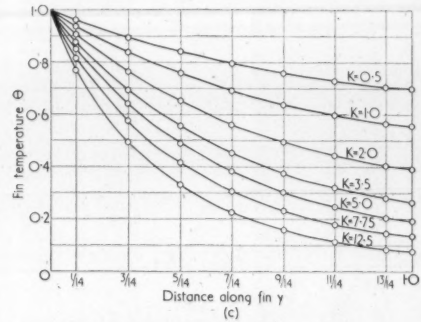

Fig. 7. Temperature distribution along fin
(*a*) $A/pl = 0$
(*b*) $A/pl = 1/7$
(*c*) $A/pl = 1/3{\cdot}5$

Examination of Fig. 8 shows that all the points do indeed lie on a single curve within the limits of experimental error. Also drawn on Fig. 8 is the line

$$y = \frac{th[(1 + A/pl)\sqrt{K}]}{(1 + A/pl)\sqrt{K}} \tag{23}$$

which represents the fin efficiency for a linear surface heat-loss law.

It is seen that, for small values of K (short fins), the analogue results agree closely with the "linear" law. For larger values of K, the analogue shows the efficiency of a fin losing heat by natural convection to be somewhat lower than that of a fin with constant heat transfer coefficient, although the difference does not exceed 10%.

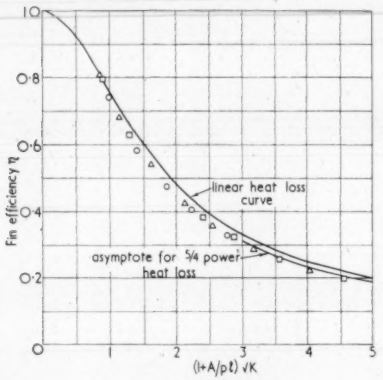

Fig. 8. Fin efficiency

○ $A/pl = 0$
△ $A/pl = 1/7$
□ $A/pl = 1/3{\cdot}5$

These results are to be expected. At low values of K, the whole fin is practically at wall temperature, so the heat transfer coefficient is practically uniform despite the 5/4 power law. As K increases, the falling surface temperature reduces the surface heat-transfer coefficient.

A check on the accuracy of the analogue is possible at high values of K, where the fin is so long that the end temperature is practically that of the surrounding fluid. For this case we can integrate equation (2), as

$$\tfrac{1}{2}[(d\theta/dy)^2]_0^1 = (4K/9)[\theta^{9/4}]_0^1 \qquad (24)$$

and put $(d\theta/dy)_1 = 0$, $\theta_1 = 0$ and $\theta_0 = 1$. Hence

$$(d\theta/dy)_0 = -\sqrt{(8K/9)}$$

and so

$$\eta = \frac{-(d\theta/dy)_0}{(1 + A/pl)K} = \frac{\sqrt{(8/9)}}{(1 + A/pl)\sqrt{K}} = \frac{0{\cdot}943}{(1 + A/pl)\sqrt{K}} \qquad (25)$$

The rectangular hyperbola $0{\cdot}943/(1 + A/pl)\sqrt{K}$ is drawn in Fig. 8. It is seen that the analogue results fall somewhat below this asymptote. This is believed to be due to the truncation error (small number of "blocks") which becomes increasingly important as the voltage distribution curve shifts to the left [Figs. 7(*a*), (*b*), (*c*)].

CONCLUSIONS

(1) Network analogues can be constructed for non-linear problems, without the necessity to use more than one non-linear element, by using a single function generator to provide iterative adjustment of a number of control elements with memory properties.

(2) This enables natural convection boundary conditions to be incorporated in network analogues for heat transfer problems.

(3) In the particular case studied, the fin of uniform cross-section, the analogue showed the fin efficiency to be practically the same as that of a fin with linear heat loss when the fin is short, but to be up to 10% less than that of the "linear" fin when the (non-dimensional) fin length is greater.

(4) The crude (seven-block) subdivision of the fin introduced truncation errors for low fin efficiencies. No difficulty of principle prevents the use of a finer sub-division however.

(5) The technique used is applicable without modification to two-dimensional problems. Variation of the surface heat-transfer coefficient by a multiplier depending only on position is also easily dealt with.

REFERENCES

(1) Schneider, P. J. *Conduction Heat Transfer* (Cambridge, Mass.: Addison-Wesley, 1955).

(2) Kayan, C. F. *Industr. Engng Chem.*, **40**, p. 1044 (1948).

(3) Liebmann, G., and Bailey, R. *Brit. J. Appl. Phys.*, **5**, p. 32 (1954).

(4) Lawson, D. I., and McGuire, J. H. *Proc. Instn Mech. Engrs, A*, **167**, p. 275 (1953).

(5) McIlroy, M. S. *J. Amer. Water Works Association*, **42**, p. 347 (1950).

(6) Karplus, W. J. *Brit. J. Appl. Phys.*, **6**, p. 356 (1955).

(7) Hutcheon, I. C. *Brit. J. Appl. Phys.*, **8**, p. 370 (1957).

(8) Harper, W. B., and Brown, D. R. *National Advisory Committee for Aeronautics Report* No. 158, p. 679 (Washington, 1922).

APPENDIX

Accuracy of analogue

Proportional band error. The current-adjusting system is a closed-loop arrangement and has a proportional band of width dependent on the characteristics of the cathode-followers and the gain of the amplifier. The proportional error can be assessed as follows. The anode-cathode voltage for any of the triodes in Fig. 3 is $V_b + v_j - V_j$ (j = 1 to 8) where:

V_b = 120 V (for all cases except $K = 12{\cdot}5$)
v_j = 0 to 100 V
V_j = 0 to 31·5 V

The range of anode-cathode voltage employed is thus approximately 120 to 190 V, while the corresponding range of cathode currents, with 10 kΩ cathode resistors, is 0–3 mA. The grid-cathode voltage required by a strapped type 12AX7 valve under these conditions varies from $-2{\cdot}0$ to $-1{\cdot}2$ V approximately, i.e. not more than $\pm 0{\cdot}5$ V about a standing bias of $-1{\cdot}5$ V. This control signal is derived from the amplifier and, if the gain is fifty, corresponds to an input signal, i.e. an error in cathode potential, of $\pm 0{\cdot}01$ V which is about $\pm 0{\cdot}03$% of the maximum cathode potential. Hence errors in current adjustment relative to the function generator output should not exceed about $\pm 0{\cdot}03$% of the maximum current plus the cathode resistor tolerance. Errors will be slightly greater for the circuit values used for the case where $K = 12{\cdot}5$ but are still small.

Other errors. Network voltages were measured and the function generator was calibrated using a Model 8 Avometer (accuracy $\pm 2\%$ of full scale) while the input current to the network was measured on a similar Model 7 meter ($\pm 1 \cdot 2\%$). Function generator errors comprise the inherent straight-line segment approximation ($\frac{1}{4}\%$) together with errors in initial setting-up and subsequent battery standardization.

It is difficult to assess the total effect of these errors on the final results and still more so to allow for truncation errors due to the lumped nature of the analogue. It is, however, clear that the system accuracy could be made quite high by the use of potentiometric methods of measurement and finer subdivision of the network, and ultimately would probably depend on that of the function generator.

A portable lamination detector for steel sheet

By B. O. Smith, M.Sc., A.Inst.P., A. P. H. Jennings, B.Sc., A.R.C.S., A.Inst.P.,* and A. G. Grimshaw,
Physics Department, The British Iron and Steel Research Association, Battersea Park Road, London

[*Paper received* 11 *October*, 1957]

This paper describes a method of detecting laminations in steel sheet based on the distortion they cause in the flow pattern of an electric current through the sheet. Direct current is passed through the sheet between two contacts on opposing faces while the potential difference between two adjacent contacts is measured. This potential difference is very small in sound material but rises sharply if a lamination is present.

Not every lamination can be detected by this method because, for this to happen, it is essential that it should form an electrical discontinuity. For example, experience has shown that in hot-rolled strip most of the laminations are not detected, but in cold-rolled strip the great majority above 0·25 in. wide do form a discontinuity and can be detected with certainty by the instrument described.

The defects in steel sheet known as laminations are the remains of cylindrical cavities in the parent ingot, which by subsequent rolling may become thin cavities of relatively large area, parallel to the surface of the sheet, and considerably extended in the direction of rolling. These defects, normally invisible at the surface, often show up when the material is pressed or deep-drawn. One characteristic of laminations is that they can impede the flow of electric current, and there is a measurable difference between the flow patterns of current in sound and in laminated material. The method employed, therefore, is to pass current perpendicularly to the plane of the material and to measure the potential gradients near the points where the current is injected.

There is a superficial resemblance between this technique, and that of Thornton and others[1, 2] for the measurement of the thickness of plate. Thornton injects current so as to flow in the plane of the material and by measurement of the resulting potential gradient can deduce a factor proportional to the resistivity and thickness of the material. The essential differences in the two techniques are that for the thickness measurement, the current flow is in the plane of the material and a uniform potential gradient is measured between the injection probes; for the lamination detection, the gradients are measured not between but in the near neighbourhood of the injection points and are changing sharply, while the current flow is perpendicular to the plane of the material.

DESIGN OF THE INSTRUMENT

The circuit arrangement employed is given in Fig. 1, and consists of a four-probe system. One pair of probes, on opposing faces of the test material, form part of a constant current circuit, while the remaining two *A* and *B* are connected to a suitable potential measuring instrument. The influence of design parameters was investigated by a simple two-dimensional model technique which will be briefly discussed. These experiments were carried out using Teledeltos recording paper as the test material, which could then readily be cut into a number of different shapes with slots cut to represent laminations. In all cases, dimensions have been quoted as ratios of strip width, *t*, since a linear change of all dimensions will not influence current flow patterns. Fig. 2

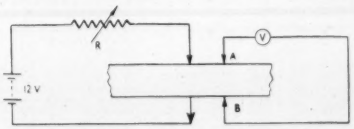

Fig. 1. Schematic circuit arrangement

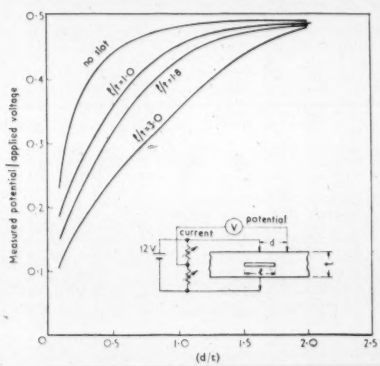

Fig. 2. Variation of potential along strip edge

* Now at Messrs. Bailey Meters and Controls Ltd., Croydon, Surrey.

gives the potential distribution along an edge of strip having a slot of length l symmetrically placed about the line of current contacts together with the simple circuit used. The potential at distance d from the current contacts is expressed as a fraction of the potential difference applied to the paper. With this circuit, the measurements were not independent of contact resistance and it is for this reason that the potential at points remote from the current contacts does not reach the expected value of 0·5. The curves do, however, show the form of variation and illustrate the fact that for a given length of slot there is a particular distance at which the potential exhibits the greatest change due to the presence of the slot. The graph also shows that since, in the case of a strip having no slot, the potential has reached a steady value at a distance given by $d/t = 2$, the current contacts could be placed at a distance from the edge of the strip of approximately this order without introducing appreciable edge effects.

Measurements were made with the final system of Fig. 1, to determine how the potential difference varied as the contact system was moved relative to the slot in the paper, for different contact spacings. Typical results are shown in Fig. 3 for one such contact spacing, $d/t = 5$. The maximum change in potential difference produced by different slots

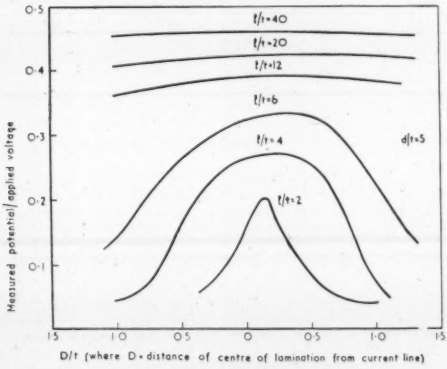

Fig. 3. Variation of potential difference during scanning of lamination

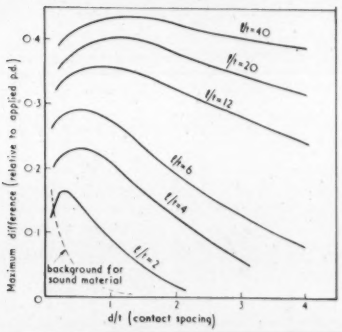

Fig. 4. Determination of optimum contact spacing

was calculated and plotted against contact spacing as shown in Fig. 4. The existence of a fairly sharply defined value of d/t for a given slot length is clearly shown. It may also be seen that while for small values of l/t small values of d/t are required, at contact spacing of $d/t = 1$ a response which is not very far removed from the maximum will be achieved for all values of l/t above 4. No attempt was made to obtain rigid design data which could be applied to a practical instrument because of the difficulty in applying the results of the two-dimensional model to the three-dimensional case, but the model results indicated that contact spacings of the order of the sheet thickness would be required. Fig. 5 shows

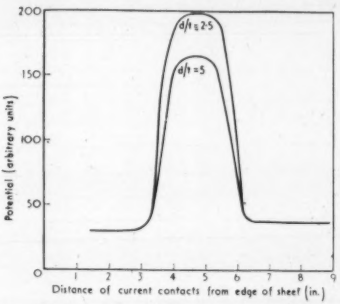

Fig. 5. Measurements on steel sheet

the results of measurements taken on a piece of laminated steel 0·05 in. thick having a lamination approximately $2\frac{1}{2}$ in. wide ($l/t = 50$). Contact spacings of $\frac{1}{4}$ in. and $\frac{1}{8}$ in. were used and the results show that yet smaller spacings would give greater response.

DESCRIPTION OF THE INSTRUMENT

A schematic arrangement of the final form of the instrument is shown in Fig. 6, while the electrical circuit conforms to Fig. 1. It consists of a pair of duralumin tongs 24 in. long pivoted near one end with the contacts mounted near the

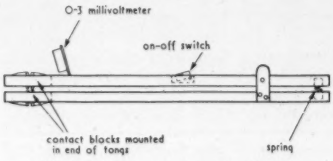

Fig. 6. Schematic diagram of tongs

other end. A 3–0–3 millivoltmeter is mounted on a bracket above the contacts. Fig. 7 shows on an enlarged scale the spring-loaded contacts, which are of "D" section silver steel $\frac{1}{4}$ in. in diameter thus obtaining maximum mechanical strength with minimum separation. A thin layer of oiled silk between the two halves provides the necessary insulation. Their points, rounded to reduce scoring of the sample, are 0·022 in. apart. A 12 V lead acid battery supplies current at 10 A through a control rheostat which acts as a "swamp" resistance giving constant current in the circuit for all normal changes in contact and specimen resistances. An on-off switch ensures that current does not flow when the sheet is

not in position between the contacts. A photograph of the instrument in use is shown in Fig. 8.

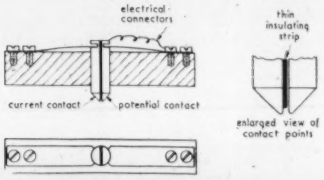

Fig. 7. Contact assembly

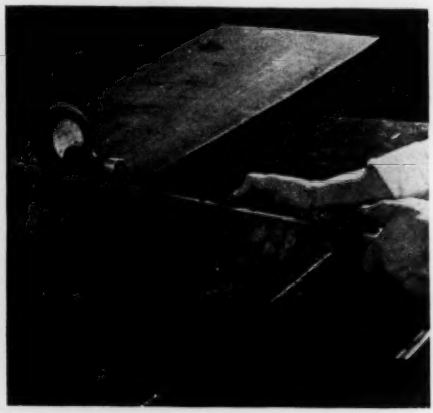

Fig. 8. The instrument in use

RESULTS OBTAINED

A number of trials of the instrument have been carried out on both cold and hot-rolled sheet. The tests on cold-rolled strip were successful, confirmation of the presence of lamination where indicated by the instrument being obtained by a destructive test. The narrowest laminations encountered were roughly $\frac{1}{2}$ in. wide, but it was not known whether smaller laminations were present. In the case of hot-rolled material no indications of lamination were obtained though wide laminations could be seen at the edge of the specimens with the naked eye. Even after the removal of the scale by pickling and rubbing down with emery cloth so that ideal contact was obtained, no lamination was detected. This was thought to be due to the two faces of a lamination being in fairly intimate contact in hot-rolled material so that electrical contact is maintained over a considerable area of the lamination. It should perhaps be emphasized here that providing a definite electrical break occurs over even small widths of lamination, then detection must be possible with the system used, the sensitivity being governed by the dimensions of the sheet and the lamination, and the contact spacing.

The idea that cold working apparently "opens" a lamination has received confirmation by some experiments made on the British Iron and Steel Research Association 14 in. Rolling Mill at Sheffield. Some hot-rolled samples suspected of being laminated were indicated by the instrument as being sound. These samples were cold-rolled from about 0·1 in. down to about 0·020 in. and after each pass were examined with the instrument. After approximately 20% reduction several of the samples showed indications of being laminated and the response of the instrument increased with increasing reduction. This indicated a gradual opening of the laminations as cold-rolling proceeded.

In a second trial, the end of a 72 in. wide coil of cold reduced strip suspected of being laminated was thoroughly inspected with the instrument and the contours of laminations in the sheet detected by the instrument marked on the surface. Sections were then cut from the sheet in the positions indicated as being laminated and in other arbitrary positions. These were mounted and the edges polished so that the presence of a lamination in a section could be detected visually. This provided a crude statistical method of checking the performance of the instrument, and of a total of 24 laminations in the sheet 16 were detected by the instrument. The widths of laminations varied from 0·01 in. approx. to 1–2 in. Below a width of 0·1 in. no laminations were detected by the instrument although two were visible from the sections taken, each approximately 0·01 in. wide. Between 0·1 in. and 0·3 in. three laminations were detected and two missed, and similar results were obtained with 0·3 in. and 0·5 in. Of the remaining twelve laminations above 0·5 in. all but two were detected by the instrument.

The instrument has more recently been applied to a number of problems of an applied nature. For example, samples of one metal bonded to another have been examined and it has been possible to detect areas of bad bonding. As would be expected, the instrument can be used on metals other than steel, although a change of operating current may be necessary to give comparable sensitivity.

In its present form, the instrument is only suitable for inspection of static samples, but the technique is being developed for continuous inspection, particularly of moving strip. It is felt, however, that the portability and simplicity of the manually operated instrument will find many applications where a thorough inspection of large areas is not required.

CONCLUSIONS

The electrical method described will detect laminations in cold reduced sheet provided that they present a definite break in electrical contact between the two faces of the sheet. Under these conditions the manual instrument will detect laminations as narrow as 0·1 in. although careful searching is required for laminations of this size. Experience gained during the development of the instrument suggests that most laminations above 0·5 in. wide are electrically "open" and that these may readily be detected.

ACKNOWLEDGEMENTS

Grateful acknowledgement is made to the following firms who provided facilities for discussion and for works trials of the instrument: Stewarts and Lloyds Ltd., Corby; Steel Company of Wales Ltd., Abbey Works; J. B. and S. Lees Ltd., West Bromwich; and to colleagues at Hoyle Street, Sheffield, who assisted with the cold rolling trials. This work was carried out on behalf of the Mechanical Working Division of the British Iron and Steel Research Association.

REFERENCES

(1) THORNTON, B. M. *Proc. Instn Mech. Engrs*, **140**, p. 349 (1938).

(2) WARREN, A. G. *Proc. Instn Elect. Engrs*, **84**, p. 91 (1939).

The high temperature stability of permanent magnets of the iron-nickel-aluminium system

By A. G. CLEGG, M.Sc., and M. MCCAIG, Ph.D., F.Inst.P., Permanent Magnet Association, Sheffield 1

[*Paper first received* 14 *October, and in final form* 16 *December*, 1957]

The open circuit magnetization of rectangular bars of various modern permanent magnet alloys has been measured at temperatures up to 550° C. A differential ballistic method has been used and, after magnetization at room temperature, both reversible and irreversible losses occur on heating. These losses vary with material and dimension ratio, and in an attempt to explain these variations demagnetization curves at 500° C have been measured. To avoid the irreversible losses, stabilization at a higher temperature is better than ageing in an alternating field.

INTRODUCTION

In an earlier paper[1] the influence of temperatures between −190° C and +60° C on permanent magnets was described. The present paper deals with the effect of temperatures up to 550° C on permanent magnets of the types indicated in Table 1. For some of the alloys the influence of the ratio, length to cross-section has been studied. The results and conclusions may be compared with those given in a recent publication by Tenzer.[2]*

EXPERIMENTAL METHOD

In the previous work[1] a magnetometer method was used. Although capable of high accuracy under ideal conditions, the method presents difficulties when applied in a laboratory in which other magnetic experiments are proceeding. These difficulties were not too serious in the previous work in which comparatively short time cycles predominated, but became more serious in the present work which involved time cycles of 24 h and more. A simple ballistic method such as that used by Tenzer[2] is not usually more accurate than 0·5% and is scarcely adequate for measuring losses of this order of magnitude.

Table 1. *Composition, treatment and properties of magnets used*

Material	*Average composition (weight %) (balance Fe)*	*Heat treatment*	B_r (G)	$(BH)_{max}$ (M.G.O.)	$-B/H$ at $(BH)_{max}$	H_c (oersteds)
Alcomax II	Al 8·1, Ni 11·9, Co 21, Cu 4·4	Cooled from 1250° C at 1·2° C/s in a magnetic field. Tempered 48 h 590° C 48 h 560° C	12 700	4·7	23·0	565
Alcomax III	Al 7·8, Ni 13·2, Co 25, Cu 3, Nb 0·8		11 900	5·14	18·1	662
Alcomax IV	Al 7·4, Ni 13·3, Co 24·5, Cu 3, Nb 2·5		11 200	4·3	17·3	725
Alnico	Al 9·7, Ni 17·5, Co 13·6, Cu 5·9	Air-cooled from 1250° C, tempered 2 h 600° C	7 500	1·68	12·7	605
Alni	Al 13·1, Ni 25·9, Cu 2	Air blast cooled from 1250° C. Tempered 1 h 700° C	6 060	1·21	10·0	520

When a magnet is heated three types of change may be expected:

(i) Metallurgical changes which remain even after remagnetization.
(ii) Irreversible magnetization changes which remain on cooling to room temperature but can be reversed by remagnetization.
(iii) Reversible magnetization changes which disappear on cooling to room temperature without remagnetization.

With these materials no metallurgical changes were expected or found with temperatures not exceeding 550° C, and the total loss of magnetization observed when a magnet is heated should be the sum of the irreversible and reversible losses (ii) and (iii). Demagnetization curves at elevated temperatures have been measured in the hope of interpreting the above irreversible and reversible losses. The efficiency of alternating field stabilization and prior heating to a higher temperature in limiting the irreversible losses has been studied.

A differential ballistic method offers the possibility of increasing the sensitivity by a factor of about ten. All that is required is to balance the flux linkage detected by pulling a coil off the test magnet by some other stable flux change. A convenient method of producing this reference flux change is by using a second permanent magnet of similar size, shape and material to the one under test. This second magnet is, of course, kept at room temperature and was always magnetized at least 24 h before starting the experiment.

The apparatus is sketched in Fig. 1. When the tube R_2 is moved from contact with stop S_1 to S_2 a galvanometer deflexion of between 1 and 6 cm/% difference in the magnetization of the two magnets can be observed. A change of 0·1% in magnetization can easily be detected.

The magnets used were bars with a 1 cm square section and various lengths. It is useful to know the ratio

* Confusion may arise because the meanings of residual magnetism and remanence approved by the British Standards Institution (B.S. 205/43 Nos. 1260 to 1262) are interchanged compared with those approved in the U.S.A. (A.S.T.M. Designation A 127–48). While Tenzer naturally uses the latter, in this paper we adhere to the British Standard, and in particular by remanence we always imply the induction at zero effective field.

$-B/H = c$, where B is the induction and H the demagnetizing field at the centre of the bar. According to Evershed[3]:

$$-B/H = K(L/A)\sqrt{S} = c \qquad (1)$$

where L = length, A = area of cross-section, and S = half the surface area of the bar. This empirical formula appears to be the best approximation available provided K is taken

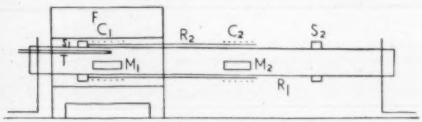

Fig. 1. Diagram of apparatus

M_1, magnet under test; M_2, reference magnet; R_1, refractory tube to which both magnets are fixed; R_2, larger refractory tube carrying two search coils; C_1, C_2, two similar search coils connected to a ballistic galvanometer in series opposition; S_1, S_2, stops to limit movement of tube R_2; F, furnace; T, platinum/platinum–rhodium thermocouple.

as 1·47, which is rather higher than originally proposed by Evershed. The lengths of bar used and calculated values of $-B/H$ are shown in Table 2.

Table 2. *Calculated values of* $-(B/H)$

Length (cm)	6·7	4·6	2·6
$-B/H$	37·4	21·6	9·5

RESULTS

Tables 3 and 4 show the total and irreversible losses of magnetization for various temperatures. The procedure adopted in compiling this data was as follows: both test and reference magnets were magnetized in a solenoid giving a field of more than 5000 oersteds, the test magnet being magnetized a few minutes before starting the experiment. The test magnet was heated to 200° C and held at this temperature for 6 h. (It has been established that all the measurable loss takes place in the first 1½ h.) The magnitude of the total loss at 200° C shown in Table 3 was then measured. The bar was allowed to cool to room temperature overnight and the irreversible loss due to heating to 200° C shown in Table 4 measured. This procedure was then repeated for each higher temperature in turn, remagnetizing the test magnet each time.

Instrument and other magnets which are required to be stable are usually given some form of magnet ageing treatment; a typical treatment is to reduce the magnetization by 5% in an alternating field. Table 5 shows the total and irreversible losses for Alcomax III bars after this treatment. Comparison of these figures with those in Tables 3 and 4 shows that this kind of ageing gives only a moderate improvement in temperature stability.

Table 3. *Total loss in magnetization at various temperatures*

Material	*Working* $-B/H$	*Total loss in magnetization (%)* 200° C	300° C	400° C	450° C	500° C	550° C
Alcomax III	37·4	4·0	6·5	9·0	10·9	12·6	14·4
Alcomax III	21·6	3·8	6·3	9·3	10·8	12·3	14·2
Alcomax III	9·5	3·2	5·4	7·9	9·5	11·5	13·2
Alcomax II	21·6	3·3	6·1	9·1	11·2	13·2	15·6
Alcomax IV	21·6	3·5	5·9	8·9	10·4	12·1	13·9
Alnico	37·4	6·0	9·2	13·4	15·8	18·2	20·8
Alnico	21·6	7·1	11·0	15·8	18·7	21·5	24·2
Alnico	9·5	5·7	10·7	15·0	18·0	20·8	23·3
Alni	37·4	8·7	14·1	19·1	22·4	27·2	32·9
Alni	21·6	10·0	16·2	22·8	27·2	32·0	36·8
Alni	9·5	11·2	17·3	25·7	30·8	37·0	42·0

Table 4. *Irreversible loss of magnetization after heating*

Material	*Working* $-B/H$	*Irreversible loss in magnetization (%)* 200° C	300° C	400° C	450° C	500° C	550° C
Alcomax III	37·4	0·4	0·6	0·75	0·85	1·0	1·15
Alcomax III	21·6	0·6	1·0	1·5	1·75	2·0	2·25
Alcomax III	9·5	0·75	1·1	1·5	1·7	1·9	2·15
Alcomax II	21·6	0·7	1·2	1·7	2·0	2·4	2·7
Alcomax IV	21·6	0·7	1·1	1·5	1·8	2·1	2·6
Alnico	37·4	2·3	3·2	4·5	5·2	5·6	6·4
Alnico	21·6	3·2	4·6	6·2	7·2	8·3	9·5
Alnico	9·5	3·2	5·4	7·3	8·7	9·7	10·8
Alni	37·4	4·0	5·9	8·5	10·3	11·5	14·1
Alni	21·6	5·4	8·3	11·6	13·8	15·6	17·2
Alni	9·5	7·6	11·1	16·2	19·4	24·1	27·8

Table 5. *Losses after 5% reduction in magnetization*

Working $-B/H$	*Total loss in magnetization (%)* 200° C	300° C	400° C
37·4	2·0	3·5	5·6
21·6	2·7	4·5	6·9
9·5	3·3	5·2	7·9
	Irreversible loss in magnetization (%)		
37·4	0·07	0·1	0·15
21·6	0·2	0·3	0·5
9·5	0·3	0·5	0·9

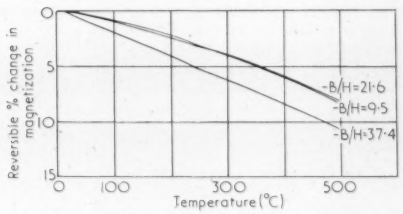

Fig. 2. Change in reversible magnetization of Alcomax III with temperature

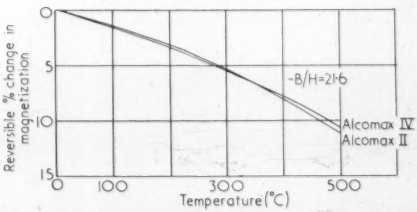

Fig. 3. Change in reversible magnetization of Alcomax II and Alcomax IV with temperature

Stabilization by an excess temperature is much more advantageous. The whole series of tests was repeated, with the test bar heated to 550° C after magnetization to saturation before commencing the experiments. The irreversible losses corresponding to the figures in Table 4 were now less than 0·1% for all bars and temperatures up to 500° C. The loss on these bars stabilized at 550° C is thus the reversible loss and is shown in Figs. 2 to 5. These direct measurements of

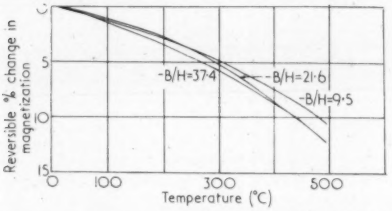

Fig. 4. Change in reversible magnetization of Alnico with temperature

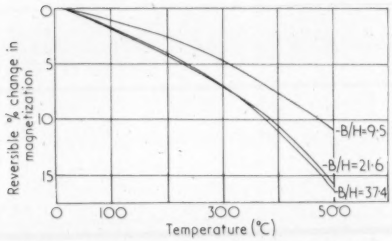

Fig. 5. Change in reversible magnetization of Alni with temperature

the reversible loss are more reliable than indirect estimates from the difference between the total loss and irreversible loss shown in Tables 3 and 4. The mean temperature coefficients of loss between room temperature and 200° C, over which range the curves are fairly linear, are given in Table 6.

Table 6. *Mean temperature coefficients of loss between room temperature and* 200° *C*

Material	*Working B/H*	*Temperature coefficient × magnetization* (%/° C)
Alcomax III	37·4	0·022
Alcomax III	21·6	0·013
Alcomax III	9·5	0·013
Alcomax II	21·6	0·018
Alcomax IV	21·6	0·019
Alnico	37·4	0·019
Alnico	21·6	0·014
Alnico	9·5	0·016
Alni	37·4	0·024
Alni	21·6	0·022
Alni	9·5	0·014

With a view to explaining the differences in their losses at high temperatures, the demagnetization curves of Alcomax III, Alnico and Alni were measured at room temperature and 500° C. The measurements at room temperature were made by the open circuit method using a magnetic potentiometer described by Margerison and Sucksmith.[4] The magnetic potentiometer could not be used at 500° C, so at this temperature it was necessary to calculate the field.

If a magnet on open circuit is subjected to an applied field H_a resulting in an induction at its central section B, then the effective field at the central section is usually obtained from:

$$H = H_a - H_d$$

where the self-demagnetizing field H_d is given by:

$$H_d = D(B - H) \qquad (2)$$

The demagnetizing factor D is calculable for ellipsoids and can be estimated approximately for other shapes from equation (1). For these measurements, values of D for

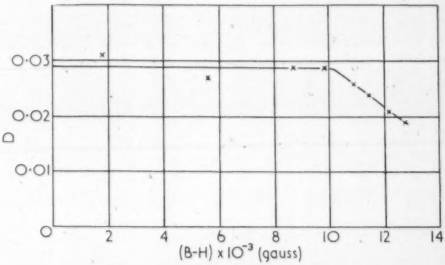

Fig. 6. Variation of demagnetizing factor for Alcomax III bar, 6·7 × 1 × 1 cm. Note that, for this dimension ratio, D is 0·0275 calculated by equation (1) and 0·044 for an ellipsoid

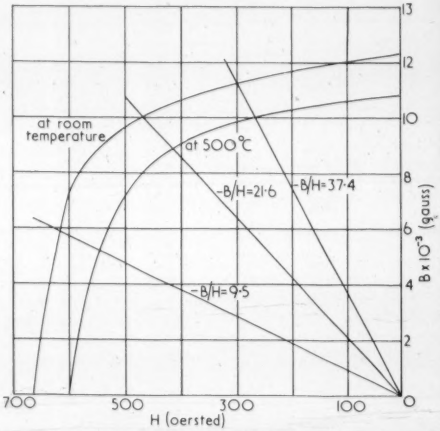

Fig. 7. Demagnetization curves of Alcomax III at room temperature and 500° C

various values of B were obtained experimentally by room temperature tests with a magnetic potentiometer. Surprisingly, it was found that the demagnetizing factor, although reasonably constant over the lower part of the demagnetization curve, decreased appreciably for magnetization approaching remanence; Fig. 6 is typical.

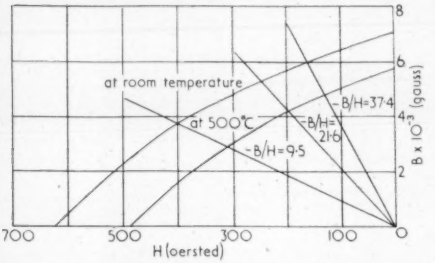

Fig. 8. Demagnetization curves of Alnico at room temperature and 500° C

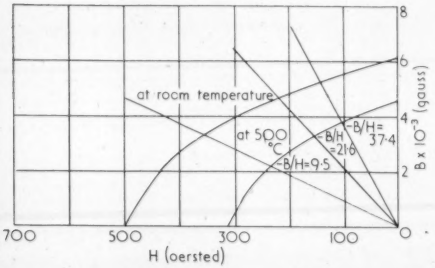

Fig. 9. Demagnetization curves of Alni at room temperature and 500° C

The variable values of D found experimentally were used in the determination of the demagnetization curves at 500° C given in Figs. 7, 8 and 9. Minor assumptions are involved but these affect only the portion of the curve near remanence. The working ratios $-B/H$ given in Figs. 7, 8 and 9 are as calculated from equation (1) for the three sizes of bar used.

DISCUSSION

When a magnet is heated the intrinsic magnetization in every domain is reduced in the same ratio. If no domain walls move and no domain directions change, the macroscopic magnetization will be reduced in the same ratio, but will be completely restored when the magnet is cooled. The actual change in macroscopic magnetization is influenced by many other factors: (1) the self-demagnetizing field is less at high temperatures because the magnetization is less; (2) crystal and strain anisotropy are sensitive to temperature and may cause reversible or irreversible rotation of domain direction; (3) it is obvious that if the coercivity is much less at high temperatures, there will be an irreversible loss of magnetization; (4) a magnet can also be demagnetized by thermal activation. This process is commonly called magnetic viscosity and may be expected to occur ten times more quickly at 250° C than at room temperature.[5]

When a magnet is working at the remanence point, processes 1 and 3 do not themselves affect the magnetization, although the changes in coercivity considered in process 3 may be partly due to the changes in anisotropy considered in process 2. Thus the percentage change of remanence with temperature should be the same as the percentage change in saturation magnetization except for processes 2 and 4. Considering for the moment the first three columns only of Table 7, it is surprising to find that the percentage remanence loss is so much less than the saturation loss as measured by the Sucksmith balance method,[6] particularly for Alcomax III. Viscosity effects would cause a discrepancy in the opposite direction and are unlikely to be large near the remanence point. Process 2, domain rotation due to changes in the anisotropy, is the only one left to account for the difference. At the remanence point the domain directions are held in equilibrium between interaction forces which tend to make them all parallel and anisotropy forces which tend to pull the domains into the preferred directions. If an increase in temperature reduces the anisotropy forces, the interaction forces will become more effective and make the domains more parallel and B_r higher than would otherwise be expected. This process must still influence magnets on open circuit, but will probably decrease the further the working point from remanence.

Neglecting process 2 for the moment, consider the effect of heating a bar magnet with some particular working point P, Fig. 10, to a temperature T. If the domains do not change their size or orientation, the magnetization of the bar will fall by the same fraction as the saturation magnetization. Suppose that as a result of this process the induction in the bar falls to Q. As a result, however, the demagnetizing field

Table 7. *Measured and estimated losses at* 500° *C*

1 *Material*	2 *Saturation* (% *loss*)	3 *Remanence* (% *loss*)	4 μ_r	5 $-B/H$	6 *Estimated loss* (%) (*a*)	7 (*b*)	8 *Measured loss* (%)
Alcomax III	17·7	12·2	3·5	37·4	16·0	11·1	12·6
Alcomax III				21·6	14·5	10·9	12·3
Alcomax III				9·5	14·0	11·1	11·5
Alnico	21·5	19·7	5	37·4	17·5	19·2	18·2
Alnico				21·6	16·8	20·5	21·5
Alnico				9·5	14·5	24·7	23·7
Alni	27·5	25·8	6	37·4	24·3	28·0	27·2
Alni				21·6	25·6	29·5	32·0
Alni				9·5	17·6	32·4	37·0

decreases and the domain configuration will change. It is tempting to see whether this change can be calculated by treating it as similar to the recoil process. This is done by drawing from Q a line QR intersecting the working line OP at R; the slope of QR should be equal to the recoil permeability μ_r. The demagnetization curve also changes with temperature for other reasons besides the change in saturation magnetization. If, however, the new curve lies above R as curve (a) in Fig. 10, there seems no reason why R should

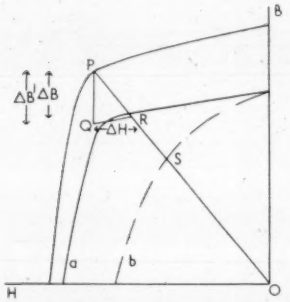

Fig. 10. Illustration of processes leading to loss of magnetization with temperature

not be the new working point. If, however, there is a large contraction of the demagnetization curve as with curve (b) R lies outside this curve. In this case R cannot be the working point which must instead be S the intersection of OP and curve (b). In Table 7, column 6 percentage losses at 500° C are calculated for various magnets by method (a), i.e. from the position of the point R. The recoil permeabilities used are shown in column 4: they are room temperature values, although it would probably be better to use values at 500° C if they were known. Column 7 shows the losses calculated by method (b), i.e. from the position of point S. It will be clear from the above argument that whichever method predicts the greater loss is expected to apply, i.e. method (a) for Alcomax and method (b) for Alnico and Alni. Allowing for the disturbing effects of processes 2 and 4, the measured total losses shown in column 8 are reasonable.

Reversible change in magnetization depends on dimension ratio, as can be seen in Table 6. Tenzer has attempted to explain this phenomenon by assuming the alloy to contain two magnetic phases. One of these he supposes has a low coercivity and a low Curie point. A magnet with a long dimension ratio is supposed to have a high temperature coefficient because of this phase. A magnet with a shorter dimension ratio is supposed to have this softer phase already demagnetized or reversed so that its temperature coefficient is less.

The authors (Clegg and McCaig[7]) have found that although magnetic phases with low Curie points can be produced in Alcomax III, there are no subsidiary Curie points above room temperature in the properly heat-treated alloy. The great squareness that can be obtained in Columax (Alcomax III with directed crystals) is also evidence against Tenzer's explanation. The processes 1 and 2 discussed in connexion with the total loss also influence the reversible change and can account for either an increase or decrease of the reversible change with dimension ratio. It is not easy to see how the effect of process 2 can be calculated but an attempt to estimate the contribution of process 1 can be made by referring again to Fig. 10. Suppose that the increase in temperature is small and represented by ΔT, $\Delta B'$ is the decrease in flux density due to the change in saturation intensity and ΔB is the actual decrease in flux density while ΔH is the decrease in demagnetizing field due to $\Delta B'$.

$$\begin{aligned} \Delta B &= \Delta B' - \mu_r \Delta H \\ &= -\Delta H \,.\, B_w/H_w \\ \Delta H &= \Delta B'/(\mu_r - B_w/H_w) \\ \Delta B &= \Delta B'[1 - \mu_r/(\mu_r - B_w/H_w)] \end{aligned} \qquad (3)$$

In the above equation H_w is, of course, negative. In Table 8 this formula has been used to calculate the temperature coefficients of magnetization of magnets of various materials and ratios of B_w/H_w. $\Delta B'/\Delta T$ is the decrease in saturation intensity per °C, and the recoil permeabilities are the same as those given in Table 7. The calculated temperature coefficients are all greater than the measured.

Table 8. *Calculated and measured temperature coefficients*

Material	$\Delta B'/\Delta T$ (%/° C)	*Temperature coefficient of magnetization in %/° C* $-B_w/H_w$	*Calculated*	*Measured*
Alcomax III	0·033	37·4	0·030	0·022
Alcomax III		21·6	0·028	0·013
Alcomax III		9·5	0·024	0·013
Alnico	0·036	37·4	0·031	0·019
Alnico		21·6	0·028	0·015
Alnico		9·5	0·022	0·016
Alni	0·052	37·4	0·046	0·024
Alni		21·6	0·042	0·022
Alni		9·5	0·034	0·014

This discrepancy is at least in part accounted for by process 2. The calculation does, however, demonstrate one way in which a decrease in temperature coefficient with dimension ratio can be explained.

CONCLUSIONS

(1) When a magnet of the iron-nickel-aluminium system is heated up to temperatures not exceeding 550° C no permanent metallurgical changes are observed but losses in magnetization occur. These losses are partly irreversible in the sense that they can be restored only by remagnetization and partly reversible meaning that they are restored by cooling.

(2) Pre-ageing by an alternating field does not eliminate the irreversible losses.

(3) On heating to any temperature up to 550° C, a magnet quickly reaches stability at that temperature, and suffers no further irreversible changes between room temperature and that temperature.

(4) The irreversible changes arise largely from changes in the demagnetization curve, and vary with dimension ratios and material, being appreciably less for the anisotropic alloys.

(5) The reversible losses are approximately linear up to 200° C with increasing curvature at higher temperatures.

(6) Temperature coefficients for all materials tested are of similar order, but tend to be less for magnets with short

dimension ratios; possible reasons for this variation are suggested.

(7) In the course of the work it was noticed that the self-demagnetizing factor of a rectangular bar magnet is not constant, but changes with the induction at the central section.

ACKNOWLEDGEMENTS

The authors wish to thank Mr. J. E. Gould for constant advice and valuable discussion. The work was carried out at the Central Research Laboratory of the Permanent Magnet Association on behalf of the Electrical Research Association.

REFERENCES

(1) CLEGG, A. G. *Brit. J. Appl. Phys.*, **6**, p. 120 (1955).
(2) TENZER, R. K. *Conference on Magnetism and Magnetic Materials* (held in Boston, Mass.), p. 203 (New York: American Inst. Elect. Engrs, 1957).
(3) EVERSHED, S. *Proc. Instn. Elect Engrs*, **58**, p. 823 (1920).
(4) MARGERISON, T. A., and SUCKSMITH, W. *J. Sci. Instrum.*, **23**, p. 182 (1946).
(5) STREET, R., and WOOLLEY, J. C. *Proc. Phys. Soc. [London] A*, **62**, p. 562 (1949).
(6) SUCKSMITH, W. *Proc. Roy. Soc. A*, **170**, p. 551 (1939).
(7) CLEGG, A. G., and MCCAIG, M. *Proc. Phys. Soc. [London] B*, **70**, p. 817 (1957).

A note on the adhesion of elastic solids

By K. L. JOHNSON, M.A., Ph.D., Engineering Laboratory, University of Cambridge

[*Paper received* 5 *November*, 1957]

A theoretical analysis is made of the stresses acting at the contact surface of two elastic spheres which are assumed to adhere to each other after the force pressing them together has been removed. The stress at the periphery of the contact area is shown to be tensile and infinite, so that adhesion is physically impossible; the spheres would peel apart. The theoretical results are consistent with the experimental work of Bowden and Tabor.

The essential feature of the commonly accepted theory of friction between unlubricated metals advanced by Bowden and Tabor[1] is the formation of metal junctions between high spots on the two contacting surfaces. Particularly if the surfaces are clean, it is maintained that in the localized areas where actual metal-to-metal contact occurs, the tips of the asperities are crushed plastically under the action of the normal pressure between them and in so doing they adhere or weld together. It is the resistance to shearing of these junctions which then provides the major contribution to the frictional resistance when the surfaces slide one upon the other.

If the surfaces do in fact adhere in this way one would expect that they would remain welded together after the normal force pressing them together has been removed, and that an additional tractive force would be required to separate them. Bowden and Tabor[2] have made sensitive experiments attempting to measure such a "force of adhesion." Even with carefully cleaned surfaces (in the absence of moisture films) no evidence could be found of an adhesive force after the initial pressure had been removed, except for the very soft metals, tin, lead and indium. The absence of any measurable adhesion with harder metals is explained mainly by suggesting that the junctions are broken by the release of *elastic* stresses in the body of the material when the load is removed. This note supports this explanation of the breakdown in adhesion of solids having a reasonably high elastic limit by a quantitative elastic analysis which demonstrates the mechanism of breakdown as the load is removed.

In common with Bowden and Tabor's experiments the analysis will be concerned with two spheres in contact. The material and radii of the spheres need not be the same and, in the limit, one sphere may become a plane.

When two spheres of radii R_1 and R_2 are pressed together with a normal force P they make contact over a circular area of radius a given by:

$$a^3 = \frac{3\pi}{4}(k_1 + k_2)\frac{R_1 R_2}{R_1 + R_2} \cdot P \qquad (1)$$

where k_1 and k_2 define the elastic constants of the material of each sphere $[k \equiv (1 - \nu^2)/\pi E]$. This result is due to the familiar Hertz theory of contact[3] which gives a distribution of pressure over the contact area:

$$p = \frac{3P}{2\pi a^2}\sqrt{\left(1 - \frac{r^2}{a^2}\right)} \qquad (2)$$

Due to local compression near to the contact area distant points in the two spheres approach each other by a distance α given by:

$$\alpha^3 = \frac{9\pi^2}{16}(k_1 + k_2)^2 \cdot \frac{R_1 + R_2}{R_1 R_2} \cdot P^2 \qquad (3)$$

Suppose that the spheres now adhere over the area defined by equation (1) whilst the load P is reduced. The new force between the spheres may be considered to be made up of the original load P with a further force P' subtracted from it. Under the action of P' the distant points in the two spheres will separate by an amount α'. This displacement will be divided between the two bodies α_1' and α_2' in the proportion of their values of $k^{2/3}$. Since the surfaces are presupposed to remain in contact over a circle of *fixed* radius a during this displacement, it follows that α_1' and α_2' must be constant for all points in the contact area. The distribution of normal surface traction which produces a constant displacement over a circular region of an elastic body corresponds to the

pressure over the face of a rigid circular die pressed on to an elastic plane. This problem has been solved by Boussinesq[4] where the relevant pressure is shown to be:

$$p' = \frac{P'}{2\pi a^2} \frac{1}{\sqrt{[1 - (r^2/a^2)]}} \quad (4)$$

giving a displacement:

$$\alpha_1' = \pi k_1 P'/2a \quad (5)$$

For our problem of adhering spheres, since with a fixed value of a the geometry remains unchanged, it is permissible to superpose the results of equations (2) and (4), also (3)

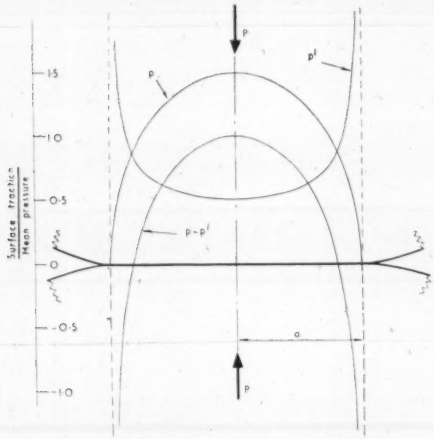

Pressure distribution over the circle of contact of two elastic spheres which are assumed to adhere together [Equations (2), (4) and (6)]

and (5) to find the net traction over the contact surface and the resultant relative displacement when the contact force has a value $(P - P')$. When the load is completely removed $P' = P$, whence:

$$p - p' = \frac{P}{2\pi a^2} \frac{2 - 3(r^2/a^2)}{\sqrt{[1 - (r^2/a^2)]}} \quad (6)$$

The tractions of equations (2), (4) and (6) are shown in the figure. It will be seen that the resultant traction which complete adhesion demands is tensile and of infinite magnitude at the periphery of the contact circle. Obviously the adhesive strength of metal junctions, however strong, cannot provide this traction, so that the surfaces peel apart from their periphery inwards. In view of the singularity exhibited by p' at $r = a$, an infinite tension is introduced by the addition of a p' component however small. We may conclude, therefore, that elastic spheres pressed together by a resultant force P cannot physically maintain contact over an area of greater radius than that given by the Hertz theory in equation (1).

The above analysis refers to contacting spheres. The more general case of contacting solids gives rise to an elliptical contact area. The situation in this case is the same; the traction p' associated with a constant displacement of the contact area rises to infinity at its periphery. For nominally flat surfaces in contact the analysis applies to the individual high spots in the surface. Such high spots may be deformed plastically near to their tips when the load is first applied, but when the load is removed the recovery is entirely elastic (see Ref. (1), p. 24) so that the theoretical elastic pressure distribution p' would still apply.

Some light is also thrown upon the function demanded of an adhesive layer applied between the contact surfaces of the solids to glue them together. The layer itself must be capable of some elastic or plastic distortion without disruption to allow sufficient peeling apart of the solids near to the edges of the contact area to relieve tension in the adhesive which would otherwise be excessively high. Soft metals such as lead and indium which exhibit considerable adhesion probably work in this way. The elastic strains in such materials are at all events small, whilst the asperities themselves constitute a plastic "layer" between the main body of each solid which is capable of considerable plastic deformation before rupture.

REFERENCES

(1) BOWDEN, F. P., and TABOR, D. *Friction and Lubrication of Solids* (London: Oxford University Press, 1950).

(2) BOWDEN, F. P., and TABOR, D. *Friction and Lubrication of Solids*, p. 306 (London: Oxford University Press, 1950).

(3) HERTZ, H., see TIMOSHENKO. *Theory of Elasticity*, p. 339 (New York: McGraw-Hill Book Co. Inc.).

(4) BOUSSINESQ, J. See Ref. (3), p. 338.

Correspondence

A method for distinguishing between sources of noise in motor-cars

The noise inside a car comes from three main sources: the engine, road excitation, and air buffeting.

At low and moderate speeds in the absence of high winds the noise due to air buffeting is small and may be neglected. And when running on a sufficiently smooth surface, noise resulting from road excitation can also be neglected.

Although the inside of a car is a closed space, and all noise therefore results from the vibration of the enclosing barriers it is possible and necessary to distinguish between:

(*a*) noise which is airborne from engine to the surfaces of the passenger compartment, or transmitted by air paths through holes in the surfaces.
(*b*) noise which results from the transmission of vibration in the structure of the vehicle, which then sets the surfaces of the passenger compartment into vibration, or from the transmission of vibration into the passenger compartment by driving controls, etc., which then radiate noise.

In considering means of reducing noise it is important to know which of these transmission paths causes the predominant noise, since the cures are generally different. More massive barriers and blocking holes are effective for (*a*) whereas vibration isolation by interposing rubber is appropriate to (*b*).

A means of investigation is to compare the noise inside the car:

(*a*) with the normal installation, engine running, car stationary;
(*b*) engine with all vibration paths disconnected and supported in the same position from a massive floor.

In the first case both airborne and structure-borne noises are present, while in the second case only the airborne noise is transmitted. The effect of structure-borne noise, if important, can then be assessed readily.

Such a test involves lengthy constructional work and a simple method was devised which has given satisfactory results in a number of applications. The method consists of measuring the attenuation of noise from engine compartment to passenger compartment. Microphone positions are fixed and noise measurements made as octave analyses. Two sets of measurements are made:

(*a*) "apparent attenuation" is measured with car stationary (or running on a very smooth surface).
(*b*) "acoustic attenuation" is measured by reproducing by means of a loudspeaker in the engine compartment the noise previously recorded during (*a*).

Provided the distribution of the loudspeaker noise in the engine compartment simulates sufficiently that of the airborne noise from the engine, (*b*) corresponds to the case in which vibration paths are disconnected and only airborne transmission is operative.

As an example, the lower (dotted) curve in the figure, drawn through the means of the points for 20, 40 and 60 m.p.h., is the "apparent attenuation." The solid curve is drawn for the means of the corresponding value of "acoustic attenuation" (points not shown) obtained by the loudspeaker method. The solid points are the corresponding values of "acoustic attenuation" measured with engine vibration paths disconnected. The agreement with the solid curve is satisfactory, which confirms the validity of the method.

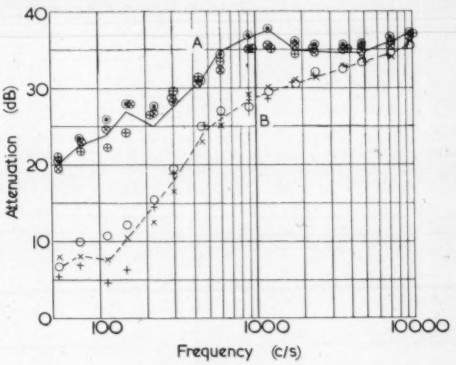

Attenuation, engine compartment to passenger compartment in a motor-car. Comparison of "acoustic attenuation" by loudspeaker method and with engine disconnected (*A*), and "apparent attenuation" (*B*)

○ 20 m.p.h.
+ 40 m.p.h.
× 60 m.p.h.
} Driving car on a smooth surface.

○ Engine running
⊕ at speeds
⊗ corresponding to
20 m.p.h.
40 m.p.h.
60 m.p.h.
} Stationary car, all vibration paths between engine and car body disconnected.

It is of interest to note that in this case, since the "acoustic attenuation" is markedly greater than the "apparent attenuation" at frequencies up to about 2000 c/s, vibration paths through the structure are the main source of noise.

C.A.V. Ltd.,
Acton,
London.

A. E. W. Austen
T. Priede

[18 January, 1958]

A rapid method for separating the principal stresses in plane photoelasticity

The main difficulty in plane photoelastic analysis lies in the fact that although photoelastic stress patterns giving fringes of constant principal stress difference are rapidly obtained, the methods available for obtaining the sum of the principal stresses are either slow and tedious or require another comparatively complicated experimental arrangement.

A very good method, originally due to Coker,[1] is to measure the change in thickness of the stressed plates, this being proportional to the sum of the principal stresses at the point. A development of this method, mentioned by

Frocht[2] and recently used by Sanks,[3] is to load the model at a high temperature where its Young's modulus is low enough to produce easily measurable deformations. The stresses and strains are then "frozen"-in as the model is allowed to cool slowly to room temperature.

The purpose of this note is to draw attention to the properties of Araldite casting resin D[4,5] which, when used with the experimental procedure described below, enables this frozen lateral strain method to be used to calculate the principal stresses quickly and with an accuracy comparable to that of graphical integration of the Lamé–Maxwell equations.

The relations used are, that at any given point, the fringe order

$$n = (P - Q)t/C \tag{1}$$

and the thickness change

$$\delta t = (P - Q)t\nu/E \tag{2}$$

where P and Q are the principal stresses, t the thickness of the model, and E, ν and C the Young's modulus, Poisson's ratio and fringe constant respectively of the model material. If P and Q are to be expressed in fringes, the thickness change corresponding to a stress sum of one fringe is required. This is given by

$$K = \nu C/E \text{ in. per fringe} \tag{3}$$

The value of K was, in fact, obtained experimentally for Araldite D at 90° C from a large number of measurements at the free edges of frozen stressed models, where the fringe meeting the edge is uniquely related to the thickness change. A value of $3{\cdot}1 \times 10^{-4}$ in. per fringe was obtained but it is worthwhile checking this calibration factor for each sheet of Araldite cast. The dial gauge comparator, described below, was able to measure changes accurately to 10^{-4} in. so that readings for $(P + Q)$ accurate to $\frac{1}{4}$ fringe could be obtained. Further, the fringe order at any point could be estimated by eye also to $\frac{1}{4}$ fringe. This means that P and Q could be found separately to $\frac{1}{4}\sqrt{[(\frac{1}{4})^2 + (\frac{1}{4})^2]}$ fringe, i.e. to about 0·25 fringe. Since the load is usually adjusted to give a maximum fringe order in the range 10–20 fringes, P and Q can therefore be found to an accuracy of better than 2·5% of the maximum stress difference.

At 90° C stresses giving up to 25 fringes produce negligible permanent yielding in Araldite D, the frozen stress model always returning to its original dimensions after annealing. The low value of Young's modulus used during stressing means that the deformations in the plane of the model are larger than usual; however, the error from this cause appears to be much less than the error in measurement.

The comparator used is shown in the figure. Two commercially available dial gauges which read to 10^{-4} in. were used. At the tip of each gauge was a steel ball 10^{-1} in. in diameter. The gauges were rigidly mounted above and below a $1\frac{1}{2}$ in. thick flat steel plate so that their axes of travel were in line and at right angles to the steel plate. The end of the lower gauge protruded a short distance through a hole in the steel plate. The double dial gauge arrangement enabled the essential requirements, that the photoelastic model be held flat and at right angles to the gauge movements whilst measurements were being made, to be fulfilled simply, and for this reason was preferred to a more complicated arrangement using only a single gauge, although it was at the expense of having a double instrument error and required two readings to be taken. The thickness of the specimen at room temperature at various points is measured before and after the stresses are "frozen" in. It has been found that the surface of the model can be marked, to locate the points where measurements are to be made, with light scratches from a sharp needle without serious loss of accuracy. The reason for this is that the error h in reading is given by

$$h = d^2/8R \tag{4}$$

where R is the radius of the dial gauge tip and d is the scratch width. Since $R = 10^{-1}$ in. and d, measured with a travelling microscope, was never greater than 2×10^{-3} in., h was always less than 5×10^{-6} in., this error being too small to affect the measurements.

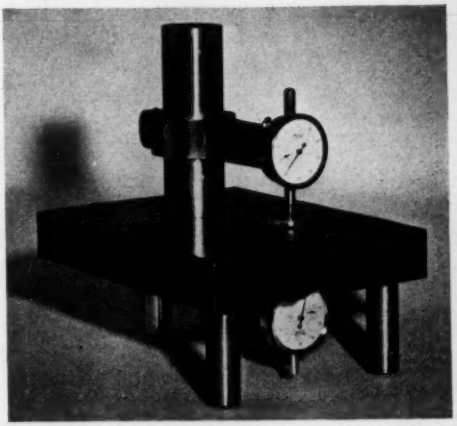

Dial gauge comparator

In order to demonstrate the range of accuracy and the usefulness of the method, the classical problem of the circular disk under diametrical compression was chosen, the reasons being that the theoretical solution is well known,[2] and Jessop and Harris[6] have given a solution using the method of graphical integration. Both of these solutions are used for comparison.

A disk 2 in. in diameter and $\frac{1}{4}$ in. thick was stressed between parallel plates in a loading frame and the whole was heated in an oven to 90° C. The load on the hot specimen was adjusted, whilst being observed in a conventional polariscope, to give a suitable number of fringes. The frame and specimen were then returned to the oven and allowed to cool slowly. A cooling rate of 10° C per hour was found adequate to prevent thermal stresses developing and the specimen was removed from the straining frame and the oven when its temperature had reached 30° C.

Measurements along the horizontal and vertical diameters were made. Since the theoretical solution is for point loading at the ends of the vertical diameter, agreement near the points of application of the load is not to be expected. Point by point comparison between the results from this method, the theoretical solution and Jessop and Harris's results are given in the table. All values were normalized to give an average vertical stress along the horizontal diameter of 100.

Comparison of results for disk in diametrical compression

	Distance	*Theoretical*	*Frozen stress*	*Graphical integration*	*Theoretical*	*Frozen stress*	*Graphical integration*
	S	*P*	*P*	*P*	$-Q$	$-Q$	$-Q$
Horizontal diameter edge → centre	0	0	0	0	0	0	0
=10 units	1	0·7	1·5	1	13·5	17	17
	2	3·0	2·5	3·8	30·3	32·5	34·7
	3	7·2	8·5	8·5	49·4	51	52
	4	13·7	13	14·9	71·5	75	72·3
	5	22·2	26	22·1	96·1	98	97·2
	6	32·4	30	29·6	122	123·5	121
	7	43·0	48	36·8	148	145	146·5
	8	52·6	59	43·6	167	167·5	169·5
	9	59·2	64	49·1	180	184	185
	10	62	66	51·5	186	191	191
Vertical diameter centre → edge	0	62	66	51·5	186	191	191
=10 units	1	62	63	53·9	187	191	194
	2	62	68	52·6	195	193	198·5
	3	62	62	55·5	210	211	208
	4	62	60	62·0	231	230	225
	5	62	60	64·0	267	258	253
	6	62	66	63·9	324	299	298
	7	62	62		421	363	

It may be concluded from these results that the frozen lateral strain method of separating the principal stresses produces results that are comparable in accuracy with the method of graphical integration. It does not require a knowledge of the stress trajectories or the isoclinic lines (except if the directions of the principal stresses are required), and the errors are not cumulative. The use of the simple comparator described enables the thickness measurements to be made extremely quickly. The use of Araldite D as the photoelastic material offers the advantage of having a suitably low Young's modulus at only 90° C so that a short cooling time can be used without introducing thermal stresses. Araldite D also shows little "time edge" effect so that the models can be stored for a short while. Owing to the comparatively large thickness changes involved, temperature control of the model during measurements need not be stringent. The method is therefore useful in finding quick, reasonably accurate solutions to a wide range of problems. It should be noted that Araldite D is supplied in the form of a very viscous liquid, and so when being cast into sheets occluded air bubbles do not have time to rise to the surface before the substance hardens. The procedure used to obtain bubble-free Araldite sheet was to heat the original oil to 65–70° C before adding the hardener. At this temperature the Araldite becomes very much less viscous and air bubbles rise to the surface immediately. The hardener takes about thirty seconds to dissolve and the mixture must be poured into the mould within a minute or two of preparation, that is before the hardening reaction begins to take effect. The mould, which in this case consisted of two ground-flat steel plates held $\frac{1}{4}$ in. apart by steel spacers, was previously heated to about 60° C so that temperature gradients were not set up in the Araldite, causing thermal stresses. The use of a silicone release agent effectively prevented the Araldite sticking to the mould.

This note forms part of the programme of research of the Mining Research Establishment and is published by permission of Dr. W. Idris Jones, Director-General of Research in the Scientific Department of the National Coal Board. The views expressed are those of the author and not necessarily those of the Board.

National Coal Board,
Mining Research Establishment,
Isleworth,
Middlesex.

I. BRODIE
[8 November, 1957]

REFERENCES

(1) COKER, E. G., and FILON, L. N. G. *A Treatise on Photoelasticity* (London: Cambridge University Press, 1931; 2nd Ed., 1957).

(2) FROCHT, M. M. *Photoelasticity*, Vol. II (New York: John Wiley and Sons Inc., 1948).

(3) SANKS, R. L. *Proc. Amer. Soc. Civil Engrs*, **81**, *Proceedings Separate* No. 693 (1955).

(4) D'AGOSTINO, J., DRUCKER, D. C., LIU, C. K., and MYLONAS, C. *Proc. Soc. Exper. Stress Anal.*, **12**, p. 123 (1955).

(5) AMBA RAO, C. L. *Brit. J. Appl. Phys.*, **7**, p. 229 (1956).

(6) JESSOP, H. T., and HARRIS, F. C. *Photoelasticity Principles and Methods* (London: Cleaver-Hume Press, 1949).

Notes and comments

Elections to The Institute of Physics

The following elections have been made by the Board of The Institute of Physics:

Fellows: F. Ashworth, G. R. A. Ellis, H. W. Emerton, A. G. Fenton, R. O. Gibson, D. M. Lucas, J. K. Mackenzie, W. P. Osmond, F. H. Sagar, D. W. Saunders, H. H. Scholefield, R. Smith, B. E. Stern, J. C. C. Stewart, N. G. Trott, W. H. Ward, G. C. Williams, E. P. Wohlfarth, M. M. Woolfson.

Associates: L. Alpin, M. H. Alston, A. J. Apostolakis, A. C. L. Barnard, C. Bristow, D. E. Bromley, K. Burrows, G. E. Cain, R. V. Coates, A. R. Collett, M. G. Davies, W. G. Davies, N. E. Dixon, J. R. Drabble, R. R. Gardner, A. Garnham, E. V. Gilby, H. W. Gosling, G. Haigh, J. K. Hargreaves, E. A. Iredale, G. W. Keeling, E. Kendrick, G. B. Marson, J. V. Major, W. W. Mapleson, W. G. Mayo, E. A. Mussett, T. P. Newcomb, A. C. Newns, E. Nicholas, E. Norcross, F. E. L. Parsons, A. R. Payne, E. R. Pike, W. E. Ribchester, E. Rowlands, K. Scott, J. S. Sivyer, L. R. Thompson, R. Ueda, G. W. Verow, E. T. Wait, R. W. Waldron, R. H. Whiddington, W. F. Williams, K. Worthington.

Fifty Graduates, ninety-four Students and four Subscribers were also elected.

User-specification for high-temperature X-ray diffraction powder cameras

The X-ray Analysis Group of The Institute of Physics announces that a panel of its Equipment Sub-Committee has completed the preparation of a user-specification dealing with the design of X-ray diffraction cameras for the examination of polycrystalline specimens at high temperatures. Copies of this specification may be had by any interested persons on application to Dr. E. G. Steward, Honorary Secretary, Equipment Sub-Committee of the X-ray Analysis Group, Research Laboratories, The General Electric Co. Ltd., Wembley, Middlesex.

Symposium on instrumentation and computation in process development and plant design

The Institution of Chemical Engineers, the Society of Instrument Technology and The British Computer Society are to hold a joint symposium on instrumentation and computation in process development. The meeting will be held in the Central Hall, Westminster, London, on the 11, 12 and 13 May, 1959, with subjects and sessions as follows:

11 May (morning session): Improving the efficiency of existing processes. (Afternoon session): The design of new processes;

12 May (morning session): The application of on-line computers. (Afternoon session): Recent developments in instruments, on-line computers and computers for design;

13 May (morning session): (*a*) The use of computer techniques in large and small companies. (*b*) The future (one paper only).

The meeting is being organized under the aegis of The British Conference on Automation and Computation. Any person wishing to present a paper at the symposium should send a summary not later than 1 June, 1958, to The General Secretary, The Institution of Chemical Engineers, 16 Belgrave Square, London, S.W.1.

Electronics exhibition and convention

The thirteenth annual electronics exhibition and convention, organized by the northern division of The Institution of Electronics, will be held during the periods 10–12 July and 14–16 July, 1958, at the Manchester College of Science and Technology. The exhibition will consist of a manufacturers' section and a scientific and industrial research section, including exhibits of interest to all branches of science and industry. The convention will include a series of lectures and film shows on electronic topics. Admission will be free of charge.

Further particulars may be obtained from the Honorary Exhibition Organizer, Mr. W. Birtwistle, 78 Shaw Road, Rochdale, Lancashire.

Journal of Scientific Instruments

Contents of the May issue

ORIGINAL CONTRIBUTIONS

Papers

Studies in microdensitometry. By A. W. Wooster and J. A. L. Fasham.

The construction and testing of a "universal" light scattering apparatus. By W. J. Hughes and P. Johnson.

A compensated moving cylinder viscometer. By G. P. Sreekantath and C. A. Verghese.

A double d.c. bridge circuit for precision measurements with load cells. By T. S. Parramore.

Derivative mass spectrometry. By J. H. Beynon, S. Clough and A. E. Williams.

An electronic feedback seismograph. By M. J. Tucker.

An instrument for the determination of potassium in sodium chloride. By G. H. Laycock.

An electrodeless method for the measurement of electrolytic conductivity and magnetic susceptibility. By W. R. Myers.

A beam-scanned rotating heavy-ice target for high loads. By J. H. Spaa.

A high stability mains-operated recording thermistor thermometer. By A. W. Melville.

Laboratory and workshop notes

A double layer-line screen for Weissenberg photography. By A. W. Hanson.

An alternative to gimbals for an ultrasonic interferometer. By A. N. Hunter.

Vacuum or low-pressure seal utilizing modified standard refrigeration-type, flare tube fittings. By B. H. Hodder.

An electrode cutter and modified arc stand for spectrochemical analysis. By J. McAndrew.

A high vacuum valve. By L. Blanaru.

A simple expansion indicator. By A. L. Sims.

Note on protective device for thermal converters. By A. G. Mungall and I. Abella.

NOTES AND NEWS

Correspondence

A narrow-band optical filter to isolate the 4245 Å spectral region. From R. P. Thorne and R. F. Warren.

Chart calibration of a photographic recording microphotometer. From M. Gadsden.

New instruments, materials and tools. New books

Manufacturers' publications Notes and comments

THIS JOURNAL is produced monthly by The Institute of Physics, in London. It deals with all branches of applied physics (including theory and technique).

All rights reserved. Responsibility for the statements contained herein attaches only to the writers.

EDITORIAL MATTER. Communications concerning editorial matter should be addressed to the Editor, The Institute of Physics, 47 Belgrave Square, London, S.W.1. (*Telephone:* Belgravia 6111.) Prospective authors are invited to prepare their scripts in accordance with the *Notes on the preparation of contributions.* (Price 2*s.* 6*d.* including postage.)

REPRODUCTION. The Institute of Physics is a signatory to The Royal Society's Fair Copying Declaration. Details may be obtained upon application from The Royal Society, London, W.1.

ADVERTISEMENTS. Communications concerning advertisements should be addressed to the agents, Messrs. Walter Judd Ltd., 47 Gresham Street, London, E.C.2. (*Telephone:* Monarch 7644.)

CLAIMS FOR MISSING JOURNALS. Claims from regular subscribers to this *Journal* for missing numbers will only be considered if received within 60 days of the date of mailing plus normal outward time of transit and time for lodging the claim. Losses attributable to failure to notify a change of address or to similar omissions will not be considered.

SUBSCRIPTION RATES. A new volume commences each January. The charge is £5 per volume ($14.25 U.S.A.), including index (post paid), payable in advance. Single parts, so far as available, may be purchased at 10*s.* each ($1.50 U.S.A.), post paid, cash with order. Orders should be sent to The Institute of Physics, 47 Belgrave Square, London, S.W.1, or to any bookseller.

Photoconductivity*

By D. A. WRIGHT, D.Sc., F.Inst.P., Research Laboratories, The General Electric Company Limited, Wembley, Middlesex

The basic factors influencing photoconductivity are first discussed, and the general pattern of behaviour to be expected is indicated. The preparation and properties of cadmium sulphide are then dealt with in some detail. Other photoconducting compounds are described more briefly, and it is shown that their properties also fit into the general pattern. Following a discussion of the nature of the impurities and defects in the crystal lattice which influence the sensitivity, the applications of photoconductors are outlined briefly.

1. INTRODUCTION

Let us consider a solid insulator or semi-conductor in thermal equilibrium in the dark. There will be a certain density of free charge carriers, *n*-electrons and *p*-holes, these quantities depending on the temperature. We then suppose that photons are injected; effects similar in many respects are produced if electrons or other charged particles are injected; however, we will consider photons in particular. Provided their energy is sufficient, they cause the formation of additional free charge carriers. In the language of energy bands and levels, we consider the conduction and valence bands (Fig. 1), and the extra levels between them due to defects of various types. As a result of the energy received from the photons, extra electrons may be raised to the conduction band either from the valence band as in (*a*) or from one of the intermediate levels as in (*b*). In the former case for every electron a free hole is formed also. Similarly electrons may be raised from the valence band to an empty intermediate level, as in (*c*), also producing a free hole. As long as the extra charge carriers, electrons or holes, or both, remain free, the electrical conductivity is raised by their presence. This is the cause of photoconductivity.

Following the excitation process, recombination takes place, by transitions in the reverse directions to (*a*), (*b*) or (*c*), Fig. 1, and if the photon input is maintained, a steady state

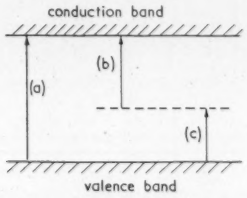

Fig. 1. Excitation of electrons

is set up, with an increased conductivity representing a balance between excitation and recombination. When the photon input ceases, the extra carrier density decays as a result of the recombination processes, and the thermal equilibrium condition is restored.

The recombination processes may be of several types. Thus there can be direct recombination of holes and electrons, either between the conduction band and the valence band, or as a result of electrons or holes returning to the centres from which they were ejected. The direct recombination between conduction band and valence band, if it occurs, will produce radiation of frequency corresponding to the absorption edge, referred to therefore frequently as "edge-emission." The transition probabilities for this process have been calculated for several types of crystal, and lead to "lifetimes" of the following order:[1]

Silicon	3·5 s
Germanium	0·3 s
Lead selenide	3 μs
Indium antimonide	0·5 μs

Here "lifetime" is the time τ defined by the relation $\tau g = \delta n = \delta p$, where g is the rate of generation of carriers in excess of the thermal rate. δn is the density of excess electrons, δp that of excess holes, maintained by the radiation in the steady state.

The long lifetimes quoted for germanium and silicon correspond to very low transition probabilities, and one therefore expects a large photoconductivity, and only a very low intensity of edge-emission. Nevertheless radiation with the corresponding frequency has been observed by Haynes[2] for germanium and even for silicon, and later by Newman and Aigrain.[3] When lifetime is studied directly, however, the measured values are much less for silicon and germanium than the values of 3·5 and 0·3 s quoted. This means that other recombination processes with higher probability are occurring in all the crystals of these materials prepared so far. The observed photoconductivity is correspondingly smaller than the theoretical value.

2. RECOMBINATION CENTRES

There is a second type of recombination process due to the presence in the crystals of specific "recombination centres." These are centres with energy levels in the forbidden gap. The capture processes occur successively, so that if radiation is emitted it is of lower energy than for edge-emission, since it corresponds to one or the other transition to the intermediate level. Transitions to such recombination centres do not necessarily, however, lead to the emission of photons. The energy may be dissipated thermally by the production of phonons, or a secondary (Auger) process may excite another free charge carrier. Recombination centres may consist in germanium for example of copper, nickel, iron or cobalt impurity atoms, or of dislocations, or of defects produced either by quenching, or by bombardment with neutrons or charged particles. Levels in the forbidden gap do not all act as recombination centres, for example those

* This article is based on a talk given to the Electronics Group of The Institute of Physics in October 1956.

near the band edges are in thermal equilibrium with the neighbouring bands, and carriers are more likely to return from them to the bands than to recombine. Rose[4] has defined the "demarcation levels" which denote energy levels at which transitions downward or upward are equally probable. In a semi-conductor the demarcation levels for electrons and holes coincide at approximately the same height above the valence band as the Fermi level is below the conduction band, as in Fig. 2(*a*). In a semi-conductor recombination occurs only at levels between the demarcation and Fermi levels. Their positions of course vary with temperature.

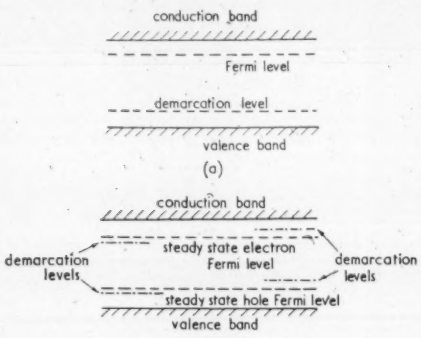

Fig. 2. (*a*) Demarcation level in a semi-conductor. (*b*) Demarcation levels in an insulator. Alternative positions are shown at left and right

In an insulator, however, the electron and hole demarcation levels are distinct, Fig. 2(*b*), and either coincide with the two corresponding steady state Fermi levels,* or are slightly displaced from these. When displaced, both levels are situated equally above the corresponding Fermi levels, as at the right in Fig. 2(*b*), or equally below them, as shown at the left. In an insulator, recombination occurs only at levels situated in the gap between the highest and the lowest of these four. Thus it is levels not too near the band edges which control recombination in both insulators and semi-conductors.

In the general case the increase in free electron density δn and in free hole density δp produce an increase in conductivity $\delta\sigma = \delta n e\mu_e + \delta p e\mu_h$, where μ_e is the electron mobility, μ_h the hole mobility and e the electronic charge. For band to band excitation and recombination processes, as we have seen, $\delta n = \delta p = g\tau_e = g\tau_p$, i.e. excess electron and hole lifetimes and densities are equal. It can be shown that under these conditions the rise and decay of photoconductivity are exponential, with a time constant equal to τ. A large value of τ is clearly necessary to give a large photoconductivity $\delta\sigma$.

If we consider the case of a crystal with ohmic contacts, flooded with light, then when carriers created by the light reach one electrode, new carriers enter *via* the opposite electrode and take their place, so that the creation of one carrier can lead to charge transfer until recombination occurs. Thus if the transit time of a carrier is T and its lifetime is τ there is a gain τ/T, and if the generation rate is g, charge transfer occurs at the rate $g\tau/T$. To obtain a large photosensitivity for a given light input and spectral distribution one requires, therefore, in this case, both a high lifetime τ and a low transit time T, i.e. a high carrier mobility.

In contrast with the case where band to band recombination occurs, the introduction of only one intermediate recombination level leads to a much more complicated theory,[5] and only special cases can be treated fully. The electron and hole lifetimes are not now necessarily equal, i.e. δn is not necessarily equal to δp; the decay curve for photoconductivity is in general the sum of two curves, and the time constants of these, if they are exponential, are not necessarily the same as the steady state lifetimes. D. H. Clarke of this Laboratory has analysed the situation in a recent paper.[6] δn will be equal to δp only when the density of recombination states is low compared with the density of carriers added by illumination. The decay curve will then be a single exponential with time constant equal to the lifetime of either carrier. Germanium can be prepared containing no more than about $10^{12}/\text{cm}^3$ recombination centres, in which case this behaviour is encountered at room temperature with quite low levels of illumination. Photoconductivity then decays exponentially with a time constant of the order 100 μs compared with the expected 0·3 s for edge recombination.

When the density of recombination levels is not low compared with that of added carriers, the behaviour is more complex. It is specially important to consider the consequences when centres are present which have widely different capture cross-sections for holes compared with electrons. Such levels tend to become occupied by an excess of the type of charge carrier most readily captured. If these levels are not fully occupied by these carriers in the dark, then under irradiation their occupancy will increase, at the expense of the population of free carriers of like sign. Recombination centres in which charges of one sign can accumulate are referred to as "traps" for those charges. Thus if the capture cross-section of a centre for an electron is s_n and for a hole s_p, and if s_n is much greater than s_p (electron trap), then there may be an increase of electron density δ_{nt} in such centres on illumination. If the increased density of free electrons is δn and of free holes δp, then $\delta n + \delta_{nt} = \delta p$, to retain charge neutrality. Thus δp may be much greater than δn when electron trapping occurs, and conversely when a centre is present with $s_p \gg s_n$ (hole trap), δn may be much greater than δp. For a given rate of generation g, the presence of hole traps can thus lead to higher values of δn and of τ_e than in the absence of such centres, and therefore to a higher photoconductive sensitivity.

The effects thus described can occur only when (*a*) the recombination centres are not fully occupied in the dark by the type of carrier which they can preferentially capture, and (*b*) when the excitation is low enough to generate free electron and hole densities less than the recombination state densities. As soon as these states are filled, further increase in excitation can only maintain δn and δp equal, with equal lifetimes and relatively low sensitivity. The values of s_p and s_n are no longer relevant.

The density of unoccupied trapping levels is very low at room temperature in good quality germanium, giving the

* The steady-state Fermi level is defined as being at an energy separation E from the appropriate band edge, where $n = N_S \exp(-E/kT)$, N_S is the density of states in the band, and n the number of free carriers. Thus for electrons the values refer to the conduction band, and for holes to the valence band. These steady state Fermi levels are separate from each other and from the ordinary Fermi level when radiation is incident and maintains electron and hole densities different from those characteristic of thermal equilibrium in the dark.

performance referred to above, i.e. lifetime near 100 μs, associated with low photoconductive response. If, however, germanium contains a transition metal impurity at a higher density, of the order 10^{15} atoms/cm^3, then [7] this impurity forms centres with a double negative charge at liquid air temperature. These have a fairly high hole capture cross-section, s_p, of the order 10^{-15} cm^2, i.e. they tend rather easily to lose an electron, and even after losing one, the capture cross-section for an electron, s_n, remains low, of the order 10^{-21} cm^2, because of the remaining negative charge. This high value of s_p relative to s_n results in a much larger photosensitivity than in the absence of impurity centres with a double negative charge, because of the increased value of δn.

The various types of level referred to, i.e. recombination centres, deep trapping levels and shallow traps, may all be present in one crystal. Thus germanium with 10^{15}/cm^3 manganese atoms will also contain about 10^{12}/cm^3 recombination centres due to vacancies or unknown impurities, together with a concentration of donor and acceptor levels near the band edges varying with the method of preparation. Moreover, there may be levels of different energies within any of these three categories, as would happen in germanium if more than one transition element and more than one group III or group V element were present. The best quality zinc or cadmium sulphide so far produced appears to contain several levels of each of the three types. It should be noted that the presence of shallow traps, i.e. levels nearer the band edges than the demarcation levels, does not affect the equilibrium values of δn and δp, and therefore does not affect the magnitude of the photoconductive response. It does, however, alter the time constants of the rise and decay of photoconductivity, because of the time necessary to bring the occupancy of the bands into equilibrium with that of the shallow traps.

For a fixed population of recombination and trapping centres, the position of the steady state Fermi levels and therefore of the demarcation levels is altered by variation of the concentration of donors and acceptors, while for a fixed concentration of donors and acceptors, these levels are altered by variation of temperature or by the actual process of illumination. The movement of the demarcation levels will alter the number of states acting as recombination centres and deep traps, if there are numerous states distributed in energy in the forbidden gap. If there are only a few such states, their occupancy will be modified by movement of the demarcation levels.

Thus raising the donor concentration in an *n*-type material will raise the Fermi level and increase the separation between the two extreme levels in Fig. 2(*a*) or 2(*b*). It will therefore increase the number of levels acting as recombination and deep trapping states; if the latter are dominating the behaviour, as in germanium with about 10^{15}/cm^3 manganese atoms, the effect will be to rise the photoconductivity. The same effect occurs in cadmium sulphide, where replacement of sulphur by a halogen or of cadmium by gallium gives increasing donor concentration, and raises both the dark conductivity and the photosensitivity.

Increased illumination will also increase the separation between the two extreme levels, and again there will be conditions under which the number of levels producing hole trapping is thereby increased. When this happens the sensitivity will rise as the level of illumination rises, so producing a "super-linear response" of photoconductivity to light.

Raising the temperature of an *n*-type material lowers the Fermi level, brings the two extreme levels closer together, and so lowers the sensitivity when hole-trapping centres are dominating the behaviour, because fewer states are embraced between the extreme levels. At a sufficiently low temperature the extreme levels may embrace all the available trapping states at low light intensity, in which case the sensitivity is high at low light intensity and super-linearity of response cannot occur. At a higher temperature, the levels will be closer, the sensitivity at low illumination will be less, but superlinearity can occur again as the extreme levels separate over an energy range where trapping states exist. The temperature at which super-linearity can occur will vary with different materials and with different distributions of trapping states in these materials. These various effects of temperature and illumination have been observed and studied in particular with cadmium sulphide and cadmium selenide, as discussed below. Some typical results for cadmium sulphide are shown in Fig. 3.

It should be noted that in the absence of any recombination or trapping centres, δn and δp would both vary with light

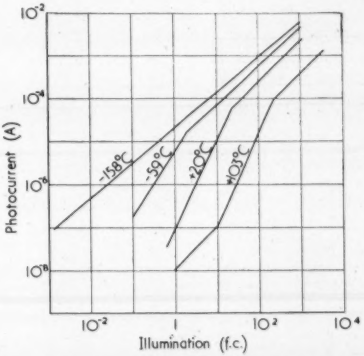

Fig. 3. Photocurrent as a function of light intensity at various temperatures. Red-sensitive cadmium sulphide: copper: chlorine crystal. 100 V applied

intensity according to a square-root law, because the recombination process would be "bi-molecular." With a single recombination level effective, the recombination process becomes "mono-molecular," and a linear law would be followed. As the level of illumination rises, the separation of the extreme levels of Fig. 2(*b*) will increase, and if they embrace an increasing number of levels which can act as recombination centres, then the sensitivity will decrease and the relation between photoconductivity and light intensity will be sub-linear. These three types of relation are encountered both when no trapping levels are present, and also when trapping levels are present but when the temperature is either above or below the range in which super-linearity occurs. The sensitivity will be low when no trapping states are present, or when the extreme levels [Fig. 2(*b*)] do not embrace any such states, i.e. at temperatures above the super-linearity range. The sensitivity will be high if trapping levels are present and are all embraced between the extreme levels, i.e. at temperature below the super-linearity range.

We have seen that the excess carrier density, and therefore the photoconductive response, is proportional to the lifetime of the carriers mainly responsible for the photoconductivity.

This lifetime is directly related to the response time, i.e. the rise and decay times observed when square light pulses are incident. Thus the more sensitive the material, the longer the response time, which moreover will vary with the level of illumination, just as the sensitivity has been shown to do. With a material having high sensitivity at low light levels, the response time and the sensitivity will fall as the level of illumination rises. It may be noted that the very shallow trapping levels already referred to will produce a "tail" on the response time, extending it beyond the value directly related to the true lifetime τ. Typical forms of the response curve of green-sensitive cadmium sulphide are shown in Fig. 4. The time constants are less for blue light than

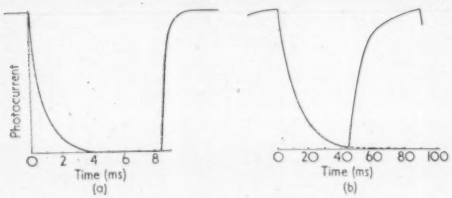

Fig. 4. Cadmium sulphide crystal with peak response at $\lambda = 5150$ Å, showing rise and decay characteristics with illumination on either side of the absorption edge

(*a*) Monochromatic illumination, $\lambda = 4790$ Å; (*b*) monochromatic illumination, $\lambda = 5450$ Å.

for red, because the penetration of blue light is much less, and the recombination processes are determined at the surface, rather than within the crystal as with red light. Recombination through levels at the surface is faster than through levels in the crystal.

3. CADMIUM SULPHIDE

3.1. *General features.*[8] Cadmium sulphide in its "pure" form has a resistivity of the order of 10^{12} Ωcm. It can be prepared as a powder, a single crystal, or as a thin film. The photosensitivity in the pure state has a peak response near the absorption edge, i.e. near 5150 Å, and is small because recombination centres are unavoidable with present techniques. The material can be made semi-conducting, with a resistivity as low as 1/10 Ωcm, by the addition of atoms of a halogen or of gallium or aluminium. These provide donor levels, situated less than 0·05 eV below the conduction band. They follow the "hydrogen model" quite well, i.e. the ionization energy corresponds with that for a hydrogen atom corrected for the dielectric constant of the crystal, 2·45,[9] and the effective mass of the electrons $m^* = 0{\cdot}25m$.[10] The provision of these donors raises the Fermi level compared with its position in the pure material, moves the two extreme levels much further apart [Fig. 2(*b*)], and so increases the sensitivity because more hole-trapping states are included between these levels. There is therefore a marked increase in photoconductivity, still with the same spectral response. The implication is that hole-trapping levels are present initially in the pure crystal as well as recombination centres, and that activation occurs mainly as a result of the movement apart of the demarcation levels when donors are added.

As the donor concentration rises, both the dark conductivity and the photoconductivity increase over a wide range. The ratio of light to dark current first increases, passes through a maximum when the dark resistivity is about 10^9 Ωcm, and then decreases again. The effect is the inverse of that when copper is added to cadmium sulphide containing chlorine, which is discussed below and shown in Fig. 5. Ultimately the photoconductivity ceases to increase when there are no further hole-trapping states to be included by further separation of the two extreme levels.

The change in dark conductivity with donor concentration is very rapid; for example, it is necessary to add only 5 parts per million of chlorine to reduce the resistivity from 10^{12} to less than 1 Ωcm. Accurate control of photoconductivity near the composition giving the maximum ratio of light to dark current is found in practice to be difficult by control of chlorine content alone. If, however, suitable acceptor levels are provided, a corresponding number of electrons from donor levels fall into these, so reducing the dark conductivity. Such acceptors are provided for example by the use of traces of copper or silver to replace cadmium. Addition of these therefore gives a further means of controlling the conductivity. It is found in practice to be simpler to add considerably more chlorine than is necessary to raise the dark conductivity to about 10^9 Ωcm, and to compensate the excess by adding copper or silver. It should be noted that continued addition of these impurities does not convert the material to a *p*-type semi-conductor.

As the copper concentration rises with a given fixed halogen concentration, the dark conductivity and the photoconductivity fall as the Fermi level moves downwards. The effect of adding acceptor centres in this way is shown in Fig. 5,

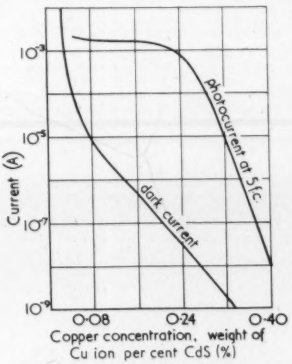

Fig. 5. Photocurrent and dark current of cadmium sulphide : copper: chlorine powder as a function of copper concentration

400 V across 1 mm gap, 2 mm long.

and is the inverse of the effect of adding donors to a pure crystal. Ultimately, provided the halogen concentration is sufficiently high, a condition is reached where the increasing copper concentration alters the spectral response. The peak response moves to 7000 Å, and the response near the absorption edge falls. When copper and chlorine have similar concentrations, near one part in a thousand, the response is as in Fig. 6, curve (*b*), contrasting with the edge response when both concentrations are low. The form of the edge response is shown at (*a*) in Fig. 6, but the height relative to the red peak (*b*) has been reduced for convenience in plotting.

The total response to a tungsten lamp is in fact similar for the two curves, provided the concentrations are adjusted to give similar dark conductivity.

Another effect of high copper concentration is that super-linearity is introduced at room temperature, as was shown in Fig. 3, whereas in the purer condition it is present only above about 100° C. This is true even when the dark conductivity is the same for the high impurity concentration as for the low; this can be achieved by appropriate balancing of

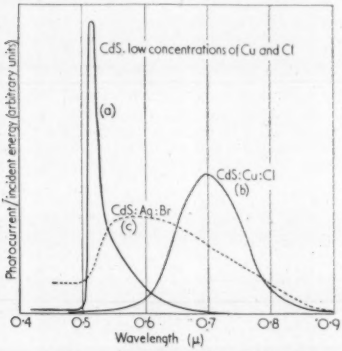

Fig. 6. Spectral distribution of cadmium sulphide photoconductors

the copper and halogen concentration whatever the concentration of either separately. When the conductivity is the same, the Fermi level is the same, unless the mobility is altered very much by the addition of the copper. Thus one must conclude that for a given position of the Fermi level, the hole demarcation level is higher relative to the hole-trapping levels when copper is present at high concentration.

The effect of temperature on photoconductivity also depends on the concentration of donors and acceptors.

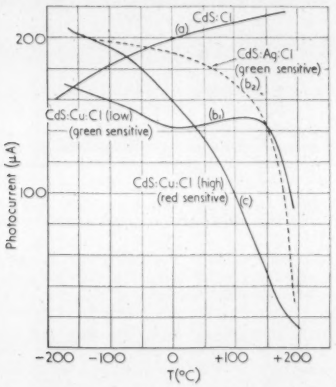

Fig. 7. Variation of photocurrent of various cadmium sulphide crystals as a function of temperature T; illumination = 30 f.c.

Crystals activated with chlorine, containing no added copper, give increasing sensitivity as temperature rises to 200° C, see curve (*a*), Fig. 7. When copper is added and the chlorine content is raised to give the same dark conductivity at room temperature, curve (b_1) is obtained. The crystals in this case are still sensitive to green light near the absorption edge. A similar curve (b_2) applies for low concentrations of silver and chlorine. Further increase in copper and chlorine content gives ultimately curve (*c*) for red-sensitive crystals. This is the condition giving superlinearity at room temperature referred to in the previous paragraph. For curves (b_1) and (b_2), super-linearity occurs near and above 150° C, when the Fermi level is 0·7 eV or more below the conduction band. This is the situation discussed in detail by Rose[4] and Bube,[8] and arises because the lower of the two extreme levels of Fig. 2(*b*) is then about 0·9 eV above the valence band, and a group of hole-trapping levels is situated near this energy. The depth of the Fermi level below the conduction band when the hole-demarcation level passes through the hole-trapping levels is indicated in Table 1 as the "critical" depth of the Fermi level.

The presence of the hole-trapping levels about 0·9 eV above the valence band for small copper concentrations is confirmed by the occurrence of infra-red quenching. Infra-red radiation reduces the photoconductivity introduced by visible radiation, the effect occurring with three maxima at 0·9, 1·35 and 1·65 eV. The lower energy maxima are the main ones in sensitive crystals, and the intensities of the quenching effects are closely related in these two bands. This can be explained assuming that transitions of electrons are induced by the infra-red radiation from the valence band to the hole-trapping levels about 1 eV higher. These transitions free holes from these levels, which increase the rate of recombination through the ordinary recombination centres, so decreasing the sensitivity. The effect can occur only when the levels are fully operative as hole traps, i.e. when the demarcation level is below them. Correspondingly the quenching can occur only at temperatures at which the sensitivity is high at low light levels, below the range where super-linearity occurs and where the response begins to decrease as temperature rises. At low copper or silver concentrations, curves (*b*) of Fig. 7, this occurs as stated above when the depth of the Fermi level is 0·7 eV and the demarcation level is 0·9 eV above the valence band. With no added copper, curve (*a*), Fig. 7, the infra-red quenching peaks occur at the same energy as with low copper content, thus the critical height of the demarcation level is 0·9 eV in this case also. To account for the difference between curves (*a*) and (*b*), one must suppose either that the Fermi level is correlated in a different way with the demarcation level in the two cases, or that the temperature variation of the Fermi level is different. The Fermi levels are similarly situated at room temperature because the conductivity is the same. The effect of temperature on the Fermi level has not been studied systematically, but it is possible for its variation with temperature to be different, and in fact smaller, for case (*a*) than for (*b*), because in the absence of copper there are many electrons in trapping levels even above room temperature. These fall into the acceptor levels as copper is added. The presence of trapped electrons at and above room temperature in crystals with very low copper concentration is shown by these observations, comparing case (*a*) with case (*b*):

(i) the response time is longer for (*a*) than for (*b*);

(ii) electrons are released from traps in a "thermal glow" experiment at higher temperatures for (*a*) than for (*b*);

(iii) the photoconductivity increases initially before the usual decrease in an infra-red quenching experiment in case (*a*), but not (*b*) [or (*c*)]. This occurs because near infra-red radiation cannot only raise electrons from the valence band to the hole-traps, but can also raise them from electron-traps to the conduction band.

The addition of silver at high concentration has the same type of effect as that of copper. The peak sensitivity is near 6000 Å (Fig. 6), thus silver produces electron-occupied levels about 2·2 eV below the conduction band, whereas the copper levels are at a depth of about 1·7 eV.

The response time after activation with copper or silver together with a halogen depends on the sensitivity achieved and on the level of illumination, as indicated at the end of section 2. Unfortunately, although with low sensitivity material or high light level the response time may be less than 1/100 s., at high sensitivity and low light level it may exceed one second. This is too slow for many applications. The variation of response time with level of illumination for red-sensitive cadmium sulphide is shown in Fig. 8.

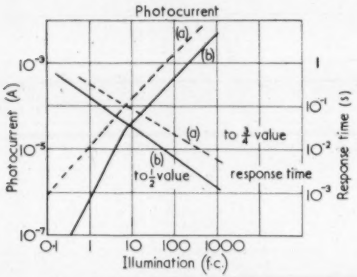

Fig. 8. Variation of photocurrent and response time with illumination for red-sensitive cadmium sulphide

(*a*) is more sensitive, the applied voltage is 10 V and the response time plotted is to $\frac{3}{4}$ value. (*b*) is less sensitive, the applied voltage is 50 V and the response time plotted is to $\frac{1}{2}$ value.

3.2. *Preparation of material.* Cadmium sulphide crystals have not so far been grown from the melt, because of the difficulties associated with the facts that the melting point is high and the dissociation pressure is high at the melting point. The procedure is either to react cadmium vapour with hydrogen sulphide,[11] and to condense the product at a constant temperature, or to sublime cadmium sulphide powder in a low pressure of hydrogen sulphide and condense the vapour.[12]

The former gives so far the purer product, though the crystals are usually more flake-like than those produced by the latter process. If activation with chlorine is desired, hydrochloric acid is added to the hydrogen sulphide. The introduction of copper is effected by washing the crystals after growth in a copper salt solution, or by evaporating copper on their surface and then firing at 700° C. It is not easy to ensure uniform distribution of chlorine or copper or similar impurities, but of course the penetration of light near the absorption edge is limited to a depth of the order 1/10 μ, so that it is the concentration in this depth which determines the photoconductive response; after activating a crystal, grinding or etching its surface produces marked changes in the behaviour. The normal situation is that both the chlorine and the copper concentrations are greatest near the surface, and decrease on entering the crystal. The ratio of the two is not necessarily constant with depth, nor does it necessarily vary in the same way in different crystals. Thus for a given photoconductivity of the surface layers, the dark conductivity of the "core" of the crystal may vary over a wide range. However, the overall dark conductivity of the crystal is much influenced by the higher-resistivity outer layers, which also determine the photoconductivity. Thus photoconductivity and the dark conductivity are well correlated in spite of the lack of homogeneity, provided that ohmic contacts are made to a part of the surface which has received the same treatment as that upon which the light is incident.

3.3. *Contacts.* Ohmic contacts are readily obtained using either indium or gallium, which can be melted or evaporated on to the crystal. Other materials such as silver, gold or graphite give ohmic contacts if special cleaning treatments are given to the crystal surface, for example electron or ion bombardment.[13] With some crystals, however, we have found that these materials give good contacts without such special cleaning. Chlorine-activated crystals containing no added copper have higher surface than bulk conductivity, due to the chlorine concentration gradient, and marked rectification effects are obtained with these crystals by making an indium contact to the surface as grown, and a silver or gold contact to the surface after etching, i.e. to a deeper seated region with lower conductivity. However, quite a small reverse voltage breaks down the rectifying barrier and lowers the resistivity of the silver or gold contact.

3.4. *Voltage response.* If a layer of powder is prepared by depositing powder in some form of binder, the current is restricted by the high resistance at the contacts between the particles. Both dark current and photocurrent are small at low voltages, but increase steeply with voltage, following approximately a fourth power law due to the breakdown of the contact resistance. Photoconducting cells made with such layers are therefore not suitable for low voltage operation. It is possible, however, to sinter cadmium sulphide powder giving a coherent block of material with ohmic resistance, and with a performance not greatly inferior to single crystals.

3.5. *Thermal activation.* Recent work in this Laboratory by Dr. J. Woods[14] has shown that the dark conductivity of pure cadmium sulphide crystals grown by the Frerichs' process can be raised by heat-treatment, and that the photoconductivity increases at the same time. The heat-treatment may either be in vacuum or in air, and may be at any temperature between 100 and 700° C, though the details of the spectral response depend upon the temperature and the ambient atmosphere. Below 300° C the effect occurs because excess cadmium is present in the crystals after growth. Above 300° C dissociation occurs, sulphur volatilizes, and further excess cadmium is produced. Thus at the higher temperatures the conductivity of all crystals rises continuously, but below 300° C there is a limit to the increase, and in fact with prolonged heating the conductivity passes through a maximum and falls again as cadmium is lost from the crystals. If a current is passed through the crystal when the temperature exceeds 300° C, the dissociation and consequent activation processes are accelerated.

When the heating is carried out in vacuum, the resultant photosensitivity is high for blue light, though the peak still occurs at the edge frequency, Fig. 9, curve (*a*). Exposure to oxygen at room temperature, curve (*b*), destroys this blue sensitivity, which is clearly due to a surface effect. Evidently oxygen introduces surface recombination centres which are

not present after heating in vacuum. After heating in air below 450° C, the sensitivity is localized near the absorption edge as with chlorine-activated crystals, or crystals heated in vacuum and then exposed to oxygen. Heating in air above

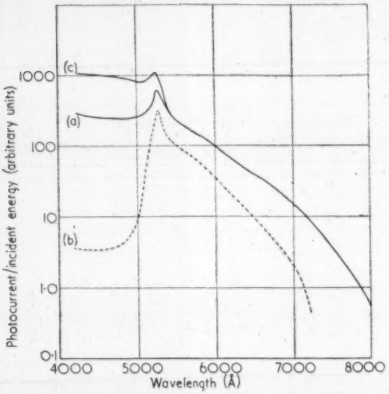

Fig. 9. Spectral sensitivity of photoconductivity of cadmium sulphide: (*a*) after heating in vacuum; (*b*) the same crystal after exposure to oxygen at room temperature; (*c*) a second crystal heated in air at 500° C

450° C, however, gives a good blue sensitivity, curve (*c*), similar to that after heating in vacuum. After this heat-treatment, the photoconductivity is maintained to higher temperatures than after heating in vacuum, in fact the two heat-treatments give curves respectively resembling (*a*) and (*b*) in Fig. 7, for chlorine/copper-activated crystals. The infra-red quenching frequencies are the same for both heat-treatments as they are after chlorine/copper activation, thus the hole-trapping levels are again the same. The good maintenance of photoconductivity with temperature for the crystals heated in air is due as in curve (*a*), Fig. 7, to a high density of trapped electrons, much higher than in crystals heated in vacuum. These electrons are mainly in the level 0·7 eV below the conduction band, which can probably therefore be attributed to oxygen in the crystals. Whether the 0·7 eV traps present in chlorine-activated crystals are due also to residual oxygen is not yet known.

4. CADMIUM SELENIDE

The properties of cadmium selenide differ in detail from those of cadmium sulphide, but follow the same general pattern. The differences arise mainly because the forbidden gap width is smaller, as shown in Table 1. The response in the pure material is therefore at a longer wavelength, while any levels in the forbidden gap are nearer to the band edges. As temperature rises the sensitivity falls almost immediately above room temperature, as the Fermi level passes through 0·3 eV below the conduction band. The lower of the two extreme levels [Fig. 2(*b*)] is then passing through the hole-trapping levels about 0·5 eV above the valence band. Correspondingly, super-linearity occurs in cadmium selenide at room temperature. The electron traps are also shallower than in cadmium sulphide, so that the long tail on the response time disappears at lower light levels.

For a particular light level, the response is between 10 and 100 times faster than for cadmium sulphide. The sensitivity at the peak in the spectral distribution is similar to that for cadmium sulphide; the overall sensitivity to light from a tungsten lamp is therefore greater because of the longer wavelength at the peak.

5. CADMIUM TELLURIDE[16]

Some of the properties of this compound are also shown in Table 1. It has been studied in less detail than the first two. An important point is that it can be made *p*-type with excess tellurium or by doping with copper or silver, whereas the others cannot. Since the gap width of 1·42 eV is near the optimum value for solar batteries,[17] there is considerable interest in the preparation and properties of *p–n* junctions in this compound, though this is a photo-voltaic effect, not photoconductive. The peak photoconductive response is found to occur at 0·84 μ, which is at the absorption edge as with cadmium sulphide and cadmium selenide.

6. ZINC TELLURIDE

Zinc sulphide and selenide have been studied in great detail, but are important primarily as phosphors. They resemble the corresponding cadmium compounds in many respects. Zinc telluride has been investigated as a photo-

Table 1. *Photoconducting cadmium and zinc compounds*

	Energy gap (eV)	*Refractive index*	*Melting point*	μ_e	μ_h	*Infra-red quenching peaks (eV)*	*Maximum electron trap depth (eV)*	*Critical depth of Fermi level (eV)*
CdS hexagonal	2·4	2·5 at 6000 Å	1475° C	~200		1·65 1·35 0·9	0·7	0·6
CdSe hexagonal	1·7		~1250° C	~200		1·20 1·0 0·8	0·4	0·3
CdTe cubic	1·42	3·3	1040° C	~600	~50			
ZnS hexagonal or cubic	3·65	2·4 at 6000 Å		~100				
ZnSe cubic	2·6							
ZnTe cubic	2·15		1240° C			0·7–1·2		0·3–0·45

Table 2. *Photoconducting lead compounds*

	Melting point (° C)	Energy gap at 300° K (eV)	Dielectric constant ε_0	Dielectric constant ε_∞	μ_e	μ_h	μ–T relation	Recombination lifetime (s)
PbS	1110	0·30	17·4	70	580	350	$T^{-5/2}$	$\sim 10^{-5}$
PbSe	1065	0·22	20·7	—	900	500	$T^{-5/2}$	$\sim 3 \cdot 10^{-6}$
PbTe	904	0·27	30·0	—	300	300	$T^{-5/2}$	$\sim 3 \cdot 10^{-6}$

conductor,[18] and all the considerations of section 2 have been found to apply. The behaviour is shown in Table 1.

7. LEAD COMPOUNDS[19]

Compounds of lead with sulphur, selenium and tellurium, are important photoconductors in the infra-red, and are usually used in the form of thin films. The details of the processes are becoming understood, and again appear to fit into the pattern of behaviour of section 2. Some properties are given in Table 2.

Recent work on lead selenide[20] has shown that thin films are initially *n*-type with low photoconductivity because of recombination centres, but sensitization with oxygen produces acceptor centres which not only make the film *p*-type, at least near the surface, but also produce marked electron trapping. The acceptor centres have s_n much greater than s_p, and therefore lead to a high photoconductivity due to holes. Excess sulphur produces electron traps also, but these are shallower and are effective in raising photoconductivity only near liquid air temperature.

In lead sulphide there has been considerable speculation as to the mechanism, and barriers have been thought to play an important part. It now appears that the considerations of section 2 may be applicable, and that the high sensitivity is associated with the production of a high majority carrier density, again probably because of minority carrier trapping.[21]

8. INDIUM ANTIMONIDE[22]

Indium antimonide has a small gap width, only 0·17 eV at room temperature, so that its absorption edge is near 7 μ. The calculated lifetime expected for direct recombination of electron and hole pairs with radiation of "edge" emission is about 0·5 μs. This is the maximum lifetime which would be observed if recombination centres were absent, or if the effect of recombination centres were reduced by the addition of appropriate minority carrier trapping centres. The observed lifetime is of the order 1/10 μs,[23] so that recombination centres may be present, but if so their effect is smaller than in any other semi-conductor when expressed as a ratio of observed lifetime to calculated recombination lifetime.

It would appear at first sight that lifetimes of 1 μs or less would not be consistent with a useful photoconductive effect. However, Moss[24] has shown that the photoconductive effect measured as a change in voltage across a specimen at constant current is dependent on the ratio of electron to hole mobility, and is large for a given gap width if the intrinsic carrier density is low, i.e. if the product of the effective masses for holes and electrons is low. Indium antimonide has the highest mobility ratio known, and this factor makes the sensitivity four times larger than that of any other material for a given lifetime. The effective mass product is also particularly low, about 10 times less than for most semi-conductors. Thus in spite of the low lifetime, this material in a state of high purity is a useful photoconductor for detection of infra-red radiation at wavelengths of 7–8 μ.

9. OTHER MATERIALS

Many other materials are of actual or potential value as photoconductors, but there is not a great deal of detailed systematic information. Their behaviour is indicated in Table 3.

Table 3. *Additional photoconductors*

		Approximate location of absorption edge (μ)	Approximate location of absorption edge (eV)	Peak response if displaced from absorption edge (μ)
ZnO	*n*	0·39	3·1	
Se	*p*	0·77	1·6	~0·7
Sb_2S_3	*n*	0·77	1·6	
Tl_2S		1·1	1·1	~1·0
Cu_2O	*p*	1·5	0·8	0·8–1·1
Ag_2S		1·4	0·9	
Mg_3Sb_2		1·55	0·8	
Cd_3As_2		2·1	0·6	
MoS_2		1·1–2·1	0·6–1·1	
ZnSb		2·2	0·55	
Te	*p*	3·9	0·34	
Mg_2Sn		3·5–5·6	0·22–0·36	

10. NATURE OF TRAPS AND RECOMBINATION CENTRES

In section 2 reference has been made to recombination centres and to trapping centres, and the later sections have shown that both are present and play an important part in all the well-known photoconductiving compounds. The recombination centres may be due to unidentified impurities, or to defects such as dislocations. Recent evidence indicates that the latter form the recombination centres in lead sulphide.[25] The hole-trapping centres in cadmium sulphide, cadmium selenide and zinc telluride may be cation vacancies. If the cation had two positive charges, its vacancy would have two effective negative charges with respect to the rest of the crystal. It could therefore trap a hole, and still have a low capture cross-section for an electron, as in the case of the Mn^{2-} ion in germanium. In fact these crystals are not fully ionic, and the cation has less than two positive changes. There are other difficulties associated with this interpretation, however, and one of the objects of the work in this Laboratory is to obtain further evidence as to the nature of the hole-trapping centres.

A sensitive material such as cadmium sulphide after activation has a hole lifetime of the order 10^{-10} s, and an electron lifetime of the order 10^{-3} s. Insensitive material has a hole lifetime exceeding 10^{-7} s and an electron lifetime of approximately 10^{-6} s. Both types of carrier injected from contacts have sufficient lifetime to give an appreciable luminescence due to recombination in insensitive crystals. This gives a d.c. electroluminescent effect at quite low field strengths.[26] The colour is green with frequency slightly less than that at the absorption edge. This is due to recombination of holes and electrons, either directly or via a level near

the band edge. It is possible similarly to obtain d.c. electroluminescence throughout the volume of single crystals of high purity zinc sulphide (J. Woods[27]), whereas in crystals containing a high concentration of copper and chlorine, the hole lifetime is small and d.c. electroluminescence is confined to the region near the cathode.

11. LUMINESCENCE

There are important correlations between photoconductivity and luminescence, which are well illustrated by the behaviour of cadmium sulphide. In the purer crystals luminescence is observable only at liquid air temperature or below, and is confined to a narrow band near the absorption edge, at slightly longer wavelengths, as in the d.c. electroluminescence. At liquid helium temperature the band is resolved into a number of lines, which may represent exciton levels, or more probably[28] levels due to shallow traps, perhaps resulting from sulphur vacancies.

When the crystals contain a halogen and sufficient copper or silver to give photoconductivity under excitation with red light, the same excitation produces infra-red luminescence, at 7800 Å for silver and 10 000 Å for copper activation.[29] This emission is due to the return of the electron from the conduction band to the emission centre. This transition is of course possible so long as there are holes in these centres, and electrons in the conduction band. After excitation ceases, the density of the latter decays in a manner indicated by the decay of photoconductivity, and it is possible for the luminescence to decay at the same rate, provided sufficient holes remain present in the emission centres.[30] However, in highly photoconducting crystals, the presence of the hole-trapping centres can lead to rapid transfer of holes from emission centres to these trapping centres, so that luminescence decays more quickly than photoconductivity.[31] The final transitions of the electrons to their ground states are in that case non-radiative.

12. APPLICATIONS

Photoconductive cells can obviously be used for detection or measurement of radiation in the appropriate part of the spectrum, and in control circuits employing radiation. The sensitivity is greatest as we have seen near to the absorption edge, except in heavily doped material. Sensitivity is often considerable on the short wavelength side of the absorption edge, but this is a surface effect greatly influenced by the ambient atmosphere. Many of the materials can be used for detection or measurement of X-rays, because these generate electron hole pairs in the body of the material, and the considerations of lifetime and trapping are applicable just as in the case of radiation near the absorption edge.

There are other less direct applications, however, arising for example from the storage of a charge pattern, in Vidicons and Xerography.[32] Another recent application arises from a combination of a photoconductive unit and an electroluminescent unit. If these are electrically in series, then the light input to the former modulates its impedance, and so modulates the voltage across the latter, and determines its light output. With suitable adjustments of resistance and capacitance, sufficiently sensitive materials will give amplification of the radiation incident on the photoconductor.[33] If the spectral sensitivities are suitably chosen, frequency conversion can be effected, in particular from X-radiation to visible radiation. X-ray intensification is very desirable in order to minimize diagnostic dosage, and this possible application is of considerable interest. Solid-state image conversion from infra-red to visible is also possible, though it does not appear to have been achieved so far. If the spectral sensitivities of the two units are matched, feedback can be obtained and bi-stable elements can be devised which can be optically switched. These and more complex developments from them have the advantage of compactness and may become important in the future. These possibilities have been discussed in a recent paper by Tomlinson of this Laboratory.[34]

For many of these applications faster response time is required than is at present available, and present work on the control of materials is therefore aimed at the reduction in density of both the shallow trap levels and the recombination levels. Their elimination requires increased purity and crystal perfection, together with, in the sulphides, selenides and tellurides, improved control of the departure from stoichiometry. Considerable progress can be expected as the techniques of preparation of the materials are improved.

REFERENCES

(1) BURSTEIN, E., and EGLI, P. H. *Adv. in Electronics and Electron Physics*, **7**, p. 56 (1955).

(2) HAYNES, J. R., and BRIGGS, H. B. *Phys. Rev.*, **86**, p. 647 (1952).
HAYNES, J. R. *Bull. Amer. Phys. Soc.*, **30**, 4, p. 30 (1955).
HAYNES, J. R., and WESTPHAL, W. C. *Phys. Rev.*, **101**, p. 1676 (1956).

(3) AIGRAIN, P., and À LA GUILLAUME, C. B. *La Luminescence des Corps Cristallins Inorganiques*, p. 101 (Paris: Éditions du Centre National de la Recherche Scientifique, 1956).
NEWMAN, R. *Phys. Rev.* **91**, p. 1313 (1953).

(4) ROSE, A. *Proc. Inst. Radio Engrs*, **43**, p. 1850 (1955); *Phys. Rev.*, **97**, p. 322 (1955).

(5) HALL, R. N. *Phys. Rev.*, **83**, p. 228 (1951); **87**, p. 387 (1952).
SHOCKLEY, W., and READ, W. T. *Phys. Rev.*, **87**, p. 835 (1952).
FAN, H. Y. *Phys. Rev.*, **92**, p. 1424 (1953).
BRECKENRIDGE, R. G., RUSSELL, B. R., and HAHN, E. E. (Editors). *Photoconductivity Conference*, p. 215 (New York: John Wiley and Sons Inc., 1956).
HAYNES, J. R., and HORNBECK, J. A. *Phys. Rev.*, **97**, p. 311 (1955); **100**, p. 606 (1955).

(6) CLARKE, D. H. *J. Electronics*, **3**, p. 375 (1957).

(7) NEWMAN, R., WOODBURY, H. H., and TYLER, W. W. *Phys. Rev.*, **102**, p. 613 (1956); **100**, p. 659 (1955); **96**, p. 882 (1954); **97**, p. 669 (1955); **98**, p. 461 (1955).

(8) BUBE, R. H. *Proc. Inst. Radio Engrs*, **43**, p. 1836 (1955).
KRÖGER, F. A., FINK, H. J., and VAN DEN BOOMGARD, J. *Z. Phys. Chem.*, **203**, p. 1 (1954).
BUBE, R. A. *Phys. Rev.*, **99**, p. 1105 (1955).

(9) CZYAK, S. J., BAKER, W. M., CRANE, R. C., and HOWE, J. B. *J. Opt. Soc. Amer.*, **47**, p. 240 (1957).

(10) KRÖGER, F. A., VINK, H. J., and VOLGER, J. *Physica*, **20**, p. 1095 (1954); *Philips Res. Repts*, **10**, p. 39 (1955).

(11) FRERICHS, R. *Phys. Rev.*, **72**, p. 594 (1947).

(12) CZYAK, S. J., and REYNOLDS, D. C. *Phys. Rev.*, **79**, p. 547 (1950); *J. App. Phys.*, **23**, p. 932 (1952); *J. Opt. Soc. Amer.*, **45**, p. 136 (1955).

(13) BUTLER, W. M., and MUSCHEID, W. *Ann. Phys. (Leipzig)*, **14**, p. 215 (1954); **15**, p. 82 (1954).

(14) WOODS, J. *J. Electronics*, **3**, p. 225 (1957).

(15) BUBE, R. H. *Proc. Inst. Radio Engrs*, **43**, p. 1836 (1955).

(16) HEINZ, D. M., and BANKS, E. *J. Chem. Phys.*, **24**, p. 391 (1956).
KRÖGER, F. A., and DE NOBEL, D. *J. Electronics*, **1**, p. 190 (1955).
VAN DOORN, C. Z., and DE NOBEL, D. *Physica*, **22**, p. 338 (1956).
(17) RITTNER, E. S. See Ref. (5).
CUMMEROW, R. L. *Phys. Rev.*, **95**, pp. 16 and 561 (1954).
CHAPIN, D. M., FULLER, C. S., and PEARSON, G. L. *J. App. Phys.*, **25**, p. 676 (1954).
(18) BUBE, R. H., and LIND, E. L. *Phys. Rev.*, **105**, p. 1711 (1957).
(19) BRECKENRIDGE, R. G., RUSSELL, B. R., and HAHN, E. E. (Editors). *Photoconductivity Conference*, pp. 463, 489, 591, 601, 619, 636 (New York: John Wiley and Sons Inc., 1956).
(20) HUMPHREY, J. N., and PETRITZ, R. L. *Phys. Rev.*, **105**, p. 1736 (1957).
(21) WOODS, J. F. *Phys. Rev.*, **106**, p. 235 (1957).
(22) WELKER, H. *Physica*, **20**, p. 893 (1955); *Ergeb. Naturwiss.*, **29**, p. 275 (1956).
KURNICK, S. W., STRAUSS, A. J., and ZITTER, R. N. *Phys. Rev.*, **94**, p. 1791 (1954).
AVERY, D. G., and JENKINS, D. P. *J. Electronics*, **1**, p. 145 (1955).
WERTHEIN, G. K. *Phys. Rev.*, **104**, p. 662 (1956).
MOSS, T. S., HAWKINS, T., and SMITH, S. D. *Report of the Meeting on Semi-conductors*, p. 133 (London: Physical Society, 1957).
(23) GOODWIN, D. W. *Report of the Meeting on Semiconductors*, p. 137 (London: Physical Society, 1957).
(24) *Photoconductivity Conference*, p. 427 (New York: John Wiley and Sons Inc., 1956).
(25) SCANLON, W. W. *Phys. Rev.*, **106**, p. 718 (1957).
(26) SMITH, R. W. *Phys. Rev.*, **105**, p. 900 (1957).
(27) WOODS, J. *J. Electronics*, **3**, p. 531 (1957).
(28) LAMBE, J. J., KLICK, C. C., and DEXTER, D. L. *Phys. Rev.*, **103**, p. 1715 (1956).
(29) GARLICK, G. F. J. *Progress in Semiconductors*, **1**, p. 101 (London: Heywood and Co., 1956).
(30) BROSER, I., and WARMINSKY, R. *Z. Phys.*, **133**, p. 340 (1952).
(31) BROSER, I., and WARMINSKY, R. *Brit. J. Appl. Phys.*, **6**, Suppl. 4, p. S90 (1955).
LAMBE, J. J. *Phys. Rev.*, **98**, p. 985 (1955).
(32) YOUNG, C. J., and GREIG, H. G. *R.C.A. Review*, **25**, p. 469 (1954).
(33) KAZAN, B., and NICOLL, F. H. *Proc. Inst. Radio Engrs*, **43**, p. 1888 (1955).
(34) TOMLINSON, T. B. *J. Brit. Instn Radio Engrs*, **17**, p. 141 (1957).

ORIGINAL CONTRIBUTIONS

Sources of error in electron stereomicroscopy

By R. I. GARROD, Ph.D., F.Inst.P., and J. F. NANKIVELL, B.Sc., A.Inst.P., Aeronautical Research Laboratories, Melbourne, Australia

[*Paper first received* 25 *April, and in final form* 11 *November*, 1957]

A theoretical examination is made of the use of the stereoscopic technique for the determination of vertical elevations in electron microscope specimens. It is shown that the variation in optical object distance due to tilting the specimen may introduce serious errors even for object points close to the optic axis of the microscope. Other possible sources of error are also analysed, and it is concluded that in practice, apart from limits due to resolution, these are likely to be of minor importance in relation to the tilt error and the precision attainable in the measurement of parallax. Consideration has been given to possible means of reducing the tilt error: no wholly satisfactory solution has been found, and it is necessary for precision work to maintain the axis of tilt of the specimen close to the optic axis within very narrow limits.

INTRODUCTION

The quantitative determination of relative elevations in a specimen is of considerable importance in some applications of electron microscopy, such as for example, in the study of particle shapes or the measurement of surface elevations by the use of a replica. It is well known that the stereoscopic technique, in which the specimen is tilted between exposures about an axis normal to the optic axis of the microscope, can be used for this purpose, and formulae have been developed that relate the relative height between two points in the object to the parallax between corresponding image points in the stereo pair.[1-4] Thus if c is the relative elevation between two points in the specimen which lie in a plane normal to the axis of tilt and y_1, y_2 are the separations of the images of the two points in the two micrographs, the relation is[3]

$$c = (y_2/M_2 - y_1/M_1)/2 \sin\theta \qquad (1)$$

where 2θ is the total angle of tilt between exposures, and M_1 and M_2 are the corresponding overall magnifications for the two micrographs.

If a stereoscope equipped with a parallax bar is used for making measurements on the micrographs, it is desirable to make M_1, M_2 as nearly identical as possible, in which case equation (1) reduces to[1, 2]

$$c = (y_2 - y_1)/2M \sin\theta \qquad (2)$$

These two equations assume that in practice the magnification is sensibly constant for each individual micrograph. Since the specimen is tilted, however, the object distance for each point in the specimen with respect to the objective lens of the microscope will vary, resulting in a continuous change in magnification across the image field and a differential magnification change between corresponding image points in the stereo pair. The effect is therefore to introduce errors in the determination of relative elevations from the above

equations, which may not be insignificant since, in contrast to aerial survey work, the object distance in electron microscopy is relatively small.

In the absolute measurement of elevation by the stereo method, several possible sources of error arise, some of which have been considered previously. It is clear from equation (1), for example, that the precision of measurement depends upon the accuracy of calibration of the magnifications M_1 and M_2 and the total stereo angle 2θ.[2, 4] Furthermore, Heidenreich and Matheson[2] and Drummond[5] have pointed out the desirability of maintaining the axis of tilt close to the optic axis of the microscope (so that $M_1 \simeq M_2$) and Rühle[6] has designed a specimen stage with this end in view. The purpose of the present paper is to assess the importance of other sources of error inherent in the stereo technique. In particular, it is shown that the implicit assumption that the magnification is constant in any one image of the stereo pair, leads, in general, to serious errors in measurement of relative heights, even for object points close to the optic axis of the microscope.

SOURCES OF ERROR

(*a*) *The tilt error*

The effect of tilting the specimen through an angle $\pm\theta$ in the stereoscopic method is illustrated in Fig. 1. The axis of tilt passes through O normal to the plane of the figure at a

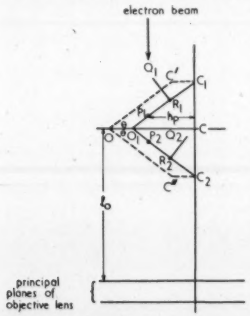

Fig. 1. Schematic diagram illustrating the effect of tilting the specimen in the stereoscopic method

distance $OC = d$ from the axis of the electron optical system, and a distance l_0 from the first principal plane of the objective lens. When the specimen is tilted anti-clockwise through an angle $+\theta$, a point C in the object originally lying on the optic axis moves to C'. The procedure is then to translate the specimen so that C' is returned to the axis at C_1, i.e. $O_1C_1 = OC = d$. Similarly for $(-\theta)$, $O_1C_2 = d$.

Consider two points P and Q in the specimen with relative elevation $QR = c$. For positive and negative tilts the positions of these points are P_1, Q_1 and P_2, Q_2 respectively. Their distances from the axis and the objective lens are given for $\pm\theta$ by

$$\left.\begin{aligned} h_P &= x_2\cos\theta \\ h_Q &= x_1\cos\theta + c\sin\theta \\ l_P &= l_0 + (d - x_2)\sin\theta \\ l_Q &= l_0 + (d - x_1)\sin\theta + c\cos\theta \end{aligned}\right\} \qquad (3)$$

where

$$C_1R_1 = C_2R_2 = x_1,\ C_1P_1 = C_2P_2 = x_2$$

From optical considerations it follows that an object point having co-ordinates (h, l) with respect to the axis and objective lens respectively, is imaged at a distance Z from the axis given by

$$Z = -Kh/l \qquad (4)$$

where K is a constant for a particular optical system and depends on the focal lengths and separation of the lenses, and the distance of the image plane from the final lens. Let y_1 and y_2 represent the separation of the images of P and Q for $\pm\theta$; and let p be the (measured) parallax between these image points in the stereo pair; i.e. $y = Z_P - Z_Q$, $p = y_2 - y_1$. It follows from (3) and (4) above that the parallax is given very closely by the relation

$$p = p_0 + (Mc^2/l_0)\sin 2\theta + 2Mc\sin\theta \qquad (5)$$

where

$$p_0 = (M/l_0)(x_2 - x_1)[d - (x_2 + x_1)]\sin 2\theta$$

and $M = -K/l_0$ is the magnification in either micrograph corresponding to the point O_1. In electron microscopy, $c \ll l_0$ and hence the second term in (5) may be ignored in comparison with the other terms, leading to

$$p \simeq p_0 + 2Mc\sin\theta \qquad (6)$$

It will be noted that equation (6) differs from the relation given in (2) by the addition of the term p_0, which is independent of the elevation and arises from the different distances of object points from the objective lens when the specimen is tilted. The term p_0 may be regarded as an "instrument parallax" and represents the parallax that would be observed in the stereomicrographs for two points P and R in a plane specimen.

The error Δc in determining the elevation from equation (2) is thus

$$\Delta c = \frac{p_0}{2M\sin\theta} = \frac{(x_2 - x_1)}{l_0}[d - (x_2 + x_1)]\cos\theta \qquad (7)$$

If parallax measurements are referred to a point on the optic axis so that $x_1 = 0$

$$\Delta c = (x_2/l_0)(d - x_2)\cos\theta \qquad (8)$$

From equation (8) it is seen that if $d \gg x_2$, Δc is nearly proportional to x_2; i.e. the error increases linearly with x if the axis of tilt is well displaced from the optic axis. On the other hand if $d \ll x_2$, the error is a parabolic function of x. An indication of the importance of the tilt error may be obtained from the following representative example.

Suppose $\theta = \pm 4°$, $l_0 = \frac{1}{8}$ in. (3·2 mm) and the width of the field of view in the microscope is 5 cm, i.e. $|x_2| \leqslant 25/M$ mm. The values of Δc obtained by the use of equation (8) are plotted in Fig. 2 for values of $d = 0$, 10^{-2} and 10^{-1} mm. The limits of x_2 for magnifications of 2500 and 25000× are also indicated in Fig. 2. Thus, for example, if the axis of tilt is displaced from the optic axis by 0·1 mm (which is roughly equivalent to one square on a 200 mesh supporting grid), the errors at the edges of the field with respect to the centre, at a magnification of 25000× are approximately ±400 Å. This value is appreciably larger than, for example, surface elevations of interest in the study of slip processes in metals.

Equation (8) has been verified experimentally by measuring the parallax on stereomicrographs from gold-shadowed carbon replicas of a plane glass surface. Prior to obtaining the micrographs, the replicas were exposed in the microscope

to a moderately intense electron beam in order to aggregate the gold film into small particles and so provide detail in the images for parallax measurements. The electron microscope

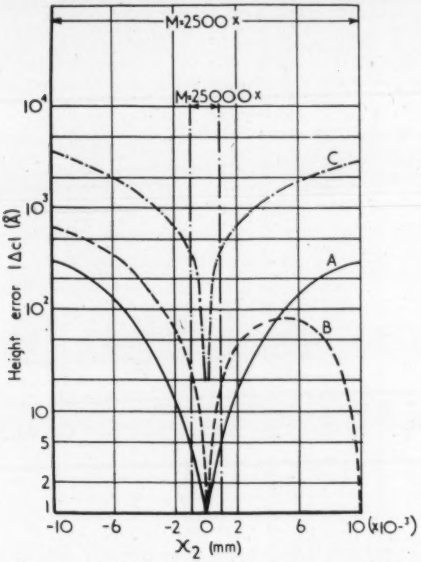

Fig. 2. Variation of height error with distance of the object point from the optic axis for the representative case of $\theta = \pm 4°$, $l_0 = 3{\cdot}2$ mm. Curves *A*, *B* and *C* correspond to displacements of the tilt axis from the optic axis of 0, 0·01 and 0·1 mm respectively. Δc is positive or negative for $\pm x_2$ respectively

used was a model EMU2B (by R.C.A. Ltd.) for which $\theta = \pm 4°$, $l_0 = \frac{1}{8}$ in. (3·2 mm), $x_{max} = \pm 1$ in. (2·5 cm). Measurements were made (i) of the total parallax across the field of view for various displacements of the tilt axis from the optic axis, and (ii) of the parallax across the micrographs for a fixed displacement of the axis of tilt ($d = 1{\cdot}9 \times 10^{-3}$ in.). As may be seen from Figs. 3 and 4, the measured and calculated values are in good agreement.

(*b*) *Other sources of error*

In addition to the error introduced through tilting the specimen, other errors may arise as a result of (i) unequal angles of tilt, (ii) variation in l_0 between the individuals of a

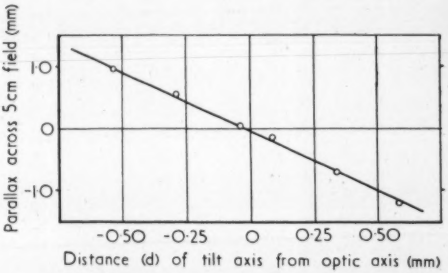

Fig. 3. Parallax on stereomicrographs of a plane replica for various displacements of the tilt axis from the optic axis. ($M = 4\,300\times$; $l_0 = 3{\cdot}2$ mm)

——— theoretical.
○ measured values.

stereo pair, (iii) variation in electron optical magnification between exposures, and (iv) the effect of refocusing, if necessary, between exposures. An analysis of these effects leads to the following results.

(i) *Unequal tilts.* Let the positive and negative angles of tilt for a stereo pair be θ_1, θ_2 respectively. If $\Delta\theta = \frac{1}{2}(\theta_1 - \theta_2)$ is small, the additional error due to this effect is given by $\Delta c_\theta \simeq (x_2 - x_1)\Delta\theta$ or referred to the centre of the field ($x_1 = 0$),

$$\Delta c_\theta \simeq x_2 \Delta\theta \qquad (9)$$

This error is therefore independent of l_0 and linear in x_2.

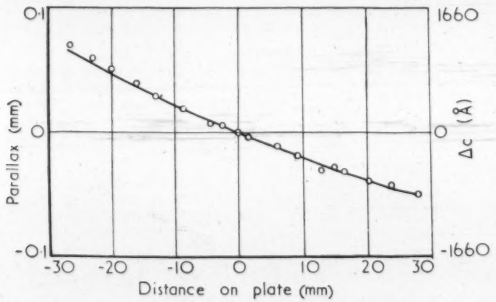

Fig. 4. Variation of parallax on stereomicrographs of a plane replica for a fixed displacement of the tilt axis from the optic axis. ($M = 4\,300\times$; $l_0 = 3{\cdot}2$ mm; $d = 0{\cdot}048$ *mm*)

——— theoretical. ○ measured values.

(ii) *Variation of* l_0. If l_0 differs between the individuals of a stereo pair by Δl_0

$$\Delta c_l \simeq \frac{x_2}{2}\frac{\Delta l_0}{l_0}\cot\theta \qquad (10)$$

(iii) *Variation in magnification.* $\Delta c_K \simeq \frac{x_2}{2}\frac{\Delta K}{K}\cot\theta$ (11)

where ΔK is the change in K between exposures, due, for example, to a slight change in current in the coil of the projector lens.

(iv) *Change in focus.* It has already been observed that if the stereomicrographs are taken with the tilt axis well displaced from the optic axis, the error in measurement of elevation increases nearly linearly with the distance of the object point from the optic axis. The effect is thus to produce a tilted baseline for the contour measurements.[2] In some applications this constant tilt can be allowed for and may be preferable to an indeterminate base of variable slope. In such circumstances, however, it may be necessary to refocus the image when the tilt is changed between exposures. The consequent change in focal length of the objective lens will alter slightly the positions of its cardinal points and thus introduce a small change in l_0. Quantitative analysis of this effect cannot readily be undertaken and indeed, numerical estimates are only possible in specific cases where detailed knowledge is available of the excitation and geometry of the actual objective lens employed. It is, however, interesting to note that for immersion type objective lenses employed in modern electron microscopes, any movements in the cardinal points that occur on refocusing are in such a direction as to partially compensate for the change in l_0 due to tilting the specimen.

PRACTICAL CONSIDERATIONS

The extent to which the effects considered above are of importance will, of course, depend upon the accuracy of measurement of parallax in the micrographs. Experience in these Laboratories has indicated that if the stereoscope is equipped with an accurate parallax bar, the standard deviation for measurements on good quality micrographs should not exceed 0·01 mm. This corresponds to an uncertainty in determination of elevations of

$$\Delta c_p = (0{\cdot}01)/2M\sin\theta \ (mm) \qquad (12)$$

As a guide to the importance of the various sources of error, Δc_p may be compared with the other errors for representative cases. Table 1 lists the magnitudes of the errors calculated from the above equations for points on the edges of an image field of $\pm 2{\cdot}5$ cm width. Values used for the various parameters are as follows:—

$\theta = \pm 4°$ and $\pm 10°$, $l_0 = \frac{1}{8}$ in. (3·2 mm), $|x_2| = 25/M$ mm, $\Delta\theta = 5'$, $\Delta l_0/l_0 = \Delta K/K = 10^{-3}$.

Table 1. *Values in Å of the various sources of error in the stereoscopic method. Values for d are in mm*

M	Δc_p	Δc (tilt)			$\theta = \pm 4°$		$\theta = \pm 10°$	
		$d=0$	$d=10^{-2}$	$d=10^{-1}$	Δc_θ	Δc_l and Δc_K	Δc_θ	Δc_l and Δc_K
			+ 0	+2840				
2500	280	±315	−630	−3460	150	715	60	280
			+ 25					
25 000	28	± 5	− 30	± 375	15	72	6	28

It should be noted that with the exception of Δc_p, all other errors given in Table 1 represent maximum values (for given parameters) in that they refer to points at the edges of the field and decrease progressively towards the centre, whereas Δc_p is independent of the lateral separation of two points in the object. In consequence, provided $\Delta\theta \gg 10'$ and $(\Delta l_0/l_0)$, $(\Delta K/K) \gg 10^{-3}$ the only error likely to be of importance is that due to tilt. In these considerations no account is taken of the resolution in the final image, which will depend principally upon the resolving power of the microscope and the resolution limit of the specimen. In some cases, e.g. if a replica technique with inherently poor resolution is employed, the minimum measurable elevation may be imposed by this limitation rather than by the factors considered above.

REDUCTION OF THE TILT ERROR

The final factor to be discussed briefly is a consideration of means for eliminating or reducing the uncertainty in measurement in the stereoscopic method due to the tilt error. Three possibilities seem open.

(i) If the axis of tilt is deliberately moved well away from the optic axis, the parallax due to tilt of the specimen increases, but becomes a linear function of x_2. This method is clearly of restricted application and with most specimen holders supplied with commercial electron microscopes will introduce a number of difficulties experimentally.

(ii) From equation (7) it is seen that within the approximations made in deriving equation (5), $\Delta c \simeq 0$ if $d = x_2 + x_1$. This implies (Fig. 1) that $C_1R_1 = O_1P_1$; i.e. the object points P and R have always to be so situated that they are equidistant along the replica from the axis of tilt and the intersection of the replica with the optic axis respectively. In general it is not possible to arrange for this condition to be fulfilled.

(iii) Thirdly, since Δc is inversely proportional to l_0, an increase in focal length of the objective lens will correspondingly reduce the tilt error. The overall magnification has then to be restored to its original value, either by increasing the power of the rest of the electron optical system or by subsequent optical enlargement of the stereomicrographs.

For the improvement to be worth while, l_0 should be increased by a factor ~ 10. In practice, however, the reduction in tilt error following upon such an increase in l_0 must be balanced against the loss in resolution that in general accompanies a reduction in lens excitation. The results given in Table 2, which have been computed from data given by Liebmann[7] and Liebmann and Grad,[8] illustrate this point for 50 kV electrons.

Table 2. *Resolution parameters for various object distances and stereo-angles*

l_0 (cm)	Lens resolution (Å)	Stereoscopic resolution (Å) $\theta = \pm 4°$	Stereoscopic resolution (Å) $\theta = \pm 10°$
0·3	7	50	20
1·0	12	90	35
3·0	24	170	70

The deterioration in resolution with reduction in lens current for a lens designed to operate at an object distance l_0 of 3 mm is shown in column 2. Heidenreich and Matheson[2] have pointed out that the minimum detectable elevation is also dependent upon the resolution limit of the objective

lens, and these corresponding minimum values are given in columns 3 and 4 for stereo angles of $\pm 4°$ and $\pm 10°$ respectively. Theoretically, an improvement in resolution at long working distances over those indicated in Table 2 could be obtained by designing a lens specifically for this purpose rather than by reduction of excitation of a short focal length lens. In practice, however, high resolution lenses having values for l_0 much in excess of 3 mm are not practical owing to their large dimensions. It therefore appears that for high stereoscopic resolution an increase in l_0 is not a promising solution to the problem.

The considerations discussed above thus suggest that the best method of reducing the tilt error is to ensure that the axis of tilt is always very close to the optic axis of the microscope. Furthermore, as Tables 1 and 2 indicate, the other errors, apart from Δc_p, reduce significantly as the stereo angle θ is increased. It should be noted, however, that in practice it may be very difficult to maintain the intersection of the tilt and optic axes within the tolerance required when small elevations are being measured. For example, from Fig. 1 it may be seen that a point C originally on the optic axis is displaced a distance $d(1 - \cos\theta)$ when the specimen is tilted. For $d = 10^{-2}$ mm, $\theta = 4°$, the displacement is approximately 2×10^{-5} mm, which at a magnification of 25000 $\times$ for example, produces a movement of the centre of the image of only 0·5 mm. Furthermore, the point of intersection on the optic axis with the image plane of the microscope is not usually known to this order of accuracy.

Although it is difficult therefore to place a quantitative lower limit to the accurate determination of elevations by the stereo method, it is believed that with present techniques this is not likely to be reliable below elevations ~100 Å.

ACKNOWLEDGEMENT

This paper is published with the permission of the Chief Scientist, Department of Supply, Australia.

REFERENCES

(1) GOTTHARDT, E. *Z. Phys.*, **118**, p. 714 (1942).

(2) HEIDENREICH, R. D., and MATHESON, L. A. *J. Appl. Phys.*, **15**, p. 423 (1944).

(3) ZWORYKIN, V. K., MORTON, G. A., RAMBERG, E. G., HILLIER, J., and VANCE, A. W. *Electron Optics and the Electron Microscope*, p. 268 (New York: John Wiley and Sons Inc., 1945).

(4) HELMCKE, J.-G., and ORTHMANN, H. J. *Optik*, **11**, p. 562 (1954).

(5) DRUMMOND, D. G. *The Practice of Electron Microscopy*, p. 109 (London: The Royal Microscopical Society, 1950).

(6) RÜHLE, R. *Optik*, **5**, p. 534 (1949).

(7) LIEBMANN, G. *Proc. Phys. Soc.* [*London*] *B*, **64**, p. 972 (1951).

(8) LIEBMANN, G., and GRAD, M. E. *Proc. Phys. Soc.* [*London*] B, **64**, p. 956 (1951).

The pneumatic conveying of spheres through straight pipes

By J. A. HITCHCOCK, B.Sc., A.R.C.S., and C. JONES, B.Sc., A.Inst.P., Mining Research Establishment, National Coal Board, Isleworth, Middlesex

[*Paper first received* 9 *December*, 1957, *and in final form* 4 *February*, 1958]

This paper reports a technique for the study of pneumatically-conveyed solids. Two equations have been established experimentally which give the pressure gradient and solid velocity along a pipe when non-adhesive spherical particles (up to 7 mm in diameter) are being conveyed with little or no acceleration by an airstream through the pipe. Straight, smooth and horizontal pipes (up to 7 cm in diameter) are considered. Included in the paper is a section examining the practical application of the equations, and a successful check of the equations is made with some values of the variables outside the range studied in the paper.

LIST OF SYMBOLS AND DIMENSIONS

d = particle diameter	L
D = pipe diameter	L
g = local acceleration due to gravity	L/T^2
g_c = conversion factor (32·17)	Non-dimensional
l = pipe length	L
M = mass flow rate of material	M/T
P_f = static pressure loss along length l of the pipe	M/LT^2
u = velocity of material	L/T
v = velocity of air	L/T
W = mass flow rate of air	M/T
ν = kinematic viscosity of air	L^2/T
ρ = density of air	M/L^3
σ = density of material	M/L^3
f = pipe friction factor $= \dfrac{2g_c DP_f}{\rho v^2 l}$	Non-dimensional
h = dynamic pressure of the air flowing in the pipe $= \dfrac{\rho v^2}{2g_c}$	M/LT^2
$\dfrac{vD}{\nu}$ = Reynolds number	Non-dimensional
$\dfrac{v^2}{gD}$ = Froude number	Non-dimensional
ΔP_f = pressure drop when only air is flowing for a length of pipe one diameter long	M/LT^2
ΔP_M = *additional* pressure drop when material is conveyed for a length of pipe one diameter long	M/LT^2
K_b, K_B = constants	
b_1, b_2, b_3, b_4, b_5, B_1, B_2, B_3, B_4 and B_5 are indices of dimensionless groups	

INTRODUCTION

Small-sized materials, such as pulverized fuel, powdered chemicals and foodstuffs, and materials like grain, which usually have reasonably constant physical properties, can be conveyed quite satisfactorily in pipelines by a stream of air. Little is known, however, about the conveyance of larger materials and, in particular, about the special problems that arise in the coal industry when shales of non-uniform physical properties are conveyed in an airstream to the coal face for roof support.

For the flow of solids in an airstream, the development of a theoretical foundation that is based on a consideration of the forces involved, such as that published by Hariu and Molstad,[1] is handicapped, as McNown shows,[2] by the lack of knowledge regarding the drag forces and also regarding the real nature of the resistance experienced by groups of particles in confined regions. Even more important is the fact that any one theory would rarely, if ever, cover the whole range of variables experienced in pneumatic conveying, since there are markedly different types of solid-fluid flow depending, as Durand has shown,[3] on the conveying conditions. Furthermore, the additional difficulties associated with irregularly shaped or sticking particles make impossible the already difficult task of theoretical development from the detailed particle dynamics.

Because of the limited success of earlier theoretical studies the authors considered that the best way to study the problem was by arranging the variables that may be effective in solid-fluid flow into conventional dimensionless groups and establishing the correlation between the groups. However, since the range and number of the variables involved in pneumatic conveying is extensive and the range of the dimensionless groups which can be derived from these variables also is large, it is necessary to confine a study of the problem in the first instance to a limited field. This report describes a study of the relatively simple case of dry spherical particles up to 7 mm in diameter moving in straight, level pipes of circular cross-section. Only that part of the pipe where the particles are fully accelerated is considered, and the air velocities are always sufficiently high to prevent slugging, i.e. the erratic motion of plugs of material along a pipe.

BASIC RELATIONSHIPS

In pneumatic conveying it is essential to know the pressure and quantity of air required to convey a given throughput of material, and it is also of importance to know the solid velocity as it moves through the pipe. Two relationships are therefore required, one to give the pressure gradient along the pipe and another to give the solid velocity when a given quantity of air conveys a measured throughput of material.

The dynamic pressure of the air flowing in the pipe $\left(h = \rho \frac{v^2}{2g_c}\right)$ is used in this report as an indication of the potential conveying power of the air,[4] and it is related to the static pressure loss along the pipe, P_f, by $P_f = \frac{fhl}{D}$. If ΔP_f is the pressure drop for a length of pipe one diameter long when air is flowing, then $\Delta P_f = hf$. The *additional* pressure drop for the same pipelength when solid is added to the airstream is ΔP_M, and the experimental work was designed to examine in what manner ΔP_M and u, the solid velocity, depended upon pipe size (D), particle size (d), air velocity (v), mass flow rate of material (M), mass flow rate of air (W), and the density of material (σ), these being the only variables that could be incorporated in the experiment at this stage. The conveying fluid used throughout was air, of density (ρ) and kinematic viscosity (ν). Conventional dimensional analysis[5] indicates that both the dimensionless groups $\frac{\Delta P_M}{h}$ and $\frac{u}{v}$ are functions of five other dimensionless groups. It is assumed that these functions are independent of one another and can be expressed as the product of powers of the other groups, giving the following relationships:

$$\frac{\Delta P_M}{h} = \frac{f \Delta P_M}{\Delta P_f} = K_b \left(\frac{M}{W}\right)^{b_1} \left(\frac{v^2}{gD}\right)^{b_2} \left(\frac{vD}{\nu}\right)^{b_3} \left(\frac{\sigma}{\rho}\right)^{b_4} \left(\frac{d}{D}\right)^{b_5} \quad (1)$$

and

$$\frac{u}{v} = K_B \left(\frac{M}{W}\right)^{B_1} \left(\frac{v^2}{gD}\right)^{B_2} \left(\frac{vD}{\nu}\right)^{B_3} \left(\frac{\sigma}{\rho}\right)^{B_4} \left(\frac{d}{D}\right)^{B_5} \quad (2)$$

where K_b, K_B are constants and b_1, b_2, b_3, b_4, b_5, B_1, B_2, B_3, B_4 and B_5 are indices of the dimensionless groups.

EXPERIMENTAL PROCEDURE

The experimental work was designed to estimate the values of the indices of the dimensionless groups and the constants K_b and K_B in equations (1) and (2), and by an examination of the deviation of the observed readings from these equations establish the validity of the multiplicative suppositions.

The study was confined to that part of the pipeline where particles were being conveyed with constant velocity, having been accelerated to this velocity from the position at which they were fed into the pipe. Straight horizontal pipes were used, as any bend or elevation retarded the particle motion. Two sizes of mild steel pipe of 2 and 3 in. internal diameter respectively were used, the cross-sections being circular. The friction factor of each size of pipe was maintained constant by occasional cleaning.

Only non-adhesive, spherical particles were conveyed, but materials of different densities and particles of different sizes were examined, as Table 1 shows. Glass balls larger than 7 mm were difficult to feed into the smaller size of pipe, and any smaller than 2 mm were difficult to measure on the velocity-measuring apparatus. The mass flow rates of the solids were decided by the fact that approximately 1 lb/s was the upper limit, common to the three materials, that could be fed into the pipe without blockage, and the minimum air velocity to convey this mass flow rate without slugging was 50 ft/s.

The length of pipe used in the work was some 100 ft, the acceleration of the particles being complete some 50 ft from the feeding hopper. It was possible to check that this was always so during the experiments, as the particle velocities were measured in short sections of clear Perspex pipe at 60 and 80 ft from the hopper, using a photographic stroboscopic technique.[6] Fig. 1 is a schematic diagram which shows the layout of the experimental apparatus.

At known distances along the 100 ft length of pipe static pressure tappings were made and these were connected to a differential manometer board. This board was photographed during an experiment in order to record the manometer readings for the same airflow both when solid was being conveyed and when it was not. The mass flow rate of the solid was controlled by a calibrated slide-valve fitted between the hopper and the pipe and it was checked by

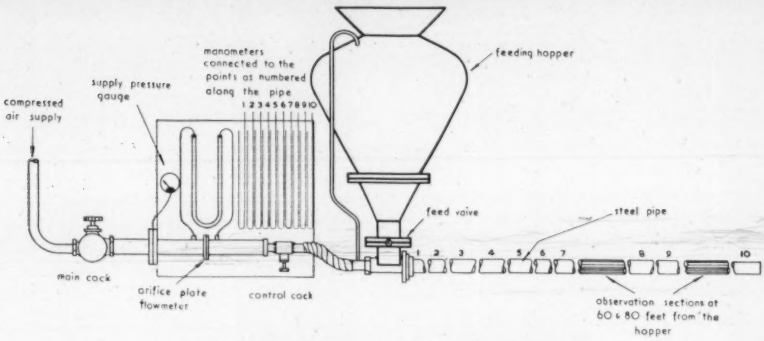
manometers connected to the points as numbered along the pipe
1 2 3 4 5 6 7 8 9 10
feeding hopper
supply pressure gauge
compressed air supply
feed valve
steel pipe
main cock
orifice plate flowmeter
control cock
observation sections at 60 & 80 feet from the hopper

Fig. 1. Schematic diagram of experimental apparatus

collecting the material for a measured time as it emerged from the other end of the pipe. The material was always examined after each experiment to check that little or no degradation had occurred.

Airflow was measured by an orifice plate flowmeter with D and $D/2$ tappings, made and used according to B.S. 1042: 1943. Air velocity was taken to be the measured volume rate of flow at standard conditions (60° F, 30 in. of mercury) divided by the cross-sectional area of the pipe. The airflow was controlled by a valve on the downstream side of the flowmeter.

It is convenient to use the word experiment as referring to a given throughput of material of one size when conveyed by a predetermined airflow along a specified size of pipe, during which time observations were recorded of air velocity, pressure gradient, solid mass flow rate and particle velocity. With three sizes of glass balls and one size each of maple peas and Blaud's pills, there were effectively five materials (see Table 1). Three mass flow rates of both air and solid

Table 1. *Materials used in the experiments*

Material	Density lb/ft³	Density g/ml	Diameter of spherical particles in.	Diameter of spherical particles mm
Maple peas	86	1·38	0·28	7
Blaud's pills	114	1·83	0·28	7
Glass balls	155	2·48	0·28	7
Glass balls	169	2·71	0·16	4
Glass balls	173	2·77	0·08	2

were possible and, as mentioned earlier, particle velocity was measured in two places. Including one repetition of each experiment there were therefore 180 experiments ($5 \times 3 \times 3 \times 2 \times 2$) for each of the two pipe sizes, i.e. 360 experiments in all. To offset any time effect, such as might have occurred, say, with the stroboscope, from wear in the pipe, or owing to degradation of material, the experiments were carried out in a random order. For experimental convenience the 360 experiments were statistically confounded into blocks for pipe size, material and observation point. All the observations of the quantities M, v, W, u and $\frac{\Delta P_M}{\Delta P_f}$ have been tabulated but, for reasons of economy of space, they are not included in the paper. They are, however, readily available for examination on request to the authors.

The experiments with the smallest size of glass ball were rejected for the following reasons. This size of glass ball showed some degradation, and as the degraded material was always removed after each experiment the stocks of the smallest balls soon became exhausted. A more serious criticism of the observations with these balls was the difficulty of measuring their velocity, for, as they were so small, there were many double images of the balls on each photograph, making identification of the pairs of images for each ball impossible. However, the pressure gradients that were observed are later compared with the values calculated from the equations obtained from the analysis of the other materials.

Before commencing the analysis, tests showed that the velocities at the two positions of 60 and 80 ft along the pipe did not differ significantly, on a significance level of 5%, and thus verified that the measurements were made in that part of the pipe where particles were not being accelerated.

ANALYSIS AND DISCUSSION OF RESULTS

Equations (1) and (2) can be written as:

$$\log\left(f\frac{\Delta P_M}{\Delta P_f}\right) = \log K_b + b_1 \log\frac{M}{W} + b_2 \log\frac{v^2}{gD} + b_3 \log\frac{vD}{\nu} + b_4 \log\frac{\sigma}{\rho} + b_5 \log\frac{d}{D}$$

and

$$\log\left(\frac{u}{v}\right) = \log K_b + B_1 \log\frac{M}{W} + B_2 \log\frac{v^2}{gD} + B_3 \log\frac{vD}{\nu} + B_4 \log\frac{\sigma}{\rho} + B_5 \log\frac{d}{D}$$

The observations were analysed to give the best estimates of K_b, b_1, b_2, b_3, b_4, b_5, K_B, B_1, B_2, B_3, B_4 and B_5, together with a measure of the experimental error and hence the conventional confidence limits within which these constants lay.

In the equation for the pressure drop ratio, b_3 and b_4, did not differ significantly from zero, at the 5% significance level, whilst the best estimates of b_1, b_2 and b_5 were 0·88, −0·45 and −0·88 respectively, with associated standard errors of 0·021, 0·019 and 0·064, each having 284 degrees

of freedom. The value of K_b was $1{\cdot}16 \times 10^{-2}$ with a standard error of $0{\cdot}10 \times 10^{-2}$ (d.f. 284). Thus,

$$\frac{\Delta P_M}{\Delta P_f} \cdot f = 1{\cdot}16 \times 10^{-2}\left(\frac{M}{W}\right)^{0{\cdot}88}\left(\frac{v^2}{gD}\right)^{-0{\cdot}45}\left(\frac{d}{D}\right)^{-0{\cdot}88} \quad (3)$$

and the 95% confidence limits of the indices were:

$$b_1 = 0{\cdot}92 \text{ to } 0{\cdot}84$$
$$b_2 = -0{\cdot}49 \text{ to } -0{\cdot}42$$
$$b_5 = -1{\cdot}01 \text{ to } -0{\cdot}76$$

The groups $\frac{\sigma}{\rho}$ and $\frac{vD}{\nu}$ do not appear, therefore, to have any directly significant effect on the pressure. The experiments were all at high Reynolds numbers where flow characteristics and drag coefficients are fairly constant, so that a Reynolds number effect was not expected.

Analysis of the results for the particle velocity gave

$$\frac{u}{v} = 6{\cdot}2\left(\frac{M}{W}\right)^{-0{\cdot}18}\left(\frac{\sigma}{\rho}\right)^{-0{\cdot}28} \quad (4)$$

With 95% limits for the indices

$$B_1 = -0{\cdot}21 \text{ to } -0{\cdot}15$$
$$B_4 = -0{\cdot}41 \text{ to } -0{\cdot}16$$

the standard errors being 0·015 and 0·054 respectively (d.f. 285). K_B was 6·2 with a standard error of 0·45 (d.f. 285). In this case the groups $\left(\frac{v^2}{gD}\right)$, $\left(\frac{d}{D}\right)$ and $\left(\frac{vd}{\nu}\right)$ do not appear to have any importance. The absence of Reynolds number is again not surprising but the absence of the Froude number, $\frac{v^2}{gD}$, is difficult to explain.

In order to facilitate a practical interpretation of the results it is helpful and sufficiently accurate to express equations (3) and (4) in the following manner:

$$f\frac{\Delta P_M}{\Delta P_f} \propto \frac{M}{d^{0{\cdot}9}\, v^{1{\cdot}8}\, \rho^{0{\cdot}9} D^{0{\cdot}4}} \quad (5)$$

$$u \propto \frac{v^{1{\cdot}2}\, \rho^{0{\cdot}5}\, D^{0{\cdot}4}}{M^{0{\cdot}2}\, \sigma^{0{\cdot}3}} \quad (6)$$

It is possible to deduce from expressions (5) and (6) the effects of changing any of the variables. For example, a change in v, keeping the other variables constant, will affect the ratio $\frac{\Delta P_M}{\Delta P_f} \cdot f$ as $v^{-1{\cdot}8}$. Since $\frac{\Delta P_f}{f}$ is proportional to v^2, then ΔP_M will vary as $v^{0{\cdot}2}$. Thus, increasing v will have small effect on ΔP_M. Similarly, the fully accelerated particle velocity will vary as $v^{1{\cdot}2}$, as expression (6) shows.

Increasing the throughput of a given material, everything else remaining constant, increases the *excess* pressure drop almost proportionally, but the maximum particle velocity is little changed. (It should be noted that in this paper the total pressure drop in a pipe is the sum of the excess pressure drop due to the material and the pressure drop that would occur if no solids were present.)

With a constant throughput of the same material and the same airflow, changing the pipe diameter changes the excess pressure drop almost inversely as the square of the diameter, since $\frac{\Delta P_f}{f}$ is proportional to $\frac{v^2}{D}$ in this case. Similarly, changing the pipe diameter changes the maximum particle velocity inversely as the square of the diameter.

Decreasing the size of material, keeping everything else constant, increases the excess pressure drop almost proportionally but does not affect the maximum particle velocity.

Changing the density of the conveyed material, keeping everything else constant, does not affect the excess pressure drop and changes the maximum velocity only a little.

APPLICATION OF THE RESULTS OUTSIDE THE RANGE OF VARIABLES STUDIED

As a practical check, equations (3) and (4) were tested by application to conveying conditions outside the range of the variables reported in this paper. The extrapolations could not be as numerous or as extensive as one would like for such a test because of limited time and lack of suitable apparatus, but they include observations with one material smaller than anything used in the analysis, a few more with a pipe of smaller diameter, and two observations with a material of much greater density.

Table 2. *Velocity ratio in a* 1 *in. pipe*

Materia	*M(lb/s)*	*v(ft/s)*	*Velocity ratio u/v* *Calculated*	*Observed*
Peas	0·59	71	0·50	0·58
Peas	0·28	75	0·57	0·55
Peas	0·28	76	0·56	0·49
Peas	0·29	53	0·54	0·56
4 mm glass balls	0·31	55	0·43	0·40
4 mm glass balls	0·32	75	0·46	0·42
4 mm glass balls	0·62	75	0·41	0·48

Table 2 shows the velocity ratio as calculated from equation (4) for peas and glass balls when conveyed in a 1 in. diameter pipe, and the calculated values agree very well with the observed values. Fig. 2 shows the velocity ratios from Table 2 plotted against the term $\left(\frac{M}{W}\right)^{-0{\cdot}18}\left(\frac{\sigma}{\rho}\right)^{-0{\cdot}28}$, and the observations are satisfactorily placed on either side of the empirical line given by equation (4). The ratio of ΔP_M to ΔP_f for the same materials in the same 1 in. pipe is plotted in Fig. 3 against the term

$$\frac{1}{f}\left(\frac{M}{W}\right)^{0{\cdot}88}\left(\frac{v^2}{gD}\right)^{-0{\cdot}45}\left(\frac{d}{D}\right)^{-0{\cdot}88}$$

and, except for one outlying point, the relationship is a linear one, as equation (3) indicates it should be.

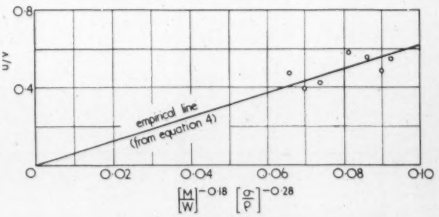

Fig. 2. Empirical and practical values of the velocity ratio for peas and 4 mm glass balls in a 1 in. pipe

Table 3 shows the only two results available with small steel balls. They are included here because the density of the material is far outside the range studied and the agreement between the calculated and observed pressure gradient ratios is good.

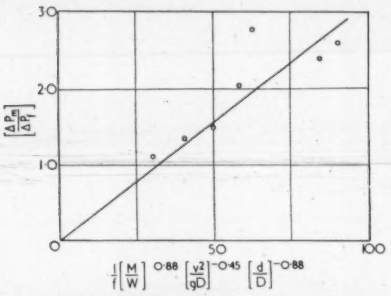

Fig. 3. Empirical and practical values of the pressure gradient ratio for peas and 4 mm glass balls in a 1 in. pipe

Table 3. *Pressure gradient ratio for steel balls in a 2 in. pipe*

Material	*M(lb/s)*	*v(ft/s)*	$\frac{\Delta P_M}{\Delta P_f}\cdot f$ *Pressure gradient ratio* *Calculated*	*Observed*
$\frac{1}{8}$–$\frac{3}{4}$ in.	0·30	74	0·012	0·011
Steel balls	0·59	74	0·021	0·022

Finally, the observed pressure gradient ratios for glass balls of the smallest diameter, which were omitted from the analysis for the reasons given earlier, are compared in Table 4 with the empirical values given by equation (4). The figures are for balls 0·08 in. in diameter when conveyed in pipes 2 or 3 in. in diameter, the observations being made at the two positions 60 and 80 ft along the pipe. The greatest disparity between the calculated and observed ratios occurs with the largest throughput of material when conveyed with the lowest air velocities. In these few cases it was possible that some degree of slugging was occurring, a condition to which the equations do not apply. In general, the agreement is very reasonable.

Table 4. *Pressure gradient ratio for 0·08 in. glass balls*

	60 ft along the pipe		$\Delta P_M/\Delta P_f$		*80 ft along the pipe*		$\Delta P_M/\Delta P_f$	
Pipe diameter	*M*	*v*	*Calculated*	*Observed*	*M*	*v*	*Calculated*	*Observed*
2 in.	0·57	54	3·1	2·5	0·54	54	3·0	1·5
	0·55	75	1·7	1·3	0·53	76	1·6	0·9
	0·55	97	1·0	0·9	0·55	102	1·0	0·8
	0·70	54	3·7	2·9	0·80	52	4·4	1·7
	0·70	74	2·1	2·3	0·75	74	2·2	1·5
	0·80	97	1·5	1·3	0·75	96	1·4	1·3
	0·97	55	4·7	3·7	1·05	54	5·3	2·1
	0·98	74	2·8	2·9	1·00	74	2·9	2·0
	0·99	99	1·7	2·0	0·95	100	1·2	1·6
3 in.	*Not observed*				0·54	55	1·7	1·7
	0·55	76	1·0	0·7	0·55	76	1·0	1·2
	0·54	97	0·6	0·5	0·54	98	0·6	1·0
	0·70	54	2·2	1·3	*Not observed*			
	0·80	75	1·4	1·0	0·75	77	1·3	1·3
	0·70	97	0·8	0·7	0·72	97	0·8	1·0
	1·10	54	3·2	1·1	1·00	55	3·0	1·9
	1·00	77	1·6	0·9	1·00	78	1·6	1·9
	1·00	98	1·1	0·8	*Not observed*			

CONCLUSIONS

(1) The experimental method and analysis form a successful technique for the study of pneumatic conveying.

(2) For pipes of a few inches in diameter, when straight, smooth and horizontal, the pressure gradient and solid velocity along the pipe when non-adhesive spherical particles are being conveyed with little or no acceleration by an airstream through the pipe are given by

(*a*) $$\frac{\Delta P_M}{\Delta P_f}\cdot f = 0{\cdot}012\left(\frac{M}{W}\right)^{0·9}\left(\frac{v^2}{gD}\right)^{-0·5}\left(\frac{d}{D}\right)^{-0·9}$$

and

(*b*) $$\frac{u}{v} = 6{\cdot}2\left(\frac{M}{W}\right)^{-0·2}\left(\frac{\sigma}{\rho}\right)^{-0·3}$$

In (*a*) it was found that the dimensionless ratios $\frac{\sigma}{\rho}$ and $\frac{vD}{\nu}$ had no significant effect and in (*b*) it was found that the dimensionless ratios $\frac{v^2}{gD}$, $\frac{d}{D}$ and $\frac{vD}{\nu}$ were not significant.

(3) The increase in pressure gradient when material is added to an airstream is proportional to the throughput and also to the size of material. It is inversely proportional to the square of the pipe diameter but is unaffected by either a change in the air velocity or a change in the density of the material.

(4) The fully accelerated particle velocity varies directly with the air velocity and inversely as the square of the pipe diameter. The size, density and throughput of material have little or no effect on it.

(5) A successful check of the two equations was made with some other values of the variables outside the range studied in this paper.

ACKNOWLEDGEMENT

The authors wish to thank Dr. Idris Jones, Director-General of Research, Scientific Department, National Coal Board, for permission to publish this paper. The opinions expressed in the paper are those of the authors and not necessarily those of the Board.

REFERENCES

(1) Hariu, O. H., and Molstad, M. C. *Industr. Engng Chem.*, **41**, p. 1148 (1949).
(2) McNown, J. S., and others. *International Congress Applied Mechanics*, **2**, p. 17 (1948).
(3) Durand, R., and Condolios, E. *Proceedings of a Colloquium on the Hydraulic Transportation of Coal*, National Coal Board Publication, November 1952.
(4) Korn, A. H. *Chemical Engineering*, p. 108 (March, 1950).
(5) Langhaar, H. L. *Dimensional Analysis and Theory of Models*, p. 18 (J. Wiley and Sons Inc., 1951).
(6) Hermges, F. G., and Jones, C. *Brit. J. Appl. Phys.*, **3**, p. 283 (1952).

The exploration of space by radio. By R. HANBURY BROWN and A. C. B. LOVELL. (London: Chapman and Hall Ltd., 1957.) Pp. xii + 207. Price 35*s*.

The completion of the 250 ft steerable radio telescope at the Jodrell Bank Experimental Station is an auspicious moment for the publication of this book describing the rich yield in new knowledge of space, and of the great variety of heavenly bodies which populate it, obtained through the new science of radio astronomy.

Written by the director of the Station, Professor A. C. B. Lovell, and one of the senior research staff, Mr. R. Hanbury Brown, the book opens with a brief review of our present knowledge of the structure of the Universe including a discussion of the relationship of our own galaxy to the extra-galactic nebulae. The radio emissions from the galaxy and from extra-galactic sources are described and the information available from the study of these emissions is discussed. The fascinating discovery that a few intense localized radio sources may be identified with visual nebulae opens up immense possibilities for the further study of these very distant objects, the radiation from which takes many millions of years to reach us. The study of discrete radio sources within the galaxy is also described, and, in particular, the important part played by the emission line from hydrogen at a wavelength near 21 cm. This hydrogen emission and corresponding absorption has played an important part in determining the spiral structure of the galaxy. The Doppler shift in this emission from distant galaxies is very large compared with the red shift in their emitted light (because of the much longer wavelength) and may also be used to determine their distance by means of Hubble's law. There is then the intriguing possibility of using radio emissions to determine the distance of objects that lie at the moment beyond the reach of the largest optical telescopes. These and many more fascinating topics are discussed. Coming nearer home we have chapters on emission from the sun and from some of the planets and a discussion of the use of radar in the study of meteors. The effect of the ionosphere on radio waves from extra-terrestrial sources is described and also the use of these to obtain further information about the ionosphere. The radio techniques and equipment required for making these observations are described in some detail including various forms of radio telescope and radio interferometer. The book ends appropriately with a description of the new 250 ft steerable telescope at Jodrell Bank.

Although the work is of a high scientific standard it is thoroughly readable and indeed makes a fascinating story. The authors are to be congratulated on compressing such a vast amount of information into just over two hundred pages without the text ever becoming a dull catalogue. For a book of this standard I must, however, make one criticism. It is astonishing that the authors should have not thought it worth while to give references in the accepted form. Practically no formal references are given in the text and only occasionally are the initials of authors given. The same criticism applies to the index in which no consistency appears—sometimes initials are given sometimes they are not. In any case the index is quite inadequate for a work of this sort.

The book is well produced and the diagrams and photographs are of the high quality we have come to expect from the publishers. Finally, the cost is very modest—a pleasant feature in these days of very expensive books—and we get extremely good value for our money. R. A. SMITH

Light, colour and vision. By Y. LE GRAND. (London: Chapman and Hall Ltd., 1957.) Pp. xiii + 512. Price 63*s*.

This book, a translation from the French and the first British edition, had its origin in a course of lectures given by the author in 1945 at the Institute of Optics in Paris, and was written as a textbook intended for use in the Institute. This excellent work has been revised and brought up to date and is very ably translated by Dr. J. W. T. Walsh, Col. F. R. W. Hunt and Dr. R. W. G. Hunt.

Professor le Grand, a physicist who has studied the physiological aspects of the subject, writes, in a very clear and interesting style, from the physicist's point of view. He claims that "the account is definitely a physical one and the aim is to give to opticians, to those who construct physical apparatus, to illuminating engineers, to architects, etc., as much information and as many numerical data as possible concerning the response of the eye to radiation."

This 500-page book is both a scientific treatise and textbook containing at the end some exercises and their solutions. It is in two sections, Section A having the sub-title "Experimental facts" and dealing with the physical and experimental approach, whilst Section B, "Theories of vision," covers the elements of anatomy, physiology and psychology necessary for an understanding of visual theories.

Section A comprises 15 chapters dealing with radiant energy, sources of radiation, the visual receptor, photometric quantities, retinal illumination, luminous efficiency curves, the trivariance of vision, the principles of colorimetry, colour vision, luminance and colour thresholds, time effects, spatial interactions, and anomalies of colour vision. Section B, chapters 16 to 20, covers the anatomy, photochemistry and electro-physiology of the retina, theories of colour vision and the thresholds. In Section A, where brief reference is made to colorimeters (pp. 203 to 205), it is disappointing to find the description of the Donaldson tristimulus visual colorimeter (1935), but no mention of Donaldson's six stimuli colorimeter (1947). With this latter instrument the spectral energy distributions of the test source can be much more closely matched than with the three stimuli instrument, and, in consequence, a large field of view may be used without introducing serious observer errors. This ensures a much better accuracy of colour measurement than is possible with the small field tristimulus instrument.

The non-specialist will find this work refreshingly clear, and at the same time forming an invaluable book of reference for those more intimately concerned with the subject. The terminology used is in accordance with the recommendations of the International Commission of Illumination.

G. T. WINCH

The reproduction of colour. By R. W. G. HUNT. (London: The Fountain Press, 1957.) Pp. 205. Price 63*s*.

The outstanding feature of this book is its lucidity. The reader is lead through the argument in so clear and logical a manner, that he will find no need to pause to resolve a difficult point or reconcile a statement with some previous one. The author has taken the trouble to do all this for him.

Yet this is no simplified guide to colour, but a precise presentation of all the difficulties and fundamental concepts involved in the physiology, psychology, physics, chemistry and technology of colour reproduction.

The first seven chapters describe the principles of colour reproduction without serious mathematics. The theory is concisely given in chapters 8 and 9, yet includes all the facts about colour essential to the subject and its development in later chapters on masking, half-tone printing, colour television and the assessment of picture quality. Throughout the book the emphasis is on how the eye sees colour, and the way in which every advantage can be taken of the characteristics of vision in deriving the best compromise between the many conflicting requirements.

The book is handsomely produced with a number of colour plates illustrating important colour effects. Only one minor misprint (a figure number) was detected. R. G. HORNER

Ferroelectricity in crystals. By HELEN D. MEGAW. (London: Methuen and Co. Ltd., 1957.) Pp. xi + 220. Price 27*s.* 6*d.*

Although the subject of ferroelectricity is still very young and imperfectly understood, the problem of the structure of ferroelectric crystals and of the relation between ferroelectric properties and crystal structure has already attracted the attention of many workers. A review of existing knowledge and an assessment of current theories is therefore timely, and Dr. Megaw's book, or monograph, meets this need admirably. It is primarily a very complete account of the properties and, more especially, of the crystal structures of ferroelectric crystals, but in the later chapters the various theories of ferroelectricity are reviewed with particular reference to their physical interpretation. Inevitably a large part of the book is concerned with crystallographic concepts but an attempt has been made to meet the needs of readers without formal training in crystal geometry by including descriptive accounts where necessary, and also a glossary of crystallographic terms.

This is not a book for the general reader, but anyone who is in any way concerned with ferroelectric materials will find it most useful and good value. A. E. DE BARR

X-ray crystal structure. By D. MCLACHLAN. (New York: McGraw-Hill Book Co. Inc.; London: McGraw-Hill Publishing Co. Ltd., 1957.) Pp. xiii + 416. Price 116*s.*

This book deals with those aspects of symmetry-theory and of X-ray diffraction on which the analysis of crystal structures is based. It includes, in addition to the topics common to all accounts of this subject, up-to-date discussions of such important developments as the use of high-speed computers in crystallographic research, and the formulation of statistical treatments leading to the so-called "direct methods" of analysis. The treatment throughout is that of the experienced teacher, able to anticipate a beginner's difficulties, careful to state arguments for and against in considering controversial matters, but always enlivening the presentation by making clear his own personal preferences or convictions. The reviewer finds some difficulty in visualizing the "lone worker" mentioned by the author, who must depend on a text such as this for instruction in the craft of structure-analysis; but for such a man the author offers reliable and brisk guidance along the main route, while finding opportunity to point the way to the more sophisticated refinements signposted "for experts only." One complaint—the title: to the reviewer, the only merit of this form of words is its brevity. One specially commendable feature: the drawings illustrating geometrical arguments. W. H. TAYLOR

Microwave measurements. By E. L. GINZTON. (New York: McGraw-Hill Co. Inc.; London: McGraw-Hill Publishing Co. Ltd., 1957.) Pp. xvii + 515. Price 90*s.*

This latest addition to the well-known International Series in pure and applied physics lives up to the high standard of previous volumes. The author acknowledges that the original plan was to write in collaboration with the late W. W. Hansen.

The volume is intended as a basic textbook for first year graduate courses in microwave measurements. It fulfils this function more than adequately. In fact, it goes a long way towards providing a very good introduction to the subject as a whole, since measurement forms so large a part of the whole science. It can be thoroughly recommended to any electronic engineer as an easily assimilated introduction to the microwave art. Unlike many textbooks on microwaves, mathematics are kept in their right perspective, and are introduced only to the extent necessary for a good understanding of the technique. The material is presented with a wealth of description and clear diagrams. It is as nearly up to date as can be expected of a textbook of this coverage.

The first chapter deals with signal sources. Magnetrons are hardly mentioned, but klystrons, travelling wave tubes and triodes are explained very fully. Their characteristics, methods of turning and conditions of operation are described. Frequency standards, harmonic and noise generators are also covered and, finally, there is a short discussion of sources for wavelengths below the limit obtainable from electron beam tubes. Chapters 2 and 3 deal very adequately with the detection and measurement of microwave power. Chapter 4 is a very clear and welcome discussion on the concept of impedance at microwave frequencies. This is followed by a chapter on the measurement of impedance. Chapter 6 discusses the microwave circuit and, as in other chapters, the connexion between microwave circuit parameters and normal circuit parameters is freely used to present a clear understanding of the concepts. The following Chapters 7–11 deal with the measurement of wavelength, frequency, Q, R_0/Q_0 and attenuation. Two appendices give useful data on field configurations and cut-off wavelengths for common wave-guides (*I*), and a series of useful formulae and constants (*II*).

In this very wide field, where security difficulties are encountered, some omissions are inevitable but this is a book written for teaching purposes. Technically, rather than scientifically, it provides an excellent grounding in the subject of microwave measurements. M. E. HAINE

Évolution des sciences. No. 9. L'Automatique des informations. By F. H. RAYMOND. (Paris: Masson et Cie, 1957.) Pp. 188. Price 1,600 fr.

The presentation in this book is at a level which aims to make it understandable to scientific workers who are not specialists in the field and, so far as a foreigner is able to judge, the style of writing is clear.

The first chapter is concerned with defining "information" and the notions which are involved in operating with it. It contains a short history of digital calculators and of the punched card, and leads naturally to the second chapter which deals with analogue and digital representations of numbers. The third chapter discusses analogue computers and the role of feedback.

The remaining five chapters describe: digital coding systems, Boolean algebra and switching circuits, the definition of universality in a computer, the detailed structure of such

computers, and programming, respectively. A short conclusion points out the fallacy of comparing computers to the human brain.

Price and language will give the book limited appeal to most British physicists. A. D. BOOTH

Feedback theory and its applications. By P. H. HAMMOND. (London: The English Universities Press Ltd., 1958.) Pp. 348. Price 35*s*.

This work is intended for post-graduate engineering and physics students but there is little doubt that many parts of it are suitable for undergraduate engineers at universities. The book could have been made even better for the latter purpose if it had included a lengthier treatment of mechanical systems and analogues, although a speed governor is treated at the very beginning of the book as an example of a non-linear element and incidental mention is made here and there of other mechanical analogues (on page 190, for instance, where a mechanical transitional lead system is treated). In this connexion, chapter 13, on electronic simulation of control systems, is especially valuable. This relatively trivial criticism, however, should not be allowed to detract from the book's value.

The diagrams are unusually well drawn and the literary style is clear and concise. There are detailed chapters on basic concepts and notation, the feedback principle, stability of linear feedback structures and graphical methods of representing the frequency response function. Chapters follow on various valve amplifier circuits (cathode followers, etc.) and on virtual earth amplifiers. Servo mechanisms are then treated in another group of chapters in which many matters such as the frequency response, non-linearities, etc., are fully discussed. Finally, there is the above mentioned chapter on electronic simulators. J. D. CRAGGS

Regelungstechnik. Moderne Theorien und ihre Verwendbarkeit. (Munchen: R. Oldenbourg Verlag g.m.b.h., 1957.) Pp. xiii + 483. Price DM. 88.

This is essentially a record of the symposium on feedback control held at Heidelberg in 1956, with the primary aim of realizing closer correlation between the theory and practice of automatic control systems. Some 90 papers are presented, many by authors of eminence in the fields of control and cybernetics, and are grouped under thirteen headings commencing with general survey papers and techniques. Linear systems, both single and multiple loop, are then considered followed by sections on non-linear and discontinuous controls, statistical methods, and optimization of performance. These latter three sections, which account for nearly half the book's contents, are likely to constitute its chief attraction to specialist control engineers. The papers in these sections are of a uniformly high standard, of wide general applicability, and in many of them the methods described are illustrated by design applications. On the other hand, the papers dealing with linear theory and the survey papers, whilst covering a wide field, contain little that is essentially new. Shorter applications sections deal with the use of analogue computers in servo-system design, steam power plant control, motor drives and industrial controls. Only one contribution approaches the problem of controlled automation of production lines, and it is disappointing to find nothing at all on the important non-linear case of nuclear reactor control. A welcome feature, however, is the use of control system theory to analyse some purely mechanical problems, such as diesel engine governing.

The compilation of the book suffers from the disadvantage common to nearly all such publications: the subject-matter is predetermined. This leads to a certain lack of continuity and an absence of impartial comparison of one system or technique against another. The multi-lingual presentation does not help: whilst some papers are presented in English, Russian or French, the major portion of the work is in German. Discussion records, particularly, are almost exclusively in German even when the original paper is in another language, and Russian contributions are repeated in German. A commendable uniformity in diagram presentation has been achieved throughout the volume: symbolism is less consistent. There are a number of printing errors; all those noted are unimportant.

This is a useful book for the specialist concerned with the more advanced techniques for control system synthesis and analysis and having a working knowledge of German.

D. ALLENDEN

The ultra high frequency performance of receiving valves. By W. E. BENHAM and I. A. HARRIS. (London: Macdonald and Co. Ltd., 1957.) Pp. ix + 173. Price 28*s*.

This work is concerned with the fundamental properties of thermionic receiving valves which arise (especially at high frequencies) from the fact that electrons have charge and mass, and therefore exhibit effects due to their finite transit times in moving between electrodes. One of the authors has studied these questions with great singleness of purpose, for at least thirty years, and may indeed be considered to have initiated the problems and recognized their importance. The treatment is largely mathematical, but although not abstruse in its nature it demands close attention from the reader, but this is indeed inseparable from an acceptable development of the subject. A valuable feature is the graphs of various transit angle functions which are given, and the representation of a valve as a two-terminal pair circuit element in Chapter VIII.

The number of misprints is commendably small. Eq. 4.5 should have an index 3/2 for V_g, but this could be inferred from 3.31 to which immediate allusion is made.

S. RODDA

Industrial electronics circuits. By R. KRETZMANN. (Eindhoven: Philips Technical Library; London: Cleaver-Hume Press, Ltd., 1957.) Pp. viii + 194. Price 35*s*.

This is a sequel and companion book to the author's *Industrial electronics handbook*, published by the Philips Technical Library. The book is divided into six sections dealing with: photoelectrically controlled apparatus; counting circuits; stabilizing circuits; contact and control devices; oscillator and amplifier circuits; rectifier and motor control circuits.

It is stated that the majority of the circuits, almost 200 in number, have been developed in the laboratory, and that some of the tubes and components are not necessarily available now. The book is not to be regarded as an exposition of the subject, although the individual items are clearly described and will be valuable to many investigators.

S. RODDA

Piezoelectricity. Post Office Research Station: Selected engineering reports. (London: Her Majesty's Stationery Office, 1957.) Pp. x + 369. Price 75*s*.

The publication in book form of a number of reports from the Post Office Research Station is a new venture which is to be applauded. In this book, eleven reports dealing with

a range of topics on piezoelectric crystals have been collected together and, although the result cannot be considered to be a textbook on the subject, it does cover a very wide field. The first five reports, dealing with piezoelectric theory and vibrations in crystals, are of value to any worker in this field and should be of interest to those working in the more general sphere of crystal physics.

The remaining works are of a more specialized nature dealing largely with the results of a comprehensive study of the properties of a number of artificially-grown water-soluble piezoelectric crystals. With the advent of more recent techniques it now appears unlikely that these materials will find extensive use commercially in frequency selective networks or electromechanical transducers. This does not, however, detract from the wealth of information to be found in these chapters nor does it reduce their value as an example of the study of the tensor properties of new materials.

The final report is a summary of published data on piezoelectric materials up to 1952 and includes a complete bibliography of original references.

Although somewhat marred by the lack of an index, this book will find its maximum use as a work of reference. It is hoped that other Government establishments can be prevailed upon to publish reports of work which would otherwise be lost to the scientific world outside these circles.

C. S. BROWN

Fundamental principles of transistors. By J. EVANS. (London: Heywood and Co. Ltd., 1957.) Pp. xii + 255. Price 45*s*.

This book is intended for users of transistors who wish to gain an intelligent insight into the physical principles of these devices. It starts from first principles and attempts in a chapter of 33 pages to convey to the uninitiated reader such notions of the quantum-mechanical theory of solids as the energy gap, holes, mobility, etc. The treatment in this and the subsequent chapters is thoroughly down-to-earth and the author consistently avoids complicated mathematics stating without proof most of the relations involved in the theory. This, for all its limitations, is the only possible way of dealing with this type of problem. The next chapter gives a brief account of measurements on semiconductors and should be very helpful to the beginner. The theory and methods of preparation of *p–n* junctions are the subjects of the next two chapters, and are followed by a discussion of junction and point-contact transistors of which the latter, a notoriously difficult subject, is not very clear in places. Measurements of transistor parameters, principles of manufacture of transistors, description of some special types and a brief but useful reference to silicon and other transistor materials complete the book. There are three appendices, one an original suggestion on the teaching of transistor physics and another a useful review of some commercial transistor data.

One's impression is that the author has given much attention to the didactic aspects of the book with, on the whole, good results. Minor criticisms are a few omissions in figure captions e.g. Fig. 45, p. 129, and scant references to most recent review articles.

A. K. JONSCHER

Fundamentals of electron devices. By K. R. SPANGENBERG. (New York: McGraw-Hill Book Co. Inc.; London: McGraw-Hill Publishing Co. Ltd., 1957.) Pp. xii + 505. Price 75*s*.

The author of this work, who is Professor of Engineering at Stamford University, is also the author of a very well-known and successful book on vacuum tubes. The volume under review contains chapters on the historical development of the subject, electrons and ions, electric and magnetic fields, and on ion emission in a vacuum in which various simple forms of field configuration are treated. Then follows a chapter on atoms of some 24 pages in which the Bohr theory and wave mechanics are briefly described at an elementary level. The next group of chapters deals with basic ideas of energy bands in solids, junction effects and electron emission, and forms with the relevant appendices a very good introduction to the electrical properties of solids. The next chapters cover thermionic vacuum tubes, starting with vacuum and semi-conductor diodes, control type vacuum tubes and transistors; then a chapter on equivalent circuits of tubes and transistors leads logically to treatments of small signal amplifiers, small signal oscillators, small signal non-linear effects in electron devices, large signal application of electron devices, photo-emission tubes, etc., and finally there is a chapter on noise. There are many useful appendices dealing mainly with mathematical formulae relating to, for example, Fermi–Dirac statistics, etc., a good collection of problems and a valuable bibliography in which the references are expressed rather curiously. The system is fully explained (p. 485) but results, for example, in Hume-Rothery's well-known book being designated as Hud and in Moullin's "Spontaneous fluctuations" appearing as Mom.

The book can be thoroughly recommended, particularly for electrical engineers taking electronics, and there is no doubt that many physics schools would find it suitable reading.

J. D. CRAGGS

Analog computer techniques. By C. L. JOHNSON. (New York: McGraw-Hill Book Co. Inc.; London: McGraw-Hill Publishing Co. Ltd., 1957.) Pp. xi + 264. Price 45*s*.

In its first chapter, this book attempts a general approach to the subject of analogue computers. Unfortunately the breadth of view of the author, who is an instructor at the U.S. Air Force Institute of Technology, does not appear entirely equal to his self-imposed task. In his initial classification of computing equipment his treatment of the subject of digital computers shows him to have little appreciation of their capabilities. Furthermore, he writes as though there are "general purpose" analogue computers of comparable flexibility to digital computers (which is not true) and thus his subsequent discussions of the use of such analogue devices lacks a sound basis. The chapters on circuitry are easy to follow, and form an adequate introduction to the subject. The mathematical analysis, however, leaves much to be desired. For instance, an account is given of the solution of partial differential equations by difference replacement without any mention being made of the mathematical as opposed to electronic stability of the processes suggested. Despite a lengthy discussion in Chapter 3 on the choice of time scales, the critical relation between δt and $(\delta r)^2$ for the diffusion equation for instance [see e.g. Courant, Friedrichs and Lewy, *Math. Annalen*, **100**, pp. 32–74 (1928)] finds no place in the text. Yet it would seem essential, in practice, to be able to distinguish between instability due to the process used and that due to circuit design.

A. S. DOUGLAS

Grundprobleme der mathematischen theorie elektromagnetischer schwingungen. By C. MULLER. (Berlin: Springer-Verlag, 1957.) Pp. viii + 344. Price DM. 52.80.

The development of the fundamental existence and uniqueness theorems for the wave equation has lagged behind the

solution of the similar problems for other of the important differential equations of mathematical physics, primarily because of the difficulty of formulating a suitable boundary condition at infinity. Already at the end of the last century Sommerfeld recognized, in connexion with acoustic waves, that the uniqueness of the solution depended on the condition of outward energy flow at infinity.

The complete evaluation of this condition had, however, to await developments in the theory of integral equations, linear transformations, etc., and it is only quite recently that these problems have been satisfactorily solved for the equations of electromagnetic waves.

The present book, which is Vol. 88 of the *Mathematischen wissenschaften*, is a series of essays on mathematical topics held together by their relevance to the basic problems just mentioned, which forms the central theme of the book. For those interested in the mathematics of electrical waves it will be indispensable, but it is not for those who merely want solutions to particular problems. A. W. GILLIES

Geometric integration theory. By H. WHITNEY. (London: Oxford University Press, 1957.) Pp. xv + 387. Price 68*s*.

One of the Princeton mathematical series, this book is concerned with integration over an r-dimensional manifold M in n-space E^n and in particular on the dependence of the integral on the position of M in E^n. In three parts, the first, Classical theory, leads up to the theory of the Riemann integral. The second develops the general theory from a postulational approach and the general study is continued in the last part, using Lebesgue theory. The approach is very abstract in character, being concerned with the rigorous foundation of the theory.

The majority of physicists will find the language of vector spaces and algebraic topology in which it is written quite unfamiliar and will be content to leave this book for the pure mathematicians. For the latter who are specially concerned with abstract integration theory, this book will be of considerable interest. It is well produced and maintains the high standard of this series. A. W. GILLIES

The physics of clouds. By B. J. MASON. (London: Oxford University Press, 1957.) Pp. xx + 481. Price 70*s*.

Water is essential for life, and the peoples of the world have been interested in rain-making throughout the ages. During the last decade or so, science has replaced magic in this field, and Langmuir claimed that, by seeding clouds with pellets of solid carbon dioxide, or with silver iodide, the natural rainfall in an area could be increased. However, the magic lingered on, and unscrupulous "rain-makers" in the United States were not slow to exploit the commercial possibilities of weather control!

British meteorologists, on the other hand, have felt that large-scale cloud-seeding trials were premature, expensive and very difficult to evaluate. They have taken the view that a better approach to the problem is to study the fundamental physics of clouds and precipitation, and try to find out just why rain falls from natural clouds, and how electricity is generated in thunderstorms. Dr. B. J. Mason has played a leading part in this work, and in the volume under review he has given a comprehensive account of the present state of the subject.

The book opens with an introduction by F. H. Ludlam on the large-scale physics of clouds, describing the principal classes of clouds and their modes of formation. This is a useful background to the main text which is concerned with the micro-physics of clouds. The first two chapters discuss atmospheric nuclei and the condensation of water vapour. Subsequent chapters deal with droplet growth; the formation of ice and snow crystals; natural precipitation processes; artificial stimulation of precipitation; and radar studies of clouds. Finally the electrification of clouds is discussed; this is usually treated as the separate subject of atmospheric electricity, but the author feels with some justification that it should be regarded as a part of cloud physics. A combined bibliography and author index is appended.

The book is beautifully produced in keeping with the high standard we have come to expect from the Oxford University Press. It gives an up-to-date and well-balanced review of recent researches in cloud physics and can be thoroughly recommended to research workers and others interested in this fascinating subject. J. S. FORREST

Rectifying semi-conductor contacts. By H. K. HENISCH. (Oxford: The Clarendon Press; London: Oxford University Press, 1957.) Pp. xii + 372. Price 70*s*.

This book is an addition to the well-established International Series of Monographs on Physics. According to the preface it "is intended mainly for physicists who require a specialized knowledge of semi-conductor contacts and related surface phenomena. The introductory chapters are included so as to make the volume self-contained for the reader not previously engaged in research on solid state physics." The book is not, however, really self-contained, for parts of these early chapters are not sufficiently clear or full for a physicist who has little acquaintance with present-day views and concepts. For example, for him the discussion on page 32 of positive holes would need considerable amplification. But these early chapters do contain some very good points which will be appreciated by those entering research, and they include a very interesting summary of the early history of work on rectifying contacts. A helpful feature is the frequent distinction between equilibrium and non-equilibrium conditions.

There are three mainly descriptive chapters on the bulk properties of important semi-conductors (Ge, Si, PbS, Se, Cu_2O), and the structure and characteristics of plate and point-contact rectifiers. These chapters are particularly well documented. It is evident that the manufacture of some efficient commercial type of rectifier is still to a large extent a culinary art in spite of all the work summarized in this book of 372 pages. The next chapter is concerned with the rectifier as a capacitive circuit element, and the experimental methods of determining the relevant parameters. There follow three chapters on theories of rectification and of the special phenomena at the contacts. Transistor action is outside the scope of the book. Chapters X and XI describe recent experimental work on injecting contacts and on plate rectifiers, and their interpretation in the light of the theories previously discussed. Throughout, Dr. Henisch naturally draws on the accumulated experience of the Reading University Group of which he is a senior member.

This is not a book for beginners, but it brings together a very large amount of information. All workers in the field will be grateful to the author for his industry in collecting all the material presented. There is a very full bibliography, and a convenient list of symbols. The book is well illustrated, though a few diagrams contain too much information for real clarity. At the rate at which papers in the field are being published it will be a difficult task to revise the book from time to time but we hope that Dr. Henisch's energy will

***

continue to be sufficiently above the Fermi level for him to attempt it.

F. A. VICK

Grain boundaries in metals. D. McLEAN. (Oxford: Clarendon Press; London: Oxford University Press, 1957.) Pp. 346. Price 50*s*.

This book is a further addition to the series of "Monographs on the physics and chemistry of metals." In it the author gives a full and up-to-date account of our present knowledge of the structure and functions of grain boundaries in metals, both from an experimental and theoretical viewpoint. The subject-matter includes such topics as the energy of a grain boundary, solute concentrations in boundaries, their influence on the deformation processes in polycrystalline metals, and the diffusion along and migration of boundaries. The book is, therefore, of paramount interest to a physical metallurgist, but much of it will also be of interest to any applied scientist working with non-metallic polycrystalline materials.

There is little that the author has either omitted or requires correction. Occasionally, however, there are slight misstatements due to the author having a particular example in mind when making a general statement. One example of this type of error occurs on page 152 where the author states that in hexagonal-close-packed metals, easy slip occurs only on one plane. Here he is thinking of metals such as zinc, cadmium and magnesium, but in fact there are many hexagonal-close-packed metals in which the basal plane is not the predominant slip plane and which do not work-harden rapidly (e.g. titanium and zirconium). Such faults as these are, it must be emphasized, rare in the book, and the author must be complimented on the excellence of his compilation of a large body of knowledge. It will be of great value for metallurgists to whom it is heartily recommended by the reviewer.

A. D. McQUILLAN

Neutron cross sections. By D. J. HUGHES. (London: Pergamon Press Ltd., 1957.) Pp. 192. Price 30*s*.

Dr. Hughes's purpose in writing this book is to assist those who require neutron cross-sections in their work to make the best use of existing tables of experimental values. The most comprehensive collection of neutron cross-sections is BNL 325* with which Dr. Hughes has been associated but for those who are unfamiliar with methods of measurement in neutron physics this book will certainly be very useful. All of the cross-sections are clearly defined and the point is well made that most neutron cross-sections are defined by the method used to measure them. The book is likely to fulfil its primary aim very well and is an excellent addition to the International Series of Monographs on Nuclear Energy. It will also be useful to research students entering the field of neutron physics as the elements of the relevant current nuclear theory are well presented. I feel it will, however, be regrettable if this book discourages the eventual appearance of a more advanced and comprehensive treatment.

A. WARD

* HUGHES, D. J., and HARVEY, J. H. *Neutron cross sections.* U.S.A.E.C. (London: McGraw-Hill Book Co. Ltd., 1955).

Electron impact phenomena and the properties of gaseous ions. By F. H. FIELD and J. L. FRANKLIN. (New York: Academic Press Inc.; London: Academic Books Ltd., 1957.) Pp. ix + 349. Price 68*s*.

This book is the first of a new series of monographs on pure and applied physics to be published under the editorship of Professor Massey. It is written by two industrial scientists with experience in the applications of mass spectrometry to oil refining studies and problems, and with commendable lack of attention to strictly practical matters. It is easily the most comprehensive and up-to-date account of the measurement, interpretation and use of ionization potentials, and there is a table, some 74 pages long, on critical potentials ("appearance potentials" to the mass spectroscopist) for positive and negative ions combined with an equally valuable list of 534 references. Atomic and molecular cross-sections for collision processes are practically ignored, but this is a legitimate and understandable limitation and does not detract from the value of the book.

The study of electronic and ionic impact phenomena has an interesting history, for in the '20's and early '30's the subject was fairly new and exciting, but gradually became less fashionable and almost died out before the last war. In the last ten years there has been (for old practitioners) a satisfying revival of interest of which the present scholarly work is another welcome sign. The book will be invaluable in every laboratory working on gaseous collision processes and discharges.

There are chapters on apparatus, methods, on the general theory of molecular ionization and dissociation, on energy relations in collision processes, on mass spectral considerations and on implications for chemical reactions.

J. D. CRAGGS

Chemistry of the rare radioelements. By K. W. BAGNALL. (London: Butterworth's Scientific Publications, 1957.) Pp. x + 177. Price 30*s*.

This excellent monograph makes a welcome addition to the small number of modern textbooks on the naturally occurring radioelements. During the last few years, Dr. Bagnall has made notable advances in the chemistry of polonium: the chapters devoted to this element include a very substantial proportion of original material, as well as a valuable summary of earlier work, a detailed description of the laboratory and its equipment, and a comprehensive bibliography. The sections on astatine, radon, francium, radium and actinium provide a critical review of published work.

L. C. MYERSCOUGH

Fundamentals of optics. 3rd ed. By F. A. JENKINS and H. E. WHITE. (London: McGraw-Hill Publishing Co. Ltd., 1957.) Pp. vi + 637. Price 64*s*.

Earlier editions of this book were well received. Its strength lies still in the section on physical optics, which offers a clear presentation of the subject at undergraduate level, and which occupies two-thirds of the space. The sections on geometrical optics and quantum optics, by the addition of which the second edition differed from the first, have been retained in the third edition. The extensive minor changes comprise improvements in presentation and a discussion of topics which are fields of contemporary activity. An entirely new set of problems is included. Particularly welcome are the references to more detailed treatments of subjects where the authors have felt obliged to be superficial.

G. W. SERIES

Theoretical physics. 3rd ed. By G. Joos, with the collaboration of IRA M. FREEMAN. (London: Blackie and Son Ltd., 1958.) Pp. xxiii + 885. Price 70*s*.

As our knowledge of the physical world expands, books such as the one under review, which seek to bring the student to "an intermediate level of attainment" from which he may

proceed to his field of research, tend to increase in size. It is a matter for regret that a greater depth of understanding produces only rarely more concise treatments. This would appear to be possible in principle by a skilful use of carefully selected and simple examples, which introduce new points of interest, while illuminating the central theme.

In this new edition Professor Joos has not followed this course. Instead, in pursuance of the general trend, the book has been increased in size by 32 pages, and in cost by 20*s*. To describe this as an additional 7*d*. per additional page would, however, be less than just, if only because this edition includes a very good revised and slightly expanded chapter on nuclear physics. The discovery of the neutrino (but not the problem of parity conservation) has already found a mention in this chapter. Apart from this, the type as set up for the second edition has been largely used again for this new edition.

The additional material includes five pages on the macroscopic theory of superconductivity, which seem to be exactly right for this type of book. There are three new and instructive pages on the part played by lattice defects. However, the opportunity of inviting the student, by way of example, to estimate the activation energy or orbital radius of ground or excited levels of a simple defect, by applying the theory of the hydrogen atom (expounded thirty pages earlier) in this slightly changed context, was unfortunately missed. Two interesting pages on chain molecules have also been added. The two remaining additions, three pages on matrices and one page on muscular action, may perhaps be regarded as of marginal value.

Faced by a new edition of a well-tried and highly successful text, such as this, a reviewer may well shrink from his traditional task of making known his personal wishes for a future edition. However, the student would probably welcome a brief account, possibly in tabular form, of the main properties of the elementary particles. Finally, in connexion with the second law of thermodynamics, it is often said that the entropy of an isolated system cannot decrease, and Professor Joos's statement to this effect has also persisted through the various editions. Yet a much stronger statement can be made by requiring the system to be merely adiabatically isolated. By moving parts of the enclosure, by mechanically operating partitions or levers from outside the enclosure, try as one may, the entropy of a thermodynamic system can still not be decreased. This point may be worth incorporating.

The text is lucid and comprehensive, and that it fulfils a real need is amply vouched for by the bare fact that it has been reprinted almost every year since 1940.

P. T. LANDSBERG

Thermodynamics of one-component systems. By W. N. LACEY and B. H. SAGE. (New York: Academic Press Inc.; London: Academic Books Ltd., 1957.) Pp. xi + 376. Price 64*s*.

The book is an example of the changing philosophical outlook in science. The choice of fundamental or undefined quantities is said to be arbitrary; and length, time, force and temperature are chosen for conventional reasons. The picture of system, boundary and surroundings—so necessary to an understanding of thermodynamics—is very clearly given; and an interesting feature is the account of the effect of friction furnished by giving certain properties to the boundary.

Part I is concerned with the system for its own sake; and Part II is concerned more with specifically engineering problems where work on the surroundings is obtained from the system. Turbines, steam engines, refrigerators, compressors and liquifiers are dealt with at a standard equal to that of a special degree in engineering. The approach by dealing with a steady flow of the working material through tubes is to be commended.

There is a unity about the book as a whole and a remarkable clarity of expression. However, a more adequate description of one or two of the machines, as, for instance, the turbine, might have been an asset. The authors leave out all reference to history, in the course of which it is seen how the concepts are created. This would have been the best way to show a present-day student why these concepts are arbitrary and why it is legitimate to choose the fundamentals in an arbitrary way. There are also no accounts of the classical experiments. Although these omissions limit the scope of the book, the authors are wise in making them, for their insertion would only lead to confusion.

The book is to be commended as a sound and clear logical exposition of its intended theme of helping science students to deal with the combination of thermodynamics and mechanics necessary for engineers.

F. I. WRIGHT

Servomecanismes: Theorie et technologie. By M. BONAMY. (Paris: Masson et Cie, Editeurs, 1957.) Pp. 284. Price 4200 fr.

There are two distinct parts to this volume, the first, consisting of three chapters, on general definitions and the influence of negative feedback on the fidelity of response; methods of analysing linear servo-mechanisms including some linear differential equation theory, Laplace transformation, and stability criteria; and on non-linear servomechanisms. This part is entirely theoretical but the various sections end with notes on practical potentialities.

The second part of the book is divided into two sections: electrical and hydraulic. The first contains three chapters which describe practical devices for control systems under the general headings: measurement, comparison and power amplification; whilst the second section contains much practical information on hydraulic relays, pumps and motors.

Presentation is clear and production good but this book appears to contain no information which cannot be obtained in works already available in English (or American!).

A. D. BOOTH

Comprehensive inorganic chemistry. Vol. 6: The alkali metals. By J. F. SUTTLE, and **Hydrogen and its isotopes.** By R. C. BRASTED. Edited by M. Cannon Sneed and R. C. Brasted. (London: D. Van Nostrand Co. Ltd., 1957.) Pp. viii + 234. Price 45*s*.

This series, to be completed in eleven volumes, is a reference work offered "to those engaged in chemical manufacture and development and to those in advanced studies in chemistry in institutions of higher learning." The volume under review contains an enormous amount of information, much of it in tabular and graphical form, many of the graphs being particularly valuable in that they reproduce the original experimental points and thus give the reader an opportunity to form a judgement about the reliability of the work. This mass of information is supported by references equally impressive for their number and variety; the reader who has been alerted by various obvious misprints may perhaps like to be assured that there really is a reputable scientific periodical called *Foote Prints*. Physicists will find much valuable information in the book, although its coverage of

chemical physics, structural chemistry and crystallography is slight. It is at its best on material which can be presented in tabular or graphical form—solubilities, phase relationships, numerical values of physical constants and the like—and is often disappointing in the more general discussion of chemical properties. Since the chemistry of the salts of the alkali metals is largely the chemistry of their anions, criticism ought perhaps to be restrained until all the relevant volumes of the series have appeared, but it is nevertheless disappointing to find (for example) that such an important substance as lithium aluminium hydride, which would receive at least half a dozen references in a modern textbook of organic chemistry, is dismissed in one short sentence.

The greatest fault of the book is its bad English. Authors endeavouring to convey to readers a large amount of information in a small space can succeed only by unremitting attention to their language, and it is only too obvious that in this book the authors have written many a sentence without stopping to think about its impact on the reader. The vagueness of "Many metals show the property of adsorbing hydrogen. The adsorption by most metals is not pronounced" is merely space-wasting and irritating, and sometimes when an author writes nonsense, as "The ionic radii are also equal to the interionic distances in ionic crystals," the informed reader can guess what he is trying to say, but what is one to make of "The selection of a constant was made as a result of several values in the vicinity of the selected value"? It is a great pity that an otherwise good book should have been spoiled in this way. E. G. Cox

Atomic energy in medicine. By K. E. Halnan. (London: Butterworth's Scientific Publications, 1957.) Pp. ix + 157. Price 15*s*.

Dr. Halnan's book is offered as an elementary account of the clinical uses of radioactive isotopes, the fundamentals of radiobiology and the treatment of cancer by high-energy radiations; it is intended for persons with little knowledge of physics or medicine. For all its faults, mistakes and misconceptions it contains a deal of interesting information on these topics. As a work of science it falls below the high standard displayed by other books from the same publisher. For example, Fig. 3 shows α- and β-rays from a radium source undergoing equal and opposite deflexions in the plane of a magnetic field between two objects labelled *positive magnetic pole* and *negative magnetic pole*; the caption describes how the rays are *split up by an electromagnetic field* and the accompanying text attributes their deflexion to *an electrical field*. The same paragraph tells us, concerning X-rays: "Roentgen soon discovered, in 1895, that they were waves (like light or radio waves)." Readers may be puzzled to see on p. 134 that "Cancer is still an uncommon disease (less than 20% of all deaths)" and, on p. 142, that "Cancer and heart disease are two of the major causes of death, especially of the young and middle-aged people expected to be still hard at work." J. M. A. Lenihan

Erzeugung sehr tiefer temperaturen. By H. Hausen. (Berlin: Springer-Verlag, 1957.) Pp. xii + 412. Price DM. 72.

This is one of the volumes in a series entitled: *Handbuch der kaltetechnik*, edited by Rudolf Plank. It deals in a comprehensive manner with the attainment of low temperatures, gas liquefaction, separation of gas mixtures and applications of gases in the liquid states. The author is a well-known authority in this field.

An indication of the contents may be formed by the following statement of some of the topics discussed: theory of liquefaction; thermodynamics; practical methods of gas liquefaction; separation of gas mixtures; theory of heat transmission; industrial practice; dehumidification; construction of low temperature equipment; working results and costs; properties of materials at very low temperatures; and application of liquefied gases.

Good descriptions are given of plants for very low temperatures such as the Kapitza, the Meissner and the Collins machines for the production of liquid helium.

Broadly the topics dealt with are those which come within the scope of the Low Temperature Group of the Physical Society.

The volume contains 307 illustrations and the line diagrams are excellent.

Many would welcome an English translation.

Ezer Griffiths

The science of engineering materials. Edited by J. E. Goldman. (New York: John Wiley and Sons, Inc., London: Chapman and Hall Ltd., 1957.) Pp. xv + 528 Price 96*s*.

This book can be recommended to every practising physicist, and could usefully be read by every student of physics. It attempts to answer the question "Why do materials behave as they do?" by applying the basic principles of solid-state physics to the explanation of the properties of materials. The treatment is almost wholly descriptive, with many well-chosen and well-drawn diagrams, and each article is an authoritative account, by an expert in that field, of the present state of knowledge of the physical reasons for the properties of some class of materials.

The materials considered include metals, magnetic, dielectric and semiconducting materials, high polymers, glass and cement, so that the book covers most of the materials used in engineering practice. Dislocation theory, and the various aspects of crystal imperfections are discussed in some detail, as also are the theories of semiconductors and of semiconductor devices, but throughout the book the emphasis is on the relation of these theories to the properties of materials as used in practice.

The book could appropriately be used for general reading as it forms a very readable account of current ideas on the properties of materials. But it could equally well be used as a textbook of applied physics for students specializing in solid-state physics, or as a supplement to the usual undergraduate course in properties of matter. A. E. De Barr

Electrostatics in the petroleum industry. Edited by A. Klinkenberg and J. L. van der Minne. (Amsterdam: Elsevier Publishing Co.; London: Cleaver-Hume Press Ltd., 1958.) Pp. 191. Price 40*s*.

This, so far as the reviewer is aware, is one of the first full-length books on the subject of "static" that has appeared in the English language. It deals, however, exclusively with one branch of the subject—that concerned with the separation of charge when a liquid of low electrical conductivity is disturbed in contact with other matter, and its relation to safety in the oil industry. This it does extremely well, with a precision and clarity that contrast strongly with that of most literature on "static" to be found in industrial journals. Indeed, the reviewer finds this book hard to fault.

After an introductory section of four chapters which, in effect, summarize the whole book (a novel scheme, but admirable where appropriate), and a further chapter ex-

pounding some of the elementary physics to be employed, the mechanism of charge separation at the interface between oils and other substances is discussed, followed by a consideration of the relevant properties of oils and how they are measured. Finally the results of large-scale tests are described with special reference to the effects of ionic impurities—natural or otherwise. These, we learn, are at once the nigger in the wood pile and the saving grace—nigger if present in minute amounts, grace if slightly more plentiful.

The editors are evidently enthusiasts for the MKS system of units; chemical readers may be a little surprised to find concentrations of solutions expressed in "kilomoles per cubic metre," but will no doubt be relieved after a moment's thought to realize that, apart from a negligible correction, these are numerically equal to their old friends "moles per litre."

There is no evidence in the book of any commercial secrecy on matters concerned with safety: the composition and concentration of the anti-static additives found most effective are given (but covered by patent). The presentation is excellent, in view of which the price can be considered moderate. P. S. H. HENRY

Solid state physics. Vol. 4. Advances in research and applications. Edited by F. SEITZ and D. TURNBULL. (New York: Academic Press Inc.; London: Academic Books Ltd., 1957.) Pp. xiv + 540. Price 96*s*.

As a result of the unmanageable flood of publications which deal with physical research the familiar review journals can no longer be relied on to provide up-to-date surveys of the literature on a level at once accessible to the non-specialist and useful to the specialist in a given topic. This has led to the appearance of a number of annual or semi-annual series which have a slightly ambiguous status, between journals and monographs, in the library shelves. *Solid state physics* is now established as one of the most useful of these semi-periodical polygraphs.

The present volume contains two substantial monographs, and three papers on mathematical and experimental methods. Känzig's article on "Ferroelectrics and antiferroelectrics" and Blatt's on "Theory of mobility of electrons in solids" occupy together some 360 pages. Ferroelectricity is a topic in which it is not easy to see wood for trees and Känzig provides a clear account of a great mass of material which complies quite well with phenomenological theory, though the detailed molecular theory is still in at least as unsatisfactory a state as the theory of other ordering phenomena. Megaw's recent book, however, is a better introduction for readers quite unfamiliar with the subject.

Blatt's article on a more coherent topic, abstracting from the complexity of experimental fact, is not only a good review of recent work but a complete monograph of its subject.

Woodruff on "The orthogonalized plane-wave method" describes one of the most straightforward and useful methods for calculating electron energy levels in solids, surveys its recent applications, and concludes with an extensive and helpful account of his own calculations on silicon, the results of which only were previously available.

Knox's bibliography of atomic wave functions is comprehensive and exactly what it claims to be, a set of references with an indication of the method used but no further discussion. It is a useful supplement to Hartree's recent book on the calculation of atomic wave functions.

Pfann describes "Techniques for zone melting and crystal growing" for the production of single crystals of great structural perfection and with controlled distribution of impurities. These methods have been enthusiastically developed for the transistor trade, but are likely to prove much more extensively useful.

This series should be in the libraries of all firms and institutions interested in the properties of solids, and of as many solid state physicists as can afford it. G. WYLLIE

Angular momentum in quantum mechanics. By A. R. EDMONDS. (New Jersey: Princeton University Press; London: Oxford University Press, 1957.) Pp. viii + 146. Price 30*s*.

The quantum mechanical theory of angular momentum is here developed on group-theoretical lines, and although the treatment has been made as simple as possible, and the exposition is generally lucid, the book will be beyond the scope of most experimental physicists. It will, on the contrary, be extremely useful to theoreticians, because not only does it give a clear and comprehensive account of the theory, but it provides also a practical manual of the associated computational methods applicable to a wide variety of problems in atomic, molecular and nuclear spectroscopy, nuclear reactions and angular correlations of successive radiations from nuclei. Tables and references are ample.

L. PINCHERLE

Quantum mechanics. By E. MANDL. 2nd ed. (London: Butterworth's Scientific Publications, 1957.) Pp. x + 267. Price 35*s*.

The present edition of Mandl's quantum mechanics is a very welcome addition to the many existing textbooks on this subject, especially since some improvements have been made and a new chapter on the relativistic theory of the electron has been added. As the author states in his preface the book is intended for a wide class of readers, including experimentalists, to enable them to perform quantum-mechanical calculations and to read the theoretical literature. It therefore concentrates on the basic principles of quantum mechanics and its mathematical formalism, without aiming at too much mathematical rigour. Applications are mainly given in the form of "exercises" for the solution of which generous hints are given at the end of the book. The reader is supposed to know some classical and quantum physics and special relativity theory, as well as calculus and vector analysis. The mathematically minded reader will have little difficulty in following the arguments and filling in the gaps, but experimentalists might find the going rather heavy and are likely to give up after the first few chapters. It would be a great help for those who wish to look up special items without willing to study the whole book if a uniform notation could be used throughout and a list of symbols provided with indications where the definitions are to be found.

R. FURTH

Russian–English atomic dictionary. By Dr. E. A. CARPOVICH. (New York: Technical Dictionaries Co., 1957.) Pp. 317. Price $12.

Dr. Carpovich has used his extensive lexicographical experience in compiling a glossary of over 23000 Russian terms pertaining to nuclear science and technology and related subjects. A fair number of these, however, consist of phrases whose meanings are obvious, and which could well have been omitted. All entries appear under the first word, even if it is a preposition, and cross-references are few. The only grammatical information provided is the listing of perfective aspects. The Russian alphabet is not given. A

curious feature is that alternative words in the Russian are separated by the *Russian* word for "or."

The book will be of little use except to an expert translator. He will find in it a number of terms not listed elsewhere, some useful distinctions between pairs of Russian words, and very full coverage of terms used in mining and crystallography. It is remarkably well printed in two foreign languages (the printer is Butow of Munich) and the binding is good. J. B. SYKES

Handbook of chemistry and physics. 39th ed. Edited by C. D. HODGMAN, in association with C. WEAST and S. M. SELBY, and in collaboration with many chemists and physicists. (Cleveland: Chemical Rubber Publishing Co., 1957.) Pp. xxii + 3213 on India paper. Price £5.

The review of the 37th edition [*Brit. J. Appl. Phys.*, **7**, p. 309 (1956)] referred to "this monumental handbook." The 39th edition is a further monument to the painstaking and affective work of the editors and their collaborators. The well-known shape is retained and, to quote the preface "there has been a deliberate endeavour . . . to exclude information which is controversial or which cannot be placed in a form as to make it readily usable." Included in the new material are tables of nuclear spin and moments; superconductivities of metals, atoms and compounds; energy, mass and velocity relations for the electron; magnetic properties of transformer steels. The pages are very thin but tough, and though a certain amount shows through from the other side they are, on the whole, very legible. The information ranges from antidotes of poisons to Laplace transforms. In most cases the sources of information are indicated. There is a particularly full section containing the main physical constants of a wide range of inorganic and organic compounds. If there are any physicists left who have never used the Handbook, they are advised to make its acquaintance without delay. Its scope is rather different from that of the new *American Institute of Physics Handbook*. F. A. VICK

Machinery's annual buyers' guide. 29th ed. 1957–58. (London: The Machinery Publishing Co. Ltd., 1957.) Pp. 993. Price 10*s*. 6*d*.

In addition to 728 pages of manufacturers' names listed under product headings and lists of their addresses and agents this volume contains French–English, German–English, Russian–English and Spanish–English glossaries. Also included are lists of professional and scientific institutions, trade associations, research organizations, etc., and some useful tables of technical data.

Elsevier's dictionary of electronics and wave guides in six languages. Compiled and arranged by W. E. CLASON. (Amsterdam: Elsevier Publishing Company; London: Cleaver-Hume Press Ltd., 1958.) Pp. 636. Price 90*s*.

This volume comprises a dictionary, giving in English, French, Spanish, Italian, Dutch and German, the terms in general use in the field of electronics and waveguides. There are 2056 numbered entries, each one comprising the term in English, a somewhat unnecessary code which is either "tron" (for electronics) or "wg" (for waveguides), a brief definition and the corresponding term in the other five languages each marked with the gender. The terms are in alphabetical order in the English language version. At the back are five glossary indices, one for each of the five languages other than English in which the terms are listed in alphabetical order for each language with a reference number corresponding to the entry in the main dictionary. Each section of this five-part glossary is marked by a thumb index.

It should be emphasized that the electronic terms contained in this dictionary refer mainly to the electronics of devices rather than to circuits. All the normal types of electron tubes, as well as semi-conductor devices, are included. The coverage is reasonably comprehensive and most useful. The format is pleasing, the printing clear, and the volume is attractively bound. M. E. HAINE

X-ray microscopy and microradiography. Edited by V. E. COSSLETT, A. ENGSTRÖM and H. H. PATTEE, JR. (New York: Academic Press Inc.; London: Academic Books Ltd., 1957.) Pp. xvii + 645. Price 118*s*.

This volume comprises the collected papers presented at a symposium on X-ray microscopy held at the Cavendish Laboratory, Cambridge, in August 1956. The 65 papers read are presented in full, although the volume includes discussions on only a few of the papers which is rather disappointing. The diagrams, however, are excellent and the volume is exceptional as a report on a symposium in that it is so well presented and has been published relatively soon after the papers were read.

The subject-matter includes the three major types of X-ray microscope, the reflexion type, the point projection type and the micro-radiography type. Papers on applications are also included, together with papers from almost all the well-known experts in the subject. The whole represents an up-to-date and comprehensive survey of this important, relatively new, and expanding field.

It is clear from the papers that considerable effort is being put into the improvement of basic apparatus and the development of the necessary theoretical background. It is also apparent that application of the techniques is proving of importance, particularly in the field of biology.

A number of closely related techniques discussed appear to offer considerable promise. M. E. HAINE

Observation and interpretation. Edited by S. KORNER. (London: Butterworth's Scientific Publications, 1957.) Pp. xiv + 218. Price 40*s*.

This is a distinguished series of essays, some by philosophers and some by physicists, presented and discussed at the ninth symposium of the Colston Research Society at Bristol.

The object was the laudable one of bringing together thinkers more particularly interested in the application of mathematics to the physical world, and the interpretation of quantum mechanics. In a very brief notice, it is impossible to do more than to select the contribution of Professor David Bohm on hidden variables as a subject of great potential interest, bringing to light (and perhaps to fruition) the abortive advance by de Broglie many years ago. The emphasis upon interpretation which underlies these papers is significant. F. I. G. RAWLINS

1957 Heat Transfer and Fluid Mechanics Institute. Preprints of papers. (California: Stanford University Press; London: Oxford University Press, 1957.) Pp. vii + 439. Price 68*s*.

In the space available it is possible to do no more than list the authors and titles of the papers contributed. They are:—

1. "The sound generated by interaction of a single vortex with a shock wave." By G. I. Ram and H. S. Ribner.
2. "On the instability of small gas bubbles moving uniformly in various liquids." By R. A. Hartunian and W. R. Sears.

3. "The fluid flow associated with the impact of liquid drops with solid surfaces." By P. Savic and G. T. Boult.
4. "Transformation of the compressible turbulent boundary layer." By Artur Mager.
5. "The unsteady laminar boundary layer of a wedge, and a related three-dimensional problem." By F. K. Moore.
6. "The laminar boundary layer near a sonic throat." By Donald Coles.
7. "Some problems of laminar boundary layer shock wave interaction." By Isaac Greber, Raimo J. Hakkinen and Leon Trilling.
8. "Cooling of solid surfaces with heat power inputs over 10^5 Watts/cm^2." By Daniel E. Bloxsom, Jr.
9. "The chemical kinetics of air at high temperatures: a problem in hypersonic aerodynamics." By Saul Feldman.
10. "Inviscid hypersonic flow over blunt-nosed slender bodies." By Toshi Kubota.
11. "General properties of normal shock waves at hypersonic speeds." By J. C. Bradley.
12. "An investigation of stagnation point heat transfer in dissociated air." By Peter H. Rose and F. R. Riddell.
13. "Heat transfer to surfaces in the neighborhood of protuberances in hypersonic flow." By M. H. Bloom and Adrian Pallone.
14. "Emissivity of high temperature air." By James Keck, Bennett Kivel and Tunis Wentink, Jr.
15. "Analysis of steady, finite-amplitude cellular flames." By G. H. Markstein.
16. "Ignition in the laminar boundary layer of a heated plate." By Donald A. Dooley.
17. "Ignition in transient flows." By D. Bitondo, N. Thomas and D. Perper.
18. "Experimental investigation of mass transfer by sublimation from sharp-edged cylinders in axisymmetric flow with laminar boundary layer." By W. J. Christian and S. P. Kezios.
19. "The heat balance integral and its application to problems involving a change of phase." By Theodore R. Goodman.
20. "The influence of solid body rotation on screen-produced turbulence." By Stephen C. Traugott and Hsuan Yeh.
21. "Some effects of isotropic turbulence on a pendulum at moderate Reynolds number." By William H. Schwarz and Stanley Corrsin.

Two invited lectures:—

"Fluid mechanical characteristics of large-scale meteorological problems illustrated by experiments." By David Fultz.

"Research in Continental Europe in engineering thermodynamics and heat transfer." By E. R. G. Eckert,

were given but are not included in this volume.

L. HOWARTH

Structure reports for 1951. Vol. 15. By A. J. C. WILSON, in association with N. C. BAENZIGER, J. WYART and J. MONTEATH ROBERTSON. (Utrecht: N.V. A. Oosthoek's Uitgevers Mij, for the International Union of Crystallography, 1957.) Pp. viii + 588. Price £10 10*s*.

The volume under review maintains the excellent standard of its predecessors and nothing more need be said by way of recommendation to those familiar with the work already done by A. J. C. Wilson and his section editors for the International Union of Crystallography. One innovation is the preparation of a separate index for the organic section, with classification first by number of carbon atoms and then by number of hydrogens. Less pleasing, but no doubt unavoidable, is the steep increase in price, calculated so that production need no longer depend upon the subvention which assisted earlier volumes. The sequence in the numbers of the volumes is interrupted (1950, volume 13: 1951, volume 15) to permit the insertion of a cumulative index, for the period 1940–1950, which will constitute volume 14. A casual scrutiny revealed a few misprints (page 98, "liqidus": page 304, legend to figure 1 should read ". . . on (0001) (III). . . ."), no doubt inevitable; but does the publisher's specimen page (492), reproduced in the advertising fly-leaf already widely distributed, have to carry the glaring misprint ". . . electron ditribution . . ."?

W. H. TAYLOR

Reports on progress in physics. Vol. 20. Edited by A. C. STICKLAND. (London: The Physical Society, 1957.) Pp. 568. Price 63*s*.

This twentieth volume includes nine reports: Plasma oscillations in metals, by S. Raimes; Theory of liquid helium (mainly concerning helium II), by J. Wilks; High energy protons, by A. E. Taylor; Theories of collective behaviour, by D. ter Haar; Strong and weak interactions of K-mesons and hyperons, by R. H. Dalitz; Microwave properties of solids, by D. M. S. Bagguley and J. Owen; Methods of high-speed photography, by J. S. Courtney-Pratt; Photographic sensitivity, by J. W. Mitchell; Theory and properties of solid argon, by E. R. Dobbs and G. O. Jones.

This group of reports not only maintains the individual standards which have come to be expected in these volumes but emphasizes once more the rapidity and scope of original "progress in physics" which is the continuing reason for their annual appearance. From this point of view the emphasis on collective phenomena on the one hand and Dalitz's exhaustive and masterly survey of the strange particle phenomena on the other are notable. The latter, in particular, occupying about one-quarter of the whole text, appears, one must remember, within ten years of the most primitive indications of the very existence of the strange particles.

A cumulative index of volumes 16–20 is also included.

J. G. WILSON

Theorie schallnaher Strömungen. By K. G. GUDERLEY. (Berlin: Springer-Verlag, 1957.) Pp. xv + 376. Price DM. 42.

It is pleasant to review a book which, I am convinced, will fill out an important area of the literature on high-speed flow. When in addition the author is so well equipped for his choice of subject as Dr. Guderley the result is a book which will certainly find a wide research and teaching public. The choice of German as its language will possibly limit its appeal here and in America but we may perhaps hope that an English edition will follow; certainly many less worthy books have been translated.

Space prevents more than a very brief survey of the contents. After an opening chapter, in which the general foundations are laid, the author goes on in Chapter 2 to derive the approximate form of the equation appropriate to transonic flow and to establish the transonic similarity law. Linear theory and its limitations are discussed in Chapter 3, and in Chapter 4 the few known exact solutions of the transonic equations are examined. The next two chapters are concerned with the hodograph form of the equations and its uses. Tricomi's equation is derived and particular solutions of it form an important study and Chapter 7, some 60 pages long, is devoted to them. The last three chapters

are concerned primarily with the flows engendered by sonic and near streams in two dimensions and in three dimensions when there is axial symmetry. Extensive use of hodograph methods is made in the two dimensional problems.

L. HOWARTH

Electric contacts handbook. 3rd ed. By R. HOLM, aided by ELSE HOLM. (Berlin: Springer-Verlag, 1958.) Pp. xviii + 522. Price DM. 52.50.

In 1941 Dr. Holm published a book entitled *Die technische Physik der elektrischen Kontakte* which was followed in 1946 by a second edition *Electric Contacts* published from Stockholm, in English. The present book, also in English, is enlarged and completely re-written: however, the authors regard it as a third edition of the original work.

The two authors have contributed much to the literature on electric contacts, firstly in Germany and later in the U.S.A. In this book they have collected what must be all the data published by other workers and have combined it into this authoritative textbook. The magnitude of this task may be judged from the length of the author and literature index: this alone occupies thirty-one pages.

The whole of the field is covered from the lightest to the heaviest contacts, stationary and sliding, and the association between electrical contact and mechanical contact, leading to frictional phenomena is discussed. The mechanism of load-carrying area, constriction resistance, tunnel and skin effects, wear and friction, lubrication, metal transfer on arcing, arc and spark suppression, and many other aspects are all fully discussed as well as many other items.

Electric Contacts Handbook will be a classic for those who want to study fully the phenomena taking place at any electric contact.

A. J. MADDOCK

Mass spectroscopy. By H. E. DUCKWORTH. (London: Cambridge University Press, 1958.) Pp. xvi + 206. Price 35*s*.

This latest addition to the literature on mass spectroscopy brings together a great deal of information which has previously been accessible only as scattered papers. Over 500 carefully selected references to the literature are in themselves sufficient to make the book of value to all students of the subject as well as workers in the field. The book is particularly easy to read in spite of the fact that the amount of information per page is large.

The first half of the book is devoted to a study of instruments and the descriptive and theoretical aspects are well balanced. The remainder of the book is devoted to applications and here clarity of description is maintained and the results quoted are set in their proper perspective in the various fields covered. One wishes, however, that Professor Duckworth had been able to devote more space to his subject, particularly to the wide variety of applications of mass spectroscopy. Those included give only a restricted coverage of the field and even so would benefit from a more detailed treatment.

J. H. BEYNON

Proceedings of the sixth international conference on spectroscopy. Edited by Prof. Dr. W. VAN TONGEREN, F. FREESE and E. H. S. VAN SOMEREN. (London: Pergamon Press Ltd., 1957.) Pp. ix + 663. Price £8 8*s*.

This volume, published as a supplement of *Spectrochimica Acta*, contains some 108 papers, a few in summary only, presented and discussed at an international conference held at Amsterdam in May 1956. The papers, printed either in English, French or German, originate from all parts of the world, including most countries in Western and Eastern Europe, the United States, Russia and China. About two-thirds of them are devoted to emission spectroscopy, with particular reference to analytical applications, dealing with flame spectroscopy, emission from arcs and sparks, spectrometry and instrumentation. Those seeking ready made analytical methods will not find them here, but they will find up-to-date articles on factors influencing analytical results, such as stability and temperature of light sources, electrical characteristics of discharges and the effects on them of ambient gases, the properties of carbon and graphite electrodes, photographic transformations, photo-electric recording, and emission of molecular spectra. The remaining third of the book is concerned with absorption and Raman spectroscopy, emphasis being on instrumental and chemical aspects. Attention is also given to the effects of environment on electronic energy changes, to absorption of powders and transient compounds and to polymorphism.

The standard of the papers is that to be found in a reputable scientific journal, with the advantage that they were all presented and edited simultaneously. In his opening address, the President of the conference expressed the satisfaction of his committee that a relatively high proportion of the communications were concerned with fundamental problems. He stated that the conference represented, in fact, the current situation in spectroscopic analysis where empiricism is being replaced by investigation, more particularly on conditions of excitation. His views are supported by the publication under review.

The price of the volume appears high, but it may be justified if one regards it as equivalent to two volumes of a scientific journal. Those who are directly concerned with applications of spectroscopy should certainly have access to it.

M. MILBOURN

The scientific papers of Sir Geoffrey Taylor. Vol. I. Mechanics of solids. Edited by G. K. BATCHELOR. (London: Cambridge University Press, 1958.) Pp. x + 593. Price 75*s*.

It is sufficient recommendation to state that this first volume of a series of four books contains all the papers written by Sir Geoffrey Taylor on the subject of the mechanics of solids. The editor has collected together forty-one papers and has arranged them in chronological order.

Scientists and technologists concerned with the study of the deformation of solids will know some of these papers almost off by heart and they will be familiar with most of them. There are, however, several papers, written for Government departments or advisory committees during the last war, which have not been published for unrestricted circulation before; these papers describe investigations carried out on the propagation of stress waves in solids resulting from the high rates of loading produced by impact and explosion.

A thorough knowledge of the work of Sir Geoffrey Taylor, particularly of his Dislocation Theory, is so important to those who wish to take part in or who wish to acquire an understanding of the developments of solid state theory that the publication of this book should be most welcome. The tasteful presentation does justice to the work it records, and it will make a valuable addition to both private and public libraries.

E. G. STANFORD

Mechanical testing of materials in the transition region between steady flow and failure

By A. Jobling, Ph.D., A.R.C.S., F.R.I.C., Ernest Oppenheimer Laboratory, University of Cambridge, and J. E. Roberts, B.Sc., A.Inst.P., Armament Research and Development Establishment, Sevenoaks, Kent

[*Paper first received* 3 *August*, 1956, *and in final form* 18 *November*, 1957]

An attempt has been made to overcome some of the defects of the standard methods of mechanical testing of materials. The new method, in which the deformation is brought about by attaching the specimen to a substrate, shows that when the final mechanical failure occurs, continuity is preceded by a region of disturbed flow in which the flow lines appear as a pattern of remarkable regularity, the direction of which is not that of maximum shear.

Materials such as dry powders, pastes, polymers and vacuum-deposited metals have been studied and show unexpected common features, e.g. fatigue and relaxation of work hardening by vibrations.

The complete examination of the mechanical properties of a given material requires its testing under conditions:

(i) in which the continuity of the sample is maintained throughout the test;

(ii) in which various disturbances to regular deformation (in general terms "flow lines") appear at some point in the test and the material ultimately fails.

Ideally one would like to have a sufficient understanding of the behaviour of the material to be able to predict its response under either set of conditions to any homogeneous mechanical action. That this perfect situation is generally far from being achieved is due, on the experimental side, to the limitations of present methods of mechanical testing, which are restricted both in the range of mechanical actions which can be applied to any one material and in the range of materials which can be examined by any particular action.

All standard testing methods for liquids employ laminar shearing movements of one type or another. Previous attempts to produce other types of rotational strain or irrotational shearing movements in liquids are not known to the authors. This limitation is not serious in the testing of Newtonian fluids but is important in the flow testing of viscoelastic liquids. It has been shown elsewhere[1] that in laminar shear of these materials, the main directions of strain velocity and stress diverge at sufficiently high values of the strain velocity, a complication which would not arise if the material could be tested in some irrotational movement.

Standard testing methods for solids employ either heterogeneous straining movements (bending tests, torsion tests) or some type of irrotational shear with cylindrical symmetry (simple axial tension or compression tests). A slightly greater degree of variability is introduced in the triaxial tests in which axial tension, compression or torsion of the sample is combined with an independently variable hydrostatic pressure. These limitations are probably not serious for materials and conditions which are adequately described by the classical elasticity theory, but they do become important in any testing involving large strains (rubber-like elasticity) or the appearance of flow disturbances preceding failure. In the study of rubber-like materials the need for a wider range of mechanical tests has already been recognized and largely met, notably by Treloar, Rivlin, and their co-workers.[2]

A further difficulty arises from the use at present of rigid grips or boundary members to hold the sample and impose on it the required deformation. If continuity is to be maintained between the grip and the specimen, then, in their interface, just where the applied action is being transmitted, no deformation occurs. The deformation produced in the interior of the specimen then depends not only on the mechanical action applied at the boundary, but also on the ability of the sample to transmit this deformation.

This paper describes the way in which some at least of these defects are overcome in a method of testing suggested by Weissenberg,[3] of which a preliminary account has been given elsewhere.[1]

TEST METHOD

In Weissenberg's method, a thin layer of the material to be examined is spread on a substrate which is itself deformable and situated in a main plane of the strain, i.e. a plane in which the *maximum* changes in length occur. The substrate can then be caused to undergo any one of a wide range of rotational or irrotational two- or three-dimensional shearing movements, the components of which in the plane of the interface are transmitted to at least the bottom layer of the sample under test, provided that the two materials adhere sufficiently.

If a straining action applied in this way is continued either in time or space to the point where failure of the specimen occurs, it is found for many materials that the final breakdown of continuity is preceded by a transition region of disturbed flow, in which the perturbations (furrows, ridges, or in general terms, flow lines) appear in a very regular pattern with a statistically well-defined periodicity, and in directions which can be related to the strain geometry of the particular movement. These features are amenable to quantitative measurement, and it should be possible by this technique to obtain much more information about the rupture process than has hitherto been available. There is no fundamental difficulty in observing the stresses and strains in the break portion, and work is now in hand for studying the possibilities of this.

A practical problem is the development of devices for producing the required movements in the deformable membrane. Even with a restriction to homogeneous strains, the complete range of available movements is very large, since one can prescribe independently the two principal strains in the plane of the substrate and their time development. Much of the experimental work to date has been performed with the

aid of a few very simple devices, each of which can produce a limited range of deformations. These are:

(i) balloons and inflatable membranes of various shapes and tensions;
(ii) membranes held in rigid grips which can be moved relative to one another, e.g. in parallel for laminar shear or apart for simple extension;
(iii) the flexible disk consisting of a sheet of some isotropic elastic material held under slight uniform tension in a ring which is inextensible along its circumference, but capable of deformation into an ellipse in the plane of the original circle. The strain geometry of this is considered more fully in the Appendix.

In most materials, failure can be produced either by a single, sufficiently large, deformation or by repeated application of a much smaller strain ("fatigue"). In the materials and tests used in the present work, failure was found to occur very frequently approximately along those directions which do not change in length in the particular deformation ("lines of zero elongation"), and the present experiments have therefore been largely restricted to movements in which these directions are well defined, i.e. to small strains.

The precise measurement of strain is conveniently made by observing the deformation of a reference grid printed on the membrane. Very small displacements can be accurately observed by the moiré technique.[4]

The problem of determining the stress developed in the sample during the test is more difficult. In all mechanical testing the ultimate aim is to be able to make a sufficient number of measurements to specify completely the angular distribution of stress at every point in the sample throughout the test. In one case, the testing of liquids in laminar flow with the Weissenberg rheogoniometer,[1] this has now been achieved, but in most mechanical tests, particularly those on solids, the stress in the interior of the specimen can only be calculated from the measured forces acting on its boundaries with the aid of certain assumptions which may or may not be justified. In the present method of testing, some at least of the components of stress in the specimen can be determined by observing the distortion of a reference grid on the substrate from the position it would have adopted under the same applied action had no test material been applied. It may also be possible to utilize stress birefringence effects in suitable cases.

The ideal requirements of the material forming the substrate are:

(i) there should be no diffusion into, chemical attack of, or swelling of one material by the other;
(ii) the two materials should "stick," i.e. maintain contact completely;
(iii) the deformation of the substrate may be plastic or elastic, but it must be uniform (i.e. without perturbations) in the region where the disturbances are appearing in the test sample.

For many experiments, the most convenient boundary material is good-quality latex rubber sheet. A rubber-like material made by fast-electron irradiation of high molecular-weight silicone oil (α of the order of 10^6 centistokes)[5] is also suitable for experiments not requiring very large strains, and has the additional considerable advantages of complete transparency and greater resistance to chemical attack. Many other materials should form suitable substrates since the main requirement is that they should deform uniformly throughout the desired range of movements. These may be very small as it is known that many metals and plastics, for example, fail under strains at least an order of magnitude smaller than those employed here to produce cracking in pastes and powders.

EXPERIMENTAL RESULTS

The behaviour of a wide range of homogeneous isotropic materials in a variety of deformations has been examined and the results will be grouped according to the orientations in the plane of the thin layer of the "flow lines" which have been observed or might be expected to appear. These may be related to:

(i) the directions of the principal strains;
(ii) the directions of maximum shear strain which lie at 45° to (i); and
(iii) the directions of zero elongation.

Failure along directions (i) or (ii) is well known in standard testing. The appearance of flow lines in a strip of aluminium in simple tension along direction (iii) has been reported by Nadai,[6] and the present series of experiments has shown this set of directions to predominate in a large group of materials and mechanical actions.

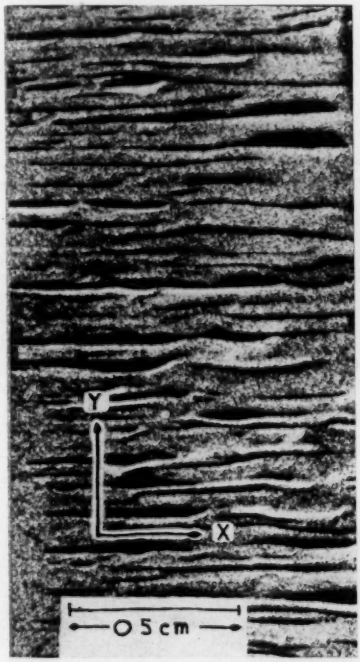

Fig. 1. Rupture of silicone bouncing putty at high rates of strain (simple extension)

(i) *Flow lines in the directions of the principal strains.* "Brittle failure" is usually understood to occur across a surface perpendicular to a direction of greatest extension and can readily be demonstrated by the thin-layer technique. Fig. 1 shows failure of this type in silicone bouncing putty

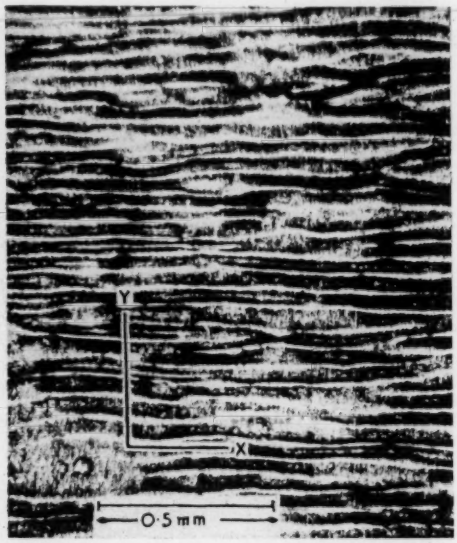

Fig. 2. Behaviour of a film of ethylcellulose on rubber in a small-amplitude oscillatory movement (simple extension and contraction)

which had been spread in a thin sandwich between two strips of rubber. A rapid lengthwise (x-direction) stretching caused regular cracking in a perpendicular plane. (Some relaxation has occurred in the brief time required to strip off one rubber support and position the sample for photography.)

A thin film of ethylcellulose deposited from solution on to a strip of rubber deforms evenly when the rubber is slightly stretched in the same way (simple extension). When the rubber is allowed to contract again regular wrinkles appear in the film perpendicular to the direction which had been extended (x-direction) (Fig. 2).

If the small-amplitude oscillatory movement is repeated a sufficient number of times, fatigue failure occurs ultimately by cracking parallel to the wrinkles.

(ii) *Flow lines in the direction of maximum shear strain.* The directions of maximum shearing strain in the plane of the film lie at an angle of 45° to the directions of the principal strains in this plane and are independent of their magnitudes. For "simple" (laminar) shear and the equivalent plane shear,[7] both of infinitesimally small amount, the directions of maximum shear correspond with those of the lines of zero elongation. In experiments with a wide range of materials subjected to deformations in which these two sets of directions do not coincide, the appearance of flow lines along direction (ii) has never been observed. This is very surprising in view of the widespread occurrence of "shear failure" in bulk tests.[6]

(iii) *Flow lines in the directions of the lines of zero elongation.* In a preliminary account of this work,[1] it has been shown that, in certain homogeneous deformations, failure in many powder aggregates and pastes occurs along certain well-defined and reproducible directions, which are definitely neither those of maximum shear strain nor of the principal strains. These directions have been interpreted as being those of the lines of zero elongation. The flexible disk technique described in the Appendix enables a whole series of such tests with different homogeneous straining actions to be condensed into a single test with a strain of known heterogeneity.

This test embraces all movements in which one major axis in the plane of the disk is expanded while the other is contracted (and *vice versa*, i.e. the two movements are 180° out of phase) and in which the ratio of the extensions in the two dimensions lies between 1 : 0 and 1 : 1. Fig. 3 shows a heterogeneous pattern produced in a lane of powdered Pyrex glass (− 200 mesh) spread along the radius of the flexible disk and subjected to a series of small-amplitude deformation

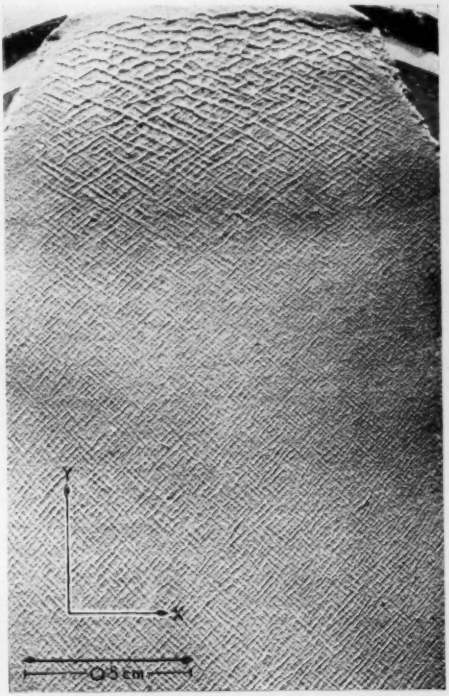

Fig. 3. Ridge and crack patterns in powdered glass spread along a radius of the flexible disk parallel to a principal strain and subjected to a small-amplitude oscillatory movement as in Fig. 5

cycles as illustrated in Fig. 5 (see Appendix). The pattern develops gradually with an increasing number of deformation cycles, thus providing a striking analogy with the phenomenon of fatigue in metals.

In Fig. 4, the observed angle between the flow lines and the width-wise dimension of the lane of powder is plotted as a function of the radial distance from the centre of the disk. In the same figure are also plotted the corresponding angles, calculated from observations with a travelling microscope, of the lateral and longitudinal changes in length in a similar

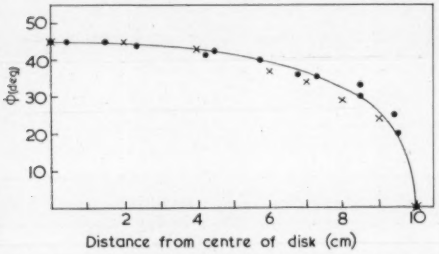

Fig. 4. Variation of the angle, ϕ, along a radius parallel to a principal strain

× = calculated from microscopic observations of the lateral and longitudinal movements at various points.
• = observed directions of cracks in cornflour powder in a pattern similar to that shown in Fig. 3.

experiment of small cells drawn on the rubber at various points along the same radius. The average experimental error in the determination of each set of angles is about $\mp 3°$, so that agreement between the two is reasonable. Experimental techniques are now being developed for the production of general homogeneous deformations, and it should then be possible to measure the directions of the flow lines with greater accuracy.

The observation of the flow lines in the direction of the lines of zero elongation is of great theoretical interest. One direct consequence is that the mode of failure, at least in these materials, must be partly dependent on the nature of the applied deformation since, in a straining movement in which both the principal directions of strain in the plane of the film expand or contract in unison, there are no lines of zero elongation and the material must then fail in some other way. Nadai[6] has remarked that "wide flat bars or strips machined from thin-rolled metal sheet when tested in cold-worked conditions in tension . . . break along an oblique plane perpendicular to the flat sides of the bar inclined at an angle of approximately 55° to the axis of the bar," clearly not a shear failure.

Nadai described this mode of rupture as depending on the shape of the specimen and occurring only in flat bars with a width: thickness ratio of 6 or 7 : 1, and it may be that the present technique, in which one dimension of the specimen is kept very small relative to the other two, predisposes failure to occur in this particular mode.

The whole question of whether or not the shape of the sample influences the mode of rupture in a homogeneous deformation (i.e. excluding notch effects and similar stress concentrations) is an open one, and should be further investigated because of its enormous practical and theoretical significance.

TIME-DEPENDENT EFFECTS: VISCOELASTICITY AND DILATANCY

In much of this experimental work, the time development of the deformation has been ignored. Fortunately, for many materials and powders in particular, it seems to be not very important. In the testing of viscoelastic materials, large time effects are well known. Thus the brittle failure of silicone bouncing putty (Fig. 1) occurs only at a sufficiently high rate of strain. In a slow deformation the material flows evenly, and no disturbances appear up to very large amounts of strain.

The other class of materials showing marked time-dependent behaviour is the dilatant pastes, for the study of which the present method is particularly suited. The term dilatancy is used here to describe not merely an increased resistance to shear with increasing rate of shear, but in the original literal sense of an increase in apparent volume accompanying shear. Thus a highly-dilatant cornflour/water paste remains mobile and deforms freely with the boundary up to very large amounts of strain if the action is slow enough. At a sufficiently high rate of strain, the surface of the material goes dry upon the imposition of a small strain. If the action is stopped at this point, rapid relaxation to a mobile fluid takes place;[5] if the apparently dry material is given a further small strain, rupture occurs, usually normal to the direction of maximum extension ("brittle fracture") if the sample is thick enough, and along the lines of zero elongation if the sample is thinly spread. Qualitatively similar results have been obtained with other pastes of very varied chemical and physical composition (e.g. metal powders, graphite in mineral oils; glass beads, powdered glass, powdered quartz in water; cornflour in glycol, glycerol, or decyl alcohol) but in most of these relaxation to a mobile fluid on cessation of shear does not occur immediately (type I) as in cornflour/water of suitable concentration. Sometimes it occurs spontaneously but much more slowly (type II), and sometimes spontaneous relaxation does not occur at all within a reasonable time, but the application of a small-amplitude oscillatory shear brings about a rapid return to the fluid state. Even the relaxation of type II materials is speeded by such mechanical vibration. Conversely, a dilatant material can, by the application of an oscillatory shear of suitable amplitude and frequency, be kept fluid throughout some shearing action under which it would normally dry out, become brittle and crack. This may have some application in any industrial process in which a dilatant material has to be pumped or spread. This relaxation effect calls to mind Freundlich's observations on "passive dilatancy,"[8] the phenomenon in which the paste is brought to a fluid state by tapping the containing vessel. Much more exact studies of mechanical relaxation can now be made since the effect can be produced by well-defined shearing movements, the type, amplitude and frequency of which can be controlled.

It is not proposed to enter here into a detailed discussion of dilatancy, but it may be remarked that the phenomenon appears to be more complex and of more widespread occurrence than is usually believed. The thin-film technique shows up clearly very slight traces of dilatancy, so that a change of surface texture on shearing has even been observed in many suspensions which are normally classified as thixotropic[8, 9] (e.g. cornflour/petroleum ether, powdered quartz/carbon tetrachloride). A surface roughening in shear is well known for many metals, and though the detailed mechanism here may well be different, it is interesting to note that relaxation (softening) of work-hardened metals (copper, aluminium, nickel, and some alloys) by the appli-

cation of small-amplitude mechanical vibrations has recently been claimed.[10, 11]

CONCLUSIONS

In order to examine completely the mechanical behaviour of a given material, one would like to be able either to subject it to any homogeneous straining movement, and to then have a complete knowledge of the angular distribution of stress at every point in the sample throughout the test (a kinematic test), or to prescribe completely any homogeneous state of stress and observe the resulting strain and its development in time (a dynamic test). It has been indicated that present standard testing methods fall far short of this ideal in many respects, and the present work should be viewed as an attempt to bridge the gap for kinematic testing.

The major advantages of the present method are that:

(i) it enables the range of deformations previously available for testing to be greatly extended. This development should assist the further study of the steady deformation and flow of viscoelastic and rubberlike materials, a topic not further considered in this paper, and is an improvement in any test on any material in which flow irregularities appear at some point in the test;

(ii) it affords improved control over the behaviour of the material in the plane of the film as evidenced by the remarkable regularity of the disturbance patterns which are produced, many of the features of which are amenable to quantitative measurement. The technique is particularly suited to the examination of the events preceding failure, since this is caused to occur not at one place, the exact site of which is not known beforehand, but regularly throughout the sample in an easily controllable manner;

(iii) it extends the range of materials that can be tested in any given deformation; for example, actions involving tensile stresses can now be applied to materials of little cohesion such as pastes or powders. As a result, striking similarities in the behaviour of materials of widely differing physical and chemical properties are now revealed (e.g. the generality of fatigue failure, dilatancy and mechanical relaxation effects, etc.).

The work so far has been restricted almost entirely to rubber substrates and materials which can be deformed on these by small easily-applied forces, but even with this limitation a wide variety of materials (powders, pastes, polymers, vacuum-deposited metals) can be investigated. In the extension of the technique to the stronger materials such as metals, in which there is most practical interest, the problems which arise are practical ones and not difficulties of principle.

In the interpretation of the results, attention has so far been concentrated on the *directions* in which the flow disturbances appear in materials which are initially isotropic, and their relation to the strain geometry. This is in contrast to the usual procedure which is chiefly concerned with the magnitudes of the various components of *stress* at failure.

If the material under test is initially anisotropic, the directional properties arising from the structure must be superimposed on those of the stress-strain geometry and either set may predominate. In crystalline substances it is probable that the structural anistropy is the more important, and deformation occurs along crystallographically important directions; whereas in polycrystalline materials, there may occur more complex effects in which microscopic flow along crystal planes in individual grains is accompanied or followed by the appearance of macroscopic flow lines along directions determined by the strain geometry.

ACKNOWLEDGEMENT

The authors are indebted to Mr. M. J. Egan for the original suggestion of the cycle of operations illustrated at the top of Fig. 5 (see Appendix), and for discussions with Dr. K. Weissenberg.

APPENDIX

Strain geometry of the flexible disk

The flexible disk consists of a sheet of some isotropic elastic material (e.g. rubber) held under slight uniform tension in a ring which is inextensible along its circumference

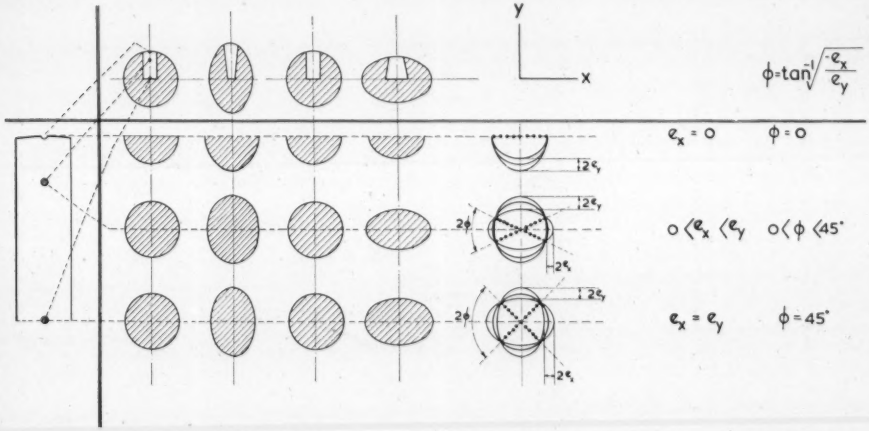

Fig. 5. Strain geometry of the flexible disk for an oscillatory irrotational movement of very small amplitude

but which can be deformed into an ellipse in the plane of the original circle. A device of this type with various geometrical figures printed on it has been used in demonstrations by Weissenberg[12] who has described the geometry of some unusual deformations that can be produced with it.

A group of irrotational straining movements can be produced simultaneously with the flexible disk by the cycle of operations illustrated at the top of Fig. 5. The disk is caused to pass through a series of elliptical shapes by alternate expansion and contraction of a diameter by an infinitesimally small amount. The strain so produced is not homogeneous over the surface of the disk. Though the two principal directions of strain in the plane of the disk are everywhere the same (and are here coincident with the x- and y-axes), the ratio of their magnitudes varies from point to point. This heterogeneity of strain is illustrated more clearly by reference to three unit circles situated along a radius of the disk, one at the centre, one at the rim, and the third intermediate between these two. These are shown in the magnified radial lane on the lower left-hand side of Fig. 5. Each circle is taken sufficiently small that the deformation over its area can be considered to be homogeneous. The deformations undergone by these unit circles during the cycle are illustrated in the lower centre of Fig. 5 and, on the right-hand side, superposition of these figures gives the orientation of the lines of zero elongation (dotted). At any given point on the surface, this direction is invariant only if the deformation is an infinitesimally small one; it then depends only on the ratio of the amplitudes, e_x, e_y, in the x- and y-directions and not on their absolute magnitudes according to the equation

$$\tan^2 \phi = -e_x/e_y$$

where 2ϕ is the minor angle between the lines of zero elongation. Since $-e_x/e_y$ varies continuously from zero at the rim to unity at the centre, the variation of ϕ is from 0° at the rim to 45° at the centre (compare Fig. 4).

REFERENCES

(1) EIRICH, F. R. (Ed.). *Rheology, Theory and Applications*, Vol. 2, Chap. 13 (New York: Academic Press Inc., 1958).
(2) TRELOAR, L. R. G. *The Physics of Rubber Elasticity* (Oxford: University Press, 1949).
(3) WEISSENBERG, K. *Bull. Brit. Soc. Rheology* (43), p. 6 (1955).
(4) BROMLEY, R. H. *Proc. Phys. Soc.* [*London*] *B*, **69**, p. 373 (1956).
(5) CHARLESBY, A. *Proc. Roy. Soc.*, *A*, **230**, p. 120 (1955).
(6) NADAI, A. *Theory of Flow and Fracture of Solids*, Vol. 1 (New York, Toronto, and London: McGraw-Hill Book Co. Inc., 1950).
(7) IBBETSON, W. J. *An Elementary Treatise on the Mathematical Theory of Perfectly Elastic Solids with a Short Account of Viscous Fluids*, Article 97 (London and New York: MacMillan and Co., 1887).
(8) FREUNDLICH, H., and JONES, A. D. *J. Phys. Chem.*, **40**, p. 1217 (1936).
(9) FREUNDLICH, H., and RODER, H. L. *Trans Faraday Soc.*, **34**, p. 308 (1938).
(10) POLAKOWSKI, N. H., and PALCHOUDHURI, A. *Proc. Amer. Soc. Test. Mat.*, **54**, p. 701 (1954).
(11) KENNEDY, A. J. *Nature* [*London*], **179**, p. 1291 (1957).
(12) WEISSENBERG, K. *Proc. First Internat. Congr. Rheology, Holland*, **1**, p. 29 (Amsterdam: North-Holland Publishing Co., 1948).

The time-constant of carbon composition resistors

By G. H. RAYNER, B.A., A.M.I.E.E., National Physical Laboratory, Teddington, Middlesex

[*Paper first received* 23 *October*, 1957, *and in final form* 8 *January*, 1958]

The inductance and capacitance of small composition resistors have been determined. It is shown that the time-constant can be obtained with high accuracy and that for a common type it does not exceed 1×10^{-9} H/Ω in magnitude for resistance values between 10 Ω and 1 kΩ and it is very close to zero for a value of 100 Ω.

The determination of the time-constant of resistors depends upon standard resistors with conductors of simple geometry for which the inductance and capacitance are calculable. The standard resistors at the N.P.L., range in value from 1 Ω to 10 kΩ, and have wires arranged in various ways: V-loops,[1] a coaxial wire in a tube and a helical coil in a tube.[2] If such resistors are not available, carbon composition resistors are sometimes employed to serve as a standard of zero time-constant since this is inherently small for such resistors. In view of this, and on account of correspondence,[3] arising from a recent paper,[4] an accurate knowledge of their time-constant was thought to be of interest.

The type of resistor investigated had an extruded composition conductor about 0·33 cm diameter, with squeezed on brass end-caps, and a ceramic sleeve overall; the outside dimensions were: length 1·2 cm, diameter 0·55 cm.

Resistors of this type have the same construction and dimensions for a very great range of values, the only difference being in the resistivity of the material of the composition conductor. It can be assumed therefore that the series inductance and the shunt capacitance are sensibly independent of the resistance value. Using this assumption, it is shown below that these resistors provide standards of which the time-constant may be known more accurately than the time-constants of the wire resistance standards.

CAPACITANCE

The capacitance has been measured for resistors of high enough value for the effect of the inductance l on the shunt capacitance, $-l/R^2$, to be negligible. The capacitance C of a single resistor was compared with the capacitance of a

parallel combination of five resistors, each having five times the resistance of the single one. The combination had a capacitance $5C$, and therefore a difference of capacitance $4C$ from that of the single resistor. This difference was measured with screened leads to the resistors, the screens being taken up to the body of the resistors and the screen capacitances eliminated; the value of C at both 1 and 10 kc/s was found to be 0·6 pF. The effect on the capacitance of leaving unscreened an inch of lead was not appreciable. An additional screen, in the form of a plate with a hole through which a resistor could pass, placed at the mid-plane of a resistor decreased the capacitance by less than 0·1 pF.

The capacitance of a smaller resistor, having a phenolic resin sleeve about 0·32 cm diameter, was also measured in this way and found to be about 1·2 pF. The approximate values of the permittivity of the sleeve materials were measured, that of the ceramic was five and that of the resin about twice as much. The capacitance of these resistors is determined largely by the permittivity of the insulating material surrounding them, and the electric field external to this makes only a small contribution to the total.

INDUCTANCE

The inductance of resistors in the range 10 to 40 Ω was determined, as for these values the effect of the shunt capacitance on the series inductance, $-CR^2$, is small, although not negligible. In order to achieve high precision it was necessary to arrange for two pairs of connexions to the resistor which provided current and potential connexions; these were disposed as shown in the figure. Measurements

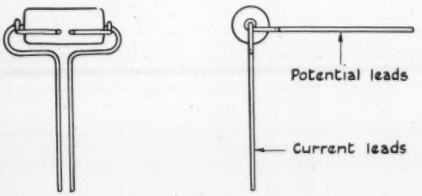

Resistor with potential and current leads

were made of the difference in the inductance of a single resistor and the inductance of a number of resistors in parallel, these being in a compact, symmetrical arrangement. The parallel combination had the same resistance as the single one, and was also provided with current and potential connexions. In one case a 10·6 Ω resistor was compared with three 32 Ω resistors in parallel, and in the second a 36 Ω resistor was compared with four 150 Ω ones in parallel.

The effects of inductance cannot be analysed as simply as the capacitance effects on account of mutual inductance. Thus, in addition to the self-inductance of the part of the current and potential circuits which is common to both, it is necessary to take into account the mutual inductance between the current circuit and the potential leads. Also, in the case of the resistors connected in parallel, there is mutual inductance that must be allowed for between each resistor and the others. The inductance L of N branches in parallel, each having a self-inductance l and a mutual inductance m to every other branch, is given by $L = [l + (N-1)m]/N$. The conditions for this relation can only be realized for two or three branches; for geometric reasons with four or more branches not all the mutual inductances can have the same value. However, their mean may be then taken as a reasonable value for m in the above formula.

If the four-terminal inductance of the single resistor R is denoted by l', then the effective inductance is $l' - CR^2$; similarly, the effective inductance of N resistors (each NR in value) in parallel is $L' - NCR^2$, where L' is the four-terminal inductance of the parallel combination. The difference of inductance is $l' - L' + (N-1)CR^2 = \Delta L$, say. A direct measurement of this difference of inductance, ΔL_m, was made at 10 kc/s using a double-bridge with capacitance ratio arms instead of the resistance arms used in Hartshorn's method.[5] Three-terminal air capacitors were used for these ratio arms, one was a fixed 1000 pF capacitor and the other was a variable capacitor to provide the ratio adjustment. The balancing and measurement of the inductance difference of the resistance arms was effected by a low range variable air capacitor connected aross the single resistor, this always being the more inductive.

The calculated values of the four-terminal inductances for the single resistor and for the parallel combination were obtained by computing the components arising from the various self- and mutual-inductances outlined above. The difference ΔL_c of the calculated effective inductances was obtained from these using the measured capacitance, and ΔL_c was compared with the observed inductance difference ΔL_m. The various quantities are summarized in the following table for the two values R of the single resistor.

Summary of inductance values

Resistance R		10·6 Ω	36 Ω
Calculated inductance l'	H $\times 10^{-9}$	6·9	6·9
Calculated inductance L'	H $\times 10^{-9}$	4·5(N=3)	3·8(N=4)
Capacitance term $(N-1)\,CR^2$	H $\times 10^{-9}$	0·1	2·3
Calculated inductance difference ΔL_c	H $\times 10^{-9}$	2·5	5·4
Measured inductance difference ΔL_m	H $\times 10^{-9}$	2·8	10·4
$\Delta L_m - \Delta L_c$	H $\times 10^{-9}$	0·3	5·0
Time-constant, $l'/R - CR$	H/Ω	$0{\cdot}7 \times 10^{-9}$	$0{\cdot}2 \times 10^{-9}$

In terms of the time-constants the differences between the measured and calculated inductance values correspond to less than 1×10^{-10} H/Ω in the case of the 10·6 Ω resistor and slightly more than this for the 36 Ω resistor. The smallness of this time-constant difference is satisfactory and it is reasonable to assume that the time-constants given in the table are correct to a similar accuracy, namely about 1×10^{-10} H/Ω. This is appreciably better than is usually achieved in standards having calculable time-constants; for example, Arnold[1] estimated the time-constant of his 1 Ω standard to be zero within $\pm 4 \times 10^{-10}$ H/Ω, while for the resistors in the range 100 Ω to 10 kΩ designed by Astbury,[2] the uncertainty is estimated not to exceed 20×10^{-10} H/Ω. The improvement in the accuracy which has been obtained with these carbon resistors is accounted for by the high resistivity of their material compared with the resistivity of normal resistance alloys; this enables a high resistance value to be obtained in a short element with a fairly large cross-section. These characteristics favour a small and accurately calculable value of inductance combined with a low value of shunt capacitance.

In conclusion it may be stated that a resistor, such as that

described, may be used as a standard with a time-constant not exceeding 1×10^{-9} H/Ω in magnitude, for values between 10 Ω and 1 kΩ; a resistor of 100 Ω is likely to have a time-constant very close to zero.

ACKNOWLEDGEMENTS

The work described above has been carried out as part of the research programme of the National Physical Laboratory, and this paper is published by permission of the Director of the Laboratory.

REFERENCES

(1) ARNOLD, A. H. M. *J. Instn Elect. Engrs*, (II), **100**, p. 319 (1953).
(2) ASTBURY, N. F. *J. Instn Elect. Engrs*, **76**, p. 389 (1935).
(3) LYNCH, A. C., RAYNER, G. H., and FORD, L. H. *J. Sci. Instrum.*, **35**, p. 36 (1958).
(4) RAYNER, G. H., and FORD, L. H. *J. Sci. Instrum.*, **34**, p. 190 (1957).
(5) HARTSHORN, L. *Proc. Phys. Soc. (London)*, **39**, p. 377 (1927).

Bonding optical components to metal mounts

By K. H. SPRING, M.Sc.,* Fighting Vehicles Research and Development Establishment, Chertsey, Surrey

[*Paper first received* 24 *October*, 1957, *and in final form* 3 *January*, 1958]

Various methods of bonding optical components to metal mounts, using synthetic resin adhesives, are described. In some cases a rubber interlayer is necessary to maintain resilience and prevent strain in the glass. A sandwich-type silicone rubber interlayer may be used to maintain resilience at temperature extremes. The tensile strength and shock resistance of the various types of bond are discussed, and a laboratory shock-tester suitable for small specimens is described.

Optical components such as prisms are usually held in position by small metal clips around their edges, sometimes with thin layers of cork to prevent strain or damage to the glass. This method of attachment is satisfactory for, say, hand-held binoculars, but is less so for the larger optical components in instruments which are likely to receive more severe shock, such as those mounted on military vehicles liable to be attacked by gunfire. The inertia of the component, in relation to the small area over which it is effectively held, may then cause it to break off and render the instrument unusable, perhaps at a critical time. The military ideal would be for all the optical instruments in a vehicle to remain usable for as long as the vehicle itself were fightable. A considerable advance towards this ideal has become possible in recent years owing to the introduction of synthetic resins which permit an optical component to be bonded to its mount over the whole common base area.

STANDARD TECHNIQUE

A technique for bonding, which has now become almost standard, was evolved mainly by the Admiralty Gunnery Establishment. The optical element is bonded to a steel plate using a rubber interlayer. Nilo 48 (by Henry Wiggin and Co. Ltd.), an alloy steel, is used to minimize differential expansion between steel and glass, and Gaco synthetic rubber (by G. Angus and Co.), which satisfactorily withstands the necessary bond-curing temperature, is used as a stress-relieving layer. Rubber of a thickness of $\frac{1}{64}$ in. and Shore hardness of 75° were found to give the most satisfactory results. The glass, steel and rubber are thoroughly cleaned with alcohol and the rubber is baked for four hours at 140° C, hanging from clips in an oven. All the components are then brought to a temperature of about 100–120° C—slowly, of course, in the case of large glass elements. The mating surfaces of glass and steel, and both sides of the rubber, are coated with a thin layer of Araldite type 1 (hot setting) cement (by Aero Research Ltd.). They are brought together under light pressure, taking care that as few air bubbles as possible remain. The assembly, usually held in a jig, is then baked for eight hours at 140° C, the lowest temperature at which satisfactory curing takes place. Considerable thought is usually needed to design a jig which holds the components with the necessary accuracy, but which does not strain the glass at any stage in the temperature cycle. Bonds produced in this manner have a tensile strength at room temperature of about 0·5–0·7 t/in.^{2}, i.e. of the same order as glass itself.

BONDING OF LARGE AREAS

Most prisms are sufficiently rigid to withstand distortion even when under strain, but this is not always true of large, comparatively thin, plates such as mirrors, for which the standard technique just described is unsuitable.

Front aluminized flats, $4 \times 2 \times \frac{3}{8}$ in. thick, were examined on the interferometer before and after being bonded on to steel plates with $\frac{1}{64}$ in. rubber interlayers. In most cases there was a slight change in fringe pattern. Much more serious distortion of the glass occurred, however, when the

* Now at Royal Aircraft Establishment, Farnborough, Hants.

Nilo steel plates were themselves attached to their supporting framework. This was so even when great care was exercised in flattening the steel plates, and in using a three-point support with spherical washers and seatings. Tests were therefore carried out with thicker interlayers, and Gaco rubber $\frac{1}{8}$ in. thick and of 75° Shore hardness was used. It was thought that with this thickness of rubber small distortions of the steel backing plate would not be transmitted to the glass plate.

To investigate this point, a glass plate 4 × 2 in. was bonded over its whole area, using a $\frac{1}{8}$ in. interlayer, to a steel plate 12 × 3 in. Provision was made for bending the steel plate longitudinally into a circular arc, the curvature of which could be increased smoothly from zero in either sense, concave or convex. Measurements of the curvature of both the steel and glass plates were obtained from observations with two autocollimators, as shown schematically in Fig. 1.

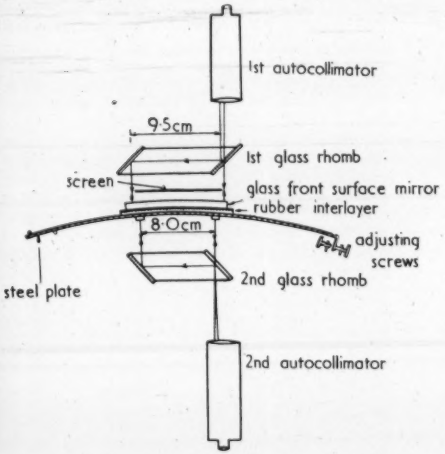

Fig. 1. Arrangement for determining curvatures of steel and glass plates. The curvature of the steel plate is greatly exaggerated

Interferograms of the glass plate are shown in Fig. 2 for five different conditions of bending of the steel plate. It will be observed that in the nominally unstrained state (*a*) the glass is slightly convex and becomes flatter on making the steel plate concave (*d* and *e*). From measurements of the fringe positions it is possible to deduce the average curvature of the glass plate under the five conditions, and these results are shown in Fig. 3.

Fig. 3 also gives the autocollimator results which are plotted to show the relation between the curvature of the glass plate and that of the steel plate. There is fairly close agreement between the slopes for the two sets of results, one of which is related to the average bending of the glass and the other to the difference between the ends. The glass must therefore have been bent almost into a circular arc. The interferograms show the smaller transverse curvature to be expected from elasticity theory. The autocollimator results pass through the origin, since only changes in curvature can be measured in this way.

It is apparent that, even for very small deflexions, the relation between the curvature of the glass and that of the steel is linear, the ratio of the two being 0·435. This means that a glass plate bonded in this manner will faithfully follow on a reduced scale the deflexions of the backing plate, the scaling factor depending, of course, on the thickness and elasticity of the glass and the rubber interlayer.

As a result of this investigation, the methods of support shown in Fig. 4 were designed for large plates. The front

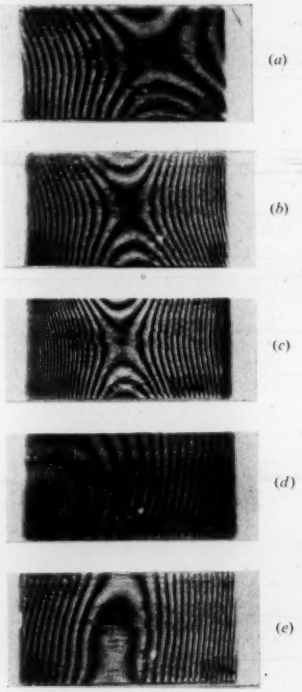

Fig. 2. Interferograms of stressed glass plate

(*a*) Steel plate unstrained.
(*b*) Steel plate 1 min. convex.
(*c*) Steel plate 2 min. convex.
(*d*) Steel plate 1 min. concave.
(*e*) Steel plate 2 min. concave.

surface reflector shown in (*a*) is bonded by a form of geometric line and point attachment and the semi-reflector in (*b*) is bonded along the edges. Both plates when mounted were found to be adequately free from strain, and they were also satisfactory as regards optical stability and shock resistance.

EXPERIMENTS WITH ARALDITE ADHESIVES

As part of a general investigation into strain-free joints, bonding tests have been made with several types of Araldite

adhesive. Tensile strength tests were made using glass specimens 1½ in. diameter (1 in.² area) bonded between steel arms of the same diameters, and shaped to fit an Avery tensile-test machine. These tests have been carried out over a range of temperatures. A laboratory shock-tester, described later, has been constructed to permit investigation of the behaviour under shock of small bonded specimens.

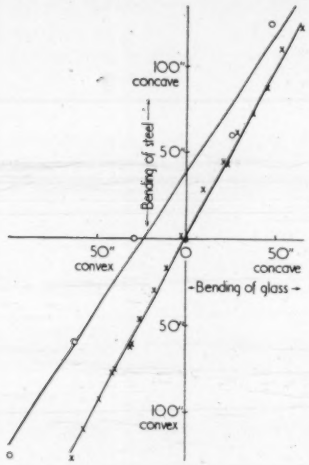

Fig. 3. Curvature of glass plate in relation to that of steel plate

○ = interferometer results; × = autocollimator results. Ratio on graph: glass/steel = 103/200. Base for glass = 9·5 cm. Base for steel = 8·0 cm. Actual ratio of curvatures:

$$\frac{\text{glass}}{\text{steel}} = \frac{103}{200} \times \frac{8{\cdot}0}{9{\cdot}5} = 0{\cdot}435$$

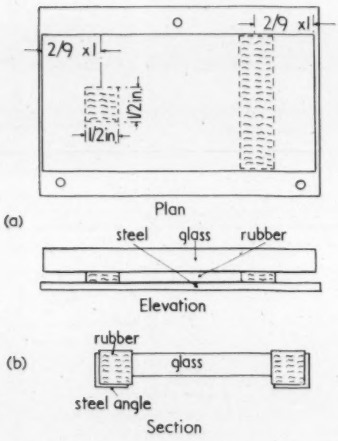

Fig. 4. Strain-free mounting of large glass plates

(*a*) Front surface reflector.
(*b*) Semi-reflector.

It would be a great convenience if a cold-setting adhesive could be used for bonding, as this would simplify procedure, and also reduce the risk of fracturing glassware from heat. Unfortunately, for Service applications the strength of the cold-setting adhesives falls off at high temperatures, but this may not be important for some uses.

Room-temperature tests with cold-setting Araldite 101 gave metal-glass tensile strengths of 0·80 t/in.², and with Araldite D, which is a later introduction, about 0·25 t/in.² Type D, however, loses less strength when hot. There was no significant difference in strength between joints made with polished glass and those with fine-ground glass. A slight increase in strength is obtained if the joints are baked at about 80° C for an hour, after cold setting, but they are relatively very weak during this phase.

At room temperature, with both type 101 and type D Araldite, failure of the joints sometimes occurred by failure of the glass, and examination of the type of fracture indicated that the glass was under strain. It was therefore decided to investigate the effects of Gaco rubber inserts in cold-setting glass-metal bonds. It was found that the highest strength was obtained when the rubber was first cleaned with acetone (or ethyl acetate) and baked for four hours (or left for twenty-four hours to dry out). Less satisfactory results were obtained if the rubber were crazed by acid pickling, with the intention of presenting a greater surface area. This may have been because, despite care in cleaning and baking, the rubber surface was still contaminated.

With Araldite 101 the tensile strength at room temperature of these rubber-glass-metal joints was about 0·2 t/in.², failure occurring at the rubber surface, and with type D about 0·1 t/in.² These figures show that the rubber insert reduces the tensile strength by a considerable factor and the resulting strength is too low for many applications. The increased resilience may, however, offset the loss of strength under shock conditions. In addition to the loss of strength at room temperature, the effects of high and low temperatures have also to be considered. A similar loss of strength factor occurs with hot-setting Araldite (type 1). The mean strength of metal-metal joints is 5·1 t/in.², whereas that with a rubber insert is 0·5–0·7 t/in.² (Glass cannot be used as the strength of the bond greatly exceeds the tensile strength of glass.)

Glass-metal joints made with cold-setting Araldite 102, to which about one-fifth by weight of powdered Gaco rubber had been added, gave strain-free joints, with a room temperature strength of 0·2 t/in.² A similar strength was attained with Araldite 15, with a rubber interlayer. This adhesive was mixed and applied cold, allowed to dry out and then cured hot, as for Araldite type 1.

The tensile strength of various types of Araldite-bonded joint over the Service temperature range of −40 to +60° C is shown in Table 1. "Type 1" refers to glass-Gaco rubber-metal joints made with hot-setting Araldite, type 1. Such joints show increasingly high strength below 0° C, owing to progressive freezing of the rubber. The high strength is, however, offset by the smaller resilience. "Type 101" in the table refers to glass-metal joints (without rubber interlayer) made with cold-setting Araldite 101, and "type D" to similar joints made with cold-setting Araldite D.

Table 1. *Strength of Araldite-bonded joints*

Temperature (°C)	Tensile strength (t/in.²) Type 1	Type 101	Type D
−40	1·8	0·8*	0·25*
−20	1·3	1·8	0·25*
0	0·75	1·2	0·25*
20	0·48	0·80	0·25*
40	0·40	0·40	0·20
60	0·40	0·12	0·20

* Denotes glass failure.

TESTS WITH "FLEXIBLE" ARALDITE

Towards the end of 1953 an experimental flexible form of Araldite was announced by Messrs. Aero Research Ltd. to be available for evaluation. The adhesive, No. 33/896, consists of three components, *A*, *B* and *C*, the proportions of *A* to *C* being kept constant, whilst that of *B* may be changed to vary the flexibility.

Initially, three mixtures were prepared, those having the maximum and minimum flexibility recommended by the manufacturers, and an intermediate mix. Subsequently a fourth mix was made and Table 2 shows the mixtures used, together with the mean tensile strength of glass-steel joints at various temperatures. Finely divided aluminium powder—as used in aluminium paint—was added to all the mixes to increase their viscosity when hot. This in turn increased the thickness of the adhesive layer, which was thought to be desirable to give greater stress relief in the joints, rubber inserts not being used. Curing was effected in all cases by baking at 100° C for three hours.

Table 2. *Flexible Araldite*

Flexibility	Proportions (by weight) *A*	*B*	*C*	*Al*	Tensile strength (t/in.²) −35° C	18° C	60° C
Minimum	100	50	6	10		1·8	1·5
	100	65	6	10	1·2	1·8	0·7
Intermediate	100	75	6	10		1·6	0·33
Maximum	100	100	6	10		1·0	0·13

As expected, flexibility is gained at the expense of strength, particularly at higher temperatures. The 100 : 65 : 6 (or 17 : 11 : 1) mix was thought to have adequate strength at all temperatures, as all joint failures occurred by at least partial rupture of the glass. Interferometric investigations showed that prisms cemented direct to Nilo plates with this mix showed little more strain than corresponding prisms bonded with a Gaco rubber insert and Araldite type 1.

Using aluminium powder as a filler the adhesive thickness was found to be about 0·004 in. Subsequently, powdered glass or silica has been substituted for the aluminium and with the mixture now used, $17A : 11B : 1C : 1{\cdot}5$ silica by weight, virtually strain-free glass-metal joints are obtained with a room temperature strength of about 2·1 t/in.² Firing trials have shown that at normal temperatures the shock-resistance of such joints is comparable with that of those made by the standard technique with Araldite type 1.

Glass-to-metal bonding with flexible Araldite is much less exacting than with Araldite type 1 as no rubber interlayer is used. Thus the usual steps of cleaning, drying, baking and coating of the rubber are eliminated. The curing process is also much shorter—three hours at 100° C compared with eight hours at 140° C. Since the glass does not have to be removed from the oven at 100° C for coating with adhesive, and the curing is at a lower temperature, the risk of fracture during processing is greatly reduced. For these reasons, much use has recently been made of flexible Araldite in the construction of prototype and other optical instruments.

TESTS WITH SILICONES

For Service use an optical instrument should be as resistant to shock as possible at temperature extremes as well as at normal temperatures. It was known that Gaco rubber lost its resilience progressively below 0° C and also during baking at temperatures above 150° C, although this is, of course, well above the highest temperature experienced in use. It was thought that silicones, as a general class of materials, deserved investigation because of their well-known property of tolerating temperature extremes.

When the investigation was started available information indicated that, whereas natural or the usual synthetic rubbers could not be bonded to glass, silicone rubber probably could be. It was also thought that Araldite-type adhesives would not adhere satisfactorily to silicone rubber. These two indications suggested that direct bonding of glass to metal with a silicone resin or rubber would be the most hopeful approach and some tests were made in conjunction with Messrs. Midland Silicones Ltd.

Tensile test specimens of glass steel bond were made with two different types of resin. In each case all surfaces were coated with resin, air-dried, assembled and then cured by placing in an oven which was raised to 200° C in two hours, and held at this temperature for a further two hours before cooling slowly. The mean tensile strength of joints made with resin MS993 was 0·33 t/in.² at 18° C, but for resin F.3044 was only 0·02 t/in.²

Some prisms and tensile test specimens were bonded by direct vulcanization of a silicone rubber layer (Silastomer 6–128) between the glass and steel. The parts were first dipped in primer MS602, air-dried and then steam vulcanized for five minutes at 25 lb/in.², followed by curing in an oven at 125° C for two hours. The glass parts were brought slowly up to temperature before vulcanization. The resulting tensile strength was only 0·04 t/in.² and the rubber layer was too soft and thick to ensure optical stability. Even so, such prisms stood up fairly well to firing trials, the low tensile strength being offset by the increased resilience.

It was appreciated that the maximum strength of bond between the Silastomer and glass or steel could only be developed by a combination of high pressure and temperature, but it did not seem advisable to exceed materially the values already used because of the risk of fracturing optical components. Tests confirmed that the tensile strength of bonds made with Silastomer and Araldite type 1 was very low—about 0·04 t/in.² It was therefore thought that the most hopeful method would be to prepare a three-ply sandwich of silicone rubber between steel plates, and to bond this between an optical component and its base, using, say, flexible Araldite. In this way it was hoped that the maximum bond strength could be obtained and the hardness and thickness of the Silastomer more closely controlled.

Initially a 4 in. square sheet was made, comprising two $\frac{1}{64}$ in. steel plates bonded with $\frac{3}{32}$ in. Silastomer 80 of about 50° Shore hardness. From this sheet were cut interlayers for tensile- and shock-testing, and for two prism assemblies for firing trials. The tensile strength appeared to depend on the region of the sheet from which the sample was cut, but was between 0·1 and 0·3 t/in.² As discussed in the next section, the results of the firing and shock-testing trials were very

satisfactory, and showed that the silicone sandwich had a substantial advantage over other methods. For these tests, flexible Araldite was used for bonding the sandwich to the glass and steel. Still better shock resistance may be obtained by bonding with Araldite type 1, using a very thin metal layer in the sandwich to prevent straining the glass.

Before the tests were undertaken, it was hoped that a fairly large sandwich could be made, from which individual requirements could be cut. However, it is now clear that small "tailor-made" sandwiches can be vulcanized more satisfactorily than large areas.

SHOCK TESTING

The resistance to shock of optical assemblies is usually studied in firing trials. The severity of attack is increased gradually by altering the calibre, velocity and angle of attack of the projectile which is fired at a structure to which the assembly is bolted. During the course of the experimental work already described the need was felt for a simple laboratory apparatus for shock testing, to supplement the results obtained from tensile tests, which give little direct information concerning resilience, and from firing trials, which are expensive and cumbersome.

The apparatus shown in Fig. 5 was designed and built for he purpose. It consists essentially of three parts, a "bomb"

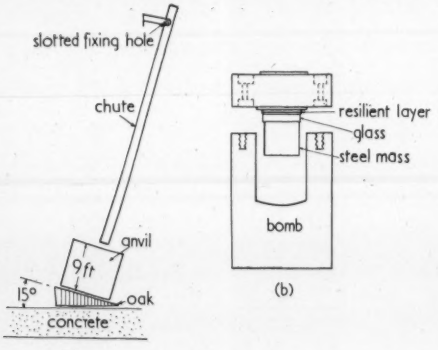

Fig. 5. Laboratory shock tester

(*a*) Chute and anvil (not to scale).
(*b*) Bomb, cap and assembly ($\times \frac{1}{4}$).

containing the assembly under test, a chute which guides the bomb during fall, and an anvil on which the bomb is suddenly brought to rest. The bomb is a steel cylinder, 3 in. in diameter and 4 in. long, with a cavity in one end. A steel cap, on to which a test assembly can be bonded, closes the end and is held in position with six screws. The total weight is about 9 lb. The chute is of machined 3 in. angle iron about 9 ft high and is inclined at 15° to the vertical. The anvil is a block of steel, of 230 lb mass supported on a 15° oak wedge, which in turn is supported by a mass concrete floor. Adjustments are provided on the chute so that its axis may be exactly normal to the striking face of the anvil; after sliding down and striking the anvil, the bomb then rebounds up the chute. Resilient material is arranged around the anvil so that no further damage is done after the primary shock. The height of drop is raised successively in steps of about 10% until failure occurs, which is readily detected by shaking the bomb.

A bonded joint can be subjected to a sudden load in either tension or compression, according to whether the bomb is dropped with the test assembly inverted or upright. The former method normally gives lower heights of failure and is mostly used. The load on a bond may be increased by adding an inertial mass of steel. Remembering that the density of steel is about three times that of glass, it is easy to calculate the thickness of steel required to simulate any given optical component.

Table 3 shows the height of failure of various types of optical bond on the shock tester, for shocks in tension. As a rough basis for comparison, the type of attack found necessary in firing trials to induce failure is also shown.

Table 3. *Comparison of shock resistance*

Type of assembly	*Adhesive*	*Height of failure, shock tester (ft)*	*Corresponding failure, firing trial*
¼ in. glass 1 in. steel	Flexible Araldite	1–2	2 pr. 30–60° 2000 f/s
¼ in. glass 1 in. steel Gaco interlayer	Araldite type 1	1–2	2 pr. 30–60° 2000 f/s or 6 pr. 60° 1600 f/s
1 in. steel, direct to cap	Araldite type 1	3	
¼ in. glass 1 in. steel 3-ply silicone sandwich	Flexible Araldite	4½	17 pr. 60° 2500 f/s
¼ in. glass 1 in. steel 3-ply silicone sandwich	Araldite type 1	6	

CONCLUSIONS

Glass-to-metal bonds of the highest strength are obtained with Araldite type 1 used in conjunction with a rubber stress-relieving layer. Flexible Araldite (used without a rubber interlayer) produces bonds of comparable strength, except at temperature extremes, using a technique which is less exacting than that for Araldite type 1. Bonds produced with the various forms of cold-setting Araldite introduce strain into all but the smallest glass components at normal temperatures and are of low strength at high temperatures. Interlayers of silicone rubber, suitable sandwiched, promise to maintain the strength and resilience of glass-to-metal bonds at temperature extremes. Special measures must be taken to prevent large, comparatively thin, components from being distorted when mounted.

ACKNOWLEDGEMENTS

The work described in this paper was carried out at the Fighting Vehicles Research and Development Establishment, and the author is indebted to his colleagues there for many useful discussions and ideas. Some aspects of the work are still being pursued. The paper is reproduced with the permission of the Controller of Her Majesty's Stationery Office, and Crown copyright is reserved.

The effective coefficient of friction for strings traversing cylinders transversely and slantwise

By C. MACK, M.A., F.Inst.P., and C. RUBENSTEIN, B.Sc., A.Inst.P., The British Cotton Industry Research Association, Shirley Institute, Didsbury, Manchester

[*Paper first received* 25 *October, and in final form* 2 *December*, 1957]

A formula is given for the effective coefficient of friction in terms of the constants of the power law of friction, the angle of wrap, and the on-going tension, for strings traversing cylinders transversely or slantwise. A table, which enables this coefficient of friction to be computed quickly and simply, is also given. Some experimental evidence for the accuracy of the formula for the slantwise case is described, while references to the experimental evidence in the transverse case are given.

It is now known that Amontons' law—that the frictional force is directly proportional to the normal load—does not hold in many cases. Over the last few years, many workers have found that, in fact, the frictional force is directly proportional to a power (less than unity) of the normal load.

It is, however, difficult to think in terms of the two constants involved in this power law, one of which has rather awkward dimensions, and in the important case of strings traversing cylinders (slantwise or transversely) the authors have defined an "effective" coefficient of friction, μ_E, which enables some well-known formulae, derived for cases where Amontons' law holds, to be applied when Amontons' law is not obeyed. (It should be noted that μ_E is not independent of the initial tension or of the cylinder radius.)

The authors certainly find it much easier to think in terms of this effective coefficient of friction than in terms of the original power law while, in addition, it shows the quantitative effects of this law quite clearly. Further, Table 1 enables computations to be carried out much more quickly and easily than by handling the power law directly.

Experimental evidence of the accuracy of the power law when strings traverse cylinders transversely has been given by various authors and is referred to here. However, in many practical cases, strings traverse cylinders in a slantwise manner and, in the last section of the present paper, some experiments carried out to verify theoretical calculations of what happens in such cases are described.

STRINGS TRAVERSING CYLINDERS TRANSVERSELY

It has now been established by a number of workers[1–9] that in many cases of sliding friction, where one surface is non-metallic, the frictional force F (per unit apparent area or per unit length, according to circumstances) is related to the normal load L (either per unit apparent area or per unit length) by a relation of the form

$$F = KL^n \tag{1}$$

where K and n are independent of L, but depend on the geometrical configuration involved (and on other factors such as the roughness, the temperature and the relative velocity of the contacting surfaces). The dependence of K and n on these factors has been discussed in some detail elsewhere by one of the present authors.[10, 11] [In reference (10), law (1) is derived from an hypothesis about the deformation of the asperities on the surfaces, assuming the validity of the adhesion theory of friction.]

In many cases of metal sliding on metal, n is unity and K (which is then usually replaced by the symbol μ and called the coefficient of friction) is independent of the apparent area of contact, and hence, of the geometrical configuration[10] and of the surface roughness, provided this is not excessive.[10, 12] [The exceptions include the cases of soft metals[13] (e.g. indium and lead) at relatively low normal loads, of harder metals at very low normal loads[14–16] and in the presence of thin film lubrication.[15, 17, 18]] Then equation (1) becomes

$$F = \mu L \tag{2}$$

which is one of Amontons' laws.

For a string traversing a cylinder transversely, where T_1, T_2 are the on-going and the off-going tensions, θ is the angle of wrap and the law of friction is given by equation (1), then it follows[11, 19–21] that

$$T_2^{1-n} - T_1^{1-n} = K(1-n)\rho^{1-n}\theta \tag{3}$$

where ρ is the radius of the cylinder. This equation has been verified experimentally in several ways, i.e. the tension T_2 has been measured:

(i) with ρ, θ maintained constant and T_1 varied [11, 20–22];
(ii) with ρ, T_1 maintained constant and θ varied[11]; and
(iii) with T_1, θ maintained constant and ρ varied.[23, 24]

When $n = 1$, equation (2) is satisfied and, taking the limiting form of equation (3) as $n \to 1$, we obtain the well-known equation

$$T_2/T_1 = \exp(\mu\theta) \tag{4}$$

Now it is not easy, given a set of values of T_1, T_2, θ, K, n and ρ satisfying equation (3), to determine the equivalent value of "μ" (which we shall call the equivalent coefficient of friction μ_E) such that T_2/T_1 is the same whether calculated by equations (3) or (4). In any case, an appreciable amount of computation is required to handle equation (3). However, we shall give a transformation of equation (3) into the form of equation (4) which gives a simple formula for μ_E, which shows clearly how T_2 depends on the other parameters and, finally, which, by means of the table below, enables computations to be carried out quickly and easily.

Dividing equation (3) by T_1^{1-n} and taking logarithms we have

$$(1-n)\log_e(T_2/T_1) = \log_e[1 + K(1-n)(\rho/T_1)^{1-n}\theta]$$

Hence, writing

$$\gamma \equiv K(\rho/T_1)^{1-n}; \quad \phi \equiv (1-n)\gamma\theta \tag{5}$$

we see that

$$\exp[\log_e(T_2/T_1)] \equiv T_2/T_1 = \exp[\mu_E\theta] \tag{6}$$

where

$$\mu_E = \gamma[(1/\phi)\log_e(1+\phi)] \tag{7}$$

By expansion, provided $|\phi| < 1$, we have

$$f(\phi) \equiv (1/\phi)\log_e(1+\phi) = 1 - \frac{\phi}{2} + \frac{\phi^2}{3} - \frac{\phi^3}{4} + \ldots \quad (8)$$

Values of this function are given in Table 1.

Table 1. *Values of function* $f(\phi) \equiv (1/\phi)\log_e(1+\phi)$

ϕ	0	0·1	0·2	0·3	0·4	0·5
$f(\phi)$	1·000	0·953	0·912	0·875	0·841	0·811
ϕ	0·6	0·7	0·8	0·9	1·0	1·1
$f(\phi)$	0·783	0·758	0·734	0·713	0·693	0·674
ϕ	1·2	1·3	1·4	1·5	1·6	1·7
$f(\phi)$	0·657	0·641	0·618	0·611	0·597	0·584
ϕ	1·8	1·9	2·0	2·1	2·2	2·3
$f(\phi)$	0·572	0·560	0·549	0·538	0·528	0·519
ϕ	2·4	2·5	2·6	2·7	2·8	2·9
$f(\phi)$	0·509	0·501	0·492	0·484	0·477	0·469

Simple approximations to $f(\phi)$ are: (i) $1 - (\phi/2)$ and (ii) $(1 + \phi/2)^{-1}$, the latter being quite close,

[thus for $\phi = 0{\cdot}2$ $0{\cdot}5$ $1{\cdot}0$ $2{\cdot}0$
$(1 + \phi/2)^{-1} = 0{\cdot}909$ $0{\cdot}800$ $0{\cdot}667$ $0{\cdot}500$].

It can be seen, from equation (7), that, for small values of ϕ,

$$\mu_E \simeq \gamma \equiv K(\rho/T_1)^{1-n}.$$

We now discuss the order of magnitude of the friction parameters so far as experiments to date have found. All the values to be quoted were obtained with the yarns traversing smooth glass rods at room temperature and at constant relative humidity.[11] The lowest value of $n = 0{\cdot}73$ was obtained with a continuous filament Nylon yarn running at a speed of 70 cm/s, while the highest value (0·98) occurred with a cotton yarn at a speed of 12 cm/s. The lowest value of $K = 0{\cdot}27$ was obtained with a spun Nylon yarn at a speed of 19 cm/s, and the highest value (1·00) was obtained with a continuous filament Nylon yarn at 70 cm/s.

If ρ is measured in cm and T_1 in g wt, ρ/T_1 will lie between 10^2 and 10^{-4} cm/g wt in all practical cases. Despite this large range in ρ/T_1, $(\rho/T_1)^{1-n}$ is a comparatively slowly varying factor as shown in Table 2, where the cases $n = 0{\cdot}90$ and $n = 0{\cdot}75$ are considered. In most practical applications outside textile technology, ropes, strings and yarns are of a "spun" nature where several strands are twisted together. For these, n usually lies between 0·89 and 1 and, as Table 2 shows, $(\rho/T_1)^{1-n}$ then will lie between 0·4 and 1·6. In some textile processes, however, monofilaments of synthetic materials (e.g. Nylon) are used and for these, n may be as low as 0·75 with, as Table 2 shows, a much larger practical range for $(\rho/T_1)^{1-n}$.

Table 2. *Typical values of* $(\rho/T_1)^{1-n}$

ρ/T_1	10^2	10	10^{-1}	10^{-2}	10^{-3}	10^{-4}
$(\rho/T_1)^{0\cdot10}$	1·59	1·26	0·79	0·63	0·50	0·40
$(\rho/T_1)^{0\cdot25}$	3·16	1·78	0·56	0·32	0·18	0·10

Finally, in handling equation (3), a point arises when the dimensions of K are considered. Now, for strings traversing cylinders, it is usual to take F and L as forces per unit length, and then K has the dimensions $[M\tau^{-2}]^{1-n}$, where $[M]$ represents the dimensions of mass and $[\tau]$ the dimensions of time. Consequently, conversion from one set of units to another is often a matter of some difficulty. If, however, we put $K \equiv \nu^{1-n}$ then ν has the dimensions $[M\tau^{-2}]$ and can be converted quite simply. In the authors' notation it can be seen, from equation (5), that $\gamma \equiv (\nu\rho/T_1)^{1-n}$. However, in the present work, values of K in $[\text{g wt/cm}]^{1-n}$ are quoted so that direct comparison with published values may be effected.

STRINGS TRAVERSING CYLINDERS SLANTWISE

In many practical cases, strings do not traverse cylinders in a transverse but in a slantwise direction, and the equations of the previous section cannot be applied without further consideration. However, one of the present authors has already considered the subject theoretically[25] and has shown that strings traversing cylinders slantwise have two important properties, namely:

(i) the tangent to the string at any point always makes the same angle (ζ say) with the cylinder axis (in other words, the string path is a helix); and
(ii) provided the power law of friction (1) holds then, if ψ is the angle between the projection of the off-going and on-going portions of the string on a plane perpendicular to the axis, relation (3) becomes modified to

$$T_2^{1-n} - T_1^{1-n} = K(1-n)\rho^{1-n}\psi\sin^{2n-1}\zeta \quad (10)$$

It can be seen by comparing equations (10) and (3) that the previous equations (5), (6) and (7) still hold, provided θ is replaced by $\psi\sin^{2n-1}\zeta$.

No experimental work on the frictional behaviour of strings traversing cylinders slantwise seems to have been published and the authors decided, therefore, to test equation (10) in a number of cases. To do this the following technique was used.

Starting with the string traversing the cylinder transversely, as shown in the figure, the cylinder was turned about the line bisecting the on-going and off-going portions of the string (in the figure this line is the co-ordinate axis OX).

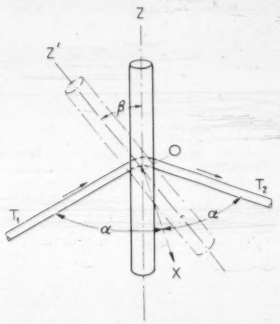

Illustration of the way in which ψ and ζ were varied

It can be proved that if the angle between off-going and on-going portions is kept fixed at 2α and that the rotation about OX is β, then ζ and ψ, as defined above, are given by

$$\cos\zeta = \sin\alpha\sin\beta, \quad \cos\psi = \cos\alpha/\sin\zeta \quad (11)$$

The angles between the cylinder axis and both the off-going and on-going portions are then the same. This may not appear so at first glance at the figure, but it should be noted that in the figure the angle between OZ' and the on-going portion (with tension T_1) is ζ and that between OZ' and the off-going portion (with tension T_2) is $\pi/2 - \zeta$.

The experimental arrangement was such that the lengths of the on-going and off-going portions were large compared with the cylinder radius, and then corrections due to the fact that these portions were not co-planar (except when $\beta = 0$ and $\beta = \pi$) were small. By altering α and β one can achieve any combination of ψ and ζ, though it is most convenient to keep α fixed and to vary β. Tests were carried out for a number of values of α, but most work was done at $\alpha = 75°$, since, from the point of view of testing equation (10), this value gave a fairly rapid change of $\psi \sin^{2n-1}\zeta$ with β (especially in the range $\pi/3 < \beta < 2\pi/3$). Again, small values of α are rather close to the purely transverse case, while for higher values of α, errors in measuring α itself become serious. T_1 was set to a predetermined value and the ratio T_2/T_1 was measured using the friction tester designed by Buckle and Pollitt.[26] A number of experiments were conducted with various types of yarn traversing glass rods and at various values of α.

Table 3 shows some of the results obtained. Here the calculated values of T_2 are obtained by using the values of n from transverse experiments[11, 24] and choosing those values of K (to two significant figures) which gave the best fit.

Table 3. *Observed and calculated values of T_2 (in g wt)*

Yarn	*Nylon monofilament*		*Spun Nylon*		*Spun viscose*		*Spun Nylon*		*Nylon monofilament*	
ρ (cm)	0·29		0·29		0·24		0·24		0·24	
n	0·76		0·89		0·89		0·89		0·76	
Best-fit K	0·61		0·31		0·32		0·31		0·69	
Transverse K	0·61–0·63		0·30–0·32		0·33–0·35		0·30–0·32		0·61–0·63	
α	15°		15°		75°		75°		75°	
T_1 (g wt)	10		15		20		20		12	
	T_2		T_2		T_2		T_2		T_2	
β	*obs.*	*calc.*	*obs.*	*calc.*	*obs.*	*calc.*	*obs.*	*calc.*	*obs.*	*calc.*
0	18·77	18·83	24·75	24·31	22·36	22·13	21·72	22·07	13·70	13·78
30°	18·90	18·89	24·75	24·39	22·42	22·21	21·72	22·10	13·98	13·96
60°	19·70	19·75	25·28	25·32	22·56	22·57	22·06	22·48	14·63	14·55
75°	20·00	20·24	25·90	25·90	23·02	23·03	22·84	22·93	16·51	15·37
90°	21·00	20·92	26·47	26·63	24·90	24·75	24·08	24·60	21·71	19·88
105°	21·52	21·50	27·30	27·40	30·46	30·85	30·04	30·42	26·58	26·02
120°	22·50	22·68	28·34	28·66	37·80	37·51	37·10	36·84	31·76	32·02
150°	23·10	23·47	29·39	29·57	51·76	51·89	50·70	50·42	—	—

The running speed of the yarns was 32·5 cm/s, the yarns were lubricated by their normal production finish, the room temperature varied between 66° and 68° F and the humidity between 64 and 66% r.h.

The agreement between observed and calculated values can be seen to be good in most conditions, except that, for Nylon monofilament at $\alpha = 75°$, $\beta = 75°$ and 90°, the calculated values were lower than the observed. In this particular experiment, too, the value of K was unusually high (0·69). However, the authors' conclusions are that equation (10) gives, in general, values of T_2 in close agreement with observed values.

REFERENCES

(1) Bowden, F. P., and Young, J. E. *Proc. Roy. Soc. A*, **208**, p. 444 (1951).
(2) Lincoln, B. *Brit. J. Appl. Phys.*, **3**, p. 260 (1952).
(3) Guthrie, J. S., and Oliver, P. H. *J. Text. Inst., Manchr.*, **43**, p. T579 (1952).
(4) Howell, H. G., and Mazur, J. *J. Text. Inst., Manchr.*, **44**, p. T59 (1953).
(5) Howell, H. G. *J. Text. Inst., Manchr.*, **45**, p. T575 (1954).
(6) Chapman, J. A., Pascoe, M. W., and Tabor, D. *J. Text. Inst., Manchr.*, **46**, p. P3 (1955).
(7) Pascoe, M. W., and Tabor, D. *Research*, **8**, p. S15 (1955).
(8) Lord, E. *J. Text. Inst., Manchr.*, **46**, p. P41 (1955).
(9) Mazur, J. *J. Text. Inst., Manchr.*, **46**, p. T712 (1955).
(10) Rubenstein, C. *Proc. Phys. Soc. [London] B*, **69**, p. 921 (1956).
(11) Rubenstein, C. *J. Text. Inst., Manchr.*, **49**, p. T13 (1958).
(12) Strang, C. D., and Lewis, C. R. *J. Appl. Phys.*, **20**, p. 1164 (1949).
(13) McFarlane, J. S., and Tabor, D. *Proc. Roy. Soc. A*, **202**, p. 244 (1950).
(14) Martin, A. J. P., and Mittelmann, R. *J. Text. Inst., Manchr.*, **37**, p. T269 (1946).
(15) Whitehead, J. R. *Proc. Roy. Soc. A*, **201**, p. 109 (1950).
(16) Wilson, R. *Proc. Roy. Soc. A*, **212**, p. 450 (1952).
(17) Barwell, F. T., and Milne, A. A. *J. Inst. Petrol.*, **35**, p. 455 (1949).
(18) Bowden, F. P., and Tabor, D. *J. Appl. Phys.*, **14**, p. 141 (1943).
(19) Howell, H. G. *Nature [London]*, **171**, p. 220 (1953); *J. Text. Inst., Manchr.*, **44**, p. T359 (1953).
(20) Lincoln, B. *J. Text. Inst., Manchr.*, **45**, p. T92 (1954).
(21) Lodge, A. S., and Howell, H. G. *Proc. Phys. Soc. [London] B*, **67**, p. 89 (1954).
(22) Baird, M. F., and Mieszkis, K. W. *J. Text. Inst., Manchr.*, **46**, p. P101 (1955).
(23) Lyne, D. G. *J. Text. Inst., Manchr.*, **46**, p. P112 (1955).
(24) Rubenstein, C. *J. Text. Inst., Manchr.* To be published.
(25) Mack, C. *Brit. J. Appl. Phys.*, **7**, p. 294 (1956).
(26) Buckle, H., and Pollitt, J. *J. Text. Inst., Manchr.*, **39**, p. T199 (1948).

A "super-elastic" single crystal calibration bar

By W. A. RACHINGER, M.Sc., Ph.D., Aeronautical Research Laboratories, Department of Supply, Box 4331 G.P.O., Melbourne, Australia

[*Paper received* 12 *November*, 1957]

Elastic strains of up to 4% can be attained in a copper–aluminium–nickel alloy in the form of a single crystal suitably heat treated. The high elasticity is due to a reversible martensite transformation induced by stressing. The methods of production and heat treatment of large crystals are described together with details of mechanical properties. The alloy can be machined by conventional methods. Suggestions are made for the development of other super-elastic alloys.

In order that electrical resistance strain gauges may be calibrated at strains of up to 2% it is necessary that the calibration bar to which the gauges are affixed must be strained to 2% and then unloaded on each calibration run. If the bar is to have a reasonable life it is necessary that it should be elastic, or very nearly so, up to 2% strain, since failure is to be expected when the total of the plastic strains suffered by the bar during cyclic straining reaches a value slightly in excess of the elongation at failure as measured in a static tensile test.

Since the limiting elastic strains of the best spring materials (e.g. phosphor-bronze, beryllium copper) are approximately 0·5%, the calibration procedure would necessitate over-straining the bar by 1·5% on each half-cycle. The ductility of these materials is very low (2%–5% elongation at fracture) and fracture of the bar would ensue after a few cycles. With more ductile, but less elastic, alloys the situation would be little improved and most materials would fail in 50 cycles or less.

During elastic deformation of most metals and alloys the application of stress causes changes in the interatomic distances, these changes increasing linearly with the applied stress. On release of the stress the atoms return to their original positions and the specimen assumes its original shape. This elastic behaviour continues until, at a certain strain, plastic flow takes place and the material acquires a permanent set.

There is one class of alloys in which the mechanism of deformation is quite different. These possess a high elasticity due to a martensitic transformation. It was alloys of this type which were considered to be possible materials for a calibration bar capable of high elastic strains.

MARTENSITE FORMATION AND SUPER-ELASTIC ALLOYS

A large number of alloys are known to undergo martensitic transformations. On cooling below a critical temperature (the M_s temperature) or stressing at a temperature slightly in excess of M_s, small lenticular regions of a new phase appear throughout the matrix. This new martensitic phase is generated by co-operative atomic movements in the parent matrix and with further cooling or increased stressing these lenticular regions increase in size and number. The martensitic phase has the same composition but a crystal structure different from that of the matrix.

On stressing, the martensite forms in such orientations as to generate strains which tend to relieve the applied stress. Accommodation stresses are set up due to the shearing movements involved in the transformation and also to the difference in specific volume of the parent and martensitic phases. In most alloys these cause plastic deformation of the matrix and consequently the martensite does not disappear on release of stress or on heating back to the M_s temperature.

There are, however, a few alloys in which the accommodation stresses are borne elastically by the matrix. In these, the martensite is both thermally and mechanically elastic. In order that these alloys should be capable of high elastic strains they must be in the form of a single crystal since in polycrystals much of the martensite formed at high strains is non-elastic. The alloys known to exhibit this phenomenon are gold–cadmium,[1] indium–thallium,[2] copper–gold–zinc,[3] and copper–aluminium–nickel,[4] the composition ranges over which the transformation takes place being very limited.

PRODUCTION OF A SUPER-ELASTIC ALLOY

(*a*) *Composition.* Of the four alloys mentioned above the copper–aluminium–nickel satisfies the requirements of both economy and corrosion resistance. The composition range over which the martensite transformation occurs with the M_s below room temperature is 1·5% to 3% nickel by weight, 14·5% aluminium and the remainder copper.[4] Preliminary experiments showed that alloys of composition 3% nickel, 14·5% aluminium, 82·5% copper were capable of high elastic strains and this composition was chosen for further work.

(*b*) *Melting and casting.* The constituent metals were electrolytic copper of 99·996% purity, aluminium of 99·995% purity and nickel of 99·9% purity. In order that melting temperatures should be kept to a reasonable level, a 50–50 copper–nickel master alloy was made by induction melting and used for all nickel additions to the melts. Melting was done in a graphite crucible heated in a gas-fired furnace. The cupro-nickel was dissolved in the molten copper and the aluminium added. The melt was cast into the form of a bar approximately $\frac{3}{4} \times \frac{3}{4} \times 18$ in. in a horizontal graphite mould pre-heated at one end to minimize pipe formation. The ingot was allowed to air-cool.

(*c*) *The growth of single crystals.* Single crystals were grown by slow cooling from the melt. The bar was embedded in alumina powder in an open-topped silica boat, the whole being heated in air in a platinum-wound horizontal tube furnace. When the bar was molten a pointed "tail" was drawn from one end of the melt and left exposed above the surface of the alumina. The temperature of the melt was raised to 1280° C, some 200° C above the liquidus temperature to aid dissolution of the impurities which might have acted as nucleation centres. The silica boat was then withdrawn from the furnace at the rate of 5 in./h. Solidification started at the pointed tail and ideally a single nucleus should have been formed here and grown throughout the bar. In many cases, however, a few crystals formed during the initial stages of solidification and usually one of these, by virtue of its orientation, soon outstripped the others in its growth and filled nearly the whole section of the bar. Nucleation sometimes took place at surface irregularities, but the growth of these nuclei could be restricted by ensuring that the solid-

liquid interface was convex towards the liquid. This was done by having a minimum of refractory packing at the "tail," allowing it to radiate freely and thus withdraw heat from the centre of the bar.

The macro-structure of the slowly cooled bar could be developed by etching in 50% nitric acid, although for reasons mentioned later, it is preferable not to etch at this stage. Single crystals of cross-section $\frac{3}{4} \times \frac{3}{4}$ in. and of maximum length 12 in. were produced. In this slowly cooled condition the alloy was rather brittle but could be machined by the usual methods of shaping, turning and grinding.

There was no marked tendency for zone refining to take place during the growth of single crystals. Typical analyses of the first-cooled and last-cooled ends of a bar are, respectively:

Copper 82·60% aluminium 14·36% nickel 3·04%
and copper 82·67% aluminium 14·25% nickel 3·08%

the nominal composition of the bar being:

Copper 82·50% aluminium 14·50% nickel 3·00%

(*d*) *Heat-treatment.* The heat treatment procedure is best understood by reference to Fig. 1 a psuedo-binary section of the copper–nickel–aluminium phase diagram at 3% nickel.[5] The alloy composition corresponds to the dotted ordinate at 14·5% aluminium.

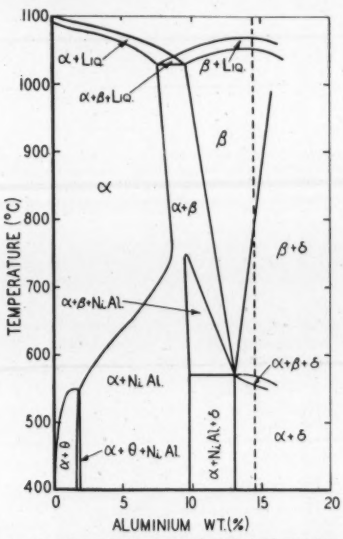

Fig. 1. Section of the copper–nickel–aluminium phase diagram at 3% nickel (after Alexander[5])

The as-grown single crystals possess an inhomogeneous cast structure. The heat-treatment necessary to bring them into a super-elastic condition is governed by three factors, namely:

(i) It is the high temperature β-phase in which the martensite transformation occurs. It is therefore necessary to homogenize the alloy by heating in the β-phase field and to retain the β-phase by quenching.

(ii) Since either cooling or stressing will cause martensite formation, the effect of internal stresses is to cause an increase of the M_s temperature. The thermal stresses produced during the quenching operation give rise to a gradient in M_s temperature through the cross-section, this being highest at the surface and decreasing with increasing distance below the surface.

If a specimen is quenched too rapidly the M_s temperature of the surface regions may be greater than room temperature. The specimen will then consist of a martensitic rim and an inner untransformed region, the M_s temperature at their junction being just below room temperature. On stressing, martensite would form firstly at this junction. As explained later this martensite would not be reversible since the M_s temperature here is not sufficiently far below room temperature. Such a specimen would not be elastic. For reversibility of the martensite it is preferable that the M_s temperature should be $-10°$ C.

Quenching stresses may be considerably reduced by ensuring that the bar is of the smallest cross-section possible and free of any sharp corners. Also the bar should be quenched slowly and in such a manner that some heat is extracted from the centre of the bar as well as from its surface. This is done by lowering the bar vertically into the quenching bath at a slow rate.

(iii) The limiting elastic strain of the alloy may be increased by hardening the β-matrix with a small amount of δ precipitate. As mentioned earlier it is necessary that the accommodation stresses around the martensite are borne elastically by the matrix. By hardening the matrix more martensite can be accommodated elastically and thus higher strains can be achieved.

Conditions (ii) and (iii) are satisfied by a slow oil quench from a temperature just above the $\beta/\beta + \delta$ boundary since δ precipitation occurs during such a quench. The heat-treatment adopted was homogenization for 15 h at 960° C, followed by furnace cooling to 800° C over a period of two hours. In quenching, the bar was lowered vertically into an oil quenching bath at the rate of approximately 3 ft/min.

During heat treatment the bar was packed in alumina powder to minimize high temperature oxidation. It was found that the composition change in oxidized regions was such as to cause an increase in the M_s temperature and thus these regions were martensitic at room temperature. This martensite could, under low stresses, propagate non-elastically along the surface of the bar and thus give rise to plastic deformation. For this reason it is preferable, as mentioned earlier, that the bar should not be macro-etched following the slow cooling from the melt since etching removes the protective aluminium oxide skin and renders the alloy more liable to high temperature oxidation. 30% nitric acid was used for macro-etching the heat-treated alloy. Any martensite present is readily distinguished since it etches to a brassy colour, whilst the β-matrix is copper-coloured.

(*e*) *Machining.* Following heat-treatment the bars were machined to remove surface irregularities and any surface crystals. If no martensite appeared on the surface of the bar on cooling to $-10°$ C, grinding, lathe turning and even milling or shaping could be carried out without fear of overstressing the bar and causing large-scale formation of martensite. Actually a very thin layer of martensite is formed at the worked surface but this does not propagate and may be removed by etching.

If the M_s temperature at the surface of the bar is greater

than $-10°$ C, the surface regions of high M_s may be removed by careful machining, light surface grinding being the most satisfactory method.

MECHANICAL PROPERTIES

Tension, compression and four-point bend tests were carried out on specimens cut from single crystal bars. A typical set of stress-strain curves is shown in Fig. 2. At

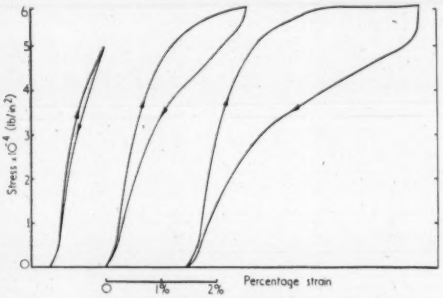

Fig. 2. Surface stress against surface strain curves in four-point bending

high strains the curve becomes almost horizontal and on unloading the stress must drop appreciably before the strain decreases, i.e. the stress required to form a particular martensite plate is greater than the stress at which this plate disappears. Microscopic observation has shown that during unloading the martensite plates disappear in the reverse order to their appearance during the loading cycle. From the few experiments carried out on specimens with various M_s temperatures, it seems that with increasing M_s there is an increase in the difference of the stresses required for the formation and the disappearance of the martensite. Thus the hysteresis loop becomes larger and, in particular, when M_s is close to room temperature the unloading curve falls almost vertically and the specimen acquires a large permanent set.

With properly heat-treated specimens the permanent set was always less than 1% of the maximum imposed strain. The nature of the curves varied with the amount of δ precipitate present and would, of course, be expected to vary with crystal orientation.

A single fatigue test was made. A cylindrical specimen was tested in plane bending, the surface strain limits being $\pm 2\%$. The fatigue life was 53 000 cycles. Under such conditions most materials would fail in 50 cycles or less.

POSSIBLE DEVELOPMENT OF SUPER ELASTIC ALLOYS

Although there are, at present, only four alloys known to exhibit elastic martensite transformations, more alloys could no doubt be developed from those known to undergo non-elastic transformations. The only requirements appear to be that the M_s temperature should be approximately $-10°$ C and that the matrix should be stiffened, either by solution or precipitation hardening, to such an extent that the accommodation stresses do not cause plastic deformation. It should be possible to adjust the M_s temperature and the strength of the matrix by alloying additions.

It is to be noted that the super-elastic behaviour need not be confined to room temperature. Either high or low temperature elasticity should be possible provided that the M_s temperature is correspondingly adjusted by alloying.

ACKNOWLEDGEMENTS

The author wishes to thank the Chief Scientist, Department of Supply, for permission to publish this paper. He also wishes to gratefully acknowledge the assistance of Mr. S. G. Glover of the University of Birmingham who made available the appropriate composition ranges of the copper–aluminium–nickel alloys.

REFERENCES

(1) CHANG, L. C., and READ, T. A. *Trans Amer. Inst. Min. Met. Engrs*, **191**, p. 47 (1951).
(2) BASINSKI, Z. S., and CHRISTIAN, J. W. *Acta Met.*, **2**, p. 148 (1954).
(3) RACHINGER, W. A. Unpublished work.
(4) GLOVER, S. G. Private communication.
(5) ALEXANDER, W. O. *J. Inst. Met.*, **63**, p. 163 (1938).

Journal of Scientific Instruments

Contents of the June issue

SPECIAL ARTICLE

The Physical Society's Exhibition—London, 1958. By A. J. Philpot.

ORIGINAL CONTRIBUTIONS

Papers

A cathode-ray tube analogue-to-serial digital converter. By J. Willis and M. G. Hartley.
An ultra-micro flame spectrophotometer. By D. Exley and D. Sproat.
The emission of light from electric discharges of microsecond durations in gases at atmospheric pressure. By D. P. C. Thackeray.
A design for a multi-channel infra-red spectrometer using transistor electronics. By D. G. Avery and R. C. Bowes.
A sensitive micrometer for measuring small displacements. By J. Norbury and D. Shewring.
Leak testing of vacuum plant by helium analysis. By E. Glueckauf and G. P. Kitt.

Laboratory and workshop notes

Calibrating manometer for pressure transducers. By J. R. Greer.
The preparation of pure sulphur for physical measurements. By R. J. Berry.
A smaller Haringx-type vibration isolating table. By J. A. Macinante.
Pot-core construction for a Hall multiplier. By D. J. Lloyd.
A constant volume pump for low flow-rates. By M. C. Corfield, S. Dilworth and G. Hines.
A vacuum evaporator for radioactive and toxic metals. By M. C. Inman and D. Quigley.
A filtration cut-off for use at low temperatures. By P. J. H. Carnell and G. W. A. Fowles.

NOTES AND NEWS

Correspondence

Obtaining rate thermal curves by a capacitor method. From B. Gregory and G. Bullock.

New instruments, materials and tools.

New books

THIS JOURNAL is produced monthly by The Institute of Physics, in London. It deals with all branches of applied physics (including theory and technique). All rights reserved. Responsibility for the statements contained herein attaches only to the writers.
EDITORIAL MATTER. Communications concerning editorial matter should be addressed to the Editor, The Institute of Physics, 47 Belgrave Square, London, S.W.1. (*Telephone:* Belgravia 6111.) Prospective authors are invited to prepare their scripts in accordance with the *Notes on the preparation of contributions*. (Price 2*s*. 6*d*. including postage.)
REPRODUCTION. The Institute of Physics is a signatory to The Royal Society's Fair Copying Declaration. Details may be obtained upon application from The Royal Society, London, W.1.
ADVERTISEMENTS. Communications concerning advertisements should be addressed to the agents, Messrs. Walter Judd Ltd., 47 Gresham Street, London, E.C.2. (*Telephone:* Monarch 7644.)
CLAIMS FOR MISSING JOURNALS. Claims from regular subscribers to this *Journal* for missing numbers will only be considered if received within 60 days of the date of mailing plus normal outward time of transit and time for lodging the claim. Losses attributable to failure to notify a change of address or to similar omissions will not be considered.
SUBSCRIPTION RATES. A new volume commences each January. The charge is £5 per volume ($14.25 U.S.A.), including index (post paid), payable in advance. Single parts, so far as available, may be purchased at 10*s*. each ($1.50 U.S.A.), post paid, cash with order. Orders should be sent to The Institute of Physics, 47 Belgrave Square, London, S.W.1, or to any bookseller.

Recent developments in electron microscopy*

By V. E. Cosslett, Ph.D., F.Inst.P., Cavendish Laboratory, Cambridge

The new high resolution electron microscopes have made possible the imaging of molecular lattices directly and of metal lattices by the moiré effects they give when superimposed. Dislocations can be observed both in such patterns and also in thin metal foils, in which their motion can be followed by electron cine-photography. In biology the trend is towards critical examination of the various stages in cutting thin sections—fixation, dehydration, embedding and sectioning—to control artefacts and to improve contrast. For this purpose the use of compounds of heavy elements as "electron stains" is being actively explored. Their value is illustrated by a study of the localization of nucleic acid in the cell nucleus and in sperm. Of two new departures in instrument design the first is the development of scanning electron microscopes: recording the scattered electrons shows the surface relief of solid specimens, recording the emitted characteristic X-rays shows the distribution of a particular element. In the second place, electron interference phenomena have been studied in some detail and the first tentative results obtained with a type of electron interference microscope, which would allow the measurement of inner potential as well as the thickness of very thin films.

Progress in electron microscopy has continued to be rapid. For purposes of convenience recent developments can be divided into those which exploit the high resolving power and high working magnification of the most modern type of instrument—these are mainly in metal physics—those which are concerned with refining and using for analytical purposes the established preparative methods at more moderate resolution—these are mainly biological—and thirdly, the exploration of some quite new electron microscopical instruments, of which the most important appear to be the interference and scanning microscopes. Any short review such as this is bound to be highly selective; only those developments have been included which promise to open up entirely new fields of research and, for the most part, they are illustrated by work in progress in this country.

DIRECT IMAGING OF MOLECULAR LATTICES

Until recently only the lattice structure of macro-molecular compounds had been made visible in the electron microscope. Hall[1, 2] obtained adequate resolution of certain planes in edestin and insulin crystals, of lattice spacing 70 and 40 Å respectively. The very high resolving power (less than 10 Å) of the new commercial models (Siemens Elmiskop; Metropolitan-Vickers EM6) offers the possibility of imaging the lattices of small-molecular compounds. Best results are obtained from crystals in which planes containing a heavy concentration of scattering centres are parallel (or almost so) to the incident electron beam. Menter[3] selected the metal phthalocyanines for investigation, in which the (201) planes are heavily loaded with metal atoms (Cu, Pt, Au, Ni) and are disposed almost normal to the extended faces of the crystals, which have a ribbon habit. He obtained excellent resolution of the copper and platinum salts and even of the simple phthalocyanine, which contains hydrogen in place of the metal atoms. This result suggested that electron diffraction rather than simple image formation was involved and detailed investigation has shown this to be correct. Independently of Menter's work, Niehrs, in von Laue's laboratory, had been investigating theoretically the possibility of resolving crystal lattices, using the dynamical theory of electron diffraction. He found[4] that it should be possible, but predicted also a dependence of "visibility" on crystal thickness which would allow quite thick layers (of the order of 2000 Å) to be resolved. So far, the results of neither Menter nor Neider[5] have supported this prediction and its detailed investigation will provide an interesting test of the dynamical theory.

The resolution of a microscope for a line object is three or four times better than that for point-point separation, on which the classical definition and test of resolving power are based. Efforts to resolve still finer lattices have, therefore, continued and Menter and Bassett[6] were able to get a clear picture of the (020) planes in molybdenum trioxide which have a spacing of only 6·9 Å (Fig. 1, p. 273). It is to be expected that spacings of 2·5–3 Å will be resolved, in existing electron microscopes, if crystals can be prepared in suitable orientation and can be kept free of the blanketing layer of carbonaceous material which only too readily forms on any surface exposed to an electron beam. That sufficient contrast would be provided, by what would be only a few rows of atoms, has been shown by the calculations of Haine[7] on electron scattering.

PATTERNS FROM CROSSED LATTICES; OBSERVATION OF DISLOCATIONS

In the experiments just described, the crystal presents in effect a plane grating to the electron wavefront. Some years ago very similar line patterns, but with much larger spacing, were observed independently by Mitsuishi, Nagasaki and Uyeda,[8] Hillier[9] and Farrant.[10] They occurred where thin lamellar crystals overlapped, as in clays, and, after some difference of opinion as to their origin, were correctly interpreted by Dowell, Farrant and Rees[11] as moiré patterns arising from diffraction by two superimposed gratings. The pattern spacing was shown to be a multiple of that of the parent lattices, depending on their relative orientation. Fig. 2 (p. 273) shows two crystals of molybdenum trioxide in crossed orientation, giving narrow spacing. The fact that the complementary pattern appeared clearly in dark field (Fig. 6 of Ref. 12) indicated that it is essentially a diffraction phenomenon. Mathematically presented, the pattern depends on the mutual positions of the scattering centres in the upper and lower lattices, and thus is related to the Patterson distribution familiar in X-ray crystallographic analysis, as shown in detail by Dowell, Farrant and Rees.[12] For crystals in almost parallel orientation they find that the fringe systems are, in fact, the terms of the Patterson series. The pattern is more complicated, but conforms to the same rules, when the two lattices are not identical. The possibility thus presents itself of crossing a crystal of known with one of unknown structure, and deducing information about the latter from the moiré pattern, which would be of great help to X-ray analysis.

It was then shown by Hashimoto and Uyeda[13] that, in

* Based on a lecture delivered to The Institute of Physics Convention, Oxford, on 12 July, 1957.

such crossed lattices, defects in one of them would still appear in the resultant pattern. This result was at once confirmed, and investigated at much higher resolution by Pashley, Menter and Bassett.[14] They obtained superimposed lattices of the same form but with slightly differing spacing, by epitaxial growth of one metal evaporated on to another—platinum or palladium on gold, for instance. The moiré spacing is then simply a beat effect: if one lattice spacing differs from the other by 5%, they reinforce at every twenty spacings of the smaller lattice. That a defect, such as an edge dislocation, in one lattice would be evident in the resultant pattern was shown by means of an optical analogue. The electron micrographs provided many examples of dislocations which had arisen during growth of the crystals (Fig. 3, p. 273). Edge dislocations had occasionally been observed by Menter[3] in crystals of phthalocyanines, but in these metal films they occur much more frequently and in circumstances where their initiation and behaviour (under thermal treatment, for instance) is more open to experimental study.

DISLOCATIONS IN MOTION: ELECTRON CINE-MICROSCOPY

It has also proved possible to identify dislocations in metals and to follow their movement under stress, by direct electron microscopy on foils thinned by beating and etching. In aluminium, Hirsch, Horne and Whelan[15] found that the individual dislocations forming sub-grain boundaries were clearly visible as dots, lines and networks. The unexpectedly high contrast of a single dislocation is explained as due to distortion of the surrounding lattice over a distance of the order of 100 Å, which results in more (or sometimes less) loss of electrons from the imaging beam by diffraction outside the objective aperture.[16] When such a plastically deformed foil is locally irradiated (over an area of a few square microns) by an intense electron beam, the dislocations are seen to move in well-defined directions, leaving slip-traces behind them. Motion appears to be produced under the stresses due to the thermal gradient in the foil. The illuminating system of the Elmiskop is so efficient that the image on the fluorescent screen at ×40 000 magnification is bright enough for external cine-photography at the normal rate of sixteen frames per second on high-speed film. In this way continuous records have been made of the complex behaviour of dislocations of different types: slow and rapid motion, break up of sub-grain boundaries, nucleation and annihilation, and cross-slip. Many of the predictions of dislocation theory have been confirmed qualitatively and some quantitatively, such as the relation between the number of dislocations per unit length of a low-angle boundary and the angular misorientation of the adjacent sub-grains, as determined by electron diffraction. The average spacing of such dislocations lies between 100 and 200 Å, the angular misorientation is of order 1°. The phenomena are particularly simple in stainless steel, where the constraints are greater than in aluminium. Rows of dislocations piled up against a grain boundary are frequently found (Fig. 4, p. 274), and the separation of a dislocation on the (110) plane into two partial dislocations on the (211) and (121) planes, with formation of a stacking fault between them, has also been observed as predicted by Heidenreich and Shockley.[17] A sequence of three shots, showing the formation and subsequent collapse of such extended dislocations is shown in Fig. 5(*a*, *b*, *c*, p. 274). The pronounced differences in behaviour between aluminium and stainless steel have been correlated with the difference in stacking fault energy by Hirsch, Horne, Whelan and Bollmann.[18] In both metals a great variety of phenomena have been observed, which remain to be elucidated by applying controlled stress at known temperature. A valuable experimental technique is thus available for checking and amplifying the theory of dislocations, which hitherto has lacked dynamical verification. At the same time, the demonstration of the possibility of filming continuous phenomena in the electron microscope is leading to the exploration of other transformations, such as the growth of "whiskers" and more complex changes which occur in microcrystals of silver and silver halides.[19] It is not too much to say that the study of the solid state has found an unexpectedly powerful tool in high resolution electron microscopy.

PROBLEMS IN BIOLOGY

In the biological field the current trend is not so much towards utilizing the high resolving power of the new electron microscopes as to stressing the need to perfect and make analytical use of existing methods of specimen preparation. The development of microtomes capable of cutting sections as thin as 100 Å has opened the way to a great deal of exploration of the micro-anatomy of tissues and indeed of micro-organisms such as bacteria and the larger viruses. The situation can only be likened to the great impetus to research provided by the perfection and general availability of the high-powered optical microscope in the second half of the nineteenth century. The subsequent development, in the 1890's, of a critical attitude to the possibility of artefact formation during specimen preparation and then of a systematic search for specific staining reagents, are now being paralleled in electron microscopy. They may best be illustrated by reference to a particular problem—one of the most interesting in its biological significance—the microstructure of the cell nucleus. Although a most complicated (and somewhat unexpected) wealth of detail has been demonstrated in the extra-nuclear region, the cytoplasm, thin sections have so far revealed little differentiation in the nucleus, where it is well known from ultra-violet and phase-contrast microscopy that well-defined chromosomes are present during at least part of the life-cycle. Comparison of adjacent thick and thin sections of locust spermatocyte, in the ultra-violet and electron microscope respectively, has recently shown that this is not due to any disruptive effect of the fixative usually used (osmium tetroxide). The chromosomes are as well defined (in ultra-violet) as after use of the fixatives usual in optical microscopy, but the nucleus remains featureless in the electron image although neighbouring mitochondria are clearly visible.[20] It appears, therefore, that the constituents of the nucleus and in particular those containing nucleic acid, do not take up osmium tetroxide in appreciable amount, a conclusion independently confirmed by Bahr.[21] Better differentiation is obtained with formalin fixation (Fig. 6, p. 274), but the chromosomes are still only faintly visible, indicating that their electron scattering power is little different from that of the rest of the nucleus after such fixation; this is to be expected, since elements of low atomic number only are involved.

It is a natural step to look for salts of heavy elements which may be taken up preferentially by nucleic acid, as phosphotungstic acid is known to be by certain constituents of muscle. Lanthanum and thorium nitrates have been found to have such a differential effect in locust spermatids.[22] The region which will ultimately form the head of the sperm shows well-defined striations in longitudinal section [Fig. 7(*a*), p. 275], clearly the basis of the pronounced birefringence observed by Caspersson.[23] In transverse section it is seen [Fig. 7(*b*), p. 275] that the structure is canalicular. It becomes

increasingly closely packed as the spermatid develops, until no structural differentiation is visible in the fully mature sperm. The hope remains that some other salt may be taken up still more selectively than is lanthanum nitrate, so that the structure which must persist at maturity may be explored.

So far such approaches to electron staining have been qualitative only. Lately Bahr and his collaborators have begun experimental studies of the rate and amount of uptake of osmium tetroxide by different tissues[24] and also theoretical calculations of their comparative electron scattering power, both in the natural state and after treatment with osmium tetroxide.[25] It may be hoped that along these lines at least a semi-quantitative analysis of the chief biochemical components of the cell may in due course become possible. Without staining the possibilities are small; with a number of specific stains, an accuracy of the order of 5–10% might be attainable.

SCANNING ELECTRON MICROSCOPES

An alternative means of obtaining information about the chemical nature of a specimen, as well as of its micromorphology, is to record the X-rays or the secondary electrons emitted from it under electron bombardment. This is best done by scanning it with a very fine electron beam. A point focus is produced by means of electron lenses, deflecting fields scan it over the surface in the same way as in a television apparatus, and an electron multiplier or counter records the emitted secondary electrons or X-rays respectively. The resulting signal is amplified and displayed on a cathode-ray tube in synchronism with the scan. A visible image is thus obtained of the surface, in which contrast variation depends on the local efficiency of X-ray or secondary electron emission. Such a system was built in the early days of electron microscopy by von Ardenne[26] in Germany and by Zworykin, Hillier and Snyder[27] in the United States, but neither was successful owing to the poor efficiency of recording systems at that time, the exposure required to obtain a picture at moderate magnification being of the order of one hour. Technical advances during the war made it a more practicable method, and MacMullan[28] obtained encouraging results with electrostatic lenses and electron multiplier recording. The sensitivity has been improved and the applications more thoroughly explored by Smith and Oatley.[29] An effective resolution of about 400 Å has now been obtained; that is to say, a useful magnification of about $\times 10000$. The method has the advantage over normal electron microscopy that dynamic effects at a surface, such as thermal or mechanical treatment, can be observed, and over the reflexion method that the intensity of electron bombardment and hence the temperature rise in the specimen is much lower at given magnification. A graphic example of its use is the examination of the tungsten-germanium contact in a transistor, as it is being "formed" by passage of a current pulse; pictures were obtained before and after passage of a current rather larger than the critical value. For thermal treatment of a specimen Smith[30] constructed a miniature hot-plate in the microscope. Fig. 8 (p. 275) shows the progress of thermal decomposition along a needle of silver azide when the centre of the plate was at a temperature of about 200° C. By this means valuable information has been obtained about this solid state reaction at a resolution beyond that of a hot-stage optical microscope.[31]

Smith has analysed the velocity distribution of the image-forming electrons and shown that they are mainly slow secondaries.[30] It should therefore be possible to explore the variation of emission coefficient over a specimen, which depends primarily on the chemical and crystallographic nature of the surface. More immediate and certain evidence of its elementary composition is obtained by recording the X-rays emitted as the surface is scanned.[32] If the X-rays are recorded in one direction by a scintillation counter and in another by a proportional counter, a picture on the display tube may be obtained in terms either of all the elements present (above a certain atomic number) or of the distribution of a selected element. A simple example of crossed silver and copper grids is shown in Fig. 9(*a*) and (*b*) (p. 275): the one or the other appears bright according to the X-ray line accepted by the counter and discriminator. The method has been used to investigate the impurities in a beryllium foil; the wavelength of beryllium K radiation is so long that it is not recorded, but foreign elements appear as bright spots on a black background.

So far this technique of micro-analysis has been employed at a resolution, as determined by the size of the electron spot, of only 1 μ. For quantitative work the number of quanta at each characteristic wavelength is recorded automatically. By inserting a crystal spectrometer before the counter, the accuracy of detection can be made high even for neighbouring elements in the periodic table. It is about 0·1% in a volume of order 1 μ^3, equivalent to a mass sensitivity of 10^{-13} to 10^{-14} g. The spot size can be made smaller, down to 1000 Å or less, but only at cost of longer "exposure" time. A visible picture could not then be obtained even on the longest delay phosphor, and counter recording only could be used. Nevertheless, the ability to carry out an elementary micro-analysis permits many useful applications even within the optical range of resolution: in metallurgy, the study of the early stages of precipitation, and in biology the identification of mineral inclusions, for instance. The extension of the method to elements of low atomic number, such as carbon and nitrogen, which are of particular interest in ferrous metallurgy, demands special precautions owing to the long wavelength (35–45 Å) of the characteristic lines; it is now under active development by Mulvey and Haine.[33]

ELECTRON INTERFERENCE MICROSCOPE

One of the most interesting and elegant of electron optical developments, in both conception and experimental execution, is the electron interferometer of Möllenstedt,[34] which he is now converting into an electron interference microscope. In principle it is the exact analogue of Fresnel's biprism: a narrow electron beam is split by a potential wedge so that two coherent beams converge and interfere (Fig. 10). The required potential distribution is obtained by applying about

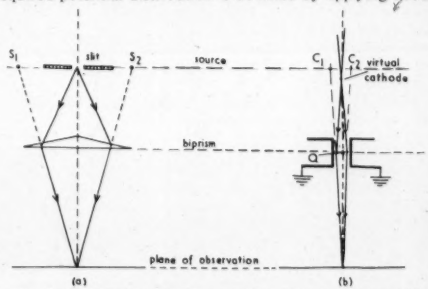

Fig. 10. Principle of the electron interferometer (*b*) compared with that of the Fresnel biprism of optics (*a*); *Q* is a metallized quartz fibre

−10 V to a metallized quartz fibre Q a few microns in diameter. Fringes are then obtained at a spacing dependent on the applied potential and on the primary accelerating voltage of the beam. If a thin object, such as a film of metal or carbon, is placed in the path of one of the beams, a fringe shift is observed, the amount of which depends on the electron optical path difference; that is to say, on the product of film thickness and refractive index. Since the latter depends on the inner potential of the material of the film, a simple method at once presents itself of measuring such inner potentials or alternatively film thicknesses of order 100 Å when the inner potential is known. Möllenstedt and Keller[35] have already applied it to evaporated carbon films and find an unexpectedly high value of 24 V for the inner potential (compare diamond 21 V; graphite 12 V), which must be accepted with reserve until the reliability of the thickness measurements has been checked.[36]

From their nature, the fringes are not localized. To convert the interferometer into an interference microscope, it is only necessary to form an image of the object in some convenient plane below the biprism. This is achieved by reversing the potential on Q; the two beams are then sufficiently separated that they pass through different regions of the objective lens. The first interference micrographs have recently been obtained with this arrangement by Möllenstedt and Bühl,[37] of which Fig. 11 (p. 275) is an example. The system needs refinement before it can become practically useful—at the moment it is too sensitive to external electromagnetic and mechanical disturbances—but its practicability has been clearly demonstrated. We thus have in prospect the ability to observe electron phase effects in sufficiently thin objects, allowing the investigation both of coherence conditions in electron beams and of local variations in thickness and inner potential of the specimen.

CONCLUSION

If any general conclusion can be drawn from the limited number of recent developments here described, it must be that electron microscopy is following the path historically pursued by optical microscopy, but at a ten-fold accelerated pace. Advances which required a century in optics are compassed in a decade or less in electron optics. One sign of this is the application of cine and interference methods. Another is the tendency to quantitative analysis, whether by measurement of the scattering of the primary electron beam or of the energy of the secondaries and X-rays which it produces. It can be anticipated that within the next few years these new developments will have been incorporated in commercial electron microscopes, providing new tools for fundamental and applied research. Meanwhile the next important step, the correction of electron lenses for spherical and perhaps also chromatic aberration is reaching the experimental stage,[38, 39, 40] preparing the way for the high-powered, wide aperture electron microscope which will be needed for resolving atomic dimensions.

REFERENCES

(1) HALL, C. E. *J. Biol. Chem.*, **185**, p. 45 (1950).
(2) HALL, C. E. *J. Biol. Chem.*, **185**, p. 749 (1950).
(3) MENTER, J. W. *Proc. Roy. Soc. A*, **236**, p. 119 (1956).
(4) NIEHRS, H. *Optik*, **13**, p. 399 (1956).
(5) NEIDER, R. *Proceedings of Electron Microscopy Conference Stockholm*, p. 93 (Stockholm: Almqvist and Wiksell, 1956).
(6) MENTER, J. W., and BASSETT, G. A. *Phil. Mag.*, **2**, p. 1482 (1957).
(7) HAINE, M. E. *J. Sci. Instrum.*, **34**, p. 9 (1957).
(8) MITSUISHI, T., NAGASAKI, H., and UYEDA, R. *Proc. Japan. Acad.*, **27**, p. 86 (1951).
(9) HILLIER, J. *Nat. Bur. Stand. Circ.* No. 527, p. 413 (1954).
(10) FARRANT, J. L., and REES, A. L. G. Quoted in Ref. 9.
(11) DOWELL, W. C. T., FARRANT, J. L., and REES, A. L. G. *Proceedings of International Conference on Electron Microscopy, London*, p. 279 (London: Royal Microscopical Society, 1954).
(12) DOWELL, W. C. T., FARRANT, J. L., and REES, A. L. G. *Proceedings of Regional Conference on Electron Microscopy, Tokyo*, p. 320 (Japan: Society of Electron Microscopy, 1956).
(13) HASHIMOTO, H., and UYEDA, R. *Acta Cryst.*, **10**, p. 143 (1957).
(14) PASHLEY, D. W., MENTER, J. W., and BASSETT, G. A. *Nature* [*London*], **179**, p. 752 (1957).
(15) HIRSCH, P. B., HORNE, R. W., and WHELAN, M. J. *Phil. Mag.*, **1**, p. 677 (1956).
(16) WHELAN, M. J., and HIRSCH, P. B. *Phil. Mag.*, **2**, p. 1121 (1957).
(17) HEIDENREICH, R. D., and SHOCKLEY, W. *Report of Conference on Strength of Solids*, p. 57 (London: Physical Society, 1948).
18) WHELAN, M. J., HIRSCH, P. B., HORNE, R. W., and BOLLMANN, W. *Proc. Roy. Soc. A*, **240**, p. 524 (1957).
(19) OTTEWILL, R. H., and HORNE, R. W. *Nature* [*London*], **180**, p. 910 (1957).
(20) GIBBONS, I. R., and BRADFIELD, J. R. G. *Biochim. Biophys. Acta*, **22**, p. 506 (1956).
(21) BAHR, G. F. *Exp. Cell Res.*, **7**, p. 457 (1954).
(22) GIBBONS, I. R., and BRADFIELD, J. R. G. *J. Biophys. Biochem. Cytology*, **3**, p. 133 (1957).
(23) CASPERSSON, T. *Chromosoma*, **1**, p. 605 (1940).
(24) BAHR, G. F., BLOOM, G., and FRIBERG, U. *Exp. Cell Res.*, **12**, p. 342 (1957).
(25) ZEITLER, E., and BAHR, G. F. *Exp. Cell Res.*, **12**, p. 44 (1957).
(26) ARDENNE, M. VON. *Z. Phys.*, **109**, p. 553 (1938).
(27) ZWORYKIN, V., HILLIER, J., and SNYDER, R. L. *Proc. Inst. Radio Engrs*, **30**, p. 255 (1942).
(28) MACMULLAN, D. *Proc. Instn Elect. Engrs* (1), **100**, p. 245 (1953).
(29) SMITH, K. C. A., and OATLEY, C. W. *Brit. J. Appl. Phys.*, **6**, p. 391 (1955).
(30) SMITH, K. C. A. *Thesis* (University of Cambridge, 1956).
(31) BOWDEN, F. P., and MCAUSLAN, J. *Nature* [*London*], **178**, p. 408 (1956).
(32) COSSLETT, V. E., and DUNCUMB, P. *Nature* [*London*], **117**, p. 1172 (1956); *Proceedings of Electron Microscopy Conference Stockholm*, p. 12 (Stockholm: Almqvist and Wiksell, 1956).
(33) MULVEY, T., and HAINE, M. E. Private communication.
(34) MÖLLENSTEDT, G., and DÜKER, H. *Naturwissenschaften*, **42**, p. 41 (1955); *Z. Phys.*, **145**, p. 377 (1956).
(35) MÖLLENSTEDT, G., and KELLER, M. *Z. Phys.*, **148**, p. 34 (1957).
(36) COSSLETT, A., and COSSLETT, V. E. *Brit. J. Appl. Phys.*, **8**, p. 374 (1957).
(37) MÖLLENSTEDT, G., and BÜHL, R. *Phys. Blatt.*, **13**, p. 357 (1957).
(38) SCHERZER, O. *Optik*, **2**, p. 114 (1947).
(39) BURFOOT, J. C. *Proc. Phys. Soc.* [*London*] *B*, **66**, p. 775 (1953).
(40) ARCHARD, G. D. *Proc. Phys. Soc.* [*London*] *B*, **68**, p. 156 (1955).

Thermionic and related properties of calcium oxide

By B. J. Hopkins, B.A., and Prof. F. A. Vick, O.B.E., Ph.D., A.M.I.E.E., F.Inst.P., Physics Department, University College of North Staffordshire, Keele, Staffs.

[*Paper first received* 19 *November*, 1957, *and in final form* 3 *January*, 1958]

Using probe diodes, changes in thermionic emission and conductivity of cathodes of calcium oxide on nickel have been followed during activation and poisoning. The effects of material liberated from the anode have been studied. The mean nominal thermionic work function is 1·69 eV for the fully activated cathode (from the slope of a Richardson line), with an estimated temperature coefficient of 1·1 mV/° K.

Three regions of conductivity have been found; the activation energies for the two at the lowest temperatures are 1·3 eV and 0·81 eV. The current-voltage characteristics between the cathode base and probe show two types of curvature, one dominant above 625° K and the other below this temperature. A linear relation extending over four orders of magnitude between the logarithms of emission and of the conductivity has been observed during activation. Assuming that semi-conductor theory may be applied the mean value of the surface work function is calculated to be 0·7 eV.

1. INTRODUCTION

During the last thirty years the bulk and surface electrical properties of barium and strontium oxides have been extensively investigated, but there have been very few measurements on calcium oxide. This oxide is used only as an additive in commercial cathodes,[1, 2] but measurements of its properties are important in addition to those on barium oxide and strontium oxide if an understanding is to be reached of how the electrical properties of alkaline-earth oxides depend on their band structure and other characteristics. It is especially important to measure thermionic emission and electrical conductivity over a wide temperature range, though such measurements are relatively difficult on calcium oxide because of the very low currents involved and because of other factors which will be discussed below. The aim of the present work is thus to relate thermionic emission and electrical conductivity of calcium oxide cathodes over as wide a temperature range as possible; to investigate how far the measurements are consistent with the Loosjes–Vink hypothesis[3]; to relate the relevant properties of calcium oxide with those of barium oxide and strontium oxide and to see how far they can be interpreted in terms of semi-conductor theory.

Summaries of the earlier work on the electrical conductivity and emission of calcium oxide may be found in a review paper by Blewett[4] and in the book by Herrmann and Wagener.[5] Apart from the effects of its incorporation with barium oxide and strontium oxide in oxide cathodes, very little work on calcium oxide appears to have been carried out recently, though a short summary of a paper by Glascock and Hensley has now appeared[6] and will be commented on below.

2. THE EXPERIMENTAL TUBES

The most satisfactory design of tube for these investigations with calcium oxide cathodes was a cylindrical diode with a helical probe wire wound into the cathode material (Fig. 1). Such an arrangement affords a means of measuring both the cathode emission and the coating conductivity, simultaneously if necessary. The great advantage of the probe method in conductivity work with calcium oxide cathodes is that the depth of the probe wire may be varied from cathode to cathode. This is important, since even in the most activated condition the resistance of calcium oxide is very much higher than the oxides of either barium or strontium. In order to bring the conduction currents between the probe and the cathode base within the range covered by the electrometer, it was essential to keep the carbonate layer sprayed beneath the probe as thin as possible. Too thick a layer of carbonate prevented the conductivity of the oxide from being

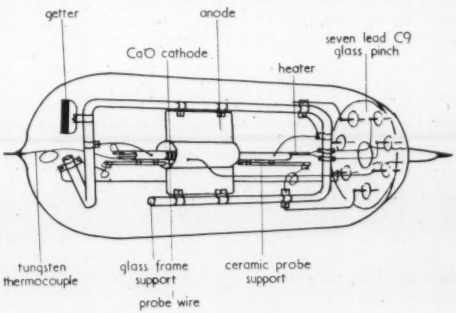

Fig. 1. The experimental tube

followed in the lower temperature ranges. Little information of value regarding the semi-conducting properties of the cathode could be obtained until the cathode temperature had been reduced to below 600° K.

The tubes were built with a view to obtaining a good vacuum before sealing off from the pumping system; the metallic parts were, therefore, reduced to a minimum and positioned so that they could readily be outgassed either by eddy-currents or by direct heating.

All of the materials used in the assembly of these diodes, i.e. nickel, tungsten and type C9 glass (by British Thomson-Houston Ltd.) were well washed in carbon tetrachloride, water, chromic acid (in the case of the glass) and finally several times in distilled water. Wherever possible the metallic components were hydrogen furnaced and subsequently handled with tweezers only. Assembly of the tubes took place in a special clean room set aside for this purpose. The cathodes were prepared from "O" nickel

sleeves 7 cm long and 0·25 cm in diameter. A tungsten thermocouple wire was welded internally to the centre of the sleeve and fitted with several fine ceramic tubes as insulation. Two other ceramic tubes fixed rigidly to the ends of the cathode serve as supports for the probe wire. A tungsten hairpin heater insulated with ceramic tubes was fitted inside the cathode sleeve and the assembly hydrogen furnaced. The cathode was then transferred to a rotating jig and sprayed over the middle 2 cm of its length with a suspension of calcium carbonate in butyl acetate (by the General Electric Co. Ltd.). Masks shielded the rest of the cathode during the spraying. A sufficiently thin and smooth surface was best obtained with a wet spray and a rapidly rotating jig. The probe wire was usually a length of "O" nickel wire, diameter 0·0013 cm. After half a dozen turns of it had been wound on to the cathode and welded into position, spraying was continued to a final thickness of about 100 μ.

Trial experiments with alternative glass and ceramic supports showed that in high vacua, taking into account ease of outgassing, a hard glass frame is more satisfactory than a ceramic one as a support for anode and cathode. The pure nickel cylindrical anodes were 0·8 cm diameter and 2·2 cm long, supported by two radial fins 1 cm wide. During assembly great care was taken to ensure that the cathode was co-axial with the anode. A sliding joint was fitted to the cathode to allow for thermal expansion. Finally a getter was welded on and the completed assembly mounted on a commercial seven-pin pinch of C9 glass (by Siemens–Edison–Swan Ltd.). The thermocouple lead was taken from a tungsten rod sealed into the top of the envelope thus ensuring a continuous tungsten path to the cold junction of the thermocouple.

3. THE PROCESSING OF THE TUBES

The completed tubes were sealed to a pumping system capable of achieving an ultimate vacuum of better than 10^{-7} mm mercury (as measured by a Bayard–Alpert type ion gauge). Immediately after pumping out the tube the whole of the glassware beyond the final liquid air trap was baked for six hours at 450° C. While the glass was still hot the metal parts in the tube were given a preliminary outgassing to a bright red heat by eddy currents.

The calcium carbonate cathode was decomposed to the oxide by heating the nickel sleeve to 900° C. This has to be done very slowly otherwise the evolution of carbon dioxide from the carbonate forces the cathode material from the metallic base and also tends to break the probe wire. A specially geared motor was built to drive a Variac transformer through the necessary voltage change in order to raise the cathode temperature from 450 to 900° C in about 48 h. At this stage the motor was stopped and the pressure brought to below 10^{-6} mm mercury with the cathode maintained at 900° C. In preliminary experiments it was often noticed at this point that the pressure in the system would not fall below 10^{-5} mm mercury, due to an accumulation of solid carbon dioxide in the liquid air trap.* (At a temperature of −183° C the vapour pressure of carbon dioxide is $2 \cdot 10^{-5}$ mm mercury.) This deposit could be readily removed from the vacuum system by the use of a large diameter stop-cock and a second liquid air trap between the tube and the contaminated trap. After the breakdown of the carbonates two liquid air traps were kept on the system throughout the further processing of the tube.

Cycles of outgassing were commenced at this stage, each consisting of four hours' baking at 450° C, eddy-current heating the metal parts to a bright red, and finally raising the cathode temperature to 900° C. The getters and the seal-off constriction were also given preliminary outgassing treatments. After several of these cycles the pressure in the tube would not rise above 10^{-6} mm mercury at any one of the stages. The getters were then fired slowly and the tube sealed slowly from the pumping system so that gas liberated as the walls collapsed could be pumped away.

4. MEASUREMENTS

(*a*) *Cathode temperature.* The tungsten lead welded inside the cathode forms one of the connexions for a tungsten–nickel thermocouple. The other tungsten–nickel junction was maintained at 0° C outside the tube and the e.m.f. developed between the two was measured by means of a potentiometer (by Muirhead and Co. Ltd.). This procedure gives the temperature of the base metal and not of the cathode surface but this does not affect the results which are all based on temperature differences and not upon the absolute temperatures.

(*b*) *Measurement of conductivity and emission.* Even in its most activated condition calcium oxide has low values of thermionic emission and electrical conductivity compared with the oxides of barium and strontium. This means that most of the measurements, especially those at the lower temperatures, involve currents of the order of 10^{-12} A. A sensitive electrometer was built around an electrometer double-beam tetrode type B.D.M. 10 (by Ferranti Ltd.). The sensitivity of the arrangement was such that an input voltage of 0·25 mV led to a galvanometer deflexion of 1 cm. For the measurements in the lower current ranges the experimental tube was placed in a screened metal box, which also contained all the components necessary for both the emission and the conduction measurements.

The voltage to the probe was drawn from a calibrated linear 1000 Ω potentiometer. This was centre-tapped so that from +100 mV to −100 mV could be applied to the probe in one continous sweep. A second potentiometer allowed this maximum of 100 mV to be varied continuously up to 3 V. A similar arrangement allowed ±4 V to be applied to the anode of the experimental tube. The only wires leaving the screened box were the cathode heater leads and the well-insulated and screened co-axial cable to the electrometer.

(*c*) *Supplies.* All the high tension supplies were obtained from batteries; the introduction of a.c. into the screened box resulted in considerable instability and zero drift in the electrometer. A 12 V accumulator in conjunction with a 10 Ω rheostat provided a good source of heater power provided that one terminal of the battery was earthed.

5. EXPERIMENTAL RESULTS

Before starting the full research programme with calcium oxide cathodes a number of preliminary investigations were undertaken. For these, diodes and probe diodes were built, some having cathodes of calcium oxide and some of the conventional barium and strontium oxides. These early measurements not only confirmed information relating to the latter oxides, but also indicated a number of snags that would be encountered in the work with calcium oxide. These may be summarized briefly:

* A report of this effect has recently been published by Curnow,[7] in which he draws the same conclusion. His experiments using an oil diffusion pump without a cold trap failed to reveal any accumulation of carbon dioxide.

(i) If the first coating on the metallic base is sprayed dry, then almost independent of how thick it is the conductivity of the resulting cathode will be too low for measurements to be made over all temperature regions of interest. Hence, in general a wet spray was used in the final tubes.

(ii) Activation of the calcium oxide cathode is a much slower process than for the other oxides. The cathode must be maintained at high temperatures for long periods during which emission current is drawn to the anode. Only after several days under these conditions is a constant activated state reached. "Flashing" the cathode to a high temperature, a common method of activation in industry, does not cause any appreciable change in cathode emission.

(iii) The search for a low-temperature conduction mechanism comparable with that obtained by Loosjes and Vink[3] for barium oxide, soon showed that if such a mechanism does exist for calcium oxide it occurs at much lower temperatures. The lower limit of current measurement is set by the leakage resistance of the ceramic insulators carrying the probe, etc.

(iv) During the early conductivity measurements it was noticed that calcium oxide cathodes showed marked photoconductivity. This was eliminated in all the subsequent tubes by means of a light-tight box. The effect is being investigated further in this laboratory and will be reported in a later paper.

(*a*) *Thermionic emission.* Following the tubes used in preliminary experiments, nine probe diodes were constructed, all similar to Fig. 1. Apart from some deliberate variations of spraying conditions, each tube was processed in the same way, as far as possible. The results of thermionic emission measurements are presented first, followed by those on electrical conductivity and then the relations between the two sets of measurements.

Tube *P.* IV was activated for 96 h with 100 V applied to the anode. Five emission characteristics (log I_A against V_A) at temperatures between 630 and 780° K were obtained and showed reasonably good saturation (Fig. 2). The Richardson plot from these curves (Fig. 3) indicates a work function of 1·73 eV. The mean contact p.d. between cathode and anode estimated from Fig. 2 averages only −0·2 V, which leads to an anode work function of about 1·5 eV, and suggests that the anode had become contaminated by electropositive material.

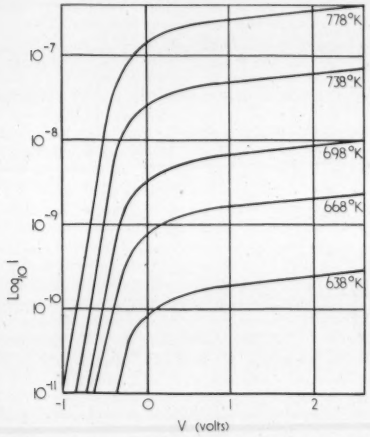

Fig. 2. Emission characteristics for tube *P.* IV

With tube *P.* V measurements were made during activation. The Richardson plots obtained at four states of activation are shown in Fig. 4. During activation the anode potential

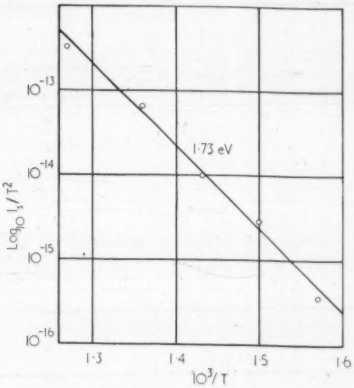

Fig. 3. Richardson plot for tube *P.* IV

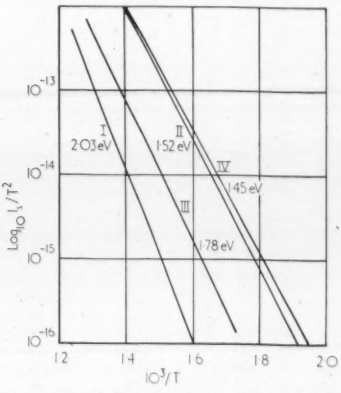

Fig. 4. Richardson plots during activation of tube *P.* V

was only 6 V, sufficient to achieve saturation but not leading to bombardment of the anode by high-energy electrons. After the cathode had reached state II, maximum activation, the anode was heated by eddy currents to a red heat. This led immediately to the poisoning of the cathode emission into the third activation state (Fig. 4). The recovery of the cathode to state IV was the result of drawing current with the anode potential raised to 8 V.

In tube *P.* VI, the whole coating was sprayed as a dry one, to verify that such a coating has a low conductivity. The cathode was activated throughout with 6 V applied to the anode, in this way poisoning by anode materials was avoided.

Richardson plots in four states of activation gave slopes of 2·2, 1·92, 1·56 and 1·50 eV respectively and the contact p.d. between anode and cathode indicated that the anode work function remained fairly constant at about 3 eV.

Six activation states were investigated with tube *P.* X; the Richardson slopes ranged from 2·44 to 1·73 eV. From the unactivated condition, state II was attained by the application of 4 V to the anode with the cathode at 850° C. Increasing the anode potential to 8 V to obtain state III caused poisoning and a fall in anode work function (see below). Then 4 V was reapplied to the anode and activation continued to state IV, for which the Richardson slope was 2·06 eV. On the application of 8 V to the anode, poisoning once again took place. Anode current was drawn until the emission indicated almost complete recovery, and the measurements of state V were taken. The Richardson slope was now 1·9 eV. Application of 8 V to the anode for 10 h produced the maximum activation of the cathode, with a Richardson slope of 1·73 eV, which remained constant even after the anode had been operated at 100 V.

With the cathode of tube *P.* XI six activation states were again investigated. Two activating anode voltages were used, 4 and 8 V. The emission measurements are summarized as follows.

Table 1. *The activation of tube P. XI*

	State I	$\phi_R = 2{\cdot}12$ eV, anode ϕ_A 3·0
4 V on anode	State II	$\phi_R = 1{\cdot}76$ eV, anode ϕ_A 4·3
4 V on anode	State III	$\phi_R = 2{\cdot}08$ eV, anode ϕ_A 3
8 V on anode, initial poisoning and then recovery	State IV	$\phi_R = 2{\cdot}18$ eV, anode ϕ_A 4·5
8 V on anode	State V	$\phi_R = 1{\cdot}85$ eV, anode ϕ_A 3·2
100 V on anode	State VI	$\phi_R = 1{\cdot}88$ eV, anode ϕ_A 2·1

The average value of cathode work function, assuming this to be given by the slopes of Richardson plots, in the fully activated states under equilibrium conditions with the anode, etc., was 1·69 eV for the five tubes. By plotting emission characteristics over a wide temperature range (644–998° K) it was possible to plot a graph of contact p.d. against temperatures and this gave a straight line (Fig. 5). Assuming that this variation of contact p.d. is due entirely to the cathode (conditions at the anode being constant), and assuming that the changes at the cathode are due to the variation in effective work function, the temperature coefficient of the work function is 1·1 mV/° K, which is similar to the values for barium oxide and (barium strontium) oxide quoted by Young.[8] These range from 0·5 to 1·0 mV/° K at 500° to 2·0 mV/° K at 1100° with a peak at 800° K of 2·5 mV/° K.

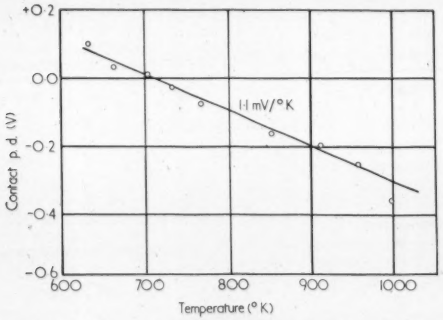

Fig. 5. The change of cathode work function with temperature

(*b*) *Cathode conductivity.* For each cathode the current between cathode and probe was plotted against probe potential over the range ±100 mV for each particular temperature and cathode state. Normally, these current-voltage characteristics did not pass through the origin because of a thermoelectric e.m.f. due to the temperature gradient between cathode and probe. To achieve greater stability the thermal e.m.f. was balanced out when taking measurements with the electrometer. The gradient of the current-voltage curves over the region of the origin gives the resistance of the cathode coating between core and probe.

For tube *P.* IV the plot of $\log(I/R)$ against $1/T$ is shown in Fig. 6. The plot consists of two slopes, just as for barium oxide, but in this case the intersection is at $T = 625°$ K instead of at about 800° K for barium oxide. To explain similar behaviour for an oxide cathode, Loosjes and Vink have suggested[3] two conduction mechanisms in parallel, one predominant at high temperatures and having the higher activation energy (given by the slope of the curve) and the other at lower temperatures. If this is so,

$$I/R = Ae^{-Q_1/kT} + Be^{-Q_2/kT} \qquad (1)$$

where Q_1 and Q_2 are the two activation energies respectively. Loosjes and Vink found that Q_1 was not very different from ϕ_R, the work function of their cathode as estimated from Richardson plots, and suggested that the high-temperature emission process consists of thermionic emission from crystal to crystal across the interstices in the cathode. At low temperatures they attributed the conductivity to movement of charge across the contacts between crystals. The slopes of the two straight lines of Fig. 6 are 0·95 and 0·77 eV, but these have to be corrected in order to obtain Q_1 and Q_2.

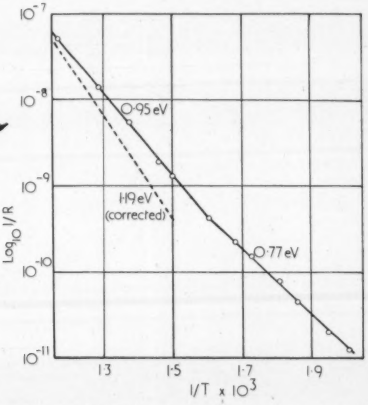

Fig. 6. Conductivity lines for tube *P.* IV (fully activated)

It has been the practice to correct the high-temperature line for the effect of the low-temperature mechanism before

attempting to interpret any activation energies. A simple correction procedure similar to that used by Shepherd[9] has been adopted in all of the tubes so far discussed. To confirm that the procedure is sufficiently accurate when the two slopes are as close together as found with calcium oxide, theoretical conductivity plots were constructed by the substitution of values for Q_1 and Q_2 into the general conduction equation (1). The results of this investigation confirm that the simple correction is justified within 4%.

For tube *P.* V the conductivity *vs.* $1/T$ plots are shown in Fig. 7. State III is incomplete because of a fault in the electrometer. States II and IV show clearly defined regions

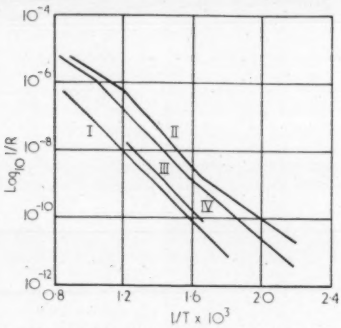

Fig. 7. Conductivity lines for tube *P.* V. After state II the anode heated to brightness. Activation was at 900° C with 8 V anode potential

State	Q_1	Q_2	Q_1 *corrected*
I	1·0	—	—
II	1·1	0·72	1·3
III	1·06	—	—
IV	1·04	0·85	1·46

completely analogous with those of the previous tube. According to the Loosjes and Vink hypothesis, the bottom line relates to semiconduction and the middle line to pore conduction. The third linear region apparent in these two activation states at the highest temperatures is thought to be due to saturation of the emission current inside the cathode pores. In the state of highest activation, the value of Q_2 is 0·72 eV, in good agreement with the previous cathode. As already described, State III was a poisoned one, and both emission and conductivity decreased by a factor of about 15 below the values for state II. Between states III and IV, the cathode was heated and the source of poisoning removed by drawing emission. Although the emission recovered fully the conductivity did not. If the poisoning agent is oxygen, as is probable (this will be discussed below), it would appear that it remains in the cathode pores after it has ceased to influence the thermionic emission to the anode.

Tube *P.* VI was allowed to activate continuously with only 6 V anode potential and not poisoned at any stage. Without disturbing factors it was possible to test whether a relationship reported by Kawamura and Nishibori[10] and confirmed by Hannay, McMair and White[11] holds for these cathodes, namely a linear relation between $\log 1/R$ and $\log j_0$, where j_0 is the thermionic emission current density. Fig. 8 shows a good linear relation over four orders of magnitude, and this interesting result will be discussed below.

Of the six activation states investigated for tube *P.* X, the low-temperature type of conductivity could be observed in three. For these Q_2 fell from 1·1 eV in state II to 0·97 in state IV and 0·84 in state VI, the fully activated condition. The corrected high-temperature slopes $Q_1 = 1{\cdot}53$ in state II and 1·44 in state IV were not the same as the Richardson slopes for the same states, being about 30% away. After poisoning, recovery of the high-temperature conductivity again lagged behind that of the thermionic emission.

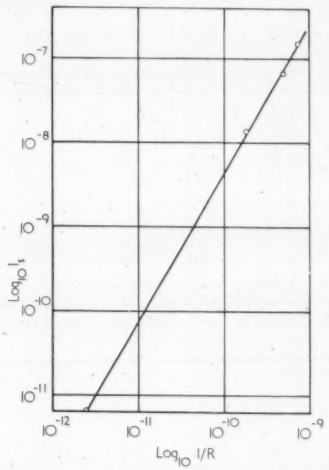

Fig. 8. Relation between conduction and emission, tube *P.* VI

The activation of tube *P.* XI was also followed through six conductivity states. In the final two states the activation energy for the low-temperature conduction mechanism changed from 1·07 to 0·92 eV. After state III, poisoning by anode materials took place and the conduction was allowed to reactivate before the measurements of state IV were obtained. Although the thermionic emission had reached its maximum activity in state V the conductivity had to be activated for a further period to state VI to attain its highest value.

Table 2. *Summary of emission and conduction measurements for the fully activated state of the oxide*

	Conductivity			*Emission*		
Tube	Q_1(eV)	Q_2(eV)	Q_1(eV) *corrected*	ϕ_H(eV)	*Final activated voltage*	ϕ_A(eV)
P. IV	0·95	0·77	1·19	1·73	100	2·0
P. V	1·1	0·72	1·30	1·52	8	3·2
P. VI	0·93	0·88	1·15	1·50	6	3·5
P. X	1·18	0·84	1·38	1·73	8	2·7
P. XI	1·16	0·92	1·36	1·88	100	2·1

(*c*) *Curvature of current-voltage characteristics for the conduction process.* In the current-voltage lines for the cathodes studied above, two regions of curvature could be distinguished. Above 1000° K the curves were linear within the ±100 mV limit applied to the probe. Below 600° K for all the cathodes, marked curvature occurred towards the current axis in the positive region and away from the current

axis in the negative region (Fig. 9). Curvature in the higher temperature region between 600 and 1000° K was not so regular and occasionally the characteristics were quite linear. When, however, curvature did occur it was always in the opposite sense to that of the low-temperature region (Fig. 10).

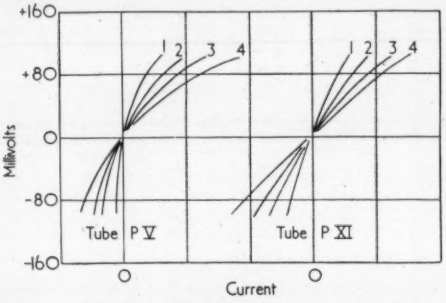

Fig. 9. Curvature of the current-voltage characteristics at low temperatures

Tube *P.* V	Tube *P.* XI
1, 518° K	1, 533° K
2, 553° K	2, 553° K
3, 603° K	3, 513° K
4, 538° K	4, 633° K

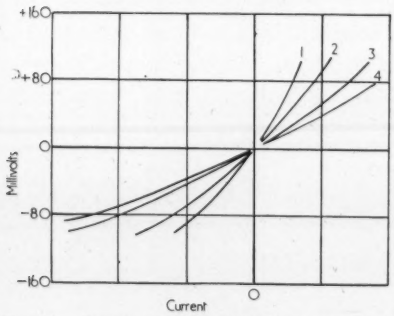

Fig. 10. Curvature of the current-voltage characteristics at high temperatures

1, 858° K; 2, 1008° K; 3, 928° K; 4, 808° K.

Cathode coloration. Within a few weeks of completing measurements with these calcium oxide cathodes, the surface of the oxide developed a marked mauve coloration. This was true only of those cathodes which had been fully activated before storage. Heating the cathode removed the colour, though within a further period of about two weeks it had returned.

Dash[12] and Sproull[13] have prepared single crystals of barium oxide with a blue colouration by heating the oxide in the presence of barium vapour. They conclude that the coloration is caused by the diffusion of neutral oxygen to leave an excess of the metallic barium. Electrons are then trapped at the oxygen vacancies to form colour centres analogous with *F* centres in the alkali halides. This coloration with calcium oxide will be investigated further.

DISCUSSION OF THE RESULTS

The maximum emission from fully-activated calcium oxide is at least two orders of magnitude below that of barium oxide. It is very slow to activate, requiring long periods at high temperatures, and is very easily poisoned. The mean thermionic work function, as measured by the Richardson line, is 1·69 eV, compared with 1·1 eV for barium oxide. The activation process appears to liberate oxygen (see below) and thus it is probable that the cathode activity is a function of the excess of metallic calcium in the cathode. The coloration observed for all fully activated cathodes seems to show that colour centres are associated with this excess of the metallic component.[13] Further work, especially on the photoconduction effect, is needed to confirm this.

A recent brief report by Glascock and Hensley[6] on thermoelectric power and electrical conductivity of calcium oxide is the only one available describing conductivity measurements on calcium oxide under high vacuum conditions. Planar nickel cathodes were mounted with their coated surfaces in contact in a manner similar to that used by Loosjes and Vink. Current measuring difficulties were encountered and the temperature range of the experiments did not extend below 650° K. Although the authors report a break in the conductivity curve at 900° K, no mention is made of any other discontinuity. It may thus be assumed that at their lowest temperature they had not reached the region of the third conduction mechanism which, according to our measurements, sets in only below about 625° K. They conclude that calcium oxide is a pore conductor with a conductivity much lower than (barium strontium) oxide.

In the results recounted above, three regions of conductivity have been observed analogous with those obtained with barium oxide cathodes.[3, 8] (A fourth region has now been found in barium oxide at lower temperatures.[14]) The lower temperature region, which is thought to be due to conduction through the crystal-to-crystal contacts, could be measured with good accuracy in four fully activated cathodes. The mean value for the activation energy of this type of conduction was 0·81 eV; the variation from cathode to cathode is less than 0·1 eV. The linear part of the conductiviy curve above 600° K is probably due to an electron emission process within the pores of the cathode; after correction the mean value of its activation energy was $1{\cdot}3 \pm 0{\cdot}1$ eV. The slope of the third linear region above 1000° K has little significance since it merely represents the onset of saturation in the cathode pores. The break at the lower end of the curve occurs at a much lower temperature (625° K) than for the corresponding point for barium oxide (800° K) and tends to be a sharp transition.

In their measurements with barium oxide, Loosjes and Vink found good agreement between the high temperature slope Q_1 and the Richardson line slope. In our work on calcium oxide in no case was such agreement found; usually ϕ_R exceeds the activation energy by about 30%. In several of the tubes (*P.* V, *P.* X and *P.* XI) the emission shows much more rapid recovery from poisoning by materials liberated from the anode surface than does the conductivity; this seems to indicate that the pore surfaces within the cathode are in a different state from the actual emitting surface of the cathode after poisoning.

It has been known for some time that deposits of cathode material on a fixed anode during operation of a diode may influence the behaviour of the diode.[15–18] Fan[19] has observed contact potential differences of between 0·1 and 0·7 V between a nickel anode and a barium oxide cathode in a diode. After high-temperature glowing of the cathode

the contact p.d. increased, whereas the drawing of a large emission had the converse effect. He concludes that the surface conditions at the anode varied with the treatment of the tube. Wright showed[16] that emission decay takes place only when the emission current is drawn to the anode used for activation of the cathode. Deb[18] has concluded that the contaminant from the anode is oxygen, though under certain circumstances it may be chlorine. During our measurements on calcium oxide it has been possible to introduce poisoning effects simply by a variation in anode potential. Measurement of the contact p.d. together with the Richardson work function in all of the activation states has allowed the condition of the anode surface to be followed continuously. A low anode potential during activation gives rise to a steadily increasing anode work function—see Table 3.

Table 3. *Tube P. XI*

Anode work function ϕ_A (eV)

State	*I*	*II*	*III*	*IV*	*V*	*VI*
Anode at 4 V	3·0	4·2	5·3			
Anode at 8 V			5·3	4·5	3·2	2·1

If, however, the tube is activated continuously with a voltage >8 V, then ϕ_A remains at a low value (about 2 eV), for example *P.* IV, $\phi_A = 1{\cdot}5$ eV. A sudden increase in the anode potential after a cathode has been activated for a time with a low voltage leads to immediate poisoning of both emission and conductivity and a gradual fall in ϕ_A (Table 3).

The most likely poisoning agent to be liberated at the anode by the higher energy electrons is oxygen, known to be liberated freely during activation.[11, 20] Thus, it appears that oxygen produced during activation is adsorbed on the anode, and when V_A exceeds 6 V it is dislodged by electrons and causes the observed poisoning of cathode emission. Electropositive elements evaporated during the breakdown of the carbonates, reduce the anode work function from 5 eV to about 2 eV. Oxygen from the cathode merely sits on top of this layer and causes the anode ϕ to rise again.

Curvature of the conductivity current-voltage characteristics for barium oxide has been observed by several other workers, for example in the temperature range 800–1100° K by Loosjes and Vink. These authors explained non-linearity in terms of their picture of conduction through the electron gas in the pores of the cathode. The extreme case they consider should in fact lead to parabolic curves. As was reported in section 5(*c*) above, our measurements on calcium oxide show the same type of curvature.

At temperatures below 600° K King[21] has observed a curvature for (barium strontium calcium) oxide which agrees in direction with that reported above though the magnitude appears to be much less in spite of the much higher potential differences applied across the oxide (14 V). King suggests that the following factors may be independently or jointly important:

(1) transitional resistances between the semi-conducting grains;
(2) increased electron mobility at high field strengths;
(3) barriers at the semi-conductor metal boundaries.

The curves published by Wright[22] for a (barium strontium) oxide coating, especially those for tube A9, have a very marked similarity with the ones of Fig. 9. From the work of Eisenstein[23] and Nergaard and Matheson[24] it may be concluded that a barrier due to an interfacial layer is responsible for this low-temperature non-linearity.

A linear relation between the logarithms of emission and conduction currents at different stages of activation was first observed by Nishibori and Kawamura[10] for a barium oxide cathode. Hannay and co-workers[11] have been able to repeat cycles of activation and deactivation over which they have shown that the logarithms of thermionic emission and conductivity are directly proportional. For one of our tubes (*P.* VI) linearity was observed over four orders of magnitude (Fig. 8). Only in the case of this cathode were homogeneous conditions maintained; no poisoning took place at any stage and the cathode was activated continuously with a low voltage on the anode. It has been noted above that reactivation after poisoning by material from the anode surface takes place more quickly in the few surface layers of the cathode, therefore homogeneous conditions cannot have been maintained in any of the cathodes which were subject to poisoning unless they were reactivated for long periods. Linearity cannot be expected, therefore, and was not observed for these cathodes.

From semi-conductor theory[11] we have

$$\frac{j_0}{\sigma} = \frac{3(1-r)kT}{4\,l_0\,e}\,e^{-\chi/kT} \qquad (2)$$

where σ = the oxide conductivity.
r = the mean reflexion coefficient for electrons at the emitting surface.
l_0 = the electron mean free path.
χ = the surface work function or electron affinity.

Thus it should be possible to estimate χ by plotting $\log j_0/\sigma T$ against $1/T$ since for any one activation state the value of l_0 will be constant. For tube *P.* VI a good linear relation was obtained, and the slope gave a value of 0·62 eV for the surface work function χ. Calculations throughout the activation stages of the other tubes have shown that the value of χ rises considerably (by about 0·3 eV) after the cathode has been poisoned by oxygen and slowly falls as the surface cleans up during reactivation. The mean value of χ for all of the fully activated cathodes investigated was 0·7 eV. Mott[25] and Wright[26] have calculated theoretical values of χ for the oxides of barium, strontium and calcium and they conclude that the value lies between 0 and 1 eV.

This value for χ is in poor agreement with the difference between ϕ_R and Q_2. The explanation for this is thought to lie in the Richardson line technique. Other methods are being investigated in this laboratory for finding the work function of the oxide cathode.

ACKNOWLEDGEMENTS

One of us (B. J. H.) makes acknowledgement to Metropolitan-Vickers Electrical Co. Ltd. for a scholarship which enabled him to take part in the work, and we thank the same company for the gift of apparatus and materials. Thanks are also due to the General Electric Co. Ltd. and to the Siemens–Edison–Swan Co. Ltd. for the gift of materials, apparatus or equipment. We also wish to thank Dr. G. S. Higginson and other colleagues for helpful discussion on some aspects of this work, and F. Rowerth and B. Bloor for help in the preparation of the paper.

REFERENCES

(1) Brodie, I., and Jenkins, R. O. *J. Appl. Phys.*, **27**, p. 4 (1956).
(2) Grey, L. E. *Nature* [*London*], **165**, p. 773 (1950).
(3) Loosjes, R., and Vink, H. J. *Philips Res. Rep.*, **4**, p. 449 (1949).

(4) BLEWETT, J. P. *J. Appl. Phys.*, **10**, p. 668 (1939).
(5) HERRMANN, G., and WAGENER, S. *The Oxide Coated Cathode*, Vol. 2 (London: Chapman and Hall Ltd., 1951).
(6) GLASCOCK, H., and HENSLEY, E. B. *Bull. Amer. Phys. Soc. Series 2*, **2** No. 5 p. 271 (1957).
(7) CURNOW, H. J. *J. Sci. Instrum.*, **34**, p. 73 (1957).
(8) YOUNG, J. R. *J. Appl. Phys.*, **23**, p. 1129 (1952).
(9) SHEPHERD, A. A. *Brit. J. Appl. Phys.*, **4**, p. 70 (1953).
(10) KAWAMURA, H., and NISHIBORI, E. *Proc. Phys. Math. Soc. Japan*, **22**, p. 378 (1940).
(11) HANNAY, N., MCNAIR, D., and WHITE, A. H. *J. Appl. Phys.*, **20**, p. 669 (1949).
(12) DASH, W. C. *Phys. Rev.*, **92**, p. 68 (1953).
(13) SPROULL, R. L. *Phys. Rev.*, **92**, p. 77 (1953).
(14) HIGGINSON, G. S. *Brit. J. Appl. Phys.*, **9**, p. 106 (1958).
(15) FEASTER, G. R. *J. Appl. Phys.*, **20**, p. 415 (1949).
(16) WRIGHT, D. A. *Proc. Phys. Soc.* [*London*], **62**, p. 398 (1949).
(17) JACOBS, H. *J. Appl. Phys.*, **17**, p. 596 (1956).
(18) DEB, S. *Indian J. Phys.*, **25**, p. 197 (1951).
(19) FAN, H. Y. *J. Appl. Phys.*, **14**, p. 552 (1943).
(20) GRATTIDGE, W., and SHEPHERD, A. A. *Proc. Phys. Soc.* [*London*] *B*, **67**, p. 177 (1954).
(21) KING, R. E. J. *Research*, **9**, p. 1 (1956).
(22) WRIGHT, D. A. *Proc. Roy. Soc. A*, **190**, p. 394 (1947).
(23) EISENSTEIN, A. *J. Appl. Phys.*, **20**, p. 776 (1949).
(24) NERGAARD, L., and MATHESON, R. *R.C.A. Rev.*, **15**, p. 3 (1954).
(25) MOTT, N. F. *Trans Farad. Soc.*, **34**, p. 500 (1938).
(26) WRIGHT, D. A. *Proc. Phys. Soc.* [*London*], **60**, p. 13 (1948).

The analysis of particle counts by the spray-drop method

By K. I. WILLIAMSON, M.Sc., A.Inst.P., Dominion Physical Laboratory, and W. B. TAYLOR, M.Sc., F.S.S., Applied Mathematics Laboratory, Department of Scientific and Industrial Research, New Zealand

[*Paper received* 29 *October*, 1957]

The spray-drop method is used in electron microscopy to determine the concentration of particles in an unknown suspension. The usual analysis procedure is criticized and a better one is given and justified. A test is included to check the presence of variations in the data due to causes other than purely random ones, e.g. inadequate mixing. The test is applied to artificial sets of data to illustrate its usefulness.

LIST OF SYMBOLS

n_i = true number of particles of n-type in ith drop.
ν_i = expected number of particles of n-type in ith drop.
m_i = true number of particles of m-type in ith drop.
μ_i = expected number of particles of m-type in ith drop.
$i = 1, 2, 3 \ldots N$, where N is the total number of drops examined.
$\kappa_i = \nu_i/\mu_i$.
ρ = expected ratio of concentration of n-type to m-type suspension.
$\hat{\rho} = r$ = best estimate of ratio ρ, where $\hat{}$ indicates best estimate from data.
σ_r^2 = variance of estimate of r.
$A = \sigma_r/r$ = coefficient of variation.

INTRODUCTION

Williams and Backus[1, 2] have described a method for the estimation of the concentration of particles in a suspension by the spray-drop method. They use as a reference a suspension of polystyrene latex spheres of known concentration. The two suspensions are mixed in known proportions, sprayed as a fine mist, collected on electron microscope specimen supports and examined in the microscope. Complete drops are photographed and the number of particles (n_i) and the number of latex spheres (m_i) in each whole drop are tabulated. The number of particles and the number of latex spheres do not bear the same ratio in all the drops. Indeed, if the counts are displayed graphically the picture they present may resemble Fig. 1 or Fig. 2. This scatter may be ascribed to random sampling errors or to bad mixing. The best estimate for the ratio of the concentrations of particles and latex in the original suspension is given by equation (1):

$$\text{best estimate of ratio} = r = \Sigma n_i/\Sigma m_i \qquad (1)$$

[the summations in this paper are taken over values of i from unity to the total number (N) of drops examined].

The concentration of particles is then obtained from the product of this ratio, the proportions used in preparing the mixture and the known concentration of latex spheres in the reference suspension.

The error of the estimated ratio is usually indicated by its variance. Luria, Williams and Backus[3] conclude that the variance of the estimated ratio is given by equation (2)

$$\text{variance of } r = \sigma_r^2 = r^2[(1/\Sigma n_i) + (1/\Sigma m_i)] \qquad (2)$$

The discussions in this paper support these two conclusions. However, it is important to know whether the scatter of the ratios of n_i/m_i for individual drops is large compared with what may be expected from, say, random errors alone. It is a common procedure to calculate the (product moment) correlation coefficient between the sets of numbers and use this as a guide.[3, 4] If the figure shows "high significance" then it is inferred that any errors arising from, say, bad mixing, are small. This procedure is quite unjustifiable and the present paper gives a better test.

It is usually considered that, for the most accurate determination of the ratio, it is best to adjust the proportion of the two suspensions in the mixture so that their ratio is unity (i.e. $r = 1$). The general tendency is to strive for $r = 1{\cdot}0$, rather than $1{\cdot}1$ or $0{\cdot}9$. It will be shown that the accuracy is indeed greatest for $r = 1$, but mixtures for which the ratio

lies between quite wide limits are not very different in the accuracy they provide.

The paper concludes with some illustrations of the power of the new test compared with the correlation coefficient, and gives a recommended analysis procedure for the spray-drop method.

VARIATION IN $(n_i m_i)$

Consider a single suspension of particles in a liquid. Let B be the total number of particles in the volume V. If the suspension were uniformly mixed we might, at first sight, expect the same number of particles in each element δV, namely $B\delta V/V$. However, particles in a suspension at ordinary temperatures exhibit considerable random movement. As a result, instead of constant numbers in each element δV, we would expect a certain randomness about some value. In fact, the numbers would form a Poisson distribution about some mean value.[5]

In the spray-drop technique, the situation is more complex. We have two sets of particles in the liquid. Each of the numbers $(n_i m_i)$ will have a randomness of the type described above which may be called an "inherent variation." Added to this are variations due to experimental factors—inadequate mixing, contamination during spraying, aggregation of particles, etc. These variations may be referred to as "induced variations."

Before any analysis procedure is begun, it is important to know whether there are any induced variations in the numbers $(n_i m_i)$. As indicated above, some authors have attempted to do this by the use of the correlation coefficient. This is not valid. The correlation between n_i and m_i has two parts:

(i) correlation between n-type and m-type particles within drops of the same size;

(ii) correlation between n-type and m-type particles within drops of differing sizes.

Considering part (i), if one assumes as above, that the two sets of particles are independent, each with independent Poisson distributions, the correlation should not differ significantly from zero (see Fig. 1). Departure from zero

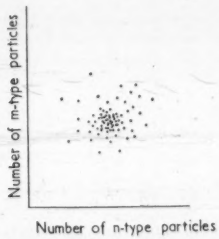

Fig. 1. Showing near-zero correlation between n-type and m-type particles in drops of the same size

would indicate either a wrong assumption as to the distributions being independent, or that excessively large numbers of one particle type are present so as to restrict the available volume of the drop left for the other particles. The latter alternative is most unlikely, but in any case the correlation would not be expected to be large.

Considering part (ii), the correlation here will depend on the range of sizes of the drop taken (see Fig. 2). In most cases, it will be high, provided a reasonable range is considered, since the numbers of n-type and m-type particles are expected to rise with drop size. The strength of the correlation indicates to some extent the range of drop size

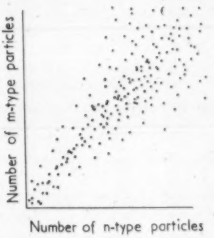

Fig. 2. Showing finite correlation between n-type and m-type particles in drops of differing sizes

considered, rather than the absence of induced variation. The correlation, in other words, is confounded with drop size and means little unless the drop sizes are given.

SUITABLE TEST FOR THE ABSENCE OF INDUCED VARIATION IN THE NUMBERS $(n_i m_i)$

For the ith drop, containing $(n_i m_i)$ particles we may consider these values each to be single numbers from two Poisson distributions of mean values $(\nu_i \mu_i)$ and

$$\nu_i/\mu_i = \kappa_i \tag{3}$$

Now the probability of obtaining m_i from a Poisson distribution, the mean of which is μ_i, is

$$p_{mi} = (e^{-\mu_i} \cdot \mu_i^{m_i})/m_i! \tag{4}$$

It follows from equations (3) and (4) that the joint probability for obtaining $(n_i m_i)$ for all drops is the product of similar expressions as (4) for $i = 1, 2, 3 \ldots N$.

i.e. joint probability or likelihood

$$= \prod_i \left[\frac{e^{-\kappa_i \mu_i} \cdot (\kappa_i \mu_i)^{n_i}}{n_i!} \cdot \frac{e^{-\mu_i} \cdot (\mu_i)^{m_i}}{m_i!} \right] \tag{5}$$

By the method of maximum likelihood[6] choice of the estimates of κ_i and μ_i which maximize the above, give the values

$$\hat{\kappa}_i = r_i = n_i/m_i \tag{6}$$

$$\hat{\mu}_i = m_i \tag{7}$$

Now, if we add the condition that there is no induced variation in the series of drops, we would expect

$$\kappa_i = \text{constant} = \rho \tag{8}$$

Replacing each κ_i by ρ in equation (3), and maximizing again, we get

$$\hat{\rho} = r = \Sigma n_i / \Sigma m_i \tag{9}$$

$$\hat{\mu}_i = (n_i + m_i)/(1 + r) \tag{10}$$

As a criterion of the absence of induced variation we test

**

the condition of κ_i = constant = ρ against κ_i not constant. To do this we compute the likelihood ratio test,[6] i.e. we compute the ratio R of the maximum value of the likelihood [equation (5)] which can be obtained when the κ_i's can be different [substituting from equations (6) and (7)], to the maximum likelihood when $\kappa_i = \rho$ [substituting from equations (9) and (10)]. It is known[6] that for large samples, minus twice the natural logarithm of this ratio is distributed as a χ-squared probability with $(N - 1)$ degrees of freedom. This distribution has been extensively tabulated by many authors and is readily available.[7, 8, 9] (Strictly, the number of observations should be large compared with the number of parameters fitted: this is not the case here, but the test should at least distinguish between those mixtures which fulfil the hypothesis and those that do not, even if the probability levels differ slightly from those given by the χ-square table.)

Thus replacing the κ_i, ρ and μ_i by their estimates in the expressions for the likelihood, we obtain

$$-2\log_e R = 2F = 2\Sigma[n_i \log_e n_i + m_i \log_e m_i - (n_i + m_i)\log_e(n_i + m_i) - n_i \log_e r + (n_i + m_i)\log_e(1 + r)] \quad (11)$$

the right-hand side being distributed as χ^2 with $(N - 1)$ degrees of freedom, if N is large.

The expression for $2F$ in equation (11) is easily computed with the aid of Table 4. The χ-squared probability P can be obtained from one of the references given above, e.g. Ref. 7. This P is the probability of obtaining by random chance a value of $2F$ as large as that computed, if there is an absence of induced variation and if the distribution is Poisson as postulated. A high value of $2F$ is indicative of unequal κ_i or non-Poisson distribution and gives a small value of P.

VALUE OF r

Having established a test for the absence of induced variation, we now proceed to find the best estimate of the ratio r, its variance and its most desirable value.

Provided there is no induced variation in the pairs $(n_i m_i)$, then the best estimate of the ratio has already been calculated in equation (9); i.e. best estimate of $r = \Sigma n_i / \Sigma m_i$, and this is the same expression as is used in the common procedures already described.

From equation (10) it follows that

$$\hat{\nu}_i = [r/(1 + r)](n_i + m_i) \quad (12)$$

Now ν_i and μ_i are means of Poisson distributions to which n_i and m_i belong respectively. It follows that the best estimates of the variance of these Poisson distributions are given by equations (10) and (12), since the variance of a Poisson distribution is equal to its mean.

By summing these two equations over all values of i, it is easy to show that the best estimate of the variance of Σn_i is Σn_i and of Σm_i is Σm_i. To obtain the variance of the ratio r, we can only use the usual approximate formula for the variance of the ratio of independent variates and this reduces to

$$\sigma_r^2 \doteq r^2[(1/\Sigma n_i) + (1/\Sigma m_i)] \quad (13)$$

This is the value obtained by Luria, Williams and Backus by a slightly different reasoning.

The labour in determining r is confined mainly to counting n_i and m_i. We may use the expression $(\Sigma n_i + \Sigma m_i)$ as a measure of the labour in determining r. For constant labour, we wish to find the value of r, which makes the proportional error of our determination a minimum. We compute the coefficient of variation $A = \sigma_r / r$ from equations (9) and (13) and the condition $\Sigma n_i + \Sigma m_i$ = constant = c. It is easy to show that the minimum value of σ_r / r is obtained when

$$\Sigma n_i = c/2, \quad \text{i.e. } r = 1$$

and that

$$A = (1 + r)/r^{1/2} c^{1/2}$$

For $r \ll 1$, A varies as $r^{-1/2}$ and for $r \gg 1$, A varies as $r^{1/2}$. At $r = 15$ or 0·065, the error A is only twice the error at $r = 1$. Thus the error in r increases slowly for r deviating from unity.

The change in the error in r, discussed above, assumes a constant amount of labour $(\Sigma n_i + \Sigma m_i)$. We may obtain a given error in r by obtaining many different pairs of n_i and m_i, the most efficient counting being obtained of course when $\Sigma n_i = \Sigma m_i$. This is illustrated in Table 1.

Table 1. *The proportional error in r obtained at constant labour for various values of r and also the amount of labour required to obtain the same error at r = 1.*

Proportional error in r (%)	*Count total of 400 particles*		*Most efficient counting r = 1*	
	Σn_i	Σm_i	Σn_i	Σm_i
10	200	200	200	200
13	100	300	125	125
20	25	375	50	50

TRIAL OF NEW TEST

It is not easy to obtain a mixture of two suspensions where the ratio of concentration is known beforehand. Instead, sets of pairs of numbers which display the same properties as $(n_i m_i)$ were obtained in the following way.

Over 400 pairs of numbers (range 1–50) were obtained on two independent counters in the same room, recording cosmic rays. The counters could be switched on and off simultaneously and were so operated for various short time intervals. The counts on both channels for a single operation of the switch were recorded as a pair and the operation was repeated over 400 times over various time intervals to obtain a table containing approximately equal numbers of integers 1–50 on the first register. The channels were then run for a long time and the ratio of these counts was used later as the "expected value" of r.

Groups of 16–20 pairs of numbers were made up by taking pairs at random from the table. The test was applied to each group and the probability P for the values of $2F$ so obtained was read from published tables.[7] The values of P and r for several sets of $(n_i m_i)$ are shown in Table 2. The expected value of the ratio r (i.e. ρ) is 0·966. The value of σ_r is approximately 0·075 for all these determinations.

Table 2. *The values of P from the test for various groups of data with ratio r*

r	0·87	0·88	0·91	0·93	0·95	0·96
P	0·68	0·62	0·53	0·25	0·77	0·92
r	0·96	1·00	1·03	1·07	1·08	1·12
P	0·83	0·91	0·53	0·85	0·02	0·09

The last two columns of Table 2 have values of r furthest from the expected value $\rho = 0{\cdot}966$. They also have the lowest value of P. This may be a coincidence, or it may indicate some dependence of P on r, or it may follow from the fact that the groups were taken from a limited universe (of the order of 400 pairs) or the approximation of N being large was unsatisfied ($N = 16 - 20$). Much further work would be needed to elucidate this.

COMPARISON OF THIS TEST WITH CORRELATION COEFFICIENT

Table 3 gives figures obtained for both tests on some groups of data. That the proposed test is a critical one is

Table 3. *Comparison of new test with correlation coefficient*

	r	P from new test	Correlation coefficient	Significance of correlation (%)
a	1·00	0·91	0·91	<0·1
b	1·12	0·09	0·76	<0·1
c	0·86	0·55	0·84	<0·1
d	0·80	0·005	0·66	<1
e	1·01	0·92	0·65	2

obvious; (*a*) and (*b*) are two results from the trial; (*c*) was obtained from a modification of the data for (*a*), in which the values of n_i for i odd were changed to $\frac{3}{4}n_i$, thus simulating bad mixing. In result (*d*), the values of n_i for i odd in (*a*) were changed further to $\frac{1}{2}n_i$. The new test showed these changes, but the correlation coefficient still showed high significance. The change in P from (*a*) to (*c*) is not as large as may at first sight be expected. The value $P = 0{\cdot}91$ in (*a*) is high and indicates that the data are exceptionally uniform. The change in the data from (*a*) to (*c*), whilst appreciable, has produced pairs ($n_i m_i$) which are still reasonably uniform. The further change in (*a*) to (*d*) has, however, produced a marked change in the uniformity.

In result (*e*), the data for (*a*) were again modified by omitting the three pairs of smallest numbers. As would be expected, the correlation coefficient has changed greatly, but the other test showed the result to be a good one, as indeed it is.

RECOMMENDED PROCEDURE

The procedure can be summarized as follows:

(1) Adjust the ratio of the number of virus particles to the number of latex particles in the suspension to be sprayed, so that the expected ratio is nearly unity (within one order of magnitude). This can be done by preliminary trials.

(2) Tabulate pairs of numbers ($n_i m_i$) for N drops from the micrographs. Compute $2F$ from equation (11) with the help of Table 4. Consult suitable tables[7, 8, 9] to obtain the probability of obtaining this value of $2F$ if there were no induced variation. If the test shows that the data are not unsatisfactory, then compute the following:

(3) best value for ratio $r = \Sigma n_i / \Sigma m_i$;

(4) variance of ratio $\sigma_r^2 = r^2[(1/\Sigma n_i) + (1/\Sigma m_i)]$.

Table 4. $n \log_e n$

n	$n \log_e n$	n	$n \log_e n$	n	$n \log_e n$
1	0	38	138·23	75	323·81
2	1·39	39	142·88	76	329·13
3	3·30	40	147·56	77	334·47
4	5·55	41	152·26	78	339·82
5	8·05	42	156·98	79	345·19
6	10·75	43	161·73	80	350·56
7	13·62	44	166·51	81	355·96
8	16·64	45	171·30	82	361·35
9	19·78	46	176·12	83	366·77
10	23·03	47	180·96	84	372·19
11	26·38	48	185·82	85	377·63
12	29·82	49	190·70	86	383·08
13	33·35	50	195·60	87	388·53
14	36·95	51	200·52	88	394·01
15	40·62	52	205·47	89	399·49
16	44·36	53	210·43	90	404·98
17	48·16	54	215·41	91	410·49
18	52·03	55	220·41	92	416·01
19	55·95	56	225·42	93	421·53
20	59·91	57	230·46	94	427·07
21	63·94	58	235·51	95	432·62
22	68·00	59	240·58	96	438·18
23	72·12	60	245·66	97	443·75
24	76·27	61	250·77	98	449·33
25	80·47	62	255·88	99	454·93
26	84·71	63	261·02	100	460·52
27	88·99	64	266·17	101	466·13
28	93·30	65	271·34	102	471·75
29	97·65	66	276·52	103	477·37
30	102·04	67	281·72	104	483·02
31	106·45	68	286·93	105	488·67
32	110·91	69	293·15	106	494·33
33	115·39	70	297·40	107	499·99
34	119·90	71	302·65	108	505·67
35	124·44	72	307·92	109	511·36
36	129·01	73	313·21	110	517·06
37	133·60	74	318·50	111	522·76

REFERENCES

(1) WILLIAMS, R. C., and BACKUS, R. C. *J. Amer. Chem. Soc.*, **71**, pp. 4052–4057 (1949).

(2) BACKUS, R. C., and WILLIAMS, R. C. *J. Appl. Phys.*, **21**, pp. 11–15 (1950).

(3) LURIA, S. E., WILLIAMS, R. C., and BACKUS, R. C. *J. Bact.*, **61**, p. 179 (1951).

(4) DONALD, H. B., and ISAACS, A. *J. Gen. Microbiol.*, **10**, p. 457 (June 1954).

(5) See, for example, FRY, T. C. *Probability and its engineering uses*, p. 410 (New York: D. Van Nostrand Co. Inc., 1928).

(6) KENDALL, M. G. *The advanced theory of statistics*, Vol. 2 (London: Cambridge University Press, 1946).

(7) PEARSON, K. *Tables for Statisticians and Biometricians, Part I*, Table 12 (London: Cambridge University Press, 1945).

(8) FISHER, R. A., and YATES, F. *Statistical tables for Biological, Agricultural and Medical Research*, 3rd Ed. (Edinburgh: Oliver and Boyd, 1948).

(9) PEARSON, E. S., and HARTLEY, H. O. *Biometrika tables for statisticians*, Vol. 1 (London: Cambridge University Press, 1954).

The chromatic field aberrations and their correction in a three lens reflexion electron microscope

By D. H. PAGE, M.A., British Paper and Board Industry Research Association, Kenley, Surrey

[*Paper received* 25 *October*, 1957]

The coefficient of the chromatic difference in magnification for a three lens reflexion electron microscope is found to be a function of the focal length of the intermediate lens and the axial position of the objective aperture. A condition is shown to exist for which the coefficient vanishes and the aberration is then corrected. The coefficient of the chromatic difference in rotation is proportional to the overall rotation of the image and can be minimized by exciting lenses in opposition. The effect on the image of a misalinement of the objective aperture is also dealt with. Tolerances in the settings of the correction conditions for the aberrations and in the alinement of the objective aperture are calculated for typical values of the energy spread in the electron beam at low and high angles of beam deviation.

INTRODUCTION

In the reflexion electron microscope the resolving power is determined by the chromatic aberration of the system because of the relatively large energy losses suffered by electrons scattered from the specimen. The resolving power d on the axis of the microscope is given by the equation

$$d = \alpha C_c \delta v / v \qquad (1)$$

where α is the semi-angle of the aperture,

C_c is the chromatic aberration constant of the objective lens,

δV is the energy spread of electrons forming the image and V is the accelerating voltage.

However, abaxial points are in general less well defined because of the chromatic field aberrations of difference in magnification and rotation. These aberrations, particularly the former, can severely limit the size of the focused region unless consideration is given to their reduction. This is particularly necessary when the angle of beam deviation, and hence the energy spread, is large.

CHROMATIC DIFFERENCE IN MAGNIFICATION

The theory of the chromatic difference in magnification of actual electron lenses has been put forward by Morito[1] and his results agree with the experimental evidence of Katagiri.[2] These results are, however, only valid for transmission electron microscopy. The only mention of this aberration in reflexion electron microscopy is by Cosslett and Jones[3] and they do not give a generally valid solution. From Morito's results it appears that the rather weak lenses used for the relatively low magnifications needed in reflexion work may be considered as "thin" to a good approximation. The treatment given here is therefore derived from the light optical analogue. The focal lengths of the lenses are considered to be proportional to a variable V corresponding to the voltage of the electrons.

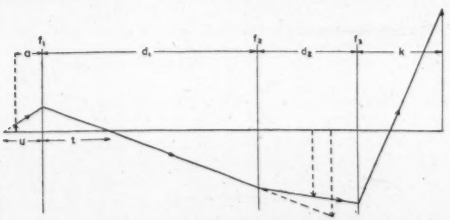

Fig. 1. Image formation in a three lens electron microscope

In calculating the chromatic aberration of magnification it is necessary to consider the general case of the unfocused image for the system focuses only those electrons of a certain energy. It is possible to derive for a system of three thin lenses an expression for the magnification on the screen in terms of a parameter u, the distance between the lens centre and the intersection with the axis of the ray leaving the object. The image formation in a three lens electron microscope operating at low magnification[4] is shown in Fig. 1.

We can then obtain the following expression:—

$$M = \frac{k}{u - a}\frac{1}{f_1 f_2 f_3}\left[(d_2 f_2 - d_1 d_2 + d_1 f_2 + d_2 f_1 - f_1 f_2)u + (d_1 d_2 - d_2 f_2 - d_1 f_2) f_1\right] \qquad (2)$$

where a is the object distance,

k is the distance from the third lens to the screen,

f_1, f_2, f_3 are the focal lengths of the three lenses,

and d_1 and d_2 are the separations between the two pairs of lenses.

This equation assumes that f_3 may be neglected in the presence of terms containing d_1, d_2, f_2 and k.

It is interesting to note in passing that the condition for a focused image may be derived from this equation. When the image is in focus the magnification is independent of u giving the condition

$$a\left(1 + \frac{d_2 f_1 - f_1 f_2}{d_1 f_2 + d_2 f_2 - d_1 d_2}\right) = f_1 \qquad (3)$$

In reflexion electron microscopy the specimen becomes effectively a secondary source of electrons. The variation in intensity of the scattered beam over an angle as small as the aperture is negligible so that the image is formed on the average by those electrons passing through the centre of the aperture. u is thus the distance between the aperture and the centre of the lens. When the aperture is on the side of the lens remote from the object, u must be replaced by the parameter t where $u(t - f_1) = f_1 t$.

From equation (2) it is possible, by differentiation with respect to V, to derive the coefficient of chromatic difference of magnification C_M given by $\delta M \,.\, V/\delta V \,.\, M$.

$$C_M = \frac{(3d_1 d_2 - 2d_2 f_2 - 2d_1 f_2 + f_1 f_2 - 2d_2 f_1)u + (d_2 f_2 + d_1 f_2 - 2d_1 d_2) f_1}{(d_2 f_2 + d_1 f_2 - d_1 d_2 + d_2 f_1 - f_1 f_2)u + (d_1 d_2 - d_1 f_2 - d_2 f_2) f_1} \qquad (4)$$

It will be seen that there is a value of f_2 for which C_M vanishes and it is this value that is required for the correction of the magnification error. The condition is

$$f_2 = \frac{(3d_1d_2 - 2f_1d_2)u - 2d_1d_2f_1}{(2d_1 + 2d_2 - f_1)u - (d_1 + d_2)f_1} \tag{5}$$

If f_1 is considered small compared with d_1 and d_2 this reduces to

$$f_2 = \frac{d_1d_2}{(d_1 + d_2)}\left(\frac{3u/f_1 - 2}{2u/f_1 - 1}\right) = \frac{d_1d_2}{(d_1 + d_2)}\left(\frac{t/f_1 + 2}{t/f_1 + 1}\right) = \gamma\frac{d_1d_2}{d_1 + d_2} \tag{6}$$

The focal length required is thus a function of the position of the aperture. When the aperture is in the back focal plane of the lens γ is 1·5. In this condition electrons leaving the specimen travelling parallel to the axis are selected by the aperture. This is similar to the case of transmission microscopy in which the image is formed largely by electrons leaving the specimen travelling parallel to the axis. This condition (with $\gamma = 1{\cdot}5$) is not explicitly stated by Morito[1] though it can readily be derived from his equations. Cosslett and Jones[3] give this condition with $\gamma = 2$ for a reflexion instrument, but make no mention of the dependence of this constant on the aperture position and do not state the position for which their equation is valid. A graph of aperture position against the value of γ for which the aberration constant is zero is shown in Fig. 2.

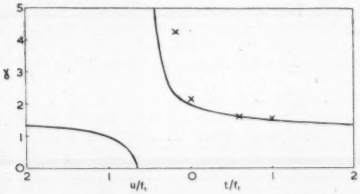

Fig. 2. Relationship between aperture position and γ [equation (6)]

For a given position of the aperture the effect on the aberration constant of an incorrect choice of the intermediate lens focal length can be determined and is given by the equation

$$C_M = \frac{(1 - \phi)[6(u/f_1)^2 - 7(u/f_1) + 2]}{(3\phi - 2)(u/f_1)^2 + (3 - 5\phi)(u/f_1) + 2\phi - 1} \tag{7}$$

where $\phi = f_2/f_{20}$, f_{20} being the value of f_2, for which $C_M = 0$. Fig. 3 shows the effect on the aberration constant of variation

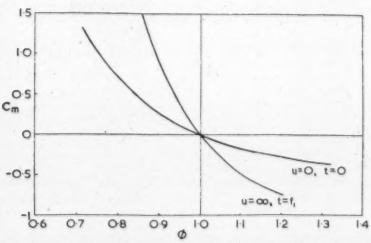

Fig. 3. Relationship between coefficient of chromatic difference in magnification C_M and ϕ [equation (7)]

in ϕ for different positions of the aperture. It is also possible to determine the effect on C_M of an incorrect choice of the aperture position. It is given by $C_M = u/(f - u)$ when the aberration is corrected for the aperture at the centre of the lens (Fig. 4, curve *A*), and $C_M = f/(f - u)$ when it is corrected at the back focal plane (Fig. 4, curve *B*).

It should be noted that the assumptions made earlier, that f_1 and f_3 may be neglected compared with d_1, d_2, f_2 and k are not strictly valid under normal working conditions. The effect of this approximation is generally small. However, equation (7) gives a value for C_M that can be appreciably lower than the correct value when ϕ is less than 0·8.

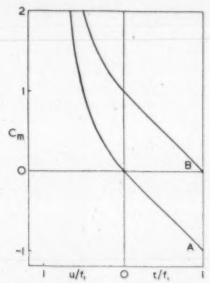

Fig. 4. Relationship between coefficient of chromatic difference in magnification C_M and aperture position

APERTURE CENTRICITY

The effect of an eccentric mounting of the aperture may be considered from equation (4) and is included here because of the importance of accurate aperture centration in reflexion work. The ray passing through the centre of an eccentric aperture does not in general cross the axis. In the special cases in which it does the position of crossing is different for each object point. It can be shown from equation (4) that an eccentricity of the aperture produces in the absence of a rotational aberration a uniform lateral blurring of the image in the direction of the eccentricity. This blurring is independent of the axial position of the aperture provided it lies between the centre of the lens and the back focal plane and is approximately given by the equation

$$\delta x = p\delta V/V \tag{8}$$

where p is the eccentricity of the aperture.

When the aperture lies between the lens and the object the centration is more critical and the aberration is given approximately by the equation

$$\delta x = (1 - u/a)^{-1}p\delta V/V \tag{9}$$

In the presence of a rotational aberration a misalinement of the aperture causes a movement of the centre of rotation in the direction perpendicular to the direction of eccentricity.

CHROMATIC DIFFERENCE IN ROTATION

The difference in rotation $\delta\psi$ of an image due to an energy spread δV is given by the equation

$$\delta\psi = \psi\delta V/2V \tag{10}$$

where ψ is the total rotation of the image.

The coefficient of chromatic difference in rotation is then simply given by:

$$C_R = V\delta\psi/\delta V = \psi/2 \qquad (11)$$

Thus the rotational aberration is only completely corrected for certain discrete values of the lens currents that make the total rotation of the image zero. Fortunately complete correction of this aberration is not necessary. The tolerance in the correction will be considered in a later section.

EXPERIMENTAL RESULTS

A quantitative verification of equation (6) has been made and the experimental points are shown in Fig. 2. The simple theory is apparently adequate in describing the relationship between the required focal length and the aperture position when the aperture is below the centre of the lens. When the aperture is above the centre of the lens the experimental points deviate from the theoretical curve but a qualitative agreement still holds. Good agreement was also obtained in a single experiment to determine the value of C_M for a given value of ϕ [equation (7), Fig. 3]. While no further verifications have been made all the results agree qualitatively and to some extent quantitatively with the author's experience in reflexion work.

PRACTICAL SIGNIFICANCES

To ensure a sharp image over the area of a lantern plate the error in the magnification $\delta M/M$ should not exceed $1{\cdot}5 \times 10^{-3}$. This would give quite a large field having 1300 resolved picture points across its width. It has been estimated that, with an angle of beam deviation of 26·5°, $\delta V/V$ is approximately 0·01,[5] whereas at low angles of beam deviation (5–10° say) it is in the region of 0·0015. C_M must therefore lie within $\pm 0{\cdot}15$ for the high angle case and within $\pm 1{\cdot}0$ for low angles. This represents quite a severe restriction at high angles for the focal length of the intermediate lens must lie between 93 and 109% of the correct value, when the aperture is at the centre of the lens. At low angles the restriction is far less severe and the magnification aberration is not troublesome provided that the focal length of the lens is greater than 75% of the calculated best value. The restriction is, however, more severe when the aperture is positioned in the back focal plane of the lens.

The effect of a vertical movement of the aperture on the constant C_M shown in Fig. 4, is of some practical importance. It is often the practice in reflexion work to raise the aperture for focusing.[6] This increases the angular aperture and gives a brighter image of poorer resolution that is more easily focused. The aperture is then lowered for recording the image. The coefficient C_M varies however with variation of the aperture position and if it is zero when the aperture is in its lowered position it can become appreciable when the aperture is raised. The effect is only noticeable at high angles of beam deviation, but under these conditions it can mar the image sufficiently to offset the advantages of this technique.

Alinement of the aperture is critical both at low and high angles of deviation. It will be seen from equation (8) that the maximum permitted eccentricity is 6 μ at high angles when a resolution of 600 Å is sought and 13 μ at low angles when a resolution of 200 Å is sought. A method by which this accuracy can be readily achieved is described elsewhere.[5] The greater sensitivity of the image quality to aperture centration when the aperture is raised [equation (9)] is another factor that makes the procedure of raising the aperture for focusing ineffective at high angles.

The reduction of the rotational aberration [equation (10)] to an insignificantly low value may be readily achieved by choosing the senses of the lens excitations so as to minimize the total rotation of the image. The aberration is unnoticeable when $\delta\psi$ is less than $1{\cdot}5 \times 10^{-3}$. This implies that ψ must be less than 17° at high angles of deviation and less than 120° at low angles. Such conditions can usually be found within the magnification range required.

CONCLUSIONS

The simple light optical analogue is adequate for an approximate quantitative treatment of the chromatic aberration of difference in magnification in the reflexion electron microscope. The coefficient of this aberration is dependent on the focal length of the intermediate lens and the axial position of the objective aperture. A focal length of the intermediate lens exists for which the coefficient is zero and at this setting the aberration is corrected. The tolerance in this setting is dependent on the energy spread of the scattered electrons and is approximately $\pm 8\%$ at the high angle of beam deviation of 26°. At low angles of beam deviation the tolerance is much wider. The effect of the chromatic difference in rotation of the image is less important and sufficient correction is normally obtained when the lenses are excited in opposition making the overall rotation of the image small. The alinement of the aperture is critical both in low and high angle reflexion work and must be made with some accuracy.

One of the main advantages of the reflexion method lies in the large overall view of the specimen that it affords, but this is only realized when the field aberrations are corrected. Micrographs showing the large attainable field of view under correction conditions, at a high angle of beam deviation have appeared in an earlier communication.[5] The author has, however, seen many reflexion electron micrographs both exhibited and published in which the field aberrations have severely limited the field of view. Much of the value of the reflexion method is then lost. It may well be that the lack of attention to these aberrations in the past is responsible in part for the general loss of interest in reflexion work.

REFERENCES

(1) MORITO, N. *J. Appl. Phys.*, **25**, p. 986 (1954).

(2) KATAGIRI, S. *Rev. Sci. Instrum.*, **26**, p. 870 (1955).

(3) COSSLETT, V. E., and JONES, D. *J. Sci. Instrum.*, **32**, p. 86 (1955).

(4) CHALLICE, C. E. *Proc. Phys. Soc.* [*London*], *B*, **63**, p. 59 (1950).

(5) PAGE, D. H. *Brit. J. Appl. Phys.*, **9**, p. 60 (1958).

(6) MENTER, J. W. *J. Inst. Metals*, **81**, p. 163 (1952).

Solid angle corrections to single scattering

By F. F. Heymann, B.Sc.(Eng.), Ph.D., and P. I. P. Kalmus, B.Sc., Ph.D., Department of Physics, University College London

[*Paper received* 25 *November*, 1957]

Corrections relating the average intensity of particles scattered into an aperture of finite solid angle to the intensity at the centre of the aperture are given for rectangular and circular apertures. The dependence of the corrections on aperture shape and scattering angle is calculated for electrons scattered according to the simple Mott formula.

In scattering experiments it is not possible to observe the number of particles scattered at a single angle θ_0 but only over a finite solid angle. In experiments where the scattered particles are detected by counters, this is usually accomplished by scattering into a collimating aperture which subtends a known solid angle at the point of scattering, having θ_0 at its centre.

If the variation of scattering intensity with angle is given by $\sigma(\theta)$ where $\sigma(\theta)d\theta$ is the differential scattering cross-section then since the particles which are counted will all have been scattered through slightly different angles, the average intensity I_A over the aperture will not in general be equal to I_0 the intensity at θ_0.

For convenience consider the angle θ_0 to be in the horizontal plane. Then if the particle is scattered into the defining aperture in such a direction as to make angles $\Delta\theta_x$, $\Delta\theta_y$ in the horizontal and vertical planes with the angle θ_0, it can be shown from spherical trigonometry that the particle has been scattered through an angle which to a second order approximation is given by

$$\theta = \theta_0 + \Delta\theta_x + \tfrac{1}{2}(\Delta\theta_y)^2 \cot\theta_0 \qquad (1)$$

The effect of the integration of this equation to cover the cases of rectangular and circular apertures is to be considered.

RECTANGULAR APERTURE

If the defining aperture is a rectangle having horizontal and vertical sides and having an angular width W and angular height h, the average intensity of scattering into this rectangle has been given by Lyman, Hanson and Scott[1] and is

$$I_A = I_0\left(1 + \frac{\sigma' h^2 \cot\theta_0}{\sigma 24} + \frac{\sigma'' W^2}{\sigma 24}\right) = I_0(1 + C) \qquad (2)$$

where σ' and σ'' represent the first and second derivatives of σ with respect to θ.

Thus it can be seen that the correction C, which must be applied in order to correlate I_A and I_0 depends on different functions of the height and width of the aperture and hence for a given angle of scattering depends on the shape of the aperture.

Furthermore it can be seen that in a particular angular range where $\sigma(\theta)$ is a monotonic function which decreases more rapidly than linearly with θ, σ' will be negative and σ'' positive, and hence while the width-dependent term in equation (2) will always be positive, the height-dependent term will be negative for values of θ_0 up to 90°. Hence in principle it would be possible to obtain a zero correction at any angle up to 90° by correct choice of the ratio h/W provided the function $\sigma(\theta)$ was of the type specified above and was known.

In practice this function is not generally known exactly and hence either an approximate angular variation of cross-section would have to be assumed, or alternatively the experimentally determined (uncorrected) variation could be used as an approximation in order to calculate the correction and hence a more accurate value of the cross-section obtained. Thus it would be desirable to keep the solid-angle correction at a fairly low value.

The solid angle correction is seen to be zero when the height to width ratio is

$$\frac{h}{W} = \sqrt{\left(-\frac{\sigma''}{\sigma}\Big/\frac{\sigma' \cot\theta_0}{\sigma}\right)} \qquad (3)$$

This ratio would be different for each angle and if cross-sections are to be measured at a series of angles it may not be very desirable to have a different defining aperture at every angle used. One reason for this which is applicable to high energy scattering is that there is another correction connected with the defining aperture, namely the correction due to multiple scattering of the particles through the material of the collimating aperture. This correction has been calculated by Courant[2] who listed values of the correction for protons collimated by long narrow slits and by Kalmus[3] who calculated corrections for electrons of a particular energy (28 MeV) collimated by circular apertures. This correction which depends on the material of the collimator and the energy resolution of the detecting apparatus (since the particles passing through the material of the collimator will have lost energy and hence could be discriminated against) results in an effective increase in aperture dimensions. Thus if this effect is important as it can be at high energies, it would be desirable to use the same collimating aperture at all angles. It is therefore instructive to calculate the solid angle corrections at various angles for rectangular apertures of different shapes which subtend a given solid angle.

CORRECTIONS FOR MOTT SCATTERING

The solid angle corrections have been calculated using the variation of $\sigma(\theta)$ given by the Mott formula in the fully relativistic case and Born approximation.

This formula which is valid for the elastic single scattering of electrons by point nuclei provided that the electron velocity approaches that of light and that $Z/137 \ll 1$ where Ze is the nuclear charge, is

$$\sigma(\theta)d\theta = \left(\frac{Ze^2}{2E}\right)^2 \frac{\cos^2\tfrac{1}{2}\theta}{\sin^2\tfrac{1}{2}\theta} \qquad (4)$$

where E is the total energy of the incoming electrons.

Since the electron energy must be relativistic and yet not sufficiently high for finite nuclear size effects to become

important, equation (4) would not be valid outside the energy range 3 to 20 MeV and would not even be strictly accurate in this range if radiative corrections as calculated by Schwinger[4] are taken into account. However, for the purposes of the solid angle corrections it should yield usable results for a much wider range of energies.

Fig. 1 shows the solid angle corrections as calculated from equations (2) and (4) for rectangular apertures of various heights to width ratios. The corrections have been expressed as percentage corrections for a solid angle of 0·01 sterad but

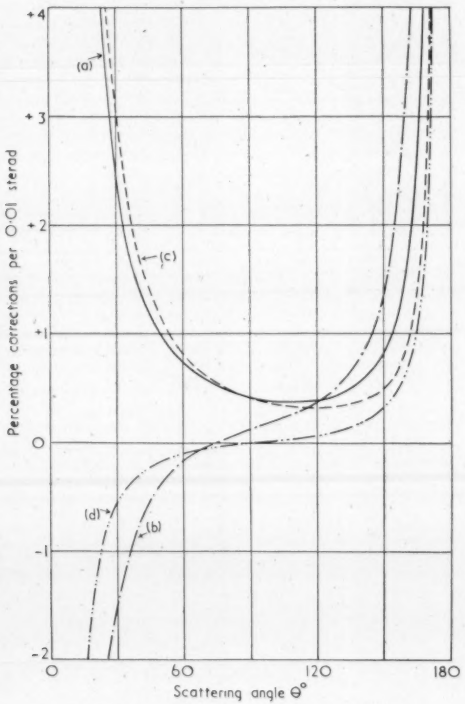

Fig. 1. Solid angle corrections for rectangular apertures of various height/width ratio

(*a*) ———— Correction for $h/W = 1$
(*b*) —— — —— Correction for $h/W = 4$
(*c*) — — — → $h/W \times$ correction for $h/W \to 0$
(*d*) —— - - —— - - $W/h \times$ correction for $h/W \to \infty$

could alternatively be regarded as fractional corrections per unit solid angle.

Fig. 2 shows the aperture height to width ratios required in order that the solid angle correction for Mott scattering should be zero. It can be seen that very high, narrow apertures are required when the angle of scattering approaches 90°. For small angles the required ratio $h/W \to \sqrt{5}$ as $\theta \to 0$, but at $\theta = 0$ a zero correction is not possible. Zero corrections also cannot be obtained for scattering angles above 90°.

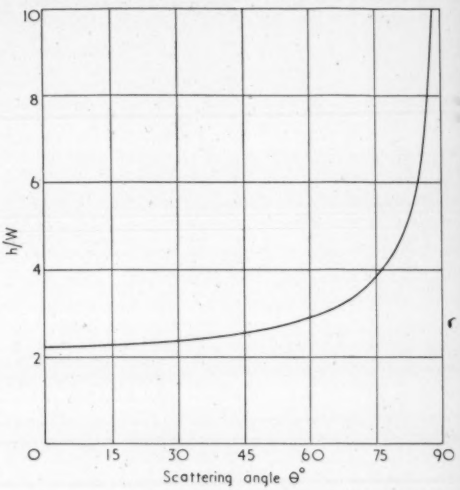

Fig. 2. Height/width ratios required for zero solid angle corrections

CIRCULAR APERTURES

By suitable integration of equation (1), over a circular aperture subtending a solid angle Ω at the point of scattering it can be shown that the average intensity I in this case is related to the intensity at the centre by

$$I = I_0\left(1 + \frac{\Omega\sigma' \cot\theta_0 + \Omega\sigma''}{8\pi\sigma}\right) \qquad (5)$$

It can be seen that this correction is almost identical to that for a square aperture ($h^2 = W^2 = \Omega$), the number 24 in the denominator of equation (2) being replaced by 8π. Thus circular aperture corrections will have exactly the same angular dependence as square apertures but will be lower by a factor of $3/\pi$, i.e. 0·955.

ACKNOWLEDGEMENTS

The authors wish to thank Prof. H. S. W. Massey for his interest in the programme of electron scattering at University College.

REFERENCES

(1) Lyman, E. M., Hanson, A. O., and Scott, M. B. *Phys. Rev.*, **84**, p. 626 (1951).
(2) Courant, E. D. *Rev. Sci. Instrum.*, **22**, p. 1003 (1951).
(3) Kalmus, P. I. P. p. 93 (London University: Ph.D. Thesis, 1957).
(4) Schwinger, J. *Phys. Rev.*, **75**, p. 898 (1949).

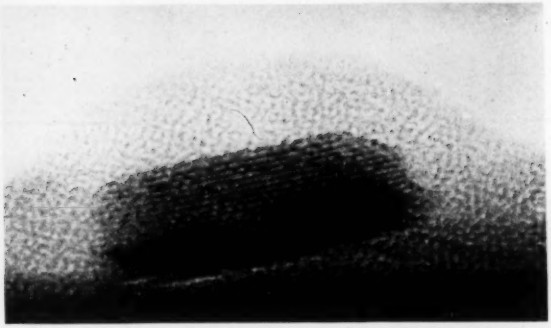

[Reproduced from *Philosophical Magazine*]

Fig. 1. Electron micrograph of a molybdenum oxide platelet, resolving the (020) planes of spacing 6·9 Å (× 1 500 000) (Menter and Bassett)

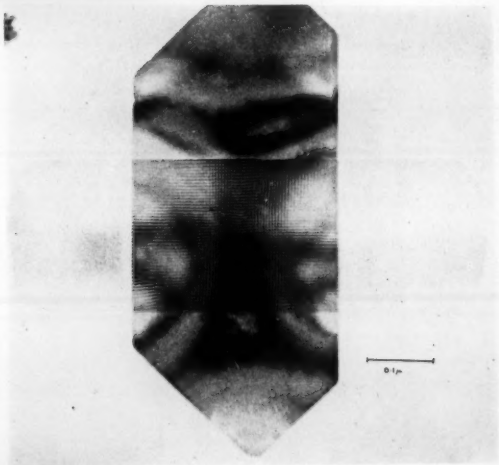

[Reproduced from *Proceedings of Regional Conference on Electron Microscopy*]

Fig. 2. Crossed molybdenum oxide lamellae, showing typical fringe pattern with spacing 110 Å (× 125 000) (Dowell, Farrant and Rees)

[Reproduced from *Nature*]

Fig. 3. Moiré pattern from superimposed gold and palladium lattices with (111) planes in parallel orientation. Edge dislocations are to be seen in several regions (× 200 000) (Pashley, Menter and Bassett)

See pages 253–256

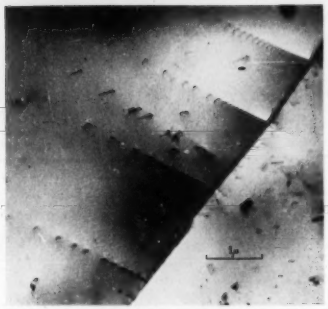

[Reproduced from *Proceedings of the Royal Society of London*]

Fig. 4. Rows of dislocations piled up against a grain boundary. Direct electron micrograph of stainless steel film (×10 500) (Bollmann)

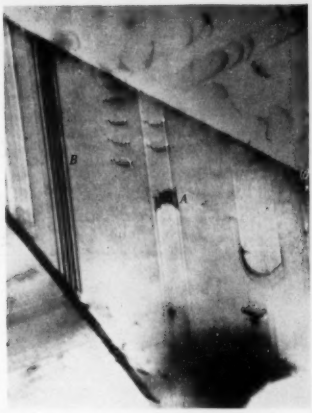

Fig. 5(*a*)

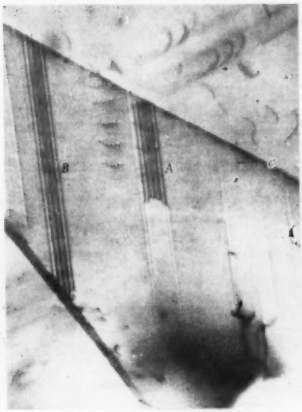

Fig. 5(*b*)

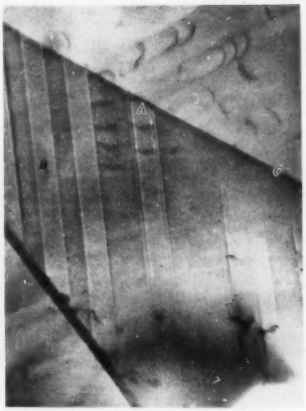

Fig. 5(*c*)

[Reproduced from *Proceedings of the Royal Society of London*]

Fig. 5. Sequence of electron micrographs of stainless steel film. Many of the dislocations are dotted and some have spread into bands (as at *A*), owing to the stacking fault formed when a dislocation splits into two partials. *B* is a wide stacking fault; *C* is a twin boundary. In (*c*) the back partials of *A* and *B* have moved up, removing the stacking fault (×32 500) (Whelan, Hirsch, Horne and Bollmann)

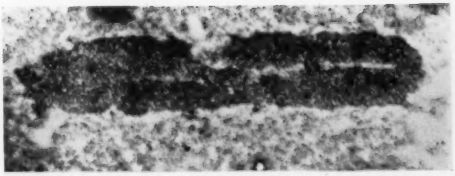

Fig. 6. Longitudinal section of metaphase chromosome from locust testis, fixed with formaldehyde and stained with lanthanum acetate (×14 000) (Gibbons and Bradfield)

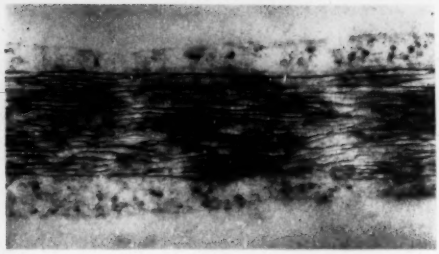

(*a*)

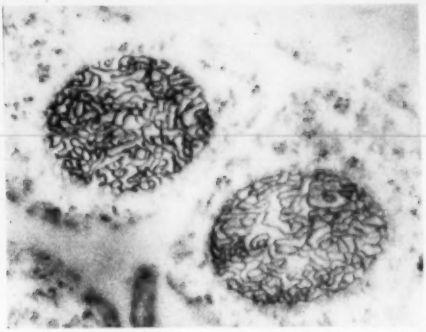

(*b*)

[Reproduced from *Journal of Biophysical and Biochemical Cytology*]

Fig. 7. Longitudinal (*a*) and transverse (*b*) sections of locust spermatid nuclei at late stage of maturation. Fixed with formaldehyde and stained with lanthanum nitrate (× 35 000) (Gibbons and Bradfield)

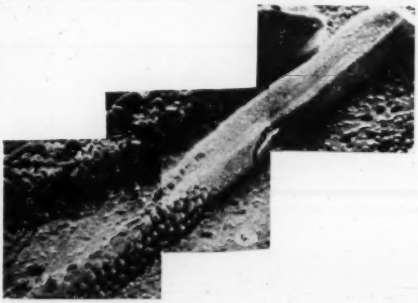

[Reproduced from *Nature*]

Fig. 8. Reflexion micrograph from the electron scanning microscope of silver azide needle on heated silver disk decomposing from lower end (× 4500 laterally, × 3250 vertically) (Bowden, McAuslan and Smith)

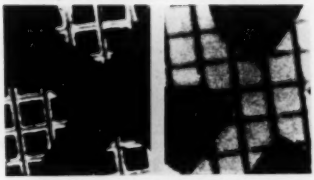

(*a*) (*b*)

Fig. 9. Silver (1500 t.p. in.) and copper (300 t.p. in.) grids in the X-ray scanning microscope (× 375). In (*a*) the analysing system records only silver K radiation, in (*b*) only copper K radiation (Cosslett and Duncumb)

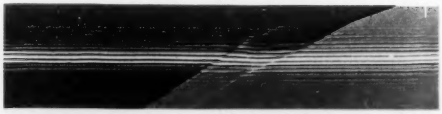

[Reproduced from *Physikalische Blätter*]

Fig. 11. Phase shift in the electron interference fringes at the edge of a carbon film, resting on another film (× 5000) (Möllenstedt and Bühl)

New techniques for the study of Bitter figures

By D. J. Craik and P. M. Griffiths

See pages 279–282

Fig. 1. ×500. Micrograph of coarse structure on cleaved surface of manganese ferrite, by normal wet colloid technique

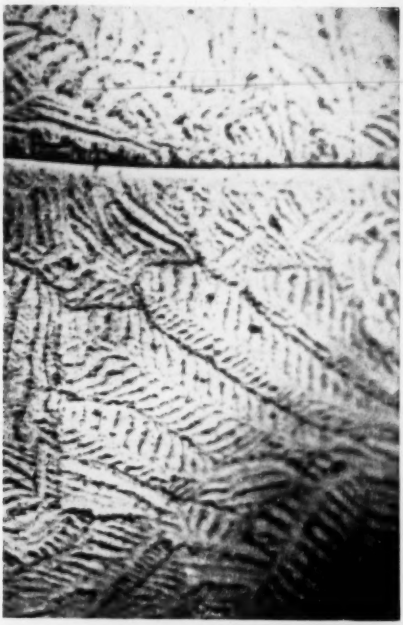

Fig. 2. ×500. Micrograph of coarse structure on cleaved surface of manganese ferrite, by "dried" film technique

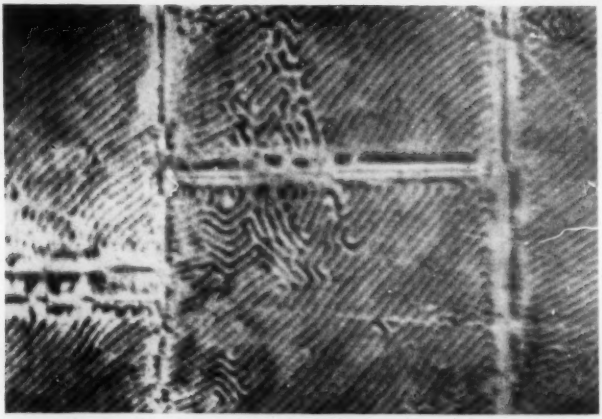

Fig. 3. ×1000. Micrograph of fine structure on cleaved surface of manganese ferrite

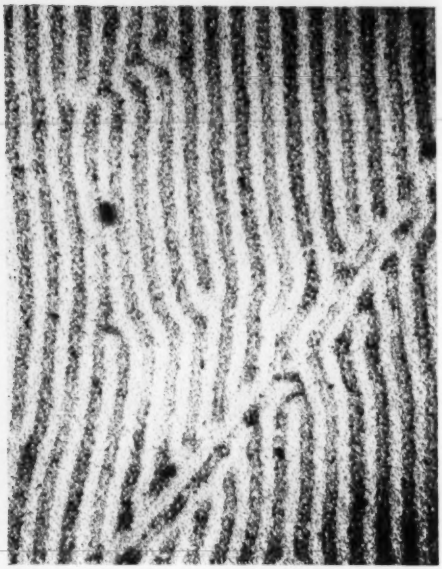

Fig. 4. ×10000. Electron micrograph of fine structure on cleaved surface of manganese ferrite

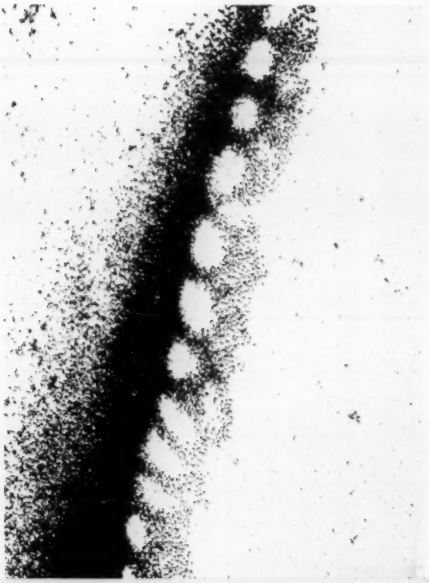

Fig. 5. ×10000. Structure at a scratch, in cobalt. Note that no particles can be seen inside closed loops

The photoelastic technique for strain measurement on flat aluminium alloy surfaces

By H. Fessler and D. J. Haines

See pages 282–287

Fig. 2. Example of stress free model

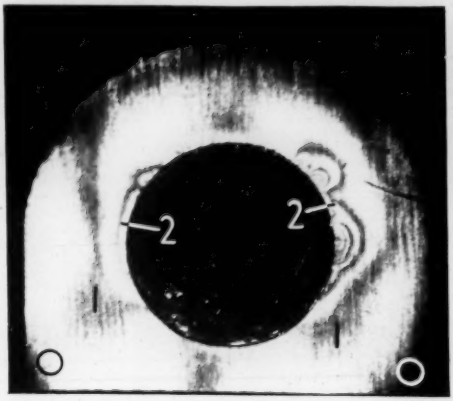

Fig. 6(*a*). Load = 1000 lb = 0·34 *Y*

Fig. 6(*b*). Load = 2000 lb = 0·68 *Y*

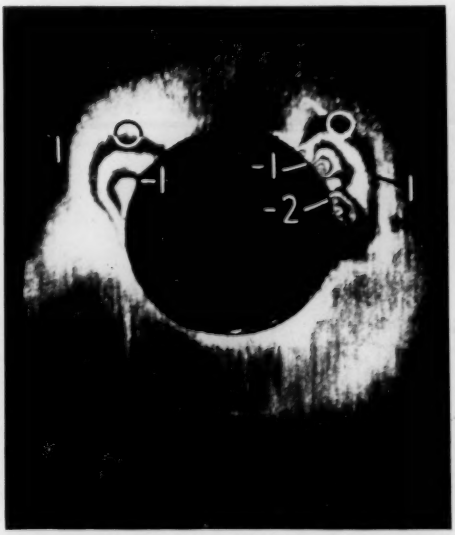

Fig. 6(*c*). Fringe pattern after removal of 2000 lb load

Fig. 6. Fringe patterns on $\frac{1}{4}$ in. wide aluminium alloy lug. Numbers indicate fringe orders. Yielding of the metal corresponds to 1·90 fringes

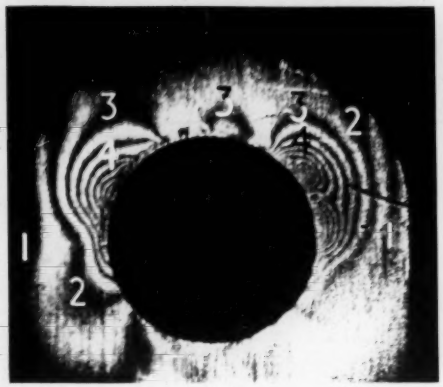

Fig. 6(*d*). Reloaded with 2000 lb — 0·68 Y

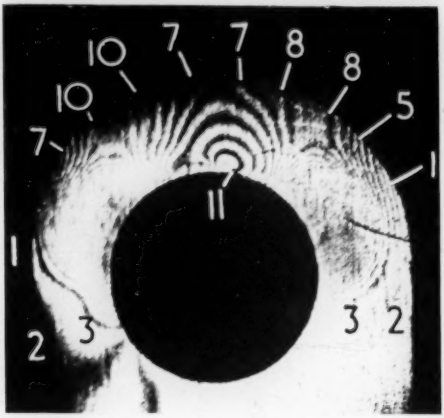

Fig. 6(*e*). Load — 2600 lb — 0·88 Y

Fig. 6. (*continued*)

New techniques for the study of Bitter figures

By D. J. Craik* B.Sc., and P. M. Griffiths, B.Sc., Department of Physics, University of Nottingham

[*Paper first received* 21 *January, and in final form* 6 *February*, 1958]

New techniques for the study of Bitter figures by optical and electron microscopy are described. In the case of the optical microscope an improved resolution and clarity is achieved. The method for the electron microscope is a modification of that previously published. Examples of the use of the methods are given.

1. Introduction

In 1931[1] Bitter first introduced what is now one of the most powerful methods for the investigation of ferromagnetic phenomena. In the demagnetized state most ferromagnetic materials have a complex structure of domains and where these domains intersect the surface, lines or sheets of magnetic poles appear. Bitter suggested that, if a sufficiently fine ferromagnetic powder or suspension of particles could be applied to the surface of a ferromagnetic crystal, these magnetic poles would attract the particles and the domain structure would be represented by a corresponding pattern formed by the powder. Satisfactory patterns are obtained by the use of a colloidal suspension of magnetite (Fe_3O_4) when a little is placed on a specially prepared crystal surface and covered with a thin glass microscope cover-slip. This forms a thin layer which may be examined under a metallurgical microscope. Generally, the surface must first be very carefully mechanically polished and finally electropolished to remove the strained layer, since what is generally desired is a pattern which is representative of the internal domain structure, and the pattern formed on a mechanically polished surface may be affected by the residual stresses in it.

The method has been extensively used, e.g. by Bates and others and Williams and others, for the study of domain configurations in very different materials in the demagnetized state, and it has provided explanations of magnetization processes in terms of changes in domain configuration.

Although so successful, this method has certain limitations with the colloids generally used in that the surface must be nearly optically flat to provide a uniform colloid layer, the surface is liable to become heavily stained by prolonged contact with the colloid, and the colloidal particles tend to lose their mobility while still in the liquid layer. In order to overcome the staining and loss of mobility, a new colloid was developed (Craik and Griffiths[2]), and it is now found that even irregular surfaces may be examined by a new method described below.

The resolution of optical microscopes limited the application of the Bitter technique until Craik[3] produced films of powder patterns which could be examined in an electron microscope. A modification of the latter method enables a higher resolution to be obtained even with an optical micro-

* Now with Boots Pure Drug Co. Ltd., Beeston, Notts.

scope. In fact, the resolution of the patterns so obtained approaches the resolution limit of the microscope itself.

2. THE NEW COLLOID

In early work one of two colloids due to Elmore[4] and to Bozorth[5] was used. For the first a slurry of magnetite is prepared, added to a 0·5% solution of sodium oleate and then peptized with 0·01 N HCl. The required dispersion of the particles is obtained by boiling for a short time. For the second, the slurry is prepared in the same manner, but is not peptized. The stabilizing substance used is *n*-dodecylamine. In this case the dispersion is obtained by stirring very rapidly; Bozorth recommended a stirring speed of about 6000 rev/min. The true particle size is the same in both cases, being governed by the preparation of the slurry, but it is generally found that the aggregate size is very much finer in the case of the former colloid.

For the new colloid the magnetite slurry is prepared according to Elmore's recipe: 2 gm $FeCl_2 4H_2O$ and 5·4 gm $FeCl_3 6H_2O$ are dissolved in 300 cm^3 of water at 70° C, to which 5 gm NaOH dissolved in 50 cm^3 of water are added with constant stirring. The heavy black precipitate of Fe_3O_4 is washed with distilled water to remove salt and excess NaOH. The slurry is added to a 0·1 N HCl solution when it is peptized to form a dense colloid. A solution of Celacol* is then added to give a final concentration of 0·5 to 1·0%. A small quantity of glycerine, approximately 10% weight for weight of Celacol, is also added. The colloid is then dialysed against distilled water through a membrane of cellophane to remove Cl radicle.

This colloid may now be used in the usual manner and it is found to have no detrimental effects on the polished surfaces, even when used for prolonged investigations. Moreover, it is a true colloid and the mobility of the particles is maintained indefinitely.

3. TECHNIQUE

Craik[3] found that when a colloid containing Celacol was allowed to dry on a smooth surface the particles remained in their dispersed state, set in a solid matrix of Celacol; the absence of coarse aggregates is shown by photographs Figs. 4 and 5 (p. 277). Generally, if a colloid is allowed to dry the particles merely form coarse aggregates which adhere to the surface and cannot give a true representation of the domain structure. The Celacol film may be removed from the surface taking with it the colloid pattern. On the surface of a ferro-magnetic crystal the particles set in regions of high magnetic divergence, and when the film of Celacol is removed, a permanent record of the domain configuration is obtained. This film may be mounted for examination in an electron microscope.

Apart from the advantages of the higher resolution of the electron microscopic examination, the fact that this colloid dries on a surface without distortion of the patterns leads to certain advantages from the point of view of optical microscopy. This method was first used in conjunction with an optical microscope by Craik and Griffiths to study an irregular surface obtained by cleavage of a single crystal of manganese ferrite. Due to heavy undulations of the surface, examination using the "wet" film technique was impossible, but a Celacol film allowed to dry on this surface followed the surface contours and gave a fine band pattern lying across several undulations upon the cleaved surface. Hence, it is possible to follow the pattern on a surface with a wide range of orientations. Once the film is formed, the pattern over the whole of the crystal surface can be examined at leisure, a great advantage in the case of complex structures.

In preparing a film for optical examination a little colloid is spread on the surface with a glass rod, the excess being removed by blotting the edge of the specimen, which is slightly inclined to ensure uniform drainage. The film should be sufficiently thick to appear a brownish-yellow colour by reflected light; when the film is somewhat thicker it appears blue. Thick films produce an effect similar to that of a photographic negative of the colloid patterns, in that the lines of domain structure appear bright against a dark background.

Occasionally it is difficult to wet the surface with colloid, so that the whole of the applied colloid drains from the surface during blotting. This is overcome by carefully washing the surface in pure ethyl alcohol, or, if the foregoing method proves unsuccessful, the surface may be degreased by pressing a piece of Sellotape against it and stripping it away. The latter procedure is not recommended in the case of loosely bound sintered ferrites. Sellotape is also used to remove the colloid film after examination, when the film leaves the surface completely clean and unstained.

The limitation of the dried film method is that it cannot be used on crystals which are readily oxidized in the presence of water. Thus, it may be used on cobalt, nickel, ferrites and any unreactive material such as Alnico, but not on iron or silicon-iron where perhaps a new colloid made by Schwartze[6] may be employed.

In electron microscopy different techniques must be employed. The essential difference lies in the fact that the film must be transferred to the microscope for examination by electron transmission. The film must therefore be stripped from the surface without tearing or distortion. The colloid used is similar to that described above, except that the colloid contains fewer magnetite particles, and to obtain the finest patterns it is also necessary to ensure that no large particle aggregates are present. The colloid should be passed through a fine filter paper before dilution to the required strength. The strength depends upon the type of pattern which is to be examined. For use with the optical microscope the colloid, when freshly prepared, has a very dense black appearance; for electron microscopy it should have a clear, deep amber colour. A greyish amber colour implies that some aggregation has taken place.

The colloid is applied in a similar way to that described above for the optical microscope; a thickness which corresponds to a pale yellow colour is most suitable to give the necessary resolution and still have sufficient strength to withstand the action of the electron beam without tearing.

In order to remove the film from the surface a thick collodion film is applied by drying a little of the solution in amyl acetate. A fine scalpel is used to lift one edge of the film without touching the specimen surface and the film is then stripped away with forceps. The composite film is laid collodion side downwards on a copper specimen grid which rests on a curved strip of wire mesh. Amyl acetate is introduced under the mesh and is periodically removed and replaced until the collodion is completely dissolved, when the Celacol film having the domain pattern alone rests on the specimen grid. This requires approximately one hour with two or three changes of the solvent. In the original method a thin plastic film was superimposed on the specimen

* Celacol is distributed by J. M. Steele and Co. Ltd., 36 Kingsway, London, W.C.2.

surface, to reduce the adhesion of the Celacol film. When glycerine is incorporated in the colloid the film may be formed directly on the surface, since the glycerine increases the equilibrium water content of the Celacol and so reduces its adhesion. For this reason it is desirable to place the specimen bearing the double film under an inverted beaker, to the inside of which a few drops of water adhere, for a little time before stripping, or alternatively to breath gently on the film. It was found in the case of cobalt, on which a very smooth surface may be obtained by electropolishing, that after the surface had been rinsed with alcohol, parts of the Celacol film still tended to adhere to the surface, even though the above precautions were taken. However, if the specimen is washed in soapy water, rinsed well with distilled water and dried by careful blotting, the film may be stripped easily, presumably because this treatment leaves a very thin layer of grease on the surface.

It is frequently necessary to study patterns on the same region by both optical and electron microscopy. In order to strip a pattern from a particular area, it is located under the optical microscope using a low power objective, and a standard electron microscope specimen grid is positioned so that the required area appears through the apertures. A small drop of a solution of 1% collodion in amyl acetate is then dropped on the grid, and allowed to dry. After checking to ensure that the grid has not been moved, a thick layer of a more concentrated solution of collodion is applied after which the specimen grid is removed with the double film.

It is usually found necessary to examine the patterns at relatively low electron optical magnifications only, and a low beam intensity may be used. When it is necessary to use a higher magnification and correspondingly higher beam intensity, the latter should be increased slowly as the film becomes tougher on exposure to the beam; presumably cross linking is induced.

The aim of the electron microscope technique is to produce and examine a Bitter figure pattern which is truly representative of the domain structure. The width of a domain wall in cobalt or iron is of the order of 10^{-5} cm. Since the diameter of the colloid particles is 10^{-6} cm it is clearly possible to obtain sufficient resolution in the patterns to give a true representation of the walls. In order to see these walls as approximately 1 mm wide, a magnification of 10000× is required, and this is sufficient for most purposes. However, high magnifications must occasionally be used, e.g. for the direct measurement of the wall thickness. This measurement was achieved by preparing a series of patterns using progressively more dilute colloids. The finest continuous line of particles which could be obtained was considered to be a fair representation of the wall itself.

4. DISCUSSION

Apart from the necessary use of the dried film technique for the optical microscopic examination of an undulatory surface, there are advantages in its use on a normally polished, flat surface. When it is required to apply a moderate field parallel to the surface of a crystal, e.g. to examine the approach to saturation of a soft magnetic material, it must be placed between the pole pieces of an electromagnet, and it is generally possible to arrange the microscope so as to observe Bitter figures by the wet film technique. However, where very large magnetic fields are necessary, as may be the case for a small specimen of a high coercivity material, large pole pieces have to be used. It would be impractical to arrange an optical microscope to focus on the specimen surface while still in the field gap. By allowing a film to dry on the specimen while in the applied field, the configuration may be studied after the specimen has been removed. Powder patterns have been obtained on a specimen of platinum–cobalt in a field range of 20000 oersteds.

To apply a normal field a bar magnet is used so that the microscope may be positioned directly over it. The magnitude of the fields which can be applied is severely limited, but with the new method the specimen may be placed between two pole pieces so that much larger fields are possible. This makes possible the observation of closure structure in both low and high coercivity materials.

The resolution which may be obtained using the dried film method is greatly enhanced compared with that obtained with a wet film. Fig. 1 (p. 276) taken with a wet film shows a typical region of the cleaved surface of a single crystal of manganese ferrite, which is an approximate (100) surface. A structure is visible, but it is somewhat "patchy." When a corresponding region was observed with a dried film (Fig. 2, p. 276) a much more clear and detailed structure was found. On examining this structure with the maximum magnification obtainable a secondary or substructure was found (Fig. 3, p. 276). This, however, was certainly not found in the "wet" condition. The substructure appears as a pattern of slab-domains of 0·7 μ spacing (Bates, Craik and Griffiths[7]), and discontinuities from a regular pattern may be readily noted. Since this resolution of 0·7 μ is obtained without the use of an oil immersion lens, it approximates closely to the maximum theoretical resolution of the optical system. For comparison with this high resolution optical micrograph an electron-micrograph of the same structure is shown in Fig. 4 (p. 277). This shows that the lines seen in the optical micrograph are in fact uniform bands with their spacing equal to their width. This is not the only instance of the revelation of extra detail which is not seen by the wet film method; patterns to be published shortly have been obtained on various polycrystalline ferrites which could not be seen at all using the wet film techniques. These patterns cannot be due to possible distortion in the Celacol film which may result from tensions set up during drying, for by allowing a film to dry on a plane glass surface no structure at all was seen with reflected light, but only a very few coarse particle aggregates. A similar conclusion was reached by electron microscopy examination. Yet these patterns can be seen to move under the effect of an applied field by a "stepping" method. This technique unfortunately does not permit the observation of a domain wall in motion. However, it is quite simple to obtain successive films in different magnetic field conditions and so observe the corresponding changes in the domain structure.

As has already been stated, much improved resolution is obtained by the dried film technique with the optical microscope, both from the point of view of the clarity of the picture obtained, and also the resolution of fine structures which are not otherwise recorded. This is because firstly, there is no film of liquid and no glass coverslip interposed between the pattern and the lens system, and secondly, and more important, the drying of the film greatly reduces its thickness. The usual liquid film is probably about 5 μ thick, since the coverslip will be largely supported by asperities of the surface, which is never perfectly flat after electropolishing. The magnetic field at a distance r from the surface, where it is intersected by a domain wall, is proportional to $1/r$ and the magnetic force on a colloidal particle is proportional to this field. Since the thickness of the Celacol film immediately before drying is of the order of 0·5 μ or less, the average magnetic force acting on a particle

at this stage will be 10× greater than in the case of a liquid film with the thickness suggested. Thus, where magnetic poles appear they will tend to collect the colloidal particles more strongly and will be particularly important in the case of materials with a low saturation magnetization, e.g. many ferrites and nickel–iron alloys. Moreover, as the film dries the liquid itself becomes more viscous and Brownian motion is inhibited, so that there will tend to be a progressive increase in the concentration of the particles in the vicinity of a source of magnetic poles. Thus, while in a wet film a statistical distribution of particles between high field and low field regions may be presumed to exist, e.g. as Kittel and Galt[8] assume, in our case (see Fig. 5, p. 277), the particles may all reside in the regions of high magnetic divergence. It may be noted that in this figure no particles whatsoever can be seen outside the dense lines.

ACKNOWLEDGEMENTS

The authors wish to thank Professor L. F. Bates for his advice and encouragement in the development of these techniques. D. J. C. wishes to thank Mr. W. J. Randall for his continued interest and encouragement and also Messrs. B. F. Miller and R. Harrison for their technical assistance. P. M. G. thanks the D.S.I.R. for a maintenance allowance.

REFERENCES

(1) Bitter, F. *Phys. Rev.*, **38**, p. 1903 (1931).
(2) Craik, D. J., and Griffiths, P. M. *Proc. Phys. Soc.* [*London*] *B*, **70**, p. 1000 (1957).
(3) Craik, D. J. *Proc. Phys. Soc.* [*London*] *B*, **69**, p. 647 (1956).
(4) Elmore, W. C. *Phys. Rev.*, **54**, p. 309 (1938).
(5) Bozorth, R. M. *Ferromagnetism*, p. 533 (New York: D Van Nostrand Co. Inc., 1951).
(6) Schwartze, W. *Ann. Phys.* [*Leipsig*], **19**, p. 322 (1956).
(7) Bates, L. F., Craik, D. J., and Griffiths, P. M. *Proc. Phys. Soc.* [*London*] (in press).
(8) Kittel, C., and Galt, J. K. *Solid State Physics*. Ed., F. Seitz and D. Turnbull, p. 437 (New York: Academic Press Inc., 1956).

A photoelastic technique for strain measurement on flat aluminium alloy surfaces

By H. Fessler, M.Sc., Ph.D., A.M.I.Mech.E., and D. J. Haines, B.Sc., The University of Nottingham

[*Paper received* 17 *October*, 1957]

A technique is described for bonding layers of an epoxy resin on flat aluminium alloy surfaces. Joints which withstood more than 4% strain were obtained by carefully controlled preparation of the metal and the adhesive. Initial birefringence was avoided by curing the joint without external pressure and by slow cooling after finish curing at 65° C.

The different types of reflexion polariscopes are discussed, the strain fringe values for the reflecting layer and for the adhesive are estimated. A test of a lug describes an application of the method.

NOTATION

C = stress optical coefficient
E = Young's modulus
P = force
R = relative retardation
T = time
Y = force to cause yielding of net section of lug, if the section were loaded in uniform tension
fr = fringes
t = thickness
δ = deformation
σ = stress
ϵ = strain
ν = Poisson's ratio
Suffix A refers to adhesive
Suffix L refers to photoelastic layer
Suffix M refers to metal
Suffices 1, 2 refer to principal directions.

INTRODUCTION

It is well known that the stress distribution in components made of ductile materials can be improved by exceeding the elastic limit in the highly stressed regions. When this occurs, parts of the component are subject to plastic stresses while the rest is stressed elastically. Plasto-elastic stress distributions occur frequently but are very difficult to determine theoretically. The experimental method described in this paper employs a birefringent layer to determine the strains on the surface of metal components. Because of the unique relationship between elastic stresses and strains, the extent of the elastic regions and stresses in these regions are readily calculated from the strain distribution when a criterion of yield has been assumed.

The method first suggested by Mesnager[1] is based on the large range of the linear relationship between birefringence and difference of principal strains which exist for some photoelastic materials; it relies on the adhesion of the birefringent layer to the surface of the metal component to strain the layer in the same manner as the component. A beam of polarized light is passed through the layer, is reflected at the metal surface, passed back through the layer and the relative retardation of the components of the beam is analysed in the usual manner. This paper describes how this simple principle can be applied.

In 1950 and 1951 Scott and Linge carried out experiments at the College of Aeronautics.[2] They coated various metals with layers of most of the photoelastic materials known at the time. Layers of Marco resin (a mixture of SB26c and SB28c) (by Scott Bader and Co. Ltd.) were cast on to the metal or bonded with Araldite 101 (by Aero Research Ltd.). The metal surfaces were prepared by sandblasting which caused warping and residual stresses near the surface. "Cast-on" and bonded layers showed considerable initial

stresses. From the published photographs of fringe patterns in lugs and holes in plates, the greatest difference of principal strains does not appear to be more than 1·5%.

In 1954 D'Agostino, Drucker, Liu and Mylonas[3] reported on the use of various resins for cast-on and bonded specimens. Because of the difference in contraction between the cast-on layer and the metal, the initial stresses which existed in the layer at room temperature are greatly reduced by testing at the curing temperature of the resin. In this way the authors obtained strains of up to 2% in cast-on specimens. Because their photoelastic layers were $\frac{1}{8}$ in. thick, they encountered appreciable errors at the boundaries of the models and at the edges of the layers. No quantitative results are given but the fringe pattern for a perforated bar shows initial stresses for the cast-on layer at the test temperature.

In 1956 Zandman[4] reported the use of what he called photoelastic varnishes. He built up layers 2 to 3 mm thick by applying thin layers of an ethoxylic resin derivative. No quantitative results are given but various field applications are quoted. Initial stresses are present in the photoelastic layers. A similar paper was published by Zandman and Wood.[5]

THE PROBLEM OF ADHESION

Murphy and Page[6] carried out a systematic investigation of the weight and porosity of the oxide layers on aluminium and of the weights of vinyl and epoxy resins which will adhere to these surfaces. They showed that porous heavy oxide films retain more resin than tightly packed films.

The nature of the oxide film depends on the temperature of the water bath in which the metal is immersed after etching. Below 71° C bayerite ($\beta Al_2O_3 . 3H_2O$) is formed on aluminium. The weight of oxide formed and the strength of the joint between oxide and resin increase with increasing water temperature and are greatest slightly above 71° C when boehmite ($\alpha Al_2O_3 . H_2O$) is formed. Above 80° C the bond between the metal and the oxide is weak. It therefore seems that a strong joint depends on the formation of a heavy, porous oxide film which firmly adheres to the surface of the metal and retains the largest possible weight of resin adhesive.

EXPERIMENTAL SEQUENCE

The method of making a specimen may be subdivided as follows:

(1) *Choice of materials.* The strongest adhesive for a particular metal and a convenient photoelastic layer must be found by experiment. In this investigation Araldite 102 (by Aero Research Ltd.) was used as the adhesive to join layers of another epoxy resin, Araldite casting resin B (by Aero Research Ltd.), to aluminium alloys.

(2) *Preparation of surfaces.* The metal surface has to be "machined" to the required surface finish, freed of grease in a detergent bath, rinsed, etched, immersed in a water bath and dried. The surface of the photoelastic layer has to be machined, cleaned and dried.

(3) *The adhesive.* The constituents of the adhesive have to be mixed in the correct proportions and the air entrained in mixing must be allowed to escape. After the two surfaces which are to form the joint have been coated with adhesive, they are both kept face upwards for a period to allow the remaining air bubbles and volatile constituents of the adhesive to escape.

(4) *Bonding.* After this evaporation period the layer is placed on the metal and the trapped air is forced out by finger pressure on the (flexible) layer. Heavy pressure is applied to the joint for a few seconds; this reduces the adhesive to a thin uniform layer. The adhesive is then allowed to gell and partly cure at room temperature without the application of pressure to the joint and the curing is completed at an elevated temperature.

(5) *Manufacture of specimen.* It was desirable to machine the metal to the required profile before bonding the layer to it; it would be impracticable to do this for the layer, because the latter would be too thin to handle and almost impossible to place exactly in the required position. The bonded specimens were therefore surface ground to obtain the desired thickness of layer and given the correct profile by very careful drilling and filing of the layer.

Whenever possible the bonded specimens were kept in a dessicator to retard the formation of (humidity caused) time edge stresses in the photoelastic layer.

VARIABLES OF THE PROCESS

The following are factors which influence the joint:

(1) *The metal surface.* The surface finish. The composition, temperature and immersion time in the detergent, etching agent and water bath. The drying time, temperature and surroundings.

(2) *The surface of the layer.* The surface finish. The composition and method of application of the cleaning agent. The drying time, temperature and surroundings.

(3) *The adhesive.* The composition, mixing procedure, method and extent of de-aeration, temperature at which adhesive is kept, the time between first mixing and coating of the surface, the time between coating and contact of the surfaces, the temperature and surroundings of the coated surfaces.

(4) *Bonding.* The way in which the surfaces are brought into contact, the method of excluding air from the joint, time and intensity of pressure on the joint, curing time and temperature, cooling rate after curing.

DEVELOPMENT OF METHOD

A beam in pure bending was chosen as a simple test to assess the effect of the different variables on the joint strength. The test beams consisted of duralumin strips as shown in Fig. 1(*a*). These beams were loaded up to failure of the $\frac{1}{8}$ in. thick photoelastic layer or of the bond. Failure, which always originated on the tensile side of the beams, was detected from discontinuities in the fringe pattern. The strain at which failure occurred was calculated from measurement of the curvature of the test beams.

Two possible methods for the preparation of the metal surface were known at the outset of the investigation. That of Mylonas and co-workers[3] consisted of:

(*a*) Immersion in a detergent solution (19 g anhydrous sodium metasilicate 2 g alkyl aryl sodium sulfonate, 710 ml. tap water) at 75° C for 4 min.
(*b*) Rinse in cold water.
(*c*) Immersion in etching solution (5% chromic acid) at 70° C for 2 min.
(*d*) Rinse in cold water.
(*e*) Drying in cool or hot air.

The method of Murphy and Page[6] consisted of:

(*a*) Immersion in detergent solution (methyl ethyl ketone) at room temperature for 10 min.
(*b*) Rinse in cold running water.

(*c*) Immersion in etching solution [15 ml. H_2SO_4 (sp. gr. = 1·84), 2·8 g $Na_2Cr_2O_7 . H_2O$ (tech), 100 ml. water] at 71° C for 5 min.
(*d*) Rinse in cold running water.
(*e*) Immersion in water (pH = 7 – 8) at 70 to 75° C for 10 min.
(*f*) Drying in air blast.
(*g*) Immersion in methyl ethyl ketone at room temperature for 16 h.
(*h*) Drying in air blast.

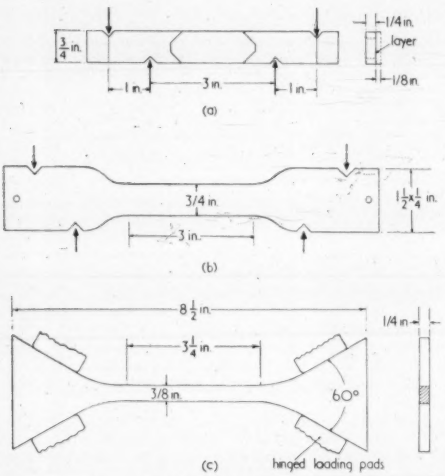

Fig. 1. Specimens

(*a*) for bending tests of joints; (*b*) for bending tests of photoelastic layer; (*c*) for calibrations.

It was decided to try Mylonas's method. The first series (specimens D1 to D4) was intended to investigate the effect of surface finish and etching time. The results given in the table show that the bonds were weak and that polishing may possibly weaken them further. The curing temperature and time refer to a finish curing of the adhesive after room temperature curing for one day. This high temperature curing was more severe than recommended by the makers of the adhesive and was intended to ensure complete curing. Heavy clamping of the joint during room temperature curing caused initial stresses in the layer which were not removed by the high temperature curing. The second series (D5 to D10) was intended to study the effects of etching time and curing temperature. The high temperature curing times were adjusted to give approximately equal intensity of curing. This was done by plotting curing temperature-time curves from the data supplied by the makers of the adhesive and arranging the tests to give a curve of the same form. The results given in the table suggest that 65° C may be a suitable curing temperature but are inconclusive regarding the effect of etching time. Light clamping of the joint caused reduced initial stresses.

Because the Araldite layer broke in some of these specimens, a bending test on Araldite Casting Resin B was carried out. The model shown in Fig. 1(*b*) was loaded in pure bending and failed in the parallel portion at more than 4·5% strain. This limits the use of this material to strains of about 4%.

Results of bending tests

Specimen	*Surface finish of metal*	*Etch time (min)*	*Cure temp. (°C)*	*Cure time (h)*	*Strain to fail (%)*
D1	Polish	2	60	7	0·9
D2	W.D. 400	2	60	7	0·9
D3	Polish	5	60	7	0·7
D4	W.D. 400	5	60	7	1·2
D5	Light polish	5	45	12·0	1·3
D6	Light polish	5	55	7·25	1·4
D7	Light polish	10	55	7·25	1·0
D8	Light polish	10	65	5·0	1·7
D9	Light polish	15	65	5·0	2·3
D10	Light polish	15	75	3·25	1·9
D11	W.D. 280	10	65	5·0	4·4+
D12	W.D. 280	10	65	5·0	3·6
D13	W.D. 280	10	65	5·0	7·4+
D14–18	W.D. 280	15	65	5·0	all 4·3+
E1	Ground	20	65	5·0	4·0+
E2	Ground	30	65	5·0	3·9+
F1–2	Ground	15	65	5·0	both 4·5+

D = duralumin strip
E = D.T.D. 683 sheet
F = D.T.D. 646 B sheet
W.D. = wet and dry emery cloth (number is grade)
\+ indicates sound at stated (greatest applied) strain

The third series was a preliminary investigation of the method of Murphy and Page. The main differences between this and Mylonas's method are the immersion of the metal in hot water and in methyl ethyl ketone. Specimens D11 to D13 were immersed in distilled water at 70° C for 10 min but only D12 was immersed in acetone at 50° C for 20 min. D13 was covered with a thick layer of adhesive only. D11 and D12 were very lightly clamped and showed small initial stresses after room temperature curing for two days, but increased stresses after the high temperature cure. The results given in the table suggested that the hot water bath was beneficial but that the acetone bath was not. The adhesive is far more ductile than Araldite Casting Resin B.

In the fourth series (D14 to D18) the successful method of D11 was repeated to test its reliability. The room temperature curing was reduced to one day without any clamping pressure (except for a few seconds after the components were joined). No initial stresses were caused in the room temperature cure. Slow cooling at 3° C per hour after the high temperature curing prevented the formation of any initial stresses. All joints remained sound at strains greater than 4%.

The last two sets of tests recorded in the table showed that the method was also successful for other aluminium alloys, that the surfaces could be ground and that long etching periods had no detrimental effect on the joint strength.

No further tests were carried out because a technique for measuring up to 4% strain was deemed sufficient.

SUCCESSFUL TECHNIQUE

(1) *Preparation of metal.* The surface ground or emeried surfaces were cleaned by immersion in a detergent solution, similar to that used by Mylonas [2 g Teepol (by Shell

Chemicals Ltd.) 21 g waterglass, 710 ml. distilled water] for 4 min at 75° C. This detergent solution becomes stale after use. After rinsing in cold distilled water, the specimen is immersed in the etching solution [15 ml. conc. H_2SO_4, 2·8 g $Na_2Cr_2O_7 . H_2O$ (tech) 100 ml. distilled water] at 65° C for 15 min. The bonding surface must be uppermost in the flat tray in which this process is conveniently carried out. The purpose of this operation is to remove the existing oxide layer from the surface; overetching does not seem to be detrimental. The solution can only be used once but one litre of the mixed solution would be sufficient to etch about 150 in.^{2} of aluminium.

After thorough rinsing in cold distilled water, the specimen is immersed for 10 min in distilled water at 70–75° C. This establishes a heavy porous oxide layer on the surface, which is soft. The oxide layer is dried and hardened for 30 min in a hot air oven at 50° C.

(2) *Preparation of the layer.* The layer was machined from $\frac{3}{16}$ in. thick flat sheets of Araldite Casting Resin B, which were cast in the usual way.[7] The bonding surface was ground and cleaned by rubbing with cotton wool impregnated with acetone, followed by cotton wool impregnated with methyl alcohol, as recommended by Mylonas.[3] After this the pieces were dried for 10 min in a hot air oven at 50° C.

No attempt was made to improve this part of the technique for, although it resulted in a weaker bond between the layer and the adhesive than between the adhesive and the metal, the resulting joints withstood strains of over 4%. Strains greater than this exceed the ductility of Araldite Casting Resin B but can be measured by a thick layer of the adhesive used as the photoelastic layer.

(3) *The adhesive.* To avoid unnecessary exposure of the prepared surfaces, the adhesive, Araldite 102, should be weighed out when the metal surfaces are being etched. It is important that the proportions of hardener 951 to the resin are exactly 6 parts to 100 because the amount of hardener controls the behaviour of the adhesive. The resin and hardener were mixed in a shallow dish and stirred at approximately five minute intervals for $\frac{1}{2}$ h to prevent segregation of the hardener. The shallow dish facilitated the escape of most of the air introduced in the mixing.

(4) *Bonding.* The warm metal and the photoelastic layer were cooled to room temperature by resting on a cold metal surface. The adhesive was applied to the prepared surfaces in moderately thick layers with a spatula and left for approximately $\frac{1}{4}$ h with the adhesive uppermost. This allowed a volatile solvent present in the adhesive and the remaining entrapped air to escape and the adhesive on the metal to thicken.

Preliminary tests showed that sliding the mating surfaces over each other shears the adhesive and entraps much air. The mating surfaces were placed in contact and the trapped air pockets, the outlines of which are visible through the layer, were expelled at the edges of the layer by finger pressure. After this the assembly was put under the greatest pressure which could be applied in an engineer's bench vice with flat smooth jaws for about $\frac{1}{4}$ min. This pressure reduced the adhesive to a constant thickness over the whole joint. The thickness varied between 0·0003 in. and 0·0025 in. for different specimens.

(5) *Curing.* After the compression of the adhesive, the specimens were kept at room temperature for 24 h. The curing of the adhesive was completed by maintaining the specimens at 65° C for 5 h in a hot air oven. During both curing cycles the only pressure on the joint was due to the weight of the photoelastic layer because it was found that pressures of only a few ounces/in.^{2} caused initial stresses in the layer. Slow cooling of the specimens at 3° C/h from 65° C to about 25° C prevented the formation of initial stresses in the final stage of the making of the joint.

Fig. 2 (p. 278) shows an example of a stress-free model of a lug, produced as described above. The actual hole was $\frac{7}{16}$ in. diameter, the photoelastic layer was 0·015 in. thick and the thickness of the adhesive was 0·001 in. The grey parts of the lug are due to light reflected from the surface of the layer. Any portion of the lug could be made to appear black by slight changes in the direction of viewing. No attempt was made to reduce this slight reflexion because it did not disturb the fringe patterns.

THE POLARISCOPE

Reflection polariscopes can be of the Vee or doubling type. In the Vee type the polarizing and analysing elements are placed side by side and the size of these elements and their distance from the model determine the angle between the incident and reflected rays. This angle may cause appreciable errors in regions of large strain gradient.

To avoid these errors the doubling polariscope shown in Fig. 3 was developed. The partial mirror makes it possible for the incident and reflected ray to be almost co-linear. A

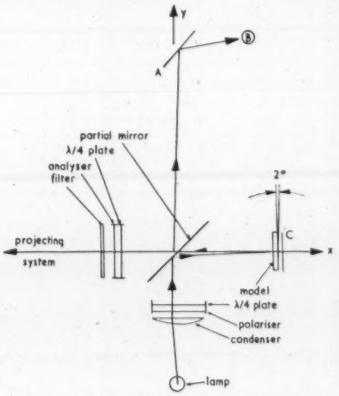

Fig. 3. Diagram of doubling polariscope

disadvantage of this type is the low intensity of the light emerging from the analyser. To photograph the fringe pattern all stray light must be excluded or absorbed. This was done by a number of black baffles. A major source of stray light arises from the part of the original beam which is transmitted through the partial mirror and reflected by any surface which obstructs its path in the y direction (Fig. 3). This was prevented by reflecting the light at A on to a large light absorbing black cloth B. The baffles also reduced the dust in the light beams and thus the amount of light scattered by dust particles.

If the model is placed normal to the x direction, the reflexion from the upper surface of the photoelastic layer tends to mask the fringe pattern. This was avoided by inclining the model through 2° as shown in Fig. 3. The

apparatus was set up with a mirror C in place of the specimen. This mirror was also used to assess the suitability of different nickel-chrome plated partial mirrors. Fig. 4 shows that the best results are obtained with mirrors of 35–40% light transmission.

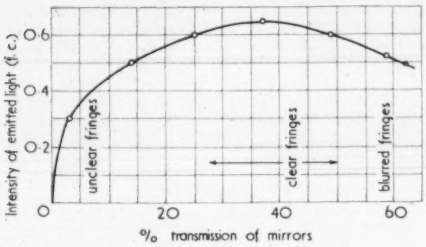

Fig. 4. Polariscope mirror characteristics

Greater intensities of emerging light could have been obtained by placing the model across the y axis, but this would have prevented Tardy compensation because of the partial polarization of the reflected beam when it is reflected (instead of transmitted) at the partial mirror.

CALIBRATIONS

Because the photoelastic layer is strained rather than stressed it is convenient to use a strain-optical coefficient. From Hooke's law, for plane stress

$$\sigma_1 - \sigma_2 = \frac{E}{1+\nu}(\epsilon_1 - \epsilon_2)$$

Therefore

$$R = C(\sigma_1 - \sigma_2)t = \frac{CE_L}{1+\nu_L}(\epsilon_1 - \epsilon_2)t$$

The calibrations were carried out in simple tension, when $\epsilon_1 - \epsilon_2 = \epsilon_1(1+\nu_M)$, for the metal. Duralumin specimens of the shape shown in Fig. 1(*c*) were used. Poisson's ratio for these specimens was determined by measurement of the transverse strain on the upper horizontal surface when this specimen was loaded as a cantilever. A Johanssen extensometer was used for this and Poisson's ratio was found to be 0·32.

To ensure that the calibrations were carried out within the elastic range of the metal a tensile test was carried out. The extension was measured with a dial gauge type extensometer of 2 in. gauge length, the weight of which was supported on soft springs to avoid bending the specimen. Young's modulus was found to be $10{\cdot}4 \times 10^6$ lb/in.^{2} and the limit of proportionality was above 0·32% direct strain. A tensile specimen of Araldite Casting Resin B was used to determine Young's modulus for the layer. This is necessary to assess the reinforcement of the metal by the layer. Two Huggenberger extensometers were used to measure the extensions and Young's modulus was found to be $0{\cdot}48 \times 10^6$ lb/in.^{2}

The strain fringe value for the adhesive was determined from a 0·032 in. thick layer of adhesive cast on to one surface of a duralumin tensile specimen and found to be 2200 fr/in. (5461 Å wavelength light) for unit strain difference. The greatest strain in this test was 0·35% to avoid errors due to creep of the adhesive. The strain fringe value for the layer was obtained from a bonded layer 0·055 in. thick and was 11000 fr/in. for unit strain difference. A correction was made for the thin layer of adhesive which formed the joint. The greatest strain in this case was 0·31%, measured with the dial gauge extensometer. The fringe order was uniform over the gauge length throughout both tests.

SOURCES OF ERRORS

In a perfectly bonded joint the adhesive may cause errors in two ways. Creep in the adhesive may change the strain (and the associated birefringence) of the layer and relaxation of birefringence in the adhesive under constant strain may reduce the total birefringence for a given condition of the metal. Both effects decrease with decreasing thickness of the adhesive.

The change in birefringence of the layer under constant strain was studied with two tensile specimens $\frac{5}{8}$ in. wide and 0·07 and 0·08 in. thick. These specimens were clamped between steel plattens approximately 4 in. apart; the plattens were displaced to give a constant strain to the specimens and the change in fringe order was observed. The results of these tests are shown in Fig. 5. The rapid fringe decay

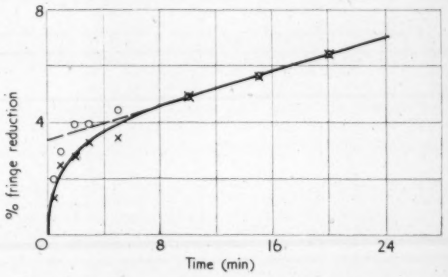

Fig. 5. Fringe decay in $\frac{5}{8}$ in. wide strips of adhesive, approximately $\frac{1}{16}$ in. thick under constant extension. Gauge lengths approximately 4 in. Results from 4% strain shown O. Results from 6% strain shown X

in the early part of the tests is attributed to the effect of the inevitable stress concentrations at the plattens. It is suggested that the dotted straight line may be a better indication of the actual fringe reduction, which would represent a decrease of 0·15%/min, independent of the original strain.

This fringe decay has little influence on the actual readings because the optical sensitivity of the adhesive is only $\frac{1}{4}$ of that of the layer. In a typical specimen the thickness of the layer would be about 20 times the thickness of the adhesive so that the adhesive only contributes about 1% to the total birefringence.

The effect of creep in the adhesive may be considered as follows. When the component is loaded, metal, adhesive and layer are subjected to the same strains. These strains produce a two-dimensional stress field in the plane of the specimen. It is assumed that the strains in the metal remain constant and that the elastic stresses in the layer try to relieve themselves and thereby cause creep in the adhesive.

When creep occurs, the strains in the adhesive vary across the thickness. The greatest change of strain occurs at the adhesive-layer interface so that any calculations based on the assumption that the interface stresses act throughout the

thickness will predict greater errors due to creep than may be expected in practice. This assumption removes the restraining effect of the metal surface so that to satisfy equilibrium, the forces in layer and adhesive acting on any area normal to the metal surface must be equal (and opposite). Because

$$P_L = P_A \quad \text{and}$$
$$P = E \times \epsilon \times (\text{area normal to metal surface})$$

$$\frac{\epsilon_L}{\epsilon_A} = \frac{E_A t_A}{E_L t_L}$$

as the widths of the normal areas are equal.

Because of creep in the adhesive ϵ_A and E_A are functions of time. After time T the change of strain is

$$\epsilon_L = \frac{t_A}{t_L E_L} [\epsilon_A E_A]_T$$

The stress field may be considered in terms of the principal stresses at any point and the strain changes can therefore be estimated from tensile tests. Specimens made of adhesive were tested under constant load and the increase of strain with time was measured. It was found that the behaviour of the adhesive in tension was complex. The strain at a given time after loading depended not only on the stress but also on the age of the specimen and its recent history. Because it is also probable that the characteristics of the adhesive may depend on the thickness of the material during curing, the results of these creep tests are not reported in detail.

For several tests at different stresses E_A was never greater than 20 000 lb/in.^{2} immediately after application of the load. Because $E_L \simeq 500\,000$ lb/in.^{2} and $t_L/t_A \simeq 20$, ϵ_L is less than $0{\cdot}2\%\ \epsilon_A$. Extrapolation of the creep curves showed that the ultimate strain was less than ten times the initial strain in the creep tests. It therefore seems unlikely that errors due to creep of the adhesive would be large.

The edges of the photoelastic layer are free boundaries and when the layer does not completely cover the metal, errors are likely to occur near the edges of the layer, due to "shear lag." If a direct or shear stress acts in the metal across the position of an edge of the layer, the stress is only transmitted to the surface of the layer in contact with the metal. The layer near such edges indicates lower strains than those occurring in the metal. The same effect may occur to a lesser degree where the stress-strain relationships of metal and layer differ, if this causes large strain gradients. Shear lag obviously depends on the thickness of the layer and is considered unimportant for layers less than $\frac{1}{2}$ in. thick on machined profiles if the layer covers the whole specimen in the region to be investigated.

EXAMPLE

The method was used to study the plasto-elastic stress distributions in semicircular ended lugs of aluminium alloy D.T.D. 646B. Fig. 6 shows some of the photographic records of the test of one of these lugs. The thicknesses of metal, adhesive and layer were 0·122 in., 0·001 in. and 0·027 in. respectively. The lower part of the lug (not shown on photographs) was clamped to the lower jaw of a small tensile testing machine and the lug was loaded through a neat fitting, hardened steel pin. The applied loads are also quoted as fractions of the load required to cause yielding in a uniform tensile specimen of the same section as the net section across the lug.

For this thickness of photoelastic layer the strain difference which marks the onset of tensile yielding corresponds to a fringe order of 1·90. Fig. 6(*a*), p. 278, shows the unsymmetrical strain distribution with pronounced local yielding in the right limb. Under the greater load for Fig. 6(*b*), p. 278, the asymmetry is reduced. The residual strains after removal of this load are shown in Fig. 6(*c*), p. 278. If the onset of compressive yielding also corresponds to 1·90 fringes, a change in fringe order of more than 3·80 between Fig. 6(*b*) and 6(*c*) probably indicates regions where reverse yielding has occurred. The residual stresses in regions where yielding has occurred during loading cannot be evaluated directly from the recorded strain distributions because there is no unique stress-strain relationship in plastic regions. Because the plastic strains in this case are small, the difference between the fringe patterns in Fig. 6(*b*) and 6(*c*) probably gives an approximate indication of the residual stresses.

Fig. 6(*d*), p. 279, shows the strain distribution on reloading with 2000 lb; this is similar to Fig. 6(*b*). One of the large-strain patterns is recorded in Fig. 6(*e*), p. 279. The fringe pattern is almost symmetrical but the fringes are too closely spaced to be distinguishable. The fringe pattern for 2700 lb applied to this lug was also recorded before it failed at this load, which corresponds to 0·91 *Y*.

CONCLUSIONS

Initial stresses in the photoelastic layer and adhesive are avoided by applying pressure to the joint for a very short time only and by slow cooling after curing.

Metal surfaces which were ground or finished with emery cloth gave satisfactory reflexion and joint strength up to 4% strain. The metal surfaces may be etched for more than 15 min but must be immersed in distilled water at 70–75° C to form a heavy oxide film. Acetone cleaning after this reduces the joint strength.

The mixed adhesive must be given time for air and the volatile constituent to escape before the joint is made. Air trapped when the layer is placed on the metal must be expelled by local finger pressure before the adhesive is reduced to a small constant thickness by a large uniform pressure.

ACKNOWLEDGEMENTS

The authors wish to thank Professor J. A. Pope, who, as Head of the Departments of Civil and Mechanical Engineering at The University of Nottingham, provided all necessary facilities for this work, and Dr. R. B. Waterhouse for his valuable advice on the metallurgical aspects of the problem.

REFERENCES

(1) MESNAGER, M. *C.R. Acad. Sci.* [*Paris*], **190**, p. 1249 (1930).
(2) LINGE, J. R. *Coll. of Aeronautics Report No.* 97, February 1956.
(3) D'AGOSTINO, J., DRUCKER, D. C., LIU, C. K., and MYLONAS, C. *Proc. Soc. Exp. Stress Anal.*, **12**, p. 115 (1955).
(4) ZANDMAN, F. *Acier Stahl Steel*, **21**, p 356 (1956).
(5) ZANDMAN, F., and WOOD, M. R. *Product Engineering*, **27**, p. 167 (1956).
(6) MURPHY, J. F., and PAGE, H. A. *Proc. Amer. Chem. Soc.* (Division of Paint, Plastics and Printing Ink Chemistry), Cincinnati Meeting, April 1955. p. 27.
(7) SPOONER, H., and MCCONNEL, L. D. *Brit. J. Appl. Phys.*, **4**, p. 181 (1953).

Stability and convergence limitations on the use of analogue computers with resistance network analogues

By M. E. FISHER, Ph.D., Wheatstone Physics Laboratory, King's College, London

[*Paper received* 4 *November*, 1957]

Various practical methods have been described for solving partial differential equations such as $\nabla^2\phi = f(\phi)$ by means of resistance networks coupled to electronic analogue computing units. These schemes are investigated mathematically to determine the conditions for which the computer remains stable, or for which the successive approximations converge to the required solution. It is shown that all the methods will break down if the gradient $df/d\phi$ is negative and sufficiently large to cause the correct solution to be "wave-like."

In recent papers Karplus[1] and Hutcheon[2] have described schemes for the automatic solution of partial differential equations of the type

$$(\partial^2\phi/\partial x^2) + (\partial^2\phi/\partial y^2) = f(\phi) \tag{1}$$

by means of resistance networks coupled to electronic analogue computing elements. The differential operators in equation (1) are approximated by finite difference operators and the network analogue is set up in the standard way.[3] Thus, if ϕ_{nm} is the potential at the node (n, m) and if i_{nm} is the current withdrawn from the same node, we have the network equations

$$(\phi_{n+1,m} + \phi_{n-1,m} + \phi_{n,m+1} + \phi_{n,m-1} - 4\phi_{nm}) = Ri_{nm} \tag{2}$$

where R is the resistance of the resistors making up the network. If the analogy (2) is to represent the partial difference equation (1), the auxiliary relations

$$Ri_{nm} = h^2u_{nm} = h^2f(\phi_{nm}) \tag{3}$$

where h is the finite difference interval, must be enforced for all n and m. In the scheme described by Karplus a set of electronic computing elements is attached to each node and these automatically alter the currents so as to fulfil the relations (3). In Hutcheon's method a single set of computing elements is used, but these are connected to each of the nodes in turn and cyclically so that the solution is approached by an automatic iterative process. A somewhat different iterative method has been used previously by Liebmann[4]. A complete trial function $\phi^{(1)}_{nm}$ is chosen and equation (2) is solved with $Ri_{nm} = h^2f(\phi^{(1)}_{nm})$ to yield a second approximation $\phi^{(2)}_{nm}$, which is again substituted into the left-hand side, and so on.

The purpose of this paper is to point out the limitations of these methods which arise from the need for stability of the total computer (in Karplus' method) and from the requirement that the iterative processes (of Hutcheon and Liebmann) should converge. Broadly speaking, it is shown that if the function $f(\phi)$ is such that the correct solution of equation (1) exhibits a "wave-like" character, then the computational schemes described above will fail. The restrictions on Liebmann's method are rather more severe. The mathematical analysis uses matrix notation and the convergence and stability criteria are derived from well-known theorems in numerical analysis.

MATHEMATICAL PRELIMINARIES

The discussion of the stability and convergence problems is facilitated by using matrix notation. For simplicity consider the one-dimensional analogue of (2) and suppose that ϕ is specified on the boundaries, i.e. that ϕ_0 and ϕ_{N+1} are given. Then the network equations are

$$h^{-2}(\phi_{n+1} - 2\phi_n + \phi_{n-1}) = u_n \qquad n = 1, 2, \ldots N-1, N, \tag{4}$$

where u_n is related to the node currents by the relations (3).

This set of equations, together with the boundary conditions, may be written in matrix notation as

$$\boldsymbol{L\varphi} = \boldsymbol{\beta} - \boldsymbol{u} \tag{5}$$

where $\boldsymbol{L}$ is an $N \times N$ square matrix given by

$$\boldsymbol{L} = +\frac{1}{h^2}\begin{bmatrix} 2 & -1 & 0 & 0 & . & . \\ -1 & 2 & -1 & 0 & . & . \\ 0 & -1 & 2 & -1 & . & . \\ . & . & . & . & . & . \\ . & . & . & . & . & . \end{bmatrix} = [l_{ij}] \tag{6}$$

and where $\boldsymbol{\varphi}$, $\boldsymbol{\beta}$ and $\boldsymbol{u}$ are $N \times 1$ column matrices (or vectors) given by

$$\boldsymbol{\varphi} = \begin{bmatrix} \phi_1 \\ \phi_2 \\ . \\ . \\ . \\ \phi_{N-1} \\ \phi_N \end{bmatrix} = [\phi_i], \quad \boldsymbol{\beta} = \frac{1}{h^2}\begin{bmatrix} \phi_0 \\ 0 \\ . \\ . \\ . \\ 0 \\ \phi_{N+1} \end{bmatrix},$$

$$\boldsymbol{u} = \begin{bmatrix} u_1 \\ u_2 \\ . \\ . \\ . \\ u_{N-1} \\ u_N \end{bmatrix} = [u_i] \tag{7}$$

If the definitions (6) and (7) are suitably generalized, equation (5) becomes a valid description of the difference approximations to partial differential equations of two or more dimensions. Similarly, if higher order difference approximations are used in place of those leading to (4), equation (5) still holds but the matrix $\boldsymbol{L}$ has a more complicated form. (Some applications of higher order difference approximations to analogue computers are discussed in Ref. 5.)

It follows by analogy with differential operators $-d^2/dx^2$, $-[(\partial^2/\partial x^2) + (\partial^2/\partial y^2)]$, etc., that the approximating matrix $\boldsymbol{L}$ is symmetric and positive definite, that is to say the eigenvalues λ_r $(r = 1, 2 \ldots N)$ of $\boldsymbol{L}$ defined by

$$\boldsymbol{Lw}_r = \lambda_r\boldsymbol{w}_r \tag{8}$$

are all real and positive. Furthermore, the lower eigenvalues of $\boldsymbol{L}$ will be good approximations to the eigenvalues ω_r^2 of the corresponding differential operators defined by

$$\frac{d^2\psi}{dx^2}(x) = -\omega^2\psi(x),$$

$$\frac{\partial^2\psi}{\partial x^2}(x, y) + \frac{\partial^2\psi}{\partial y^2}(x, y) = -\omega^2\psi(x, y), \text{ etc.} \quad (9)$$

where $\psi(x)$, $\psi(x, y)$ fulfil appropriate homogeneous conditions on the specified boundaries. (ω is the characteristic frequency of the corresponding "string" or "membrane.") Thus, in one dimension for a region of length $l = h(N + 1)$, the smallest eigenvalue is

$$\lambda_1 \simeq \pi^2/l^2 \quad (10)$$

whilst for a two-dimensional rectangular region of sides length l and m,

$$\lambda_1 \simeq (\pi^2/l^2) + (\pi^2/m^2). \quad (11)$$

For the matrix (6) we actually have the exact result

$$\lambda_r = (2/h)^2 \sin^2 [\pi r/2(N + 1)] = \pi^2 r^2/h^2(N + 1)^2\{1 + 0[\pi^4 r^4/(N + 1)^4]\}$$

so that equation (10) is indeed a good first approximation for $r = 1$.

SIMULTANEOUS ADJUSTMENT

In Karplus's parallel method of solving the partial differential equation the elements u_i of the matrix $\boldsymbol{u}$ in equation (4) (i.e. the currents) are simultaneously adjusted by function generators so as to fulfil the conditions (3). If there were no dynamic lag in the function generators, or (equivalently) if they had an infinite bandwidth, the relations (3) would always hold identically and the analogy would be complete. In practice, however, there is lag and the bandwidth is necessarily finite. The true dynamic performance of a function generator with an input $\phi_i(t)$, may, in most cases, be represented by a single (small) time constant τ, so that, in place of relations (3) we have

$$\tau(du_i/dt) + u_i = f(\phi_i), \quad i = 1, 2 \ldots N. \quad (12)$$

To carry the analysis further we suppose that $f(\phi)$ is a linear function of ϕ, or that, over the relevant range, $f(\phi)$ may reasonably be approximated by a linear function. (This point is discussed further below.) Thus, taking

$$f(\phi) = a + b\phi \quad (13)$$

equation (12) can be written in matrix notation as

$$\tau(d\boldsymbol{u}/dt) + \boldsymbol{u} = \boldsymbol{f}(\boldsymbol{\phi}) = \boldsymbol{a} + b\boldsymbol{\varphi} \quad (14)$$

where $\boldsymbol{a}$ is the column matrix $[a_i] = [a]$. On substituting for $\boldsymbol{u}$ from equation (5) we obtain the dynamic equation

$$\tau\boldsymbol{L}(d\boldsymbol{\varphi}/dt) + (\boldsymbol{L} + b\boldsymbol{I})\boldsymbol{\varphi} = \boldsymbol{\beta} - \boldsymbol{a} \quad (15)$$

for the potentials $\boldsymbol{\varphi}(t)$. The solution of this linear differential equation may be written

$$\boldsymbol{\varphi}(t) = \boldsymbol{\varphi}_S + \sum_{r=1}^{N} \boldsymbol{\psi}_r \exp(-\mu_r t/\tau) \quad (16)$$

where

$$\boldsymbol{\varphi}_S = [\boldsymbol{L} + b\boldsymbol{I}]^{-1}(\boldsymbol{\beta} - \boldsymbol{a}) \quad (17)$$

is the required potential distribution representing the solution of the original partial differential equation. The $\boldsymbol{\psi}_r$ are determined by the initial (arbitrary) settings of the function generators and the μ_r are the roots of the equation

$$|\boldsymbol{L} + b\boldsymbol{I} - \mu\boldsymbol{L}| = 0 \quad (18)$$

In other words, the μ_r are the eigenvalues of the matrix $\boldsymbol{I} + b\boldsymbol{L}^{-1}$, and so

$$\mu_r = 1 + b/\lambda_r \quad (r = 1, 2, \ldots N). \quad (19)$$

For stability, that is to ensure that $\boldsymbol{\varphi}(t) \to \boldsymbol{\varphi}_S$ as $t \to \infty$, whatever the initial conditions or subsequent disturbances (noise), the real parts of all the μ_r must be positive and by equation (19) this will be the case if, and only if,

$$b > -\lambda_1. \quad (20)$$

Thus we have shown that apparatus such as described by Karplus will only be stable and yield the correct solution of partial differential equations like (1), if the gradient of the function $f(\phi)$ is positive, or, if negative, is smaller in absolute value than λ_1, the lowest eigenvalue of the operator $\boldsymbol{L}$.

ITERATIVE ADJUSTMENTS

In the iterative scheme of adjustment described by Hutcheon, all the elements u_i of the matrix $\boldsymbol{u}$ are held stationary except for one, u_j, which is varied (automatically or manually) until the jth auxiliary relation (3),

$$u_j = f(\phi_j) \quad (21)$$

is fulfilled. During this variation all the potentials ϕ_i will, in general, change so that, substituting from equation (5), the equation

$$u_j = f(\{\boldsymbol{L}^{-1}[\boldsymbol{\beta} - \boldsymbol{u}]\}_j) \quad (22)$$

is actually solved for u_j at each successive adjustment, ($j = 1, 2 \ldots N, 1, 2 \ldots$). [The notation $\{\boldsymbol{w}\}_j$ signifies the jth component of the vector $\boldsymbol{w}$.] Taking $f(\phi)$ to be linear, as previously, equation (22) becomes

$$u_j = a + b\{\boldsymbol{L}^{-1}(\boldsymbol{\beta} - \boldsymbol{u})\}_j$$

which may be rewritten as

$$\{(\boldsymbol{I} + b\boldsymbol{L}^{-1})\boldsymbol{u}\}_j = \{\boldsymbol{a} + b\boldsymbol{L}^{-1}\boldsymbol{\beta}\}_j \quad (23)$$
$$j = 1, 2, \ldots N, 1, 2, \ldots$$

The iterative process specified by equation (23) is none other than the classical "single-step" process (also known as the "Gauss–Seidel" method)[6–9] for the solution of the set of simultaneous equations

$$\boldsymbol{A}\boldsymbol{u} = \boldsymbol{g} \quad (24)$$

where $\boldsymbol{A} = \boldsymbol{I} + b\boldsymbol{L}^{-1}$. If the adjustments are not made in strict cyclic order then we have a "relaxation process."[10] (Such a relaxation method has, in fact, been used by Liebmann and Bailey in solving the related problem of finding the lowest normal mode and "cut off" frequency of a waveguide.[11]) In either case it is known[9] that when the matrix $\boldsymbol{A} = \boldsymbol{I} + b\boldsymbol{L}^{-1}$ is symmetric, the method converges if, and only if, the matrix $\boldsymbol{A}$ is also positive definite. This criterion is quite equivalent to the condition for stability of the last section and so we conclude that the method of successive single adjustments converges to yield the correct solution, if, and only if, the function $f(\phi)$ is such that

$$b > -\lambda_1. \quad (25)$$

Liebmann's iterative scheme, on the other hand, is given by

$$\boldsymbol{L}\boldsymbol{\varphi}^{(k+1)} = \boldsymbol{\beta} - \boldsymbol{u}^{(k)} \quad (26)$$

and

$$u_i^{(k)} = f(\phi_i^{(k)}) \quad i = 1, 2, \ldots N \quad (27)$$

where $\boldsymbol{\varphi}^{(k)}$ is the kth approximation to the required solution. This method is a "total-step" iteration in that all the components of $\boldsymbol{u}$ are adjusted simultaneously on the basis of the previously computed values of the potentials. When $f(\phi)$ is linear, equations (26) and (27) become

$$\boldsymbol{\varphi}^{(k+1)} = \boldsymbol{L}^{-1}(\boldsymbol{\beta} - \boldsymbol{a}) - b\boldsymbol{L}^{-1}\boldsymbol{\varphi}^{(k)}. \tag{28}$$

It is readily shown[6, 9] that with this iterative process $\boldsymbol{\varphi}^{(k)}$ converges to the correct solution $\boldsymbol{\varphi}_S$ if, and only if, all the eigenvalues of the "kernel matrix" $b\boldsymbol{L}^{-1}$ lie within the unit circle $|z| = 1$ in the complex plane. In the present case this implies that Liebmann's computational scheme using "total adjustments" will diverge unless

$$|b| < \lambda_1. \tag{29}$$

This is a more restrictive condition than equation (25) since it rules out large positive values of b ($> \lambda_1$) which are allowed by equation (25). The method may be modified, however, by replacing equation (27) by

$$u_i^{(k)} = f(\psi_i^{(k)}) \tag{30}$$

where

$$\boldsymbol{\psi}^{(k)} = \theta\boldsymbol{\varphi}^{(k)} + (1 - \theta)\boldsymbol{\psi}^{(k-1)}, \quad \boldsymbol{\psi}^{(1)} = \boldsymbol{\varphi}^{(1)} \tag{31}$$

and where θ is a fixed parameter. This is equivalent to calculating the new approximation at each stage by taking a weighted average with the previous approximation; the procedure would be quite straightforward in practice. The resulting iterative equation for $\boldsymbol{\psi}^{(k)}$ has the "kernel matrix" $\boldsymbol{I} - \theta(\boldsymbol{I} + b\boldsymbol{L}^{-1})$. Provided the condition (25) is fulfilled, the eigenvalues of this matrix can be made to lie within the unit circle by taking θ less than $2\lambda_1/(\lambda_1 + b)$, and in this case $\boldsymbol{\psi}^{(k)}$ and $\boldsymbol{\varphi}^{(k)}$ will both converge to the correct solution $\boldsymbol{\varphi}_S$. Consequently the modified Liebmann scheme would yield solutions under the same conditions as Hutcheon's "single-step" method. (The iterative process for $\boldsymbol{\psi}^{(k)}$ is sometimes called a "mixed iteration" and has been discussed by Wiarda.[13])

GENERALIZATIONS

The arguments of the preceding sections can readily be generalized to the cases in which, (i) $f(\phi)$ is also a function of the independent variables x, y, etc., (ii) $f(\phi)$ involves operations on ϕ such as integration or differentiation, (iii) $f(\phi)$ is a non-linear function of ϕ.

Firstly suppose that $f(\phi)$ is linear in ϕ but depends on the variable x. Thus

$$f(\phi; x) = a(x) + b(x)\phi \tag{32}$$

so that, in matrix notation, equation (13) must be replaced by

$$f(\boldsymbol{\varphi}) = \boldsymbol{a} + \boldsymbol{B}\boldsymbol{\varphi} \tag{33}$$

where the components of $\boldsymbol{a}$ are no longer constant but are given by $a_j = a(jh)$ and where $\boldsymbol{B}$ is a diagonal matrix with $b_{jj} = b(jh)$.

Secondly, suppose, for example, that $f(\phi)$ includes a differentiation of ϕ. Then, by using finite difference approximations, we can replace

$$f(\phi) = a(x) + b(x)\phi + c(x)(d\phi/dx) \tag{34}$$

by

$$f(\phi_j) = a(jh) + b(jh)\phi_j + c(jh)(\phi_{j+1} - \phi_j)/h \tag{35}$$

which can also be written in the form of equation (33), provided the matrix $\boldsymbol{B}$ is defined by

$$b_{jj} = b(jh) - c(jh)/h, \quad b_{jj+1} = c(jh)/h$$

$$\text{and } b_{jk} = 0 \text{ if } k \neq j \text{ or } \neq j + 1.$$

In such cases $\boldsymbol{B}$ will not be diagonal. Definite or indefinite integrals of $\phi(x)$ and other combinations of linear operations can obviously be included by the same device.

The analysis now proceeds as before except that equation (33) is used in place of equation (13). It then follows that, for stability and convergence, *the eigenvalues μ_r of the matrix $\boldsymbol{I} + \boldsymbol{B}\boldsymbol{L}^{-1}$ must have positive real parts.* Since $\boldsymbol{B}$ is a matrix the μ_r cannot be expressed by the simple formula (19). First-order perturbation theory, however, enables us to conclude that

$$\mu_r \simeq 1 + \sum_{ij} b_{ij} w_{ri} w_{rj}/\lambda_r \sum_i w_{ri}^2 \tag{36}$$

where w_{ri} is the ith component of the rth eigenvector of $\boldsymbol{L}$. From this result the approximate criterion

$$\bar{b} = \sum_{ij} b_{ij} w_{1i} w_{1j} / \sum_i w_{1i}^2 > -\lambda_1 \tag{37}$$

may be derived. This is the same condition as (20) and (25), except that the parameter b has been replaced by $\bar{b}$, an average over the elements b_{ij} weighted by the lowest eigenfunction of $\boldsymbol{L}$. (This eigenfunction would, in most cases, be known at least roughly.)

Finally, suppose that $f(\phi)$ is a non-linear function of ϕ. To establish stability or convergence it is sufficient to consider the behaviour of small deviations from the true solution $\boldsymbol{\varphi}_S$. On defining the deviations by

$$\boldsymbol{e} = \boldsymbol{\varphi} - \boldsymbol{\varphi}_S \text{ and } \boldsymbol{v} = \boldsymbol{u} - f(\boldsymbol{\varphi}_S) \tag{38}$$

the basic network equation (5) becomes

$$\boldsymbol{L}\boldsymbol{e} = -\boldsymbol{v}. \tag{39}$$

By Taylor's theorem the auxiliary conditions (3) may be written

$$u_i = f(\phi_{Si}) + \frac{df}{d\phi}(\phi_{Si})e_i + 0(e_i^2). \tag{40}$$

Since the deviations can be taken arbitrarily small the correction term $0(e_i^2)$ may be omitted safely so that we have the auxiliary condition

$$\boldsymbol{v} = \boldsymbol{B}\boldsymbol{e} \tag{41}$$

where

$$b_{ii} = \frac{df}{d\phi}(\phi_{Si}), \qquad b_{ij} = 0 \ (i \neq j). \tag{42}$$

The dynamic equation corresponding to equation (15) then reads

$$\tau\boldsymbol{L}(d\boldsymbol{e}/dt) + (\boldsymbol{L} + \boldsymbol{B})\boldsymbol{e} = 0 \tag{43}$$

whilst the iterative equation (23) becomes

$$\{(\boldsymbol{I} + \boldsymbol{B}\boldsymbol{L}^{-1})\boldsymbol{u}\}_j = 0, \qquad j = 1, 2, \ldots N, 1, 2, \ldots \tag{44}$$

These two results both lead to the previous conclusion regarding the eigenvalues of the matrix $\boldsymbol{I} + \boldsymbol{B}\boldsymbol{L}^{-1}$. The only new feature is that, in this case, the matrix $\boldsymbol{B}$ depends on the correct solution $\boldsymbol{\varphi}_S$ which, of course, is not generally known beforehand. For practical applications of the criterion, however, quite crude approximations to the solution should suffice for estimating the likelihood of instability or non-convergence.

CONCLUSIONS

The foregoing analysis has shown that the methods of Karplus, Hutcheon and Liebmann (the last suitably modified) for obtaining analogue solutions to partial differential equations of the type (1) will be satisfactory, provided the gradient of the function $f(\phi)$ is positive or, if negative, is not too large. More specifically, all these schemes will break

down by reason of instability or non-convergence if $\bar{b}$ [which measures the gradient of $f(\phi)$] is more negative than $-\lambda_1$, λ_1 being the lowest eigenvalue of the matrix $\boldsymbol{L}$ approximating the differential operator.

Thus it will not be possible to solve the equation

$$(\partial^2\phi/\partial x^2) + (\partial^2\phi/\partial y^2) = -k^2\phi \qquad (33)$$

when k is greater than ω_1, the "frequency of the lowest mode." (The related fact that it is not possible to determine the higher normal modes and their frequencies by a direct iterative method was discovered experimentally by Liebmann but he noted it only in passing.[12]) Below the lowest mode frequency the solution ϕ displays only a single maximum (or minimum). For $k > \omega_1$, however, when the computational procedure fails, the solution has a number of maxima or minima (and points of inflexion or saddle points) and so exhibits a "wave-like" character. On the other hand, if it is known from physical insight that the required solution of a particular equation is not of an oscillatory nature, then any of the computing schemes will probably be satisfactory. The applications described in Refs. (1), (2) and (4) have been to the "space-charge" equation in which $f(\phi) = c^2\phi^{1/2}$. In this case the gradient of $f(\phi)$ is always positive, and so (except possibly in the case of Liebmann's method) there is no danger of instability or non-convergence.

It should be noted that similar stability and convergence questions arise in many branches of analogue computing, particularly in connexion with simultaneous equation solvers where they have been considered by Murray[7] and others.

REFERENCES

(1) KARPLUS, W. J. *Brit. J. Appl. Phys.*, **6**, p. 356 (1955).
(2) HUTCHEON, I. C. *Brit. J. Appl. Phys.*, **8**, p. 370 (1957).
(3) LIEBMANN, G. *Proceedings of the International Analogy Computation Meeting*, pp. 346–369 (Brussels: Association Internationale pour le calcul Analogique, 1955).
(4) LIEBMANN, G. Ref. 3, p. 355, and *Nature* [*London*], **164**, p. 149 (1949).
(5) FISHER, M. E. *J. Assoc. Comp. Machinery*, **3**, p. 325 (1956).
(6) FORSYTHE, G. E. *Bull. Amer. Math. Soc.*, **59**, p. 299 (1953).
(7) MURRAY, F. J. *The Theory of Mathematical Machines*, 2nd Ed., pp. 111–13 (New York: King's Crown Press, 1948).
(8) HOUSEHOLDER, A. S. *Principles of Numerical Analysis*, Ed. 2.1 (New York: McGraw-Hill Book Co., 1953).
(9) HOUSEHOLDER, A. S. *On the Convergence of Matrix Operations*, Report No. ORNL–1883 (U.S. Atomic Energy Commission, May 1955).
(10) TEMPLE, G. *Proc. Roy. Soc. A*, **169**, p. 476 (1939).
(11) LIEBMANN, G., and BAILEY, R. *Brit. J. Appl. Phys.*, **5**, p. 32 (1954).
(12) LIEBMANN, G. *Proc. Instn Elect. Engrs*, **99** (IV), footnote p. 267 (1952).
(13) BÜCKNER, H. *Die praktische Behandlung von Integralgleichungen*. Ergebnisse der angewandten Mathematik, no. 1, § 19 (Berlin: Springer-Verlag, 1952).

The performance of infra-red photoconductive cells

By D. H. ROBERTS, B.Sc., and B. L. H. WILSON, M.A., The Plessey Co. Ltd., Caswell, Towcester, Northants

[*Paper first received* 22 *November*, 1957, *and in final form* 18 *February*, 1958]

Expressions are derived for the responsivity and signal/noise ratio of photoconductive detectors under various conditions of noise limitation. These are used to show the basis for McAlister's relation, $E.N.I./\tau \simeq K$, and also the reasons for its failure to apply in the case of lead selenide cells. Experimental data obtained on lead selenide cells are presented, and a simple model for the flicker noise is shown to be consistent with the experimental observations.

LIST OF SYMBOLS

(Additional symbols required in the Appendices are defined therein.)

α = absorption coefficient for radiation
b = ratio of electron to hole mobility = μ_n/μ_p
β = recombination coefficient for hole-electron pairs
C_1, C_2 = constants describing fluctuations in shot, photon noise, usually approximately equal to unity
γ = generation coefficient for hole-electron pairs
D = diffusion constant of electrons
δ = phase shift in photoconductive response = $\tan^{-1}\omega\tau$
e = electronic charge
$\Delta\epsilon$ = energy gap between valence and conduction band
E, E' = constants describing flicker noise
$E.N.I.$ = equivalent noise input
f = frequency, modulation frequency
Δf = (amplifier) band width
FN (subscript) = flicker noise
F = ratio of noise power to Johnson noise
h = Planck's constant
H = energy dissipation per unit area
$\overline{i_N^2}$ = mean square noise current
I = d.c. bias current
I_0 = current corresponding to incident radiation flux $\bar{Q}_0$
JN (subscript) = Johnson noise
k = Boltzmann's constant
λ = wavelength
λ_{max} = wavelength of maximum response
$\lambda_{cut\ off}$ = long wavelength limit of sensitivity
m_{eff} = effective mass of the electron
μ_n, μ_p = electron, hole mobility
n = electron density
$\bar{n}$ = equilibrium electron density
$\Delta n = n - \bar{n}$
N_c = effective density of states in conduction band
ν = frequency of radiation
ω = angular frequency = $2\pi f$
p = hole density
$\bar{p}$ = equilibrium hole density
$\Delta p = p - \bar{p}$
PN (subscript) = photon noise
Q = quantum flux density
$\bar{Q}$ = mean quantum flux density
$\bar{Q}_0$ = mean quantum flux density at surface $Z = 0$
SN (subscript) = shot noise

S (subscript) = signal
S/N = voltage ratio of signal to noise
t = time
τ = decay constant of excess carriers
τ' = transit time of a carrier between electrodes
u = index of the power describing the dependence of $\overline{i_{FN}^2}$ on bias current
$\overline{V_N^2}$ = mean square noise voltage
V_c = bias voltage
V_N = r.m.s. noise voltage
$V_s = V_s'/\sin wt$
V_s' = signal voltage
V_{SN} = r.m.s. noise voltage due to shot noise, etc.
w = index of the power describing the dependence of $\overline{i_{FN}^2}$ on frequency
x = co-ordinate in direction of applied field
X = length of specimen in direction of applied field, inter electrode distance
χ = conductance of specimen $= 1/R_c$
$\bar{\chi}$ = conductance of specimen at equilibrium
y = co-ordinate at right angles to field and photon flux
Y = breadth of specimen
$\mathscr{Y}$ = admittance
z = co-ordinate in direction of photon flux
Z = thickness of specimen
$\mathscr{Z}$ = impedance

1. INTRODUCTION

As it appears likely that photoconductive cells of such materials as lead sulphide, lead selenide, lead telluride and indium antimonide will come into increasingly wide use as infra-red detectors, it is considered worthwhile to draw attention to the conditions desirable in the design and application of such detectors. The bias and measuring circuits required are discussed, and the noise sources and signal level in photocells are related to the basic material parameters (carrier density, mobility, lifetime, effective mass, etc.). The effects on performance of such factors as cell area, chopping frequency, operating temperature and ambient illumination are pointed out.

2. PHOTOCONDUCTIVE RESPONSE

2.1 *Introduction.* In a semiconductor the electrical conductivity is due to the free charge carriers—i.e. electrons in the conduction band and holes in the full band. It is necessary to supply energy equal to or greater than $\Delta\epsilon$ to such a system to produce an additional free electron-hole pair. This energy can be supplied in many ways—thermal energy *via* the lattice, bombardment with high energy particles or the absorption of electromagnetic radiation. Only the latter will be considered here.

The absorption of a quantum of radiation of energy equal to or greater than $\Delta\epsilon$ produces a free electron-hole pair, and hence a change in the conductivity of the specimen. The long wavelength limit of photoconductivity is determined by

$$h\nu = \Delta\epsilon$$

Whence
$$\lambda_{cut\ off} = hc/\Delta\epsilon \qquad (1)$$

Typical values for commercial photocells are given in the table.

2.2 *Theory.* Consider a uniform slab of photoconductor as shown in Fig. 1, uniformly illuminated in the z-direction.

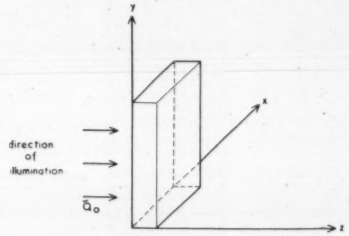

Fig. 1. Slab of photoconductor

The differential equation describing the rate of change of the carrier density is

$$dn/dt = \alpha Q - \beta(\bar{n} + \Delta n)(\bar{p} + \Delta p) + \gamma(\bar{n}\bar{p}) + D(\partial n/\partial z) \qquad (2)$$

Three assumptions will be made to simplify the solution of this equation:

(i) surface recombination is negligible. (This will be discussed later);
(ii) the signal is linear with respect to Δn and Δp, i.e. Δn, $\Delta p \ll \bar{n}$ or $\bar{p}$;
(iii) $\Delta n = \Delta p$. This is necessary to preserve charge neutrality.

If one considers the case where $Q = 0$ everywhere at all times,

$$\gamma = \beta$$

The first two assumptions allow the diffusion term, $D(dn/dz)$ to be ignored providing one later integrates to obtain the integral of Δn over the complete specimen. (Amongst others, Kurnick and Zitter[1] give a treatment which takes account of surface recombination—and hence of diffusion.)

So
$$dn/dt = \alpha Q - \beta(\bar{n} + \bar{p})\Delta n \qquad (3)$$

ignoring second-order terms in Δn.

If we now let $Q = 0$ for $t > 0$, the excess carriers decay according to

$$\Delta n(t) = \Delta n_0 \exp\left[-\beta(\bar{n} + \bar{p})\right]t \qquad (4)$$

$1/\beta(\bar{n} + \bar{p})$ is known as the lifetime τ, and is a characteristic

Properties of common photoconductors

	Si	*Ge*	*PbS*	*PbSe*	*InSb*
$\Delta\epsilon(eV)$	1·1	0·72	0·37	0·25	0·17
τ (s)	$<2 \times 10^{-3}$	$<5 \times 10^{-3}$	$\sim 75 \times 10^{-6}$	$\sim 10^{-6}$	$<10^{-7}$
λ_{max} (μ)	0·8	1·7	2·5	2·8	7·0
$\lambda_{cut\ off}$ (μ)	1·1	2·1	~3·5	~4·5	~8·0
$\bar{n}$ (*intrinsic at* 300° *K*)(cm^{-3})	$1{\cdot}3 \times 10^{10}$	$2{\cdot}10^{13}$	3×10^{15}	$\sim 4 \times 10^{16}$	2×10^{16}
E.N.I. at λ_{max} (*W*)*			$\sim 10^{-11}$	$\sim 10^{-10}$	10^{-9}

* Normalized for an area of 2 mm².

of the sample such that at time $t = \tau$ the number of excess carriers has decayed to $1/e$ of its original value, that is

$$\Delta n(t) = \Delta n_0 \exp(-t/\tau) \tag{5}$$

A similar expression holds for recombination *via* centres at which the recombining carrier is held for a negligible time. Cases in which more than one characteristic time occur are found in larger energy gap materials[2] (e.g. cadmium sulphide). These will not be considered here as they occur chiefly in detectors of visible rather than infra-red radiation. (Scanlon[3] has, however, observed two time constants in lead telluride.)

If we now return to equation (3) and consider the steady state solution

$$dn/dt = 0$$

then
$$\Delta n = \alpha Q \tau \tag{6}$$

or
$$n(z) = \bar{n}(z) + \alpha Q(z)\tau \tag{7}$$

If the incident radiation is modulated sinusoidally at frequency $f = \omega/2\pi$ so that

$$Q = \bar{Q}(1 + \sin \omega t)$$

then the solution of equation (3) is

$$n(z) = \bar{n}(z) + \frac{\alpha \bar{Q}(z)\tau}{(1 + \omega^2\tau^2)^{1/2}} \sin(\omega t + \delta) + \alpha \bar{Q}(z)\tau \tag{8}$$

where $\tan \delta = \omega\tau$.

Now, the conductance X of a film of length X, width Y and thickness Z is

$$X = \frac{Y}{X}\int_0^Z \sigma(z)dz$$

$$= \overline{X} + \Delta X \sin(\omega t + \delta)$$

where in the small signal case,

$$\overline{X} = (Y/X)eZ(\bar{n}\mu_n + \bar{p}\mu_p) \tag{9}$$

since the conductivity $\sigma = \bar{n}e\mu_n + \bar{p}e\mu_p$

and
$$\Delta X = (Y/X)e(\mu_n + \mu_p)\frac{\tau}{(1 + \omega^2\tau^2)^{1/2}}\int_0^Z \alpha Q(z)dz \tag{10}$$

Initially we shall consider the case where $\omega\tau \ll 1$ that is where

$$\delta \to 0 \text{ and } 1 + \omega^2\tau^2 \to 1$$

By Lambert's law we know that

$$\bar{Q}(z) = \bar{Q}_0 \exp(-\alpha z) \tag{11}$$

This ignores reflexion losses and interference effects. The former will reduce $\bar{Q}_0$ by a constant factor, given by Fresnel's reflexion coefficient. Interference effects can be ignored at this stage.

Therefore,

$$\Delta X = (Y/X)e(\mu_n + \mu_p)\bar{Q}_0\tau[1 - \exp(-\alpha Z)] \tag{12}$$

It is shown in Appendix II that the signal voltage is given by

$$V_s' = V_c \Delta\chi/\overline{\chi} \tag{13}$$

$$= V_c \bar{Q}_0 \tau \frac{1 - \exp(-\alpha Z)}{Z} \frac{\mu_n + \mu_p}{\bar{n}\mu_n + \bar{p}\mu_p} \sin \omega t \tag{14}$$

One can now consider two cases of intrinsic or extrinsic conduction:

(*a*) *Intrinsic case* $\bar{n} = \bar{p}$ $\qquad \dfrac{\mu_n + \mu_p}{\bar{n}\mu_n + \bar{p}\mu_p} = \dfrac{1}{\bar{n}}$

(*b*) *Extrinsic case* $\bar{n}$ (or $\bar{p}$) $= 0$ $\qquad \dfrac{\mu_n + \mu_p}{\bar{n}\mu_n + \bar{p}\mu_p} = \dfrac{1 + b}{\bar{p}}$

Only the intrinsic case will be dealt with at this stage. The importance of b in the extrinsic case will be discussed in a later section. In the intrinsic case,

$$V_s' = \frac{V_c \bar{Q}_0 \tau}{\bar{n}}\left[\frac{1 - \exp(-\alpha Z)}{Z}\right] \sin \omega t \tag{15}$$

It can be seen from equation (15) that the responsivity, defined as signal volts per watt incident power, is independent of carrier mobility, and is directly proportional to $\tau/\bar{n}$. This result will be discussed later.

On re-inserting the $(1 + \omega^2\tau^2)^{-1/2}$ term to assess performance at high frequencies, it is apparent that unless one requires a fast time constant (i.e. small τ) in order to study transient phenomena and avoid high frequency distortion of the incident waveform, it is always the detector with the longest time constant which gives the highest responsivity at any modulation frequency (other things being equal).[4]

3. NOISE

There are four types of noise generally occurring in any photoconductive element. More detailed information and a fuller bibliography are given in papers by Burgess[5] and Wilson.[6]

3.1 *Johnson noise.* The voltage fluctuations across any two terminal impedance $\mathscr{Z}$ in thermal equilibrium at absolute temperature T may be deduced from purely thermodynamic considerations. The Fourier components are given by Nyquist's theorem:

$$\overline{V_{JN}^2} = 4\mathscr{R}(\mathscr{Z})hf[\exp(hf/kT) - 1]^{-1}\Delta f \tag{16}$$

Except at very high frequencies and reduced temperatures this reduces to the well-known expression

$$\overline{V_{JN}^2} = 4kT\mathscr{R}(\mathscr{Z})\Delta f \tag{17}$$

The corresponding parallel current fluctuations across an admittance $\mathscr{Y}$ are

$$\overline{i_{JN}^2} = 4kT\mathscr{R}(\mathscr{Y})\Delta f \tag{18}$$

These fluctuations can be related to particular models of conduction. In a uniform conductor they are usually related to the velocity fluctuations of the charge carriers. (This is by no means always true for non-uniform conductors. For example, the noise in a semiconductor diode without applied bias is related to the numbers of carriers crossing the junction rather than their velocity.) The same fluctuations are found even under bias if, as is usual, the velocity distribution is substantially unchanged by the drift velocity produced by the applied field.

3.2 *Shot noise.* As the excitation and recombination processes governing the number of free charge carriers are randomly occurring discrete events, there will be an excess noise in a semiconductor carrying current.

In the case of an *n*-type semiconductor with a single lifetime,

$$(\overline{\Delta n})^2 = C_1\bar{n} = (\overline{\Delta p})^2 \tag{19}$$

where $\bar{n}$ = mean number of electrons present and $(\overline{\Delta n})^2$, $(\overline{\Delta p})^2$ are the variances in the numbers of electrons and holes. In a complete treatment, Burgess[7, 8] derives a value for C_1 which, in the intrinsic case, reduces to a half.

The frequency dependence of the shot noise has also been considered by Burgess[5] for the important case of carriers in

a uniform rod of semiconductor under bias, when the carriers decay with time constant τ and the transit time is τ'.

The shot noise current is given by

$$\overline{i_{SN}^2} = 2C_1 eIW(\omega\tau, \omega\tau')\Delta f \qquad (20)$$

where W is a rather complicated expression given by Burgess.[5] Important special cases are:

(i) $\tau \ll \tau'$ $\quad W = \dfrac{2\tau}{\tau'} \dfrac{1}{1+\omega^2\tau^2}$

this is the case obtained in practice.

(ii) $\omega\tau \ll 1$, $\omega\tau' \ll 1$ $\quad W = \dfrac{\tau^2}{\tau'^2}\left[\dfrac{\tau'}{\tau} - 1 + \exp(-\tau'/\tau)\right]$

(iii) $\tau \gg \tau'$ $\quad W = 2(1 - \cos\omega\tau')/\omega^2\tau'^2$

In the last case, $W \to 1$ as $\omega\tau' \to 0$. This is analagous to the shot noise in a temperature-limited vacuum diode, for which

$$\overline{i_{SN}^2} = 2eI\Delta f$$

when the frequency is much less than the reciprocal of the transit time.

Inserting the result of case (i) above into equation (20)

$$\overline{i_{SN}^2} = 4C_1 eI\{\tau/[\tau'(1+\omega^2\tau^2)]\}\Delta f \qquad (21)$$

Equation (21) indicates that shot noise has a white spectrum except at high frequencies. Here $\omega^2\tau^2$ becomes greater than unity and the noise current varies inversely with frequency.

3.3 *Photon noise.* The radiation incident on a photoconductive element consists of a fluctuating number of quanta. If $\bar{Q}$ is the mean number of quanta arriving per second, the mean square fluctuation is given by

$$(\overline{\Delta Q})^2 = C_2\bar{Q} \qquad (22)$$

The coefficient C_2 is determined by the statistics of the radiation stream, being greater when the source is hotter, so that more multiple quanta are emitted. It is, in practice, near unity. The photon noise in a uniform photoconductor produced by the fluctuations in the incident radiation stream is

$$(\overline{\Delta I})^2 = 2C_2 eI_0\Delta f \qquad (23)$$

where I_0 is the d.c. photocurrent corresponding to signal $\bar{Q}_0$. Additional shot noise is generated in the recombination process.[9] The photon noise in the signal radiation is the ultimate limit to the sensitivity of a radiation detector. Photon noise is also generated owing to ambient radiation. The increase in sensitivity in cooled lead telluride cells and lead sulphide cells on cooling their surroundings, has been adduced as evidence that the photon noise limit is being reached in this type of detector when operated at reduced temperatures.[10]

3.4 *Flicker noise.* It is found that over and above the types of noise previously mentioned there exists a noise current dependent on the frequency and the bias current I. This noise may be denoted by

$$\overline{i_{FN}^2} = E'I^w f^{-u}\Delta f \qquad (24)$$

where u is of the order of 2, and w is equal to or just over unity. E' is a constant for the cell dependent on the material, the cell dimensions, the state of the surface[11] and the contacts.[12]

If we suppose that satisfactory (i.e. not noisy) contacts are made to the material and X, $Y \gg Z$, as is usual, dimensional arguments show, if $u = 2$,

$$E' = E/(XY) \qquad E \neq E(X,Y)$$

This may be proved most simply by considering the combination of two cells in series or parallel.

The Z-dependence is more complicated. If the noise is generated by centres distributed throughout the volume and if volume recombination is dominant, similar arguments give

$$E \propto Z^{-1}$$

However a surface distribution of noise centres would tend to make E decrease more rapidly with Z (than Z^{-1}) and a surface distribution of recombination centres less rapidly.

4. SIGNAL/NOISE RATIO, S/N

4.1 *Johnson noise limited.*

R.m.s. signal voltage, $V_s = \dfrac{V_c}{\sqrt{2}} \dfrac{\bar{Q}_0\tau}{\bar{n}} \dfrac{1-\exp(-\alpha Z)}{Z}$

where $V_s' = \sqrt{2}\,.\,V_s \sin\omega t$

r.m.s. noise voltage $V_{JN} = (4kT\Delta f/X)^{1/2}$ (25)

$$(S/N)_{JN} = \frac{V_c X^{1/2}}{(8kT\Delta f)^{1/2}} \frac{\bar{Q}_0\tau}{\bar{n}} \frac{1-\exp(-\alpha Z)}{Z} \qquad (26)$$

Obviously, the signal-to-noise ratio increases with the applied voltage. The limitation is set by the dissipation of heat by the detector.

Suppose the detector can dissipate a maximum of $H/2$ (W/cm^2)

$$(V_{cmax})^2 X = HXY \qquad (27)$$

$$(S/N)_{JN} = \frac{H^{1/2}(XY)^{1/2}}{(8kT\Delta f)^{1/2}} \frac{\bar{Q}_0\tau}{\bar{n}} \frac{1-\exp(-\alpha Z)}{Z} \qquad (28)$$

4.2 *Shot noise limited.* From equation (21),

$$V_{SN} = (4C_1 eV_c X^{-1}\tau\tau'^{-1}\Delta f)^{1/2} \qquad (29)$$

$$(S/N)_{SN} = \frac{(V_c X)^{1/2}}{(8C_1 e\Delta f)^{1/2}} \frac{\bar{Q}_0\tau}{\bar{n}} \frac{1-\exp(-\alpha Z)}{Z} \left(\frac{\tau'}{\tau}\right)^{1/2} \qquad (30)$$

Now, τ' the transit time is given by

$$\tau' = X^2/(\mu_n V_c) \text{ for voltage applied in the } x\text{-direction} \qquad (31)$$

Therefore

$$(S/N)_{SN} = \frac{X^{1/2}X}{(8C_1 e\mu_n\Delta f)^{1/2}} \frac{\bar{Q}_0\tau^{1/2}}{\bar{n}} \frac{1-\exp(-\alpha Z)}{Z} \qquad (32)$$

$$= \frac{(XY)^{1/2}\bar{Q}_0\tau^{1/2}}{(8C_1 e\bar{n}\Delta f)^{1/2}} \frac{1-\exp(-\alpha Z)}{Z^{1/2}} \qquad (33)$$

4.3 *Photon noise limited.* From equation (23),

noise voltage, $V_{PN} = (2eC_2 V_c X^{-1}\Delta f)^{1/2}$

Therefore

$$(S/N)_{PN} = \frac{V_c^{1/2}X^{1/2}}{2(C_2 e\Delta f)^{1/2}}\left[\frac{\bar{Q}_0\tau}{\bar{n}} \frac{1-\exp(-\alpha Z)}{Z}\right]^{1/2} \qquad (34)$$

$$= \frac{1}{2}\left(\frac{H\mu_n}{\bar{n}e}\right)^{1/4}\left[\frac{Y\bar{Q}_0\tau}{C_2\Delta f} \frac{1-\exp(-\alpha Z)}{Z^{1/2}}\right]^{1/2} \qquad (35)$$

4.4 *Flicker noise limited.* We shall assume $u = 2$, $w = 1$ initially

$$V_{FN} = \left[\frac{E^{1/2}V_c}{(XY)^{1/2}}\right]\left(\frac{\Delta f}{f}\right)^{1/2}$$

Whence

$$(S/N)_{FN} = \frac{(XY)^{1/2}}{\sqrt{2}}\,\frac{\bar{Q}_0\tau}{\bar{n}}\left(\frac{f}{E\Delta f}\right)^{1/2}\frac{1-\exp(-\alpha Z)}{Z} \quad (36)$$

The general expression for the signal-to-noise ratio will be of the form

$$(S/N)_{FN} \propto V_c^{1-u/2}$$

The variation in the signal-to-noise ratio with voltage for a combination of Johnson and flicker noise is sketched in Fig. 2 for the three cases $u < 2$, $u = 2$ and $u > 2$. In all three cases the initial rise occurs in the region where Johnson noise is still predominant.

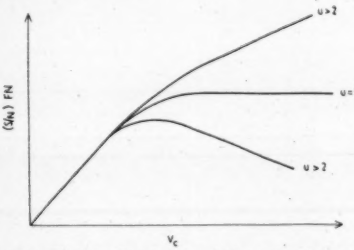

Fig. 2. Variation in signal-to-noise ratio with voltage for a combination of Johnson and flicker noise

Measurements carried out by the authors on photoconductive films of lead selenide indicate that for that particular detector, $2 < u < 2{\cdot}3$ so that there is an optimum bias condition. The case $u = 2$ is the one already dealt with in equation (36).

The case of $u < 2$ is the rarest and, when encountered, the solution is as for the case of Johnson noise limited, in so far as the limitation is set by dissipation of heat owing to Joule heating.

4.5 *Responsivity and equivalent noise input.* Responsivity is the term given to the output signal (usually in volts) of a detector per watt incident radiant power (usually monochromatic at the wavelength of peak response).

The equivalent noise input (*E.N.I.*) is defined as the minimum energy flux density required to give a (S/N) ratio of 1, when measured in a 1 c/s bandwidth.

Example. If a detector has a (S/N) ratio of 100 : 1 in an energy flux density of $7{\cdot}2 \times 10^{-6}$ W/cm^2 (r.m.s.) measured with an amplifier bandwidth of 50 c/s.

Then, *E.N.I.*

$$= \frac{7{\cdot}2 \times 10^{-6}}{100\sqrt{50}} = 10^{-8}\ \text{W/cm}^2$$

5. EFFECT OF CELL AREA ON E.N.I.

Equations (28), (33) and (36) contain the terms

$$(S/N) \propto (XY)^{1/2}\bar{Q}_0 \quad (37)$$

Now if $\bar{Q}_0$ is constant, i.e. the detector is placed in a uniform field of radiation,

$$(S/N) \propto (\text{area})^{1/2} \quad (38)$$

On the other hand, if Q^*, the total number of photons, $= \bar{Q}_0 \times$ area $=$ constant

$$(S/N) \propto (XY)^{1/2}Q^*/(XY)$$
$$\propto (\text{area})^{-1/2} \quad (39)$$

In the case of photon noise limited detectors, equation (35) shows that (S/N) is proportional to the square root of the width and independent of the length.

6. EFFECT OF FILM THICKNESS

The responsivity is shown in equation (14), where surface recombination is neglected, to have a Z-dependence given by

$$[1 - \exp(-\alpha Z)]/Z$$

under these conditions the responsivity tends to a limit when $\alpha Z \ll 1$. In other words at the absorption edge the photoconductive responsive is independent of film thickness and the spectral response follows the absorption curve. If Z is sufficiently small, this condition applies for all values of α, i.e. all wavelengths. In thin films of lead selenide it has been postulated[13] that the reason for the departure from this dependence is the presence of potential barriers in certain types of film which inhibit the long wavelength photoconductive response.

The signal-to-noise ratio shows the same Z-dependence for Johnson noise limited cells.

The shot noise limited case gives

$$(S/N)_{SN} \propto [1 - \exp(-\alpha Z)]/Z^{1/2}$$

and the signal-to-noise ratio shows a maximum when $Z = 1{\cdot}25/\alpha$. Equation (35) shows that the photon noise limited case gives $(S/N)_{PN} \propto \{[1 - \exp(-\alpha Z)]/Z^{1/2}\}^{1/2}$ which is a maximum when $Z = 1{\cdot}25/\alpha$ as in the previous case.

The only simple case for the flicker noise limited detector is when flicker noise generation and carrier recombination occur in the volume. The Z-dependence of the signal-to-noise ratio is then the same as for the shot noise limited detector. This result may be obtained from equation (36) by putting $E \propto Z^{-1}$ as discussed in Section 3.4. The matter is discussed in Appendix IV. It is possible that thin films will exhibit interference effects, but none have been observed by the authors even in lead selenide films only $0{\cdot}3\ \mu$ thick.

7. EFFECT OF SURFACE RECOMBINATION

The effect of surface recombination on the photoconductive spectral response has been considered by Moss[14] and De Vore[15] who point out that it is usual to find a peak in the photoconductive response in the neighbourhood of the absorption edge. De Vore shows that this is due to surface recombination. The response is reduced at short wavelengths where the carriers are produced in the surface, but at the edge, where α is low, carriers are produced in the body of the material away from the high recombination surface. It is found experimentally that then films show a broad maximum, whereas thick samples show a sharper peak and a greater reduction in the short wavelength response. This is in agreement with De Vore's theory. Earlier ideas ascribed this effect to high recombination in the surface due to the high density of photocarriers, when the incident radiation is of wavelength less than the cut-off wavelength.

8. IMPORTANCE OF EFFECTIVE MASS AND MOBILITY RATIO

It can be shown[16] that the density of excess carriers in the conduction band is given by

$$\bar{n} = N_c \exp(-\Delta\epsilon/kT) \tag{40}$$

where the effective density of states in the conduction band N_c, is given by

$$N_c = 2(2\pi m_{eff} kT/h^2)^{3/2} \tag{41}$$

where m_{eff} is the effective mass of the charge carrier. In other words

$$\bar{n} \propto (m_{eff})^{3/2} \tag{42}$$

For all the cases considered, the signal/noise ratio is an inverse function of $\bar{n}$. Therefore for a high value of (S/N) a low effective mass is advantageous. This is particularly important in the case of an intermetallic semiconductor such as indium antimonide, where the effective masses of electrons and holes are respectively 0·03 and 0·2 times the free electron mass.

In Section 2.2 the distinction was drawn between the intrinsic and extrinsic photoconductor, and only the intrinsic case was considered in detail. It is worth noting that for p-type extrinsic material, the solution in the case of Johnson noise limited operation, for example, is

$$(S/N)_{JN} = \frac{H^{1/2}(XY)^{1/2}}{(8kT\Delta f)^{1/2}} \frac{\bar{Q}_0\tau(1+b)}{\bar{p}} \frac{1-\exp(-\alpha Z)}{Z} \tag{43}$$

so that there is every advantage to be gained by having a high value of b. Once again, indium antimonide ($b \simeq 30$) is a good example, and this material is most efficient as a photoconductor when slightly p-type material is used.[17] In the case of impurity photoconduction (in silicon and germanium), there is an advantage in using donor levels rather than acceptors, for the same reason.

There are theoretical reasons[18] for expecting $\mu_n \propto m_{eff}^{-5/2}$ when only lattice scattering is taken into account. Thus materials such as indium antimonide, where the ratio of electron to hole effective mass is small, have the additional advantage of a high ratio of mobilities b.

9. EFFECT OF AMBIENT TEMPERATURE AND ILLUMINATION

(i) In the case of a Johnson noise limited detector the noise voltage, V_{JN}, is proportional to the square root of the temperature.

(ii) Increasing temperature and background illumination both lead to an increase in $\bar{n}$ and hence a reduction in sensitivity.

(iii) The carrier lifetime τ is usually reduced by background illumination, and the effect of temperature depends on the recombination process:

- (*a*) for photon-radiative recombination τ increases as T decreases;
- (*b*) when recombination occurs *via* centres of the Shockley-Read type[19] the variation of τ with T depends on the position of the centres relative to the Fermi level, and the subsequent movement of the Fermi level with temperature. In practice τ can either increase or decrease with increasing T.

(iv) A further effect of temperature is on the energy gap $\Delta\epsilon$. In the case of the lead sulphide group, $\Delta\epsilon$ decreases as T decreases,[10] so that at reduced temperatures these detectors are sensitive to longer wavelengths than at room temperatures. On the other hand, $\Delta\epsilon$ increases as T decreases in the case of germanium, silicon and indium antimonide, so that if one gains sensitivity by cooling it is at the expense of the spectral response.

10. OPTIMUM CHOPPING FREQUENCY

For many applications of photoconductive cells there will some freedom in the choice of modulation frequency.

As implied by equations (10) and (24), the signal-to-noise ratio for cells dominated by flicker noise is such that

$$(S/N)_{FN} \propto \left(\frac{f}{1+4\pi^2 f^2\tau^2}\right)^{1/2}$$

putting $W = 1$ in equation (24).

The ratio rises initially as $f^{1/2}$ reaches a maximum when $2\pi f\tau = 1$, and finally falls as $f^{-1/2}$.

For Johnson noise limited detectors,

$$(S/N)_{JN} \propto (1+4\pi^2 f^2\tau^2)^{-1/2}$$

that is, the ratio remains substantially constant until $2\pi ft = 1$, and then finally falls as f^{-1}; ($f^{-1/2}$ in the case of a photon noise limited detector). The shot noise limited case gives signal-to-noise ratio independent of frequency.

The common chopping frequency of 800 c/s is suitable for lead sulphide, but for other flicker noise limited detectors a higher signal-to-noise ratio may be obtained at higher frequencies. It is no longer easy to chop with a simple toothed wheel and more refined techniques are required.

It must be stressed that spectroscopists who replace a thermal detector by a photoconductive cell will usually gain considerably by changing their frequency from 5–20 c/s to 1 kc/s or more. In addition, the amplifier design is simpler in this frequency range.

11. THE MCALISTER RELATION

In a paper on the detectivity of lead sulphide cells, Dr. R. Clark Jones[20] reports experimental results obtained by Dr. E. D. McAlister of the Eastman Kodak Co.

Dr. McAlister plotted *E.N.I. versus* τ for about eighty different lead sulphide cells, manufactured by various groups in America and Great Britain, and found the empirical relationship

$$E.N.I./\tau \simeq K \tag{44}$$

to apply within a factor of three for nearly all of the eighty cells.

This result was obtained with cells, the response times of which varied from 3 to 3000 μs. Presumably the values of *E.N.I.* also covered three decades, so that not all the cells were of the most sensitive type. For this type of detector, flicker noise predominates, and so inspection of equation (36) should indicate to what extent McAlister's relation is to be expected theoretically:

$$(S/N)_{FN} = (XY)^{1/2} \frac{\bar{Q}_0\tau}{\bar{n}} \left(\frac{f}{E\Delta f}\right)^{1/2} \frac{1-\exp(-\alpha Z)}{Z}$$

Because these measurements were presumably made under identical conditions, and the value of *E.N.I.* would be

normalized to a standard detector area, this equation can be simplified to

$$(S/N)_{FN} \propto \frac{\tau}{\bar{n}E^{1/2}} \frac{1 - \exp(-\alpha Z)}{Z} \qquad (45)$$

whence it is quite apparent that, all other things being equal,

$$E.N.I./\tau \simeq K$$

Three other factors, $\bar{n}$, E and Z are, however, variables, and McAlister's relation would appear to be somewhat fortuitous. For comparison, results of measurements carried out on lead selenide cells are given in Appendix I. These do not conform to McAlister's relation, and part of the reason for this is shown in the scatter of the value of E for these detectors. For this batch of detectors, the thickness Z is constant within a factor of 2.

12. CONCLUSIONS

The importance of the results obtained above may best be summarized by suggesting a few "golden rules" which should govern the choice of the most suitable detector for a particular application.

(i) *Size.* Whenever an optical condensing system can be used, so that the total number of available quanta is constant, the detector should be as small as possible. If, on the other hand, focusing is impossible and the detector is to be placed in a uniform radiation field, it should be as large as possible. The above remarks do not apply to photon noise limited detectors, as was indicated in Section 5.

(ii) *Response time.* The highest value of (S/N) will always be obtained with the slowest detector[4] (other things being equal). Only if a high frequency response is required to avoid distortion of a pulse waveform is this not so (e.g. in the study of transient phenomena). Even in this case, however, it is sometimes better to use the slowest detector in conjunction with a compensated amplifier, so that the responsivity of the whole is flat to the required high frequency.

(iii) *Chopping frequency.* In the case of a flicker noise limited detector it is obviously profitable to modulate the signal at the highest possible frequency, providing $2\pi f\tau < 1$. In the case of other detectors the more important consideration is of a simplicity of amplifier design. It is generally found that a frequency of 800 c/s is quite satisfactory.

(iv) *Choice of photoconductive material.* The important fact here is that it is detrimental to use a detector which is sensitive to wavelengths longer than the region in which sensitivity is actually required. This is because the reduction of $\Delta\epsilon$ (see Section 2.1) results in an increase in $\bar{n}$ and decrease in τ, as can be seen from the results given in the table.

Furthermore, in the case of a cooled, photon noise limited detector, the noise will be greater in the long wavelength detector, as a larger band of thermal radiation will be capable of producing electron hole pairs.[21, 22, 23]

(v) *Responsivity or E.N.I.* When working at low signal levels with a low noise amplifier, where detector noise dominates, the criterion applied to a detector should be the value of its *E.N.I.* However, if amplifier noise dominates, the detector with the highest responsivity should be used.

ACKNOWLEDGEMENTS

Our thanks are due to Messrs. N. F. Durrant and W. M. Wallbank for much helpful criticism and to the Plessey Co. Ltd. for permission to publish this paper.

REFERENCES

(1) KURNICK, S. W., and ZITTER, R. N. *J. Appl. Phys.*, **27**, p. 278 (1956).
(2) ROSE, A. *Progress in Semiconductors*, Vol. II, p. 109 (London: Heyward and Co., 1957).
(3) SCANLON, W. W., PETRITZ, R. L., and LUMMIS, F. L. *Phys. Rev.*, **86**, p. 659 (1952).
(4) CLARK JONES, R. *Advances in Electronics*, Vol. V, p. 1 (New York: Academic Press Inc., 1953).
(5) BURGESS, R. E. *Brit. J. Appl. Phys.*, **6**, p. 185 (1955).
(6) WILSON, B. L. H. *J. Brit. Instn Radio Engrs*, **18**, p. 208 (1958).
(7) BURGESS, R. E. *Proc. Phys. Soc.* [*London*] *B*, **68**, p. 666 (1955).
(8) BURGESS, R. E. *Proc. Phys. Soc.* [*London*] *B*, **69**, p. 1020 (1956).
(9) ROSE, A. *Proc. Inst. Radio Engrs*, **43**, p. 1850 (1955).
(10) MOSS, T. S. *Pros. Inst. Radio Engrs*, **43**, p. 1869 (1955).
(11) PEARSON, G. L., MONTGOMERY, H. C., and FELDMANN, W. L. *J. Appl. Phys.*, **27**, p. 51 (1956).
(12) BURGESS, R. E. *Brit. J. Appl. Phys.*, **6**, p. 385 (1955).
(13) ROBERTS, D. H., and BAINES, J. E. *Physics and Chemistry of Solids*. To be published.
(14) MOSS, T. S. *J. Electronics*, **1**, p. 126 (1955).
(15) DE VORE, H. B. *Phys. Rev.*, **102**, p. 86 (1956).
(16) SHOCKLEY, W. *Electrons and Holes in Semiconductors* (New York: D. Van Nostrand Co. Inc., 1950).
(17) MOSS, T. S. *Photoconductivity Conference* (New York: J. Wiley and Sons Inc., 1956).
(18) BLATT, F. J. *Solid state physics*, Vol. IV, p. 199 (New York: Academic Press Inc., 1957).
(19) SHOCKLEY, W., and READ, W. T. *Phys. Rev.*, **87**, p. 835 (1952).
(20) CLARK JONES, R. *J. Opt. Soc. Amer.*, **43**, p. 1008 (1953).
(21) MOSS, T. S. *J. Opt. Soc. Amer.*, **40**, p. 603 (1950).
(22) FELLGETT, P. *J. Opt. Soc. Amer.*, **39**, p. 970 (1949).
(23) PLATT, J. R. *J. Opt. Soc. Amer.*, **46**, p. 609 (1956).
(24) OLIVER, D. J. *Proc. Phys. Soc.* [*London*], *B*, **70**, p. 331 (1957).

APPENDIX I

Test of McAlister's relationship for lead selenide photoconductive cells

The following data was obtained from measurements performed by Mr. T. C. Denton on lead selenide photocells prepared by Mr. P. E. Cotterrell at this laboratory. All measurements were carried out at 800 c/s with an amplifier bandwidth of 50 c/s. The signal source was a black body at 200° C. The values of S/N ratio were obtained at the optimum bias condition (see Section 4.4) and the noise voltages were measured at constant current ($I = 40\ \mu A$). The response time was found by direct observation of the photoconductive decay on illumination with radiation from a spark gap, the duration of the spark being about $0{\cdot}4\ \mu s$.

In Fig. 3 the values of signal-to-noise ratio and response time are plotted for fifty-two lead selenide cells. The line indicates the curve one would expect from McAlister's relation. These results are given for a constant cell area of 15 mm^2 and a constant level of illumination.

Fig. 4 is a plot of noise voltage (at constant current) *versus* resistance for the same batch of lead selenide cells.

From equation (24)

$$V_{FN} = (E' I^{\mu} f^{-w} \Delta f)^{1/2} R_c \qquad (46)$$

whence a plot of V_{FN} *versus* R_c should yield a straight line of slope $(E'I^u f^{-w}\Delta f)^{1/2}$. Any deviations from this result can only be due to variation of E', u or w. It has been found that $w = 1$ substantially, $u = 2 - 2{\cdot}3$, so that the large deviations from the expected straight line are due to variations in E'.

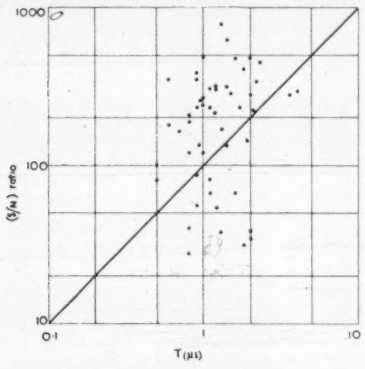

Fig. 3. Values of signal-to-noise ratio and response time plotted with fifty-two lead selenide cells

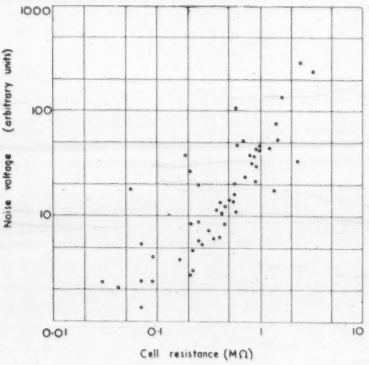

Fig. 4. Relation between noise voltage (at constant current) and resistance for the same batch of lead selenide cells as used for Fig. 3

APPENDIX II

Bias conditions for photoconductive cells

Suppose that a photoconductive cell of dark resistance $\bar{R}_c$ is put in series with a load R_L and battery V_0. Under dark conditions the current $\bar{I}$ flowing is given by

$$\bar{I} = V_0/(\bar{R}_c + R_L) \tag{47}$$

Suppose the effect of the incident radiation is to produce a small change in resistance ΔR_c, then the change in current through the load $\Delta I = V_0\Delta R_c/(\bar{R}_c + R_L)^2$. In terms of the d.c. voltage V_c across the cell, the signal voltage V_s' across the load is given by

$$V_s' = V_c R_L \Delta R_c/\bar{R}_c(R_L + \bar{R}_c) \tag{48}$$

It will be seen that the cell acts as a voltage generator of value $V_c\Delta R_c/\bar{R}_c$ or a current generator $V_c\Delta R_c/\bar{R}_c^2$. For maximum voltage output $R_L \gg \bar{R}_c$.

when
$$V_s' = V_c\Delta R_c/\bar{R}_c$$
$$= V_c\Delta\chi/\bar{\chi} \tag{49}$$

APPENDIX III

Dependence of the signal-to-noise ratio of flicker noise limited detectors on thickness and minority carrier lifetime

While the authors have no wish to join the ranks of those who have been able to explain the inverse frequency dependence of flicker noise, it seems worthwhile to deduce a few results on the dependence of noise on other parameters using a simple model. The charge flowing through the external circuit due to the generation of one minority carrier is given by

$$q = e\mu V\tau/X^2 \tag{50}$$

If the flow of minority carriers is controlled by a number N of centres, the noise current may be written

$$\bar{i}_{FN}^2(f) = Nq^2\psi(f)\Delta f \tag{51}$$

The function $\psi(f)$ is determined by some activation process or diffusive motion of the centres, which we suppose takes place slowly compared with the minority carrier lifetime. Equation (51) should be compared with the equation (20) for shot noise, which may be rewritten

$$\bar{i}_{SN}^2(f) = 2C_1N'e^2W(f)\Delta f/T' \tag{52}$$

where N' is the number of electrons flowing in a long time interval T'.

If we use equation (50) in (51), and put

$$V = IX/(YZne\mu) \tag{53}$$

we have
$$\bar{i}_{FN}^2 = N\psi(f)(I^2\tau^2/X^2Y^2Z^2)\Delta f \tag{54}$$

In terms of the noise voltage

$$V_{FN} = (N\psi)^{1/2}(V_c\tau/XYZ)\Delta f \tag{55}$$

The number of centres may be characterized either by a surface concentration $N_s = N/XY$ or a volume concentration $N_v = N/(XYZ)$. In terms of N_s or N_v equation (55) becomes

$$V_{FNS} = (N_s\psi/XY)^{1/2}(V_c\tau/Z)\Delta f \tag{56}$$

or
$$V_{FNV} = (N_v\psi/XYZ)^{1/2}V_c\tau\Delta f \tag{57}$$

This dependence upon τ probably explains the failure to observe flicker noise in an indium antimonide filament,[24] the value of τ being less than 10^{-7} s compared with values of the order of 10^{-4} or 10^{-3} for silicon and germanium respectively (see the table).

The corresponding signal-to-noise ratios are given by

$$(S/N)_{FNS} = \frac{\bar{Q}_0}{\bar{n}N_s^{1/2}\psi^{1/2}}\left(\frac{XY}{\Delta f}\right)^{1/2}[1 - \exp(-\alpha Z)] \tag{58}$$

or
$$(S/N)_{FNV} = \frac{\bar{Q}_0}{\bar{n}N_v^{1/2}\psi^{1/2}}\left(\frac{XY}{\Delta f}\right)^{1/2}\left[\frac{1 - \exp(-\alpha Z)}{Z^{1/2}}\right] \tag{59}$$

As the diffusion length is, in practice, greater than the thickness, it is justifiable to cancel out the τ-dependence of the signal and noise voltages. The resultant independence of lifetime is consistent with the use of low lifetime materials (lead selenide and lead telluride) in flicker noise limited detectors, and with the experimental evidence of Appendix I.

The Z-dependence of the signal-to-noise ratio is the same for a volume distribution of noise centres as for the shot noise limited detector. This result was obtained on general grounds in Section 6 for the case where τ is determined by volume recombination. For a surface distribution of noise centres the signal-to-noise ratio increases asymptotically to a maximum for large Z.

NOTES AND NEWS

Correspondence

A note on the calculation of second moments of nuclear magnetic resonance absorption lines

We report a convenient method for calculating the second moments of broad nuclear magnetic resonance absorption lines. The calculation of second moments is very tedious and there may be large numbers of such calculations to be made. In view of the importance of second moment values in the interpretation of the results of nuclear magnetic resonance experiments,* it is worth while finding a method of calculation which involves a minimum of work for a given accuracy and which can be performed by relatively unskilled assistants. It is likely that in many papers in this field second moment values are not given because of the tediousness of the calculations.

If the nuclear magnetic resonance absorption at a field H is $\zeta(H)$ the second moment, ΔH_2^2, is defined, as,

$$\Delta H_2^2 = \int_{line} \zeta(H)(H - H_0)^2 dH \Big/ \int_{line} \zeta(H) dH \qquad (1)$$

where H_0 is the field at the centre of the absorption line. The limits of integration extend sufficiently far from H_0 to include the absorption due to the nucleus concerned.

However, these weak broad lines are usually observed as a plot of $\zeta'(H) = d\zeta(H)/dH$ as a function of H. Calculation of ΔH_2^2 using equation (1) would therefore involve two numerical double integrations. A better method is to use the equivalent form,

$$\Delta H_2^2 = \tfrac{1}{3} \int \zeta'(H)(H - H_0)^3 dH \Big/ \int \zeta'(H)(H - H_0) dH \qquad (2)$$

for which two single integrations must be performed. Nevertheless, it is found that use of equation (2) is extremely tedious in practice, particularly if the line shape is complex. The chart of ζ' *versus* H usually involves a certain amount of noise and possibly zero drift (Fig. 1) and the record may not be in rectangular Cartesian co-ordinates, so that in practice one reads off a series of values of ζ' at various values of H at equal increments. The integrals in equation (2) can then be calculated using, say, the trapezoidal rule, but in any case a large number of individual operations have to be performed for which the accuracy hardly demands the use of a machine.

We propose a graphical method which is appreciably more rapid and convenient and depends on the fact that equation (2) can be written

$$\Delta H_2^2 = \tfrac{1}{6} \int \zeta'(H) d[(H - H_0)^4] \Big/ \int \zeta'(H) d[(H - H_0)^2] \qquad (3)$$

$\zeta'(H)$ is read from the chart at convenient equal intervals of $(H - H_0)$ independent of the actual width in gauss, so that numerical values of the independent variable can be chosen always to be about the same (in practice one arranges the "length" of the plot on the chart to be always much the same).

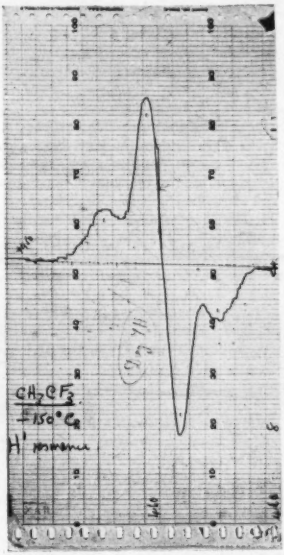

Fig. 1. A typical derivative absorption line for which a second moment value is required. Proton resonance in methyl fluoroform at -150° C

Similarly, the maximum ordinate $\zeta'(H)$ is always much the same and is determined by the chart width. We now plot $\zeta'(H)$ against $(H - H_0)^2$ but mark the abscissae by the values of $(H - H_0)$. One then plots the curve of $\zeta'(H)$ *versus* $(5/3)(H - H_0)^4$ which is very rapid since one merely moves the ordinates of the first curve already plotted to the new positions. The pairs of points are usually quite close. Moreover, the areas under the two curves (A_1 and A_2) are

* Van Vleck, J. H. *Phys. Rev.*, **74**, p. 1168 (1948).

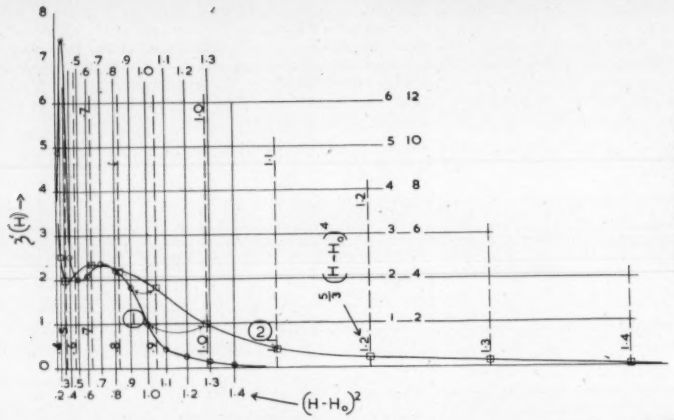

Fig. 2. Plots for the same curve as in Fig. 1. Curve 1 against $(H - H_0)^2$ and curve 2 against $\frac{5}{3}(H - H_0)^4$. Notice that the outer peak is much more important than the inner in contributing to the areas A_1 and A_2 under 1 and 2 and that A_1 and A_2 are similar in magnitude

similar in magnitude and are therefore measured with a planimeter with comparable accuracy. The second moment is then $A_2/10A_1$ apart from a scale factor which relates chart travel to field sweep.

The method has the advantages that it is at least twice as fast as by a desk machine and it is easy to maintain a given accuracy. It is easy to judge the contribution of the "tails" of the absorption curves to the second moment, and this has a sobering effect on claims as to the accuracy of measurement of second moments.

Since all the plots are relatively similar the method is well adapted to mass production. The writer uses a small number of basic sheets, one of which is shown in Fig. 2. The curves are plotted on a piece of transparent paper held on the basic sheet by Perspex laths with bevelled edges defining the co-ordinate axes. It is rather rare in broad line work to find that $\zeta'(H)$ has both positive and negative values in the half line, but this is easily accommodated.

Fig. 1 shows a photograph of an actual recording. Fig. 2 shows the curves (1) and (2) the areas under which are the A_1 and A_2 already referred to.

It is also possible to make the calculations with comparable speed and accuracy on a National Accounting Machine class 3000 with six registers,* but only because two calculations can be run simultaneously. The writer will be glad to provide a "programme" for this machine to anyone who has access to one.

The writer is grateful to Dr. J. C. E. Jennings of Birkbeck College (University of London) for assistance in the use of his machine.

Queen Mary College,
University of London,
London, E.1.

J. G. POWLES.

[10 *January*, 1958]

* COMRIE, L. J. *J. Roy. Stat. Soc. Suppl. III*, (2), p. 103 (1936).

Journal of Scientific Instruments

Contents of the July issue

ORIGINAL CONTRIBUTIONS

Papers

A mechanical version of the Smith Chart. By J. E. Knowles.
An electrically-driven disk atomizer for high speeds of rotation. By D. J. Ryley.
An improved electromagnetic integrator. By A. J. Dyer.
A compact and versatile fraction collector. By A. Snow, F. A. E. Porter and A. W. Tomalin.
A high voltage electron injector gun for synchrotrons. By E. W. V. Action and K. T. W. Milne.
A spectrograph attachment for high speed cameras. By D. P. C. Thackeray.
A simple, automatic, high-temperature thermal analysis apparatus. By S. L. Lloyd and J. R. Murray.
A method of obtaining accurate relative pressures in the range 20 to 200 mm mercury. By G. A. Bottomley.
On numerical Fourier transformation, with special reference to Lipson–Beevers strips. By P. Fellgett.
A portable apparatus for recording the rate of clearance of radioactive sodium from human calf muscle. By L. Molyneux, J. Turnbull and D. N. Walder.
Jigs for making crystallographic wire models. By W. Hughes and C. A. Taylor.

Laboratory and workshop notes

A high sensitivity d.c. cull indicator with automatic reduction of sensitivity for large inputs. By R. Thorn.
Some factors influencing the optimum design of cascade image intensifiers. By L. Mandel.

NOTES AND NEWS

Correspondence

A double layer-line screen for Weissenberg photography. From A. W. Hanson.
A valve for the grease-free manipulation of mercury. From J. A. Frost.

New book
New instruments, materials and tools
Notes and comments

THIS JOURNAL is produced monthly by The Institute of Physics, in London. It deals with all branches of applied physics (including theory and technique).
All rights reserved. Responsibility for the statements contained herein attaches only to the writers.
EDITORIAL MATTER. Communications concerning editorial matter should be addressed to the Editor, The Institute of Physics, 47 Belgrave Square, London, S.W.1. (*Telephone:* Belgravia 6111.) Prospective authors are invited to prepare their scripts in accordance with the *Notes on the preparation of contributions*. (Price 2*s.* 6*d.* including postage.)
REPRODUCTION. The Institute of Physics is a signatory to The Royal Society's Fair Copying Declaration. Details may be obtained upon application from The Royal Society, London, W.1.
ADVERTISEMENTS. Communications concerning advertisements should be addressed to the agents, Messrs. Walter Judd Ltd., 47 Gresham Street, London, E.C.2. (*Telephone:* Monarch 7644.)
CLAIMS FOR MISSING JOURNALS. Claims from regular subscribers to this *Journal* for missing numbers will only be considered if received within 60 days of the date of mailing plus normal outward time of transit and time for lodging the claim. Losses attributable to failure to notify a change of address or to similar omissions will not be considered.
SUBSCRIPTION RATES. A new volume commences each January. The charge is £5 per volume ($14.25 U.S.A.), including index (post paid), payable in advance. Single parts, so far as available, may be purchased at 10*s.* each ($1.50 U.S.A.), post paid, cash with order. Orders should be sent to The Institute of Physics, 47 Belgrave Square, London, S.W.1, or to any bookseller.

Atmospheric pollution and the soiling of textile materials*

By W. H. Rees, M.Sc., F.Inst.P., The British Cotton Industry Research Association, Shirley Institute, Didsbury, Manchester

The article opens with a discussion of the factors which influence the soiling of textile materials by airborne dirt and of a method for measuring and expressing the extent of soiling of textile materials. An account is then given, with experimental data, of the soiling of textile fabrics by exposure to moving air, by thermal precipitation and by electrostatic attraction of airborne particles, and of the effect of fabric wettability on the appearance of a cotton fabric soiled by exposure to a damp polluted atmosphere. Finally, the article introduces the "murk" unit of air dirtiness and deals briefly with the measurement of atmospheric murk values. Typical data for a residential district are given showing differences in the magnitude and diurnal variation of air dirtiness in summer and autumn.

INTRODUCTION

The soiling of textile materials is a familiar phenomenon, generally accepted as an unavoidable nuisance, which has been a source of domestic drudgery for centuries. Soiling of clothing is a matter of universal concern, for in addition to reducing the aesthetic appeal of garments, soiling may also reduce their functional effectiveness, and a garment which soils readily will not have the same user appeal as one which does not, even though its functional performance may be supreme. It is therefore highly desirable that textile materials intended for clothing and furnishings should possess high resistance to soiling matter in daily use.

There are two distinct processes by which soiling matter may be deposited on or within a textile material: first, by exposure to air containing soiling matter in suspension, and second, by contact with a soiled surface or with a liquid dispersion or solution of soiling matter. This is a very wide field and the present article deals exclusively with the soiling of textile materials by airborne matter.

The extent of soiling of a textile material on exposure to a polluted atmosphere is influenced by various factors which may be external to the textile, e.g. the temperature, relative humidity and rate of movement of the atmosphere, and the nature and size of dirt particles, or directly related to the textile itself, e.g. the construction and finish of the textile material and the type of fibre from which it is made. By construction is meant the thickness and twist of the yarns and the manner in which they are woven or knitted to form the fabric; by finish is meant the chemical or mechanical treatment given to the fabric, e.g. it may be given a water-repellent treatment or it may be calendered to give a smooth, flat surface.

SOILING DURING NORMAL USE

Suspended solid matter is a constituent feature of the earth's atmosphere, the size and concentration of the individual particles often varying enormously from place to place. This matter ranges from extremely fine smoke particles of diameter about 0·01 μ to heavy industrial dusts whose diameters are reckoned in hundreds of microns. Particles of diameter less than about 0·3 μ exhibit such minute rates of settling in still air that they may be classed as permanent atmospheric impurities. In a normal atmosphere, the majority of suspended particles range from about 0·1–10 μ in diameter, particles larger than about 1 μ being generally classed as temporary atmospheric impurities to an extent depending on their size and on the degree of atmospheric disturbance. The concentration of suspended matter is naturally greatest in industrial areas and least in rural areas.

When textile materials are exposed to a polluted atmosphere they become soiled when suspended particles impinge on them and adhere to their surface. Large particles may be deposited on the material as they settle out under gravity. In moving air, particles may be directly intercepted by individual fibres or may be thrown on to the fibres as air sweeps through the intricate channels between them—in other words, the material behaves as a filter. Soiling of curtains, of flags and bunting and of filter cloths in ventilating systems are familiar examples of soiling by airborne dirt which can also affect the cleanliness of garments during wear and of yarns and fabrics during their manufacture. A further example is the soiling of the fabric frontispiece of a radio receiver over an area covering the cone of the loudspeaker where, owing to the vibrations of the speech coil, air is continually drawn in and forced out through the fabric.

Soiling of walls above hot water pipes is of common occurrence and is due to the thermal precipitation of airborne dirt particles which are subjected to differential molecular bombardment by air molecules in the region of temperature gradient near the cool wall. Soiling of a textile fabric by thermal precipation will occur if the temperature of the exposed surface of the fabric is below that of the ambient air; this type of soiling will not therefore occur with garments in use as they will be warmer than the air, but it can occur with furnishing fabrics in rooms especially where convection heating is used.

There are in the atmosphere numerous fast-moving positive and negative ions of molecular size. The presence in the air of minute particles of dust, of the products of combustion and of extremely small drops of water often leads to the capture of a small ion by one of these condensation nuclei and so to the formation of large slow-moving positive and negative ions called "Langevin" ions after their discoverer. Roughly one-third of the condensation nuclei in the air is electrically neutral, the other two-thirds being charged by the capture of small ions and being more numerously negative than positive. If an exposed textile material acquires an electrostatic charge as, for example, by friction and is able to retain its charge, uncharged airborne particles and large ions of opposite sign will be attracted to it, thereby increasing its rate of soiling. Cellulose acetate and some of the synthetic textiles acquire electrostatic charges by friction during spinning and weaving which, because of the high insulating properties of these materials are retained for a considerable time; in dirty air, this results in troublesome "fog-marking" caused by the attraction of airborne particles to the charged textile.

* Based on a lecture delivered to the Manchester Branch on 11 February, 1955, and to the Midland Branch on 16 October, 1956.

ASSESSMENT OF SOILING

The first practical consideration in an investigation of the soiling problem is to establish a method for measuring and for expressing the extent of soiling of textile materials. One method is the gravimetric technique where the material is weighed before and after soiling and the result expressed as the mass of soil acquired by a certain quantity of the material. Early tests showed, however, that marked visible soiling is produced by minute quantities of soil, so the gravimetric method is impracticable. In most uses the appearance and not the soil content of the textile is the standard by which cleanliness or dirtiness is judged; thus a convenient method for assessing soiling is an optical one in which the intensity of light reflected by, say, a fabric is compared with that reflected by a standard white surface. This is the method adopted for general use in these laboratories, measurements being made with a photo-electric reflectometer using magnesium carbonate as the comparison surface.

Any expression for the extent of soiling derived from optical measurements must include data for both the soiled and the unsoiled material. The index of soiling adopted in these laboratories is the increase in the reflexion density of the textile material due to soiling. This index is called the "Soiling Additional Density" (S.A.D.). Thus if R_0 is the reflexion factor of the unsoiled, and R_s the reflexion factor of the soiled material, then

$$\text{S.A.D.} = \log_{10} 1/R_s - \log_{10} 1/Ro = \log_{10} Ro/R_s \qquad (1)$$

Equation (1) shows that S.A.D. values can range from zero to infinity. In practice, however, the upper limit is never attained owing to the imperfect blackness of soiling matter, the practical limits of S.A.D. being zero to about 1·5. An S.A.D. value of 1·5 corresponds to a reflexion factor of the soiled material of only about 3%, which represents extremely severe soiling—the housewife is unlikely to tolerate a soiling level greater than that represented by an S.A.D. value of about 0·01. By analogy with the non-linear relation between transmission optical density and the weight of silver deposit in a photographic negative, the S.A.D. values will not be proportional to the amount of soil on the fabric over the practical range of soiling levels, although they are very nearly so in the early stages of soiling, and there comes a stage where further acquisition of soil by the fabric produces no change in S.A.D. It is thus of fundamental interest to know the relation between S.A.D. and the quantity of soil on a fabric, and this matter will be dealt with in a forthcoming paper by the writer to be published elsewhere.

EXPOSURE TO MOVING AIR

To investigate the soiling of textile materials by airborne matter, samples may be exposed to the normal atmosphere outdoors, but this requires a long exposure even in town air, during which atmospheric conditions, and particularly the concentration of soiling matter in the air, can vary considerably. Such a procedure, although forming a necessary part of the investigations, is not therefore a convenient method of experimentation in an extensive research programme, and accordingly, a laboratory apparatus was developed in which air laden with particulate soiling matter (such as powdered carbon) to a controlled concentration is circulated past the textile material under test at a known speed. With this "dust circulating apparatus," the dust concentration, air speed, orientation of the test specimen with respect to the air stream, and the exposure may be varied independently. With this apparatus, exposures of 5 min or less are adequate under conditions which are strictly reproducible from sample to sample. Fig. 1 shows a photograph of the apparatus in operation.

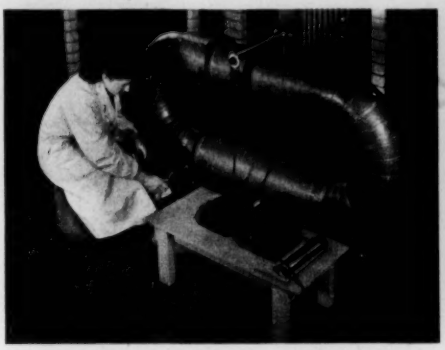

Fig. 1. Dust circulating apparatus

The dust circulating apparatus was used to test specimens of each of a series of fourteen scoured and bleached woven cotton fabrics of various constructions. The specimen under test was clamped in a brass frame mounted centrally inside the apparatus with the fabric surface perpendicular to the air stream, the area of the specimen being one-fifth the cross-sectional area of the stream. Activated charcoal powder was used as soiling matter dispersed in the air stream, moving at 15 ft/s, to a concentration about 2000 times that of soiling matter in average town air. Each exposure was of 5 min duration. The S.A.D. values attained in these tests are given in Table 1. Air permeability values are given as an indication of the closeness of construction of the various samples.

The data in Table 1 show clearly that S.A.D. is closely related to air permeability, thus illustrating the important influence of fabric structure on the soiling of fabrics by airborne matter. The same trend was observed when the same fabrics were soiled by exposure to the normal atmosphere outdoors. The experiments show that in a polluted atmosphere, a close structure giving a fabric of low porosity is required to give resistance to soiling by airborne impurities.

Table 1. *Soiling additional density values obtained in test*

Cotton fabric	*Weight* (oz/yd²)	*Air* Permeability*	*S.A.D.†*
Canvas	5·3	0·4	0·13
Poplin *A*	4·8	1·5	0·21
Plain cloth *A*	2·4	4·4	0·39
Poplin *B*	3·0	6·3	0·40
Plain cloth *B*	3·2	6·3	0·45
Twill	5·4	12·5	0·51
Sateen	4·9	12·5	0·52
Plain cloth *C*	2·8	14·3	0·54
Poplinette	3·2	16·7	0·59
Plain cloth *D*	4·1	20·0	0·61
Plain cloth *E*	2·4	20·0	0·64
Plain cloth *F*	2·5	33·3	0·70
Plain cloth *G*	2·0	45·0	0·81
Plain cloth *H*	1·8	50·0	1·14

* Cm^3/cm^2 s under pressure difference of 1 cm water.
† Each value is the mean of three determinations and has a standard error of about 2½%.

THERMAL PRECIPITATION

Soiling of textile materials by thermal precipitation of airborne particles can only occur if the surface temperature of the fabric is below that of the ambient dusty air. The apparatus used in this study consists of two brass cylinders of the same dimensions mounted vertically side by side within a large open-ended metal tube also mounted vertically. A current of air, heated by an electric element at the lower end of the tube, flows upwards past the cylinders. A specimen of the fabric under test is wrapped around each cylinder, one of which is open at both ends so that its surface assumes the temperature of the heated air (75° C) and the other closed and fitted with inlet and outlet tubes through which a stream of cold water (at about 18° C) is passed continuously from a constant head source. The specimens were exposed under these conditions in the laboratory for several weeks. To overcome the effect of varying dirt content of the atmosphere from day to day in making comparative studies of the soiling of different fabrics, a duplicate apparatus is mounted alongside the original, on which specimens of a particular fabric are mounted in each experiment to serve as a control.

Under the experimental conditions described, the surface temperature of a fabric exposed on the cooled cylinder will lie between that of the water and of the hot air, and since most textile fabrics have approximately the same thermal conductivity, the surface temperature will increase with increasing fabric thickness. The surface temperature of each fabric specimen exposed on the apparatus was measured with the aid of fine wire copper-Constantan thermocouples (48 s.w.g.). Surface temperature values are given in Table 2 for various fabrics along with corresponding thickness data and S.A.D. values after an exposure of three weeks in midsummer.

Table 2. *Variation of S.A.D. with surface temperature*

		Exposed on cylinder at air temperature		*Exposed on cooled cylinder*	
*Sample**	*Thickness* (1/1000 in.)	*Surface temp.* (° C)	*S.A.D.*	*Surface temp.* (° C)	*S.A.D.*
Bare cylinder	—	75	—	21·4	—
Nylon fabric	7	75	<0·01	24·0	0·12
Acetate rayon fabric	7	75	<0·01	25·0	0·12
Viscose rayon fabric	10	75	<0·01	26·9	0·11
Cotton poplin	18	75	<0·01	28·0	0·10
Fibro fabric	24	75	<0·01	28·9	0·09
Cotton sateen	30	75	<0·01	31·4	0·08

* Nylon and acetate rayon samples scoured, other samples scoured and bleached.

It is seen that the cooled specimen is in each case soiled to a much greater extent than the corresponding specimen exposed at the temperature of the air. The results show further that the greater the temperature difference between the fabric surface and the ambient air, the greater is the extent of soiling. The thicker the fabric in contact with the cooled cylinder, the smaller is the temperature difference between fabric surface and air, and the smaller is the extent of soiling. Differential molecular bombardment of suspended particles in a warm air stream contacting a cool surface creates a resultant force which drives the particles on to the surface. The greater the temperature gradient, the greater is the driving force acting on the particles and hence the greater is the rate of soiling of the cool surface.

ELECTROSTATIC ATTRACTION

"Fog-marking" of acetate rayon and nylon fabrics during weaving is caused by electrostatic attraction of airborne dirt particles by the textile which has become charged by friction with the metallic parts of the loom and which, because of its high insulating property, retains its charge for a considerable time. With relatively conducting materials like cotton and viscose rayon, the electrostatic charges developed are rapidly dissipated and fog-marking does not occur.

Investigations of the electrostatic attraction of airborne dirt particles to cotton textiles were made in the laboratory by maintaining fabric specimens at certain electrical potentials throughout their exposure to the atmosphere, the specimens being mounted in separate brass frames suspended vertically, some frames being connected to a positive d.c. supply, some to a negative d.c. supply and some to earth. Fig. 2 shows

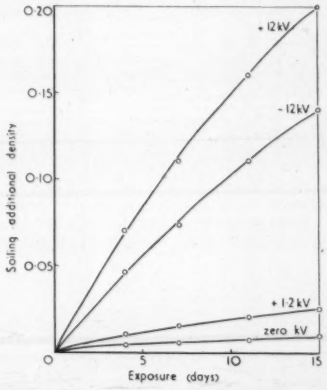

Fig. 2. Progress in electrostatic soiling of scoured and bleached cotton fabric

graphically the progress of soiling of a scoured and bleached cotton fabric in such an experiment when maintained at various d.c. potentials. It is seen that soiling is more rapid when the fabric is charged than when uncharged, and that the rate of soiling is increased by stepping up the applied potential, i.e. by increasing the charge density on the fabric. Further, at a given potential, the rate of soiling is seen to be greater for the positively charged than for the negatively charged specimen: this is attributable to a preponderance of negatively charged dirt particles in the atmosphere.

In a particular experiment, specimens of the cotton fabric were exposed at +1200 V, −1200 V and at earth potential to the laboratory air for five weeks, and a nitrocellulose film mounted on an electron microscope grid was attached to each specimen throughout the exposure. Electron micrographs of the exposed films are shown in Fig. 3. Inspection of the micrographs showed that most of the particles, which were roughly circular in shape, lay within diameter limits of 0·05 and 0·1 μ. The number of particles of all sizes on the micrographs were counted, and the results are given in Table 3 along with the S.A.D. values of the exposed fabric specimens.

The data show that soiling is heavier on the positively than on the negatively charged fabric, with both showing much greater soiling than the uncharged fabric. The S.A.D. data are in agreement with the particle count values.

Fog-marking on fabrics is strikingly apparent to the eye,

yet the individual dirt particles on fog-marked fabrics are so fine as to be invisible under the ordinary microscope. The large majority of the particles shown in the electron micrographs (Fig. 3) are too small to be seen under the optical microscope.

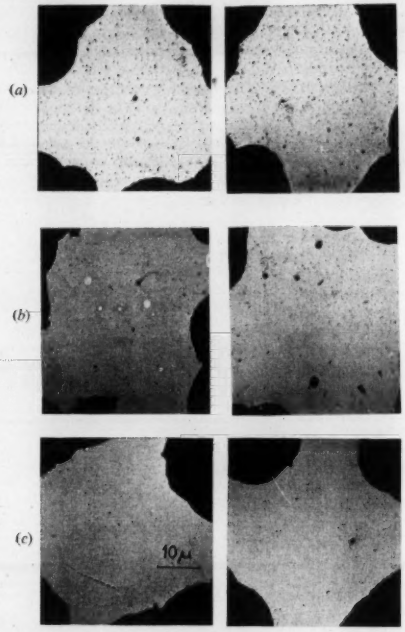

Fig. 3. Electron micrographs of exposed films
(*a*) +1200 V; (*b*) −1200 V; (*c*) zero V.

Table 3. *Variation of soiling with electrostatic charge*

Specimen at	*Fabric S.A.D.* actual	relative	*Number of particles/cm² of film* actual	relative
+1200 V	0·064	7·1	140×10^3	6·4
−1200 V	0·050	5·6	106×10^3	4·8
zero V	0·009	1·0	22×10^3	1·0

FABRIC FINISH

One example will be given of the effect of fabric finish on the appearance of a soiled textile fabric, namely, the effect of a waterproofing treatment on the soiling of a cotton fabric in a damp atmosphere.

A technique for investigating airborne soiling of textiles was developed in which fabrics are exposed to a cloud of soil particles which may be either wet or dry. An aqueous dispersion of insoluble particles (e.g. carbon) is converted into a fine mist with the aid of a suitable spraying device. This mist is allowed to settle under gravity on to the surface of the fabric, the air within the test chamber being maintained at saturation point throughout the exposure. Alternatively, by means of a roof heater, the relative humidity within the chamber can be maintained at a value below 40%, and under these conditions the water droplets evaporate, leaving a dry particulate cloud which is deposited on the fabric surface. Fig. 4 shows a photograph of two samples of the cotton poplin *B* (see Table 1) after exposure in this manner to a wet particulate cloud, sample (*a*) representing the scoured and bleached fabric and sample (*b*) the same fabric after receiving

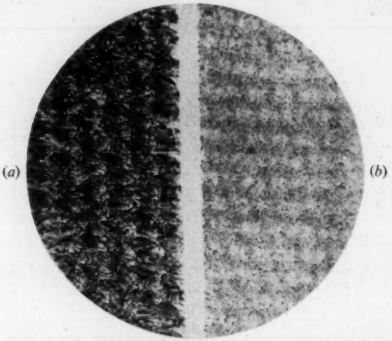

Fig. 4. Samples soiled by exposure to wet particulate carbon cloud (×10)
(*a*) Scoured and bleached poplin *B*.
(*b*) Dipsanil proofed poplin *B*.

a water repellency treatment in a 10% dispersion of Dipsanil V. The experimental technique employed ensures that the mass deposit of soiling matter on each sample is the same (namely 47 $\mu g/cm^2$ of the sample), yet the visual appearance is strikingly different for the two samples, the wettable sample (*a*) appearing much dirtier than the unwettable sample (*b*), the S.A.D. values being 0·54 for (*a*) and 0·30 for (*b*), a ratio of 1·8 to 1. Microscopical examination showed that the different visual effects are due to different distributions of the soiling matter; the particles are evenly spread over the surface of the bleached sample, but are distributed in discrete groups on the surface of the proofed sample. This is attributable to the different wettabilities of the samples. This conclusion was confirmed by a similar experiment with a dry cloud of particles instead of a wet cloud; the bleached and the proofed samples then showed equal visible soiling. Thus whereas under the dry conditions the appearance of both soiled samples is the same, a marked difference in appearance occurs under the saturated conditions because of the different distributions of the particles resulting from a difference in wettability.

AIR DIRTINESS

Several examples have been given of factors which can influence the extent of soiling of textiles by airborne dirt, but, of course, all these factors are of secondary importance compared with the dirt content of the air itself. If the atmosphere is entirely free of suspended dirt, the textile will remain clean however one varies the construction and finish of the materials or the type of fibre incorporated in them or the temperature and relative humidity of the atmosphere, but since the atmosphere is never perfectly clean, the extent of soiling of textile materials will increase with increasing dirt content of the air. Thus the concentration of airborne matter is an important factor, but it is not necessarily the major factor—the nature of airborne dirt is important since

different types of suspended matter can produce different visual effects on textiles.

Dirty atmospheres can be a serious source of trouble in the textile industry, and, indeed, in other industries, and can cause considerable economic loss to manufacturers by contaminating their goods to such an extent that at best they are of "seconds" quality. Many manufacturers have installed air-filtering plants, but experience has shown that such plants sometimes fail to achieve the desired level of cleanliness in mills. It therefore became important to be able to make an assessment of the dirtiness of, say, mill atmospheres and of the filtering efficiency of complete air-cleaning plants or of various stages of such plants on the site. An air dirtiness sampler was developed at the Shirley Institute to enable rapid assessments to be made in this respect. This instrument will be described elsewhere in due course.

In a test for air dirtiness, a certain volume of air is pumped through a disk of Whatman No. 1 filter paper of known area, and the air dirtiness value is calculated in terms of these quantities and the measured change in the reflexion factor of the paper. The unit of air dirtiness has been named the "murk"; air is said to have unit murk value when 0·1 m^3 of the air drawn through 1 mm^2 of the filter paper produces an increase in reflexion density, i.e. a decrease in $\log_{10}$ (reflexion factor), of 0·1. The derivation of the murk unit and a discussion of the various factors affecting its assessment will be published elsewhere. The murk value of the atmosphere ranges from about 1, obtained in mid-summer within a mill equipped with a highly efficient air-cleaning plant, to about 13 000 outdoors during very severe fog. A murk value of 1 represents exceptionally clean air, and is not in the writer's experience representative of the outdoor atmosphere in or near towns, for which the lowest value obtained so far is 6·3 murks on the outskirts of a north-east Lancashire town with the wind blowing from open moorland. At the other extreme, values around 10 000 murks, representing really filthy atmospheres, occur only very rarely. The scale of murk values given in Table 4 will usefully describe the cleanliness or dirtiness of the atmosphere.

Table 4. *Scale of murk values*

0–50 murks	Outstandingly clean air
50–100 murks	Clean air
100–250 murks	Moderately clean air
250–500 murks	Fairly dirty air
500–1000 murks	Unpleasantly dirty air
1000 murks	Light fog
3000–5000 murks	Dense town fog
Over 10 000 murks	"Pea-souper" fog

Naturally if the same volume of air is always sampled, the stain on the filter paper disk will be much denser when the air being tested is very dirty than when it is very clean, and under very clean conditions the stain may be too faint to be observed or even to be measured. Thus under clean air conditions a larger volume of air must be sampled than under dirty air conditions. The sampler has been designed to meet these requirements; different volumes may be selected at will by turning a switch and the sampler automatically switches itself off after the selected volume of air has been sampled. As the filter paper becomes clogged with airborne dirt, the pumping rate will decrease, but the sampler is so designed that it ensures that the same volume of air is sampled for any particular setting of the instrument under all conditions.

The dirtiness of the outdoor atmosphere of towns is rarely

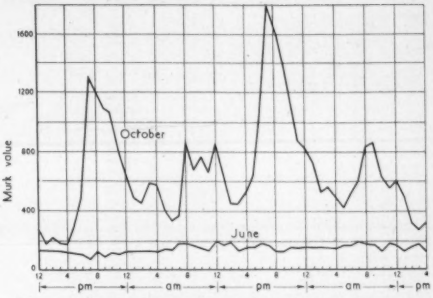

Fig. 5. Variation in dirtiness of air during typical day in June and October in Manchester

constant for more than a few minutes and it is often important to know how much it varies during the day and whether there is a regular pattern in the variation throughout each day. In order to obtain this information, another version of the air dirtiness sampler was developed which samples the air automatically at pre-determined intervals throughout the day and night for many days. Typical trends are shown in Fig. 5 for the outdoor air in a residential district of Manchester. Whereas in June the air is moderately clean and there is no appreciable change in air dirtiness throughout day and night, an entirely different pattern occurs in October. The level of dirtiness is appreciably higher than in June and a remarkably consistent diurnal trend exists in normal settled weather showing maximum cleanliness at 5–6 a.m. and maximum dirtiness at 6–7 p.m. On any particular day the ratio of air dirtiness at these two times ranges from about 4 : 1 to 12 : 1 in normal settled weather. In unsettled and foggy weather, however, atmospheric dirtiness can change rapidly; for example, during one foggy period the murk value rose from 750 to 2000 in twenty minutes.

Without doubt, the major contribution to atmospheric pollution is attributable to the combustion of fuels. The polluting matter from this source consists of incompletely burned particles of fuel, ash, grit, dust and tarry soot, all of which give rise to visible pollution, and also of gases, mainly sulphur oxides, which, although invisible, are, nevertheless, damaging, for the sulphuric acid into which they become converted in the atmosphere decays stonework, corrodes metals, sours the soil and tenders textiles.

It is, admittedly, the solid components of polluted air which manifest themselves most readily as far as textiles are concerned, resulting in soiled clothing and curtains and furnishing fabrics; but we cannot ignore the deleterious effects of the invisible gases, particularly the sulphur oxides. Visible smoke pollution and invisible gas pollution do not necessarily go hand in hand. It has been found, for example, that, although cotton fabrics exposed outdoors in a residential district of Manchester were soiled to a less extent than similar fabrics similarly exposed in an industrial area of Sheffield, the tendering of the Manchester fabrics was on average greater than that of those exposed in Sheffield. Admittedly, the soiling and tendering of textiles cannot be attributed wholly to atmospheric pollution, but there is no doubt that the existence and maintenance of clean air in hitherto polluted areas will substantially decrease these undesirable phenomena and also contribute in other ways to a happier existence.

CONFERENCE REPORT

Summarized proceedings of a conference on electron microscopy—Bangor, September 1957

The Annual Conference of the Electron Microscopy Group of The Institute of Physics was held in the Department of Botany, University College of North Wales, Bangor, from 10 to 12 September, 1957. The papers presented, and discussion on them, are summarized in this report.

ELECTRON OPTICS

The opening session contained two papers by Mr. D. H. PAGE (British Paper and Board Industry Research Association, Kenley, Surrey). In the first of these, on the chromatic field aberrations in reflexion electron microscopy,[1] Mr. Page showed that the coefficient of the chromatic difference in magnification in a triple-lens reflexion electron microscope is a function of the axial position of the aperture and the focal length of the intermediate lens. The magnitude of the coefficient may be calculated as a function of these variables. It was shown that there is a focal length of the intermediate lens for which the coefficient vanishes and this condition is required for the correction of the aberration. The coefficient of chromatic difference in rotation is dependent on the overall rotation of the image and may be minimized by exciting the lenses in opposition. The effect on the image of a misalinement of the objective aperture was also dealt with. The tolerances in the conditions for the correction of the field aberrations and the alinement of the aperture were calculated for typical values of the energy spread in the electron beam for reflexion work at both low and high angles of beam deviation.

In his second paper, Mr. Page described how the Metropolitan-Vickers type EM3 microscope may be adapted for use as a reflexion instrument with an angle of beam deviation as high as $26 \cdot 5°$[2] (Fig. 1, p. 319). It was necessary to minimize both the axial and field components of the chromatic aberration, within the limits imposed by the use of a commercial instrument. Under these conditions, a resolution of 600 Å can be achieved with a depth of field of 200 μ. Although the resolution is inferior to that of the conventional reflexion instrument, the comparatively low degree of foreshortening ($2 \cdot 6 : 1$) and the very high depth of field give rise to a highly informative and readily interpreted image. Micrographs were shown illustrating the method applied to problems in the chemical, biological and metallurgical fields.

INSTRUMENTATION

A small universal electron microscope was described by Dr. V. DRAHOS and Dr. A. DELONG (Laboratory of Electron Optics, Czechoslovak Academy of Sciences, Prague). The column and the high tension unit may be placed on a normal laboratory table, because the dimension and weight of both are as small as possible. The illuminating system is formed by an electrostatic lens, permitting the elimination of the condenser lens. The magnifying system has four magnetic lenses, the magnification ranging from 1000 to 30 000. This system also facilitates electron diffraction. The final image is recorded on 35 mm film or 5 × 5 cm lantern slides. There are two adjustable apertures: one above the specimen and the other between the objective pole-pieces. The instrument is provided with a magnetic stigmator, an object air lock and a stereo-device. The resolving power attainable is about 20 Å.

The accelerating potential of 60 kV is formed by a high-frequency circuit with a degenerative feedback stabilization securing a stability of ±2 V. The coils are fed from a 24 V battery with a capacity of 120 Ah. The vacuum system employs an air-cooled oil diffusion pump backed by a two-stage oil rotary pump and a very simply operated distribution system.

The instrument may be used as a reflexion electron microscope; only the insertion of an oblique flange between the illuminating system and the specimen chamber is necessary. The electron beam can be tilted through any angle between 5 and 11°. The tilt of the specimen is continuously variable within a desirable range. For emission microscopy the illuminating system is replaced by a special adaptor. It is possible to activate the specimen in the instrument without disturbing the vacuum. The temperature of the specimen can be measured by means of a thermocouple.

The construction of a high-temperature stage for the Elmiskop 1 (by Siemens and Halske) was described by Dr. M. J. WHELAN (Cavendish Laboratory, University of Cambridge). This requires a new object carriage [Fig. 2(*a*), p. 319], similar to the conventional one but without the stereo attachment. Except for stereo work, this carriage may therefore be used for routine work. The object holder [Fig. 2(*b*), p. 319] is similar in external appearance to the conventional one and is inserted through the air lock in the usual manner. The holder contains a two-pin socket which makes contact with a two-pin plug [Fig. 2(*c*), p. 319] inserted through the hole normally occupied by the stereo control. The plug can be withdrawn and the object holder removed while the instrument is under high vacuum. Temperatures of the order of 800–1000° C can be attained by passing a direct current of up to 3 A through the 200-mesh stainless steel specimen-supporting grid. The effect of the heating current on the performance of the objective is not noticeable in transmission work on thin metal foils; the main factor limiting resolution appears to be drift of the filament specimen support during the warming-up period.

Mr. J. CARTWRIGHT and Mr. G. WILLIAMSON (Safety in Mines Research Establishment, Sheffield) described an integrating exposure indicator. This shows the total exposure from the moment of opening the shutter, which the operator closes when the indicator reaches a predetermined mark. When it is opened, a pair of contacts on the shutter starts a count of X-ray quanta emitted from the photographic emulsion and resets the indicator to zero when the shutter is closed. The instrument may be adjusted so that, for a given type of photographic plate, the mid-scale reading on the meter corresponds to normal exposure.

The resolution available with present-day electron microscopes enables defects in shadow-casting methods to be detected. In order to evaluate the use of shadow-casting techniques in electron microscopy, a special evaporator unit has been constructed by Mr. R. W. HORNE (Cavendish Laboratory, University of Cambridge). The essential

features consist of a large demountable metal chamber pumped by a mercury diffusion pump fitted with cold traps. Specimen angles and position can be changed by external controls. Facilities for introducing suitable apertures above the point source are provided, together with methods for introducing cold fingers into the chamber. Freeze-drying spray tubes can also be mounted to the unit. It is proposed to study the "background" structures produced by different metals over a range of substrate temperatures. Initial experiments using uranium evaporated on to carbon films stripped from mica suggested an improvement in the sharpness of the shadow, but considerable background structure was observed within the range of 15–25 Å.

Mr. A. C. VAN DORSTEN (Philips Research Laboratories, Eindhoven) then outlined recent modifications to Philips electron microscopes and described a correlation method for the identification of grain patterns.

SPECIMEN TECHNIQUES

Mr. A. W. AGAR (Aeon Laboratories, Englefield Green, Surrey) discussed the potential advantages of thin sections of inorganic material, using a diamond knife as developed by Moran, and presented some preliminary results. Sections of a pure, coarse-grained, polycrystalline aluminium of relatively uniform thickness (about 500 Å) were shown, together with a micro-diffraction pattern from a selected area of one of these micrographs. Other applications of thin sectioning described were the distribution of the carbon particles in their matrix of resin in a carbon resistor and the structure of carbon rods of the type used in Bradley's replication method.

The use of an Araldite resin for embedding was the subject of a paper by Mr. M. S. C. BIRBECK and Dr. E. H. MERCER (Chester Beatty Research Institute, London). The widespread use of methacrylate polymers as embedding materials is due to their admirable cutting qualities. However, it has been found that certain materials consistently contain a type of artefact that arises during the polymerization process and reveals itself as localized swellings. It may be slight or it may result in a complete destruction of the tissue ("explosion"). The cause is probably the catalytic effect of the tissue itself. The idea of using epoxide resins, where hardening does not depend on the presence of a catalyst, is due to Maaløe and Birch-Anderson,[3] but the most satisfactory mixture is that devised by Glauert, Rogers and Glauert[4] and based on the Araldite resins. Mr. Birbeck and Dr. Mercer have tested this mixture over a large range of tissues, e.g. materials noted for their poor preservation in methacrylate: liver, spleen, bone marrow and protozoa; tissues of abnormal hardness; hair; tissues having variable texture; glands with a dense secretion and bacteria. In all cases extremely good preservation was obtained. Cutting is a little more difficult and is improved by using a glass knife with an angle less than 45°.

ELECTRON DIFFRACTION

Dr. M. J. WHELAN and Dr. P. B. HIRSCH (Cavendish Laboratory, University of Cambridge) presented a paper on electron diffraction from crystals containing stacking faults. In this they showed that the well-known dynamical equations of electron diffraction can be extended to the case of overlapping crystals, so that the diffraction of electrons by crystals containing imperfections, such as grain boundaries and stacking faults, could be predicted. The theory had been developed in detail for the case of a single stacking fault traversing a thin parallel-sided metal foil.[5] It can also be applied to the case of overlapping crystal stacking faults on neighbouring crystal planes. The predicted contrast variations are observed directly on transmission electron micrographs of metals of low stacking-fault energy, where stacking faults are produced as a result of splitting of dislocations into partial dislocations (Fig. 3, p. 319).

Mr. J. A. GARD (Department of Chemistry, University of Aberdeen) described three instances where information about structures of silicate minerals had been derived from electron diffraction of small single crystals. X-ray data for the fibrous zerolite erionite had indicated an orthorhombic unit cell, but electron diffraction clearly showed that the cell is a closely related hexagonal one, and revealed the presence of glide planes which restricted the permitted space groups to five.[6] Secondly, a provisional structure for zeophyllite, $Ca_4Si_3O_8F_2(OH)_2$, $2H_2O$, had been derived on the assumption that the more intense spots in the diffraction pattern were related to the positions of the heavy calcium atoms.[7] Finally, the derivation of the unit cell of foshagite, $Ca_4Si_3O_9 . H_2O$, was described. The cell is closely related to that of β–$CaSiO_3$, one of the products of dehydration at 700° C, and it was shown that the orientation is preserved. A mechanism for the dehydration and a provisional structure for foshagite were proposed.[8]

Experiments using various methods have suggested that particles of quartz dust have an external layer of amorphous silica. The thickness of this has been investigated by Mr. J. CARTWRIGHT (Safety in Mines Research Establishment, Sheffield). Experiments with an artificially applied amorphous layer on quartz powders showed that with an applied layer 100 Å thick there was a detectable reduction in the clarity of the electron diffraction patterns; the amorphous silica layer must therefore be thinner than this. Specific surface measurements based on electron microscope counts and low-temperature nitrogen sorption revealed a layer thickness in the range 10 to 50 Å.

PHYSICAL APPLICATIONS

The session held under this title contained five papers contributed by members of the group working at the Tube Investments Research Laboratories, Hinxton, under Dr. J. W. Menter. In the first of these, Dr. D. W. PASHLEY described a method of preparing thin (200 Å upwards) single-crystal, coherent and uniform films of gold and the observation of dislocation features in them. Electron diffraction examination showed that the films were highly oriented with (111) planes parallel to the plane of the film. Electron microscopic examination showed that they were very coherent and uniform in thickness. Dislocations could be observed in the films by means of diffraction contrast, and the motion of these dislocations and the effect of annealing at about 500° C was studied when the specimen was illuminated by means of the double condenser system in the Siemens Elmiskop I. It was also found possible to prepare films of gold in (100) orientation.

Moiré patterns on electron micrographs were described by Mr. G. A. BASSETT, Dr. J. W. MENTER and Dr. D. W. PASHLEY. There are two basic methods of preparing these patterns. In the first, two identical overlapping crystals are used with a small relative rotational misorientation (rotation moiré patterns); in the second method, two crystals of slightly different lattice spacings are overlapped in parallel orientation (parallel moiré patterns). The authors have developed a method[9] of preparing such specimens in a controlled manner.

In each case single crystal gold films (as described in the preceding paper) are used as the first crystal. Either a second gold crystal is mounted on this (rotation) or else a second metal (copper, nickel, palladium or platinum) is evaporated on it (parallel). The mechanism of formation of moiré patterns was then considered in some detail and it was shown that both types of pattern may be thought of as enlarged images of the projected lattice planes. Thus the moiré patterns provide an indirect method of resolving a crystal lattice. This technique is extremely valuable because a dislocation in one of the two lattices will appear as an extra half-line or lines on the moiré pattern as shown in the two-dimensional optical analogue (Fig. 4, p. 320) and in the example of Fig. 5 (p. 320). The movement of dislocations may be observed by means of the associated changes in the patterns. An example of this was shown for the case where the movement resulted from thermal stresses induced by the electron beam.

An apparatus was described by Dr. D. W. PASHLEY which permitted thin metal films to be put under stress inside the electron microscope (Siemens Elmiskop I) so that simultaneous examination of the microscope image or electron diffraction pattern could be made. Preliminary experiments have been carried out with single crystal gold films in (111) orientation and about 1000 Å in thickness. These were described in some detail. One interesting conclusion from preliminary diffraction measurements was that, while the spacing of the lattice planes parallel to the direction of stressing remained unchanged, that perpendicular to the direction of stressing increased by at least 0·7%, an amount of elastic strain at least an order of magnitude greater than that observed in a bulk specimen of gold.

The observation of small periodic structures by electron microscopy was next discussed by Mr. G. A. BASSETT. Following earlier work on the direct resolution of the crystal lattice (about 12 Å spacing) of phthalocyanine crystals, successful results have been obtained with molybdenum trioxide in which the (020) planes have a spacing of 6·93 Å (Fig. 6, p. 320). It is not thought that this represents the limit of what is possible with existing microscope. The moiré pattern method described above had already resolved lattice spacings of 5·8 Å and direct observation should be possible down to 5 Å. Moiré patterns from gold/nickel specimens have also been recorded with a periodicity in two directions with a spacing of 9·2 Å, thus demonstrating that astigmatism is not a limiting factor at this level.

Also considered in this session was a new crystallographic replica method described by Dr. T. EVANS. This had been designed to permit the study of the slip process in silver crystals. The principle is to grow a thin film of gold by evaporation on the silver surface which had been electropolished. The gold forms a coherent film which is oriented with respect to the underlying silver. As the lattice parameters of silver and gold differ by only 0·5%, the gold film may be considered, to a first approximation, as a continuation of the silver lattice. The composite specimen may be deformed in tension and the gold film stripped by dissolving the silver in dilute nitric acid. The deformation studied by this technique is characteristic of the bulk material and not of the thin films themselves. The results obtained were described.

CHEMICAL APPLICATIONS

The so-called "whiskers" that can be grown from thin layers of electrodeposited tin compressed between two clamping plates were described by Mr. D. E. BRADLEY, Mr. J. FRANKS and Mr. P. E. RUSH (Associated Electrical Industries, Aldermaston). The light microscope was found inadequate for revealing the surface structure of the filaments, the diameters of which were less than 5 μ, and direct electron micrographs gave only a silhouette. Carbon replicas were therefore used and gave satisfactory results (Fig. 7, p. 320). Various different forms of whisker were found, including smooth cylinders, ribbons and whiskers with irregular cross-sections. Bundles of whiskers were also found and were thought to be due to a number of adjacent sources.

Mr. R. W. HORNE (Cavendish Laboratory) and Mr. R. H. OTTEWILL (Department of Colloid Science, University of Cambridge) showed a 16 mm ciné film, obtained by direct photography of the fluorescent viewing screen of a Siemens Elmiskop I, of studies on particles of colloidal silver iodide (single crystals). Under certain electron optical conditions two interesting phenomena had been observed. Highly mobile changes of contrast occurred within the particles, the speed of which could be accentuated by increasing the electron beam intensity and decreased, or apparently stopped, by reducing the beam to low intensity; the variations in contrast appeared to continue indefinitely without decomposition of the particle provided that the beam intensity was maintained constant. These changes are thought to be associated with the defect lattice of silver iodide and the high transport number of the silver ion. Secondly, with certain types of particles, notably tetrahedra, the formation of filaments was observed. These were pushed outwards very rapidly, often in a series of jerks, many filaments having diameters as low as 30 Å and yet remaining quite rigid. With thicker filaments (about 100 Å diameter) changes of contrast were observed during growth. Micro-diffraction patterns indicated that the filaments consisted of silver iodide.

Mr. P. CHARSLEY and Mr. P. E. RUSH (Associated Electrical Industries, Aldermaston) had studied sodium chloride whiskers, grown from solution by the Gyulai technique,[10] using carbon replicas, electron diffraction and direct observation in the electron microscope. The orientations of the whiskers were found to be in the [001] direction and occasionally in the [110] direction. The whisker shapes were various, the most common type being bounded by two parallel (100) planes and two irregular surfaces which were formed by the edges of growth layers on the (100) planes. A small number of whiskers were of highly regular cross-sections—usually rectangular or square and very occasionally triangular. Other observations were described which indicated that the thickening of the whiskers (which occurs at a late stage during growth) results from growth in layers initiated by two-dimensional nucleation (Fig. 8, p. 321). Nucleation occurs when the thin film of solution adhering to the whisker surfaces becomes highly supersaturated. It was thought that the substructure revealed during the destruction of the whiskers under electron bombardment might be a result of this mode of growth.

The fine structure of unstretched regenerated cellulose, which had not hitherto been elucidated satisfactorily, was described by Dr. A. SHARPLES, Mr. R. I. C. MICHIE and Dr. J. DLUGOSZ (British Rayon Research Association, Manchester). The usual ultrasonic disintegration technique, prior to electron microscopy, yields characteristically irreproducible results, there being occasionally an indication of some sort of microfibrillar structure but more often just an apparently amorphous mass. In the present investigation unstretched regenerated cellulose had been subjected to swelling in 35% w/w hydrochloric acid for 5–10 min at room temperature prior to ultrasonic disintegration. The

resulting picture in the electron microscope was quite different from that observed previously, and indicated a conglomeration of short, rather irregular microfibrils possibly associated in a network. This result had been obtained with saponified cellulose acetate film (secondary and primary), freeze-dried saponified cellulose triacetate and viscose model filament. The picture was completely reproducible and was held to be correspondingly significant.

Mr. A. KELLER (H. H. Wills Physics Laboratory, University of Bristol) showed evidence of chain folding in single crystals of polymers. Polyethylenes, polyamides, nylons and guttapercha had been studied. In the course of this work, single crystals, confirmed by electron diffraction, had been prepared. The most striking results had been obtained with the linear polyethylene Marlex 50. Polygonal areas in continuous films (Fig. 9, p. 321) could be identified as single crystals with the molecules essentially perpendicular to the film surface. The striations visible in the figure are along the *b* crystallographic axis and are most probably slip lines. In another method of preparation, the same polymer was allowed to crystallize while the solution was cooled, resulting in a suspension of single crystals that resembled those of paraffins. They consisted of flat layers, with well-defined faces, and grew by spiral terrace formation centred on screw dislocations. The basic layers, and those of subsequent growth steps, were about 80–150 Å thick. The most striking feature was the orientation of these molecules; electron diffraction had revealed that the molecules are perpendicular to the flat surface of the crystals. The molecules must therefore be sharply folded back on themselves. Keller indicated supporting evidence for this and discussed the parallel between paraffin and polymer crystals.

Mr. M. W. ANDREWS, Mr. S. C. ROY and Dr. J. SIKORSKI (Textile Physics Laboratory, University of Leeds) discussed the significance of the now well-established microfibrillar character of most natural and synthetic fibres in relation to the old concept of their two-phase (crystalline and amorphous) structure, suggested mainly on the basis of X-ray work, on the one hand, and to more recent considerations of their typical dimensions (about 200 Å) as the manifestations of thermodynamic equilibrium,[11] on the other. In agreement with the latter views, the presence of microfibrils was clearly demonstrated in crystalline polyethylene terephthalate (drawn Terylene), using the usual mechanical and chemical techniques of specimen preparation, thus confirming the conclusions obtained from early work involving replica techniques. However, more significant is evidence suggesting that the tendency to form microfibrillar units is inherent also in amorphous polyethylene terephthalate (undrawn Terylene) (Fig. 10, p. 322). The interaction between some organic solvents and amorphous polyethylene terephthalate showed many interesting (though, at present, not fully explained) features of partial crystallization or progressive dissolution. More detailed studies are now being undertaken of the varying character and size of microfibrillar material recrystallized from different solvents.

In two brief communications, Dr. D. G. DRUMMOND (British Cotton Industry Research Association, Manchester) showed micrographs of a viscose filament in cross-section and some observations on vat dyes.

METALLURGICAL APPLICATIONS

Five papers were contributed by members of the Department of Metallurgy, University of Cambridge. Dr. G. THOMAS described a technique for obtaining thin metal foils of aluminium alloys for transmission electron microscopy. The thickness of the foils is reduced mechanically and by controlled electropolishing, the remaining oxide film being removed chemically. Details of the method have since been published in this *Journal*.[12]

Mr. R. B. NICHOLSON had examined by transmission thin foils of aluminium 4% copper heat-treated in the bulk state. Preferential arrays of the θ' phase had been frequently observed and these were thought to be due to precipitation on slip lines, subgrain boundaries and single dislocations. The use of thin foils rather than oxide replicas had enabled studies of the shapes and orientations of the precipitates to be made. It had been found that only one or two of the three orientations of θ' present in bulk material are seen in the preferential arrays.

An electron metallographic study of fatigue in aluminium 4% copper alloys was reported by Mr. W. I. MITCHELL for which oxide replicas had been used. These had been made by anodizing at 40 V in di-sodium hydrogen phosphate solution and stripped by electropolishing away the metal beneath them. This gave a strong replica showing slip lines and extrusion on the surface of the specimen. Some workers have assumed the existence of localized over-ageing on the slip lines but no evidence was found to support this view. To produce softening θ' precipitation would be required and, although the oxide replica would show this from its earliest stages, none could be found in specimens fatigued in the as-quenched stage.

The results of a metallographic study of the changes associated with creep in a tempered steel were reported by Mr. R. G. BAKER and Dr. J. NUTTING. The steel investigated was a commercial creep-resisting HGT. 3 type which had been solution treated, quenched and tempered. Creep tests to rupture were then carried out over a range of stresses at three different temperatures and, after testing, the microstructure was examined in the electron microscope using the carbon extraction replica technique. The creep ductility varied considerably with testing conditions. High ductility was favoured by high stresses but at low stress levels intergranular fracture resulted after very little deformation. It was thought that at low stresses the grain deformation was very slow compared with the intergranular sliding and that this led to stress concentration at the boundaries, eventually resulting in cavitation and fracture. Raising the testing temperature lowered the creep strength considerably, but increased the ductility. This was due to the changes which took place in the microstructure during testing at higher temperatures; coarsening of the carbide structure and a decrease of the grain strength.

The metallography of surface structure resulting from deformation was investigated by Mr. D. G. BRANDON using direct-carbon replicas. The wavy slip lines characteristic of α-iron were not generally resolvable into lamellae and their diffuse nature indicated that slip occurred on a wide band of slip planes, and not on one or two planes as in α-brass. Cross-slip and sharp slip lines were also observed, and at grain boundaries slip lines faded out, "crossed" into the next grain or were deflected parallel to the boundary. After abrading and electropolishing deformed specimens to remove slip traces, etching in 1% nital revealed banded markings. Electron microscopical examination resolved a background etch-structure with a density of $10^{10} - 10^{11}$ bumps/cm^2. In the etchbands this structure was absent and it was thought that these regions were bands in which slip had occurred and the dislocations had been torn from their Cottrell atmospheres, the background structure being due to the formation of segregates at dislocations and other imperfections during heat treatment.

Mr. R. PHILLIPS (Associated Electrical Industries, Aldermaston) showed some transmission electron micrographs of arrays of dislocations at sub-boundaries in thin films of aluminium and bismuth telluride. These included examples of interference phenomena of the moiré pattern type. Mr. Phillips explained certain apparently anomalous arrangements on the observation that certain elements of dislocation give rise to very little contrast. He also discussed the problem of distinguishing between patterns at sub-boundaries due to dislocations and those due to interference and indicated differences in the general appearance and in the behaviour under stress of these patterns.

Dr. M. J. WHELAN, Dr. P. B. HIRSCH and Mr. R. W. HORNE (Cavendish Laboratory, University of Cambridge) and Dr. W. BOLLMANN (Batelle Memorial Institute, Geneva) described experiments by transmission electron microscopy on thin sections of stainless steel.[13] After small deformations the dislocations were found to occur in pile-ups against grain boundaries. Many of these pile-ups were found to have interacted with dislocations on other slip planes and certain specific reactions could be recognized. Under suitable conditions, the partial dislocations are driven apart, leaving wide stacking faults (Fig. 3, p. 319). It has been possible to estimate the stacking fault energy and this had been found to be low. In contrast to the case of aluminium, cross-slip was only observed in exceptional circumstances. Several other observations were described and illustrated by ciné film, including the interaction between dislocations that result from the stresses induced when thin films are heated by the electron beam.

The results of a study of etching structure on aluminium were presented by Mr. R. PHILLIPS and Mr. N. C. WELSH (Associated Electrical Industries, Aldermaston). Typical sub-grains, 1 to 3 μ in diameter, were revealed but, in addition, an etching structure consisting of cells of about 0·2 μ spacing was found. The latter structure closely resembled patterns observed by Hunter and Robinson[14] on replicas from chemically polished aluminium surfaces. The postulate by these workers that misorientation boundaries are revealed by the chemical polishing process was therefore rejected.

Mr. W. F. JACK and Mr. J. W. SHARPE (Royal College of Science and Technology, Glasgow) described an investigation of pure and corrosion fatigue cracks in a mild steel. A replica method due to Page[15, 16] was used and particular attention was paid to the region near the tip of the crack. Very striking differences were observed between pure and corrosion fatigue. In pure fatigue the crack was generally extremely fine (less than 1 μ) and of fairly uniform width, even at a considerable distance from the tip, while in corrosion fatigue the crack widened rapidly to 10 μ or more. The cracks were always transcrystalline in ferrite, and when intercrystalline cracks did occur they were always between ferrite and pearlite. They tended to avoid pearlite grains and where they did pass through pearlite it was usually at a weak or thin part of the grain. In all the samples examined, the tip of the crack was in the ferrite and it appeared that the crack was propagated very rapidly through pearlite. In the case of corrosion fatigue, evidence of corrosion products could be observed right to the tip of the crack.

The last four papers of this session were contributed by members of the group working at the Research Laboratories of Richard Thomas and Baldwin Ltd., Aylesbury. Dr. G. R. BOOKER and Dr. J. NORBURY outlined a scheme for the examination of inclusions and precipitates occurring in steels, based on techniques previously described by these authors.[17, 18] The use of an extraction replica method allows the isolated material to be examined in transmission by optical and electron microscopy, and electron diffraction, and yields sufficient extracted material for X-ray diffraction, X-ray fluorescent analysis and spectrographic studies. The scheme has been devised to allow most types of included material to be studied, but the information yielded by the various phases of the examination may depend on the shape, size and distribution of the included material. Examples were given of the application of the scheme to the study of carbides, nitrides and inclusions in plain and alloy steels.

Dr. G. R. BOOKER, Dr. J. NORBURY and Mr. A. L. SUTTON used previously described[17, 18] techniques to identify the precipitates formed during the nitriding of pure iron and open hearth steel. Two types of precipitate were observed, a "large" type shown to be γ'–Fe_4N, and a "small" type, the identity of which had been established as α''–$Fe_{16}N_2$. Transmission studies on the extracted material yielded much detailed information concerning the morphology and substructure of the two precipitates. The identification of the small type was facilitated by tilting the replica at a large angle to the beam and by scanning the replica whilst recording the diffraction pattern. The "large" type of precipitate occurred as plates up to 25 μ in size and was found to grow with the plane of the plates parallel to the (112) γ'-crystallographic planes. The "small" types were also plate-like, did not exceed 6 μ in size, and formed with the plane of the plates parallel to the (001) α''-crystallographic planes. They had similarly identified the same types of precipitates sometimes found in commercial open hearth steel (Fig. 11, p. 322).

Dr. G. R. BOOKER, Dr. J. NORBURY and Mr. A. WESTROPE described how they had isolated, by extraction replicas using the single-etch technique,[17, 18] the inclusions present in the aluminium deoxidation series ingots of Sloman and Evans. These had been examined by optical and electron microscopy and by X-ray and electron diffraction. Some additional morphology of the particles had been revealed and the identity of the particles proposed by previous investigators confirmed. In particular, inclusions in the oxygen-rich ingots were found to contain appreciable amounts of magnetite.

This session ended with a general contribution by Dr. G. R. BOOKER and Dr. J. NORBURY on the use of the electron microscope for day-to-day problems in the steel industry.

BIOLOGICAL APPLICATIONS

With the increased use of selective weedkillers, insecticides, and foliar applied fertilizers, characteristics of leaf surfaces have become increasingly important. For example, a herbicide which fails to wet the surface of a particular leaf, is unlikely to have the desired effect on the plant. Mr. B. E. JUNIPER (Department of Botany, University of Oxford), who had investigated this problem, had found the light microscope inadequate for detecting differences between certain wettable and non-wettable leaf surfaces and had therefore studied these in the electron microscope. A single-stage replica technique was used to avoid affecting the delicate nature of the leaf surfaces with organic solvents. Evaporated carbon was employed, deposited directly on to the leaf and stripped mechanically. The leaf surface was not apparently affected in any way by being placed in a vacuum, nor did it gas to any significant extent. Either true replicas or pseudo-replicas were produced by this method, the latter containing some of the original wax structures torn from the leaf surface. Mr. Juniper showed examples of the leaf surfaces of a number of different species obtained in this way (Fig. 12, p. 322).

A method devised by Mr. D. H. PAGE (British Paper and Board Industry Research Association, Kenley, Surrey) for the replication of pulp fibres[15] was found not to be applicable to dry macerated wood fibres (tracheids), owing to their rigidity and inability to bond securely to a glass substrate. Furthermore, the lumen was uncollapsed and filled with air which escaped during the replication. These difficulties had been overcome by a simple partial embedding technique, followed by vacuum impregnation of the fibres with methacrylate monomer. The replication then followed the method previously described.

Dr. A. M. GLAUERT (Strangeways Research Laboratory, Cambridge) and Mr. D. A. HOPWOOD (Department of Botany, University of Cambridge) described an investigation of the fine structure of *Streptomyces coelicolor*. Colonies were embedded in methacrylate or Araldite and thin sections were examined in a Siemens Elmiskop I. A series of changes was observed in the nuclear material of the hyphae during spore formation. These changes could be correlated with observations with the light microscope on colonies stained with chromatinic stains. *Streptomyces* has a greater structural complexity than other bacteria, as indicated by the presence of laminated structures and electron-dense polymetaphosphate bodies in the cytoplasm.

The problems arising from the application of the electron microscope to histological problems, and particularly to pathological material, were discussed by Dr. K. LITTLE (Nuffield Orthopaedic Centre, Oxford). Emphasizing the importance of the fixative used, Miss Little pointed out that in many cases a choice between alternative interpretations of the final photograph would be impossible without a detailed knowledge both of the history of the specimen and its processing.

Mr. D. E. BRADLEY (Associated Electrical Industries, Aldermaston) and Mr. D. J. WILLIAMS (National Institute for Research in Dairying, Shinfield) showed carbon replicas of *Bacillus* spores which revealed unexpected surface sculpturing (Fig. 13, p. 322). This had been found to vary according to the species, and in those so far examined the variation was sufficiently well-defined to permit identification at species level. Less marked, though definite, differences had also been detected in different strains of the same species. It had been found that biochemically similar species have nearly similar spores. The only case in which different species had been found to have identical spores was that of *Bacillus polymyxa* and *Bacillus macerans*.

The structure of chloroplasts in *Tradescantia* and maize was described by Mr. J. C. W. CRAWLEY (John Innes Horticultural Institution, Bayfordbury). The amount of chlorophyll extracted from pieces of leaf from *Zea mais* during preparation for electron microscopy was estimated by measuring light absorption in the 660 mμ region. Comparison with chlorophyll extracts from unfixed material from the same leaves showed that 10 to 24% of the chlorophyll is removed depending upon the fixation and dehydration procedure. Chloroplasts in the leaves of *Zea mais* that had been fixed in a buffered osmium solution at 0·35 M showed the well-known structure of grana linked by lamellae in the stroma. Fixation at 0·2 M gave rise to a swelling that disrupted the stroma but showed that the grana consist of systems of closed membranes. Chloroplasts in the leaves of *Tradescantia bracteata* contain large rectangular bodies, and these could be related to the large crystals that occur in the leaf cells of this plant, but may, in fact, be large starch grains. The grana of these chloroplasts appeared in the swollen state to have a somewhat different structure to those in maize, a system of triple membranes being more typical.

Mr. A. D. HALLY (Department of Anatomy, University of Glasgow) reported on the fine structure of the Paneth cell. Portions of mouse jejunum were fixed with osmium tetroxide solution and embedded in methacrylate. The Paneth cells were readily distinguished from the neighbouring cells of the crypt. The features of the Paneth cell were found to be large secretory granules, extensive endoplasmic reticulum and clusters of dense particles. The Golgi complex was supranuclear and appeared to give rise to small vacuoles which incorporated Golgi vesicles and became small secretory granules. Mr. Hally therefore concluded that the Golgi vesicles, a component of the Golgi complex, form part of the final secretory product of the Paneth cell.

Dr. A. O. T. CHARLES (Departments of Dermatology and Biomolecular Structure, University of Leeds), postulated a two-ended attachment for the tonofibrils of the human epidermis. The points of attachment are at the prickles of the epidermal cells, where adjacent cell walls adhere together. In this way the relationship of the tonofibrils and the prickles are made clear, since, efficiently utilizing the elastic α–β transformation of the tonofibrils and their ultimate resistance to further stretching, they form a continuous system throughout the epidermis, a system well suited to the environmental conditions met by the body surface.

A study of connective tissue growth in normal and scorbutic granuloma was reported by Dr. J. A. CHAPMAN and Mr. R. PEACH (Rheumatism Research Laboratory, University of Manchester). The injection of carrageenin, a sulphated polygalactose obtained from seaweed, into the skin of the guinea-pig stimulates the rapid formation of connective tissue. An electron microscope study of this tissue showed the occurrence of normal collagen fibres and intermediate stages in their development. The reprecipitated neutral-salt-soluble collagen fraction extracted from the tissue was found to consist of thin fibres, some of them showing 220 Å striations; the reprecipitated citrate-soluble fraction consisted of normal fibres. In scorbutic animals the amount of tissue formed is smaller and no new fibres are visible histologically. The electron microscope showed the presence of collagen fibres with the normal structure, but in addition, thin beaded fibrils, not present in normal animals, were found. In phosphotungstic-acid-stained specimens of reprecipitated citrate-soluble collagen from scorbutic animals, a highly abnormal type of fibre with diagonal banding was observed.

H. W. EMERTON

REFERENCES

(1) PAGE, D. H. *Brit. J. Appl. Phys.*, **9**, p. 268 (1958).
(2) PAGE, D. H. *Brit. J. Appl. Phys.*, **9**, p. 60 (1958).
(3) MAALØE, O., and BIRCH-ANDERSON, A. *Sixth Symposium of Gen. Microbiol. Bacterial Anatomy*, p. 261 (London: Cambridge University Press, 1956).
(4) GLAUERT, A. M., ROGERS, G. E., and GLAUERT, R. M. *Nature (London)*, **178**, p. 803 (1956).
(5) WHELAN, M. J., and HIRSCH, P. B. *Phil. Mag.* To be published.
(6) STAPLES, L. W., and GARD, J. A. To be published.
(7) CHALMERS, R. A., DENT, L. S., and TAYLOR, H. F. W. *Min. Mag.*, **31**. To be published.
(8) GARD, J. A., and TAYLOR, H. F. W. *Amer. Mineralogist*, **43**, p. 3 (1958).
(9) PASHLEY, D. W., MENTER, J. W., and BASSETT, G. A. *Nature (London)*, **179**, p. 752 (1957).
(10) GYULAI, Z. *Z. Phys.*, **138**, p. 317 (1954).

**

(11) BALASHOV, V., and PRESTON, R. D. *Nature (London)*, **176**, p. 64 (1955).
(12) NICHOLSON, R. B., THOMAS, G., and NUTTING, J. *Brit. J. Appl. Phys.*, **9**, p. 25 (1958).
(13) WHELAN, M. J., HIRSCH, P. B., HORNE, R. W., and BOLLMANN, W. *Proc. Roy. Soc. A*, **240**, p. 524 (1957).
(14) HUNTER, M. S., and ROBINSON, D. L. *J. Metals*, **5**, p. 717 (1953).
(15) PAGE, D. H. *Electron Microscopy: Proceedings of the Stockholm Conference, September* 1956, p. 285 (Stockholm: Almquist and Wiksell, 1957).
(16) PAGE, D. H. *Research Suppl.*, **9**, p. S10 (1956).
(17) BOOKER, G. R., and NORBURY, J. *Brit. J. Appl. Phys.*, **8**, p. 109 (1957).
(18) BOOKER, G. R., NORBURY, J., and SUTTON, A. L. *Brit. J. Appl. Phys.*, **8**, p. 154 (1957).

ORIGINAL CONTRIBUTIONS

The ratio of characteristic to white X-radiation from a copper target

By E. G. BENDIT, B.Sc., M.Sc., Wool Textile Research Laboratories, Commonwealth Scientific and Industrial Research Organization, Ryde, New South Wales, Australia

[*Paper received* 5 *December*, 1957]

The ratio (k) of the total Kα radiation to the total white radiation emitted by copper target X-ray tubes has been estimated by isolating the contribution of wavelengths near λKα with balanced nickel and iron filters. The total radiations leaving the tube have been inferred from the counting rates of a Geiger counter exposed to the direct beam from the X-ray tube (suitably attenuated by a pinhole system). Corrections for transmission of the air path and quantum efficiency of the Geiger counter as functions of wavelength were applied to an assumed spectral distribution for the white radiation. The assumed spectral distribution was selected on the basis of a literature survey of investigations on continuous spectra, a brief outline of which is given. It is found that at 35 kVp, $k = 2{\cdot}2$, a result which lies between those of Arndt and Riley,[12] who found $k = 5{\cdot}4$, and of Parrish and Kohler,[13] from whose curves a value of $k = 0{\cdot}35$ is deduced. A measure of reconciliation between these results is achieved if various corrections and different experimental conditions are taken into consideration. Curves show the variation of k over the target area, with take-off angle, and with voltage; the form of the voltage variation agrees with the results of Guinier.[21]

For the purpose of testing a correction applied to experimental data obtained during an investigation of the X-ray diagram of wool,[1] the author required a knowledge of the approximate distribution of the continuous spectrum, and the approximate ratio of the integrated intensity of the characteristic to that of the continuous radiation. A Norelco Geiger counter diffractometer was used for the investigation on wool, and the standard four-window X-ray tube was operated at 35 kVp (full-wave rectified), and at 3° take-off angle.

The literature on X-ray spectra deals mainly with precise determinations of emission wavelengths of the K, L and M series, and relatively little work has been carried out on investigations of spectral intensities. Some workers, Ulrey,[2] Deauvillier,[3] Kulenkampff,[4] Kirkpatrick,[5] and Pike,[6] concentrated mainly on the distribution of the continuous spectrum, while amongst others, Webster and Clark,[7] Unnewehr,[8] Allison,[9] Webster and others,[10] and Worthington and Tomlin,[11] dealt with the intensities of characteristic spectra. There appears to be a lack of work on the determination of intensities of complete spectra, and it is only in recent years that any information on such spectra has been published.[12, 13]

Arndt and Riley[12] used an almost new copper X-ray tube at unspecified take-off angle, and at 30 kV d.c. Their results, which were obtained by combining data from Geiger counter and proportional counter measurements, were corrected for absorption in the air, the nickel filter, the counter window and the counter gas, and for wavelength variation of reflexion from the calcite crystal. Subject to a correction for higher order reflexions from the crystal and a correction for lack of linearity in the dispersion curve of the spectrometer, their curve represents the spectral distribution at the window of the X-ray tube. They state that the integrated intensities of the Kα, Kβ and white radiations are in the ratio of 100 : 13·3 : 18·5, i.e. a Kα/white ratio of 5·4 : 1.

Parrish and Kohler[13] operated their copper X-ray tube, which was old and tungsten-contaminated, at 3° take-off angle and at 40 kVp (full-wave rectified). They used a silicon (111) crystal monochromator, and their detector was a NaI.T*l* scintillation counter without peak height discrimination. The results are apparently not corrected for air absorption, etc., and it is difficult to estimate the magnitude of the necessary corrections. They state that "the continuous spectra at moderately high operating voltages have an integrated intensity of more than an order of magnitude greater than that of the Kα lines." Actual integration of the areas under their curve gives a Kα/white ratio of about 0·35 : 1. (The spectral curve shown in Parrish and Kohler's article is rather small, and the integration was performed, using an evidently identical curve, but drawn to

a larger scale, contained in an article by Parrish and Taylor.[14])

The large discrepancy between these results, which is not explained by differences in operating conditions, caused the author to carry out his own determination of this ratio. A suitable X-ray spectrometer not being available, it was decided to use the copper X-ray tube in conjunction with balanced nickel and iron filters. By a method described in detail later, the ratio of the intensities transmitted through these filters was used to calculate the Kα/white ratio, which was found to be about 2 : 1.

EXPERIMENTAL

In principle, the experimental arrangement is very simple. The direct beam from the X-ray tube is stopped down to a few hundred counts per second; at counting rates above about 800 counts per second, the long resolving time of the Geiger counter, about 150 μs at constant potential, does not permit accurate corrections for coincidence losses to be made.[15] [In calculating corrections for counting losses, the effective dead time of the Geiger counter (Norelco type 62019), which takes account of alternating potentials, was taken as 270 μs.[16]] The intensities transmitted through the nickel and iron filters are then obtained in turn, and their ratio calculated.

A number of complications arise in practice. The intensity of the direct beam from the copper target of the Norelco four-window X-ray tube, at 3° take-off angle, when reduced by the standard 0·003 in. slit in front of the Geiger counter, is of the order of 10^6–10^7 counts per second at normal operating voltages. This intensity has to be reduced by a factor of about 10^4 before it can be used for absorption tests involving the direct beam. If this reduction is effected by the use of a series of narrow slits, erroneous results are obtained, as even a small misalinement of the slits changes the spectral character of the observed intensity, probably due to diffraction at the slits. Similarly, the use of long fine-bore capillary tubes is unsatisfactory, because of total external reflexion effects in the bore, which tend to monochromatize the resultant beam.[17] The final arrangement, which gave consistent results, was a pair of circular apertures, one 80 μ diameter, mounted in front of the X-ray tube, and the other, 200 μ diameter, in front of the Geiger counter. As the diameters of these apertures were sufficiently large, and their lengths sufficiently short (about 1·5 mm), errors due to diffraction at the apertures and total external reflexion were eliminated. This method of direct beam reduction was used with the Geiger counter in its normal goniometer mounting, but it was found necessary to remove the Soller slit assemblies, as these also markedly changed the character of the radiation, presumably again owing to total external reflexion effects.

The 80 μ aperture in front of the X-ray tube was held in a universal mounting, which permitted correct alinement and change of take-off angle. By moving this aperture horizontally parallel to the line focus of the X-ray tube, the Kα/white ratio of different parts of the target could be investigated.

As a check on the above procedure, the reduction of the direct beam intensity was also effected by placing the Geiger counter at a distance of about 350 cm from the X-ray tube. An evacuated tube with thin mica windows was placed between source and detector, and the thickness of the mica windows chosen so as to be equivalent to the normal air path of 34 cm. Without the evacuated tube, this method of determining the Kα/white ratio is too insensitive, because absorption in 350 cm of air reduces the copper characteristic radiation to about 1% of its original intensity. The mica window near the X-ray tube was large, and permitted the entire focal area to be seen from the other window, which had a diameter of 140 μ. With this arrangement, therefore, the spectral character of the radiation from the entire target area could be determined, compared with about one-hundredth of the target area for the two-pinhole system. Consistent results were obtained with these two methods.

As a further check, the direct beam was attenuated also by reducing the X-ray tube current to a few microamperes. The advantage of this method lies in its simplicity: the normal X-ray optical arrangement is used, and there is no need to remove the Soller slit assemblies. At the same time it should be noted that some de-focusing of the electron beam may occur when an X-ray tube is operated under current conditions greatly different from those for which it was designed: parts of the target not kept "clean" by evaporation of tungsten deposits owing to constant electron bombardment may then be caused to emit X-rays, and this radiation will have a different spectral quality from that produced under normal operating conditions. In the event, however, the results obtained with this method were entirely consistent with those obtained by stopping down the direct beam, which suggests that no significant de-focusing takes place.

THEORETICAL

The spectral distribution of the radiation from an X-ray target is usually obtained with a suitable X-ray spectrometer, an instrument which consists essentially of a crystal analyser and a detector of X-rays. The original radiation is modified by the following factors:

(1) absorption in the X-ray target;
(2) absorption in the window of the X-ray tube;
(3) absorption in the air path between X-ray tube and detector;
(4) reflectivity of the crystal analyser;
(5) correction for lack of linearity in the dispersion curve of the spectrometer (this is often ignored);
(6) correction for orders of reflexion from crystal analyser;
(7) quantum efficiency of the detector.

All these corrections must be applied in order to obtain the true spectrum from that observed with the spectrometer. In practice, only the spectrum at the window of the X-ray tube is of interest, and only corrections (3–7) need be applied. Once this spectrum has been calculated, the Kα/white ratio is found from the areas under the spectral curve.

In the case of the direct-beam method employed by the author, the Kα/white ratio cannot be found as easily, because the Geiger counter detector is not capable of discriminating between intensity contributions from different parts of the spectrum. Instead, use is made of the fact that nickel is relatively transparent, while iron is practically opaque to the copper Kα line. The ratio of the intensity transmitted by the nickel and iron foils of suitable thickness, the nickel/iron ratio, is therefore some measure of the Kα/white ratio of the radiation. The method of calculating the actual Kα/white ratio is described below; it involves a knowledge of the spectral distribution at the window of the X-ray tube, and as the distribution is not known, a reasonable spectrum must be assumed. This can only be done on the basis of the various spectral curves reported in the literature, and

proved to be rather difficult, because, for a variety of reasons, most published spectra are unsatisfactory.

Spectral distributions. Ulrey,[2] who was the first to attempt a determination of the spectral distribution of X-rays, and whose curves are still frequently found in reference works and textbooks, only covers the range up to 1 Å, and does not apply any corrections at all. His results are therefore of little value for quantitative work. Ulrey's data were re-computed by Pike,[6] who only applied corrections (2), (4) and (7). Deauvillier's curves[3] are corrected for (2), (6) and (7), but his upper wavelength limit is only 0·8 Å. Kulenkampff[4] corrects for (1–5) and (7), and he circumvents the need to apply correction (6) by limiting the wavelength region to $\lambda_0 < \lambda < 2\lambda_0$ at any particular X-ray tube voltage. He fitted his curves to the empirical equation

$$I_\lambda = \frac{CZ}{\lambda^2}\left(\frac{1}{\lambda_0} - \frac{1}{\lambda}\right) + \frac{bZ^2}{\lambda^2} \qquad (1)$$

where I_λ is the intensity of the radiation at wavelength λ, λ_0 is the Duane–Hunt short-wavelength limit, and Z is the atomic number of the target material; C and b are constants, but b is so small that the second term is generally omitted. Kulenkampff's curves only cover the wavelength range from about 1 to 3 Å, and his voltages range from 7 to 12 kV. Kirkpatrick[5] applies all the corrections, except (1), and he determines the spectrum inside the X-ray tube. Again, however, only wavelengths up to 1 Å are covered, and all the tests are carried out at relatively high voltages (51·4 to 70·7 kV). Arndt and Riley's curve is claimed to represent the spectrum at the window of the X-ray tube, but unfortunately corrections (5) and (6) do not appear to have been applied. Parrish and Kohler's curves, which were reported with the primary object of showing the effect of pulse height discrimination on spectra obtained with scintillation counters, are apparently uncorrected experimental records, and do not show true spectral distributions.

Of all the curves available in the literature, it appears that only Arndt and Riley's data can be used as a reasonable basis for the present investigation. In Fig. 1, Arndt and Riley's and Kirkpatrick's curves are compared with those given by Kulenkampff's equation. Also shown is the curve by Parrish and Kohler, and that assumed by the author for 35 kVp.

It is seen that the general shape of the family of Kulenkampff's curves differs from that of the experimental curves. This is to be expected, in view of the different experimental conditions and correction procedures already referred to, and also because Kulenkampff tested his expression only in a limited voltage and wavelength range. Nevertheless, the author found the Kulenkampff expression convenient, because it permits a whole set of mutually consistent spectral distributions to be drawn. It should be noted here that a theoretical expression obtained by Kramers[18] from quantum principles is in good agreement with the experimental expression obtained by Kulenkampff.

The assumed spectral curve for 35 kVp was drawn on the basis of Arndt and Riley's curve at 30 kV d.c., and using Kulenkampff's curves as a general guide. Some allowance was made for Arndt and Riley's curve not being corrected for the effect of higher orders, by reducing the height of the tail level of the assumed curve. This reduction could only be guessed, but some indication of its magnitude was obtained from Kirkpatrick's work. The effect of higher orders is to some extent compensated by Arndt and Riley's omission to apply the probably small correction for spectrometer dispersion. It is further compensated by the author's use of a.c.: Deauvillier found that the tail levels of a.c. spectral curves are higher than that of corresponding d.c. curves.

In view of the uncertainty concerning the true spectral distribution, the effect of different assumed distributions on the Kα/white ratio was investigated, and was found to be relatively small (see below).

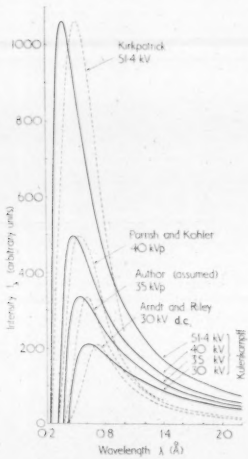

Fig. 1. Comparison of Kulenkampff's spectral distributions with various experimental curves, and the author's assumed curve for 35 kVp. All the experimental curves are normalized to make their peak intensities equal to the corresponding Kulenkampff curves

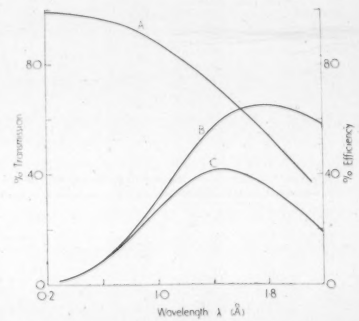

Fig. 2. Efficiency of X-ray detection as a function of wavelength. Curves (*A*) and (*B*) are taken from a report by Taylor and Parrish.[19] Curve (*C*) is obtained by multiplying corresponding ordinates of curves (*A*) and (*B*)

Curve (*A*), transmission of 34·0 cm of air; curve (*B*), Geiger counter quantum efficiency (Norelco No. 62019); curve (*C*), overall efficiency of instrument.

The Kα/white ratio (k). The curve at 35 kV assumed by the author (Fig. 1 and Fig. 3, curve *A*) is taken to represent the spectrum at the window of the X-ray tube. This spectrum is corrected for absorption in the air path, and for Geiger counter quantum efficiency, using the curves shown in Fig. 2. The resulting "instrumental spectrum" (Fig. 3, curve *B*) is next corrected for absorption in the nearly balanced nickel and iron filters, of thicknesses 0·00070 and 0·00095 in. respectively (Fig. 3, curves *C* and *D*), on the basis of mass absorption coefficients reported by Allen.[20]

In order to obtain an expression for the desired Kα/white ratio, let the total white intensity of the spectra shown in Fig. 3, as determined by integration under the curves, be $\overset{A}{\Sigma} I_\lambda d\lambda$, etc., and let the corresponding characteristic intensities be $I\alpha_A$, $I\beta_A$, etc. The Kα/white ratio is then given by

$$k = I\alpha_A / \overset{A}{\Sigma} I_\lambda d\lambda = \kappa / \overset{A}{\Sigma} I_\lambda d\lambda \qquad (2)$$

where $\kappa = I\alpha_A$. The value of $\overset{A}{\Sigma} I_\lambda d\lambda$ is calculated in arbitrary units, and k is known, if κ can be determined in the same units.

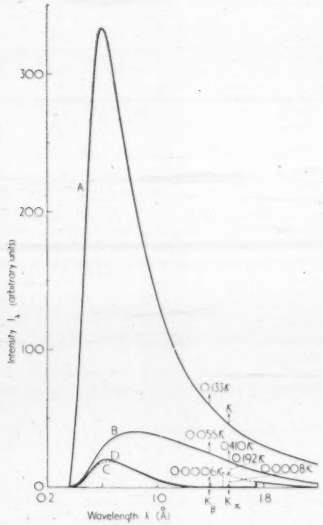

Fig. 3. Effect of corrections on the spectral distribution at 35 kVp assumed by the author. Integrated white intensities are given in arbitrary units, and intensities of the Kα and Kβ lines are shown as a function of κ, the Kα intensity of the spectrum at the window of the X-ray tube. The ratio of the Kα to the Kβ intensity (1 : 0·133) is taken from Arndt and Riley's report[12]

Curve *A*, spectrum at window of X-ray tube; curve *B*, "instrumental spectrum"; curve *C*, nickel-filtered "instrumental spectrum"; curve *D*, iron-filtered "instrumental spectrum."

$\overset{A}{\Sigma} I_\lambda d\lambda = 210$ $\qquad$ $\overset{C}{\Sigma} I_\lambda d\lambda = 10{\cdot}7$

$\overset{B}{\Sigma} I_\lambda d\lambda = 40$ $\qquad$ $\overset{D}{\Sigma} I_\lambda d\lambda = 9{\cdot}2$

The ratio of the intensity transmitted by the nickel foil to that of the iron foil, the nickel/iron ratio, is given by

$$k' = \frac{\overset{C}{\Sigma} I_\lambda d\lambda + I\alpha_C + I\beta_C}{\overset{D}{\Sigma} I_\lambda d\lambda + I\alpha_D + I\beta_D}$$

Using the intensity data shown in Fig. 3, this equation becomes

$$k' = \frac{10{\cdot}7 + (0{\cdot}192 + 0{\cdot}0006)\kappa}{9{\cdot}2 + (0{\cdot}0008 + 0{\cdot}0006)\kappa} = \frac{10{\cdot}7 + 0{\cdot}193\kappa}{9{\cdot}2 + 0{\cdot}001\kappa}$$

or $$\kappa = \frac{9{\cdot}2k' - 10{\cdot}7}{0{\cdot}193 - 0{\cdot}001k'} \qquad (3)$$

Substitution of the value of κ in equation (2) gives

$$k = \frac{1}{210} \cdot \frac{9{\cdot}2k' - 10{\cdot}7}{0{\cdot}193 - 0{\cdot}001k'} \qquad (4)$$

The value of k' is determined by experiment, and hence k can be calculated.

RESULTS

Two Norelco four-window copper tubes were investigated; one tube was old (about 1500 hours use), and the other new (about 150 hours use). Surprisingly, the old tube gave a higher value of k, despite a presumably larger amount of tungsten contamination. A single-crystal oscillation photograph was therefore taken, and it was found that the new tube was heavily contaminated with iron. As the iron lines lie outside the "window" of the balanced nickel–iron filter combination, their contribution forms, in effect, part of the white spectrum, and this results in a lower Kα/white ratio for the new copper tube. A small amount of iron was also found to be present in the old copper tube. Two different Geiger tubes were tested, one supplied by North American Philips, and the other by Philips, Eindhoven. Both gave almost identical results.

The variation of k across the Geiger counter window was investigated by moving the Geiger counter across the pinhole at the end of the 350 cm evacuated tube. In the central

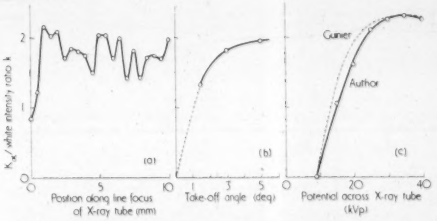

Fig. 4. (*a*) Variation of k along line focus of X-ray tube. New copper tube, 35 kVp, 3 mA, 3° take-off angle. Geiger counter in normal position on goniometer. No Soller slits. (*b*) Variation of k with take-off angle. New copper tube, 25 kVp, 3 mA. Geiger counter in normal position on goniometer. No Soller slits. (*c*) Variation of k with applied voltage. Old copper tube, X-ray tube current about 3 μA, 3° take-off angle, normal X-ray optical arrangement, Soller slits in position. Guinier's original curve has arbitrary units of k. It is normalized here to agree with the author's curve at 35 kVp

region of the window (about 10 mm) where the variation is small, the mean value of k is about 2·2 for the old copper tube, and about 1·7 for the new copper tube. There is no significant difference between spot focus and line focus.

The variation of k along the line focus of the X-ray tube was investigated by moving the two-pinhole system horizontally across the window of the new X-ray tube [Fig. 4(*a*)]. The large fluctuations in the value of k, which are only to a minor extent statistical, are thought to be due mainly to slight variations in the surface structure of the target. The mean value of k is about 1·7, which is consistent with the already quoted result obtained with this tube. The variation of k with take-off angle was determined by rotating the two-pinhole system in a vertical plane. The results clearly show a rise of k with increasing take-off angle [Fig. 4(*b*)]. The variation of k with voltage is shown in Fig. 4(*c*).

All the results reported here, as well as others not included for reasons of space, show that at normal take-off angle (3°) and 35 kVp, the Kα/white ratio (k) for the old copper tube is about 2·2, while that for the new copper tube is about 1·7. The latter result is of little significance, because of the iron contamination of the target. Some comment is called for on the variation of k with voltage. Equation (3) can only be used at 35 kVp. At other voltages, other equations, based on different assumed spectra, have to be used: when this is done, the graph shown in Fig. 4(*c*) is obtained. For comparison, a curve reported by Guinier[21] is also shown.

Because of the many uncertainties in determining the value of k, some estimate of the accuracy of the procedure must be given. In order of importance, the main sources of error are: choice of spectrum at the window of the X-ray tube, Geiger counter efficiency and thickness of balanced filters. The magnitude of the first of these can only be assessed by assuming different distributions, and calculating the effect on the Kα/white ratio, as shown in Fig. 5. The

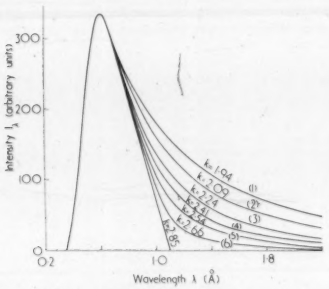

Fig. 5. Effect of different assumed spectra at the window of the X-ray tube on the Kα/white ratio. All curves are drawn for 35 kVp

position of maximum intensity is not seriously in dispute, and all the curves are identical up to 0·7 Å, the wavelength at which higher order reflexions first occur. Curve (1) is essentially that assumed by Kulenkampff, and must be too high, because he corrects for absorption in the target and the window of the X-ray tube. Curve (3) is the one assumed by the author, and is identical with curve *A* of Fig. 3. The correct curve could be lower, as has already been mentioned, and possibly curves (4) or (5) should have been chosen, but it can be seen this uncertainty is not likely to affect the final value of k by more than ±10%. The error in k due to a 10% variation (at all wavelengths) of the Geiger counter quantum efficiency (Fig. 2) is ±10%, and that due to a 3% variation of filter thickness is ±5%. The overall error in the Kα/white ratio is therefore of the order of 30%, possibly considerably less.

DISCUSSION

The result of this investigation ($k = 2 \pm 0{\cdot}5$) differs greatly from that obtained by Arndt and Riley[12] ($k = 5{\cdot}4$) and Parrish and Kohler[13] ($k \simeq 0{\cdot}35$). A measure of reconciliation between these results can be achieved, however, if the different experimental conditions are taken into consideration. In Arndt and Riley's case, their use of a new copper X-ray tube operated at d.c., and possibly at large take-off angle, would undoubtedly lead to a greater Kα/white ratio than that obtained by the author, particularly as the target of even the old copper tube used by the author contained some iron contamination. While the effect of these factors cannot be estimated quantitatively, it is possible that after correction the results could agree within experimental error. In Parrish and Kohler's case, omission of the necessary corrections (air absorption, etc.) must have resulted in their Kα/white ratio being considerably too low, but the discrepancy between their result and the author's, which is of the order of 10 : 1, would still be expected to be large after correction.

ACKNOWLEDGEMENTS

The author is indebted to Prof. C. J. Milner, head of the School of Applied Physics, N.S.W. University of Technology, Sydney, for the use of the Norelco Geiger-counter diffractometer, and for pointing out to him the need for the spectrometer dispersion correction. Thanks are also due to two members of his staff, Associate Prof. J. F. McConnell and Mr. N. R. Hansen, for valuable discussions.

REFERENCES

(1) Bendit, E. G. *Nature* (*London*), **179**, p. 535 (1957).
(2) Ulrey, C. T. *Phys. Rev.*, **11**, p. 401 (1918).
(3) Deauvillier, A. *Ann. Phys.* (*Paris*), **13**, p. 49 (1920).
(4) Kulenkampff, H. *Ann. Phys.* (*Leipzig*), **69**, p. 548 (1922).
(5) Kirkpatrick, P. *Phys. Rev.*, **22**, p. 37 (1923).
(6) Pike, E. W. *J. Appl. Phys.*, **12**, p. 206 (1941).
(7) Webster, D. L., and Clark, H. *Proc. Nat. Acad. Sci., U.S.A.*, **3**, p. 181 (1917).
(8) Unnewehr, E. C. *Phys. Rev.*, **22**, p. 529 (1923).
(9) Allison, S. K. *Phys. Rev.*, **32**, p. 1 (1928).
(10) Webster, D. L., Hansen, W. W., and Duveneck, F. B. *Phys. Rev.*, **44**, p. 258 (1933).
(11) Worthington, C. R., and Tomlin, S. G. *Proc. Phys. Soc.* (*London*) *A*, **69**, p. 401 (1956).
(12) Arndt, U. W., and Riley, D. P. *Proc. Phys. Soc.* (*London*) *A*, **65**, p. 74 (1952).
(13) Parrish, W., and Kohler, T. R. *J. Appl. Phys.*, **27**, p. 1215 (1956).
(14) Parrish, W., and Taylor, J. *Norelco Reporter*, **3**, p. 105 (1956).

(15) KLUG, H. P., and ALEXANDER, L. E. *X-ray Diffraction Procedures for Polycrystalline and Amorphous Materials*, p. 281 (New York: John Wiley and Sons Inc., 1954).

(16) PARRISH, W., and KOHLER, T. R. *Rev. Sci. Instrum.*, **27**, p. 795 (1956).

(17) HIRSCH, P. B. *X-ray Diffraction by Polycrystalline Materials* (Edited by Peiser, Rooksby and Wilson), p. 285 (London: The Institute of Physics, 1955).

(18) KRAMERS, H. A. *Phil. Mag.*, **46**, p. 836 (1923).

(19) TAYLOR, J., and PARRISH, W. *Rev. Sci. Instrum.*, **26**, p. 367 (1955).

(20) ALLEN, S. J. M. *Handbook of Chemistry and Physics*, 38th Ed., p. 2427 (Cleveland, Ohio: Chemical Rubber Publishing Co. 1956–57).

(21) GUINIER, A. *X-ray Crystallographic Technology*, p. 6 (London: Hilger and Watts Ltd., 1952).

The ageing of vacuum standard lamps on a.c. and d.c.

By W. BARNETT, R. G. BERRY, B.Sc., Grad.I.E.E., and J. S. PRESTON, M.A., M.I.E.E., F.Inst.P., F.I.E.S., Light Division, National Physical Laboratory, Teddington, Middlesex

[*Paper received* 20 *December*, 1957]

A comparison is made of the rates of fall of luminous intensity and current, at constant voltage and colour temperature 2390° K approximately, of 100 V 30 W vacuum photometric standard lamps, on a.c. and d.c. supplies. The rate for intensity is considerably higher on d.c. than on a.c., while the rate for current is lower. These specific effects of d.c. operation can be accounted for simply by changes in filament emissivity. There is no necessity to postulate a migration of tungsten along the surface of the filament, as in the authors' previous work on gasfilled lamps. The effects are shown to be almost fully reversible, after many hours of burning, by suitable application of reversed d.c., and a.c., supplies. As for gasfilled lamps, the usefully smaller rate of depreciation characteristic of a.c. operation may be fully retained on d.c. by reversal of polarity at regular convenient intervals, so that the use of a.c. becomes legitimate for the normal preliminary ageing tests.

INTRODUCTION

In a previous paper,[1] the authors dealt with the ageing of gasfilled standard lamps run at constant voltage. With a d.c. supply of fixed polarity, the rates of fall of luminous flux and of current were found to be, respectively, some four times and twice the rates observed with an a.c. supply of the same r.m.s. voltage. These effects, peculiar to d.c., were ascribed partly to migration of tungsten along the filament, producing a greater rate of increase in filament resistance, and partly to faster roughening of the filament surface, decreasing the proportion of radiation emitted selectively in the visible region of the spectrum. The effects were reversible, for both light output and lamp current were observed to *increase* for many hours after reversal of the previously fixed d.c. polarity. Moreover, with regular reversals of d.c. at intervals of a couple of hours or less, the lamps settled down to behave, in these respects, exactly as though running on 50 c/s a.c.

The present paper describes similar work on tungsten filament vacuum lamps. They were of the 100 V 30 W type (by the General Electric Co. Ltd.) for use as secondary standards of luminous intensity.[2,3] The filament is a uniplanar grid of straight tungsten wire. The lamps were set at 100 V with colour temperatures near 2390° K. These and some other conditions were dictated by the ultimate purpose of using the lamps as N.P.L. standards. In particular the photometer measured not the luminous flux but the luminous intensity. This may be taken as approximately proportional to the flux. However, the ratio of the two does not necessarily remain exactly constant with time of burning, for any progressive change in the surface-structure of the filament would presumably alter to some extent the polar distribution of light from it. This point—interesting, though in practice only incidental—was not investigated.

EXPERIMENTAL OBSERVATIONS

Of a group of fourteen lamps, ten were aged continuously on an a.c. supply for just over 240 h. The broken lines in the figure show the average depreciation in luminous intensity and lamp-current. Over the later part of the period the luminous intensity was falling at the rate of 0·32% per 100 h, and the current at 0·11% per 100 h.

The remaining four lamps were differently treated, with results shown by the full lines in the figure. For the first ninety hours or so, terminating at *A* on the graph, they also were run on a.c. This provided initial stabilization under the same conditions as for the other ten lamps. Then for the period *AB* of about 200 h, the four lamps were run on d.c. of fixed polarity. It is seen that the intensity soon began to fall more rapidly than on a.c. At the end of the period it was falling at the rate of 2·5% per 100 h—about eight times the a.c. rate. On the other hand, the rate of fall in current diminished, and was only about 0·07% per 100 h, averaged over the period—about two-thirds the a.c. rate.

It was then decided to attempt a "recovery programme" for the four lamps, as for the gasfilled lamps which had been run on d.c. in the previous work. It was not clear, however, whether the better treatment would be, simply, reversal of the d.c. polarity, or an immediate change to an a.c. supply.

Therefore at B the lamps were divided into two pairs. One pair, run on a.c. from B onward, followed the course $C_1D_1E_1$. The other pair, placed on reversed d.c. at B, showed an initial rise in intensity to C_2, followed by a fall to D_2. This pair was then also placed on a.c. for the run D_2E_2, during which the intensity again rose. For both pairs, the lamp-currents throughout this treatment showed a trend consistently opposite in sign to that of the intensity. The final

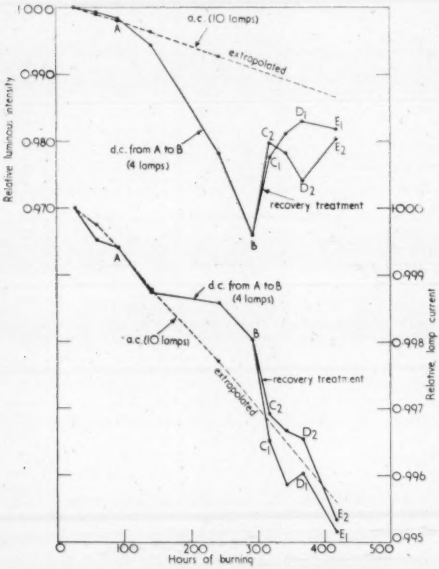

Changes in light output (*upper diagram*) and lamp current (*lower diagram*) during the ageing, and subsequent recovery, of uniplanar-filament vacuum lamps at constant voltage. Broken lines relate to lamps run throughout on a.c. Full lines relate to lamps run steadily on d.c. of constant polarity from A to B, and then subjected to "recovery treatment," as described in the text, from B to E_1 or E_2

result was that for both pairs, the luminous intensity had recovered to nearly as high a value as it would have taken had the lamps been run throughout on a.c. The lamp currents also are seen to have returned to values quite close to the extrapolation of the a.c. ageing characteristic established by the measurements on the group of ten lamps.

At this stage measurements were discontinued in order to conserve the lamps for their intended use as standards.

DISCUSSION

Of the ageing of the lamps on a.c. there is little to be said. By the reasoning followed previously,[1] the rate of fall of 0·32% per 100 h, in luminous intensity, may be split very roughly into 0·2% due to decrease in current and power consumed, and 0·12% due to blackening of the bulb.

Of the d.c. ageing the striking feature is the lower rate of fall of current. It seems inconceivable that this could be due to any less rapid evaporation of the filament. The most direct conclusion is that it results from a more rapid fall in filament temperature on d.c. than on a.c., having regard to the temperature coefficient of the resistance of tungsten at the filament-temperature. This, together with the greater rate of fall in luminous intensity, can best be accounted for by a greater rate of roughening of the surface-structure of the filament. The resulting increase in total emissivity would lower the temperature and also, *a fortiori*, the proportion of radiation emitted selectively in the visible spectrum.

An emissivity-effect, it will be recalled, was found to occur in gasfilled lamps on d.c., and so is not unexpected. It is surprising, however, to find it even greater in vacuum lamps at so much lower a temperature, the respective components of the fall in light output in the two cases being 1·37% per 100 h and 2·18% per 100 h. On the other hand, the present results for vacuum lamps show no evidence of any migration of the material of the filament such as was found for gasfilled lamps on d.c.

In gasfilled lamps, migration is no doubt facilitated by the higher operating temperature and consequent greater mobility of tungsten over the filament-surface. Also, it may be accentuated by the effect of the gasfilling in partially confining the evaporating tungsten to a sheath closely surrounding the filament. The same factors may explain the slower change in the emissive properties of the filament of a gasfilled lamp on d.c., for they could conceivably retard the development of surface-asperities which must be the direct cause of this, and which seem to be provoked by operation on d.c. The coiled form of the filament in a gasfilled lamp may also contribute to these subtler differences in behaviour between gasfilled and vacuum lamps. At least it may endow the gasfilled lamp initially with a spectral emissivity curve nearer to that of a true grey body, and so with less room—so to speak—for subsequent change in emissivity, due to any cause whatever.

Once again, for vacuum lamps as for gasfilled, the effects of d.c. operation are seen to be largely reversible, so that regular periodic reversal of the supply, when d.c. must be used, should help to retain the low ageing rates characteristic of burning on a.c. For gasfilled lamps, regular reversal every two hours or less was shown to be certainly adequate for this. The steepness of the effect on the vacuum lamps resulting from the reversal of polarity at B (see figure) suggests that for these the reversals should preferably be at shorter intervals than two hours. Reversal on each normal occasion of use should again in practice be a convenient way of fully retaining the low a.c. rate of ageing while actually using the lamps on a d.c. supply.

ACKNOWLEDGEMENT

The work described above has been done as part of the research programme of the National Physical Laboratory, and this paper is published by permission of the Director of the Laboratory.

REFERENCES

(1) BARNETT, W., BERRY, R. G., and PRESTON, J. S. *Brit. J. Appl. Phys.*, **8**, p. 363 (1957).
(2) LEEDS, R. E., and WINCH, G. T. *G.E.C. J.*, **22**, p. 232 (1955).
(3) WINCH, G. T. *Trans Illum. Engng Soc.*, **21**, p. 92 (1956).

By H. W. Emerton

See pages 306–312

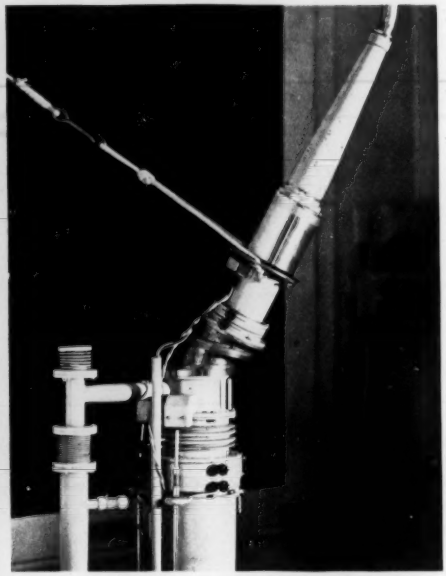

Fig. 1. The type EM3 microscope (by Metropolitan-Vickers Electrical Co. Ltd.) adapted for reflexion work at an angle of beam deviation of 26·5°

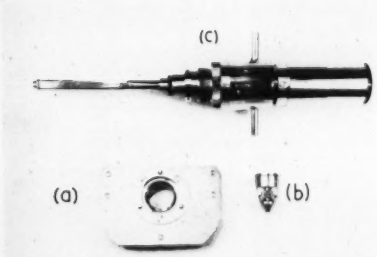

Fig. 2. Heating stage for the Elmiskop 1 electron microscope (by Siemens and Halske), showing new object carriage (*a*), high temperature object holder (*b*), and the two-pin plug rod insert (*c*)

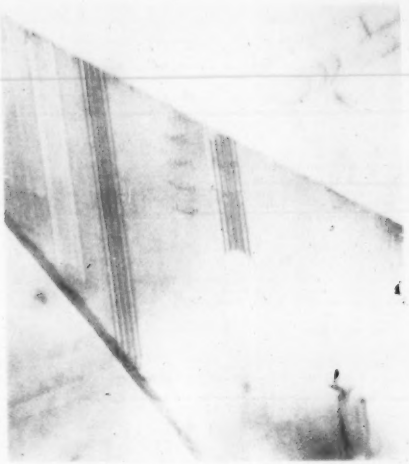

Fig. 3(*a*). A thin, stainless steel crystal showing electron optical interference fringes at the stacking faults, produced by the splitting of dislocations into widely separated partial dislocations under the action of the thermal stresses produced by the fine focus electron beam (×40 000)

Fig. 3(*b*). The same area as in Fig. 3(*a*) after the partial dislocations have recombined. The stacking faults, and hence the interference fringes, have been removed. The slip trace bands are interpreted in terms of the interaction of the moving dislocation with the oxide film on the surfaces of the foil (×40 000)

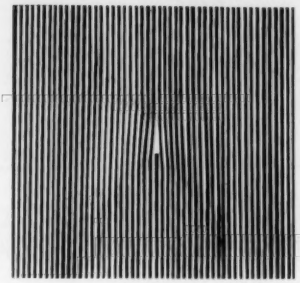

Fig. 4(*a*). A line grating containing a dislocation

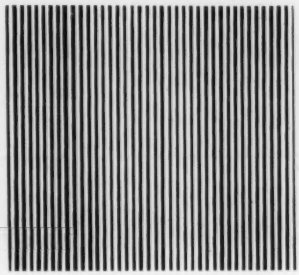

Fig. 4(*b*). A line grating without a dislocation and of slightly larger spacing than Fig. 4(*a*)

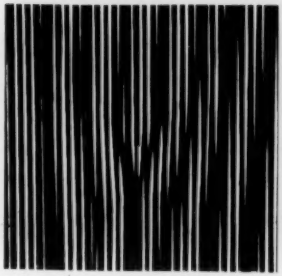

Fig. 4(*c*). "Parallel" moiré pattern formed by superposing Figs. 4(*a*) and (*b*) and illustrating appearance of dislocation in the moiré pattern

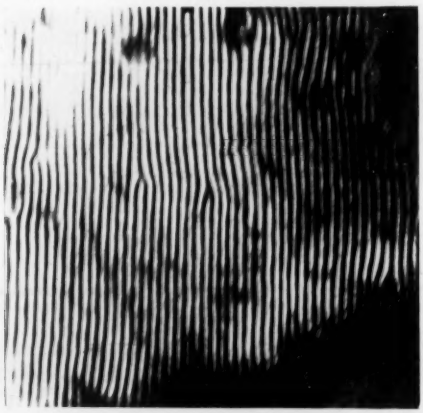

Fig. 5. Moiré pattern from parallel gold and palladium crystals, showing indirect resolution of (220) planes. Spacing of pattern is 35 Å approximately (× 500 000)

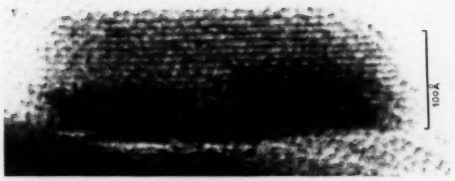

Fig. 6. Direct resolution of (020) planes of molybdenum trioxide; the spacing of the planes is 6·93 Å

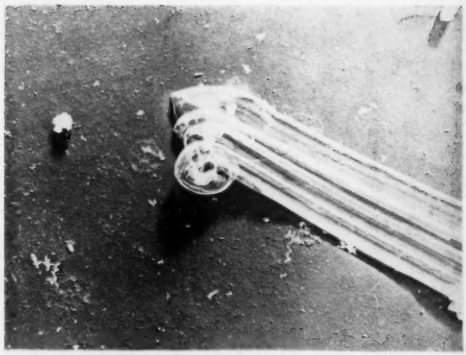

Fig. 7. Carbon replica of a tin whisker (ribbon form) which has its tip curled over (× 9000)

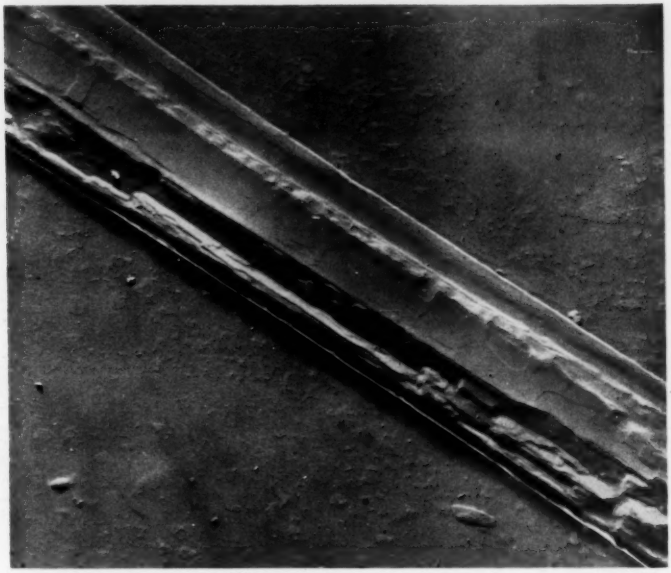

Fig. 8. Carbon replica of a sodium chloride whisker shadowed 2 : 1 with gold-palladium. The edges of growth layers can be clearly seen on the sides of the central ridge (×9900)

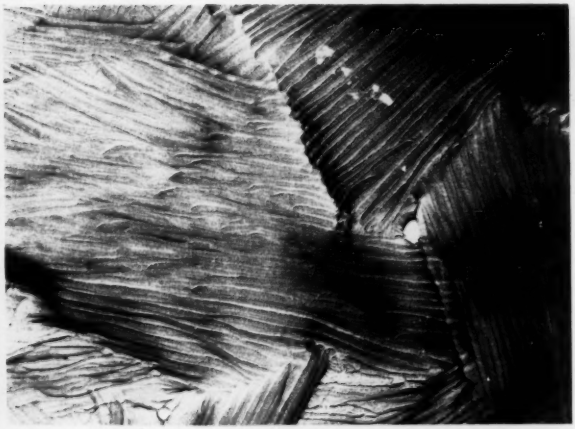

Fig. 9. Polygonal areas in continuous film of linear polyethylene Marlex 50 (×12000)

Fig. 10. Amorphous polyethylene terephthalate (undrawn Terylene) (×15 000)

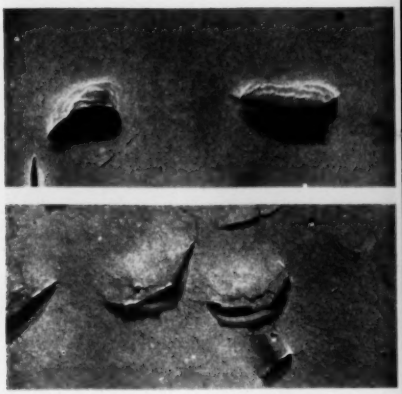

Fig. 11. α''–$Fe_{16}N_2$ iron nitride precipitates formed in an open hearth steel (×10 000)

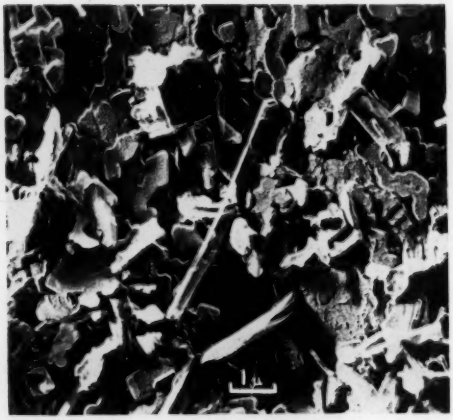

Fig. 12. Adaxial leaf surface of a daffodil

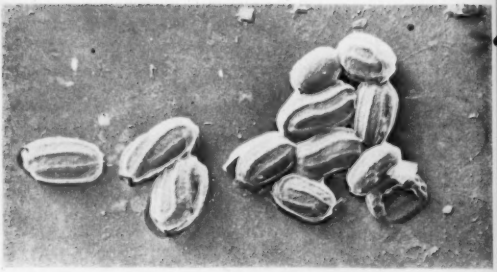

Fig. 13. Carbon replica of spores of *Bacillus macerans* (×8500)

The dependence of stress distribution on elastic constants

By MARGERY CLUTTERBUCK, M.Sc., A.Inst.P.,* University College, London

[*Paper first received* 30 *September*, 1957, *and in final form* 7 *February*, 1958]

Experimental methods in stress analysis are becoming increasingly important in the design of engineering structures, particularly in the aircraft and associated industries. In this paper, the effect of the elastic constants on certain stress distributions is investigated using the photoelastic technique. Similarity in stress distributions is obtained by suitable adjustment of the loads with respect to the Young's moduli of the materials from which the models are made, but no such adjustment is possible to compensate for the differences in their Poisson's ratios. The error introduced by this effect is considered by reference to problems of a particular type, from which some general conclusions are drawn.

The study of stress distribution in elastic plates has many important applications in engineering practice; such variations as may be due to different values of the elastic constants are therefore of great interest, particularly in the use of photoelasticity as a method of exploring practically the stress distribution in elastic plates and other models.

The dependence of the stress distribution on the two constants of elasticity for three-dimensional models has been shown in the theoretical solutions of the few problems which have been considered. It follows from the fact that all isotropic elastic non-accelerating stress states are solutions of the equation in the displacement **D** given by

$$\text{grad div } \mathbf{D} + 2(1 - 2\eta)\nabla^2\mathbf{D} = 0 \qquad (1)$$

where η is Poisson's ratio.

For a given geometrical shape loaded in a given manner, the stress in a model of a given material divided by some relevant nominal stress is a non-dimensional quantity. Since it involves the elastic constants, it must involve them in a non-dimensional manner, and with two arbitrary elastic constants E and $G = E(1 + \eta)$ this implies a function of η only. It does not follow that the difference in the stresses expressed non-dimensionally for two different materials is a function only of the difference of the Poisson's ratio. The dependence of stress on η will also apply to two-dimensional stress systems, except in one particular case when the resultant force over each boundary vanishes separately and the boundary conditions only involve the stresses. It has been shown theoretically that under these conditions for "plane strain" or "generalized plane stress" the stress distribution in a body is independent of the constants of elasticity. When the boundary displacements are specified, the boundary conditions for the stress functions involve the elastic constants, and the dependence of the stress distribution on the elastic constants will be much more complex.

Problems of this type are very varied. Very simple general conclusions are drawn concerning these later on. First the two- and three-dimensional stress distributions produced by stated stresses or point loads applied to the boundary were investigated experimentally and theoretically.

PREVIOUS WORK

Few quantitative results are available from the theoretical considerations of previous authors. Most important of these is a result first due to Michell[1] which is most adequately summarized by Muskhelishvili[2] who states that "The same stress functions (and therefore the same stresses) will give the solution for the distribution of stress for bodies of different materials with different values of Poisson's ratio if, and only if, the resultant vectors of the external forces applied to each boundary of the body separately are zero, then, and only then, the state of stress does not depend on the elastic constants." Furthermore, a resultant force over any boundary can only exist in multiply-connected regions.

The most powerful attempt to assess the effect of Poisson's ratio on stresses in multiply-connected regions of this type was made by Filon.[3] He showed that if the distribution of stress for a given material with modulus of elasticity E_0 and Poisson's ratio η_0 under given boundary conditions is known, then the distribution for any other material of Poisson's ratio η_1 can be obtained by the addition of certain stress distributions obtained by what Volterra[4] has named "distortions" and for which Professor Love[5] proposed the term "dislocations." (The work by Filon can also be approached by the complex potential method, giving the same result.)

Filon applied this method to finding the corrective terms which have to be added to the stress system observed in a ring, and his investigations showed that, in this case, the correction due to variation in the ratio of the elastic constants is very small.

Another important result stated by Filon is that these corrective terms are proportional to the difference of the two values of Poisson's ratio and to the force resultant, and are independent of the way in which the force is applied. The application of a dislocation is discussed later.

Two conclusions can be noted from Bickley's[6] results in his paper on the stresses around a circular hole in a plate under several different methods of application of the load to the boundary of the hole. The general effect of an increase in Poisson's ratio is in the direction of diminishing the maximum stress intensities, and in considering those modes of loading on the hole which give a net resultant force, the terms dependent on Poisson's ratio are the same. Bickley does not draw attention to this latter fact. It is possible to show that these terms are the same for any distributions of boundary stress with distributed or point loads.

All the cases quoted by Bickley can be derived from a later and more general treatment by Stevenson,[7] with whose results there is complete agreement, and the general solution for any type of distributed load on the hole boundary has already been published. The theory as used by Stevenson involving complex potentials has been used[8] to give a perfectly general theorem for dislocations as well as for exact values of stress for comparison between theory and experiment.

There are very few complete solutions for general three-dimensional stress problems of practical significance. The most widely used solutions are those due to Neuber which involve infinite bodies with either internal cavities or external notches. The three-dimensional deep external

* Now at the General Electric Co. Ltd., Stanmore, Middlesex.

circumferential notch in an infinite cylinder loaded under pure tension is considered later.

THEORETICAL CONSIDERATIONS

Two dimensional

Considering a specific case, the simplest multiply-connected region is the hole in the infinite plate. This corresponds to the practical case of rivets or bolt holes in large plates. The simplest form of loading is that due to a point load, which will tend to the case for real bolt or rivet loads except near to the contact areas. For this case, the errors involved in model tests are given by:

$$\left.\begin{aligned}\widehat{rr} &= \frac{-P\,.\,\Delta\eta\,.\cos\theta}{4\pi r^3}(r^2-a^2)\\ \widehat{\theta\theta} &= \frac{-P\,.\,\Delta\eta\,.\cos\theta}{4\pi r^3}(r^2+a^2)\\ \widehat{r\theta} &= \frac{-P\,.\,\Delta\eta\,.\sin\theta}{4\pi r^3}(r^2-a^2)\end{aligned}\right\} \qquad (2)$$

where r, a, P and θ are defined by Fig. 1 and $\Delta\eta$ is the difference in the Poisson's ratio of the two specified materials. It can be seen from these equations that the maximum value of $\Delta\widehat{rr}$ and $\Delta\widehat{\theta\theta}$ occurs on the line $\theta = 0°$ and the maximum value of $\Delta\widehat{r\theta}$ occurs on the line $\theta = 90°$.

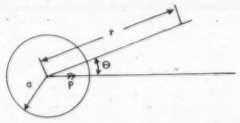

Fig. 1. Loaded hole in an infinite plate

The actual stress distribution due to a point load applied to the boundary of the hole in the plate was obtained in "closed form."[7] These stresses are given by the following equations:

$$\left.\begin{aligned}\widehat{rr}+\widehat{\theta\theta} &= \frac{-2P(r\,.\cos\theta-a)}{\pi(r^2+a^2-2ar\cos\theta)}+(3-\eta)\,.\,\frac{P\cos\theta}{2\pi r}\\ \widehat{rr}-\widehat{\theta\theta} &= \frac{P[-2r^5\cos\theta+2a(r^2+a^2)r^2\cos 2\theta-5a^2r^3\cos\theta-a^2r^3\cos 3\theta+4ar^4]}{\pi r^2(r^2+a^2-2ar\cos\theta)^2}\\ &\quad+\frac{(3-\eta)P(r^2-2a^2)\cos\theta}{4\pi r^3}+\frac{P[-4a+r\cos\theta(1+\eta)]}{4\pi r^2}\\ \widehat{r\theta} &= \frac{P[-r^2\sin 2\theta(2ar^2+2a^3)+5a^2r^3\sin\theta+a^2r^3\sin 3\theta]}{2\pi r^2(r^2+a^2-2ar\cos\theta)^2}\\ &\quad+\frac{(3-\eta)P(r^2-2a^2)\sin\theta}{8\pi r^3}-\frac{Pr^2(1+\eta)\sin\theta}{8\pi r^3}\end{aligned}\right\} \qquad (3)$$

in which the η dependent terms are in agreement with those given in equations (2).

The theoretical values of the principal stresses on line A with $\theta = 0°$ and line B with $\theta = 90°$ were calculated from equations (3) for $\eta = 0{\cdot}36$ and a load of 40 lb/in. thickness, so as to be directly comparable with experiment; the differences in the principal stresses due to a change of $0{\cdot}12$ in the value of Poisson's ratio were also calculated from equation (2).

Values of the principal stresses and their differences due to the change in Poisson's ratio are shown in Table 1. These

Table 1. *Two-dimensional theoretical investigation*

Principal stresses and their differences due to a change in Poisson's ratio

r/a	$\widehat{rr}$	$\Delta\widehat{rr}$	$\widehat{\theta\theta}$	$\Delta\widehat{\theta\theta}$	$\widehat{r\theta}$	$\Delta\widehat{r\theta}$
10	−12	−0·30	+2	−0·30	+1·8	−0·32
8	−16	−0·38	+3	−0·40	+2·3	−0·40
6	−23	−0·50	+4	−0·53	+3·3	−0·52
4	−42	−0·72	+9	−0·8	+5·9	−0·72
3	−80	−0·9	+15	−1·2	+9·1	−0·88
2	−160	−1·15	+30	−1·9	+16	−1·16
1·5	−370	−1·16	+54	−2·9	+20	−1·16
1·25	−800	−0·88	+80	−4·0	+17·6	−0·88
1·12	−1860	−0·56	+100	−4·87	+11·6	−0·56
1·05	−5100	−0·23	+120	−5·64	+4·8	−0·23
1·0	—	0	+135	−6·12	0	0

$\widehat{rr}$, $\widehat{\theta\theta}$ and $\widehat{r\theta}$ are quoted in lb/in.^{2}

results demonstrate the rapid increase in the stress $\widehat{rr}$ in the immediate vicinity of the load and the small differences in the principal stresses due to a change in Poisson's ratio of $0{\cdot}12$.

Near to the load, the stress distribution is dependent on the contact conditions, and comparable results can only be obtained by ensuring exact similarity of contact. If the load is transmitted through an effectively rigid pin, the contact area varies inversely with the elastic modulus, and stresses very near to the loaded surface can be obtained to a reasonable degree of accuracy from model tests if the loads are in the proportion of the moduli, as shown in Fig. 2.

This is in accordance with theoretical predictions by Hertz[9] and others, that where two elastic regions of general shape are pressed into contact, the local stresses are likely to depend on the two elastic constants of each of the two materials.

Three-dimensional

The stresses for a deep external circumferential hyperbolic notch loaded under pure tension were calculated according to the solution of Neuber.[10]

The hyperbolic notch considered is given by curvilinear co-ordinates.

$$\left.\begin{aligned}x &= K\sinh u\cos v\\ y &= K\cosh u\sin v\cos w\\ z &= K\cosh u\sin v\sin w\end{aligned}\right\} \qquad (4)$$

The plane of minimum cross-section is given by $u = 0$, thus for this plane, $\sinh u = \tanh u = 0$ and $\cosh u = 1$. The notch boundary is given by $v = v_0$ and the x-axis by $v = 0$, thus the limiting values of $\cos v$ are $\cos v_0$ and 1. Radius of the narrowest section is a; radius of curvature at the base of notch is ρ; Poisson's ratio is η.

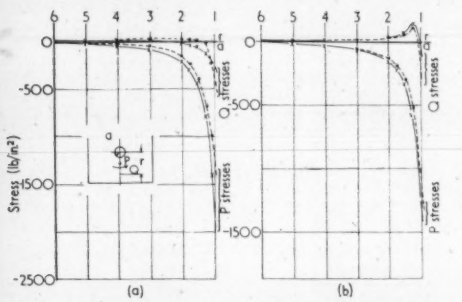

Fig. 2. Effect of change of Poisson's ratio on the stresses around a loaded hole in a plate. (One loaded hole.)
(*a*) Normal loading. (*b*) Equal strains
× —— × = cold loading. • - - - • = frozen stress.

The stresses on the narrowest section P, Q and R are

$$\left.\begin{aligned} P(\sigma_w) &= \frac{1}{h^2}\left[B\cos v + C(-3+2\eta)\cos v\right] + \\ &\quad + \cos v\,(-A+B+C\cos^2 v)\frac{1}{h^4} \\ Q(\sigma_w) &= \frac{1}{h^2}\left[\frac{A\cos v}{1+\cos v} - B\cos v + \right. \\ &\quad \left. + C(-2\eta)\cos v\right] \\ R(\sigma_v) &= \frac{1}{h^2}\left[\frac{-A\cos v}{1+\cos v} + (1-2\eta)\,C\cos v\right] + \\ &\quad + \cos v(A-B-C\cos^2 v)\frac{1}{h^4} \end{aligned}\right\} \quad (5)$$

where $A = (1-2\eta)(1+\cos v_0)C$; $B = A - C\cos^2 v_0$

$$C = -\frac{W}{2}\left[\frac{1+\cos v_0}{1+\cos v_0 \,.\, 2\eta + \cos^2 v_0}\right]$$

and $h = \cos v$, $\tan v_0 = \sqrt{(a/\rho)}$ and $W = T/\pi a^2$, T being the load applied to the model. (P is the axial, Q the circumferential and R the radial stress.)

These equations show that the dependence on Poisson's ratio of the stresses P, Q and R on the narrowest section of the model is not linear.

The values of the constants for the particular model that was examined experimentally were

$a = 0{\cdot}25$ in. $\qquad \eta = 0{\cdot}36$ and $0{\cdot}48$
$\rho = 0{\cdot}12$ in. $\qquad T = 50$ lb

giving the theoretical stresses P, Q and R, and the differences in the stresses ΔP, ΔQ and ΔR due to the change in Poisson's ratio of $0{\cdot}12$, shown in Table 2. They demonstrate that there is a difference of less than 2% everywhere on the section for the P and R stresses with an 8% difference on the circumferential stress Q at the notch boundary, this difference decreasing to zero at the centre of the model.

Table 2. *Three-dimensional theoretical investigation*

Principal stresses and their differences due to a change in Poisson's ratio

r/a	P	ΔP	Q	ΔQ	R	ΔR
0	437	+4	113	−10	0	0
0·1	342	+1	101	−8	40	+2
0·215	263	0	90	−5	61	+1
0·375	219	−2	81	−3	69	0
0·48	200	−3	77	−2	71	+1
0·63	184	−3	74	−1	71·4	+0·4
1·0	171	−3	71	0	71	0

P, Q and R are quoted in lb/in.²

The values of the stress differences $(P - Q)$ and $(P - R)$ were also calculated and the largest variation of stress difference was 4½% in values of $(P - Q)$. These differences are compared with experimental values in Table 4.

METHODS OF MEASUREMENT

Two-dimensional models

The two-dimensional models considered were plates of various widths made of glass and Araldite type B. They were loaded by a pin through a hole in the plate in which the resultant force on the hole boundary is not zero, and the stress distribution across any section is dependent on the value of Poisson's ratio. The Araldite models were loaded at room temperature when the Poisson's ratio of the material is 0·36 and secondly they were subjected to a heat cycle during which the stresses were "frozen" into the model,[11] the Poisson's ratio of the material at the elevated temperature being 0·48; the Poisson's ratio for glass is 0·25.

The models were examined in the normal polariscope, sketches being made of the isoclinic and isochromatic fringes in plane and circularly polarized light; fractional fringe measurements were made on some sections of the models using the Sénarmont method.

As it was impossible to estimate visually the number of fringes under the loading pin in some cases, a special form of measurement was used. The projection lens and screen of the normal polariscope were replaced by a travelling microscope, the collecting lens being positioned so as to produce an enlarged image, suitably placed for the objective of the miscoscope. The number of fringes under the load and their distance apart could then be measured very accurately.

Three-dimensional model

The three-dimensional model was a cylinder of Araldite type B with a symmetrically placed hyperbolic groove. It was first loaded under compression at room temperature and examined in the scattered light apparatus, values being obtained of the principal stress differences across the diameter of the narrowest section. The same model was then loaded under a compressive load at an elevated temperature, so that the stresses were "frozen" into the model. It was examined in the scattered light apparatus as for the cold-loaded model, and similar measurements of principal stress differences recorded.

The models were set up as shown in Fig. 3 in order that maximum intensity of the scattered light fringes could be obtained, the measurements being made in the normal manner using a uniform field compensator and travelling microscope.

A more complete comparison of the experimental and theoretical results was obtained by the calculation of the separate stresses in the frozen stress three-dimensional model, employing the usual slicing technique[12] and viewing the slices of the model in the normal polariscope.

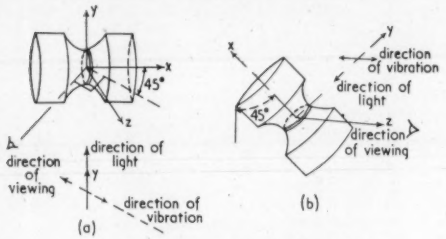

Fig. 3. The three-dimensional model
(*a*) Frozen-stressed model. (*b*) Cold-loaded model.

SEPARATING THE STRESSES IN THE TWO-DIMENSIONAL MODELS

The Lamé–Maxwell equations

These equations were used for separating the stresses along a line of symmetry—that for integration along a p line being equation

$$\partial P/\partial s = -(P - Q)/\rho_1$$

where s is the increment along the p line, and ρ_1 the radius of curvature of the transverse q line of stress.

The shear difference method

This method was used for separating the stresses along any line other than a line of symmetry.

The normal stress σ_x is calculated from

$$\partial\sigma_x/\partial x = -\delta\tau_{xy}/\delta y$$

where $\delta\tau_{xy}$ is the change in shear stress in the y-direction. If both $(P - Q)$ and σ_x are known, P and Q can be found.

TWO-DIMENSIONAL INVESTIGATION

Dislocation stresses

Before considering the experimental work, the practical application of dislocation stresses in transferring states of stress from one material to another was investigated.

It has been shown[8] that for any stress (normal or shear) at any point in a given geometric shape subjected to given boundary stress conditions, the following conditions apply:

$$[\sigma_{metal}]_{load} = [\sigma_{model}]_{load} + [\sigma_{model}]_{dislocation} \qquad (6)$$

where for any load there is unique dislocation of a particular type and magnitude.

Dislocations are defined as states of stress arising from continuous strains *but* from discontinuous displacements. These can happen in only two ways as illustrated in Fig. 4. The multiply-connected region bounded outside by the contour L and inside by the contours $L_1 \ldots L_m$ can have dislocations arising from each of the interior contours $L_1 - L_m$. Considering L_1, let a cut, not necessarily straight, have two faces CDE and $C^1D^1E^1$ which are coincident in the unstrained state. Dislocations are such that curve CDE is moved as a rigid body relative to $C^1D^1E^1$ and there are two possibilities, the angles between the two faces are preserved, as in Fig. 4(*b*), or the edges suffer relative rotation as in (*c*). The dislocation required for this "stress correction" is that of pure translation. The dislocation is defined from the vector displacement of each point **D** by the quantities

$\alpha_1 + i\alpha_2 = \oint d\mathbf{D}$ for a complete path enclosing the contour L_1 in an anti-clockwise direction. It is therefore the displacement of the face $C^1D^1E^1$ minus the displacement of face CDE and in Figs. 4(*b*) and (*c*) both α_1 and α_2 are negative, α_1 and α_2 being the x and y components of this dislocation.

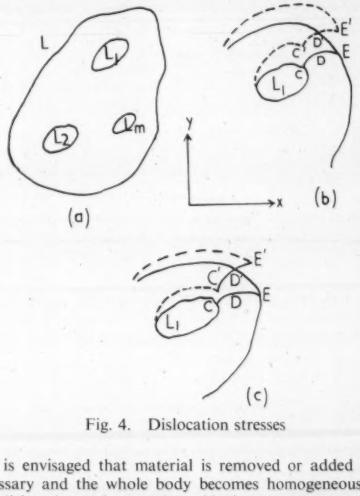

Fig. 4. Dislocation stresses

It is envisaged that material is removed or added where necessary and the whole body becomes homogeneous after the dislocation. In practice, this is not necessary if we appeal to St. Venant's principle, so long as moments and forces are applied at the cut corresponding to the appropriate dislocation.

The magnitude of this dislocation is given by:

$$\alpha_1 + i\alpha_2 = i[(X + iY)/E_{model}](\eta_{metal} - \eta_{model}) \qquad (7)$$

where X and Y are the resolutes of the force resultant per unit thickness acting on the contour L_1, independent of the shape of L_1 and of the way in which the force is applied.

Thus

$$\alpha_1 = -(Y/E_{model}) \times \Delta\eta \text{ and } \alpha_2 = (X/E_{model}) \times \Delta\eta \qquad (8)$$

As an example, a lifting bolt was given a load of 30 lb in an Araldite model $\frac{1}{4}$ in. thick; with normal Cartesian co-ordinates $X = 0$, $Y = -120$ lb in.

$$\alpha_1 = [120/(5 \times 10^5)](0{\cdot}29 - 0{\cdot}36) = -1{\cdot}7 \times 10^{-5}$$

Such a dislocation is too small to measure, so in practice it is preferable to obtain a suitable dislocation, measure it and apply the information obtained to the problem. Fig. 5 shows a reasonably successfully translation, a separation of a vertical cut by an amount 0·062 in. Thus the stress from Fig. 5 at any point must be *divided* by a factor

$$-0{\cdot}062/(-1{\cdot}7 \times 10^{-5})$$

i.e. 4000 and added to the stress obtained from the first Araldite model. It should be noted how small such additions would be, in this case, 0·025% of the stresses at any point of the model.

The separation in Fig. 5 was achieved by forces and moments applied to brass strips riveted to the Araldite. Owing to pin yield and other causes, the true dislocation to which the stresses in Fig. 5 correspond may differ from 0·062 in. by an error which may be as large as 10%.

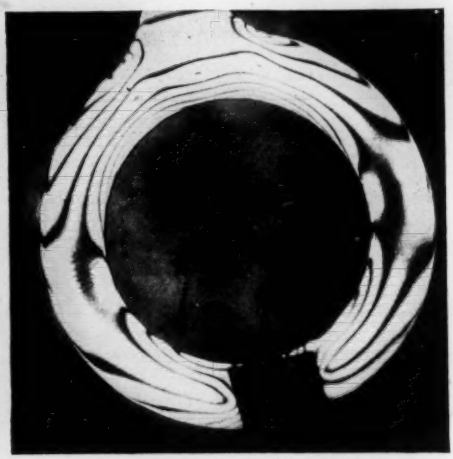

Fig. 5. Dislocation stresses in a lifting bolt

In order to apply St. Venant's principle in this work—that the stresses produced differ from those for the dislocation envisaged in the theory, only in the neighbourhood of the cut—it is essential to remove the cut as far as possible from the points of interest.

Experimental work

In order to establish the accuracy with which measurements could be made on two-dimensional models, a test was made on a tension bar with a symmetrically placed hole, both under cold-loaded and frozen-stressed conditions. The results are shown diagrammatically in Fig. 6 for the principal stress difference along the extended diameter of the unloaded hole, perpendicular to the line of loading. The actual differences for the maximum values of stress difference in the regions of highest stress are, for the two types of loading, of the order of 3%, representing an error of 45 lb/in.^{2}; the differences for the remainder are less than 4%.

These are all within the limits of experimental error, estimated from observations taken for the calibration of the material, the loads applied to the model, and the direct polariscope and linear measurements. Moreover, it is not possible to improve the accuracy of such observations using the existing photoelastic methods and materials.

As the tests on the other two-dimensional models are of a similar nature the errors of observation may be expected to be similar to those encountered in this model.

(*a*) *One loaded hole in an Araldite plate.* The first two-dimensional model to be investigated for the Poisson's ratio effect was a $\frac{1}{4}$ in. thick plate loaded by a $\frac{1}{8}$ in. diameter pin through a symmetrically placed $\frac{1}{4}$ in. diameter hole in the plate. Initially a steel loading pin was used, but as the contact area was small and the stress concentration immediately under the pin excessive, an Araldite loading pin with a steel core was used in all the remaining experimental work. The plate was examined in the polariscope both when cold loaded and after it had been subjected to a frozen stress cycle.

A second pair of plates, with a load per unit thickness proportional to the Young's moduli of the cold-loaded and frozen-stressed Araldite (ensuring approximately equal area of contact between the pin and the hole boundary) were also examined.

The results of subsequent measurements and calculations on these plates are shown in Figs. 2(*a*) and (*b*). The very large differences in the stresses immediately below the load shown in Fig. 2(*a*) are modified considerably in Fig. 2(*b*), although the differences decrease rapidly away from the boundary of the hole in both cases. (It should be stated that a further error is introduced to those already considered when line integrations are made for the principal stresses.) Similarly, the difference in boundary stresses around the loaded hole is generally small, and within the limits of experimental error except in the immediate vicinity of the load.

The conclusions which can be drawn from these investigations is that, in the first plate examined, the loading conditions influence the state of stress between the pin and the plate,

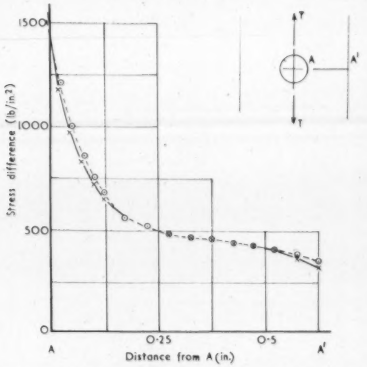

Fig. 6. Unloaded hole in a tension bar. Principal stress difference along A–A'
× — × = cold loading. ○ - - - ○ = frozen stress.

as well as the effects due to changes in Poisson's ratio. One of these effects, namely the contact area between the pin and the plate, is reduced considerably in the stress investigation of the second pair of plates, although the difference in contact conditions is not entirely eliminated. It is inevitable that there will be certain differences in the tangential forces due to friction between the pin and the hole, since changes in temperature in the frozen stress method will produce a certain amount of relative contraction between the pin and the plate. The results of these effects would be to produce differences of the type observed in the normal and tangential stresses directly under the pin.

No differences in the principal stresses on the sections examined were observed which could be attributed to the different values of Poisson's ratio.

(*b*) *Three horizontal and three vertical holes in an Araldite plate.* Real problems are likely to have more than one loaded boundary. The possibility that errors due to a difference in Poisson's ratio might be additive was investigated, using plates with multiple-loaded holes. Two similar plates with three symmetrically placed holes, the centres of which were either on a line perpendicular to the line of loading or on the line of loading, were examined, the same load being applied to each hole.

The results of these investigations followed the same pattern as for the first one-loaded hole plate of the previous section. The differences in boundary stresses around the loaded holes and along the line of symmetry are again within the limits of experimental error except in the immediate vicinity of the load, where differences due to different contact conditions inevitably occur. There was no evidence of a measurable difference in stress distribution due to a change in value of Poisson's ratio, or of an additive effect attributable to the latter in the case of multiply-loaded holes.

(*c*) *The round-ended bar.* A further engineering practical shape is the lug. This was the last type of two-dimensional model to be investigated, the round-ended bar being loaded first by a small pin and then by a fitting pin through a hole in the bar, the latter being concentric with the round end of the bar, and of diameter one-third the width of the bar.

The results, calculated from the measurements made on these models for the principal stresses on the line of symmetry and under the load, are shown in Figs. 7(*a*, *b*). The trend of

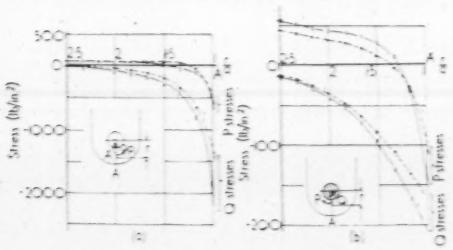

Fig. 7. Effect of change of Poisson's ratio on the stresses around a loaded hole in a plate. (Round-ended bars.) Principal stresses on the line of symmetry. (*a*) Small loading pin. (*b*) Large loading pin
× —— × = cold loading. ● - - - - ● = frozen stress.

these results is very similar to those for the preceding models and it can be concluded that the contact area between the pin and the plate is again the important factor. Away from this area, the differences between the principal stresses of the cold-loaded and frozen-stressed models are within the limits of experimental error, and no differences were observed which could be attributed to the change in the value of Poisson's ratio.

Comparison of the theoretical and experimental results

The theoretical calculations made for the two-dimensional plate give directly the principal stresses on certain sections, whilst the measurements made on the experimental plates were of the principal stress differences and directions, line integrations being necessary to find the principal stresses. As errors are likely to occur in the latter, consideration is first given to the values of principal stress differences, and secondly, to the principal stresses.

A separate table of such values of principal stress differences for the one-loaded hole models and for the theoretical results for the point load on an infinite plate are given in Table 3.

Table 3. *The two-dimensional models*

Comparison of the theoretical and experimental results. Principal stress differences on the line of symmetry

	Theoretical results		*Unequal strains*		*Equal strains*	
r/a	*Cold loading*	*Frozen stress*	*Cold loading*	*Frozen stress*	*Cold loading*	*Frozen stress*
10	−14	−15	−42	−40	−36	−44
8	−19	−20	−17	−7	−15	−16
6	−27	−28	−21	−16	−18	−20
4	−51	−53	−52	−35	−42	−41
2	−190	−193	−185	−180	−175	−174
1·75	−280	−284	−255	−250	−250	−237
1·5	−424	−428	−386	−380	−372	−352
1·25	−880	−885	−670	−660	−710	−633
1·12	−1960	−1965	−1225	−925	−1150	−1000
1·0	—	—	−1900	−910	−1313	−960

Principal stress differences are quoted in lb/in.²

In comparing these values, the differences, both from plate-to-plate and from cold loading to frozen stress, are within the limits of experimental error up to ¼ in. from the boundary of the loaded hole on the actual model. Between this point and the boundary of the loaded hole, the theoretical values of the principal stress difference increase markedly over the experimental value, a result due directly to the method of loading which has been adopted in the theoretical calculations. The theoretical and experimental results for the principal stresses show the same trend as for the principal stress differences.

Although the measurements quoted from the dislocation work were obtained on a different type of two-dimensional model, the order of the differences in the stresses due to a change in Poisson's ratio was also very small.

THE THREE-DIMENSIONAL INVESTIGATION

The three-dimensional model was a cylinder with a symmetrically placed hyperbolic groove, the model being made from Araldite B. A little finely divided silica was added to the Araldite to improve the light scattering properties of the latter. The same model was cold-loaded and examined in the scattered light apparatus, placed under a frozen stress cycle and then re-examined, both in its entirety and when sliced, in the scattered light apparatus and normal polariscope (see Fig. 3).

The same measurements were taken on the model for both types of loading and gave values of the stress differences $(P - Q)$ and $(P - R)$ where P is the axial stress, Q the circumferential stress and R the radial stress on the section of minimum area. These stress differences, calculated from a load of 50 lb are given in Fig. 8.

Considering first the experimental error of this type of measurement, it is impossible to measure the position of the black zero fringe very close to the entry of the beam of light into the model; the tangent to the graph at the origin of such a series of scattered light observations, and thus the

stress differences represented by this tangent, is therefore liable to a large error. This is estimated to be of the order of 30 lb/in.^{2} for the maximum stress difference at the boundary in both the cold-loaded and frozen-stressed models, or an error of 150 in the scale used in Fig. 8.

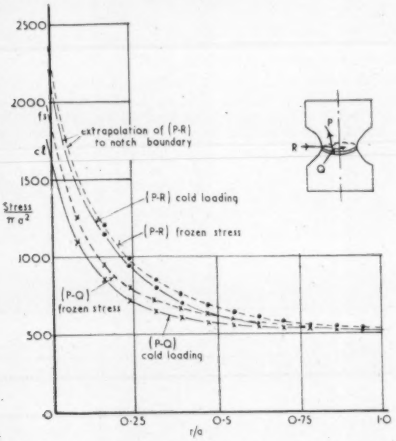

Fig. 8. Deep external hyperbolic notch. Scattered light measurements

Thus an examination of the values of the stress differences $(P - Q)$ and $(P - R)$ obtained in the two models divided by the minimum area of cross-section and illustrated in Fig. 8 shows that any variations are of the same order as the possible errors of observation. (It should be pointed out that the stress differences $(P - R)$ can, however, only be compared in the central region over which measurements were possible. Measurements for values of $(P - R)$ cannot be made very near to the boundary and thus the extrapolations of the $(P - R)$ curves to the boundary are unreliable, the value of $(P - R)$ increasing rapidly in this region.)

It must therefore be concluded that any effect due to the change in Poisson's ratio is of an order not greater than that of the errors of observation, that is, about 7%.

Further results were obtained as to the principal stresses on the plane of minimum cross-section for the frozen stress model, but these are not given here as they can only be compared with the theoretical result.

Comparison of the theoretical and experimental results

Comparisons can be made between the principal stress differences $(P - Q)$ and $(P - R)$, the values of the former being given in Table 4.

Considering first the theoretical values, there is little difference between the two sets of figures calculated for the values of Poisson's ratio which are appropriate to the two types of loading used on the Araldite models in the experimental work. Such a difference as does exist is a maximum at the notch boundary, and is of a magnitude less than the possible experimental error. Such differences would thus be impossible to measure.

Table 4. *The three-dimensional model*

Comparison of the theoretical and experimental results. Principal stress differences $(P - Q)$

	Theoretical results		*Experimental results*	
	Cold loading	*Frozen stress*	*Cold loading*	*Frozen stress*
r/a	$\tau_i = 0{\cdot}36$	$\tau_i = 0{\cdot}48$		
0	−325	−310	−340	−383
0·08	−260	−247	−223	−251
0·16	−208	−200	−177	−189
0·24	−169	−162	−144	−162
0·31	−150	−144	−128	−147
0·39	−134	−130	−123	−136
0·55	−114	−113	−113	−120
0·7	−106	−106	−110	−114
0·86	−103	−104	−108	−108
1·0	−100	−103	−107	−105

Principal stress differences are quoted in lb/in.^{2}

CONCLUSIONS

The main conclusion which can be drawn from this work is that differences in experimentally determined stress distributions due to Poisson's ratio effects are less than the errors which would be introduced by other factors.

A further conclusion is that the complete transfer of stress, from the photoelastic two-dimensional models considered to the metal prototype, is possible if the loading conditions are accurately reproduced. If this type of loading is impractical, then the results obtained from the model can be transferred to the prototype, except in the immediate vicinity of the point of application of the load.

ACKNOWLEDGEMENTS

My thanks are due to Colonel H. T. Jessop and Mr. C. Snell for advice and encouragement in this work, and to Prof. H. St. J. Collins for his help in securing facilities for the completion of the research.

REFERENCES

(1) MICHELL, J. H. *London Math. Soc. Proc.*, **31** (1900).

(2) MUSKHELISHVILI, N. I. *Some Basis Problems of the Mathematical Theory of Elasticity* (Translated by J. R. M. Radok) (Groningen: P. Noordhoff Ltd., 1953).

(3) FILON, N. G. *Brit. Assoc. Rep.*, pp. 305–315 (1921).

(4) VOLTERRA, V. *Ann L'Ecole Normale* (III), **24** (1907).

(5) LOVE, A. E. H. *Treatise on the Mathematical Theory of Elasticity* (London: Cambridge University Press).

(6) BICKLEY, W. G. *Phil. Trans A*, **227**, p. 383 (1928).

(7) STEVENSON, A. C. *Phil. Mag.*, **34**, p. 766 (1943).

(8) CLUTTERBUCK, M. *M. Sc. Thesis* (University of London, 1955).

(9) HERTZ, H. *Gesammelte Werke*, **1**.

(10) NEUBER, H. *Theory of Notch Stresses.* David Taylor Model Bason Translation No. 74 (Berlin: Julius Springer, 1937).

(11) HETÉNYI, M. *J. Appl. Mech. A*, p. 149 (1938).

(12) JESSOP, H. T. *Brit. J. Appl. Phys.*, **2**, p. 249 (1951).

Pulse-annealing technique for metals and alloys

By P. WRIGHT, Ph.D., F.Inst.P., and K. THOMAS, B.Sc., Grad.Inst.P.,* University College of North Wales, Bangor, Caerns.

[*Paper received* 11 *December*, 1957]

An account is given of some improvements in the technique of pulse-annealing. Procedures for sharpening up the pulsing and quenching processes, and for accurately controlling the annealing temperature, are described. Some experimental results on Cu_3Au are given to illustrate the special uses of the pulse-annealing method.

1. INTRODUCTION

In the pulse-annealing method, a small solid specimen is rapidly heated to a predetermined temperature, annealed, and then quenched to a fixed temperature at which some physical property may be conveniently measured. Provided the lattice configurations corresponding to different annealing temperatures are retained during quenching, variations in the property due to changes in configuration can be studied in the absence of relatively large variations due to temperature. The advantages of this method in the study of relaxation processes have been discussed in detail by Parkins, Dienes and Brown,[1] who also developed a technique suitable for materials which can be heated directly by an electric current. Dienes[2] employed the pulse-annealing method to investigate the kinetics of ordering in the alloy AuCu, using electrical resistivity as an indicator. The conclusion reached by Bowen,[3] who analysed Dienes' results, was that the data were not sufficiently accurate to determine the kinetics of the transformation.

In developing a more precise method, the present writers have found it necessary to sharpen up the pulsing and quenching processes, and also to devise a means of accurately re-establishing and maintaining the required annealing temperature. The apparatus and techniques to be described are suitable for observing resistivity changes in metals.

2. APPARATUS

2.1 *Specimen holder*. A general view, with glass bell-jar enclosure removed, is given in Fig. 1. The specimen, a wire 1 mm in diameter and 6 cm long, is flattened near its ends and clamped between two copper blocks. The blocks are bolted to sheets of copper, and water-cooling pipes soft-soldered to the sheets serve both as supports and current leads. The pipes pass through a Perspex base-plate *via* brass bushes to which they are silver-soldered. Connexion to a vacuum system is made by a pipe passing through the base, the pipe terminating close to the middle part of the specimen.

2.2 *Thermocouples*. Platinum/platinum : 13% rhodium thermocouples, s.w.g. 44, are spot-welded to the specimen as indicated in Fig. 2(*a*). Three platinum wires on one side of the specimen serve as potential tappings for resistance measurement, and, with the platinum: 13% rhodium wires opposite to them, they form three thermojunctions for measuring the temperature of the intermediate metal. The brass bolts [Fig. 2(*b*)] through which the fine wires leave the base are designed to minimize stray thermo-electromotive forces.

It is desirable to have the thermocouple wires diametrically opposite on the specimen wire, and essential to avoid damaging the specimen in the process of spot-welding. Both objects may be accomplished by using an ordinary spot-welder with suitably designed electrodes, provided the welding current is reduced to the necessary minimum. As a lower electrode, a grooved copper plate will preserve wires

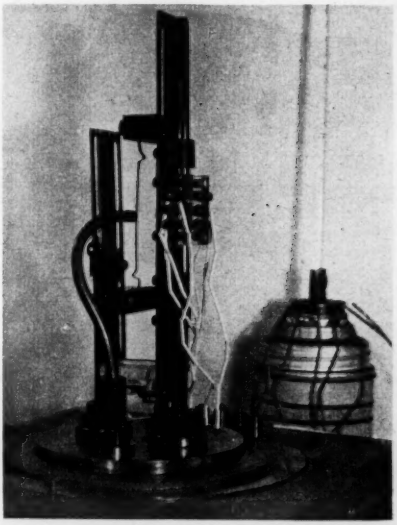

Fig. 1. Specimen holder

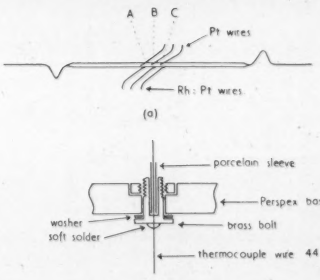

Fig. 2. (*a*) Specimen with thermocouples attached
(*b*) Brass bolt carrying thermocouple wire through base

* Now at the National Physical Laboratory, Teddington, Middlesex.

attached to one side of the specimen whilst wires are welded to the opposite side.

2.3 *Electrical circuits.* The specimen S is heated by current from a step-down transformer T (Fig. 3), rapid pulsing being produced by short-circuiting a resistance R_2 in the transformer primary circuit. Control of the annealing temperature is effected by balancing the electromotive force from one of the specimen thermocouples against a preset steady potential difference provided by a potential divider D; the out-of-balance potential difference due to temperature variation in the specimen is applied to a thermo-regulator which appropriately re-adjusts the heating current. A detailed account of the regulator has been given by Wright[4];

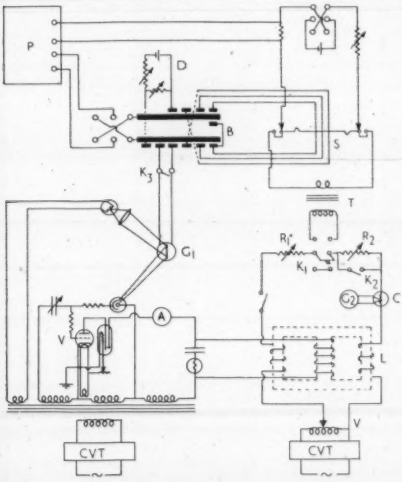

Fig. 3. Pulsing, measuring and thermo-regulator-circuits

A, milliameter; *B*, plug-board; *C*, vacuum thermocouple; *CVT*, constant voltage transformer; *D*, potential divider; G_1, thermo-regulator galvanometer; G_2, vacuum thermocouple galvanometer; K_1, change over key; K_2, K_3, shorting keys; *L*, part-saturated choke; *P*, Cambridge vernier potentiometer; R_1, R_2, resistances for adjustment of heating currents; *S*, specimen; *T*, step-down transformer; *V*, phase-controlled thyratron.

the circuit diagram is reproduced on the left-hand side of Fig. 3. The out-of-balance potential difference is applied to a galvanometer, the mirror of which reflects the image of a lamp filament on the cathode of a photocell. The amount of light falling on the cell determines the anode current in a phase-controlled thyratron. The anode load includes many turns on the centre limb of a partly saturated choke in series with the primary of the transformer T; thus by varying the inductance of the choke, a small anode current can control a heavy current through the specimen. The feedback reacts so rapidly on the temperature of the specimen that electrical or mechanical disturbances of the galvanometer cannot be tolerated; it may be found necessary to provide electrical screening and an anti-vibration support. A base for the galvanometer which can be rotated by a worm and pinion greatly facilitates the "zero adjustment" of the light falling upon the photocell.

A Cambridge vernier potentiometer P, with a d'Arsonval galvanometer (deflexion 175 mm/uA at 1 m), is used for measuring the temperature and resistivity of the specimen. The potentiometer is graduated in microvolts and the galvanometer gives a deflexion of 5 mm/μV; with certain precautions (see Section 3.3), measurements can thus be made to 0·2 μV. Resistivity observations are carried out at two or more temperatures near room temperature and the resistivity at a reference temperature, say 20° C, found by extrapolation. The steady current which produces the potential differences to be measured, across the specimen and a series standard resistance, also serves to heat the specimen to the required temperature. If a 200 ampere-hour, 2 V, accumulator is used to supply the current, the temperature of the specimen in a vacuum reaches a maximum value in about $\frac{1}{2}$ h, and variations in temperature whilst making resistance measurements rarely exceed 0·2° C.

For convenience and rapidity in the processes of pulsing, quenching, temperature and resistance measurement, copper wires from the thermocouple cold junctions, together with leads from potentiometers and thermostat, are all brought to a plug-board (*B*, Fig. 3). Here the wires are soft-soldered to terminal strips of copper on an insulating base.

2.4 *Vacuum system.* Annealing operations and resistivity measurements are conducted with the specimen in a vacuum. An oil diffusion pump, with charcoal trap, backed by a rotary pump is used to evacuate the bell-jar. Nitrogen is stored at atmospheric pressure in a large reservoir connected to the vacuum system near the bell-jar; an additional rotary pump is useful for removing nitrogen from the system after quenching.

3. EXPERIMENTAL PROCEDURE

3.1 *Preliminary operations.* To avoid straining the specimen when it expands, the flattened parts at the ends are given one or more "V" bends [Fig. 2(*a*)]. As this may produce appreciable local increases in resistivity, the specimen should be cautiously annealed in position at moderate temperatures before attempting any high temperature pulses. The settings of the Variac V and resistances R_1 and R_2 (Fig. 3), for a given annealing temperature are first found by trial. The key K_1 is then changed over and the current in the *primary* circuit of the transformer T measured by the vacuum thermocouple C. The heating current may then be preset for subsequent annealing at the same temperature without actually passing current through the specimen. The current settings are not highly critical since the final adjustment is made automatically by the thermo-regulator. Temperature gradients along the part of the specimen between the thermocouples can be eliminated, within the limits of accuracy of the thermocouple measurement of temperature (see Section 3.3), by a process of trial and error in which tests are made with the vital part in slightly different positions relative to the clamps.

3.2 *Pulsing, annealing and quenching.* Ideally, the temperature-time relation for a pulse-anneal has the form of a "square-wave"; the annealing periods are then additive and isothermals can be derived for kinetic analysis. Though, in practice, the pulsing and quenching periods are finite, it is necessary and sufficient only that they should be short compared with the relaxation period of the changes in the property under investigation. Further, it is often the case that, during pulsing and quenching, the specimen spends only a fraction of the time at temperatures high enough to produce changes in the property.

Quenching is performed by switching off the heating current and simultaneously opening a tap between the nitrogen reservoir and the (evacuated) bell-jar. The jet of nitrogen directed on the specimen appreciably accelerates the quench and a specimen can be cooled by this means from 500° C to room temperature in a few seconds.

The pulsing process will now be described. The settings of the Variac and resistances in the primary of the heating circuit are first adjusted for the required annealing temperature as already explained above (Section 3.2). The rheostat R_2 is then short-circuited; the value of R_2 is chosen so that the pulsing current will be roughly twice the annealing current. A measured balancing potential difference from the potential divider, corresponding to the annealing temperature, is then applied to one of the end thermocouples on the specimen, with the thermostat galvanometer, its terminals short-circuited, in series. The centre thermocouple is connected to the vernier potentiometer, the dials of the latter being set for the annealing temperature; a universal shunt is used across the potentiometer galvanometer to reduce its sensitivity and produce a full-scale deflexion. When the key K_1 is thrown over, the galvanometer deflexion falls sharply towards the zero as the specimen temperature rises. As the deflexion approaches zero, the heating current is reduced by opening the key K_2 and the thermostat is placed in control by opening its galvanometer key K_3. The temperature of the specimen may now be followed accurately by adjusting the universal shunt for greater sensitivity. The thermostat quickly stabilizes the temperature at the preset value and variations exceeding 0·2° C during an anneal can be avoided by occasional re-adjustment of the potential divider. With a Cu_3Au alloy wire of the form shown in Fig. 2(*a*), the temperature is raised from room temperature to 500° C in about ½ min. Attempts to shorten the pulse by using heavier heating currents tend to be frustrated by intense local heating of the specimen or instability of the thermostatic control. A faster pulse can be achieved with a short specimen, but tests with a number of different specimens showed that one of the form chosen affords the best compromise between the various conflicting requirements. If, during a pulsing or quenching process the property under investigation undergoes any change, a cumulative error is involved in determining the isothermal. The error can be restricted to that incurred in a single pulse-annealing process by carrying out a series of pulse-anneals, each longer than its predecessor, starting each time with the specimen in the same initial state.

3.3 *Resistivity and temperature measurement.* A resistance of 400 $\mu\Omega$ (3 mm of Cu_3Au wire) can be measured to 1/1000 if a suitable measuring procedure is used to eliminate the effects of spurious thermal electromotive forces. The errors arising from constant electromotive forces due to temperature gradient along the specimen, contacts in leads to potentiometer, etc., can be eliminated in the usual manner by reversing the current through the specimen. By measuring in turn the resistances between *A* and *B*, *B* and *C*, *A* and *C* [Fig. 2(*a*)], the error (of the order of 1μV in the present case) due to the potentiometer itself may be determined and allowed for.

Temperature measurement during annealing presents no difficulty since the heating current through the specimen is alternating. When the resistivity of the specimen is being measured, however, the direct current produces a potential difference between thermocouple contacts if the latter are not diametrically opposite. Here again the errors, in this case in determining the true electromotive force of the thermocouple, can be eliminated by reversals. With such precautions, relative values of temperature may be determined to 0·2° C. For the absolute measurement of temperature the authors cannot improve on the maker's calibration tables[5]; the uncertainty is about ±1° C at 1000° C.

4. RESULTS

The relation between measurements made by the pulse-annealing method and those made at the annealing temperature is illustrated by Fig. 4. In Fig. 4(*a*), the quenched resistivity at 20° C of a Cu_3Au wire, in which the equilibrium degree of order has been established by pulse-annealing, is plotted against the annealing temperature. The corresponding curve which would have been obtained by making resistivity measurements at the annealing temperature is constructed from curve (*a*) by using the measured temperature coefficients. The resulting equilibrium curve (*b*) which has the well-known form associated with this alloy, tends to obscure finer detail such as the small rise in resistivity as the critical temperature (approximately 380° C) is approached from higher temperatures.

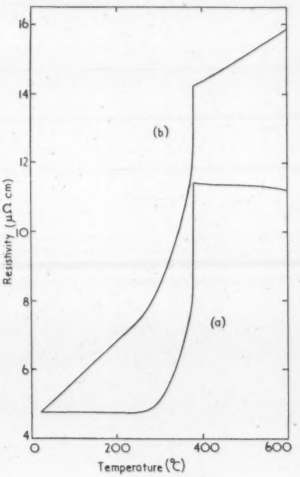

Fig. 4. Resistivity of ordered Cu_3Au

Curve (*a*) Resistivity at 20° C measured after pulse-annealing. Curve (*b*) Resistivity "at temperature" calculated from curve (*a*) using observed temperature coefficients.

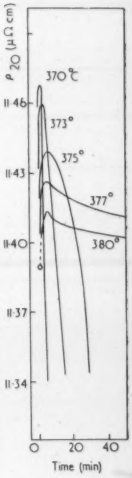

Fig. 5. Isothermals, resistivity at 20° C, ρ_{20}, *versus* time, for Cu_3Au initially disordered at 390° C and pulse-annealed at the temperatures indicated

The isothermals shown in Fig. 5, of quenched resistivity at 20° C *versus* time, were obtained by pulse-annealing the Cu_3Au wire at the temperatures indicated. In each case the alloy was initially in an equilibrium disordered state produced by annealing at 390° C and quenching to room temperature. Owing to the short relaxation period of the ordering transformation it was necessary to return the alloy to the dis-

ordered state at 390° C before each annealing pulse. Curves of similar form, but with less pronounced peaks, have been obtained by Burns and Quimby[6] by measuring the resistivity of Cu_3Au at the annealing temperature. They attribute the rise in resistivity during the first few minutes of the anneal to the formation of antiphase nuclei.[7]

The authors have used the pulse-annealing apparatus to investigate the influence of vacancy migration on ordering in the alloy Cu_3Au. It will be seen from the equilibrium curves (Fig. 4) that under ordinary conditions long-range ordering ceases at about 250° C. The authors found, however, that if the alloy is quenched from temperatures above the critical value, the vacancy concentration in the quenched alloy is sufficient to induce ordering at temperatures as low as 100° C. From this it was concluded that the nitrogen quench is rapid enough to trap vacancies considerably in excess of the equilibrium concentration.

ACKNOWLEDGEMENT

We are pleased to have this opportunity of recording our thanks to the Royal Society to whom we are indebted for a grant.

REFERENCES

(1) PARKINS, W. E., DIENES, G. J., and BROWN, F. W. *J. Appl. Phys.*, **22**, p. 1012 (1951).
(2) DIENES, G. J. *J. Appl. Phys.*, **22**, p. 1020 (1951).
(3) BOWEN, D. B. *U.S. Atomic Energy Commission Publ. (NAA–SR–154)*, (1951).
(4) WRIGHT, P. *J. Sci. Instrum.*, **24**, p. 258 (1947).
(5) *Pt : Pt.* 13% *Rh* (Johnson, Matthey and Co. Ltd., 1952).
(6) BURNS, F. P., and QUIMBY, S. L. *Phys. Rev.*, **97**, p. 1567 (1955).
(7) SYKES, C., and JONES, F. W. *Proc. Roy. Soc. A.*, **157**, p. 213 (1936).

A constant liquid flow device

By G. H. LAYCOCK, B.Sc., A.Inst.P.,* Imperial Chemical Industries Ltd., Nobel Division, Stevenston, Ayrshire

[*Paper first received* 16 *December*, 1957, *and in final form* 20 *February*, 1958]

The theoretical design is given for a device, which passes a constant liquid-flow irrespective of wide viscosity variations, consisting of an orifice in series with a capillary restrictor. A device based on this design is described and experimental results showing that a constant flow is obtained are quoted. An alternative means of rendering the flow automatically independent of viscosity is suggested.

LIST OF SYMBOLS

W = flow in g/min
ρ = density of liquid in g/cm^3
C = orifice discharge coefficient
D_1 = diameter of bore of tube containing the orifice in cm
D_2 = diameter of orifice in cm
P = pressure drop across the unit in g/cm^2
P_1 = pressure drop across the orifice in g/cm^2
P_2 = pressure drop across the capillary tube in g/cm^2
R = Reynolds's number
η = liquid viscosity in cP
n = number of capillary tubes in parallel
l = length of each capillary tube in cm
a = internal diameter of capillary tube in cm

INTRODUCTION

A liquid flowing through a sharp-edged orifice within a certain range of Reynolds numbers will increase in flow rate with increased viscosity if the pressure drop is constant, or alternatively, for a constant flow rate through the orifice, a decreased pressure drop is obtained with increased viscosity.

A liquid flowing under laminar flow conditions in a capillary tube will, however, decrease flow rate with increased viscosity at constant pressure drop or alternatively, at constant flow rate, increase pressure drop with increased viscosity.

A unit can therefore be designed consisting of an orifice in series with a multiplicity of capillary tubes, such that a constant flow rate of liquid will pass through the unit for a constant pressure drop across it, irrespective of wide variations in the viscosity of the liquid.

Poiseulle's formula for laminar flow of liquids in long capillary tubes gives, in general:

$$w = \frac{\pi P a^4 \rho g n}{128 l \mu}$$

where μ = absolute viscosity, which by reference to the list of symbols, gives:

$$W = 144465\,(P_2 a^4 \rho n/\eta l)\ \text{g/min} \qquad (1)$$

The general formula (2) for liquid flow through a sharp edged orifice is:

$$w = CA\sqrt{2g\rho P_1}$$

where A = area of orifice, which gives:

$$W = 2087 C D_2^2 \sqrt{\rho P_1}\ \text{g/min} \qquad (2)$$

The value of the discharge coefficient C is a function of the Reynolds number at the orifice which is found from:

$$R = 2{\cdot}122\,(W/D_2\eta) \qquad (3)$$

From the value of Reynolds number one can obtain a value for discharge coefficient from the tables published by Tuve and Sprenkle[1] and summarized in Fig. 1.[2]

It can be seen from Fig. 1 that, for $D_1/D_2 = 0{\cdot}20$, as R increases, in the range from 200 upwards, C decreases. With an increase in viscosity there is a decrease in R and an increase in C. Therefore if one maintains W at a constant value one must decrease P_1.

* Now at Alkali Division, Northwich, Cheshire.

To a first approximation in the range $R = 200$ to $R = 2000$, with diameter ratio 0·20:

$$C = 0{\cdot}814 - 0{\cdot}054 \log_{10} R \qquad (4)$$

DESIGN CALCULATION

The following calculation was made to design a unit in order to make practical measurements to verify the theory of an accurate constant flow device. The liquid chosen was a transformer oil with a large temperature coefficient of viscosity. The results of a series of measurements of viscosity and density of the oil are shown in Fig. 2.

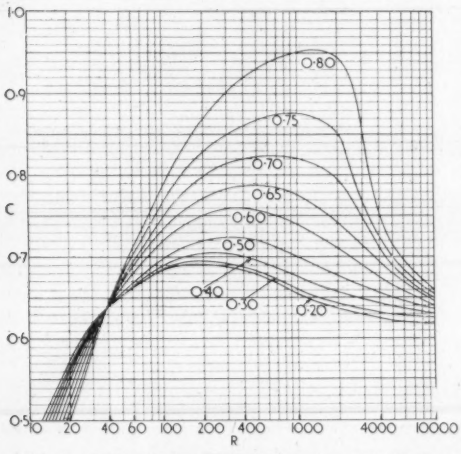

Fig. 1. Orifice discharge coefficient curves for viscous liquids. Values of D_1/D_2 are indicated on each curve

D_1 = diameter of orifice.
D_2 = diameter of tube containing orifice.

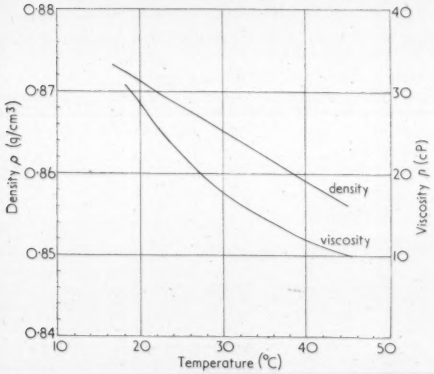

Fig. 2. Density and viscosity curves for transformer oil

At 27° C. $\rho = 0{\cdot}8668$ g/cm³ and $\eta = 20$ cP.

Let $W = 400$ g/min, $P_1 = 1900$ g/cm² and assume $C = 0{\cdot}66$.

From equation (2) $D_2 = 0{\cdot}084\,59$ cm, and from equation (3) $R = 502$.

From Fig. 1, if $D_1/D_2 = 0{\cdot}20$, $C = 0{\cdot}678$.

Substituting this correct value of C in equation (2), $D_2 = 0{\cdot}083\,46$ cm.

Using this value of D_2 with $\eta = 10$ cP, $\rho = 0{\cdot}856$ g/cm³, and with $\eta = 30$ cP, $\rho = 0{\cdot}872$ g/cm³, when $W = 400$ g/min, values of R, C, and P_1 were successively calculated, giving:

P_1 (when $\eta = 10$ cP) $= 2060{\cdot}9$ g/cm² and P_1 (when $\eta = 30$ cP) $= 1839{\cdot}0$ g/cm².

As the total pressure drop is to be independent of viscosity

$2060{\cdot}9 + P_2$ (when $\eta = 10$ cP) $= 1839{\cdot}0 + P_2$ (when $\eta = 30$ cP).

But from equation (1), with W, a, n and l constant, $P_2 \propto \eta/\rho$. So approximately:

$$P_2(\eta = 30\text{ cP}) = 3P_2(\eta = 10\text{ cP})$$

Whence
$$P_2(\eta = 10\text{ cP}) = 111\text{ g/cm}^2$$
$$P_2(\eta = 30\text{ cP}) = 333\text{ g/cm}^2$$

and
$$P = P_1 + P_2 = 2172\text{ g/cm}^2.$$

Calculating a capillary flow restriction to give these values of P_2 under the relevant viscosity conditions, W being 400 g/min, let $n = 32$ and $a = 0{\cdot}20$ cm (the bore of available tubing); then from equation (1) $l = 176$ cm.

THE APPARATUS

A unit was constructed with dimensions as near as possible to those found in the design calculation (Figs. 3 and 4). The orifice plate had an orifice diameter of 0·033 in. and was mounted in a short tube of 0·166 in. bore, giving a diameter ratio of 0·20. The upstream end of this tube was connected to a wide bore tube, reaching below the liquid surface inside a pressure vessel, and the downstream end was connected to an adaptor to which thirty-two plastic tubes of 2 mm bore and 180 cm length were connected.

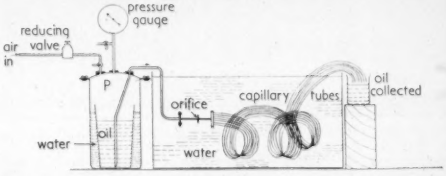

Fig. 3. The flow unit in a constant temperature bath

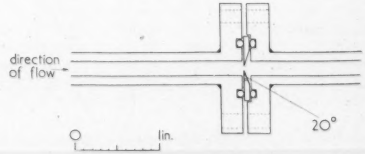

Fig. 4. Details of orifice

To ensure that the oil remained at the same temperature during its passage through the unit, a sample of oil was heated to the required temperature and a large volume of water was heated to the same temperature. The oil was placed in a container inside the pressure vessel and surrounded by water at the same temperature. The orifice and capillary tubes were also immersed in the water, apart from a very short length at the end of each capillary tube leading to a collecting vessel. This was found to be essential since the capillary tubes form an efficient heat exchanger. Air pressure was applied to the pressure vessel from a source of compressed air *via* an accurate reducing valve. The pressure was indicated on a standard pressure gauge.

Oil was passed through the unit at a series of pressures P and at a series of temperatures, and measurements were made of the flow by weighing the amount delivered in a known time. Sufficient time was allowed before each measurement for steady flow conditions to be set up.

RESULTS

The results obtained are plotted in Figs. 5 and 6. At a pressure P of 2110 g/cm^2 the flow was constant over a range of temperatures of from 18 to 42° C to within ±0·6% of flow. As the pressure deviated from this value the errors increased, as shown in Fig. 5. However, in the pressure range 1406 to 2812 g/cm^2 the flow was constant at a particular pressure over the same temperature range to within ±1·5%. The range of temperature is equivalent to a change in viscosity of from 10 to 30 cP. It was found that, using the orifice only, the change in flow within the temperature range at constant pressure was ±6%, and, using the capillary restrictor only, the equivalent change in flow was three times, i.e. ±50%.

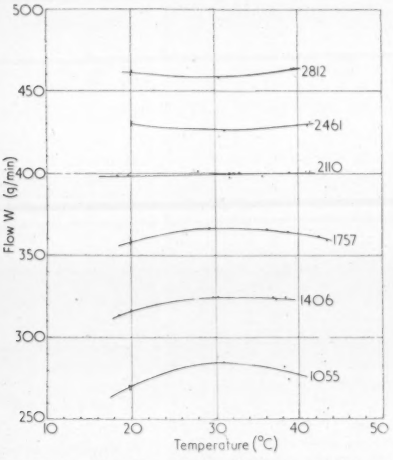

Fig. 5. Relation between temperatures and flow at a series of pressures P given on each curve

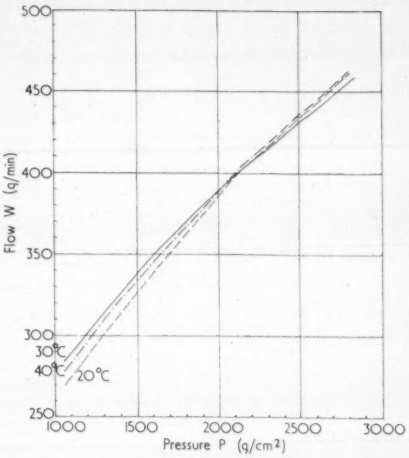

Fig. 6. Relation between pressure and flow at a series of temperatures

DISCUSSION

Since the unit behaved as predicted in the design calculation, the experimental results of Tuve and Sprenkle[1] are further verified. Devices of this type could be designed for a wide variety of liquids, flow conditions and restrictors. For example, based on the principle verified for one case above, a constant flow device could be designed using two orifices of different diameters placed in series in a carrier tube such that the Reynolds number for one varies in the range 15 to 150 and for the other varies in the range 300 to 3000 (Fig. 1). For constant flow through this device an increase in viscosity would have the effect of increasing the pressure drop at the first orifice and decreasing the pressure drop at the second orifice. The orifice diameters could be arranged so that the total pressure drop was a constant for constant flow with varying viscosity. It is probable, therefore, that a flow indicator measuring the pressure drop across a unit of two orifices in series designed as indicated would be more accurate than the conventional single orifice plate flow-meter.

ACKNOWLEDGEMENT

The writer wishes to thank Mr. R. M. Dawson for his assistance in making the experimental measurements.

REFERENCES

(1) TUVE, G. L., and SPRENKLE, R. E. *Instruments*, **6**, p. 201 (1933).

(2) PERRY, J. H. *Chemical Engineers' Handbook*, 3rd ed., p. 403 (London: McGraw-Hill Publishing Co. Ltd., 1950).

The effect of gettering on the reflectivity of aluminium films

By L. HOLLAND, F.Inst.P., Research Laboratories, Edwards High Vacuum Ltd., Manor Royal, Crawley, Sussex

[*Paper received* 28 *November*, 1957]

Aluminium films evaporated on glass from a single vapour source are more optically absorbing at high angles of vapour incidence if the films are slowly deposited or prepared in a poor vacuum. The rise in the optical absorption with vapour incidence angle is attributed to the degree of gas contamination of the growing film increasing as the deposition becomes more oblique. Such an effect could arise from a greater ratio of the number of gas molecules to vapour atoms combining at the receiver in regions of low vapour intensity. The reflectivities of aluminium films prepared at different gas pressures and rates of deposition show qualitative agreement with the hypothesis when plotted as a function of vapour incidence angle. The simple theory advanced is not applicable at gas pressures above 1 μ mercury because the vapour atoms are scattered by gas molecules before striking the receiver.

Both optical[1] and electron microscopy[2] studies have shown that evaporated aluminium films may develop a coarse texture when deposited at oblique angles of vapour incidence, because the film nuclei can only grow on restricted surfaces. Also, it has been found that the residual gas in the vacuum chamber is gettered by the evaporated aluminium which combines during condensation with the gas molecules striking the receiver.[3,4] Thus the reflectivity of an aluminium front surface mirror may be reduced, particularly for blue light, if the film is either granular and scatters the incident light or is impure and optically absorbing. Gas contaminated deposits have a lowered reflectivity at both film boundaries if the deposition rate and gas pressure are constant during deposition, whereas diffusely reflecting deposits arising from preferred growth have a reduced reflectivity only at the air to film boundary.

The writer has observed the formation of poorly reflecting aluminium films in the region of oblique incidence when evaporating on plane mirrors from a single vapour source. The fall in reflectivity did not arise from the formation of an irregular texture because a bluish bloom, characteristic of light scattering, was not present on the mirror surface. Measurement of the reflectivity over the surface of such mirrors showed that the obliquely deposited regions were more optically absorbing indicating that the purity of the deposit had fallen.

It can be shown that the gas contamination of an aluminium film should vary with the vapour incidence angle if the vapour intensity is not uniform over the receiver surface and this could explain the formation of optically absorbing films at oblique incidence. The gas absorbed by an aluminium film during deposition depends upon the gas pressure and rate of deposition, i.e. the gas contamination increases with a rise in the ratio of the number of gas molecules to metal atoms striking the receiver in unit time. Thus when evaporating on a plane surface from a tungsten filament with approximately spherical vapour emission the gas contamination of the deposit should be greater at oblique incidence where the intensity of the vapour reaching the receiver is weakest. If the rate of absorption of gas is independent of the level of gas content in the film, then it can be shown for a point source, that the percentage gas absorbed (Ns) by a portion of the deposit at point S on the receiver plane relative to that (No) at $S = 0$ normal to the emitter is given by

$$\frac{Ns}{No} = \frac{(h^2 + S^2)^{3/2}}{h^3}$$

where h is the normal distance between the emitter and the receiver plane. The vapour angle θ is measured from the surface normal. Thus for a source at $h = 6$ in. the gas contamination at $S = 10{\cdot}34$ in. (i.e. $\theta = 60°$) should be eight times greater than that of the deposit at normal incidence. Under the dynamic conditions of evaporation the gas pressure momentarily falls as gas is removed by the deposit which functions as a pump. The pressure reduction is greatest where the vapour atoms incident on the surface are most intense, i.e. at normal incidence where the film is least saturated with gas, and this should enhance the relative gas contamination of the deposit.

EXPERIMENTAL METHOD

Tests have been made to determine the qualitative effects of the gas pressure and angle of vapour incidence on the gas contamination of thin films by measuring the reflectivity of aluminium mirrors. The coatings were prepared in a horizontal 24 in. diameter metal chamber exhausted by a silicone oil diffusion pump of 1500 l./s. A number of glass slides were arranged on a long holder with a vapour source placed under one end at a normal distance of 6 in. with θ varying from 0 to 60°.

The aluminium films were made sufficiently thick for the deposit to be optically opaque and thus if pure fully reflecting

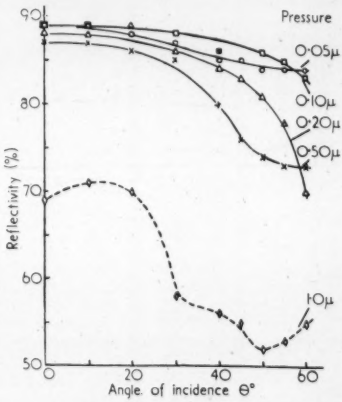

Fig. 1. Aluminium evaporated in 8–10 s with initial gas pressure adjusted by admitting air to the vacuum chamber

within the incident angles examined. Some 0·37 g of alumium, i.e. a 9 in. length of 20 s.w.g. wire, was evaporated and this produced a film of about 600 Å thick at $\theta = 60°$. The wire was placed inside a stranded tungsten filament and pre-melted to fuse it to the heater. The output potential of the low tension supply was adjusted so that the complete charge of aluminium could be evaporated in a known time interval. The glasses were cleaned chemically and by a glow discharge, and then coated as follows:

(1) The aluminium films were evaporated at a constant time of 8–10 s after the gas pressure had been adjusted to an initial value in the range 0·05–1 μ mercury by admitting air to the vacuum chamber *via* a needle valve. The reflectivities at $\lambda = 5300$ Å of the mirrors produced on each cycle are shown in Fig. 1.

(2) Aluminium films were produced in a similar manner to the above but the evaporation time on each cycle was reduced to a constant value of 3–4 s. The film reflectivities are plotted in Fig. 2.

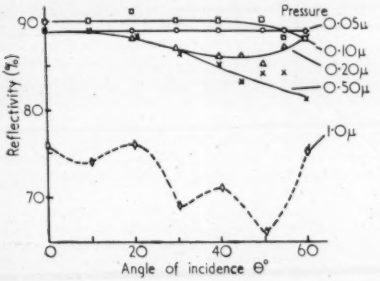

Fig. 2. Aluminium evaporated in 3–4 s with initial gas pressure adjusted by admitting air to the vacuum chamber

(3) The ultimate pressure of the residual gas in the coating chamber was raised by partially closing the high vacuum valve above the diffusion pump. Aluminium films were prepared on all cycles at a constant evaporation time of 3–4 s with the initial pressure adjusted between 0·05 and 1 μ mercury.

DISCUSSION OF RESULTS

The results show that as the gas pressure or the evaporation time is raised the reflectivities of the mirrors tend to fall, the reduction being most marked at oblique incidence for pressures up to 0·5 μ mercury. The films produced by method (2) in the degassed atmosphere show less reduction in reflectivity than those produced with a constant leak of air to the system. This was because the pressure of the degassed components momentarily fell to a lower value than with a constant flow of gas into the vapour stream. It is obvious, however, that a badly degassing plant could give similar results to that obtained in Figs. 2 and 3, because the major component of the residual atmosphere is usually water vapour which readily reacts with aluminium.

Films prepared at 1 μ mercury with a constant leak had low reflectivities but the minimum values sometimes occurred at θ equal to 30–50° instead of at higher angles as expected. At this high pressure the vapour atoms cannot travel to the receiver unimpeded by gas molecules and the evaporation must be compared to the expansion of a cloud so that the simple theory advanced for the variation in the gas absorption would no longer apply.

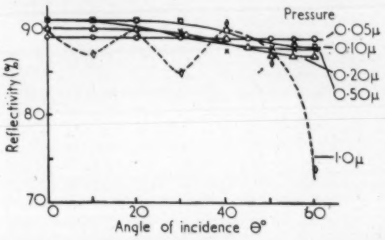

Fig. 3. Aluminium evaporated in 3–4 s with initial gas pressure raised by partially closing high vacuum valve

The high reflectivities reached at all angles of vapour incidence for films evaporated rapidly (3–4 s) at low pressure (0·05 μ mercury) showed that the films were below the minimum thickness required for the onset of a light scattering film, which, from reported values[1] at $\theta = 60°$, required a thickness above the 600 Å used.

Thus, it can be inferred that the reduction in the reflectivity of aluminium films in regions of oblique vapour incidence when evaporating in a poor vacuum or at slow deposition rates arises from their high degree of gas absorption. This may also explain the reason why a masked deposit forms a discoloured zone at the metal boundary when the film is condensed through a thick stencil. The vapour intensity is greatly reduced in the region of the penumbra cast by the stencil edge and the amount of gas absorbed at the edges of the film is consequently greater. The foregoing is not necessarily applicable when the receiver is of a type which degasses freely with rise in temperature, e.g. an organic substance, because the gas contamination of the deposit may be greatest in the region of normal incidence where the temperature rise in the base is highest.[5]

ACKNOWLEDGEMENTS

Acknowledgements are made to Mr. T. Koot who prepared many of the films used in this investigation, and to Mr. A. S. D. Barrett, Technical Director of Edwards High Vacuum Ltd., for permission to publish this report.

REFERENCES

(1) HOLLAND, L. *J. Opt. Soc. Amer.*, **43**, p. 376 (1953).

(2) KOENIG, H., and HELWIG, G. *Optik*, **6**, p. 111 (1950).

(3) HOLLAND, L. *Vacuum Deposition of Thin Films* p. 6 (London: Chapman and Hall, Ltd., 1956).

(4) BURRIDGE, J. C., KUHN, H., and PERY, A. *Proc. Phys. Soc. (London) B*, **66**, p. 963 (1953).

(5) HOLLAND, L. *Trans Plastic Inst.*, **24**, p. 153 (1956).

Correspondence

Frictional behaviour and structure of the surface oxides of steel

We have recently investigated the frictional behaviour of high carbon steel which had been treated in seven different ways; i.e. *A*-0 freshly abraded, *B*-0 left in a desiccator at room temperature for half a year, *B*-1 first left for half a year and then heated in air to produce a reddish-yellow oxide film (thickness: ca. 500 Å), *B*-2 heated until blue (about 700 Å) in the same way, *B*-3 heated until colourless again (about 1000 Å) like above, *B*-4 heated until dark grey ($>10^3$ Å) like above, and *A*-4 heated until dark grey immediately after abrasion. These deductions of oxide-film thickness from the colour of the oxide are relatively crude but appear sufficient for the present investigation.

The coefficient of friction μ was measured with a pendulum-type apparatus identical in principle with that of Kyropoulos,[1] in which the steel specimens were arranged in the form of "crossed cylinders." The frictional sliding was therefore reciprocating and the condition seemed more severe and more likely to cause breakdown of the surface oxide film than in unidirectional sliding. The measurements were made at loads of 100 g and 25 g per contact and at the maximum speed of about 3 mm s^{-1}. The period of swing was about 2 c/s. The specimens were degreased in a boiling mixture of alcohol and KOH (5%).

The results shown in Fig. 1 indicate *B*-series specimens at a load of 100 g; Fig. 2, *B*-series specimens at a load of 25 g; and Fig. 3, comparison of *A*- and *B*-series at a load of 100 g. In these figures the abscissa m represents the number of successive measurements, during which the contact of the specimens was not changed.

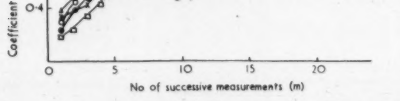

Fig. 1. Change of coefficient of friction μ with number of successive measurements m in *B*-series (aged specimens) at a load of 100 g

B-0, no treatment; *B*-1, heated, 500 Å; *B*-2, heated, 700 Å; *B*-3, heated, 1000 Å; *B*-4, heated, above 10^3 Å.

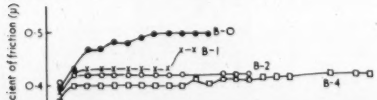

Fig. 2. Change of coefficient of friction μ with number of successive measurements m in *B*-series (aged specimens) at a load of 25 g

B-0, no treatment; *B*-1, heated, 500 Å; *B*-2, heated, 700 Å; *B*-4, heated, above 10^3 Å.

Early experiments[2] on the breakdown of the oxide film in metallic friction have been carried out under the condition of unidirectional sliding, showing that the change of μ corresponds to the degree of oxide breakdown and that this, in turn, is determined by the applied load. In the present work the value of μ was slowly increased as the reciprocating rubbing was repeated. This suggests that the breakdown of the oxide film occurred despite the fact that the load was kept constant and was lower than the critical value which is, in unidirectional sliding, sufficient to cause breakdown of the film. Comparing Fig. 1 with Fig. 2, it is readily seen that not only the heavy load but the repeated rubbing ruptures the film. It is worthwhile to note in Figs. 1 and 2 that all surfaces showed a similar frictional behaviour at the early stages of successive measurements. This suggests that for these specimens the oxide layer had the same structure independent of its thickness. It is probable that this thin surface layer of amorphous Fe_2O_3 or FeO(OH) was abraded away in the course of $m = 1 \sim 4$. The values of μ, 0·50 and 0·45, correspond to the values which Bisson and Johnson attribute to "dry" steel and to Fe_3O_4, respectively.[3] It has also been reported that the natural surface oxide, produced by oxidizing for a prolonged period at room temperature, is more protective,[4] and the difference between *A*-0 and *B*-0 in Fig. 3 showed this is true for the repeated rubbing as well as for the heavy load.

The friction results also show an interesting difference in the type of surface oxide produced. Comparing *A*-0 and *A*-4 with *B*-0 and *B*-4 in Fig. 3, it is clear that the protective

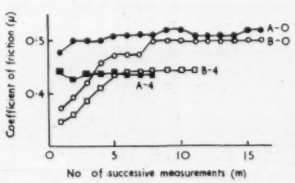

Fig. 3. Comparison of *A*- and *B*-series (fresh and aged) at a load of 100 g

m, no. of successive measurements; *A*-0, fresh, no treatment; *A*-4, fresh, heated, above 10^3 Å; *B*-0, aged, no treatment; *B*-4, aged, heated, above 10^3 Å.

oxide formed at room temperature on *B*-0 survived after heating at a higher temperature and still existed on the outermost surface. According to the present theory of the tarnishing process,[5] it is usually assumed that the surface of a ferrous material is covered with FeO, then Fe_3O_4 and finally (as the outermost layer) Fe_2O_3. The growth of Fe_3O_4 presumably means diffusion of oxygen through the Fe_2O_3 and growth from the FeO upwards so that the outermost layer of Fe_2O_3 persists after further oxidation. Our results were in good agreement with this tarnishing feature.

Although the changes in coefficient of friction are relatively small (generally from 0·4 to 0·5) it is felt that the differences in friction are significant and meaningful. The results

suggest, in agreement with earlier work, that for steel surfaces from which most of the oxide is removed (the surface is probably covered with FeO) the friction has a value of about $\mu = 0{\cdot}5$, for steel covered with Fe_3O_4 the friction is about $\mu = 0{\cdot}45$ and for surfaces covered with Fe_2O_3 [or FeO(OH)] the friction is between $\mu = 0{\cdot}35$ and $0{\cdot}4$.

The writer wishes to thank Profs. S. Makishima and N. Soda for their interest and encouragement.

Institute of Science and Technology,
University of Tokyo,
Meguro, Tokyo, Japan.

YASUKATSU TAMAI

[10 March, 1958]

REFERENCES

(1) KYROPOULOS, S., and SHOBER, E. I. *Rev. Sci. Instr.*, **8**, p. 151 (1937).

(2) WILSON, R. *Proc. Phys. Soc. B*, **68**, p. 625 (1955).

(3) BISSON, E. E., and JOHNSON, R. L. *S.A.E. Journal*, **58**, No. 3, p. 39 (1950).

(4) HIRST, W., and LANCASTER, J. K. *Proc. Roy. Soc.* [*London*] *A*, **223**, p. 324 (1954).

(5) DAVIES, M. H., and BIRCHENALL, C. E. *J. Metals*, **3**, p. 889 (1951).

Notes and comments

Elections to The Institute of Physics

The following elections have been made by the Board of The Institute of Physics:

Fellows: H. Adam, J. F. Archard, J. J. Benbow, M. M. Bluhm, A. W. Crook, J. Darbyshire, L. R. B. Elton, J. H. Jaffe, E. W. Kellerman, C. N. W. Litting, D. McGill, E. G. Steward, A. N. Stroh.

Associates: H. S. Adams, G. J. Ames, M. I. Andrews, R. G. Angus, D. G. Baldwin, B. Barber, D. A. Calder, J. A. Carruthers, L. G. S. Clark, P. R. Cloud, J. K. Easlea, R. H. Haynes, D. G. Holloway, H. M. McGeachin, D. H. Morton, A. P. Rouse, M. Seal, D. G. Singleton, M. J. Smith, W. S. Symes, R. Thorburn, D. R. Tibbetts, A. H. Truelove, C. Turner, C. H. Ward, R. West, R. W. Whitworth.

Thirty-five Graduates, one hundred and two Students and five Subscribers were also elected.

Symposium on nuclear fuel cycles

The Institute of Physics, one of the constituent bodies of the British Nuclear Energy Conference, announces that it is arranging a symposium in London on nuclear fuel cycles on 22 and 23 January, 1959. The programme is as follows:

Session 1: (*a*) Long term reactivity changes; (*b*) Theory of once-through fuel cycles; (*c*) Perturbations due to fuel cycles.

Session 2: Optimization of fuel cycles for nuclear power stations.

Session 3: Fuel cycle operational problems.

The papers which have been invited will cater mainly for persons working in the field, and will deal with the applied physics aspects of the fuel cycles which form the basis of the immediate nuclear power programme. Abstracts (but not pre-prints) of the papers to be read or presented at the symposium will be available early in January.

Application forms for tickets to attend the symposium are obtainable from the Secretary of The Institute of Physics, 47 Belgrave Square, London, S.W.1, and should be returned as soon as possible.

The symposium will be published in the *Journal of the British Nuclear Energy Conference*.

Instrument enquiries service

In order to help prospective instrument users to find the sources of supply and particulars of the type of instrument best suited to their needs, the Scientific Instrument Manufacturers' Association of Great Britain Ltd. have established a technical enquiry service in collaboration with the British Scientific Instrument Research Association. It is hoped that, through this service, enquirers may be able to obtain the most accurate and up-to-date information on all products manufactured by the members of the Association. The telephone number of the service is IMPerial 6000.

Notes for prospective authors

Authors preparing contributions for submission to this *Journal* are invited to make use of the guidance available in a 32-page booklet entitled *Notes on the preparation of contributions to the Institute's Journals and other publications*. It is intended to assist less-experienced authors and to serve as a reference booklet for all who wish to contribute to the Institute's publications. It gives hints on the preparation of scripts and diagrams, on the lay-out of mathematics for the printer, the correction of proofs and so on. In addition to a short bibliography of reference books and works on technical writing, there are lists of the spellings, symbols and abbreviations used by the Institute. These conform with British Standard 1991, Part 1: 1954: *Letter symbols, signs and abbreviations, Part* 1, *General*, which authors of mathematical papers are also advised to consult.

Copies of the booklet may be obtained from The Institute of Physics for 2*s*. 6*d*. (including postage).

International conference on the peaceful uses of atomic energy

The list of 2500 scientific papers to be presented before the 1958 International Conference on the Peaceful Uses of Atomic Energy, 1–13 September, 1958, is being made available by the Document Service of The Chronicle of United Nations Activities.

The subject-matter ranges through all the aspects of the peaceful uses of atomic energy, including the production and control of thermo-nuclear power; advances in reactor technology; extraction and refining of nuclear materials; effects and control of radiation; uses of isotopes in industry, agriculture, and medicine; and many other research developments from the major laboratories of the world. Copies of the list, free of charge, may be obtained from the Atomic Energy Document Service, The Chronicle of United Nations Activities, 234 West 26 Street, New York 1, N.Y., U.S.A.

The Geophysical Journal

The first issue of *The Geophysical Journal* was published in March this year. This is a journal intended for the publication of papers on research and progress in geophysics and related subjects. It incorporates the earlier *Geophysical*

Supplement to the *Monthly Notices of the Royal Astronomical Society*; by widening its scope to include, in addition to original papers, such matters as reports of geophysical discussions, short notes and letters and book reviews, it is hoped to increase its circulation throughout the large body of exploration geophysicists.

There is no limit to the range of geophysical subjects which the journal covers. Contributions to the first number come from Australia, Canada, the U.K., the U.S.A. and the U.S.S.R. and the papers cover such varied subjects as the use of hydrogen bomb explosions for seismological purposes; the application of geomagnetic measurements to studies of ionic density in the outer atmosphere; polar wandering; the theory underlying calibration of travimeters by comparison with pendulums, and a review of the recent Toronto U.G.G.I. conference. Of more immediate practical nature is a paper on a seismic refraction survey off the north coast of Cornwall. At the end of the journal there is a series of Russian translations of summaries of the original papers.

We welcome this new periodical and wish it success.

The *Journal* is published quarterly by The Royal Astronomical Society, Burlington House, London, W.1. The annual subscription is £3 (U.S.A. $9).

Pakistan journal of scientific and industrial research

We have received the first issue of a new quarterly periodical entitled *Pakistan journal of scientific and industrial research*, edited by Dr. M. M. Qurashi and published by the Pakistan Council of Scientific and Industrial Research, Karachi. Among the papers included are the following: Radio frequency transmission system of a 30 MEV electron cyclotron; Scattering of high energy electrons by electrons in nuclear emulsion; Proton-proton scattering at medium-high energies; Design and study of audio-amplifier and radio-receiver using transistors; Design of an improved type of dry cell; Studies in the properties of heat insulating building materials. Part I —Cement-rice husk ash mixtures.

The price of the annual volume is Rs. 15, post free, and single parts Rs. 4, post free. Further details may be obtained from the publishers.

We wish the latest of the many additions to our contemporaries all success.

Wear

The aim of a new "international" Journal entitled *Wear*, which commenced publication in August 1957, is to report on basic research on friction, lubrication, and wear and the application of the results to industry. The Editor is Dr. G. Salomon of Delft and he is supported by international editorial and advisory boards. Papers and review articles are published in English, French or German, and are supplemented by a section containing book reviews, abstracts of papers appearing elsewhere, and brief reports on current events.

Wear will have six issues to the volume of about 500 pages and is published by Elsevier Publishing Co. of Amsterdam at £5 7*s.* 6*d.* or $15 per volume. Once again it is our pleasure to wish success to yet another contemporary.

Erratum

The paper by B. Meltzer and P. L. Holmes which appeared on page 139 of the April issue of this Journal contained the following printing errors: In Figs. 7 and 8 "Log S_2/S_1" should read "Lag S_2/S_1". On page 140, second line below Fig. 2, "$2 \cdot 303a$" should read "$a/2 \cdot 303$".

Journal of Scientific Instruments

Contents of the August issue

SPECIAL ARTICLE

Infra-red and microwave modulation using free carriers in semiconductors. By A. F. Gibson.

ORIGINAL CONTRIBUTIONS

Papers

Magnetic deflexion of electron beams without astigmatism. By G. D. Archard and T. Mulvey.

Error in temperature measurement due to the interdiffusion at the hot junction of a thermocouple. By A. J. Mortlock.

A simple phase sensitive rectifier for use with radiation detectors. By J. C. S. Richards.

A nuclear plate camera for angular distribution measurements with gaseous or solid targets over a wide range of angles. By W. M. Jones and D. G. Waters.

A mass spectrometer mass marker. By J. H. Beynon and S. Clough.

An apparatus for the viscometry of organic liquids at high temperature. By W. G. Burns, B. Morris and R. W. Wilkinson.

A critical method of focusing an optical diffractometer. By C. A. Taylor and B. J. Thompson.

A double γ-ray spectrometer for coincidence counting of positrons. By J. W. Weale.

The use of a manometric densitometer for molten salts. By the late L. J. B. Husband.

The preparation of powder specimens from active and toxic metals for use in conventional X-ray diffraction studies. By A. Moore, D. B. Wright and A. J. Martin.

Photoelectric indicator for precision setting in co-ordinate measurements. By E. Djurle and G. Gran.

Laboratory and workshop notes

The use of coarse gratings to find the refractive index of liquids. By G. M. Sreekantath and C. A. Verghese.

Inventoried storage of large numbers of small radioactive particles. By L. E. Preuss.

A metal through glass seal. By E. J. Davis.

A null-point pressure indicator for use at high temperature. By P. E. Liley.

A general purpose electronic timer particularly suitable for time-lapse kinemicrography. By D. McNish and R. E. Trotman.

NOTES AND NEWS

New instruments, materials and tools

BINDING ORDERS

From the date of this announcement, orders and enquiries about the binding of back-numbers of the *Journal of Scientific Instruments* and of the *British Journal of Applied Physics* should now be sent direct to Messrs. E. A. Weeks and Son, 168 Gower Street, London, N.W.1 (EUSton 4674), and *not* to The Institute of Physics. This new arrangement does not involve any change in price.

THIS JOURNAL is produced monthly by The Institute of Physics, in London. It deals with all branches of applied physics (including theory and technique).
All rights reserved. Responsibility for the statements contained herein attaches only to the writers.
EDITORIAL MATTER. Communications concerning editorial matter should be addressed to the Editor, The Institute of Physics, 47 Belgrave Square, London, S.W.1. (*Telephone*: Belgravia 6111.) Prospective authors are invited to prepare their scripts in accordance with the *Notes on the preparation of contributions*. (Price 2*s.* 6*d.* including postage.)

REPRODUCTION. The Institute of Physics is a signatory to The Royal Society's Fair Copying Declaration. Details may be obtained upon application from The Royal Society, London, W.1.

ADVERTISEMENTS. Communications concerning advertisements should be addressed to the agents, Messrs. Walter Judd Ltd., 47 Gresham Street, London, E.C.2. (*Telephone*: Monarch 7644.)

CLAIMS FOR MISSING JOURNALS. Claims from regular subscribers to this *Journal* for missing numbers will only be considered if received within 60 days of the date of mailing plus normal outward time of transit and time for lodging the claim. Losses attributable to failure to notify a change of address or to similar omissions will not be considered.

SUBSCRIPTION RATES. A new volume commences each January. The charge is £5 per volume ($14.25 U.S.A.), including index (post paid), payable in advance. Single parts, so far as available, may be purchased at 10*s.* each ($1.50 U.S.A.), post paid, cash with order. Orders should be sent to The Institute of Physics, 47 Belgrave Square, London, S.W.1, or to any bookseller.

SPECIAL ARTICLE

The physics of fibres with special reference to wool*

By A. B. D. Cassie, C.B.E., M.A., D.Sc., F.Inst.P., Wool Industries Research Association, Headingley, Leeds 6

There are many angles from which one could approach the physical study of fibrous materials. In the book under a similar title published in the Physics in Industry series Woods[1] has dealt largely, but not exclusively, with those aspects of the study which are concerned with the consequences of the molecular structure of fibrous substances. On the other hand, there are many interesting physical problems, particularly in relation to fibre assemblies such as fabrics, which arise purely from the geometrical form of the fibres and their ability to exchange water vapour with the atmosphere. This paper is largely concerned with these aspects of the subject.

AIR PERMEABILITY

The fibres used in textiles are usually fine and long and hence have a very large surface-volume ratio. This has a number of interesting consequences. Take, for example, an ordinary wool suiting material; this may look pretty solid but, in fact, even the most closely packed wool fabrics have about 60% air space, and only 40% wool. Such a material cannot interpose a solid barrier to the passage of a fluid, the resistance to the passage of air, for example, through a wool fabric being caused mainly by friction at the enormous fibre surface to which any air being driven through the fabric is exposed. As examples of the large surface areas involved the following figures may be quoted. The surface area of 1 lb of a typical merino wool is about 800 ft^2, that of 1 lb of silk is 3200 ft^2. A wool clothing fabric may weigh over 1 lb/yd^2 so that the fibre surface area may be anything up to 80 times the fabric area. Although the area of 1 lb of silk is so much greater than that of 1 lb of wool, silk fabrics are usually much lighter than are wool fabrics and the total fibre surface is correspondingly less.

The surface drag on a fluid flowing through an assembly of fibres is only fully effective when the fibres are approximately uniformly distributed. Except for pressed felts, this implies that the fabric density shall not differ very greatly from the yarn density. If this is not so, the air will pass mainly through the comparatively large spaces between the yarns rather than through the fine spaces between the fibres in the yarn. The air drag will then be greatly reduced, particularly with smooth yarns which have no loose fibres to break up the inter-yarn spaces. There will, however, usually be an additional resistance to air flow under these conditions which arises from the turbulence set up. This will normally be much less than the loss of frictional drag.

Kozeny[2] has made an extended study of the resistance to fluid flow through approximately uniform beds, based essentially on the theories developed for the air drag of cylinders which have, of course, been applied to the very different problems of airplane wings and the like. Kozeny's theory when applied to air flow through a plug of fibres gives the formula

$$d^2 = 16\,k\eta l\,\frac{v}{\Delta P}\,\frac{\rho V m^2}{(\rho V - m)^3}$$

where d is the fibre diameter, v is the rate of air flow measured outside the plug, l is the thickness of the plug, V is the volume of the plug, m is the mass of fibres therein, ρ is the fibre density, η is the viscosity of air, ΔP is the pressure drop across the plug, and k is a dimensionless shape factor, depending on fibre orientation and the uniformity of packing, relating the mean diameter of the fibres to the rate of air flow through the plug. In this formula $v/\Delta P$ is the air permeability.

There is one unknown in this equation, namely the shape factor k. It has been worked on from both theoretical and practical angles, and we now know that for fibres randomly oriented in a plane perpendicular to the air flow, it has a value of about 6·6. If this value is substituted in the Kozeny equation and the latter applied to flow through a fabric, we obtain the formula

$$A = \frac{(1-\phi_f)^3}{l\phi_f^2}d^2$$

where A is air permeability in ft/min × in. (water gauge), ϕ_f is the volume fraction of fibres in the fabric (i.e. the ratio of fabric density to fibre density), l is the fabric thickness in mils (1/1000 in.) and d is the fibre diameter in microns.

Table 1. *Low woollen fabric fibre diameter* 23·7 μ

Stage	ϕ_f	l (1/1000 in.)	*Air permeability ft/min × in.* Calc.	*Obs.*	*Ratio*
Greasy	0·201	71·0	97·5	405	4·15
Scoured	0·170	78·3	142	173	1·22
Milled 1 hour	0·160	86·1	150	157	1·05
Milled 2 hours and washed off	0·162	97·6	132	112	0·85
As above with surface cover removed	0·214	65·8	90·5	110	1·22

Tables 1 and 2 give a comparison between the air permeability as calculated on the above theory and that determined experimentally. The material referred to in Table 1 as "greasy" is the fabric as it comes from the loom, when it has the appearance of canvas rather than of wool; but after scouring and milling—which is really a prolonged scour—the calculated and observed air permeabilities agree surprisingly closely. These results show how uniform the packing of wool fibres is in a typical milled fabric, and that the resistance to penetration by wind or other air movement is entirely due to the ordinary effects of drag. The fibres have an enormous surface area and it is the drag of this

* Based on a lecture given to the North Eastern Branch of The Institute of Physics in Newcastle upon Tyne on 4 December, 1957.

Table 2. *Air permeability of milled fabrics*

Fabric	ϕ_f	d (microns)	l (1/1000 in.)	Air permeability ft/min × in. Calc.	Obs.	Ratio	Notes
A	0·137	21·8	143	114	79·5	0·697	
B	0·135	22·3	137	129	81	0·625	
C	0·095	31·5	177	458	400	0·872	
D	0·092	31·4	196	474	400	0·845	
E	0·114	31·0	153	339	300	0·881	
F	0·132	33·4	170	232	281	1·21	Raised, but open weave
G	0·197	31·0	140	91	94·6	1·04	Very little surface cover
H	0·203	32·0	126	100	111	1·11	
I	0·135	31·8	178	202	157	0·78	
J	0·177	32·0	157	115	118	1·03	Little cover
K	0·131	32·7	266	146	121	0·83	
L	0·263	22·2	54·4	53·6	35·6	0·66	Very compact fabric; fibres varying in diameter
M	0·310	22·7	57·1	31·5	24·9	0·79	
N	0·164	43·0	100	400	209	0·53	
O	0·262	28·6	75·5	63·2	49·1	0·78	

Note.—Fabric N contained a large number of medullated fibres.

enormous surface that brings the air movement to rest and so protects the body against heat loss by moving air.

FIBRE DISTRIBUTION IN WOOL FABRICS

The relatively uniform fibre distribution found with wool fabrics occurs because wool yarns (whether worsted or woollen) are very loosely packed compared with some of those made from cellulosic materials. It does not, therefore, require a tight weave and a high fabric density to produce a uniform fibre distribution in the fabric. This loose structure of wool yarns is no doubt partly the result of the crimp of most wool fibres—the loftiness of yarns made of synthetic fibres can be improved by giving them an artificial crimp. The elastic properties of the fibre, however, also contribute to this effect. The essential requirement here is that a given length of fibre can be bent into a circle for the expenditure of less work than is required to twist it through one revolution.[3] For a cylindrical fibre this requires a relatively low longitudinal Young's modulus combined with a high rigidity modulus in torsion, the actual relation being

$$(E - 2G)/G < 0$$

where E and G are the relevant Young's modulus and rigidity modulus respectively.

There is some doubt as to whether this is actually negative for wool, but the value of the ratio is certainly much less than it is for other fibres. Flat ribbons are usually more easily bent in the plane of the ribbon than twisted, but they are much more difficult to bend at right angles to this plane. One might expect, therefore, that cotton fibres which are ribbon-like in their structure might give lofty yarns; however, the plane of the ribbon in cotton fibre is not constant, but twists to and fro down the fibre so that the application of the criterion for loftiness given above to cotton is more likely to be justified than would appear at first sight.

A second deduction which can be made from the low packing density of many fibres is that fabrics have thermal conductivities which are more or less those of still air.[4] The thermal conductivity of wool felts of different densities are shown in Fig. 1. The curious rise in thermal conductivity above that for still air, at very low packing densities has not been satisfactorily explained. Schuhmeister[5] has given an equation which relates the conductivity of mixtures of solid cylinders in a fluid to the conductivity of the components and the proportion and orientation of the cylinders. The curves in Fig. 1 represent the conductivity of the fabrics as calculated with this relation assuming that the conductivity of the fibres is the same as that of horn keratin. The latter was separately measured and found to be $4{\cdot}6 \times 10^{-4}$ cal/cm × s × °C at low regains and 5·1 cal/cm × s × °C at medium regains, i.e. the thermal conductivity of keratin (the wool substance) is about ten times as great as that of air.

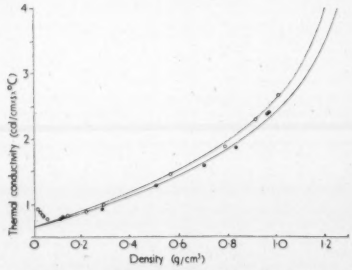

[Reproduced from *Wool Research, Vol.* 2]

Fig. 1. Relation between thermal conductivity and bulk density for wool felts

○ medium regain (10·7%) • low regain (0·7%)

THE EFFECTS OF WATER SORPTION

As is well known, wool is a hygroscopic substance absorbing up to 33% of its weight of water in a saturated atmosphere. This implies that at saturation, when the density of wool is about 1·28, the concentration of water in the wool fibre is about 0·32 g/cm^3, whereas at 25° C the water vapour concentration in the atmosphere is only 23 mg/l; i.e. when wool is in moisture equilibrium with the atmosphere at normal temperatures, the concentration of water in wool is about 10^4 that in the atmosphere. This fact taken in conjunction with the small diameter of fibres means that a wool fibre rapidly comes into moisture equilibrium with the atmosphere in its immediate neighbourhood despite the low coefficient of diffusion of water in wool. This is because equilibrium is attained by changing the moisture content of the atmosphere

rather than that of the wool. This is true even with fabrics because the low packing density maintains the fibres everywhere in contact with the atmosphere.

Fig. 2 shows the variation in the diffusion coefficient of water in keratin[6] at various regains. This coefficient is only of the order of 10^{-7} cm^2/s. Even when allowance is made for the greater concentration gradients in wool, as

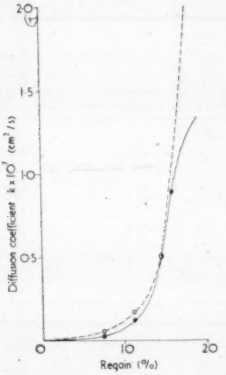

[Reproduced from the *Transactions of the Faraday Society*]

Fig. 2. Variation in diffusion coefficient of water in keratin at various regains

- - - - - theoretical
——— experimental: curves made to coincide at *A*

compared with air for two different equilibrium conditions between air and wool, this means that the rate of diffusion through keratin is only 1/100 of that through a corresponding air layer for which the diffusion coefficient is of the order of 10^{-1} cm^2/s. Nevertheless, because of the small diameter of the wool fibre sufficient water to reduce the moisture content of its surroundings to equilibrium is rapidly absorbed. Further absorption is then controlled by the rate of diffusion through the atmosphere.[7]

This argument also applies to a large mass of wool. Just as with the flow of heat, the flow of water vapour through a mass of wool largely takes place through the air. The only difference is that since the diffusion coefficient in wool is less than that in air, the diffusion coefficient for a fabric is slightly less than that of air, whereas the thermal conductivity is slightly higher.

When there is a difference in both temperature and moisture content between the atmosphere on the two sides of a fabric the direction of flow of moisture is controlled by the water vapour concentration gradient in the atmosphere rather than by that in the wool. Because of the rapid variation of saturation vapour pressure with temperature, the humidity on the high temperature side, and hence the regain of wool, may be less than that on the low temperature side, even though the water vapour concentration and the water vapour pressure is higher. The data recorded in Fig. 3 show the vapour pressure and temperature between different layers of clothing and also the saturation vapour pressure curve. It will be noticed that the relative humidity is much lower next to the skin, although the vapour pressure is higher. It is for this reason that the body can lose heat by insensible perspiration even to a saturated atmosphere. Because the thermal conductivity of a fabric is slightly higher than that of air and increases with fabric density whereas the diffusion coefficient is lower, the temperature drop across a dense fabric layer will be less than across an equivalent air layer and the vapour pressure drop greater. This will cause the vapour pressure-temperature curve to be steeper. If such a fabric forms the outer garment (as is often the case) the curve through the clothing assembly will be concave downwards (as shown by the dotted curve) and there is a risk of this curve cutting the saturation curve, particularly with high humidities near the skin (approaching sweating), and condensation will occur on the inner surface of the outer garments.[8]

Another consequence of the large moisture content of wool, and indeed of most natural fibres, is that they tend to

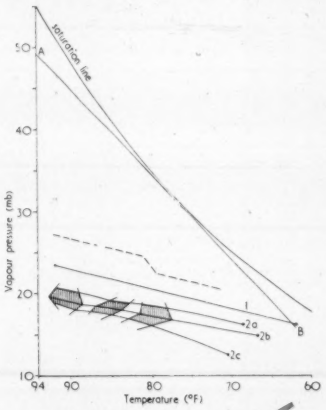

[Reproduced from *Wool Research, Vol.* 2]

Fig. 3. Microclimatic conditions within clothing

1, Cassie; 2, Ogden and Rees: 2*a*, sitting resting; 2*b*, sitting writing; 2*c*, prone; shaded areas, fabric layer.
● ambient conditions.

control the humidity of their surroundings instead of vice versa. Thus at 65° F (18½° C) it will take as much water to change the regain of 10 lb of wool by a given amount as it would to change the humidity of a room of 2000 ft^3 capacity by an equivalent amount. This is about the size of a medium living room (14 × 14 ft) and the wool in the carpets alone would weigh much more than this. This example shows the value of soft furnishings made of the natural and regenerated fibres as a humidistat. This fact is realized by the curators of many of our art galleries who make use of curtains and draperies as an invaluable aid to the preservation of our art treasures,[9] where air conditioning is not available.

The deduction that the air in immediate contact with a wool material is always in moisture and thermal equilibrium with it means that the theory developed for the wet bulb thermometer can be applied to discussion of the transfer of heat and moisture between wool and the surrounding atmosphere. August's hypothesis, on which all wet bulb theory is based, states that the air stream flowing over a wet bulb supplies the heat necessary to evaporate sufficient water from the bulb to saturate itself at the wet bulb temperature. This

hypothesis has been verified by much experimental work, but it has never been satisfactorily deduced from theory. Taylor[10] probably got closest to it, but even his theory is not entirely convincing. Taylor's theory rests on the fact that the ratio of the heat and water vapour transfer coefficient is the same whether transfer takes place by bulk transport as in August's simple hypothesis, or by diffusion of water vapour and conduction of heat. The heat balance that results from this hypothesis is

$$L_w k_V (p_w - p_a) = k_T (t_a - t_w)$$

where L_w is latent heat of evaporation of water from the wet bulb, t_a, p_a are the temperature and water vapour pressure in the ambient atmosphere, t_w, p_w are those for air in equilibrium with the wet bulb, and k_V, k_T are the transfer coefficients for water vapour and heat respectively.

Putting in the value of the ratio of the two coefficients this leads to the wet bulb equation

$$(p_w - p_a) = \frac{P - p_w}{2{\cdot}6L_w}(t_a - t_w)$$

or at ordinary temperatures when p_w can be neglected in comparison with P, the atmospheric pressure

$$(p_w - p_a) = (P/2{\cdot}6L_w)(t_a - t_w)$$

The equation requires modification for unventilated hygrometers, not because of the difference in the ratio of k_V and k_T for diffusion and bulk transport, but because in still air the heat received by the wet bulb from radiation from solid bodies at the ambient temperature becomes comparable in amount to that received by conduction and the basic assumption no longer holds.

In transferring this equation to exchange of water vapour with fibres[11] at regains below saturation the only modifications required are that the latent heat is now that of evaporation of water from wool and that p_w and t_w are the vapour pressure and temperature of the air in equilibrium with wool at the appropriate regain. The condition that the regain of the wool remains sensibly unchanged during the short time taken for the wool to reach the temperature given by the wet bulb equation gives the appropriate relation between t_w and p_w. This relation is Kirchhoff's relation which can be used to relate t_w and p_w to the original temperature and pressure t_0 and p_0, to which the wool has been conditioned. We have, therefore, two relations between the unknowns t_w and p_w and so we can obtain the temperature and water vapour pressure of the air in contact with the textile material. These values will, of course, only apply initially because as soon as the regain of the material is changed appreciably, new values will have to be used in Kirchhoff's equation. A different value of t_w will of course result, and this means that the temperature of the textile material must be changed. August's hypothesis does not, therefore, strictly hold because heat will be required for this temperature change; the amount of heat required for this purpose is, however, negligible in comparison with that used in evaporating water and so can be safely ignored.

The two simultaneous equations used for obtaining t_w

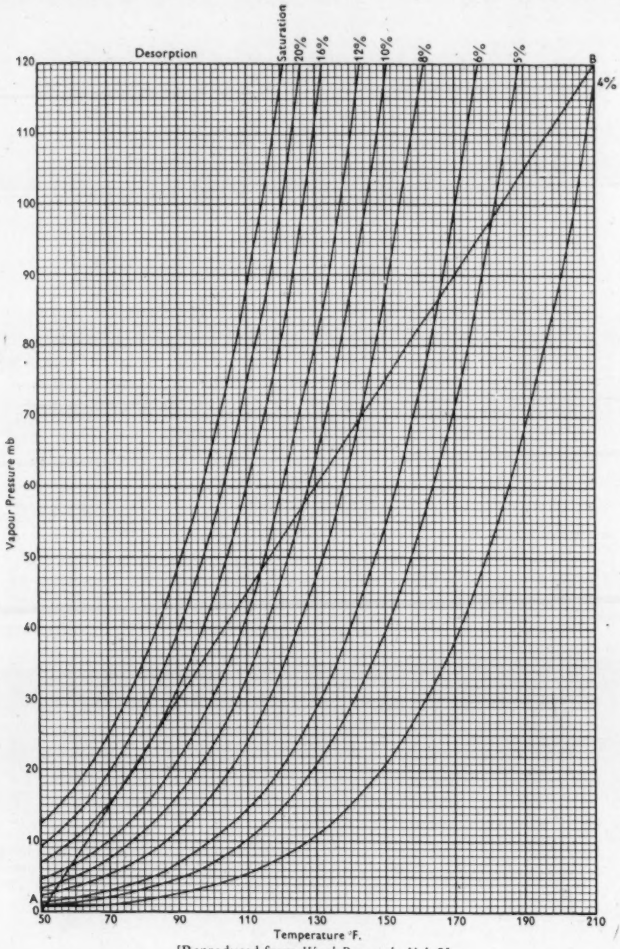

[Reproduced from *Wool Research*, *Vol.* 2]

Fig. 4. Relation between vapour pressure and temperature for wool at different regains (desorption)

and p_w cannot be solved formally and recourse must be had to numerical or graphical methods.[12] Figs. 4 and 5 provide a convenient means of carrying out the solution by the latter method. The curves represent Kirchhoff's relation for a number of wool regains under desorption and absorption conditions respectively. All that is needed to solve the equations is to draw the wet bulb line through the point representing the ambient conditions. The point at which this line cuts the curve for the appropriate Kirchhoff relation then gives the values of t_w and p_w. The sloping line running across the graph is perpendicular to the average value of the slope of the wet-bulb line and so can be used in conjunction with a set-square in drawing this line.

The simplest application of these equations is to a change of temperature. If a mass of textile material is in equilibrium with air of 20° C (68° F) and 60% r.h. or of water vapour pressure 14 mb and air at 35° C (95° F) and of water vapour pressure 14 mb is forced through it, then it can be shown from these relations that the temperature of the air issuing from the textile material should be 26° C (78° F). The water vapour pressure in the air should be 20 mb.

An experiment[13] was carried through to test this theory; in particular it tests our basic assumption that wool fibres are always in equilibrium with the air surrounding them or that the keratin material is so exposed to the air that its low diffusion coefficient causes no delay. Fig. 6 shows the apparatus that was used for the experiment. A cylinder *ABCD* of textile material was conditioned by air at 20° C after which the air temperature was changed to 35° C whilst maintaining the water vapour pressure at 14 mb. The air temperature before and after passing through the cylinder was measured by means of the thermocouples T_1 and T_2. The resulting temperature-time relations are shown in Fig. 7. The results for all textiles show an initial rapid increase in the temperature of the air which has passed through the textile to about 26° C. This is in excellent agreement with value obtained by application of the wet bulb theory. When this "wet bulb" temperature has been attained there follows a gradual increase in the temperature of the exit air until it reaches the value of the incident air, i.e. 35° C. During this period the regain of wool slowly decreases from 16% regain to 10% which is consistent with the new conditions.

A change of this type generally occurs in clothing when the wearer proceeds from indoors to outdoors. The water vapour content of the atmosphere is roughly the same in a well-ventilated room indoors as it is outdoors, and in winter a change in conditions corresponds to a decrease in temperature accompanied by an increase in relative humidity.

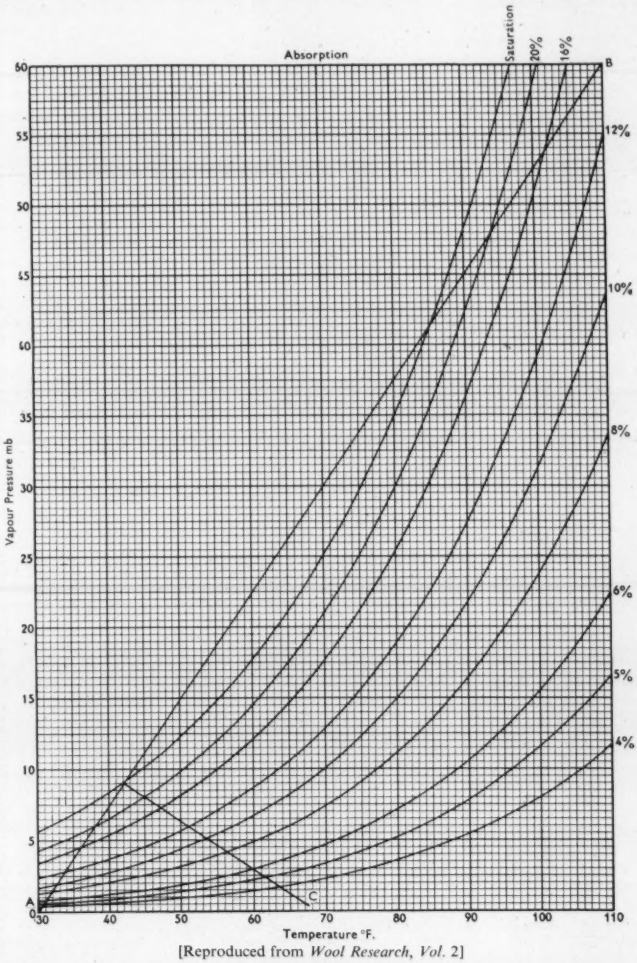

[Reproduced from *Wool Research, Vol.* 2]

Fig. 5. Relation between vapour pressure and temperature for wool at different regains (absorption)

Let us consider what happens when outside air at 45° F (7·2° C) and 8 mb vapour pressure (79% r.h.) is blown on to clothing initially in equilibrium with air at 65° F (18½° C) and 8 mb vapour pressure (38% r.h.) which are not uncommon conditions indoors on a cold winter's day. Reference to Fig. 5 shows that assuming the wool has

attained its original equilibrium from the dry state, the equilibrium regains will be 10% and 20% respectively. Immediately the cold air comes into contact with the outer layers of the clothing it will come to equilibrium with wool at 10% regain under the conditions given by the wet bulb equation, the wool being assumed to attain the correct temperature with negligible evolution of heat. These conditions would take place, possibly twice as great, leading to an even greater evolution of heat.

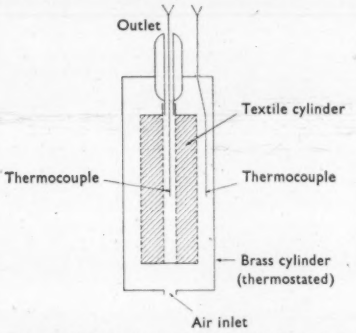

[Reproduced from the *Transactions of the Faraday Society*]

Fig. 6. Apparatus for measuring rate of transmission of temperature changes

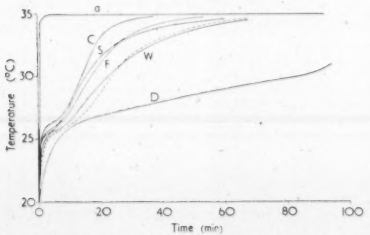

[Reproduced from the *Transactions of the Faraday Society*]

Fig. 7. Rate of propagation of temperature changes

a, outside air temperature; - - - - theoretical curve; *C*, cotton; *S*, silk; *F*, Fibro; *W*, wool; *D*, curve for diffusion through cotton.

are given by the line C in Fig. 5, and it will be seen that the initial equilibrium is attained at about 54° F. This "initial" temperature is about half-way between the original and final temperatures (65° F and 45° F respectively). This comes about because at normal temperatures the slopes of the wet bulb line and the Kirchhoff line are approximately equal and opposite.

In the above example the regain of the wool has been changed by 10% so that the wool in a man's clothing, which weighs about 5 lb will absorb ½ lb of water. The heat liberated by this absorption is about 600 B.t.u. (666 cal/g water); this may be compared with the heat normally generated by the body which is about 400 B.t.u./h. The heat liberated by the clothing in going from indoors to outdoors is, therefore, about the same as that produced by the body in 1½ h. If the outside temperature were lower and the humidity consequently higher, an even greater regain change

WATER REPELLENCY

Apart from these thermal effects the fibrous structure of textile materials also contributes in a considerable degree to their water repellency. The ordinary formula for the angle of contact between a liquid and a solid is

$$\cos\theta = (\gamma_{SA} - \gamma_{SL})/\gamma_{LA}$$

where θ is the contact angle measured in the liquid, γ_{SA} is the solid-air interfacial energy, γ_{SL} is the solid-liquid interfacial energy, and γ_{LA} is liquid-air interfacial energy.

This equation shows that the cosine of the contact angle is the ratio of the energy required to replace unit area of solid-liquid interface by a solid-air interface to that required to produce unit area of liquid-air interface. This equation only holds for contact with a smooth surface for which unit area is covered per unit length when the line of contact moves forward unit distance. With rough and porous surfaces this simple relation between the advance of the line of contact and the surface area covered no longer holds.

If a smooth solid surface is roughened so that unit plane geometrical area has an actual surface area σ times that of the "smooth" surface, the energy gained in forming the solid-liquid interface will be $\sigma(\gamma_{SA} - \gamma_{SL})$, and the contact angle, θ', for the rough surface will be given by[14]

$$\cos\theta' = \sigma(\gamma_{SA} - \gamma_{SL})/\gamma_{LA}$$

This equation explains the apparently high advancing contact angles obtained when a wool fibre is partly immersed in water. The wool fibre has a rough scaley surface and because of the roughness the apparent contact angle is large, being around 120°. The true contact angle for smooth keratin is probably between 90 and 100°.

We have seen, however, that a wool textile material is very porous, and that the surface of a fabric is a heterogeneous one, consisting of rather more air spaces than there are solid fibres. We can extend this argument to a heterogeneous surface of this type;[15] in fact, if unit geometrical area of a surface has an actual surface area σ_1 of real contact angle θ_1 and an area σ_2 of contact angle θ_2, the apparent contact angle θ'' for the composite surface is given by

$$\cos\theta'' = \sigma_1 \cos\theta_1 + \sigma_2 \cos\theta_2$$

This equation reduces to the previous one when σ_2 is zero. The interesting case for textiles is that when σ_2 is composed of air spaces, θ_2 is then 180° and the equation for the apparent contact angle becomes

$$\cos\theta'' = \sigma_1 \cos\theta_1 - \sigma_2$$

This formula was tested by forming a cage of fine wires which were waxed to give an advancing contact angle of 105° and a receding one of 93°. The areas σ_1 and σ_2 can then be obtained from the geometry of the system, and the apparent contact angle for a surface of the cage can be calculated. Table 3 shows how very well the calculated and observed angles agree.

The existence of these very large contact angles means that a drop of water placed on the cage is extremely mobile and, in fact, this is a characteristic of such a structure. Raindrops that fall on it immediately pearl into drops and run off. The same phenomenon arises when a fabric is first exposed to rain. The apparent advancing and receding angles can be calculated for fabrics of different density.[16] The results are shown in Figs. 8(*a*) and (*b*). The bulk density of wool yarn and fabrics is usually around 0·4, and these

Table 3. *Theoretical and observed contact angles for a grid*

$2r$ (cm)	$2(r+d)$ (cm)	σ_s	σ_A	θ''_A Calc.	θ''_A Obs.	θ''_R Calc.	θ''_R Obs.
0·007	0·025	0·366	0·730	145½°	143°	138½°	138°
0·007	0·0404	0·227	0·833	153°	152°	147½°	148°
0·013	0·025	0·680	0·498	132½°	133°	122°	118°
0·013	0·0404	0·422	0·689	143°	143°	135½°	135½°

figures show how important the porosity is in increasing the apparent advancing and receding angles.

These phenomena are, of course, most strikingly brought out in the case of ducks' feathers. It has often been assumed that a duck uses some remarkably water repellent material, but even the advancing contact angle for the stem of a duck's feather is around 90 to 100°. The receding angle is approximately 60°. However, the feather is formed of a very open framework of barbules which are roughly 8 μ in diameter, and the ratio of $(r + d)/r$ for one layer of parallel barbules is roughly 5 (Fig. 9). This geometry of the feather means that the true advancing contact angle of 90 to 100° becomes 150° and the receding one 130°. It is because of these very large apparent advancing and receding contact angles that water runs off a duck's back. Hens' feathers often fail to show this phenomenon because there is almost a continuous film of grease between the barbules, and, of course, sea birds suffer from the same fate when oil becomes prevalent and forms a film over the fine structure of their feathers.

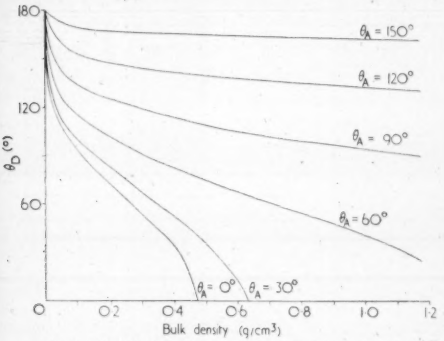

[Reproduced from the *Journal of the Textile Institute*]

Fig. 8(*a*). Variation of apparent yarn advancing contact angle with density

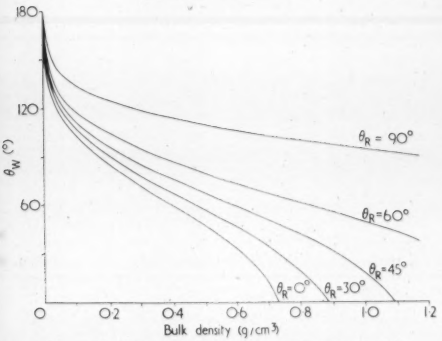

[Reproduced from the *Journal of the Textile Institute*]

Fig. 8(*b*). Variation of apparent yarn receding contact angle with density for true fibre advancing contact angle 90°

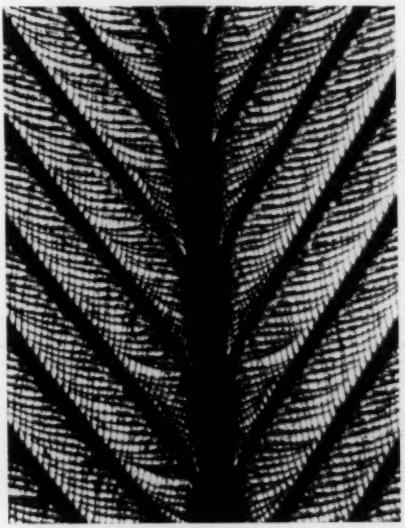

[Reproduced from *Wool Research*, *Vol.* 2]

Fig. 9. Photomicrograph of duck's feather

Although the porous structure of textile materials contributes to their water repellency by increasing the contact angle between water drops and the fabric, water can be forced through the pores if sufficient pressure is applied. The force required to effect this will depend on the separation of the yarns or fibres and the contact angle with them. If water is forced sufficiently far into the pores of yarn some will be left behind when the water recedes, thereby reducing the contact angle. With the larger holes found between yarns in some fabrics, the impact pressure of a large raindrop may be sufficient to produce penetration. It is important, therefore, to determine the pressure required to produce penetration for the different types of assembly. As water is forced into the space between two fibres the curvature will at first increase, thereby increasing the force resisting penetration, and then decrease (Fig. 10). It can be seen from the

geometry of the figure that the radius of curvature of the drop will be a minimum when the line PO is a minimum, i.e. when the centre of curvature is mid-way between the centres of the two fibres. This minimum radius r_S is given by

$$r_S = r\cos\theta_A + \sqrt{(r^2 + d^2 - r^2\sin^2\theta_A)}$$

where r is the fibre radius, d is the fibre separation, and θ_A is the fibre advancing contact angle. The minimum pressure required for penetration is therefore

$$\Delta P = \gamma/[r\cos\theta_A + \sqrt{(r^2 + d^2 - r^2\sin^2\theta_A)}]$$

for long narrow pores, and

$$\Delta P = 2\gamma/[r\cos\theta_A + \sqrt{(r^2 + d^2 - r^2\sin^2\theta_A)}]$$

for square pores (as between yarns in a fabric).

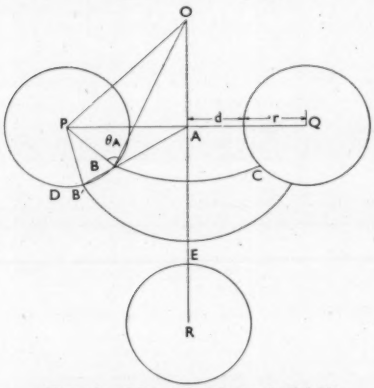

[Reproduced from *Wool Research, Vol.* 2]

Fig. 10. Variation of curvature of interface with depth of penetration

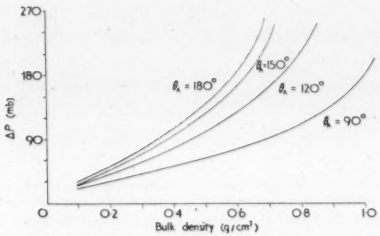

[Reproduced from *The Journal of the Textile Institute*]

Fig. 11. Pressure for penetration into yarns

Fig. 11 shows the pressure required to produce penetration into a yarn of various densities, assuming a hexagonal packing of fibres of 20 μ diameter, and Fig. 12 the pressure required to produce penetration through the pores of fabrics with yarn diameter (a) 0·05 cm for different types of weave (b/a is the product of the number of threads per cm and the thread diameter). The fibre advancing contact angle has been used in constructing Fig. 11 and the yarn contact angle in constructing Fig. 12.

The discussion given above suggests that the ideal water repellent porous fabric will have a low bulk density with as uniform a structure as possible so that there are no inter-yarn interstices. It has already been shown that wool fibres easily lend themselves to structures of this type in which the fabric density is made equal to yarn density at comparatively low densities. The ideas expressed here on factors determining water repellency were tested using a fabric composed of card web (similar in structure to a roll of cotton wool) lightly felted to a piece of muslin. When subjected to test this stood up indefinitely to a shower (equivalent to 3 in. of rain per hour) which penetrated a close woven gaberdine within a few minutes.

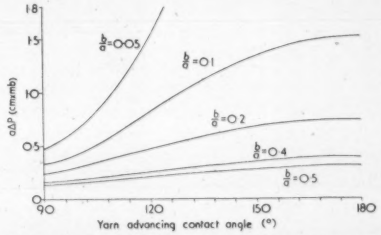

[Reproduced from the *Journal of the Textile Institute*]

Fig. 12. Pressure required to force water through a fabric

ACKNOWLEDGEMENT

I am much indebted to Mr. F. L. Warburton who has prepared this paper from rough lecture notes.

REFERENCES

(1) Woods, H. J. *Physics of Fibres* (London: Institute of Physics, 1955).
(2) Kozeny. *Wasserkraft und Wasserwirtschaft*, **67,** p. 1 (1931).
Sullivan, R. R., and Hertel, K. L. *Advances in Colloid Science*, **1,** p. 37 (1942).
(3) Cassie, A. B. D. *J. Text. Inst.*, **37,** p. P154 (1946).
(4) Baxter, S. *Proc. Phys. Soc.* [*London*], **58,** p. 105 (1946).
(5) Schuhmeister, J. *Ber. K. Akad. Wien.* (*Math–Naturw. Klasse*), **76,** p. 283 (1877).
(6) King, G. *Trans Faraday Soc.*, **41,** p. 479 (1945).
(7) King, G., and Cassie, A. B. D. *Trans Faraday Soc.*, **36,** p. 445 (1940).
(8) Warburton, F. L. *Wool Research, Vol.* 2, *Physical Properties*, p. 73. (Leeds: Wool Industries Research Association, 1955.)
(9) Rawlins, F. I. G. *Research*, **11,** p. 5 (1958).
(10) *See* Whipple, F. J. W. *Proc. Phys. Soc.* [*London*], **45,** p. 310 (1933).
(11) Cassie, A. B. D. *Trans Faraday Soc.*, **36,** p. 453 (1940).
(12) Warburton, F. L. *Wool Research Vol.* 2, *Physical Properties*, p. 25 (Leeds: Wool Industries Research Association, 1955).
(13) Cassie, A. B. D., and Baxter, S. *Trans Faraday Soc.*, **36,** p. 458 (1940).
(14) Wenzel, R. N. *Industr. engng Chem.*, **28,** p. 988 (1936).
(15) Cassie, A. B. D., and Baxter, S. *Trans Faraday Soc.*, **40,** p. 546 (1944).
(16) Baxter, S., and Cassie, A. B. D. *J. Text. Inst.*, **36,** p. T67 (1945).

Some developments and applications of microfocus X-ray diffraction techniques

By A. FRANKS, Ph.D., Metallurgy Division, National Physical Laboratory, Teddington, Middlesex

[*Paper received* 8 *January*, 1958]

This paper describes a low angle X-ray scattering camera, a microbeam camera and an electron gun for a microfocus X-ray tube. In the low angle scattering camera which can resolve a spacing of 1000 Å using CuK radiation, the X-ray beam is totally reflected by two crossed bent glass plates, which focus the relatively intense beam on to a small spot on the film. Provision is made for accurately positioning a selected area of the specimen in the path of the beam. This facility is also provided in the microbeam camera for transmission and back reflexion work. In the electron gun, focusing is facilitated by independent adjustments of the positions of the filament and grid cylinder, while the tube is in operation.

A LOW ANGLE SCATTERING CAMERA

Low angle scattering studies of fatigued metal foil[1] which have been carried out have indicated the usefulness of a camera embodying the following features:

(1) An intense beam with high resolution achieved in all directions on the film; the beam must therefore be of the "pinhole" type;
(2) A monochromatic beam;
(3) Small area of specimen irradiated.

The last feature is of particular importance in the examination of fine grained polycrystalline material, but is not usually embodied in the more conventional low angle scattering cameras.

The design of the present camera is based on two physical considerations. Firstly, X-rays are totally reflected when incident on a surface at a sufficiently small glancing angle (approximately 11′ for CuK radiation on glass), and by suitably adjusting the glancing angle, partial monochromatization may be achieved, the characteristic and softer radiation only being reflected. Secondly, rays diverging from the focus of a mirror of elliptical cross-section will, after reflexion, reunite to form a line image passing through the other focus. In practice, it is more convenient to use a mirror of circular cross-section, the curvature being obtained by applying equal bending couples near the edges of a rectangular plate. Fig. 1 is a diagrammatic representation of the camera, the arrows representing the traverses. A photograph of the camera clamped to the X-ray tube is shown in Fig. 2.

The camera was designed to resolve a spacing of 1000 Å in the first order using CuK radiation and its dimensions were chosen to achieve this resolution with the minimum loss of intensity, using the calculated data of Franks.[2] The

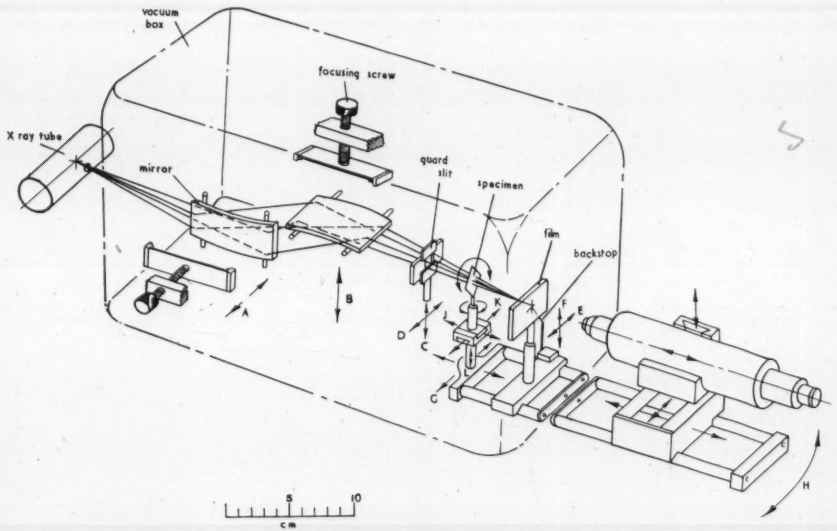

Fig. 1. The low angle scattering camera

principal dimensions of the camera are: X-ray focus to film distance 34 cm, the length of each reflector 6 cm, specimen to film distance 5 cm, area of beam at specimen 40 × 80 μ.

Description of the apparatus. The X-ray source is a microfocus tube[3] (by Hilger and Watts Ltd.), mounted on a concrete table top to ensure stability. The component parts of the camera are screwed to a 1 in. thick plate of mild steel which is supported by legs bolted to steel plates sunk into the concrete. The X-ray tube is clamped to the base plate by means of a trunnion, so that it can rotate about a vertical axis passing through (or close to) the focal spot.

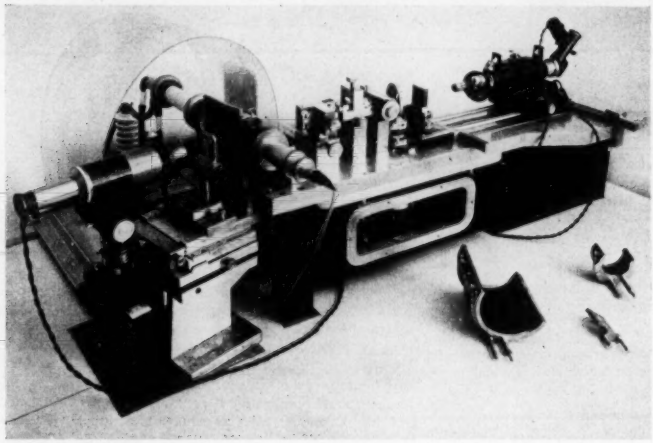

Fig. 2. From left to right: microbeam camera, X-ray tube with modified electron gun, low angle scattering camera. The cylindrical film holders and fluorescent crystal mount are in the foreground

The bending couple is applied to the mirrors by means of a focusing screw (Fig. 1). The main features of the reflector units are also shown in Fig. 1. The nozzle-shaped guard slit (Fig. 3) allows a specimen in the form of a sheet to be oscillated about a vertical axis while in close proximity to the slit; this is desirable to ensure high resolution. To set the slit, the two fixed jaws are first positioned by means of the traverses *C* and *D* (Fig. 1) followed by adjustment of the movable jaws. The specimen holder, backstop, film holder and microscope are mounted on an optical bench which has a vertical axis of rotation coincident with the axis of rotation of the specimen. This arrangement is useful, though not essential, in many applications of microbeam techniques, since it facilitates the irradiation of a selected area of the specimen and also ensures that the film is perpendicular to the X-ray beam. The end portion of the bench, between the normal position of the film holder and the microscope can be detached. This allows a vacuum tight box (Fig. 1) to be placed over the camera, the seal being effected by means of an O-ring clamped against the steel base plate. A box of the same dimensions is permanently bolted in the corresponding position below the base plate and contains the mechanism for oscillating and rotating the specimen. The use of two similar boxes ensures that no distortion of the base takes place on evacuation. The operation of the camera in vacuum (or hydrogen) is essential only when using the longer wavelength radiations.

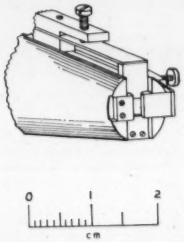

Fig. 3. The guard slit

The lower container has a vacuum tight cover plate (removed in Fig. 2) which allows easy access to the motorized drive and the associated circular scale used for setting the specimen at a specific orientation with respect to the beam. The specimen is mounted on two cross slides *J* and *K* (Fig. 1), which are used to centre it. For the thin metallurgical specimens [Fig. 4(*b*)], employed in low angle scattering

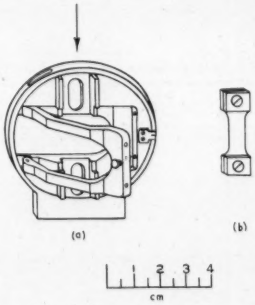

Fig. 4. (*a*) Retaining ring and specimen clamp (*b*) Specimen
The arrow indicates position of specimen in clamp

studies of fatigue, a vertical retaining ring [Fig. 4(*a*)], in which the specimen clamp is free to rotate about a horizontal axis, is screwed to the cross slides. The specimen clamp can be accommodated both on the camera and on the fatigue machine, in order that handling of the delicate specimen is reduced to a minimum.

Adjustment of the camera. The X-ray tube is clamped to its trunnion so that the beam passes approximately along the centre of the base plate. The vertical reflector is then rotated until the reflecting surface is roughly parallel to the X-ray beam. A small adjustment of the horizontal traverse *A*, is sufficient to produce a reflected beam which can clearly be seen on a fluorescent screen held near the film holder. The horizontal mirror is then adjusted in a similar way. Having obtained a beam reflected in turn from both mirrors, a critical focusing adjustment can be made. The beam may be focused photographically by taking a series of trial photographs for different settings of the focusing screws. A more rapid and convenient method relies on the use of a single crystal of CsI–Tl[4] as a high resolution fluorescent screen. This is shown in its mount in Fig. 2, lying between the two cylindrical film holders; when in use, it is placed in the film holder base and may be observed under high magnification (×400). The adjustments consist of translating each reflector (traverses *A* and *B*) to obtain the maximum glancing angle of incidence consistent with X-ray reflexion: the reflected beam flashes into view at the critical angle and the focusing screws are then used to form a sharp image. The whole procedure can be completed in a matter of minutes. Finally, the guard slit is set so that the jaws are just clear of the main beam while the backstop (a 0·006 in. tungsten wire) is positioned to intercept the beam, by means of the two micrometer controls *E* and *F*.

The optical bench is used in the following manner. The axis of rotation of the bench is translated laterally (*G*) until it intersects the X-ray beam after which the bench is aligned parallel to the beam by means of traverse *H*. Both these operations are conveniently carried out using the microscope and a fluorescent crystal, a thin wire on the specimen holder serving to define the axis of rotation. It is observed with the microscope which can be brought close to it after removing the film holder from its base and rotating the backstop out of the path of the microscope. The microscope can now be used either at the focal spot to examine the focus and to position the backstop, or at the specimen, without requiring any further lateral adjustment.

To irradiate a selected area of the specimen, a fluorescent crystal is placed in the beam at the specimen position and the microscope is so adjusted that its cross wires coincide with the fluorescent image. The crystal is then replaced by the specimen which is positioned by means of the traverses *J*, *K* and *L*, until the required area coincides with the cross wires. The microscope is not moved during this operation, so that the accuracy of location of the selected area depends only on the accuracy with which it can be located in the microscope and not on the mechanical perfection of the slideways.

Two cylindrical film holders (Fig. 2) are used for large angle diffraction work. With the larger one, which has a radius of 5 cm, both the low angle scattering and Bragg diffraction patterns are obtained on one film. This is convenient for obtaining orientation relationships. The smaller film holder is a 5 cm diameter focusing camera of the Seemann–Bohlin type. It can be used to great advantage to obtain sharp, well defined diffraction lines owing to the narrowness of the focused beam. This leads to high accuracy in measurement: the width of the (111) reflexion from an annealed silicon powder specimen was less than 20 μ. An unfavourable feature of this arrangement is that the volume of the specimen irradiated is much smaller than that in a Seemann–Bohlin camera with a crystal monochromator. The exposure times are therefore correspondingly longer, while scanning of the specimen will usually be required.

Performance of the camera. Fig. 5 is the diffraction photograph of collagen from a rat tail tendon stained in

Fig. 5. Diffraction pattern of collagen from stained rat tail tendon

phosphotungstic acid. The first order reflexion (approximately 640 Å) is clearly visible and the maximum spacing which can be resolved is about 1000 Å. The exposure time was 10 min. For longer exposures, the resolution decreases owing to parasitic scatter. Fig. 6 is the diffraction photograph of collagen from a kangaroo tail tendon, the exposure time was 2½ h. The first order reflexion is still visible; since it is heavily overexposed the true resolution is somewhat greater than suggested by the photograph. The increase in length of successive orders is similar to the patterns obtained by Bear and Bolduan.[5] For the sake of clarity of reproduction, Fig. 6 is a composite enlargement. The technique is due to Mr. Hammond of the Pest Infestation Laboratory and will be published elsewhere.

The camera is being used at present to study the low angle scattering from a fatigued metal foil. Results will be published elsewhere, but it is of interest to note the importance of irradiating small accurately selected areas. Fig. 7(*a* and *b*) shows typical patterns from one grain of a fatigued polycrystalline copper foil. The change in the patterns result from a rotation of the specimen through 2½° about a vertical axis.

Fig. 6. Diffraction pattern of collagen from kangaroo tail tendon

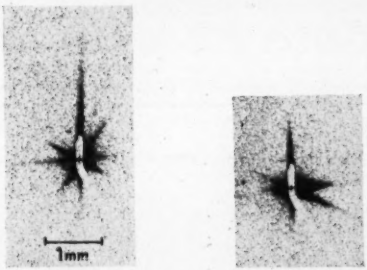

(*a*) (*b*)

Fig. 7. (*a*) Low angle scattering pattern from grain of fatigued copper foil. (*b*) Same as (*a*) with grain rotated through 2½° about a vertical axis

(Scale on Fig. 7(*a*) represents 1 mm on original photographs of Figs. 5, 6 and 7.)

A MICROBEAM CAMERA

Several methods have been developed to irradiate a selected area of a specimen with a microbeam. Lewis[6] describes a direct and accurate optical technique; however, relatively small specimens are required and the optical system employed is not conductive to high definition. A modification by Holmes and Fochs[7] eliminates the restriction on specimen size, but at the expense of a loss in the accuracy of location. A combination of various features of both these cameras has been used to build an instrument capable of examining large specimens, either in transmission or back reflexion, with a precision limited only by the accuracy with which the required area can be centred on the cross wires of a high power microscope.

The camera is shown in Fig. 2. Collimation is provided by a conical hole machined in tantalum or gold disks, 1 mm thick, using the technique described by Middleton.[8] The diameter of the smallest pinhole is 10 μ. The specimen is placed on a rotary table shown diagrammatically in Fig. 8.

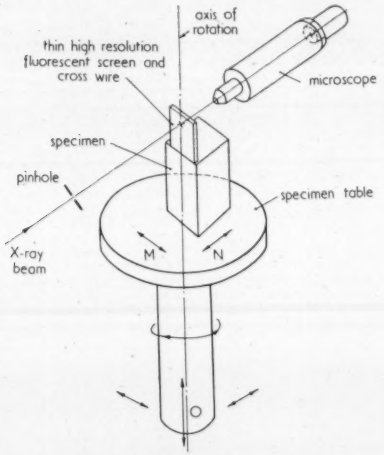

Fig. 8. The microbeam camera

The bearing is long steel rod held in a closed vee block, all the bearing surfaces being hardened and lapped. The specimen to film distance may be varied between 1 cm and 4 cm. Integral with the specimen holder is a mount for both a single crystal fluorescent screen and a fine cross wire which is coplanar with it.

To align the camera, collimators are placed in the transmission (not shown) and back reflexion film holders which are kinematically mounted on the upper plate (Fig. 2) together with the specimen holder. Adjustment of the plate, to allow the beam to pass through the system, ensures that the beam is perpendicular to the film holders and parallel to the slideway.

For back reflexion work, the following procedure is used in selecting a specific area for examination. The specimen mount cross wires are made coincident with the vertical axis of rotation using traverses M and N (Fig. 8), the microscope cross wires are then focused on the image of the beam on a high resolution fluorescent screen. Within the limits of the precision of this setting, any object which is focused on the microscope cross wires will be both on the vertical axis of rotation and in the path of the X-ray beam. Errors which arise due to the depth of focus of the objective are unimportant, because the microscope can be aligned parallel to the X-ray beam. The required area of the specimen is brought into coincidence with the microscope cross wires using traverses M, N and O. The microscope is then withdrawn and the specimen is rotated through 180° about the vertical axis to bring it into the path of the beam. The camera has been employed in the study of imperfections in metal crystals and has also been used successfully in analysing an inclusion of cross-section 40 × 50 μ.

A MODIFIED ELECTRON GUN

In the auto-biasing electron optical system used in the Ehrenberg and Spear[3] microfocus tube, it has been found that for the best focus, the position of the filament within the grid cylinder of the electron gun is critical to less than 0·1 mm along the axis of the tube. It is therefore convenient to be able to adjust the filament independently of the grid cylinder while the tube is in operation. The method by which this is achieved is shown diagrammatically in Fig. 9, while the gun

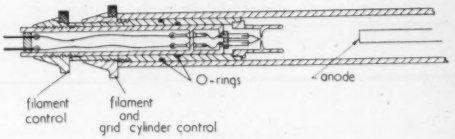

Fig. 9. The electron gun

is shown attached to the X-ray tube in Fig. 2. Care has been taken to provide a good bearing surface for the filament slide, in order to prevent radial movement of the filament.

ACKNOWLEDGEMENTS

The author desires to acknowledge the assistance rendered by his colleague Mr. K. Thomas who took the diffraction photographs and also by the staff of the Central Drawing Office for contributing greatly to the design of the apparatus. The low angle scattering camera was constructed by Mr. G. V. Anthony and the microbeam camera by Mr. K. Young, both of the Metrology Division Workshop.

The work described above has been carried out as part of the General Research Programme of the National Physical Laboratory and this paper is published by permission of the Director of the Laboratory.

REFERENCES

(1) Franks, A., and Holden, J. *Nature* [*London*], **176,** p. 1022 (1955).
(2) Franks, A. *Proc. Phys. Soc.* [*London*] *B*, **68,** p. 1054 (1955).
(3) Ehrenberg, W., and Spear, W. E. *Proc. Phys. Soc.* [*London*] *B*, **64,** p. 67 (1951).
(4) Franks, J. *Brit. J. Appl. Phys.*, **4,** p. 377 (1953).
(5) Bear, R. S., and Bolduan, O. E. A. *Acta Cryst.*, **3,** p. 236 (1950).
(6) Lewis, D. *J. Sci. Instrum.*, **32,** p. 467 (1955).
(7) Holmes, P. J., and Fochs, P. D. *J. Sci. Instrum.*, **33,** p. 239 (1956).
(8) Middleton, S. P. *J. Sci. Instrum.*, **32,** p. 399 (1955).

Temperature distribution throughout a stack of electrical sheet steel during annealing

By R. J. WAKELIN, Ph.D., A.I.M., A.Inst.P., Atomic Weapons Research Establishment, Aldermaston, Berks.

[*Paper received* 9 *December*, 1957]

During the final annealing process in the manufacture of 4% silicon–iron electrical sheet, the temperature at any one time varies horizontally across the plane of the sheets and vertically up the stack. The temperature distribution in the horizontal plane of sheets 8 ft × 3 ft × 0·014 in. thick has been calculated theoretically and compared with that determined experimentally. By combining the results from a number of experiments, the temperature distribution throughout a stack of sheets has been obtained at all times during the three-day annealing cycle.

The final process during the manufacture of hot-rolled silicon steel to be used for electrical laminations consists of an anneal which lasts for a number of days. The hot-rolled sheets are produced in large sizes, up to 10 × 3 ft in area and are frequently about 0·014 in. thick. Many hundreds of these sheets are annealed at a time and from consideration of the method of heating, it was apparent that some parts of the stack of sheets received a different heat treatment from others. As heat treatment could be related to electrical quality, it was hoped to improve the latter by investigating the former. Further, during the subsequent stamping of electrical sheet into large rotors and stators, distortion took place which was thought to be due to internal stresses in the steel sheet. This investigation was undertaken to discover the manner in which these stresses were caused and, if possible, to suggest means whereby they could be reduced.

WORKS PROCEDURE

The sheets are stacked on the furnace hearth in the manner shown in Fig. 1. The stack is built up on a 1 in. thick steel plate which is raised above the solid foundation of the refractory brick hearth, so that heat can penetrate underneath. It has been found by years of experience that the curvature of the stack is essential to avoid buckling of the sheets during the annealing process. This curvature is obtained by placing a large cast iron wedge under each corner of the stack and packing the space between them with sand which is smoothed into a curve before the sheets are loaded.

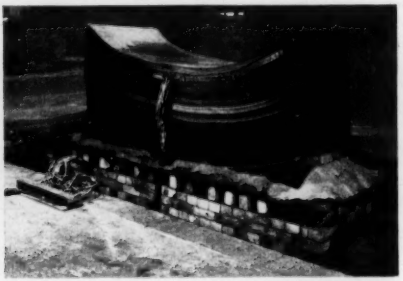

Fig. 1. Photograph of stack with thermocouple sheet in position

When the stack is loaded, it is covered by an "inner cover" made of ¼ in. thick corrugated mild steel. This inner cover rests on the steel base plate and is made "air-tight" by a sand seal: it remains in position throughout the whole anneal until the sheets are unloaded.

The stack is heated by a rectangular bell-type electric furnace which is lowered on to the stack directly after lifting off another hot stack. The temperature of the furnace is about 500° C when lowered on to the stack, and is raised to 830° C in about eighteen hours. It is maintained at this temperature for a further period of about eighteen hours, the actual soaking time being a function of the load of the furnace. The furnace is then removed and replaced by an "outer cover" made of welded ¼ in. steel plate, which is left in position until the stack is cool. To reduce oxidation, a coal-gas atmosphere is introduced into the outer cover during the cooling part of the cycle; this latter can be as long as fifty hours.

THEORY

Apart from the maximum temperature reached by any part of the stack, and the time at that temperature, the temperature distribution over any one sheet during the cooling part of the cycle is probably the most important factor in the production of satisfactory sheet steel. Consider the case of one sheet half-way up the stack. The thermal conductivity of a stack of sheets in a vertical direction has been shown experimentally to be only about one-fiftieth of that in the plane of the sheet. As the sheet is very thin compared with its length and breadth, it may be treated as a two-dimensional problem instead of three-dimensional.

Consider the cooling of a sheet which is initially at a uniform temperature V, and losing heat by radiating from its edges into an atmosphere at zero temperature. According to Stefan's law, the sheet will lose heat at the rate

$$Q = \sigma E(v^4 - v_0^4)$$

per unit area, where σ is the Stefan–Boltzman constant, E the emissivity of the surface, v the absolute temperature of the sheet and v_0 that of the surroundings. Exact solutions of problems on heat conduction in the variable state with this accurate boundary condition have not been found[1,2] owing to the complexity of the mathematics. An approximate solution, however, may be obtained by assuming that Newton's law of cooling is obeyed, i.e. that the heat flux across the boundary is proportional to the temperature difference between the surface and the surrounding medium. Consider the sheet to lie in the (x, y) plane. The heat flux across the boundary is given by $-K\partial v/\partial x$, where K is the thermal conductivity. Assuming Newton's law, this equals $H(v - v_0)$ where H is called the outer conductivity.

So $$K\partial v/\partial x + H(v - v_0) = 0$$

i.e. $$\partial v/\partial x + h(v - v_0) = 0 \qquad (1)$$

where $h = H/K$.

**

Consider the sheet to be a rectangle of length $2l$ in the x-direction and $2b$ in the y-direction; take the origin of the co-ordinate axes at one corner of the sheet.

Then $0 < x < 2l$

and $0 < y < 2b$

Carslaw and Jaeger[1] have shown that the temperature at any time t in this two-variable plane (x and y) may be expressed as the product of the solution of uni-variant problems. Thus if $v = f(x, l, t)$ is the solution to the case of a region $0 < x < 2l$ bounded by two infinite planes $x = 0$ and $x = 2l$, and if $v = f'(y, b, t)$ is the solution in the y-direction, then the solution to the two-variable problem is

$$v = f(x, l, t)\, f'(y, b, t) \tag{2}$$

Let us first examine, then, the uni-variant problem of heat flow between two infinite planes $x = 0$ and $x = 2l$ with uniform initial temperature V, and the planes radiating heat into an atmosphere at zero temperature.

The equation of conduction may be written in the form

$$\partial v/\partial t = \kappa \partial^2 v/\partial x^2 \tag{3}$$

where κ is the diffusivity and equals $K/\rho s$, ρ being the density and s the specific heat.

The boundary conditions may be considered as

$$hv - \partial v/\partial x = 0 \text{ at } x = 0 \tag{4}$$

$$hv + \partial v/\partial x = 0 \text{ at } x = 2l \tag{5}$$

$$v = V \text{ when } t = 0 \tag{6}$$

The expression

$$\exp(-\kappa\alpha^2 t)(A \cos \alpha x + B \sin \alpha x) \tag{7}$$

satisfies equation (3). It also satisfies conditions (4) and (5) provided that

$$-\alpha B + hA = 0$$

and

$$\alpha(B \cos 2\alpha l - A \sin 2\alpha l) + h(B \sin 2\alpha l + A \cos 2\alpha l) = 0$$

From these $A/B = \alpha/h$

and $$\tan 2\alpha l = 2\alpha h/(\alpha^2 - h^2) \tag{8}$$

Hence expression (7) becomes

$$A[\cos \alpha x + (h/\alpha) \sin \alpha x] \exp(-\kappa\alpha^2 t) \tag{9}$$

which satisfies equations (3), (4) and (5), where A is an arbitrary constant and α is any root (except zero) of equation (8).

The solution to the problem, then, is given by the series:—

$$v = \sum_{n=1}^{n=\infty} A_n \left(\cos \alpha_n x + \frac{h}{\alpha_n} \sin \alpha_n x\right) \exp(-\kappa\alpha_n^2 t) \tag{10}$$

This series can be integrated term by term, and the values of the coefficients $A_1, A_2 \ldots A_n$ can be obtained in a similar way to that for a Fourier series.

It can be shown simply that

$$A_n = \frac{\alpha_n^2}{(\alpha_n^2 + h^2)l + h} \int_0^{2l} V \left(\cos \alpha_n x + \frac{h}{\alpha_n} \sin \alpha_n x\right) dx \tag{11}$$

So by equations (10) and (11)

$$v = \sum_{n=1}^{n=\infty} \exp(-\kappa\alpha_n^2 t) \frac{\alpha_n \cos \alpha_n x + h \sin \alpha_n x}{(\alpha_n^2 + h^2)l + h} \int_0^{2l} V(\alpha_n \cos \alpha_n x + h \sin \alpha_n x) dx \tag{12}$$

where α_n are the positive roots of equation (8).

Equation (8) may be put in the form

$$\frac{\sin 2\alpha l}{\cos 2\alpha l} = \frac{2\alpha h}{\alpha^2 - h^2}$$

i.e. $$\frac{\sin \alpha l \cos \alpha l}{(\cos^2 \alpha l - \sin^2 \alpha l)} = \frac{2\alpha h}{\alpha^2 - h^2}$$

whence

$$(h \sin \alpha l + \alpha \cos \alpha l)(h \cos \alpha l - \alpha \sin \alpha l) = 0 \tag{13}$$

Thus by equation (13) the positive roots of equation (12) comprise the positive roots of the two equations

$$\alpha \tan \alpha l - h = 0 \tag{14}$$

and $$\alpha \cot \alpha l + h = 0 \tag{15}$$

From physical considerations there must be optical symmetry about the plane $x = l$. To allow for this the axes are now transferred to have their origin at the point (l, b) and the region is bounded by the infinite planes $x = +l$ and $x = -l$. Then only the cosine terms of the infinite series of equation (12) will be operative which reduces to

$$\frac{v}{V} = \sum_{n=1}^{n=\infty} \exp(-\kappa\alpha_n^2 t) \frac{(h^2 + \alpha_n^2) \cos \alpha_n x}{(\alpha_n^2 + h^2)l + h} \int_{-l}^{+l} \cos \alpha_n x dx$$

where α_n are the positive roots of equation (14).

By equation (14)

$$\alpha_n = h \cos \alpha_n l / \sin \alpha_n l$$

so $$\frac{v}{V} = \sum_{n=1}^{n=\infty} \exp(-\kappa\alpha_n^2 t) \frac{h^2[1 + (\cos^2 \alpha l/\sin^2 \alpha l)]}{(\alpha_n^2 + h^2)l + h} \cos \alpha_n x \left(\frac{\sin \alpha_n x}{\alpha_n}\right)_{-l}^{+}$$

$$= \sum_{n=1}^{n=\infty} \exp(-\kappa\alpha_n^2 t) \frac{2h^2 \cos \alpha_n x \,.\, \sin^2 \alpha l}{[(\alpha_n^2 + h^2)l + h] \sin^2 \alpha l . h \cos \alpha l}$$

$$= \sum_{n=1}^{n=\infty} \frac{2h \cos \alpha_n x \exp(-\kappa\alpha_n^2 t)}{[(\alpha_n^2 + h^2)l + h] \cos \alpha_n l} \tag{16}$$

It has been found more convenient to express this solution in terms of the dimensionless quantities:—

$$\xi = x/l, \quad T = \kappa t/l^2, \quad L = lh$$

Using these and putting $\beta_n = l\alpha_n$, equation (16) becomes

$$\frac{v}{V} = \sum_{n=1}^{n=\infty} \frac{2L \cos \beta_n \xi}{(\beta_n^2 + L + L^2) \cos \beta_n} \exp(-\beta_n^2 T) \tag{17}$$

where β_n are the positive roots of

$$\beta \tan \beta = L \tag{18}$$

Thus by the equations (2) and (17) the temperature at any point in the sheet at any time is given by

$$\frac{v}{V} = \sum_{n=1}^{n=\infty} \frac{2L \cos \beta_n \xi}{(\beta_n^2 + L + L^2) \cos \beta_n} \exp(-\beta_n^2 T) \sum_{m=1}^{m=\infty} \frac{2L' \cos \beta_m \xi'}{(\beta_m^2 + L' + L'^2) \cos \beta_m} \exp(-\beta_m^2 T) \tag{19}$$

where L' and ξ' are the quantities in the y-direction corresponding to L and ξ.

From this calculation it is possible to predict the temperature distribution, i.e. the pattern of the isotherms for any time of cooling t. As an example, let us consider the conditions after eight hours cooling.

Thermal conductivity at 830° C = 0·06 cal cm^{-1} s^{-1} C^{-1}

Emissivity value used = 0·65

Stefan's constant $= 5{\cdot}72 \times 10^{-5}$ erg cm^{-2} s^{-1} ° C^{-4}
l (in the x-direction) $= 122$ cm
b (in the y-direction) $= 45$ cm
Initial temperature $V = 1100°$ K
Density $= 7{\cdot}75$ g/cm^3
Specific heat s at $800° C = 0{\cdot}159$
$t = 8$ h

The positive roots β_n of equation (18) $\beta \tan \beta = 3{\cdot}165$ can be determined graphically (by plotting $y = \tan x$ and $y = 3{\cdot}165/x$). The expression

$$\frac{2L \cos \beta_n \xi \exp(-\beta_n^2 T)}{(\beta_n^2 + L + L^2) \cos \beta_n}$$

can then be evaluated for each value of β_n and summed to infinity. This procedure can be undertaken for each value of ξ (from 0 to 1) and a graph of

$$\sum_{n=1}^{n=\infty} \frac{2L \cos \beta_n \xi \exp(-\beta_n^2 T)}{(\beta_n^2 + L + L^2) \cos \beta_n}$$

against ξ plotted. This is shown in Fig. 2.

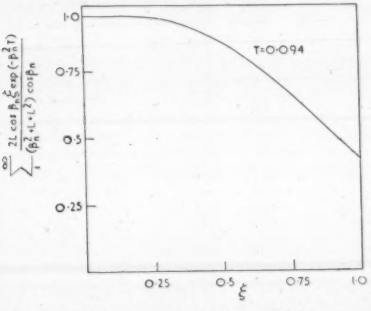

Fig. 2. Graph for x-direction after eight hours cooling

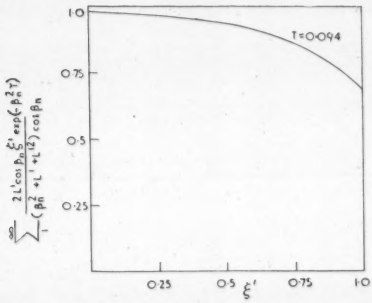

Fig. 3. Graph for y-direction after eight hours cooling

A similar graph can be plotted of

$$\sum_{n=1}^{n=\infty} \frac{2L' \cos \beta_n \xi' \exp(-\beta_n^2 T)}{(\beta_n^2 + L' + L'^2) \cos \beta_n}$$

against ξ' for the variation in the y-direction (Fig. 3) for the same value of t. From these two graphs it is possible to plot ξ against ξ' for fixed values of v/V as given by equation (19).

These curves (i.e. the isotherms for $v/V = 0{\cdot}9$, $0{\cdot}8$, $0{\cdot}7$, etc., are shown in Fig. 4.

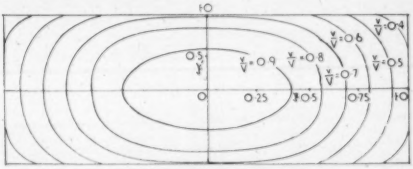

Fig. 4. Theoretical isotherms after eight hours cooling

METHOD OF MEASUREMENT

In order to measure the true temperature distribution it is important to disturb this as little as possible by the measuring device. The obvious choice for the latter was to use thermocouples owing to their small size and the availability of recording equipment. Equipment was available for recording the output of twenty-four thermocouples simultaneously. It would be impossible to get an accurate picture of the temperature distribution of the whole stack for one annealing cycle (one heat) with only twenty-four thermocouples, so it was decided to arrange the thermocouples at one height only for each heat, and to repeat the measurements at a different height for the next heat. Care had to be taken to ensure that the different stacks investigated were, as near as possible, identical. By measuring temperatures at seven heights the effective number of measuring points was increased to 168.

In order to position the thermocouples accurately in the stack a thin "sandwich" sheet had to be designed to conform to the following requirements:

(i) it had to be kept as thin as possible to minimize the effect on the temperature of the stack;

(ii) it had to be flexible in order to take up the various curvatures at different heights in the stack; and

(iii) its surfaces had to be smooth, as any projections would cause buckling in sheets placed on top of it. The "sandwich" was made from two mild steel sheets 8 ft × 3 ft × 0·030 in. thick separated by strips of mild steel $\frac{1}{8}$ in. thick. Portions of these strips were cut away, and insulated thermocouple wire placed in the spaces. A close-up view of the sandwich sheet with the top 0·030 in. sheet removed is shown in Fig. 5. The assembly is fixed together with small countersunk steel

Fig. 5. Close-up view of "sandwich" sheet

screws. The distribution of thermocouples over the area of the sandwich sheet is illustrated in Fig. 6.

Chromel–alumel 20 s.w.g. thermocouples were used, each thermocouple being individually checked against a standard before incorporating in the sandwich sheet. The leads were

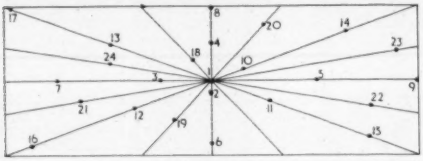

Fig. 6. Distribution of thermocouples over the area of the sheet

insulated with $\frac{1}{8}$ in. thick re-crystallized alumina twin-bore insulators over the lengths within the sandwich where compactness was an important consideration. Outside the sandwich a cheaper, more bulky type of insulator was used. In the initial experiments the thermocouple leads hung freely from the edge of the sandwich. After annealing the wires became rather brittle, and handling caused fractures. In order to protect these leads a simple gutter was fixed to the sandwich sheet. This may be seen in Fig. 1: it was supported by creep resistant steel brackets.

The output from the thermocouples was recorded on four six-point potentiometric recorders; the time between consecutive records on any one trace was about four minutes.

EXPERIMENTAL PROCEDURE

The sandwich sheet was first loaded on to the stack by means of a crane and specially constructed lifting tackle. The thermocouple leads were led through a hole in the furnace hearth and through a 2 in. steel pipe under the sand seal to a cold junction box outside the furnace as shown in Fig. 7. From the junction box copper leads were taken to the recorders. The stack was then annealed in the normal way and the temperatures were continuously recorded over the complete heating and cooling cycle until the furnace was unloaded, a minimum time of seventy-eight hours. In this way temperatures were measured at one height in the stack for one heating cycle. In order that results for each height in the stack could be compared and correlated, the weight of steel used for each heat was kept constant (eleven tons): this produced a stack 31 in. high above the furnace hearth. The material used throughout was a 4% silicon–iron alloy and the size of sheets was 8 ft $\times$ 3 ft $\times$ 0·014 in.

RESULTS

Temperature measurements were obtained with the sandwich on top of the stack, at the bottom of the stack and at heights of 5, 10, 15, 22 and 29 in. above the furnace hearth.

By considering the thermocouples to lie all in one quarter of the sheet, and plotting the temperature gradients along *OA*, *OB*, *OC*, *OD* and *OE*, of Fig. 6 at any one height, no assumption was made that the temperature distribution of the sheet was symmetrical. The small and random scatter on the temperature gradient graphs indicated that the temperature distribution was indeed symmetrical and the symmetrical drawing of the isotherms was justified. Temperature gradients were plotted along each of the above directions at 4, 24, 36, 44 and 60 h after the furnace was placed on the stack, at each of the seven heights above the base-plate. The times were chosen as they represent various stages of the annealing cycle, thus 36 h represents the end of the soaking period, just before the furnace is removed from the stack. The 44 h gradients were plotted as at this time the temperature difference between the centre and the edges of any sheet was a maximum. From the charts of the temperature recorders it would be possible to obtain temperature gradients at any time during the cycle. From these gradient curves it was possible to construct isothermal contour lines over the area of the sheets. These isothermal contours in the (curved) plane of the sheets will be referred to as horizontal isotherms. From a consideration of all the horizontal isotherms at any given time it was possible to construct vertical isothermal diagrams. The sections *ABCD* and *WXYZ* of Fig. 8 were chosen to be representative of the state of the stack. As an example of the isotherm patterns occurring during the heating part of the cycle, Figs. 9, 10 and 11 show the horizontal isotherms at a height of 15 in. and the vertical isotherms, after four hours heating. Figs. 12 and 13 show the vertical isotherms at the end of the soaking period.

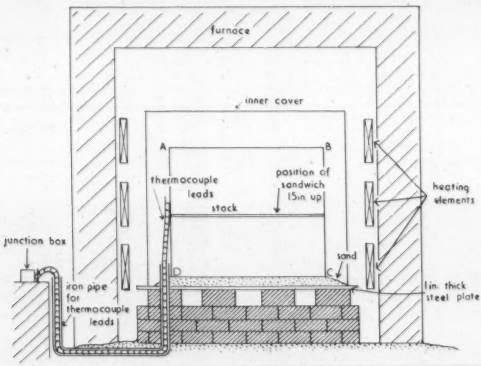

Fig. 7. Vertical section *ABCD* through the stack in the furnace

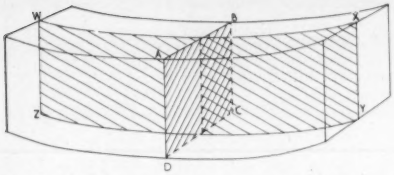

Fig. 8. Diagram showing sections on which vertical isotherms were plotted

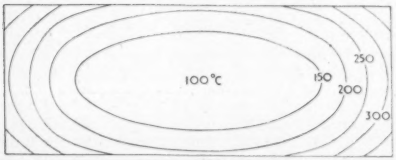

Fig. 9. Horizontal isotherms, 15 in. up, after four hours heating

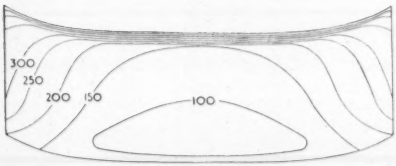

Fig. 10. Vertical isotherms, section *WXYZ* after four hours heating

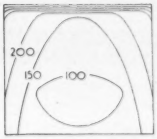

Fig. 11. Vertical isotherms, section *ABCD* after four hours heating

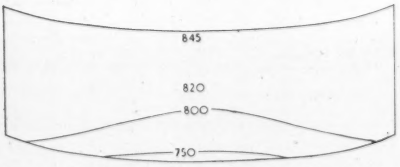

Fig. 12. Vertical isotherms, section *WXYZ* after thirty-six hours heating

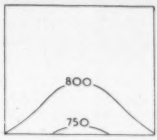

Fig. 13. Vertical isotherms, section *ABCD* after thirty-six hours heating

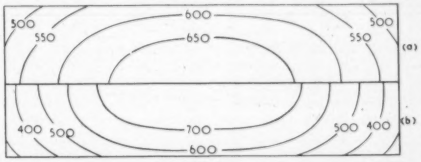

Fig. 14. Horizontal isotherms, 15 in. up, after eight hours cooling
(*a*) experimental (*b*) theoretical

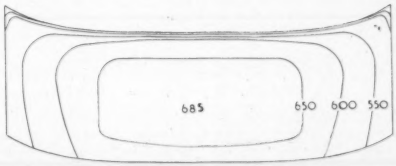

Fig. 15. Vertical isotherms, section *WXYZ* after eight hours cooling

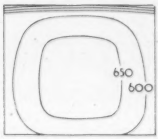

Fig. 16. Vertical isotherms, section *ABCD* after eight hours cooling

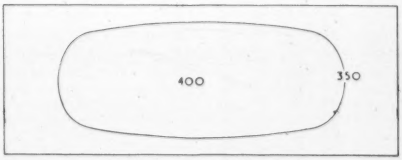

Fig. 17. Horizontal isotherms, 15 in. up, after twenty-four hours cooling

The horizontal isotherms, 15 in. up the stack, after eight hours cooling (forty-four hours from the start of the cycle) are shown in Fig. 14(*a*). The horizontal isotherms 5, 10 and 22 in. up, after the same eight hours cooling, showed very similar patterns. The vertical isotherms at this time are given in Figs. 15 and 16. The thermal condition of the stack later in the cooling cycle, sixty hours after the furnace was lowered on to the stack, is illustrated in Figs. 17, 18 and 19.

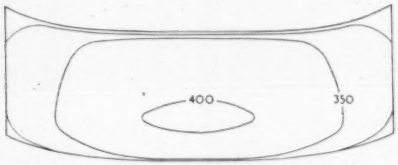

Fig. 18. Vertical isotherms, section *WXYZ* after twenty-four hours cooling

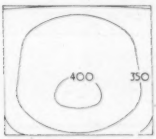

Fig. 19. Vertical isotherms, section *ABCD* after twenty-four hours cooling

The accuracy with which temperatures could be read from the recorder charts was of the order of $\pm 1^\circ$ C for each individual thermocouple. A maximum spread of $\pm 10^\circ$ C occurred on the thermal gradient curves: the horizontal isotherms could therefore be expected to have the same degree of uncertainty. This uncertainty was due in part to slight variations occurring in the thermocouples with time, but was mainly due to the fact that each quarter of the stack was not identical. The vertical isotherms, made by combining the results of several different anneals, will be subject to slightly greater errors owing to small differences in loading and other small uncontrollable variables, although every effort was made to keep each heat identical. They were calculated to be correct within $\pm 15^\circ$ C.

DISCUSSION OF RESULTS

The results of the experimental work show that the corners of the sheets heat up quicker than the edges, owing to the fact that they are heated from two sides; also the time lags in both heating and cooling are very great. A scientific investigation of this nature into a well-established industrial process often shows that the process is very close to the ideal: in this case the time of annealing (36 h) has been determined in the past without any measurements of the temperature of the stack. These measurements (Figs. 12 and 13) show that the majority of the sheets have reached a temperature of 800° C all over.

The horizontal isotherms after eight hours cooling indicate that a surprisingly large temperature difference exists between the centre and the outside edges of the sheets (about 200° C). This determination of the thermal conditions occurring during the annealing cycle is a necessary preliminary to a determination of the thermal stresses during annealing. From these it should be possible to evaluate the residual stresses in the cool sheets. Lack of reliable data has held up this work.

The close agreement between the experimental work and the theoretical is apparent from a comparison of Figs. 14(*a*) and (*b*), the latter being calculated from Fig. 4, with V, the temperature at the start of the cooling cycle, equal to 830° C. The general shape of the curves is identical and agreement for isotherms in the region of 600° C is good. The numerical value of the outer isotherms in the theoretical distribution is, however, lower than that found in practice. The predicted 400° C isotherm was found experimentally to be about 540° C. This discrepancy is to be expected as the theoretical curves were calculated for a sheet radiating heat into an atmosphere at zero temperature, whereas, in practice, the stack radiates heat into an atmosphere well above zero, owing to the inter-position of the inner cover (see Fig. 7) between the stack and zero temperature. The temperature of this inner cover falls rapidly from 830 to 350° C after eight hours cooling. Furthermore, radiation from the edges of the sheet was assumed to obey Newton's law of cooling, whereas, in fact, Stefan's law holds.

A more accurate calculation, with the correct boundary condition, is possible using numerical computing techniques; these, however, are likely to be excessively lengthy.

From the experimental work it is possible to trace the thermal history of any part of any sheet in the stack. By measuring the electrical watts loss on small strips cut from the large sheets, it has been possible using statistical techniques to correlate the watts loss (i.e. the quality) of the material with the amount of annealing it has received, i.e. the time it has been above a specified temperature.

ACKNOWLEDGEMENTS

This investigation was carried out while the author was a member of the G.K.N. Group Research Laboratory. He is grateful to the Director, Dr. T. Emmerson, for suggesting the problem and for permission to publish. He also wishes to acknowledge the assistance of Mr. D. B. Clayton and Mr. W. H. Eliot with the practical work, this being carried out at Messrs. Joseph Sankey and Sons, Manor Works, Ltd.

REFERENCES

(1) CARSLAW, H. S., and JAEGER, J. C. *Conduction of Heat in Solids* (London: Oxford University Press, 1950).

(2) FISHENDEN, M., and SAUNDERS, O. A. *The Calculation of Heat Transmission* (London: H.M. Stationery Office, 1932).

Heat-reflecting windows using gold and bismuth oxide films

By L. HOLLAND, F.Inst.P., and G. SIDDALL, Edwards High Vacuum Ltd., Crawley, Sussex

[*Paper first received* 20 *February, and in final form* 16 *April*, 1958]

Thin gold films sandwiched between certain metal oxide layers possess a high electrical conductivity and high optical transparency. They also have a high infra-red reflectance, and may be used as transparent heat-reflecting coatings if their yellowish tinted colour in transmitted light can be tolerated. The observation window of an enclosure exposed to infra-red radiation was coated with different film combinations, and their effectiveness in reducing the internal temperature rise determined. The reflectance and transmittance of the coatings were measured at $\lambda = 0{\cdot}56\,\mu$ and in the infra-red region using a photometer with a broad bandwidth ($0{\cdot}8$–$2\,\mu$). Results are given for the following: plain glass; a high reflecting bismuth oxide film on glass; gold film on glass; and gold films sandwiched between bismuth oxide and silicon monoxide coatings. Optimum performance was obtained with a $Bi_2O_3/Au/Bi_2O_3$ multi-layer of 450/130/450 Å thickness which had a transmittance of 73% for green light and a reflectance of 74% in the near infra-red region, compared with values of 55 and 35% respectively for a gold film of the same thickness without the oxide layers.

Thin films of gold deposited on base layers of certain metal oxides have been found to possess a higher transparency for light and a greater electrical conductivity than gold films deposited directly on glass. Gillham, Preston and Williams[1] have shown that sputtered base layers of bismuth oxide improve these physical properties of thin gold films because the texture of the superimposed metal coating is made more compact and uniform. They also found that the transparency and conductivity may be further enhanced by coating the outer surface of the gold with a top layer of bismuth oxide. When used as a transparent heating element the metal coating must be heat treated, at least up to the temperature of its subsequent use (usually a maximum of about 250° C), to enable defects in the lattice structure to decay and thus produce a stable resistance. These results have been confirmed by Holland and Siddall[2] who also found that the temperature coefficient of resistivity was dependent on the film thickness. Ennos[3] has repeated this work using evaporated gold and bismuth oxide films, and claims that evaporated films are more conducting than sputtered layers. However, recent tests by the writers have not shown a fundamental difference between films prepared by the two techniques.

It has been reported[4] recently in the U.S.A. that thin conducting coatings will strongly reflect infra-red radiation up to centimetric wavelengths, whilst giving a high transmission for visible light. The particular film combination used was not stated, and experiments have been made by the present authors to determine the value of gold films on metal oxide base coatings as transparent heat-reflecting mirrors. It was expected that such a film combination would be highly efficient for this purpose because of its low optical absorption and high electrical conductivity.

FILM PREPARATION

Films of gold sandwiched between two bismuth oxide layers were prepared on glass plates from nine inches up to about two feet square, in order to determine their efficiency as viewing windows in enclosures exposed to infra-red radiation. The vacuum deposition chamber was three feet in diameter and exhausted by silicone oil diffusion pumps. The bismuth oxide was sputtered from sector-shaped cathodes on to a rotary holder as described by Holland,[5] and the gold evaporated from a vapour source arranged under the edge of the rotary holder to give a uniform coating. The sector cathodes were operated from an a.c. high tension supply so that each electrode sputtered alternately on to the work plane. The bismuth oxide was deposited in pure oxygen at a rate of 1 Å/s, using a power input of 3 kV and $0{\cdot}5$ mA/cm^2 of work plate, and the gold volatilized from a molybdenum boat at about 20 Å/s. Both materials were deposited in sequence without breaking the vacuum.

Some experiments were also made using gold films sandwiched between silica layers prepared by evaporating silicon monoxide. These films were deposited from molybdenum boats placed under the circumference of the rotary holder.

The test glasses were cleaned before coating by washing in Teepol and water, followed by vapour degreasing in *iso*propyl alcohol for ten minutes. Film thickness measurements were made by multiple beam interferometry.

OPTICAL MEASUREMENTS

The transmittance and reflectance of the coatings were measured in the visible region using a tungsten lamp, photomultiplier cell and Wratten filters. Measurements were also made in the near infra-red region with a simple photometer using a Sentercel germanium junction diode, type P50A, and infra-red lamp. The relative and combined sensitivities of the lamp and photocell as a function of wavelength are shown in Fig. 1. It can be seen from the curves that the photometer has a fairly flat response between $0{\cdot}8$ to $2\,\mu$ with a slight maximum at $1{\cdot}5\,\mu$, so that the measured reflectance and transmittance values tend to be integrated values over this

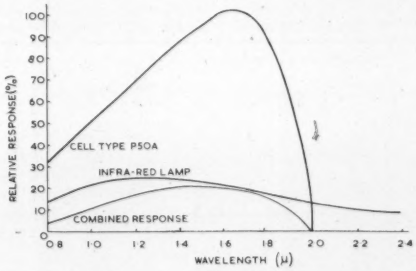

Fig. 1. Relative and combined sensitivity as a function of wavelength of components used in infra-red photometer

wavelength interval. The bandwidth of the photometer also covers the wavelength range in which maximum suppression of infra-red radiation is usually required.

HEAT-REFLECTING WINDOWS

An apparatus was made for determining the relative temperature rise in an enclosure when using observation windows coated with different types of infra-red reflecting films. The apparatus consisted of a steel box with sides of nine inches in length, painted matt black on the inside and silver-grey on the outside. The box was heated by a 250 W Crompton infra-red lamp which radiated on to a glass window coated with the heat-reflecting film under test. The effectiveness of a particular film combination as a heat-reflecting window could be determined by measuring the temperature rise in the interior of the enclosure with a mercury thermometer. The results for a range of films have been plotted in Fig. 2. The windows tested were as follows: (*A*) uncoated glass; (*B*) a single layer film of bismuth oxide of $\lambda/2$ optical thickness for a wavelength of 5000 Å, so that a high reflexion was obtained in the infra-red region at about 1 μ; (*C*) a plain gold film of 130 Å thickness; (*D*, *E* and *F*) bismuth oxide gold sandwich films with different metal and oxide film thicknesses; and (*G*) a silicon monoxide gold sandwich layer. All of the trial coatings were deposited on $\frac{1}{8}$ in. thick green plate glass.

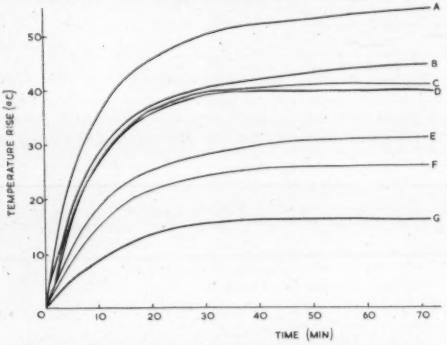

Fig. 2. The temperature rise in an enclosure using glass windows coated with different film materials

Curve (*A*) glass; curve (*B*) 1200 Å Bi_2O_3-film; curve (*C*) 130 Å Au-film; curve (*D*) 65 Å Au-film between 80 Å thick Bi_2O_3-films; curve (*E*) 100 Å Au-film between 80 Å thick Bi_2O_3-films; curve (*F*) 130 Å Au-film between 450 Å thick Bi_2O_3-films; curve (*G*) 130 Å Au-film between 200 Å thick SiO_2-films.

The optical properties of some of the different film combinations tested, together with their film thicknesses and the maximum rise in the enclosure temperature are given in the table. The resistance values, in Ω per square, are those obtained after annealing the film at 300° C. They have been included in the table because this affords a simple method for roughly estimating film thickness and optical properties. From the table it can be seen that a transparent gold film on glass is inefficient for reducing the temperature rise of an enclosure. This is because it possesses a high absorption in the infra-red region and energy is dissipated in the coating so that the enclosure is heated by convection. A $\lambda/2$-film of bismuth oxide gives almost the same performance as the plain gold film, but with the advantage of a much higher transmission of visible light. Also a gold film of 65 Å thickness sandwiched between bismuth oxide layers gives a temperature rise and visible transmittance which is only comparable with the single-layer bismuth oxide film. However, sandwich layers with a gold film of a 100 Å thick or higher produce a marked reduction in the enclosure temperature, whilst possessing a reasonable transmittance in the visible region. The best compromise was obtained with a 130 Å thick gold film sandwiched between bismuth oxide films of 450 Å thickness. Gillham, Preston and Williams[1] have shown that the bismuth oxide films act as anti-reflexion coatings on the gold layer when they are 450 Å thick.

It was found that the sputtered bismuth oxide films of 1200 Å thickness were incompletely oxidized because they possessed a high absorption in the visible region. Heating the coated glass to about 300° C in air was sufficient to reduce the absorption to a low value, but in both cases the infra-red absorption was small and unchanged as shown in the table. More recent experiments have shown that rapid sputtering produces highly oxidized deposits.

Heat-reflecting glasses using gold films between oxide layers are much easier to produce than the all-dielectric multi-layer filters used as heat-reflecting mirrors. Unfortunately, the gold films are yellow coloured in transmission and are not suitable for use in projectors, etc., where the illumination must be untinted. The writers understand that the British Scientific Instrument Research Association[6] have incorporated highly conducting gold films in multi-layer interference filters to improve their infra-red reflectivity. Such filters are strongly yellow tinted in transmission.

The gold sandwich films may be used as observation windows for use near furnaces and for reflecting solar radiation. After satisfactory tests a number of windows have been prepared for installation in a crane cabin operating near an annealing furnace.

Some typical properties of thin films used for heat-reflecting windows

Window	*Gold thickness* (Å)	*Total resistance* (Ω/*square*)	*Total oxide thickness* (Å)	$\lambda = 0{\cdot}8 - 2\ \mu$†			$\lambda = 0{\cdot}56\ \mu$†			*Maximum temperature rise in enclosure** (°C)
				T (%)	R (%)	A (%)	T (%)	R (%)	A (%)	
$Bi_2O_3/Au/Bi_2O_3$	65	30	160	42·5	50	7·5	73	4	23	40
$Bi_2O_3/Au/Bi_2O_3$	100	10	160	31	64·5	4·5	71·5	6	22·5	30·5
$Bi_2O_3/Au/Bi_2O_3$	130	7	900	23·5	74	2·5	73	8	19	23
$SiO/Au/SiO$	130	4	400	12·5	87	0·5	68	8	24	16
$\lambda/2$-film Bi_2O_3	—	—	1200	64	34	2	78	10	12	44
$\lambda/2$-film Bi_2O_3 (fully oxidized by heating in air)	—	—	1200	65	32·5	2·5	82·5	13	4·5	44
Au-film	130	—		22	35	43	55	12	33	40·2

* Maximum temperature rise in enclosure with plain glass = 56° C. † T = transmittance; R = reflectance; A = absorption.

The gold and bismuth oxide films could be cleaned with a cloth, but, unprotected, would not withstand the harsh conditions of a steel factory. Some films were prepared using silicon monoxide in place of bismuth oxide, but although the resultant film combination was an efficient heat-reflecting window, as shown in the table and Fig. 2, the durability of the coating was poor. In fact, the results obtained with silicon monoxide were contradictory, because films of exceptional conductivity were prepared on this material but the gold layers were less thermally stable than those on bismuth oxide.

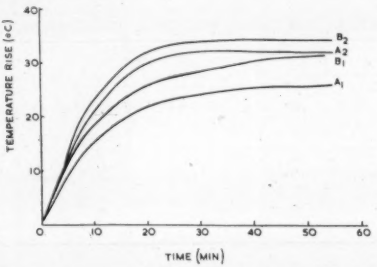

Fig. 3. The temperature rise in an enclosure using glass windows coated with bismuth oxide and gold of different thicknesses ($A = 130$ Å, $B = 100$ Å). The suffix 1 refers to a window with its coating on the inside, and the suffix 2 refers to a coating on the outside facing the lamp; curves A_2 and B_2 are also obtained with an air-spaced glass protecting the metal film

When the coated glass was mounted with the unfilmed side facing the radiation, the high reflectance of the gold film produced a double absorption of heat by the glass which, under the conditions of test used here, often resulted in the glass rapidly breaking. The temperature rise measured in the enclosure with gold films of two different thicknesses when facing and remote from the radiation are shown in Fig. 3. The temperature rise was also measured for a coated window with the metal film facing the infra-red lamp, but protected on the outside with a glass separated from the window by an air space which was not sealed at the window edges. With this arrangement the protective glass could rise in temperature without directly heating the metallized glass and thereby the enclosure. No difference could be measured in the temperature rise of the enclosure, with and without the cover glass, and this was the preferred protective method.

ACKNOWLEDGEMENTS

Acknowledgements are made to Mr. A. S. D. Barrett, Technical Director of Edwards High Vacuum Ltd., for permission to publish this report.

REFERENCES

(1) GILLHAM, E. J., PRESTON, J. S., and WILLIAMS, B. E. *Phil. Mag.*, **46**, p. 1051 (1955).
(2) HOLLAND, L., and SIDDALL, G. *Vacuum*, **3**, p. 375 (1953).
(3) ENNOS, A. E. *Brit. J. Appl. Phys.*, **8**, p. 113 (1957).
(4) *The Properties and Application of Sierracote* (California: The Sierracin Corporation, 1956).
(5) HOLLAND, L. *Nature* [*London*], **177**, p. 1229 (1956).
(6) *Research Report R191* (London: British Scientific Instrument Research Association, 1955).

A general scheme for the examination of precipitates and inclusions in steels*

By G. R. BOOKER, B.Sc., A.Inst.P., and J. NORBURY, B.Sc., Ph.D., A.R.T.C.S., F.Inst.P., Richard Thomas and Baldwins Ltd., Aylesbury, Bucks.

[*Paper received* 19 *February*, 1958]

A comprehensive scheme is described for the examination of included materials occurring in steels using the newer physical techniques. The material is isolated by extraction replicas in a form suitable for examination by optical and electron microscopy, electron and X-ray diffraction, and X-ray fluorescent and spectrographic analysis.

Application of the scheme allows the precise form and identity of the included material to be determined, even when only small amounts of specimen are available. The extraction replica method enables particles up to about 50 μ and less than 0·01 μ in size to be satisfactorily isolated and retained for examination. The possibility of modification of the included material during isolation is small because only mild chemical treatments are used. The scheme has been satisfactorily applied so far to iron and alloy carbides and nitrides, and simple and mixed oxides and sulphides present in steels.

Metallographic methods for the examination of precipitates and inclusions in steels are well established, but since they are confined mainly to optical microscope studies on polished sections and etching tests, they are subject to certain limitations. The newer physical techniques, e.g. electron microscopy and diffraction, X-ray diffraction and fluorescence, and optical spectroscopy, have been used to obtain more precise information about included material occurring in steels, but up to the present a comprehensive scheme embracing all these methods of examination has not been available. However, following extensive studies made by the authors during the last three years, such a scheme has now been established which provides detailed information concerning the distribution, morphology, crystal structure and composition of included material occurring in steels. The material is isolated by the extraction replica method previously described in detail,[1,2] and then examined successively by each of the physical methods enumerated above. The complete sequence of operations which experience has shown to be most suitable

* This paper was presented at the Annual Conference of the Electron Microscopy Group of The Institute of Physics held in Bangor, September 1957.

for precipitates and inclusions in steels is given, but it may sometimes prove convenient or advantageous to change the order, or omit some phases, of the examination.

The main advantages of using the scheme of examination are that:

(i) its comprehensive nature enables the precise form and identity of the included material to be determined;

(ii) significant results can be obtained from small amounts of specimen; and

(iii) there is little possibility of modification of the included material prior to its examination, since only mild chemical treatments are used to effect isolation.

(iii) The specimen is re-examined with the optical microscope. This allows a check to be made on the depth of etch and frequently shows more detail of the three-dimensional form of the included material.

(iv) A Formvar replica film and a collodion backing film are applied to the etched metal surface, allowed to dry, and the composite film dry stripped.

(v) The replica film is examined in transmitted light with the optical microscope in the normal manner, thus enabling the success of the extraction process to be determined except when the included material is very small. This examination reveals additional information concerning the morphology of the included material, and enables the colour by transmitted

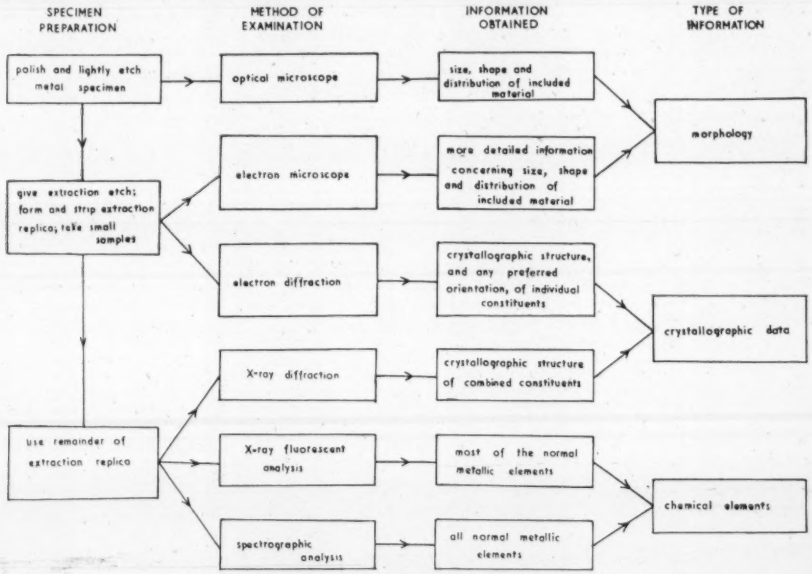
SPECIMEN PREPARATION
METHOD OF EXAMINATION
INFORMATION OBTAINED
TYPE OF INFORMATION
polish and lightly etch metal specimen
optical microscope
size, shape and distribution of included material
morphology
give extraction etch; form and strip extraction replica; take small samples
electron microscope
more detailed information concerning size, shape and distribution of included material
electron diffraction
crystallographic structure, and any preferred orientation, of individual constituents
crystallographic data
X-ray diffraction
crystallographic structure of combined constituents
use remainder of extraction replica
X-ray fluorescent analysis
most of the normal metallic elements
chemical elements
spectrographic analysis
all normal metallic elements

Summary of the scheme of examination

SCHEME OF EXAMINATION

The general features of the scheme of examination and the type of information obtained are summarized in the figure, whilst the essential practical details are as follows.

(i) Polished sections of the specimen are prepared, given a normal metallographic etch where necessary, and examined with the optical microscope at magnifications of ×100, ×600 and ×1000. The types, distribution, size, shape, colour and birefringence of the included material are noted.

(ii) The specimen is etched to a mean depth equal to about half the average size of the included material being investigated, carefully washed with alcohol and dried. Experience has shown 10% alcohol-iodine solution to be a satisfactory etchant for most types of included material in steels, but 10% nital is also often suitable. Etch times at 18° C are usually in the range half to ten minutes, the actual time used in a particular instance depending on the etchant, type of steel, and size of particles.

white light to be observed directly. In addition, transmission optical microscope studies on the replicas using polarized light may aid in assessing the birefringent properties of the material.

(vi) Disks $\frac{1}{8}$ in. in diameter are punched from the replica film, mounted on electron microscope grids, the collodion backing is dissolved and the films allowed to dry.

(vii) These films are examined in the electron microscope, generally at selected magnifications of ×1500 and ×4000 (but higher if necessary). The examination provides more detailed information of the morphology of the included material and reveals the presence of any sub-optical microscopic particles.

(viii) The same films are then examined by electron diffraction. The use of the selected-area method, which is available with three-stage electron microscopes, enables transmission electron diffraction patterns to be recorded from individual constituents of the extracted material, thus

allowing the determination of the crystalline structure and any preferred orientation of separate constituents.

(ix) The collodion backing film is dissolved from the remaining, and by far larger, portion of the extraction replica, and the resulting film compressed and extruded through a fine capillary tube to form a small cylindrical specimen about 0·5 mm in diameter.

(x) Using a powder camera, X-ray diffraction patterns are recorded from this specimen, and the crystalline structure of the bulk included material in the extraction replica thus determined.

(xi) The same specimen is then examined by the X-ray fluorescent analysis method, and the metallic elements of the included material in the replica thereby determined, with the exception of some of the commonly occurring light elements, e.g. aluminium, boron and silicon.

(xii) The same specimen is then available for examination by optical spectroscopy which enables all the metallic elements present in the isolated included material to be determined. Since this latter examination destroys the specimen, it is always the last phase in the scheme of examination.

ADVANTAGES OF THE SCHEME OF EXAMINATION

The examination of an extraction replica is, in effect, an examination of the included material present in a shallow surface layer of a metal specimen, without the inconvenience of a metallic matrix. Consequently, if only extraction replicas are to be examined, the high standard of polishing of metal specimens required for normal metallographic examinations and electron microscope examinations of ordinary replicas is not necessary, and hence a saving in polishing time results. In addition, difficulty experienced in the examination of the included material present in heavily cold-worked specimens due to the presence of a severely strained matrix does not occur in extraction replica examinations, because the matrix is no longer present.

As the relative positions of the included material in the metal specimen are maintained in the stripped extraction replica, the microscope observations made at each stage of extraction [i.e. paragraphs (i), (iii), (v) and (vii) above] readily allow the types of isolated material observed in the extraction replica to be directly related to the types of included material originally observed in the matrix. Individual particles can be examined at the various stages of extraction if the matrix in the neighbourhood of the particles is marked before extraction.

The electron microscope examination of samples from the extraction replica yields detailed information concerning the size, shape and distribution of the isolated material, including particles in a size range below that which could usefully be studied in a normal metallographic examination.

If the material isolated in the replica is crystalline and of suitable shape and size, then the X-ray diffraction analysis gives accurate crystallographic data concerning the types of included material in the extraction replicas, whilst the electron diffraction studies establish the crystallographic structure and any preferred crystallographic orientation of individual constituents.

The X-ray fluorescent and spectrographic examinations show which metallic elements are present in the isolated material, and hence considerably aid the identification. As these analyses and the X-ray diffraction analysis are all performed on the same specimen, the results may be directly correlated.

AMOUNTS OF INCLUDED MATERIAL REQUIRED

Sufficient included material for the optical microscope, electron microscope and electron diffraction studies is normally readily available in the extraction replicas, as the amounts required are extremely small. On the other hand, experimental results have indicated that about 20 μg of isolated material is necessary for X-ray diffraction and X-ray fluorescent analyses and about 100 μg for spectrographic analysis.

The amount of material isolated depends on the surface area covered by the extraction replicas, the weight per cent of included material in the metal specimen, the depth of etch, and the shape, size and distribution of the particles. However, for normal commercial steels, experience has shown that about 20 μg of isolated material can be obtained using extraction replicas from specimen areas about 10 cm^2 in size.

For convenience of preparation and storage, the metal specimens are usually cut with cross-sections about 2 cm square, and mounted in Bakelite to yield a cylindrical mount 1$\frac{1}{4}$ in. in diameter. Polyvinyl formal (Formvar) is not recommended as a mounting material, since it is softened during the replica-making process. If one extraction replica from the 4 cm^2 surface area of the specimen proves inadequate, additional extraction replicas are obtained and combined for subsequent analysis. In some instances, suitable extraction replicas may be obtained successively without repolishing the specimen. Experience has shown that this procedure may be used satisfactorily for profusely distributed carbide and nitride precipitates, but should not be used for non-metallic inclusions, as these latter particles are generally present in steels to only a small extent, and extraction replicas containing the largest possible number of such particles are desirable.

The cutting and orienting of metal specimens for mounting usually presents little difficulty when the specimens are originally in the form of slabs or plates. Thin sheet specimens can conveniently be mounted with the plane of the sheets parallel to the Bakelite mount surface that is to be polished, and the polishing continued until the region of interest is exposed over the whole area of the specimen. The same procedure can be employed with metal specimens containing parallel surface layers of differing composition, such as steels that have been case-hardened by nitriding or carburizing.

TYPES OF INCLUDED MATERIAL

Included material occurring in steels is normally present as particles up to about 25 μ in size, although larger particles sometimes occur. The particles may be in the form of rods, plates, globules, or irregularly shaped material. The suitability of the electron and X-ray diffraction methods for examining such material, if crystalline, depends on the size and shape of the particles. Thus, electron diffraction patterns from solid particles greater than about 0·1 μ in size are not necessarily characteristic of the bulk of the material comprising the particles, since such particles are in general not completely penetrated by the electrons. Significant electron diffraction patterns can be obtained, however, from particles having appreciable maximum dimensions (e.g. 10 μ), if they are sufficiently small in other directions. Hence, the large rod-like and plate-like precipitates occurring in steels frequently yield good electron diffraction patterns. Individual plate-like precipitates usually give regular "two-dimensional" spot patterns, indicating that they are single crystals. Since the nature of the patterns from such precipitates depends on their orientation with respect to the electron beam, additional information may be obtained by recording further patterns

with the replica inclined at large angles to the electron beam, and by scanning the replica during the exposure. The former technique is useful when examining individual precipitates because it enables further atomic planes to contribute to the diffraction pattern, whilst the latter allows the relative average intensities of individual diffraction rings from a large number of randomly oriented precipitates to be ascertained.

On the other hand, in X-ray diffraction analysis, solid particles less than about 0·1 μ in size may be difficult to detect, as broadening of the diffraction lines will probably occur. X-ray diffraction effects from particles of large maximum dimension, but of the order of 0·1 μ or less in other directions, may also be difficult to detect. Furthermore, X-ray diffraction patterns from such particles may differ from the normal "powder"-type pattern in that the relative intensities of the lines are altered.

The types of diffraction pattern normally obtained from precipitates and inclusions encountered in steels, and their relationship to the shape and size of the particles, are summarized in the table.

The types of electron diffraction and X-ray diffraction patterns normally obtained from included materials occurring in steels

Type of material	*Physical form*	*Size range*	*Types of diffraction pattern obtained*
Precipitates	"One-dimensional" (rods)	< About 0·1 μ in diameter	*ED*—Good: spotty ring patterns from groups. *XRD*—None, or poor.
		> About 0·1 μ in diameter	*ED*—None, or poor. *XRD*—Good.
	"Two-dimensional" (plates)	< About 0·1 μ in thickness	*ED*—Good*: "two-dimensional" single crystal patterns from individual plates, spotty ring patterns from groups. *XRD*—None, or poor.
		> About 0·1 μ in thickness	*ED*—None, or poor. *XRD*—Good.
	"Three-dimensional" (e.g. globules)	< About 0·1 μ in diameter	*ED*—Good: spotty or continuous ring patterns from groups. *XRD*—None, or poor.
		> About 0·1 μ in diameter	*ED*—None, or poor. *XRD*—Good.
Inclusions	Mostly "three-dimensional"	Normally about 1–25 μ	*ED*—None, or poor.† *XRD*—Good.

ED, electron diffraction; *XRD*, X-ray diffraction.

* Additional information often obtained by tilting the replica and/or scanning the replica during the exposure.

† The small and/or irregularly shaped particles are more likely to give electron diffraction patterns.

In some investigations, constituents of one type may possess a size range sufficient to enable electron diffraction patterns to be obtained from the smaller, and X-ray patterns from the larger, particles.

REMOVAL OF INTERFERING CARBIDES

Extracted material from commercial steels often contains a large amount of cementite (Fe_3C). This is unfortunate for X-ray diffraction studies, because the diffraction pattern from cementite consists of many lines, which may obscure weaker lines from other constituents. The method found most effective in eliminating the pronounced cementite pattern has been to remove the interfering carbides prior to extraction, by annealing the steel specimen at a temperature slightly in excess of that necessary to put the carbides into solid solution, and then rapidly quenching it. This temperature depends mainly on the carbon and alloy content of the steel, and is normally in the range 700 to 1000° C. Sometimes a weak γ–Fe pattern is obtained from retained austenite, but this comprises only a few lines and has a negligible interfering effect. The heat-treatment does not appear to have any effect on the composition of the normal types of inclusions occurring in steels.

DISCUSSION

The application of the newer physical techniques allows significant results to be obtained from very small amounts of isolated material and, therefore, since small steel specimens are suitable, information beyond the scope of other methods can often be obtained. The use of the same extraction replicas for all the phases of the scheme of examination, and the comprehensive nature of the examination, enable the precise form and identity of most types of included material to be determined.

Several advantages result from using the extraction replica method described herein for isolating the included material from the matrix as follows.

(i) The technique involves the minimum dissolution of the matrix for isolation, the depth of etch being merely that necessary to loosen the particles lying in the surface of polished metal sections. As this depth normally corresponds to about one-half of the average size of the included material, any chemical reactions between the etchant and the included material is likely to be extremely small. For example, using a 10% alcohol-iodine solution, the period for which the specimen and included material are in contact with the etchant is only a few minutes, compared with several hours for normal bulk extraction methods.

(ii) Previous investigators[3,4] using extraction replica

techniques have encountered difficulty in isolating particles greater in size than about 1 μ due to the lack of strength of the plastic replica film after etching through it. The present technique, however, does not suffer from this limitation. Particles up to about 50 μ, and less than 0·01 μ, in size are satisfactorily extracted and retained for subsequent examination.

(iii) Since the replica films are applied after the specimen has been etched, carefully washed with alcohol and dried, they are completely free from etching debris and staining.

(iv) Fragile particles, such as thin plates and small-diameter rods, receive substantial mechanical support from the replica film, and so do not disintegrate during isolation or subsequent examination.

Although the scheme enables the form and identity of the included material to be precisely determined, estimations of the relative amounts of the various types of material may not be quantitative, especially if the mean sizes of the particles of each type are widely different. The scheme is, however, particularly useful for the study and identification of non-metallic constituents which are not satisfactorily isolated and retained for examination by some of the conventional bulk extraction methods. Consequently, although the scheme may not give strictly quantitative results, it enables considerably more information to be obtained concerning many types of included material than has been previously possible.

It is not always essential, nor advisable, to carry out the whole scheme of examination on each specimen. The results of the early parts of the examination often indicate whether succeeding parts may be omitted. Thus, if the extracted material is found to consist of very small, thin particles, it is unlikely that X-ray diffraction studies will give useful information, whilst in all probability electron diffraction will not make a significant contribution towards the identification of large solid particles.

The general scheme of examination as a whole or in part has been applied to the examination of iron and alloy carbides and nitrides,[5] and simple and mixed oxides and sulphides present in steels. The only material hitherto encountered with a composition which has been difficult to determine has been the glassy, amorphous type of inclusion.

ACKNOWLEDGEMENTS

The authors wish to express their thanks to colleagues in these Laboratories for practical assistance in the development of the scheme of examination. Thanks are also due to Mr. R. A. Hacking, Director of Research, for permission to publish this paper.

REFERENCES

(1) BOOKER, G. R., and NORBURY, J. *Brit. J. Appl. Phys.*, **8**, pp. 109–113 (1957).
(2) BOOKER, G. R., NORBURY, J., and SUTTON, A. L. *Brit. J. Appl. Phys.*, **8**, pp. 155–157 (1957).
(3) FISHER, R. M. *Amer. Soc. Test. Mater. Special Tech. Publication No.* 155, p. 51 (1953).
(4) WILLIAMS, B. E. *Brit. J. Appl. Phys.*, **8**, p. 242 (1957).
(5) BOOKER, G. R., NORBURY, J., and SUTTON, A. L. *J. Iron Steel Inst.*, **187**, pp. 205–215 (1957).

The performance of bismuth telluride thermojunctions*

By H. J. GOLDSMID, B.Sc., Ph.D., A. R. SHEARD, B.Sc., A.R.I.C., and D. A. WRIGHT, D.Sc., F.Inst.P.,
The General Electric Co. Ltd., Wembley, Middlesex

[*Paper received* 24 *January*, 1958]

The thermoelectric properties of *n*-type and *p*-type bismuth telluride between 150 and 300° K have been measured and the figure of merit for thermoelectric applications has been calculated. This figure of merit has been shown to be highest for material with an electrical conductivity of about 1000 Ω^{-1} cm^{-1} with current flow parallel to the cleavage planes. Its value at 290° K corresponds to a maximum cooling by means of the Peltier effect of about 65° C, and an efficiency of thermoelectric generation of 1% for a 25° C temperature difference.

1. INTRODUCTION

The possibility of refrigeration by means of the Peltier effect using semiconductor thermocouples was considered in 1954.[1] At that time some preliminary experiments had been carried out using the semiconductor bismuth telluride (Bi_2Te_3) for the positive branch of a thermocouple in which the negative branch was the metal bismuth. It was reported that a cooling of 26° C below the ambient temperature had been achieved. Later, when both *p*-type and *n*-type Bi_2Te_3 were available, a cooling effect of 40° C was observed,[2] but even this is considerably less than the peak performance that is possible. The results which will be reported here show that, at a mean temperature of 17° C (290° K), the maximum cooling effect that may be obtained with the compound is about 65° C. Estimates of the coefficient of performance for thermoelectric refrigeration and of the efficiency for thermoelectric generation will be made, and the possibility of further improvement will be discussed.

2. FIGURE OF MERIT FOR THERMOELECTRIC APPLICATIONS

Altenkirch[3] showed that the performance of a thermoelectric refrigerator could be related to the thermoelectric power, the electrical conductivity and the thermal conductivity of the thermocouple elements. A figure of merit involving these quantities may be defined as

$$\theta = \frac{(\alpha_p - \alpha_n)T^{\frac{1}{2}}}{(\kappa_p/\sigma_p)^{\frac{1}{2}} + (\kappa_n/\sigma_n)^{\frac{1}{2}}} \qquad (1)$$

where α = thermoelectric power (V °C^{-1})
κ = thermal conductivity (W cm^{-1} °C^{-1})
σ = electrical conductivity (Ω^{-1} cm^{-1})
T = mean absolute temperature (°K).

The suffixes *p* and *n* refer to the positive and negative branches of the thermocouple; for semiconductors they refer to *p*-type and *n*-type material respectively.

The maximum coefficient of performance for refrigeration

* G.E.C. Communication No. 762.

ϕ, defined as the ratio of the heat extracted to the electrical energy supplied, is given in terms of θ by

$$\phi = \frac{T[(1+\theta^2)^{\frac{1}{2}} - 1]}{\Delta T[(1+\theta^2)^{\frac{1}{2}} + 1]} - \frac{1}{2} \qquad (2)$$

where ΔT = temperature difference between the thermocouple junctions.

This coefficient of performance can only be realized if an optimum current is passed, and if the dimensions of the thermocouple branches obey a certain simple relationship.[3] However, Ioffe and others[4] have shown that this last condition is not critical and have also demonstrated that, if the values of the parameters which determine θ are temperature dependent, and if the Thomson effect is taken into account, then the mean value of θ, over the range of temperature, may be used in equation (2) to a high degree of accuracy. The maximum temperature difference is obtained by setting $\phi = 0$ in equation (2), and then

$$\Delta T_{max} = 2T\frac{(1+\theta^2)^{\frac{1}{2}} - 1}{(1+\theta^2)^{\frac{1}{2}} + 1} \qquad (3)$$

The same figure of merit θ applies equally well to thermoelectric generation. In this case the quantity of interest is the efficiency ψ. When the resistances of the load and the generator are equal:[5]

$$\psi = 1/[1 + 2T/\Delta T(1 + 2/\theta^2)] \qquad (4)$$

A slight improvement in the efficiency may be obtained by adjustment of the load resistance,[6] but for materials at present available the effect is very small.[7]

Equation (4) shows that, as for an ideal thermodynamic machine, the efficiency is improved if the temperature difference ΔT is increased. Otherwise, for both generation and refrigeration, the problem reduces to that of finding the thermocouple combination which gives the highest value of the figure of merit θ.

It is now generally realized that some semiconductor thermocouples are preferable to the best metallic thermocouples, since the higher thermoelectric power more than compensates for a reduction in the ratio of electrical to thermal conductivity.[8] It has been shown[1] that the highest figures of merit are obtained by the use of semiconductors in which the factor F, given by

$$F = (\mu/\kappa_0)\,(m^*/m)^{3/2} \qquad (5)$$

is as great as possible. Here κ_0 is the lattice component of the thermal conductivity, μ is the mobility of the charge carriers and m^*/m is the ratio of their density-of-states effective mass to the free-electron mass.

For a series of elements in a group of the periodic table, e.g. diamond, silicon, germanium, the thermal conductivity decreases with rise of atomic weight. A similar trend is found for a series of compounds such as the alkali halides, or the III – V intermetallic compounds.[9] Since the carrier mobility does not appear to decrease with rise of atomic weight it is clear that a high atomic weight (or mean atomic weight in the case of compounds), is favourable. It is, however, difficult to predict the best series of semiconductors since, for a series with a range of high mobilities (corresponding to covalent-bonding), the thermal conductivities are also high. Conversely, ionic compounds having low thermal conductivities also have low carrier mobilities. Possibly some of the best materials may have bonding which is intermediate between covalent and ionic.

A more detailed consideration is complicated by the fact that the mobility and the effective mass are interdependent. For a simple covalent-type semiconductor with a single conduction or valence band, having spherical energy surfaces, the mobility depends on the effective mass according to[10]

$$\mu \propto m^{*-5/2}$$

The factor F is then proportional to m^{*-1}. However, if the binding were partly ionic in nature, the mobility would be less dependent on the effective mass. Moreover, for ionized-impurity scattering[11]

$$\mu \propto m^{*-\frac{1}{2}}$$

and Ioffe[8] has suggested that a certain amount of impurity scattering could be advantageous if the increase of the kinetic energy term in the expression for the thermoelectric power more than compensated for the decrease in mobility. However, we shall confine our attention to covalent-type scattering since this would seem to be predominant in Bi_2Te_3, the semiconductor with which we are particularly concerned.

For non-spherical energy surfaces there is no longer a single effective mass.[12] It is important to distinguish between an inertial mass m_i and a density-of-states mass m^*. For a single-valley semiconductor

$$\mu \propto m_i^{-1}\, m^{*-3/2}$$

so F is inversely proportional to m_i. For a many-valley semiconductor,[13] ignoring inter-valley scattering,

$$\mu \propto N m_i^{-1}\, m^{*-3/2} \qquad (6)$$

where N is the number of valleys. In effect, this relation implies that the mobility depends on the inertial mass m_i and also on a density-of-states mass for a single valley which is $N^{-2/3}$ times the overall density-of-states mass m^*. Thus

$$F \propto N/m_i$$

It is therefore concluded that the inertial mass should be low and the number of valleys should be high, with the reservations that too low an inertial mass may make ionized-impurity scattering important, and that multiplicity of valleys could lead to inter-valley scattering.

Drabble and Wolfe[14] have shown that a six- or possibly a twelve-valley model is applicable to Bi_2Te_3, and that the inertial mass is low, so that the above requirement is met. This, combined with the effect of the high mean atomic weight, would account for the large figure of merit of Bi_2Te_3.

3. THERMOELECTRIC PROPERTIES OF BISMUTH TELLURIDE

3.1 *Thermoelectric power and electrical conductivity.* An ingot of Bi_2Te_3 may be formed by heating an evacuated sealed tube, containing the elements in the correct proportions, to about 600–700° C, and allowing it to cool slowly. However, such an ingot is found to be inhomogeneous and to consist of small, randomly orientated crystals.

If Bi_2Te_3 is zone-melted, very much improved ingots are obtained, and, furthermore, the addition of impurities can be adequately controlled. Although the cleavage planes within such ingots are not coplanar, they are alined with the direction of zone-refining. Samples cut from such ingots have, therefore, been suitable for use in measurements with gradients parallel to the cleavage planes. Most of the results outlined in this Section have been obtained with such samples, but some single crystals have also been measured and their properties have not been found to differ from those of zone-refined material. The discussion in Section 3.3 of the

anisotropy of Bi_2Te_3 is based on results obtained from single-crystal specimens only.

Bismuth telluride, when prepared from the pure elements in the atomic proportions 2 : 3, is always *p*-type with an electrical resistivity at room temperature of about $2 \times 10^{-3}\,\Omega\,cm$. *N*-type material may be produced by the addition of one of the halogens. *P*-type Bi_2Te_3 of reduced resistivity is obtained using, for example, lead or cadmium as the acceptor impurity.

The measurements of thermoelectric power, electrical conductivity and thermal conductivity over the temperature range 150–300° K have been reported in detail elsewhere.[15, 16] Here, only the results which affect the performance of Bi_2Te_3 thermocouples will be considered. Fig. 1 shows a plot of thermoelectric power against electrical conductivity for *p*-type and *n*-type material at 300° K.

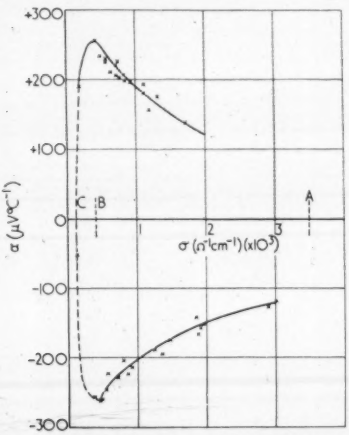

Fig. 1. Thermoelectric power against electrical conductivity for Bi_2Te_3 at 300° K

Over most of the range covered *A*–*B*, the thermoelectric power increased as the electrical conductivity decreased, but, for low electrical conductivities *B*–*C*, the thermoelectric power was again reduced. This was due to the presence of both electrons and holes, resulting in mixed conduction; the energy gap of Bi_2Te_3 is only about 0·16 eV.[17] Clearly, material in the range *B*–*C* is unsuitable for thermoelectric applications.

The plots of thermoelectric power against electrical conductivity, other than in the range of mixed conduction, were found to depend very little on the temperature. No dependence on temperature at all would be expected if, as in the simplest semiconductor model, the mobility were proportional to $T^{-3/2}$ and the effective density of states[18] were proportional to $T^{3/2}$. However, for non-degenerate Bi_2Te_3 the hole mobility is proportional to $T^{-1\cdot94}$ and the electron mobility is proportional to $T^{-1\cdot72}$.[15] Thus, in both cases, the variation of mobility is greater than for simple covalent lattice scattering. This is, however, compensated for by a more rapid variation of thermoelectric power with temperature than would be expected from the simple theory.

3.2 *Thermal conductivity*. Fig. 2 shows the variation of thermal conductivity with electrical conductivity for *n*-type and *p*-type Bi_2Te_3 at 300° K. The total thermal conductivity κ is the sum of a lattice component κ_0 and an electronic component κ_e. For a non-degenerate semiconductor, in which the mean free path of the charge carriers is independent of their energy, it is to be expected that[10]

$$\kappa_e = 2(k/e)^2\sigma T \qquad (7)$$

where k = Boltzmann's constant
and e = electronic charge.

Thus, if the lattice component is constant, the plot of thermal conductivity against electrical conductivity, at a given

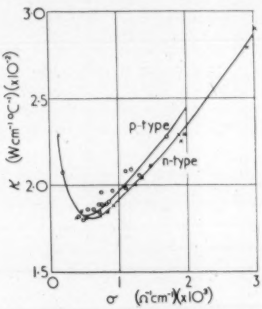

Fig. 2. Thermal conductivity against electrical conductivity for Bi_2Te_3 at 300° K
× = n-type ○ = p-type

temperature, should be a straight line of slope $2(k/e)^2T$. The fact that the results, shown in Fig. 2, differ for *n*-type and *p*-type material is due partly to a difference in the dependence of mobility on temperature for electrons and holes, and partly to the dependence of the lattice thermal conductivity on the electrical conductivity for *n*-type Bi_2Te_3 when doped, as in this case, with iodine.[16] The curvature for the higher electrical conductivities is due to an increase in the Lorenz number in the range of partial degeneracy, and the rise of thermal conductivity for low electrical conductivities, in the range of mixed conduction, is due to the transport of ionization energy by hole-electron pairs.[19] Since we are concerned with substantially extrinsic Bi_2Te_3 this last effect is not important in thermoelectric applications.

As will be seen from equation (7), the electronic component of the thermal conductivity rises with temperature, but the lattice component falls from a value of 0·0268 W cm^{-1} $°C^{-1}$ at 150° K to 0·0157 W cm^{-1} $°C^{-1}$ at 300° K. The variation of the total thermal conductivity with temperature depends on the particular value of the electrical conductivity.

3.3 *Anisotropy*. Bismuth telluride forms trigonal crystals which cleave very readily perpendicular to the *c*-axis. Of the properties with which we are concerned, the least dependent on orientation is the thermoelectric power. In fact, for *p*-type Bi_2Te_3 the thermoelectric power appears to be isotropic,[20] but for *n*-type material having a thermoelectric power of about $-200\,\mu V°C^{-1}$ with the thermal gradient parallel to the cleavage planes, the thermoelectric power in the perpendicular direction is about $20\,\mu V°C^{-1}$ less.

The ratio of the electrical conductivity in the cleavage planes to that in the perpendicular direction is about 2·7 : 1 for *p*-type material over the whole temperature range which

has been covered. For *n*-type material the same ratio rises from 4·0 : 1 at 150° K to 4·75 : 1 at 300° K. The lattice component of the thermal conductivity with the gradient along the cleavage planes is about 2·1 times its value for the perpendicular direction.

3.4 *Figure of merit for Bi_2Te_3 thermocouples.* The results given in Sections 3.1 and 3.2 enable the figure of merit at 300° K to be calculated for thermocouples consisting of *n*-type and *p*-type Bi_2Te_3 covering a wide range of conductivity. There are three variables, namely, the figure of merit, the electrical conductivity of the *p*-type branch and the electrical conductivity of the *n*-type branch, but it is found that the optimum figure of merit occurs for a couple consisting of *n*-type and *p*-type Bi_2Te_3 of approximately equal conductivities. Consequently, in Fig. 3, the figure of merit θ has been plotted against the electrical conductivity which has been assumed to be the same for *n*-type and the *p*-type material. It will be seen that the electrical conductivity can depart quite widely from the optimum value before the figure

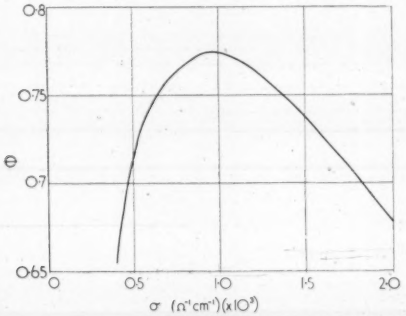

Fig. 3. Figure of merit against electrical conductivity at 300° K

of merit is reduced below, say, 90% of the maximum value. It is interesting to note that the optimum thermoelectric power for both *p*-type and *n*-type Bi_2Te_3 is quite close to $\pm 200\ \mu V°C^{-1}$ in good agreement with the theoretical predictions.[2, 8]

The optimum thermoelectric power below 300° K should not be very dependent on temperature, so, since the relationship between thermoelectric power and electrical conductivity does not change appreciably with change of temperature, the optimum electrical conductivity should still be quite close to $1000\ \Omega^{-1}\,cm^{-1}$ as the temperature is lowered. In order to determine the change of the maximum figure of merit with temperature it is necessary to know the variation of the thermal conductivity. Fig. 4 shows the variation of thermal conductivity and thermoelectric power with temperature, for *n*-type and *p*-type Bi_2Te_3 with an electrical conductivity of $1000\ \Omega^{-1}\,cm^{-1}$. In Fig. 5 the corresponding figure of merit is plotted against temperature. In view of the fairly flat maximum of Fig. 3 it is thought that Fig. 5 should equally well represent the plot of *maximum* figure of merit against temperature.

Above room temperature it is probable that the optimum electrical conductivity would rise above $1000\ \Omega^{-1}\,cm^{-1}$, since, at higher temperatures, this electrical conductivity would correspond to the range of mixed conduction. However, the maximum figure of merit should continue to increase up to about 150° C, and should not fall below the room temperature value until about 300° C is reached unless the temperature dependence of one or other of the relevant

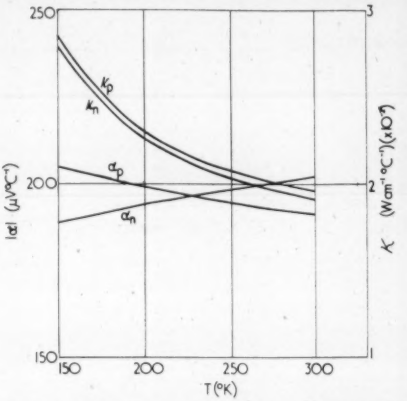

Fig. 4. Thermoelectric power and thermal conductivity against temperature for an electrical conductivity of $1000\ \Omega^{-1}\,cm^{-1}$

semiconductor properties changed. For example, the work of Vlasova and Stil'bans[21] suggests that the rate of change of carrier mobility with temperature is more rapid above 300° K than below this temperature.

4. COEFFICIENT OF PERFORMANCE FOR REFRIGERATION WITH BISMUTH TELLURIDE COUPLES

It will be seen from Fig. 5 that the figure of merit for a Bi_2Te_3 couple at 290° K is 0·76. The coefficient of performance for refrigeration can be calculated from equation (2)

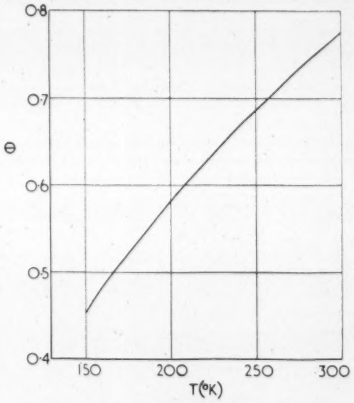

Fig. 5. Figure of merit against temperature $\sigma_n = \sigma_p = 1000\ \Omega^{-1}cm^{-1}$

using this value for θ. In Fig. 6 the coefficient of performance has been plotted against the temperature difference for a mean temperature of 290° K (17° C). It will be noticed that the maximum temperature difference is 66° C; this difference should become higher at greater mean temperatures than 290° K and correspondingly lower at lower mean temperatures. At 150° K the maximum temperature difference would be not more than about 14° C.

The attainment of the maximum temperature difference requires perfect thermal insulation of the cold junction and of the thermocouple branches. The nearest approach to this condition is obtained in a high vacuum and the performance of a Bi_2Te_3 couple in a vacuum has therefore been studied. The temperature of the cold junction of the couple, which consisted of a negative branch with a thermoelectric power of $-210\,\mu V°C^{-1}$ and a positive branch with a thermoelectric power of $+190\,\mu V°C^{-1}$, was measured with a very fine gauge copper-constantan thermocouple. With a mean temperature of 292° K a cooling effect of 64° C was observed. The fact that this is so close to the theoretical maximum cooling shows that contact resistances at the junctions must have been negligible.[22]

Fig. 6 shows that a coefficient of performance of unity can be attained only when the temperature difference is less than

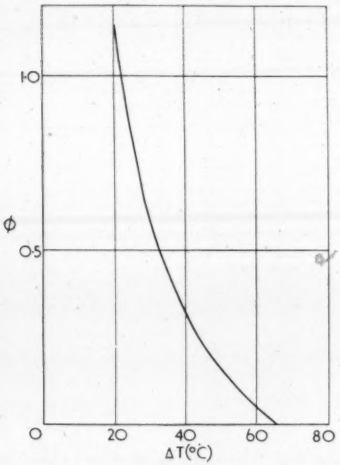

Fig. 6. Coefficient of performance for refrigeration against temperature difference for Bi_2Te_3 thermocouples at a mean temperature of 290° K

22° C. Since part of the overall temperature difference must be associated with the transfer of heat between the thermocouple junctions and the surroundings, it is clear that the coefficient of performance of a thermoelectric refrigerator consisting of Bi_2Te_3 couples must be considerably less than that for a conventional compressor-type refrigerator.

5. EFFICIENCY OF GENERATION WITH Bi_2Te_3 COUPLES

In Fig. 7 the efficiency of thermoelectric generation with Bi_2Te_3 couples, calculated from equation (4), has been plotted against the temperature difference, again assuming a mean temperature of 290° K. This diagram shows that the efficiency would be about 1% for every 25° C temperature difference available.

It is difficult to envisage many applications where the mean temperature would be as low as 290° K. The use of large

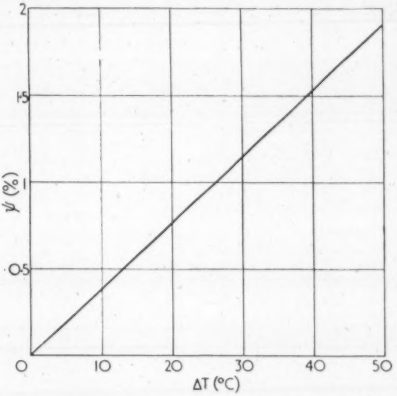

Fig. 7. Efficiency for generation against temperature difference for Bi_2Te_3 thermocouples at a mean temperature of 290° K

temperature differences, in order to obtain increased efficiencies according to equation (4), might involve mean operating temperatures of 200° C (about 500° K) or higher. Measurements of the thermoelectric properties of Bi_2Te_3 have not so far been made above 300° K so the prediction of efficiencies at higher temperatures can only be speculative. It is, however, apparent that the efficiency for a given temperature difference will be higher than that given in Fig. 7 if the mean temperature rises above 290° K, in view of the rise of the figure of merit θ with temperature shown in Fig. 5.

6. CONCLUSIONS

The measurements on the properties of Bi_2Te_3 have confirmed its early promise as a thermoelectric material. It has been found possible to achieve a figure of merit, as defined in equation (1), of 0·76, at a mean temperature of 290° K. This corresponds to a maximum cooling by means of the Peltier effect of 66° C and an efficiency of thermoelectric generation of 1% for a 25° C temperature difference.

Bismuth telluride couples should find immediate laboratory applications in cooling units for dew-point hygrometers and in vacuum thermopiles for which the same criteria apply.

The comparatively high figure of merit makes thermoelectric refrigeration on a larger scale a practical proposition. It appears, however, that still higher values of the figure of merit are needed to make it attractive commercially.

Ioffe and others[23] have shown that the thermal conductivity of a semiconductor may be reduced by the addition of an isomorphous material, and that the carrier mobility need not be affected. One alloy of Bi_2Te_3 with Bi_2Se_3 seems promising[24] and a study of Bi_2Te_3 alloys should lead to a

further improvement in the figure of merit. Our most recent work has confirmed this expectation.[25]

REFERENCES

(1) GOLDSMID, H. J., and DOUGLAS, R. W. *Brit. J. Appl. Phys.*, **5**, pp. 386, 458 (1954).
(2) GOLDSMID, H. J. *J. Electronics*, **1**, p. 218 (1955).
(3) ALTENKIRCH, E. *Phys. Z.*, **12**, p. 920 (1911).
(4) IOFFE, A. F., STIL'BANS, L. S., IORDANISHVILI, E. K., and STAVITSKAYA, T. S. *Thermoelectric Cooling** (Moscow: Akademii Nauk SSSR, 1956).
(5) TELKES, M. *J. Appl. Phys.*, **18**, p. 1116 (1947).
(6) PAPET, R. M. *J. Appl. Phys.*, **19**, p. 1180 (1948).
(7) GOLDSMID, H. J. *Research*, **8**, p. 172 (1955).
(8) IOFFE, A. F. *Semiconductor Thermoelements** (Moscow: Akademii Nauk SSSR, 1956).
(9) IOFFE, A. V., and IOFFE, A. F. *Dokl. Akad. Nauk. SSSR*, **97**, p. 821 (1954).
(10) WILSON, A. H. *The Theory of Metals*, 2nd Ed. (London: Cambridge University Press, 1953).
(11) CONWELL, E., and WEISSKOPF, V. F. *Phys. Rev.*, **77**, p. 388 (1950).
(12) BROOKS, H. *Advances in Electronics and Electron Physics*, **7**, p. 85 (1955).
(13) HERRING, C. *Bell. Syst. Tech. J.*, **34**, p. 1342 (1956).
(14) DRABBLE, J. R., and WOLFE, R. *Proc. Phys. Soc. [London] B*, **69**, p. 1101 (1956).
(15) GOLDSMID, H. J. *Proc. Phys. Soc. [London]*, **71**, p. 633 (1958).
(16) GOLDSMID, H. J. *Proc. Phys. Soc. [London]*, **72**, p. 17 (1958).
(17) BLACK, J., CONWELL, E. M., SEIGLE, L., and SPENCER, C. W. *J. Phys. Chem. Solids*, **2**, p. 240 (1957).
(18) SHOCKLEY, W. *Electrons and Holes in Semiconductors* (New York: D. Van Nostrand Co. Inc., 1950).
(19) PRICE, P. J. *Phil. Mag.*, **46**, p. 1252 (1955).
(20) WRIGHT, D. A. *Halbleiter-Probleme*, **4**. "Proceedings of Garmisch Conference, 1956." To be published.
(21) VLASOVA, R. M., and STIL'BANS, L. S. *Z. Tekh. Fiz.*, **25**, p. 569 (1955).
(22) GEHLHOFF, P. O., JUSTI, E., and KOHLER, M. *Abhandl. Braunschw. Wiss Gesell.*, **2**, p. 149 (1950).
(23) IOFFE, A. F., AIRAPETYANTS, S. V., IOFFE, A. V., KOLOMOETS, N. V., and STIL'BANS, L. S. *Dokl. Akad. Nauk. SSSR*, **106**, p. 981 (1956).
(24) SINANI, S. S., and GORDYAKOVA, G. N. *Z. Tekh. Fiz.*, **26**, p. 2398 (1956).
(25) WRIGHT, D. A. *Nature [London]*, **181**, p. 834 (1958).

* These two books have been combined in an English edition, *Semiconductor Thermoelements and Thermoelectric Cooling* (London: Infosearch, 1957).

The flow of heat in a parallel-faced infinite solid

By T. P. NEWCOMB, M.Sc., A.Inst.P., Ferodo Ltd., Chapel-en-le-Frith, Stockport, Cheshire

[*Paper received* 29 *March*, 1958]

A solution is given for the problem of heat conduction in an infinite slab in which one face is subjected to a linearly decreasing thermal flux $Q(1 - at)$, there being no flow of heat at the parallel boundary. This solution may be applied to the problem of braking with uniform deceleration. Typical curves illustrating the agreement between transient temperatures determined theoretically and experimentally at different points in the slab are given.

In a recent series of papers,[1–3] solutions have been presented for the flow of heat through an infinite slab in which one face is subjected to a thermal flux linearly decreasing with time, the methods used being based on the Fourier series and on the method of images. By using the Laplace transformation, however, a more elegant solution of the problem can be obtained.

This method of analysis is described below. It is of interest as it enables the temperatures reached at the interface between a brake drum and lining, or at any point within the contacting bodies, to be readily calculated provided the deceleration is constant. The errors introduced by considering the cylindrical portion of the drum to be developed into a flat rectangular plate and the heat flow to be uni-dimensional are small enough to be neglected. For constant deceleration, the rate of heat generation H can be shown to diminish linearly with time t, i.e. $H = Q(1 - at)$ where Q and a are constants.

THE EQUATIONS AND THEIR FORMAL SOLUTION

Consider the linear flow of heat in a solid initially at zero temperature and bounded by a pair of infinite parallel planes at $x = 0$ and $x = d$, such that at $x = 0$ there is no flow of heat perpendicular to the plane and at $x = d$ there is a flux $Q(1 - at)$ into the solid. If v, K and k denote the temperature, thermal conductivity and diffusivity respectively, the solution of the following differential equation is required:

$$\frac{\partial^2 v}{\partial x^2} - \frac{1}{k}\frac{\partial v}{\partial t} = 0 (0 < x < d) \tag{1}$$

with the conditions

$$\partial v/\partial x = 0 \text{ at } x = 0 \tag{2}$$

and

$$K(\partial v/\partial x) = Q(1 - at) \text{ at } x = d \tag{3}$$

Introducing the Laplace transform of v, defined as

$$\bar{v} = \int_0^\infty \exp(-pt) \cdot v(x, t)\, dt$$

the equation to be solved becomes

$$(d^2\bar{v}/dx^2) - (p/k)\bar{v} = 0 \quad (0 < x < d) \tag{4}$$

subject to

$$d\bar{v}/dx = 0 \text{ at } x = 0 \tag{5}$$

and

$$\frac{d\bar{v}}{dx} = \frac{Q}{K}\left(\frac{1}{p} - \frac{a}{p^2}\right) \text{ at } x = d \tag{6}$$

The solution to equation (4) is

$$\bar{v} = A \cosh qx + B \sinh qx \tag{7}$$

where $q = (p/k)^{\frac{1}{2}}$.

Using the boundary conditions (5) and (6), $\bar{v}$ finally reduces to

$$\bar{v} = \frac{Q}{K}\left(\frac{1}{p} - \frac{a}{p^2}\right)\frac{\cosh qx}{q \sinh qd} \tag{8}$$

Expressing the hyperbolic functions in terms of negative exponentials and expanding in a series by the binomial theorem, one obtains

$$\bar{v} = \frac{Q}{K}\left(\frac{1}{p} - \frac{a}{p^2}\right)\frac{1}{q}\{\exp[-q(d-x)] + \exp[-q(d+x)]\}\sum_{n=0}^{\infty}\exp(-2nqd) \tag{9}$$

$$= \frac{Q}{K}\left(\frac{1}{pq} - \frac{a}{p^2 q}\right)\left(\sum_{n=0}^{\infty}\exp\{-q[(2n+1)d+x]\} + \sum_{n=0}^{\infty}\exp\{-q[(2n+1)d+x]\}\right) \tag{10}$$

Inverting the transform[4] gives

$$\frac{Kv}{Qk^{\frac{1}{2}}} = 2t^{\frac{1}{2}}\sum_{n=0}^{\infty}\left[i\operatorname{erf}c\frac{(2n+1)d-x}{2(kt)^{\frac{1}{2}}} + i\operatorname{erf}c\frac{(2n+1)d+x}{2(kt)^{\frac{1}{2}}}\right] - a8t^{\frac{1}{2}}\sum_{n=0}^{\infty}\left[i^3\operatorname{erf}c\frac{(2n+1)d-x}{2(kt)^{\frac{1}{2}}} + i^3\operatorname{erf}c\frac{(2n+1)d+x}{2(kt)^{\frac{1}{2}}}\right] \tag{11}$$

where $i^n \operatorname{erf} c\, x = \int_x^{\infty} i^{n-1}\operatorname{erf} c\, y dy \quad (n = 1, 2, 3 \ldots)$

with $i^0 \operatorname{erf} c\, x = \operatorname{erf} c\, x = \frac{2}{\pi^{\frac{1}{2}}}\int_x^{\infty}\exp(-y^2)dy$

The function $i^n \operatorname{erf} c\, x$ for various values of n and x has been considered by Hartree,[5] the results being given in tabular form (see also Carslaw and Jaeger,[4] Appendix II).

If T is the total time for which the flux is applied, then $a = 1/T$.

Further, if we put $x = sd (0 < s < 1)$ and $\lambda = d/[2(kt)^{\frac{1}{2}}]$ equation (11) may be expressed as

$$\frac{Kv}{Qk^{\frac{1}{2}}} = 2t^{\frac{1}{2}}\sum_{n=0}^{\infty}\left[i\operatorname{erf}c(2n+1-s)\lambda + i\operatorname{erf}c(2n+1+s)\lambda\right] - \frac{8t^{\frac{1}{2}}}{T}\sum_{n=0}^{\infty}\left[i^3\operatorname{erf}c(2n+1-s)\lambda + i^3\operatorname{erf}c(2n+1+s)\lambda\right] \tag{12}$$

Therefore, if Q, K, T, d and k are known, the transient temperatures for particular values of the parameters t/T and s may be evaluated from equation (12).

The above relationship can readily be used to determine the temperature reached at the interface between a brake lining and a brake drum which is being uniformly decelerated. In this case $s = 1$ and the expression reduces to

$$\frac{Kv}{Qk^{\frac{1}{2}}} = \frac{2t^{\frac{1}{2}}}{\pi^{\frac{1}{2}}}\left(1 - \frac{2}{3}\frac{t}{T}\right) + 4t^{\frac{1}{2}}\sum_{n=1}^{\infty} i\operatorname{erf}c2n\lambda - \frac{16t^{\frac{1}{2}}}{T}\sum_{n=1}^{\infty} i^3\operatorname{erf}c2n\lambda \tag{13}$$

Equation (13) is rapidly convergent for values of λ normally encountered, the number of terms required increasing only when d is small or t large.

The temperature gradient at any point in the solid $\partial v/\partial x$ may be determined by differentiation of equation (12)

$$\text{i.e. } \frac{\partial v}{\partial x} = \frac{Q}{K}\sum_{n=0}^{\infty}\left[\operatorname{erf}c(2n+1-s)\lambda - \operatorname{erf}c(2n+1+s)\lambda\right] - \frac{Q}{K}\frac{4t}{T}\sum_{n=0}^{\infty}\left[i^2\operatorname{erf}c(2n+1-s)\lambda - i^2\operatorname{erf}c(2n+1+s)\lambda\right] \tag{14}$$

APPLICATION OF THEORY

If a brake lining slides against a rotating cast iron drum and produces a constant drum deceleration f cm/s^2, then after t seconds of braking from an initial speed u cm/s the instantaneous speed is $(u - ft)$ cm/s. Hence, the instantaneous energy H generated at the friction surface is

$$H = (Fu/A_2J)\left[1 - (ft/u)\right] = Q(1 - at) \tag{15}$$

where A_2 = area of brake linings (cm^2); F = tangential force acting at the friction surface (dyn); J = mechanical equivalent of heat, taken as $4{\cdot}18 \times 10^7$ erg/cal; $Q = Fu/A_2J$; and $a = f/u$.

Using suffixes 1 and 2 for drum and lining respectively, the heat dissipated into each solid is

$$H_1 = Q_1(1 - at), \quad H_2 = Q_2(1 - at)$$

where $$H_1 + H_2 = H$$

The values of Q_1 and Q_2 may be determined by the condition of equal temperatures at the common surface of drum and lining. To a first approximation this is given by the first term of equation (13)

$$\frac{v_1K_1}{2Q_1(k_1t)^{\frac{1}{2}}} = \frac{1}{\pi^{\frac{1}{2}}}\left(1 - \frac{2}{3}\frac{t}{T}\right) = \frac{v_2K_2}{2Q_2(k_2t)^{\frac{1}{2}}} \tag{16}$$

where v_1, v_2 are the temperatures of drum and lining respectively, relative to the ambient temperature, during one application of the brake, from which

$$\frac{Q_2}{Q_1} = \frac{K_2(k_1)^{\frac{1}{2}}}{K_1(k_2)^{\frac{1}{2}}} = \frac{H_2}{H_1} \tag{17}$$

Since the working surface areas A_1 and A_2 of drum and lining are different, the net heat absorptions are in the ratio

$$\frac{H_2A_2}{H_1A_1} = \frac{A_2K_2(k_1)^{\frac{1}{2}}}{A_1K_1(k_2)^{\frac{1}{2}}} \tag{18}$$

In the brake of a typical family saloon car, A_1 and A_2 were 238 and 146 cm^2 respectively, $K_1 = 0{\cdot}12$ cal/cm $\times$ s $\times$ °C, $k_1 = 0{\cdot}12$ cm^2/s, $d_1 = 0{\cdot}64$ cm and $K_2 = 0{\cdot}0018$ cal/cm $\times$ s $\times$ °C, $k_2 = 0{\cdot}0033$ cm^2/s, $d_2 = 0{\cdot}48$ cm. The term H_2A_2/H_1A_1 represents the fraction of the total energy dissipated in the brake lining, which for the above example is 1/18·08. Hence, from a knowledge of H and the physical properties of the contacting bodies, Q_1 and Q_2 may be evaluated. Finally, from equation (12) the temperature at any position in the drum or lining may be calculated.

Experimental verification of equation (12) for the case when the lining possesses the physical quantities given above (from which $\lambda_2 = 4{\cdot}38/t^{\frac{1}{2}}$) has been obtained by measuring transient temperatures inside the linings at positions $s = 0{\cdot}6$, $0{\cdot}85$ and near $s = 1{\cdot}0$. The stopping time T, from an initial sliding surface speed of 436 cm/s, was 5 s, thereby resulting in a value of $1{\cdot}96$ cal/cm^2 $\times$ s for Q_2.

Temperature measurements during each application of the brake were made by copper-constantan thermocouples, the outputs of which were fed into an amplifier and then to an

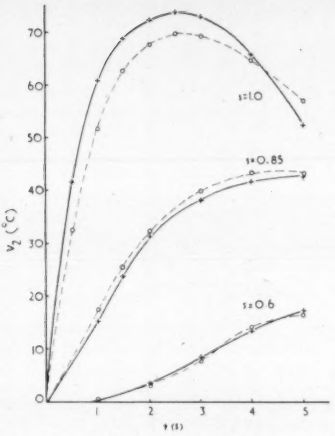

Typical curves of transient temperatures at different positions in a brake lining

○ = experimental measurements
+ = calculated temperatures

Evershed and Vignoles recorder having a response of approximately $\frac{1}{10}$ s. The agreement between temperatures determined experimentally and theoretically from equation (12) at various times during the braking application are illustrated graphically in the figure. Each experimental point contains the mean of at least four measurements, the scatter in individual measurements about their mean being of the order $\pm 5\%$. These experimental curves show agreement to within 10% of the theoretical values.

ACKNOWLEDGEMENTS

The author wishes to thank Dr. R. T. Spurr and Mr. A. D. M. Frood of the Research Division of Ferodo Ltd. for assistance and criticism, and the Directors of Ferodo Ltd. for permission to publish this paper.

REFERENCES

(1) ODIER, J., and LEUTARD, P. *C.R. Acad. Sci. (Paris)*, **244**, p. 1141 (1957).
(2) ODIER, J., and LEUTARD, P. *C.R. Acad. Sci. (Paris)*, **244**, p. 1321 (1957).
(3) BANNISTER, F. K. *Engineering (London)*, **183**, p. 304 (1957).
(4) CARSLAW, H. S., and JAEGER, J. C. *Conduction of heat in solids*, 1st Ed., Appendix V (Oxford: Clarendon Press, 1947).
(5) HARTREE, D. R. *Mem. Manchester Lit. Phil. Soc.*, **80**, p. 85 (1935).

Studies of the viscosity and sedimentation of suspensions

Part 4.—Capillary-tube viscometry applied to stable suspensions of spherical particles*

By G. H. HIGGINBOTHAM, Ph.D.,† D. R. OLIVER, Ph.D.,‡ and Prof. S. G. WARD, Ph.D., D.I.C.,
Department of Mining, University of Birmingham

[*Paper first received* 23 *January, and in final form* 7 *May*, 1958]

A description is given of a series of measurements of the viscosity of stable suspensions of spherical particles in an efflux-type capillary-tube viscometer.

It is shown that a form of wall-effect is present in the tube, which causes the apparent viscosity of the suspensions to decrease with decreasing tube-size. The suspensions are shown to behave as though a layer of pure liquid were present along the tube walls, though the layer appears to be only hypothetical in nature. The values of the wall-layer thickness obtained in the present work are used in a brief assessment of a recently-proposed "concentration" theory of wall effect.[10]

The final values of the relative viscosity, corrected for wall effect, show no dependence on absolute particle size or particle size-range. All series of results are shown to be governed by a single type of equation, which reduces to that of Einstein at very low values of the volume concentration.

INTRODUCTION

The well-known equation of Einstein[1] for the relative viscosity η_r of a stable suspension of smooth, equisized, rigid spheres is

$$\eta_r = \eta/\eta_0 = 1 + kc \qquad (1)$$

where η and η_0 are the absolute viscosities of the suspension and dispersing liquid respectively, c is the volumetric concentration of the spheres and k is a constant equal to 2·5. The relationship applies only to very dilute suspensions, the upper limit of concentration, according to Roscoe,[2] being well below 0·05. Several workers[2–9] have made theoretical and experimental attempts to develop a relationship which would be valid over a wider range of volume concentrations.

Vand[6] included in his work a theoretical examination of the change of behaviour produced by the presence of a rigid boundary on a flowing suspension of spherical particles. He proposed the hypothesis that the suspension would behave as if there were, along the wall, a layer of fluid of viscosity equal to that of the pure liquid. The thickness D of the layer was

* Parts 1 and 2 of this paper, "The viscosity of suspensions of spherical particles" and "The viscosity and sedimentation of suspensions of rough powders," were published on pp. 286 and 325 of Volume 1 (1950) of this *Journal*. Part 3, "The sedimentation of isometric and compact particles," was published on p. 83 of Volume 6 (1955) of this *Journal*.

† Now at Simon Carves Ltd., Cheadle Heath, Stockport.

‡ Now at Department of Chemical Engineering, University of Birmingham.

related to the radius r of the particles by the expression $D = 1{\cdot}301r$. Measurements carried out using Ostwald viscometers showed effects which could be attributed to a wall layer of the above type, but the thickness of the layer was found to vary considerably with the solids concentration of the suspensions.

Maude and Whitmore[10] have recently suggested that wall effects in capillary tubes can be explained in terms of a reduction of solids concentration in the tube, caused by a reduced stay-time of certain particles which travel close to the walls. These particles, it is argued, are constrained by the wall to travel along faster-moving streamlines than they otherwise would have done; their time-average concentration is therefore reduced. The theory was tested by actual measurements of the solids concentration in a flowing suspension, and the results were in fairly good agreement with the theory. It was shown that, with a few simplifying assumptions, the postulated change of concentration could be related to the thickness of a hypothetical layer of fluid, of the Vand type, along the tube wall.

The work now to be described was carried out in an efflux-type capillary-tube viscometer and was designed to investigate not only wall effects but also the relative viscosities of stable suspensions of spherical particles, as measured in such an instrument.

FUNDAMENTAL APPROACH

Vand[6] considered that the effect of the constraint of the tube walls on the spherical particles of a flowing suspension would be to *increase* their volume concentration in the ratio $1/(1 - r/a)^2$, where r and a are the respective radii of the particles and tube. This concentration correction factor was not proved, but may be obtained by assuming that, since no sphere centre can lie within a distance r of the tube wall, the effective increase of concentration of sphere centres in the central region of the tube is

$$a^2/(a - r)^2 \quad \text{or} \quad 1/(1 - r/a)^2$$

It is submitted that this factor gives merely the geometrical increase of concentration of sphere centres in the central region of the tube (radius $a - r$) and not the change of concentration of solid matter in the tube as a whole. The constraint of the walls results only in the displacement of certain particles towards the centre of the tube, the change in the concentration distribution constituting a form of wall effect. It does not seem justifiable to apply the above ratio as a concentration correction factor; it is omitted in the present work.

Maude and Whitmore's work led to the conclusion that the concentration of spherical particles in a flowing suspension should be *decreased*, and not *increased*, as a result of the constraint of the tube walls on the particles. Since, however, the concentration change was assumed to account directly for the wall effect, the phenomenon being investigated, it would be unsound to attempt to apply a concentration correction factor.

In this paper, therefore, the volumetric concentration c of spherical particles in a suspension is taken to equal the solids concentration in the clean vessel into which the suspension flows after passage down the capillary tube.

Regarding the wall effect, the following principles will be followed:

(1) any redistribution or change of concentration of the particles in the suspension resulting directly from the mechanical constraining effect of the walls will be treated as part of the wall effect itself; and

(2) since the exact nature of the wall effect is open to some doubt, hydrodynamical and concentration effects being difficult to separate, a simple model of the Vand "fluid layer" type will be used where practicable. The test of the model will be that it gives consistent and reproducible results for viscosities measured in tubes of different diameters, the particle size and volumetric concentration of the solids in the suspensions being varied over a wide range of values.

SUSPENSIONS

The systems used were suspensions of sieved size-fractions of spherical particles of a methyl methacrylate polymer in an aqueous glycerol solution of lead nitrate containing 0·01% dispersing agent (Dispersol O.G.). The density of the liquid was adjusted to equal that of the particles. The size-distributions of the spheres were substantially flat-topped; size characteristics are shown in Table 1.

Table 1. *Size characteristics of spherical powders used*

Sample	*Nominal size-range* (μ)	*Mean diameter* (μ)	*Size ratio* $\frac{\text{largest particle}}{\text{smallest particle}}$
(*a*)	178 — 152	165	1·17
(*b*)	176 — 76	127	2·34
(*c*)	89 — 76	82·5	1·17
(*d*)	76 — 53	64·5	1·43

THE EFFLUX-TYPE CAPILLARY-TUBE VISCOMETER

This instrument, described in Appendix 1, is a development of the consistometer of DeVaney and Shelton.[11] Important improvements were the provision of accurate systems of temperature and flow-rate control, and the replacement of an open discharge by a suspended level discharge. The instrument could be used to measure absolute viscosities with an accuracy of ±1% in capillary tubes of three different diameters. All measurements were made at a temperature of 20 ± 0·1° C; the flow in each capillary tube was laminar in character.

CONCENTRATION MEASUREMENT

Suspensions of approximately the required concentrations were prepared, poured into the upper vessel of the instrument and stirred. The accurate value of the concentration of each suspension was obtained after timings of the flow had been carried out. A sample of the suspension was allowed to pass from the capillary tube into a weighed beaker, after which the beaker was re-weighed. A final weighing of the washed, dried particles completed the information required to calculate the volume concentration of solids in the suspension.

VISCOSITY MEASUREMENTS

A series of preliminary tests using liquids of standard viscosities showed that, for the present instrument, the capillary-tube end correction factor n was zero whilst the kinetic energy correction factor m was equal to unity. The viscosities of the suspensions and dispersing liquids could therefore be calculated from a suitably modified Poiseuille equation.[12] For each suspension prepared, three series of three measurements of the time taken for the lower bulb to fill were made, each series being carried out with a different back pressure applied at the lower end of the capillary tube. The object of this procedure was to find out whether the viscosity of the suspensions varied with the rate of flow down the tube. No such non-Newtonian behaviour was

observed in any suspension of volume concentration below 40%.

The mean value of the measured viscosity of each suspension was divided by the viscosity of the pure dispersing liquid to give the apparent relative viscosity of the suspension in the particular tube used. Curves were drawn showing the variation of apparent relative viscosity with the volume concentration of the suspensions; typical examples are shown in Fig. 1. These curves were of the same form, illustrating clearly the breakdown of the Einstein equation[1] for suspensions of finite concentration. The dependence of the relative viscosity on tube size is also illustrated by the curves; this is in accordance with the theories of Vand[6] and of Maude and Whitmore.[10] Table 2 summarizes the measures values of the relative viscosity η_r obtained in different-sized tubes, read off at intervals of concentration of 2·5%.

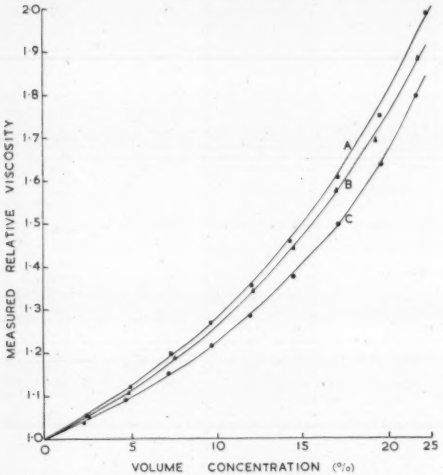

Fig. 1. Typical examples of curves showing variation of apparent viscosity of suspensions with volume concentration of solid phase for particles in the size range 89 — 76 μ

Curve *A*, tube diameter 3 mm; curve *B*, tube diameter 2 mm; curve *C*, tube diameter 1 mm.

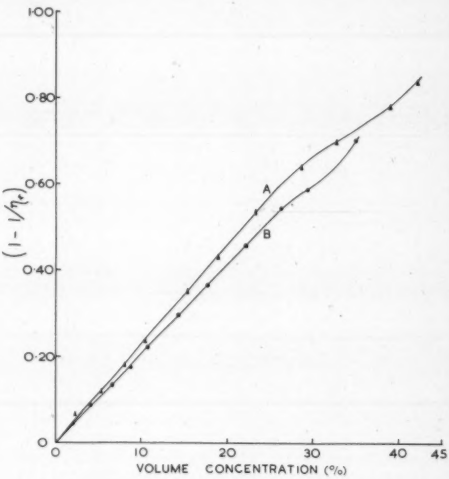

Fig. 2. Typical curves showing relationship between the quantity $(1 - 1/\eta_r)$ and volume concentration for particles in the size range 76 — 53 μ

Curve *A*, tube diameter 2 mm; curve *B*, tube diameter 1 mm.

Table 2. *Measured values of relative viscosity*

Size range of spheres (μ)	178 — 152			178 — 76		89 — 76			76 — 53	
Capillary-tube diameter (mm)	1·0	2·0	3·0	2·0	3·0	1·0	2·0	3·0	1·0	2·0
Volume concentration (%)										
2·5	1·04	1·05	1·05	1·05	1·06	1·04	1·05	1·06	1·05	1·06
5·0	1·07	1·10	1·11	1·11	1·12	1·10	1·12	1·12	1·11	1·12
7·5	1·12	1·16	1·18	1·17	1·18	1·16	1·19	1·20	1·18	1·20
10·0	1·17	1·23	1·25	1·24	1·26	1·23	1·27	1·28	1·25	1·29
12·5	1·24	1·30	1·34	1·32	1·35	1·30	1·36	1·38	1·34	1·39
15·0	1·33	1·39	1·43	1·41	1·45	1·39	1·47	1·49	1·44	1·51
17·5	1·45	1·48	1·54	1·52	1·55	1·52	1·60	1·63	1·56	1·65
20·0	1·63	1·59	1·67	1·64	1·71	1·65	1·75	1·79	1·69	1·82
22·5	1·86	1·75	1·83	1·79	1·86	1·85	1·92	1·98	1·86	2·03
25·0									2·05	2·29
27·5									2·26	2·59
30·0									2·48	2·91
32·5									2·75	3·30

In order to provide the data required for the application of Vand's method* of determining the thickness D of the hypothetical layer of pure liquid along the tube walls, values of the quantity $(1 - 1/\eta_r)$ were plotted against the volume

* See Appendix 2.

Table 3. *Values of D/r*

Mean diameter of spheres (μ)	165		127	82·5		64·5
Capillary-tube diameters (mm)	1·0 *and* 2·0	2·0 *and* 3·0	2·0 *and* 3·0	1·0 *and* 2·0	2·0 *and* 3·0	1·0 *and* 2·0
Concentration range over which D/r is constant (%)	0–10	0–20	0–22·5+	0–18	0–22·5+	0–30
Value of D/r	0·802	0·717	0·631	0·776	0·665	0·695
Mean values of D/r	0·76		0·63	0·72		0·70

Table 4. *Values of relative viscosity corrected for wall effect*

$D/r = 0·70$ (*mean value*)

Size range of spheres (μ)	178 — 152			178 — 76		89 — 76			76 — 53	
Capillary-tube diameter (mm)	1·0	2·0	3·0	2·0	3·0	1·0	2·0	3·0	1·0	2·0
Volume concentration (%)										
2·5		1·07	1·06	1·06	1·07	1·05	1·06	1·07	1·06	1·06
5·0		1·13	1·13	1·14	1·14	1·13	1·14	1·13	1·14	1·14
7·5		1·21	1·22	1·21	1·21	1·21	1·22	1·22	1·22	1·22
10·0		1·31	1·31	1·30	1·30	1·31	1·31	1·31	1·32	1·32
12·5		1·41	1·42	1·41	1·40	1·41	1·43	1·42	1·44	1·44
15·0		1·55	1·54	1·54	1·54	1·55	1·56	1·55	1·59	1·58
17·5		1·70	1·70	1·70	1·69	1·76	1·73	1·72	1·76	1·76
20·0		1·89	1·88	1·88	1·88	1·99	1·93	1·91	1·98	1·98
22·5		2·19	2·13	2·12	2·08	2·39	2·17	2·15	2·26	2·26
25·0									2·62	2·62
27·5									3·06	3·07
30·0									3·56	3·57
32·5									4·29	4·27
Values of K in equation $\eta_r = (1 - Kc)^{-1}$		2·36	2·34	2·34	2·33	2·39	2·35	2·35	2·46	2·46

* Viscosities not corrected due to early curvature of graph of $(1 - 1/\eta_r)$ against concentration.

concentration of the suspensions. Typical results are shown in Fig. 2. The lines were straight, in some cases up to concentrations of nearly 30%, and this led Oliver and Ward[9] to suggest a modified form of the Einstein relationship

$$\eta_r = (1 - Kc)^{-1} \qquad (2)$$

In this equation K is an experimentally determined constant evaluated after correction of the viscosities for wall effect.

The values of D/r, obtained as in Appendix 2, are summarized in Table 3. The mean of these figures, $D/r = 0·70$, was used to correct the measured relative viscosities for wall effect, giving the results listed in Table 4. The values of K for these series of viscosity measurements vary between 2·33 and 2·46.

DISCUSSION OF RESULTS

The results confirm the conclusion of previous workers[6, 10] that the tube radius affects values of the measured viscosity. Moreover, the Vand "fluid layer" hypothesis provides a satisfactory basis for assessing the wall effect in capillary tubes.

The values of D/r do not show the type of variation with volume concentration which was noted in the experimental work of Vand,[6] though at the higher concentrations a fall in the apparent value of D/r occurs. The effect is most noticeable in measurements where the tube diameter is small, and always results in the bending of the graph of $(1 - 1/\eta_r)$ against concentration towards the corresponding line for a larger diameter tube (Fig. 2). It is felt that the deviation of this line is due to particle-particle or particle-wall interactions which depend on the freedom of movement permitted to the particles in the tube. It is significant that the upward curvature of the lines always begins for values of cr/a between 1·5 and 2·0; thus for a given particle size the curvature begins at smaller concentrations in tubes of lower diameters. It was originally thought that the above effects might be obtained if there were actually present at the walls a layer of pure liquid, which the particles could penetrate at sufficiently high volume concentrations. A high-speed ciné film, however, showed particles rolling down the walls and in contact with them. This indicated that Vand's wall layer was, at best, hypothetical in nature.

For results unaffected by the above type of behaviour, the line relating $(1 - 1/\eta_r)$ and concentration begins to bend slowly away from the axis of $(1 - 1/\eta_r)$ at a concentration of approximately 28%. The position of this point of breakdown of the viscosity-concentration equation[2] has been shown to vary slightly with the type of instrument used.[9]

The mean values of D/r, for particles of mean diameters 165, 127, 82·5 and 64·5 μ, were 0·76, 0·63, 0·72 and 0·70 respectively. These figures may be compared with Vand's

theoretical value of 1·301. Maude and Whitmore's theory, in its simplest form,[10] gives $D/r = 0·50$, though reasons are suggested for this figure being too low. Experimental measurements by these workers, based on the change of concentration observed in a flowing suspension, gave values of D/r varying between 0·57 and 0·74 for a tube of diameter 1·876 mm and particles of mean diameter 96·5 μ. The scatter of these figures is largely due to the difficulty of measuring the solids concentration in the tube. A suspension was allowed to flow steadily down a capillary tube, after which a finger was placed over the lower end of the tube and a microscope cover-slip over the upper end. The concentration of the solids in the capillary was then obtained by washing, drying and weighing the particles present in the tube. This figure was compared with the solids concentration of the suspension which had flowed out of the tube. Results are quoted for only one tube size and one particle size range, the concentration range being reported as 16 to 21%; it is not therefore clear whether the values of D/r would show variation with any of these factors. There is, nevertheless, fair agreement between the figures given by Maude and Whitmore and those reported in this paper. A concentration change is therefore the possible cause of the major part of the wall effect though more experimental evidence is required to substantiate the theory.

The "concentration" theory offers a satisfactory explanation of the fact that no appreciable wall effect has been discovered in rotating-cylinder viscometers.[10] It should be pointed out, however, that in their proof of the proposition that the distribution of spheres should not alter the measured viscosity in this type of instrument, Maude and Whitmore assume the validity of Oliver and Ward's empirical equation.[9] If an equation such as that of Einstein[1] is used, the concentration distribution appears to affect the measured viscosity. The absence of a significant wall effect in rotating cylinder viscometers therefore provides evidence in favour of the use of the empirical equation, if the "concentration" theory is to be accepted.

The final series of corrected relative viscosities show consistency, which is reflected in the values of K quoted at the foot of the Table 4. These figures may be compared with Einstein's theoretical value of 2·50, since the equation $\eta_r = (1 - Kc)^{-1}$ reduces to that of Einstein at very low values of the concentration. The measured values are all somewhat below 2·50, but it is worthy of note that measurements in rotating cylinder viscometers have been found to give values slightly higher than 2·50.[9] It is possible that the different conditions of shear encountered in these types of instrument affect the value of K, provided the particles in the suspensions are not extremely small with respect to the instrument; in this case the local shear distributions around each particle should be the same as that obtaining if the suspension were being sheared ideally, i.e. between infinite parallel plates. Under these circumstances the viscosity of the suspension should not be dependent on the type of instrument used. The results confirm the value of Einstein's constant 2·50, though his equation can only be used for very dilute suspensions of spherical particles. The modified equation

$$\eta_r = (1 - 2·5c)^{-1}$$

gives satisfactory agreement with experimental results up to volume concentrations of approximately 30%.

CONCLUSIONS

The suspensions of spherical particles behaved as Newtonian fluids at volume concentrations below 40%. For each size-range of particles used, the viscosity of the suspensions showed marked dependence on the diameter of the tube in which the measurement was carried out. Following Vand,[6] the behaviour was described in terms of the thickness D of a hypothetical layer of pure liquid at the tube wall. The ratio between the value of D and the mean particle radius r was found to vary little over wide ranges of volume concentration, a mean value of the ratio being 0·70. This figure is in fair agreement with those obtained by Maude and Whitmore,[10] from measurements of the concentration of a suspension flowing down a capillary tube.

The final series of relative viscosities, corrected for wall effect, can be described by the equation

$$\eta_r = (1 - Kc)^{-1}$$

where $2·33 < K < 2·46$ and $c < 0·28$. At higher values of the concentration the actual viscosities were lower than those predicted by the equation.

ACKNOWLEDGEMENTS

The authors wish to acknowledge the assistance given by Dr. R. L. Whitmore in the early stages of the work and the assistance given by Dr. G. F. Eveson in discussions. One of the authors (D. R. O.) wishes to acknowledge with appreciation a D.S.I.R. maintenance grant which enabled him to undertake part of the work.

APPENDIX 1

The efflux-type capillary-tube viscometer

The instrument (Fig. 3) is constructed of glass and consists of three main sections, connected by ground glass joints (E and K). The sections may be conveniently termed the

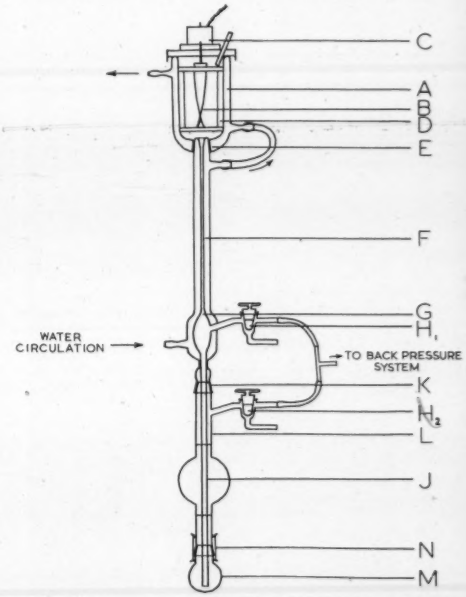

Fig. 3. Diagram of the capillary-tube efflux viscometer

reservoir, the capillary and the receiver. Support is provided by an adjustable mounting (not shown) which enables the capillary section to be set exactly vertical.

The upper reservoir A is a cylindrical vessel surrounded by a jacket through which water of controlled temperature may be circulated. A twisted nickel-plated stirrer B driven by a motor C is fitted to the removable lid of the vessel; excessive swirling of the liquid is prevented by nickel-plated baffles D connected to metal rings at the upper and lower ends of the vessel.

The viscometer has six interchangeable water-jacketed capillary sections F, of nominal lengths 15 and 25 cm (1 mm diam.), 30 and 50 cm (2 mm diam.); 45 and 75 cm (3 mm diam.). The upper end of the capillary section is a ground glass cone which fits into the socket situated centrally in the hemispherical base of the reservoir. The entrance of each capillary tube is bell-mouthed; the lower end widens into a small egg-shaped bulb G. Liquid flows down the walls of this bulb to form a "suspended level" discharge. The bulb carries a side-arm and three-way cock H_1, which may be connected to a back-pressure system. The lower end of the bulb leads into a vertical drain tube J, which passes through the second ground glass joint K and ends in the lower bulb of the receiving section. The water jackets surrounding the upper reservoir and capillary section are connected in series and the temperature of the water is controlled thermostatically to within 0·05° C.

Each of four receiving flasks, of either 30 or 100 ml. capacity, consists of a central bulb calibrated between fiducial marks on upper and lower cylindrical extensions, the ends of which carry ground-glass joints. The upper joint K fits into the capillary section; the lower fits into a small spherical bulb M held in place by rubber bands N. A side-arm with a three-way tap H_2 is attached to the flask L above the central bulb and may be connected to the back-pressure system. This system enables positive or negative pressures to be applied to the base of the capillary tube and to the receiving flask, so that the rate of shear of the fluid in the capillary may be varied.

In using the instrument the time required for the level of the fluid in the receiving flask to rise from the lower to the upper fiducial mark is measured. The effective mean forward pressure causing flow of liquid through the capillary tube is taken as the logarithmic mean of the initial and final forward pressures.

APPENDIX 2

Vand's method of determining the thickness D of the hypothetical layer of pure liquid at the tube wall

The following method, due to Vand,[6] was used in order to obtain the values of D from the measured series of relative viscosities of the suspensions.

From the usual equations for the flow of a liquid through a capillary tube in which a wall layer of lower viscosity is present, it may be shown that

$$1/\eta_r - 1 = H_x(1/\eta_{rx} - 1) \qquad (1)$$

where η_r = correct relative viscosity of the suspension
η_{rx} = apparent relative viscosity of the suspension as measured in tube "x"
and H_x = correction factor due to the presence of the hypothetical layer of liquid at the wall, appropriate to be "x."

The value of H_x is defined by the equation

$$H_x = (1 - D/a_x)^{-4} \qquad 2$$

where D = thickness of hypothetical layer of pure liquid
and a_x = radius of capillary tube "x."

With similar notation, for apparent viscosities measured in two capillary tubes "x" and "y" of different diameters, the ratio H_x/H_y may be obtained from equation (1), i.e.

$$H_x/H_y = (1 - 1/\eta_{ry})/(1 - 1/\eta_{rx}) \qquad (3)$$

It now follows from equation (2) that

$$(H_x/H_y)^{1/4} = (1 - D/a_y)/(1 - D/a_x) \qquad (4)$$

Since $(H_x/H_y)^{1/4}$, a_y and a_x are known, the value of D may be calculated from this equation for viscosities measured in any pair of tubes of different radii. The figures were divided by the mean particle radius r to give the values of D/r summarized in Table 3.

REFERENCES

(1) Einstein, A. *Ann. Phys.* [*Leipzig*], **19**, p. 289 (1906); **34**, p. 591 (1911).
(2) Roscoe, R. *Brit. J. Appl. Phys.*, **3**, p. 267 (1952).
(3) Kunitz, M. *J. Ges. Physiol.*, **9**, p. 715 (1926).
(4) Guth, E., and Simha, R. *Kolloid Z.*, **74**, p. 226 (1936).
(5) Guth, E., and Gold I. *Phys. Rev.*, **53**, p. 322 (1938).
(6) Vand, V. *J. phys. Coll. Chem.*, **52**, pp. 277, 300 (1948).
(7) Weissberg, M., Simha, R., and Rothman, N. *J. Res. Nat. Bur. Stand.*, **47**, p. 298 (1951).
(8) Brinkman, H. C. *J. chem. Phys.*, **20**, p. 571 (1952).
(9) Oliver, D. R., and Ward, S. G. *Nature* [*London*], **171**, p. 396 (1953).
(10) Maude, A. D., and Whitmore, R. L. *Brit. J. Appl. Phys.*, **7**, p. 98 (1956).
(11) DeVaney, F., and Shelton, S. *U.S. Bureau of Mines, R.I.* 3469(R) (1940).
(12) Higginbotham, G. Thesis for Ph.D. Univ. of Birmingham (1951).

Energy balance in disk seal oscillators at ultra-high frequencies

By M. R. Gavin,* D.Sc., and L. J. Herbst,† Ph.D., College of Technology, Birmingham

[*Paper received* 9 *December*, 1957]

Energy measurements were made on DET 22 (CV 273) disk seal triode oscillators in the frequency range 500–2000 Mc/s. It was found that most of the input power from the d.c. supplies could be accounted for by the a.c. output power and the power dissipated at the electrodes, including the heating of the cathode coating by h.f. currents.

1. INTRODUCTION

The use of valves for the conversion of energy from d.c. to a.c. always involves some inefficiency. Under favourable conditions a triode oscillator may convert about 70% of the power taken from the anode d.c. power supply to useful alternating power in the load. The remaining 30% is dissipated as heat by electron bombardment of the anode and grid electrodes, or by ohmic, dielectric or radiation losses in the associated circuits. As the frequency of operation is

* Now at the University College of North Wales, Bangor.
† Now at British Telecommunications Research Ltd., Taplow.

increased not only do the losses increase but also charging currents to the circuit and valve capacitances increase. As a result the efficiency of power conversion decreases at high frequencies. The drop in efficiency can be offset to some extent by the use of low-loss circuits. In the case of disk seal triodes, coaxial line circuits with appreciable surface area are used and there is very little dielectric material in the regions where the alternating voltages are large. Practically the only dielectric loss is in the glass of the valve itself. Radiation loss is also eliminated very largely with such circuits (see Fig. 1). With certain disk seal valves it has

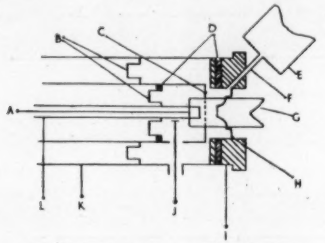

Fig. 1. Arrangement of apparatus

A, heater terminal; *B*, shorting bridges; *C*, grid thermocouple; *D*, insulating mica capacitors; *E*, box containing photocell and amplifier; *F*, light slot; *G*, valve; *H*, anode thermocouple; *I*, anode terminal; *J*, r.f. input; *K*, grid terminal; *L*, cathode terminal.

been found that the bulk resistance of the oxide coating on the cathode causes an appreciable dissipation of power at frequencies of the order of 1000 Mc/s. The resulting increase in cathode temperature has been used to determine the value of the coating resistance.[1]

At high frequencies, where the inter-electrode electron transit time becomes comparable with the alternating period, electrons may acquire additional energy from the alternating components of the fields. This energy is ultimately dissipated as heat at the electrodes.

Thus the power P_i taken from the anode supply is expended somewhat as follows:

P_0 = useful h.f. power in the load.
P_a = power dissipated at the anode.
P_g = power dissipated at the grid.
P_k = power dissipated at the cathode, including heating of the coating by r.f. current.
P_l = power dissipated in the circuit resistance and insulators.

and P_r = power radiated from the circuit.

i.e. $P_i = P_0 + P_a + P_g + P_k + P_l + P_r$.

The electrode dissipations P_a, P_g and P_k have been determined under operating conditions by the measurement of the electrode temperatures as described in the next section.

2. Measurement of Electrode Dissipations

2.1 *Cathode.* The cathode temperature was determined by the photo-electric method already described.[1, 2] Changes of temperature of the order of 1° C could be detected and the change in cathode dissipation was found by restoring the temperature by adjustment of heater power. It had already been established on d.c. tests that 95% of the heater power is passed on to the cathode.

Cathode power measurements can also be effected by using the heater resistance as the active element of a resistance thermometer. The relation between heater d.c. resistance and the r.f. heating power in the cathode was determined over a frequency range of 500–2000 Mc/s. A certain amount of r.f. energy was fed to a valve from a separate oscillator. This caused cathode heating and a change in cathode surface temperature, which was observed with the photocell. The original cathode temperature was restored by changing the d.c. heater power. The d.c. heater resistance was measured in both cases. It was found that the change in heater resistance was proportional to the change in heater power, i.e. to the r.f. heating power in the cathode, and that the constant of proportionality was independent of frequency. The heater resistance method of determining the cathode dissipation was particularly useful when valves were studied in self-oscillating circuits. Then, under some conditions, a glow was observed in the cathode-grid space and it was feared that the photocell readings might be unreliable. It was found in most cases that, even with the glow, the two methods of determining the r.f. dissipation in the cathode gave identical results. The glow was probably due to the high r.f. voltage between grid and cathode.

In determining the cathode dissipation under oscillatory conditions it is necessary to allow for the evaporation cooling of the cathode due to the mean component of the anode current.[1, 3] The heater resistance was also measured with steady currents of 20 and 40 mA when the evaporation cooling greatly exceeded the i^2R heating. The change in heater resistance was found to be proportional to the cooling power in the cathode coating, and the constant of proportionality was the same as that obtained in the h.f. tests.

2.2 *Anode and grid.* In the DET 22 triodes the anode and grid electrodes are integral parts of two copper disks. It is therefore possible to get a measure of the electrode temperatures by attaching thermocouples to the external disks. For the anode, one junction of a copper-eureka couple was attached on the inner surface of the brass retaining ring which clamped the valve to the co-axial line circuit (see Fig. 1). The junction was therefore in close contact with the anode flange but was outside the r.f. field.

Since both outer and inner surfaces of the grid tube are necessarily in the high frequency fields of the oscillator, the attachment of the grid thermocouple presents some difficulty. This was overcome by milling a V-shaped slot along the outer surface of the whole length of the grid tube. Insulated copper and eureka wires were put inside an aluminium sleeve, of diameter 1 mm and wall thickness 0·1 mm, and the sleeve was pressed into the groove so that there was virtually no disturbance of the surface of the grid tube. The bared ends of the two wires were joined and soldered close to the spring fingers which were in contact with the grid disk (see Fig. 1).

Calibrations of the thermocouples under static conditions were made for each valve immediately before the oscillatory tests; this was done by measuring t_a and t_g, the increases in the galvanometer deflexions above the values at room temperature for the anode and grid couples respectively. First t_a and t_g were found when heater power only was applied. Then with the grid biased negatively the anode dissipation P_a was varied and t_a and t_g again measured. In all cases t_a and t_g were proportional to P_a; typical results are shown in Fig. 2. In this figure P_{a0}, the negative value of P_a when $t_a = 0$, represents the proportion of the radiated cathode power which is intercepted by the anode.

Calibration of the grid thermocouple against P_g, the grid dissipation, is not easy on account of the limitations imposed

by the valve ratings. Even when all the maximum cathode emission is taken to the grid under static conditions, the grid dissipation is only about 0·25 W. The resulting change in grid temperature is fairly small in comparison with the

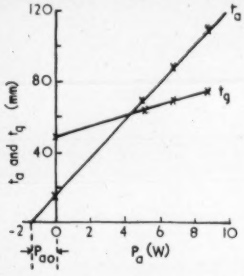

Fig. 2. Thermocouple calibrations

change due to the power intercepted from the cathode. Also, under working conditions with appreciable anode dissipation, the change in grid temperature due to P_a is considerable and may be more than the change due to $P_g = 0{\cdot}25$ W. However, an approximate calibration of t_g against P_g can be

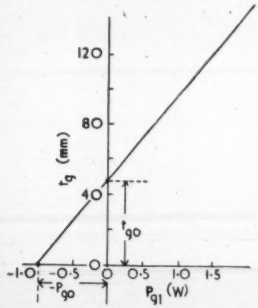

Fig. 3. Grid thermocouple calibration

effected by assuming that practically all the cathode power is radiated and is intercepted by the grid and the anode together. The difference between the cathode power and P_{a0} gives P_{g0}, the proportion of the cathode power intercepted by the grid. Then $(-P_{g0}, 0)$ is a point on the grid calibration curve. A second point is $(0, t_g')$, where t_g' is the increase in the grid thermocouple reading when the cathode is heated. The grid calibration is then assumed to be a straight line through these points as shown in Fig. 3 in which P_{g1}, the total grid power is plotted against t_g. From Figs. 2 and 3 the contribution to the grid heating due to the anode dissipation P_a can be determined and this is shown as P_{g2} in Fig. 4. This curve is subsequently used under oscillatory

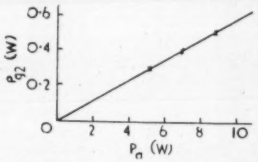

Fig. 4. Grid dissipation calibration

conditions to find the true grid dissipation P_g due to electron bombardment, where $P_g = P_{g1} - P_{g2}$. The anode temperature is also affected by the grid dissipation but the effect is small, as the grid dissipation is much less than the anode dissipation; this correction has been neglected. A check of the grid calibration was made with one valve on d.c. taking the full emission to the grid and good agreement was obtained. Even so no great accuracy can be claimed for the grid dissipations.

When the cathode temperature changes under oscillating conditions, this change affects the grid and anode temperatures. However, this effect is also small and it has been neglected.

3. OSCILLATORY MEASUREMENTS

Power measurements were made at frequencies ranging from 500 to 2000 Mc/s on ten different valves. The electrode dissipations were determined by the methods described in section 2 and the r.f. power P_0 was measured in a lamp load. The oscillator was adjusted to optimum operation and then left until stable conditions were reached. Typical results for three different valves are shown in the table. In this table P_i, P_0, P_a, P_g and P_k are the quantities already defined; P_b is the power in the grid bias resistor and

$$P_s = P_0 + P_a + P_g + P_k + P_b$$

4. DISCUSSION OF THE RESULTS

It may be seen that the difference between P_s and P_i varies from 0 to about 1 W. In view of the inaccuracies in deter-

Power distribution in oscillating triode

Valve No.	f (Mc/s)	P_i (W)	P_o (W)	P_a (W)	P_g (W)	P_k (W)	P_b (W)	P_s (W)	P_k/P_o	P_g/P_a
1	696	8·4	2·20	4·42	0·91	0·20	0·18	7·9	0·1	0·4
	900	9·6	1·97	5·42	0·73	0·21	0·23	8·6	0·1	0·4
	1400	9·7	0·88	6·80	0·81	0·21	0·09	8·8	0·2	0·9
	1830	9·8	0·38	7·20	0·96	0·44	0·12	9·1	1·1	2·5
2	540	6·6	1·64	3·32	0·33	0·21	0·40	5·9	0·1	0·2
	675	6·7	2·22	3·48	0·21	0·22	0·32	6·5	0·1	0·1
	920	8·7	1·76	5·15	0·29	0·37	0·31	7·9	0·2	0·2
	1530	9·2	0·77	6·90	0·46	0·40	0·12	8·7	0·5	0·6
	1805	8·6	0·64	5·55	0·68	0·63	0·20	7·7	1·0	1·1
3	734	10·0	1·28	6·45	1·09	0·31	0·20	9·3	0·2	0·9
	989	10·1	1·18	7·20	0·67	0·18	0·20	9·4	0·2	0·6
	1400	9·6	0·54	7·51	0·79	0·24	0·06	9·1	0·4	1·5
	1840	9·9	0·33	8·48	0·75	0·15	0·08	9·8	0·5	2·3

(N.B.—The values of P_0 in this table are not necessarily indicative of the best performance that can be obtained from the DET22 triode.)

mining the various components of P_s it would seem that on average 0·5 W, or 5% of the d.c. anode power, were unaccounted for and must be attributed to resistive, dielectric or radiation losses in the valve and circuit.

An interesting feature of these results is the magnitude of P_k, the cathode-coating loss, and its variation with frequency. Its importance as a limiting factor on the performance may be seen from the ratio P_k/P_0. This shows that, at the higher frequencies, the power lost in the coating becomes comparable with the power delivered to the load.

The importance of the grid dissipation may also be seen from the table. The grid power is always appreciable and its value relative to the power output increases with frequency, as shown by the ratio P_g/P_0.

An attempt was made to calculate the power dissipated in the coating using low frequency class C oscillator theory. Fairly good agreement was obtained with the measured values even at high frequencies.[4]

4.1 *Effect of the grid-cathode clearance.* Some power tests were also carried out on disk seal triodes which were the same as the DET 22 but with different cathode-grid spacings. The cathodes were identical and the valve ratings the same, so that the valves operated at approximately the same value of anode current. All the valves had high amplification factor and the flow of current was controlled mainly by the grid voltage. Treating the valve as a simple diode the current is proportional to $v_g^{3/2}/d^2$, where v_g is the grid voltage and d is the cathode grid spacing. Thus, for the same anode current, v_g is proportional to $d^{4/3}$. The power dissipated in the cathode coating is proportional to i_g^2 and to the effective conductance G between the grid and cathode. The grid-cathode circuit may be represented by Fig. 5(*a*). Here

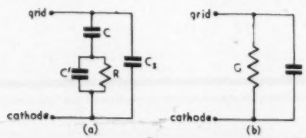

Fig. 5. Grid-cathode circuit
(*a*) actual circuit
(*b*) equivalent circuit

$$G = \omega^2 C^2 R^2/[1 + \omega^2(C + C')^2 R^2]$$

C is the capacitance between the grid wires and the coating surface; C' and R represent the impedance of the actual coating and C_s represents stray capacitance including edge effects, etc. The circuit may be drawn as shown in Fig. 5(*b*) in which

$$G = \omega^2 C^2 R/[1 + \omega^2(C + C')^2 R^2] \qquad (1)$$

When the cathode-grid spacing is varied, C is proportional to $1/d$. Also provided the frequency is not too high

$$G = \omega^2 C^2 R \qquad (2)$$

Hence the coating dissipation at a given frequency is proportional to $v_g^2 C^2$, i.e. $P_k \propto d^{2/3}$.

If we assume that the proportion of the total current flowing to the grid does not alter when the clearance is changed the grid dissipation is proportional to v_g, i.e. $P_g \propto d^{4/3}$. Thus when the clearance is increased the cathode heating and grid dissipation both increase but the latter more rapidly. These relations are subject to wide variations depending on the oscillator conditions but the power tests on valves with large clearances confirm the general trends qualitatively.

4.2 *Factors affecting coating loss.* Equation (1) shows that the equivalent grid-cathode conductance arising from the coating resistance varies as the square of the frequency, provided

$$\omega^2(C + C')^2 R^2 \ll 1$$

As the frequency is increased the rate of increase of G is reduced and ultimately it reaches a limiting value of

$$G = \frac{1}{R}\left(\frac{C}{C + C'}\right)^2 \simeq \frac{1}{R}\left(\frac{C}{C'}\right)^2 \qquad (3)$$

The variation of G with frequency for the DET 22 is shown in Fig. 6. Values of 0·8 $\mu\mu$F, 7·0 $\mu\mu$F and 15 Ω have

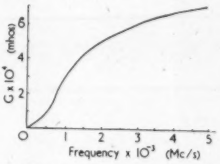

Fig. 6. Variation of equivalent grid conductance with frequency

been taken for C, C' and R respectively.[2] The coating resistance R varies directly as the coating thickness and its capacitance C' varies inversely as the thickness. Equation (3) emphasizes the importance of a thin coating. Two of the most successful present-day microwave triodes are the VX3061 and the EC57. The former has a much thinner cathode coating than the DET22. The EC57 has a dispenser cathode with negligible coating thickness.[5]

REFERENCES

(1) Herbst, L. J., and Houldin, J. E. *Brit. J. Appl. Phys.*, **6**, p. 236 (1955).
(2) Herbst, L. J. *Brit. J. Appl. Phys.*, **8**, p. 277 (1957).
(3) Hermann, G., and Wagener, S. *The Oxide-coated Cathode* (London: Chapman and Hall Ltd., 1951).
(4) Herbst, L. J. Ph.D. thesis, University of London (1956).
(5) Diemer, G., Rodenhuis, K., and van Wijngaarden, J. G. *Philips tech. Rev.*, **18**, p. 317 (1957).

THIS JOURNAL is produced monthly by The Institute of Physics, in London. It deals with all branches of applied physics (including theory and technique).
All rights reserved. Responsibility for the statements contained herein attaches only to the writers.
EDITORIAL MATTER. Communications concerning editorial matter should be addressed to the Editor, The Institute of Physics, 47 Belgrave Square, London, S.W.1. (*Telephone:* Belgravia 6111.) Prospective authors are invited to prepare their scripts in accordance with the *Notes on the preparation of contributions.* (Price 2*s.* 6*d.* including postage.)
REPRODUCTION. The Institute of Physics is a signatory to The Royal Society's Fair Copying Declaration. Details may be obtained upon application from The Royal Society, London, W.1.
ADVERTISEMENTS. Communications concerning advertisements should be addressed to the agents, Messrs. Walter Judd Ltd., 47 Gresham Street, London, E.C.2. (*Telephone:* Monarch 7644.)
CLAIMS FOR MISSING JOURNALS. Claims from regular subscribers to this *Journal* for missing numbers will only be considered if received within 60 days of the date of mailing plus normal outward time of transit and time for lodging the claim. Losses attributable to failure to notify a change of address or to similar omissions will not be considered.
SUBSCRIPTION RATES. A new volume commences each January. The charge is £5 per volume ($14.25 U.S.A.), including index (post paid), payable in advance. Single parts, so far as available, may be purchased at 10*s.* each ($1.50 U.S.A.), post paid, cash with order. Orders should be sent to The Institute of Physics, 47 Belgrave Square, London, S.W.1, or to any bookseller.

The influence of shear and rotatory inertia on the free flexural vibration of wooden beams

By R. F. S. HEARMON, F.Inst.P., Forest Products Research Laboratory, Princes Risborough, Bucks.

[*Paper first received* 26 *February, and in final form* 19 *May*, 1958]

The existence of shear and rotatory inertia effects leads to a reduction in the frequency of flexural vibration of beams as compared with the frequencies predicted by the simple Rayleigh treatment. Tables and graphs, based on the Timoshenko–Goens theory, are given to facilitate the estimation of the correction factor in the case of free-free beams. Experiments are described in which the frequencies of wooden beams are measured up to the 16th mode, and a least-squares method is described for analysing the results. Effects introduced by the anisotropic nature of wood are also investigated and discussed.

1. INTRODUCTION

Considerable interest has been shown recently in the vibration characteristics of wood, especially in connexion with non-destructive testing and with the determination of elastic constants and damping. The elastic constant of major interest is the Young's modulus along the grain and, in addition to the more usual static methods, both longitudinal and flexural vibration methods have been used in its measurement. Of these, the flexural vibration method has been the more popular, mainly because the vibrations are easier to excite and detect. The frequency of flexural vibration is, however, influenced by the occurrence of shear and rotatory inertia effects in the beam, and the purpose of the present paper is to examine the extent to which the frequencies of vibration and the derived elastic constants are altered by the occurrence of these effects. Wood is particularly interesting as an experimental material in this connexion because it is anisotropic and also has a very low shear modulus.

2. THEORY

Assuming pure bending, the differential equation governing the flexural vibrations of a beam is:

$$\frac{Ei^2}{\rho}\frac{\partial^4 y}{\partial x^4}+\frac{\partial^2 y}{\partial t^2}=0, \tag{1}$$

where

E = Young's modulus,
i = radius of gyration of cross-section,
ρ = density,
y = lateral deflexion,
x = distance along the beam,
t = time.

For a beam of rectangular cross-section

$$i^2=h^2/12, \tag{2}$$

where h is the thickness of the beam in the plane of bending.

Solutions of equation (1) appropriate to various end conditions have been given by Rayleigh.[1] If both ends of the beam are free, the frequencies f_r are

$$f_r=\frac{im^2}{2\pi l^2}\sqrt{\frac{E}{\rho}}, \tag{3}$$

where l is the length of the beam and the values of m appropriate to the successive modes of vibration are the roots of

$$\cos m \cosh m = 1, \tag{4}$$

i.e. $m_1 = 4{\cdot}730$, and subsequently, to sufficient accuracy

$$m_p=\tfrac{1}{2}(2p+1)\pi, \tag{5}$$

where p denotes the order of the mode. Values of m^2 and m^4 up to the 16th mode are given in columns 2 and 5 of Table 1 below.

The above treatment ignores the occurrence of shear deflexion and of rotatory inertia effects in the bar. The full differential equation taking both of these effects into account was first discussed by Timoshenko[2] and, in the present notation, is:

$$\frac{Ei^2}{\rho}\frac{\partial^4 y}{\partial x^4}+\frac{\partial^2 y}{\partial t^2}-i^2\left(1+\frac{sE}{G}\right)\frac{\partial^4 y}{\partial x^2\partial t^2}+\frac{\rho si^2}{G}\frac{\partial^4 y}{\partial t^4}=0, \tag{6}$$

where G = shear modulus.

The shear deflexion coefficient s is introduced to allow for the fact that the shear stress is not uniform over the cross-section; if, in fact, the stress were uniform, the value of s would be unity. Several attempts[3–7] have been made to evaluate s from theoretical considerations, but there is no general agreement as to its exact value. The various estimates, however, indicate that its approximate value is 1·2; further discussion of s is given in Section 5 below.

Solutions of equation (6), or of equivalent equations, appropriate to various boundary conditions have been obtained by a number of workers.[8–17] The experiments described later were carried out on free-free beams, and solutions corresponding to these boundary conditions have been given by Goens,[10] Howe and Howe,[11] Kruzewski,[13] Traill-Nash and Collar[15] and Wuolijoki.[16] Howe and Howe[11] solve the differential equation by means of an electronic differential analyser, but the other three workers obtain an analytical solution, which gives the frequencies in the form of a rather involved transcendental equation. Kruzewski,[13] and Howe and Howe[11] present graphs from which some of the frequencies can be obtained, but these graphs do not cover the full range of the variables required in the present work. Wuolijoki[16] gives a graphical method which is of unlimited range, but which is rather time consuming in practice. Goens,[10] on the other hand, develops the transcendental equation into a relatively simple, though approximate, equation which gives the effect of shear and rotatory inertia explicitly.

According to Goens, the theoretical frequency (f_g) is

$$f_g=f_r/\sqrt{T}, \tag{7}$$

where f_r is calculated from equation (3) and T is given by

$$T=1+\frac{i^2}{l^2}[m^2F^2(m)+6mF(m)]+\frac{i^2}{l^2}\frac{sE}{G}[m^2F^2(m)-2mF(m)]-\frac{4\pi^2\rho si^2 f_g^2}{G}. \tag{7a}$$

The function $F(m)$ is found by Goens to be

$$\left.\begin{aligned} 0{\cdot}9825 \text{ for } p = 1, \\ 1{\cdot}0008 \text{ for } p = 2, \end{aligned}\right\} \qquad (7b)$$

and subsequently $F(m) = 1$ for all values of p.

Writing

$$\left.\begin{aligned} m^2F^2(m) + 6mF(m) &= F_1(m), \\ m^2F^2(m) - 2mF(m) &= F_2(m), \end{aligned}\right\} \qquad (7c)$$

equation (7*a*) becomes

$$T = 1 + \frac{i^2}{l^2}F_1(m) + \frac{i^2}{l^2}\frac{sE}{G}F_2(m) - \frac{4\pi^2\rho s i^2 f_g^2}{G}. \qquad (8)$$

The values of $F_1(m)$ and $F_2(m)$, computed from equation (7*b*) and (7*c*) in conjunction with the known values of m (Table 1), are entered in columns 3 and 4, Table 1.

Table 1. *Values of* m^2, $F_1(m)$, $F_2(m)$ and m^4

p	m^2	$F_1(m)$	$F_2(m)$	$m^4 \times 10^{-3}$
1	22·37	49·48	12·30	0·5006
2	61·67	108·9	46·05	3·804
3	120·9	186·9	98·9	14·62
4	199·9	284·7	171·6	39·94
5	298·6	402·3	264·0	89·13
6	417·0	539·5	376·1	173·9
7	555·2	696·5	508·0	308·2
8	713·1	873·3	659·7	508·5
9	890·7	1070	831·0	793·4
10	1088	1286	1022	1184
11	1305	1522	1233	1704
12	1542	1778	1464	2378
13	1799	2053	1714	3235
14	2075	2348	1984	4306
15	2371	2663	2274	5622
16	2687	2998	2583	7220

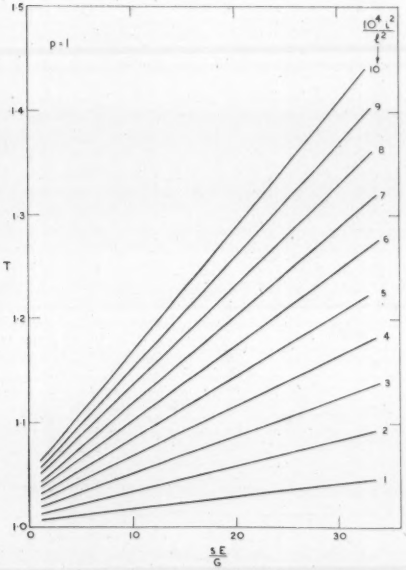

Fig. 1. T as function of i^2/l^2 and sE/G, 1st mode

From equations (3) and (7) we have

$$f_g^2 = \frac{i^2m^4E}{4\pi^2l^4\rho T}, \qquad (9)$$

and substituting for f_g^2 in equation (8)

$$T = 1 + \frac{i^2}{l^2}\left\{F_1(m) + \frac{sE}{G}F_2(m)\left[1 - \frac{m^4i^2}{F_2(m)l^2T}\right]\right\}. \qquad (10)$$

The last term in equations (8) and (10) is only a rough approximation, but its numerical value is small in comparison with 1, and T itself is not very different from 1. A good first approximation to T can therefore be obtained by setting T

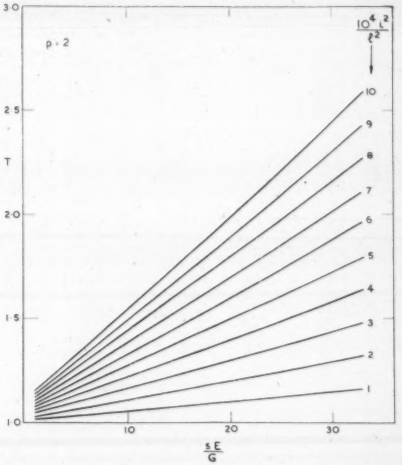

Fig. 2. T as function of i^2/l^2 and sE/G, 2nd mode

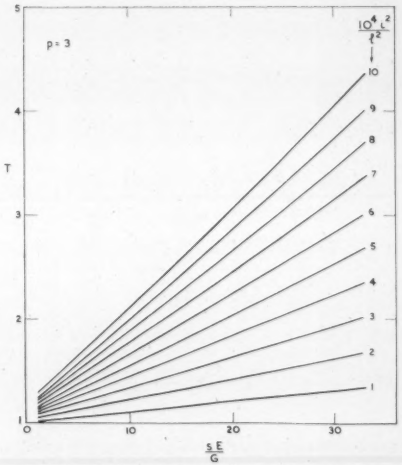

Fig. 3. T as function of i^2/l^2 and sE/G, 3rd mode

on the right-hand side of equation (10) equal to 1. The value of T obtained in this way is then inserted on the right of equation (10), thus improving the first estimate; a third and further improved estimate of T can be obtained similarly if necessary. Values of T obtained in this way for the first three modes of vibration are shown in Figs. 1–3 as functions of sE/G and i^2/l^2.

3. EXPERIMENTAL

Experiments similar in some respects to the present ones have previously been made by Adamson[18] on simply supported beams and by Goens[10] and Wuolijoki[16] on free-free beams; Traill-Nash and Collar[15] have also compared theoretical and experimental frequencies for free-free box-beams.

The experiments reported below were carried out on one beam of brown sterculia (*Sterculia rhinopetala*) and two each of Sitka spruce (*Picea sitchensis*) European beech (*Fagus sylvatica*) and European ash (*Fraxinus excelsior*). The grain-direction in the wooden beams was parallel to their lengths; the cross-sectional dimensions were approximately 5 × 2·5cm. One beam each of the Sitka spruce, beech and ash were cut as shown in Fig. 4(*a*), with the longer side of the rectangular cross-section parallel to the radial direction in the tree R,

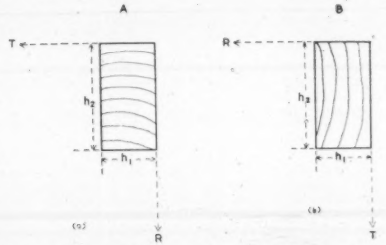

Fig. 4. Cross-sections of A and B specimens showing annual rings of wood

and the shorter side as nearly tangential as possible to the annual rings (the tangential direction T). The other beams of Sitka spruce, beech and ash were each cut as shown in Fig. 4(*b*); the single sterculia beam was cut as in Fig. 4(*a*). The densities and dimensions of the beams are given in Table 2.

Table 2. *Dimensions and densities of beams*

Beam	*Initial Length (cm)*	h_1 *(cm)*	h_2 *(cm)*	ρ *(g/cm³)*
Brown sterculia	183·1	2·510	5·033	0·900
Sitka spruce *A*	144·3	2·555	5·105	0·543
Sitka spruce *B*	107·0	2·530	5·061	0·535
Beech *A*	160·8	2·548	5·088	0·672
Beech B	160·9	2·545	5·069	0·684
Ash *A*	161·2	2·502	4·761	0·702
Ash *B*	161·2	2·505	5·004	0·686

A circuit diagram of the exciting and measuring apparatus is shown in Fig. 5. The specimen was suspended by means of threads AA, which should ideally be located at the nodal points of the mode under investigation. It was found experimentally, however, that for the 4th and higher modes the location of the threads had an insignificant effect on the frequency. The nodal points shown in Table 3 were therefore marked on the specimen which was suspended from these points as appropriate.

Table 3. *Distance (x/l) of nodal points from free ends of specimen*

p	x/l
1	0·2241
2	0·1321
3	0·0944
4	0·0735

The distances in Table 3 are based on the simple Rayleigh theory[1,19] and will be affected to some extent by the existence of shear and rotatory inertia. The effect of shear

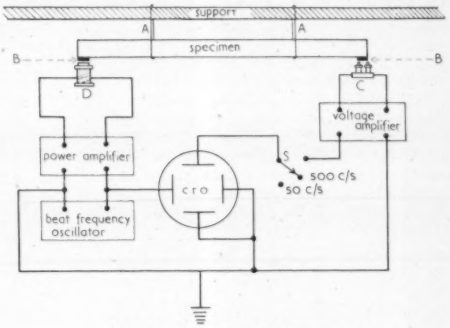

Fig. 5. Diagram of apparatus

and rotatory inertia on the position of the nodal points is not known, but it will be least in the fundamental mode, where the need for accurate location of the supporting threads was found to be greatest. The effect of shear and rotatory inertia on nodal position almost certainly increases as the mode number increases, but on the other hand, the need for accurate positioning of the supporting threads decreases, and it is thus unlikely that uncertainty in the exact nodal positions will lead to serious errors in the measurements.

In order to excite the specimens and to detect their response, small iron plates B were attached near the ends. One of these plates was close to the magnets of a telephone receiver C which served as a pick-up. The other iron plate was near the magnet of the driving coil D, which was supplied with amplified current from a beat frequency oscillator. In order to increase the effect of the alternating current, a subsidiary coil carrying direct current to polarize the magnet was wound over the driving coil. (The subsidiary coil is not shown in Fig. 5.)

This feature of the apparatus prevented the use of elastic threads for the supports AA. Such threads would have made the exact positioning of the supports even less critical than it proved to be with the normal thread actually used. It was found, however, that with elastic thread supports the distance between the iron plate B and the magnetic core of coil D (Fig. 5) decreased when the polarizing current was switched on, owing to the extension of the threads caused by the attraction between the plate and the core; under these circumstances it was extremely difficult to adjust the initial distance between the two so that the distance was optimum for good response of the specimen when the polarizing current was switched on.

The horizontal-deflexion plates of the cathode ray oscilloscope (*CRO*) were permanently connected to the oscillator. By means of a three-way selector switch *S*, the vertical plates could be connected either to the amplified output from the pick-up, or to sources of frequency 500 c/s or 50 c/s. The 500 c/s source was a valve-maintained tuning fork; that of 50 c/s was derived from the mains supply, which was always checked against the tuning fork before being used as a frequency standard.

In measuring a response frequency of the specimen, the following procedure was adopted. The output from the pick-up was connected to the oscilloscope, and the coarse dials of the oscillator adjusted until the response as indicated on the oscilloscope screen was a maximum. The switch *S* was then connected to the 500 c/s or the 50 c/s source, whichever was the more convenient, and the oscillator adjusted until the oscilloscope showed a recognizable Lissajous figure from which the oscillator frequency could be found exactly. The pick-up output was reconnected to the oscilloscope, and the frequency of the oscillator adjusted by means of a calibrated incremental condenser until the response on the oscilloscope screen was again a maximum. The resonant frequency was then obtained from the sum of the known initial oscillator frequency and the increment of frequency corresponding to the amount of adjustment of the incremental condenser. In this way the frequencies were measured independently of the main graduations on the oscillator dials, and the accuracy of measurement, estimated as about 0·2%, depended only on the accuracy of the standard frequency, and on the calibration of the incremental condenser.

Complete series of measurements were taken with the plane of vibration parallel to the shorter side of the cross-section (Type 1 vibrations, see Fig. 4) and to the longer side (Type 2 vibrations). In a typical series the specimen was first weighed and measured, and the nodal positions were marked in. The plates *B* (Fig. 5) were then attached to the specimen in positions such that Type 1 vibrations would be excited. With the specimen suspended at the 1st nodal positions, the frequencies of the 1st, 5th and higher modes were determined. The position of the supporting threads was then altered to the 2nd nodal positions, and the frequencies of the 2nd, 5th and higher modes determined. This procedure was repeated with the threads at the 3rd and 4th nodal positions, thus yielding one estimate of the frequencies of the 1st to 4th modes, and 4 estimates of the frequencies of the 5th and higher modes. The measurements on the 1st to 4th modes were repeated at least twice, after which the plates *B* were removed and reattached so as to excite type 2 vibrations, the frequencies of which were measured exactly as described above. After the measurements had been completed, the specimens were successively shortened, complete frequency measurements being taken on each length.

The measurements were not made under controlled conditions of relative humidity and temperature, but approximate corrections were applied to the frequencies to adjust them to a standard moisture content (approximately 11%). Over the small range of moisture contents involved it can be assumed that the change in longitudinal dimensions is negligible, and that the changes in lateral dimensions and Young's modulus are small and proportional to the moisture content change. The frequency is proportional to $i\sqrt{(E/\rho)}$, and on the above assumptions, for a type 1 vibration, it can be shown that

$$f_a/f_b \simeq 1 + (\tfrac{3}{2}\alpha_1 + \tfrac{1}{2}\alpha_2 - \tfrac{1}{2}\alpha_E - 0{\cdot}005)\Delta m, \qquad (11)$$

where f_b and f_a are the frequencies before and after an increase in moisture content of $\Delta m\%$ and the coefficients α are defined by the equations

$$(h_1)_a/(h_1)_b = 1 + \alpha_1\Delta m;$$
$$(h_2)_a/(h_2)_b = 1 + \alpha_2\Delta m;$$
$$E_a/E_b = 1 - \alpha_E\Delta m.$$

The directly observed frequencies were corrected by means of equation (11) before the results were finally analysed. As an indication of the order of magnitude of the correction, the value of α_E was about 0·01 and of α_1 and α_2 about 0·003. With these values, equation (11) reduces to

$$f_a/f_b = 1 - 0{\cdot}004\Delta m,$$

and for a moisture content increase of, say, 2%,

$$f_a/f_b = 0{\cdot}992.$$

4. RESULTS AND DISCUSSION

The observed frequencies, corrected where necessary for changes in moisture content, are given in Table 4 under the heading f_0. The complete results are tabulated for brown sterculia, but to save space, further results are given for two lengths only of the beech and ash specimens. The remaining columns in Table 4, headed $\sqrt{T}$ and f_0/f_g, were computed in the following way.

From equation (3), the true Young's modulus E is

$$E = 4\pi^2 l^4 \rho f_r^2/m^4 i^2. \qquad (12)$$

Similarly the apparent Young's modulus E_A, calculated directly from the observed frequencies is

$$E_A = 4\pi^2 l^4 \rho f_0^2/m^4 i^2. \qquad (13)$$

Thus, from equations (7) (9) and (13), assuming f_0 and f_g are identical,

$$E = E_A T. \qquad (14)$$

For present purposes, the most convenient form of the equation for T is (8). In this equation, the last term is small in comparison with unity, and it is therefore possible to use a provisional value of s/G in it. (If the provisional value proves to be seriously in error, the calculations can be repeated using an improved value of s/G). Thus if we write

$$c = E_A\left[1 + \frac{i^2}{l^2}F_1(m) - \frac{4\pi^2\rho s i^2 f_0^2}{G}\right], \qquad (15)$$

$$b = \frac{E_A i^2}{l^2}F_2(m);\ x = E;\ y = sE/G$$

then from equations (8), (14) and (15):

$$x = c + by, \qquad (16)$$

in which the unknowns are x and y. To each measured frequency there corresponds an equation of the form (16) and we thus have a series of equations

$$\left.\begin{aligned} x &= c_1 + b_1 y,\\ x &= c_2 + b_2 y,\\ &\cdots\cdots\cdots\\ x &= c_n + b_n y, \end{aligned}\right\} \qquad (17)$$

where n is the number of observations (e.g. for brown sterculia, Table 4(*a*), type 1 vibrations, $n = 35$; type 2 vibrations, $n = 27$). The "best" values of x and y consistent with the set of equations (17) can then be found by the method of least squares[20] as the solution of the simultaneous equations

$$\left.\begin{aligned} nx &= [c] + [b]y,\\ [b]x &= [bc] + [b^2]y, \end{aligned}\right\} \qquad (18)$$

where the square brackets indicate summation (e.g. $[bc] =$

Table 4. *Observed and calculated results* (l *in cm;* f_0 *in c/s;* $R = 10^4 i^2/l^2$)

(a) *Brown sterculia*

Type 1 vibrations

p	f_0	$\sqrt{T}$	f_0/f_θ
$l = 183{\cdot}1$; $R = 0{\cdot}1565$			
1	37·1	1·002	1·003
2	101·8	1·007	1·002
3	198·0	1·017	1·004
4	323·7	1·030	1·005
5	475·0	1·045	1·002
6	654·2	1·062	1·004
7	855·4	1·082	1·005
8	1075	1·105	1·004
9	1309	1·130	1·001
10	1560	1·158	1·001
$l = 151{\cdot}8$; $R = 0{\cdot}2278$			
1	53·9	1·003	1·002
2	147·0	1·011	0·999
3	285·0	1·024	1·000
4	465·1	1·041	1·004
5	679·9	1·062	1·002
6	927·1	1·087	1·002
7	1198	1·115	0·997

Type 2 vibrations

p	f_0	$\sqrt{T}$	f_0/f_θ
$l = 120{\cdot}8$; $R = 0{\cdot}3596$			
1	84·5	1·005	0·996
2	230·2	1·018	0·997
3	444·2	1·039	1·002
4	717·5	1·064	1·002
5	1037	1·096	0·999
$l = 105{\cdot}2$; $R = 0{\cdot}4744$			
1	111·4	1·007	0·998
2	302·0	1·024	0·998
3	580·0	1·050	1·002
4	928·4	1·084	1·002
5	1333	1·125	1·000
$l = 89{\cdot}8$; $R = 0{\cdot}6510$			
1	152·2	1·009	0·995
2	411·6	1·033	0·999
3	780·6	1·068	0·999
4	1234	1·114	0·997
$l = 74{\cdot}3$; $R = 0{\cdot}9511$			
1	222·0	1·014	0·999
2	587·9	1·047	0·990
3	1110	1·097	0·999
4	1725	1·161	0·994

Type 1 vibrations

p	f_0	$\sqrt{T}$	f_0/f_θ
$l = 183{\cdot}1$; $R = 0{\cdot}6295$			
1	73·9	1·008	1·003
2	200·2	1·029	1·007
3	380·4	1·059	1·004
4	607·6	1·098	1·006
5	869·1	1·145	1·004
6	1157	1·201	1·004
7	1462	1·262	1·001
$l = 151{\cdot}8$; $R = 0{\cdot}9158$			
1	107·7	1·012	1·009
2	288·1	1·041	1·007
3	543·8	1·084	1·010
4	854·5	1·139	1·008
5	1206	1·205	1·008
6	1576	1·280	1·002

Type 2 vibrations

p	f_0	$\sqrt{T}$	f_0/f_θ
$l = 120{\cdot}8$; $R = 1{\cdot}445$			
1	166·9	1·019	0·998
2	443·3	1·063	1·002
3	822·3	1·128	1·006
4	1265	1·211	1·006
5	1748	1·308	1·004
$l = 105{\cdot}2$; $R = 1{\cdot}907$			
1	220·4	1·025	1·005
2	573·0	1·083	1·001
3	1048	1·166	1·006
4	1585	1·270	1·002
$l = 89{\cdot}8$; $R = 2{\cdot}618$			
1	297·8	1·035	0·999
2	766·0	1·112	1·001
3	1362	1·222	0·998
$l = 74{\cdot}3$; $R = 3{\cdot}824$			
1	428·5	1·049	0·997
2	1069	1·160	0·998

(b) *Beech A*

Type 1 vibrations

p	f_0	$\sqrt{T}$	f_0/f_θ
$l = 160{\cdot}8$; $R = 0{\cdot}2092$			
1	45·5	1·003	0·970
2	127·3	1·009	1·003
3	246·3	1·022	1·003
4	402·2	1·036	1·004
5	588·7	1·055	1·002
6	807·7	1·077	1·005
7	1049	1·102	1·003
8	1308	1·130	0·999
$l = 67{\cdot}3$; $R = 1{\cdot}195$			
1	260·6	1·017	1·000
2	693·0	1·057	1·002
3	1293	1·115	1·006
4	1999	1·190	1·005
5	2768	1·278	1·000
6	3619	1·376	1·007
7	4405	1·483	0·993
8	5266	1·597	0·995
9	6100	1·716	0·992
10	7068	1·838	1·008
11	7888	1·965	1·002

Type 2 vibrations

p	f_0	$\sqrt{T}$	f_0/f_θ
$l = 160{\cdot}8$; $R = 0{\cdot}8348$			
1	90·0	1·008	0·983
2	250·8	1·025	1·010
3	473·0	1·052	0·998
4	760·0	1·087	1·002
5	1094	1·127	1·001
6	1459	1·174	0·995
$l = 67{\cdot}3$; $R = 4{\cdot}763$			
1	507·4	1·043	1·004
2	1278	1·134	0·998
3	2281	1·258	1·008
4	3362	1·407	1·004
5	4477	1·573	1·001
6	5582	1·753	0·996
7	6726	1·941	0·998

(c) *Beech B*

Type 1 vibrations

p	f_0	$\sqrt{T}$	f_0/f_θ
$l = 160{\cdot}9$; $R = 0{\cdot}2085$			
1	41·4	1·002	0·958
2	119·5	1·005	1·006
3	229·0	1·012	0·990
4	380·5	1·019	1·002
5	561·0	1·028	0·998
6	782·0	1·039	1·006
7	1028	1·052	1·006
8	1293	1·067	0·999
9	1586	1·083	0·996
$l = 67{\cdot}15$; $R = 1{\cdot}197$			
1	242·4	1·009	0·984
2	664·6	1·031	1·000
3	1274	1·061	1·006
4	1984	1·101	0·984
5	2907	1·149	1·007
6	3877	1·205	1·008
7	4878	1·265	1·000
8	5907	1·331	0·992
9	7012	1·401	0·993

Type 2 vibrations

p	f_0	$\sqrt{T}$	f_0/f_θ
$l = 160{\cdot}9$; $R = 0{\cdot}8271$			
1	84·2	1·010	0·985
2	232·2	1·035	1·010
3	435·0	1·071	0·999
4	691·0	1·119	1·003
5	976·0	1·176	0·996
6	1271	1·241	0·981
$l = 67{\cdot}15$; $R = 4{\cdot}748$			
1	467·1	1·057	0·997
2	1169	1·183	1·013
3	1986	1·354	1·005
4	2865	1·552	1·005
5	3753	1·773	1·007
6	4601	2·007	1·000
7	5389	2·253	0·988
8	6312	2·501	1·000
9	7256	2·755	1·014

(d) *Ash A*

Type 1 vibrations

p	f_0	$\sqrt{T}$	f_0/f_θ
$l = 161{\cdot}2$; $R = 0{\cdot}2007$			
1	45·8	1·002	0·993
2	126·8	1·007	1·002
3	246·6	1·016	1·002
4	403·0	1·027	1·002
5	592·9	1·041	1·000
6	817·5	1·057	1·003
7	1068	1·076	1·001
8	1344	1·098	1·001
9	1648	1·120	1·002
10	1964	1·146	1·001
11	2303	1·173	1·001
12	2643	1·202	0·997
13	3006	1·232	0·996
14	3367	1·265	0·993
15	3766	1·298	0·997
16	4140	1·332	0·993
$l = 46{\cdot}9$; $R = 2{\cdot}371$			
1	531·6	1·027	0·999
2	1384	1·085	0·997
3	2520	1·170	0·999
4	3816	1·275	0·997
5	5218	1·396	0·999
6	6631	1·530	0·996

Type 2 vibrations

p	f_0	$\sqrt{T}$	f_0/f_θ
$l = 161{\cdot}2$; $R = 0{\cdot}7271$			
1	85·3	1·007	0·994
2	233·0	1·021	0·998
3	447·3	1·043	0·999
4	717·7	1·073	0·997
5	1041	1·108	0·999
6	1401	1·149	0·999
7	1790	1·195	0·997
8	2201	1·245	0·995
9	2637	1·299	0·995
10	3075	1·357	0·993
11	3535	1·417	0·993
12	3990	1·480	0·991
13	4469	1·545	0·994
14	4877	1·613	0·981
15	5363	1·682	0·985
$l = 46{\cdot}9$; $R = 8{\cdot}586$			
1	952·0	1·072	1·000
2	2297	1·221	0·997
3	3916	1·413	1·003
4	5574	1·637	1·000

(e) *Ash B*

Type 1 vibrations

p	f_0	$\sqrt{T}$	f_0/f_θ
$l = 161{\cdot}2$; $R = 0{\cdot}2013$			
1	47·4	1·002	0·994
2	131·0	1·007	1·000
3	254·8	1·014	1·000
4	419·2	1·023	1·004
5	620·2	1·035	1·006
6	857·7	1·049	1·009
7	1123	1·065	1·007
8	1421	1·084	1·010
9	1735	1·104	1·006
10	2087	1·125	1·009
11	2450	1·149	1·009
12	2843	1·174	1·012
13	3231	1·200	1·008
14	3643	1·228	1·008
15	4064	1·258	1·008
16	4506	1·288	1·010
$l = 46{\cdot}9$; $R = 2{\cdot}377$			
1	550·4	1·023	0·997
2	1443	1·075	0·997
3	2645	1·147	0·994
4	4035	1·240	0·992
5	5512	1·335	0·976

Type 2 vibrations

p	f_0	$\sqrt{T}$	f_0/f_θ
$l = 161{\cdot}2$; $R = 0{\cdot}8032$			
1	94·7	1·009	1·001
2	256·7	1·032	1·006
3	484·4	1·065	1·000
4	770·4	1·109	1·001
5	1099	1·161	1·001
6	1466	1·221	1·005
7	1842	1·287	1·001
8	2253	1·359	1·006
9	2658	1·436	1·004
10	3094	1·516	1·010
11	3504	1·600	1·006
12	3928	1·687	1·007
13	4357	1·775	1·007
$l = 46{\cdot}9$; $R = 9{\cdot}490$			
1	1021	1·104	0·999
2	2354	1·318	0·997
3	3801	1·589	0·991
4	5275	1·895	0·992
5	6759	2·222	0·997

$= b_1c_1 + b_2c_2 + \ldots + b_nc_n$). A similar method involving least squares was used by Wuolojoki[16] in analysing his experimental results.

The values of E and sE/G found in this way are given in Table 5.

Table 5. *Least square values of E and sE/G (E in 10^{11} dyn/cm²)*

Material	Type 1 vibrations			Type 2 vibrations		
	n	E	sE/G	n	E	sE/G
Brown sterculia	35	2·094	19·99	27	2·086	17·63
Sitka spruce *A*	60	1·193	11·50	47	1·210	10·98
Sitka spruce *B*	24	1·427	14·72	19	1·482	15·70
Beech *A*	68	1·413	19·02	46	1·401	10·98
Beech *B*	59	1·256	8·90	50	1·258	16·46
Ash *A*	74	1·533	14·24	57	1·480	10·54
Ash *B*	69	1·598	11·93	64	1·596	15·19

Using the values of E and sE/G from Table 5, T was obtained from equation (8), and its square-root for each individual case is given in Table 4. Finally, f_r was calculated from equation (3), f_g from equation (7) and the ratio f_0/f_g is also given in Table 4. This table, however, contains a part only of the complete results, and a better picture of the data as a whole is gained from Table 6 in which the averages and standard deviations of the ratio f_0/f_g are given.

Table 6. *Averages ($\bar{x}$) and standard deviations (σ) of the ratio f_0/f_g*

Material	Type 1 vibrations		Type 2 vibrations	
	$\bar{x}$	σ	$\bar{x}$	σ
Brown sterculia	1·000	0·003	1·004	0·004
Sitka spruce *A*	1·004	0·006	1·001	0·006
Sitka spruce *B*	1·001	0·005	0·999	0·008
Beech *A*	1·000	0·007	1·000	0·006
Beech *B*	1·000	0·012	1·001	0·008
Ash *A*	1·000	0·005	1·000	0·006
Ash *B*	1·000	0·008	1·001	0·004

It is evident from Tables 4 and 6 that the ratio is unity to within experimental error and that the Goens' solution of equation (6), in conjunction with the least squares fitting of the data is adequate for values of l^2/l^2 up to at least 10^{-3}, and sE/G up to at least 20. The highest tabulated value of $\sqrt{T}$ is 2·755, and a number of others are greater than 2, which means that owing to the effects of shear and rotatory inertia, the actual frequency of the beam is less than half the frequency which would be expected when these effects are ignored, as in the Rayleigh treatment.

It is assumed in the theoretical treatment that the elastic constants are independent of frequency and this assumption is supported by the fact that the ratio f_0/f_g in Table 4 shows no tendency to change regularly with frequency. Further evidence that there is no significant effect of frequency on Young's modulus is obtained by finding the least square values of E individually for each length of the specimens. These values are given in Table 7, together with the associated values of G/s. In general, the elastic constants will refer to a higher average frequency the shorter the specimen, but the table does not reveal any tendency to regular change in the elastic constants with decreasing length.

Table 7. *Least square values of E and G/s (10^{11} dyn/cm²)*

Material	l (cm)	Type 1 vibrations			Type 2 vibrations		
		n	E	G/s	n	E	G/s
	183·1	10	2·11	0·103	7	2·11	0·118
	151·8	7	2·09	0·102	6	2·12	0·118
Brown sterculia	120·8	5	2·08	0·110	5	2·08	0·122
	105·2	5	2·09	0·108	4	2·10	0·119
	89·8	4	2·08	0·104	3	2·08	0·118
	74·3	4	2·08	0·103	2	2·07	0·119
	144·3	10	1·21	0·105	8	1·22	0·109
	122·6	7	1·18	0·114	5	1·19	0·114
	107·1	7	1·18	0·112	5	1·19	0·111
Sitka spruce	96·8	7	1·18	0·112	5	1·19	0·115
A	88·9	7	1·19	0·105	5	1·21	0·111
	82·8	7	1·19	0·110	7	1·23	0·111
	74·8	8	1·20	0·101	6	1·21	0·109
	67·2	7	1·19	0·100	6	1·21	0·107
Sitka spruce	107·0	13	1·42	0·098	11	1·47	0·094
B	71·75	11	1·43	0·095	8	1·50	0·095
	160·8	8	1·41	0·077	6	1·39	0·132
	122·6	7	1·42	0·074	5	1·40	0·128
	107·3	7	1·42	0·073	5	1·41	0·129
	96·9	7	1·42	0·071	5	1·41	0·119
Beech *A*	88·95	7	1·39	0·076	5	1·40	0·122
	82·6	10	1·42	0·075	7	1·42	0·127
	74·9	11	1·42	0·073	6	1·41	0·128
	67·3	11	1·42	0·074	7	1·41	0·128
	160·9	9	1·23	0·182	6	1·26	0·073
	122·4	8	1·27	0·156	6	1·26	0·078
	107·3	7	1·26	0·147	5	1·28	0·072
Beech *B*	97·0	7	1·24	0·158	6	1·26	0·072
	82·7	9	1·26	0·147	8	1·25	0·078
	74·95	10	1·24	0·139	10	1·27	0·076
	67·15	9	1·24	0·142	9	1·27	0·077
	161·2	16	1·54	0·105	15	1·48	0·135
	119·8	13	1·54	0·111	9	1·48	0·146
	104·55	12	1·53	0·110	9	1·48	0·143
Ash *A*	90·0	11	1·53	0·111	8	1·48	0·144
	75·0	9	1·53	0·105	7	1·48	0·139
	60·0	7	1·53	0·104	5	1·48	0·142
	46·9	6	1·53	0·107	4	1·47	0·141
	161·2	16	1·60	0·142	13	1·60	0·108
	119·75	12	1·60	0·132	12	1·59	0·106
	104·35	13	1·59	0·135	10	1·59	0·106
Ash *B*	89·95	9	1·60	0·132	11	1·60	0·106
	74·85	8	1·59	0·132	8	1·59	0·103
	60·0	6	1·60	0·132	5	1·61	0·102
	46·9	5	1·59	0·126	5	1·59	0·103

5. A NOTE ON THE SHEAR DEFLECTION COEFFICIENT s

The analysis of the experimental results carried out above shows that good agreement between calculated and observed frequencies is obtained on the basis of the Goens' equation for T [equation (8) above], supplemented by least squares determination of the constants E and sE/G which occur in the equation. This procedure is evidently equivalent to determining E and G/s, and is quite satisfactory for all practical purposes. Nevertheless, it may sometimes be necessary to calculate T from G and s separately. Unfortunately, the available theoretical estimates of s show a rather large scatter, and the effects of shape of cross-section and of mode number do not seem to have been

investigated fully. Föppl[4] dealt with the case of static deflexions and obtained $s = 1{\cdot}2$ for a rectangular cross-section. This value was adopted, with some reservations, by Goens[10] as applying to a free-free vibrating bar. For a circular cross-section, Goens assumed $s = 1{\cdot}11$. Timoshenko[2] quotes $s = 1{\cdot}5$ for a simply supported beam, and has also used $s = 1{\cdot}125$. Mindlin[6] has solved the three dimensional elasticity equations to obtain the velocity of flexural and shear waves. In the limit of very short flexural waves (high frequencies) the wave velocity should coincide with that of the Rayleigh surface waves. Equating the two velocities leads to

$$4\left[\left(1-\frac{\alpha}{s}\right)\left(1-\frac{1}{s}\right)\right]^{1/2} = \left(2-\frac{1}{s}\right)^2, \qquad (19)$$

where $\alpha = (1-2\mu)/2(1-\mu)$,
μ = Poisson's ratio.

On the other hand, Mindlin's solution for shear waves, when compared with the known solution for thickness-shear vibrations, leads to

$$s = 12/\pi^2 = 1{\cdot}216, \qquad (20)$$

and Mindlin shows that the solution of equation (19) coincides with equation (20) when $\mu = 0{\cdot}176$. He adds: "For other values of μ, one must choose or compromise in accordance with the relative importance of the two modes of motion."

Pickett[7] had previously solved the three-dimensional elasticity equations and concluded that the "best" values of s were 1·2, 1·12 and 1·18 for $\mu = 0$, 1/6, 1/3 respectively; the corresponding values obtained from equation (19) are 1·31, 1·22 and 1·15 respectively. More recently, Mindlin and Deresiewicz[6] quote $s = 1{\cdot}216$ for a rectangular cross-section and $s = 1{\cdot}181$ for a circular cross-section. These results show considerable uncertainty in s even when the material is isotropic, and the uncertainty is not likely to be less when the material is anisotropic, e.g. wood.

A review of the derivation of the Timoshenko equation (6) shows that it is not free from objection, and suggests that s may be a function of wavelength.[21] This possibility is also mentioned by Mindlin and Deresiewicz,[6] although the final value of s obtained by them is a constant, independent not only of wavelength, but of Poisson's ratio as well. An extension of the treatment of Higuchi, Saito and Hashimoto[22] indicates, however, that for the wavelengths and specimen dimensions encountered in the present paper, any variation of s with wavelength is probably not greater than a few parts in a thousand, and for practical purposes is negligible.[21]

In the absence of an unambiguous theoretical estimate of s, an attempt was made to determine its value by a purely experimental approach. This was done by cutting strips (approximately 30 × 2·5 × 0·5 cm) from the beams and estimating the shear modulus G by a torsional vibration method.[23] These values of G were then used together with the values of E and sE/G from Table 5 to estimate s. The results are given in Table 8.

In examining the figures in Table 8 it must be remembered that wood is not an ideal material for these experiments because of its variability and because the moisture content may change between the respective tests. The uncertainty in s due to these causes is estimated at about ±5%, and perhaps more. The uncertainty in the average s will be about ±2%, and it appears that to this accuracy, the average value (1·06 for both types of vibration) is smaller than many of the theoretical estimates of s.

If the main object of the experiments is a measurement of Young's modulus, the best procedure seems to be to measure the frequency of as many modes as possible and to analyse the results by the least squares procedure. If this cannot be done (for instance, because of a limited frequency range in the measuring apparatus) then approximate correction factors can be obtained from the shear modulus and an assumed s of 1·06.

Table 8. *Values of G (10^{11} dyn/cm^2) and s*

Material	*Type 1 vibrations*		*Type 2 vibrations*	
	G	s	G	s
Brown sterculia	0·112	1·07	0·132	1·12
Sitka spruce *A*	0·104	1·00	0·106	0·96
Sitka spruce *B*	0·107	1·10	0·108	1·14
Beech *A*	0·085	1·14	0·135	1·06
Beech *B*	0·140	0·99	0·084	1·10
Ash *A*	0·107	0·99	0·139	0·99
Ash *B*	0·149	1·11	0·109	1·04
Average	—	1·06	—	1·06

It is worth pointing out that for the low modes of vibration of a slender beam, it is not necessary to know s, E or G very accurately in order to calculate an accurate correction factor. The quantity T [equations (8) and (10)] is of the form $1 + t$, where t depends on sE/G, and, for example, if t is 0·01, then sE/G need only be known to about 10% in order to calculate T correct to 1 part in 1000.

ACKNOWLEDGEMENTS

The work described above was carried out as part of the programme of the Forest Products Research Board, and is published by permission of the Department of Scientific and Industrial Research. Acknowledgement is also made to Mr. H. L. Cox, of the National Physical Laboratory, and to the referee, for criticisms and suggestions.

REFERENCES

(1) Rayleigh, Lord. *Theory of Sound.* Vol. 1, Ch. vii (London: Macmillan and Co., 1877; Reprinted by Dover Publications, New York).
(2) Timoshenko, S. *Phil. Mag.*, **41**, p. 744 (1921); **43**, p. 125 (1922); *Collected Papers*, p. 288 (New York: McGraw-Hill Book Co. Inc., 1953); *Vibration Problems in Engineering* (New York: D. Van Nostrand Inc., 1955).
(3) Anderson, R. A. *J. Appl. Mech.*, **21**, p. 203 (1954).
(4) Föppl, O. *Vorlesungen über Technische Mechanik*, Vol. 3, 10th Ed. (Leipzig-Berlin: Teubner, 1927).
(5) Goodman, L. E., and Sutherland, J. G. *J. Appl. Mech.*, **18**, p. 217 (1951); Goodman, L. E. *J. Appl. Mech.*, **21**, p. 203 (1954).
(6) Mindlin, R. D. *J. Appl. Mech.*, **18**, p. 31 (1951); Mindlin, R. D., and Deresiewicz, H. *Proc. 2nd Nat. Congr. Appl. Mech.*, p. 175 (New York: American Society of Mechanical Engineers, 1955).
(7) Pickett, G. *Proc. Amer. Soc. Test. Mater.*, **45**, p. 846 (1945); *J. Appl. Phys.*, **16**, p. 820 (1945).
(8) Davies, R. M. *Phil. Mag.*, **23**, p. 1129 (1937).
(9) Dolph, C. L. *Quart. Appl. Math.*, **12**, p. 175 (1954).
(10) Goens, E. *Ann. Phys. (Leipzig)*, **11**, p. 649 (1931).
(11) Howe, C. E., and Howe, R. M. *J. Appl. Mech.*, **22**, p. 13 (1955).
(12) Jacobsen, L. S. *J. Appl. Mech.*, **5**, p. A-1 (1938).
(13) Kruzewski, E. T. *Tech. Notes Nat. Adv. Comm. Aero., Wash.*, 1909 (1949).
(14) Miklowitz, J. *J. Appl. Mech.*, **20**, p. 511 (1953).

(15) Traill-Nash, R. W., and Collar, A. R. *Quart. J. Mech. Appl. Math.*, **6**, p. 186 (1953).

(16) Wuolijoki, J. R. Thesis, Finnish Technical High School (Helsinki, 1947).

(17) Wuolijoki, J. R. *Valt. Tekn. Tutkimusl. Julk.* 6 (1948); *Valt. Tekn. Tutkimusl. Julk.* 20 (1950).

(18) Adamson, B. *Publ. Int. Assn. Bridge Struct. Engng*, **15**, p. 1 (1955).

(19) Heller, R. *J. Acoust. Soc. Amer.*, **24**, p. 273 (1952).

(20) Whittaker, E. T., and Robinson, G. *The Calculus of Observations.* Sections 107, 108 (London: Blackie and Sons, 1954).

(21) Cox, H. L. Private communication (1957).

(22) Higuchi, S., Saito, H., and Hashimoto, C. *Canad. J. Phys.*, **35**, p. 757 (1957).

(23) Hearmon, R. F. S. *Elasticity of Wood and Plywood.* Pp. 13–14 (London: H.M. Stationery Office, 1948).

Photoelastic properties of plasticised polymethyl methacrylate in the glassy state

By J. H. Lamble, D.Sc., and E. S. Dahmouch, B.Sc., Mechanical Engineering Department, Manchester College of Science and Technology

[*Paper first received* 28 *August, and in final form* 23 *December*, 1957]

The stress-optical coefficient of polymethyl methacrylate plasticised with dibutyl phthalate varies linearly from −4·55 Brewsters (18° C) for the unplasticised polymer to +4·4 Brewsters for the polymer plasticised with 20% by weight dibutyl phthalate, being zero when the percentage of this plasticiser is about ten. Another plasticiser, polyethylene glycol, when used in the same proportion by weight as for dibutyl phthalate, has a much smaller influence on the stress-optical coefficient. Optical creep reduces algebraically the value of the stress-optical coefficients. The influence of the proportion of the plasticiser on the refractive index and the mechanical properties of the plasticised polymers is also studied.

INTRODUCTION

There are two classes of natural doubly refracting uniaxial crystals,[1] namely, positive and negative. The extraordinary index of refraction is greater than the ordinary index in a positive crystal (quartz) and is smaller than the ordinary index in a negative crystal (calcite).

Most transparent materials become doubly refracting (birefringent) when stressed, with the line of stress corresponding to the optic axis in a natural doubly refracting crystal. The stress-optical coefficient of a material is measured in Brewsters, one Brewster being 10^{-13} cm^2/dyn. The relationship between the stress-optical coefficient C in Brewsters and the material fringe value F in lb/in.^{2} per in. per fringe, for sodium light ($\lambda = 5893$ Å), is given by $C = 3363/F$.

In general, a material under a simple tension acquires the properties of a positive uniaxial crystal (positive birefringence), and under a simple compressive stress those of a negative uniaxial crystal (negative birefringence). The convention is to consider the sign of the stress-optical coefficient, under these circumstances, to be positive. However, there are exceptional cases in which the above order is reversed as in certain very dense flint glasses,[2] polystyrene above its softening temperature,[3] and polymethyl methacrylate (Perspex).[4, 5] The sign of the stress-optical coefficient is then considered negative.

The authors were interested in obtaining a transparent, rigid material showing no stress-birefringence. The only known such material is Pockels' glass.

Pockels[2] observed that the stress-optical coefficients of a series of Jena glasses, with silica and lead oxide as their main constituents, varied with the percentage of lead oxide present, and that a very dense flint containing 80% lead oxide had a negative stress-optical coefficient. The curve showing the relationship between the stress-optical coefficient and the percentage of lead oxide indicated that the stress-optical coefficient should vanish for a percentage of lead oxide of about 75. Pockels had a glass of approximately this composition cast and the result obtained verified his prediction. Filon[2] and, more recently, Waxler and Napolitano[6] repeated the tests on flint glasses and obtained similar results to those of Pockels.

POLYMETHYL METHACRYLATE

Polymethyl methacrylate is an amorphous linear polymer of very high transparency and good machinability. It is known under different trade names: I.C.I., Perspex in the United Kingdom, Röhm and Haas Plexiglas and E.I. Du Pont de Nemours Lucite in the United States of America. The stress-optical sensitivity of this material is very low compared with most other photoelastic materials. Its use in photoelasticity has, therefore, been confined to exploring isoclinic lines and to such cases where its relative insensitivity is desirable, e.g. in making transparent loading tackle.

Kolsky and Shearman[4] found that the stress-optical coefficient of this material is negative. Robinson, Ruggy and Slantz[5] showed that the stress-optical coefficient varies markedly with temperature, showing a sharp maximum of −45 Brewsters at 93° C (compared with −3·8 Brewsters at 21° C). Tsvetkov[7] showed that the sign of the streaming (or flow) birefringence of polymethyl methacrylate solutions in various solvents is positive. He also showed that the streaming birefringence is a parabolic function of the refractive index of the solvent and has a minimum value when the solvent has the same refractive index as the polymer.

The present authors measured the stress-optical coefficient of commercial plasticised Perspex (5% dibutyl phthalate), and found it to be −2·3 Brewsters (18° C). This is almost half as much as that of the unplasticised Perspex. If, by increasing the proportion of the plasticiser, the stress-optical coefficient of plasticised polymethyl methacrylate can be reduced numerically still further and its sign reversed, it will then be possible to prepare a polymer with a stress-optical coefficient of zero Brewsters.

MATERIALS USED IN THE PRESENT WORK

For the purpose of this work, $\frac{1}{4}$ in. thick sheets of polymethyl methacrylate plasticised with various proportions (0 to 20% by weight) of dibutyl phthalate were specially prepared. In addition, for comparison purposes, two samples plasticised with 5 and 10% by weight respectively of polyethylene glycol were also prepared. The plasticiser was added to the methyl methacrylate monomer before polymerization.

METHODS OF MEASUREMENT

All tests were made at room temperature (18° C), and sodium light ($\lambda = 5890$ Å) was used unless otherwise stated.

The refractive index was measured by an Abbé refractometer with sodium light illumination; readings to the fourth decimal place could be conveniently observed. Four separate readings of each of two specimens of the same sheet were made and the average recorded.

Young's modulus was determined only in tension, flat tensile specimens of uniform thickness, $\frac{1}{4}$ in. (see Fig. 2), being strained in the vertical loading frame of a diffused light polariscope. Load was applied by means of dead weights through a lever having a 10 : 1 ratio. Two Johansson extensometers (8 mm gauge length, forty divisions on the scale, each division equal to $8{\cdot}5 \times 10^{-6}$ in., and with provision for re-setting) were lightly clamped, one on each face of the specimen, with their knife edges placed on its centre line. The absence of any bending was ensured by a preliminary loading of very short duration, during which the readings of the two extensometers were taken and the colour pattern, developed in the specimen in white plane polarized light (plane of polarization at 45° to the direction of stress), was observed for symmetry. Any bending which existed was eliminated by adjustment of the loading pins until proper alinement in all directions was obtained.

Birefringence tests were made under tension and compression on flat specimens of uniform thickness, $\frac{1}{4}$ in. (see Fig. 4). The compression specimens were loaded through flat pins in a compression attachment taken from the Hounsfield tensometer. Fractional fringe orders were measured by the Sénarmont method. All sheets tested were optically isotropic in the unstressed condition, with the polished surfaces normal to the direction of propagation of polarized light.

Mechanical and optical creep occurred when the specimens were left under constant load. For stresses up to 1200 lb/in.^{2}, creep was complete ten minutes after application of the load in any of the specimens tested. The strain or the relative retardation was measured directly after loading and again after ten minutes for all stresses. The load was then removed and, in birefringence tests, the residual birefringence was measured. The same specimen was used for successive loadings with a recovery time of one hour between two loadings. However, when very high stresses had been applied, particularly on specimens containing a high proportion of plasticiser, a large part of the residual birefringence remained permanent and other specimens of the same sheet had to be used for each subsequent loading.

RESULTS AND DISCUSSION

The influence of the proportion of dibutyl phthalate (D.B.P.)

(*a*) *On refractive index.* D.B.P. has almost the same refractive index as unplasticised polymethyl methacrylate (1·4925 and 1·4909 respectively, sodium light, 18° C). Fig. 1 shows the refractive index of the plasticised polymer plotted against the proportion of the plasticiser. It should be noticed that the rise in the refractive index is higher than that for an ideal mixture.

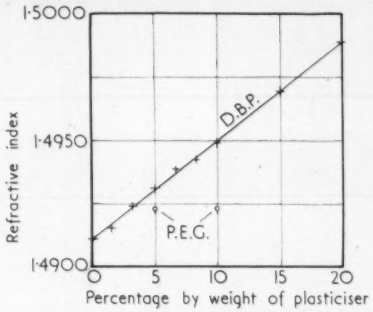

Fig. 1. Change in the refractive index
$\lambda = 5890$ Å. Temperature, 18° C.

(*b*) *On mechanical properties.* Fig. 2 shows the stress *versus* strain curves in tension of unplasticised polymethyl methacrylate and the polymer plasticised with 20% by weight D.B.P., the values of stress being based on the dimensions of the specimens before loading. The stress *versus* strain curves of the polymers plasticised with intermediate proportions of D.B.P. lie between the two extremes shown and have been omitted for clarity.

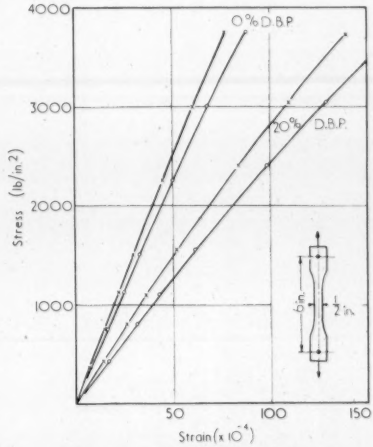

Fig. 2. Stress-strain curves in tension
Temperature, 18° C. ×: for 0 min. ○: for 10 min.

The departure from linearity of the nominally instantaneous (0 min) curves may be due in part to the higher rate of creep directly after loading in the high stress region. It can be seen from Fig. 2 that both the extension and the strain-creep produced by any tensile stress are higher in the plasticised polymer. The stress *versus* strain curves are straight in the

**

stress range 0 to 1200 lb/in.^{2} and Young's modulus was determined from the slopes of these lines. In Fig. 3 Young's modulus, before and after creep, is plotted against the proportion of D.B.P.

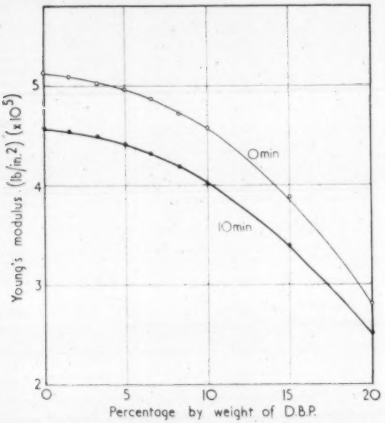

Fig. 3. Change in Young's modulus
Temperature, 18° C.

(c) *On birefringence.* Fig. 4 shows the birefringence *versus* stress curves under tension and under compression for polymethyl methacrylate plasticised with 0, 5, 10, 15 and 20% by weight D.B.P.

Both the unplasticised polymer and the polymer plasticised with 5% D.B.P. show negative birefringence under tension,

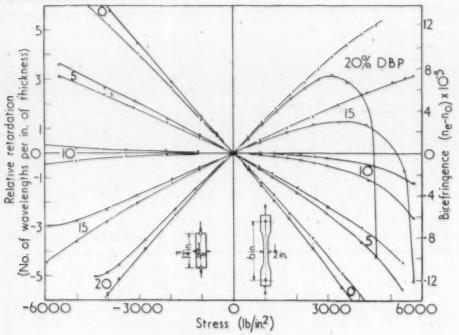

Fig. 4. Birefringence—stress curves
λ = 5890 Å. Temperature, 18° C.
×: for 0 min. ○: for 10 min.

and positive birefringence under compression. The effect of optical creep is to increase numerically the relative retardation in either case in the two polymers.

The polymer plasticised with 10% D.B.P. is of particular interest. Directly after loading no birefringence is obtained for stresses below ±1000 lb/in.^{2}, but negative birefringence is obtained under higher stresses, either tensile or compressive. The effect of optical creep is to increase numerically the negative birefringence under tension, while under compression the negative birefringence is numerically reduced, goes through zero and then becomes positive.

The polymers plasticised with 15 and 20% D.B.P. show positive birefringence under tension and negative birefringence under compression. The effect of optical creep is to reduce numerically the birefringence in either case in the two polymers. Under sufficiently high tensile stresses the positive birefringence obtained directly after loading in the two polymers decreases with time, passes through zero and becomes negative. The tensile stress at which this may occur depends on the length of time for which the load is maintained, but for the same period it is lower in the more highly plasticised polymer. This change is usually rapid, is accompanied by large plastic flow and crazing marks are produced on the surfaces of the specimen. Such a reversal of the sign of birefringence due to optical creep does not take place in either polymer under compression, for even higher stresses.

The residual birefringence, upon removal of the load, is negative in all specimens tested under tension and positive in all specimens tested under compression, and is equal to the change in birefringence due to optical creep.

The stress-optical coefficients were determined from the average slopes of the curves in Fig. 4 in the stress range −1200 to +1200 lb/in.^{2}, and are plotted in Fig. 5 against

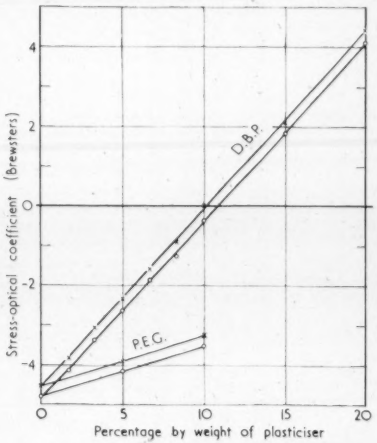

Fig. 5. Change in stress-optical coefficient
Temperature, 18° C. ×: for 0 min. ○: for 10 min.

the proportion of the plasticiser. The stress-optical coefficient (0 min) varies linearly from −4·55 Brewsters for unplasticised polymethyl methacrylate to +4·4 Brewsters for the polymer plasticised with 20% D.B.P., and vanishes when the percentage of D.B.P. is ten.

The effect of optical creep is to reduce algebraically the value of the stress-optical coefficient by almost the same amount in all polymers tested. As a result, the percentage of D.B.P. at which the stress-optical coefficient vanishes is

greater than ten, when the effect of optical creep is taken into account.

Polyethylene glycol (P.E.G.)

The refractive index of P.E.G., mol. wt 600, is 1·4651 (sodium light, 18° C). The two samples of polymethyl methacrylate plasticised with 5 and 10% by weight P.E.G. respectively, have the same refractive index of 1·4922. The birefringence *versus* stress curves lie between those of the unplasticised polymer and those of the polymer plasticised with 5% D.B.P. (Fig. 4) and are of the same shape.

The effect of P.E.G. is also to increase algebraically the stress-optical coefficient, but to a much smaller extent compared with the effect of D.B.P. used in the same proportion. The stress-optical coefficient appears to vary linearly from −4·55 Brewsters for the unplasticised polymethyl methacrylate to −3·25 Brewsters for the polymer plasticised with 10% by weight P.E.G. The effect of optical creep and the sign of the residual birefringence after the removal of the load are the same as when D.B.P. is used.

CONCLUSIONS

It is considered that the results obtained from the present investigation throw more light on the mechanisms of birefringence in linear amorphous polymers, and also on the action of plasticisers.

It is now possible to prepare a rigid plastic, of high transparency and good machining properties, with a stress-optical coefficient at room temperature of zero Brewsters. This is polymethyl methacrylate plasticised with 10% by weight dibutyl phthalate. This material shows no stress birefringence under a limited range of stress, ±1000 lb/in.^{2}, but a slightly higher proportion of plasticiser has to be used if the effect of optical creep is taken into account.

ACKNOWLEDGEMENTS

The authors wish to express their gratitude to I.C.I. Ltd., (Plastics Division) for the manufacture and supply of the materials used in this work. They also wish to thank Prof. H. Wright Baker for his encouragement during the course of the work.

REFERENCES

(1) JENKINS, F. A., and WHITE, H. E. *Fundamentals of Optics*, 2nd Ed., p. 507 (New York: McGraw-Hill Publishing Co., 1951).
(2) COKER, E. G., and FILON, L. N. G. *Photoelasticity*, p. 217 (London: Cambridge University Press, 1931).
(3) KAWATA, K. *J. Polymer Sci.*, **19**, p. 359 (1956).
(4) KOLSKY, H., and SHEARMAN, A. C. *Proc. Phys. Soc. (London)*, **55**, p. 383 (1943).
(5) ROBINSON, H. A., RUGGY, R., and SLANTZ, E. *J. Appl. Phys.*, **15**, p. 343 (1944).
(6) WAXLER, R. M., and NAPOLITANO, A. *J. Res. Nat. Bur. Stand.*, **59**, p. 121 (1957).
(7) TSVETKOV, V. N. *International Symposium on Macromolecule Chemistry*, 1954, *Milano-Torino*. Suppl. to *La Ricerca Scientifica*, **25**, p. 413 (1955).

The theory of ballast tubes or barretters

By R. O. JENKINS, A.R.C.S., D.I.C., Ph.D., F.Inst.P., The General Electric Co. Ltd., Wembley, Middlesex

[*Paper received* 20 *March*, 1958]

The theory is based on a simple graphical method of solving the equation of thermal equilibrium of an electrically heated wire in a gas-filled enclosure. The results account for the main operating characteristics and have accurately predicted the ratings of various low voltage barretters. It is also shown why, in practice, barretters have always consisted of an iron wire in hydrogen.

INTRODUCTION

Two papers[1-2] have appeared recently discussing the theory of the action of ballast tubes or, as they are often called, barretters. A barretter consists essentially of an electrically heated iron wire mounted in an enclosure containing hydrogen. As the voltage applied across the wire is increased, the current increases steadily up to a certain value. Beyond this point it remains sensibly constant while the voltage is approximately doubled. Yet a further increase in voltage causes the current to rise again. This results in a current-voltage characteristic as shown in Fig. 1 (curve *c*). As the voltage is increased along the "plateau," visible hot spots develop along the wire, and gradually extend till the whole wire is at an approximately uniform temperature (about 800° C) when the upper end of the plateau is reached. These barretter tubes are used to absorb fluctuations in the voltage applied to circuits such as thermionic valve heater chains in which it is desired to maintain a constant current.

The recent paper of Minter[1] sought to explain the hot spot formation by a phenomenological approach, while the paper of Armstrong[2] discussed the action in more general terms using the simpler approach of considering a uniform wire temperature. These two approaches do not appear to account completely for all the properties observed nor do they lead to numerical values.

In this paper a simple approach to the problem is described

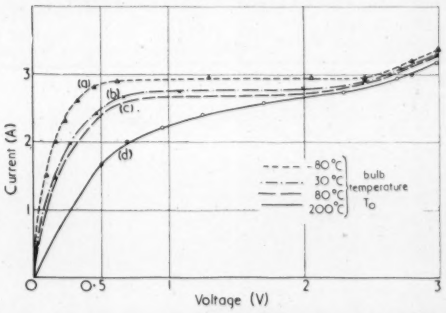

Fig. 1. Current-voltage characteristic curves of a low voltage barretter

which accounts for the plateau accompanied by the hot spot formation, and also for the effect of bulb temperature on the plateau characteristic. Numerical formulae are also derived which have been used during the last two years in these laboratories to design barretters. These formulae have predicted ratings of various types to an accuracy of about 10%.

DEVELOPMENT OF THEORY

The approach adopted is a graphical method of solving a simple equation of thermal equilibrium for the hot wire. Consider a wire of uniform radius r cm and length l cm carrying a current i A and operating at a uniform temperature T° C. If its specific resistivity at temperature T° C is $\sigma_T\,\Omega$ cm, then W, the heat generated in watts is given by

$$W = i^2\sigma_T l/\pi r^2 \qquad (1)$$

If the rate of heat loss from the wire is uniform along its length and is only by thermal conduction through the gas, then for thermal equilibrium in the wire

$$W = Kg(T - T_0) \qquad (2)$$

where K is a constant depending on the geometry of the wire and envelope, g the thermal conductivity of the gas, and T_0 the temperature of the envelope.

At this point the validity of the assumptions made in equation (2) should be examined. It may be shown by consideration of thermal radiation and conduction constants that below a temperature of about 800° C, the heat lost by radiation in a typical barretter is less than about 10% of that lost by conduction. The relative loss through the wire supports depends on their number and spacing and also on the diameter of the wire. It is likely to be negligible for a low current high voltage barretter but begins to become apparent for tubes with operating resistances of below about 1 Ω. The assumption that heat is lost by thermal conduction and not by convection appears justified for the usual pressure of hydrogen, because the thickness of the stagnant gas layer should be much greater than the diameter of the bulb. The thermal conductivity g varies only slightly with temperature so that a constant value corresponding to about 400° C can be assumed. It may thus be seen that for an approximate theory the assumptions inherent in equation (2) are justified.

By combining equations (1) and (2) it may be seen that

$$\sigma_T = \frac{Kg\pi r^2}{i^2 l}(T - T_0) \qquad (3)$$

This equation may be solved graphically as follows. σ_T is plotted as a function of T. The data for this was obtained by combining values for 0–600° C from the International Critical tables with values for the 600°–1000° C range obtained experimentally.

The right-hand side of equation (3) when plotted as a function of T is a straight line through $T = T_0$ with a slope ϕ where

$$\tan\phi = Kg\pi r^2/i^2 l \qquad (4)$$

The solution of the equation (3) is thus the intersection of the σ_T curve and this straight line.

APPLICATION OF THEORY

The plateau characteristic and formation of hot spots. This graphical procedure is shown in Fig. 2. The bulb temperature T_0 is assumed to be about 80° C which is a reasonable practical value. A family of lines through $T_0 = 80$° C may be drawn intersecting the σ_T curve giving corresponding values for T and σ_T.

The line with $\phi = 90°$ corresponds from equation (4), to zero current, and reducing the angle ϕ corresponds to increasing i. It will be seen that as i increases, the intersection of the σ_T curve and line moves steadily up the σ_T

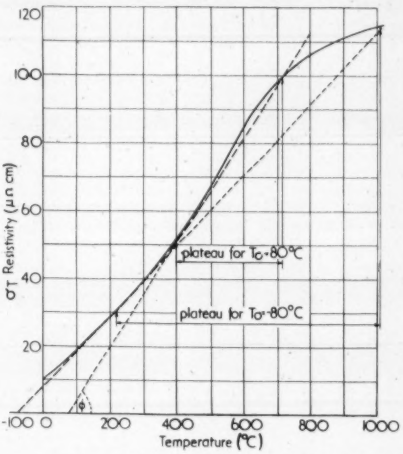

Fig. 2. Resistivity temperature curves for iron

curve, corresponding to a steady increase in temperature and resistivity. When T reaches 400° C the straight line becomes just tangential to the σ_T curve and the slightest decrease in ϕ, corresponding to an increase in i, results in T rising to over 700° C. This causes a large increase in σ_T and hence in the voltage across the wire for a negligible increase in current. It is this transition which results in the plateau.

This transition occurs at any point along the wire which reaches the critical temperature of 400° C. As a result of thermal conductivity along the wire, the centre of a limb usually reaches this temperature first, and a hot spot forms there. With an increase in applied voltage, it generally spreads until an obstruction such as a support is reached. When this happens, a further increase in applied voltage results in another hot spot forming on an hitherto cool section of the wire, and so on until all the wire has risen to the upper temperature.

Variation of plateau characteristic with bulb temperature. It is of interest to consider what happens if the bulb temperature T_0 is varied. Experimental curves for a particular barretter are shown in Fig. 1 corresponding to bulb temperatures of −80° C, 30° C, 80° C and 200° C. It will be seen by drawing the family of lines corresponding to a variation in i through the point $T_0 = 200$° C on Fig. 2 that for no value of ϕ does the line become tangential to the curve, thus explaining why a flat plateau is not observed. Hot spot formation should be absent and is, in fact, very considerably reduced and what remains is probably due to local inhomogeneities in the wire or variations in geometry. It will be observed that between 500° and 700° C, T and σ_T are varying rapidly with ϕ, thus giving a short section of current voltage characteristic with a fairly low slope.

Considering now $T_0 = 30°$ C it may be seen that the plateau should start at $T = 370°$ C, $\sigma_1 = 48\ \mu\Omega$ cm and end at $T = 750°$ C, $\sigma_2 = 103\ \mu\Omega$ cm. This means that the voltage ratio between top and bottom of the plateau should be 2·18. Curve (*b*) of Fig. 1 indicates a ratio of 2/0·9 which is 2·22.

Considering $T_0 = -80°$ C the line becomes tangential to the curve at $T = 230°$ C, $\sigma_1 = 30\ \mu\Omega$ cm, and intersects the curve again at $T = 1000°$ C, $\sigma_2 = 114\ \mu\Omega$ cm, resulting in a voltage ratio of 3·8. The experimental voltage ratio from curve (*d*) of Fig. 1 is 2·4/0·65 which is 3·7.

It may thus be seen that this simple approach has accounted at least qualitatively for the main features of barretter operation.

Derivation of numerical formulae. Perhaps the most attractive feature of this method of treating the problem is that it leads to simple numerical formulae which have been valuable in designing barretters. Referring to Fig. 2 and assuming $T_0 = 80°$ C it may be seen that the plateau corresponds to a rise in σ_T from $\sigma_1 = 50$ to $\sigma_2 = 100\ \mu\Omega$ cm approximately and to a line for which $\tan\phi = 0{\cdot}15\ \mu\Omega$ cm/°C.

To derive a value of i for a particular wire from equation (4) it is essential also to know K and g. A value for g of 6×10^{-4} cal cm for hydrogen at a pressure of 10 cm mercury has been assumed. This pressure has been chosen as the thermal conductivity varies only slowly with the pressure in this region.

K can only be calculated analytically for very simple configurations, the most useful of these being a wire along the axis of a cylinder. In this case

$$K = \frac{2\pi Jl}{\log_e (a/r)} \tag{5}$$

where $J = 4{\cdot}2$ W/cal and a is the radius of the bulb in cm.

Combining equations (4) and (5) and using the appropriate figures derived from the graphical solution, we have

$$i = \frac{3800r}{[\log_{10} (a/r)]^{\frac{1}{2}}} \tag{6}$$

The corresponding voltages across the wire at the beginning and end of the plateau are given by

$$V_1 = \frac{i\sigma_1 l}{\pi r^2} = \frac{6{\cdot}04 \times 10^{-3} l}{r[\log_{10} (a/r)]^{\frac{1}{2}}} \tag{7}$$

$$V_2 = \frac{i\sigma_2 l}{\pi r^2} = \frac{12{\cdot}08 \times 10^{-3} l}{r[\log_{10} (a/r)]^{\frac{1}{2}}} \tag{8}$$

For other arrangements of the wire and enclosure the value of K may be derived by using the electrolytic analogue. In the design of low voltage barretters in which equations (6) (7) and (8) have been used, the wire was generally in the form of an open coil. It was found by using the electrolytic analogue that the effect of coiling on K was in many cases negligible, although for close coiling it could have a large effect. As an illustration of the use of these numerical formulae the barretter whose curves are shown in Fig. 1 had values of $r = 0{\cdot}01$ cm, $l = 2{\cdot}5$ cm, and $a = 1{\cdot}2$ cm while the effect of coiling was found by a simple electrolytic experiment to be negligible. Inserting these figures in equations (6), (7) and (8) $i = 2{\cdot}63$ A, $V_1 = 1{\cdot}04$ V, $V_2 = 2{\cdot}09$ V compared with the experimental values for Fig. 1 (curve *c*) of $i = 2{\cdot}65$ A, $V_1 = 0{\cdot}85$ V, $V_2 = 1{\cdot}75$ V.

The experimental values of V are slightly low because of the end cooling of the wire which shortens its effective length. From observation, this end cooling prevents about 2–3 mm of each end of the wire from reaching a visible temperature in operation. As the wire is a single length and is relatively large in diameter, only a single hot spot, at the centre of the wire, is observed, and this spreads as the voltage is increased along the plateau.

DISCUSSION

It will be seen that this very simple approach to the problem not only accounts for the main operational features of the barretter but gives a surprisingly accurate estimate of the ratings.

It also clearly demonstrates that the truly flat plateau in the operational current-voltage characteristic is the result of losing most of the heat by gaseous conduction, combined with an inflexion in the resistivity-temperature curve for iron. This allows a straight line through $T_0 = 50$–$100°$ C, corresponding to thermal conduction, to become tangential with the resistivity temperature curve and to intersect it again at a higher temperature. It appears that iron is unique in this respect, in that the inflexion point is at a sufficiently high temperature and is also accompanied by a rapid rise in resistance below the point of inflexion.

Nickel also has a point of inflexion in the resistivity-temperature curve as shown in Fig. 3. This is at a lower temperature than iron, and results in a plateau of negligible length as may be seen from the diagram. A useful plateau would be obtained with a bulb temperature of about −100° C. The case of tungsten is also of interest as this metal has no inflexion, but has a greater rate of rise of resistivity with temperature than most other metals. Fig. 3 shows the resistivity-temperature curve with a family of lines drawn through $T_0 = 80°$ C. It will be seen that no true plateau is possible in this case.

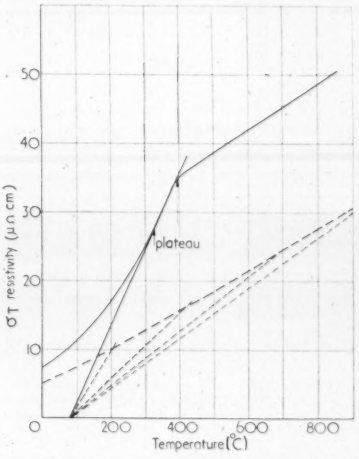

Fig. 3. Resistivity temperature curves for nickel and tungsten

——— nickel.
– – – tungsten.

One other point meriting discussion is the effect of using other gases. Any other gas than hydrogen will have a lower thermal conductivity and the heat lost by radiation may become significant. Equation (2) would then be augmented by a term $R(T^4 - T_0^4)$ for radiation heat loss. This results in the family of lines through T_0 deviating from the straight in an upward direction. It can be seen that a significant curvature may cause the lines always to intersect the resistivity curve, even for iron, in one point, and never become tangential. This would result in a current-voltage relationship similar to curve (*d*) of Fig. 1. In any case the plateau obtained with any other gas will tend to be shorter than that obtained with hydrogen at the usual filling pressure.

The conclusion of this analysis is that a better combination than iron wire in hydrogen is unlikely to be found.

ACKNOWLEDGEMENT

In conclusion, the author wishes to thank the Marconi–Osram Valve Co. Ltd., on whose behalf this work was carried out, for permission to publish this paper.

REFERENCES

(1) MINTER, C. C. *Rev. Sci. Instrum.*, **28**, p. 569 (1957).
(2) ARMSTRONG, H. L. *Rev. Sci. Instrum.*, **28**, p. 1088 (1957).

The bistable behaviour of the magnetic transductor

By E. H. FREI, Ph.D., S. SHTRIKMAN, M.Sc., and D. TREVES, M.Sc., The Weizmann Institute of Science, Rehovot, Israel

[*Paper first received* 16 *January and in final form* 11 *March*, 1958]

It is already well known that the second harmonic magnetic transductor has instability regions.[1-3] It has been found experimentally that in each region two modes of output current exist, differing only by the phase, which these currents have with respect to the exciting voltage. Under suitable parameters and excitation conditions, the transductor will jump from one mode of operation to the other, whenever the exciting current is modulated with a negative pulse. It therefore operates like a bistable element.

It has been shown by various authors that the capacity loaded second harmonic magnetic amplifier has instability regions where a current will flow in the output winding even in the absence of a signal current.[1-3] The frequency of the output current in unstable operation is equal to, or a harmonic of the frequency of the exciting current.

In the course of investigation of the properties of the second harmonic magnetic amplifier, it was found that there exist two modes of oscillation which differ only by the phase the output currents have with respect to the exciting voltage, but are otherwise identical. This effect was experimentally found at oscillations of the fundamental, second[4] and up to the eleventh harmonic of the exciting current frequency. The explanation of this phenomenon lies in the fact that to a good approximation the inductance is a function of the absolute value of the exciting current,[3] and if the latter is an odd function, the output circuit does not distinguish between the positive and negative half-cycles of exciting current, leading to the above-mentioned two modes. When operating at the second harmonic frequency, either of these modes can be forced by injecting a pulse of direct current in the signal winding. By reversing the sign of the pulse, the other mode will occur. The same result is obtained by inducing a small remanent magnetization in the desired direction when the exciting current is cut off. When the amplitude of the exciting current is raised enough to reach instability, oscillation will start in the same mode that would occur in the presence of a direct signal current inducing a magnetization in the direction of the remanance.

With suitable circuit parameters and excitation conditions, each time the exciting current is decreased and increased again (modulated) the phase of the oscillating current with respect to the exciting current reverses. The device operates then as a single stage binary counter, with an exciting current modulation pulse as the signal. The mode is remembered even after the exciting current has been switched off for days. However, if after each reduction of exciting current the core is demagnetized with a slowly decaying alternating current, oscillations will occur in an unpredictable mode. The bistable behaviour was also found at other harmonics. It may perhaps be of interest to mention that in one-crossed field ferrite transductor, oscillation of the fundamental frequency always began in the same mode, obviously due to a screw-type asymmetry of the material. With a proper adjustable biasing field this asymmetry was nullified and the bistable behaviour occurred.

Experiments suggest that bistable behaviour occurs only when the amplitude of oscillation increases and decreases abruptly, as in a ferroresonant circuit, and not reversibly. This can easily be achieved as the values of the parameters are not critical. Furthermore it should be noted that the waveform of the modulating pulse of exciting current need not be of a specific shape, and modulation depth need only be a small fraction of the exciting current amplitude. Flipping can also be brought about by frequency-modulation of the exciting current and in some cases by a modulation of a circuit parameter such as the loading condenser.

Ferrite transductors of various types including the usual parallel field amplifier,[5] the hollow toroid[6] (Fig. 1) and the McCreary cross valve type[7] (Fig. 2) were built in order to test the bistable behaviour. The hollow toroid crossed field transductor of Fig. 1 was operated as a bistable device when oscillating at the second harmonic. The loading capacitor was 9 μF, the exciting current approximately 7·5 A peak and its frequency 320 c/s. The waveforms of the exciting current and the voltage on the capacitor are shown in Fig. 3. The complete cycle of the bistable device can be followed. The pairs of lines, *a* to *e*, in the oscillogram are taken simultaneously. The upper line in each pair is the voltage in the loading condenser and the lower line is the exciting current taken for phase comparison. If the exciting current is increased from zero, the voltage on the condenser increases reversibly up to a certain amplitude, and this amplitude is shown in *a*. By further increasing the excitation, the output voltage increases irreversibly to the amplitude shown in *b*. On lowering the exciting current, the output

voltage decreases irreversibly to the value shown in *c*. It can be seen that the phase of oscillation with respect to the exciting current reverses during this irreversible change. On increasing the excitation again, the output voltage increases reversibly up to the amplitude shown in *d*, and then jumps irreversibly to the value in *e*. On now decreasing the exciting current, the output voltage will decrease irreversibly and its phase will reverse again to that of *a*, thus completing the cycle. The transductor of Fig. 2 was operated as a bistable device oscillating at the fundamental frequency. The exciting current was about 1 A peak at 7·5 kc/s driven from an approximately sinusoidal voltage generator. The load consisted of a resistance of 15 Ω in series with 0·15 μF. The waveforms of the exciting and output current are shown in Fig. 4. The bistable cycle, *a* to *e*, is as in Fig. 3 except that *a*, *c* and *d* have been amplified on this oscillogram by 40 dB. In *b* the amplitude of the output current was 0·25 A peak. One can observe in Figs. 3 and 4 that the reversing of the phase of the output voltage or current occurs during the irreversible decrease of oscillation. A small transductor for higher frequencies was also built. It consisted of a ring of ferrite (Ferroxcube 3 *c*) with a hole drilled through its wall to accommodate the output winding. It operated satisfactorily as a bistable device oscillating at the second harmonic with the exciting frequency of 200 kc/s.

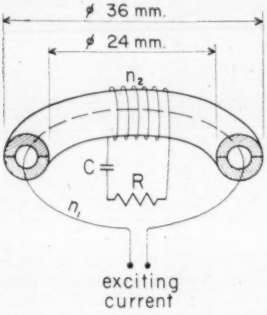

Fig. 1. Hollow toroid transductor operating as a bistable device. The core is of ferrite material (Ferroxcube II B2). The exciting winding n_1 consists of one turn 0·7 mm wire and the output winding n_2 of 200 turns of the same wire

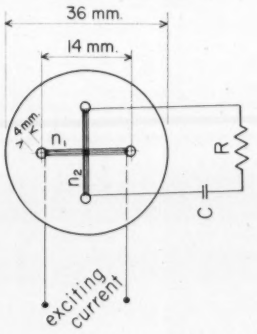

Fig. 2. Transductor of the McCreary type of ferrite (Ferroxcube III B2) the exciting winding n_1 consists of 6 turns of 0·7 mm and the output winding n_2 of 31 turns of 0·25 mm wire. The thickness of the ferrite is 6 mm

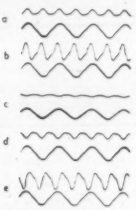

Fig. 3. Complete bistable cycles of hollow toroid transductor oscillating at second harmonic, operated by changes in amplitude of exciting current. Upper line in each pair is the voltage on the capacitor, lower line is the exciting current

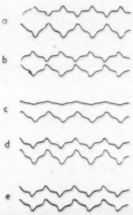

Fig. 4. Complete bistable cycle of the McCreary transductor oscillating at fundamental frequency operated by changes in amplitude of exciting current. Upper line in each pair is the output current, lower line is the exciting current

In conclusion, it can be said that two modes of current occur in each instability region of the magnetic transductor. The phases of these two modes differ by π. Under easily obtainable and not critical parameters the transductors will jump from the one mode of oscillation to the other mode, if the exciting current is temporarily reduced or the loading capacity is temporarily changed.

REFERENCES

(1) BRILLOUIN, L. *Wave Propagation in Periodic Structures*, 2nd ed., p. 186 (New York: Dover Publications Inc., 1953).
(2) SERSON, P. H., and HANNAFORD, W. L. W. *Canad. J. Tech.*, **34**, p. 232 (1956).
(3) FREI, E. H., and TREVES, D. *Conference on Magnetism and Magnetic Materials, Boston*, 1956 (New York: American Institution of Electrical Engineers, 1957).
(4) CUNNINGHAM, W. J. *J. Appl. Phys.*, **27**, p. 1373 (1956).
(5) MANLEY, J. M. *Proc. Inst. Radio Engrs*, **39**, p. 242 (1951).
(6) FREI, E. H., SHTRIKMAN, S., and TREVES, D. *Bull. Res. Counc. of Israel*, **3**, p. 443 (1954).
(7) MCCREARY, H. J. *Proc. Nat. Electronics Conf.*, **5**, p. 450 (1949).

Proceedings of the congress on modern analytical chemistry in industry. (Cambridge: W. Heffer and Sons Ltd., for The Society for Analytical Chemistry, 1958.) Pp. vii + 244. Price £2 2*s*.

The papers presented to the Congress held in June 1957, are recorded in this well-produced volume, with the discussions appropriate to each. They purposely contain little specialized detail, but they are directed primarily to those who wish to know how analysts can best be of service to them. Modern techniques and applications in various organizations are reviewed broadly, so that both the analyst and the user of analytical facilities have standards of comparison for re-appraising their own practices. The physicist will be interested in the expanding use of physical techniques, particularly for control purposes, but he will also be made aware that instrumentation can only be successful when it is backed by first-class analytical research and standardization. The volume could be studied with profit by several different types of people, and the Society for Analytical Chemistry is to be complimented on expeditious publication before the subject-matter is out of date.

M. MILBOURN

Proceedings of the international conference on fatigue of metals, 1956. (London: The Institution of Mechanical Engineers; New York: The American Society of Mechanical Engineers, 1958.) Pp. v + 961. Price £4 10*s*.

The subject of the fatigue of metals has engaged the attention of a considerable number of eminent investigators during the past 40 years. The *Proceedings* of an international conference on the subject, held under the sponsorship of the Institution of Mechanical Engineers and the American Society of Mechanical Engineers in 1956, have now been published and show very clearly that world activity in this important field, which is of such significance to engineers, is still very great. Over 80 papers were presented to the conference, and with the rapporteurs' summaries and the discussion these occupy over 900 pages. That the conference was truly international in character is shown by the fact that papers were submitted from Great Britain, United States, France, Germany, U.S.S.R., Australia, and Japan. It is of interest to note that nearly half the total number of papers were from Great Britain.

The conference was arranged in sessions so that each session dealt with a specific aspect of the subject and the *Proceedings* are correspondingly arranged so that reference to the most recent work on a particular aspect can be very conveniently made.

It is impossible, in such a short review as this, to do justice to the really vast amount of valuable and up-to-date information given in this single volume. One can therefore give only general, overall impressions, which can be summarized as follows:

(i) Since a *very* large proportion of the failures of metals in service is due to fatigue it is not surprising that these *Proceedings* reveal the great effort going on in the world to enlarge our knowledge of the subject.

(ii) Despite the considerable work that has been, and is still being, done there is still a very large area to be explored and many more data are required. The present papers show, for example, that the effect of very high speed alternations of stress is still far from clear and more information on fretting and ways and means of minimizing it is urgently required. Additional work is necessary on the size effect, more information is desirable on the cumulative effect of fatigue so that the designer can predict the likely performance of members subject to random service loads, whilst the basic studies of the subject have still not produced an acceptable understanding of what happens when a metal is fatigued.

(iii) On the one hand one must have sympathy with the engineering designer who, when fixing his working stress may have to take account of stress raisers, random overloads, fretting, corrosion, temperature, etc., whilst on the other hand there must be some impatience with him because it is clear from the papers that many failures still occur due to ungenerous fillet radii and other unnecessary stress raisers and hence imply that the designer has not yet learned lessons taught long ago.

As one would expect from such eminent sponsors, the *Proceedings* are well arranged, well printed, with graphs of sensible size and well reproduced microphotographs. The volume will be a "must" for all students of the subject but it is important to add that many of the papers are of an essentially practical character and are of clear and immediate value to many branches of engineering design.

N. P. INGLIS

International Scientific Radio Union: Proceedings of the XIIth general assembly. Vol. XI, Part 1, Commission 1: On radio measurements and standards. (Brussels: International Scientific Radio Union, 1957.) Pp. 78. Price 14*s*. 6*d*.

The contents of this publication follow closely the objects of the International Scientific Radio Union, which are to review at regular intervals the state of scientific knowledge in each of seven fields into which the subject is divided, to provide opportunities for discussion and to formulate programmes of work particularly where international co-operation is needed.

The reports of 12 national committees give a broad survey of the developments in standards and measuring techniques made during the period 1954–57, and the comprehensive list of references facilitates a thorough study of the field. Short accounts are given of the meetings of Commission 1 held at Boulder, of the resolutions that were passed and of the summary of the Chairman, Mr. B. Decaux. Mr. Decaux stressed particularly the importance of the development of atomic standards and the need for comparing standards of different types and constructions. One way of effecting this was the use of low frequency standard transmissions such as the MSF transmissions from Rugby.

It will be recalled that the Union was the first international body to adopt the improved value for the velocity of light determined by the use of short radio waves. The value adopted at Sydney in 1952 was 299 792 ± 2 km/s. In view of the more precise measurements made since then a new resolution recommends the use of the value 299 792·5 ± 0·4 km/s.

L. ESSEN

Proceedings of the international symposium on isotope separation. Edited by J. KISTEMAKER, J. BIGELEISEN and A. O. C. NIER. (Amsterdam: North-Holland Publishing Co., 1958.) Pp. xx + 704. Price 110*s*.

This book consists of a collection of somewhat expanded versions of the papers presented at the symposium on isotope separation held in Amsterdam in April 1957. There are 63

chapters, one for each of the papers presented. These are grouped according to the method of separation adopted. Thus, for example, Part III of the book consists of 10 chapters on the chemical exchange method of separation. There are 2 chapters on ultracentrifuges, 13 on electromagnetic separation, 10 on diffusion, 7 on thermal diffusion, 11 on distillation and related topics, 6 on electromigration and 4 on chemical engineering aspects. Five chapters are in French, 11 in German, and the remainder in English. The papers in French and German have abstracts in English.

The contributions differ very widely in their nature and in their length. A few chapters are mere abstracts of one or two pages, some consist of reviews, while many refer to particular experimental or theoretical work, most of which has not previously been published in detailed form.

This book will be welcomed by all who work in the field of isotope separation. Never before have so many papers on the many and diverse methods of isotope separation been gathered together under one cover. It is, of course, not a textbook, but it contains enough authoritative articles to ensure its success as a reference book.

The publishers are to be congratulated on the excellence of the production; after having seen the book one is less shocked by the price.

T. F. JOHNS

Electromagnetic isotope separators and applications of electromagnetically enriched isotopes. By J. KOCH (Editor), R. H. V. M. DAWTON, M. L. SMITH and W. WALCHER. (Amsterdam: North Holland Publishing Co., 1958.) Pp. xi + 314. Price 53*s*.

This is a very welcome book on a subject which had its beginnings 24 years back, which has grown to undreamt-of proportions during and after the war, and of which this is the first comprehensive monograph. It is written by a team of experts with first-hand experience in electromagnetic separators. The Editor, J. Koch, is in charge of the isotope separator of the Institute of Theoretical Physics in Copenhagen. W. Walcher, who started working in this field in 1937, is the designer of the Marburg separator, while R. H. V. M. Dawton and M. L. Smith are in a position to report competently not only on the British but also on the American work, during and after the war.

The first four chapters, by J. Koch, contain a historical introduction which leads up to the modern medium-size separators of Marburg (Walcher), to the four, essentially similar, separators of Copenhagen, Stockholm, Uppsala and Gothenburg, and to the Saclay separator (Bernas), which has many striking original features. Chapters V–VIII, by Dawton and Smith, are perhaps the most impressive, as they give a brief but comprehensive description of the astounding wartime development in the United States, which, within a few years raised the electromagnetically separated quantities from micrograms to grams in the largest electromagnetic machines ever built, the separators of Oak Ridge which weigh over 5000 tons each. The authors describe in more detail the smaller but still gigantic Harwell machines, the 180° separator (with a magnet weighing 400 tons), and the 90° separator for radioactive materials (HERMES), with its almost fantastic safety precautions. Dawton and Smith contribute three further chapters on operational experiences, and on the chemistry and applications of enriched isotopes. The last three chapters are the work of W. Walcher, which treat somewhat briefly but competently the ion-optics of separators, the physics of arc sources, and the mechanism of space charge neutralization. If the chapter on the physics of arc sources appears less satisfactory than the rest, this is not the fault of the author but of the subject. The arc "played such phantastic tricks under High Heaven" as to beat the brilliant British-U.S. team, but by rousing the permanent interest of some members of the team, it became one of the main causes of our present better understanding of plasmas in magnetic fields.

By the nature of things only a small number of physicists or engineers will ever be required to design or to operate electromagnetic separators. The chapter on the application of isotopes on the other hand may appeal to a very wide circle of scientists. But the book may be recommended also to those who have no professional connexion with electromagnetic separators or isotopes, because it tells in a masterly way the fascinating "success story" of a physical instrument which has grown into a giant.

D. GABOR

Physics of nuclear fission. Translated from the Russian by J. E. S. BRADLEY. (London: Pergamon Press Ltd., 1958.) Pp. vi + 182. Price 60*s*.

The U.S.S.R. Academy of Sciences held a conference in January 1956, to discuss the physics of fission, and the papers presented to the conference subsequently appeared in book form. Dr. Bradley has made an excellent translation of the text and the English reader is now able to judge the level which Russian work on the subject had reached at that time.

Those physicists who have only a slight knowledge of fission physics will find this volume to be a valuable textbook for introducing them to the subject. Fission theory is briefly described, and this is followed by chapters dealing with fission cross-sections, and the other well-known features of neutron induced fission, the charge and mass distributions of the fission products, the number of neutrons emitted and their energy spectrum. Separate chapters cover spontaneous fission, photofission and fission thresholds. Over four hundred references to original work are given, and a large proportion of them refer to work printed in English. The book is well printed and is well illustrated by diagrams.

D. J. LITTLER

Progress in nuclear physics. Vol. 6. Edited by O. R. FRISCH. (London: Pergamon Press, 1957.) Pp. vii + 297. Price 84*s*.

The main emphasis in Vol. 6 of Professor Frisch's *Progress in nuclear physics* is on isotopic masses and isotope separation. On the first topic, there are two very comprehensive articles by H. E. Duckworth for $A > 40$ and by J. Mattauch and F. Everling for $A < 40$. These describe in full detail both direct determinations and the data obtained in nuclear disintegrations. The description of isotope separation methods fulfils a real need, since very little has been written on the subject. M. L. Smith gives an excellent account of the electromagnetic separation process, originally designed for separating uranium, but now mainly used for the preparation of targets of various indispensable isotopes for nuclear physics work. The general article on multistage methods by T. F. Johns is unfortunately too brief and, presumably for reasons of secrecy, the most important process, that of membrane diffusion, is hardly referred to at all.

Related to the articles on masses, there is a very useful article on nuclear moment and spins by K. F. Smith which surveys the experimental methods and the results obtained. G. N. Walton contributes an article on fission recoils, most of which is concerned with slowing down effects, and chemical effects in materials.

There is a valuable article on mesonic X-rays by M. B. Stearns, and the volume is completed by two articles on

***

theoretical physics, one by R. J. Eden on nuclear models and the other a rather brief account by O. R. Frisch and T. H. R. Skyrme on parity non-conservation in weak interactions. Unfortunately the subject of the last has moved so rapidly, both experimentally and theoretically, that the description given is already somewhat incomplete.

H. W. B. SKINNER

Nuclear masses and their determination. By H. HINTENBERGER. (London: Pergammon Press Ltd., 1957.) Pp. vi + 267. Price 84*s*.

The need for more precise measurement of the nuclear masses became apparent some ten years ago when it was found that the values accepted at that time did not always satisfy the energy equation in the study of a nuclear reaction. This led to an extensive redetermination of the masses by both mass spectroscopists and nuclear physicists. The book reports the problems encountered in those measurements and is the proceedings of a conference held in July 1956 at the Max Plank Institute for Chemistry, Mainz, Germany.

The methods of mass spectrography and of nuclear reaction studies are described in detail. The results obtained are critically discussed and some of the papers attempt to resolve the discrepancies which still exist. The papers are largely concerned with the experimental techniques and instruments constructed for this field of research. It is an authoritative publication, containing a wealth of practical information which will be invaluable to mass spectroscopists and nuclear physicists concerned with the problems of mass measurement.

The inclusion of a table summarizing the accepted values for the nuclear masses would have been useful.

G. H. PALMER

The cosmic radiation. By J. E. HOOPER and M. SCHARFF. (London: Methuen and Co. Ltd., 1958.) Pp. 172. Price 12*s*. 6*d*.

During the last decade our knowledge of the properties of the primary cosmic radiation and its behaviour in the earth's atmosphere has developed enormously. Several long monographs and very many review articles on this work have appeared; the present book, however, is a very useful introduction to the subject, covering almost all the main topics of current activity. Naturally, in the space of 172 small pages, the authors have only been able to give a sketchy treatment of the subject, nevertheless, the treatment is not superficial or even elementary.

The plan of the book is conventional, it contains chapters dealing with experimental techniques, the nature of the primary radiation, the properties of nuclear and electromagnetic interactions, the unstable particles produced by the radiation in the atmosphere, a general description of the degradation of the primary energy in the atmosphere and finally some brief comments on the spectra of the cosmic-ray particles at sea-level and underground.

The book is well written and produced and should be particularly valuable to the physicist who wants a brief but reasonably up to date (January 1957) account of the subject. It will also have a limited use as an introductory book for intending research workers in the field of cosmic-ray or high-energy physics.

C. C. BUTLER

Cosmic electrodynamics. By J. W. DUNGEY. (London: Cambridge University Press, 1958.) Pp. ix + 183. Price 32*s*. 6*d*.

Dr. Dungey's book on cosmic rays has appeared at a very opportune moment. It is quite clear now that the evolution of the galactic system has been governed in large measure by electromagnetic effects. Since the pioneer work of Alfvén on magnetohydrodynamics very great interest has developed in this complicated subject. Only the elements of it are understood and there is immense scope for further work, both mathematical and experimental. Quite independently of the realization of the importance on a cosmic scale of the properties of highly ionized matter moving in electric and magnetic fields, the exciting problem of obtaining controlled fusion reactions brings in very nearly the same physical principles. At the recent Atoms for Peace Conference at Geneva there were very many contributions to the theory and experiment of obtaining high temperatures essentially by magnetohydrodynamic means. Though it may take several decades to achieve success, many scientists believe that it should be possible to harness the energy of the fusion of the light elements for producing useful power. This, at any rate, is the main incentive for the vast amount of work in progress all over the world in this field.

This book covers in an elegant and straightforward fashion the physics of motion of highly ionized matter under the influence of electromagnetic fields. Dr. Dungey's special interest is towards the galactic and solar applications, and his book can be strongly recommended to any student of this subject. A considerable part of the book, however, is also applicable to students of plasma physics in the laboratory, and is greatly to be welcomed.

P. M. S. BLACKETT

Missile engineering handbook. By C. W. BESSERER. (New York: D. Van Nostrand Co. Inc.; London: D. Van Nostrand Co. Ltd., 1958.) Pp. xi + 600. Price 109*s*.

This American book is one of a series on principles of guided missile design. The volume on "Guidance" was reviewed in this *Journal* in May, 1956, and was considered a worthwhile addition to the literature generally available in this field. The present volume is not likely to prove so useful, at least to readers in this country. In judging it, one has to remember that it is primarily a handbook intended for American designers, but even so one is left with an impression of lack of selectivity.

The book is intended to be a compendium of design data appearing in the series and other unclassified literature, together with a glossary of terms for those needing a working vocabulary in this field. The glossary occupies about one third of the book and covers terms in fields from nuclear physics to contract documents, production and service use. The author says in his foreword that he hopes to contribute to standardization of terminology and to understanding between different technical disciplines. No authorities are given for the terms and definitions, jargon is admitted, and some of the information is of a transient nature.

The first section of the book, "General data," opens with a table of U.S. guided missiles, which must quickly be out of date, and continues with data and conversion tables of the type generally available. A 24-page section on properties of the atmosphere follows. The third section, of about 50 pages, covers environmental data and reliability. About one half is general information and the rest covers requirements of American military specifications. The largest section, after the Glossary, deals with "Properties of materials structures" and, not unnaturally, is largely concerned with properties of materials available to American designers. There are short sections on aerodynamics, propulsion and "avionics" and a section on space flight is included. The "avionics" section is similar to a fairly simple radio engineer's handbook, with

more emphasis than usual on radar. Even so, the radar range equation gets only elementary treatment. The electronics of control, and control as a subject, receive only about three pages outside the glossary.

The design of guided weapons embraces so many techniques that it is doubtful if one handbook can usefully cover the whole field. If it contains information on military specifications and proprietary materials it will quickly be out of date. The present book will be of most use to anyone who has to deal with American equipment or information. Even so, it may have to be treated as a year-book rather than a handbook.

R. J. CLAYTON

The exterior ballistics of rockets. By L. DAVIS, Jr., J. W. FOLLIN, Jr., and L. BLITZER. (New York: D. Van Nostrand Co. Inc.; London: D. Van Nostrand Co. Ltd., 1958.) Pp. v + 457. Price 64*s*.

Those who expect to find an up-to-date account of modern rockets in this book will be disappointed. This is no fault of the authors but is an inevitable consequence of the fact that modern rockets are weapons of war and published accounts of them are subject to security regulations. In fact, the book deals with the basic theory of the exterior ballistics of simple rockets which have no moving control surfaces, operated by human or automatic pilots, and is based on a number of originally confidential reports about developments during World War II. Since that time, significant advances have been made but it is the authors' contention that the basic concepts and treatments of solid-fuel rockets which they present remain still, and indeed permanently, useful as a foundation for more advanced treatments. Whether this is adequate justification for a book of this magnitude, detail and price, is for the reader to judge.

The trajectory of a rocket depends very much on its motion during the burning of the propellant, and so the study of this motion, and of that after the jet force ceases, constitutes the principal problem of exterior ballistics. The study of the burning process, of the flow of gas through the nozzle, and the production of the force that accelerates the rocket is the concern of internal ballistics and so is outside the scope of the book.

The treatment is mathematical throughout but necessarily incorporates a good deal of experimental data, particularly about the aerodynamical forces opposing the rocket's motion. After a general introduction the account is grouped under the two main self-explanatory headings of fin-stabilized rockets and spin-stabilized rockets. The forces on each type of rocket are considered and general equations are set up describing the rocket's motion during burning and launching and also after burning has ceased. Considerable attention is devoted to an examination of sundry approximations which render the differential equations solvable by formal methods. Comparatively little use appears to have been made at this stage of numerical methods though doubtless subsequent technical developments have been greatly influenced by the advent of high-speed computers. Numerous graphs are presented to help with the evaluation of the functions describing the behaviour of the rockets. In addition, tables of some of the more important functions are given to five decimal places. Fresenel integrals and associated functions feature largely in the theory and tabulations.

Parts of the book, such as the treatment of the dynamics of axially symmetric rigid bodies, are of interest in themselves apart from their application to rockets. The book is lucidly written and excellently produced. The reviewer looks forward to the publication of a further edition which will contain much information at present classified as "top secret" or even higher.

J. CRANK

Numerical analysis. 2nd ed. By D. R. HARTREE. (London: Oxford University Press, 1958.) Pp. xvi + 302. Price 42*s*.

It is fitting that this second edition should appear so soon after the author's untimely death since it reflects so much of his interests and personality. The book is essentially a record of the late Professor Hartree's teaching of numerical analysis in Cambridge. There are many books on this subject in these days, but this one is outstanding for its severely practical approach so typical of the author. This is the book for those who wish to practise numerical methods rather than to read about the formal theory of them.

There are a number of additions to the first edition. Gaussian quadrature formulae, using values of the integrand at unequal intervals in the independent variable, are treated more fully, as also are differential equations with two-point boundary conditions. The chapter on partial differential equations has been enlarged. An introduction to Whittaker's cardinal function has been included. The final chapter on automatic digital computers has been considerably shortened in view of other publications on the subject.

This is likely to remain a standard textbook on numerical analysis for many years.

J. CRANK

Digital computer components and circuits. By R. K. RICHARDS. (London: D. Van Nostrand Co. Ltd., 1957.) Pp. vii + 511. Price 64*s*.

This is essentially a textbook on the engineering side of computer design, and is intended as a sequel to the author's earlier book, *Arithmetic operation in digital computers*, which dealt with the overall organization of a computer. It is clearly and carefully written, the bibliography is comprehensive and the author gives a well-balanced account of design problems over which some controversy still exists, such as the merits and demerits of synchronous and asynchronous circuitry. From the point of view of the physicist interest will mainly centre on the accounts of transistor and magnetic core circuits given in Chapters 4 and 5, since these elements are still to some extent under development in the laboratory. However, increasing numbers of applications of computers to physical problems demand efficient methods of recording data in a form that can be assimilated directly into a digital machine. There is, therefore, much of importance in the last three chapters, and particularly in the discussion of analogue-to-digital conversion in Chapter 11. In view of the general excellence of the book it may appear carping in me to criticize Chapter 1. However, having now read at least five conflicting accounts of the history of computer development, I must protest at yet another incomplete version of the story being given. The author attempts to evade responsibility by phrases like "it is reported that," "so far as is known," and "are generally credited with." If he is so uncertain of who did what, would it not be better to omit names altogether and merely state results? It is only fair to say that he is better informed than most American authors on developments on this side of the water, but I think there is a good case, on the grounds of scholarship as much as those of national prestige, for the preparation of a version acceptable on both sides of the Atlantic—Scientific Historians please note!

A. S. DOUGLAS

Theory of dielectrics: dielectric constant and dielectric loss. 2nd ed. By H. FRÖHLICH. (London: Oxford University Press, 1958.) Pp. vii + 192. Price 30*s*.

In its original edition this book gave a lucid account of dielectric polarization and energy loss, with emphasis on modern mathematical methods of handling these phenomena—a subject to which the author has made many contributions.

The value of the work is attested by the issue, after no long interval, of this second edition. The main text remains unchanged, but is supplemented by new appendices which extend the author's derivation of some very general expressions for dielectric constant in terms of dipolar moment. They also elucidate a crucial point in the theory on which there has been recent controversy. The additions, though described as "paragraphs," in fact run to a dozen pages with some 70 equations.

The only significant error noticed is an obvious inversion of one side of the last equation in the book.

The work can be warmly recommended, especially for its clarity, to all interested in the dielectric properties of matter.

C. G. GARTON

The rheology of elastomers. By P. MASON and N. WOOKEY. (London: Pergamon Press Ltd., 1958.) Pp. viii + 202. Price 50*s*.

This book contains the papers, and discussions on them, read at a conference organized by the British Society of Rheology. It is not a treatise on a particular aspect of the subject since the subject-matter was selected by the individual authors. Apart from three theoretical papers which are of wide application, the contributions are reports of experimental work on a specific property of one material. The substances studied included rubber, gelatine, polythene, Terylene and irradiated polymers. In addition to elasticity measurements there is a paper on each of photo-elasticity and oscillatory testing, mechanical and electrical.

This collection of papers provides a summary of experimental techniques and data which could be useful to other workers with this class of material. The book is well presented and free from typographical errors except for a few divergences between the text and legends of the tables and figures.

C. C. MILL

Rheology. Theory and applications. Vol. II. By F. R. EIRICH. (New York: Academic Press Inc.; London: Academic Books Ltd., 1958.) Pp. xiii + 591. Price 128*s*. 6*d*.

In this short review it is hardly possible to do more than indicate the contents of Vol. II in this series of three volumes on rheology. The volume opens with a chapter by H. Leaderman on the general phenomena of viscoelasticity, with particular reference to high polymers. This is followed by a closely-related treatment of stress-relaxation phenomena by A. V. Tobolsky. Various aspects of transport phenomena, including non-Newtonian flow and diffusion, are then discussed by Taikyue Rhee and H. Eyring in terms of the latter's well-known molecular theory. Later chapters are concerned more specifically with the rheology of particular materials. Thus, organic glasses are dealt with by R. Buchdahl, raw elastomers (mainly rubbers) by M. Mooney, cellulose derivatives by E. B. Atkinson, fibres by R. Meredith, gelatin by A. G. Ward and P. R. Saunders, and asphalts by R. N. J. Saal and J. W. A. Labout. There follows an unusual chapter on rheological problems of the earth's interior by B. Gutenberg, after which it reverts to fundamental methods and techniques for the study of viscoelastic phenomena by J. D. Ferry and by B. A. Toms. The final chapter, entitled "Goniometry of flow and rupture," by A. Jobling and J. E. Roberts, is concerned with effects associated with the normal stress components in viscoelastic liquids.

The Editor, Dr. F. R. Eirich, has performed a valuable service in bringing together so many well-known exponents of the various branches of the subject in this international compilation. He disarms criticism by the admission that a certain amount of overlap or repetition is inevitable in a work of this kind, claiming that the presentation of varying viewpoints on the same subjects may be an advantage. Not all the contributions are equally good, and there is a tendency in certain sections to adopt a somewhat narrow theoretical outlook. Taken as a whole, however, this work provides a balanced view of the rapidly expanding science of rheology, and will be an important source of information for the more mature research worker who is able to bring a critical judgment to bear upon its contents.

L. R. G. TRELOAR

Flame photometry. A manual of methods and applications. By F. BURRIEL-MARTÍ and J. RAMÍREZ-MUÑOZ. (Amsterdam: Elsevier Publishing Co.; London: Cleaver-Hume Press Ltd., 1958.) Pp. xii + 531. Price 65*s*.

The original method of qualitative spectroscopic analysis depending on flame excitation was due to Bunsen and Kirchoff in 1859. Such flame tests were first used for spectrography by Gouy in 1879, who atomized solutions of samples by compressed air and introduced them into a coal gas flame and photographed the spectrum. The earliest direct measurements by visual matching using a spectrograph and a flame were made by Klemperer in 1910 and the first flame photometer constructed on the basis of what is to-day considered characteristic of this apparatus for quantitative determinations, was due to W. Schuknecht about 1937.

In the past twenty years or so there have been notable advances in flame photometry and it has come into use extensively in a number of different fields, especially in the analysis of biological and agricultural materials. The importance of this technique depends on it providing a method of analysis for specific substances, rather than a measurement of some property that is a compounded result of many substances. Further, the equipment required is less expensive than for spectrography and simpler to use. About fifty elements can be detected on excitation to relatively low levels attainable by different types of flames. In quantitative determinations it is possible to obtain results, in general, with an accuracy of about 2%, which can be regarded as satisfactory when it is realized that the concentrations being dealt with are of the order of parts per million. The amount of sample required for many determinations need not be more than 10 mg, and 0·01 mg may serve for some.

The present book on this subject, written by the Professor and the Senior Lecturer in Analytical Chemistry in the University of Madrid, is a comprehensive manual, the first of its kind to be published in English. It will remain, almost certainly, the authoritative work for some time to come. It gives information on the principles and applications of flame photometry, together with accounts of instrumental systems and experimental methods. There is a bibliography of over nine hundred items and, worthy of special commendation, a subject index of fifty-two pages. The book is admirably produced.

W. A. KIRKBY

Surface chemistry. Theory and applications. 2nd ed. By J. J. BIKERMANN. (New York: Academic Press Inc.; London: Academic Books Ltd., 1958.) Pp. x + 501. Price $15.

This is the second edition of Bikermann's *Surface chemistry for industrial research*, and represents a considerable improvement on its forerunner. Theory and applications have been brought up to date, and "chaff" has been deleted.

The book is divided into five chapters on liquid-gas, liquid-liquid, solid-gas, solid-liquid, and solid-liquid-gas, solid-liquid-liquid interfaces, and a final chapter on electric surface phenomena. The subject-matter is independently divided into 340 sections which are articles in themselves. There are ample cross-references, and the author and subject indices are good.

In his treatment of each topic, Dr. Bikermann gives the general theory without rigorous proof and then gives some recent numerical results. After commenting on these he gives some examples from everyday life, and presents the uses to which they have been or could be put. One of the author's aims was to treat his subject as an integral part of physical chemistry, and the reviewer reached the end of the book with the impression that it was as essential a component as, say, the kinetic theory of gases.

The importance of the inhomogeneity of surfaces is emphasized throughout the book, and the author's criticism of surface tension measurements on mercury and industrial mixtures deserves wider dissemination. On pp. 249 ff. elutriation might have been included as a method of particle size determination, and work has been done by the Joint Fire Research Association on the correlation between fire-fighting foam efficiencies and the physico-chemical features of the bubbles (p. 108).

In general the book is well written by one who is not afraid of exhibiting a sense of humour. The printing is good and the text is amply illustrated by line drawings and tables.

J. S. TAYLOR

Chemical engineering practice. Vol. 4. Fluid state. Edited by H. W. Cremer and T. Davies. (London: Butterworths Scientific Publications, 1957.) Pp. 623 + xix. Price 95*s*.

This book, the fourth of twelve volumes on chemical engineering practice deals with the fluid state. The detailed treatment is subdivided into three sections.

The first section on the thermodynamic properties of physical systems is concerned with the theoretical background of the subject. An elementary knowledge of thermodynamics is assumed, and the work is admirably suited for the trained chemical engineer. The subject-matter covers the wide field of physical thermodynamics as required by the chemical engineer including the definition of the thermodynamic functions and the development of their more important relations, the properties of perfect and imperfect gases together with a consideration of the high pressure régime, the liquid phase, the properties of mixtures, and the development of the fundamental equations of fluid flow.

The second section likewise presents a review of the theoretical background of the transport properties of fluids and covers a wide field including fluid statics, the flow of viscous fluids, turbulence, flow within tubes and ducts, flow around objects, and compressible fluids. Many of the formulae of practical interest are derived from basic principles, while the text properly introduces such aspects as relaxation methods, dimensional analysis and modelling. The chapter on turbulence deals extensively with the concept of the boundary layer and is a most useful contribution to the work.

This volume concludes with a section on the measurement of process variables. The chemical engineer should be familiar with the basic principles underlying the design and construction of many instruments now used on chemical plant, and this section thus fulfils an instructive purpose in presenting the principles involved in the measurement of pressure, fluid flow, both in closed and open conduits, liquid level and temperature.

The editors and contributors are to be congratulated on producing a volume which will be an invaluable work for reference to the practising chemical engineer. H. THOMAS

Free radicals in solution. By C. WALLING. (New York: John Wiley and Sons Inc.; London: Chapman and Hall Ltd., 1957.) Pp. xii + 631. Price 116*s*.

Free radicals may be defined as monatomic or polyatomic species having at least one unpaired electron. Since the discovery in 1900 of the triphenyl methyl radical an immense, coherent, body of knowledge concerning them has developed. Their stabilities, defined as the average lifetimes between creation and destruction, are determined on the one hand by the mode and rate of their formation, and on the other by their reactivity with themselves and their environment, and range from microseconds to years. The reactivity depends upon such intrinsic properties of the radical as the ionization potential, electron affinity, degree of delocalization of the unpaired electron and on the nature of the medium which may solvate the radical and control its mobility, and on the concentration and nature of potentially reactive solutes. Their main importance is the role which they occupy as the intermediates in a very large number of chemical reactions—especially chain reactions.

Dr. Walling has made his own considerable and distinctive contribution to knowledge of this field and his book is an admirably balanced and lucid account of free radicals in liquid solutions. After describing the structure and physical properties, with justifiable emphasis on the magnetic properties, the author devotes about 200 pages to free radicals in reactions which result in the formation of macromolecules. This is followed by approximately another 200 pages dealing with non-polymeric systems such as oxidation, halogenation and related reactions. The book concludes rather curiously with two chapters on radical formation which might more logically have appeared at the beginning. Throughout, the author's attitude is a splendid blend of the imaginative and realistic, nowhere better expressed than in footnote 23 on page 38, and Dr. Walling combines the disciplines of physics, reaction kinetics and organic chemistry in a most illuminating fashion. There is no doubt that it will achieve the author's object of clarifying existing knowledge and stimulating further research. Its weaknesses lie, as they inevitably must, in those fields with which the author has least direct acquaintance, e.g. radiation chemistry and free radicals in aqueous solution where the virtual omission of reference to the reactions between metal ions and organic free radicals has made the discussion unnecessarily obscure. However, such criticisms of emphasis are somewhat subjective and will inevitably arise if a book on this vast subject is to be a single volume of manageable dimensions. The book is remarkably free from typographical errors—misspellings were detected only on page 191 line 8, pages 354 and 600 (Chanmugam) and reference 57 page 555. F. S. DAINTON

The powder method in X-ray crystallography. By L. V. AZÁROFF and M. J. BUERGER. (New York: McGraw-Hill Book Co. Inc.; London: McGraw-Hill Publishing Co. Ltd., 1958.) Pp. xv + 342. Price 68*s*.

The introduction states that the purpose of this book is to guide the physicist, chemist, metallurgist, or even someone without much scientific background, in the taking of powder photographs and the interpretation of them. Its 16 chapters cover a wide field, and are of very uneven merit. The best sections are those devoted to the indexing of powder photographs and the deduction of the unit cell. There is a very full treatment of Ito's method, and of the Delaunay reduction. The beginners postulated by the authors in their introduction, however, will find these sections very tough going. Although the book is called "the powder method" the discussion is confined entirely to powder photography. Diffractometers get 12 lines on p. 3.

There are a number of ambiguities likely to confuse the beginner. For example, on p. 217 and again on p. 236 it is stated that the error due to vertical divergence is proportional to $\cot^2\theta - 1$. On the first of these pages there is a footnote pointing out that this expression is incorrect, but your reviewer was unable to find the correct expression anywhere in the book. Again, on p. 262, in describing the appearance of powder photographs, it is stated that stacking faults leave the small-angle side of a line sharp, whereas on the high-angle side the intensity of the line declines very gradually. This description is correct for photographs of random layer structures, discussed on p. 263.

The reviewer's conclusion is that the beginner would be well advised to avoid this book, but the worker with enough experience to sort out pitfalls of the kind just mentioned will find much to interest him.

The book ends with a number of tables, including an extensive one (45 pages) of the relation between d and $1/d^2$. There is a good index.

A. J. C. WILSON

Spectrochemical abstracts. Vol. 5. *1952–1953.* By E. H. S. VAN SOMEREN and F. LACHMAN. (London: Hilger and Watts Ltd., 1958.) Pp. 66. Price 20*s*.

The abstracts contained in this volume cover papers for the years 1952–1953 and relate to emission spectroscopy in its analytical applications. Flame spectroscopy is included, but not X-ray emission spectroscopy. The publishers hope that a further volume covering the years 1954–1955 will appear shortly.

Magnetohydrodynamics. By T. G. COWLING. (New York: Interscience Publishers Inc.; London: Interscience Publishers Ltd., 1958.) Pp. viii + 115. Price 25*s*. (paper bound 14*s*.).

The author mentions in his preface that when work on this book began its main applications were to geophysical and astronomical problems, but that now engineering applications are evident. The master work by Chapman and Cowling has long been a classical study in the physics of gases and the present, much shorter, work is of the same high scholarly standard. It forms a companion volume to that of Spitzer in the same series (Interscience tracts on physics and astronomy). It will be quite invaluable for those working on gaseous discharges, particularly those on high temperatures.

Astrophysics still claims a large share of the work, including chapters 2, 3 and 4, which are respectively on magnetohydrostatics, wave motion (as applied to sun spots, etc.), and magnetic fields. Chapter 1 is a general introduction and chapter 5 is on dynamo theories (magnetic field of the earth, etc.). Chapter 6 is on ionized gases and is of very great topical interest and many will hope that it may be expanded by the same author, in the near future, to a full book.

J. D. CRAGGS

The measurement of colour. 2nd ed. By W. D. WRIGHT. (Hilger and Watts Ltd., 1958.) Pp. ix + 263. Price 52*s*.

The new edition of this excellent book has been largely re-written and brought up to date, and is attractively produced. Many of the less important sections have been omitted or condensed and the opportunity taken to expand the treatment of the principles of photometry and colorimetry, and to explain more fully the origins of the CIE system in which the author took so much part. Particular pains are taken to explain, by simple analogy, the meaning and use of that confusing (and by many thought to be unnecessary) concept—the trichromatic unit. The chapter on colour atlases is much enlarged and skilfully developed from the general standpoint of the problem of colour spacing by subjective judgments. There is a new chapter on colour reproduction processes including colour television which includes an interesting discussion on the assessment of picture quality.

R. G. HORNER

Modern electroanalytical methods. Edited by G. CHARLOT. (Amsterdam: Elsevier Publishing Company; London: Cleaver-Hume Press Ltd., 1958.) Pp. ix + 186. Price 24*s*.

In 1957, a symposium on modern electrochemical methods of analysis was held in Paris under the auspices of the International Committee for Electrochemical Thermodynamics and Kinetics (C.I.T.C.E.); twenty-two papers were presented and these papers, in different languages, were subsequently published in *Analytica Chimica Acta*, Nos. 1 and 2, 1958. The opportunity has now been taken to bring the papers together under one cover. Many of the authors of the papers are of international repute, e.g. Kolthoff, Laitinen, Barker and Delahay, and the emphasis throughout is on *modern* methods. The field covered is very wide indeed.

The subjects discussed include the reduction of fused chlorides such as cobalt chloride in eutectic mixtures of alkali chlorides, new developments in "dead stop" end point titrations, potentiometry at constant intensity and the plotting of intensity potential curves in ion exchange resins. Coulometry, millicoulometry and the coulomb as a universal standard in analytical work, adsorption kinetics and electrode process are all dealt with. New developments in radiochemical procedures and in the use of the rotated dropping mercury electrode are described and attention is drawn to the application of the hanging mercury drop electrode in analysis. Current scanning polarography, square wave polarography and oscillopolarographic micro-analysis all find a place, whilst there are papers which deal with high frequency titrimetry in analysis and a final paper on new methods of determination of electrical conductivity. Most of the papers conclude with a useful bibliography and a valuable feature is the inclusion of the discussion on the individual papers.

This is definitely not a book for the casual reader. It will be useful to those analytical chemists interested in electrochemical procedures who wish to obtain new ideas by the intensive study of original papers; though not always the most popular, this method is usually the most rewarding.

Moreover, instrument manufacturers seeking to get the right ideas about the best instruments to develop in this particular field will do well to bear this collection of papers in mind.

J. HASLAM

Dictionary of physics. By H. J. GRAY. (London: Longmans, Green & Co., Ltd. 1958.) Pp. x + 544. Price 84*s*.

Aldous Huxley once said that the best reading on holiday was to be found in a volume of the *Encyclopaedia Brittanica* chosen at random; a dictionary provides something of the same inconsequent fascination, but unless it is of monumental size suffers from the defect that it dispenses its information in exasperatingly small doses. The *Dictionary of Physics* succeeds in satisfying the enquirer because many articles are long enough to give a bird's-eye view of the subject, and references to other authorities are frequent and to the point. Browsing within its covers is insidiously easy, cross references leading one from entry to entry.

Generally speaking it is true to say that modern developments and discoveries are well represented, especially in the field of nuclear physics. There are however gaps, some of them surprising. For instance, on looking up "Coriolis," one is directed to an entry under "Force," where Coriolis forces are mentioned as being involved in problems of projectiles shot from the surface of the rotating earth; artificial satellites are not listed, so naturally "sputniks" are not to be found, but under "rockets" there is no entry save a reference to "astronautics" where, at last, the reader may learn that the Russians launched earth satellites in 1957.

An even more surprising example is the lack of all reference to radio-telescopes, steerable or fixed, and though four lines are devoted to "radio-astronomy" the only reference is to an article in *Nature* six years old. The editor asks for suggestions for future editions and will doubtless have a ready response. His task is unenviable but he has achieved much and many readers will be grateful to him and his contributors. The inclusion of numerous biographical notes will gladden the hearts of those older physicists to whom ignorance of the great names of science is a distressing characteristic of the younger generation in whose eyes history is often of little consequence.

A. M. TAYLOR

Television in science and industry. By V. K. ZWORYKIN, E. G. RAMBERG and L. E. FLORY. (New York: John Wiley and Sons Inc.; London: Chapman and Hall Ltd., 1958.) Pp. xii + 300. Price 80*s*.

This book is written by three well-known specialists of the R.C.A. Laboratories and headed by that remarkably active pioneer of television, Dr. Zworykin. It may be regarded as the industrial user's guide to television.

The first chapter gives an historical outline of the technical development of television from early myth to the modern electronic systems. This is well done, except for the selective reporting which ignores the fact that the regular electronic television service, substantially as it is to-day, was begun in London in 1936—some nine years before it began in the U.S.A.

Then follows a chapter devoted to outlining ways in which closed circuit television might be used to advantage. This seems slightly redundant as it could have been covered in the later chapter dealing with actual applications.

The third chapter is devoted to a technical outline of closed circuit television channels. The authors describe the principal pick-up tubes, the camera optical systems, the basic operating circuitry and picture display apparatus. This is done for single- and multi-channel monochrome, for field-sequential and simultaneous (N.T.S.C.) colour television, and stereoscopic systems. In addition, the two types of television microscope and the colour translating television microscope are described.

Having laid down the essential technical basis a long list of possible and actual applications are described in Chapter 4. These cover a wide field of physical, engineering and biological research and practical applications in medical, engineering, business, educational, and military fields.

The book will be very useful to those who wish to find out if television can help them solve their problems which may range from baby-supervision to space-vehicle instrumentation.

J. D. MCGEE

Transistor technology. Vol. 1. By the members of the technical staff of Bell Telephone Laboratories. Edited by H. E. BRIDGERS, J. H. SCAFF and J. N. SHIVE. (London: D. Van Nostrand Co. Ltd., 1958.) Pp. xxxvii + 661. Price 131*s*. 6*d*.

This book is based on the texts presented at a symposium on transistors in 1952. It presents the fundamental principles of the subject, and is intended to provide a basis for two further volumes, dealing with modern developments in transistor materials, and in the design of devices and the techniques for producing them.

Volume 1 deals exclusively with germanium and devices made from this material. The first section, of 60 pages, covers the preparation of the semiconductor and includes a detailed account of zone-melting. The second section (100 pages) deals with the growing of high quality single crystals by the pulling process.

The third section, of 280 pages, discusses the principles of device fabrication. There is a short treatment of the basic theory of p–n junction diodes and triodes, followed by an account of the physical properties of the germanium appropriate for different types of device. This leads to a description of methods of evaluating the material, especially by measurement of resistivity and lifetime. Methods for locating junctions in grown crystals are then discussed. The preparation of the germanium by cutting, lapping, surface treatment, etching and plating is dealt with in detail, followed by the provision of contacts of various types, the problems of hermetic sealing and capsulation, and the final electrical processes for forming and pre-aging of devices.

Section 4 (150 pages) deals with transistors as circuit elements, and the different means of characterizing their performance. Various types of characterization parameter can be defined, and the measurement of these is described in detail for both the small- and large-signal cases.

The final section, of 20 pages, deals with the reliability of transistors and their specification and evaluation.

The book is well produced and will be regarded as a standard text on the subject.

D. A. WRIGHT

Advances in electronics and electron physics. Vol. IX. By L. MARTON. (New York: Academic Press Inc.; London: Academic Books Ltd., 1957.) Pp. x + 347. Price $9.00.

The present volume in this series represents a departure from previous practice in that it is devoted to topics which may be broadly described as geophysical. Electronics and electron physics are featured only in so far as they are relevant to these topics. There are seven separate articles covering the Aurora Borealis, negative ions, radio observation of meteors, intensity variations in cosmic rays, radio-wave

propagation, oceanography and finally seismology and geomagnetism. Each article is authoritatively written and the whole will make valuable and informative reading for anyone generally interested in geophysics. To the expert in electronics, however, it must represent a rather heterogeneous collection of articles for general reading, even during the International Geophysical Year. H. ELLIOT

Electronic semiconductors. By E. SPENKE. (New York: McGraw-Hill Book Co. Inc.; London: McGraw-Hill Publishing Co. Ltd., 1958.) Pp. xxvi + 402. Price 85*s*. 6*d*.

This book is a translation of the 2nd edition of *Elektronische Halbleiter*, by Dr. Spenke. The original German text was reviewed by Dr. Jonscher in 1955.* A full account was given there of the contents of the book, and it is only necessary for the present reviewer to point out significant changes.

The translators (Drs. D. A. Jenny, H. Kroemer, E. G. Ramberg and A. H. Sommer of the R.C.A. Laboratories) have presented us with an excellent translation of this most useful book. In accordance with American practice they have added a series of problems at the end of every chapter. They have also augmented Chapter IV with a section on junction capacitance, which is omitted from the German text.

A novel feature of the original text has been lost in this edition of the translation. The coloured diagrams of the various band models now appear in black and white and the clarity of these diagrams has been lost. No doubt the publishers had considered that this would have added to the already very high cost.

This book is to be commended to both the student and the expert for a fully authoritative account of the fundamental physics of semiconductors. P. A. LEE

* *British J. Appl. Phys.* **6**, p. 341 (1955).

The kinetics of vinyl polymerization by radical mechanisms. By C. H. BAMFORD, W. G. BARB, A. D. JENKINS and P. F. ONYON. (New York: Academic Press Inc.; London: Butterworths Scientific Publications, 1958.) Pp. xii + 318. Price 50*s*.

The scientific interest and industrial importance of polymerization reactions with free-radical mechanisms have led to the publication of a vast bulk of work in the last ten to fifteen years. The chemistry of these reactions is complex, and it is only during this period that their mechanisms have been understood in any detail; many obscurities still remain.

This book is an able and critical survey of the field. Its main emphasis is on the principles that are applied to the analysis of the kinetics of free-radical polymerizations, and on the results that have been obtained, rather than on detailed experimental techniques. The last chapter is mainly mathematical and discusses the distributions of such properties as molecular weight, and composition in copolymers. References are plentiful.

Most polymer chemists will find something of interest in this book, and to some it will be a valuable work of reference. An author index, however, would have enhanced its value. P. A. SMALL

Les ondes centimétriques. By G. Raoult. (Paris: Masson et Cie., 1958.) Pp. vii + 401. Price 6 500 fr. (paper bound), 7 300 fr. (linen bound).

The author acknowledges in his introduction that much of the original work in this field was carried out "in the Anglo-Saxon countries" and was consequently described in English. The compliment may be returned for it is unfortunate that the present work is not in English and so tends to be rather beyond the reach of those who have not even troubled to keep up to date their schoolboy French. Fortunately, however, the literary style is simple and thus can be easily followed by the most casual linguist.

The work is more comprehensive than most of its kind. It covers all the usual introductory theoretical matters (propagation in unbounded and bounded media, etc.), technical subjects (oscillators, amplifiers, wave-guide techniques, antennae, etc.), and techniques of measurements, etc. There are interesting chapters on optical analogues, radio astronomy and paramagnetic resonance, and, even in the chapter on detectors, an excursion into elementary solid state theory. J. D. CRAGGS

Mesure et détection des rayonnements nucléaires. By J. SHARPE and D. TAYLOR. Translated by J. CHATELET. (Paris: Dunod, 1958.) Pp. xi + 319. Price 3400 fr.

This book is a French translation from the second editions of two well-known Methuen Monographs, namely *Nuclear radiation detectors* by J. Sharpe and *The measurement of radioisotopes* by Dennis Taylor. The translator has combined these two monographs into a single volume, dividing the subject-matter into three parts with a short introduction. In the introduction the translator has used sections from the introduction of both the original works which fit together extraordinarily well. The first part of the book deals with measurements of radioactivity, and is taken entirely from Taylor and the second part about the physical phenomena of detection is taken from Sharpe. The third part concerning apparatus is taken from the relevant sections of both the original works.

The translator has not altered the text more than is necessary for the purposes of the translation and has added brief footnotes where he considers some small point requires clarification for French readers. The presentation of the book on larger sized paper and in larger print makes it easier to use than the English originals, but the French reader certainly has to pay for this privilege. G. W. DOLPHIN

Les piles atomiques à neutrons lents. By J. MAURIN. (Paris: Dunod, 1958.) Pp. xii + 197. Price 980 fr.

This book is an introduction to the physics of thermal neutron reactors for French readers. After a short qualitative account of the subject, a description is given of the calculation of neutron behaviour in thermal reactors, including a detailed account of the calculation of the critical size of a heterogeneous thermal reactor by diffusion theory. The book consists of more detailed mathematical analysis than is necessary for the beginner in the field though the practising reactor engineer or physicist may find a need to refer to the standard works on the subject. The book does not discuss in detail the implications of the results derived, the limitations of the methods used, and the important experimental aspects of the subject. J. J. SYRETT

Elektronik freier Raumladungen. By F. OLLENDORFF. (Wien: Springer-Verlag, 1957.) Pp. xii + 620. Price £8 7*s*.

This book is the result of a sustained effort in applied mathematics of which only its author is capable. For more than 30 years Professor Franz Ollendorff of the Technion, Haifa, has produced well-known textbooks on potential

theory, earth currents, high frequency theory and electronics. This volume is the third of his monumental *Technical Electrodynamics*. The first was on the "Calculation of magnetic fields," the second on "Electronics of single electrons" (electron optics), and the present volume will be followed by three others on "Kinetic theory of electrons" (noise and quantum mechanics), "Crystal electronics" and "Ionics."

The present volume displays on every page the individual characteristics of its author. It covers the vast field of space charge phenomena more thoroughly than any other known to the reviewer, and it covers it in a very systematic way. Yet the result is not a textbook but a reference book. The treatment is "atomistic"—that is to say each problem is considered by itself. A few assumptions are made, the equations are quickly set up, and the mathematical machine is set into operation until it has ground out the result in the form of long formulae, displayed in great detail and at full length, made even longer by the German standards of mathematical printing. Though the formulae are often illustrated by painstakingly computed curves there is hardly ever an illuminating remark throwing light on their physical content. General principles, if they appear for a moment in the introduction of the problem, are soon hidden from sight. No intuitive insight is granted to the reader, nor is he given any hint of the historical origin of the problem, and (with rare exceptions) of the author who first solved it.

Though an enormous bibliography is attached to the book, this is subdivided by chapters only, and there are no detailed references to it in the text, hence the reader will have great difficulty in locating the relevant papers. This "anonymous" method is hardly fair in a field which owes so much to brilliant individuals such as Langmuir, Schottky, Brillouin and Pierce. Besides, the field is not as closed and dead as the author seems to believe, and the student who diligently plods through the 600 pages of this work has a right to expect some indication of unsolved problems, and of unexplained discrepancies between theory and experiment on which he could start exercising his powers. It is quite likely that, owing to his long isolation from practical electronics, the author himself was not sufficiently aware of such discrepancies as arise for instance in magnetrons. This isolation explains also his overrating of the value of long final formulae, which are too complicated to give physical insight, but which might help the tube designer. He does not seem to be aware of the fact that tube designers have never used anything but the simplest approximate formulae, and nowadays they use no formulae at all, because their vast accumulated data enable them to obtain any new designs (on the rare occasions when they are needed), by interpolation and by scaling methods, checked by experiments.

As one may well expect from a book by Prof. Ollendorff, the text contains many original contributions, such as, quoting from the blurb, "the derivation of the Maxwellian velocity distribution from a phenomenological integral equation, the introduction of Green's function in the potential theory of valves, the simplified treatment of electron trajectories in the grid zone, the synthesis of the field of oscillating electrons by means of moving plane surface charges, and the description of electronic travelling waves by means of generalized Hertz and Fitzgerald vectors." Whether the first-mentioned of these represents a gain in physical insight or not, a complaint must be made on behalf of the novice reader against the way in which the author deals with the integral equation. He goes through all the motions of solving it, without mentioning in so much as a word that it is an equation of the well-known Abel type. Later, when the equation crops up again, on pp. 217–19, he goes through all the motions again, though this time he discloses that it is an Abel-type equation. If this sort of repetition had been avoided, the book may well have been shortened by a third. A little contact with practical electronic research workers would have made the remaining two-thirds twice as valuable.

With all its failings as a textbook, this work remains a unique reference book, and as such can be recommended, in spite of its high price, to the libraries of universities and of electronic laboratories. D. GABOR

Der transistor. By J. DOSSE. (München: R. Oldenbourg GmbH., 1957.) Pp. 207. Price 19.80 DM.

This introduction to transistor techniques starts with simplified physical concepts, explains the operating principles of transistors and reviews the various types that have appeared up to the beginning of 1957. The fourth chapter discusses the various systems of parameters and equivalent circuits used to represent the transistor and includes sections on noise and other practical considerations such as temperature effects, while the next and longest chapter describes a representative selection of transistor circuits.

The reduction of mathematics to a minimum, the lucidity of the presentation—enhanced by the use of coloured diagrams in various sections—and the inclusion of an excellent bibliography to offset the limited scope of this book render it useful to those wishing to acquaint themselves easily and rapidly with basic transistor techniques; an edition in English would be welcome. E. ADLER

Achema Year Book 1956/1958. European catalogue of chemical apparatus and equipment. (Frankfurt: Deutsche Gesellschaft fur Chemisches Apparatewesen, 1957.) Pp. 1068. Price 25 DM.

The *Achema Yearbook* is, essentially, a triennial journal of the German chemical engineering industry justifying its subtitle by including a not too liberal sprinkling of non-German firms. Out of 100 firms, chosen at random throughout this tome, 82 were German, 7 Swiss, 4 French, 3 British, 1 each Danish, Dutch and Italian and 1 American. Geographically, at least, the editors have answered the questions: "Who can supply? Who can furnish information?" which are given as the aims of the *Yearbook*.

Although impressive in its layout and indexed with all the thoroughness usually associated with German publications, the *Yearbook* is poorer than most trade journals in that it attempts too much, covering as it does the manufacture of filter papers and filter plants, of nuts and bolts and entire chemical factories. In providing translations into two and at times four languages, the section "Technical achievements" has been condensed to the point where it is difficult to maintain interest.

But whatever criticism may be levelled against the *Yearbook* as a whole, the section entitled "Research institutions" is excellent, giving concisely the teaching methods and the research projects of 65 major technical colleges teaching one branch or another of chemical engineering in 10 European countries. I know of no other publication which presents the information contained in this section in so readable a manner, each report being written by a prominent faculty member. This section alone makes the *Achema Yearbook* an important reference book for the educationalist, the research director and the employer. H. W. HOLY

Proportional counters in X-ray spectro-chemical analysis

By T. Mulvey and A. J. Campbell,* Research Laboratory, Associated Electrical Industries Ltd., Aldermaston, Berks.

[*Paper first received* 14 *February, and in final form* 22 *April*, 1958]

Proportional counters have been used as spectrometers in experiments in nuclear physics for some time, but their general application to problems of X-ray analysis has been delayed partly for technical reasons and partly through lack of information. The present report reviews existing theories on the proportional counter in order to determine the fundamental limits of resolving power when used as a spectrometer for light elements such as magnesium. A survey of experimental results indicates that only a slight further improvement in performance is required to enable proportional counters to analyse adjacent elements such as magnesium and aluminium, thus allowing one to dispense with an analysing crystal.

INTRODUCTION

In X-ray analysis, difficulties arise in performing an analysis on elements lighter than potassium (19), since it is not easy to find suitable analysing crystals and sufficiently sensitive detectors. The use of a proportional counter is attractive in this region since it can be designed to have a high quantum counting efficiency, a high counting rate (20 000/s), and, furthermore, it is intrinsically energy-sensitive and therefore capable of being used as a spectrometer to perform a chemical analysis without the use of an analysing crystal. The group of elements suitable for analysis by this technique includes silicon, aluminium and magnesium.

A proportional counter consists essentially of a smooth metal wire about 0·1 mm in diameter, accurately aligned along the axis of a metal cylinder, a few centimetres in diameter; the cylinder is filled with a heavy gas such as argon or xenon, which serves to absorb incident X-ray photons. The wire is maintained at a high positive potential, usually about 2 kV, relative to the cylinder. Incident X-ray photons ionize the gas, thus forming a number of pairs of electrons and positive ions; the number formed is proportional to the energy of the incident photon. If the average gas amplification is kept constant, then the average height of the voltage pulse on the central wire is proportional to the energy of the incident X-ray photons and the proportional counter becomes a useful spectrometer for X-ray analysis. The energy resolution of a proportional counter is limited by statistical considerations and by purely technical difficulties. It is the purpose of the present paper to determine the fundamental statistical limit and to suggest means of attaining it in practice.

STATISTICAL LIMITATIONS

In the absence of purely instrumental defects, the mean pulse height from a proportional counter varies directly as the energy of the incident photons. The resolving power is limited by statistical fluctuations in the number of initial electrons N formed by each photon, and in the number of ion pairs A produced by each electron in an avalanche. Frisch[1] has shown theoretically that the relative variance of the output pulse height $(\sigma_P/\bar{P})^2$ is practically independent of the gas amplification factor $\bar{A}$, where σ_P is the standard deviation, and $\bar{P}$ the mean of the pulse height; this has been verified experimentally by Hanna, Kirkwood and Pontecorvo[2] for $\bar{A}E < 10^5$, where E is the energy of the incident photons in keV.

As N is small and $\bar{P} \propto E$, it is reasonable to assume that A is independent of N and it can be shown that

$$\left(\frac{\sigma_P}{\bar{P}}\right)^2 = \frac{1}{\bar{N}}\left(\frac{\sigma_A}{\bar{A}}\right)^2 + \left(\frac{\sigma_N}{\bar{N}}\right)^2 \qquad (1)$$

Snyder[3] and Frisch[1] have shown theoretically that

$$\frac{\sigma_A}{\bar{A}} = 1 \text{ and } \left(\frac{\sigma_N}{\bar{N}}\right)^2 \propto \frac{1}{\bar{N}} \qquad (2)$$

and hence

$$\left(\frac{\sigma_P}{\bar{P}}\right)^2 = \frac{1}{\bar{N}} + \frac{1}{k\bar{N}} \propto \frac{1}{\bar{N}} \qquad (3)$$

Fano[4] has discussed the value of k, the coefficient associated with the formation of initial ions, and estimated it to be between 2 and 3. Hence, taking an average value for k

$$\left(\frac{\sigma_P}{\bar{P}}\right)^2 \simeq \frac{1{\cdot}4}{\bar{N}} \qquad (4)$$

Valentine[5] and Weiss and Bernstein[6] have determined the energy loss per collision in argon and found that $E/N = 0{\cdot}0264$ and $0{\cdot}0255$ keV respectively. If a value $E/N = 0{\cdot}026$ keV is accepted (4) becomes

$$\left(\frac{\sigma_P}{\bar{P}}\right)^2 \simeq \frac{0{\cdot}0364}{E}$$

Therefore

$$\frac{\sigma_P}{\bar{P}} \simeq \frac{0{\cdot}19}{E^{1/2}} \quad (E \text{ measured in keV}) \qquad (5)$$

Values of $\sigma_P/\bar{P}$ for energies between 0·25 and 70 keV have been found experimentally by Hanna and his co-workers,[2] Curran, Cockroft and Angus,[7] Arndt, Coates and Crathorn,[8] Bisi and Zappa,[9] Lang,[10] West and Bradley,[11] and by the present authors; the results are plotted in Fig. 1. It will be sufficient to remark at this stage that the values of $\sigma_P/\bar{P}$ obtained here are in agreement with the early work of Curran and his co-workers, but higher than those of Bisi and Zappa.

It is difficult to assess the comparative accuracy of the experiments mentioned above, but certain tests can be applied, particularly where data have been obtained over a wide energy range. In this connexion, it is of great interest to separate the variance $(\sigma_P/\bar{P})^2$ into its components

$$\frac{1}{\bar{N}}\left(\frac{\sigma_A}{\bar{A}}\right)^2 \text{ and } \left(\frac{\sigma_N}{\bar{N}}\right)^2$$

as given by equation (1). Curran and his co-workers have

* Now at Trinity College, Cambridge.

done this by investigating the pulse height distribution from single electrons (i.e. $N = 1$) and found that, in this case

$$\left(\frac{\sigma_P}{\bar{P}}\right)^2 = \left(\frac{\sigma_A}{\bar{A}}\right)^2 = 0{\cdot}681$$

Hence, (1) may be written

$$\left(\frac{\sigma_P}{\bar{P}}\right)^2 = \frac{0{\cdot}681}{N} + \left(\frac{\sigma_N}{\bar{N}}\right)^2 \qquad (6)$$

so, taking $E/N = 0{\cdot}026$ as before

$$\left(\frac{\sigma_P}{\bar{P}}\right)^2 = \frac{0{\cdot}0177}{E} + \left(\frac{\sigma_N}{\bar{N}}\right)^2 \qquad (7)$$

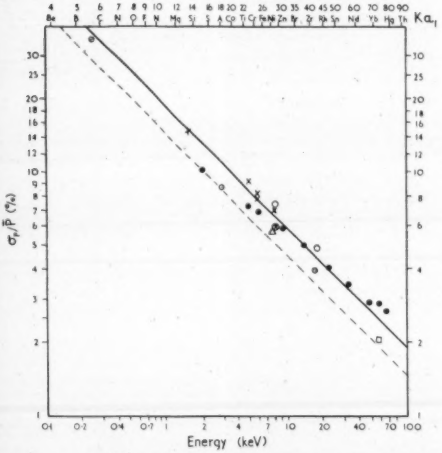

Fig. 1. Relative standard deviation of pulse height distribution with energy

——— theoretical (Snyder, Frisch, Fano).
– – – empirical [equation (8)].
× Mulvey and Campbell.
● Bisi and Zappa.
○ Hanna, Kirkwood and Pontecorvo.
△ Arndt, Coates and Riley.
○ Curran, Cockroft and Angus.
⊗ Lang.
□ West and Bradley.

In Fig. 2, the data of Bisi and Zappa have been used to plot $(\sigma_P/\bar{P})^2$ and $0{\cdot}0177/E$ as functions of E. The difference between them is also plotted, giving a curve for the variance $(\sigma_N/\bar{N})^2$ associated with the initial electrons. This does not give the surprising peak at 5 keV which Bisi and Zappa found by using an earlier value $E/N = 0{\cdot}0286$ determined by Curran, Cockroft and Insch.[12]

It is fairly clear from Fig. 1 that the results of Curran and his co-workers and the present writers for $(\sigma_P/\bar{P})^2$ are on the high side; this can almost certainly be ascribed to end effects in the particular counters employed, since the active volume was not defined with sufficient precision (e.g. by the use of field tubes). It is probable that Curran and his co-workers' value $\sigma_A/\bar{A} = 0{\cdot}681$ is also too high, and hence that the value of $\sigma_N/\bar{N}$ is in fact larger than is shown in Fig. 2, particularly for lower energies, as would be expected on theoretical grounds. The nature of possible improvements in the counters is discussed in a later section.

Bisi and Zappa's results fit the curve $\sigma_P/\bar{P} = \dfrac{0{\cdot}138}{E^{0{\cdot}395}}$ very closely, but it is difficult to reconcile the exponent of E with the physical processes involved. The general form of

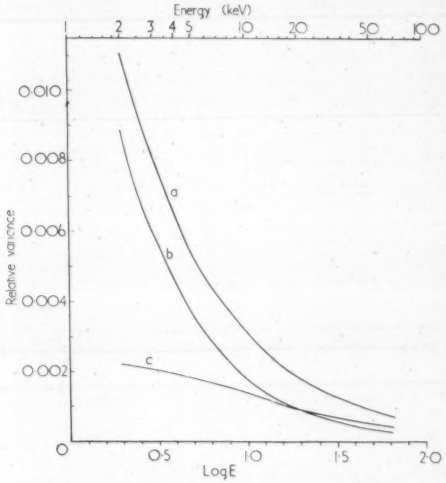

Fig. 2. Relative variance of the number of initial electrons

Curve (*a*), $(\sigma_P/\bar{P})^2$; curve (*b*) $1/N\,(\sigma_A/\bar{A})^2$; curve (*c*) $(\sigma_N)^2/\bar{N}$.

equation (5) is probably correct, but it appears that the factor 0·19 is somewhat higher than the value suggested by experiment; consideration of all available results suggests the adoption of

$$\frac{\sigma_P}{\bar{P}} = \frac{0{\cdot}15}{E^{1/2}} \qquad (8)$$

as being the most probable value.

The experimental evidence would be greatly clarified if values of $\sigma_P/\bar{P}$ could be obtained

(i) in an ionization chamber ($\bar{A} = 1$, $\sigma_A = 0$),

(ii) in a proportional counter, particularly in the range $0{\cdot}1 < E < 2$ keV, and

(iii) in a proportional counter with single electrons ($\bar{N} = 1$, $\sigma_N = 0$) to verify the work of Curran and his co-workers.[7]

APPLICATION TO X-RAY SPECTRO-CHEMICAL ANALYSIS

In the analysis of the X-ray K spectra of the elements, it is important to determine the resolving power needed to separate the spectra of neighbouring elements. The problem is complicated by the fact that the relative spacing of the Kα and Kβ lines varies through the spectrum; this could make the resolution of neighbouring elements a difficult task in certain parts of the spectrum.

In order to determine the power of a proportional counter to separate the K emission lines of neighbouring elements, Hendee and Fine[13] considered the ratio

$$R(Z) = \frac{B(Z)}{E(Z+1) - E(Z)} \qquad (9)$$

where Z is the atomic number of an element, $E(Z)$ is the energy of its Kα line, and $B(Z)$ is the width of the pulse height distribution curve at half the maximum height. $B(Z)$ is sometimes known as the "half-width" of the distribution. Hanna and his co-workers[2] and Bisi and Zappa[9] have found that the distribution may be fitted with a normal curve, at least within $\pm 3\sigma$ of the maximum.

Applying Moseley's law to equation (9) and using the relation that the half-width is proportional to $E^{1/2}$, Hendee and Fine showed that $R(Z)$ is independent of Z. If their analysis is repeated using equation (8) to obtain the half-width, then $R(Z)$ has the value 1·8 (compare Appendix A) and is independent of atomic number.

Fig. 3 shows the predicted pulse height distribution curves calculated for $R(Z) = 2$, i.e. a slightly inferior resolving power compared with the best that has been obtained. Fig. 3(*a*) shows the distribution that would be obtained from various alloy compositions of elements separated by two atomic numbers, for example magnesium (12) and phosphorus (15). Fig. 3(*b*) shows the corresponding distributions for elements separated by one atomic number, for example magnesium (12) and silicon (14). With the aid of such curves, accurate analysis should not be difficult. Fig. 3(*c*) shows the more difficult case of neighbouring elements such as magnesium (12) and aluminium (13). The curves for alloys of different composition are not so readily distinguished, but even this case should not prove intractable, given the necessary instrumental stability.

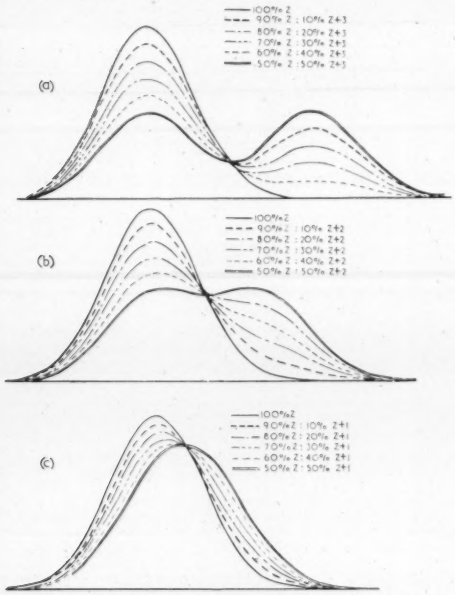

Fig. 3. Calculated pulse height distributions from alloys of different compositions

(*a*) separated by two elements; (*b*) separated by one element; (*c*) neighbouring elements.

THE INFLUENCE OF WEAK LINES

The above expression for the resolving power of a proportional counter is strictly valid only if the pulse height distribution from the Kα_1 line is not affected by weaker lines, such as the Kα_2 or Kβ_1 lines. This holds only for elements of atomic number lower than sulphur. For elements of higher atomic number than sulphur but less than that of silver the Kβ_1 line causes a broadening which amounts to a maximum of 7% for cobalt. For elements of still higher atomic number the Kα_2 line is mainly responsible for the broadening which reaches 20% for lead.

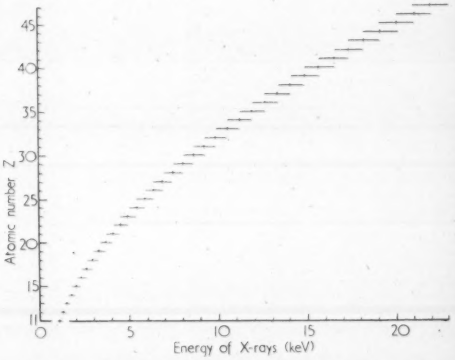

Fig. 4. Calculated half-widths of K emission pulse distribution from sodium to silver

——— half-width of counter distribution.

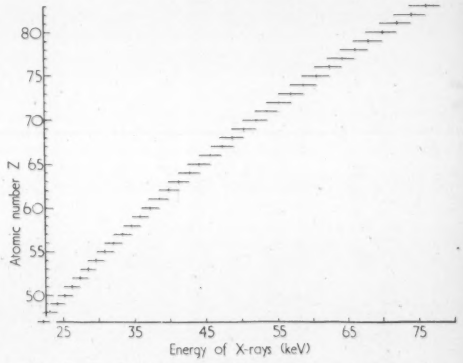

Fig. 5. Calculated half-width of K emission pulse distribution from silver to bismuth

——— half-width of counter distribution.

The actual half-widths are shown in Figs. 4 and 5 for the elements sodium (11) to bismuth (83). The layout is taken from Hendee and Fine,[13] whose figure is based on $R(Z) = 2{\cdot}1$ but neglects the effect of weak lines. The half-widths in Figs. 4 and 5 are based on the experimental data of Bisi and Zappa; this results in smaller half-widths for the lighter elements than those given by Hendee and Fine. On the other hand, elements heavier than lanthanum give rise to distributions with greater half-widths because of substantial broadening by the $K\alpha_2$ line.

One may conclude that when Z is less than 20, the most important region for proportional counters in spectro-chemical analysis, the resolving power will be almost independent of atomic number. Curves similar to those of Fig. 3 may be expected in which only adjacent elements should cause any difficulty and even these should not prove intractable. In this region, even a modest improvement in the present-day resolving power of the proportional counter would be of great benefit in X-ray analysis.

EXPERIMENTAL

No published accounts are available of the pulse height distribution from elements such as magnesium or aluminium. The distribution for aluminium K radiation was measured with a gas-flow proportional counter of conventional design. The K radiation was excited by bombarding an aluminium target in the electrons in an X-ray micro-analyser[14] developed in this laboratory. Such an instrument is suited to investigations in the soft X-ray region since the electron bombardment can be closely controlled and a vacuum path is available between target and counter.

The pulse height distributions from vanadium, chromium and copper K radiations were also obtained, either by electron bombardment or from radioactive isotopes such as Cr^{51} or Fe^{55}. The relative standard deviations $\sigma_P/\bar{P}$, which have already been referred to, are plotted in Fig. 1.

Although these results are in excellent agreement with the extrapolated values of Curran, Cockroft and Angus, and confirm the general form of equation (5), they are nevertheless significantly higher than the results of Bisi and Zappa.

A subsequent check on possible instrument errors indicated that the lack of roundness of the central wire, as shown by optical micrographs of the cross-section, could be a cause of the discrepancy. The lack of field tubes in the present counter could also affect the results. More experimental evidence for $\sigma_P/\bar{P}$ is required in the soft X-ray region, and the counter is being re-designed to eliminate these geometrical effects as far as possible.

CONCLUSIONS

A critical review of the present writers' experiments, in the light of theoretical and experimental work by previous authors, suggests that the limit of the spread of the pulse height distributions (due to statistical fluctuations) has not yet been reached for the characteristic radiation of elements from potassium to magnesium. The further slight improvement in proportional counters that is required is possible and worth while for X-ray analysis for these elements owing to the favourable nature of their K spectra. The improvement to the counter is likely to be in the use of field tubes,[15] the perfection of methods of lapping the central wire and the removal of electro-negative impurities from the gas.[16] Arndt and his co-workers[8] and Lang[10] have described proportional counters for use with the more energetic copper $K\alpha$ radiation, in which instrument defects are negligible; the smaller spreads reported by Bisi and Zappa[9] also point to the feasibility of such improvements, but their results as a whole are difficult to reconcile with existing theory and require further experimental support.

A suitable counter of improved design is being developed.

ACKNOWLEDGEMENTS

The authors wish to thank many colleagues in the Laboratory for helpful discussions, and Dr. T. E. Allibone, Director of the Research Laboratory, Associated Electrical Industries, for permission to publish this paper.

APPENDIX A

Proof that $R(Z) \simeq 1{\cdot}8$

Assuming that the pulse-height distribution is Gaussian,

$$B(Z) = 2{\cdot}36\sigma_E = 2{\cdot}36(\sigma_P/\bar{P})E$$

From equation (8)

$$\sigma_P/\bar{P} = 0{\cdot}15/E^{1/2}$$

i.e. $B(Z) = 2{\cdot}36 \times 0{\cdot}15E^{1/2} = 0{\cdot}0354E^{1/2}$

Percentage standard deviation of pulse height distribution $\sigma_P/\bar{P}$ (%)

Energy (keV)	*Curran and co-workers*	*Hanna and co-workers*	*Lang*	*Arndt and co-workers*	*Bisi and Zappa*	*West and Bradley*	*Present authors*
0·250		36 ± 4					
1·49							15·4 (Probe on Al)
2·00					10·5		
2·8		8·8					
4·95					7·3		9·3 (Cr^{51})
5·86					6·9		8·0 (Fe^{55})
							8·2 (Probe on Mn)
8·0	7·43		6·0	5·8			7·2 (Probe on Cu)
9·25					5·9		
13·37					5·1		
17·4	5·00	4·0					
22·10					4·10		
32·05					3·50		
46·7					2·94		
57·15					2·92		
59·6						2·1	
66·20					2·70		

By Moseley's law

$$E \simeq 0{\cdot}01(Z-1)^2$$

i.e. $$B(Z) = 2{\cdot}36 \times 0{\cdot}15E^{1/2}$$

i.e. $$B(Z) = 0{\cdot}0354(Z-1)$$

But $$E(Z+1) - E(Z) = 0{\cdot}01(2Z-1)$$
$$\simeq 0{\cdot}02(Z-1)$$

i.e. $$R(Z) \simeq 1{\cdot}8$$

Note added in proof

Considerably smaller standard deviations than those reported above have recently been observed by the authors using a proportional counter of improved design. In order to avoid instrumental errors the pulse height distributions were recorded on a Sunvic 100-channel pulse height analyser, kindly loaned by the manufacturers for the purpose. The relative standard deviation ($\sigma_p/\bar{P}$) for copper radiation was 2·6% and for aluminium 6·1%; both being excited by direct electron bombardment. With such low standard deviations the analysis of adjacent elements should be greatly simplified.

REFERENCES

(1) Frisch O. R. Statistics of Multiplicative Processes (unpublished lectures, 1948).

(2) Hanna, G. C., Kirkwood, D. H. W., and Pontecorvo, B. *Phys. Rev.*, **75**, p. 985 (1949).

(3) Snyder, H. S. *Phys. Rev.*, **72**, p. 181 (1947).

(4) Fano, U. *Phys. Rev.*, **70**, p. 44 (1946), and **72**, p. 26 (1947).

(5) Valentine, J. M. *Proc. Roy. Soc.* **211 A**, p. 75 (1952).

(6) Weiss, J., and Bernstein, W. *Phys. Rev.*, **98**, p. 1828 (1955).

(7) Curran, S. C., Cockroft, A. L., and Angus, J. *Phil. Mag.*, **40**, p. 929 (1949).

(8) Arndt, U. W., Coates, W. A., and Crathorn, A. R. *Proc. Phys. Soc.* (*London*) **67 B**, p. 357 (1954).

(9) Bisi, A., and Zappa, L. *Nuovo Cimento*, **2**, p. 988 (1955).

(10) Lang, A. R. *J. Sci. Instrum.*, **33**, p. 96 (1956).

(11) West, D., and Bradley, E. F. *Phil. Mag.*, **2**, p. 957 (1957).

(12) Curran, S. C., Cockroft, A. L., and Insch, G. M. *Phil. Mag.*, **41**, p. 517 (1950).

(13) Hendee, C. F., and Fine, S. *Phys. Rev.*, **95**, p. 281 (1954).

(14) *Proceedings of a Conference on Electron Microscopy*, Reading, 1956.

(15) Cockroft, A. L., and Curran, S. C. *Rev. Sci. Instrum.*, **22**, p. 37 (1951).

(16) Bertolini, G., Bisi, A., and Zappa, L. *Nuovo Cimento*, **10**, p. 1424 (1953).

The cleaning of glass in a glow discharge

By L. Holland, F.Inst.P., Research Laboratory, Edwards High Vacuum Ltd., Crawley, Sussex

[*Paper first received* 17 *March, and in final form* 23 *May*, 1958]

An investigation into the glow discharge cleaning of glass in kinetic vacuum systems is described. The cleanliness of the treated glasses is assessed by their coefficient of friction μ, freedom from optical absorption and wetting characteristics. Glasses bombarded by high energy electrons from the cathode dark space in the presence of hydrocarbon vapours are coated with organic layers, whereas glasses bombarded in the positive column are cleaned. Deposits formed in hydrocarbon vapours have a value of $\mu = 0{\cdot}3$ and cannot be wetted, whereas those formed in silicone vapour are wettable and have a value of $\mu = 0{\cdot}6$. An electrode system is described for use in evaporation plant in which the high energy electrons traversing the cathode dark space are prevented from bombarding the glass. Random bombardment by positive ions and neutral molecules in air, A, N_2, H_2 and O_2 produces clean glass with $\mu = 0{\cdot}7 - 0{\cdot}9$. The contamination of the cleaned surfaces by hydrocarbon and silicone molecules is discussed. Freshly deposited silica films and glass surfaces prepared by fracture *in vacuo* become contaminated by strongly adsorbed silicone molecules, whereas clean aged surfaces of glass and silica are not contaminated because the cations are screened by OH-ions.

1. INTRODUCTION

Clean glass possesses a number of distinguishing features such as the ability to condense a uniform water layer when breathed upon, known as a "black breath figure" to differentiate it from the "grey figure" that forms on a hydrophobic surface. Clean glass also has an abnormally high coefficient of friction when rubbed with glass or metal, and Langmuir[1] has demonstrated that an adsorbed mono-molecular layer of a fatty acid is sufficient to have a marked lubricating effect. Many workers have shown that clean glass possessing such properties may be produced by treatment with hot acids,[2] high temperature flames,[3–5] electrical sparking[6, 7] and glow discharge cleaning at low pressures.[8-10]

In spite of the extensive literature on the properties of clean glass and the techniques for its production, there has been little attempt to determine the manner in which cleaning occurs, particularly when using flames and ionized gases. The cleaning of glass in a glow discharge is now a commonly practised method of preparing a substrate before evaporation of thin films in vacuum, but in spite of its general use the technique has developed more as an *art* than a *science*.

An investigation is being made by the writer into the effects of treating glass in a glow discharge at voltages between 0·5–5 kV, and it has been shown elsewhere[11] that bombardment by high energy electrons deposits organic films on glass surfaces when using a kinetic pumping system. Similar coatings are formed by electron bombardment in high vacuum and have been attributed by Ennos[12, 13] to the decomposition of hydrocarbon molecules adsorbed to the target surface. It has also been found that bombardment of glass by positive ions traversing the cathode dark space removes contaminants remaining after chemical cleaning or organic film condensed by electron impact. At high current densities components are selectively removed from the glass, thereby lowering the refractive index of the surface.[11] More recent results indicate that the glass components are

removed by cathodic sputtering, an effect which could explain the surface changes noted by Koch[14] and Hines[15] who bombarded glasses with 40 keV ions, and attributed the lowering of the refractive index to alterations in the internal structure of the glass.

This account deals with the development of electrode systems for cleaning glass in a glow discharge in the presence of organic vapours such as are found in kinetic pumping systems. Attention is also given to the use of the electrodes in vacuum evaporation plant and the properties of the cleaned glass surface.

2. EXPERIMENTAL METHOD

The experimental electrode systems were mounted in a metal vessel fitted with rubber seals and exhausted by a silicone oil diffusion pump with a water-cooled vapour baffle. The arrangement of the high tension power supply and the gas pressure control were those described by Holland.[16] Power for the glow discharge was obtained from a high reactance transformer, the output of which could be varied between 0 and 5 kV at a current of up to 500 mA. The pressure was roughly set by admitting gas to the vacuum vessel through a needle valve and finely adjusted by varying the pumping speed. The speed of the diffusion pump after baffling was 1000 l/s below 1 micron of mercury, and in the pressure range used for the glow discharge (5 to 1000 μ Hg) the rate of leaking gas into the system was equal to 1 c^3/s at atmospheric pressure so that the contamination from degassed vapours was a minimum. The plant could be exhausted to an ultimate pressure of 0·01 μ Hg before admitting gas.

The glass specimens were cut from plate glass and cleaned with a detergent (Teepol) before treatment in the glow discharge. The cleanliness of the treated glasses was assessed by determining their coefficient of friction, optical absorption and wetting properties.

The reflectance, transmittance and absorption ($R + T + A = 100\%$) of the treated glasses were measured with a photometer fitted with a chopped light source (33 c/s) and a high gain amplifier which permitted an accuracy of $\pm\frac{1}{2}\%$ when determining the absorption.

3. GLOW DISCHARGE ELECTRODES

Glass slides may be cleaned by the bombardment of positive ions traversing the cathode dark space of a glow discharge if the glass is rested on a plane cathode electrode. Clean surfaces may be obtained even in the presence of hydrocarbon vapour. However, there are many obstacles to the use of such a simple arrangement, particularly in vacuum evaporation plant. At high current densities (0·2 mA/cm^2) the glass surface may be damaged by the removal of components of the glass. Also, the bombarded surface becomes electrically charged so that ions in the glass such as sodium, migrate to the surface under the induced field. The system can only be used with a glass of limited area, otherwise the configuration of the cathode dark space is affected, and only the edges of the glass are bombarded by positive ions. Finally, when used in evaporation plant volatilized films may be deposited on the open cathode electrode and sputter on to the glass during a subsequent cleaning operation. For these reasons experiments were made to find whether a glass could be cleaned by random bombardment of positive ions in a glow discharge in the presence of hydrocarbon vapour.

(*a*) *Cleaning in the positive column.* A cathode of 18 cm diameter made of pure aluminium was mounted with a long glass slide arranged at an angle to the normal to the cathode surface so that the glass was bombarded at different distances from the cathode. In this experiment only, a tray of butyl phthalate was placed in the chamber to maintain a high hydrocarbon vapour pressure ($\simeq 0{\cdot}1\ \mu$ Hg) throughout the bombardment period. Glass slides were bombarded in air for 5 min at a current density of 0·2 mA/cm^2 and at different voltages and gas pressures. The optical transmittance of the glasses was measured at $\lambda = 4600$ Å as a function of the distance from the cathode and is plotted in Fig. 1. Similar curves have been obtained, but with less reduction in transmittance, when the hydrocarbon vapour present was solely that from the vacuum system.

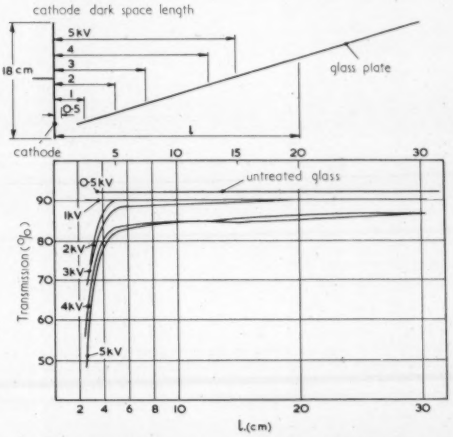

Fig. 1. Reduction in transmission of glass plate measured at $\lambda = 4600$ Å after 5 min bombardment in air at constant current density (0·2 mA/cm^2) and different voltages and gas pressures

The curves in Fig. 1 show that the optically absorbing deposit is concentrated near the cathode where the glass is exposed to bombardment of high energy electrons traversing the cathode dark space. Glasses bombarded at a high pressure and low voltage (500 V) were completely immersed in the positive column and did not become optically absorbing. Near to the cathode the exposed glass surface was hydrophobic indicating that the glass was not free from electron induced contaminants, but at the anode end of the positive column both sides of the glass showed a black breath figure and had a high coefficient of friction.

If a glass previously contaminated with a hydrocarbon film by electron bombardment was exposed in the anode end of the positive column, the coating was not removed. This showed that the electrons in the plasma had insufficient energy to dissociate the hydrocarbon molecules because the random ion bombardment could not have removed the decomposition products had they formed. However, the random bombardment of positive ions was sufficient to remove weakly absorbed contaminants remaining after chemical cleaning.

The arrangement shown in Fig. 1 is unsatisfactory for

cleaning purposes even when using low voltages because if the pressure should fall, the cathode dark space lengthens so that the glass is exposed to the bombardment of high energy electrons, which quickly induce surface contamination. This may be avoided with the apparatus described below which permits the use of an extended cathode dark space without the risk of electron induced contamination.

(*b*) *Shielded cathode system.* The electrons liberated from or near the cathode in a glow discharge tend to travel in straight paths through the cathode dark space, whereas the ions with their smaller mean free path are scattered by colliding with gas molecules. The rectilinearly propagated electrons can be prevented from striking the work by shielding the cathode, and an alternative path made available to sustain ionization. Thus, the high velocity electrons can be made to travel in directions which will avoid collisions with the work surface, whereas the positive ions and neutral molecules of high velocity may be considerably scattered and strike the work.

Electrode systems* based on this simple design principle have been used effectively in several different evaporation plants, and we shall deal here with that used in a plant fitted with a rotary plane work holder. For purposes of comparison a conventional system has been used consisting of a pair of sector-shaped electrodes mounted under the work holder and connected to an a.c. power supply as shown

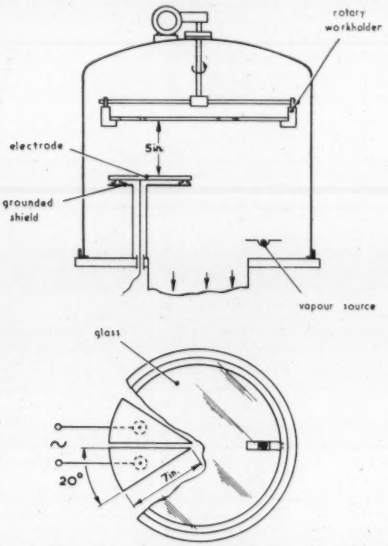

Fig. 2. Sector cathodes used with a rotary work holder in a vacuum evaporation plant (dimensions are given in inches)

in Fig. 2. Hiesinger[17] has described a similar system using a single sector cathode.

Shown in Fig. 3 is the modified electrode system. It consists of two electrodes made from aluminium bar arranged radially under the work holder. The gap between the electrodes is too small for sustained ionization at the pressure and current density used, and the discharge follows the longer path shown. The electrodes are covered with a shield so that the electrons traversing the cathode dark spaces are accelerated parallel to the plane of the glass. When operated at high pressures (0·5 mm Hg) and low voltage (500 V) the glass is exposed only to the positive column and

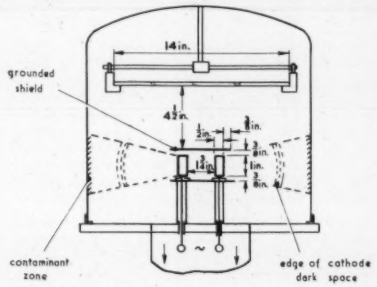

Fig. 3. Shielded electrodes used with a rotary work holder in a vacuum evaporation plant (dimensions are given in inches)

at low pressures (0·01 mm Hg) and high voltages (5 kV) the glass is exposed to the random bombardment of high energy ions and neutral molecules from the greatly extended cathode dark space, but under neither condition can high energy electrons reach the glass. Operation of the electrode system at high voltages and low pressures results in intense heating of the glass, which is useful when the properties of an evaporated deposit are improved by deposition on to a hot substrate.

4. OPTICAL MEASUREMENTS

Table 1 compares the optical absorption produced in glasses by contaminating films using the unshielded sector cathodes and those of the new design. Both systems were operated at 5 kV and 160 mA at 10^{-2} mm Hg pressure with a cathode dark space of about 4 in. in depth. Under these conditions the edge of the cathode dark space almost reaches the work surface when using the open sector electrodes. The exposed glass remained free from absorption even when a piece of Neoprene rubber was placed in the cathode dark space near to one of the shielded electrodes, whereas a dense

Table 1. *The effect of the glow discharge on the optical absorption of glass at* $\lambda = 5300$ Å *when treated in a demountable metal vessel with different electrode arrangements*

H.T. electrode design	*Residual gas*	*Treatment time (min.)*	*T*(%)	*R*(%)	*A*(%)
Unshielded	air	60	88	8·5	3·5
Unshielded	air	180	86·5	7·5	6
Shielded	air	60	91	9	0
Unshielded	argon	60	88	8	4
Shielded	argon	60	91	9	0
Unshielded	air-Neoprene	10	10	10	80
Shielded	air-Neoprene	10	91	9	0

All glasses were mounted on a 14 in. diam. rotary holder and exposed to a glow discharge of 5 kV at 160 mA with flowing gas at 10^{-2} mm Hg pressure.

* Subject of a provisional patent specification.

brown deposit was formed on the glass using unshielded electrodes, as shown in Fig. 4(*a*). Fairly clean glass could, in fact, be prepared in the presence of the Neoprene so that when a stick of titanium was lightly rubbed over the glass surface, a heavy trace of metal was left on the treated portion of the glass as shown in Fig. 4(*b*). Undecomposed hydrocarbon molecules would not be readily adsorbed to the glass because its temperature rose to about 150° C during the treatment. The electrons accelerated in the cathode dark

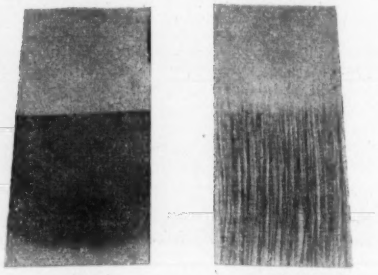

(*a*) (*b*)

Fig. 4. The glasses have been partially masked and exposed to a glow discharge using a rotary holder with Neoprene rubber in the cathode dark space. Glass (*a*) shows on the exposed half of the surface the pattern of hydrocarbon decomposition which varies with the intensity of the impinging electrons. Glass (*b*) cleaned with shielded cathodes has a high coefficient of friction on the treated surface which has been permanently exposed by rubbing the surface with titanium

space of the shielded electrodes struck the wall of the vessel where an organic deposit slowly appeared as shown in Fig. 3.

It has been claimed[18] that a chemically cleaned glass surface may be protected against contamination whilst in the atmosphere by a film of an organic fluid which is thermally evaporated or oxidized in a glow discharge. Tests have shown that at low pressures the electrode system in Fig. 2 decomposes grease films (e.g. Apiezon "L") spread on a glass surface because the glass is exposed to bombardment by high energy electrons, whereas grease layers are removed from glass using the shielded electrodes.

5. SOME PROPERTIES OF CLEAN GLASS

(*a*) *The coefficient of friction*

The coefficient of friction μ was measured for glasses cleaned in a glow discharge and by other means using a glass rider with an area of $2{\cdot}5 \times 5$ cm under a load of 120 g.

Vapour degreasing both the test glass and the rider in iso-propyl alcohol produced a surface with a static value of $\mu = 0{\cdot}6$. When the glass was cleaned in a glow discharge with shielded electrodes the value of μ measured in air immediately after treatment was substantially the same whether the rider was glow-discharge cleaned or vapour degreased. A vapour degreased rider was normally used in the experiments to be described. Table 2 shows the values of μ measured using different cleaning techniques and is largely self-explanatory. The values given are the average of five or more measurements. Measurement of the kinetic friction with the test glass vibrated at 50 c/s gave values some 15% under those in Table 2, but with the same relative order.

Of interest is the low value of μ obtained with a chemically cleaned glass after baking for 1 h at 300° C at $0{\cdot}1\ \mu$ Hg pressure. The surface could not be wetted with water and it was concluded that the glass was contaminated with hydrocarbons. It is not usually possible to produce durable evaporated films on glasses which have been baked in vacuum. Rayleigh found that a black breath figure could only be obtained by heating if the glass temperature was raised to the softening point.

Table 2. *The coefficient of friction of glass on glass using different cleaning techniques*

*Cleaning techniques**	μ
Teepol and Selvyt polished	0·05
Vapour degreased (*iso-propyl* alcohol)	0·6
Baked in vacuo (300° C 1 h)	0·2
Flamed (coal gas and air)	0·4
Unshielded h.t. electrodes in air (silicone contamination)	0·7
Unshielded h.t. electrodes with silicone oil bath	0·6
Unshielded h.t. electrodes in air/Neoprene rubber	0·3
Shielded h.t. electrodes in air	0·8
Shielded h.t. electrodes in air/Neoprene rubber	0·6
Shielded h.t. electrodes in A, N_2, H_2 and O_2	0·7–0·9
Evaporated silica on silica	0·7
Evaporated cryolite on cryolite	0·55

* All glasses treated in a glow discharge were mounted on a rotary support of 14 in. diameter and exposed for 10 min. at 5 kV and 160 mA in flowing gas at 10^{-2} mm Hg pressure, unless otherwise specified.

The glasses treated in a glow discharge were mounted on a rotary support and exposed for 10 min at 5 kV and 160 mA in flowing gas at 10^{-2} mm Hg pressure, using the apparatus shown in Figs. 2 and 3. The surprising observation was made that glasses bombarded with the open sector cathodes as shown in Fig. 2 were coated with optically absorbing deposits which were readily wetted by water and possessed a high value of μ. The effect was attributed to the decomposition of silicone vapours emitted by the diffusion pump which formed silica films on the glass surface. To confirm this a tray of silicone oil was placed near to the sector electrodes and the treated glass still had a high value of μ and could be wetted. If the electron bombardment was very intense the deposit showed interference colours and had negligible absorption. Using a method based on Brewster angle measurement, Mr. T. Putner found that the deposits had a refractive index of 1·58. Durable coatings of aluminium have been produced on glasses coated with decomposed silicone films and undoubtedly many workers using these fluids must have unwittingly produced such base coatings. The values of μ for glasses treated in the presence of hydrocarbon vapours from Neoprene rubber were low and the decomposed deposits could not be wetted.

Absorption-free glasses with a high coefficient of friction and showing a black breath figure were always obtained with the shielded electrodes irrespective of the nature of the residual gas. As the friction was not measured *in vacuo* it would be dangerous to attribute different cleaning efficiencies to the different gases because the test glasses must have been partially contaminated by exposure to air.

When the shielded electrodes were operated at high pressure and low voltage (500 V) so that the glass was in the positive

column between the electrodes clean glass was obtained with $\mu = 0{\cdot}75$. Karasev and Izmailova[19] have reported a value of 0·8 for clean quartz and 1·07 for clean glass, compared with the average value measured here for clean glass of 0·8; from their experimental data it would appear that their surfaces were cleaned in the positive column of the discharge.

An attempt to produce a very clean surface was made by evaporating $\lambda/4$-films of silica and cryolite on to the test glass and the rider. The static coefficient of friction for a silica film was 0·7 and for cryolite 0·55. The coatings were disrupted by the sliding action, and it was apparent that the frictional force had been overcome by shearing at the glass-to-film boundary. The values, therefore, cannot be taken as those of bulk material, but they are a useful indication of the bonding of a film. Thus, silica deposited on Teepol-cleaned glass without glow-discharge cleaning gave a value of $\mu = 0{\cdot}3$.

(*b*) *Contamination of the cleaned surface*

Bateson[20] has shown that a glass surface cleaned in a glow discharge becomes contaminated by hydrocarbon molecules if left for a few minutes in the vacuum of a kinetic pumping system. However, when making the tests discussed here the glasses were removed from the vessel immediately the cleaning was completed. Tests were made to find the speed of surface contamination in a normal kinetic plant. Fresh evaporated films of silica-on-glass were prepared and exposed for different periods *in vacuo* after deposition. It was observed that the silica deposits could be readily wetted with water for a certain exposure period, and then their surfaces rapidly became hydrophobic so that spherical water droplets were formed. All of the coatings possessed a high coefficient of friction, and it was deduced that the adsorbed layer was silicone oil from the diffusion pump, which is a poor lubricant and strongly water repellant.

A series of clean silica and glass surfaces were prepared and exposed in air and vacuo and the following observations made:

(*a*) *Silica coated glass.* Films which had been rendered hydrophobic by exposure *in vacuo* could not be made wettable by vapour degreasing in iso-propyl alcohol vapour, but could be by flaming or glow-discharge cleaning. However, the cleaned films did not become hydrophobic as found with new coatings when re-exposed *in vacuo*. Evaporated silica films initially exposed to the atmosphere immediately after formation also did not become hydrophobic after long periods *in vacuo*.

(*b*) *Fractured glass surfaces.* The fresh surface of a fractured piece of glass was readily wetted by water and showed a black breath figure when the glass was broken in air. The surfaces of broken glass prepared *in vacuo* could not be wetted after exposure for 4 min at the reduced pressure. However, glass fractured in air and transferred to the vacuum plant continued to be wettable after hours of exposure *in vacuo*.

(*c*) *Clean glass.* Glasses cleaned by a glow discharge or chemical methods remained wettable and did not develop a hydrophobic surface after hours of exposure *in vacuo*.

From these observations it is obvious that a new surface of glass or silica rapidly becomes contaminated by strongly adsorbed substances when exposed in air and these screen the cations in the glass surface and prevent the subsequent adsorption of silicone molecules. (It should be noted that the vapour pressure of the silicones in the vacuum chamber was below the saturated value so that oil could not condense on the glass.) Water vapour would have been present in the glow discharge gas and also formed in the flame so that cleaned surfaces would constantly be covered with OH^- ions. It is known that silicone molecules can be chemisorbed to glass by using dimethyl silicon chloride which chemically reacts with the OH^- ions and removes them from the surface.

An experiment was made to ensure that the hydrophobic surface was not produced by hydrocarbon vapours emitted from rubber gaskets. A quantity of rubber shielded from heat radiation was placed inside the vacuum vessel and a silica film deposited. When removed from the vessel the coating smelt strongly of sulphur and was obviously contaminated, but a black breath figure could still be condensed and the surface was readily wetted. This proved that the principal material emitted by the rubber at normal temperature was not hydrophobic and also that a black breath figure was not a criterion of cleanliness under all conditions.

From the earlier measurements of the different times required to render a silica film hydrophobic, it was concluded that the silicone vapour pressure was less than the equilibrium amount due to the fresh coating on the chamber interior having a gettering action. To avoid this, a tray of silicone oil was placed in the coating vessel. The coating vessel was exhausted by a fractionating oil diffusion pump charged with Silicone 704 and fitted with a cooled baffle (15° C). With Silicone 704 in the vessel the contamination time was constant at 3 min and with Silicone 703 the time was 1 min. Silicone 704 is a new fluid consisting of molecules with a constant molecular weight of 484. Assuming that some 10^{14} molecules per square centimetre are required to cover the surface and that the molecules condense on first impact, then this would give a vapour pressure of about 7×10^{-9} mm Hg. The ion gauge reading of the ultimate of a fractionating pump charged with this fluid is 4×10^{-6} mm Hg, but this is in error due to the unknown ionization coefficient of the vapour. An estimate of the vapour pressure obtained by extrapolating a curve determined at high pressures, has recently been reported[21] as 9×10^{-9} mm Hg at 20° C. If one allows for the uncertainty in the area of the silica surface, the two values are in good agreement. It is likely that the surface of the silica available for adsorption approximates to that of a plane, because the large oil molecules are unable to penetrate the porous structure of the evaporated film.

5. CONCLUSIONS

It has been shown that bombardment of glass surfaces by the electrons traversing the cathode dark space in a glow discharge may produce surface coatings if hydrocarbon molecules are adsorbed to the glass. Further, that decomposition of silicone molecules forms coatings which are readily wetted with water and have a high coefficient of friction as found with clean glass. Random bombardment by positive ions (or neutral molecules), from the cathode dark space or positive column, produces clean glass in air or argon. Glass may be cleaned without risk of hydrocarbon contamination using a cathode electrode which is shielded to prevent direct electron bombardment of the glass.

Glasses cleaned in a glow discharge or by flaming cannot be rendered hydrophobic by exposure to silicone vapour as can freshly fractured surfaces and those of evaporated silica. Aged glass surfaces are covered by OH^- ions which are not removed by the cleaning techniques discussed here.

6. ACKNOWLEDGEMENTS

My thanks are due to Mr. T. Putner and Mr. L. Elsworth for their valuable assistance during this work, and to

Mr. A. S. D. Barrett, Technical Director of Edwards High Vacuum Ltd., for permission to publish this report.

REFERENCES

(1) LANGMUIR, I. *J. Franklin Inst.*, **218**, p. 143 (1934).
(2) QUINCKE, G. H. *Wied. Ann.*, **2**, p. 145 (1877).
(3) AITKEN, J. *Proc. Roy. Soc. Edin.*, **20**, p. 94 (1893).
(4) RAYLEIGH, LORD. *Nature* [*London*], **86**, p. 416 (1911).
(5) RAYLEIGH, LORD. *Nature* [*London*], **90**, p. 436 (1912).
(6) CROFT, W. B. *Phil. Mag.*, **34**, p. 180 (1892).
(7) BAKER, T. J. *Phil. Mag.*, **44**, p. 752 (1922).
(8) RITSCHL, R. *Z. Phys.*, **69**, p. 578 (1931).
(9) STRONG, J. *Pacific Publ. Astro. Soc.*, **46**, p. 18 (1934).
(10) STRONG, J. *Rev. Sci. Instrum.*, **6**, p. 97 (1935).
(11) HOLLAND, L. *Nature* [*London*], **181**, p. 1451 (1958).
(12) ENNOS, A. E. *Brit. J. Appl. Phys.*, **4**, p. 101 (1953).
(13) ENNOS, A. E. *Brit. J. Appl. Phys.*, **5**, p. 27 (1954).
(14) KOCH, J. *Nature* [*London*], **164**, p. 19 (1949).
(15) HINES, R. L. *J. Appl. Phys.*, **28**, p. 587 (1957).
(16) HOLLAND, L. *Vacuum Deposition of Thin Films* (London: Chapman and Hall Ltd., 1956).
(17) HIESINGER, L. *Sonderdruck aus der Festschrift*, p. 17 (Hanau: W. C. Heraeus, 1951).
(18) COLBERT, W. H., and WEINRICH, A. R. U.S. Pat. 2,383,469 (1945).
(19) KARASEV, V. V., and ISMAILOVA, G. I. *Zh. Tekh. Fiz.*, **24**, p. 871 (1954).
(20) BATESON, S. *Vacuum*, **2**, p. 365 (1952).
(21) HUNTRESS, A. R., SMITH, A. L., POWER, B. D., and DENNIS, N. T. M. *Symposium on Vacuum Technology*, 1957. To be published.

Structure-cell data and expansion coefficients of bismuth telluride*

By M. H. FRANCOMBE, M.Sc., A.Inst.P., The General Electric Co. Ltd., Wembley, Middlesex

[*Paper first received* 20 *February, and in final form* 15 *April*, 1958]

Accurate measurements of the structure-cell parameters of bismuth telluride, Bi_2Te_3, have been made using annealed powders and etched rods cut from single-crystal ingots. Previously reported anomalies in the X-ray powder intensity data are found to originate entirely in preferred orientation of the crystallites.

A study of the thermal expansion of the unit cell over the temperature range −195 to 400° C has revealed a marked anisotropy between the axial expansion coefficients, that for the *c* axis ($22{\cdot}2 \times 10^{-6}$ per °C at 20° C) being almost twice that for the *a* axis ($12{\cdot}9 \times 10^{-6}$). Near 200° C changes occur in both the principal axial expansions, comparable with those observed at low temperatures in certain hexagonal metal structures.

A great deal of interest has been focused on bismuth telluride (Bi_2Te_3) in recent years because of its potential value in thermoelectric applications.[1] Crystallographic data for this compound were originally published by Lange[2] who described the structure as rhombohedral with the space group D^5_{3d} ($R\bar{3}m$), and structure-cell parameters

$$a_R = 10{\cdot}45 \text{ Å}, \alpha = 24° 8'$$

The structure consists of layers of atoms stacked in the rhombohedral [111] direction in approximately cubic close packing. The sequence of layers is

Bi–Te–Bi–Te–Te–Bi–Te–Bi–Te– – –

A striking feature of single crystals is the ease with which they can be cleaved and bent along the basal (0001) planes (referred to hexagonal axes). It has been suggested by Drabble and Goodman[3] that the bonding between Bi–Te layers is predominantly homopolar in character, while that between Te–Te layers is of the van der Waals type, and that cleavage occurs between the weakly bonded Te layers.

In a previous communication from these laboratories[4] significant differences were reported for the structure-cell dimensions of single-crystal samples of bismuth telluride prepared by different methods. It therefore seemed desirable to measure the lattice dimensions of stoichiometric bismuth telluride with high accuracy, so that the influence of possible variations of composition on electrical characteristics could be appraised. This paper presents the results of such measurements made on annealed powders and etched single crystals. The X-ray studies have also been extended to cover a range of temperatures, and thermal expansion data are given for the range −195 to 400° C.

EXPERIMENTAL

The X-ray studies were carried out on powdered and single-crystal material obtained from zone-melted ingots, prepared from zone-refined bismuth and tellurium. This material was prepared by Mr. A. R. Sheard as part of the general programme on thermoelectric materials in the Solid Physics Laboratory. Because of the softness and cleavage properties of bismuth telluride, special precautions had to be taken to obtain diffraction lines and reflexions with high definition suitable for accurate measurement. All powder specimens were annealed in evacuated, sealed, vitreous silica tubes for four to six days at 425° C, while single-crystal fragments were etched in a 1 : 1 mixture of HNO_3 and distilled water to remove the strained surfaces.

The X-ray powder photographs were taken, with specimens held in thin-walled silica tubes, using a 19 cm Unicam camera and nickel-filtered copper radiation. Measurements of the hexagonal *c* parameter were also made separately, using long, thin, rod-shaped crystals cut parallel to the basal (0001) cleavage planes and mounted in the same 19 cm powder camera. Diffraction-line intensities were determined with the aid of a manually-operated microdensitometer, supplementary observations being made on loosely-packed flat powder samples with a Philips high-angle diffractometer.

For the high-temperature studies a 19 cm Unicam high-temperature powder camera was used. Low-temperature measurements were made by employing a modified 19 cm Unicam powder camera with the liquid- and gas-cooling techniques described previously in the literature.[5, 6]

* G.E.C. Communication No. 780.

X-RAY STUDIES AT ROOM TEMPERATURE

Single-crystal rotation photographs obtained with the 19 cm powder camera enabled zero and first-order layer-line reflexions with indices of the type 0, 0, *l* and 1, 0, *l* to be recorded. These were used to calculate the *c* parameter and, by direct comparison, to index many of the diffraction lines in X-ray powder photographs of annealed powders. Unfortunately it was not found possible to adopt similar methods to determine the *a* parameter, because of the difficulty in cutting single crystals of suitable shape. Interplanar spacing data and peak intensities obtained with powdered samples are given in the table.

Final determinations of the hexagonal unit-cell dimensions were made from the powder photographs, using the extrapolation method of Thewlis,[8] which gave

$$a = 4{\cdot}3835 \pm 0{\cdot}0005\ \text{Å},\ c = 30{\cdot}487 \pm 0{\cdot}001\ \text{Å}$$

The rhombohedral unit-cell dimensions calculated from these are

$$a_R = 10{\cdot}473\ \text{Å},\ \alpha = 24^\circ\ 9'\ 32''$$

THERMAL EXPANSION MEASUREMENTS

The variations of hexagonal *a* and *c* parameters with temperature are shown graphically in Fig. 1(*a*) and (*b*)

X-ray powder difraction data for bismuth telluride

(19 cm camera and diffractometer, Cu Kα radiation)

*hkl**	*d*(Å)	*I*	*hkl*	*d*(Å)	*I*	*hkl*	*d*(Å)	*I*
006	5·09	20	1, 0, 23	1·252	3	1, 1, 30	0·9218	6
101	3·78	8	306	1·228	2	1, 3, 17 2, 1, 26	0·9078	3
105	3·22	100	2, 0, 19	1·225	2	4, 0, 10	0·9060	2
108	2·694	5	1, 1, 21	1·211	5	2, 2, 21	0·8748	2
1, 0, 10	2·378	55	2, 0, 20	1·189	5	2, 0, 31	0·8730	2
1, 0, 11	2·237	11	1, 0, 25	1·161	6	1, 2, 28	0·8672	2
110	2·191	35	2, 1, 16	1·146	2	1, 3, 20	0·8663	3
113	2·144	4	1, 0, 26 2, 1, 17	1·120	4	3, 2, 5	0·8623	4
0, 0, 15	2·032	40	220	1·0955	3	0, 2, 32	0·8513	4
116	2·014	8	2, 0, 23	1·0865	1	328	0·8490	4
1, 0, 13	1·995	6	3, 0, 15	1·0750	6	2, 3, 10	0·8378	4
1, 0, 14	1·890	3	1, 0, 28	1·0463	2	3, 2, 11	0·8310	1
205	1·810	20	2, 1, 20	1·0452	6	410	0·8280	5
1, 0, 16	1·703	8	3, 1, 5	1·0380	4	1, 3, 23	0·8245	2
0, 0, 18	1·694	5	2, 0, 25	1·0260	3	416	0·8175	1
2, 0, 10	1·610	16	0, 0, 30	1·0163	2	2, 1, 31	0·8113	3
2, 0, 11	1·567	3	3, 0, 18	1·0135	2	4, 0, 20	0·8058	3
1, 1, 15	1·489	25	2, 0, 26	0·9970	2	3, 1, 25	0·7970	4
2, 0, 13	1·476	2	3, 1, 10	0·9953	6	2, 1, 32	0·7935	1
0, 0, 21	1·452	6	3, 1, 11	0·9848	2	2, 3, 16	0·7922	4
121	1·434	2	2, 1, 23	0·9735	2	0, 2, 35	0·7915	1
1, 0, 20	1·415	12	2, 2, 15	0·9648	5	1, 1, 36	0·7900	3
215	1·398	13	3, 0, 21	0·9538	3	2, 2, 27	0·7865	1
2, 0, 16	1·345	2	1, 0, 31	0·9517	4	1, 0, 38	0·7849	2
1, 1, 18	1·340	3	2, 0, 28	0·9445	2	3, 2, 17 1, 3, 26	0·7835	2
2, 1, 10	1·299	10	4, 0, 5	0·9377	4			
2, 1, 11	1·274	2	2, 1, 25	0·9290	5			
3, 0, 0	1·265	5	1, 0, 32	0·9240	2			

* The *hkl* indices are referred to the hexagonal structure cell.

There is a marked tendency for the relative line intensities to be influenced by preferred orientation effects, particularly with diffractometer measurements. The effect is more pronounced in tightly packed specimens and leads to anomalies in the intensities of the diffraction lines with high "*l*" indices. This fact would appear to explain the diffraction-peak intensity variations found by Vasenin and Konovalov[7] in their diffractometer studies of sintered powder blocks, and which were interpreted as evidence for the coexistence of rhombohedral and hexagonal polymorphic structures in bismuth telluride. The inconsistencies occurring between powder photograph diffraction-line intensities and those measured with the diffractometer are found to be very small, providing that the powders are loosely packed either in the vitreous silica tubes or plate holders.

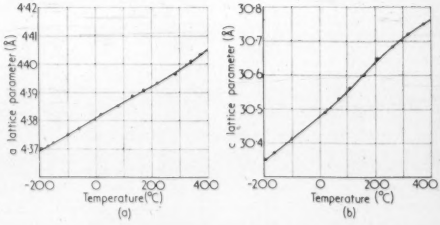

Fig. 1. Temperature variation of lattice parameters of bismuth telluride

respectively. Values of c/a axial ratio and unit-cell volume have been derived from these curves, and are plotted against temperature in Fig. 2. The coefficients of expansion at different temperatures T along the two principal axes were also calculated, using the expressions

$$\alpha_{T[100]} = (da/dt)_T/a_T$$

and

$$\alpha_{T[001]} = (dc/dt)_T/c_T$$

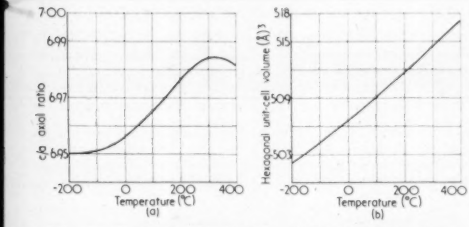

Fig. 2. Temperature variation of axial ratio and volume of structure cell of bismuth telluride

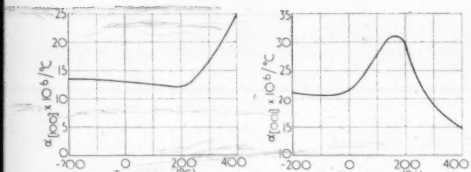

Fig. 3. Temperature variation of axial expansion coefficients of bismuth telluride

The temperature derivatives of the values of a and c at different temperatures were obtained from Fig. 1. Plots of the coefficients against temperature are shown in Fig. 3.

SUMMARY AND CONCLUSIONS

By using etched single crystals and annealed powders, the unit structure cell dimensions of pure bismuth telluride have been re-determined to a high order of accuracy. These accurate values should provide a standard of reference for appraising the purity and homogeneity of bismuth telluride crystals intended for thermoelectric applications.

The suggestion, based on anomalies in X-ray intensity data, that bismuth telluride can possess rhombohedral and hexagonal polymorphic forms, is not confirmed. It is shown that preferential orientation arrangements of the plate-like crystals in the samples examined probably account for the intensity variations previously reported.

A marked anisotropy is shown in the thermal expansion of bismuth telluride, the values of the coefficients at 20° C for the a and c axial directions being respectively 12·9 and $22{\cdot}2 \times 10^{-6}$ per °C. Anomalous changes are found in the coefficients as the temperature rises above 200° C. Thus while the expansion rate in the a direction increases above this temperature, that in the c direction first reaches a maximum and then decreases. This behaviour is consistent with the observed anisotropy in mechanical strength, and is similar to that displayed at lower temperatures by certain hexagonal metal structures such as zinc and cadmium.

REFERENCES

(1) GOLDSMID, H. J., and DOUGLAS, R. W. *J. Appl. Phys.*, **5**, p. 386 (1954).

(2) LANGE, P. W. *Naturwissenschaften*, **27**, p. 133 (1939).

(3) DRABBLE, J. R., and GOODMAN, C. H. L. *J. Phys. Chem. Solids*, **5**, p. 142 (1958).

(4) AINSWORTH, L. *Proc. Phys. Soc. (London)* **69B**, p. 606 (1956).

(5) TOMBS, N. C. *J. Sci. Instrum.*, **29**, p. 364 (1952).

(6) FRANCOMBE, M. H. *J. Sci. Instrum.*, **34**, p. 35 (1957).

(7) VASENIN, E. I., and KONOVALOV, P. F. *Zh. Tekh. Fiz.*, **26**, p. 1406 (1956).

(8) THEWLIS, J. *Acta Cryst.*, **5**, p. 849 (1952).

NOTES AND NEWS

Correspondence

A note on the paper "The oxidation of evaporated barium films (getters)"[1]

A recent paper by R. N. Bloomer[1] has dealt with the kinetics of the oxidation of barium in oxygen, and it has been shown that there exists a critical temperature below which the oxide film is protective and above which the barium oxidizes to completion. It is concluded that the results are in accord with Mott's theory of oxidation, the critical temperature being identified with that calculated by Mott[2] as

$$T_c = W/32k$$

the oxidation being regarded as ceasing when the rate of growth of the oxide layer has fallen to 10^{-10} cm/s. (W is the sum of the heat of solution of the metal ion and the activation energy for diffusion; k is the Boltzmann constant.)

It is implicit in Bloomer's paper though perhaps insufficiently emphasized that the conclusions drawn from the experimental results are only valid when the thickness of the oxide film formed by the total oxidation of the barium getter is still within the "thin film" region of Mott.

Bloomer states that "above the critical temperature, the capacity will be limited only by the thickness of barium deposited when the getter is fired." Whilst oxidation of the whole of the metal is consistent with the Mott theory for the thin films which Bloomer has in mind, it should not be inferred from the theory that the oxide film on a layer of "massive" barium can similarly continue to increase in thickness until all the metal has been consumed. At temperatures greater than T_c the fairly rapid rate of growth will pass over into the "thin film" mechanism where the rate

of diffusion of the metal ions through the film is proportional to the electrostatic field across it so that the film will thicken according to the parabolic law. Since the theory only applies to regions of film thickness where the concentrations of metal ions and electrons can become unequal without the setting up of a space charge, it cannot be argued that an indefinite thickening of the oxide layer is a consequence of the Mott theory. As space charge effects become appreciable, the oxide film can be expected to thicken from the thin film region into that described by the Wagner[3] theory of parabolic oxidation; however, it may happen in practice that when the film has grown to some particular thickness, the rate of oxidation falls off to a negligible value. This is illustrated by the oxidation of aluminium in oxygen for which Bloomer quotes a value of T_c thus implying that above this temperature the metal will oxidize indefinitely. That this does not occur is shown by the work of Smeltzer[4] who stresses that oxidation virtually ceases at elevated temperatures.

An alternative explanation of the non-protective oxidation of barium at temperatures greater than T_c is suggested by reference to the oxidation behaviour of two other alkaline earth metals, magnesium and calcium. When magnesium is oxidized in dry oxygen at temperatures below about 450° C it follows an approximate parabolic law[5] whereas above this temperature the oxidation is no longer protective and the metal oxidizes until it is all consumed.[6, 7] With calcium the kinetics of the oxidation have not been investigated in such detail, but the general features are analogous: thus the metal oxidizes to completion in dry oxygen at temperatures of 300° C and above and, like magnesium, does so at a constant rate.[8] The transition temperature corresponding to the change from protective to non-protective oxidation has not been determined but it must lie between room temperature and 300° C.

It would seem that the transition temperature is determined by the physical properties of the oxide film in that at temperatures above it the oxide film develops cracks and becomes porous to oxygen gas. Leontis and Rhines[6] suppose that the magnesium oxide film spontaneously ruptures when some critical thickness is reached so that reaction then takes place at the metal surface between magnesium and oxygen gas to give a non-adherent oxide product. Alternatively, a thin uncracked layer of oxide may remain next to the metal through which the metal ions must diffuse before reacting.[9] If the thin layer of oxide remains of an effective constant thickness because growth and cracking proceed at equal and opposite rates, oxidation will take place at a constant rate.[7] Either of these mechanisms will explain the linear oxidation observed for magnesium and calcium but evidence we have recently accumulated in these laboratories indicates that the latter is the more likely.

It seems probable that the cracks are formed by a recrystallization mechanism, and support for this concept is provided by an examination of the kinetic data relating to the very early stages of the oxidation, full details of which will be published elsewhere. That the oxide scale formed on magnesium is highly porous has been shown by specific surface measurements.[10] We know of no work which enables an estimate of T_c to be made for the oxidation of either calcium or magnesium in oxygen.

It is possible that a similar mechanism of film recrystallization operates in the case of barium at temperatures greater than 40° C. Bloomer has shown that the oxidation curves at temperatures below 40° C follow the temperature dependence predicted by the Mott theory (see Fig. 5 of Bloomer's paper) so that the value 40° C can in fact be identified with T_c. Above 40° C, then, the barium oxide film might be expected to thicken according to a parabolic law and even possibly to reach a limiting thickness (compare magnesium at temperatures below about 450° C), but instead the conversion to oxide is complete. What probably in fact happens is that the barium first oxidizes according to the thin film mechanism, but when the film has grown to a particular thickness it recrystallizes in the manner already explained, so that the film through which the barium ions now have to diffuse is thinner and remains of an effective constant thickness. The linear rate thus predicted has been observed for barium oxidized in moist oxygen,[11] but unfortunately there is no similar data for the oxidation in dry oxygen.

Thus the oxidation of barium appears to present the interesting case where the transition temperature and the critical temperature happen to coincide.

Department of Chemistry,
The University of Exeter,
The Washington Singer Laboratories,
Prince of Wales Road,
Exeter.

S. J. GREGG and
W. B. JEPSON

[14 May, 1958]

REFERENCES

(1) BLOOMER, R. N. *Brit. J. Appl. Phys.*, **8**, p. 321 (1957).
(2) *See for example*: CABRERA, N., and MOTT, N. F. *Rep. Progr. Phys.*, **12**, p. 163 (1948).
(3) WAGNER, C. *Z. Phys. Chem.* (Leipzig), **B21**, p. 25 (1933).
(4) SMELTZER, W. W. *J. Electrochem. Soc.*, **103**, p. 209 (1956).
(5) GULBRANSEN, E. A. *Trans Electrochem. Soc.*, **87**, p. 589 (1945).
(6) LEONTIS, T., and RHINES, N. F. *Trans Amer. Inst. Min. Met. Eng.*, **166**, p. 265 (1946).
(7) GREGG, S. J., and JEPSON, W. B. Unpublished work.
(8) PILLING, N. B., and BEDWORTH, R. E. *J. Inst. Metals*, **75**, p. 529 (1923).
(9) *See for example*: EVANS, U. R. *Metallic Corrosion, Passivity and Protection* (London: Edward Arnold and Co. Ltd., 1946).
(10) GREGG, S. J., and SMITH, D. G. Unpublished work.
(11) KUBASCHEWSKI, O., and HOPKINS, B. E. *Oxidation of Metals and Alloys* (London: Butterworths Scientific Publications, 1952).

Thanks are due to Drs. Gregg and Jepson for pointing out that in this paper it is not sufficiently emphasized that the conclusions which may be drawn from the experimental results are valid only for oxide films which are within the "thin film" range of Mott. It is regretted that it was wrongfully thought unnecessary to emphasize this, once reference had been made to the papers by Mott and his co-workers. Care was taken, of course, to confine the experimental testing within the prescribed bounds of the theory, which are set at film thicknesses of a few hundred Angstrom units. (See, for example, the paper by Cabrera and Mott,[1] p. 176.) Therefore, in making some deductions from the Mott theory relevant to the experimental studies it was correct to state that above the critical temperature the capacity (oxide film thickness) will be limited by the thickness of barium deposited when the getter is fired.

Some of the misunderstanding of the paper arises from the different use of the word "indefinitely" by Gregg and Jepson and myself. Above the critical temperature no limit to growth is defined by deductions from the Mott theory, in

particular from equation (1) of Appendix 1 to the paper, (although the theory as a whole is valid only when the assumption about the absence of space charge is true). In other words, according to the Mott theory, the growth of oxide is indefinite. Thus, in his paper,[2] Mott uses the words "for temperatures above this, (the critical temperature) growth continues indefinitely." The argument which Gregg and Jepson disallow in their third paragraph must, on the contrary, be upheld when "indefinitely" has this meaning. Gregg and Jepson use "indefinitely" differently, as a synonym for "endlessly."

Furthermore, there is danger of confusion because the word "protective" us used to describe films of very different thicknesses. In their opening sentence Gregg and Jepson use the word, in the same way as it was used in the criticized paper, to describe oxide layers, about 50 Å thick, whose rate of growth has fallen to some low, arbitrarily selected, value. But elsewhere, Gregg and Jepson must use the word to describe a property of films so thick as to be outside the prescribed bounds of the Mott theory discussed and tested in the criticized paper. Otherwise, their final conclusion—that the transition temperature (defined by Gregg and Jepson as that "corresponding to the change from protective to non-protective oxidation") and the critical temperature (defined in equation (1) of the criticized paper) happen to coincide in the case of barium—cannot be avoided in the cases of all those other metals upon which oxide layers grow at a rapidly decreasing rate as the thickness increases beyond about 50 Å (the greatest thickness for electron transfer by quantum mechanical tunnel effect).

As commentary upon the note by Gregg and Jepson it must be pointed out that since it is implicit in the paper that the conclusions to be deduced from the experimental results with the barium films are valid only within the prescribed limits of the Mott theory, then the quotation therein of the critical temperature for any metal cannot be treated as an implication of endless growth of oxide at higher temperatures, although the extent of growth is indefinite in the theory.

Finally, Gregg and Jepson state that an alternative explanation of the non-protective oxidation of barium at temperatures greater than the critical temperature is suggested by reference to the oxidation behaviour of magnesium and calcium, for which metals the critical temperature is apparently not known. The evidence adduced is obtained from studies with oxide films much thicker than those for which the Mott theory is relevant. The suggestion that it is possible that a mechanism of film recrystallization operates in the case of barium at temperatures above 40° C is based on the assumption that since the thin barium films used in the work with getters did oxidize right through then much thicker films would have done so as well. Hence the conclusion that the critical and transition temperatures coincide for barium is reached through the inference that Gregg and Jepson rightly condemn in their third paragraph. The conclusion reached by this wrong inference might be right or wrong. Judgement can be made only after appeal to other theories and experimental results outside the scope of the work with barium films.

Research Laboratory,
Associated Electrical Industries Ltd.
Aldermaston, Berks.

R. N. BLOOMER
[23 May, 1958]

REFERENCES

(1) CABRERA, N., and MOTT, N. F. *Rep. Progr. Phys.*, **12**, p. 163 (1948).
(2) MOTT, N. F. *Trans Faraday Soc.*, **43**, p. 429 (1947).

Selected area microdiffraction in the electron microscope

Selected area microdiffraction is being increasingly used as an adjunct to studies in the electron microscope. In order to record exactly the part of the specimen giving rise to the diffraction pattern, it is necessary to photograph the specimen with the selector aperture in position. Such a photograph may be almost meaningless unless a survey micrograph is also recorded to show the relation of the selected area to the rest of the specimen. The necessity to make two photographs may be avoided very simply by the following procedure:

(1) record the diffraction pattern from the required area;
(2) adjust the strength of the intermediate lens to produce an image of the selected area and focus it;
(3) adjust the intensity of the illumination so that a five to six second exposure is required;
(4) open the shutter to expose the plate;
(5) after one to two seconds withdraw the selector aperture;
(6) close the shutter after the full exposure time of five to to six seconds.

The resulting micrograph will be as shown in the figure, with the required information on one plate. It has been found that the selector aperture can be withdrawn quickly

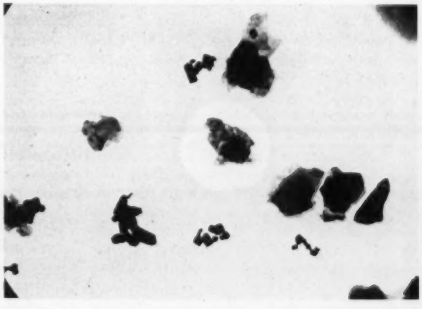

Dispersion of face powder. Light circle shows area selected for microdiffraction. (×8000)

enough to avoid streaks on the picture without causing vibration which would reduce the quality of the micrograph.

Strictly speaking, the area selected for diffraction can only be reproduced with accuracy at one magnification, namely that at which the image plane of the intermediate lens coincides with the plane of the selector aperture. At other settings of the intermediate lens the selected area shown on the micrograph will be only approximately correct. When a low magnification survey picture of the region around the selected area is required, however, the inaccuracy in the selected area shown will generally be unimportant.

Aeon Laboratories,
Beech Hill,
Englefield Green,
Surrey.

A. W. AGAR
[13 May, 1958]

Notes and comments

Proceedings of the Royal Institution

The Friday evening discourses given at the Royal Institution of Great Britain in the heart of London are well known to most of our readers as understandable yet authoritative accounts by specialists of recent advances in a wide field of learning. These discourses, concerned mainly with scientific subjects, are published in the *Proceedings* which have appeared annually. In future the *Proceedings* will appear three times a year at a charge of 8*s*. 6*d*. a part or 21*s*. p.a., commencing January next. The first of the new series contains the following discourses: Sir Lawrence Bragg on "Gemstones," Mr. John M. Allegro on "The Dead Sea Scrolls," Dr. L. Radzinowicz on "Changing attitudes towards crime and the devices used to combat it," Professor W. R. Hawthorne on "Aero-thermodynamics," Professor C. D. Darlington on "The control of evolution in man" and Professor R. J. Pumphrey on "Hearing in man and animals."

Orders for these *Proceedings* should be sent to the Royal Institution, 21 Albemarle Street, London, W.1.

User-specification for sealed X-ray tubes for use in X-ray diffraction

The X-ray Analysis Group of the Institute of Physics announces that a panel of its Equipment Sub-Committee has completed the preparation of a user-specification dealing with the design of sealed X-ray tubes for use in X-ray diffraction and similar applications. Copies of this specification may be had by anyone interested on application to the Honorary Secretary of the Equipment Sub-Committee of the X-ray Analysis Group, Dr. E. G. Steward, Research Laboratories of The General Electric Co. Ltd., Wembley, Middlesex.

British Nuclear Energy Conference: lecture symposium on the Geneva conference.

To help scientists and engineers to assimilate the large amount of material (over 2000 papers) produced for the second International conference on the peaceful uses of atomic energy (Geneva, 1–13th September 1958), the British Nuclear Energy Conference (of which the Institute of Physics is a constituent body) has planned a one-day lecture symposium to take place on Thursday, 11 March, 1959.

For the purpose of the symposium, the Geneva conference papers will be classified into 6 or 7 groups, and leading experts in each field will attempt to highlight the most important aspects of the new information.

The lectures will be printed in the April 1959 issue of the *Journal of the British Nuclear Energy Conference* and further details will be announced in due course.

Journal of Scientific Instruments

Contents of the September issue

ORIGINAL CONTRIBUTIONS

Papers

A calculator for numerical Fourier synthesis. By V. Timbrell.
A microwave spectrometer for the study of free radicals. By I. R. Hurle and T. M. Sugden.
X-ray absorption microanalysis with fine-focus tubes. By J. V. P. Long.
An airborne infra-red solar spectrometer. By J. T. Houghton, T. S. Moss and J. P. Chamberlain.
The influence of rate of cooling on the zeros of mercury-in-glass thermometers. By Sj. Van Dijk, J. A. Hall and Vera M. Leaver.
A method of flash synchronization for high-speed cinematography. By J. D. Lewis and G. T. Peck.
A vibration pick-up which does not load the system being examined. By S. K. Rushforth and A. Selwood.
A permeameter controller for magnetic measurements. By M. J. Swan.
A piezo-electric pressure bar gauge. By D. H. Edwards.

Laboratory and workshop notes

Electrodes for thin metal films. By S. Chandra and G. D. Scott.
An electrode holder for the porous cup technique of spectrographic analysis. By G. W. J. Kingsbury and Anita Farsey.

NOTES AND NEWS

Correspondence

A precise reference inductor. From A. C. Lynch; D. Gugan.

New instruments, materials and tools

Journal of Scientific Instruments

Contents of the October issue

ORIGINAL CONTRIBUTIONS

Papers

A decade of stable resistors for calibration of the Smith resistance thermometry bridge (type 3). By G. G. Lowenthal and R. G. Ackland.
Computing plates. By J. de Meulenaer.
An electrostatic-magnetic alinement section for the electron microscope. By M. E. Haine, A. W. Agar and T. Mulvey.
The preparation of single-crystal ingots of silicon by the pulling technique. By E. Billig and D. B. Gasson.
The sensitivity of low-frequency valve amplifiers for electromyography. By A. Nightingale.
An alternating-beam spectrophotometer. By R. V. Hesketh.
An electrodynamic magnetic field gradiometer employing a microvibration technique. By Y. L. Yousef and H. Mikhail.

Laboratory and workshop notes

A method of programming the speed of linear traverse. By P. H. Hollins and D. W. Skidmore.
A note on the use of polytetrafluoroethylene in vacuum seals. By A. J. Davies.
A simple creep strain recorder for use with wire specimens. By J. Congleton and R. N. Parkins.
Stabilization of air flow through a filter. By S. H. Small.
A high-speed relay self-rectifying circuit for conductivity measurements. By D. M. G. Armstrong.
A buckling spring calibrator for thread strength machines. By S. L. Anderson.
A neoprene vacuum gasket for wires. By A. C. Prior.
The use of germanium junction cells for photoelectric control circuits. By R. F. Peart, T. B. Rymer and D. H. Tomlin.

NOTES AND NEWS

Correspondence

Modifications to the collimating system of the Unicam 9 cm X-ray powder camera. From R. L. Gordon, O. G. Griffin and E. P. Rodgers.
A corrosion proof vacuum controller for pressures under 1 mm of mercury. From I. Amariglio and M. M. Benarie.

New books — New instruments, materials and tools
Manufacturers' publications — Notes and comments

BINDING ORDERS

Orders and enquiries about the binding of back-numbers of the *Journal of Scientific Instruments* and of the *British Journal of Applied Physics* should now be sent direct to Messrs. E. A. Weeks and Son, 168 Gower Street, London, N.W.1 (EUSton 4674), and *not* to The Institute of Physics. This new arrangement does not involve any change in price.

THIS JOURNAL is produced monthly by The Institute of Physics, in London.

It deals with all branches of applied physics (including theory and technique). All rights reserved. Responsibility for the statements contained herein attaches only to the writers.

EDITORIAL MATTER. Communications concerning editorial matter should be addressed to the Editor, The Institute of Physics, 47 Belgrave Square, London, S.W.1. (*Telephone:* Belgravia 6111.) Prospective authors are invited to prepare their scripts in accordance with the *Notes on the preparation of contributions*. (Price 2*s*. 6*d*. including postage.)

REPRODUCTION. The Institute of Physics is a signatory to The Royal Society's Fair Copying Declaration. Details may be obtained upon application from The Royal Society, London, W.1.

ADVERTISEMENTS. Communications concerning advertisements should be addressed to the agents, Messrs. Walter Judd Ltd., 47 Gresham Street, London, E.C.2. (*Telephone:* Monarch 7644.)

CLAIMS FOR MISSING JOURNALS. Claims from regular subscribers to this *Journal* for missing numbers will only be considered if received within 60 days of the date of mailing plus normal outward time of transit and time for lodging the claim. Losses attributable to failure to notify a change of address or to similar omissions will not be considered.

SUBSCRIPTION RATES. A new volume commences each January. The charge is £5 per volume ($14.25 U.S.A.), including index (post paid), payable in advance. Single parts, so far as available, may be purchased at 10*s*. each ($1.50 U.S.A.), post paid, cash with order. Orders should be sent to The Institute of Physics, 47 Belgrave Square, London, S.W.1, or to any bookseller.

The relationship between surface texture and rolling resistance of steel

By J. HALLING, B.Sc.(Eng.), Mechanical Engineering Department, University of Liverpool

[*Paper first received* 3 *April, and in final form* 1 *July*, 1958]

The paper describes two series of experiments which were designed to investigate the relationship between the surface texture of ground mild steel surfaces and the resistance to rolling of hard steel rollers on these surfaces. In the first series of experiments the rollers were unloaded whilst in the second series of tests the rollers were subjected to a load range of 15–80 lb. In both cases it was found that the coefficient of rolling resistance increased with increasing roughness of the surface. By extrapolation of the results from the second series of tests, agreement with the results of the first series was obtained. The coefficient of rolling resistance was found to decrease with increasing load.

The variation of the coefficient of rolling resistance with load is obtained in the form of an experimental law which is compared with the various theories of the mechanism of rolling resistance.

The widespread awareness of the low resistance to motion exhibited by rolling elements is apparent from the extensive application of the phenomenon. Nevertheless, there appears to be very little published information giving experimental results which can be used to establish the probable causes of this type of resistance. The results from tests on ball and roller bearings are of little use because of the complicating effects of other variables such as lubricant effects and the existence of sliding conditions between the rolling elements and their cages and races. This paper describes some experiments designed to establish the degree of dependence of pure rolling resistance on the surface texture of machined surfaces. The tests here reported were carried out using rollers rather than balls since it is probable that with line contact the conditions of pure rolling are most nearly attained.

THE NATURE OF ROLLING RESISTANCE

The earliest attempt to describe the nature of rolling resistance appears to be due to Leonardo da Vinci (1452–1519). He stated that: "This kind of friction is caused, not by rubbing, but by contact in what might be described as progress by infinitely small steps."

The first experimental investigation of the phenomenon is credited to Coulomb (1736–1806) who obtained the resistance to motion of rollers of *lignum vitae* and elm resting on oak supports. He found that the resistance was directly proportional to the load and was inversely proportional to the radius of the roller. Subsequent experiments by Morrin on the resistance of wagons moving along roads appeared to confirm Coulomb's results.

(1) *Interfacial slip theories.* Towards the end of the last century this problem was studied both experimentally and analytically by Reynolds.[1] He introduced the concept of zones of sticking and sliding inside the contact area between the roller and the surface. These sliding regions on either side of a central region of sticking are then assumed to be responsible for the resistance to motion.

Recently several mathematical relationships have been developed to deal with the resistance to rolling from the standpoint of the sliding zones originally postulated by Reynolds. Glagolev[2] has considered three possibilities for the condition of sliding in the contact zone: (*a*) Forward and rearward areas of sliding bounding a central region of sticking; (*b*) sliding over the whole of the contact zone which is assumed to be a limiting condition; (*c*) one zone of sliding combined with one zone of sticking, which is not supported by the mathematical solution.

Another solution for this problem was developed by Föppl[3] and later modified by Heinrick[4] to satisfy the contact conditions postulated by Hertz.[5] In this solution the slipping is assumed to occur over a single rearward area of the contact zone. An alternative solution for the same contact conditions has also been produced by Poritsky.[6]

These solutions may all be represented by the following equation for a cylinder rolling along a plane surface:

$$\lambda = \mu R\left[1 - \left(\frac{\alpha}{a}\right)^2\right] \qquad (1)$$

where λ = coefficient of rolling resistance
μ = coefficient of sliding friction
R = radius of the cylinder
$2a$ = width of the contact zone
2α = width of the zone of sticking.

For a cylinder subjected to a normal load P and a torque M

$$\lambda = M/P = QR/P \qquad (2)$$

where Q is the tangential traction in the contact zone. The coefficient λ may be given the physical significance shown in Fig. 1 where the normal reaction P is supposed to act at a distance λ from the axis of rotation.

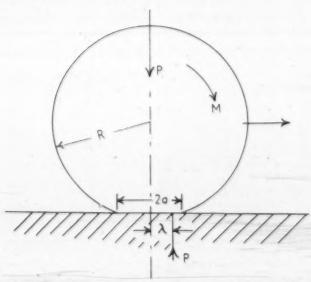

Fig. 1. The representation of the coefficient of rolling resistance

(2) *Molecular adhesion theory.* Tomlinson[7] carried out careful experiments on the rolling of metal cylinders at light loads and explained his results on the assumption that the resistance was due to molecular adhesion between the surfaces arising from interfacial forces. Thus he concluded that both sliding and rolling friction are manifestations of the same phenomenon and may be simply related one to the other.

For a cylinder rolling along a plane surface his theoretical equation may be expressed as:

$$\lambda = 3Re\mu/4a \tag{3}$$

where μ, λ, R and a have the same meaning as before and e represents the mean molecular spacing, i.e. lattice constant, for the material of the plane and the roller.

Substituting the value of a (Prescott[8]) yields the equation for the coefficient of rolling resistance:

$$\lambda = \frac{3}{8} Re\mu \cdot \frac{1}{\sqrt{P}} \sqrt{\left[\frac{\pi E}{2R(1-\sigma^2)}\right]} \tag{4}$$

(3) *The surface irregularities theory.* Another possible cause of the resistance to rolling has been suggested by Bikerman.[9] He postulates that the resistance to motion is due to the requirements for the rolling element to surmount the irregularities which are present on any machined surface. The inclined plate method was used to determine the resistance to motion of steel balls rolling along steel plates having a variety of surface textures. If h is the average height of the surface irregularities and θ is the angle of inclination necessary to either initiate, or arrest, motion then:

$$h = R(1 - \cos\theta) \tag{5}$$

and

$$\lambda = R \tan\theta \tag{6}$$

The values of h predicted using equation (5) showed an approximate correlation with the values of h as measured by a stylus type of surface texture instrument.

(4) *The hysteresis theory.* In view of the forward compression and rearward expansion of the material as motion proceeds the possible contribution of hysteresis losses to the overall resistance has been suggested by Palmegren,[10] and Allan.[11] This effect has been investigated experimentally by Tabor[12, 13] for the case of steel balls rolling along rubber sheets having differing hysteresis properties. The results show good agreement with the theoretical predictions on the assumption that the resistance is entirely due to hysteresis effects. It is possible that the large magnitude of the hysteresis losses for rubber as compared with losses due to other causes in these tests leads to such good agreement. For the smaller order of magnitude of the hysteresis effects with metals such good correlation with theoretical predictions was not obtained.

TESTS WITH UNLOADED ROLLERS

These tests were designed to determine the effect of surface texture of ground steel surfaces on the resistance to rolling of relatively smooth rollers.

Apparatus. The apparatus, shown in Fig. 2, was designed to measure accurately that inclination of the test surface which initiated rolling. The roller *D* rests on the test surface *C* which is located on the tilting table *E* mounted in the trunnions *A*. The pin *G*, which may be adjusted to any desired eccentricity to the axis of the drive, engaged in a slot cut along the arm of the table *E*. A control *J* operates the eccentric pin *via* a 40 : 1 reduction gear *H*, to produce angular displacement of the test surface. The angular position of the test surface was obtained from the reading of the dial gauge *F* (1×10^{-4} in./division) whose anvil rests on the table at a fixed distance from the trunnions. Two stops *B*, resting on the test surface, were used to set the initial position of the roller for motion to the right and to the left respectively. A traversing microscope *K* was used to ascertain the initial movement of the roller as the inclination of the table was increased.

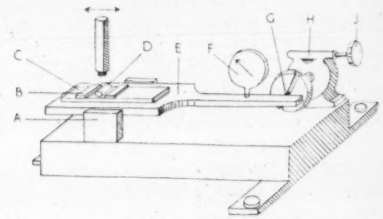

Fig. 2. Apparatus used in the first test series

Test specimens. For these tests twelve surfaces were produced by surface grinding on the larger face of $4 \times 1\frac{1}{4} \times \frac{1}{4}$ in. steel plates. The material of the plates had a yield strength of approximately 25 tons/in.^{2} and a Vickers diamond pyramid hardness number of 197. The finishes obtained by grinding ranged from 10 to 68 μ in. c.l.a. (centre line average) as measured across the direction of machining by a Talysurf (by Taylor, Taylor and Hobson Ltd.), at a wavelength cut off setting of 0·03 in.

A set of rollers of $\frac{1}{2}$ in. diameter and of lengths $\frac{1}{2}$, $\frac{5}{8}$, $\frac{3}{4}$ and 1 in. respectively were used. These were produced by grinding from a roller bearing steel having a yield strength in excess of 100 tons/in.^{2} The Vickers diamond pyramid hardness number was 835. The finish of all the rollers was better than 3 μ in. c.l.a.

Experimental technique. The rollers, stops and test surfaces were cleansed by successive washing in ethylene trichloride vapour and acetone, followed by drying in air. The test surface and stops were then located on the tilting table, the roller being placed in contact with one of the stops. The inclination of the table was then increased until the first motion of the roller away from the stop was detected by observation through the microscope. On numerous occasions the initial movement of the roller was exceedingly small, and further inclinations of the surface was necessary to obtain further movement of the roller. The angle of inclination necessary to produce motion in the opposite direction away from the second stop, placed about $\frac{3}{4}$ in. along the surface from the first stop, was then obtained.

This procedure was repeated for ten positions of the stops at equal intervals along the length of the test surface.

Results. The readings of the angle dial gauge for the ten positions along the test surface using the various lengths of roller are shown for two of the test surfaces in Table 1. The average values of the inclination for each of the twelve test surfaces is shown in Table 2 together with the derived values of the coefficient of rolling resistance obtained from equation (6). The value of the coefficient of rolling resistance is plotted to a base of the c.l.a. for each surface in Fig. 3.

Table 1. *Typical experimental observations for the first test series*

Surface No. 2

Roller length (in.)	*Direction of motion*	*Dial gauge reading* 1×10^{-4} *in.*										*Mean value* 1×10^{-4} *in.*
1	To right:	43	55	58	38	131	110	39	36	48	53	60
	to left	14	141	123	68	165	44	9	91	77	67	
$\frac{3}{4}$	To right:	85	89	94	96	89	5	19	125	54	58	62
	to left	48	65	78	34	9	16	93	143	25	110	
$\frac{5}{8}$	To right:	48	87	64	4	7	30	89	91	77	120	64
	to left	1	77	66	57	158	16	26	90	86	94	
$\frac{1}{2}$	To right:	13	67	93	45	51	78	65	153	93	55	62
	to left	25	44	5	61	18	21	50	23	177	170	

The mean value of the dial gauge reading = 62 × 10^{-4} in.

Surface No. 8

Roller length (in.)	*Direction of motion*	*Dial gauge reading* 1×10^{-4} *in.*										*Mean value* 1×10^{-4} *in.*
1	To right:	28	195	148	98	176	209	196	35	42	133	79
	to left	34	78	154	27	86	95	83	122	104	46	
$\frac{3}{4}$	To right:	92	65	214	144	30	85	135	137	83	83	77
	to left	22	233	37	88	71	24	58	87	76	19	
$\frac{5}{8}$	To right:	146	34	46	146	104	157	126	180	182	64	82
	to left	10	181	7	52	127	211	25	71	39	16	
$\frac{1}{2}$	To right:	45	30	28	127	48	95	222	24	15	85	79
	to left	98	64	92	95	92	57	157	57	189	129	

The mean value of the dial gauge reading = 79 × 10^{-4} in.

Table 2. *Results derived from the first test series*

Each c.l.a. value is the average of five determinations.
(Cut-off wavelength 0·03 in.)

Test plate	*C.l.a. value (μ in.)* *Transverse*	*Longitudinal*	*Dial gauge reading average value* 10^{-4} *in.*	*Angle of inclination (rad.)*	*Coefficient of resistance* λ
1	10	5·2	50	0·001 60	0·000 400
2	16	6·4	62	0·001 90	0·000 498
3	25	7·5	75	0·002 40	0·000 600
4	37	7·5	73	0·002 35	0·000 578
5	21	7·8	71	0·002 27	0·000 568
6	28	8·9	80	0·002 56	0·000 640
7	45	12	78	0·002 50	0·000 625
8	23	8·7	79	0·002 53	0·000 632
9	68	14	84	0·002 70	0·000 675
10	55	15	84	0·002 75	0·000 688
11	58	15	87	0·002 79	0·000 698
12	41	11	82	0·002 63	0·000 658

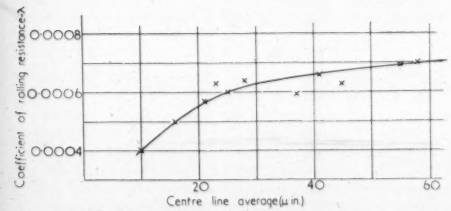

Fig. 3. Relationship between the coefficient of rolling resistance and the surface texture

Discussion of the results. In these tests the angle of inclination which is required to initiate motion will depend on the following factors:

(*a*) The accuracy of the initial levelling of the test surface which dictates the accuracy of the zero setting of the angle dial gauge.

(*b*) The dimensional truth, i.e. flatness, of the test surface.

(*c*) Those properties of the surface and roller which are responsible for the phenomenon of rolling resistance.

(*d*) The resistance to motion created by the capillarity of traces of liquid on the surface.

The method of testing which was adopted and in which readings were obtained for both direction of inclination at a number of positions along the surface minimized the effect of (*a*) and (*b*).

If the surface textures is a significant variable affecting the value of the rolling resistance, as is suggested by the results, any particular determination in these tests will be dependent on the position of the roller with relation to the surface irregularities. Since the surface irregularities are of varying size and shape, randomly distributed over the surface, the reason for the considerable scatter of the results becomes accountable. Such scatter of results has been noted by previous investigators, and is typical of much experimental work on friction. A small amount of initial movement followed by an arrest, which was often observed, could also be accountable to the size and disposition of the irregularities.

The axial pressure distribution is not uniform due to the lateral displacement of material at the extremities of the roller. From the results, however, the length of the roller does not appear to be significant so that these effects have been discounted.

Deformation of the surfaces. For a roller of length l in. and radius R in. resting on a plane surface, the maximum vertical elastic deformation δ in., due to an applied load of P lb, is given by Föppl (Allan[11], p. 147) as:

$$\delta = \frac{2}{\pi E}(1 - \sigma^2)\frac{P}{l}\left(1{\cdot}207 + \log_e \frac{l.E.R}{P}\right) \qquad (7)$$

In these tests the value of δ is found to be 0·03 μ in. For

the same conditions the maximum stress in the contact zone is given by Prescott[8]:

$$p_{max} = \sqrt{\frac{P \cdot E}{2\pi \cdot l \cdot R \cdot (1 - \sigma^2)}} = \frac{2P}{\pi \cdot a \cdot l} \qquad (8)$$

which gives a value for p_{max} of 0·501 tons/in.^{2} For these values of δ and p_{max} the surfaces of the contacting bodies are assumed to be ideal. The existence of surface irregularities, and consequently smaller real areas of contact, will result in considerably higher values for the deformation and contact stresses. Indeed, it is probable that some plastic deformation of the tips of the irregularities occurs although such deformation was not detectable in stylus records of the surface before and after the tests.

The effects of capillarity. To check the possible effect of capillarity a separate test series was carried out with the apparatus inside a sealed cabinet containing trays of silica gel drying agent. The control *J* (Fig. 2) protruded through a greased felt seal. The roller and angle dial could be observed through a Perspex panel, the microscope being mounted externally.

The tests were conducted after sealing the cabinet and allowing to dry out overnight. The results from such tests on two of the test surfaces were not significantly different from the results obtained for the previous tests.

TESTS WITH LOADED ROLLERS

The tests already reported were extended in this section by the development of a technique which enabled normal loads to be applied to the rollers.

Apparatus. The apparatus[14] is shown diagrammatically in Fig. 4 and a general view is shown in Fig. 5. The compression system consists essentially of three blocks, *A*, *B* and *C*, which are separated by pairs of identical rollers *D* resting between similar test plates *E*. The system is loaded by the nut and screw *G*, the rotation of the screw being prevented by a pin located in a slot cut along the length of the screw. The upper and lower blocks are constrained by the end plates *F* such that they have no lateral movement. The central block *B* has limited lateral freedom by virtue of the two pairs of rollers. Alignment of the applied load is achieved by locating the compression system between ball and cone seatings situated at the centre of the loading beam *H* and at the base of the lower block *C*. The applied load is indicated by the dial gauge which is attached to, and indicates the deflection of the loading beam *H* by means of the extensions *K*.

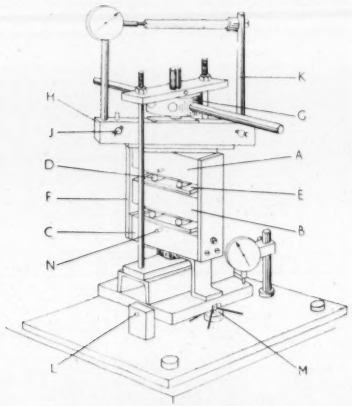

Fig. 4. Rolling friction machine

The compression system is pivoted at *L*, the angle of inclination being adjusted by the screw *M*. The angle of inclination is computed from the reading of the second dial gauge (1×10^{-3} in./division). The position of the rollers must be such that they are equally disposed on each side of the loading axis and with their axes parallel. This condition is ensured by the use of setting gauges (not shown) which are located by two plates which are indexed by the two pins *N*.

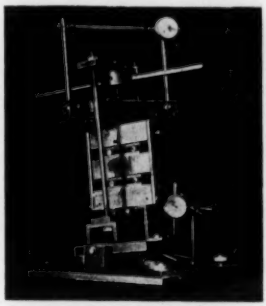

Fig. 5. Photograph of the apparatus shown in Fig. 4

Test specimens. Test specimens similar to those previously described were used in these tests. It was necessary to produce these specimens in sets of four, i.e. four plates and four rollers. The plates in each group had similar c.l.a. values; the average values for each group are shown in Table 3.

Table 3. *Values of surface texture for the test surfaces used in the second test series*

(Cut-off wave length 0·03 in.)

Direction of measurement of c.l.a. value	*Average c.l.a. value for group (μ in.)*				
	Group A	*Group B*	*Group C*	*Group D*	*Group E*
Longitudinal	14·5	12·2	7·8	6·9	4·9
Transverse	59	43	27	15	7·6

Experimental technique. The rollers, plates and setting gauges were cleansed by the method described previously, and the apparatus was assembled with the rollers correctly located by the setting gauges. The central block *B* was then released and oscillated ten times over its full traverse (about $\frac{1}{4}$ in.). This procedure was adopted to ensure that the surface irregularities were plastically deformed before measurements of the resistance to motion were made. It was found that five readings of the inclination necessary to initiate motion of the central block gave a repeatable average value. Similar determinations were obtained for a series of loads up to 80 lb and at each load setting the central block was oscillated over its full traverse ten times before any measurement was attempted. Each of the sets of specimens

designated in Table 3 were tested in this manner, using the same set of $\frac{1}{4}$ in. diameter $1\frac{1}{4}$ in. long rollers.

The very limited scatter of the experimental results observed in these tests compared to that obtained previously is attributable to:

(*a*) The averaging effect of having eight contact surfaces.
(*b*) The increased resistance due to the applied loading.

The minimum load used in these tests was 15·7 lb for each roller arising from the dead weight of those parts of the apparatus which were supported by the roller.

Determination of the coefficient of rolling resistance. In Fig. 6 the normal reaction P is assumed to be displaced

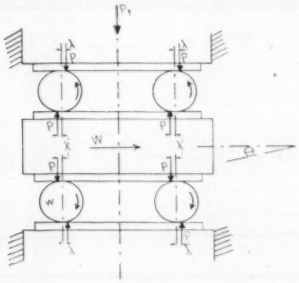

Fig. 6. The method of determining the coefficient of rolling resistance in the second test series

by a distance λ from the axis of rotation for each of the eight contact zones. It is assumed that P and λ have the same values in each contact zone although in fact they differ slightly due to the weight W of the central block and the weight w of the rollers. Such an assumption will produce the greatest errors at low loads where W is significant with respect to the thrust load Pt. The average load per contact surface is

$$P = P_t/2 + W/4 + w \tag{9}$$

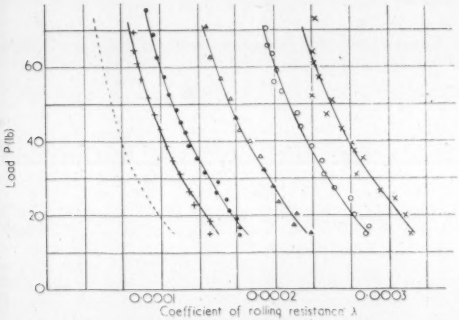

Fig. 7. The variation of the coefficient of rolling resistance with load for different surfaces

× Group *A*, average c.l.a. 59 μ in.
○ Group *B*, average c.l.a. 43 μ in.
△ Group *C*, average c.l.a. 27 μ in.
● Group *D*, average c.l.a. 15 μ in.
+ Group *E*, average c.l.a. 7·6 μ in.
– – – – derived for a c.l.a. of 0 μ in.

Also
$$2WR\sin\theta + 4wR\sin\theta = 8\,.\,P\,.\,\lambda \tag{10}$$

Therefore
$$\lambda = \frac{(W + 2w)R\sin\theta}{2P_t + W + 4w} \tag{11}$$

Results. The curves of Fig. 7 show the experimental values of λ and P obtained for the five sets of test surfaces described in Table 3. The curves in Fig. 7 are redrawn on a semi-logarithmic base in Fig. 8 which indicates an

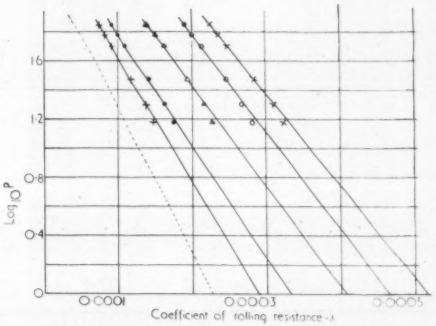

Fig. 8. The relationship between $\log_{10} P$ and the coefficient of rolling resistance for different surfaces

× Group *A*, average c.l.a. 59 μ in.
○ Group *B*, average c.l.a. 43 μ in.
△ Group *C*, average c.l.a. 27 μ in.
● Group *D*, average c.l.a. 15 μ in.
+ Group *E*, average c.l.a. 7·6 μ in.
– – – – derived for a c.l.a. of 0 μ in.

experimental law relating the applied load and the coefficient of rolling resistance of the form

$$\lambda = \frac{K}{n}\left(1 - \frac{\log_{10} P}{K}\right) \tag{12}$$

The values of K and n in equation (12) for the several values of surface texture are shown in Fig. 9. Using the values of K and n for the ideal smooth surface obtained from Fig. 9

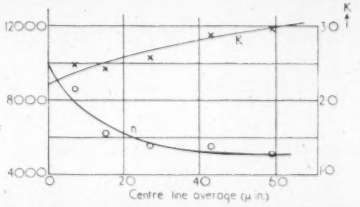

Fig. 9. The relationship between n and K and the surface texture

○ values of n
× values of K

the relationship of λ with P for such a surface is shown dotted in Fig. 7. Furthermore, from the curves in Fig. 7 and from equation (12) the variation of λ with surface texture at a variety of loads are shown in Fig. 10. The predicted curve for an applied load of 0·06 lb is shown in

Fig. 10 together with the original curve obtained experimentally in the first series of tests for this load condition. The agreement obtained by this extrapolation of the experimental results from the second series to the conditions of the first series is sufficient justification for the validity of equation (12) over the range of loads here considered. Tests on the surfaces in groups A and E in the presence of

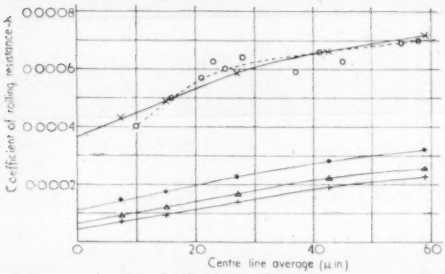

Fig. 10. The relationship of the coefficient of rolling resistance with surface texture at various loads

+ applied load 70 lb.
△ applied load 45 lb.
● applied load 15 lb.
× applied load 0·06 lb derived by extrapolation from Fig. 11.
○ applied load 0·06 lb obtained experimentally in the first test series.

a lubricant showed no significant variation from the results already reported.

DISCUSSION OF RESULTS

The results of these tests show a definite dependence of the resistance to rolling on surface texture and it is interesting to compare these results in the context of the respective theories.

The interfacial slip theories. An immediate similarity of form is apparent between the experimental equation (12) which may be written:

$$\lambda = \left(\frac{K}{nR}\right) R\left(1 - \frac{\log_{10} P}{K}\right) \tag{13}$$

and equation (1)

$$\lambda = \mu R\left[1 - \left(\frac{\alpha}{a}\right)^2\right] \tag{1}$$

These equations suggest that the ratio (α/a) is a function of P and K, the latter term being dependent upon the surface texture, i.e. K increases with the roughness of the surfaces as shown in Fig. 9. Thus the degree of sticking should increase with increasing load and will be less, at any given load, for the rougher surface. Furthermore, there should be sticking over the whole contact zone for values of load such that $\log_{10} P$ is equal to the appropriate value of K for the surface and the value of λ would then be zero.

Because of the very small width of the contact zone for rolling bodies any slip in this zone must be in the nature of microslip. Cocks,[15] Johnson,[16] Courtney-Pratt and Eisner[17] have shown that such slip conditions yield reduced values of the coefficient of sliding friction. Despite this the values required to correlate equations (1) and (14), which are shown in Fig. 11, are still impossibly small. For this reason it is concluded that the interfacial slip theory cannot explain the experimental results.

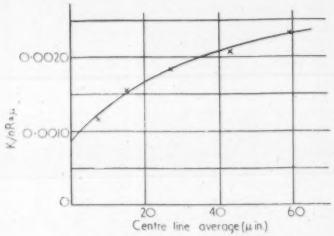

Fig. 11. The relationship between the apparent coefficient of sliding friction ($\mu \equiv K/nR$) and the surface texture

Molecular adhesion theory. Using equation (4) and the results from Fig. 7 for the ideal surface (c.l.a. zero), the values of the product $e\mu$ have been calculated and are shown in Table 4. Although these values are reasonably

Table 4. *Values of $e\mu$ for the ideal surface at various values of applied loads*

P (lb) Load	*Value of $e\mu$ for the ideal surface*
15	$3{\cdot}16 \times 10^{-7}$
20	$3{\cdot}20 \times 10^{-7}$
30	$3{\cdot}13 \times 10^{-7}$
40	$3{\cdot}10 \times 10^{-7}$
50	$3{\cdot}07 \times 10^{-7}$
60	$2{\cdot}95 \times 10^{-7}$
70	$2{\cdot}76 \times 10^{-7}$

constant with increasing load they yield a larger value for e than would be expected if any typical value for steel on steel is ascribed to μ.

The surface irregularities theories. On the basis of this theory the decrease in the coefficient of rolling resistance with increasing load is accountable to the plastic deformation of the tips of the irregularities. The nature of this deformation is illustrated by the surface records (Fig. 12) at various loads, due to a roller moving along the surface. For the range of loading employed in these tests the first two records are of interest. The actual deformation of the tips of the irregularities becomes more apparent by considering the shape of the bearing area curves shown in Fig. 13, where the deformation is indicated by the flattening of the portion AB of this curve after the first loading. These small changes in magnitude of the irregularities could produce a significant change in λ since the roller will only penetrate the depth of the texture to a slight degree due to its axial length, and large radius relative to the size of the irregularities. It is, however, apparent that since for the ideal surface (c.l.a. zero) there still remains a finite value of the coefficient of resistance this explanation cannot account for the whole of the rolling resistance.

Hysteresis theory. The elastic work done in rolling a given distance will be a function of the applied load and the elastic deflexion. The majority of this work done in the

forward compression region will be recovered due to the rearward expansion region. Any loss due to hysteresis effects will produce a resistance to motion.

A loaded cylinder rolling a distance x along a plane will map out an area lx where l is the axial length of the cylinder. Neglecting small end effects each element of this area will be subjected to a stress p_{max} given by equation (8) and will undergo a deflexion δ given by equation (7).

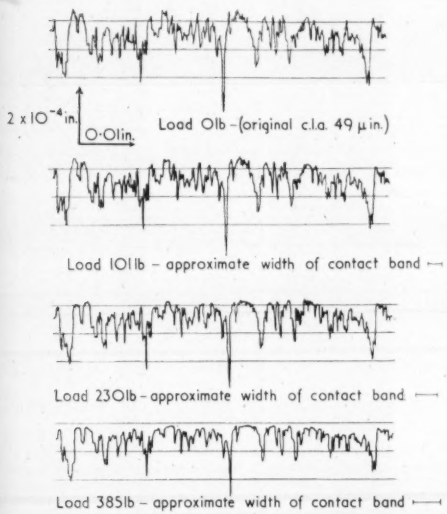
2 x 10⁻⁴ in.
0·01in.
Load 0lb – (original c.l.a. 49 μ in.)
Load 101lb – approximate width of contact band
Load 230lb – approximate width of contact band
Load 385lb – approximate width of contact band

Fig. 12. The deformed texture due to rolling at various values of load. The approximate width of the contact band at each load is also shown

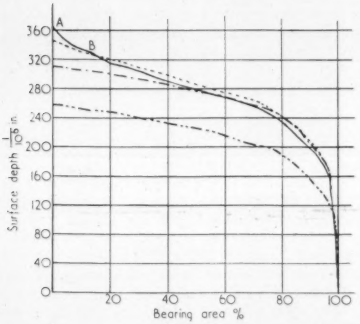

Fig. 13. Bearing area curves for the profiles shown in Fig. 12

——— Load 0 lb.
– – – – – Load 101 lb.
— — — Load 230 lb.
— – — – Load 385 lb.

Thus the elastic work done in compressing the material is given by:

$$\frac{2P}{\pi \,.\, a \,.\, l} \cdot lx \cdot \frac{2}{\pi E}(1 - \sigma^2)\frac{P}{l}\left(1{\cdot}207 + \log_e \frac{l \,.\, E \,.\, R}{P}\right)$$

If ϕ is the hysteresis loss factor, the work done, expressed in terms of the coefficient of rolling resistance, may be equated to the energy loss as follows:

$$P \,.\, \lambda \cdot \frac{x}{R} = \phi\left[\frac{2P}{\pi a l} \cdot lx \cdot \frac{2}{\pi E}(1 - \sigma^2)\frac{P}{l}\left(1{\cdot}207 + \log_e \frac{lER}{P}\right)\right]$$

$$\text{Thus} \quad \lambda = \phi\left[\frac{4P}{\pi^2 Ela}(1 - \sigma^2)\left(1{\cdot}207 + \log_e \frac{lER}{P}\right)\right]$$

Inserting appropriate numerical values for the constants of these experiments and converting to a $\log_{10}$ basis yields:

$$\lambda = 0{\cdot}003 \,.\, \phi \,.\, (P)^{\frac{1}{2}}[1 - (\log_{10} P/7{\cdot}5] \qquad (14)$$

If ϕ is assumed to be constant, equation (14) yields an increasing value of λ with increasing load which is contrary to the experimental observations. Furthermore, if ϕ is assumed to increase with increasing load[13] the divergence between equation (14) and the experimental results is even more apparent. Although the hysteresis loss may be a contributory factor in the rolling resistance it is not possible to correlate the results of these experiments with this factor alone.

CONCLUSIONS

It appears from the experimental results that the resistance to motion of steel rollers moving along steel surfaces cannot be attributed to any single theory of those which have been proposed to explain the phenomenon. The surface texture theory offers the simplest explanation of the phenomenon and is in agreement with the observed decrease in the coefficient of resistance with increasing load. The hysteresis theory is in all probability a further contributory factor but a smaller order effect than the other factors.

The primary purpose of the investigation is fulfilled in that it shows a definite dependence of the rolling resistance on surface texture.

ACKNOWLEDGEMENTS

I would like to express my thanks to Professor H. Ford of the Imperial College of Science and Technology and to Professor W. J. Kearton of the University of Liverpool for their help and suggestions during the progress of this investigation. Finally my thanks are due to British Timken Ltd. for the generous supply of test specimens which they have provided.

REFERENCES

(1) Reynolds, O. *Phil. Trans*, **166,** p. 155 (1876).
(2) Glagolev, N. I. *Appl. Math. Mech. Leningr.*, **9** (4), p. 318 (1945).
(3) Föppl, L. *Die Strenge Lösung för die Rollende Reigung* (Munich: Leibniz–Verlag, 1947).
(4) Heinrick, G. *Ost. Ingen. Arch.*, **4** (5), p. 363 (1950).
(5) Hertz, H. *J. reine angew Math.*, **92,** p. 156 (1886).
(6) Poritsky, H. *J. Appl. Mech.*, **17,** p. 191 (1950).
(7) Tomlinson, G. *Phil. Mag.*, **7,** p. 905 (1929).
(8) Prescott, J. *Applied Elasticity* (London: Longmans, Green and Co., 1924).

(9) BIKERMAN, J. J. *J. Appl. Phys.*, **28**, p. 971 (1949).
(10) PALMEGREN, A. *Ball and Roller Bearing Engineering*, 2nd ed. (Philadelphia: S.K.F. Industries Inc., 1945).
(11) ALLAN, R. K. *Rolling Bearings* (London: Sir Isaac Pitman and Sons Ltd., 1948).
(12) TABOR, D. *Phil. Mag.*, **43**, p. 1055 (1952).
(13) TABOR, D. *Proc. Roy. Soc. A*, **229**, p. 198 (1955).
(14) HALLING, J. *J. Sci. Instrum.*, **32**, p. 8 (1955).
(15) COCKS, M. *Nature* [*London*], **170**, p. 203 (1952).
(16) JOHNSON, K. L. *Proc. Roy. Soc. A*, **230**, p. 531 (1955).
(17) COURTNEY-PRATT, J. S., and EISNER, E. *Proc. Roy. Soc. A*, **238**, p. 529 (1957).

Apparent slip between metal and rubber-covered pressure rollers

By G. J. PARISH, B.Sc., The British Cotton Industry Research Association, Shirley Institute, Manchester, 20

[*Paper first received* 3 *March, and in final form* 10 *June*, 1958]

Measurements are described which indicate that in a roller system consisting of a metal and a rubber-covered roller rotating in contact under load, the metal roller always has the higher apparent peripheral speed whether it is driving or is driven by the rubber roller. This behaviour is similar to that observed when a wheel or cylinder is rolled over a stationary surface, and is attributed to extension of the rubber surface in the region of the nip, the extension being due in part to the contact pressure and in part to the presence of shear strains consequent on the transmission of torque through the nip. The theoretical distribution of surface strain in the rubber due to the contact pressure is derived, and the theoretical results are found to be in fair agreement with the experimental. Some further experiments designed to measure the rubber extension are described.

It is commonly found when one pressure roller drives another that the driven roller has a lower peripheral speed than the driving roller. The peripheral speeds may be measured by wheels running on the rollers, but it is perhaps more usual to compute them from the angular velocities and the free circumferences of the rollers.

It is well known that this effect is observed when the driving roller is of metal and the driven roller consists of a metal shell carrying a rubber cover, but it is perhaps less well known that when this system is reversed, the rubber driving the metal, the metal roller still has the higher peripheral speed. These phenomena might be described as slip and gain, respectively, of the driven roller, but these terms imply that there is a true difference in surface speed where the rollers are in contact, whereas in fact such a speed difference almost certainly does not occur.

A close parallel to one aspect of this behaviour of rotating rollers is found in the behaviour observed by Tabor[1] in experiments in which metal cylinders and spheres were rolled over a stationary, flat, rubber block; a somewhat less close parallel to the converse aspect is provided by experiments on the rolling of pneumatic tyred wheels over hard surfaces.[2] Tabor[1] has shown that the effects observed with a metal cylinder rolling over rubber may be explained by an extension of the rubber surface in the contact region. The use of the term "peripheral speed" in the present instance is therefore inadvisable, since it cannot safely be assumed to have a unique meaning for a roller with an elastic cover. It is better to adopt the concept of "effective rolling radius" of the rubber-covered roller and to express the behaviour in terms of variations in this radius. In the present context the effective rolling radius may be defined as follows:

$$\frac{\text{effective rolling radius of rubber-covered roller}}{\text{radius of metal roller}} = \frac{\text{angular velocity of metal roller}}{\text{angular velocity of rubber roller}}$$

MEASUREMENTS OF EFFECTIVE ROLLING RADIUS

The experiments described in this paper were carried out on a small three-roller experimental calender of 16 in. working face. This machine is hydraulically loaded and has a top roller of mild steel 14 in. in diameter and a bottom roller of chilled iron 20 in. in diameter. For the present experiments the centre position was occupied by a rubber-covered roller of 11 in. diameter, with a cover thickness of 1¼ in. and a cover hardness of 71° B.S. The top roller alone was positively driven, so that at the upper nip the drive was from metal to rubber and at the lower nip from rubber to metal. All the experiments were carried out with the rollers directly in contact; that is, without any material interposed.

The relative angular velocities of each pair of rollers were obtained by counting the number of revolutions made by each roller of the pair in a given time interval. For convenience this time interval was made to correspond to an integral number of revolutions of the metal roller (*A*, say). An effective datum line is provided on each roller by a cam which operates a spring set, and the timing interval thus starts and finishes with the operation of the spring set associated with roller *A*. At these instants the cam on the rubber-covered roller (*B*) will not in general be in contact with its spring set, and the angular separation of these two is equivalent to a fractional revolution of roller *B* at each end of the timing interval. These fractional revolutions are computed from the times between the appropriate operation of spring set *A* and the next operation of spring set *B* and the time for one revolution of roller *B*. With the apparatus used an accuracy of 0·1% was obtainable by timing over an interval of about one minute.

A series of measurements, consisting of three readings on each nip, was made at a number of applied loads and at two speeds; the results, expressed as the ratio r_e/r_0 where r_0 is the free radius of the rubber-covered roller, are shown in Fig. 1. This ignores the effect of indentation of the rubber

in the nip, which gives a radius in the plane of the roller axes smaller than the free radius. Measurements of indentation have been made; the indented radius was found to be virtually the same at each nip and the ratio r_i/r_0 varied from 0·99 at a load of 100 lb/in. to 0·98 at 500 lb/in. However, since over the contact region the rubber surface must conform to the surface of the metal roller, the indented radius

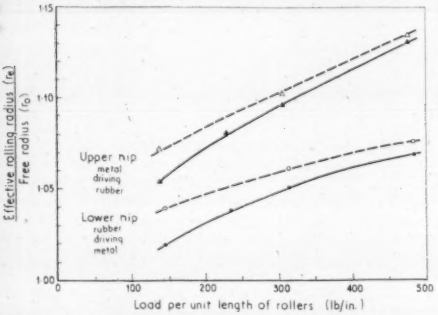

Fig. 1. Variation with load of effective rolling radius of rubber-covered roller

Top roller speed: —— = 42 ft/min; – – – = 7 ft/min.

has no unique meaning unless the position in the nip is specified. The variation of r_i with position is as large as the difference between $(r_i)_{min}$ and r_0; for points on the edge of the nip the ratio $(r_i)_h/r_0$ has the value 1·000 at 100 lb/in. and 1·006 at 500 lb/in. It seems, therefore, more reasonable to express the measured effective rolling radii in terms of the free radius rather than of an indented radius of uncertain meaning.

The effective rolling radius is always greater than the free radius, increases with load, and is larger at the lower speed. It is greater at the upper nip, where the metal roller drives the rubber, than at the lower nip; this difference can hardly be accounted for by the difference in diameter of the metal rollers, and it seems certain that there are two effects superimposed at each nip. The larger of these leads to an effective rolling radius greater than the free radius whether the rubber-covered roller is driving or is driven; it is attributed to an extension of the rubber surface in the contact region resulting from the contact pressure on the nip.

The second, smaller, effect changes sign with the drive, increasing the effective rolling radius when the rubber-covered roller is driven, and *vice versa*. It thus behaves as though it were always slip of the driven roller, but almost certainly it is not true slip, but is an increase or decrease of the primary surface extension caused by shear strains set up in the rubber by the transmission of torque from driving to driven roller.

The behaviour may then be expressed by the equation

$$r_e = r_0(1 + \alpha \pm \beta),$$

where α represents the contribution of the contact pressure and β that of the shear strains.

It will be seen from Fig. 1 that the change in r_e brought about by a change in speed is very nearly the same at each nip. This suggests that the change is primarily due to a change in α (probably the result of a time-effect in the rubber elasticity), and that β varies little with speed.

It is impossible to obtain an accurate figure for the relative proportions of α and β at a given load. If the difference in metal roller diameters is ignored, α must have the same value at each nip, but the torque transmitted must be greater at the upper nip than at the lower. The main sources of power consumption are hysteresis losses in the rubber at each nip and frictional losses at the bottom roller bearings. An estimate of these losses (using the formula given by Evans[3] for the determination of hysteresis loss) suggests that they are of roughly the same magnitude. It will be assumed therefore, that $\beta_U = 2\beta_L$ throughout the load range, where the subscripts U and L indicate upper and the lower nip, respectively. With this assumption the values of α, β_U and β_L can be determined for a given load from the data in Fig. 1. The values of α and of β_L are shown in Fig. 2. Wide varia-

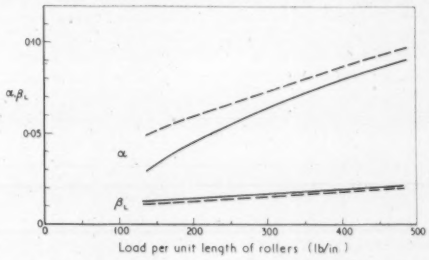

Fig. 2. Components α and β_L of effective rolling radius

Top roller speed: —— = 42 ft/min; – – – = 7 ft/min.

tions in the ratio β_U/β_L make only small differences to the value of α. For example, if $\beta_U = \beta_L$ (negligible hysteresis loss) α at 7 ft/min and 400 lb/in. has a value of 0·095; if $\beta_U = 3\beta_L$ its value is 0·080.

THEORY OF SURFACE STRAIN

Although the theory of stress distribution between bodies in contact has been extensively studied, little or no attention has been paid to the distribution of tangential strain at the surfaces in contact. A solution of the stress distribution between homogeneous elastic rollers has been given by Thomas and Hoersch[4] for conditions of plane strain, and a treatment of the problem when one of the rollers is assumed to be perfectly hard and the other to consist of an elastic layer on a perfectly hard shell has been given by Hannah.[5]

In this section of the present paper the distribution of surface strain will be derived from the results given by Thomas and Hoersch and by Hannah. That is, the solution will give the surface strain due only to the contact pressure distribution, and with the assumption that the rollers are stationary. Some justification is desirable for the application to the problem of a theoretical treatment which assumes stationary contacting surfaces and infinitesimal strains. In a recent paper[6] some measurements of the distribution of normal pressure between rotating rollers under conditions similar to those in the present experiments have been compared with the predictions of Hannah's theory. The results were found to be in qualitative agreement, and although there were quantitative differences they were not attributable to the failure of these assumptions. They were, in fact, attributed to imperfect elastic properties of the rubber roller coverings. This effect will presumably be operative here also,

and probably accounts for the variation in effective rolling radius with roller speed. The assumption of infinitesimal strains, while satisfactory for the determination of normal pressure distribution, cannot be completely satisfactory here, since it includes the assumption that the roller indentation is negligible, whereas, as was discussed above, although the indentation is small it is not negligibly so. The main function of this theoretical investigation is to determine whether a surface extension of the correct order of magnitude is predicted.

The present experimental conditions correspond, of course, to those studied by Hannah, but as no solution of the other case has been given it seems desirable to include it. Hannah's results are given for generalized plane stress, but the experimental conditions correspond much more closely to plane strain, and the following treatment will be given for this condition. In view of the mathematical identity of plane strain and generalized plane stress solutions, the difference corresponds merely to the usual modifications of

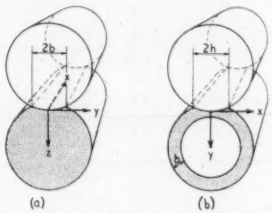

Fig. 3. Notations used by (*a*) Thomas and Hoersch and (*b*) Hannah. Hannah's notation is followed here

the elastic constants. The notations used by Thomas and Hoersch and by Hannah differ appreciably; the relevant symbols are listed below and shown in Fig. 3. Hannah's notation is followed here, the bracketed symbols being used here only.

		Thomas and Hoersch	*Hannah*
Axes	axial	x	(z)
	normal	z	y
	tangential	y	x
Tangential displacement		v	(u)
Stress components	axial	X_x	(Z_z)
	normal	Z_z	(Y_y)
Modulus of rigidity		μ	(μ)
Poisson's ratio		σ	η
Young's modulus		E	E
Applied load per unit length of rollers		$\bar{P}$	W
Nip width		$2b$	$2h$
Cover thickness		—	b
$\eta/(1+\eta)$		—	σ

Homogeneous rollers. Attention will be confined to the case of a perfectly hard roller in contact with a homogeneous elastic roller, the roller axes being parallel. The surface strain in the elastic roller is conveniently derived in the following manner.

From Thomas and Hoersch's equations (3), (81), and (82) we obtain with the appropriate changes in notation

$$2\mu\frac{\partial u}{\partial x} = Z_z\left(\frac{1-\eta}{\eta}\right) - Y_y \qquad (1)$$

The surface strain is given by $\partial u/\partial x$ for $y = 0$, and the appropriate values of Z_z and Y_y are readily found from Thomas and Hoersch's equations (73) to be

$$(Z_z)_{y=0} = -\frac{4\eta W}{\pi h}\left(1-\frac{x^2}{h^2}\right)^{1/2} \quad -h \leqslant x \leqslant h$$

$$(Y_y)_{y=0} = -\frac{2W}{\pi h}\left(1-\frac{x^2}{h^2}\right)^{1/2} \quad -h \leqslant x \leqslant h$$

Hence, since $2\mu = E/(1+\eta)$,

$$\left(\frac{\partial u}{\partial x}\right)_{y=0} = -\frac{2W}{\pi Eh}(1+\eta)(1-2\eta)\left(1-\frac{x^2}{h^2}\right)^{1/2} - \quad -h \leqslant x \leqslant h \qquad (2)$$

The negative sign indicates a compressive strain.

Thin elastic cover. It is assumed that the cover is firmly bonded to its underlying shell; that is, that there is no normal or tangential displacement at this boundary.

A solution for the tangential strain in terms of the stress function, X, in the absence of body forces is (Coker and Filon,[7] with a slight change in notation)

$$2\mu\frac{\partial u}{\partial x} = -\sigma\frac{\partial^2 X}{\partial x^2} + (1-\sigma)\frac{\partial^2 X}{\partial y^2}$$

for conditions of generalized plane stress.

Using the solution for the stress function given by Hannah for an isolated force on a thin elastic layer, the surface strain is given by

$$2\mu\left(\frac{\partial u}{\partial x}\right)_{y=0} = \frac{1}{2}\int_0^\infty [\phi_1(m) + 2(1-\sigma)\phi_4(m)]\cos mx\,.dm \qquad (3)$$

The values of $\phi_1(m)$ and $\phi_4(m)$ appropriate to the above conditions are given by Hannah in her equation (9); in fact Hannah's value for $\phi_4(m)$ is in error, and should read

$$\phi_4(m) = \frac{2W}{\pi}\left[\frac{1-2\sigma-(3-4\sigma)\cosh^2 mb}{(mb)^2+(1-2\sigma)^2+(3-4\sigma)\cosh^2 mb}\right]$$

The value of $\phi_1(m)$ is

$$\phi_1(m) = 2W/\pi$$

These values are for conditions of generalized plane stress. For plane strain σ must be replaced by η. For plane strain we also have $2\mu = E/(1+\eta)$. For a pressure distribution $P(x)$ over $-h \leqslant x \leqslant h$, equation (3) then leads to, putting $2mb = z$ and inverting the order of integration,

$$\left(\frac{\partial u}{\partial x}\right)_0 = \frac{(1+\eta)}{2\pi Eb}\int_0^\infty R(z)\,.dz\int_{-h}^{h} P(x')\cos\left[\frac{z(x-x')}{2b}\right]dx' \qquad (4)$$

where

$$R(z) = \frac{\frac{1}{2}z^2-(1-2\eta)(3-4\eta)(\cosh z-1)}{\frac{1}{2}z^2+2(1-2\eta)^2+(3-4\eta)(\cosh z+1)} \qquad (5)$$

Hannah assumes a pressure distribution of the form

$$P(x) = w\left[(1-x^2/h^2)^{1/2} + \sum_{n=1} a_n\cos\frac{(2n-1)\pi x}{2h}\right] \qquad (6)$$

an even function which makes

$$P(x) = 0 \quad \text{at} \quad x = \pm h.$$

Then

$$W = \int_{-h}^{h} P(x)dx = wh\left[\tfrac{1}{2}\pi + \sum_{n=1}(-1)^{n-1}\frac{4a_n}{(2n-1)\pi}\right] \qquad (7)$$

Equation (4) is closely related to the integral developed by Hannah, and with the value of $P(x)$ given by equation (6) it is readily shown that

$$\int_{-h}^{h} P(x') \cos\left[\frac{z(x-x')}{2b}\right] dx' = 2b\pi w\left\{\frac{J_1(zh/2b)}{z} + \left(\frac{h}{2b}\right)\sum_{n=1}(-1)^n \frac{a_n(2n-1)\cos(zh/2b)}{(zh/2b)^2 - [(2n-1)\pi/2]^2}\right\}\cos\left(\frac{zx}{2b}\right)$$

where $J_1(\xi)$ denotes the Bessel function of the first order. Putting $h/2b = K$, $x/h = X$, $(2n-1)\pi/2 = \psi_n$, $J_1(\xi)/\xi = F(\xi)$ and

$$(-1)^n \frac{(2n-1)\cos\xi}{\xi^2 - \psi_n^2} = F_n(\xi)$$

and inserting the value of w from equation (7), we obtain from (4)

$$\left(\frac{\partial u}{\partial x}\right)_0 = \frac{2W(1+\eta)}{\pi Eh\left[1 + \sum_{n=1}(-1)^{n-1}\dfrac{8a_n}{(2n-1)\pi^2}\right]} \int_0^\infty R(z)\left[F(Kz) + \sum_{n=1} a_n F_n(Kz)\right] K\cos KXz\,.dz \quad (8)$$

Condition of infinite cover thickness. Inspection of equation (8), remembering that $z = 2mb$, shows that only the term $R(z)$ involves b. Further, equation (5) shows that

$$R(z) \to -(1-2\eta) \text{ as } b \to \infty$$

Hence, in the limit,

$$\left(\frac{\partial u}{\partial x}\right)_{0,\,b=\infty} = -\frac{2W(1+\eta)(1-2\eta)}{\pi Eh\left[1 + \sum_{n=1}(-1)^{n-1}\dfrac{8a_n}{(2n-1)\pi^2}\right]} \int_0^\infty \left[F(Kz) + \sum_{n=1} a_n F_n(Kz)\right] K\cos KXz\,.dz$$

$$= -\frac{2W(1+\eta)(1-2\eta)}{\pi Eh}\int_0^\infty F(Kz) K\cos KXz\,.dz \quad (9)$$

since Hannah has shown that $a_n \to 0$ for all values of n as $b \to \infty$.

The integral in equation (9) is known[8]; it is

$$\int_0^\infty F(Kz)\, K\cos KXz\,.dz = (1-X^2)^{1/2} - 1 \leqslant X \leqslant 1 \quad (10)$$

Hence

$$\left(\frac{\partial u}{\partial x}\right)_{0,\,b=\infty} = -\frac{2W(1+\eta)(1-2\eta)}{\pi Eh}(1-X^2)^{1/2}$$

in agreement with the value derived from Thomas and Hoersch's data and given in equation (2).

Solution of the general equation. For the case we are particularly concerned with here, that is, with a rubber-covered roller, we have $\eta = \frac{1}{2}$, and hence $R(z) \to 0$ as $z \to \infty$. The solution of equation (8) can then be carried out directly by numerical integration for stated values of K and X. (The values of a_n are obtained for given values of K from the normal displacement conditions treated by Hannah.) The details of this computation will be described in the next section. It is desirable at this point to indicate the method of solution for values of η other than $\frac{1}{2}$; since $R(z) \to -(1-2\eta)$ as $z \to \infty$ the integral in equation (8) is only slowly convergent, and we follow Hannah in writing

$$\int_0^\infty F(Kz) K\cos KXz\,.dz = M(X)$$

$$\int_0^\infty F_n(Kz) K\cos KXz\,.dz = M_n(X)$$

$$\int_0^\infty [R(z) + 1 - 2\eta] F(Kz) K\cos KXz\,.dz = N(K, X)$$

$$\int_0^\infty [R(z) + 1 - 2\eta] F_n(Kz) K\cos KXz\,.dz = N_n(K, X)$$

We then have

$$\left(\frac{\partial u}{\partial x}\right)_0 = \left\{[2W(1+\eta)]\Big/\pi Eh\left[1 + \sum_{n=1}(-1)^{n-1}\frac{8a_n}{(2n-1)\pi^2}\right]\right\} \left\{N(K, X) - (1-2\eta)M(X) + \sum_{n=1} a_n[N_n(K, X) - (1-2\eta)M_n(X)]\right\}$$

The value of $M(X)$ has already been given [equation (10)]. The value of $M_n(X)$ is also known[9]; it is

$$M_n(X) = [(-1)^{n-1}/2][\sin(1+X)\psi_n + \sin(1-X)\psi_n]$$

The values of $N(K, X)$ and $N_n(K, X)$ are to be determined by numerical integration.

APPLICATION OF THE THEORY

Attention will be confined to the case $\eta = \frac{1}{2}$, and we note first that for a homogeneous roller [equation (2)] the surface is unstrained throughout the nip. For a roller with a finite cover thickness the surface strain is given by equation (8), which reduces with $\eta = \frac{1}{2}$ to

$$(\partial u/\partial x)_0 = (3W/\pi Eh)\Psi'(K, X)$$

where

$$\Psi'(K, X) = 1\Big/\left[1 + \sum_{n=1}(-1)^{n-1}\frac{8a_n}{(2n-1)\pi^2}\right] \int_0^\infty R(z)\left[F(Kz) + \sum_{n=1} a_n F_n(Kz)\right] K\cos KXz\,.dz$$

and

$$R(z) = (\tfrac{1}{2}z^2)/(\tfrac{1}{2}z^2 + \cosh z + 1)$$

The values of a_n given by Hannah are for conditions of generalized plane stress. In a recent paper[6] the present author has given the values of a_1, a_2, a_3 for plane strain and $\eta = \frac{1}{2}$ for $K = 0{\cdot}4$, $0{\cdot}7$, $1{\cdot}0$. From the values at $K = 0{\cdot}4$, $1{\cdot}0$ and from interpolated values at $K = 0{\cdot}2$, the values of $\Psi'(K, X)$ have been computed for $X = 0$, $0{\cdot}2$, $0{\cdot}4$, $0{\cdot}6$, $0{\cdot}8$, $1{\cdot}0$. The integration was carried out by Simpson's rule with half-integral values of z up to 4 and integral values from 4 to 10. The results are shown in Fig. 4. A few additional values of $\Psi'(K, 0)$ were calculated and a plot of $\Psi'(K, 0)$ against K is shown in Fig. 5.

It may be pointed out first that the maximum value of $\Psi'(K, X)$ always occurs at $X = 0$, and from Fig. 5 it will be seen that this value is positive throughout the range $0 < K \leqslant 1$; that is, the rubber surface is always stretched at the centre of the nip. For values of K below $0{\cdot}2$ (Fig. 4) the surface extension varies very little with X, but for larger values the

variation becomes more pronounced, and at $K = 1$ the surface is in compression near the ends of the nip.

In order to determine actual values of strain for given conditions of load, roller diameters, etc., it is necessary to determine the appropriate values of h and of K. This can

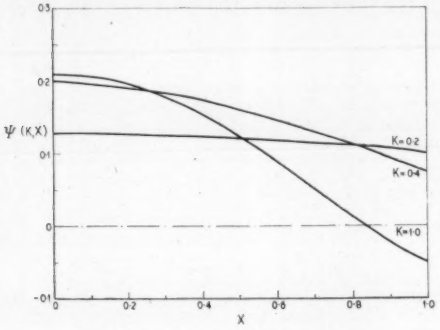

Fig. 4. Variation of $\Psi(K, X)$ with X

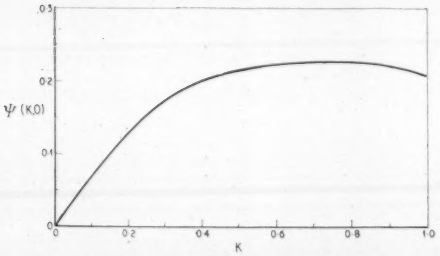

Fig. 5. Variation of $\Psi(K, O)$ with K

conveniently be done as follows. If a hard roller of diameter D_1 is pressed against a homogeneous elastic roller of diameter D_2 the nip width, assuming plane strain, is given by

$$h_0^2 = [2WD(1 - \eta^2)]/\pi E$$

where $2h_0$ = nip width ($K = 0$)

and $1/D = 1/D_1 + 1/D_2$.

Denoting by $2h_K$ the nip width obtained with a cover of thickness b for the same values of W, D, and E, Hannah gives

$$h_K = h_0 C_1(K) \tag{11}$$

where $C_1(K)$ is obtained from Hannah's solution of the normal stress distribution.

From equation (11)

$$h_0/2b = K/C_1(K) \tag{12}$$

and from this relation the value of K can be obtained from given values of h_0 and b. This is conveniently carried out by means of a graphical plot of $K/C_1(K)$ against K; values of $C_1(K)$ for plane strain and $\eta = \frac{1}{2}$ are given in Ref. (6). The value of K, being determined, gives h directly and enables the value of $\Psi(K, X)$ to be obtained for any desired value of X.

Proceeding in this way the values of maximum strain ($X = 0$) have been calculated for the conditions obtaining in the experiments described above. The value of E for the rubber cover of the middle roller was taken[6] as 900 lb/in.^{2}, and the strains were calculated for applied loads up to 500 lb/in. It was found that the greatest difference between the strains at the upper and lower nips (due to the different metal roller diameters) was 3%. This is negligible and supports the assumption to this effect made earlier in the discussion of the experimental results.

In Fig. 6 the theoretical maximum strains are compared with the values of α (the estimated contribution to r_e/r_0 of

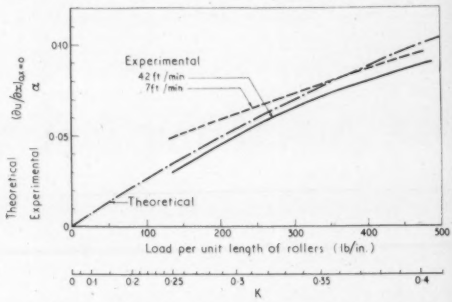

Fig. 6. Comparison of theoretical and experimental rubber surface extensions

the normal loading) taken from Fig. 2. The theoretical values of K are indicated along the horizontal axis, and it will be seen that the maximum value of K attained in the experiments is about 0·4. The theoretical and experimental results are in reasonable agreement. In view of uncertainties in the values of α, of the simplifying theoretical assumption, and of the discrepancies reported elsewhere,[6] the closeness of agreement must be to some extent fortuitous.

MEASUREMENT OF RUBBER EXTENSION

A series of measurements has been made of changes in the disposition of the rubber in the region of the nip. This was done by drawing a number of radial lines on one end face of the rubber roller cover and photographing them with the roller free and, using flash illumination, with it rotating under load. The results are not of high accuracy and, because of the conditions under which they were obtained, they cannot be expected to represent very closely the behaviour at interior parts of the roller. The free rubber surface at the end of the roller suffers appreciable axial displacement under load. This displacement was found to distort the shapes of the lines drawn on the rubber; however, it was observed that at the cylindrical roller surface the axial displacement was very slight. For this reason measurements were made only of the separations of the ends of the lines, at the cylindrical surface of the roller. The measurements were made at a speed of 7 ft/min only.

In all cases the changes in line separation between the free and loaded conditions were plotted as percentage extension against position in the nip, the positions of the ends of

the nip being estimated from the photographs. The results are shown in Fig. 7, where the quoted loads are the average values for the whole length of the rollers; because of the axial displacement of the rubber the loads at the roller ends are appreciably lower than these figures. The illumination over one half of the lower nip at 145 lb/in. was insufficient for the line positions to be measured.

Even allowing for the appreciable errors in the individual points in Fig. 7, it is clearly shown that the rubber surface is extended, and the maximum values of extension are in good agreement with the measured values of effective rolling radius (Fig. 1). Too much significance should not be attached to this agreement in view of the remarks made above, but these extension measurements may be tentatively taken as supporting the view that the whole of the observed behaviour is due to extension of the rubber surface, and that there is a true difference in the extensions at the two nips.

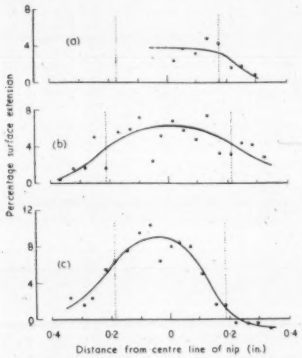

Fig. 7. Measured rubber surface extensions. The dotted lines indicate the nip edges

(*a*) Lower nip, 145 lb/in., 7 ft/min; (*b*) lower nip, 315 lb/in., 7 ft/min; (*c*) upper nip, 305 lb/in., 7 ft/min.

CONCLUSIONS

The experiments described show that the apparent slip between metal and rubber-covered rollers is due, in fact, to extension of the rubber surface in the nip. This extension may be regarded as having two components, one (appreciably the larger in the present experiments) being due to the normal loading and the other being ascribed to the forces necessary for torque transmission through the nip.

The theoretical treatment of the component of surface extension due to the normal loading gives values of maximum extension in reasonable agreement with the experimental results, and shows that the distribution of this strain component through the nip is dependent upon the parameter $K = h/2b$, where $2h$ is the nip width and b is the thickness of the rubber cover. The theoretical results are supported by measurements of surface extension in showing that at small values of K the extension is practically uniform throughout the nip. Under these conditions the metal and rubber-covered rollers will have very nearly the same surface speed at each point in the nip.

At larger values of K the situation is more complicated. The theoretical treatment indicates that, although the rollers may have the same surface speed on the centre line of the nip, there must be some relative movement elsewhere because of the non-uniformity in the rubber extension. However, the tendency to slip must give rise to frictional forces, which are not considered in the theoretical treatment. It is possible, considering the extreme case, that these frictional forces may constrain the rubber to have the same extension at all points in the nip.

The true state of affairs must lie between these extremes. The measurements of surface extension made at the higher load apparently show that the extension does vary through the nip. Although these results may not reliably represent the conditions elsewhere than at the roller edges, it seems certain that a variation in rubber extension must occur at high values of K, although it probably does not attain the full theoretical value. Under these conditions there must therefore be some relative movement between the roller surfaces within the nip.

ACKNOWLEDGEMENTS

The author wishes to thank Mr. L. A. Logue for assistance in carrying out the measurements and Mr. H. Catling for helpful discussions. Acknowledgement is also due to the Director of the Shirley Institute for permission to publish this paper.

REFERENCES

(1) TABOR, D. *Proc. Roy. Soc. A*, **229**, p. 198 (1955).

(2) FLOOR, W. K. G. *The effective rolling radii of pneumatic tyred wheels* (Amsterdam: Nationaal Luchtvaart-laboratorium Report S428, 1954).

(3) EVANS, I. *Brit. J. Appl. Phys.*, **5**, p. 187 (1954).

(4) THOMAS, H. R., and HOERSCH, V. A. *Bull. Univ. Illinois Engng Exper. Sta.*, **212**, p. 7 (1930).

(5) HANNAH, M. *Quart. J. Mech. Appl. Math.*, **4**, p. 94 (1951).

(6) PARISH, G. J. *Brit. J. Appl. Phys.*, **9**, p. 158 (1958).

(7) COKER, E. G., and FILON, L. N. G. *Photoelasticity*, p. 130 (Cambridge: University Press, 1931).

(8) WATSON, G. N. *Theory of Bessel Functions*, 2nd Ed., p. 405 (Cambridge: University Press, 1944).

(9) GRÖBNER, W., and HOFFREITER, N. *Integraltafel*, Vol. 2, p. 128 (Vienna: Springer Verlag, 1950).

The measurement of the strain-dependent damping of metals vibrating torsionally

By G. SUMNER, Ph.D.,* and K. M. ENTWISTLE, M.Sc., Ph.D., Department of Metallurgy, University of Manchester

[*Paper first received* 21 *March, and in final form* 7 *May*, 1958]

Apparatus is described for the measurement at room temperature of the mechanical damping of torsionally vibrating metal specimens up to shear strains of about 2×10^{-3} for mild steel. Vibrations are maintained by a moving-coil exciter which is energized by an electronic feedback circuit and controlled by a Rochelle salt detector coupled to the end of the specimen. The phase of the exciter current is adjusted to coincide with that of the angular velocity of the specimen so that absolute values of energy loss can be obtained by measuring the exciter current, the exciter force constant and the frequency and amplitude of vibration. Values so obtained for an aluminium alloy agree with the decrement measured by a free-decay test to about 1%. Evidence is reported which shows that such agreement would not be expected with ferromagnetic specimens because the free decay tests do not allow enough time for a cyclic condition to be attained at intermediate strains. The total extraneous energy loss in the apparatus is shown to be less than 3×10^{-5} of the vibrational energy of the system.

In connexion with an investigation of the relation between magnetic properties, magneto-mechanical damping and fatigue behaviour, apparatus was required which would measure the damping capacity of ferromagnetic specimens vibrating over a wide range of strain at room temperature. The present paper describes the development of this apparatus; the preliminary results of the investigation for which it was used will appear in the *Journal of the Iron and Steel Institute*.[1] Although the method was designed specifically for magnetic materials it can be used equally effectively for the study of amplitude-dependent damping in non-ferrous materials.

Hanstock and Murray[2] devised a highly effective method of damping measurement, which is particularly suited to testing aluminium alloys; the present technique owes much in general inspiration to their work but differs from it mainly through modifications which are desirable for tests on magnetic specimens. The important differences include the use of a moving coil exciter, which overcomes the difficulties encountered in using an eddy current device with ferromagnetic test-pieces; it also allows the specimen to be well removed from stray magnetic fields, which are known profoundly to influence the damping capacity. The frequency of vibration, about 20 c/s, is lower, and a different form of electronic feed-back circuit is adopted.

GENERAL OUTLINE OF THE APPARATUS

Torsional vibration was selected because earlier research[3] had produced a vibrating system of low extraneous loss comprising a vertical solid cylindrical specimen with enlarged tapered ends, each expanded into a disk-shaped inertia (Fig. 1). The lower inertia was securely bolted to a large steel base in a heavy concrete bed, leaving the upper disk free to execute torsional vibration controlled by the torsional stiffness of the specimen. Hitherto damping measurements had been made by timing the decay of free vibrations, but for the present work an electronic feed-back system was devised to maintain vibration of the specimen. The damping was measured by the alternating torque required to sustain a pre-determined amplitude of vibration.

The feed-back circuit comprises a Rochelle salt torsional pick-up coupled to the oscillating inertia and delivering a voltage proportional to its angular displacement. This voltage is amplified, limited to a selected level, adjusted in phase and fed to a power amplifier which delivers alternating current to a moving coil exciter fixed to the free end of the specimen. The current is adjusted to be exactly in phase with the angular velocity of the inertia, that is to give maximum reinforcement to the vibration of the specimen. This condition is secured when the exciter current is at a minimum for a constant amplitude of vibration of the specimen, and

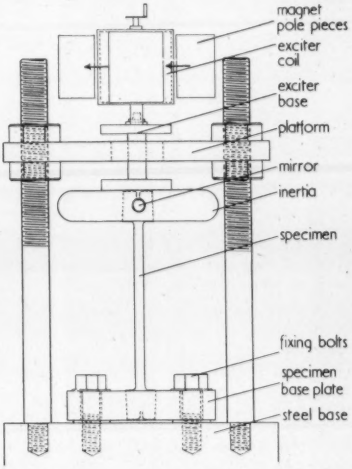

Fig. 1. Diagram showing the damping specimen, method of gripping and position of the exciter

then the torque exerted by the exciter is determined by (*a*) the level at which the amplified pick-up voltage is limited, and (*b*) the gain of the power amplifier.

Manual adjustment of controls affecting these two quantities therefore allows the alternating torque to be adjusted within a range limited only by the maximum power available.

Measurement of energy dissipation. If a purely sinusoidal torque of maximum value T_m is applied to the oscillating inertia so that it is displaced in phase by $\pi/2$ relative to the

* Now at United Kingdom Atomic Energy Authority, Springfields Works, nr. Preston.

purely sinusoidal resonant angular displacement of maximum value θ_m, the work done by T_m per cycle is

$$\Delta E = \pi T_m \theta_m$$

The measurement of energy dissipation is based on this relation. θ_m was measured optically by reflecting a beam of light from a plane mirror fixed to the inertia on to a scale graduated in millimetres. T_m is the product of the exciter force constant K, and the maximum exciter current i_m.

The complete expression for the energy dissipation per cycle therefore is

$$\Delta E = \sqrt{2}\pi K i \theta_m \text{ ergs/cycle}$$

where i is the r.m.s. exciter current.

The results which follow are expressed in terms of the fractional vibrational energy loss, P, defined by

$$P = \frac{\Delta E}{\frac{1}{2} I\omega^2 \theta_m^2} = \frac{2\sqrt{2}\pi K i}{I\omega^2 \theta_m}$$

where I is the effective moment of inertia of the vibrating system. At lower damping levels $\frac{1}{2} I\omega^2\theta_m^2$ is the maximum vibrational energy during the cycle, but as P rises it becomes difficult to give this denominator a unique physical meaning; it is always, however, a precisely measurable quantity. Where necessary, P has been related to the logarithmic decrement δ using

$$P = 1 - \exp(-2\delta)$$

The expression for P assumes that both T and θ are described by pure sine curves. The waveform of T, that is i, approaches this very closely because of a highly selective amplifier in the feed-back circuit tuned to the specimen vibration frequency and so drastically attenuating any harmonics. The complex elastic hysteresis loops for iron must cause the θ wave-form to contain harmonics, but inspection of the detector voltage waveform on an oscillograph screen failed to reveal any significant distortion.

Inhomogeneous stress. The radial stress gradient in a solid cylinder strained in torsion has objections for high stress work which can largely be overcome by the use of thin tubes. Solid cylinders were used, however, and the damping P_ϕ which would be measured on a specimen deformed homogeneously to a shear strain ϕ was derived from the relation between the measured damping P_m and surface shear strain ϕ for a solid cylinder by a graphical construction based on

$$P_\phi = P_m + \frac{\phi}{4} \cdot \frac{dP_m}{d\phi}$$

Choice of vibration frequency. The vibration frequency was chosen to give the highest attainable stress. The mechanical energy supplied by the exciter to the specimen during one vibration cycle is $\Delta E = e_b i/f$, where i is the exciter current, f is the frequency and e_b the exciter back e.m.f. For a given amplitude e_b is proportional to f so that $\Delta E \propto i$.

If it is assumed that the total power supplied to the exciter, W, is a constant independent of frequency, then under these conditions i falls as f increases at a rate dependent on the ratio of motional to clamped resistance. Hence for maximum ΔE and hence the highest stress, f should be low. There is, however, a limit to the increase of ΔE secured by decreasing f, since W falls with f in a conventional power amplifier because of a drop in efficiency of the coupling transformer. This effect became marked at about 15 c/s with the transformer available and in consequence an operating frequency of about 20 c/s was selected as about the best compromise. Although this frequency gives the highest stress it is still possible to make useful damping measurements at frequencies as low as 5 c/s and well above 100 c/s.

Two additional advantages which accrue from the use of a low vibration frequency are the reduced temperature rise in high damping specimens and the ability to follow damping changes in the early stages of a fatigue test.

DETAILS OF THE DAMPING APPARATUS

The detector. The detector was based on a design by Berry[4] and is illustrated in Fig. 2. A Rochelle salt bimorph sensitive to torsion is coupled to a torsion wire and cross-arm.

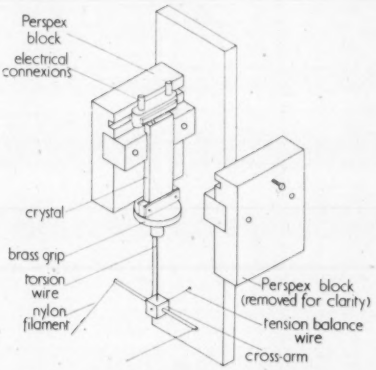

Fig. 2. Detailed diagram of crystal detector

A loop of nylon filament fixed to the ends of the cross-arm (Fig. 3) wraps round one of a set of cylinders fixed on the axis of the oscillating inertia. The overall detector sensitivity can be increased by selecting a cylinder of larger diameter or by fitting a stiffer coupling torsion wire. Most of the measurements were made with a detector giving 4·5 V/rad rotation of the cross-arm and coupled to the specimen assembly to give a sensitivity of 1·0 V/rad rotation of the inertia for tests at high stress and 4 V/rad for tests at lower stress. The maximum safe crystal output voltage is about 0·12 V.

At a frequency of about 20 c/s there is appreciable phase shift at room temperature between the twist of the crystal and its output voltage. This is a consequence of the ferroelectric characteristics of Rochelle salt and complicates the use of the crystal voltage as an indication of the phase of the specimen vibration, for example to set the exciter current exactly in quadrature to the vibrational strain. However, the phase shift did not appear to vary within the range of room temperatures which was normally encountered, since the phase shift setting for maximum reinforcement of the vibrations did not vary during any test. An alternative to the crystal detector, which is being developed, is a moving coil system. This will have a simpler phase relation but must be heavily screened from the magnetic fields of the exciter. From this point of view the crystal detector is much simpler.

The exciter. The exciter resembles a large moving coil galvanometer element; the coil has a cross-section of $2 \times 2\frac{1}{4}$ in. and is wound with about 350 turns of 34 s.w.g. enamelled wire on an acrylic moulding. The wires are

securely bonded with acrylic cement. The coil is rigidly fixed to the top of the inertia and with its axis collinear with that of the specimen (Fig. 3). Current is fed into the coil through a stout copper–beryllium hair spring and out along the specimen and through the machine base. A radial magnetic field is defined by shaped pole pieces and a central

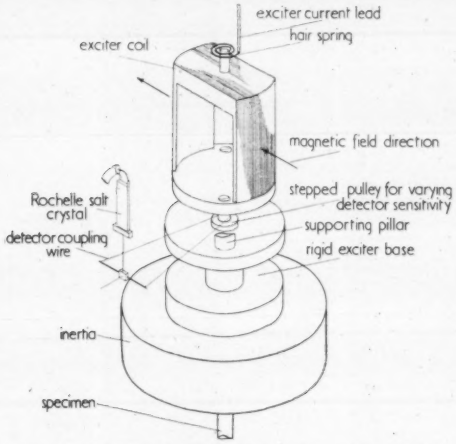

Fig. 3. Diagram showing the moving coil exciter and the method of coupling the detector to the oscillating inertia

soft iron core and supplied either by an Alcomax III permanent magnet (about 350 oersted) or, where higher torques are required, an electro-magnet (about 2000 oersted). The exciter force constant K was measured by two methods giving results in good agreement.

(i) The maximum voltage, e_m, generated by the exciter on

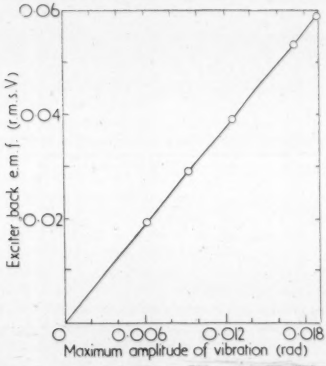

Fig. 4. Typical relation between open-circuit voltage generated by the exciter and amplitude of oscillation. Slope gives $K = 3{\cdot}69 \times 10^5$ dyn cm/A. Vibration frequency = 19·25 c/s

open circuit at maximum angular displacement θ_m and angular frequency ω is

$$e_m = K\omega\theta_m \times 10^{-8}\ \text{V};$$

e_m was measured with a carefully calibrated valve voltmeter as a function of θ_m during a slowly decaying free vibration. The gradient of the linear relation between e_m and θ_m (Fig. 4), coupled with a measurement of ω by timing the interval for, say, 1000 cycles to be recorded on Dekatron counters, gave K in dyn cm/A.

(ii) If a direct current i is passed through the exciter when it is coupled to a slender specimen of known torsional stiffness C, the resulting static rotation θ when i is reversed is given by

$$Ki = \tfrac{1}{2}C\theta$$

C was calculated from the measured vibration frequency of the specimen when attached to a disk of known moment of inertia.

Method (i) was preferred because in many cases it allowed K to be checked with the damping specimens in the machine; these were usually too stiff for accurate measurement by (ii). Typical exciter characteristics are given in the Appendix.

The exciter current was measured with a vacuum thermojunction. Seven shunts were provided to permit accurate current measurement to be made from 0·0005 to 2·0 A. Each range was calibrated with direct current; the thermocouple voltage was compared potentiometrically with the voltage drop across a standard resistor in series with the heater. The maximum couple voltage was 7 mV and could be measured to 10^{-6} V.

The feedback circuit. A block diagram of the feedback circuit is given in Fig. 5.

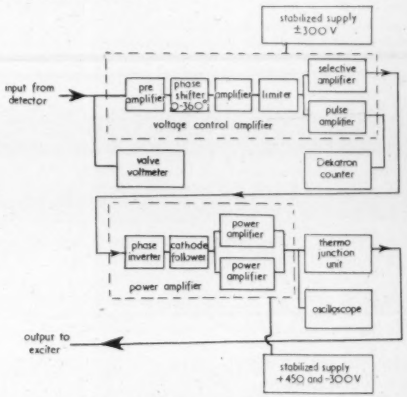

Fig. 5. Block diagram of the feedback circuit

The pre-amplifier has an input impedance of 50 000 Ω and ensures that the voltage eventually delivered to the limiter is always well above the maximum voltage which this stage will pass; this is an essential condition for stable vibration.

The phase-shift stage can be adjusted to displace the phase of its output voltage relative to the input voltage over the range 0–360°. This allows all possible phase displacements round the system to be corrected. The circuit compounds two vectors, displaced $\pi/2$ relative to each other in time

phase and variable in magnitude between equal positive and negative limits. The controls are usually manipulated so that the resultant vector traces a square locus; the fact that this causes the output voltage to vary in magnitude by a factor of $\sqrt{2}$ is not important since the voltage is later heavily clipped.

The limiter is a "soft spring" feedback amplifier which cuts off all the incoming voltage wave above a well defined and adjustable level. Thus the output from this stage is very nearly a square wave, the height of which defines the voltage ultimately fed to the power amplifier and hence the alternating torque exerted on the specimen.

In order to measure energy dissipation it is necessary to abstract from the square wave only the component which can do work on the specimen, that is the fundamental of its Fourier series. A highly selective amplifier[5] performs this function; the selectivity derives from a "twin-T" resistance-capacity feedback circuit tuned to the vibration frequency of the specimen.

The phase inverter allows the output of the tuned amplifier to be fed to the push-pull power amplifier, which incorporates negative feed-back and has a power rating of 25 W. Of this only about 4 W can be delivered at 20 c/s in undistorted form by the coupling transformer. This can be improved.

It may be possible to use one of the commercially available high fidelity audio amplifiers in place of part of the circuit labelled "power amplifier" in Fig. 5, but the authors have not tried this substitution.

The stabilized power supply for the power amplifier is of the simple form which uses neon tubes, since the voltages required are multiples of 150 V.

The square wave from the limiter is used to supply a conventional counting circuit. Pulses are recorded up to 1000 on Dekatron counters; units of 1000 are transferred to a 6 digit post-office counter storing therefore up to 10^{10} cycles. The Dekatron circuit allows accurate measurements of vibration frequency to be made by timing a count of several thousand cycles.

Characteristics of the feedback system. Because of the negative feedback in the power amplifier, change of motional impedance of the exciter caused by a change of specimen damping gives rise to only secondary changes of exciter current. The exciter therefore imposes a constant torque on the specimen for fixed control settings and in consequence damping changes produce variation of amplitude of vibration.

A disadvantage of such a constant torque system of control became evident during tests on magnetic materials, where often a range of strain exists over which P varies almost inversely with shear strain; that is ΔE increases linearly with amplitude. The maximum torque T_m required to supply this loss is

$$T_m = \frac{\Delta E}{\pi \theta_m}$$

and is therefore constant. This means that a slight variation of torque, or exciter current, produces a large change of θ_m and close control of amplitude is not preserved. Fortunately it never became necessary to sustain vibration for long periods in this range and in most cases a stable amplitude could be maintained for sufficient time to allow an accurate measurement to be made. The exceptions were well annealed pure iron and nickel, in which a range of strain existed over which P fell more steeply than $1/\phi$; this means that T falls with increasing θ and the vibration amplitude rises uncontrolled to the strain at which T begins to rise again.

The natural frequency of vibration of the specimen falls with increase of damping, so, because the phase shift in the feedback circuit varies with frequency, the phase relation between T and θ in principle depends on the specimen damping. In practice this effect was found to be unimportant in almost all cases, since the phase setting for minimum exciter current at constant amplitude of vibration was found to be independent of amplitude and therefore of damping. A notable exception was annealed nickel in which a range of damping from 0·0048 to 0·5 was measured, corresponding to natural frequencies of 20·4 and 17·4 c/s respectively. Here slight phase correction was necessary during a test.

The frequency-dependence of phase shift complicates the use of this circuit for maintaining vibration over a wide range of frequency, such as would be met in tests over a range of temperature.

Extraneous energy loss. The magnitude of energy losses arising outside the specimen was measured directly by tests on an aluminium alloy specimen (R.R.56) vibrating at strains known from earlier work to correspond to a low and stable damping capacity. Fig. 6 shows the relation between P and

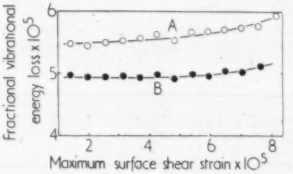

Fig. 6. The effect of attaching the exciter and detector on the measured damping of an aluminium alloy (R.R.56) specimen. Vibration frequency = 12·8 c/s

Curve A represents test on complete machine, exciter electrically disconnected; curve B represents test with exciter and detector removed.

ϕ for this specimen measured at atmospheric pressure by timing the optically-indicated decay of free vibrations. Curve B was measured with the exciter and detector completely removed; before determining curve A the exciter and detector were connected mechanically but not electrically and it is evident that a fractional energy loss of $5{\cdot}5 \times 10^{-6}$ is introduced. This would not be serious even in tests on materials of low damping such as aluminium alloys. In assessing how this loss would affect the measured damping of, for example, a steel specimen, allowance must be made for possible differences of specimen strain energy.

A further test showed that the loss contributed by the hair spring above the exciter was undetectable; thus, if it were undesirable to pass the exciter current along the specimen, two hair springs could be used.

One check measurement confirmed the magnitude of the air friction loss predicted from earlier work[3] to be about $2{\cdot}5 \times 10^{-5}$ of the total vibrational energy of the system.

It is concluded that the total extraneous energy loss in tests with standard sized steel specimens vibrating at about 20 c/s never exceeds 3×10^{-5} of the energy of the vibrating system; this is a small fraction of even the lowest damping encountered which in ferromagnetic specimens was about 10^{-3} of the vibrational energy.

VERIFICATION OF THE ACCURACY OF DAMPING MEASUREMENT

A comparison was made between the damping of an aluminium alloy specimen measured respectively by a free

decay test and by the electrical feedback technique in order to confirm the predicted operation of the regenerative system. The results are listed in Table 1. Corresponding values are in excellent agreement and it should be noted that no arbitrary parameter is used. The low damping of the specimen caused about 1½ h to elapse before the equilibrium amplitude was attained during self-excited vibration. The free-decay tests were carried out with the exciter on open circuit.

Table 1. *Comparison between damping measured on an aluminium alloy (R.R.56) specimen by free-decay and electrical methods*

Specimen diameter 0·320$_5$ *in.*; *length* 6·125 *in.*; *frequency* 12·66 *c/s*. $K = 3{\cdot}69 \times 10^5$ *dyn cm/A*. $I = 112000$ *gm cm*^{2}

Surface shear strain $\bar{\gamma}$	*Exciter current (r.m.s. A)*	P *(Electrical)*	P *(free decay)*
$13{\cdot}7 \times 10^{-4}$	$1{\cdot}29 \times 10^{-3}$	$1{\cdot}13_7 \times 10^{-4}$	$1{\cdot}15_4 \times 10^{-4}$
$9{\cdot}38 \times 10^{-4}$	$0{\cdot}76_4 \times 10^{-3}$	$0{\cdot}98_4 \times 10^{-4}$	$1{\cdot}01_2 \times 10^{-4}$
$6{\cdot}99 \times 10^{-4}$	$0{\cdot}51_0 \times 10^{-3}$	$0{\cdot}88_2 \times 10^{-4}$	$0{\cdot}88_0 \times 10^{-4}$

The table shows:

(i) the ability of the apparatus to measure a damping below 10^{-4} of the energy of the vibrating system, which is of the order of one hundredth of typical values for unmagnetized mild steel;

(ii) the absence of any loss associated with vibration excitation.

It must be admitted that only small torques were involved in this test so that losses arising from inelastic distortion of the exciter coil and former may not be critically assessed. It is not easy to secure a reliable comparison between the results of free decay and sustained vibration techniques on high damping specimens because of variation of damping with vibration history. Magnetic damping behaviour illustrates this point. An attempt was made to compare the damping of mild steel, measured by photographically recording a freely decaying vibration [curve (*a*)], with values obtained by the present method [curve (*b*)]. The results are shown in Fig. 7,

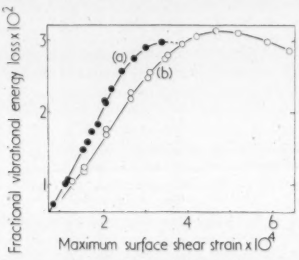

Fig. 7. Comparison between the damping of a mild steel specimen measured (*a*) by recording photographically a freely decaying vibration and (*b*) by the sustained vibration method. The free-decay test was begun at a surface shear strain of $3{\cdot}9 \times 10^{-4}$

where each curve includes points from two separate tests. The relation between damping and vibrational strain for mild steel shows a characteristic peak of magnetic origin and the damping curve for an initially demagnetized specimen measured with progressively rising strain lies below that for decreasing strain. Thus in order to make the conditions of the electrically measured damping approach as closely as possible to those of the free decay tests, the electrical measurements of Fig. 7, were made with a sequence of strains decreasing from the maximum value. Even so the free decay results are higher than the electrically measured values, except at the strain at which the free decay test was begun and at which vibration had been maintained for some minutes before the excitation force was removed. This suggests that the rapid fall of amplitude during free vibration prevents the attainment of a cyclic magnetic condition, whereas in forced vibration, where about 3 min elapse during each measurement, equilibrium can be attained. Confirmation of this explanation was obtained by reducing the amplitude setting after maintaining vibration for several minutes. The exciter current was observed to reach a lower steady value quickly but the swift fall of amplitude was followed by a slower rise which persisted for about a minute after this, indicating a fall of damping capacity. In material of this class, therefore, damping values measured by a free vibration technique must be expected to differ from those measured during sustained vibration.

APPENDIX

Typical exciter characteristics

Clamped resistance of exciter = 34·0 Ω at 20 c/s. Force constants: $K = 3{\cdot}65 \times 10^5$ dyn cm/A (with permanent magnet). $K = 21{\cdot}4 \times 10^5$ dyn cm/A (with electromagnet).

After dismantling the exciter and reassembly, variations in K of not more than 1% may arise.

Typical exciter efficiency at maximum power. When coupled to a mild steel specimen and polarized with the electromagnet the damping was 0·287 of the vibrational energy of the specimen at $\theta_m = 0{\cdot}116$ rad (specimen surface shear strain $1{\cdot}95 \times 10^{-3}$). The exciter current was 0·329 A, the applied e.m.f. 14·8 V and the back e.m.f. 3·61 V. Hence the efficiency was $3{\cdot}61/14{\cdot}8 = 24{\cdot}2\%$ and the specimen was dissipating 1·19 W.

These figures indicate, too, that at this frequency the exciter impedance is almost wholly resistive.

The exciter efficiency will rise as the damping falls; with aluminium alloy specimens efficiencies of over 80% were achieved even with lower polarizing fields.

ACKNOWLEDGEMENTS

The authors thank Prof. F. C. Thompson for research facilities and Mr. M. J. Somerville for invaluable advice on electronic matters.

One of the authors (G. S.) acknowledges his indebtedness to the Council of the Iron and Steel Institute for the award of a maintenance grant from the Andrew Carnegie Research Fund.

REFERENCES

(1) Sumner, G., and Entwistle, K. M. *J. Iron Steel Inst.* To be published.
(2) Hanstock, R. F., and Murray, A. *J. Inst. Metals*, **72**, p. 97 (1946).
(3) Cottell, G. A., Entwistle, K. M., and Thompson, F. C. *J. Inst. Metals*, **74**, p. 373 (1948).
(4) Berry, B. S. *Rev. sci. Instrum.*, **26**, p. 884 (1955).
(5) Sturtevant, J. M. *Rev. sci. Instrum.*, **18**, p. 124 (1947).

Resonant cavity methods of measuring ferrite properties

By R. A. WALDRON, B.A., A.Inst.P., Marconi's Wireless Telegraph Co. Ltd., Great Baddow, Essex

[*Paper first received* 19 *March, and in final form* 20 *June*, 1958]

Formulae are given for the frequency shift on introducing a ferrite sample into a resonant cavity. Cylindrical rod, circular disk, and spherical samples are considered; the sample may be placed in a region of zero electric or magnetic field, enabling magnetic and dielectric properties to be separately determined. The merits and demerits of the various sample shapes are discussed, and it is concluded that a spherical sample is usually best; in particular, with such a sample, the dielectric constant and permeability can be measured on the same sample, in the same cavity, working in the same mode.

LIST OF PRINCIPAL SYMBOLS

$\boldsymbol{E}_0, \boldsymbol{D}_0, \boldsymbol{H}_0, \boldsymbol{B}_0$ = electric and magnetic fields and inductions in the cavity in the unperturbed state.

$\boldsymbol{E}_1, \boldsymbol{D}_1, \boldsymbol{H}_1, \boldsymbol{B}_1$ = fields and inductions which must be added to $\boldsymbol{E}_0$, $\boldsymbol{D}_0$, $\boldsymbol{H}_0$ and $\boldsymbol{B}_0$ to give the quantities appropriate to the perturbed state.

$\boldsymbol{H}$ = magnetic field external to sample. H_z is a direct field; the component of $\boldsymbol{H}$ perpendicular to z is a microwave quantity.

$\boldsymbol{h}$ = field internal to specimen due to $\boldsymbol{H}$.

$\boldsymbol{b}$ = magnetic induction internal to specimen.

μ_0, ε_0 = permeability and permittivity of free space.

ε = relative permittivity of ferrite.

μ, α = components of relative permeability tensor of ferrite.

M_s = saturation (direct) magnetization of ferrite (in z direction).

V_1, V_0 = volume of sample and cavity, respectively.

Q_0, Q_1 = "Q" of cavity in absence and presence of sample, respectively.

INTRODUCTION

Resonant cavity methods have long been in use for measuring dielectric constants of materials, and in recent years these techniques have been adapted to the measurement of the permeability of a ferrite. Ferrites are substances having a tensor permeability in the presence of a direct polarizing magnetic field. Provided that this field is sufficiently great to cause saturation, the induction in the ferrite is related to the field in the ferrite at microwave frequencies by

$$\boldsymbol{b} = \mu_0 \begin{bmatrix} \mu & -j\alpha & 0 \\ j\alpha & \mu & 0 \\ 0 & 0 & 1 \end{bmatrix} \boldsymbol{h} \qquad (1)$$

Polder[1] has given the following formulae for μ and α:

$$\mu = 1 + \frac{h_z M_s}{\mu_0(h_z^2 - H_r^2)} \qquad \alpha = \frac{H_r M_s}{\mu_0(h_z^2 - H_r^2)} \qquad (2)$$

where h_z is the direct polarizing field in the sample and M_s is the saturation magnetization in the z direction. If the working frequency is $\omega/2\pi$, H_r is given by ω/γ, where γ is the reciprocal of the gyromagnetic ratio. Polder's expressions hold for the lossless case; Hogan[2] has obtained similar expressions involving loss terms.

In order to measure both μ and α, it is customary to use a cavity in a degenerate mode; by applying two input signals in space and time quadrature, it is possible to generate, at least in some part of the cavity, a circularly polarized oscillation. This may be polarized in either sense, and different values of the frequency shift obtained in the two cases. In this way, a pair of equations is obtained from which μ and α may be determined. Experimental methods of generating circularly-polarized oscillations have been described by several authors.[3–6]

Formulae have been given by Berk and Lengyel,[7] Rowen and von Aulock,[8] and the present author[9, 10] for the frequency shift due to a small spherical sample. Berk and Lengyel also give formulae for a small disk sample and a cylindrical rod sample. Recently, Rowen and von Aulock have suggested the use of large disks situated at the end of a cavity.[11]

The aim of the present paper is to gather together the various methods of measuring ferrite properties in one and the same treatment of the subject, and to discuss the merits and demerits of these methods both from the point of view of the technique of measurement and in relation to the purpose for which the ferrite is intended. We shall also pay some attention to the problem of measuring the dielectric constant on the same sample as the permeability. Such a discussion does not appear to have been previously given; various authors have brought up some point or other in connexion with a new method of carrying out a measurement, but have not given a complete discussion of the topic. Also, the concept of "external permeability" is still not dead, in spite of the confusion it causes. It is hoped that the discussion given in the present paper will prove helpful to workers, particularly newcomers to the field, in planning experimental work.

PERTURBATION THEORY OF A RESONANT CAVITY

It may be shown[10, 12] that if a small body of volume V_1 is inserted in a cavity of volume V_0, and if $\boldsymbol{E}_0$, $\boldsymbol{H}_0$ are the fields in the cavity in the absence of the body, the frequency shift that takes place is

$$\frac{\delta\omega}{\omega} = \frac{\iiint_{V_1} [(\boldsymbol{E}_1 \cdot \boldsymbol{D}_0 - \boldsymbol{E}_0 \cdot \boldsymbol{D}_1) - (\boldsymbol{H}_1 \cdot \boldsymbol{B}_0 - \boldsymbol{H}_0 \cdot \boldsymbol{B}_1)]dV}{\iiint_{V_0} (\boldsymbol{E}_0 \cdot \boldsymbol{D}_0 - \boldsymbol{H}_0 \cdot \boldsymbol{B}_0)dV} \qquad (3)$$

It is assumed here that if the fields and inductions in the unperturbed condition can be represented as $\boldsymbol{X}_0 \exp(j\omega t)$, where $\boldsymbol{X} = \boldsymbol{E}$, $\boldsymbol{D}$, $\boldsymbol{H}$ or $\boldsymbol{B}$, then in the perturbed condition they become $(\boldsymbol{X}_0 + \boldsymbol{X}_1) \exp[j(\omega + \delta\omega)t]$. In the unperturbed condition, the inductions are given by

$$\boldsymbol{D}_0 = \varepsilon_0 \boldsymbol{E}_0 \qquad \boldsymbol{B}_0 = \mu_0 \boldsymbol{H}_0 \qquad (4)$$

while in the perturbed condition we have, in the sample,

$$\left.\begin{aligned} \boldsymbol{D}_1 &= \varepsilon_0 \varepsilon (\boldsymbol{E}_1 + \boldsymbol{E}_0) - \varepsilon_0 \boldsymbol{E}_0 \\ \boldsymbol{B}_1 &= \mu_0 [\mu](\boldsymbol{H}_1 + \boldsymbol{H}_0) - \mu_0 \boldsymbol{H}_0 \end{aligned}\right\} \qquad (5)$$

$[\mu]$ denoting the tensor relative permeability of equation (1).

Equation (3) can be applied in principle to any cavity, working in any mode, and containing a sample of any shape. In practice, however, it is convenient to limit cavity shapes to rectangular and cylindrical, and to consider samples which are spheres, cylindrical rods, or circular disks, as it is only in these cases that the results can be calculated conveniently and the sample and cavity conveniently made.

It is the usual practice to make magnetic measurements with the sample at a position of zero electric field, and to make dielectric measurements with the sample at a position of zero magnetic field. Thus in the numerator of equation (3) either $(\boldsymbol{E}_1 \cdot \boldsymbol{D}_0 - \boldsymbol{E}_0 \cdot \boldsymbol{D}_1)$ or $(\boldsymbol{H}_1 \cdot \boldsymbol{B}_0 - \boldsymbol{H}_0 \cdot \boldsymbol{B}_1)$ will be zero.

SPHERICAL SAMPLES

With a cylindrical cavity in which oscillations are generated which are circularly polarized on the axis, and with the polarizing field for the ferrite directed along the axis, the frequency shift for a spherical sample in a region of uniform magnetic field is[7-10]

$$\frac{\delta\omega}{\omega} \propto \frac{\mu - 1 \pm \alpha}{\mu + 2 \pm \alpha} \cdot \frac{V_1}{V_0} \tag{6}$$

the positive or negative sign being taken according to the sense of circular polarization. To take into account losses, we write $\mu = \mu' - j\mu''$, $\alpha = \alpha' - j\alpha''$, and then have[10]

$$\frac{\delta\omega}{\omega} \propto \frac{\mu' - 1 \pm \alpha'}{\mu' + 2 \pm \alpha'} \cdot \frac{V_1}{V_0} \tag{7}$$

$$\frac{1}{Q_1} - \frac{1}{Q_0} \propto \frac{-6(\mu'' \pm \alpha'')}{(\mu' + 2 \pm \alpha')^2} \cdot \frac{V_1}{V_0} \tag{8}$$

where Q_0 is the "Q" of the empty cavity and Q_1 that of the cavity containing the sample. These equations were deduced directly from Maxwell's equations by the present author.

A suitable mode for this measurement is the H_{112} mode, with the sample at the centre of the cavity. It will be noticed that at a distance of a quarter of the cavity length from one end, the magnetic field components are all zero, while the electric field is uniform and perpendicular to the axis of the cavity. It is well known that for a dielectric sphere in a uniform field E_0 the internal field in the sphere, $E_0 + E_1$, is given by

$$E_1 + E_0 = 3E_0/(\varepsilon + 2)$$

so that

$$E_1 = -[(\varepsilon - 1)/(\varepsilon + 2)]E_0$$

Thus in the numerator of equation (3), bearing in mind equations (5)

$$\iiint_{V_1} (\boldsymbol{E}_1 \cdot \boldsymbol{D}_0 - \boldsymbol{E}_0 \cdot \boldsymbol{D}_1) dV = \iiint_{V_1} \varepsilon_0 E_0^2 \left[-\frac{(\varepsilon - 1)}{(\varepsilon + 2)} - \frac{3\varepsilon}{\varepsilon + 2} + 1 \right] dV$$

Since $\boldsymbol{E}_0$ is uniform over V_1, and since the denominator of equation (3) is a constant, we obtain

$$\frac{\delta\omega}{\omega} \propto \frac{\varepsilon - 1}{\varepsilon + 2} \cdot \frac{V_1}{V_0} \tag{9}$$

Losses may be treated by writing $\varepsilon = \varepsilon' - j\varepsilon''$, and we have then

$$\frac{\delta\omega}{\omega} \propto \frac{\varepsilon' - 1}{\varepsilon' + 2} \cdot \frac{V_1}{V_0} \tag{10}$$

$$\frac{1}{Q_1} - \frac{1}{Q_0} \propto \frac{-6j\varepsilon''}{(\varepsilon' + 2)^2} \cdot \frac{V_1}{V_0} \tag{11}$$

It may be noted that the proportionality constant is the same in equations (6), (7) and (8). In equations (9), (10) and (11) the proportionality constant has a value l^2/λ_0^2 times that in equations (6), (7) and (8), l being the length of the cavity and λ_0 the free-space wavelength. Since l and λ_0 are comparable in magnitude, the frequency shifts and changes in "Q" may be expected to give comparable accuracy in the measurement of dielectric and magnetic properties.

CYLINDRICAL ROD SAMPLES

It is common practice to measure the dielectric constant of a dielectric material by taking a cylindrical rod sample, concentrically placed in a cylindrical cavity oscillating in the E_{010} mode, when the electric field is directed parallel to the cavity axis, and is constant over the whole volume of the sample. This technique can be used in the case of a ferrite, since the magnetic field vanishes on the cavity axis. Alternatively, the circular cavity may be replaced by a rectangular cavity oscillating in the E_{110} mode; the only field components are then H_x, H_y and E_z. If the cavity is bounded by the faces $x = 0$, $x = a$; $y = 0$, $y = b$; $z = 0$, $z = c$; then along the line $x = a/2$, $y = b/2$, H_x and H_y vanish, while E_z is constant. This mode may therefore be used to measure the dielectric constant of a ferrite rod. Since the electric field is parallel to the axis of the rod, we shall have $\boldsymbol{E}_1 = \boldsymbol{0}$ in equation (3). Hence

$$\iiint_{V_1} (\boldsymbol{E}_1 \cdot \boldsymbol{D}_0 - \boldsymbol{E}_0 \cdot \boldsymbol{D}_1) dV = \iiint_{V_1} -\varepsilon_0 E_0^2 (\varepsilon - 1) dV$$

so that

$$\delta\omega/\omega \propto (\varepsilon - 1)(V_1/V_0) \tag{10}$$

It was suggested by Berk and Lengyel[7] that the rectangular cavity arrangement could be used to measure the magnetic properties of a ferrite rod if the E_{210} mode is used. All the field components except H_y vanish on the axis ($x = a/2$, $y = b/2$); H_y is uniform and independent of z. If a square cavity is used ($a = b$), and is stimulated to oscillate in both the E_{210} and E_{120} modes with equal amplitude, the oscillations being in time quadrature, H_x and H_y are connected by the relation $H_y = \pm jH_x$ on the axis, i.e. there is circular polarization.

From Maxwell's equations, it can be shown that the magnetic potential equation satisfied in a ferrite is[7, 10]

$$\mu\left(\frac{\partial^2\psi}{\partial x^2} + \frac{\partial^2\psi}{\partial y^2}\right) + \frac{\partial^2\psi}{\partial z^2} = 0 \tag{13}$$

For the present case, $\partial^2\psi/\partial z^2 = 0$, and we have

$$(\partial^2\psi/\partial x^2) + (\partial^2\psi/\partial y^2) = 0 \tag{14}$$

which is the two-dimensional form of Laplace's equation. Solving this subject to the boundary conditions, we find that if $\boldsymbol{H}$ is the external microwave field, perpendicular to z, the internal field $\boldsymbol{h}$ is given by

$$\left.\begin{aligned} h_x &= 2\left[\frac{(\mu + 1)H_x + j\alpha H_y}{(\mu + 1)^2 - \alpha^2}\right] \\ h_y &= 2\left[\frac{-j\alpha H_x + (\mu + 1)H_y}{(\mu + 1)^2 - \alpha^2}\right] \end{aligned}\right\} \tag{15}$$

If we substitute from equations (15) into equation (3), and use equations (5), we find

$$\frac{\delta\omega}{\omega} \propto \frac{(\mu-1)(\mu+1)-\alpha^2}{(\mu+1)^2-\alpha^2} \cdot \frac{V_1}{V_0}$$

For the case of circular polarization, we replace α by zero and μ by $\mu \pm \alpha$, thus obtaining

$$\frac{\delta\omega}{\omega} \propto \frac{\mu-1\pm\alpha}{\mu+1\pm\alpha} \cdot \frac{V_1}{V_0}$$

Since the rod and the cavity both have the same length, this may be written

$$\frac{\delta\omega}{\omega} \pm \frac{\mu-1\pm\alpha}{\mu+1\pm\alpha} \cdot \frac{S_1}{S_0} \tag{16}$$

S_1 and S_0 being the cross-sectional areas of the rod and the cavity respectively. This formula was given by Berk and Lengyel.

CIRCULAR DISK SAMPLES

The disk is supposed to have a thickness very small compared with its diameter, so that the magnetic field in the disk can be taken to be the same as that which exists when the disk is absent, i.e. $\boldsymbol{h} = \boldsymbol{H}$ and $\boldsymbol{H}_1 = O$. For a cylindrical cavity oscillating in a circularly-polarized H_{112} mode, the frequency shift is

$$\delta\omega/\omega \propto (\mu \pm \alpha - 1)(V_1/V_0) \tag{17}$$

when the sample is placed at the centre of the cavity with its axis along the cavity axis. When the sample is placed one-quarter of the way along the cavity, at a position of maximum electric and minimum magnetic field, the frequency shift is

$$\delta\omega/\omega \propto (\varepsilon - 1)(V_1/V_0) \tag{18}$$

Rowen and von Aulock[11] have suggested the use of a fairly large disk, centrally placed at the end of a cylindrical cavity oscillating in the H_{111} mode. They show that provided the radius of the disk is less than about half that of the cavity, the frequency shift is given approximately by

$$\delta\omega/\omega \propto (\mu \pm \alpha - 1)(V_1/V_0) \tag{19}$$

A dielectric measurement could be made on such a sample by placing it with its centre at the centre of a cylindrical cavity oscillating in the E_{111} mode.

FERROMAGNETIC RESONANCE

Ferromagnetic resonance is said to occur when the frequency shift becomes very large. The values of μ and α are given in terms of frequency and polarizing field by equation (2); they may be varied, at a constant working frequency, by varying the polarizing field H_z, and the resonance phenomenon may thus be brought about.

Spherical samples. From equations (2) and (6), it may be seen that $\delta\omega/\omega \to \infty$ when

$$\left.\begin{aligned} h_z &\simeq H_r - M_s/3\mu_0 \\ H_z &\simeq H_r \end{aligned}\right\} \tag{20}$$

Circular disk samples. From equations (2) and (17), it may be seen that $\delta\omega/\omega \to \infty$ when

$$\left.\begin{aligned} h_z &\simeq H_r \\ H_z &\simeq H_r + M_s/\mu_0 \end{aligned}\right\} \tag{21}$$

Cylindrical rod samples. In this case $h_z = H_z$ and $\delta\omega/\omega \to \infty$ when

$$h_z = H_z \simeq H_r - M_s/2\mu_0 \tag{22}$$

EXTERNAL PERMEABILITY

In the early days of measurements of ferrite permeabilities spherical samples were used, and the problem arose of calculating the quantities $\boldsymbol{H}_1$ and $\boldsymbol{B}_1$ of equation (3), which is equivalent to calculating the magnetic field $\boldsymbol{h}$ in a ferrite due to an external uniform field $\boldsymbol{H}$, perpendicular to the polarizing field. The early workers made the assumption that to a first approximation $\boldsymbol{h}$ could be taken equal to $\boldsymbol{H}$, which, however, only gives accurate results when $\mu \sim 1$ and $\alpha \sim 0$, and does not give a useful result when μ and α differ considerably from 1 and 0. The error was pointed out by Rowen and von Aulock[8] and the present author[9]; the latter has given a formula for $\boldsymbol{h}$ in terms of $\boldsymbol{H}$.[10] Rowen and von Aulock introduced the concept of external permeability, relating the induction $\boldsymbol{b}$ in the ferrite sphere to the external field $\boldsymbol{H}$ thus:

$$\boldsymbol{b} = \mu_0 \begin{bmatrix} \eta & -j\kappa & 0 \\ j\kappa & \eta & 0 \\ 0 & 0 & 1 \end{bmatrix} \boldsymbol{H} \tag{23}$$

Results previously erroneously calculated for μ and α now become correct if they are taken to refer to η and κ. However, η and κ depend not only on the material of the ferrite, but also on its shape, while μ and α are properties of the material only. It is thus desirable to measure μ and α, not η and κ; the only reason for discussing η and κ further is that if results have previously been given in terms of η and κ, it is necessary to know the relations between these quantities and μ and α in order to calculate μ and α. Relations between μ and α and η and κ were given by the present author,[10] who also gave η and κ as functions of the external polarizing field H_z. These functions were derived from Polder's equations for μ and α in terms of h_z.

DISCUSSION

In planning to make measurements of ferrite properties, it is important to choose a sample shape that has a bearing on the use to which the ferrite is to be put. The properties of a ferrite depend on how it is made; a moulded disk may have appreciably different values of μ, α and ϵ from those possessed by an extruded rod, although the ingredients and firing conditions are the same. Therefore, if it is desired to use extruded ferrite rods, either circular for Faraday rotation devices, or rectangular for use in rectangular guides, a circular rod is a suitable specimen for cavity measurements. On the other hand, if ferrites are to be moulded—e.g. in the form of large disks for magnetic tuning of cavities—then a large disk sample is suitable, having also been moulded.

Small disk-shaped or spherical samples can always be used; if a number of rods or disks are made for some purpose, one or more of these, chosen at random, may be broken into pieces and the pieces rolled in a mill with carborundum; after a time the pieces are ground into spheres. Alternatively, if a piece is broken from a cylindrical rod, it may be ground flat to give a circular disk.

One is usually concerned to measure μ and α as functions of the polarizing field. Rowen and von Aulock[11] have

pointed out that the polarizing field for which magnetic resonance occurs is higher for a disk-shaped sample than for samples of other shapes, as can be seen from equations (20), (21), (22), and for this reason suggest that disk-shaped samples are particularly suitable at low frequencies, since other-shaped samples exhibit resonance in this range. It is doubtful, however, whether this constitutes any advantage, since it is not the observation of a large frequency shift that causes difficulty, but the calculation of μ and α, when these are large, from the observed frequency shift, whether this is large or small (depending on the sample shape). The values of μ and α become large when $h_z \simeq H_r$; this phenomenon is independent of the sample shape, as can be seen from equations (2), so that on this score there is no advantage in any particular sample shape.

Disk-shaped samples are likely to give less reliable results than rod-shaped or spherical samples because the formula for the frequency shift [equation (17)] is less accurate than in the case of a spherical or rod-shaped sample. The assumption has had to be made that the microwave field in the sample is the same as in the external field, which is only true for an infinitesimally thin sample. If the sample is sufficiently thin to justify this assumption, then the sample volume V_1 is small and the frequency shift measurement correspondingly less accurate.

The field in the specimen can be expressed exactly in terms of the external field if the specimen is a sphere or an infinitely long circular rod. The latter is achieved in practice if the actual rod fits flush with the ends of the cavity; if these are perfect reflectors, both cavity and rod may be regarded as part of an infinitely long system. The only inaccuracies that now appear in the formula for the frequency shift [equations (6) and (16)] are due to the non-uniformity of the microwave magnetic field in the neighbourhood of the sample, and a small effect due to the non-uniformity of the polarizing field at the ends of the sample. The best way to deal with the first difficulty is to start with a comparatively large sample (spherical or rod-shaped) and take a series of readings; then grind a little off the sample and repeat the readings. For sufficiently small values of the radius, the frequency shift will depend linearly on the sample volume, and in this range of values of radius the frequency shift readings may be used to determine μ and α. Also, for sufficiently small values of radius, the second difficulty will become negligible.

There are several other points to bear in mind in choosing the sample shape. With a rod, there is a tendency to average out local inhomogeneities; several spheres, all made from the same rod, can be used to indicate whether or not the rod is uniform. This applies equally to spheres made from a large disk. A spherical sample is much less likely to be damaged by mechanical shock than any other shape; many a worker has spent a week grinding a rod, only to have his work ruined in a second by dropping it. A spherical sample is easier to mount than a small disk, because it is only necessary to locate its centre; the orientation is unimportant. A large disk may be easily mounted at the end of a cavity for the magnetic measurement, but its mounting in the centre of a cavity for the dielectric measurement presents a difficulty.

Perhaps the decisive point in favour of a spherical sample is that measurements of μ, α and ϵ can probably all be made together on the same sample, in the same cavity, oscillating in the same mode. This minimizes the effects of extraneous factors, requires the design and manufacture of only one cavity instead of two and saves time in experiment, since it is only necessary to set up the apparatus once instead of twice. The sphere may be mounted on a fine fibre of silk or Nylon, passing through minute holes in the ends of the cavity. The change of position from the half-way to the quarter-way position may then be effected quite simply by drawing the thread along an appropriate distance, without otherwise disturbing the apparatus. The experiment has not been tried, but there is no apparent reason why it should not work.

In conclusion, the spherical sample shape is probably to be preferred in most cases for the elegance of experimental technique which it permits, for the reliability of the frequency shift formula, which is not subject to errors due to edge effects, and because a spherical sample can always be prepared from a given specimen. In special cases, however, other factors may be more important, and this possibility should be examined in relation to the discussion given here. A final point is that the concept of external permeability has outlived its usefulness and should be dropped.

ACKNOWLEDGEMENT

The author wishes to express his gratitude to the Engineer-in-Chief of Marconi's Wireless Telegraph Co. for permission to publish this paper.

REFERENCES

(1) POLDER, D. *Phil. Mag.*, **40**, pp. 99–115 (1949).

(2) HOGAN, C. L. *Bell Syst. Tech. J.*, **31**, pp. 1–31 (1952).

(3) SPENCER, E. G., LECRAW, R. C., and REGGIA, F. *Convention Record of the Institute of Radio Engineers* (8), pp. 113–21 (1955).

(4) ARTMAN, J. O., and TANNENWALD, P. E. *J. Appl. Phys.*, **26**, pp. 1124–32 (1955).

(5) LAX, B., and BERK, A. D. *Convention Record of the Institute of Radio Engineers* (10), pp. 70–4 (1953).

(6) TINKHAM, M., and STRANDBERG, M. W. P. *Proc. Inst. Radio Engrs*, **43**, pp. 734–38 (1955).

(7) LENGYEL, B. A., and BERK, A. D. *Proc. Inst. Radio Engrs*, **43**, pp. 1587–91 (1955).

(8) ROWEN, J. H., and VON AULOCK, W. *Phys. Rev.*, **96**, pp. 1151–3 (1954).

(9) WALDRON, R. A. *Brit. J. Appl. Phys.*, **7**, p. 114 (1956).

(10) WALDRON, R. A. *Convention on Ferrites*, Paper No. 2225R (London: The Institution of Electrical Engineers, October–November 1956).

(11) ROWEN, J. H., and VON AULOCK, W. *Bell Syst. Tech. J.*, **36**, pp. 427–48 (1957).

(12) CASIMIR, H. B. G. *Philips Res. Rep.*, **6**, pp. 162–82 (1951).

γ-ray yield and spectra produced by irradiating backing materials with protons

By S. E. Hunt, B.Sc., Ph.D., F.Inst.P., R. A. Pope, B.Sc., W. W. Evans and D. A. Hancock,
Associated Electrical Industries Ltd., Aldermaston, Berks.

[*Paper first received* 19 *February, and in final form* 2 *June*, 1958]

Thick targets of copper, silver, gold, tungsten, molybdenum, titanium, tantalum and tin were irradiated by protons in the energy range 0·6 to 2·8 MeV and the total γ-ray yield measured as a function of proton energy. The γ-ray spectra were also measured for a fixed proton energy of 2·2 MeV.

The total γ-ray yields of the materials were found to decrease in the order given above, indicating that tungsten backings produce less total γ-ray background than any other. If high energy γ-rays are being investigated it may be advisable to use tin or gold backings since the γ-ray spectrum from these is concentrated towards the lower energies and can consequently be biased out in the counting equipment, but both materials are rather fragile under heavy proton irradiation.

1. Introduction

Targets used for investigating γ-rays resulting from the proton irradiation of an element often consist of a thin layer of the element deposited on some backing material. γ-rays from the backing material itself provide an unwanted background and may completely mask those from the material under investigation.[1] A knowledge of its γ-ray yield under proton irradiation is therefore necessary in choosing a target backing material, and it is also essential to know the γ-ray spectrum produced, in order to assess the possibility of separating this from the γ-rays under investigation by biasing the counting equipment.

2. Target Preparation

The targets consisted of foils or disks about one square centimetre in area and of sufficient thickness to stop completely the protons of highest energy used. The following materials were tested (percentage purities are given in brackets): copper (99·5%); silver (99·999%); gold (99·999%); tungsten (99·8%); molybdenum (99·5%); titanium (99·9%); tantalum (99·9%); tin (99·998%).

The targets were first abraded using fine emery cloth to remove surface impurities, cleaned with acetone, washed in hot water and finally rinsed in distilled water. The gold target consisted of four 0·001 in. thick foils which were placed one on top of the other in order to provide the requisite thickness to stop the beam, and because of the fragility of the material the initial abrasion with emery cloth was omitted.

The cleaning process was carried out immediately before the targets were placed in the vacuum system for irradiation, and whilst they were under vacuum a liquid air trap was placed in their immediate vicinity. This had previously been found to greatly reduce the deposition of impurities such as carbon from the vacuum system on to the surface of the targets.[2]

3. Geometrical Arrangement

The beam from a vertical pressurized Van de Graaff accelerator[3] was first deflected through an angle of 63·6° by means of an absolute electrostatic analyser.[4] This provided a beam homogeneous in energy to about 6 parts in 10^4, which was then deflected through a further angle of 26·4° by a deflecting magnet which also separated out the particles of unwanted mass and provided a horizontal and approximately parallel beam of protons of the required energy. The beam was focused to a spot of about 5 mm diameter on the targets using a strong focusing magnet.

The target arrangement is shown in Fig. 1. This consisted of target 1 mounted on a flap so that it could either intercept

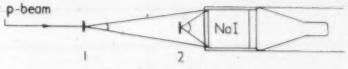

Fig. 1. Experimental arrangement for recording γ-spectra

or be withdrawn from the path of the beam and target 2 which was fixed and positioned 8 in. away from target 1.

In measuring the γ-ray spectra a 10 cm diameter sodium iodide crystal was placed 8 in. behind target 2, so that it subtended a solid angle of approximately 0·2 steradian at target 2 and 0·05 steradian at target 1.

The 36 mm diameter crystal used to estimate the total γ-ray yield was placed 1 in. behind target 2 so that it subtended a solid angle of 1·75 steradian at target 2 and 0·02 steradian at target 1.

4. γ-ray Detection and Energy Measurement

The γ-ray energy spectra were measured using a 10 cm diameter by 10 cm long sodium iodide crystal optically coupled to a photomultiplier type 6099A (by E.M.I. Ltd.). This large crystal produced effectively a single total-absorption peak for each γ-ray. Pulses were fed through a cathode follower and linear amplifier to a 120-channel pulse height analyser of the Hutchinson Scarrott type[5] made by Sunvic Controls Ltd. The spectrometer was calibrated using radioactive sources ^{22}Na (E_γ = 1·28 MeV and 0·51 MeV) ^{124}Sb (E_γ = 1·71 MeV) ThC″ (E_γ = 2·62 MeV) and the 6·14 MeV γ-ray from the ^{19}F ($p \propto \gamma$) ^{16}O reaction which was produced by irradiating a thin calcium fluoride target. The crystal and photomultiplier were surrounded by a lead shield of thickness 5½ in. which protruded 6 in. in front of the crystal to provide increased protection from machine X-rays.

In estimating the total γ-ray yields as a function of proton energy the γ-rays were detected by a 36 mm diameter by 25 mm long sodium iodide crystal, shielded by a 1 in. thick lead screen and optically coupled to a type 6262A photo-

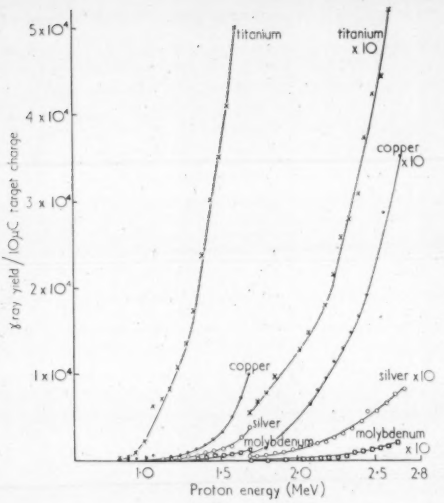

Fig. 2. γ-ray yield curves for titanium, copper, silver and molybdenum

× = titanium. ● = copper. ○ = silver. □ = molybenum.

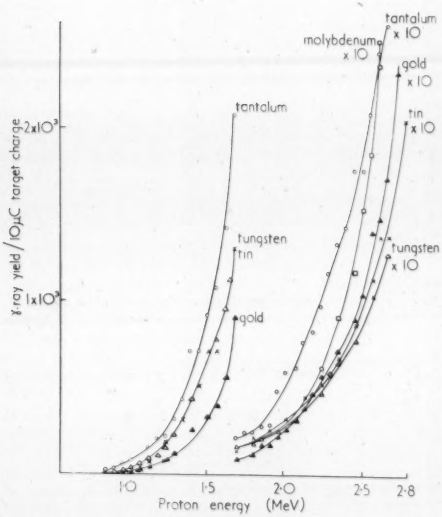

Fig. 3. γ-ray yield curves for tungsten, tantalum, gold, tin and molybdenum

△ = tungsten. ○ = tantalum. ▲ = gold. × = tin. □ = molybdenum.

multiplier (by E.M.I. Ltd.), which fed into a standard scaler *via* a cathode follower and linear amplifier. Zero bias setting was used on the discriminator of the scaler in order to record the low energy γ-rays, the lower limit of detection being about 200 keV, so that essentially all the γ-ray peaks observed in the spectra were recorded in the total yield measurements.

The total counts obtained from the target materials, using the large crystal, were estimated by measuring the areas under the γ-ray spectra curves (Figs. 4–11) and it was found that the relative yields computed in this manner were closely similar to those obtained from the total yield curves for a proton energy of 2·2 MeV (Figs. 2 and 3). This indicates that the reduced sensitivity of the small crystal to high energy γ-rays had not greatly affected the total yield curves, a result which was anticipated in view of the predominance of low energy radiation in all the spectra.

5. EXPERIMENTAL PROCEDURE

Appreciable background counting rates were observed due to X-rays from the Van de Graaff accelerator and γ-rays produced by accelerated particles striking the electrodes and slits of the electrostatic analyser and the brass walls of the magnet box. In initial irradiations, attempts were made to estimate these by intercepting the beam on a tungsten flap which could be placed in front of the target, but the γ-ray yield from this interceptor was appreciable and the double target system already described, and shown in Fig. 1, was therefore used. A steady beam was first allowed to fall on target 2 until the required target charge had been received. The beam was then intercepted by target 1, and the irradiation repeated. The machine conditions were kept constant during the two irradiations and identical target charges were received by each of the two targets in times which were equal to within one or two per cent. This was necessary since the background counts from the accelerator were strongly time dependent. Since the machine conditions were extremely stable the background counts were approximately equal in the two irradiations, the difference in the two total counts being equal to the counts from each of the targets multiplied by the difference in the solid angle subtended at the counter by target 2 and target 1. Reproducible counts were obtained in this way even for the targets of very low yield, when the background counting rate was of the same order as that from the target.

Both targets were connected to a beam current integrator, and in estimating the total yield curves this was arranged to switch off the counting circuits when the target had received a charge of 10 μC. Irradiations were repeated at proton energy intervals of about 50 keV through the range 0·6 to 2·8 MeV.

In measuring the γ-ray spectra the irradiation was continued at a fixed beam energy of 2·2 MeV until acceptable counting statistics had been obtained, the total target charge being recorded. In order to obtain acceptable statistics at the higher energy end of the spectrum for some low-yield targets it was necessary to increase the solid angle of observation by moving the counter nearer the target. The counts shown in Figs. 4 to 11 have been normalized to refer to the geometry described in Section 3 in the few instances where this was necessary.

In general, target currents of between 2 and 5 μA were used, but these had to be reduced for materials of higher yield to avoid large counting losses, and, for the tin target, to avoid melting the material.

6. RESULTS

The γ-ray yield curves as a function of proton energy are shown in Figs. 2 and 3. It will be noted that at the higher proton energies the yields vary by a factor of forty or more between the higher-yielding materials, titanium and copper, and those of lower yield, tungsten and tin. Figs. 4 to 11 show the γ-ray spectra produced by irradiating the materials with 2·2 MeV protons. The spectra are normalized to the same solid angle subtended at the counter by target 2. γ-ray energies given are subject to an experimental uncertainty of ±0·03 MeV for the sharper peaks.

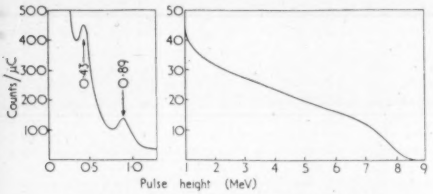

Fig. 4. Pulse height spectrum resulting from bombardment of titanium with 2·2 MeV protons

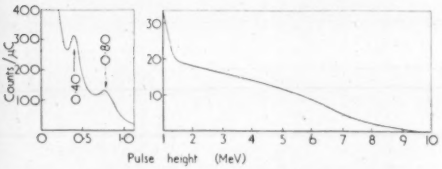

Fig. 5. Pulse height spectrum resulting from bombardment of copper with 2·2 MeV protons

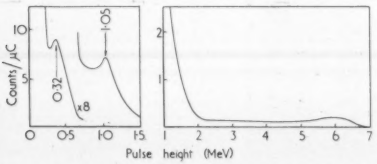

Fig. 6. Pulse height spectrum resulting from bombardment of silver with 2·2 MeV protons

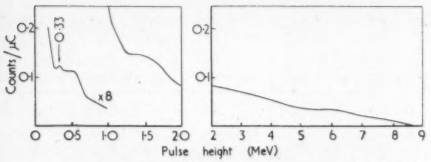

Fig. 7. Pulse height spectrum resulting from bombardment of molybdenum with 2·2 MeV protons

Titanium and copper both have a considerable high-energy yield, extending up to 9 or 10 MeV. The slight prominence at about 6 MeV apparent for silver, tantalum and tungsten indicates that an appreciable part of their high energy spectrum could be due to 6·14 MeV radiation from ^{19}F contamination of the targets. Molybdenum has a high-energy spectrum which shows no significant evidence of ^{19}F radiation, while gold and tin appear to yield nothing above about 2 MeV. The 0·33 MeV γ-ray from tantalum is probably the Coulomb excitation γ-ray measured as 0·303 MeV by

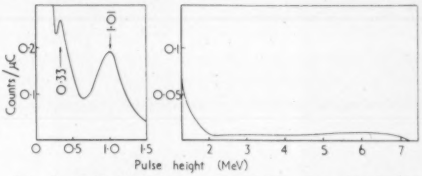

Fig. 8. Pulse height spectrum resulting from bombardment of tantalum with 2·2 MeV protons

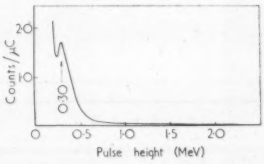

Fig. 9. Pulse height spectrum resulting from bombardment of gold with 2·2 MeV protons

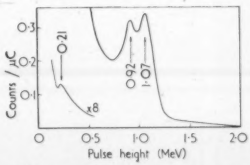

Fig. 10. Pulse height spectrum resulting from bombardment of tin with 2·2 MeV protons

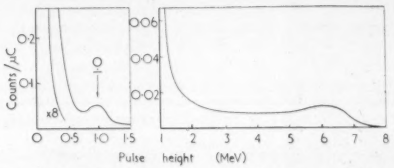

Fig. 11. Pulse height spectrum resulting from bombardment of tungsten with 2·2 MeV protons

Goldburg and Williamson,[6] and the 0·30 MeV γ-ray from gold is probably the same as that measured as 0·277 MeV by the same workers. The 0·32 MeV γ-ray from silver is a composite line of the Coulomb excitation γ-rays from the two isotopes ^{107}Ag and ^{109}Ag.[7] γ-ray spectra from separated isotopes of copper have been investigated in detail by Weller and Grosskreutz,[8] who also reported the absence of any structure in the spectrum from their tin backing.

7. CONCLUSIONS

The materials investigated give γ-ray yields under proton bombardment decreasing in the order titanium, copper, silver, molybdenum, tantalum, gold, tin and tungsten. Therefore, the most suitable target backing material for γ-ray yield and spectroscopy work, in general, is tungsten. While suitable for high-energy spectra, tin is easily melted unless the beam intensity is low, and gold, too, suffers from the same disadvantage unless adequate cooling facilities can be provided.

ACKNOWLEDGEMENTS

The authors are pleased to acknowledge the assistance of G. Hunt with the experimental work.

Thanks are also due to Dr. T. E. Allibone, Director of the Research Laboratory, Associated Electrical Industries Ltd., for permission to publish this work.

REFERENCES

(1) HUNT, S. E., POPE, R. A., and EVANS, W. W. *Phys. Rev.*, **106**, p. 1012 (1957).
(2) HUNT, S. E. *Proc. Phys. Soc.* [*London*] *A*, **65**, p. 982 (1952).
(3) CHICK, D. R., and PETRIE, D. P. R. *Proc. Instn Elect. Engrs*, *B*, **103**, p. 132 (1955).
(4) HUNT, S. E., PETRIE, D. P. R., FIRTH, K. A., and TROTT, A. J. *Proc. Instn Elect. Engrs*, *B*, **103**, p. 146 (1955).
(5) HUTCHINSON, G. W., and SCARROTT, G. G. *Phil. Mag.*, **42**, p. 792 (1951).
(6) GOLDBURG, W. I., and WILLIAMSON, R. M. *Phys. Rev.*, **95**, p. 767 (1954).
(7) FAGG, L. W., WOLICKI, E. A., BONDELID, R. O., DUNNING, K. L., and SNYDER, S. *Phys. Rev.*, **100**, p. 1299 (1955).
(8) WELLER, C. E., and GROSSKREUTZ, J. C. *Phys. Rev.*, **102**, p. 1149 (1956).

Crystallographic programmes for a computer

By J. C. GOWER, B.A., and J. H. RAYNER, M.A., D.Phil., A.Inst.P., Rothamsted Experimental Station, Harpenden, Herts.

[*Paper first received* 18 *March and in final form* 9 *April*, 1958]

A brief description is given of programmes developed for the calculations involved in the X-ray analysis of crystal structures. The programmes calculate three dimensional structure factors, one and two dimensional Fourier syntheses and *R*-factors.

Although several programmes to facilitate crystallographic calculation have been described in the past [see, for example, references (1–4)], these have been mostly for use on computers having much larger fast access storage than the Elliott–N.R.D.C. 401. It may be of interest to describe some of the devices used to speed up the programmes when fast access storage is limited. So far programmes have been written to calculate structure factors, one- and two-dimensional Fourier synthesis and *R*-factors. These programmes are not written for particular space groups but are general ones which ignore all the symmetry, although it has been found a trival matter to modify them for the case of centro-symmetric cells.

The Elliott 401 has a magnetic disk store consisting of 23 tracks each holding 128 numbers or instructions, each of 32 binary digits. There are only three fast access stores, besides the accumulator and the multiplier register. Only the one number or instruction on each track which is under the reading head is available for calculation at any given moment. For the calculation to proceed rapidly the orders and numbers must be arranged around the disk in such a way that the delay between successive operations is as small as possible—so-called optimum programming. A one-plus-one address code is used, each instruction specifying an address in the store and also the address of the next instruction to be obeyed. This machine can use its three fast access stores as *B*-registers. This means that the contents of one of these registers may be added to an order before it is obeyed; a common use of this is to enable numbers to be picked up in sequence from consecutive addresses.

The structure factor programme works out A, B and $|F| = \sqrt{(A^2 + B^2)}$ where

$$A(h, k, l) + iB(h, k, l) = \sum_j f_j(\sin\theta) \sum_{nj} \exp\left[2\pi i(hx_{nj} + k\,y_{nj} + lz_{nj})\right] \quad (1)$$

Here f_j is the atomic scattering factor of the j^{th} type of atom and (x_{nj}, y_{nj}, z_{nj}) are the co-ordinates of the n^{th} atom of type j. The inner loop of the programme calculates simultaneously the cosine and sine of $2\pi(hx + k\,y + lz)$, which, since we are not dealing with special space groups, is better than calculating expressions of the form

$$\begin{matrix}\cos\\ \sin\end{matrix} 2\pi hx \quad \begin{matrix}\cos\\ \sin\end{matrix} 2\pi ky \quad \begin{matrix}\cos\\ \sin\end{matrix} 2\pi lz.$$

It is in this inner loop that the timing is most critical and two devices are used to increase the efficiency of this part of the calculation. By storing the numbers between the instructions, the co-ordinates x, y, z can be picked up quickly. In this way speed can be increased three-fold at the expense of a two-thirds increase in the storage space for co-ordinates. If the n^{th} set of co-ordinates are wanted the first order is *B*-modified to pick up x_n and to take the next instruction from the address following that occupied by x_n. This instruction in turn picks up y_n and gives the address of the instruction to pick up z_n (which is, in fact, the location following that where y_n is stored). The second device evaluates the sine and cosine terms. A sine/cosine table is stored, the argument running in steps of $\frac{2\pi}{1024}$ in the range $0 \leqslant \phi \leqslant \pi/4$. Both the sine and cosine are picked up together and each is used to interpolate linearly in the table of the other. This depends on the fact that $\sin(\phi + \delta) \simeq \sin\phi + \delta\cos\phi$ and $\cos(\phi + \delta) \simeq \cos\phi - \delta\sin\phi$ for small δ. Such a method gives a maximum error of 2×10^{-5}. By incorporating these two devices the inner loop has been programmed to take only seven revolutions of the disk (7/80 s).

Much of this complication could have been avoided, if the three co-ordinates for one atom could have been packed

to sufficient accuracy in one store, as should be possible in those machines which work with 40 binary digit numbers.

A method similar to that described for picking up the co-ordinates is also used for selecting the appropriate value of f as a function of $\sin\theta$. In order to give a close approximation to the f-curve by a series of linear segments and thus to improve the accuracy of linear interpolation, the f-table is stored at unequal intervals of the argument. The problem is to interpolate in a table of n values of X (equivalent to $\sin\theta$) and Y (equivalent to the f values) when it is no longer possible

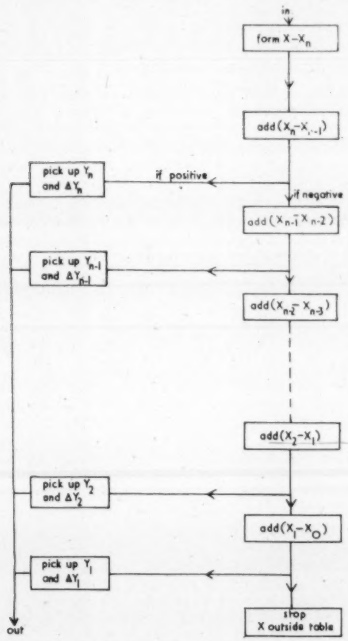

Diagrammatic representation of scheme used to pick up values to interpolate in f-tables

to determine the entry point of the table by B-modification. The value of X for which Y is required must lie on one or between two of the tabulated values of X. In the first case no interpolation is necessary and in the second these two tabular values of X are found by subtracting from X the largest value X_n and adding the successive X-differences until the total becomes positive (see figure). When this happens the next instruction is to pick up the corresponding value of Y together with its first difference, the two being packed in the same store. The registers now contain all that is required for the linear interpolation and this information has all been obtained in one revolution of the disk. The process is performed by a series of instructions interspersed between the tabulated values of X and this interspersion is most easily arranged by first putting the table entries into consecutive stores and then reorganizing them, as a preliminary part of the calculation.

When care has been taken to make the programme fast the output time becomes an appreciable part of the total computing time. In the structure factor programme computing and printing are suppressed when the reflection would lie outside the unit sphere. If B is known to be zero, B and F are not printed (however, if B is printed it acts as a partial check on the computed value of A).

For Fourier synthesis separate programmes have been written for the one- and two-dimensional cases, but there is as yet no three-dimensional programme.

The one-dimensional programme operates in a straightforward manner using a cosine table which it prepares at intervals corresponding to the chosen division of the unit cell. The two-dimensional programme, which was written by way of experiment, uses trigonometrical formulae of the type $\sin(hx + ky)$ rather than using two stages of one-dimensional synthesis. The method used has been shown[1] to be the slower and although it is adequately fast for our present purposes we shall use the other method for the three-dimensional case.

The structure factor and two-dimensional Fourier programmes are used to find by successive approximation the best set of atomic co-ordinates for a projection of a crystal structure. Each cycle of refinement involves the calculation of structure factors, the agreement factor R, the differences between the observed and calculated structure factors, and a difference synthesis. To complete this cycle a programme has been written which will read in a tape with F (observed) punched on it together with the tape actually produced by the structure factor programme containing F (calculated). When both of these tapes have been read in

$$R = \frac{\Sigma||F_0'| - |F_c||}{\Sigma|F_c|}$$

is calculated, where F_0' is the value of F_0 scaled to be comparable with F_c. In addition $F_0' - F_c$ is printed, where F_0' is given the sign of F_c, the quantities required for the difference synthesis to be computed.

In the structure factor programme speed has been gained at the expense of an extravagant use of storage space. This limits the number of atoms and the number of types of atom that can be handled in our case to, say, 325 atoms of one type or 200 atoms of six types, but this is sufficient for any of the smaller structures for which general (all space group) programmes are suitable [Trueblood, in reference (4)].

The programmes have been used to refine the co-ordinates in a projection of the structure of sodium formaldeyde bisulphite. For the 28 atoms (one of each pair of centrosymmetrically related atoms) of four types, the 64 structure factors were calculated in about 6 minutes and the difference synthesis calculated at 297 points in about 40 minutes.

REFERENCES

(1) Bennett, J. M., and Kendrew, J. C. *Acta cryst.*, **5**, p. 109 (1952).

(2) Mayer, S. W., and Trueblood, K. N. *Acta cryst.*, **6**, p. 427 (1953).

(3) Ahmed, F. R., and Cruickshank, D. W. J. *Acta cryst.*, **6**, p. 765 (1953).

(4) Finch, J., Green, D. W., Holmes, K. C., and North, A. C. T. *Brit. J. Appl. Phys.*, **9**, p. 1 (1958).

Stresses and strains in an infinite elastic sheet under a tension applied at two rigid pairs of square jaws

By DAPHNE G. PADFIELD, Ph.D., and NORA B. DICKINSON, B.Sc., Wool Industries Research Association, Leeds

[*Paper first received* 14 *May*, 1957, *and in final form* 10 *April*, 1958]

First-order elastic theory of plane stresses is applied numerically to obtain estimates of the stresses in an infinite elastic sheet stretched in its own plane by forces applied at two rigid jaws. A similar method is applied (largely for purposes of comparison) to the stress in a strip tensioned by forces applied at rigid jaws extending across the whole width of the strip. As contrasted with relaxation methods, the procedure is well-suited to use with electronic computers.

1. INTRODUCTION

Tests of two types are commonly used to find the breakage strength of fabrics: in the first type a straight strip of material is subjected to a load by means of jaws at the two ends of the strip, each pair of jaws extending across the whole width of the strip; while in the second type (grab test) the load is applied at small jaws placed well in from the edges of a larger area of fabric. No theory has yet been found which adequately relates the results of the two types of test: even if the load-extension curve as well as the breakage point is known for one kind of test, neither the breakage point nor the load-extension curve can be reliably predicted for the other kind.

It was as a preliminary to tackling this question that the present work was undertaken, though the results as they stand are far from being directly applicable to fabric strength tests, in which large deformations occur and in which the materials are anything but isotropic.

2. APPROXIMATION TO THE STRESSES IN THE IDEALIZED GRAB TEST

Consider the stresses which arise in samples under test when the deformations are sufficiently small for the ordinary linear equations of elasticity theory to be used. It is assumed that the sample may be considered to be a plane sheet of

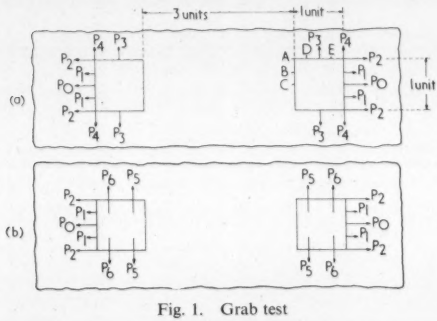

Fig. 1. Grab test

homogeneous, isotropic material of modulus E and Poisson's ratio ν. The forces exerted by the jaws are approximated in the case of the grab test, by a system of point forces. Two variations of a symmetrical system with five unknowns were investigated, namely, the system $P_0P_1P_2P_3P_4$ shown in Fig. 1(*a*) and the system $P_0P_1P_2P_5P_6$ of Fig. 1(*b*). The original idea behind the choice of the forces was to keep them as far away as possible from the region between the two jaws in which we are primarily interested, so that the irregularities caused by these point discontinuities would be unimportant, and the stresses predicted for the region between the jaws be a good approximation to the actual values (as in Saint-Venant's principle). Subsequently, to improve the fit, two versions of the seven-force system P_0–P_6 were worked out: the first, a linear combination (one extra unknown therefore) of the two five-force solutions, the second, an independent treatment starting from the seven unknowns P_0–P_6.

The geometrical proportions were chosen to correspond to a common practical set-up, jaws one unit square situated three units apart; the edges of the sample were supposed to be sufficiently far away from the jaws for the stresses to be the same as for an infinite sheet of material.

Five conditions are necessary to complete the formulation of the five-force problem. The following set of conditions was imposed:

(i) $P_0 + 2P_1 + 2P_2 =$ applied load P;

(ii and iii) the displacements of points A, B, C in the x-direction are equal;

(iv) the y-displacement of point A is zero;

(v) the y-displacement of point D is zero.

For the combination of the two five-force solutions the additional boundary condition was

(vi) the y-displacement of point E is zero;

and for the full seven-force problem we also put

(vii) the x-displacement of point E equal to that of A, B and C.

All these conditions are, of course, necessarily satisfied in the actual experimental conditions if there is no slipping.

The stresses at any point (x_1, y) due to a point force P at the origin in the direction of the x-axis are given by:

$$\sigma_x = \frac{P}{4\pi}\left[\frac{-(3+\nu)x}{x^2+y^2} + \frac{2(1+\nu)xy^2}{(x^2+y^2)^2}\right] \quad (1)$$

$$\sigma_y = \frac{P}{4\pi}\left[\frac{(1-\nu)x}{x^2+y^2} - \frac{2(1+\nu)xy^2}{(x^2+y^2)^2}\right] \quad (2)$$

(see Timoshenko*), and the corresponding strains are given by $\epsilon_x = (\sigma_x - \nu\sigma_y)/E$; $\epsilon_y = (\sigma_y - \nu\sigma_x)/E$. The extension along the line (x_0, y) to (x_1, y) can therefore be evaluated as

$$\text{extension} = \int_{x_0}^{x_1} \epsilon_x \, dx$$

* TIMOSHENKO. *Theory of Elasticity*, p. 111 (New York: McGraw-Hill Book Co. Inc., 1934).

Table 1. *Magnitudes of the forces P_0–P_6 in three versions of the grab calculation [namely, (i) first five-force method, (ii) second five-force method, (iii) seven-force method]*

ν	0			0·2			0·4			0·6			0·8	
	(i)	(ii)	(iii)	(i)	(ii)	(iii)	(ii)	(iii)	(i)	(ii)	(iii)	(ii)	(iii)
P_0	+1·6880P	−32·4138P	+20·3157P	+1·8383P	−55·1332P	+17·1955P	−91·1585P	+13·8636P	−2·8414P	−154·842P	+11·1349P	−292·644P	+ 4·4210P
P_1	−2·1280P	+22·9676P	−13·7971P	−2·5383P	+39·6156P	−11·4876P	+66·0808P	− 9·1252P	−2·2362P	+112·972P	− 7·3691P	+214·638P	− 4·5625P
P_2	−1·7840P	− 6·2606P	+ 4·1392P	+2·1192P	−11·5490P	+ 3·3898P	−20·0015P	+ 2·6934P	+4·1569P	− 35·0511P	+ 2·3450P	− 67·8165P	+ 2·8519P
P_3	−0·31172P	—	+ 0·7382P	−0·4656P	—	+ 0·61605P	—	+ 0·4763P	−1·5911P	—	+ 0·3011P	—	− 0·4777P
P_4	+1·1734P	—	+ 1·9187P	+1·8577P	—	+ 2·3809P	—	+ 3·3659P	+7·3388P	—	+ 6·5132P	—	+23·8037P
P_5	—	+ 0·6020P	+ 0·3545P	—	+ 0·8979P	+ 0·3997P	+ 1·3622P	+ 0·4824P	—	+ 2·1771P	+ 0·7574P	+ 3·9353P	+ 2·1719P
P_6	—	+ 1·5343P	− 5·2005P	—	− 2·3498P	− 5·3274P	− 3·6623P	− 5·8822P	—	− 6·0136P	− 8·4968P	− 11·1764P	−22·6906P

Table 2. *Comparison of stresses predicted by different methods of calculation (grab test)*

*Points** (x, y)	*Value of* ν	*First five-force solution* (P_0-P_4) *for* $P=1$			*Second five-force solution* $(P_0, P_1, P_2, P_5, P_6)$ *for* $P=1$			*First seven-force solution* (λ) *for* $P=1$			*Full seven-force solution* (P_0-P_6) *for* $P=1$		
		σ_x	σ_y	τ_{xy}	σ_x	σ_y	τ_{xy}	σ_x	σ_y	τ_{xy}	σ_x	σ_y	τ_{xy}
(0, 0)	0·2	+0·2007	−0·0054	0	+0·2149	−0·0789	0	+0·2097	−0·0255	0	+0·2002	−0·0306	0
	0·6	+0·4380	+0·0915	0	+0·3052	−0·1294	0	+0·4054	+0·0372	0	+0·3801	+0·0207	0
(0, ½)	0·2	+0·2049	−0·0039	0	+0·2100	−0·0762	0	+0·2063	−0·0237	0	+0·1976	−0·0304	0
	0·6	+0·4284	+0·0966	0	+0·2917	−0·1214	0	+0·3949	+0·0431	0	+0·3709	+0·0237	0
(0, ½)	0·2	+0·1970	−0·0015	0	+0·1968	−0·0688	0	+0·1970	−0·0199	0	+0·1893	−0·0269	0
	0·6	+0·4005	+0·1043	0	+0·2563	−0·1008	0	+0·3651	+0·0539	0	+0·3447	+0·0337	0
(0, 1)	0·2	+0·1660	+0·0083	0	+0·1582	−0·0468	0	+0·1639	−0·0068	0	+0·1607	−0·0150	0
	0·6	+0·2948	+0·1337	0	+0·1652	−0·0482	0	+0·2629	+0·0890	0	+0·2585	+0·0633	0
(½, 0)	0·2	+0·2102	+0·0001	0	+0·2271	−0·0831	0	+0·2148	−0·0227	0	+0·2066	−0·0345	0
	0·6	+0·4465	+0·1130	0	+0·3407	−0·1441	0	+0·4205	+0·0499	0	+0·3956	+0·0205	0
(½, ¼)	0·2	+0·2080	+0·0004	−0·0026	+0·2196	−0·0777	−0·0111	+0·2112	−0·0210	−0·0049	+0·2021	−0·0284	−0·0046
	0·6	+0·4384	+0·1142	−0·0084	+0·3184	−0·1272	−0·0333	+0·4089	+0·0549	−0·0146	+0·3837	+0·0332	−0·0138
(½, ½)	0·2	+0·2008	+0·0020	−0·0060	+0·2025	−0·0700	−0·0186	+0·2012	−0·0177	−0·0095	+0·1930	−0·0253	−0·0086
	0·6	+0·4117	+0·1192	−0·0193	+0·2669	−0·1028	−0·0517	+0·3761	+0·0647	−0·0273	+0·3539	+0·0424	−0·0248
(½, 1)	0·2	+0·1677	+0·0115	−0·0128	+0·1584	−0·0479	−0·0230	+0·1652	−0·0048	−0·0148	+0·1623	−0·0140	−0·0143
	0·6	+0·2954	+0·1483	−0·0355	+0·1573	−0·0483	−0·0496	+0·2615	+0·1000	−0·0390	+0·1560	+0·0731	−0·0343
(1, 0)	0·2	+0·2143	+0·0174	0	+0·2622	−0·0664	0	+0·2274	−0·0055	0	+0·2180	−0·0142	0
	0·6	+0·4593	+0·1812	0	+0·4641	−0·1130	0	+0 4605	+0·1090	0	+0 4355	+0·0798	0
(1, ¼)	0·2	+0·2151	+0·0160	−0·0014	+0·2452	−0·0698	−0·0175	+0·2234	−0·0075	−0·0058	+0·2130	−0·0174	−0·0056
	0·6	+0·4616	+0·1762	−0·0041	+0·3956	−0·1102	−0·0702	+0·4454	+0·1059	−0·0203	+0·4171	+0·0754	−0·0209
(1, ½)	0·2	+0·2139	+0·0136	−0·0080	+0·2180	−0·0781	−0·0272	+0·2150	−0·0115	−0·0133	+0·2035	−0·0208	−0·0108
	0·6	+0·4537	+0·1683	−0·0267	+0·2869	−0·1150	−0·0884	+0·4134	+0·0987	−0·0418	+0·3815	+0·0704	−0·0367
(1, 1)	0·2	+0·1732	+0·0231	−0·0277	+0·1640	−0·0609	−0·0558	+0·1707	+0·0001	−0·0354	+0·1701	−0·0144	−0·0310
	0·6	+0·2945	+0·2034	−0·0792	+0·1406	−0·0746	−0·1130	+0·2567	+0·1351	−0·0875	+0·2562	+0·0946	−0·0750

* Note. The origin is at the centre of symmetry, i.e. at the mid-point of the sample, and the x, y axes are respectively parallel and perpendicular to the applied force P.

Table 3. *Stresses in material under grab test for* $\nu = 0, 0{\cdot}2, 0{\cdot}4, 0{\cdot}6, 0{\cdot}8$ *(seven-force calculation)*

ν / (x, y)	0			0·2			0·4			0·6			0·8		
	σ_x	σ_y	τ_{xy}	σ_x	σ_y	τ_{xy}	σ_x	σ_y	τ_{xy}	σ_x	σ_y	τ_{xy}	σ_x	σ_y	τ_{xy}
(0, 0)	+0·1755P	−0·0481P	0	+0·2002P	−0·0306P	0	+0·2444P	−0·0115P	0	+0·3801P	+0·0207P	0	+1·0284P	+0·1358P	0
(0, ¼)	+0·1735P	−0·0472P	0	+0·1976P	−0·0304P	0	+0·2398P	−0·0097P	0	+0·3709P	+0·0237P	0	+0·9943P	+0·1487P	0
(0, ½)	+0·1678P	−0·0446P	0	+0·1893P	−0·0269P	0	+0·2270P	−0·0046P	0	+0·3447P	+0·0337P	0	+0·8970P	+0·1849P	0
(0, 1)	+0·1473P	−0·0351P	0	+0 1607P	−0·0150P	0	+0·1833P	+0·0120P	0	+0·2585P	+0·0633P	0	+0·5738P	+0·2964P	0
(¼, 0)	+0·1806P	−0·0517P	0	+0·2066P	−0·0345P	0	+0·2527P	−0·0133P	0	+0·3956P	+0·0205P	0	+1·0824P	+0·1467P	0
(¼, ¼)	+0·1768P	−0·0463P	−0·0034P	+0·2021P	−0·0284P	−0·0046P	+0·2464P	−0·0055P	−0·0070P	+0·3837P	+0·0332P	−0·0138P	+1·0412P	+0·1853P	−0·0504P
(¼, ½)	+0·1747P	−0·0455P	−0·0064P	+0·1930P	−0·0253P	−0·0086P	+0·2336P	−0·0013P	−0·0126P	+0·3539P	+0·0424P	−0·0248P	+0·9318P	+0·2196P	−0·0906P
(¼, 1)	+0·1494P	−0·0353P	−0·0120P	+0·1623P	−0·0140P	−0·0143P	+0·1841P	+0·0150P	−0·0190P	+0·2560P	+0·0731P	−0·0343P	+0·5642P	+0·3314P	−0·1187P
(1, 0)	+0·1873P	−0·0371P	0	+0·2180P	−0·0142P	0	+0·2718P	+0·0171P	0	+0 4355P	+0·0798P	0	+1·2313P	+0·3557P	0
(1, ¼)	+0·1849P	−0·0404P	−0·0032P	+0·2130P	−0·0174P	−0·0056P	+0·1630P	+0·0138P	−0·0097P	+0·5171P	+0·0754P	−0·0209P	+1·1655P	+0·3449P	−0·0796P
(1, ½)	+0·1798P	−0·0437P	−0·0074P	+0·2035P	−0·0208P	−0·0108P	+0·2463P	+0·0101P	−0·0174P	+0·3815P	−0·0704P	−0·0367P	+1·0334P	+0·3330P	−0·1425P
(1, 1)	+0·1587P	−0·0391P	−0·0262P	+0·1701P	−0·0144P	−0·0310P	+0·1894P	+0·0207P	−0·0412P	+0·2562P	+0·0946P	−0·0750P	+0·5355P	+0·4363P	−0·2620P

which can be written explicitly

$$= -\frac{P(1+\nu)}{2\pi E}\left[\frac{(3-\nu)}{4}\log\left(\frac{x_1^2+y^2}{x_0^2+y^2}\right)+\right.$$
$$\left.+\frac{(1+\nu)y^2}{2(x_1^2+y^2)}-\frac{(1+\nu)y^2}{2(x_0^2+y^2)}\right] \quad (3)$$

and similarly, extensions in the y-direction take the form

$$\int_{y_0}^{y_1}\epsilon_y\,dy = -\frac{P(1+\nu)}{2\pi E}\cdot\frac{(1+\nu)}{2}\left(\frac{xy_0}{x^2+y_0^2}-\frac{xy_1}{x^2+y_1^2}\right) \quad (4)$$

By simple addition of such expressions as these, the displacements of points A, B, C, D, etc., can be expressed as linear expressions in P_0, P_1, ... Take the first five-force problem. Conditions (i)–(v) give the five linear equations in five unknowns, so we can solve for P_0–P_4 in terms of P, and hence evaluate the stresses and strains at any point in terms of the applied force P. The other versions of the grab-problem calculation follow a similar course.

Solutions of the equations for P_0–P_6 are tabulated for values of ν between 0 and 0·8 in Table 1, and corresponding values of the stresses, putting $P = 1$, in Tables 2 and 3. The seven-force solution should, of course, be the most accurate, but the values in the other cases are useful as an aid to estimating the probable accuracy of this solution (see Section 4).

3. APPROXIMATION TO THE STRESSES DURING A STRIP TEST

In the case of a strip, the previous boundary conditions at infinity ($\sigma_x \to 0$, $\sigma_y \to 0$, $\tau_{xy} \to 0$) are replaced by boundary conditions at the edge of the strip, namely, $\sigma_y = \tau_{xy} = 0$ at the edges.

With the idea of preserving a close correspondence with the grab case, the following procedure was adopted. Forces $P_0P_1P_2P_5P_6$ were found exactly as for the grab problem except for one modification: condition (v) was replaced by

(v′) the y-displacement of point B is zero.

On to this system of point forces was superposed a continuous polynomial-type distribution, the coefficients being chosen so as to cancel out the values of σ_y, τ_{xy} produced by the point forces along the edges of the strip, while not disturbing conditions (i)–(v′).

We cannot, of course, expect to make the resultant $\sigma_y = 0$ and $\tau_{xy} = 0$ at all points along the edges, but are content with satisfying these conditions at the points L, M, N in Fig. 2. It was found, however, that the force P_5, being rather

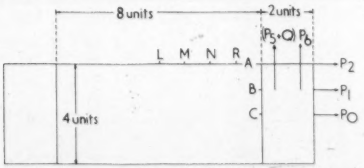

Fig. 2. Strip test

close to the edge AC of the jaws, created an effect somewhat difficult to compensate by the polynomial. For this reason we also superposed a force Q on top of P_5 at the same time as fitting the polynomial. The force Q largely cancelled out

Table 4. *Stresses during strip test*

ν	0·2			0·4			0·6			0·8		
(x, y)	σ_x	σ_y	τ_{xy}	σ_x	σ_y	τ_{xy}	σ_x	σ_y	τ_{xy}	σ_x	σ_y	τ_{xy}
(0, 0)	+0·2641P	−0·0016P	0	+0·2767P	−0·0037P	0	+0·2889P	−0·0063P	0	+0·3013P	−0·0091P	0
(0, 1)	+0·2621P	−0·0009P	0	+0·2725P	−0·0021P	0	+0·2824P	−0·0036P	0	+0·2924P	−0·0052P	0
(0, 2)	+0·2589P	0	0	+0·2663P	0	0	+0·2732P	0	0	+0·2807P	0	0
(1, 0)	+0·2647P	−0·0006P	0	+0·2780P	−0·0019P	0	+0·2927P	−0·0043P	0	+0·3057P	−0·0071P	0
(1, 1)	+0·2640P	−0·0005P	−0·0009P	+0·2731P	−0·0014P	−0·0024P	+0·2834P	−0·0027P	−0·0042P	+0·2937P	−0·0043P	−0·0064P
(1, 2)	+0·2567P	0	0	+0·2617P	0	0	+0·2660P	0	0	+0·2702P	0	0
(2, 0)	+0·2654P	+0·0052P	0	+0·2809P	+0·0086P	0	+0·2975P	+0·0104P	0	+0·3155P	+0·0107P	0
(2, 1)	+0·2653P	+0·0032P	+0·0003P	+0·2744P	+0·0054P	−0·0009P	+0·2855P	+0·0068P	−0·0033P	+0·2967P	+0·0073P	−0·0069P
(2, 2)	+0·2348P	0	0	+0·2539P	0	0	+0·2519P	0	0	+0·2485P	0	0
(3, 0)	+0·2613P	+0·0249P	0	+0·2755P	+0·0478P	0	+0·2935P	+0·0687P	0	+0·3254P	+0·0874P	0
(3, 1)	+0·2500P	+0·0174P	+0·0083P	+0·2335P	+0·0332P	+0·0138P	+0·2605P	+0·0478P	+0·0164P	+0·2691P	+0·0611P	+0·0162P
(3, 2)	+0·2583P	0	+0·0072P	+0·2580P	0	+0·0134P	+0·2516P	0	+0·0195P	+0·1400P	0	+0·0257P

the force P_5 and led to smoother values of the stresses near the jaws: it also allowed us to fit one extra condition, namely, $\sigma_y = 0$ at the point R shown in Fig. 2. The polynomial forms used were:

$$\sigma_x = \frac{\partial^2\phi}{\partial y^2}; \quad \sigma_y = \frac{\partial^2\phi}{\partial x^2}; \quad \tau_{xy} = \frac{-\partial^2\phi}{\partial x \partial y} \tag{5}$$

where $\phi = a_1x^2 + b_1y^2$

$$+a_2x^4 + b_2x^2y^2 + c_2y^4$$
$$+a_3x^6 + b_3x^4y^2 + c_3x^2y^4 + d_3y^6$$
$$+a_4x^8 + b_4x^6y^2 + c_4x^4y^4 + d_4x^2y^6 + e4y^8$$

and, in order to satisfy the elastic equation

$$\frac{\partial^4\phi}{\partial x^4} + 2\frac{\partial^4\phi}{\partial x^2\partial y^2} + \frac{\partial^4\phi}{\partial y^4} = 0 \tag{6}$$

the coefficients are related by the equations

$$b_2 = -3(a_2 + c_2); \quad 15a_3 = -(2b_3 + c_3);$$
$$15d_3 = -(b_3 + 2c_3); \quad 70a_4 = -(5b_4 + c_4);$$
$$5d_4 = -(5b_4 + 4c_4); \quad 70e_4 = 3c_4 + 5b_4 \tag{7}$$

The conditions stated are sufficient to determine the coefficients uniquely, whence the stresses at all points of the strip can be evaluated. Since it was anticipated that the stresses in a narrow strip would differ little from a uniform stress system ($\phi = ky^2$, $\sigma_x = 2k$, $\sigma_y = \tau_{xy} = 0$), a wide strip, with width equal to half the length, was chosen for the calculations.

Stresses were evaluated for $\nu = 0{\cdot}2$, $0{\cdot}4$, $0{\cdot}6$, $0{\cdot}8$ and the results are shown in Table 4.

4. DISCUSSION OF ACCURACY OF RESULTS

We must now assess the errors which are likely to spring from the representation of the forces at the jaws of the testing equipment by a system of point forces at arbitrarily chosen points within the jaw area.

In the case of the strip test, an estimate can be made from the difference between the applied load P and the calculated value of $\int\sigma_x dy$ along any line across the strip, which should be equal to P for all sections. The discrepancy varies from about 4% at $\nu = 0{\cdot}2$ to about 15% at $\nu = 0{\cdot}8$. It is possible, of course, to apply a corresponding correction factor to all calculated stresses so that the integral across at least one section has the correct value. This has been done, but even then a residual discrepancy for other sections of about 2½% at $\nu = 0{\cdot}2$ to 5½% at $\nu = 0{\cdot}8$ remains. One might guess at intermediate figures, say 3% of the maximum stress at $\nu = 0{\cdot}2$ to 10% at $\nu = 0{\cdot}8$ as the estimate of probable error in the calculated strip values of σ_x. There is no obvious way of estimating the errors of σ_y and τ_{xy} values; but these values are, in any case, not big enough to have much effect on the quantity in which we are primarily interested, namely, the tendency to break, at least if the classical methods of estimation from strain energy, etc., are valid.

Within a single strip test calculation, the values of σ_x differ from one another by about 3% at $\nu = 0{\cdot}2$ and by 25% at $\nu = 0{\cdot}8$. Thus at $\nu = 0{\cdot}2$, the departures from σ_x = constant are no greater than the probable error, but at $\nu = 0{\cdot}8$ the overall variations of σ_x are at least qualitatively significant.

Turning to the grab test, examination of $\int\sigma_x dy$ will tell us nothing since it is bound to be equal to P. We can therefore only compare results given by different systems of forces, with a backward look at the strip problem where comparison is possible.

The discrepancy between the two five-force grab calculations of σ_x ranges from 4–15% at $\nu = 0{\cdot}2$ to 30–50% at $\nu = 0{\cdot}6$ (values for $\nu = 0{\cdot}8$ were not worked out). The discrepancy between the two seven-force calculations (one with six, the other with seven relevant boundary conditions including total force equal to P) was from 0–4% at $\nu = 0{\cdot}2$ to 0–6½% at $\nu = 0{\cdot}6$. One hesitates to accept these latter figures unquestioningly as estimates of accuracy, since the choice both of the positions of the applied forces and of six of the seven boundary conditions were identical. Let us therefore make a comparison with the strip problem. The argument—one can hardly call it a justification—for doing this would run roughly as follows.

The mode of calculating strip stresses involves similar approximations in the first step to those involved in a grab calculation. Since the methods and postulates are similar, the consequent error will be of the same order of magnitude provided the number of boundary conditions satisfied in the two cases is the same. A solution with a greater number of boundary conditions satisfied should be more accurate than a solution with a lower number. The fact that the strip test calculations involve two different kinds of approximation, point force and polynomial, the errors of which are unlikely to cancel out, makes it probable that the accuracy of a grab calculation will be greater than that of a strip calculation with the same number of point forces. The accuracy estimates we have made above of 3% of the maximum stress at $0{\cdot}2$ and 10% at $0{\cdot}8$ (or, say, 8% at $0{\cdot}6$) refer to a strip problem with twelve boundary conditions satisfied, namely, (i) to (v) and $\sigma_y = \tau_{xy} = 0$ at L, M, N and $\sigma_y = 0$ at R. The seven-force grab problem satisfied conditions (i) to (vii) and also σ_x, σ_y, $\tau_{xy} \to 0$ as $x \to \infty$ and as $y \to \infty$. If we regard this as thirteen conditions we should expect the error of the seven-force *grab* problem to be something like or less than the error of the twelve-condition *strip* problem, i.e. of the order of 3% at $\nu = 0{\cdot}2$ to 8% at $0{\cdot}6$. These second estimates are close enough to the upper limits of the first, namely, 4 to 6½% to be accepted as a rough guide to the reliability of the calculated values of σ_x in the grab problem. The values of σ_x, τ_{xy} are again small enough to be ignored in first approximation for strength estimates.

5. CHECK BY RELAXATION

A final test of accuracy can be obtained by relaxing the problem. This was done for the single case $\nu = 0{\cdot}8$ for the grab problem. (This case was chosen because the values of P_0–P_6 are particularly large and erratic, and the point-force approximation seems therefore particularly liable to large errors.) As the boundary conditions essentially refer to displacements—the displacements of all points on the edges of the square jaws are equal—it is most convenient to use the equations of elasticity in the form:

$$\frac{1-\nu}{1+\nu}\nabla^2 u + \frac{\partial^2 u}{\partial x^2} + \frac{\partial^2 v}{\partial x \partial y} = 0 \tag{8}$$

$$\frac{1-\nu}{1+\nu}\nabla^2 v + \frac{\partial^2 v}{\partial y^2} + \frac{\partial^2 u}{\partial x \partial y} = 0 \tag{9}$$

where u and v are the components of displacement (see, for example, Allen*).

* ALLEN. *Relaxation Methods*, p. 125 (London: McGraw-Hill Ltd., 1954).

A good starting point for the relaxation calculation is given by the values of u, v calculated from our point-force approximation, so the labour of relaxation is not too formidable. However, the mixing of the two methods (point force and relaxation) has two demerits. First, the evaluation of u, v at all net points from the point forces, i.e. from algebraic expressions of the forms

$$-\frac{(1+\nu)}{2\pi E}\sum_i\left[\frac{3-\nu}{4}\log\frac{(x-x_i)^2+(y-y_i)^2}{x_i^2+(y-y_i)^2}+\right.$$
$$\left.+\frac{\frac{1}{2}(1+\nu)(y-y_i)^2}{(x-x_i)^2+(y-y_i)^2}-\frac{\frac{1}{2}(1+\nu)(y-y_i)^2}{x_i^2+(y-y_i)^2}\right]Pi \quad (10)$$

and

$$\frac{(1+\nu)^2}{4\pi E}\sum_j\left[\frac{(x-x_j)y_j}{(x-x_j)^2+y_j^2}+\right.$$
$$\left.+\frac{(x-x_j)(y-y_j)}{(x-x_j)^2+(y-y_j)^2}\right]P_j \quad (11)$$

is distinctly tedious using a desk calculating machine. Secondly, the relaxation solution in terms of displacements is far less convenient for the evaluation of stresses than the original point force solution, and any values derived for the stresses from the displacements will be of a lower order of reliability than that of the displacements themselves, since a process of numerical differentiation is involved.

For these reasons the mixed method does not entirely recommend itself as a general technique; it is introduced here purely for checking purposes. One may remark in passing that if a range of problems were being tackled, the use of an electronic machine—especially with an autocode programme—would reduce the labour of the point-force method, and of the calculation of u, v if required, to very modest proportions.

For the relaxation a square net was used of side equal to a quarter of a unit, i.e. a quarter of the linear dimensions of the square jaws, or one-twelfth of the distance between the jaws. In the immediate "frame" round the jaws large residuals are to be expected from the point-force solution values. Elsewhere the residuals differ from zero only because of effects due to the net size, i.e. due to neglect of fourth and higher order derivatives of u, v in the finite difference formulae. These false residuals enable a useful estimate to be made of the level of relaxation which is profitable with a given net size. For displacement d of each pair of jaws, i.e. for a separation of $2d$, the largest false residual at any point in front of the jaws ($x \leqslant 1$) was $0{\cdot}017d$; the largest behind the front edge of the jaws was $0{\cdot}65d$ but this could be directly attributed to a nearby point force. When large false residuals directly attributable to neighbouring point forces were disregarded, the greatest remaining false residuals were approximately $0{\cdot}1d$. This compares with residuals of up to $10{\cdot}5d$ in the "frame," see Table 5. With a quarter-unit net, it therefore seemed reasonable to pursue the process of relaxation until the residuals at points in front of or level with the front edge of the jaws were less than $0{\cdot}03d$, and those behind this level were less than $0{\cdot}2d$.

In this relaxation no changes were required in the u, v values at any of the points at which values of σ_x, σ_y were quoted in Table 3, i.e. for any of the points (0, 0)–(1, 1). Behind the jaws, of course, and particularly in the "frame," large changes were necessary, e.g. original values of $(-2{\cdot}48d, 3{\cdot}17d)$ at the point $(2\frac{1}{4}, \frac{1}{4})$ were replaced by $(0{\cdot}24d, 0{\cdot}75d)$: but it was precisely because this region was of no interest as far as the strength tests were concerned that the point forces were applied nearby.

Finally, a one-eighth unit net was considered in the region $x \leqslant 1\frac{1}{2}$ and the residuals were reduced to $<0{\cdot}01d$. This still left the (u, v) values at the points (0, 0)–(1, 1) almost undisturbed: only at the points (1, 0), (1, $\frac{1}{4}$) and (1, 1) were values altered, and of these the change at the first point (on the axis of symmetry) may well be due to a high fourth derivative and corresponding false residual. The necessary changes at the other two points were from $(0{\cdot}608, -0{\cdot}227)$ and $(0{\cdot}231, -0{\cdot}349)$ to $(0{\cdot}608\ -0{\cdot}242)$ and $(0{\cdot}228, -0{\cdot}341)$ respectively in units of d.

Table 5. *Residuals in the "frame" of points adjacent to the jaws using values of u, v obtained in the point-force approximation*

($\nu = 0{\cdot}8$: $\frac{1}{4}$ unit net: δu, δv in units of d)

Point x, y	δu	δv
$1\frac{1}{4}$, 0	−0·035	0
$1\frac{1}{4}$, $\frac{1}{4}$	−0·011	+0·026
$1\frac{1}{4}$, $\frac{1}{2}$	+0·049	−0·013
$1\frac{1}{4}$, $\frac{3}{4}$	+0·015	−0·007
$1\frac{1}{2}$, $\frac{3}{4}$	−0·014	+0·173
$1\frac{3}{4}$, $\frac{3}{4}$	−0·715	+0·671
2, $\frac{3}{4}$	−1·069	+2·212
$2\frac{1}{4}$, $\frac{3}{4}$	+4·177	−0·230
$2\frac{1}{2}$, $\frac{3}{4}$	+1·030	−10·522
$2\frac{3}{4}$, $\frac{3}{4}$	−3·948	−0·982
$2\frac{3}{4}$, $\frac{1}{2}$	+0·114	+1·260
$2\frac{3}{4}$, $\frac{1}{4}$	+4·499	−3·829
$2\frac{3}{4}$, 0	−0·950	0

At points nearer the jaws than the set (0, 0)–(1, 1) rather larger modifications were involved, e.g. the values at $(1\frac{1}{4}, 0)$, $(1\frac{1}{4}, \frac{1}{4})$, $(1\frac{1}{4}, \frac{1}{2})$, $(1\frac{1}{4}, 1)$, were changed from $(0{\cdot}920, 0)$, $(0{\cdot}885, -0{\cdot}077)$, $(0{\cdot}768, -0{\cdot}166)$, $(0{\cdot}258, -0{\cdot}318)$, to $(0{\cdot}906, 0)$, $(0{\cdot}877, -0{\cdot}077)$, $(0{\cdot}783, -0{\cdot}199)$, $(0{\cdot}237, -0{\cdot}287)$ respectively.

In view of these findings it is apparent that the greatest errors in the quoted values of σ_x, σ_y (Table 3) are to be expected at $x = 1$.

Prior to numerical differentiation, a smoothing operation was performed on each of the sets of collinear points to be used in the differentiations; the smoothing consisted of further relaxation at these points so that all the corresponding residuals were less than $0{\cdot}001d$. Numerical differentiations were then carried out on the differences between the point-force values and the smoothed relaxation values of u, v at (1, 0), (1, $\frac{1}{4}$), (1, $\frac{1}{2}$), (1, 1) so that the ϵ_x, ϵ_y and hence the σ_x, σ_y corrections could be deduced. By this means the errors in the point-force values of σ_x, σ_y were found to be $(0{\cdot}039, 0{\cdot}019)$, $(0{\cdot}072, 0{\cdot}116)$, $(-0{\cdot}026, -0{\cdot}016)$, $(0{\cdot}117, 0{\cdot}119)$ respectively. The greatest of these, $0{\cdot}119$, is $9{\cdot}7\%$ of the greatest stress value, $1{\cdot}231$. We conclude that the error estimate of 10% made in Section 4 is realistic, and there is no ground for supposing that the other error estimates are any less satisfactory.

ACKNOWLEDGEMENTS

We wish to express our thanks to Messrs. D. Newton and N. Warner of the Wool Industries Research Association for their valuable assistance in some of the numerical calculations.

The dielectric constant of zinc oxide over a range of frequencies

By N. H. LANGTON, Ph.D., A.M.Brit.I.R.E., A.Inst.P., and D. MATTHEWS, A.N.C.R.T., D.P.I., The National College of Rubber Technology, Northern Polytechnic, Holloway Road, London, N.7

[*Paper first received* 28 *March, and in final form* 19 *May*, 1958]

The dielectric constant of a colloidal zinc oxide has been measured by the method of mixtures, using cyclohexanol and ethyl acetate as the suspending liquids. The dielectric constant has been found to be 10·4 over the frequency range 105 kc/s to 10 Mc/s, falling to 9·4 at 25 Mc/s, measurements being made at 25° C with an accuracy of 2·3%. The dielectric constant of an acicular zinc oxide has been found to have an apparent value of about 40, over the frequency range 100 kc/s to 10 Mc/s. Results are given of dielectric constant measurements on mixtures of cyclohexanol and ethyl acetate, which appear to disobey Lichteneker's empirical logarithmic mixing rule.

INTRODUCTION

During an investigation into a proposed electrical method of measuring the degree of dispersion of zinc oxide particles in rubber, the value of the dielectric constant of zinc oxide over a range of frequencies from 100 kc/s or lower to 25 Mc/s was required. A few figures are available, but the values given vary widely from $K = 3 \cdot 5$[1] to $K = 36 \cdot 5$.[2] The frequency at which measurements were made is often not given. Some work has been done in Russia at a frequency of 3800 Mc/s,[3] but this is rather outside the scope of the present work.

Measurements at a frequency of 1 kc/s have been made by Mujamoto and his co-workers,[4] the value found for the dielectric constant of zinc oxide being 11·0, at a temperature of 15° C. No details are given in any of these references of the particle size or shape of the zinc oxides used.

Some measurements made by the authors on nominally identical mixes of zinc oxide and rubber show that different grades of zinc oxide give mixes of greatly differing dielectric constants, a mix containing an acicular zinc oxide having a higher dielectric constant than an otherwise identical mix made with a colloidal zinc oxide. This paper describes some experiments carried out to measure the dielectric constant of zinc oxide particles of known shape and size over the frequency range quoted above.

One of the main difficulties in measuring this property of zinc oxide is that it is almost impossible to obtain large crystals of the pure material. Crystals of cylindrical shape, about 1 in. in diameter by a few millimetres thick, were required for the capacitor used. Such blanks cannot be made directly, and compressing the powder is unsatisfactory because it is impossible to remove all the voids, and the presence of even a small quantity of air would lead to significant errors in the results. Zinc oxide occurs naturally in the massive crystalline form as the mineral zincite, but this is usually contaminated with traces of iron and other elements. For these reasons, the dielectric constant is measured by the method of mixtures.[5]

METHOD

The zinc oxide powder is suspended in an inactive liquid of known dielectric constant, and the dielectric constant of the resulting suspension is determined. By using a pair of mutually soluble inactive liquids, and altering the proportions of each, a range of dielectric constants can be covered. If a solution is obtained which shows no change of dielectric constant when zinc oxide is added, the dielectric constant of the liquid is the same as that of the zinc oxide.

APPARATUS

The test capacitor cell used for determining the dielectric constants of the liquids and suspensions was specially constructed to plug directly into the capacitor terminal sockets of a Marconi Q-meter, model 329E, thus eliminating errors due to the movement of flexible leads. It consisted of a cylindrical brass tube, silver plated inside and bonded with Araldite resin to a piece of $\frac{1}{4}$ in. Tufnol sheet. In the centre of this was mounted the second electrode, a piece of silver plated brass rod, this being bonded with Araldite to the Tufnol. Leads, of 13 gauge brass wire, were taken from each electrode to a pair of plugs at the side of the base spaced to plug directly into the Q-meter (see Fig. 1).

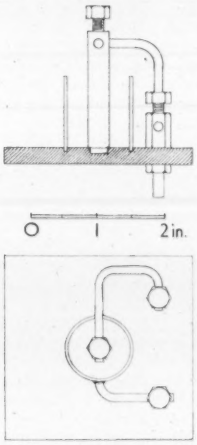

Fig. 1. Test capacitor cell

Before use, the effective capacity of the empty cell was found by using two liquids of known dielectric constant: benzene, of "Analytical Reagent" quality, supplied by British Drug Houses Ltd., and a specially purified sample of carbon tetrachloride. The sample of benzene was dried for a week over fused calcium chloride before use, whilst the carbon tetrachloride was a dry sample. Calibration measurements on the cell were made at a temperature of 25° C. The dielectric constant of benzene has been determined by Hartshorn and his co-workers,[6] using a number of different specimens. A sample of benzene from the same source as that used in these experiments has a dielectric constant of 2·2890 at a temperature of 20° C with a temperature coefficient of $-0 \cdot 0020^{\circ} C^{-1}$, in the "as received" condition.

After redistillation and drying for a week the dielectric constant has a value of 2·2850 at a temperature of 20° C and a temperature coefficient of $-0{\cdot}00185\ ^\circ C^{-1}$. Accordingly a value of 2·276 was taken for the dielectric constant of benzene at a temperature of 25° C, the possible error being of the order of 0·2%.

The dielectric constant of carbon tetrachloride at 25° C is 2·17.[7] All these values remain constant over the required frequency range. A number of measurements were made to calibrate the cell, which was found to have an effective capacity of 1·33 pF, the accuracy of measurement being ±2·3%.

EXPERIMENTAL

As the approximate value of the dielectric constant of the zinc oxide was not known, a range of liquids was selected and their dielectric constants were found at a frequency of 1 Mc/s and at 25° C. By this means a dielectric constant range from approximately 2 to 40 was covered. Many organic liquids of high dielectric constant, for example alcohols and ketones, were found to be unsuitable as their electrical conductivities were too great. Eventually it was found that the dielectric constant of the colloidal zinc oxide lay between those of cyclohexanol and ethyl acetate. These two liquids were found to be mutually soluble in all proportions, and to have no chemical action on the zinc oxide, which was satisfactorily wetted by them.

Six different mixtures of cyclohexanol and ethyl acetate were made up containing from 0 to 100% by volume of ethyl acetate in steps of 20%. After mixing they were stored in well stoppered bottles. As a check on the composition of the mixtures the refractive indices were measured using an Abbé refractometer, and a graph plotted of refractive index against the percentage of one component, giving a smooth curve. Any wrongly made solution was thus easily discovered, and by measuring the refractive indices of the liquids at various times during the experimental work and comparing the values obtained with the originals, any evaporation of the components could be detected.

The samples of zinc oxide were very carefully dried before use to remove moisture, the presence of which could otherwise cause large errors in the measured dielectric constant values. Each sample was spread over a piece of clean paper, the depth of the layer not exceeding $\frac{1}{16}$ in., and dried in an electric oven for at least 12 h at 120° C. The samples were then transferred to dry jars and left open in a dessicator to cool before use.

25 ml. portions of the solutions were taken and mixed with 4 g of the dried zinc oxide by shaking in the special irradiation tube. The mixture after being roughly dispersed was subjected to ultrasonic irradiation at a frequency of 1 Mc/s for 1 h to remove occluded air and to aid dispersion. The ultrasonic power in the tube was measured calorimetrically and found to be 5 W, the method of irradiation and apparatus being the same as that used by Langton and Vaughan,[8] when measuring the ultrasonic degradation of polystyrene. After irradiation, the zinc oxide mixtures were transferred to tightly stoppered storage bottles until required.

Control experiments were carried out to determine whether the dielectric constants of the ethyl acetate and cyclohexanol were affected by the ultrasonic irradiation, but no effect could be found after irradiation for 1 h.

Throughout these experiments a colloidal grade of zinc oxide, supplied by Amalgamated Oxides (1939) Ltd., was used. This particular sample was stated by the makers to have a particle size of 0·085 μ,[9] measured by an air permeability method. Very few acicular particles are present as can be seen from the electron micrograph (Fig. 2).

An attempt was made to measure the dielectric constant of an acicular zinc oxide of particle size 0·845 μ supplied by the same company, but the dielectric constant of this was found to be greater than that of the cyclohexanol over the whole frequency range. An experiment was carried out using a sample of nitrobenzene, the dielectric constant of which was found to be 37·1. On adding zinc oxide a small rise in dielectric constant was noted, measurements being made at frequencies of 100 kc/s, 1 Mc/s and 10 Mc/s, suggesting a value of about 40 for the apparent dielectric constant of the acicular zinc oxide. An electron micrograph showing the crystal form of the acicular zinc oxide is shown in Fig. 3.

Fig. 2. Colloidal zinc oxide

Fig. 3. Acicular zinc oxide

Since no suitable liquid of sufficiently high dielectric constant was available, it was not possible to use the method of mixtures to determine the dielectric constant of the acicular oxide with greater accuracy.

The ethyl acetate used throughout the experiments was of "Analytical Reagent" quality, and the cyclohexanol of "Laboratory Reagent" quality, supplied by the General Chemical and Pharmaceutical Company Ltd. Both were used in the "as received" condition, without any drying or

other treatment. The purity of the cyclohexanol was checked by infra-red methods, but no impurity could be discovered. It will be noted, however, that since the dielectric constant of the zinc oxide is found by a null method, the presence of impurities in the liquids, providing they do not give rise to chemical reactions, would not affect the accuracy of the measurements.

After preparation, samples of the liquids and zinc oxide suspensions were placed in tightly corked test tubes and left in a thermostat at 25° C. The test cell was conditioned before each measurement by being placed in a deep empty beaker held in the thermostat bath for at least 15 min. The dielectric constant measurements on each sample were completed within 30 s of its being removed from the thermostat, during which time only a negligible fall of temperature took place. For each reading the cell was very carefully filled to the brim to minimize errors caused by changes in the height of the electrolyte.

RESULTS

The dielectric constant for each liquid mixture was noted, together with that of the corresponding zinc oxide suspension at each different frequency, measurements being made at 11 different frequencies over the range 50 kc/s to 25 Mc/s. For each frequency a graph was drawn of the dielectric constants K of the liquid mixtures, against the difference in dielectric constant δK on adding zinc oxide. As an example, Fig. 4 gives the results obtained at a frequency of 800 kc/s. The point at which the curve crosses the axis $\delta K = 0$ gives the dielectric constant of the zinc oxide, in this case 10·4.

In addition, results were obtained for the dielectric constants of cyclohexanol and ethyl acetate over the frequency range, and these, with the values found for colloidal zinc oxide, are shown graphically in Fig. 5. It will be noted that no results are given for the zinc oxide below a frequency of 105 kc/s as the Q-meter was insufficiently sensitive at this frequency to give a reliable figure. The dielectric constant of zinc oxide is shown to have a value of 10·4 over the frequency range 0·1 Mc/s to about 10 Mc/s. As the frequency rises above this value the dielectric constant falls off, having a value of 9·4 at 25 Mc/s, all dielectric constant values having an accuracy of $\pm 2{\cdot}3\%$. In comparison, the acicular type of zinc oxide appears to have a dielectric constant of the order of 40 over the frequency range 0·1 to 10 Mc/s.

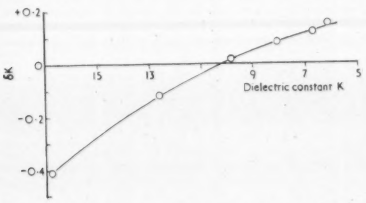

Fig. 4. Curve showing method of determining K

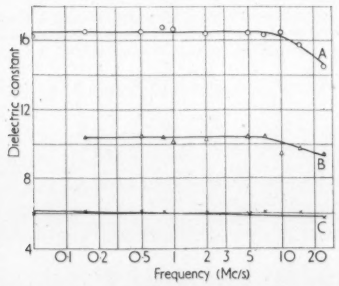

Fig. 5. Variation of dielectric constant with frequency
A, cyclohexanol; *B*, colloidal zinc oxide; *C*, ethyl acetate.

The dielectric constant of the cyclohexanol used in the experiments is shown to have a value of 16·5 over the frequency range 50 kc/s to 8 Mc/s, the value falling as the frequency is increased to 25 Mc/s. The dielectric constant of the ethyl acetate falls steadily with increasing frequency from a value of 6·12 at 50 kc/s to 5·78 at 25 Mc/s.

Published data gives the dielectric constant of ethyl acetate as 6·4 at 20° C and at 10 kc/s,[10] that of cyclohexanol being 15·0 at 25° C and at 10 kc/s.[10,11]

DISCUSSION

The dielectric constants of the colloidal and acicular types of zinc oxide differ greatly. Although that of the acicular type is not known accurately, it seems to have a value about four times that of the colloidal oxide. Both samples of the oxide were very carefully dried before use, under similar conditions, suggesting that the change in dielectric constant is due to some difference between the oxides themselves. The authors have noted that the loss tangent of rubber mixes loaded with acicular zinc oxide is greater than that of colloidal zinc oxide mixes.

The difference between the dielectric constant values found here for the two types of zinc oxide may be due to the differences in the particle shape. There are, however, other factors which may have caused this difference. Zinc oxide is known to be a non-stoichiometric substance, with an unstable oxygen content. It also has semi-conducting properties which are not constant. The high dielectric constant value for the acicular zinc oxide may be due to a conductivity effect. It seems possible that the different values for the dielectric constant of zinc oxide found by previous workers were due to the use of different, unspecified types of zinc oxide.

Application of Lichteneker's equation to mixtures of ethyl acetate, and cyclohexanol. The dielectric constants of mixtures of varying proportions of these two liquids have been measured at a temperature of 25° C. In calculating the dielectric constant of a mixed dielectric, Lichteneker's empirical logarithmic mixing rule[12] is often employed. Thus,

$$\log K = p_1 \log K_1 + p_2 \log K_2 + \ldots + p_n \log K_n$$

where K is the dielectric constant of the final mixture, $K_1, K_2, \ldots K_n$ are the dielectric constants of the 1st, 2nd . . . nth components, $p_1, p_2, \ldots p_n$ are the proportions by volume of these components, such that $p_1 + p_2 + \ldots + p_n = 1$.

This rule is put forward for uniform dispersions of the components. It was assumed that a good dispersion of ethyl acetate and cyclohexanol could be obtained since the two liquids were perfectly miscible, and as a matter of interest, a check was made between the values expected from Lichteneker's rule, and the experimental results, assuming the dielectric constants of the pure liquids. The results of this comparison are shown in Fig. 6, from which it can be

seen that the two liquids do not appear to conform to Lichteneker's rule.

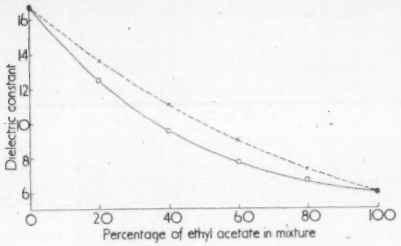

Fig. 6. The application of Lichteneker's equation to mixtures of cyclohexanol and ethyl acetate

× - - - × - - - × Lichteneker's relation.
○——○——○ experimental results.

ACKNOWLEDGEMENTS

One of the authors (D. Matthews) is indebted to Amalgamated Oxides (1939) Ltd. for a Research Fellowship enabling him to carry out this work at the National College of Rubber Technology.

REFERENCES

(1) WILDSCHUT, A. J. *India Rubber J.*, **92**, No. 18A, p. 19 (1936).
(2) GLEMSER, O. *Z. Electrochem.*, **45**, p. 865 (1939).
(3) SUS, A. N. *C.R. Acad. Sci. U.R.S.S.*, **33**, p. 210 (1940).
(4) MUJAMOTO, OKITA and KITAOKA. *Summitomo Elect. Rev.*, **26**, p. 1 (1942).
(5) WHITEHEAD and HACKETT. *Proc. Phys. Soc.* [*London*], **51**, p. 173 (1939).
(6) HARTSHORN, L., and co-workers. *Proc. Phys. Soc.* [*London*] *B*, **68**, p. 422 (1955).
(7) VON HIPPEL, A. *Dielectric Materials and Applications*, p. 362 (New York: John Wiley and Sons Inc., 1954).
(8) LANGTON, N. H., and VAUGHAN, P. *Brit. J. Appl. Phys.*, **8**, p. 289 (1957).
(9) Amalgamated Oxides (1939) Ltd. Private Communication.
(10) *Handbook of Chemistry and Physics*, 34th Ed., p. 2162 (Ohio: Chemical Rubber Publishing Co., 1952).
(11) *American Institute of Physics Handbook*, **5**, p. 137 (New York: McGraw-Hill Book Co. Inc., 1957).
(12) LICHTENEKER, K. *Physik. Z.*, **27**, p. 115 (1926).

The radial flow of heat in an infinite cylinder

By T. P. NEWCOMB, M.Sc., A.Inst.P., Ferodo Ltd., Chapel-en-le-Frith, Stockport, Cheshire

[*Paper received* 16 *June*, 1958]

A solution is given to the problem of heat conduction in a solid cylinder of infinite length, the surface of which is subjected to a thermal flux which decreases linearly with time. This solution may be used to determine the transient temperatures occurring at the interface or at any point within two concentric cylinders which are in contact, one of which is rotating relative to the other. The solution is of importance as it permits calculation of the temperatures reached in the lining and drum of a band brake during a brake application. Typical curves illustrating the agreement between transient temperatures determined theoretically and experimentally at the surface of the cylinder are given.

A type of brake used extensively in the industrial field is the band brake which consists essentially of a strip of friction material fastened to a thin flexible metal backing member. This strip is then "wrapped round" the periphery of the body, the motion of which requires to be retarded. Provided the brake lining material is of sufficient width, the flow of heat produced during a brake application can be considered to be radial, with the boundary conditions of a thermal flux $Q(1 - at)$ at the surface of contact and a finite temperature at the axis of the cylinder. The term $Q(1 - at)$ where Q and a are constants and t is time (in seconds), assumes that the deceleration during a single brake application is uniform.

The method of analysis used is based on the Laplace transformation and enables the temperature distribution in a band brake to be determined. Extending this analysis to the case of a cylinder of large radius reduces the solution to that of the flow of heat through an infinite slab in which one face is subjected to a thermal flux which decreases linearly with time.[1]

THE EQUATIONS AND THEIR FORMAL SOLUTION

Consider the radial flow of heat in a circular cylinder $0 \leqslant r \leqslant d$ infinite in length which is initially at zero temperature and such that there is a thermal flux $Q(1 - at)$ at the cylinder surface of radius $r = d$. The temperature of the cylinder is finite at the axis $r = 0$. If v, K and k denote the temperature, thermal conductivity and diffusivity respectively, we require the solution of the partial differential equation

$$\frac{\partial^2 v}{\partial r^2} + \frac{1}{r}\frac{\partial v}{\partial r} - \frac{1}{k}\frac{\partial v}{\partial t} = 0 \qquad 0 \leqslant r < d \qquad t > 0 \qquad (1)$$

subject to the boundary conditions

$$v = 0 \text{ when } t = 0 \qquad 0 < r < d \qquad (2)$$

$$K(\partial v/\partial r) = Q(1 - at) \text{ for } r = d,\ t > 0 \qquad (3)$$

and v is to remain finite as $r \to 0$ for $t > 0$.

Introducing the Laplace transform defined as

$$\bar{v} = \int_0^\infty \exp(-pt)v(r, t)dt$$

the differential equation to be solved reduces to

$$\frac{d^2\bar{v}}{dr^2} + \frac{1}{r}\frac{d\bar{v}}{dr} - \frac{p\bar{v}}{k} = 0 \qquad 0 \leqslant r < d \qquad (4)$$

subject to the conditions

$$\frac{d\bar{v}}{dr} = \frac{Q}{K}\left(\frac{1}{p} - \frac{a}{p^2}\right) \quad \text{at } r = d \tag{5}$$

$$\text{and } \bar{v} \text{ is finite as } r \to 0 \tag{6}$$

The solution of equations (4), (5) and (6) is

$$\bar{v} = \frac{Q}{K}\left(1 - \frac{a}{p}\right)\frac{k^{1/2}I_0(rq)}{p^{3/2}I_1(dq)} \quad \text{where } q = \left(\frac{p}{k}\right)^{1/2} \tag{7}$$

and I_0 and I_1 are the modified Bessel functions of the first kind of order zero and unity respectively.

Applying the inversion theorem for the Laplace transformation[2] to equation (7), one obtains

$$v = \frac{Q}{Kd}\left\{2kt + \frac{r^2}{2} - \frac{d^2}{4} - a\left[kt^2 + \frac{t}{2}\left(r^2 - \frac{d^2}{2}\right) + \frac{r^4}{16k} - \frac{r^2d^2}{16k} + \frac{d^4}{48k}\right]\right\} - \frac{2Q}{dK}\sum_{s=1}^{\infty}\exp(-k\alpha_s^2 t)\frac{J_0(r\alpha_s)}{\alpha_s^2 J_0(d\alpha_s)} - \frac{2a}{Kkd}Q\sum_{s=1}^{\infty}\exp(-k\alpha_s^2 t) \times \frac{J_0(r\alpha_s)}{\alpha_s^4 J_0(d\alpha_s)} \tag{8}$$

where the $\alpha_s (s = 1, 2, 3 \ldots)$ are the positive roots of

$$J_1(d\alpha) = 0 \tag{9}$$

where $J_1(d\alpha)$ is the Bessel function of the first kind of order unity. The first few roots are given in Carslaw and Jaeger,[2] Appendix IV, Table 3.

This solution converges slowly for small values of kt/d^2 and is of little value as a basis for calculations of the transient temperatures in brake linings where kt/d^2 is generally less than 0·02. When this is the case and when r/d is not small a solution may be obtained by substituting the asymptotic expansion of the Bessel functions in equation (7) and expanding as a series in $1/p$.

Applying this process the first few terms are given by

$$\bar{v} = \frac{Q}{K}\left(1 - \frac{a}{p}\right) \times \exp\left[-q(d-r)\right]\left[\frac{d^{1/2}k^{1/2}}{r^{1/2}p^{3/2}} + \frac{k}{8p^2r^{1/2}d^{1/2}}\left(3 + \frac{a}{r}\right) + \frac{k^{3/2}}{128d^{3/2}r^{1/2}p^{5/2}}\left(33 + \frac{6d}{r} + \frac{9d^2}{r^2}\right) + \ldots\right] \tag{10}$$

Thus, using Appendix V of Carslaw and Jaeger (Ref. 2, p. 380) to evaluate each term of the transform, we have

$$v = \frac{Q}{K}\left(\frac{kt}{r}\right)^{1/2}\left\{2i\,\mathrm{erfc}\left[\frac{d-r}{2(kt)^{1/2}}\right] + \frac{1}{2}\frac{k^{1/2}t^{1/2}}{dr}(a+3r)i^2\,\mathrm{erfc}\left[\frac{d-r}{2(kt)^{1/2}}\right] + \left[\frac{kt}{16d^2r^2}(33r^2 + 6dr + 9d^2) - 8at\right]i^3\mathrm{erfc}\left[\frac{d-r}{2(kt)^{1/2}}\right] \tag{11}$$

where $i^n \mathrm{erfc}\, x = \int_x^{\infty} i^{n-1}\,\mathrm{erfc}\, y\,dy \quad n = 1, 2, 3 \ldots$

with $i^0 \mathrm{erfc}\, x = \mathrm{erfc}\, x = \frac{2}{\pi^{1/2}}\int_x^{\infty}\exp(-y^2)dy$

The function $i^n \mathrm{erfc}\, x$ for various values of n and x has been considered by Hartree,[3] the results being given in tabular form (see also Carslaw and Jaeger, Ref. 2, p. 373).

In practice, the important temperature is that attained at the surface of the cylinder where $r = d$ and with this substitution, equation (11) reduces to

$$v = \frac{Q}{K}(kt)^{1/2}\left[\frac{2}{\pi^{1/2}}\left(1 - \frac{2at}{3}\right) + \frac{k^{1/2}t^{1/2}}{2d} + \frac{kt}{2\pi^{1/2}d^2}\right] \tag{12}$$

Thus, if Q, K, k, a, d are known for the contacting body considered, provided that $kt/d^2 < 0{\cdot}02$, the temperature at a given radial position at any instant during a brake application may be determined from equation (11).

APPLICATION OF THEORY

If a band brake slides against a cast iron cylinder from an initial surface speed u cm/s and produces a constant linear deceleration of f cm/s^2, then after t seconds of braking the instantaneous speed is $(u - ft)$ cm/s. Hence the instantaneous energy H generated at the friction surface is

$$H = \frac{Fu}{A_2 J}\left(1 - \frac{ft}{u}\right) = Q(1 - at) \tag{13}$$

where A_2 = area of brake lining (cm^2)
F = total frictional force acting at the interface of drum and lining (dyn.)
J = mechanical equivalent of heat, taken as $4{\cdot}18 \times 10^7$ erg/cal
$Q = Fu/A_2J$
$a = f/u$

Using suffixes 1 and 2 for drum and lining respectively the heat dissipated into each solid is

$$H_1 = Q_1(1 - at) \quad \text{and} \quad H_2 = Q_2(1 - at) \tag{14}$$

where $H_1 + H_2 = H$

The values Q_1 and Q_2 may be determined by the condition of equal temperatures at the common surface of drum and lining. To a first approximation this is given by the first term of equation (12)

$$\frac{v_1K_1}{2Q_1(k_1t)^{1/2}} = \frac{1}{\pi^{1/2}}\left(1 - \frac{2}{3}at\right) = \frac{v_2K_2}{2Q_2(k_2t)^{1/2}} \tag{15}$$

where v_1, v_2 are the temperatures of cylinder and lining respectively, relative to the ambient temperature, during one application of the brake, from which

$$\frac{Q_2}{Q_1} = \frac{K_2(k_1)^{1/2}}{K_1(k_2)^{1/2}} = \frac{H_2}{H_1} \tag{16}$$

In a typical band brake $K_1 = 1{\cdot}2 \times 10^{-1}$ cal cm^{-1} s^{-1} °C^{-1}, $k_1 = 1{\cdot}2 \times 10^{-1}$ cm^2/s, $K_2 = 1{\cdot}9 \times 10^{-3}$ cal cm^{-1} s^{-1} °C^{-1}, $k_2 = 3{\cdot}8 \times 10^{-3}$ cm^2/s giving a value for Q_2/Q_1 of 1/11·19, i.e. approximately 9% of the total heat generated by friction enters the lining. Hence, from a knowledge of H and the thermal properties of the contacting bodies, Q_1 and Q_2 may be evaluated. Finally, from equation (11) provided that $kt/d^2 < 0{\cdot}02$ the temperature at any radial position in the drum or lining may be calculated.

Experimental verification of equation (11) has been obtained by measuring the transient temperature at a position extremely close to the contacting surface of a band brake during single uniform brake applications. The method of measurement was to insert a fine gauge copper-constantan thermocouple inside the lining and feed its output during

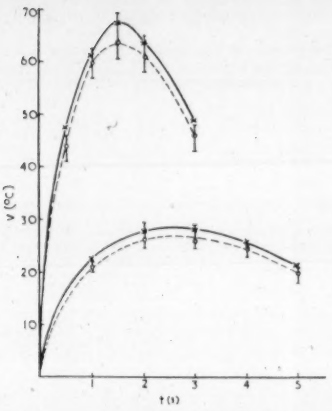

A typical curve of transient temperature near the surface of a band brake during a brake application

× = calculated values; ○ = mean experimental values; the range of values is also shown.

braking to an amplifier and then to an Evershed and Vignoles recorder, the overall system having a response time of approximately 10^{-1} s. The rotating cylinder of diameter 3·75 cm had an initial linear surface speed of 1273 cm/s and was braked to rest in 3 s or in 5 s, the corresponding values of Q_2 were 2·169 cal/s and $7{\cdot}23 \times 10^{-1}$ cal/s.

The agreement between temperatures determined experimentally (broken line) and theoretically from equation (11) (full line) at various times during a single uniform braking application are illustrated graphically in the figure. These curves agree to within 10%.

ACKNOWLEDGEMENTS

The author wishes to thank Dr. R. T. Spurr, Mr. A. Jenkins and Mr. A. D. M. Frood of the Research Division of Ferodo Ltd. for assistance and criticism, and the directors of Ferodo Ltd. for permission to publish this paper.

REFERENCES

(1) NEWCOMB, T. P. *Brit. J. Appl. Phys.* To be published.
(2) CARSLAW, H. S., and JAEGER, J. C. *Conduction of heat in solids*, 1st Ed., p. 244 (Oxford: Clarendon Press, 1947).
(3) HARTREE, D. R. *Mem. Manchester Lit. Phil. Soc.*, **80**, p. 85 (1935).

The temperature dependence of noise temperature ratio in germanium diodes

By A. HENDRY, B.Sc., National Research Council, Ottawa, Canada

[*Paper first received* 21 *April, and in final form* 29 *May*, 1958]

Measurements of the 30 Mc/s noise temperature ratio of a d.c. biased germanium mixer diode at various mixer temperatures are reported. The noise temperature ratio is observed to increase as the temperature is lowered, indicating the presence of noise which is substantially in excess of thermal and shot noise, and which increases in magnitude as the temperature is lowered.

A semiconductor diode exhibits noise at its terminals which is composed of three types, which are:

(i) thermal noise in the spreading resistance of the diode;
(ii) shot noise due to thermal excitation of current carriers over the barrier; and
(iii) excess noise, characterized by a (frequency) dependence, which is believed to be due to modulation of the barrier height.

Of these various types of noise, the first two are proportional in magnitude to the absolute temperature of the device.

It has been predicted[1] that the noise temperature ratio of germanium mixer diodes can be lowered by mixer cooling; however, the anticipated improvements in noise temperature ratio due to cooling have not been observed,[2] indicating the presence of appreciable noise in excess of any thermal or shot noise in the diode.

There is some evidence that excess noise varies inversely with temperature. Miller,[3] for example, states that the magnitude of the noise power from a silicon diode is the same at liquid air temperature as at room temperature, which indicates that not all the noise from the diode can be shot or thermal noise (both of which are proportional to temperature). Furthermore, there must be an increase in the excess noise to offset the decrease in shot and thermal noise which occurs as the temperature is lowered.

The work reported in this paper was undertaken to determine the magnitude and variation of the noise temperature ratio of a type 1N263 germanium point contact diode with crystal temperature and d.c. bias current. The noise temperature ratio of the crystal is defined as

$$t = N/kT_0B \qquad (1)$$

where N = available noise power output from the crystal in bandwidth B; $T_0 = 290°$ K, the standard reference temperature; and k = Boltzman's constant.

From the observed variations of t, the variation of excess noise with temperature and current will be inferred.

APPARATUS AND EXPERIMENTAL TECHNIQUES

Fig. 1 is a block diagram of the test set-up used. The method used for the determination of t is largely that of Torrey and Whitmer.[4] The output meter was calibrated in terms of noise temperature ratio t, by the use of resistance cartridges in place of the crystal. By making a resistance cartridge noisy using the diode noise generator, the noise temperature ratio (n.t.r.) of the resistor becomes

$$t = 1 + (eIR/2kT_0) \qquad (2)$$

where R = resistance of cartridge and I = diode current.

Thus the output meter may be calibrated in terms of t by

varying I, for values of t greater than unity. The output meter was calibrated for t less than unity by physically cooling the resistance cartridge to a temperature T. The n.t.r. of such a resistor is then T/T_0, if it is assumed that the resistor

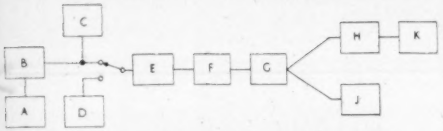

Fig. 1. Block diagram of test set-up

A, bias supply; *B*, crystal holder; *C*, noise diode; *D*, standard resistor; *E*, Roberts coupling circuit; *F*, 30 Mc/s pre-amplifier; *G*, 30 Mc/s intermediate frequency amplifier; *H*, detector; *J*, 30 Mc/s barretter bridge; *K*, output meter.

itself has no excess noise. This assumption may be checked by making the cooled resistor noisy as before, until its n.t.r. is again unity. The current required to reach unity n.t.r. may then be compared with the theoretical value:

$$I_D = \frac{2kT_0}{eR}\left(1 - \frac{T}{T_0}\right) \qquad (3)$$

The agreement between measured and calculated values of the diode currents is a measure of the validity of the assumption that the resistor generates only thermal noise. In the calibration made for the work reported here, calculated and observed values of I_D agreed to within a few per cent.

In order that the calibration of the output meter in terms of n.t.r. would be approximately independent of the intermediate frequency (i.f.) resistance of the crystal over the range 100 to 200 Ω, a Roberts coupling circuit (Ref. 4, p. 223) was used between the crystal and the pre-amplifier. This restriction on the allowable i.f. resistance of the crystal made it necessary to provide means for the determination of $R_{i.f.}$. This measurement was made by the method outlined by Torrey and Whitmer. A bolometer bridge was used to measure the change in output power of the i.f. amplifier which occurs during this measurement, thus obviating the necessity for a correction due to detector non-linearity. (The i.f. amplifier, however, must still be operated in a linear region.)

The diode under test was mounted in a crystal mount which could be lowered into a flask containing liquid nitrogen. Temperatures were determined by measurement of the e.m.f. of a thermocouple which had one junction attached to the crystal mount. By suitable positioning of the mount relative to the liquid nitrogen level, any temperature between room temperature and 77° K could be obtained. Rapid changes in temperature were avoided to minimize the danger of permanently damaging the crystal, and for each determination of t, sufficient time was allowed for the crystal to reach thermal equilibrium with the mount.

To reduce errors due to drifts in the gain, the i.f. amplifier was connected to a standard resistor, the temperature of which was T_0, and the gain adjusted to give an output corresponding to $t = 1{\cdot}00$, before each determination of t.

Checks of receiver noise factor, crystal conversion loss and noise temperature ratio before and after temperature cycling, indicated that no damage occurred to the crystal.

EXPERIMENTAL RESULTS

Measurements of the n.t.r. of the crystal were made at bias currents of 0·1, 0·15, 0·2 and 0·3 mA, at several temperatures in the range 77 to 300° K. The results of these measurements are given in Fig. 2.

These curves indicate a striking increase in noise temperature ratio as the temperature is lowered. Thus the noise power output of the crystal does not have the linear dependence on absolute temperature that has been suggested. Because of the observed temperature dependence, a large fraction of the noise power available from the crystal must be in excess of any shot or thermal noise. It is also evident from the curves that t varies approximately linearly with I over the range plotted.

On the basis of simple diode theory[5] shot noise in the barrier is such that the noise temperature ratio tends to a

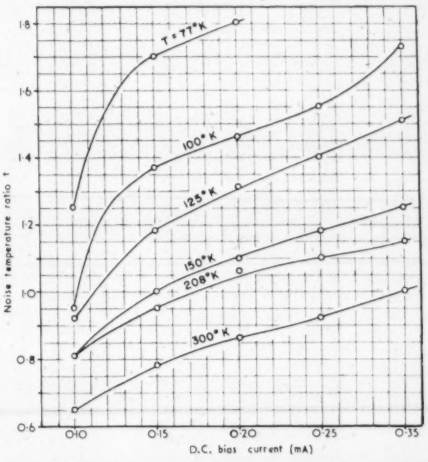

Fig. 2. Noise temperature ratio *versus* bias current for type 1N263 germanium mixer

half for large forward biases (large being much greater than $kT/e = 1/40$ V at room temperature). This limit is, of course, dependent on absolute temperature. Thus in an attempt to separate the excess noise from shot noise, one may subtract $\frac{1}{2}(T/T_0)$ from the observed values of n.t.r. to obtain

$$t' = t - \tfrac{1}{2}\frac{T}{T_0} \qquad (4)$$

where t' is a measure of the excess noise from the diode. Thermal noise in the spreading resistance is assumed to contribute little to the total noise because of the small value of R_s in this diode.

Fig. 3 is a plot of $\log t'$ *versus* $\log T$, from which it may be seen that t' has an approximate dependence of T^{-2} in the region of 300° K, and T^{-1} over the range 77 to 200° K.

Excess noise in semiconductor diodes, which is believed to be due to modulation of the barrier height[5,6] in a fluctuating manner has been assumed to have the following pattern:

$$\overline{(\Delta I)^2} = \left(\frac{eI}{kT}\right)^2 \overline{(\Delta\phi)^2} \qquad (5)$$

where I = mean current through the diode, e = electronic

charge, k = Boltzman's constant, T = absolute temperature (° K), and ϕ = barrier height (V).

The causes of barrier height fluctuation are as yet not clear. On the basis of this simple model, the modulation noise current should be proportional to $(I/T)^2$, if $\overline{(\Delta\phi)^2}$ is independent of I and T. Hence i' should be proportional to I/T^2.

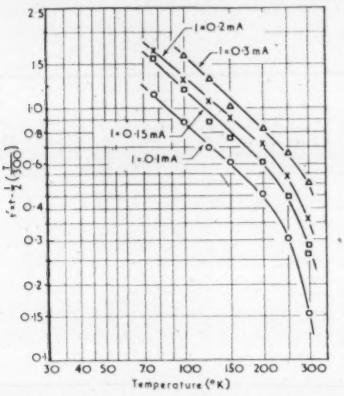

Fig. 3. Variation of crystal excess noise with temperature

It appears, therefore, that a different model is necessary to explain the observed deviations from a T^{-2} dependency at low temperatures. The model satisfactorily explains the linear current dependency observed, which is in contrast to the commonly reported I^2 dependency for current noise. A similar dependence has been reported for excess noise in iron oxide flakes.(7)

CONCLUSIONS

It has been shown experimentally that the noise temperature ratio of a 1N263 germanium diode under positive d.c. bias varies widely in the region 77 to 300° K. On the basis of an approximate division of the observed noise into shot and excess noise, the temperature dependence of excess noise between these temperatures has been established. The excess noise has been observed to vary approximately as the first power of I, and as T^{-2} in the region of 300° K, and as T^{-1} from 77 to 200° K.

REFERENCES

(1) MESSENGER, G. C. *I.R.E. Trans*, MTT-**5**, pp. 62–3 (1957).

(2) ANDERSON, L. K., and HENDRY, A. *An Investigation of the Properties of X-Band Germanium Mixer Crystals at Low Temperatures*. To be published in *I.R.E. Trans.*

(3) MILLER, P. H. *Proc. Inst. Radio Engrs*, **35**, p. 252 (1947).

(4) TORREY, H. C., and WHITMER, C. A. *Crystal Rectifiers*, pp. 226–32 (New York: McGraw-Hill Book Co. Inc., 1948).

(5) NICOLL, G. R. *Proc. Instn Elect. Engrs* (3), **101**, pp. 317–24 (1954).

(6) BURGESS, R. E. *Brit. J. Appl. Phys.*, **6**, pp. 185–90 (1955).

(7) BROPHY, J. J. *J. Appl. Phys.*, **25** (2), p. 222 (1954).

Journal of Scientific Instruments

Contents of the November issue

ORIGINAL CONTRIBUTIONS

Papers

Soft X-ray spectroscopy using an electron multiplier. By J. A. Catterall, L. F. Wilson and J. Trotter.

A method of maintaining temperature control over a wide range. By H. L. Allsopp and D. F. Gibbs.

A cryostat for reactor irradiations in liquid nitrogen. By M. W. Thompson and D. W. Jefferson-Loveday.

A variable radio-frequency inductance for the Birmingham proton synchrotron. By P. H. Rose.

A differential thermal analysis apparatus. By F. W. Wilburn.

The effect of variations in ambient temperature upon the optical alinement of an X-ray fluorescence spectrometer. By T. A. Davies.

X-ray spectrographs for rapid X-ray fluorescence analysis with photographic recording. By E. F. Priestley.

A two co-ordinate light pointer and its application to a recording interferometer. By H. G. Kuhn and H. J. Lucas-Tooth.

A rotational viscometer employing a reference liquid. By J. F. Hills.

A method of correcting for the response time delays of measuring equipment. By J. A. Sirs.

Laboratory and workshop notes

The use of argon at atmospheric pressure as Geiger counting gas in a windowless counter. By S. Lovell.

Metallic contacts to germanium and silicon. By L. W. Davies and D. K. Milne.

The mounting of fibres and organic crystals for spectroscopy in the near infra-red region. By B. R. Malcolm.

Two capacitance transducer circuits. By K. E. Machin.

A simple apparatus for electrolytic polishing of metallographic specimens. By F. Brossa and C. Sari.

A modification to the Cambridge rocking microtome to facilitate the cutting of thin sections for electron microscopy. By E. H. Mercer.

A modified X-ray powder camera. By A. Franks.

An apparatus, capable of being heated, for high vacuum grinding of solids. By E. Baronetzky.

The construction of small vacuum leaks of constant value. By R. O. Jenkins.

NOTES AND NEWS

Correspondence

A modified mass spectrometer ion source for the study of solid samples. From G. A. Heath, and R. M. Hobson.

New books

New instruments, materials and tools

BINDING ORDERS

Orders and enquiries about the binding of back-numbers of the *Journal of Scientific Instruments* and of the *British Journal of Applied Physics* should now be sent direct to Messrs. E. A. Weeks and Son, 168 Gower Street, London, N.W.1 (EUSton 4674), and *not* to The Institute of Physics. This new arrangement does not involve any change in price.

THIS JOURNAL is produced monthly by The Institute of Physics, in London.

It deals with all branches of applied physics (including theory and technique). All rights reserved. Responsibility for the statements contained herein attaches only to the writers.

EDITORIAL MATTER. Communications concerning editorial matter should be addressed to the Editor, The Institute of Physics, 47 Belgrave Square, London, S.W.1. (*Telephone:* Belgravia 6111.) Prospective authors are invited to prepare their scripts in accordance with the *Notes on the preparation of contributions*. (Price 2*s.* 6*d.* including postage.)

REPRODUCTION. The Institute of Physics is a signatory to The Royal Society's Fair Copying Declaration. Details may be obtained upon application from The Royal Society, London, W.1.

ADVERTISEMENTS. Communications concerning advertisements should be addressed to the agents, Messrs. Walter Judd Ltd., 47 Gresham Street, London, E.C.2. (*Telephone:* Monarch 7644.)

CLAIMS FOR MISSING JOURNALS. Claims from regular subscribers to this *Journal* for missing numbers will only be considered if received within 60 days of the date of mailing plus normal outward time of transit and time for lodging the claim. Losses attributable to failure to notify a change of address or to similar omissions will not be considered.

SUBSCRIPTION RATES. A new volume commences each January. The charge is £5 per volume ($14.25 U.S.A.), including index (post paid), payable in advance. Single parts, so far as available, may be purchased at 10*s.* each ($1.50 U.S.A.), post paid, cash with order. Orders should be sent to The Institute of Physics, 47 Belgrave Square, London, S.W.1, or to any bookseller.

The choice of resilient materials for anti-vibration mountings

By J. C. SNOWDON, B.Sc., Ph.D., D.I.C.,* Physics Department, Imperial College of Science and Technology, London

This article attempts to determine, solely from the aspect of vibration reduction, the criteria which define a good anti-vibration mount material. It concludes firstly that such a material should possess a high damping factor which does not increase greatly with frequency, and secondly, that it should be free from any major increase in dynamic modulus with frequency.

Results of transmissibility measurements on a variety of resilient materials indicate that high damping synthetic rubbers normally possess a dynamic modulus which increases rapidly with frequency. It is shown that this modulus increase is responsible for the poor isolation afforded by these rubbers at frequencies above the resonant frequency of the mounting system, and not their inherent high damping as commonly supposed.

Filled butyl rubber is an exception, affording an isolation at high frequencies not greatly inferior to that of natural rubber, yet at the same time possessing much higher damping.

1. REPRESENTATION OF THE MECHANICAL PROPERTIES OF A VISCOELASTIC MATERIAL

The relation existing between small values of stress and strain in a linear viscoelastic medium can be most generally represented by a linear partial differential equation of arbitrary order. This equation becomes algebraic when both stress and strain vary sinusoidally with time, because the operator

$$\partial^n/\partial t^n = (j\omega)^n \qquad (1)$$

where t is time, ω is angular frequency, and $j = (-1)^{1/2}$. The ratio of stress to strain in a viscoelastic material can therefore be expressed as a complex quantity,[1] and the mechanical properties of the material represented not by a real, but by a complex "elastic" modulus, possessing real and imaginary parts that are both, in general, functions of frequency. The damping factor of the material is defined as the ratio of the imaginary to the real part of the modulus, and is analogous to the reciprocal of the magnification Q which is employed in electrical circuit theory to describe the ratio of an inductive reactance to a resistance.

2. THE GENERAL TRANSMISSIBILITY EQUATION

Fig. 1(*a*) diagrammatically shows an item of mass M resiliently mounted on an infinitely massive foundation, and sinusoidally vibrating at an angular frequency ω. The item is said to be simply mounted, and the item plus mounting

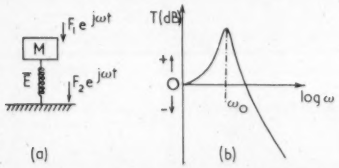

Fig. 1. Diagrammatic representation of the simple mounting system

is known as the simple mounting system.[2] Let the resilient isolator possess a complex modulus $\bar{E}$, with a real part E' and an imaginary part E''. Transmissibility T is defined as that fraction of the force exciting the mounted item which is transmitted to the foundation, and is given by the relation:

$$T^2 = \left|\frac{F_2}{F_1}\right|^2 = (1+\delta^2)\Big/\left[\left(1-\frac{\omega^2 M}{kE'}\right)^2 + \delta^2\right] \qquad (2)$$

where the damping factor $\delta = E''/E'$. The quantity k is a constant determined solely by the mount geometry, for example, when the mount possesses uniform cross-section, k is equal to the ratio of the cross-sectional area to the mount thickness.

In practice, the quantities E' and δ are not constant, but functions of frequency. Thus, suppose that the real part of the modulus $E' = E_\omega$, and the damping factor $\delta = \delta_\omega$ at an angular frequency ω, and suppose that the resonance of the mounting system occurs at an angular frequency ω_0 (Fig. 1*b*), when $E' = E_0$, such that $\omega_0^2 = kE_0/M$. (Transmissibility is presented here on a decibel scale; thus, a force ratio equal to T appears on a decibel scale as $20\log_{10}(T)$ decibels.) It then follows that the quantity

$$\frac{\omega^2 M}{kE'} = \frac{\omega^2}{\omega_0^2}\cdot\frac{E_0}{E_\omega} \qquad (3)$$

so that if the frequency ratio ω/ω_0 is equal to x, equation (2) becomes:

$$T^2 = \frac{(1+\delta_\omega^2)}{[1-x^2(E_0/E_\omega)]^2 + \delta_\omega^2} \qquad (4)$$

From this equation the transmissibility of any linear rubber-like material can be derived when the variation with frequency of the dynamic modulus (namely, that of the real part of the complex modulus) and damping factor possessed by the material are inserted.

3. CHOICE OF ISOLATING MATERIAL

The transmissibility of an anti-vibration mounting should be small at all frequencies which it is required to isolate, and the resilient mount material should therefore be chosen to provide:

(i) a low natural mounting frequency ω_0;

(ii) a low transmissibility at resonance; and

(iii) a rapid decrease of the transmitted force with increase in frequency above ω_0.

A low natural frequency can be obtained by employing a mount of suitably low stiffness (or by increasing the mass of

* Now at The University of Michigan Research Institute, Ann Arbor, Michigan, U.S.A.

the mounted item). The use of a high damping mount material ensures that the resonant transmissibility is small and, in addition, when the vibrating item is resiliently mounted on a non-rigid foundation, it is valuable in suppressing the natural modes of vibration of the foundation.[2] The decrease in the transmitted force at frequencies above ω_0 varies considerably with the rubber-like material employed in the mounting. The comparative behaviour of different resilient materials is discussed in later sections.

4. APPLICATION OF THE GENERAL TRANSMISSIBILITY EQUATION

4.1 *Damping of the solid type.* A number of materials, including natural rubber, are found in practice to possess a damping factor which is largely independent of frequency. The real and imaginary parts of the complex elastic moduli possessed by these materials, E' and E'' respectively, must therefore be approximately constant, or show a similar frequency dependence. Such materials are said to possess solid-type damping.

The mechanical behaviour of a linear viscoelastic material subject to sinusoidal variations of stress and strain can be represented by a parallel spring and dashpot which will, in general, possess both frequency-dependent modulus of elasticity (E), and viscosity coefficient (η) (Fig. 2). For sinusoidal

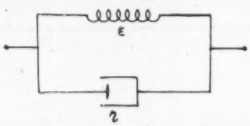

Fig. 2. Representation of linear viscoelastic material

excitation the complex ratio of stress to strain in such an element is equal to $E + j\omega\eta$. The real part of the complex modulus (E') possessed by the material is therefore represented by E, and the damping factor (E''/E') by $\omega\eta/E$.

It is sometimes possible to describe approximately the behaviour of a rubber-like material by assuming either (i) that E' and E'' are constant, or (ii) that E' and E'' are both directly proportional to frequency.

(i) *Both E' and E'' constant.* Namely, E constant and δ constant (hence, η inversely proportional to frequency). Equation (4) becomes:

$$T^2 = \frac{1 + \delta^2}{(1 - x^2)^2 + \delta^2} \tag{5}$$

At frequencies well above the natural mounting frequency, T is therefore inversely proportional to the square of the frequency, that is, T decreases at 12 dB/octave. The transmissibility of a resilient isolator possessing constant modulus and damping factor is shown as a function of frequency in Figs. 3 and 4. The damping factor is assigned values 0·1 and 1, which respectively typify the damping possessed by natural and some high damping rubbers.

(ii) *Both E' and E'' proportional to frequency.* Namely, E proportional to frequency, and δ constant (hence, η constant). Equation (4) becomes:

$$T^2 = \frac{1 + \delta^2}{(1 - x)^2 + \delta^2} \tag{6}$$

since $E_0/E_\omega = \omega_0/\omega$.

Therefore, at frequencies well above the natural frequency, T is now inversely proportional to frequency, that is, T decreases at 6 dB/octave. The transmissibility of an isolator possessing a constant damping factor, and an elastic modulus directly proportional to frequency is shown as a function of frequency in Figs. 3 and 4. The damping factor is again assigned the values 0·1 and 1.

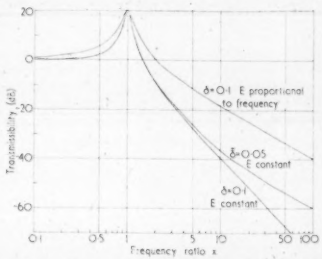

Fig. 3. The transmissibility of a parallel spring-dashpot element in the simple mounting system. Damping factor $\delta = 0{\cdot}1$

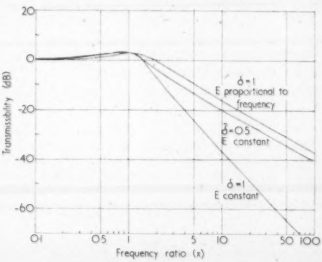

Fig. 4. The transmissibility of a parallel spring-dashpot element in the simple mounting system. Damping factor $\delta = 1{\cdot}0$

4.2 *Damping of the viscous type.* This is the type of damping most commonly discussed in literature concerned with vibration isolation. The elastic modulus E and the viscosity coefficient η are considered constant, so that the damping factor δ is directly proportional to frequency.

In the case of viscous damping it is found convenient to define a damping ratio $\bar{\delta}$ which is characteristic of the mounting system as a whole. The damping ratio is defined as the ratio of the viscosity coefficient actually possessed by the isolator and that required to damp the system critically. It can be shown[3] that $\bar{\delta} = \omega_0\eta/2E$. The damping factor, which previously has been shown equal to $\omega\eta/E$, can therefore be replaced by the quantity $2(\omega/\omega_0)\bar{\delta}$. Equation (4) then becomes:

$$T^2 = \frac{1 + (2x\bar{\delta})^2}{(1 - x^2)^2 + (2x\bar{\delta})^2} \tag{7}$$

Since E and η are considered independent of frequency, the damping ratio $\bar{\delta}$ will be constant. At frequencies well above the natural frequency T is therefore inversely proportional to frequency, that is, T decreases at 6 dB/octave. Since the

increase in high frequency isolation is now less rapid than when the mount possessed solid-type damping (with constant modulus E), it may be concluded (Section 3) that a vibration isolator should preferably possess damping of the latter type. The transmissibility of an isolator assumed to possess constant elastic modulus and viscosity coefficient is shown as a function of frequency in Figs. 3 and 4. The damping ratio is assigned the values 0·05 and 0·5.

4.3 *The relaxation of rubber-like materials.* Fig. 5 shows the variation of the dynamic modulus and damping factor exhibited by the synthetic rubber G.R.-S. at room temperature.[4] The frequency at which the damping factor

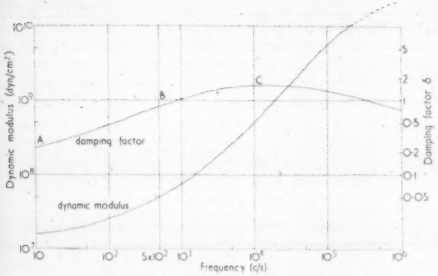

[Reproduced from *Journal of Applied Physics*]

Fig. 5. The damping factor and dynamic modulus of G.R.-S. rubber at 20° C. (Due to Ivey, Mrowca, and Guth)

possesses a maximum value is known here as the transition frequency; a rapid increase in modulus with frequency occurs in this region. The frequency variation of the dynamic modulus and damping factor in any viscoelastic material are of an essentially similar nature to the curves shown in Fig. 5.

At room temperature the transition frequency of natural and other low damping rubbers occurs at very high frequencies, so that over the frequency range normally of interest in vibration isolation (namely, well below the transition frequency) the damping factor is small, and, in fact, both the damping factor and the dynamic modulus may be considered sensibly independent of frequency. [Section 4.1, example (i).]

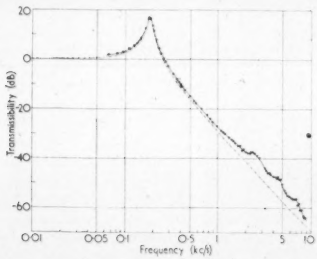

Fig. 6. The transmissibility of natural rubber in the simple mounting system. Temperature 19° C. Mounts contain forty parts channel black in one hundred parts natural rubber. Broken curve calculated assuming constant damping factor δ and modulus E

Fig. 6 shows the experimentally determined transmissibility of a natural rubber specimen in the simple mounting system. The specimen contains forty parts channel black in one hundred parts natural rubber, and is $\frac{1}{2}$ in. long and $\frac{7}{8}$ in. in diameter. These results are compared with the theoretical transmissibility (broken curve) calculated from equation (5). Values of the equation parameters are chosen so that the theoretical transmissibility coincides with the experimental curve at the observed resonant frequency. "Wave effects" are observed at high frequencies[5] when the mount length is equal to, or greater than, a half-wavelength of the elastic wave passing through the mounting.

In general, the transition frequency of synthetic high-damping rubber-like materials is much lower than for natural rubber or G.R.-S., occurring at frequencies which are normally of interest at room temperature. The damping factor is therefore large over a range of frequencies within which the natural mounting frequency will occur, and may be considered approximately constant, while the dynamic modulus is approximately proportional to frequency. [Section 4.1, example (ii).] Fig. 7 shows the experimentally determined

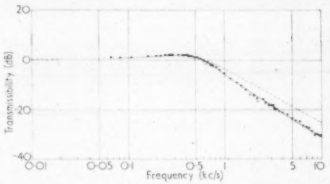

Fig. 7. The transmissibility of Hycar 1001 in the simple mounting system. Temperature 16·5° C. Broken curve calculated assuming constant damping factor δ and frequency proportional modulus E

transmissibility of Hycar 1001 (a butadiene acrylonitrile copolymer) in the simple mounting system, for a specimen $\frac{5}{8}$ in. long and $\frac{3}{4}$ in. in diameter. These results are compared with the theoretical transmissibility (broken curve) calculated from equation (6). Values of the equation parameters are again chosen so that the theoretical and experimental curves coincide at the observed resonant frequency.

4.4 *Substitution in the general transmissibility equation of the dynamic modulus and damping factor possessed by a rubber-like material.* The frequency dependence of the elastic modulus and the damping factor possessed by rubber-like materials is typified by that of G.R.-S. rubber shown in Fig. 5. The curves of this figure are used here to determine how the vibration isolation provided by high damping rubbers is related to the frequency variation of their mechanical properties. Thus, the form of the isolation afforded by relatively low, high, and very high damping rubbers is apparent when the frequencies A, B and C (Fig. 5) are taken as unity on a relative frequency scale, and the resonant frequency of a vibrating item mounted on each "material" made to coincide with the corresponding unit frequency. The quantity E_0 (Section 2) is equated to the value of the dynamic modulus at the frequencies A, B and C, the corresponding values of the damping factor being 0·23, 0·82 and 1·60. The transmissibility of the three mounting systems can be calculated from the general equation:

$$T^2 = \frac{1 + \delta_{E_0}^2}{[1 - x^2(E_0/E_\omega)]^2 + \delta_{E_0}^2}$$

The calculated transmissibility is presented in Fig. 8. Curves *a*, *b* and *c* correspond to the resonance of the mounted item at *A*, *B* and *C*.

The general transmissibility equation shows that at very high frequencies the transmissibility is sensibly proportional to $(1/x^2)(E_\omega/E_0)$, provided that the variation of the damping factor with frequency is not large. Any increase in modulus E_ω with frequency implies that the high frequency transmissibility ceases to decrease as the square of the frequency, that is, at 12 dB/octave. Since for natural and low damping rubbers, E_ω does not increase with frequency to any great extent, the high frequency loss in isolation, or the departure from 12 dB/octave fall-off, is not large. (Fig. 6; Fig. 8, curve *a*.) For high damping rubbers, however, the increase in E_ω with frequency, and the resulting departure from 12 dB/octave fall off, is appreciable (Fig. 7; Fig. 8, curve *c*).

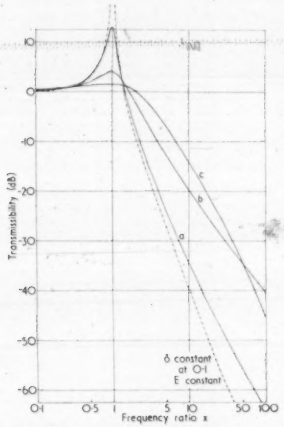

Fig. 8. Calculated transmissibility curves for a rubber-like material. Curve (*a*) derived from the low damping region of the G.R.-S. relaxation curve, curve (*b*) intermediate damping, and curve (*c*) high damping region

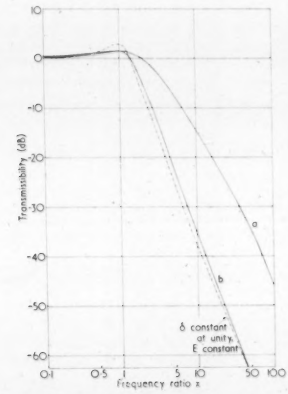

Fig. 9. Showing how the rapid increase in modulus about the transition frequency is responsible for the loss in high frequency isolation. Curve (*a*) is identical with curve (*c*) of Fig. 8, curve (*b*) is derived from curve (*c*) assuming that the dynamic modulus is independent of frequency

High damping rubbers may therefore be undesirable mount materials because their elastic modulus increases greatly with frequency, and not because of their inherent high damping as commonly supposed. Fig. 9 illustrates how closely the loss in high frequency isolation is related to the rapid increase in modulus at frequencies near to the transition frequency. Curve *a* is identical with curve *c* of Fig. 8; curve *b* is derived from curve *c* of Fig. 8 assuming that the modulus is frequency-independent, but with the variation of the damping factor with frequency unaltered. It is seen that virtually the entire departure from 12 dB/octave fall-off is due to the frequency dependence of the dynamic modulus.

4.5 *Criteria defining a good resilient vibration isolator.* It can be concluded from Fig. 9 that a good anti-vibration mount material (Section 3) should:

(i) possess a large damping factor—to provide a low resonant transmissibility;

(ii) be free from any major increase in dynamic modulus or damping factor with frequency—to ensure a rapid decrease of transmissibility with increase in frequency above resonance.

5. THE COMPOUND MOUNTING SYSTEM

5.1 *Introduction.* It has been shown that the high frequency isolation afforded by the simple mounting system (Fig. 10*a*) increases as the square of the frequency, providing that the damping factor and elastic modulus of the mounting are constant. Fig. 6 shows that the transmissibility calculated for such conditions is in reasonable agreement with the experimentally determined transmissibility of natural rubber.

Isolation superior to that of the simple system can be obtained above a certain frequency by introducing a secondary

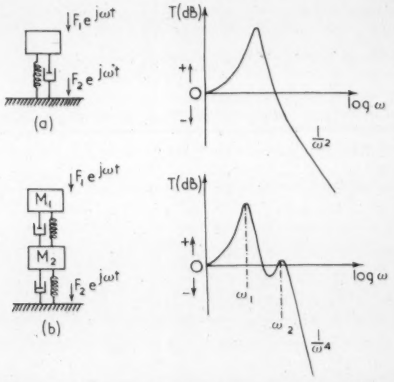

Fig. 10. Diagrammatic representation of the simple and compound mounting systems

mass into the resilient mounting, as M_2 in Fig. 10(*b*), to form what is known as the compound mounting system.[2] The form of the transmissibility possessed by the compound system is shown as a function of frequency in Fig. 10(*b*). This system possesses a secondary as well as a primary resonance, but above the secondary resonant frequency ω_2, the isolation increases as the fourth power of the frequency, that is, at 24 dB/octave.

5.2 *Properties and applications of the compound mounting system.* The mass ratio β is defined as the ratio of the secondary and principal masses M_2/M_1 (Fig. 10*b*). For a given mass ratio, optimum conditions are realized when the frequency separation of the primary and secondary resonances is least. This occurs when the ratio θ of the lower to the upper mount stiffness is equal to $(1 + \beta)$, providing that the mount damping factors are negligible. Under these conditions the ratio of the secondary and primary resonant frequencies, namely, ω_2/ω_1 (Fig. 10*b*) is given by the relation:

$$\frac{\omega_2^2}{\omega_1^2} = \frac{(1+\beta) + (1+\beta)^{1/2}}{(1+\beta) - (1+\beta)^{1/2}} \qquad (8)$$

Providing that the mass ratio is small and the mount damping factors remain negligible, optimum conditions are practically realized when the mount stiffness ratio is equal to unity. For example:

	β	0·1	0·2	0·5	1·0
$\theta = (1 + \beta)$	ω_2/ω_1	6·48	4·69	3·15	2·41
$\theta = 1$	ω_2/ω_1	6·49	4·71	3·23	2·62

At frequencies above the secondary resonance, the compound system affords greater isolation than the simple system, the difference in isolation increasing at 12 dB/octave. The compound system can, therefore, be advantageously employed when especially good isolation is required. The secondary resonance is an undesirable feature of this system, but it can be suppressed by suitably high mount damping, in common with the primary resonance.

The compound system is of especial value in mitigating the isolation loss always occurring at the natural frequencies possessed by non-rigid foundations.[2] For example, the resonant modes of vibration excited in the structural girders supporting a vibrating machine, or the resonance of a rigid machine foundation with the "elastic" sub-soil (plus its associated "mass") beneath it.[6] The isolation loss at the natural frequencies of such relatively undamped foundations is normally considerable.[2, 6]

6. RESULTS OF TRANSMISSIBILITY MEASUREMENTS ON RUBBER-LIKE MATERIALS IN THE SIMPLE AND COMPOUND MOUNTING SYSTEMS

(*a*) *The simple mounting system*

6.1 *The transmissibility of natural rubber.* Results of transmissibility measurements on natural rubber at 19° C have been previously presented in Fig. 6, for a specimen containing forty parts channel black in one hundred parts natural rubber.

The damping factor of the rubber at the resonant frequency is equal to 0·14. The close correspondence of the experimental and theoretical transmissibility curves below the first standing wave frequency indicates (Section 4) that the increase in elastic modulus of the rubber with frequency is not large.

It has been shown[5] that the first standing wave resonance occurs when the mount length is equal to a half wavelength of the elastic wave passing through the mounting, and that other wave resonances occur at integral multiples of this frequency. Inspection of Fig. 6 shows that if the first resonant wave frequency is taken as 2·3 kc/s, then the second and third wave resonances do occur at, or in the immediate neighbourhood of 4·6 and 6·9 kc/s.

6.2 *The transmissibility of Hycar* 1001. Results of transmissibility measurements on Hycar 1001 at 16·5° C have previously been presented in Fig. 7.

Hycar 1001 possesses a large damping factor of the order unity, which together with the dynamic modulus is very sensitive to variations in temperature. The transmissibility at resonance is heavily suppressed by this high damping. At frequencies above resonance, the isolation afforded by the Hycar increases at 8 dB/octave only, indicating (Section 4) that the increase in modulus with frequency is appreciable.

6.3 *The transmissibility of Heveaplus M–G.* Heveaplus M–G[7] is a rubber free from conventional fillers such as carbon black, which derives its reinforcement from polymethyl methacrylate. It is prepared by polymerizing polymethyl methacrylate in rubber latex to give a graft polymer in which the rubber molecules have attached side chains of methyl methacrylate.

Under low amplitude vibration Heveaplus M–G possesses a much lower dynamic modulus and damping factor than a black-reinforced compound with similar static properties.

The transmissibility of Heveaplus M–G at 21·5° C is shown in Fig. 11. The specimen contains five per cent methyl methacrylate in the total polymer. It is $\frac{7}{16}$ in. long and $\frac{3}{8}$ in. in diameter. The transmissibility curve reflects the low damping characteristics of the polymer, namely, a relatively sharp resonance (damping factor $\delta = 0{\cdot}08$ at the resonant frequency), a rapid decrease in transmissibility with frequency above resonance, and pronounced wave effects at high frequencies. The standing wave resonances appear to be less regular in nature than those of the natural rubber specimen previously discussed. The first wave resonance is clearly defined, and occurs at 2·66 kc/s. There is no evidence of equally well defined wave resonances at 5·32 and 7·98 kc/s, although a broad maximum does exist in the region of 5·5 kc/s.

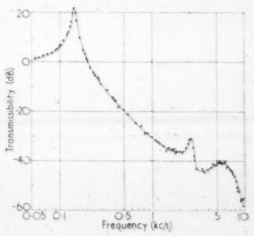

Fig. 11. The transmissibility of Heveaplus M–G in the simple mounting system. Temperature 21·5° C

6.4 *The transmissibility of castor oil urethane.* Castor oil urethanes are produced by cross-linking castor oil with a di-isocyanate, and are characterized by their flexibility and high damping factor.[8]

The transmissibility of castor oil urethane at 22° C is shown in Fig. 12. The specimen contains forty parts di-isocyanate in one hundred parts castor oil. It is $\frac{3}{8}$ in. long and $\frac{13}{16}$ in. in diameter.

The damping factor at the resonant frequency is equal to 0·89. Above resonance the isolation afforded by the castor oil urethane increases with frequency at 10 dB/octave, more

**

rapidly than normally found for a material (for example, Hycar 1001) with such a high damping factor.

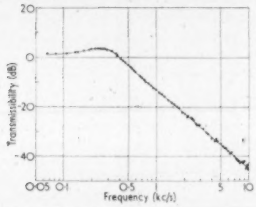

Fig. 12. The transmissibility of castor oil urethane in the simple mounting system. Temperature 22° C. Mounts contain forty parts di-isocyanate in one hundred parts castor oil

6.5 *The transmissibility of irradiated polythene.* High polymers are essentially composed of chains of large numbers of monomeric units; the main chain may not always be linear, and branched side chains may be present. Exposure to nuclear irradiation either degrades the main or side chains, or produces cross-links between them.[9, 10]

Polythene is readily cross-linked, primary bonds forming between adjacent carbon atoms. The degree of cross-linking is dependent on the radiation dose. At room temperature polythene is largely crystalline and, although cross-linking occurs when polythene is irradiated, the crystallinity it possesses is destroyed. Cross-linking increases the elastic modulus of the polymer, but the decrease in crystallinity is reflected as a decrease in modulus.

The reduction in modulus at room temperature as the radiation dose is increased from zero to eight units is due to the decrease in crystallinity outweighing the effect of the cross-linking produced by the irradiation. (One radiation unit is defined as an integrated flux of 10^{17} slow neutrons per square centimetre, plus associated fast neutrons and γ-rays.) Above eight units the modulus increases as the degree of cross-linking increases still further, and the material becomes more rigid and eventually brittle and glass-like.

The damping factor of polythene exhibits a maximum, and the elastic modulus a minimum value, after approximately eight units of irradiation. Both the damping factor and the modulus are extremely temperature and frequency-sensitive for this dosage, and at room temperature the polythene exhibits typically rubber-like behaviour.

The transmissibility of irradiated polythene at 18° C is shown in Fig. 13. The specimens are $\frac{3}{8}$ in. long and $\frac{1}{4}$ in.

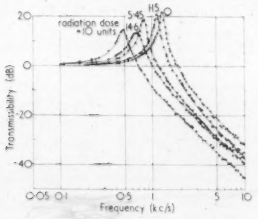

Fig. 13. The transmissibility of neutron irradiated polythene in the simple mounting system. Temperature 18° C

in diameter. The nature of the transmissibility curves at resonance reflects the behaviour of the modulus and damping factor possessed by irradiated polythene described above. At first sight it would be expected that the resonant transmissibility of polythene at 14·6 units of irradiation would be greater than at ten units. That this is not so may probably be ascribed to the increase of the damping factor with frequency being greater than the reduction of the damping factor that occurs as the polythene moves further towards the brittle or glass-like state.

(*b*) *The compound mounting system*

6.6 *The transmissibility of natural rubber.* Results of transmissibility measurements on natural rubber specimens in the compound system at 19° C are presented in Fig. 14, together with the transmissibility of an identical specimen

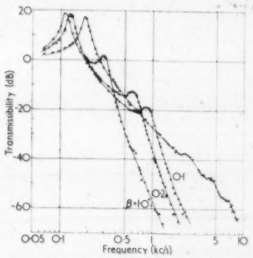

Fig. 14. The transmissibility of natural rubber in the simple and compound mounting systems. Temperature 19° C. Mounts contain forty parts channel black in one hundred parts natural rubber

in the simple system, shown previously in Fig. 6. The test specimens contain forty parts channel black in one hundred parts natural rubber.

The transmissibility curves for the compound mounting systems with mass ratios $\beta = 0{\cdot}1$, $0{\cdot}2$, $1{\cdot}0$ are in good agreement with their theoretical form (Section 5). The ratios of the secondary and primary resonant frequencies ω_2/ω_1, agree with the values which were calculated (equation 8) on the assumption that the mount damping was very small. Thus:

	β	$0{\cdot}1$	$0{\cdot}2$	$1{\cdot}0$
ω_2/ω_1	Calculated	2·62	4·71	6·49
	Measured	2·66	4·69	6·62

At frequencies above the secondary resonance, the isolation provided by the compound system becomes rapidly superior to that of the simple system, and Fig. 14 indicates the considerable increase in isolation afforded by the former at high frequencies.

6.7 *The transmissibility of Hycar* 1001. Results of transmissibility measurements on Hycar specimens in the simple and compound mounting systems at 17° C are presented in Fig. 15. The mounts are $\frac{3}{8}$ in. long and $\frac{1}{4}$ in. in diameter.

The primary and secondary resonances of the compound system are heavily suppressed by the high damping possessed by the Hycar rubber. Above the secondary resonant frequency the isolation afforded by Hycar 1001 increases at 16 dB-octave only, as might be expected from consideration of the simple system, where the high frequency isolation increases at 8 dB/octave. In addition, the secondary resonant frequency is displaced towards higher frequencies, namely,

the ratio of the secondary and primary resonant frequencies is significantly larger than for natural rubber (Fig. 14). The increase in the dynamic modulus of the mounting with frequency is primarily responsible for this behaviour (Section 4).

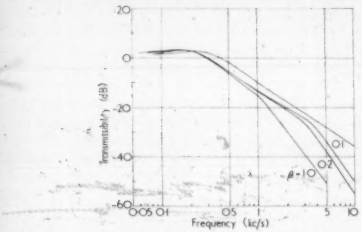

Fig. 15. The transmissibility of Hycar 1001 in the simple and compound mounting systems. Temperature 17° C. (Experimental points omitted to ensure clarity of figure)

At frequencies above the primary resonance, the isolation provided by Hycar 1001 in the compound system is never inferior to that of the simple system, but the overall increase in isolation afforded by the compound systems employing small secondary masses is very poor.

6.8 *The transmissibility of butyl rubber.* The transmissibility of butyl rubber in the simple and compound mounting systems at 18° C is shown in Fig. 16. The specimens are $\frac{1}{2}$ in. long and $\frac{7}{8}$ in. in diameter, and contain fifty parts furnace black in one hundred parts butyl rubber. This proportion of carbon black ensures that a good bond is obtained between the rubber and the metal end pieces of the mounting.

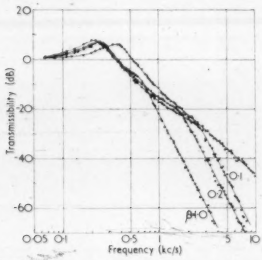

Fig. 16. The transmissibility of butyl rubber in the simple and compound mounting systems. Temperature 18° C. Mounts contain fifty parts furnace black in one hundred parts butyl rubber

The damping factor of the butyl rubber is equal to 0·58 at a frequency of 360 c/s. Although the resonances occurring in the simple and compound systems are well suppressed by this high damping, the displacement of the secondary resonance of the compound system towards higher frequencies is appreciably less than when Hycar mounts are employed. The isolation afforded by the simple system above its resonant frequency increases at approximately 10·5 dB/octave, while above the secondary resonance of the compound system, the isolation increases at 22 dB/octave.

Both the relatively small departure made by the rates of high frequency increase in isolation from 12 and 24 dB/octave, and the frequency displacement of the secondary resonance, indicate that the elastic modulus of butyl rubber does not increase greatly with frequency. This is remarkable considering that at the same time the rubber possesses a high damping factor.

7. CONCLUSIONS

7.1 A good anti-vibration mount material should: (i) possess a large damping factor, and (ii) be free from any major increase in dynamic modulus or damping factor with frequency. Thus:

(i) a high mount damping factor provides a low transmissibility at the resonant frequencies of the simple and compound mounting systems, and reduces the loss in isolation occurring at the resonant modes of vibration possessed by non-rigid foundations;

(ii) if the dynamic modulus of the mount material does not increase greatly with frequency, the anti-vibration mounting provides an isolation at high frequencies which rapidly increases with frequency.

7.2 Figs. 17, 18, 19 and 20 show previously presented results of transmissibility measurements on natural rubber, the copolymer Hycar 1001, and butyl rubber, redrawn on a relative frequency scale.

It is seen from these figures that natural and butyl rubbers most closely satisfy the above criteria (Section 7.1), although:

(i) the damping factor of natural rubber is not sufficiently high to suppress resonant transmissibility greatly;

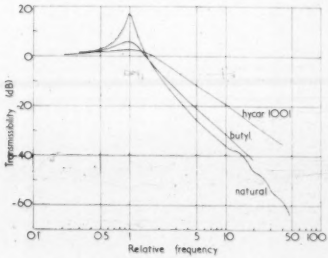

Fig. 17. The transmissibility of natural, Hycar, and butyl rubbers in the simple mounting system

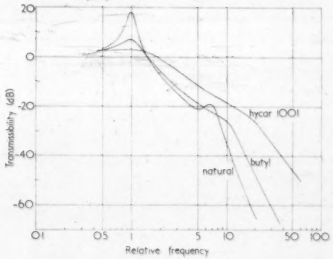

Fig. 18. The transmissibility of natural, Hycar, and butyl rubbers in the compound mounting system. Mass ratio $\beta = 0{\cdot}1$

(ii) the dynamic modulus of butyl rubber does increase somewhat with frequency.

The inferior high frequency isolation associated with Hycar 1001 makes its use as a mount material undesirable.

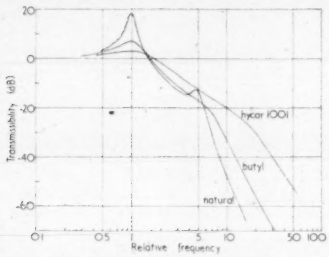

Fig. 19. The transmissibility of natural, Hycar, and butyl rubbers in the compound mounting system. Mass ratio $\beta = 0{\cdot}2$

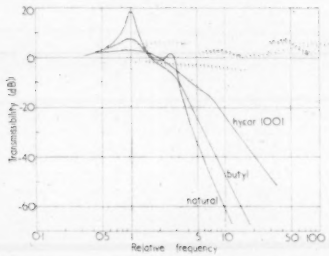

Fig. 20. The transmissibility of natural, Hycar, and butyl rubbers in the compound mounting system. Mass ratio $\beta = 1{\cdot}0$

7.3 The high frequency isolation provided by castor oil urethane is good, considering the high damping that it possesses, but inferior to that of butyl rubber. Judged by the above criteria, Heveaplus M–G and ordinary polythene are undesirable mount materials because of their relatively low damping. Irradiated polythene in the "rubber-like" state possesses higher damping, but the rate of increase of high frequency isolation is not superior to that of butyl rubber, and the transmissibility at resonance is much greater.

7.4 It can be concluded from the results of transmissibility measurements on the above variety of resilient materials that, solely from the aspect of vibration reduction, butyl rubber:

(i) is superior to any of the synthetic materials examined;

(ii) may well compete with natural rubber, because although it exhibits inferior high frequency isolation, this difference:

(*a*) is not excessive and, in fact, is greatest at frequencies where appreciable isolation already exists;

(*b*) may be more than compensated by the lower resonant transmissibility in the simple and compound systems, and the much greater suppression of foundation resonances which butyl rubber affords.

8. NOTE

The criteria which define a good anti-vibration mount material have been determined solely from the aspect of vibration reduction. No account has been taken of practical problems such as the creep and oil resisting properties of the resilient materials considered above, or of the temperature rise occurring if they are subject to large-amplitude vibration (which in the case of high damping rubbers can cause bond failure after a relatively short mount life).

Rubbers containing a high proportion of carbon black, such as the specimens of natural and butyl rubber employed in the transmissibility measurements above, characteristically possess a modulus that decreases, and a damping factor which increases with the impressed amplitude of vibration.[11] The vibrational amplitudes experienced by the resilient materials in the transmissibility measurements were insufficiently large, however, to invoke such non-linear properties.

The conclusions drawn from the transmissibility measurements made on the resilient materials considered in this article only apply strictly to the frequency range in which the measurements were made. In practice, the resonant frequency of a vibrating item on its resilient mounting will be the order of one decade lower than in the above measurements. The resonant transmissibility of the resilient materials at the lower frequencies will be somewhat greater than depicted here, as will be the rate of increase in high frequency isolation which they afford. This improvement in isolation will be rather more apparent for the high damping materials, since their elastic modulus decreases more rapidly with frequency than that of low damping materials. It is felt, however, that the conclusions of Section 7 can correctly guide the choice of mount materials for use at frequencies where, in practice, mounting resonances occur. For example, the conclusions drawn from the critical comparison of natural and butyl rubber remain unchanged. Thus, although the suppression of resonant transmissibility afforded by butyl rubber in the simple and compound systems will be less at lower frequencies, it will still be superior to that afforded by natural rubber, but probably by a reduced amount.[12] There is no doubt that at frequencies above the mounting resonances, butyl rubber will continue to offer far greater suppression of foundation resonances than natural rubber.

Reference must also be made to the temperature dependence of the resilient materials considered in this article. The mechanical properties of high damping materials will be the most temperature sensitive. Any temperature variation will be reflected as a change in the suppression of mounting and foundation resonances, and in the high frequency isolation which the materials afford. It is felt that the conclusions of Section 7 will remain valid for all the ambient temperatures commonly met with in practice. For example, in the particular case of a mounting of filled butyl rubber in the simple system, it is thought most unlikely that a change in temperature of plus or minus 10° C from room temperature (20° C) would produce more than plus or minus 2·5 dB change in the resonant transmissibility. Even at higher temperatures it is very probable that the damping of butyl rubber will continue to exceed that of natural rubber. The rate of increase in high frequency isolation which butyl rubber affords will become favourably greater. At lower temperatures, however, the damping factor of butyl rubber will increase, and the high frequency isolation which butyl rubber affords will become less as the temperature decreases. At sub-zero temperatures the high frequency isolation will possibly be much inferior to that of natural rubber. If this is the case, and the mounting is required to operate continually at such temperatures, then

natural rubber will definitely prove a more suitable mount material.

APPENDIX

The experimental determination of transmissibility

Transmissibility measurements have been made on small cylindrical specimens of natural rubber and synthetic rubber-like materials using a method previously employed by Harrison, Sykes, and Martin.[5] These workers have shown from a reciprocity theorem that when the mass M_1 of Fig. 21(*a*) is driven at an angular frequency ω, the ratio of the accelerations A_2/A_1 is identical with the ratio of the forces F_2/F_1 in Fig. 21(*b*). This force ratio is by definition the transmissibility of the simple system with a mount of elastic modulus E, and mass M which vibrates at the angular frequency ω. Transmissibility measurements on resilient specimens in the compound system may equally well be made in this way.

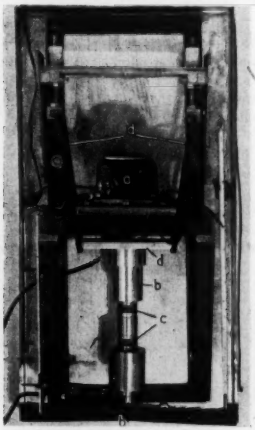

a, vibration generator; *b*, accelerometers; *c*, test specimen E in the compound system; *d*, the elements M_1, E_1.

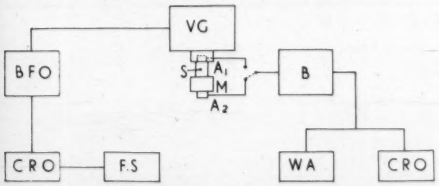

(*d*) F.S., frequency standard; *C.R.O.*, cathode ray oscillograph; B.F.O., beat-frequency oscillator; V.G., vibration generator; *S*, specimen; A_1, A_2, accelerometers; B, amplifier; W.A., wave analyser.

Fig. 21. The experimental determination of transmissibility

A photograph of the apparatus is shown in Fig. 21(*c*). The mass represented by M_1 in Fig. 21(*a*) is comprised of a short aluminium beam and aluminium housing, which contains the accelerometer A_1. The elastic modulus represented by E_1 in Fig. 21(*a*) is provided by catapult elastic, which softly suspends the beam and mounting system which is fastened to it. The beam is excited at its mid-point by a small vibration generator, which is driven by a beat-frequency oscillator (Fig. 21*d*) at accurately known frequencies in the range 60 c/s to 10 kc/s.

The accelerations A_1 and A_2 are measured by barium titanate accelerometers. The amplified accelerometer outputs are compared by a wave analyser possessing a logarithmic output meter, so that the transmissibility of the test specimen in decibels can be read directly.

The amplitudes of vibration suffered by the resilient materials during transmissibility measurements are very small, and are such that in all cases the materials exhibit linear behaviour. For example, with reference to the transmissibility of natural rubber in the simple mounting system (Fig. 6), the peak displacement suffered by the rubber at 500 c/s is $5{\cdot}5 \times 10^{-5}$ cm, and the associated dynamic strain is $4{\cdot}3 \times 10^{-5}$.

ACKNOWLEDGEMENTS

The author wishes to thank Dr. R. W. B. Stephens and Dr. G. G. Parfitt for their advice and encouragement during the course of this work.

The author also wishes to thank the Andre Rubber Co. for providing specimens of natural rubber, butyl rubber, and Heveaplus M-G, the British Rubber Producers' Research Association for providing the specimen of Hycar 1001; Gestetner Ltd., for providing the specimen of castor oil urethane; and the United Kingdom Atomic Energy Authority for providing the specimens of irradiated polythene.

REFERENCES

(1) NOLLE, A. W. *J. Polymer Science*, **5**, p. 1 (1950).
(2) SNOWDON, J. C. *Akust. Beih.*, **1**, p. 118 (1956).
(3) TIMOSHENKO, S. *Vibration Problems in Engineering* (New York: D. Van Nostrand Co., 1928).
(4) IVEY, D. G., MROWCA, B. A., and GUTH, E. *J. Appl. Phys.*, **20**, p. 486 (1949).
(5) HARRISON, M., SYKES, A. O., and MARTIN, M. *J. Acoust. Soc. Amer.*, **24**, p. 62 (1952).
(6) CROCKETT, J. A., and HAMMOND, R. E. R. *Proc. Instn Mech. Engrs*, **160**, p. 512 (1949).
(7) HEVEAPLUS, M. *British Rubber Producers' Research Association Technical Bulletin*, No. 1 (1955).
(8) DUMMER, G. W. A., and JOHNSTON, D. L. *Proc. Inst. Elec. Engrs*, (III), **100**, p. 177 (1953).
(9) CHARLESBY, A. *Nucleonics*, **12**, p. 18 (1954).
(10) CHARLESBY, A., and HANCOCK, N. H. *Proc. Roy. Soc. A*, **218**, p. 245 (1953).
(11) FLETCHER, W. P., and GENT, A. N. *Instn Rubber Ind.*, **29**, p. 266 (1953).
(12) JACKSON, R. S., KING, A. J., and MAGUIRE, C. R. *Proc. Instn Elect. Engrs*, (II), **101**, p. 512 (1954).

The performance of spark guards*

By J. H. McGuire, B.Sc., A.M.I.E.E., A.Inst.P., and Margaret Law, B.Sc., Fire Research Station, Boreham Wood, Herts.

[*Paper received* 23 *April*, 1958]

The probabilities that various sizes of live coal will ignite various domestic materials have been determined. In addition the maximum probability that a coal will pass through a mesh has been calculated. Combining the two results has given a measure of the efficiency of spark guards in reducing fire risk. It is suggested that non-flammable Nylon net is a suitable material for a combined fire and spark guard.

INTRODUCTION

The Fire Brigades in the United Kingdom are notified of about 6000 incidents each year in which domestic open fires, either guarded or not, are responsible for igniting nearby materials other than structural timber underneath the hearth. Although all means of ignition (e.g. clothing falling on to the fire whilst being aired, ignition by radiation, etc.) are included in arriving at the above figure, it is probable that the use of almost any form of spark or fireguard would substantially reduce the figure since it would ensure that combustible materials were kept clear of hot coals. (A fireguard is a rigidly fixed device intended, firstly, to prevent children and infirm people from falling on to the fire, and secondly, to reduce the risk of ignition of clothing which, whilst being worn, might otherwise be brought into contact with hot coals. A spark guard is a device intended to retain flying coals and sparks, and is usually not as robust as a fireguard.) The importance of guarding an open fire, with a view to reducing burn injuries caused by contact with hot coals and by clothing igniting, has been stressed by Colebrook and Colebrook[1] and has been recognized in law.[2] The scope of this paper is confined to the fire risk created by flying coals and sparks, and the reduction in this risk which can be brought about by the use of a spark guard. The ignitability of materials by flying coals and sparks has been determined experimentally, and the effect of using a spark guard has been assessed by combining the above results with predictions of the probability that a live coal will pass through a specified spark guard mesh.

The effect of the use of a spark guard on room heating is also discussed, and the possible use of non-flammable Nylon net as a spark guard is examined.

THE IGNITION OF DOMESTIC MATERIALS BY LIVE COALS

The coal used in all the tests was Midland Singles, which is a bituminous, high volatile, non-coking coal. Standard conditions were obtained by heating the coals in a bunsen flame. They were thus ignited quickly and could be projected on to the samples of material whilst still distilling volatiles at a rate sufficient to maintain flaming. To represent the most hazardous conditions likely to be encountered in practice, the coals were dropped directly on to the material, a distance of about 3 in.

Table 1 lists the materials tested for ignition by burning coals. They were chosen as examples of the more easily ignitable materials likely to be found near to an open fire.

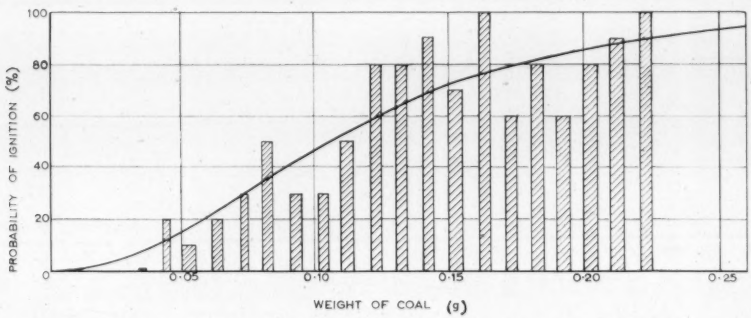

Fig. 1. Probability of a piece of burning coal igniting brushed scrim

Table 1. *Materials tested*

Material	*Weight/unit area (g/cm²)*
Cotton	$1{\cdot}2 \times 10^{-2}$
Viscose rayon net	$1{\cdot}8 \times 10^{-3}$
Hessian scrim	$2{\cdot}2 \times 10^{-2}$
Newspaper	$5{\cdot}5 \times 10^{-3}$
Belgian cotton carpet	0·12
Surgical cotton wool	—

* Crown copyright reserved.

All the specimens of material were dried before testing and the scrim was brushed, since it was found to be more easily ignited in this condition. Its appearance, when brushed, resembled that of the scrim commonly found underneath arm chairs.

Cotton wool, irrespective of its disposition, was readily ignited by pieces of coal weighing only 0·005 g. As this weight corresponds to a diameter of only 0·075 in. for a spherical particle, it was concluded that cotton wool would always present a hazard and that it would not be practicable to design a spark guard to overcome this.

With Belgian cotton carpet, laid horizontally, no continuing fire was started when pieces of flaming coal with dimensions of the order of 0·5 in. were dropped on it. It was therefore concluded that this material did not present an appreciable hazard from this point of view and no further tests were made on it.

The results for brushed scrim are shown in Fig. 1 in the form of a histogram in which each block represents ten experiments. It has been assumed that a finite probability of igniting materials exists for coals even smaller than those tested and a probability curve for all ranges of weight of coal has been calculated by probit analysis (see Appendix I). This is also shown in Fig. 1. The adoption of probit analysis automatically involves the assumption that a finite (though very small) probability of igniting a material exists for every size of coal however small, whereas theoretically there is possibly a threshold energy level below which a fire cannot be initiated. The consequent exaggeration of the hazard where very small coals are concerned will not greatly influence the estimation of the performance of spark guards.

A probit analysis was made of the histograms derived from testing the remaining materials and the resulting probability curves (including that for brushed scrim) are shown in Fig. 2.

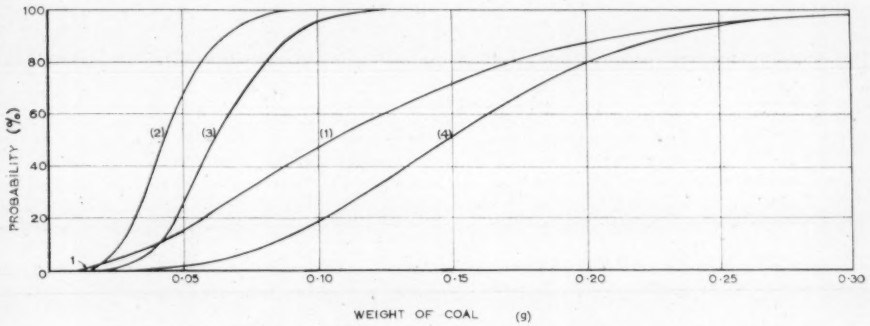

Fig. 2. Probability of a piece of burning coal igniting various materials

Curve (1), scrim; curve (2), viscose rayon net; curve (3), newspaper; curve (4), cotton.

THE PERFORMANCE OF SPARK GUARDS

The reduction in fire risk. No information is available as to the distribution of the geometrical shapes of the particles emitted by a domestic open fire. In deriving expressions for the probability that a piece of coal will pass through a mesh (Appendix II), two shapes, a sphere and a cylindrical particle, with a length/diameter ratio of eight have therefore been assumed as the practical extremes. The probability for a spherical particle may be greater or less than that for a cylindrical particle, depending on the actual mass and on the size of the mesh. Whichever is the larger is referred to as the probability for any given mass. Some calculated results are shown in Fig. 3. From these and the experimental results for the probability of ignition of a fabric by a given mass of coal, the combined probability that a coal will both pass through a mesh and ignite a fabric can be obtained.

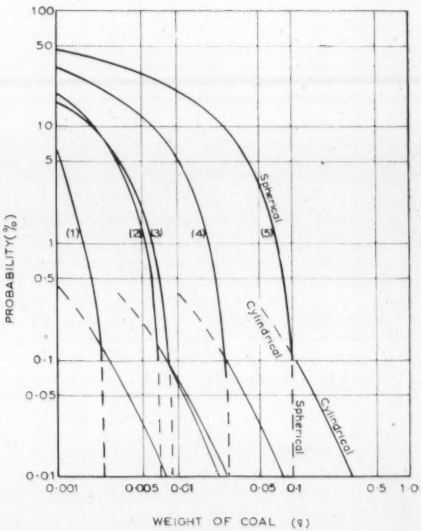

Fig. 3. Probability of a piece of coal passing freely through a mesh

Curve (1), non-flammable Nylon net *A*; curve (2), non-flammable Nylon net *B*; curve (3), 8-mesh (22 s.w.g.); curve (4), 6-mesh (22 s.w.g.); curve (5), 4-mesh (20 s.w.g.).

Fig. 4 shows the combined probability curves for an eight-mesh (22 s.w.g.) guard. Similar curves have been obtained for six-mesh (22 s.w.g.) and four-mesh (20 s.w.g.) guards and for two permanent finish non-flammable Nylon meshes, *A*, 45 denier, and *B*, 150 denier. For any given

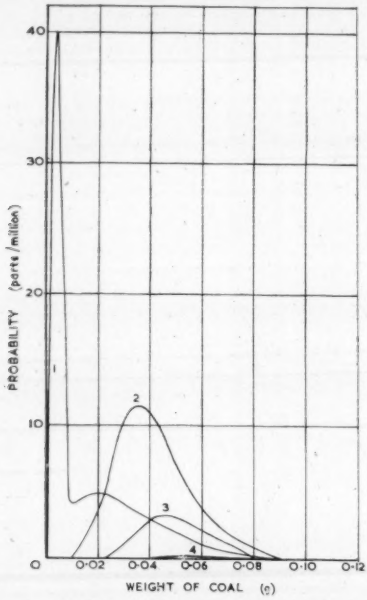

Fig. 4. Probability of a piece of coal both passing through eight-mesh (22 s.w.g.) and igniting various materials

Curve (1), scrim; curve (2), viscose rayon net; curve (3), newspaper; curve (4), cotton.

mesh size and fabric there is a mass of coal for which this combined probability is greatest. The largest of these peak values for the four materials tested has been called the maximum probability, and for the various meshes considered these values are given in Table 2.

Table 2. *Maximum probabilities of ignition of the materials listed in Table 1 (excluding cotton wool and Belgian cotton carpet)*

Guard	*Maximum probability of ignition (parts per million)*
8-mesh (22 s.w.g.)	40
6-mesh (22 s.w.g.)	340
4-mesh (20 s.w.g.)	24 000
Non-flammable Nylon *A*	3·3
Non-flammable Nylon *B*	34

To confirm that the non-flammable Nylon nets would, in fact, not melt in practice, they were hung vertically and, whilst subjected to an intensity of radiation of 0·5 cal $cm^{-2} s^{-1}$ (representing the maximum intensity they would receive from an open fire), flaming coals with linear dimensions up to ½ in. were projected on to them. The nets were structurally undamaged. If a hot coal rested against either of the nets, however, the Nylon in contact with the coal melted.

The effect on room heating. A domestic open fire heats a room largely by radiation and the use of a guard will, to a close approximation, reduce radiative heating by the amount which is intercepted by the elements of the mesh. The consequent heating of the guard contributes little to the heating of a room because the guard is cooled by the substantial air flow from the room which passes directly up the flue. As a measure of the reduction in radiation the obscuration has been calculated in the case of the metal meshes and measured experimentally in the case of the Nylon nets. The results are given in Table 3.

Table 3. *Obscuration of radiation by guards*

Guard	*Obscuration (%)*
8-mesh (22 s.w.g.)	40
6-mesh (22 s.w.g.)	30
4-mesh (20 s.w.g.)	27
Non-flammable Nylon *A*	13
Non-flammable Nylon *B*	18

Strength of meshes. Spark guards with metal meshes have been widely used for many years and have been found to be satisfactory from the strength point of view. The three meshes considered are typical of those on the market and are adequately strong. Nylon net guards, however, have never been available, and although they are strong enough to deflect hot coals they might be damaged by misuse. It was found that Nylon *A* could be punctured by forcing a pencil against it, but that Nylon *B* was considerably more robust and should be able to stand considerable rough usage.

CONCLUSIONS

The results in Tables 2 and 3 show that the six- and eight-mesh guards are far more effective than the four-mesh guard in reducing fire risk, whilst the amounts by which they reduce room heating are increased by much smaller factors.

The Nylon meshes are superior to the wire meshes both in their efficiency in reducing fire risk and in the extent to which they reduce obstruction of radiation. They are, however, not quite so robust and if hot coals come to rest against them they will melt. This might happen if the Nylon net extends down to hearth level and large coals fall on the hearth.

Nylon net will have a valuable application in the manufacture of combined fire and spark guards. To date these have not been popular since, if constructed of fine wire mesh, they substantially reduce room heating. By using a Nylon instead of a fine wire mesh this effect will be much less marked.

It should be noted that, of the domestic materials tested, cotton wool was found to present so exceptional a hazard that it would not be practicable to design a spark guard giving a substantial reduction in the risk.

ACKNOWLEDGEMENT

The work described in this paper forms part of the programme of the Joint Fire Research Organization of the Department of Scientific and Industrial Research and Fire Offices' Committee; the paper is published by permission of the Director of Fire Research.

Acknowledgement is due to the Assistant Director, Mr. D. I. Lawson, for drawing attention to the potentialities of non-flammable Nylon net as a spark guard, and to Miss J. E. Miller for undertaking much of the work described.

REFERENCES

(1) COLEBROOK, L., and COLEBROOK, V. *Lancet*, **2** (6570), pp. 181–188 (1949).
(2) *Children and Young Persons (Amendment) Act*, 1952 (London: H.M. Stationery Office, 1952).
(3) FINNEY, D. J. *Probit analysis. A statistical treatment of the Sigmoid response curve*. 2nd Ed. Chapters 3 and 4 (London: Cambridge University Press, 1952).

APPENDIX I

Probit analysis

Analysis of the experimental results has been carried out on the hypothesis that the probability of ignition is Gaussian with respect to the cube root of the mass of the coal. Probit lines have been calculated on this assumption; their linearity has been tested by the χ^2 test and there is no significant heterogeneity.(3)

The equations of the probit lines for the four materials are given in Table 4, together with the 95% confidence limits,

where y is the probit corresponding to a probability of ignition p

$x = m^{\frac{1}{3}} \times 10$

and m is the mass of coal in grammes which gives probability of ignition p

APPENDIX II

The probability of a particle passing freely through a mesh

Spherical particle. The total probability may be considered as the product of the probability of a sphere not engaging on a horizontal wire and the probability of a sphere not striking a vertical wire (Fig. 5). The probability of a particle not

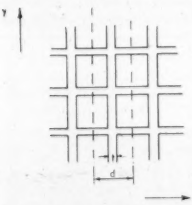

Fig. 5. Section of guard

striking a vertical wire will now be discussed. If the centre of a particle of diameter D lies within the x co-ordinate zero and d, the probability of its centre lying in any range δx is $\delta x/d$. The particle will not strike the wire if the x co-ordinate of its centre lies within the range zero and $\frac{d}{2} - \frac{t}{2} - \frac{D}{2}$ or the range $\frac{d}{2} + \frac{t}{2} + \frac{D}{2}$ and d, i.e. a range $d - t - D$. The probability of this occurring is $\frac{(d - t - D)}{d} = 1 - [(D + t)/d]$

Of the particles which will not strike the vertical wires the fraction which will not strike the horizontal wires is also $1 - [(D + t)/d]$. The probability of a particle passing freely through the mesh is therefore $\{1 - [(D + t)/d]\}^2$.

Cylindrical particle. The particle is considered to have random orientation and direction of flight normal to the mesh (Fig. 6). This latter assumption will lead to the hazard

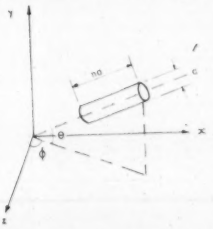

Fig. 6. Orientation of particle to mesh in yx plane

being somewhat over-estimated and the results will therefore be conservative. From symmetry, only values of ϕ and θ between zero and $\pi/2$ need be considered.

Table 4. *Probit analysis of the ignition of various materials*

Material	*Probit line*	*95% confidence limits to x*
Cotton	$y = 1{\cdot}441x - 2{\cdot}634$	$1{\cdot}12x - 0{\cdot}65 \pm 1{\cdot}52\sqrt{[0{\cdot}018 + 0{\cdot}057\,(x - 5{\cdot}45)^2]}$
Viscose rayon net	$y = 2{\cdot}509x - 3{\cdot}842$	$1{\cdot}17x - 0{\cdot}62 \pm 0{\cdot}92\sqrt{[0{\cdot}034 + 0{\cdot}241\,(x - 3{\cdot}62)^2]}$
Hessian scrim	$y = 0{\cdot}986x + 0{\cdot}338$	$1{\cdot}08x - 0{\cdot}37 \pm 2{\cdot}14\sqrt{[0{\cdot}009 + 0{\cdot}018\,(x - 4{\cdot}9)^2]}$
Newspaper	$y = 2{\cdot}437x - 4{\cdot}634$	$1{\cdot}15x - 0{\cdot}61 \pm 0{\cdot}93\sqrt{[0{\cdot}026 + 0{\cdot}204\,(x - 4{\cdot}04)^2]}$

If the cylinder has diameter a and length na and the axis makes an angle θ with the zx plane, then the projection of the cylinder in the y dimension is

$$D_H = na \sin\theta + a\cos\theta$$

For a given value of θ the probability of passing freely between the horizontal wires is (from above)

$$P_H = 1 - \left(\frac{D_H + t}{d} = 1 - \right)\frac{a}{d}(n\sin\theta + \cos\theta) - \frac{t}{d}$$

The probability that θ will lie within the limits θ and $\theta + \delta\theta$ is $\cos\theta\delta\theta$. Combining these two probabilities gives

$$dP_H = \left[1 - \frac{a}{d}(n\sin\theta + \cos\theta) - \frac{t}{d}\right]\cos\theta d\theta$$

where the limits of θ are 0 and θ'

and $$a(n\sin\theta' + \cos\theta') = d - t$$

If the projection of the cylinder in the xz plane makes an angle ϕ with the z axis then the projection of the cylinder in the x dimension is given, for small values of θ

by $$D_V \simeq na\cos\theta\sin\phi + a\cos\phi$$

***

The probability of passing between the vertical wires for a given value of θ and ϕ is

$$P_V = 1 - \frac{D_V + t}{d} = 1 - \frac{a}{d}(n\cos\theta\sin\phi + \cos\phi) - \frac{t}{d}$$

The probability that ϕ will lie between ϕ and $\phi + \delta\phi$ is $2\delta\phi/\pi$. Combining these two probabilities gives

$$dP_V = \frac{2}{\pi}\left[1 - \frac{a}{d}(n\cos\theta\sin\phi + \cos\phi) - \frac{t}{d}\right]d\phi$$

where the limits of ϕ are 0 and ϕ'

and $$a(n\cos\theta\sin\phi' + \cos\phi') = d - t$$

The total probability of passing freely through the mesh is given by

$$P = \int_0^{\theta'}\int_0^{\phi'} dP_H dP_V$$

For particles of such dimensions that θ' and ϕ' are small, this expression reduces to

$$P = (d - t - a)/2\pi n^2 a^2 d^2$$

Combination of results. The two expressions derived in the above paragraphs have been evaluated and plotted in Fig. 3 for the various meshes, taking the density of coal as $1{\cdot}27$ g/cm^3 and $n = 8$ in the case of the cylinders. The extreme probabilities for all shapes of particle are given by the solid curves in Fig. 3.

Electrical properties of chalcopyrite

By B. Donovan, Ph.D., A.R.C.S., F.Inst.P., Department of Physics, Bedford College, London,
and G. Reichenbaum, M.Sc., Ph.D., Grad.Inst.P.,* Department of Physics, Northern Polytechnic, London

[*Paper first received* 24 *April, and in final form* 10 *July*, 1958]

The conductivity σ and thermoelectric power ϕ of synthetic and natural specimens of chalcopyrite have been investigated in the temperature range -140 to 300° C. The Hall coefficient R of the natural specimens has also been measured in this region, but in the case of the synthetic specimens is too small to be detected. For the majority of the specimens the product $R\sigma$ varies approximately as $T^{0\cdot7}$ from about 100 to -140° C. This is taken to indicate that impurity scattering of the carriers is predominant, and on this basis the effective mass is estimated to be roughly equal to the free electron mass. The low mobility values encountered suggest that the samples are markedly inhomogeneous and this is further borne out by the decrease in the measured resistance at high frequencies.

The possibility of a group of ternary semiconducting compounds with diamond type structure was first discussed by Goodman and Douglas,[1] who pointed out their relationship with the binary II–VI zinc blende compounds and mentioned preliminary results obtained with $CuInSe_2$ and $AgInSe_2$. Subsequently, further details of the preparation of these and other ternary compounds were published, together with values for the optically determined energy gaps.[2, 3]

Few systematic experiments on the electrical properties of these compounds have been carried out, and the object of the present paper is to discuss briefly the results of some measurements made on synthetic and natural samples of copper iron sulphide, $CuFeS_2$. This compound occurs naturally as chalcopyrite and its structure is a slightly tetragonal distortion of a perfect diamond lattice.

During the course of the present work a paper by Boltaks and Tarnovski[4] came to the authors' notice, in which experimental results on the electrical conductivity and thermoelectric power of synthetic and natural chalcopyrite were presented, in addition to a study of rectifying properties. These results were obtained in the temperature range 20–600° C and differ from those of the present paper in several respects; in particular, the deduction of the energy gap appears to be of doubtful validity owing to the changes in composition which occur at high temperatures.

EXPERIMENTAL PROCEDURES AND RESULTS

Specimens. In view of the serious difficulties encountered with ternary compounds,[3] and with sulphides in general, no attempt was made to grow single crystals and the synthetic samples were all obtained in the form of compressed powders. The compound was prepared by melting the components together in stoichiometric proportions (copper and iron, prepared electrolytically; sulphur from Johnson Matthey Ltd.). The synthesis was carried out in a sealed silica tube which fitted exactly into a stainless steel bomb. The temperature was maintained at a value in the range 900–1100° C for a period of 8–10 hours; after cooling the compound was ground and compressed in a specially constructed mould. No X-ray investigation of the material was carried out, but by examination under an electron microscope it was verified that the grain size in the powder was very nearly uniform. No evidence at all was obtained to indicate that the specimens contained any free copper, iron or sulphur, and it is reasonable to suppose that departures from stoichiometry were extremely small.

The natural specimens were supplied by the Geology Department of the Northern Polytechnic and the cutting of selected portions was carried out by Hilger and Watts Ltd.

Electrical conductivity. Measurements of the electrical properties were carried out over the temperature range -140–300° C using specimens with approximate dimensions $30 \times 7 \times 2$ mm. The ends of the specimens were coated by vacuum evaporation, firstly with a layer of silver and then with a thicker layer of copper. The current leads were soldered to these contacts. The potential probes (and Hall electrodes) were formed by lengths of tungsten wire, with electrolytically sharpened tips, held in position by short flat brass springs.

Typical conductivity curves for synthetic and natural specimens are shown in Figs. 1(*a*) and (*b*) respectively. All

* Now at English Electric Valve Co. Ltd., Chelmsford.

the natural specimens and all the synthetic specimens except two were found to be *n*-type semiconductors, in agreement with Boltaks and Tarnovski[4]; S_3 and S_4 were the two exceptional *p*-type specimens. In general, the orders of

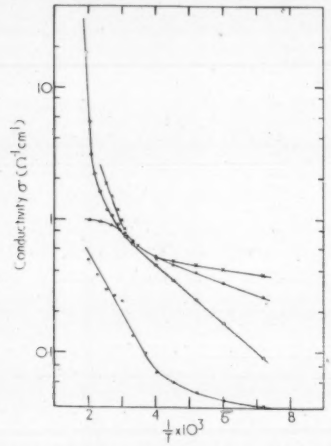

Fig. 1(*a*). Conductivity of various synthetic specimens
△ = S_1. ○ = S_2. • = S_3. × = S_4.

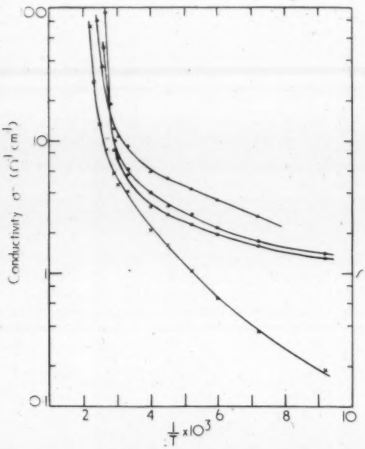

Fig. 1(*b*). Conductivity of various natural specimens
• = A_1. ○ = A_2. × = A_3. △ = A_4.

magnitude of conductivity were appreciably lower than those reported by Boltaks and Tarnovski,[4] and no minimum was found in the conductivity for any of the specimens studied. At high temperatures (effectively above about 200° C) the readings are less significant, owing to the tendency of the compound to lose sulphur and the occurrence of irreversible effects similar to those observed in binary compounds.[5] For this reason it is not possible to make reliable estimates of activation energies from readings in this region.

Hall effect. The Hall coefficient was measured by conventional methods and in all cases was found to be extremely small. For the synthetic specimens, in fact, the effect was too small to be observable. No previous measurements of Hall effect appear to have been published. The results for four natural specimens are shown in Fig. 2 and these show that, on the basis of a single-carrier model, the carrier density at room temperature is of order of magnitude 10^{19}. It is therefore reasonable to suppose that we are dealing with very impure samples which are strongly degenerate over most of the temperature range considered. Further evidence from the behaviour of the thermoelectric power is consistent with

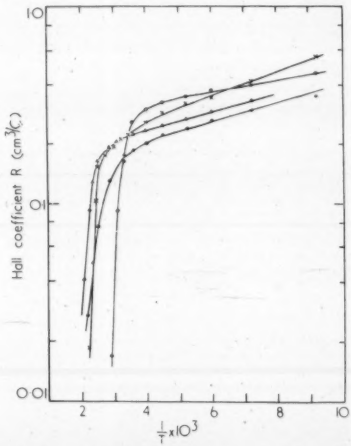

Fig. 2. Hall coefficient of various natural specimens
• = A_1. ○ = A_2. × = A_3. △ = A_4.

this view. The form of the curves in Fig. 2 is typical of all the specimens investigated and shows that the carrier density is roughly constant at low temperatures. No quantitative information can be obtained from the steep portion at high temperatures, which is a consequence of the composition changes previously mentioned.

Attempts were made to measure the magneto-resistance effect in specimens having various geometrical forms, including a Corbino disk. No change in resistivity could be detected in any of the specimens, synthetic or natural, and for highly degenerate samples such a zero result would not be unexpected.

Thermoelectric power. The thermoelectric power was determined with respect to platinum for several samples and the results are shown in Fig. 3. The results for the two *p*-type synthetic specimens are illustrated in Fig. 3(*a*) and the curves for typical *n*-type specimens (two synthetic and two natural) are given in Fig. 3(*b*). The thermoelectric power of the natural specimens was in general higher than that of the synthetic specimens and reached a maximum value in the region of 300–380 μV/° C. The orders of magnitude and the form of the curves are similar to those given by Boltaks and Tarnovski,[4] but in the present work

the maximum value was found to occur at a lower temperature in most cases.

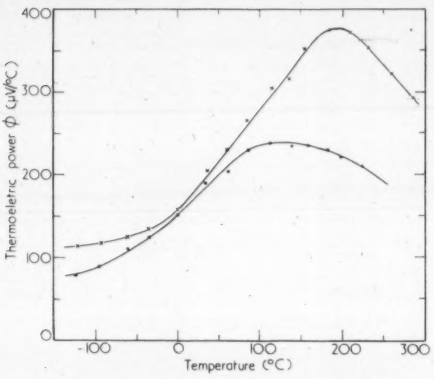

Fig. 3(*a*). Thermoelectric power: *p*-type specimens
× = S_4. • = S_3.

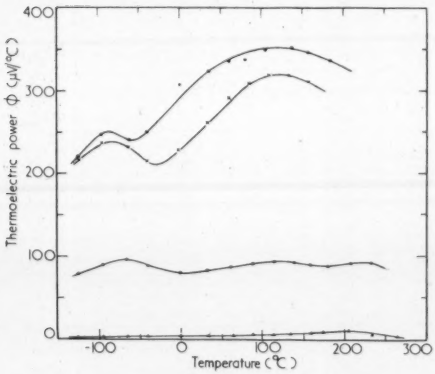

Fig. 3(*b*). Thermoelectric power: *n*-type specimens
• = A_1. × = A_3. ○ = S_2. △ = S_1.

DISCUSSION

The carrier mobility may be calculated from the Hall coefficient R and the conductivity σ by using an expression of the form

$$\mu = R\sigma/r \tag{1}$$

where r is a factor depending upon the scattering mechanism, the state of degeneracy and the form of the constant energy surfaces in k-space. The temperature dependence of the product $R\sigma$ for four natural specimens is illustrated in Fig. 4 and, since r is approximately unity for degenerate specimens, these curves may be taken as providing a good indication of the behaviour of the electron mobility.

The mobility values thus estimated are all extremely small (of the order of 1·0 cm^2/V s at room temperature) and far below the value 32 quoted in Ref. 3 for a *p*-type sample at room temperature. These low mobility values are undoubtedly due to the polycrystalline structure of the specimens, which gives rise to considerable scattering from grain boundaries and inhomogeneities, and to the high concentration of impurities. The variation of mobility with temperature may be represented with reasonable accuracy by a power law, $\mu \propto T^s$, below about 100° C, as shown in Fig. 4. In most cases a value around 0·7 was obtained for the index s, as illustrated by specimens A_1, A_2 and A_4; the behaviour of

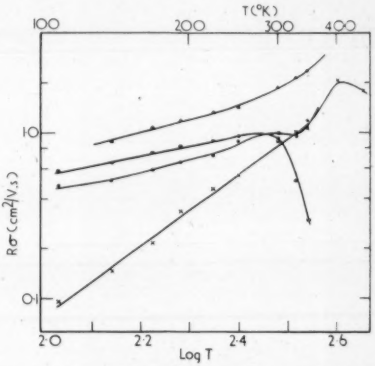

Fig. 4. Temperature dependence of $R\sigma$ for natural specimens
• = A_1. ○ = A_2. × = A_3. △ = A_4.

specimen A_3 was exceptional and the explanation of such a rapid variation of mobility ($s \simeq 2{\cdot}0$) would appear to be obscure.

Although these results do not permit a clear-cut interpretation in terms of any one scattering mechanism, it is not unreasonable to suppose that the scattering is predominantly due to ionized impurity centres. If this were the only mechanism present, the index s would have the value 1·5 in the nondegenerate range and would be approximately zero for degenerate specimens.

On the basis of the above ideas, rough values for the effective mass m^* may be derived from the results for the Hall coefficient and thermoelectric power. For a single-carrier system with impurity scattering only, the carrier density n, Hall coefficient R and thermoelectric power ϕ are given by[6]

$$n = 5{\cdot}54 \times 10^{15} T^{3/2} (m^*/m)^{3/2} F_{1/2}(\xi) \tag{2}$$

$$R = -\left(\frac{3}{4ne}\right) F_{7/2}(\xi) \cdot F_{1/2}(\xi)/F_2^2 \tag{3}$$

$$\phi = -\frac{k}{e}\left[\frac{4}{3}\cdot\frac{F_3(\xi)}{F_2(\xi)} - \xi\right] \tag{4}$$

where ξ is the reduced thermodynamic potential and the $F_r(\xi)$ are Fermi–Dirac functions.

Measurements of ϕ enable the parameter ξ to be calculated from equation (4), hence n and m^*/m may be evaluated from equations (2) and (3). Values for three specimens at −40, 0 and 40° C are given in the table.

Typical values of effective mass

Temperature (°C)	Specimen	ξ	n (cm^{-3}) ($\times 10^{19}$)	m^*/m
−40	A_1	1·85	4·08	0·97
	A_2	2·42	2·88	0·61
	A_3	2·64	3·26	0·62
0	A_1	1·07	5·29	1·28
	A_2	2·22	3·50	0·61
	A_3	2·26	3·78	0·66
+40	A_1	0·60	6·62	1·61
	A_2	1·53	8·04	1·22
	A_3	1·52	4·61	0·85

Finally, it is of interest to report briefly the results of some measurements of the conductivity at high frequencies. It is well known that in the case of compressed powder specimens the possibility of irregular contact between grains may give rise to spuriously low values of the d.c. conductivity and that this effect may be investigated by measurements at high frequencies.[7] For this purpose the resistance of various specially made samples at room temperature was determined up to 50 Mc/s, using a Q-meter technique, and typical results are illustrated in Fig. 5. It was not possible to obtain natural specimens in a form suitable for these measurements and the three curves shown in Fig. 5 are typical of the behaviour of the synthetic specimens investigated. The specimen resistance at 50 Mc/s was found to be smaller than the d.c. value by a factor of about two to three, and this may be regarded as a further consequence of the granular structure of the specimens. While no useful purpose would be served by analysing these results in detail, they serve to emphasize that the experimental values of the d.c. conductivity have only limited quantitative significance and that the true values may well be appreciably higher.

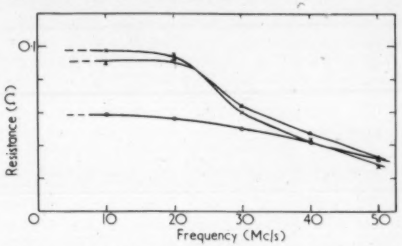

Fig. 5. High frequency resistance of various synthetic specimens

REFERENCES

(1) GOODMAN, C. H. L., and DOUGLAS, R. W. *Physica*, **20**, p. 1107 (1954).
(2) AUSTIN, I. G., GOODMAN, C. H. L., and PENGELLY, A. E. *Nature* [*London*], **178**, p. 433 (1956).
(3) AUSTIN, I. G., GOODMAN, C. H. L., and PENGELLY, A. E. *J. Electrochem. Soc.*, **103**, p. 609 (1956).
(4) BOLTAKS, B. I., and TARNOVSKI, N. N. *Zh. Tekh. Fiz.*, **25**, p. 402 (1955).
(5) SCANLON, W. W. *Phys. Rev.*, **92**, p. 1573 (1953).
(6) See, for example, WEISS, H. *Z. Naturforsch.*, **11**a, p. 131 (1956).
(7) HAHN, E. E. *J. Appl. Phys.*, **22**, p. 855 (1951).

A generalized theory of sedimentation

By A. D. MAUDE, B.Sc., Ph.D., A.Inst.P.,* and R. L. WHITMORE, B.Sc., Ph.D., A.Inst.P., Department of Mining and Fuels, University of Nottingham

[*Paper first received* 3 *January, and in final form* 25 *June*, 1958]

A theoretical relationship between the concentration and the sedimentation velocity of non-flocculated suspensions of particles is derived. It is shown that the settling velocity relative to that of a single particle in the suspension is $(1 - c)^{\beta}$ where β is a function of particle shape, size distribution and Reynolds number and c is the volume of solid per unit volume of suspension. The expression is shown to satisfy the experimental results of other workers. An empirical relationship between β and the Reynolds number is suggested.

1. INTRODUCTION

When a body falls through a fluid, it accelerates until it reaches a constant terminal velocity. This velocity is determined by the density of the fluid ρ_f, the density of the body ρ_s, the viscosity of the fluid η, the shape and orientation of the body and by some length characterizing the size of the body d. The velocity may also depend, to some extent, upon the size and shape of the containing vessel, but if this is large its influence may be neglected.

The problem becomes more complicated if many bodies are present and the system becomes a sedimenting suspension. When the bodies are more or less evenly dispersed throughout the fluid, their rate of fall is decreased, and it is of considerable practical interest to know the relation between the concentration of bodies and the magnitude of this decrease.

Many theoretical and empirical relations[1-8] have been proposed to solve this problem, but they suffer from various defects, in particular they lack generality. It would be of considerable practical value if an equation could be derived which would cover a wide range of particle shapes, size ranges and rates of fall, and in the following paper an attempt is made to do this.

2. FALL OF SPHERES AT LOW REYNOLDS NUMBER

Consider a mass of equi-velocity particles falling through a pure fluid. If v is the average volume of one particle, and g is the acceleration due to gravity, then the average force on one particle is $F = (\rho_s - \rho_f)gv$. If c is the volume of solid in unit form of suspension, then it may be shown from

* Now at the City of Liverpool College of Technology.

dimensional reasoning that, if inertial forces may be neglected, the sedimentation velocity is given by:

$$U = K(F/d\eta)\phi(c) \tag{1}$$

where K is a constant, and $\phi(c)$ is a function of c.

For spheres, from Stokes' law, $K = \frac{1}{3}\pi$ if $\phi(0) = 1$, but in general K is a function of particle shape, orientation and size distribution, and is constant for any one set of particles.

The problem is to find the function ϕ, and most investigators, both theoretical and experimental, have taken $KF/d\eta$ as constant, and have found the function ϕ as a relation between U and c. In the following theoretical investigation it has been found more convenient to maintain $Ud\eta/K$ constant, and to consider the function ϕ as expressing the relation between F and c. That is, as the concentration is varied the gravitational force is altered in such a manner that the settling velocity is unchanged. This might be achieved experimentally, for example, in a centrifuge.

It is also convenient to take a frame of reference which is stationary with respect to the particles, so that the liquid flows past them at a velocity which reduces to U above the surface of the suspension. Within the suspension the velocity will vary from place to place, and will on the average exceed U. If this average velocity is U' it may easily be shown that

$$U'(1 - c) = U \tag{2}$$

The theory is first developed for the case of equi-sized, equi-density spheres, and it is then shown how variations of size, density and shape affect the expression obtained.

Consider a suspension supported by an upward current in a vessel, which is sufficiently large to allow edge effects to be neglected. Suppose that a small number of spheres is added to the suspension, increasing its concentration by dc, and at the same time the gravitational force on each particle F is increased by an amount dF so that U remains unaltered. For simplicity, suppose that the added spheres enter the fluid at places where the average velocity before the addition was U'. When the concentration is very low all portions of the liquid will have an equal probability of being entered, so that this will on the average be true. Reasons for the belief that it is also true at high concentrations are advanced later.

When finding the velocity distribution caused by the introduction of a stationary body into a moving fluid when all movements are slow, it is usual to consider a velocity field which possesses the following characteristics:

(*a*) it obeys the linearized Navier–Stokes equations for all points outside the surface of the body;
(*b*) it is equal and opposite to the original velocity at all points on the surface of the body;
(*c*) it obeys appropriate boundary conditions at the surfaces of other bodies and the containing vessel;
(*d*) it obeys the continuity equation (i.e. is non-divergent) for points within the volume of the body. For the present argument the fact that a force must be applied to this liquid so that discontinuities occur in the stresses is unimportant so long as the velocity remains finite.

Whilst for all hydrodynamical considerations the addition of such a field to the existing velocity field will produce the same result as the addition of the body, it is not sufficient for mechanical considerations. The condition must also be included that all points on what would otherwise be the surface of the body cannot be penetrated by solid bodies. For convenience, all points within this surface will be called "within the added body."

Following this method, the added spheres may be considered as replaced by a velocity field of average value $-U'$ within the volume of the spheres, and some form of return flow through the suspension. It is apparent that as this flow is non-divergent within the volume of the added spheres, it will be circulatory in form, i.e. the streamlines will form closed loops, and there will be no net flow across any infinite plane.

From equation (1) we may write:

total force on volume V of suspension,

$$F' = (\text{average force per particle}) \times (\text{number of particles in } V) = U\eta d/K\phi(c) \times V(c/v)$$

which may be written as

$$F' = \frac{\eta cd}{Kv\phi(c)} \times UV \tag{3}$$

Equation (3) shows that for given particles, a given liquid and a given concentration, the total force exerted by the liquid is proportional to the product of the velocity and the volume. It will be noted that the velocity referred to is an average velocity which may be found by dividing the volume rate of flow by the total area of cross-section, including the area occupied by particles. As the integral of the product of volume and velocity defined as above is zero for a circulating current, it follows that if a current circulates through an array of stationary particles, it will exert no net force on them. If the particles of a suspension are randomly, rather than evenly positioned, any one circulatory flow may exert a force, but the average over a large number of similar currents will be zero.

It does not follow, however, that the circulatory flow which replaced the added spheres, exerts no force on the remainder of the suspension, for no other particle may penetrate the position of the surface of the added spheres, and hence the current within the volume of the added spheres can exert no force on the other particles. The product of volume and velocity within the added spheres in unit volume of suspension is $-U'dc$ so that the product of volume and velocity over the remainder of the circulatory currents in unit volume is $+U'dc$. Therefore, the total force per unit volume which this uncompensated return flow exerts is, from equation (3),

$$U'dc\left(\frac{\eta d}{K}\,\frac{c}{\phi(c)}\,\frac{1}{v}\right)$$

As there are c/v particles per unit volume, the average force dF which the circulatory currents exert on a single particle is given by

$$dF = U'dc\left[\frac{\eta d}{K\phi(c)}\right] = \frac{F}{U}U'dc \tag{4}$$

Using equation (2)

$$dF/F = dc/(1 - c) \tag{5}$$

Integrating

$$F = F_0/(1 - c)$$

where F_0 is the value of F when $c = 0$

so that $$\phi(c) = (1 - c)$$

and $$U = U_0(1 - c) \tag{6}$$

where U_0 is the value of U when $c = 0$, and is assumed to be the velocity of fall of a single sphere. Equation (6) expresses the fact, recognized by Steinour[1] and by Hawksley[5], that the increase in the velocity of flow within a suspension over

its value above a suspension, leads to a change in the settling velocity by a factor of $(1 - c)$.

Equation (5) contains certain simplifications which must now be considered. As no sphere centre can exist within one sphere radius of the surface of the added particles without the spheres overlapping, the concentration of solid near to the surface of the added spheres is less than the concentration elsewhere. Not only does the circulatory current through the volume of the added spheres exert no force on other particles, but that part of it within one sphere radius of the surface of the added spheres exerts a reduced force. Thus the term for the product of volume and velocity of the uncompensated return flow is increased by some constant α.

Equation (4) now becomes

$$dF = (F/U)\alpha U' dc \tag{7}$$

and equation (5)

$$dF/F = \alpha dc/(1 - c) \tag{8}$$

the solution of which is

$$F = F_0(1 - c)^{-\alpha}$$

so that $$\phi(c) = (1 - c)^{\alpha}$$

or $$U = U_0(1 - c)^{\alpha} \tag{9}$$

No theoretical value can be assigned to α but limiting values may be set for it. The upper limit is reached when the concentration within one sphere radius of the surface of the added sphere is zero, and the circulatory flow within this volume is $-U'$. Under these circumstances the product of volume and velocity of the added flow which exerts no force on the suspension already present is $-8U'dc$. (The volume possessing zero concentration is assumed to be eight times the volume of a single sphere.) The lower limit is reached when the effect of the reduced concentration near to the added sphere is ignored, and equation (5) is true. Thus for equi-sized sphere $1 < \alpha < 8$.

3. FALL OF SPHERES AT ANY REYNOLDS NUMBER

It is possible to derive equation (9) by an argument which does not necessitate the assumption of negligible inertial forces and streamlined conditions of flow in the suspension, but the physical significance of the constant α disappears.

Thus, if a small number of new particles is added to the suspension in which the velocity of sedimentation is held constant, the fluid is unable to pass through the position occupied by the added particles, and the fluid velocity through the suspension is raised. The increase of the average force on the particles already present, which may be expressed as $(\partial F/\partial c)_u dc$, is caused by a rise in the velocity of fluid through the suspension, and is the same as would have been produced if U had been increased by some small amount dU. That is, it may be expressed as $(\partial F/\partial U)_c dU$.

Thus $$(\partial F/\partial c)_u dc = (\partial F/\partial U)_c dU \tag{10}$$

The extra volume of fluid passing through any horizontal plane in a given time is the fluid which would otherwise have passed through the position now occupied by the new particles, so that dU must be proportional both to dc and U'.

That is $$dU = \beta U' dc \tag{11}$$

where β is some constant. If the extra flow were uniformly distributed in a manner similar to the original flow, β would be unity. As the extra flow will be unevenly distributed, some form of averaging its effect must be adopted and the numerical factor β will result. Its value will thus depend on the pattern in which the extra flow distributes itself around an isolated added sphere; the further re-distribution caused by other spheres (constituting the interaction between them) is involved in the term $(\partial F/\partial U)_c$ and not in the value of dU. It is thus expected that β would depend not upon the concentration, but upon the Drag coefficient and Reynolds number in unhindered settling.

From equations (10) and (11)

$$\left(\frac{\partial F}{\partial c}\right)_u dc = \left(\frac{\partial F}{\partial U}\right)_c U' \beta dc$$

or $$\left(\frac{\partial F}{\partial c}\right)_u = \left(\frac{\partial F}{\partial U}\right)_c \frac{\beta U}{1 - c}$$

The solution of this partial differential equation is

$$F = \psi[U(1 - c)^{-\beta}] \tag{12}$$

where ψ is an arbitary function.

Equation (12) implies that

$$U = U_0(1 - c)^{\beta} \tag{13}$$

In both this and the preceding section it has been assumed that the spheres enter the fluid where the average velocity was U'. This may not be true for individual spheres, but it will be true on the average for a large number. At high concentrations it might appear that the fluid near to the surface of the particles already present has less chance of being entered than the fluid elsewhere. However, the virtual extension of the volume of the added particles by a factor α or β combined with the non-rigid nature of this extension allows the probability of such regions being entered to be as great as for other regions.

4. SEDIMENTATION OF COMPLEX SYSTEM

Whilst for simplicity the theory has been developed above for equi-sized, equi-settling spheres, the argument remains valid if the particles vary in size, shape and settling rate, except that the value of α or β may be changed. It should be noted, however, that the rate of fall which is being considered is that of the centre of gravity of the volume occupied by the falling solids, and this need not always equal the mass rate of fall.

It has been implicitly assumed that no ordering of the particles occurs and that the added particles were randomly placed. The opposite assumption has been made by some workers[3, 5] but appears to be unlikely. If one portion of the suspension began to form a regular array, and if this portion fell at a rate different from that of the remainder of the suspension, it would mix with further particles, and the ordering would be destroyed. Also in any practical case, slight differences between individual particles would cause them to fall at different rates so that any pattern which formed would be destroyed by the motion of one particle relative to the others.

It was also assumed that there was always room for the added fraction without rearrangement of the particles already present. This will not be true at very high concentrations, and sets a limit to the highest concentration to which the theory is applicable.

5. COMPARISON WITH EXPERIMENT

A considerable number of published experimental results are available which may be used for comparison with equations (9) and (13). For a variety of reasons, not all the

evidence is equally reliable, but it was considered that it would not be appropriate to enter into a critical comparison of the techniques of the various workers here.

Where individual readings were presented, $\log U/U_0$ has been plotted against $\log(1-c)$. From equation (13) this should result in a straight line of slope β. Fig. 1 presents nineteen such graphs; details of the various experiments are given in the table.

Certain workers have produced empirical equations to fit experimental results, which are identical with equation (13). The results of Hirst[9] on mineral particles have been shown by Hancock[7] to fit an empirical formula, which, at any one value of Reynolds number, reduces to equation (13). The value of β obtained for streamlined condition is 6. Lewis, Gilliland and Bauer[8] fit their experimental results on equi-sized spheres to an equation identical with (13) for any one value of Reynolds number, the value of β for streamlined conditions being 4·65. Richardson and Zaki[10] have plotted $\log U$ against $\log(1-c)$ for results covering a large range of shapes, particle densities and rates of fall. In every case they obtain a straight line, indicating a relation of the form of equation (13). They obtain results for α which depend upon the vessel size, but which extrapolate to $\alpha = 4{\cdot}65$ for infinite vessels.

Bearing in mind the many potential sources of error in making sedimentation velocity measurements, the experimental evidence summarized in Fig. 1 and the table is in good agreement with equations (9) and (13).

6. RELATION BETWEEN α AND β

From dimensional reasoning it can be shown that for a mass of particles sedimenting in a fluid

$$\frac{F\rho_i}{\eta^2} = \psi_1\left(\frac{U\rho_i d}{\eta},\ c\right) \tag{14}$$

where ψ_1 is some function of the two groups of variables and depends upon the shapes of the particles. The experimental results on the fall of a single body may be expressed as

$$\frac{F\rho_i}{\eta^2} \propto \left(\frac{U\rho_i d}{\eta}\right)^m \tag{15}$$

where $m = 1$ for Reynolds number <1
$m = 2$ for Reynolds number $>10^3$

and m is some constant between 1 and 2 for any limited range of values of Reynolds number between 1 and 1000.

If we assume that the variables of equation (14) are separable, it may be written as

$$\frac{F\rho_i}{\eta^2} \propto \psi_2\left(\frac{U\rho_i d}{\eta}\right)\psi_3(c) \tag{16}$$

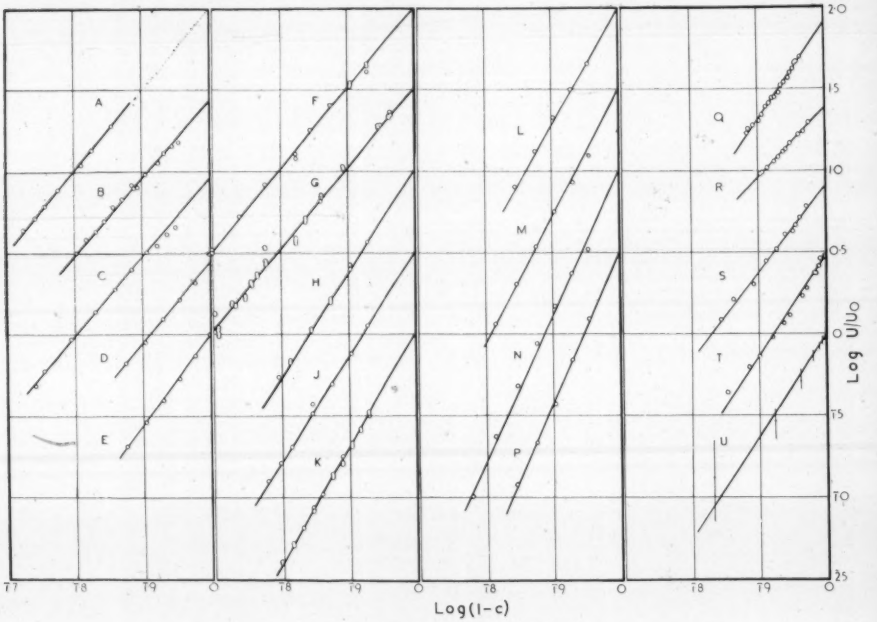

Fig. 1. Collected results of sedimentation experiments

When U_0 was not reported its value has been deduced by extrapolation. Successive curves have been displaced vertically by 0·5. The key to the various curves is given in the table.

Sedimentation experiments

Graph (Fig. 1)	Ref.	Particles	Fluid	Investigator	α
A	12	147–152 μ Kallodoc spheres 147–152 μ glass spheres	Aqueous glycerol Aqueous mercuric nitrate	Gurel	4·95*
B	12	152–178 μ Kallodoc spheres	Aqueous glycerol	Gurel	4·95
C	12	104–124 μ glass spheres	Aqueous mercuric nitrate	Gurel	4·80
D	13	81–104 μ polystyrene spheres	Aqueous lead nitrate	Whitmore	5·00
E	13	89–104 μ Kallodoc spheres	Aqueous lead nitrate	Whitmore	5·60
F	1	Glass spheres	Water	Steinour	5·00
G	1	Tapioca spheres	Oil	Steinour	4·90
H	2	10–14 μ emery *A*	Water	Steinour	6·80
J	2	7–10 μ emery *B*	Water	Steinour	6·80
K	2	62–74 μ emery *E*	Diethyl Phthalate	Steinour	7·00
L	14	Rough acrylic powder (*a*) 72–85 B.S.S.	Water	Whitmore	6·75
M	14	Rough acrylic powder (*b*) 100–120 B.S.S.	Water	Whitmore	7·65
N	14	Rough acrylic powder (*c*) 150–170 B.S.S.	Water	Whitmore	8·50
P	14	Rough acrylic powder (*d*) 200–300 B.S.S.	Water	Whitmore	9·35
Q	12	Cubes	Aqueous glycerol	Gurel	5·85
R	12	Disks	Aqueous glycerol	Gurel	4·15
S	12	Cylinders	Aqueous glycerol	Gurel	5·15
T	12	Cylinders	Paraffin	Gurel	5·35
U	15	Red blood cells	Water	Kermack, McKendrick and Ponder	6·50†

* The large number of results at low concentrations has made ringing these points impossible.
† The vertical line represents the experimental spread. The central spot represents the average result.

From equation (15)

$$\psi_2\left(\frac{U\rho_l d}{\eta}\right) = \left(\frac{U\rho_l d}{\eta}\right)^m$$

From equation (9)

$$\psi_3(c) = (1 - c)^\alpha$$

Thus equation (16) becomes

$$\frac{F\rho_l}{\eta^2} \propto \left(\frac{U\rho_l d}{\eta}\right)^m (1 - c)^\alpha$$

which gives

$$U = U_0(1 - c)^{\alpha/m} \qquad (17)$$

It is seen that the assumption that the variables are separable leads to a conclusion consistent with Section 3, and also leads to an expression for the variation of β with Reynolds number.

In the previous section it was stated that Lewis, Gilliland and Bauer,[8] Hancock[7] and Hirst[9] derived equation (13) empirically for spheres and mineral particles respectively. They both extended their equations to cover the effect of change of Reynolds number. Examination of their equations shows that they are identical with equation (17), with, of course, different numerical values for α. Richardson and Zaki[10] obtained experimentally the variation with Reynolds number of their equivalent of β for suspensions of spheres. Their values (extrapolated to represent an infinitely-large containing vessel) are presented in Fig. 2.

If the variation of m with Reynolds number for the fall of a single sphere is taken from the work of Needham and Hill,[11] and Richardson and Zaki's streamline-flow value of 4·65 is assumed for α, β may be calculated and in Fig. 2 is plotted as a continuous line against the Reynolds number. It will be observed that while the agreement of this line with Richardson and Zaki's experimental points is not perfect, it is sufficiently good for equation (17) to be used as a useful approximation.

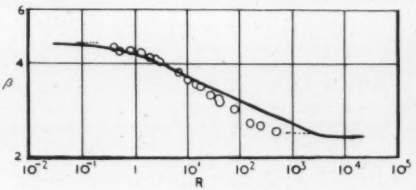

Fig. 2. Variation of the exponent of $(1 - c)$ with Reynolds number

——— = the theoretical result obtained in Section 6.
○ = experimental results of Richardson and Zaki.[10]

7. CONCLUSIONS

The theoretical expression $U = U_0(1 - c)^\beta$ appears to satisfy available experimental data on the sedimentation of suspensions of particles. The variation of β with Reynolds number can be expressed by the equation $\beta = \alpha/m$ where α is the value of β for streamlined flow and m is defined by equation (15).

The value of α has been found to vary from one suspension to another and may be considered to represent a shape factor. Its exact value for equi-sized, equi-density spheres is uncertain but is approximately 5.

The simple form of the equations makes them suitable for

general application and the physical picture used in their theoretical derivation may aid in the solution of related problems.

ACKNOWLEDGEMENTS

The authors would like to express their indebtedness to Dr. E. E. Jones for his help in arranging the paper, to Prof. F. B. Hinsley for valuable discussions and to the Scientific Department of the National Coal Board for financing the work.

REFERENCES

(1) STEINOUR, H. *Industr. Engng Chem.*, **36**, p. 618 (1944).
(2) STEINOUR, H. *Industr. Engng Chem.*, **36**, p. 840 (1944).
(3) RICHARDSON, J. F., and ZAKI, W. N. *Chem. Eng. Sci.*, **3**, p. 65 (1954).
(4) BURGERS, J. M. *Proc. K. Ned. Akad. Wetensch.*, **44**, p. 1177 (1941).
(5) HAWKSLEY, P. G. W. *Conference on some aspects of fluid flow*, The Institute of Physics, 1950, p. 114 (London: Edward Arnold and Co., 1951).
(6) ROBINSON, J. *J. Phys. Coll. Chem.*, **53**, p. 1042 (1949).
(7) HANCOCK, R. T. *Trans Inst. Min. Engrs*, **94**, p. 114 (1937–38).
(8) LEWIS, W. K., GILLILAND, E. R., and BAUER, W. C. *Industr. Engng Chem.*, **41**, p. 1104 (1949).
(9) HIRST, A. A. *Trans Inst. Min. Engrs*, **85**, p. 236 (1932–33).
(10) RICHARDSON, J. F., and ZAKI, W. N. *Trans Inst. Chem. Engrs (London)*, **32**, p. 35 (1954).
(11) NEEDHAM, L. W., and HILL, N. W. *Fuel (London)*, **26**, p. 101 (1947).
(12) GUREL, S. Ph.D. Thesis (University of Birmingham, 1951).
(13) WHITMORE, R. L. *Brit. J. Appl. Phys.*, **6**, p. 239 (1955).
(14) WHITMORE, R. L. Ph.D. Thesis (University of Birmingham, 1949).
(15) KERMACK, W. O., MCKENDRICK, A. G., and PONDER, E. *Proc. Roy. Soc. Edinburgh*, **44**, p. 170 (1928).

Resistance bias characteristic of the electron microscope gun

By M. E. HAINE, D.Sc., M.I.E.E., F.Inst.P.,* P. A. EINSTEIN, M.Sc., A.M.I.E.E.,* and P. H. BORCHERDS, B.Sc., Grad.I.E.E.,† Associated Electrical Industries Ltd., Research Laboratory, Aldermaston Court, Aldermaston, Berkshire.

[*Paper first received* 14 *April, and in final form* 30 *May*, 1958]

It has been shown in a previous paper[1] that the theoretical value of current density per unit solid angle (brightness) could be obtained from the hairpin cathode electron microscope gun for a wide range of geometrical design, provided an optimum bias voltage, which depended on the geometrical design, was applied between shield and cathode. When using a self-biasing arrangement, the total beam current tends to become stabilized by negative feed-back action. This is a valuable advantage but may lead to the impossibility of operating the gun at the optimum bias voltage. The present investigation shows that for a reasonably wide range of geometrical design, conditions can be established, with the correct choice of bias resistance, whereby the gun can be operated at theoretical brightness and with current stabilization, for a reasonable choice of filament temperature, giving a range for choice in beam angle or beam current.

INTRODUCTION

In a previous paper,[1] the measured characteristics of the high-voltage hot-cathode electron gun of the type commonly used in the electron microscope were described and discussed. Such a gun consists of a tungsten hair-pin filamentary cathode, a negatively-biased cathode shield electrode and an anode (Fig. 1). The shield has a circular hole on the axis, and may be shaped in a number of ways, as shown. It is usually flat or in the form of a re-entrant cone. The anode is flat and has a circular hole on the axis through which the beam emerges.

The factors most affecting the gun performance for a given anode voltage are the cathode temperature, the shield aperture diameter d, the shield shape, the filament height h (measured in thousandths of an inch, to the front edge) behind the shield, and the bias voltage.

When the emergent beam is focused to form a spot of minimum diameter, some virtual beam cross-section is imaged. This was termed the virtual source. Since, in many applications, the maximum usable beam angle is fixed by the aberrations of the imaging system, and, since the requirement, e.g. in the electron microscope, is usually to obtain a final image of maximum current density, the most important performance parameter of the gun is the current density per unit solid angle. This is called the electron beam brightness β and, in theory,[2] has a maximum value given by

$$\beta = \rho_c \phi_0 / \pi k T \qquad (1)$$

where ρ_c is the cathode current density, ϕ_0 the accelerating voltage, k is Boltzmann's constant (1/11 600 eV/° K), and T the absolute temperature of the cathode.

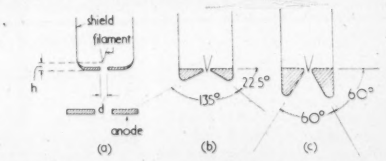

Fig. 1. Geometrical designs investigated
(*a*) flat, h measured in thousandths of an inch to the front edge.
(*b*) 22½° re-entrant; (*c*) 60° re-entrant.

It is sometimes important to operate the gun so as to obtain a specific value of beam angle, but more often this angle is determined by a physical aperture in the system,

*Now at Siemens Edison Swan Ltd., Research Laboratory, Templefields, Harlow, Essex.
† Now at the University, Cape Town, South Africa.

e.g. condenser lens aperture, in which case the beam angle from the gun need only be larger than the angle defined by this aperture.

Since the current density across the beam, emerging from the gun, has a Gaussian distribution, it is usually advantageous to make the beam angle sufficiently large so that the current density across the limiting aperture becomes fairly uniform. In addition, the use of a large total beam angle simplifies alignment of the beam and aperture. On the other hand, it may often be necessary to restrict the total beam current because of limitations in the high-voltage supply unit or for reasons of heat dissipation. This would set an upper limit to the beam angle, since the total beam current drawn from the gun increases as the square of this angle.

The maximum brightness for a given anode-voltage is limited by the cathode emission current density which in turn is governed by the cathode temperature; in practice, the latter should not exceed a value consistent with a reasonable filament life. Tungsten wire is generally used as a cathode material. Bloomer[3, 4] has investigated the variation of tungsten filament life and electron emission with temperature. From his results, a simple empirical relation (to a first approximation) between emission current density and life for a 0·005 in. diam. wire has been deduced, namely

$$t_l = 50/\rho_c \quad \text{h} \qquad (2)$$

where ρ_c is the cathode emission current density in A/cm^2.

From the earlier paper,[1] it was concluded that, for a fairly wide variation of the geometrical parameters (cathode height, shield aperture diameter and shield shape), there could always be found a value of bias voltage which would give a brightness substantially equal to the theoretical value of equation (1). At this optimum bias, however, the total current I_B and beam semi-angle α were found to vary for different geometrical designs. It is thus possible to select a required beam angle or total current by choice of geometrical design while maintaining the theoretical brightness.

It was shown that for cathode temperatures below about 2700° K (at this temperature, the cathode life is about 30 h), space-charge limitation of emission could be neglected. This last result was unexpected since previous papers had ascribed certain effects observed in this type of gun to space charge. Thus, the apparently most convincing evidence in favour of space-charge limitation of emission had been the observation that the total current is sharply saturated on increasing the temperature, an effect well known to electron microscopists. In the previous paper[1] it was, however, shown that this effect is solely due to the negative feedback action of the series cathode resistor used to generate the bias voltage, a gun using such a biasing arrangement being known as an automatically biased gun [see Fig. 2(*a*)]. With bias supplied from an independent (or "free") supply, no such "saturation" occurs until the temperature reaches higher values, and, even then, such saturation takes effect only gradually with increasing cathode temperature. The negative feedback action in the automatic bias gun is extremely useful in such instruments as the electron microscope, since it provides stabilization of the total beam current. It is the usual practice to raise the filament temperature until the total beam current reading shows that the "saturation knee" has been reached.

The use of a series resistor to generate the bias voltage leads to a difficulty in that the value of bias cannot easily be set to the value corresponding to optimum brightness. The setting is simplified if an adjustable bias resistor is used, but even then it cannot be guaranteed that the value of bias voltage generated across the bias resistor at the current saturation point is the "optimum value," i.e. value giving maximum brightness. The requirement for working at, or beyond, the current saturation point imposes yet a further limitation restricting the freedom of choice of the gun design.

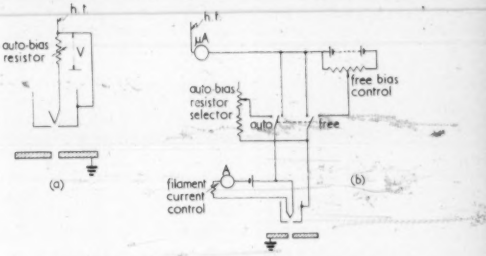

Fig. 2. (*a*) Resistor bias circuit. (*b*) Switching arrangement

It is the purpose of this paper to describe some measurements made to determine the conditions under which the theoretical brightness can be obtained at and near the current saturation point and at cathode temperatures at which it is desired to work.

EXPERIMENTAL ARRANGEMENT

The measurements were made on substantially the same apparatus as used for the earlier work.[1] Various electrode geometrical designs were investigated, and the bias resistor varied in value while the brightness and total beam current were measured as a function of the cathode heating current. At the same time, the maximum brightness under independent bias conditions was also measured as a function of the cathode heating current. This could be done quite quickly by operating the change-over switch to independent bias in the circuit of Fig. 2(*b*) while the gun was working. The ratio of the brightnesses under automatic bias and independent bias β/β_0 was noted for different filament currents.

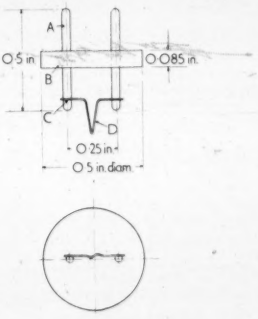

Fig. 3. Standard filament

A, 0·040 in. diam. nickel legs; *B*, ceramic insulator; *C*, beginning of weld; *D*, 0·005 in. diam. tungsten wire. Length of tungsten wire to beginning of weld = 13 mm.

The filaments used were made from 0·005 in. diam. tungsten wire, 13 mm long, bent into the shape shown in Fig. 3. The relation between life, theoretical brightness and filament heating current and temperature are shown in Fig. 4, some of the results being taken from the paper by Bloomer,[3] and also compounded from observed filament temperature end corrections.

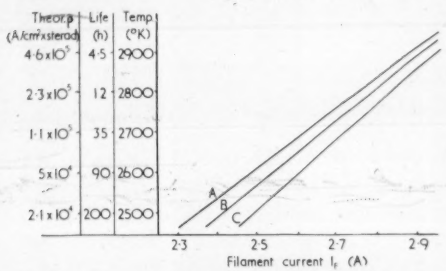

Fig. 4. Relation between filament current, temperature, life and β. Filament diameter = 0·005 in.

A, standard 13 mm filament; *B*, 12 mm filament; *C*, 11 mm filament.

RESULTS

The results are summarized in Fig. 5. The ratio β/β_0—shown dotted—of the brightness with automatic bias to the maximum brightness with free bias, and the total beam current I_B (for automatic bias) are ploted as a function of the filament heating current I_F, for a range of values of the filament height h behind the shield aperture and for various values of bias resistance. (Up to about 2700° K, β_0 has the theoretical value; above this temperature, the emission falls below the theoretical value as a result of space-charge limitation.) Results are given for the flat-ended shield, a 22½° conical shield and a 60° conical shield (Fig. 1). The shield hole aperture was 0·05 in. in diam. in the first two cases and 0·07 in. in the 60° re-entrant cone shield. The cathode-anode spacing was 0·5 in. and the accelerating voltage was 50 kV in each case. The values of β/β_0 for any given value of bias resistor vary so little with h for the flat shield that this ratio is shown plotted as a single curve for this geometrical design.

It will be noted that for any particular geometrical design the variation of β/β_0 with filament heating current shows a fairly broad maximum (of unity); the theoretical brightness can thus be obtained with automatic bias over a fairly useful range of filament temperatures. The temperature for which maximum brightness is obtained with automatic bias is a function of the cathode shield geometrical design, the value of the bias resistor and, with the exception of the flat shield, the filament height. It is thus possible to choose a bias resistor so that the maximum brightness occurs at any desired cathode temperature. It may also be desirable to obtain the maximum brightness with a reasonable economy of total beam current (i.e. for a small beam angle) and, furthermore, to operate beyond the beam current "saturation" point for reasons of current stability. The "saturation knees" are located on the $I_B - I_F$ curves, as indicated by dashed lines crossing the I_B curves on Fig. 5; the position of

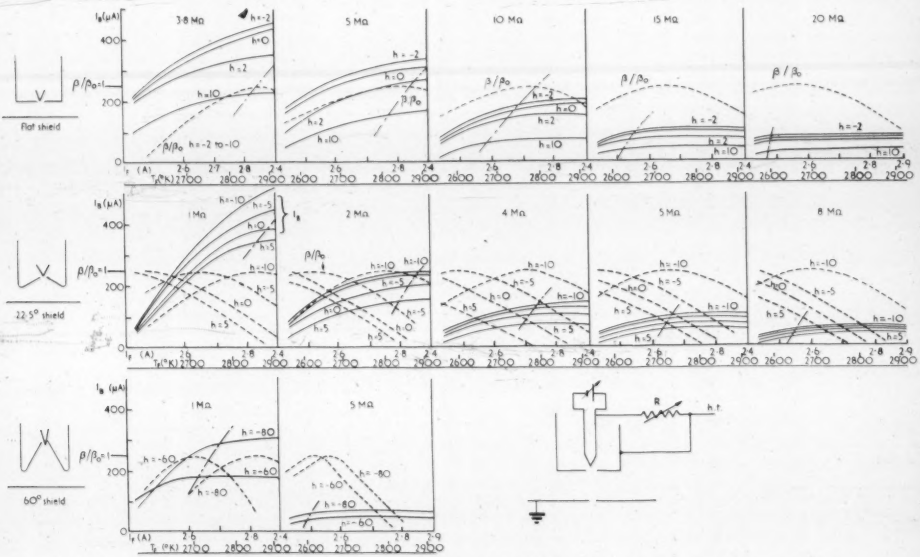

Fig. 5. Automatic bias characteristics for 50 kV and h measured in in. $\times 10^{-3}$

——— = I_B.

- - - - - = β/β_0.

·—·—· = saturation knee line.

the knee varies both with filament height and bias resistance although more markedly so with resistance.

To illustrate the use of the results, consider a case where maximum brightness is desired consistent with a filament life of, say, 12 h. From Fig. 4, it is seen that this corresponds to an operating temperature of 2800° K and a brightness of $2{\cdot}3 \times 10^5$ A/cm^2 × sterad in the absence of space-charge limitation. (In practice, the corresponding brightness obtained would be around $1{\cdot}6 \times 10^5$ for this temperature [see Fig. 5(*b*), reference (1)]. There is evidence that the temperature at which space-charge limitation commences becomes lower for more re-entrant shields.) The 13 mm filament will require a heating current of 2·75 A. With the flat shield, values of β/β_0 near unity will be obtained for values of bias resistor between 3·5 and 15 MΩ, but to operate also above the saturation knee, these values are restricted to 8–15 MΩ. The greater current economy is obtained with the higher bias resistors and larger values of h, i.e. with the filament behind the shield. A lower limit must, however, be set to the beam current since otherwise the beam angle becomes too small. For example, if a minimum beam semi-angle α of 0·005 rad is specified, the total current, which is given by

$$I = \beta \times \pi\alpha^2 \times \pi r_s^2 \qquad (3)$$

is about 130 μA, taking $\beta = 1{\cdot}6 \times 10^5$ A/cm^2 × sterad and the virtual source radius $r_s = 0{\cdot}0018$ cm, the latter varying only slightly with operating conditions [Fig. 4 of reference (1)]. Thus, for this minimum beam angle, the total current must not be less than this value. The curves (Fig. 5) show that this condition prescribes a value of h of about −0·002 in.

For the 22½° re-entrant shield, the "saturation" condition requires the use of a bias resistor of greater value than 5 MΩ, which, at the same time, brings the total current to less than 100 μA. Thus, a specified beam semi-angle greater than 0·005 rad cannot be achieved coincidentally with the other desired conditions. However, for normal electron microscope applications, a beam semi-angle of 0·003 rad is sufficient. This would be obtained at a total current of 50 μA. The gun alignment might now be rather critical as a result of the small beam angle, but, in any case, such high brightness and short filament life would only be required for most critical operation at the highest magnification.

In the table, which has been abstracted from Fig. 5, is set down a range of conditions for different filament temperatures or lives at which the maximum brightness would be obtained for currents which are saturated. The final two columns give the corresponding values of beam current and beam semi-angle. It is seen that any one of the three shield geometrical designs gives conditions which meet typical requirements, but the flat shield allows the greatest flexibility. There is some advantage in using a re-entrant shield since a lower bias voltage is required.

LIMITATION TO MAXIMUM CURRENT AND BEAM ANGLE

It will be noted that for the range of parameters covered by the table, the beam angle range is small, lying between 0·003 and 0·008 rad. It is of interest to consider the upper limitation imposed on this angle. For a given cathode temperature and with optimum bias the theoretical brightness is obtained. The total current and beam angle for this condition can be varied by varying the geometrical design. If the geometrical design is varied to give larger and larger total beam current, keeping the bias condition always optimum, the increasing current can only result from an increased emission area. When this area reaches a value equal to about half that of the roughly spherical cathode tip the beam begins to depart from its Gaussian angular distribution and tends to become hollow—a well-known effect which is associated with the formation of multiple spots in a focused image of the source [see reference (1)]. This effect sets an upper limit to the total current which is drawn at theoretical brightness and for a given source size.

Table 1. 50 *kV*

Shield	I_F (*A*)	T_F (*temp.*) (°*K*)	t_l (*life*) (*h*)	β_T (*theoret.*) (*A/cm²/sterad*)	β_0 (*sp. charge limited*)* (*A/cm²/sterad*)	*R, bias resist.* (MΩ)	*h (fil. height)* (*in.* × 10⁻³)	I_B (*beam current*) (μ*A*)	α, (*semi angle*) $= \sqrt{I_B/\beta\pi^2 r_s^2}$ (r_s = 0·0018 cm)
Flat shield	2·5	2615	80	$5{\cdot}8 \times 10^4$	$5{\cdot}8 \times 10^4$	20–15	−2 to +10	80 to 30	0·0065–0·004
	2·6	2680	40	$9{\cdot}6 \times 10^4$	$9{\cdot}6 \times 10^4$	15–20	0 to +10	100 to 50	0·0057–0·004
	2·7	2760	16	$1{\cdot}75 \times 10^5$	$1{\cdot}40 \times 10^5$	10–15	2 to +10	150 to 50	0·0057–0·0033
	2·8	2840	8	$3{\cdot}10 \times 10^5$	$1{\cdot}70 \times 10^5$	5–10	5 to +10	200 to 80	0·006 –0·004
22½° shield	2·5	2615	80	$5{\cdot}8 \times 10^4$	$5{\cdot}8 \times 10^4$	∼ 10	∼ −10	∼ 50	0·0052
	2·6	2680	40	$9{\cdot}6 \times 10^4$	$9{\cdot}6 \times 10^4$	8–10	−10	∼ 60	0·0045
	2·7	2760	16	$1{\cdot}75 \times 10^5$	$1{\cdot}40 \times 10^5$	6–8	−10	∼ 80	0·0042
	2·8	2840	8	$3{\cdot}10 \times 10^5$	$1{\cdot}70 \times 10^5$	3–4	−10	∼ 200	0·0060
60° shield	2·6	2680	40	$9{\cdot}6 \times 10^4$	$9{\cdot}0 \times 10^4$	2–5	−60 to −80	180 to 70	0·008 –0·005
	2·7	2760	16	$1{\cdot}75 \times 10^5$	$1{\cdot}40 \times 10^5$	1–2	∼ −70	∼ 230	0·007
	2·8	2840	8	$3{\cdot}10 \times 10^5$	$1{\cdot}70 \times 10^5$	1	∼ −80	∼ 300	0·007

* *See Fig. 5(b) of reference* 1.

EFFECT OF ACCELERATING VOLTAGE

All the present results were obtained at an accelerating voltage of 50 kV. For other voltages, if the small space charge effects are neglected, results may be deduced from the present ones as follows. If the anode voltage and at the same time the bias voltage are multiplied by a factor n, the emitting area and hence the total current will remain unchanged. To achieve this, the bias resistance must therefore be multiplied n times. The brightness will increase n times (because of the increase in anode voltage), and, if the virtual source size is unchanged, the beam angle will be reduced n times. From the small amount of data available,[1] it appears that the source size is little affected by h.t. voltage,

Thus, the present curves can be applied to obtain information at voltages equal to $50 \times n$ kV, if the bias resistor values are multiplied by n.

ACKNOWLEDGEMENT

The authors are indebted to Dr. T. E. Allibone, Director of the Research Laboratory, Associated Electrical Industries, for permission to publish this paper.

REFERENCES

(1) HAINE, M. E., and EINSTEIN, P. A. *Brit. J. Appl. Phys.*, **3**, p. 40 (1952)
(2) LANGMUIR, D. B. *Proc. Inst. Radio Engrs*, **25**, p. 977 (1937).
(3) BLOOMER, R. N. *Brit. J. Appl. Phys.*, **8**, p. 83 (1957).
(4) BLOOMER, R. N. *Proc. Instn Elect. Engrs B*, **104**, p. 153 (1957).

The friction of mineral particles

By R. T. SPURR, Ph.D., B.Sc., Ferodo Limited, Chapel-en-le-Frith, Stockport, Cheshire

[*Paper received* 3 *April*, 1958]

The coefficient of friction of loose particles slid between parallel plates is approximately proportional to the Mohs hardness of the particles. The particles are crushed during sliding.

In general no quantitative relationships have been observed between the physical properties of surfaces and their coefficients of friction. Parker and Whittaker,(1) however, found that under certain circumstances the friction of resin blocks filled with mineral powders was related to the Mohs hardness H of the mineral. They loaded the resin specimens against a rotating cast iron annulus driven by an electric motor and found that when the surfaces came to rest on switching off the motor, the friction increased to a value such that μ (the coefficient of friction) was proportional to H. As μ depended upon the hardness of the filler alone, and not upon the resin matrix, the filler was presumably carrying all of the normal load at the end of a stop; consequently the μ of the mineral filler must have been proportional to its Mohs hardness. An investigation was therefore made of the relationship between the friction and hardness of minerals. It was found that there was no correlation between the μ and the hardness of minerals in bulk form but that there was correlation when the mineral was in powder form and so the friction of powders has been examined in some detail. The results are of some practical interest as mineral particles are sometimes used to increase the friction between railway wheels and the rails.

EXPERIMENTAL DETAILS

Static friction was measured on a trolley apparatus described elsewhere.(2) The powders were very lightly sprinkled on to a plate mounted on the trolley, the distance between the particles being greater than their diameter. Smooth flat blocks about $1\frac{1}{2}$ in. square were then loaded by a lever against the powders and the friction determined by applying a horizontal force to the trolley through a spring balance. A normal load of 1 kg was generally used and the particles were in the size range 70–120 I.M.M.

RESULTS AND DISCUSSION

The friction of particles of twelve different materials sliding between smooth copper surfaces was measured. The μ of the various minerals are shown plotted against their Mohs hardness H in Fig. 1. Each point represents the average of at least fifty measurements, and the ranges indicate the range of the averages of sets of ten measurements, not of individual measurements. Some of the scatter in the results was due to the difficulty of getting all the particles to the same state of cleanliness and dryness; furthermore some of the minerals could not be obtained in the desired particle size range. The values of Mohs hardness were obtained mainly from the Handbook of Chemistry and Physics 1943–4.(3) It can be seen from Fig. 1 that most of the experimental points lie about a straight line. The points lie

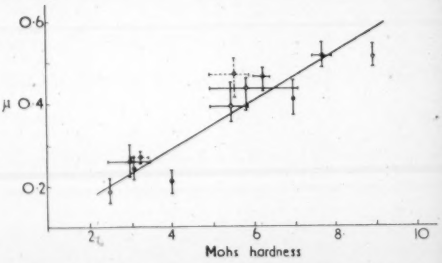

Fig. 1. μ of particles plotted against Mohs hardness

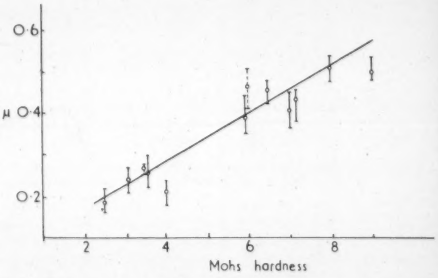

Fig. 2. μ plotted against the maximum Mohs hardness

closer to such a line if μ is plotted against the maximum value of H (Fig. 2).

Some measurements were made using normal loads of 100 to 4000 g and particle sizes ranging from $-20 + 40$, to -200 I.M.M. There was a tendency for μ to increase with

load at light loads, and to increase slightly with increasing particle size.

A range of particles was slid between blocks of metals and non-metals and a polished copper plate. The harder surfaces tended to give the lower frictions but the effect of surface hardness was small compared with that of the particle hardness. Perspex and polythene surfaces, however, gave much lower frictions with the harder particles than metals of comparable hardness and were not so badly damaged during sliding. Presumably materials of low elastic modulus can deform sufficiently to make small particles relatively ineffective. The friction of the particles was influenced by the roughness of the surfaces. If copper surfaces were abraded with 000 emery the μ, particularly of the softer particles, was greater when the scratches were perpendicular than when parallel to the direction of sliding. All the particles had much the same μ when slid between copper surfaces abraded with 2 emery, the scratches being perpendicular to the direction of sliding. The particles are more or less keyed into place in rough surfaces, consequently if the opposing surface is soft compared with the particles it suffers considerable damage and the friction is no longer determined by the particles themselves for the ploughing of the surface also contributes to the friction. Rather similar results were obtained when the particles were glued to the lower surface, the plate being covered with a very thin film of Durofix and the particles sprinkled on to the Durofix. Measurements were made with the surfaces covered with a very thin film of oleic acid. The results were similar to those obtained with uncontaminated surfaces, but the μ was reduced by about 0·1 for each mineral.

Particles were slid between a glass and a metal plate and their behaviour observed with a binocular microscope. The load bearing particles did not roll but tended to be crushed during sliding, even in the case of hard particles, of e.g. silica, suggesting that the particles have to be fractured before sliding can occur. The "fracture strength" F of the minerals available in bulk form was therefore measured by loading a $\frac{1}{2}$ in. steel ball against $\frac{1}{2}$ in. cubes of the minerals in a Howden test machine (500 lb capacity) and increasing the load until the specimen fractured. Generally the specimen broke into only two or three pieces, the augite and celestite, however, crumbled. The measurements were reasonably

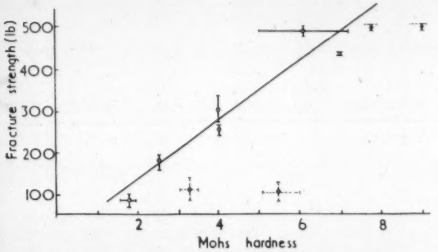

Fig. 3. Fracture strength plotted against Mohs hardness

reproducible except in the case of calcite. The fracture strength of the minerals was approximately proportional to their Mohs hardness (Fig. 3) except for the minerals that crumbled (represented by dotted lines in the figures). A relationship between F and H is not altogether surprising for when one mineral is scratched by another, fragmentation occurs along the track. In Fig. 4 μ is plotted against F; provided the augite and celestite results are omitted, the experimental points fall about a straight line.

Presumably the relationship that exists between the stress required to fracture a specimen and its load carrying capacity

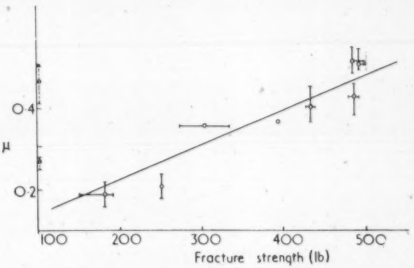

Fig. 4. μ plotted against fracture strength

when fractured on the Howden machine, is similar to that existing between the force required to fracture a particle and so permit sliding and the load it carries when tested on the friction apparatus.

The sliding behaviour of the minerals in bulk form is quite different to that of the minerals in particle form. Hemispherical specimens of rocksalt were made by compacting sodium chloride in a cylindrical die, one end of which was closed by a polished plate containing a large Brinell impression. The hemispheres were slid against glass plates and at the same time the apparent contact area between specimen and plate was examined microscopically. No fracture or fragmentation occurred, instead the rocksalt flowed in a plastic manner and the constant area remained smooth and polished (compare King and Tabor[4]). Rocksalt particles, however, fractured when slid between glass plates. Bulk specimen of other minerals were slid on metal and glass surfaces and very little damage occurred.

The equation relating μ and H for loose particles obviously does not apply when H is small. It is difficult to reconcile this equation, and the relationship between F and H, with Tabor's linear relationship[5] between H and log (indentation hardness) for minerals. The latter relationship involves only the plastic properties of the minerals whereas the "fracture strength" involves other properties as well.

ACKNOWLEDGEMENTS

The author would like to thank Mr. G. Parker who carried out most of the experimental work, and the Directors of Ferodo Ltd. for permission to publish this paper.

REFERENCES

(1) PARKER, R. C., and WHITTAKER, E. J. W. *Proc. Phys. Soc. B*, **64**, p. 126 (1951).

(2) SPURR, R. T. *Brit. J. Appl. Phys.*, **6**, p. 402 (1955).

(3) *Handbook of Chemistry and Physics*. Pp. 1188–1203 (Cleveland: Chemical Rubber Publishing Co., 1943–4).

(4) KING, R. F., and TABOR, D. *Proc. Roy. Soc. A*, **223**, p. 225. (1954).

(5) TABOR, D. *Proc. Phys. Soc. B*, **67**, p. 249 (1954).

The magnetic stabilization of low pressure d.c. arcs

By H. Wroe, M.Sc., Metropolitan-Vickers Electrical Co. Ltd., Trafford Park, Manchester

[*Paper received* 2 *May*, 1958]

Self-sustaining d.c. arc discharges between solid metal electrodes at pressures down to 10^{-4} mm of mercury have been investigated. At pressures below a few millimetres of mercury, arcs on both refractory and non-refractory metals behaved like "cold cathode" arcs. "Spot-splitting" and "reverse driving" of the cathode spot were observed and a form of instability is described. Reverse driving of the cathode spot or spots by the magnetic field set up by the current in the electrodes themselves is suggested as the cause of the instability.

A magnetic method of stabilizing the discharge is described, requiring an axial magnetic field of at least 500 G. A marked constriction of the positive column was caused with this value of field.

The magnetically stabilized discharge has been used experimentally to produce short welds on $\frac{1}{8}$ in. thick mild steel plate at 1 μ of mercury pressure using about 40 A at 30 V.

There is a growing interest at the present time in the uses of arc discharges between solid metal electrodes at low gas pressures, for the production and fabrication of the rare metals without contamination. High temperatures can be produced at the electrodes of an arc, thus enabling the refractory metals, like molybdenum, to be melted. Also, an arc discharge at low gas pressure, say a few microns of mercury, reduces contamination to a minimum. The production of ingots, alloys and the welding of the rare metals is becoming an important aspect of nuclear reactor technology.

Little fundamental work has been done on low pressure arcs between refractory electrodes, and the present paper deals with some results obtained from such an investigation. Direct currents up to 400 A were available, and most of the work was done with currents of the order of 100 A and pressures down to 10^{-4} mm of mercury.

General Form of Low Pressure Discharges between Solid Metals

The behaviour of an arc between refractory metal electrodes, e.g. tungsten, at a pressure of 1 μ of mercury is quite different to that at a pressure of a few centimetres of mercury. A photograph of a 120 A arc between tungsten electrodes in argon at a pressure of 10 cm of mercury is shown in Fig. 1.

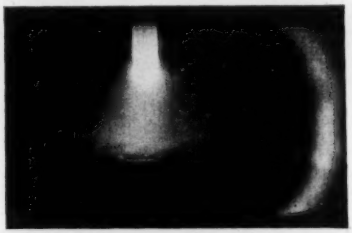

Fig. 1. Photograph showing 120 A d.c. arc in argon at 10 cm mercury pressure, between $\frac{1}{8}$ in. diameter tungsten cathode (above) and tungsten block anode; 12 mm gap

It is quite stable and is a typical thermionic arc.[1] Also it is the type of discharge utilized in small, inert electrode arc furnaces which operate in a gas atmosphere in this pressure range. When the gas pressure is reduced, this arc either extinguishes or goes over to a completely different mode of operation, which seems to be typical of vacuum arcs whatever the electrode metal. This is illustrated in Fig. 2, which was obtained at a pressure of 15 mm of mercury. The behaviour at the lowest pressures is identical to that shown in Fig. 2, except that the positive column tends to fill the whole arc chamber. Thus the discharge resembles a low pressure mercury arc in having a small, luminous cathode spot region in random motion and a diffuse positive column—often called the "cold cathode" arc.

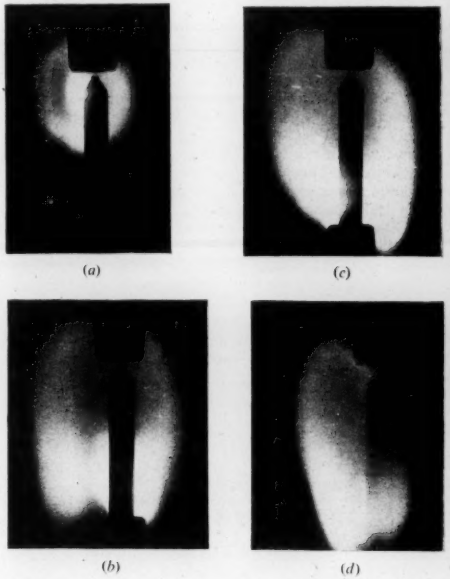

Fig. 2. Photograph showing 70 A arc in argon at 15 mm of mercury pressure, between $\frac{1}{8}$ in. diameter tungsten cathode (below) and $\frac{1}{4}$ in. diameter tungsten anode. Electrodes have just separated. Cine photograph at 1120 frames per second, time increasing from left to right

For currents up to a few hundred amperes, it exhibits a peculiar instability in the sense that the cathode spot will not

remain near the end of a cylindrical cathode, but always moves along it in the direction of current flow in the electrode itself. Thus in Fig. 2, the arc was started by touching the electrodes together and, although they have only separated about 0·8 mm, the cathode spot has moved an appreciable distance along the electrode. It is suggested that this is an effect due to the magnetic field of the current in the electrode itself, but no detailed discussion will be given at this stage. For much experimental work on continuously running arcs and for some practical applications, e.g. welding at low gas pressures, the phenomenon presents a serious problem. Also, for welding, the current density at the anode at low pressures is much too low to provide the concentrated heat source which is required for good welds. The remainder of the paper describes a solution to these problems.

MAGNETIC EFFECTS WITH LOW PRESSURE D.C. ARCS

It has been stated by Smith[2] that a magnetic field at an angle to a surface on which a cathode spot exists, will deflect the spot from the obtuse angle between the field and the surface and towards the acute angle (see Fig. 3). This effect

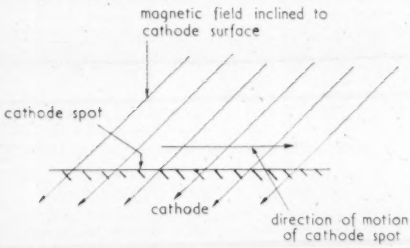

Fig. 3. Diagrammatic representation of effect on a cathode spot of a magnetic field inclined to the cathode surface

was found to occur in the present work and has been utilized to control the motion of the cathode spot as indicated in Fig. 4. Here the pointed magnet pole-piece provides a shaped field which intersects the cathode surface at an angle, the arrangement being symmetrical with respect to the axis of the system. Thus the cathode spot always has a tendency to move towards the axis, and in practice the motion is confined to a small region as shown in Fig. 4.

An alternative arrangement, often more convenient in practice, is shown in Fig. 5. The shaped cathode is in a uniform axial magnetic field which is thus at an angle to the conical surface and the cathode spot is confined to a small region near the tip.

It was found that field strengths of at least 500 G were required at the cathode for reliable stabilization, the direction of the field being immaterial. The inclination of the field does not seem to be very critical and an angle of about 45° is normally used. It was found that a field strength of 1000 G would stabilize an arc on a cathode $\frac{1}{4}$ in. in diameter. With the uniform field arrangement (Fig. 5) a pronounced constriction of the positive column was produced, as shown in Fig. 6, thus giving rise to a much more concentrated energy input to the anode than exists with the unstabilized arc. Short welds have been produced with this discharge (see the next Section).

The phenomenon of "spot splitting" is well known for mercury arcs[3]—the discharge preferring to carry a high current in a number of spots rather than the whole current in one spot—and it has been observed in the present work with magnetically stabilized arcs.

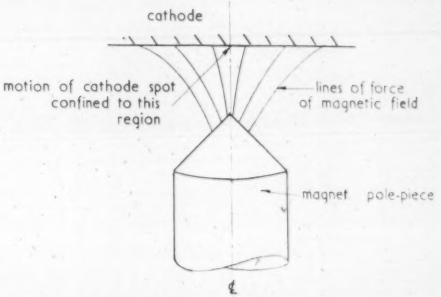

Fig. 4. Diagrammatic representation of method of stabilizing a cathode spot on a plane cathode by means of a shaped magnetic field. The magnet pole-piece may or may not be the anode of the discharge

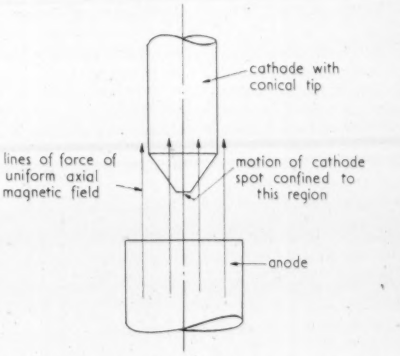
cathode with conical tip
lines of force of uniform axial magnetic field
motion of cathode spot confined to this region
anode

Fig. 5. Diagrammatic representation of method of stabilizing a cathode spot on the end of a cylindrical cathode by means of a uniform magnetic field

If the cathode is allowed to melt so that its shape alters then the stabilization often breaks down. Thus for small cathodes (say $\frac{1}{4}$ in. in diameter) which cannot be water cooled, the arc current cannot exceed a few tens of amperes for reliable stabilization. Material is lost from the cathode by evaporation from the spot region and also (mostly) by the ejection of small globules of molten metal. This is probably due to the violent evolution of gas from the metal under the cathode spot, and the rate of loss of metal was found to increase as the temperature of the cathode as a whole increased. Thus with a given water-cooling system a copper cathode was eroded at a lower rate than a steel one of identical shape and size, owing to the greater thermal conductivity of the copper.

Arcs have been stabilized on copper, steel, aluminium and

aluminium alloys, nickel, germanium, zirconium, molybdenum and tungsten—most of these being of ordinary commercial purity. It was found that a low pressure arc could be maintained most easily on the more readily vaporizable metals. In the case of tungsten, the discharge always extinguished after a fraction of a second.

Fig. 6. Magnetically stabilized arc. Current, 30 A; arc voltage, 30 V; axial magnetic field, 800 G; pressure, 8×10^{-4} mm of mercury; residual gas, air; gap length, 1 cm. Water-cooled copper cathode (above) machined to conical shape. Steel anode. One frame of a cine photograph at 450 frames per second

Returning to Fig. 3, the component of the magnetic field which is parallel to the surface will deflect the cathode spot in a direction which is perpendicular to the plane of the paper. At low pressures the direction of this motion was found to be opposite to that predicted by the left-hand rule—the well-known phenomenon of "reverse driving". It is suggested that the basic cause of many instability troubles with vacuum arcs is reverse driving of the cathode spot or spots by the magnetic field due to the current flowing in the electrodes themselves.

THE APPLICATION OF MAGNETICALLY STABILIZED ARCS TO WELDING AT LOW PRESSURES

Provided the conditions set out in the previous section are complied with, a magnetically stabilized arc can be used for welding at pressures of the order of 1 μ of mercury.[4] The magnetic field can be produced by a coil placed outside the vacuum chamber, with suitable design of the latter, or by permanent magnets carried with the cathode inside the chamber, as shown in Fig. 7. This device has been used experimentally to produce short runs of weld on $\frac{1}{8}$ in. thick mild steel plate at a pressure of 1 μ of mercury with an arc current of about 40 A at 30 V. The guard ring is necessary when using a cathode of magnetic material, e.g. steel, in order to preserve the correct field shape at the cathode surface. In this case, of course, the cathode is non-consumable and either a separate filler rod must be used in the weld, or the joint must be such that two edges have merely to be fused together.

A possible extension of the method to enable a consumable steel electrode to be used is shown in Fig. 8. Here the steel tube forms a guard ring and provides a symmetrical field inclined to the side of the cathode as shown, and thus the motion of the spot is confined to the end portion. This arrangement was successful in stabilizing the arc but has not yet been tried for welding.

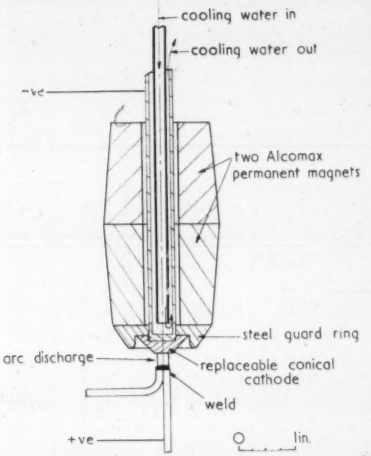

Fig. 7. Cross-section of electrode arrangement for vacuum welding with stabilizing field produced by permanent magnets

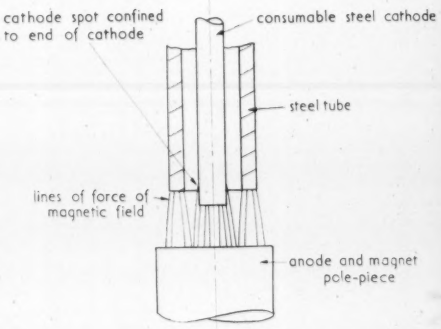
cathode spot confined to end of cathode
consumable steel cathode
steel tube
lines of force of magnetic field
anode and magnet pole-piece

Fig. 8. Diagrammatic arrangement for magnetic stabilization permitting a consumable cathode to be used

CONCLUSIONS

At pressures below a few millimetres of mercury self-sustained d.c. arc discharges behave like "cold cathode arcs" whether the cathode material is refractory, like tungsten, or non-refractory, like copper. Some of the phenomena associated with the mercury arc cathode, such as "spot splitting" and "reverse driving", have been observed with arcs on refractory metals in vacuum.

It is suggested that instability of the d.c. vacuum arc is often due to reverse driving of the cathode spot in magnetic fields set up by the current flowing in the electrodes themselves.

The motion of the cathode spot can be confined to a small area on a plane cathode by a suitably shaped magnetic field. Also it can be confined to the end of a cylindrical cathode by a uniform, axial magnetic field, provided the end of the electrode is conical in shape. Field strengths of at least 500 G are required at the cathode surface for reliable stabilization. Such a field gives rise to a marked constricting of the arc positive column.

It is considered that a magnetically stabilized arc could be used for welding in vacuum.

ACKNOWLEDGEMENTS

The author thanks Dr. Willis Jackson, Director of Research and Education, Metropolitan-Vickers Electrical Co. Ltd., for permission to publish.

REFERENCES

(1) DRUVESTYEN, M. J., and PENNING, F. M. *Rev. Mod. Phys.*, **12**, p. 142 (April, 1940).
(2) SMITH, C. G. *Phys. Rev.*, **69**, p. 96 (1946).
(3) FROOME, K. D. *Proc. Phys. Soc.* [*London*], **60**, p. 424 (1948).
(4) Improvements relating to the stabilization of low-pressure d.c. arc discharges. Patent application No. 16569/57.

The grid emitting properties of titanium

By J. A. CHAMPION, M.Sc., A.Inst.P., Research Laboratories of The General Electric Co. Ltd., Wembley, England

[*Paper first received* 6 *May, and in final form* 29 *May*, 1958]

Experiments are described in which the emission from thin films of barium and barium oxide deposited on titanium is compared with that from similar deposits on tungsten. With deposits of both barium and barium oxide the emission from titanium is very much less than that from tungsten throughout the temperature range investigated (700–1000° C). Above about 900° C the evaporation of titanium will poison the emission of an adjacent oxide cathode, but it is concluded that from 700° C up to this temperature titanium would possess good grid emission suppression properties. This could enable titanium to be used as a screen grid winding wire in the place of carbonized molybdenum wire in a number of receiving valves, and as an electrode material in other electronic devices where hot electrodes become contaminated with cathode material.

INTRODUCTION

The problem of stray thermionic emission from hot electrodes, usually known as "grid emission" occurs in both radio valves and in electron beam devices. In radio receiving valves control grids are usually heated only by radiation from the oxide-coated cathode and to temperatures not exceeding 500° C. Unwanted emission from deposits evaporated from the cathode on to such grids may be suppressed adequately by plating the grid winding wires with gold. This has been reported by Baker[1] and by others.

The winding wires of screen grids in tetrode or pentode valves may, however, reach considerably higher temperatures as they are heated by electron bombardment as well as by radiation; and the operation of circuits containing such valves may be impaired if the screen grid emission is excessive. For example, the line time base circuit in a television set will not function satisfactorily if the screen grid emission from the valve used is greater than about 0·1 mA, corresponding to about 0·1 mA cm^{-2} for a typical valve screen grid. If, however, the emission from the screen grid wound with untreated tungsten or molybdenum wire were so restricted, the output obtainable from an acceptable size of valve would only be about a fifth of the desired level. It is inadvisable to use gold-plated material for the winding wire of screen grids since, although gold will adequately suppress the grid emission there is considerable likelihood of the gold evaporating in sufficient quantities to "poison" the emission from the cathode within a relatively short period. As discussed in a previous paper[2] carbon may be satisfactorily used for the suppression of screen grid emission, but it does suffer from certain undesirable features.

The problem of stray emission from hot electrodes also occurs in electron beam devices containing either oxide-coated or barium dispenser cathodes. In such cases the electrode temperatures may be too high for gold plating to be used and it may well be impracticable to process carbonized electrodes to a sufficiently high temperature.

For these several reasons an alternative method would be very welcome for suppressing emission from electrodes at temperatures above 600° C on to which evaporation products from oxide or barium dispenser cathodes have been deposited. Some previous observations in these laboratories suggested that titanium probably possessed good grid emission suppressive properties. In a recent paper Espersen and Rogers[3] studied the grid emission from titanium, as well as other materials, when contaminated with the evaporation products from "L" cathodes and concluded that it possessed excellent grid emission inhibiting properties. In the present work experiments have been performed in which the emission from separate barium and barium oxide deposits on titanium was compared with that from similar deposits on tungsten, which behaves in much the same way as molybdenum[2] but is easier to clean.

Experiments were also carried out to determine whether a titanium wire heated in the presence of an oxide-coated cathode had any harmful effect on the cathode emission and if so, the maximum permissible operating temperature for titanium.

DEPOSITION EXPERIMENTS

Experimental valve. The valve used for the deposition experiments was similar in design to that used in earlier work[2] and is shown in Fig. 1. Either barium or barium oxide could be evaporated on to a titanium wire and on to a tungsten wire. The barium source was a "batalum" getter, consisting of a reaction mixture of barium orthotitanate and beryllium deposited on a molybdenum strip. The barium oxide source was a spiral of platinum wire coated by spraying with a barium carbonate suspension. The two sources were shielded from each other. Both wires and sources could be heated independently electrically and the thermionic emission

from the wires could be drawn to a surrounding nickel anode. The temperature of the elements could be observed optically through slots in the anode and, unless otherwise stated, all temperatures quoted for the wires include a correction for the spectral emissivity. A getter assembly which releases barium when heated was also fixed to the bottom of the foot tube.

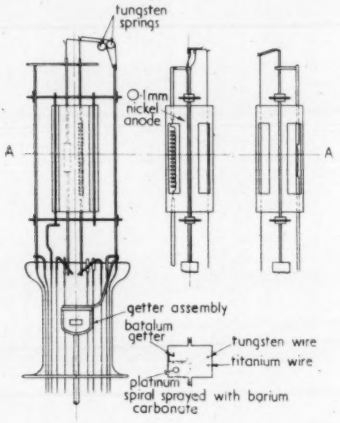

Fig. 1. Valve assembly used for deposition experiments
Inset, section through *A–A*.

The valve was evacuated and baked on a mercury diffusion pump with liquid air trap, after which the anode and getter assembly were outgassed by eddy current heating. Next the "batalum" getter was outgassed and the barium carbonate on the spiral converted to the oxide, both by electrical resistance heating. The titanium wire was outgassed by heating to about 1000° C for 2 min and the tungsten wire was heated to about 2300° C for 2 min to clean it. Finally the barium was evaporated from the getter assembly and the valve sealed off from the pump.

In order that the temperature of the titanium and tungsten wires would be known during subsequent experiments, temperature-current graphs were constructed for both using an optical background pyrometer.

Deposition of barium. Experiments by Brodie and Jenkins[4] on the evaporation from dispenser cathodes have shown that the evaporation increases rapidly with temperature, but for typical operating conditions an impregnated cathode at 1030° C has a rate of evaporation of about 1 monolayer in 8 min, the evaporant being barium with a small amount of barium oxide. The rate of evaporation increases to about one monolayer/min at 1100° C. Since in most valves the distance between grids and cathode is small, the rate of deposition on to the grids may be taken as equal to the rate of evaporation from the cathode.

Calculations based on the lives of receiving valves show that the rate of evaporation of barium from oxide-coated cathodes when run under very onerous conditions is just under 1 monolayer/min and when run under more normal conditions is a factor of about 10 less than this. During the processing of a normal receiving valve the temperature of the cathode ranges from 900–1050° C, and the vacuum is considerably worse than that maintained during normal operation. As a result of this the deposit is likely to be mainly barium oxide and the rate of deposition of the order of 20 monolayers/min. The experiments therefore used deposition rates corresponding approximately to the foregoing figures.

In the first experiment barium was deposited with the receptors cold. At intervals the saturated emission was measured at 700° C for an anode potential of 50 V. It was found that the emission from the tungsten wire reached a maximum of about 1 mA cm^{-2} after about 22 min of deposition. This maximum would correspond to a deposit one monolayer thick.[5] The emission from the titanium wire reached a maximum of 0·55 mA cm^{-2} after about 22 min of deposition, but in this case the maximum was not so well defined. After about 2 monolayers the deposition was stopped, the temperature of the titanium wire maintained at 700° C and the change of emission with time observed. The result is shown in Fig. 2. When the tungsten wire was

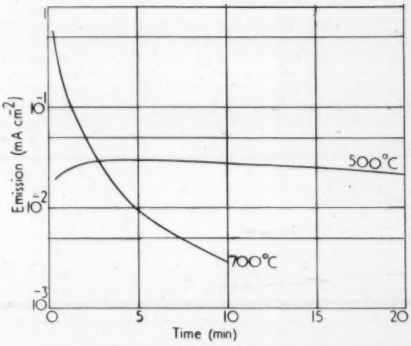

Fig. 2. Change of emission with time from titanium wire when heated to different temperatures after about 2 monolayers of barium had been deposited on to it

heated to 700° C the emission remained steady. After this experiment the wires were cleaned, the tungsten wire by heating to 2300° C and the titanium wire by heating to 1000° C.

The experiment was repeated for titanium with the emission measurements made at 500° C instead of 700° C. The emission from the titanium wire reached a maximum of 0·018 mA cm^{-2} after about 20 min of deposition. After about 2 monolayers the deposition was stopped, the titanium wire was kept at 500° C and the change of emission with time observed, and this is also shown in Fig. 2. After these experiments the wires were again cleaned as described above.

Further experiments were carried out in which barium was deposited at the rates of 1 monolayer in 1, 3 and 10 min on to tungsten and titanium wires heated to a temperature of 700° C. Fig. 3 shows the achievement of steady emission in each of these experiments. It will be noticed that in each of the experiments performed with titanium the steady emission is about two orders of magnitude lower than the corresponding steady emission from tungsten.

After the above experiments had been carried out, the effect of operating the tungsten and titanium wires at successively higher temperatures was investigated with barium deposited continuously at the rate of 1 monolayer in 1, 3 and

10 min. The results are given in Table 1. It was noticed that when the temperature of tungsten was raised to 1000° C the emission at first rose somewhat, but soon settled to a steady value less than that at 700° C. Presumably this was due to the re-evaporation of the barium from the tungsten wire at the higher temperature till a new equilibrium was reached. The behaviour of the titanium wire at temperatures between 700° C and 850° C was investigated in more detail for the most severe case and the results are shown in Table 2.

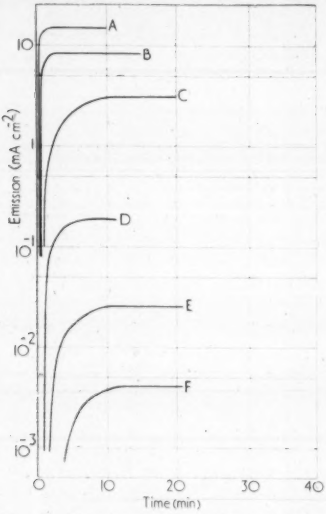

Fig. 3. Change of emission with time from tungsten and titanium wires heated to 700° C as barium was deposited on to them for three different rates of deposition

A, tungsten: 1 monolayer in 1 min; *B*, tungsten: 1 monolayer in 3 min; *C*, tungsten: 1 monolayer in 10 min; *D*, titanium: 1 monolayer in 1 min; *E*, titanium: 1 monolayer in 3 min; *F*, titanium: 1 monolayer in 10 min.

Table 1. *Steady emission achieved when barium was deposited at various rates on to heated tungsten and titanium*

Rate of deposition of barium	*Temperature of tungsten and titanium* (° C)	*Steady emission from tungsten* (mA cm^{-2})	*Steady emission from titanium* (mA cm^{-2})
1 monolayer in	700	15	0·18
1 minute	850	65	<0·00002
	1000	13	<0·00002
1 monolayer in	700	8·5	0·025
3 minutes	850	27	<0·00002
	1000	3·3	<0·00002
1 monolayer in	700	3·1	0·004
10 minutes	850	13	<0·00002
	1000	0·7	<0·00002

Deposition of barium oxide. It has previously been deduced from measurements of deposited material that during the processing of receiving valves with oxide-coated cathodes a layer of barium oxide of the order of 10^{-5} cm or about 500 monolayers thick is deposited on the screen grids. Also previous estimates from the appearance of interference fringes showed that when the platinum spiral coated with barium oxide was heated to 1100° C barium oxide is deposited at a rate of about 20 monolayers/min. At 1150° C the rate would be about 100 monolayers/min and at 1050° C about 5 monolayers/min.

Table 2. *Steady emission achieved when barium was deposited at a rate of* 1 *monolayer/min on to heated titanium*

Temperature of titanium (° C)	*Steady emission from titanium* (mA cm^{-2})
700	0·18
740	0·50
770	0·33
800	0·15
850	<0·00002
1000	<0·00002

In a further series of experiments the emission from layers of barium oxide on titanium was compared with that from similar deposits on tungsten. The evaporation took place from the platinum spiral coated with barium oxide and heated electrically to a luminance temperature of 1150° C at the rate of about 100 monolayers/min. During deposition the receptors were cold. At intervals the titanium and tungsten wire were in turn heated to a temperature of 700° C and the emission measured by applying a potential of 50 V to the anode. After 15 min the emission from the titanium had reached a steady value of 0·45 mA cm^{-2} and that from the tungsten had reached a steady value of 4·4 mA cm^{-2}.

The deposition of barium oxide was continued subsequently for a further 45 min, the emission from the tungsten and titanium wires remaining fairly steady. By the end of this time it was estimated that a layer of barium oxide about 10^{-4} cm thick had been deposited. The tungsten and titanium wires were then heated to 700° C and the change of emission with time observed and after 10 min the tem-

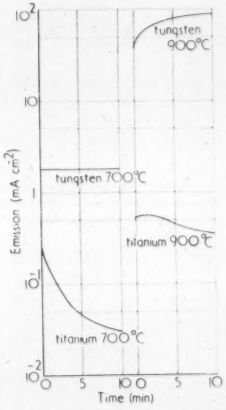

Fig. 4. Change of emission with time from tungsten and titanium wires when heated to different temperatures after about 10^{-4} cm barium oxide had been deposited on to them

perature of the wires was raised to 900° C. The results are shown in Fig. 4.

Further experiments were carried out in which barium oxide was deposited at a rate of about 20 monolayers/min on to heated tungsten and titanium wires. The temperature of the wires was initially 700° C and was subsequently increased to 850° C and later to 1000° C. In each case the wires were maintained at temperature until the emission became steady, and the results are shown in Table 3.

Table 3. *Steady emission achieved when barium oxide was deposited at a rate of about 20 monolayers/min on to heated tungsten and titanium*

Temperature of tungsten and titanium (° C)	*Steady emission from tungsten* ($mA\ cm^{-2}$)	*Time for emission from tungsten to become steady* (*min*)	*Steady emission from titanium* ($mA\ cm^{-2}$)	*Time for emission from titanium to become steady* (*min*)
700	17	20	2·9	15
increased to 850	110	1 (after increasing temperature from 700° C)	0·0017	10 (after increasing temperature from 700° C)
increased to 1000	87	8 (after increasing temperature from 850° C)	0·0008	4 (after increasing temperature from 850° C)

POISONING EXPERIMENTS

The tubes used for the poisoning experiment contained a rectangular conventional oxide cathode sprayed on one side only, and a titanium wire 0·25 mm diameter was supported 2 mm in front of the coated face. A nickel anode was placed between the wire and the cathode. This anode could slide on supporting rods so that the cathode could either be shielded from, or exposed to, the titanium wire. A barium getter was fixed to the bottom of the assembly. In those tubes in which the titanium wire was heated above 1000° C a further shield was included to prevent blackening of the glass envelope by deposition of titanium.

After evacuating and baking the valve on a mercury diffusion pump with liquid air trap, the anode and getter were outgassed, following which the carbonate cathode coating was converted to oxide. Finally the barium was evaporated from the getter and the valve sealed off from the pump. The tube was given a normal activation and a run under operating conditions to stabilize the emission and vacuum. In these experiments the cathode activity was estimated by measuring the total emission at reduced temperature. Between measurements the titanium wire was heated and the cathode run at the typical operating temperature of 700° C. A separate tube was used for each temperature run.

Table 4. *Change in emission from an oxide-coated cathode when exposed to a heated titanium wire*

Temperature of titanium (° C)	*Time* (*h*)	*Emission change (at "knee" with cathode temperature reduced)*
900 (i)	12	none
900 (ii)	153	increase from 4·3 mA to 5·6 mA during first 20 h, steady at 5·6 mA thereafter.
950 (i)	5	decrease from 6·3 mA to 3·5 mA.
950 (ii)	5½	decrease from 5·0 mA to 4·0 mA.
1000	1¾	decrease from 7·3 mA to 3·7 mA.

By operating the titanium wire with the shield interposed, it was found that any gas released from the titanium at temperatures between 900° C and 1100° C had a negligible poisoning effect. When the titanium wire was heated to 1100° C with the cathode exposed, serious poisoning could take place within an hour although the emission could be partially recovered by a reactivating process; but the emission was permanently reduced to an extremely low level after 15 h. At 1000° C the poisoning was still becoming apparent within a few hours. The results obtained when the titanium wire was operated at temperatures below 1000° C are shown in Table 4 from which it is seen that the maximum safe operating temperature is about 900° C.

DISCUSSION OF RESULTS

A comparison may be made between these results and those of Esperson and Rogers. The latter gave all their results in terms of the actual emission measured and not as emission density. Estimating the effective area of their grids as about 0·02 cm^2, the present results for the steady emission from heated tungsten wire on to which barium is deposited would agree with those of Espersen and Rogers if their "L" cathode operating at 1000° C was evaporating barium at a rate of about 1 monolayer in 4 min. Such a rate of evaporation is within a factor of two of the value obtained by Brodie and Jenkins[4] for an "L" cathode, so that there is reasonable agreement.

The deposition experiments with titanium show that if after a thin film of barium has been deposited on to a cold titanium wire the titanium wire is heated, then at 700° C the emission falls fairly rapidly. A similar comparatively rapid initial fall was found by Espersen and Rogers for a much thicker deposit evaporated from an "L" cathode on to titanium.

When the deposition of barium was carried out with the titanium wire heated to 500° C, however, there was initially a slight rise (see Fig. 2) followed by a very slow decay. This indicates that migration of the barium over the surface of the wire is probably taking place accompanied by a very slow re-evaporation of the barium. This makes it seem unlikely that there is an appreciable re-evaporation of barium from titanium at temperatures as low as 600° K (327° C) as suggested by Espersen and Rogers.

The results in Table 2 show that even when the rate of deposition is as high as 1 monolayer/min the high rate of re-evaporation makes it impossible to maintain a complete monolayer on the titanium surface above about 740° C. Below 740° C the coverage is probably fairly complete and the emission varies according to the Richardson law.

When a titanium wire, on to which barium oxide had been

deposited while cold, was heated, an appreciable decay in emission with time was obtained at 700° C (see Fig. 4). As barium oxide is not appreciably volatile at this temperature this would support the conclusion of Espersen and Rogers that titanium converts barium oxide to barium which in turn evaporates.

GENERAL CONCLUSIONS

It is concluded that in the range of temperatures investigated (700–1000° C) titanium would possess good screen grid emission suppression properties in the presence of an oxide-coated cathode. In use it would generally be necessary to limit the operating temperature of the titanium to 900° C to avoid poisoning the cathode emission. During activation, however, when the deposit would consist largely of barium oxide it might be necessary to maintain a screen grid at somewhat greater temperature for a short period which would not cause damage to the cathode. During subsequent operation when the deposit would be mainly barium the emission should maintain at a very low value.

Titanium should also be suitable for electrodes in electron beam devices. Although these may employ impregnated cathodes which are less likely to be poisoned than oxide cathodes, it would be unwise for the temperature of the electrodes to exceed 900° C as evaporated titanium could cause electrical breakdown over insulators.

ACKNOWLEDGEMENT

The author is indebted to the M.O. Valve Co. Ltd., on whose behalf the work described in this paper was carried out, for permission to publish the paper.

REFERENCES

(1) BAKER, B. O. *Brit. J. Appl. Phys.*, **4**, p. 311 (1953).
(2) CHAMPION, J. A. *Brit. J. Appl. Phys.*, **7**, p. 395 (1956).
(3) ESPERSEN, G. A., and ROGERS, J. W. *I.R.E. Trans*, **ED-3**, p. 100 (1956).
(4) BRODIE, I., and JENKINS, R. O. *J. Electronics*, **2**, p. 33 (1956).
(5) BECKER, J. A. *Trans Faraday Soc.*, **28**, p. 151 (1932).

The influence of the method of demagnetization on the reversible permeability of a high-permeability nickel-iron alloy

By R. C. JACKSON, B.Sc., Ph.D.,* E. W. LEE, B.Sc., Ph.D., and A. G. H. TROUGHTON, B.Sc.,†
Department of Physics, University of Nottingham

[*Paper received* 10 *June*, 1958]

Measurement of the reversible permeability of a high-permeability nickel-iron alloy shows that its dependence upon biasing field depends upon the method of demagnetization used. Results are found to be partially explicable in terms of residual magnetization, some specimens possessing residual magnetization even after a high-temperature anneal.

It is well known that the behaviour of a ferromagnetic substance in low and moderate fields depends on its magnetic and thermal histories. Recently, evidence has been presented which indicates that the low field properties of a ferromagnetic substance may depend also on the manner in which it has been demagnetized:[1,2] e.g. by heating above the Curie temperature or by gradual reduction of an alternating field. These observations are usually ascribed to differences in domain structure brought about by the different methods. In other words, there may exist a large number of possible domain configurations resulting in zero net magnetization, of which some are more likely to result from one form of the demagnetization process, others from another.

The authors have encountered this phenomenon during an investigation into the magnetic properties of certain high-permeability alloys and it is hoped that the following observations, although incomplete, may be of interest.

Fig. 1 shows the initial *B–H* characteristic of an alloy of composition 80% nickel, 11% iron, 5% copper, 4% molybdenum, supplied by the Post Office Research Station. The initial permeability as received, i.e. after annealing, is seen to be less than that after demagnetizing by gradual reduction of a 50 c/s, a.c. field to zero. Small differences in the initial domain structure and the shape of the initial *B–H* curve show up more clearly in the incremental (μ_I) or reversible permeability (μ_R) rather than their integrated contribution. The authors investigated μ_R since this is rather easier to measure than μ_I. The specimens, of composition 77% nickel, 14% iron; 5% copper, 4% molybdenum, were in the form of stamped rings 1 in. external diameter, $\frac{1}{16}$ in. internal dia-

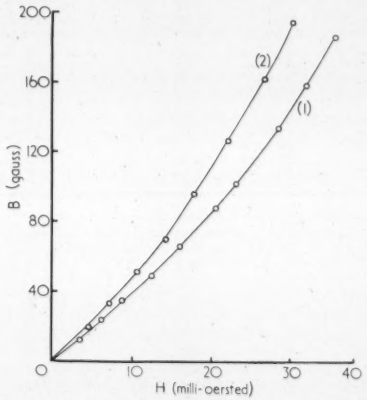

Fig. 1. Initial *B–H* characteristics for alloy of composition 80% nickel, 11% iron, 5% copper, 4% molybdenum Curve (1) was obtained after annealing at 1050° C; curve (2) after demagnetizing by gradual reduction of an alternative field to zero.

* Now at The Plessey Co. Ltd., Towcester, Northants.
† Now at S.E.R.L., Baldock, Herts.

meter. Rings were available in five different thicknesses, 15, 29, 49, 100 and 200 μ. Reversible permeability was measured on an a.c. bridge similar to that employed by Richards, Walker and Lynch,[3] at a frequency of 2·7 kc/s, but with provision for application of a polarizing field. Corrections were applied for eddy-current shielding and the exciting field was kept sufficiently low to ensure that the

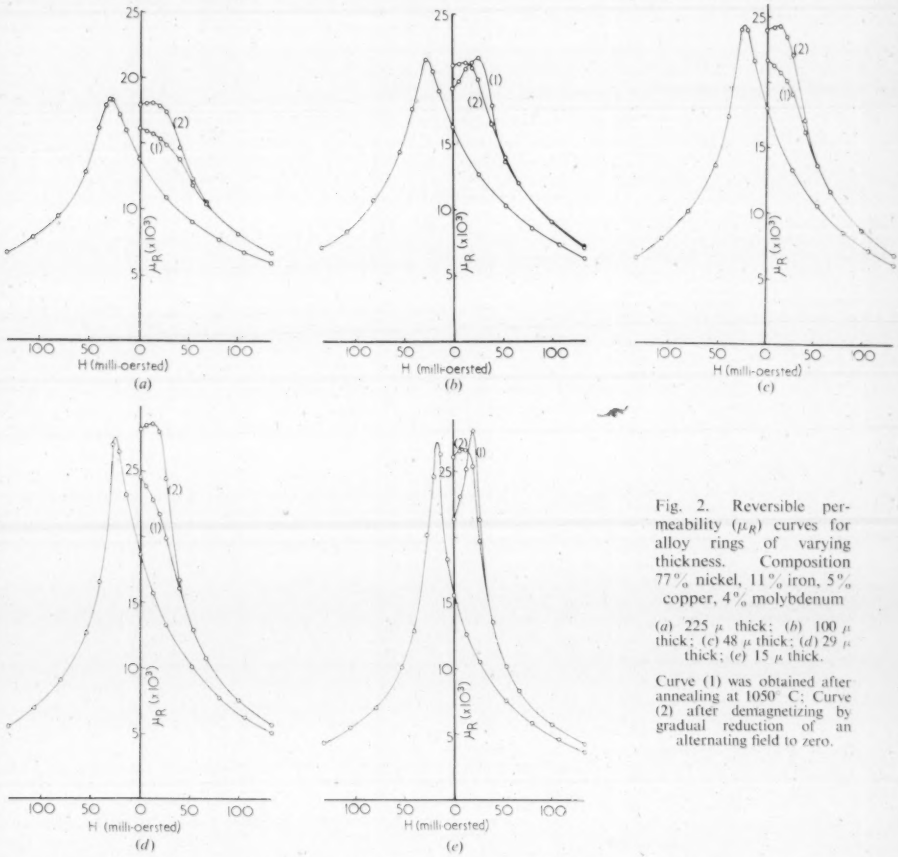

Fig. 2. Reversible permeability (μ_R) curves for alloy rings of varying thickness. Composition 77% nickel, 11% iron, 5% copper, 4% molybdenum

(*a*) 225 μ thick; (*b*) 100 μ thick; (*c*) 48 μ thick; (*d*) 29 μ thick; (*e*) 15 μ thick.

Curve (1) was obtained after annealing at 1050° C; Curve (2) after demagnetizing by gradual reduction of an alternating field to zero.

to the initial magnetization curve. For the latter, curve (1) represents the first measurements made on the specimens after an anneal at 1050° C, and therefore originates from a demagnetized state obtained by heating above the Curie temperature. Curve (2) originates from a demagnetized state obtained by gradual reduction of an alternating field to zero.

permeability thus measured was the true reversible permeability. In an attempt to avoid spurious effects due to stray magnetic fields, the specimens were magnetically shielded by placing them in a thick-walled, soft iron cylinder closed at both ends.

Results are shown in Fig. 2. The fact that these results apply to specimens of different thickness is purely incidental. No systematic differences in the effect described below were found which could be attributed to variations in the specimen thickness. Each figure shows the reversible permeability μ_R over a complete half cycle, together with that corresponding

In the first place it is evident that for all specimens the initial permeability is greater after a.c. demagnetization than after demagnetization by heating above the Curie temperature. For the latter μ_R increases with increasing biasing field to some maximum value for the 15 and 100 μ specimens, whilst for the 29, 49 and 225 μ specimens, μ_R decreases monotonically with field. It is difficult to avoid the inference that after annealing, each specimen is magnetized at $H = 0$, the 15 and 100 μ specimens being magnetized in a direction opposite to that of the biasing field, the reverse being the case for the three others.

To confirm this a further set of specimens was taken as annealed. A large field was applied, sufficient to saturate the specimens, and the change in induction was measured ballistically. The ballistic deflexion obtained (θ) was then compared with that obtained by reversing the magnetization (ϕ). Then

$$\Delta I/I = (2\theta - \phi)/\phi$$

where ΔI is the initial magnetization. The values of $\Delta I/I$ obtained for the five rings were $+0{\cdot}1$, $-0{\cdot}85$, 0, $-2{\cdot}8$ and $+1{\cdot}9\%$.

An attempt was then made to demagnetize these specimens in an alternating field, ascertaining the success of the procedure by the same ballistic method. The specimens were again found to be magnetized, but in this case always in the same direction. Similar behaviour can be seen in curves (2) of Figs. 2(*a*)–2(*e*).

Repeating the process with the leads to the specimens reversed gave similar results, but with the sign of the residual magnetization also reversed. This result might be caused by the presence of stray magnetic fields which may be negligible with alloys of lower permeability. However, the conditions of both methods of demagnetization are very similar to those under which the anhysteretic permeability is measured. This is very much higher than the usual d.c. permeability. Measurement by Polivanov and Braude[4] on Russian Mumetal (d.c. permeability 12 000) indicate a value of $2{\cdot}3 \times 10^7$, for the anhysteretic permeability at $H = 2 \times 10^{-5}$ oersted, the lowest field at which measurements were made. Moreover, this permeability increases rapidly with decreasing field strength. The alloys used in the present investigation possess initial permeabilities somewhat greater than those used by the Russian workers and the anhysteretic permeability may be very high, perhaps as much as 10^9. Under these circumstances the most minute stray field may be important.

It thus appears that the different demagnetizing procedures do indeed give rise to different magnetic states, but rarely reduce the magnetization to zero. This fact is by itself capable of providing an explanation for the observed difference in initial permeability. However, the fact that the initial permeability after a.c. demagnetization is always greater than after thermal demagnetization indicates that some other effect must be present as well. It is possible that this genuine effect is caused by a change in the number of domain walls.

ACKNOWLEDGEMENTS

It is a pleasure to thank Prof. L. F. Bates for his interest in this work and for many useful comments. We have benefited greatly from discussions with Mr. A. C. Lynch of the Post Office Research Station.

REFERENCES

(1) Broz, J., and Shernberk, J. *Czech. J. Phys.*, **5**, p. 425 (1955).
(2) Drokin, A. I., and Il'yushenko, V. L. *Zh. Éksper. Teor. Fiz.*, **29**, p. 339 (1955).
(3) Richards, C. E., Walker, E. V., and Lynch, A. C., *Proc. Instn Elect. Engrs*, **104**, *B*, p. 343 (1957).
(4) Polivanov, K. M., and Braude, A. A. *Trudy Moskovskogo Energeticheskogo Instituta*, **18**, p. 135 (1956).

NOTES AND NEWS

Correspondence

Deuterium-filled thyratrons

Hot cathode hydrogen thyratrons are now widely used as pulse modulators in radar equipments and recently have been used as grid controlled rectifiers.

The main advantages of hydrogen are (*a*) that the deionization time of the gas is very short and (*b*) that gas which is lost owing to "clean up" when the valve is operating, can be replenished using a reservoir such as a capsule of titanium hydride.

The disadvantage of hydrogen is the relatively high cathode–anode arc voltage which is realized in these devices. In simple diodes the voltage with mercury or xenon filling is about 10 V and with hydrogen about 20 V. These voltages are near the ionization potential of the gas concerned. If any obstacle, such as a grid electrode, is placed between the cathode and anode, it is found that the voltage with mercury and xenon is substantially unchanged, whereas with hydrogen it may rise to 50 or even 100 V.

A possible explanation is as follows. The positive ions in a hot cathode discharge are only required to neutralize the negative space charge of electrons which would otherwise form. If these ions remained permanently in the discharge space, only a few tenths of a volt would be required to draw the cathode current across to the anode. In practice, ions are lost by diffusion to the electrodes or walls of the device, where recombination can take place. These must be replaced by further ionizing collisions in the discharge and this implies that some electrons are accelerated to the ionization potential of the gas.

If the rate of loss of ions is small, as it is in a diode, very few electrons need make ionizing collisions in order to replace the losses, and with a cathode-anode voltage near to the ionization potential, the rate of production of ions will be

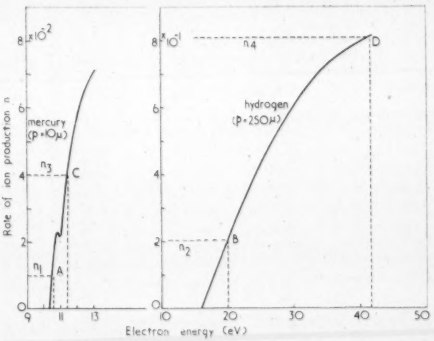

Fig. 1. Number of ions (n) generated per electron per centimetre of path as a function of electron energy (eV)

sufficient. This is illustrated very approximately in Fig. 1 (based on measurements by Smith and Tate,[1] and Nottingham[2]) which shows the rate of ion production n as a function of electron energy. For simplicity, it is assumed that the electron energy is proportional to the voltage across the device. In the case of mercury, the n_1 ions which are required to replace losses are produced at the point A on the curve; the electron energy is then almost equal to the ionization potential. In the hydrogen diode, although the losses are higher owing to the higher mobility and diffusion rate of the ions, and require n_2 ions to replace them, the electron energy at point B is only a few volts above the ionization potential of hydrogen.

If any obstacle is placed in the path of the discharge, the rate of loss of ions is increased. In the case of mercury (or xenon), if the rate of loss of ions is quadrupled, and n_3 ions are required to replace them, the electron energy required rises only slightly to point C on the curve. With hydrogen, if the losses are quadrupled the n_4 ions needed are produced at point D at considerably increased electron energy.

These considerations suggested the use of deuterium in a gas-filled valve since the lower mobility and diffusion rate of the heavier ion will result in reduced losses.

Fig. 2(*a*) shows the voltage across a cathode-grid discharge in hydrogen-filled and deuterium-filled thyratrons of exactly similar construction. Fig. 2(*b*) gives the corresponding

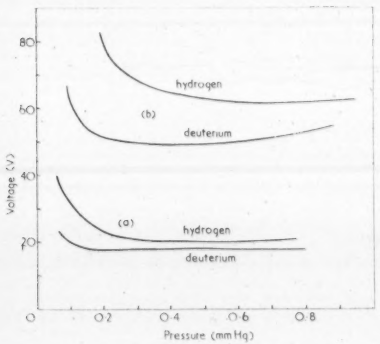

Fig. 2. Pressure-voltage characteristics for hydrogen and deuterium filled thyratrons

(*a*) cathode-grid voltage; (*b*) cathode-anode voltage.

cathode–anode discharge voltages, the grid being connected to cathode. In the cathode-grid case, in which no obstacle is present between the two electrodes, the voltages are similar, both being a little above the ionization potential of hydrogen. The cathode–anode voltage of the deuterium valve is, however, significantly lower than that of the hydrogen valve.

An additional advantage of deuterium is that the anode-cathode voltage begins to rise at a rather lower pressure than with hydrogen. This may well be associated with the difference in Townsend's α for the two gases.[3]

Further observations are as follows:

(i) the deionization time of the deuterium valve was found to be 40% longer than that of the hydrogen valve; this increase is not significant in most applications;

(ii) deuterium can be replenished from a reservoir of titanium or zirconium "deuterides" in a similar manner to hydrogen;

(iii) there is some evidence that the Paschen sparking potential, between anode and grid, is higher in the deuterium valve. This allows the use of higher gas pressure at a given anode hold-off voltage.

The use of deuterium as a filling in thyratrons and grid-controlled rectifiers would therefore appear to offer considerable advantages over hydrogen.

The writers are indebted to the Admiralty for permission to publish this note.

Research Laboratories of
The General Electric Co. Ltd.
Wembley, England.

K. G. Cook
G. G. Isaacs

[13 June, 1958]

REFERENCES

(1) Smith, P. T., and Tate, J. T. *Phys. Rev.*, **39**, p. 270 (1932).
(2) Nottingham, W. B. *Phys. Rev.*, **55**, p. 203 (1939).
(3) Rose, D. J. *Phys. Rev.*, **104**, p. 273 (1956).

Deuterium as a filling for high-voltage thyratrons

To explore the usefulness of deuterium in high-voltage thyratrons, and to illuminate the already successful application of hydrogen in such valves, an experimental study has been made of the characteristics of a particular thyratron (type G.H.T. 1) when filled with deuterium. An identical valve filled with hydrogen was used for comparison.

The recovery time was measured by passing a current of 100 A and subsequently applying a probing pulse of 1·5 kV to the anode* (Fig. 1). The results are in agreement with the

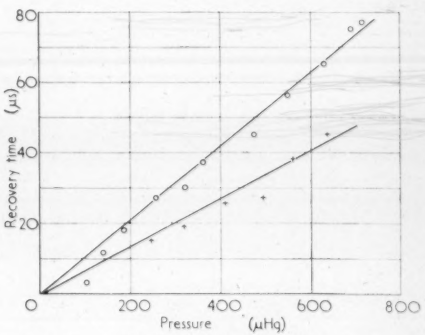

[Crown copyright reserved]

Fig. 1. Recovery time of thyratron
○ = deuterium. + = hydrogen.

generally accepted theory that the deionization is governed by diffusion.† The arc drop and grid-cathode potential during conduction to the anode were measured at a current of 100 A at 1·5 μs after the initiation of the discharge (Fig. 2). The values are higher than for direct current in all cases, presumably owing to the absence of thermal equilibrium.

* *Technical Note No.* 604 (Radar Research Establishment, unpublished report).

† Malter, L. and Johnson, E. O., *R.C.A. Review*, **11**, pp. 165, 178 (1950).

Paschen breakdown curves were taken with −100 V grid bias by determining the anode potential at which di/dv (which is defined as the derivative of anode current with respect to anode voltage—other parameters being held constant) became infinite (Fig. 3). This occurred at currents up to 0·5 mA at the higher voltages.

The peak value of the rate of fall of anode voltage during the initiation of the discharge was measured by means of a capacitance-resistance differentiating circuit and a high-speed oscilloscope (Fig. 4). The upper curve was obtained with the thyratron anode charged to a potential of 10 kV through a resistor of 25 MΩ. For the lower curve the thyratron was in series with an inductor of 2·8 μH and a capacitor of 1250 pF charged to 10 kV. It is estimated that the difference between the curves is attributable to the effect of the cathode lead inductance (0·4 μH approximately). The peak value of the rate of rise of current was measured by means of a mutual inductor and high-speed oscilloscope, with a capacitor of 500 pF connected from anode to cathode of the thyratron and charged to 10 kV (Fig. 5).

All the observations were made with a sufficient interval between successive discharges for the initial state of the gas and electrode temperatures to be restored. Deuterium shows equal or superior properties to hydrogen in every respect except for recovery time. The difference in the Paschen breakdown characteristics is attributed to a difference in γ (which represents the second Townsend breakdown coefficient) between the two gases. Their equality in respect of rate of fall of voltage indicates a controlling mechanism independent of γ and of the mass of the ion.

The valves were constructed by the Research Laboratories of The General Electric Co. Ltd.

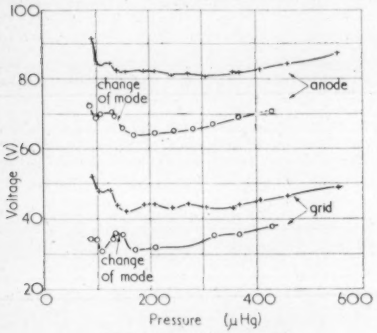

[Crown copyright reserved]

Fig. 2. Arc drop of thyratron
○ = deuterium. + = hydrogen.

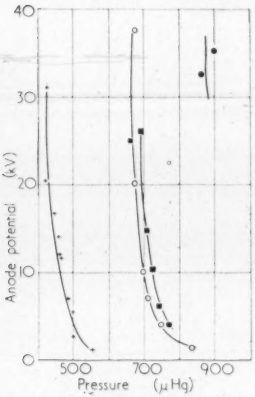

[Crown copyright reserved]

Fig. 3. Paschen breakdown curves
+ = hydrogen, cathode cold. ■ = hydrogen, cathode hot.
○ = deuterium, cathode cold. ● = deuterium, cathode hot.

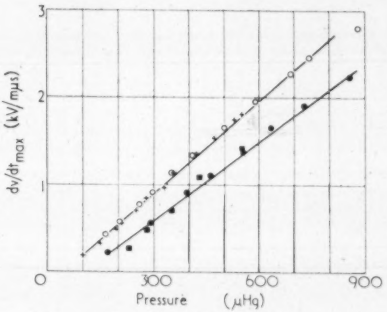

[Crown copyright reserved]

Fig. 4. Maximum rate of fall of voltage
+ = hydrogen, 25 MΩ. ■ = hydrogen, 1250 pF, 2·8 μH.
○ = deuterium, 25 MΩ. ● = deuterium, 1250 pF, 2·8 μH.

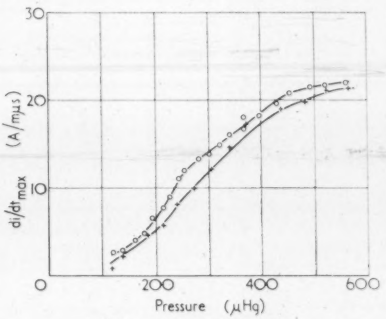

[Crown copyright reserved]

Fig. 5. Maximum rate of rise of current
+ = hydrogen. ○ = deuterium.
500 pF capacitor; 0·4 μH residual inductance (estimated).

Royal Radar Establishment, R. J. ARMSTRONG
Ministry of Supply, Malvern. N. S. NICHOLLS

[11 *July*, 1958]

Notes and comments

Congress of the International Federation of Automatic Control, Moscow, 1960

The first International Congress of the International Federation of Automatic Control is to be held in Moscow from 25 June to 5 July, 1960. The British Conference on Automation and Computation has been asked by the Executive Council of the International Federation of Automatic Control for their co-operation in arranging for the submission of papers for the Congress from British sources and, in accordance with this request, the British contribution to the Congress will be co-ordinated through the General Committee of the British Conference on Automation and Computation with the assistance of its three Groups.

The Congress will cover the following three fields:

Section I, Theoretical and experimental investigations on automatic control and servomechanisms;

Section II, Instrumentation and investigations connected with the development of automatic control systems;

Section III, Industrial applications of automatic control (including the application of prediction and computing devices).

The Congress will include: (*a*) the presentation and discussion of scientific reports, (*b*) excursions to scientific institutions and also to various automatic undertakings, (*c*) visits to centres of culture in Moscow.

Intending authors should submit abstracts of their proposed papers, not exceeding 500 words in length, and not later than 1 February, 1959, to Mr. W. Bamford, Honorary Secretary, Group B, British Conference on Automation and Computation, c/o The Institution of Electrical Engineers, Savoy Place, London, W.C.2.

The Physical Society's annual exhibition of scientific instruments and apparatus

The Physical Society announces that its forty-third annual exhibition will be held at the Royal Horticultural Society's Old and New Halls, Westminster, London, S.W.1, from 19–22 January, 1959 (inclusive).

Entrance to the exhibition is by ticket only and these may be obtained, free of charge, from the offices of the Society, 1 Lowther Gardens, Prince Consort Road, London, S.W.1. Members of The Institute of Physics may obtain tickets from the Institute. The handbook of scientific instruments and apparatus published in connexion with the exhibition is available from the Society, price 6*s.*; by post 7*s.* 8*d.*

Medical electronics discussion group

An Interim Committee composed of members of The Institution of Electrical Engineers and of the medical profession, having a common interest in medical electronics, discussed at a recent meeting the scope and future activities of the Medical electronics discussion group which has been set up by the Council of The Institution.

It has been decided that the activities of the Group should be centred round advanced electronic techniques applied or related to medical and biological problems, and there will be a program of informal discussion meetings which will provide a forum for the exchange of information between the two professions on subjects coming within this field.

It is proposed to provide an opportunity in the course of each discussion meeting for members present to give notice of any problems which they have encountered (not necessarily related to the topic discussed at the meeting), in the hope that others present may be able to offer suggestions for their resolution.

A mailing list has been compiled of those who have expressed interest in the Group's activities. Any interested reader should send his name and address to the Secretary of The Institution of Electrical Engineers, Savoy Place, London, W.C.2.

Journal of Scientific Instruments

Contents of the December issue

ORIGINAL CONTRIBUTIONS

Papers

A thermometer for high-speed aircraft. By D. D. Clark.

The measurement of the dielectric properties of liquids in an H_{01} resonator. By J. S. Dryden.

A self-adjusting unit for the control of an animal calorimeter. By A. E. Hawkins.

A thermocouple method for measuring relative humidity in the range 95–100%. By J. E. Monteith and P. C. Owen.

A simple orbit contractor for betatron-started synchrotrons. By J. Moffatt.

A precision, direct-reading, colour temperature meter. By P. Hariharan and M. S. Bhalla.

A temperature-chlorinity-depth recorder for use at sea. By B. V. Hamon and N. L. Brown.

A technique for the measurement of diffusion coefficients in molten salts. By C. A. Angell and J. O'M. Bockris.

An apparatus for visual and acoustical display of electrocardiograms. By A. Strojnik.

A very sensitive relay, able to withstand heavy overloading. By F. H. Plankeel.

Image intensifier for the electron microscope. By M. E. Haine, A. E. Ennos and P. A. Einstein.

Laboratory and workshop notes

A low-temperature resistance thermometer using p-type gallium arsenide. By R. F. Broom.

An attachment for measuring reflexion interference spectra in the Beckman DK2 ratio-recording spectrophotometer. By D. G. Lloyd.

A method of completely filling capillary tubes with mercury for diameter determination. By G. F. Whitty.

An X-ray tube target current stabilizer. By R. S. Crisp.

A triode-connected pentode with stabilized anode current. By B. C. Cox.

A high-pressure electrical lead-in. By D. F. Gibbs and M. Jarman.

Improvements in photographic printing of electron micrographs. By D. M. Hall.

An improvement to the multi-stage impulse generator. By W. A. Smith.

NOTES AND NEWS

Correspondence

The magnetic spectra of some ferrites. From E. A. Faulkner and J. F. Werner.

New instruments, materials and tools — New books

Notes and comments

THIS JOURNAL is produced monthly by The Institute of Physics, in London. It deals with all branches of applied physics (including theory and technique).

All rights reserved. Responsibility for the statements contained herein attaches only to the writers.

EDITORIAL MATTER. Communications concerning editorial matter should be addressed to the Editor, The Institute of Physics, 47 Belgrave Square, London, S.W.1. (*Telephone:* Belgravia 6111.) Prospective authors are invited to prepare their scripts in accordance with the *Notes on the preparation of contributions*. (Price 2*s.* 6*d.* including postage.)

REPRODUCTION. The Institute of Physics is a signatory to The Royal Society's Fair Copying Declaration. Details may be obtained upon application from The Royal Society, London, W.1.

ADVERTISEMENTS. Communications concerning advertisements should be addressed to the agents, Messrs. Walter Judd Ltd., 47 Gresham Street, London, E.C.2. (*Telephone:* Monarch 7644.)

CLAIMS FOR MISSING JOURNALS. Claims from regular subscribers to this *Journal* for missing numbers will only be considered if received within 60 days of the date of mailing plus normal outward time of transit and time for lodging the claim. Losses attributable to failure to notify a change of address or to similar omissions will not be considered.

SUBSCRIPTION RATES. A new volume commences each January. The charge is £6 per volume ($17 U.S.A.), including index (post paid), payable in advance. Single parts, so far as available, may be purchased at 12*s.* 6*d.* each ($1.75 U.S.A.), post paid, cash with order. Orders should be sent to The Institute of Physics, 47 Belgrave Square, London, S.W.1, or to any bookseller.